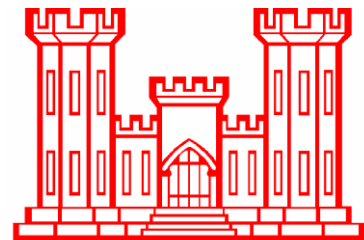
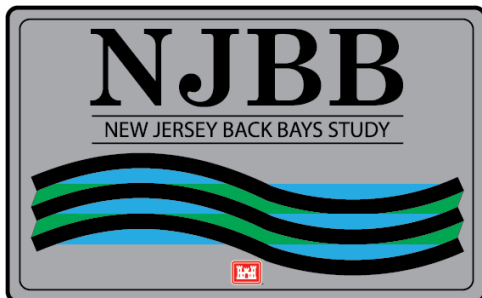

**ENGINEER RESEARCH AND
DEVELOPMENT CENTER APPENDIX**

**NEW JERSEY BACK BAYS
COASTAL STORM RISK MANAGEMENT
FEASIBILITY STUDY**

PHILADELPHIA, PENNSYLVANIA

APPENDIX H

August 2021



**U.S. Army Corps of Engineers
Philadelphia District**

THIS PAGE INTENTIONALLY LEFT BLANK

Table of Contents

H-1) ANALYSIS OF PROPOSED STORM PROTECTION STRUCTURES ON THE HYDRODYNAMICS AND SALINITY IN NEW JERSEY BACK BAYS (NJBB)

H-2) NUMERICAL STORM SURGE MODELING AND PROBABILISTIC ANALYSIS FOR EVALUATING PROPOSED NEW JERSEY BACK BAYS INLET CLOSURES

H-3) RESIDENCE TIME ANALYSIS TO PREDICT IMPACT OF PROPOSED STORM PROTECTION STRUCTURES IN NEW JERSEY BACK BAYS (NJBB)

H-1) ANALYSIS OF PROPOSED STORM PROTECTION
STRUCTURES ON THE HYDRODYNAMICS AND SALINITY
IN NEW JERSEY BACK BAYS (NJBB)

ERDC/CHL TR-20-X

Coastal and Hydraulics Laboratory



**US Army Corps
of Engineers®**
Engineer Research and
Development Center



DRAFT: Analysis of Proposed Storm Protection Structures on the Hydrodynamics and Salinity in New Jersey Back Bays (NJBB)

Jennifer McAlpin and Cassandra Ross

February 2020

The U.S. Army Engineer Research and Development Center (ERDC) solves the nation's toughest engineering and environmental challenges. ERDC develops innovative solutions in civil and military engineering, geospatial sciences, water resources, and environmental sciences for the Army, the Department of Defense, civilian agencies, and our nation's public good. Find out more at www.erdclibrary.usace.army.mil.

To search for other technical reports published by ERDC, visit the ERDC online library at <http://acwc.sdp.sirsi.net/client/default>.

DRAFT: Analysis of Proposed Storm Protection Structures on the Hydrodynamics and Salinity in New Jersey Back Bays (NJBB)

Jennifer McAlpin and Cassandra Ross

*Coastal and Hydraulics Laboratory
U.S. Army Engineer Research and Development Center
3909 Halls Ferry Road
Vicksburg, MS 39180-6199*

Final report

Approved for public release; distribution is unlimited.

Prepared for U.S. Army Corps of Engineers, Philadelphia District
Under Work Unit

Abstract

The New Jersey Back Bay area consists of X acres of estuarine and marsh environments. The U.S. Army Engineer District, Philadelphia, requested the U.S. Army Engineer Research and Development Center, Coastal and Hydraulics Laboratory, to perform hydrodynamic and salinity modeling of proposed storm surge protection measures at several inlets from the Atlantic Ocean. The modeling results are necessary to provide data for environmental analysis. The model setup and validation are presented as well as the results of several proposed alternatives for with and without project results.

DISCLAIMER: The contents of this report are not to be used for advertising, publication, or promotional purposes. Citation of trade names does not constitute an official endorsement or approval of the use of such commercial products. All product names and trademarks cited are the property of their respective owners. The findings of this report are not to be construed as an official Department of the Army position unless so designated by other authorized documents.

DESTROY THIS REPORT WHEN NO LONGER NEEDED. DO NOT RETURN IT TO THE ORIGINATOR.

Contents

Abstract	2
Figures and Tables	6
Preface	9
1 Introduction	11
Background	11
Objective	11
Approach.....	11
2 Model Development	13
Numerical code	13
Mesh development.....	13
Boundary conditions	17
<i>Tide Boundary Condition</i>	17
<i>Freshwater River Inflows</i>	20
<i>Meteorological Input (Wind)</i>	23
<i>Ocean Salinity Boundary</i>	25
<i>Precipitation</i>	27
<i>AdH model parameters</i>	28
3 Model/Field Comparison – Calibration and Validation	31
Field Data Collection	31
Hydrodynamic comparisons	31
<i>Water surface elevation</i>	32
<i>Harmonic Analysis</i>	39
<i>Discharge</i>	44
Salinity comparisons.....	50
4 Inlet Area of Influence	56
5 Plan Alternatives	64
6 Alternative Result Analysis	75
Analysis Locations.....	75
Model Results.....	78
<i>Percentile Analysis</i>	79
<i>Tidal Prism</i>	79
<i>Tidal Amplitude</i>	82
<i>Salinity</i>	86
<i>Velocity Magnitude</i>	89
<i>Residual Velocity</i>	91
7 Discussion of Alternatives	92

Tidal Prism	92
Water Surface Elevation and Tidal Amplitude	92
Salinity	92
Velocity.....	93
In General	93
8 Conclusions.....	94
References.....	95
Appendix A: Model Bathymetry Development.....	97
Appendix B: Tide Boundary Condition Development	103
Appendix C: Model/Field Comparisons	112
Water Surface Elevation	112
Harmonic Analysis.....	129
Salinity	145
Appendix D: Alternative Water Surface Elevation and Tidal Comparisons	157
Comparison to Base.....	157
<i>Water Surface Elevation Plots</i>	157
<i>Tidal Amplitude Plots</i>	173
<i>Tidal Prism Plots</i>	189
Comparisons to Base with Sea Level Rise.....	194
<i>Water Surface Elevation Plots</i>	194
<i>Tidal Amplitude Plots</i>	212
<i>Tidal Prism Plots</i>	228
Appendix E: Alternative Salinity Comparisons	233
Comparisons to Base.....	233
<i>Maximum, Mean, Minimum</i>	233
<i>Point Comparisons</i>	236
<i>Regional Mean</i>	282
Comparisons to Base with Sea Level Rise.....	303
<i>Maximum, Mean, Minimum</i>	303
<i>Point Comparisons</i>	306
<i>Regional Mean with Sea Level Rise</i>	352
Appendix F: Alternative Velocity Comparisons.....	361
Comparisons to Base.....	361
<i>Maximum, Mean, Minimum</i>	361
<i>Point Comparisons</i>	364
<i>Regional Mean</i>	410
<i>Flood/Ebb Velocity Comparison at Structures</i>	430
<i>Residual Velocity at Structures</i>	469
Comparisons to Base with Sea Level Rise.....	489
<i>Maximum, Mean, Minimum</i>	489

Point Comparisons492
Regional Mean with Sea Level Rise.....538
Flood/ebb Velocity Comparison at Structures with Sea Level Rise547
Residual Velocity at Structures with Sea Level Rise.....566

Appendix G: Field Data Collection Reportdlxxvii

Introductiondlxxviii
Summary of workdlxxviii
 Site conditions.....dlxxviii
General methods.....dlxxix
 Survey procedure dlxxix
 Data processing dlxxix
 Data products..... dlxxx
Great Egg Inlet..... dlxxx
Little Egg Inlet..... dxciii
Barnegat Inlet..... dxcvii

Report Documentation Page

Figures and Tables

Figures

Figure 1. NJBB area map.....	12
Figure 2. Proposed coastal protection.	12
Figure 3. Model domain bathymetry.	15
Figure 4. Mesh resolution.....	16
Figure 5. Little Egg Inlet mesh resolution	17
Figure 6. AdH tide boundary	18
Figure 7. Complete tidal boundary condition	19
Figure 8. Tidal boundary condition (subset).....	20
Figure 9. Freshwater inflow locations.....	21
Figure 10. NJBB freshwater river inflows.	22
Figure 11. Delaware River freshwater inflow.	22
Figure 12. 2018 wind speed and direction for JACNCMET.	24
Figure 13. JACNCMET wind speed components.	25
Figure 14. UK Met Office salinity data in model domain vicinity.	26
Figure 15. UK Met Office salinity data (ppt).	27
Figure 16. JACNCMET precipitation.....	28
Figure 17. Material designations.....	29
Figure 18. Barnegat Inlet material designations (showing jetties).....	30
Figure 19. Water surface elevation comparison locations.....	33
Figure 20. Water surface elevation comparisons over time for Barnegat Bay at Mantoloking.....	35
Figure 21. Water surface elevation comparison box plot for Barnegat Bay at Mantoloking.....	35
Figure 22. Water surface elevation comparisons over time for Barnegat Bay at Barnegat Light.....	36
Figure 23. Water surface elevation comparison box plot for Barnegat Bay at Barnegat Light.....	36
Figure 24. Water surface elevation comparisons over time for Inside Thorofare.	37
Figure 25. Water surface elevation comparison box plot for Inside Thorofare.	37
Figure 26. Water surface elevation comparisons over time for Ingram Thorofare.	38
Figure 27. Water surface elevation calibration comparison box plot for Ingram Thorofare.	38
Figure 28. Barnegat Inlet discharge transect.....	44
Figure 29. Barnegat Inlet discharge comparison.....	45
Figure 30. Little Egg Inlet discharge transects.	45
Figure 31. Little Egg Inlet discharge comparison at Transect 1.....	46
Figure 32. Little Egg Inlet discharge comparison at Transect 2.	46
Figure 33. Little Egg Inlet discharge comparison at Transect 3.	47
Figure 34. Little Egg Inlet discharge comparison at Transect 4.	47

Figure 35. Great Egg Inlet discharge transects..... 48

Figure 36. Great Egg Inlet discharge comparison at Transect 41. 48

Figure 37. Great Egg Inlet discharge comparison at Transect 2. 49

Figure 38. Great Egg Inlet discharge comparison at Transect 3. 49

Figure 39. Great Egg Inlet discharge comparison at Transect 4. 50

Figure 40. Salinity comparison locations..... 51

Figure 41. Historic salinity comparison locations..... 52

Figure 42. Mantoloking salinity comparison. 53

Figure 43. Barnegat Light salinity comparison..... 53

Figure 44. JACB6WQ salinity comparison..... 54

Figure 45. JACNEWQ salinity comparison..... 54

Figure 46. Inlet labels. 56

Figure 47. Salinity comparison locations. JACBAWQ will not be compared. 57

Figure 48. Inlet influence comparison at Brick. 58

Figure 49. Inlet influence comparison at Barnegat Bay at Mantoloking. 58

Figure 50. Inlet influence comparison at Berkeley. 59

Figure 51. Inlet influence comparison at Barnegat Light. 59

Figure 52. Inlet influence comparison at Stafford. 60

Figure 53. Inlet influence comparison at Westecunk..... 60

Figure 54. Inlet influence comparison at Beach Haven. 61

Figure 55. Inlet influence comparison at Little Egg. 61

Figure 56. Inlet influence comparison at JACB6WQ..... 62

Figure 57. Inlet influence comparison at JACB9WQ..... 62

Figure 58. Inlet influence comparison at JACNEWQ..... 63

Figure 59. Manasquan structure A1 and A2..... 65

Figure 60. Barnegat structure A1 and A2..... 66

Figure 61. Barnegat structure A3 and A4..... 67

Figure 62. Great Egg structures A1 and A2..... 69

Figure 63. Absecon structures A1 and A2..... 71

Figure 64. Absecon Bay Boulevard structures. 72

Figure 65. Southern Ocean City Bay (72nd Street) structures. 73

Figure 66. NACCS bathymetry showing area that could wet under the 0.445m sea level rise. Points are the NACCS data and the brown line is the AdH model domain..... 74

Figure 67. Northern Region Analysis Locations..... 76

Figure 68. Central Region Analysis Locations 77

Figure 69. Southern Region Analysis Locations..... 78

Figure 70. Tidal prism analysis regions..... 80

Figure 71. VDatum computed conversion from MLLW to NAVD88 (ft) 98

Figure 72. Converted survey data 99

Figure 73. NED dataset quadrants..... 100

Figure 74. AdH model bathymetry 102

Figure 75. Model domain and tidal boundary location. 103

Figure 76. Tidal constituent amplitude comparisons. 104

Figure 77. NACCS and ADCIRC database harmonic tide comparison..... 105

Figure 78. NACCS and ADCIRC database harmonic tide difference. 105

Figure 79. ADCIRC database and Atlantic City harmonic tide comparison. 106

Figure 80. ADCIRC database and Atlantic City harmonic tide difference. 107

Figure 81. NOAA gage secondary harmonic constituent tide comparison. 108

Figure 82. NOAA gage secondary harmonic constituent tide difference..... 109

Figure 83. NOAA gage nonharmonic tide comparison. 110

Figure 84. AdH model boundary tide at select locations and comparison to other components. 111

Tables

Table 1. USGS gage information for freshwater flows. 21

Table 2. Model parameters. 28

Table 3. Statistical model/field calibration comparison of water surface elevation. 34

Table 4. With project alternative combinations..... 74

Table 5. Mean tidal prism comparison to base..... 81

Table 6. Mean tidal prism comparison to base sea level rise..... 81

Table 7. Mean tidal amplitude..... 82

Table 8. Mean tidal amplitude comparison to base. 83

Table 9. Mean tidal amplitude for sea level rise alternatives..... 84

Table 10. Mean tidal amplitude comparison to base for sea level rise alternatives. 85

Table 11. Mean salinity..... 86

Table 12. Mean salinity for sea level rise alternatives. 87

Table 13. Mean velocity magnitude. 89

Table 14. Mean velocity magnitude for sea level rise alternatives..... 90

Preface

The model investigation presented in this report was authorized and funded by the U.S. Army Corps of Engineers, Philadelphia District.

The work was performed at the U.S. Army Engineer Research and Development Center, Coastal and Hydraulics Laboratory (ERDC-CHL), Vicksburg, MS. At the time of publication of this report, Dr. Ty V. Wamsley was Director, and Mr. Jeffrey R. Eckstein was Deputy Director, ERDC-CHL. Direct supervision was provided by Dr. Cary Talbot, Chief, Flood and Storm Protection Division, and **Mr. Keith Flowers**, Chief, River and Estuarine Engineering Branch.

COL Teresa Schlosser was Commander of ERDC, and Dr. David W. Pittman was Director.

1 Introduction

Background

After hurricane Sandy wreaked havoc along the east coast of the United States in the fall of 2012, the desire for more robust coastal protection along the Atlantic coastline grew rapidly. The North Atlantic Coast Comprehensive Study (NACCS) included a large scale storm surge modeling effort to analyze potential flooding due to various storm conditions (USACE 2015 and Cialone et al. 2017). The NACCS risk study identified several areas of further detailed evaluation - New Jersey Back Bays being one of these (Figure 1). This area extends from Brick, NJ, to the southern tip of the state at Delaware Bay. The area of interest includes the inlets where the Atlantic Ocean joins the back bays as well as the area between the barrier islands and the mainland where large areas of wetland habitat reside.

Objective

In 2018, NAP requested the ERDC-CHL perform hydrodynamic and salinity modeling of proposed storm surge protection measures. The modeling results are necessary to provide data for hydrodynamic and salinity analysis as well as ecological models to determine impacts on aquatic habitat. The model setup, validation and results for with and without project are documented.

Approach

A two-dimensional (2D) Adaptive Hydraulics (AdH) model was developed and validated for simulation of hydrodynamics and salinity. The model was validated to available field data for all parameters and then utilized to test project alternatives for present and future sea level rise conditions. A field data collection effort was performed in February 2019 to collect salinity and discharge/velocity data at three major inlets over a 13-hour tidal cycle – Barnegat, Little Egg, and Great Egg. The field data collection supported the use of a 2D model as opposed to a three-dimensional (3D) model due to the little salinity stratification that was measured in the field.

Chapter 2 discusses the model development and boundary condition definitions for the hydrodynamic and salinity transport model. Chapter 3 documents the model to field data comparisons for hydrodynamics and salinity. Chapter 4 focuses on the plan alternatives and simulation periods.

Chapter 5 focuses on the comparisons of these modifications to the present condition for hydrodynamics and salinity. Chapter 6 provides the conclusions of this numerical model investigation. Appendix G gives information on the field data collection effort.

Figure 1. NJBB area map.

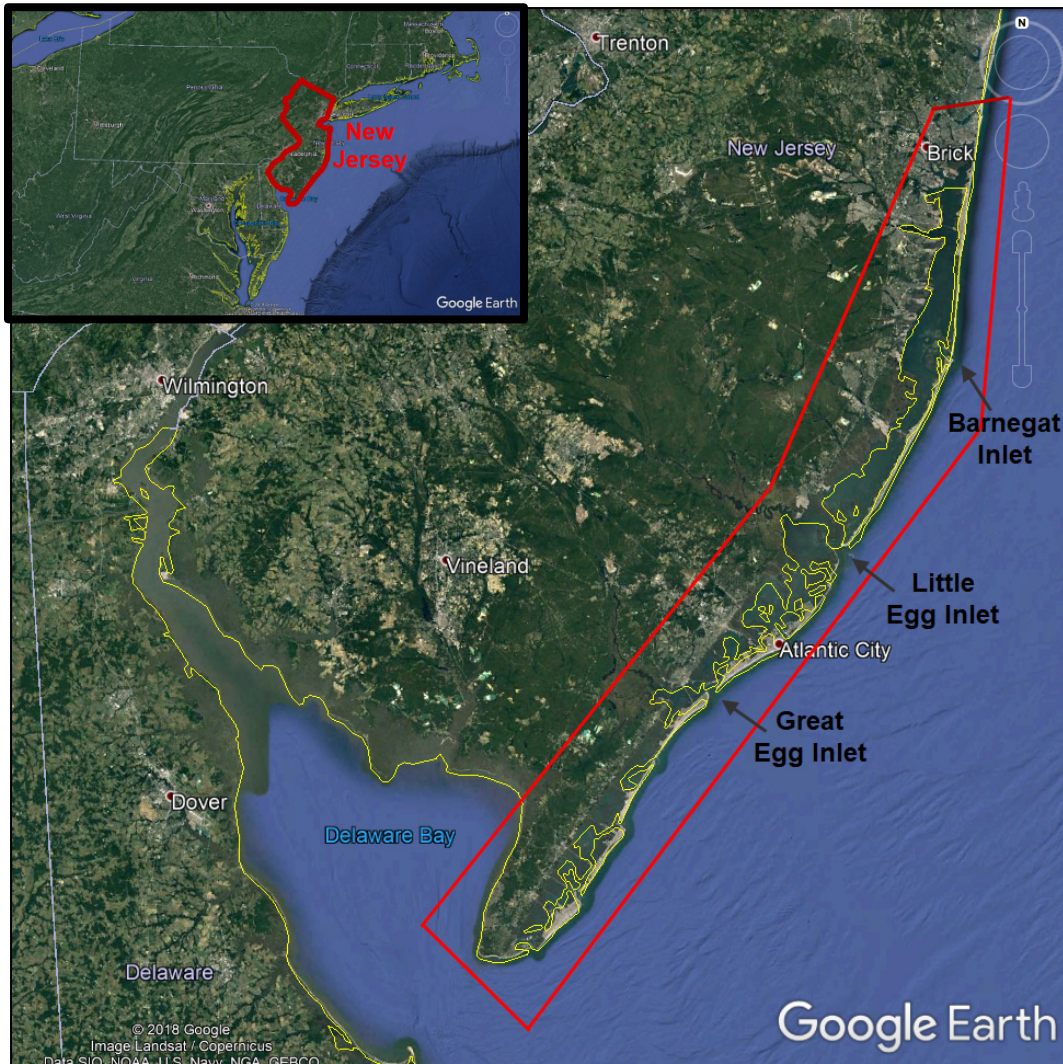


Figure 2. Proposed coastal protection.

2 Model Development

A numerical model was developed to analyze alternative plans for coastal protection of the NJBB. The model was developed such that the natural driving forces of the system are included — winds, tides, salinity, freshwater inflows, and friction effects. The model results are compared to field data collected during the simulation period to ensure an accurate representation of nature. This model is calibrated and validated using data from 2018 and 2019.

Numerical code

AdH is the numerical model code applied for the simulations in this study (Savant et al. 2014; Savant and Berger 2015). AdH is a finite element code that is capable of simulating 3D Navier-Stokes equations, 2D and 3D shallow water equations, and groundwater equations. It can be used in a serial or multiprocessor mode on personal computers and high-performance computing systems. AdH can refine the domain mesh in areas where more resolution is needed at certain times due to changes in the flow conditions and then remove the added resolution when it is no longer needed, to minimize computational burden. The code also includes automatic time-step adaption, as needed. AdH can simulate the transport of conservative constituents, such as dye clouds, as well as simulate sediment transport, when used with SEDLIB, that is coupled to bed and hydrodynamic changes. This code has been applied to model riverine flow (Bell et al. 2017; Clifton et al. 2017) estuarine circulation (Tate et al. 2009; McAlpin et al. 2013), and sediment transport (Sharp et al. 2013; Heath et al. 2015; Letter et al. 2015).

For this study, the 2D shallow water module of AdH is applied for all simulations. This code solves for depth-averaged depth, velocity and salinity throughout the model domain. (More details of the 2D shallow water module of AdH and its computational philosophy and equations are available in Savant et al. 2014 and Savant and Berger 2015.) AdH version 4.6 was applied for this study.

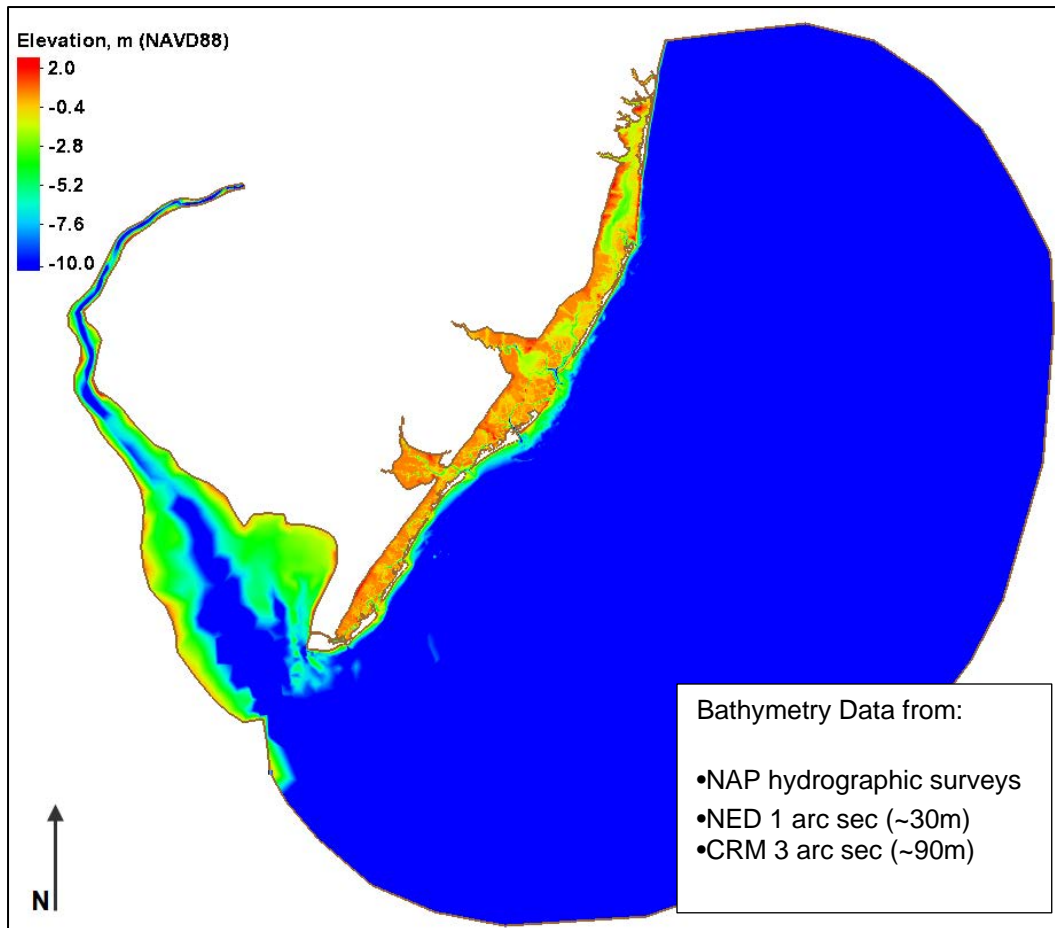
Mesh development

The model domain was determined using aerial images and bathymetry/topographic data for the area. The Surface Water Modeling

System was used to generate a 2D surface mesh and define material regions for applying specific model features, such as bed roughness. The domain is defined horizontally in Universal Transverse Mercator, zone 18 coordinates with units of meters. Vertically it is based on North American Vertical Datum of 1988 (NAVD88) with units of meters. All data applied to the model are shifted to this datum and coordinate system.

Bathymetry data for the model were obtained from several sources: the Coastal Relief Model (CRM), sponsor-collected hydrographic surveys, and the National Elevation Dataset (NED). These data sets were combined such that the latest data were made a priority as well as data collected at finer resolution. The 2D AdH code can include areas that wet/dry; therefore, elevations were included in the domain up to 2 m NAVD88. Figure 3 shows the model domain and bathymetry. Additional details of the bathymetry dataset generation are provided in Appendix A.

Figure 3. Model domain bathymetry.



The model domain includes over 9,867 square miles, extending approximately 115 miles along the New Jersey Atlantic Ocean coastline from Lewes, DE, to Manasquan, NJ. The 2D mesh contains 324,881 elements and 165,514 nodes. Figure 4 shows the horizontal mesh resolution for the model domain with a close-up image of Little Egg Inlet. Resolution is finest in the small wetland channels to accurately capture the conveyance of flow in these areas as well as the salinity that migrates upstream in deeper channels. Finer resolution is also seen in areas where geometric features need to be defined accurately, such as in the inlets and around jetties.

Figure 4. Mesh resolution.

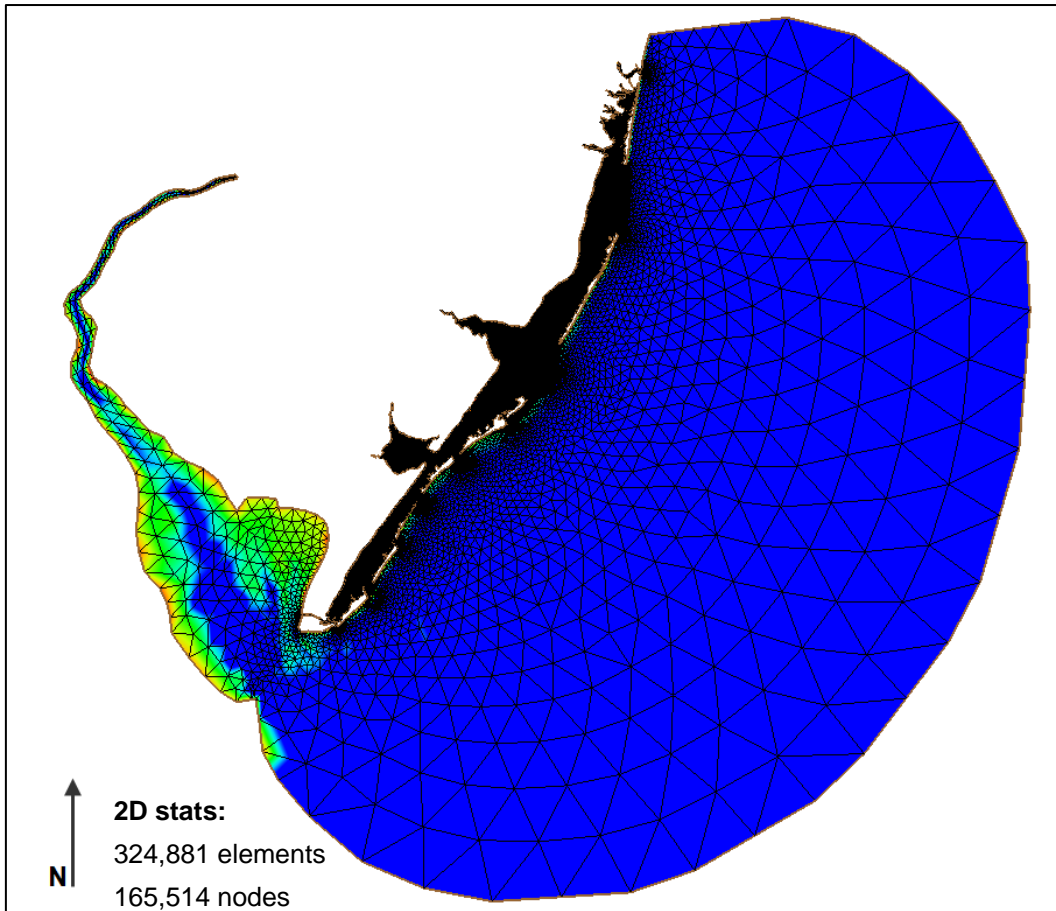
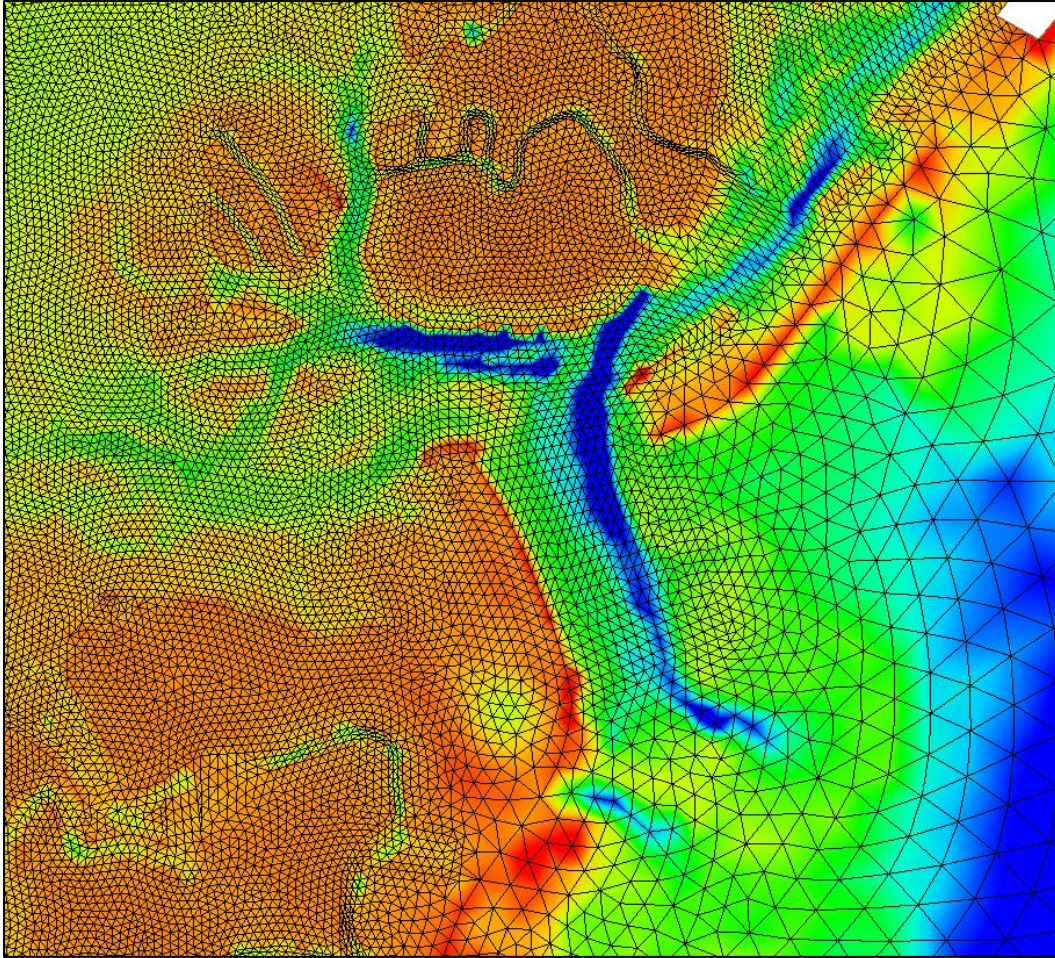


Figure 5. Little Egg Inlet mesh resolution



Boundary conditions

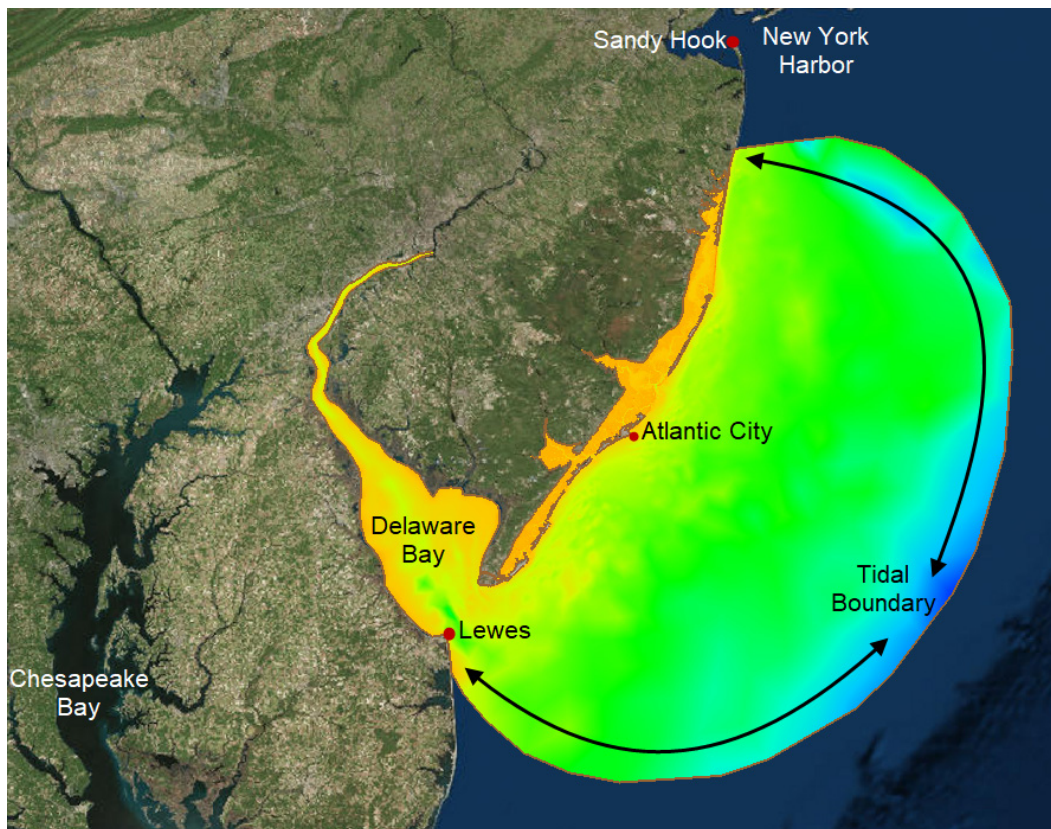
The boundary conditions for this study are set up in the typical manner for any numerical model studies. Tidal water surface elevations and salinity are applied at the ocean boundary. Winds are included throughout the model domain. Freshwater inflow is applied for the measured flow locations.

Tide Boundary Condition

The tidal boundary condition was created using harmonic and nonharmonic components from various sources in an effort to build the most representative condition for the AdH model boundary location. The semi-circular AdH model boundary lies approximately 70 miles offshore at its greatest distance. Figure 6 shows the location of the tidal boundary.

The tide boundary condition for January 2018 through February 2019 was generated by combining harmonic constituents from the ADCIRC tidal database and the Atlantic City NOAA gage as well as the nonharmonic signal from the Atlantic City NOAA gage.

Figure 6. AdH tide boundary



It was determined that since NOAA uses a much longer time history of data than the ADCIRC database to determine the harmonic constituents, the NOAA constituents should be used as the base values. Then, based on the component comparisons provided in Appendix B, it was determined that the ADCIRC database constituents are best for the major 8 – M2, S2, N2, K2, K1, O1, Q1, P1 – since they can be obtained for each edge along the AdH model boundary. Therefore, the harmonic signal along the AdH model boundary will include variable amplitudes and phases for the eight constituents noted and constant amplitudes and phases for the other 29 constituents.

The nonharmonic signal must also be included in the AdH model tidal boundary condition to account for storms and other nonharmonic events. This information is determined from measured (observed) values and must come from the NOAA gages (observed – predicted). In the area of the AdH model domain, NOAA data are available at Lewes, DE, Atlantic City, NJ, and Sandy Hook, NY. Based on comparisons among the NOAA gages, presented in Appendix B, the nonharmonic component of the AdH model boundary tide condition will be applied from Atlantic City and applied equally along the model boundary.

The AdH model boundary consists of 30 edges that will each have a time-varying elevation boundary condition. As determined from the analysis detailed in Appendix B, the harmonic signal along the AdH model boundary will include variable amplitudes and phases for eight constituents – M2, S2, N2, K2, K1, O1, Q1, P1 – and constant amplitudes and phases from NOAA’s Atlantic City gage for the other 29 harmonic constituents and the nonharmonic signal. Figure 8 shows the generated tidal signal at the AdH northernmost boundary edge and the southernmost boundary edge for the full simulation period. Figure 8 shows the first 200 hours of the tidal signal such that the variation along the boundary edge is visible.

Figure 7. Complete tidal boundary condition

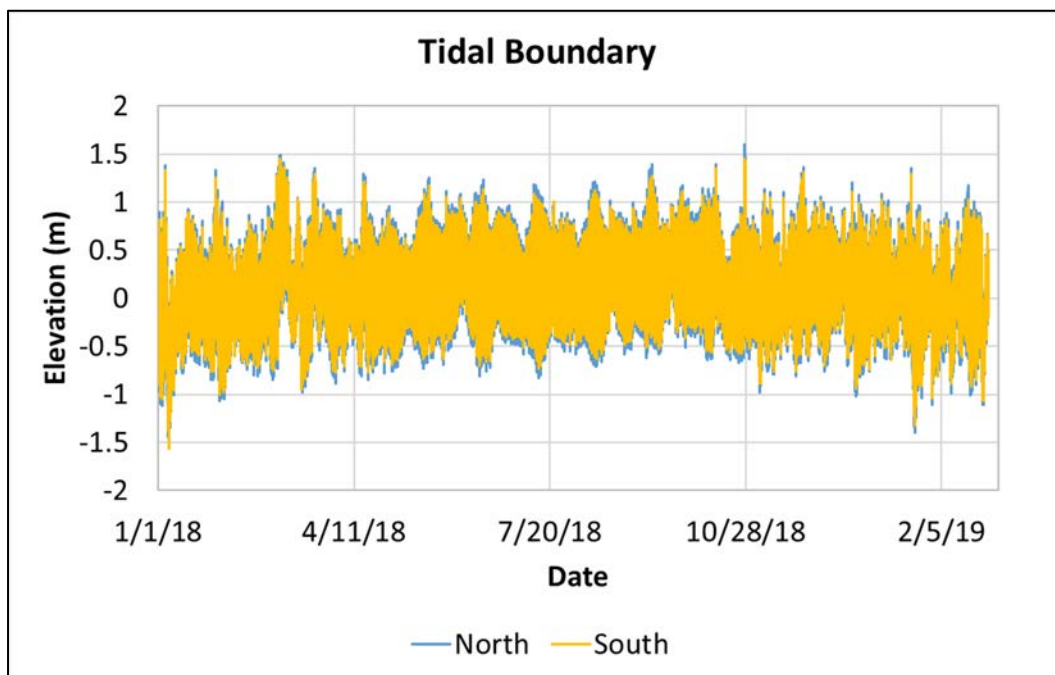
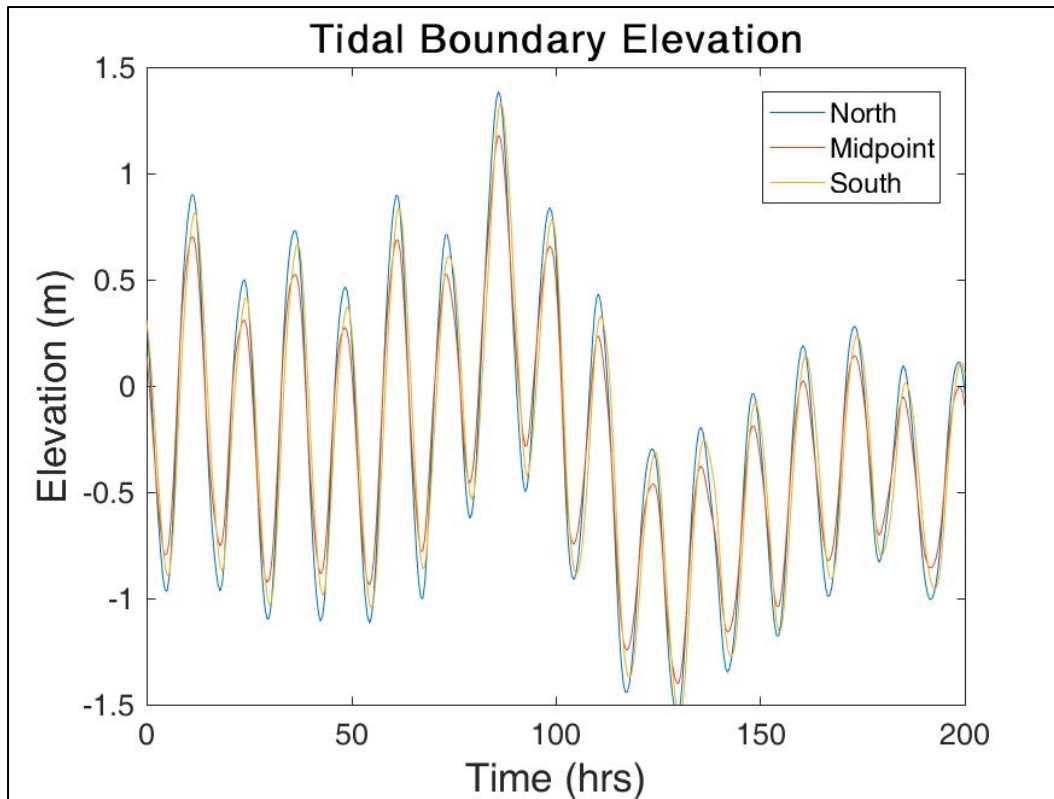


Figure 8. Tidal boundary condition (subset)



Freshwater River Inflows

Twelve freshwater flow locations are included in the model boundary conditions. These data were obtained from USGS over the model simulation period – 1 January 2018 through 28 February 2019. The inflow locations are shown in Figure 9 and the USGS gage numbers are provided in Table 1. These data were applied as discharge inflows and the Delaware River inflow includes data from multiple sites. Figure 10 and Figure 11 show the discharge values over the simulation period for all of the freshwater flow locations. The flow into the back bay area is much lower in magnitude than the flow into Delaware Bay from the Delaware River.

Figure 9. Freshwater inflow locations.

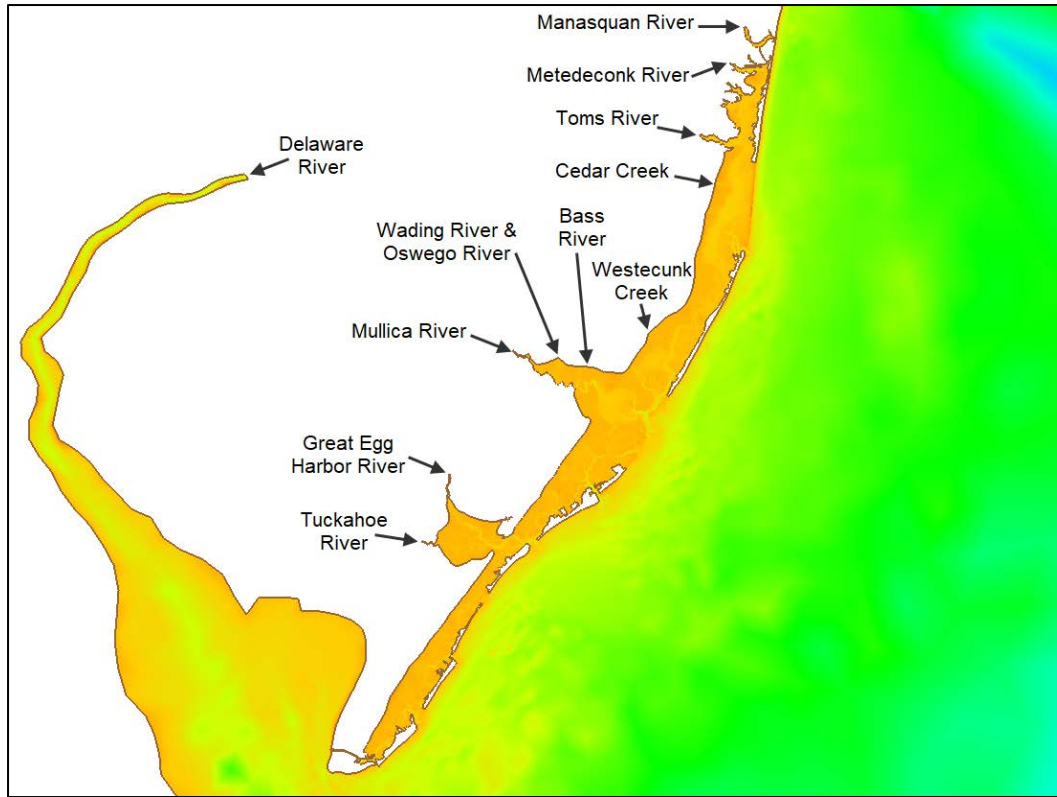


Table 1. USGS gage information for freshwater flows.

Model Input River	USGS gage number	USGS gage name
Manasquan River	01408029	Manasquan River near Allenwood, NJ
Metedeconk River	01408120	North Branch Metedeconk River near Lakewood, NJ
Toms River	01408500	Toms River near Toms River, NJ
Cedar Creek	01408900	Cedar Creek at Western Blvd near Lanoka Harbor, NJ
Westecunk Creek	01409280	Westecunk Creek at Stafford Forge, NJ
Bass River	01410150	East Branch Bass River near New Gretna, NJ
Wading River	01409810	West Branch Wading River near Jenkins, NJ
Oswego River	01410000	Oswego River at Harrisville, NJ
Mullica River	01409400	Mullica River near Batsto, NJ
Great Egg Harbor River	01411000	Great Egg Harbor River at Folsom, NJ
Tuckahoe River	01411300	Tuckahoe River at Head of River, NJ
Delaware River	01463500	Delaware River at Trenton, NJ
	01467087	Frankford Creek at Castor Ave, Philadelphia, PA
	01474500	Schuylkill River at Philadelphia, PA
	01477000	Chester Creek near Chester, PA

Figure 10. NJBB freshwater river inflows.

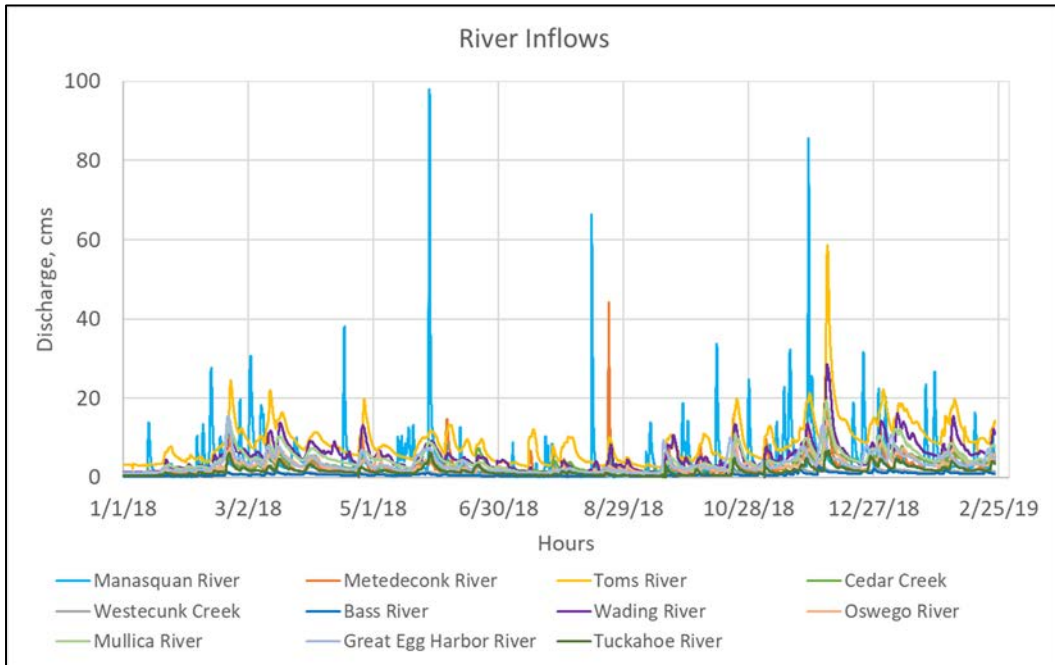
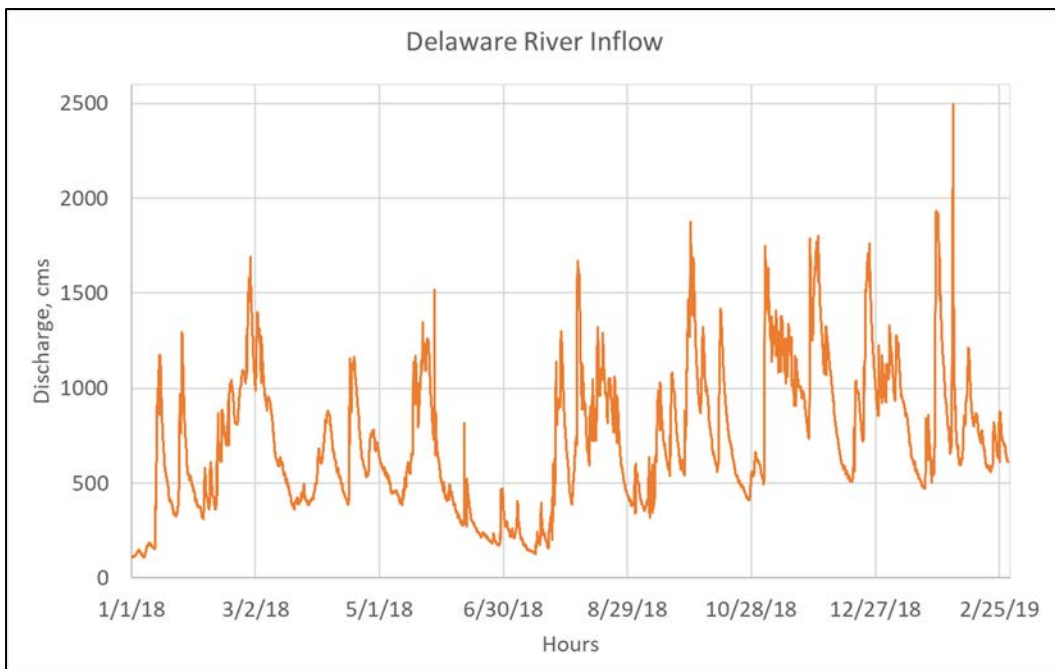
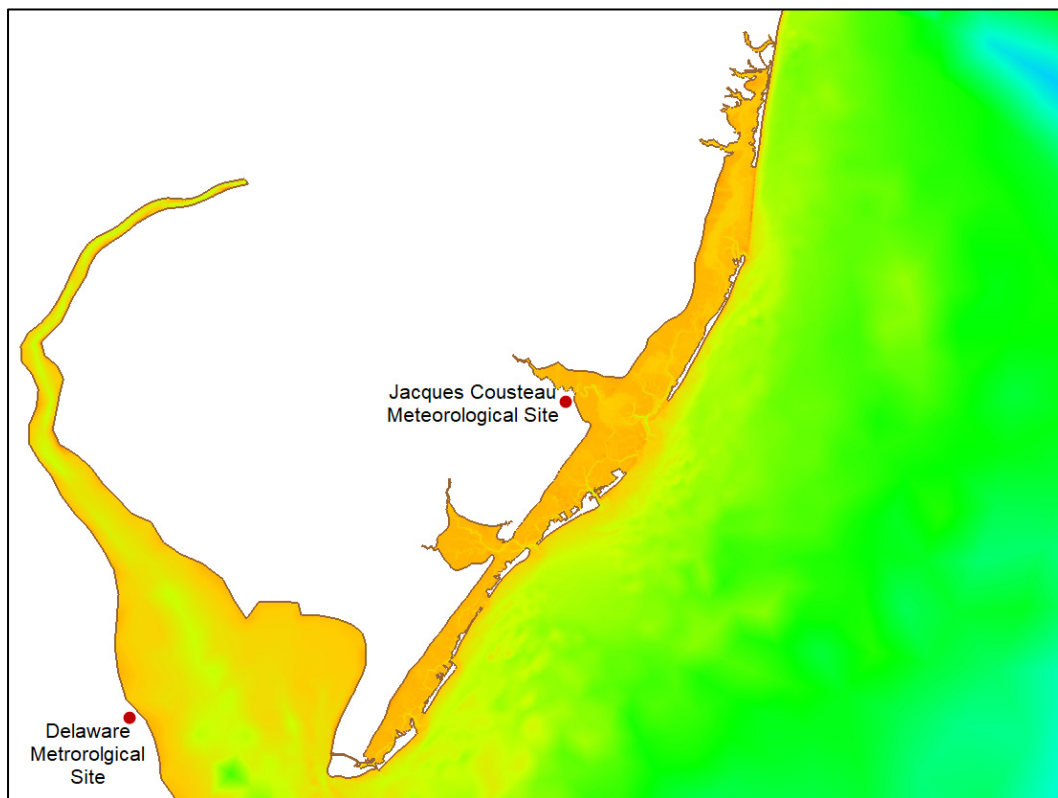


Figure 11. Delaware River freshwater inflow.



Meteorological Input (Wind)

Wind data were available from NOAA's National Estuarine Research Reserve System (NERRS) National Monitoring Program for Nacote Creek in the Jacques Cousteau Reserve (JACNCMET) and Saint Jones River in the Delaware Reserve (DELSJMET). The Delaware site is located on the western shore of Delaware Bay and at the boundary of the AdH model domain. However, the Jacques Cousteau site is located on the western side of Great Bay, near Little Egg Inlet, which is central to the AdH model domain and used for this model.



The wind speed and direction were converted to Cartesian components and filtered to remove signals less than 3 hours so that random data spikes do not generate model instability. Figure 12 shows a 2018 wind rose for the Jacques Cousteau site. These wind data are oriented in the “from” direction measured clockwise from North. The speed is measured in meters per second. These data indicate that the dominant wind direction is from west to east whereas the strongest winds generally come from the east, northeast. Figure 13 shows the Cartesian wind speed components with direction converted to “toward” measured counter-clockwise from East.

The AdH code can take supplied wind stress components or wind speed and direction and compute the wind stress internally. In this model, the Wu formulation (Wu 1982) is used in the ocean and inlet areas – the deeper areas of the domain. The Teeter formulation (Teeter 2002) is used in the back bays and wetland areas.

Figure 12. 2018 wind speed and direction for JACNCMET.

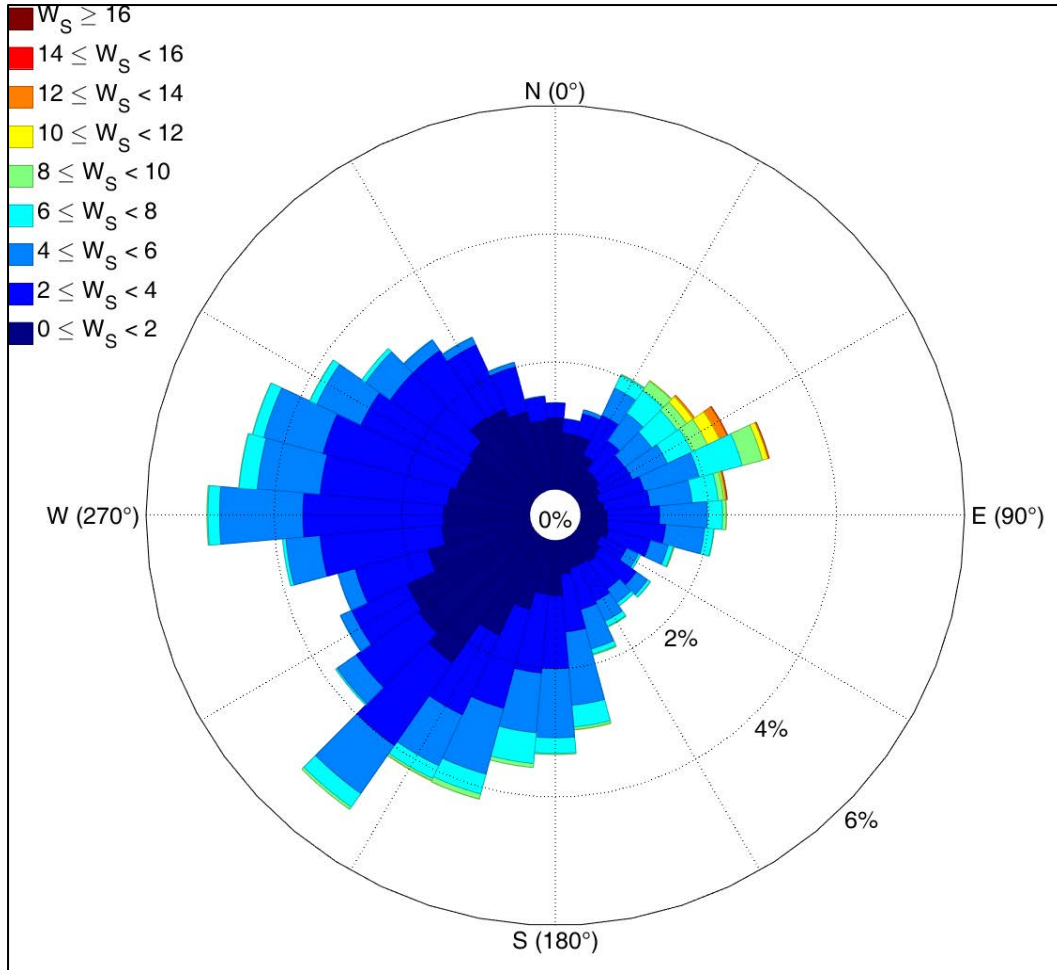
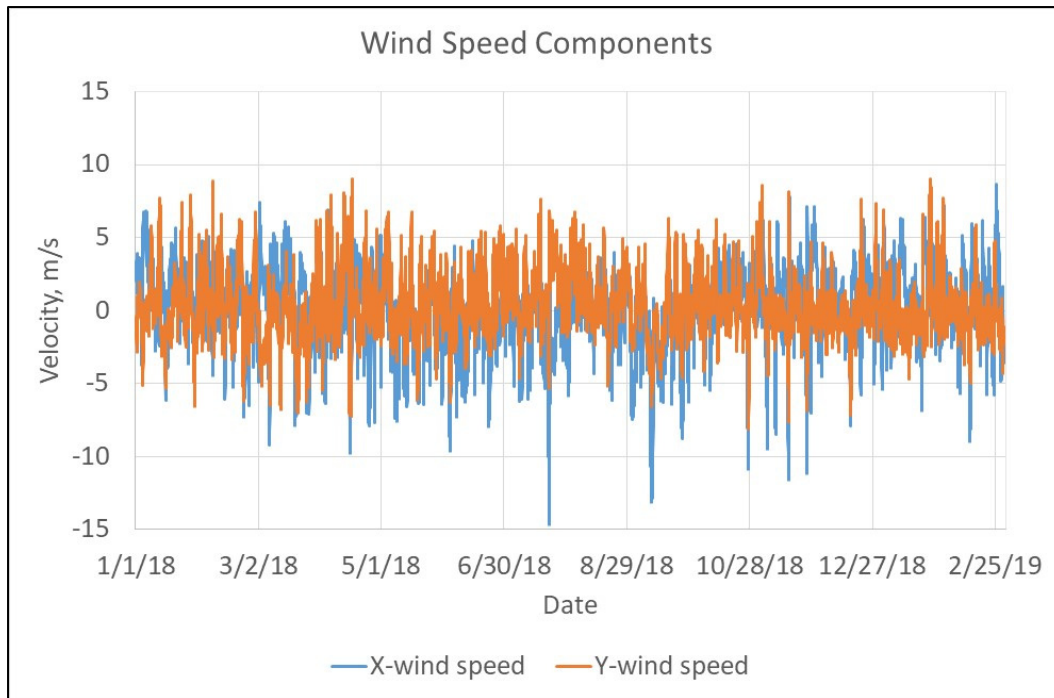


Figure 13. JACNCMET wind speed components.



Ocean Salinity Boundary

The UK Met Office Hadley Center provides model computed salinity results for locations throughout the world (Good et al.). 2018 monthly average salinity were downloaded for all points and compared at locations closest to the model domain (based on latitude/longitude). Figure 14 shows the locations of salinity model data in relation to the AdH model domain. The degree of variation among the points will indicate if a single salinity boundary can be applied or if a variable boundary will be necessary. There is no salinity data at location -75, 40 since this location is on land. Salinity at the other five locations are shown in Figure 15. The range of salinity variation among the locations is at most 3 ppt over the year and within 1.3 ppt for any given month. Given the small salinity difference among the computed locations, a single location (-73, 39) will be used to drive the AdH model ocean salinity boundary (see Figure 15).

Based on the model calibration/validation effort, the boundary salinity values were reduced by 3 ppt to better match the field data.

Figure 14. UK Met Office salinity data in model domain vicinity.

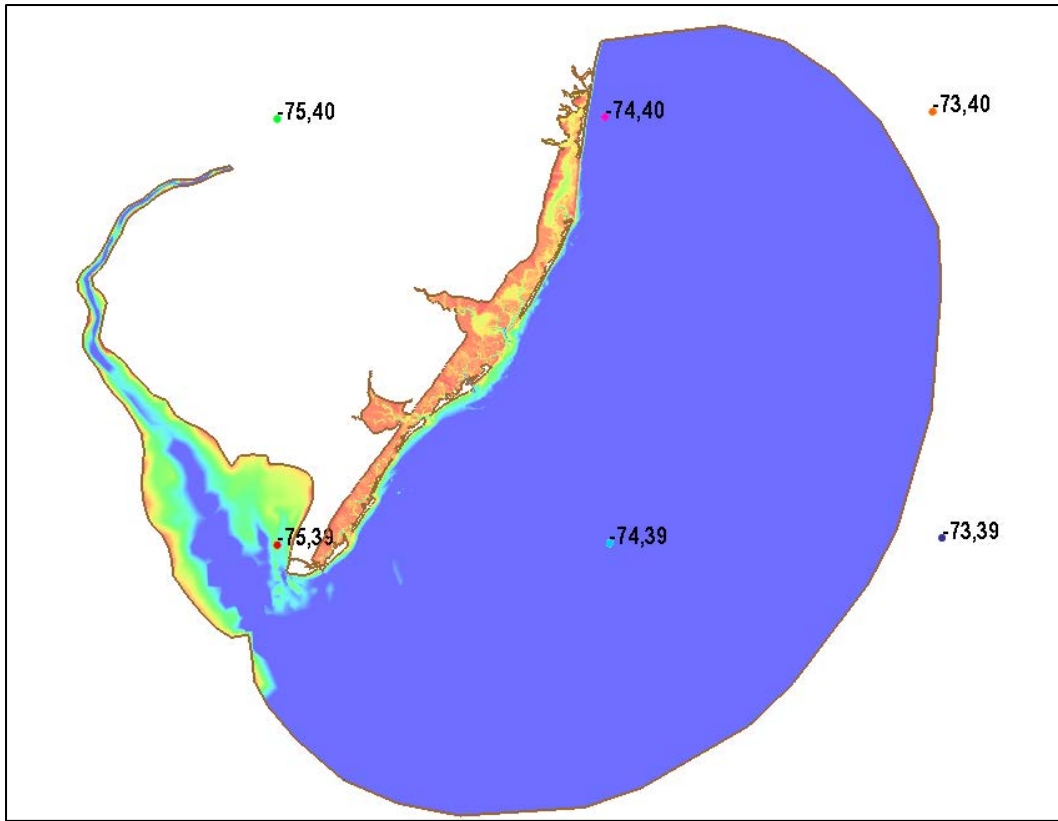


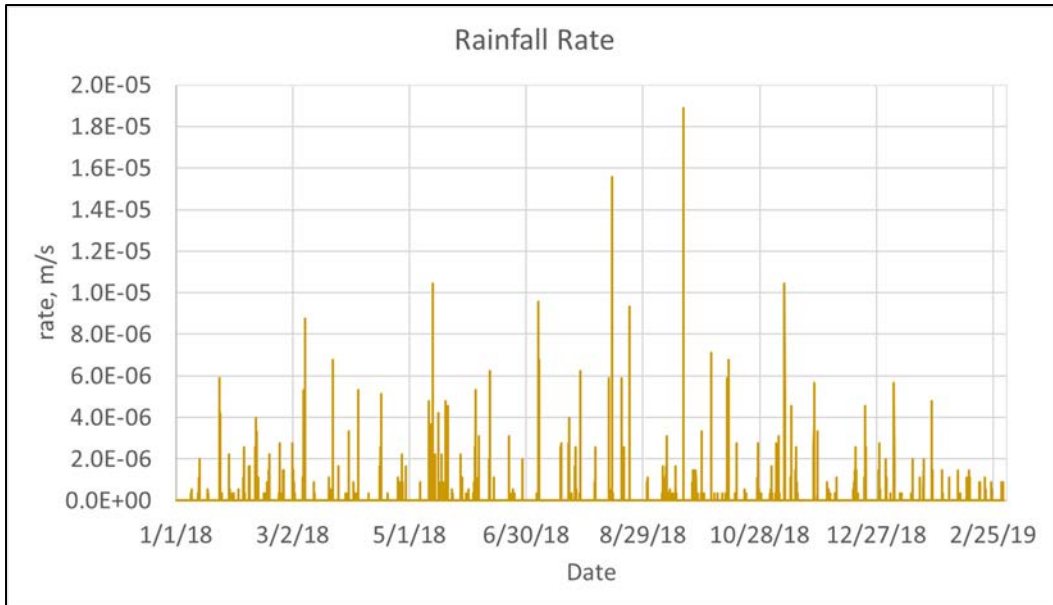
Figure 15. UK Met Office salinity data (ppt).



Precipitation

The NEERS Jacques Cousteau Meteorological site also collects precipitation data. This time-varying rainfall rate, shown in Figure 16, was applied over the entire wetted model domain.

Figure 16. JACNCMET precipitation.



AdH model parameters

The parameters used by AdH to achieve the validated model (discussed in the following sections) are provided in Table 2. This table provides the specific or range of values used for various model properties such as bed roughness, diffusion, eddy viscosity, and turbulence. The values vary by location as defined in Figure 17 and Figure 18. The salinity was modeled as a generic constituent to remove unrealistic salinity gradient driven velocity fields in the ocean.

Table 2. Model parameters.

Parameter	Value	
Estimated Eddy Viscosity Coefficient	0.5 (Isotropic)	
Wetting/Drying Tolerance	2.7 - 3.2 m	
Bed Roughness	Equivalent Roughness Height	0.0034 - 0.072 m
	Unsubmerged Rigid Vegetation (Wetland)	0.02 m, 0.01 m, 50
	Submerged Aquatic Vegetation	0.025 m, 0.25 m
Time Stepping	First-order	
Time-Step Maximum	100 s	
Convergence	Residual Norm	0.001
	Increment Norm	0.01

Figure 17. Material designations.

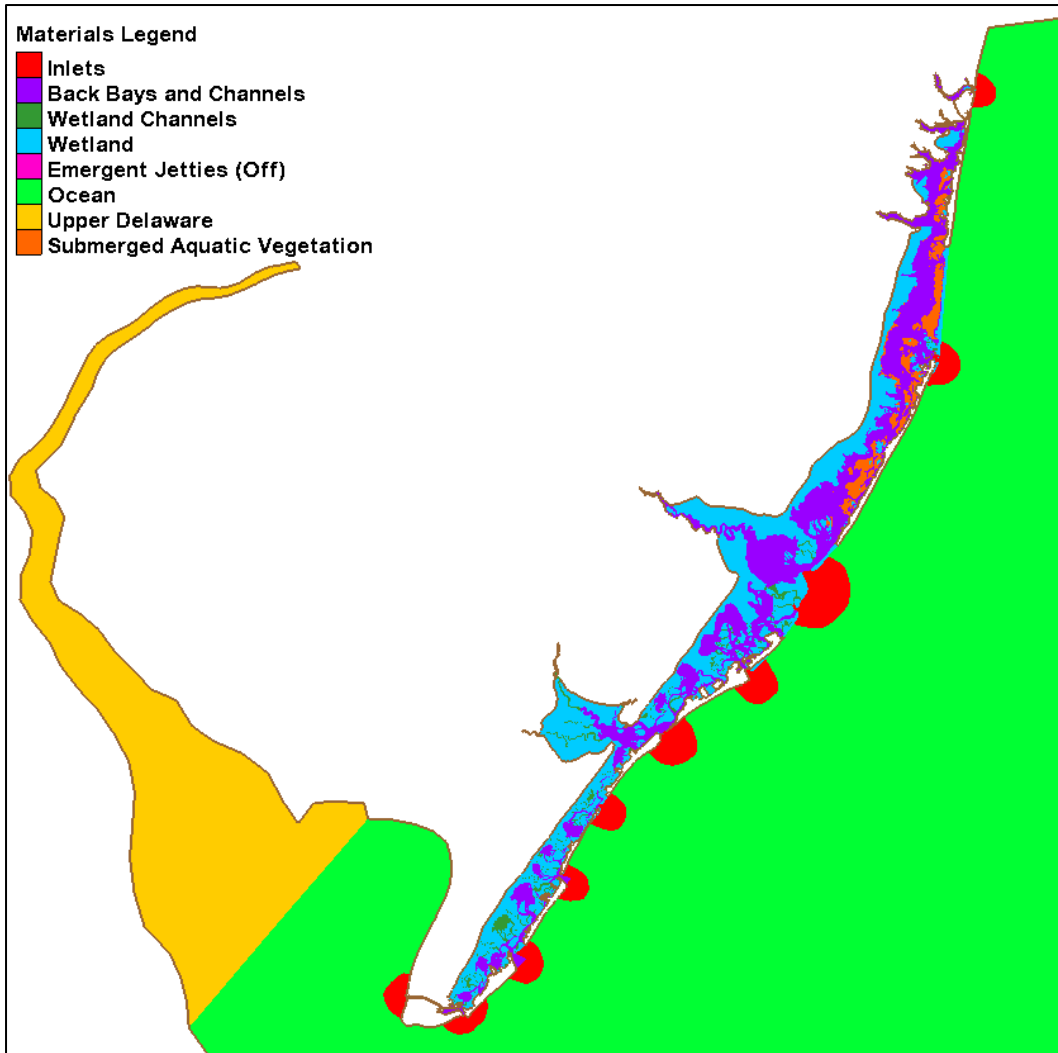
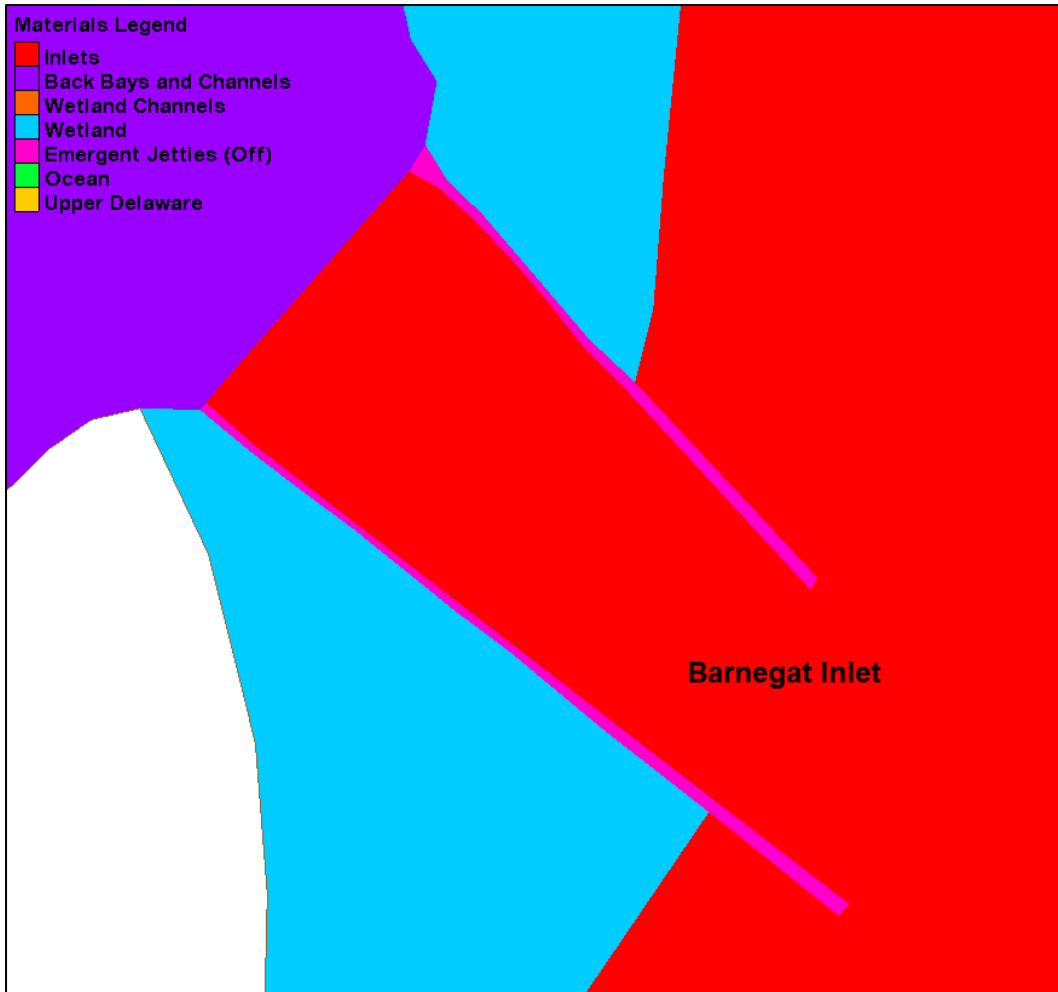


Figure 18. Barnegat Inlet material designations (showing jetties).



3 Model/Field Comparison – Calibration and Validation

The model is calibrated/validated by comparing to measured field data from 2018 and February 2019. These 2 time periods were used to take advantage of various data sets for hydrodynamics and salinity transport as well as provide a wide range of conditions over which the model is considered accurate. Part of the time served as a calibration period such that parameters — such as bed roughness, salinity diffusion, and viscosity — were adjusted, within a physically reasonable range, to get the best match to the field data. Those parameters were then unchanged when the model was simulated and compared to the field (validated) for the remainder of the comparison time. Most data were obtained from publicly accessible data websites. For all comparison types — hydrodynamic and salinity — a subset of the sites are provided in the body of the report with all site comparisons provided in the appendices.

Field Data Collection

CHL performed a 13 hour field data collection effort on 21 February 2019 at three of the inlets – Barnegat, Little Egg, and Great Egg – to collect vertical salinity measurements as well as discharge transects at the inlets. This data collection is detailed in Appendix G.

The field data showed very little, less than 2 ppt, vertical stratification at the inlets. These data supported the use of a 2D model. It is likely that there are times of high wind or freshwater flows that may generate some vertical stratification in the deep channels but this is not the case under typical conditions.

Discharge transects were taken on the bay side of the inlets to track the distribution of flow into the system. These data transects are used in the model calibration/validation effort.

Hydrodynamic comparisons

The model is compared to water surface elevation and discharge at several locations during the 2018 and 2019 calibration/validation period. Water surface elevation data were obtained from the NOAA Co-Ops for Atlantic City and the USGS for 15 other locations throughout the model domain.

Salinity data were obtained from USGS, NOAA's National Estuarine Research Reserve System (NEERS), and New Jersey Department of Environmental Protection (NJDEP). Discharge data were obtained from the CHL data collection effort.

Water surface elevation

Water surface elevation results are compared to the field at 16 locations as shown in Figure 19. Statistical comparisons for root-mean-square and correlation coefficient are provided in Table 3. Time history and box plot comparisons at selected sites (those circled in red in Figure 19) are shown in Figure 20 through Figure 27. The full set of comparisons is provided in Appendix C.

Figure 19. Water surface elevation comparison locations.

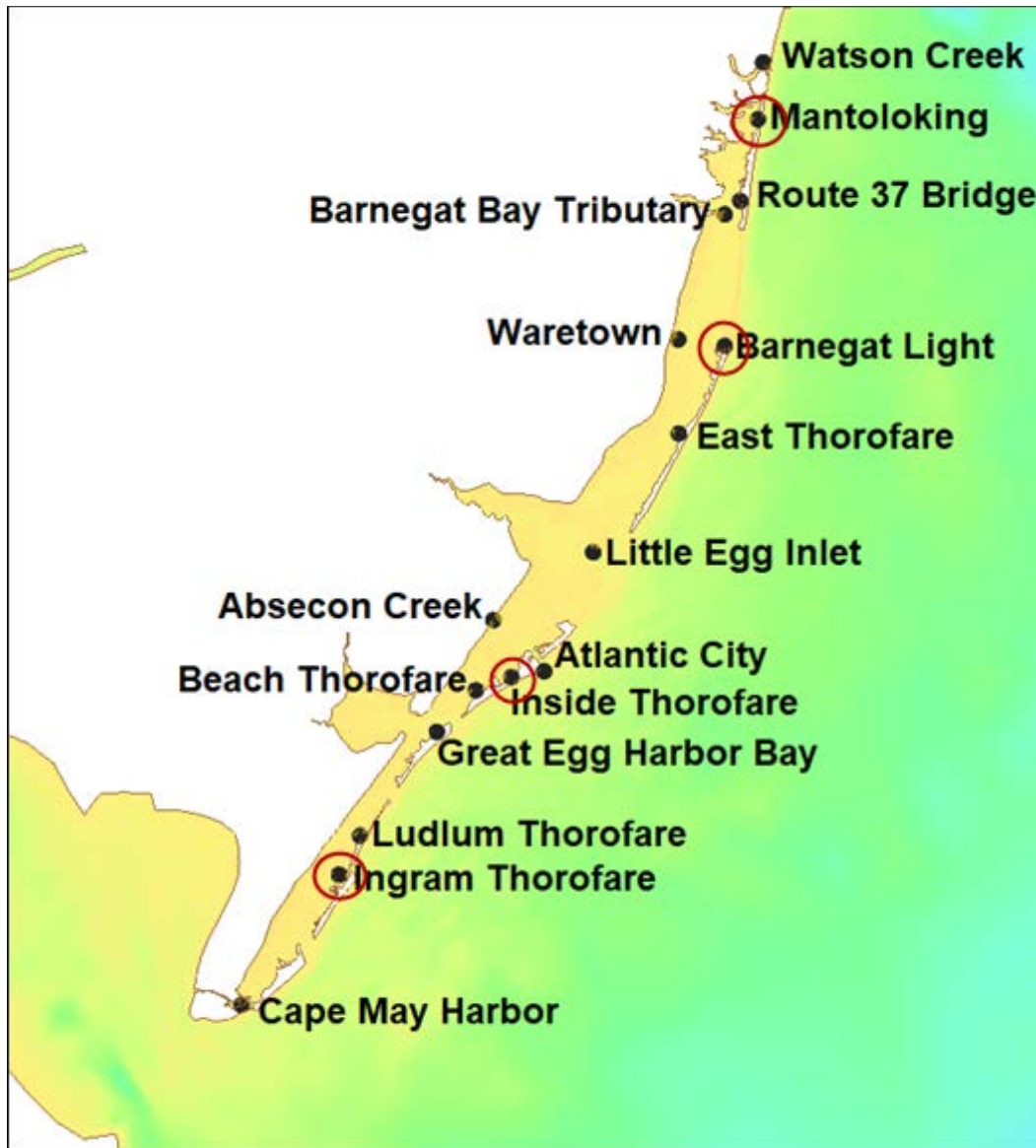


Table 3. Statistical model/field calibration comparison of water surface elevation.

	Root Mean Square Error	Correlation Coefficient
Watson Creek	0.11	0.98
Barnegat Bay at Mantoloking	0.10	0.86
Barnegat Bay at Route 37 Bridge	0.07	0.89
Barnegat Bay Tributary	0.06	0.93
Barnegat Bay near Waretown	0.05	0.94
Barnegat Bay at Barnegat Light	0.08	0.97
East Thorofare	0.08	0.94
Little Egg Inlet	0.13	0.93
Absecon Creek	0.21	0.92
Atlantic City	0.18	0.93
Inside Thorofare	0.17	0.94
Beach Thorofare	0.17	0.93
Great Egg Harbor Bay	0.18	0.92
Ludlum Thorofare	0.24	0.90
Ingram Thorofare	0.16	0.95
Cape May Harbor	0.13	0.97

For the time history plots, the red line represents the measured field data, and the blue line represents the model computed values. Each comparison location also includes a box plot showing the relationship between the measured field data (x -axis) and the modeled data (y -axis). A perfect match would yield points on the black 1:1 line.

Figure 20. Water surface elevation comparisons over time for Barnegat Bay at Mantoloking.

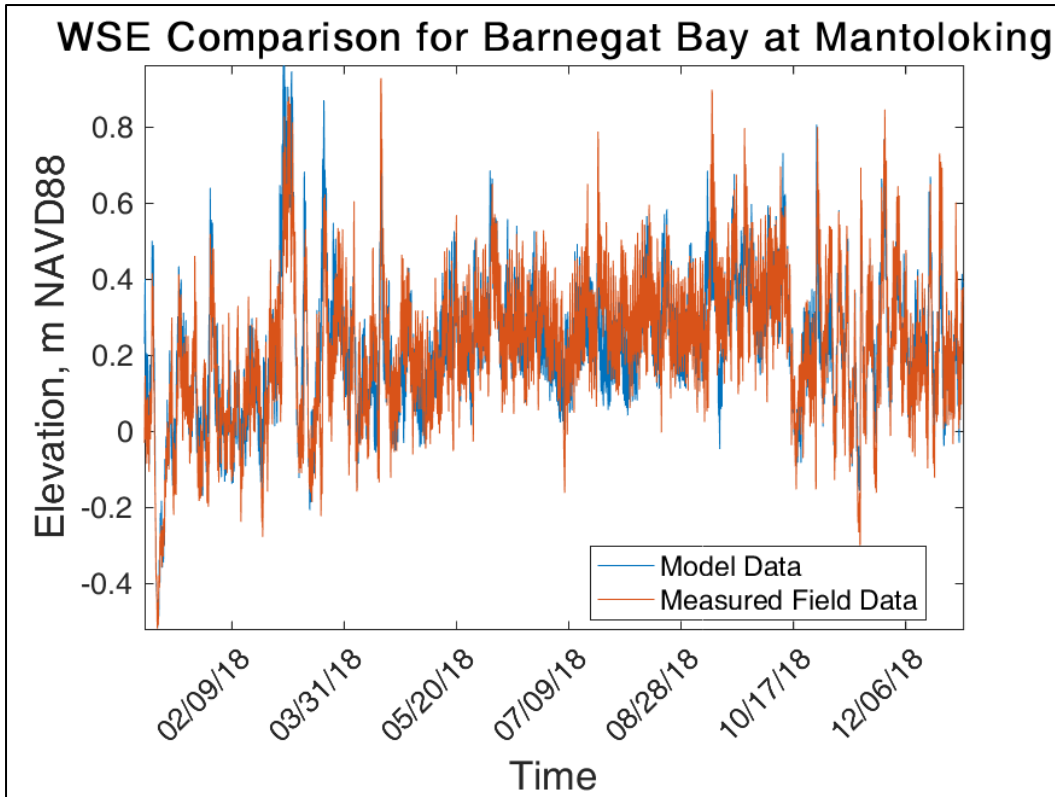


Figure 21. Water surface elevation comparison box plot for Barnegat Bay at Mantoloking.

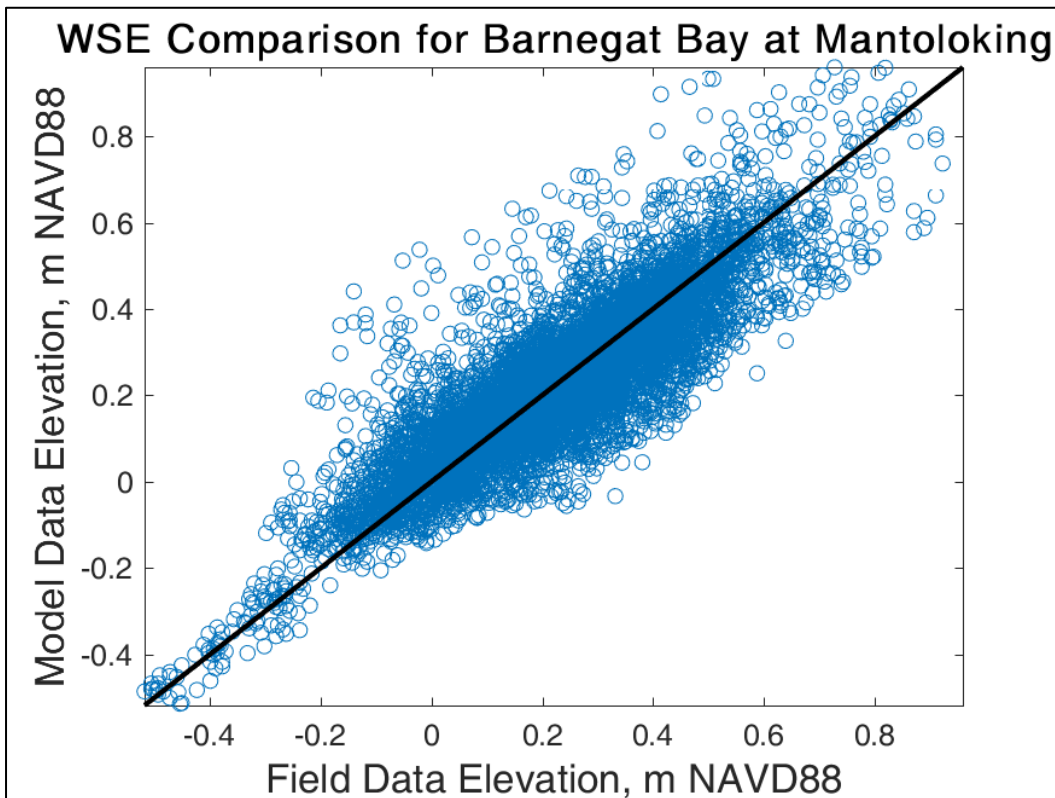


Figure 22. Water surface elevation comparisons over time for Barnegat Bay at Barnegat Light.

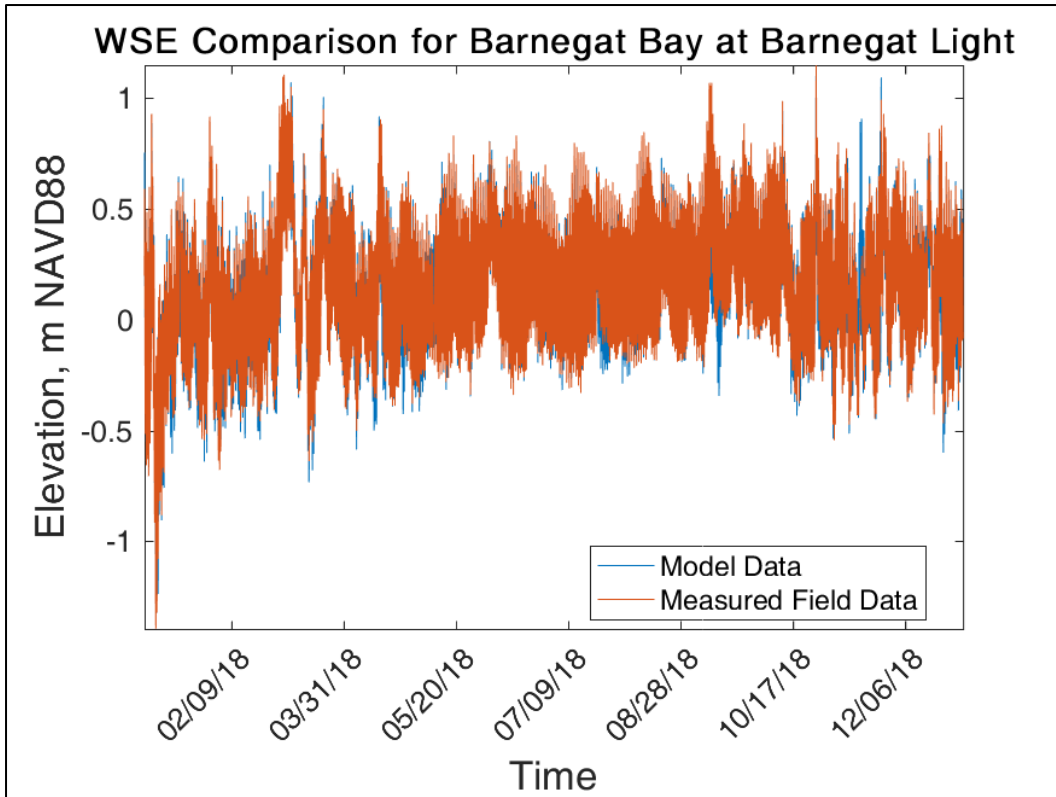


Figure 23. Water surface elevation comparison box plot for Barnegat Bay at Barnegat Light.

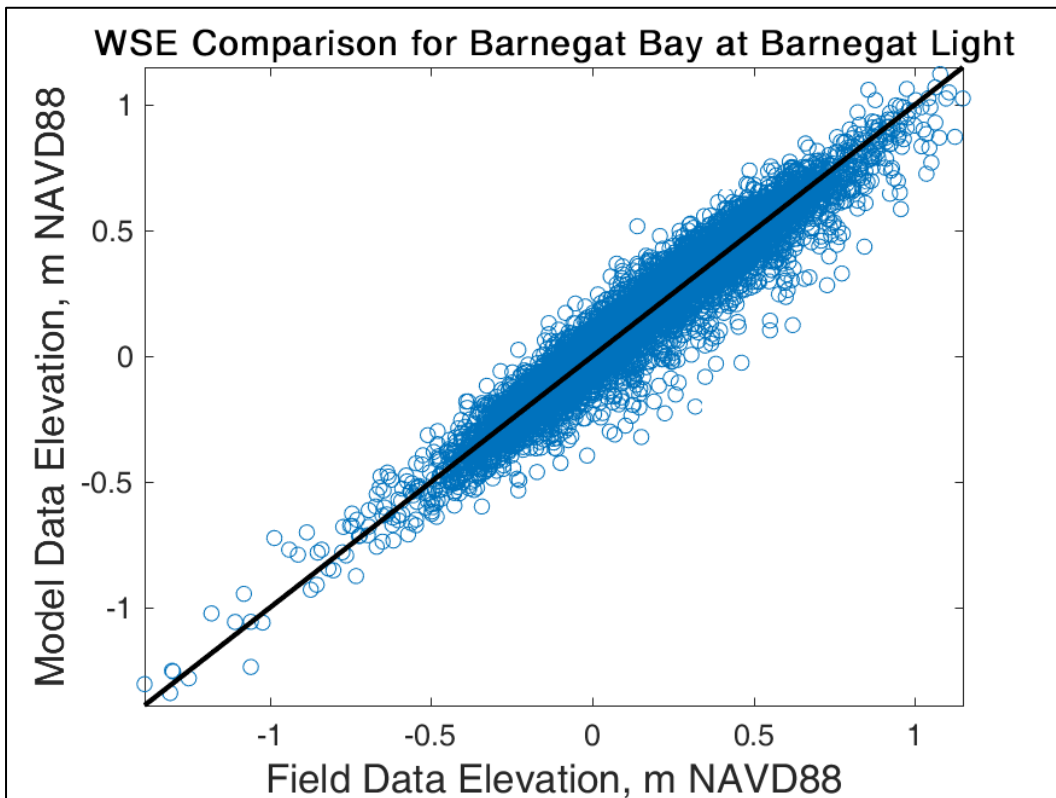


Figure 24. Water surface elevation comparisons over time for Inside Thorofare.

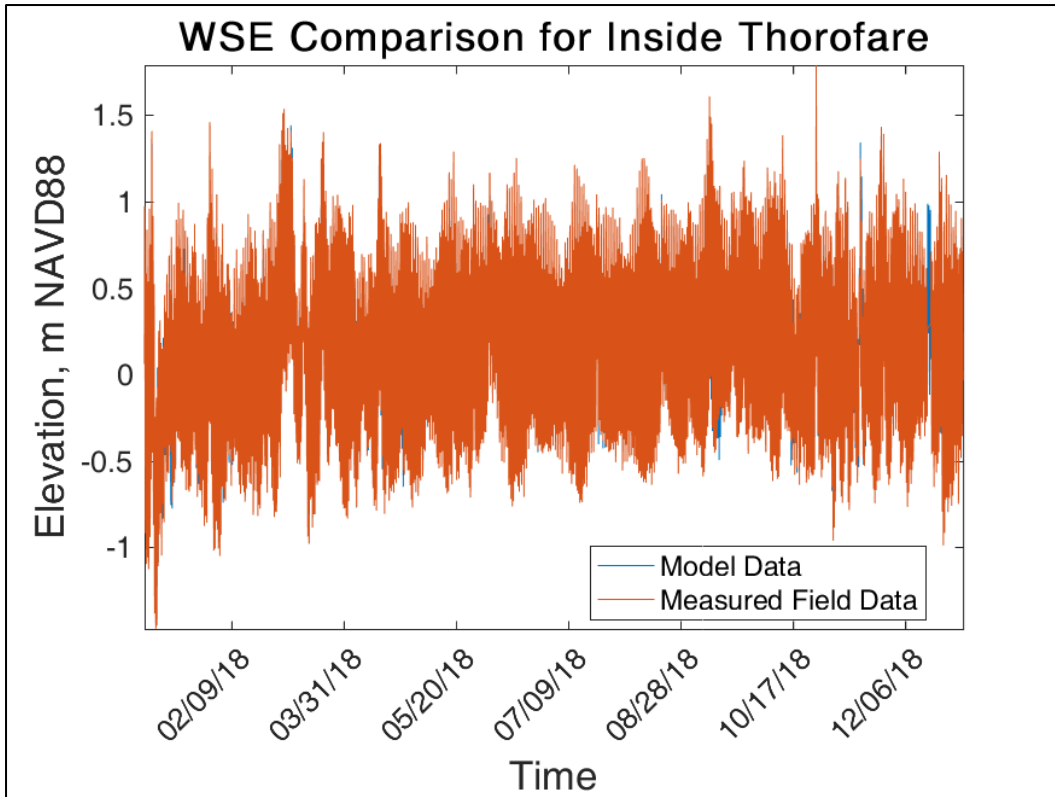


Figure 25. Water surface elevation comparison box plot for Inside Thorofare.

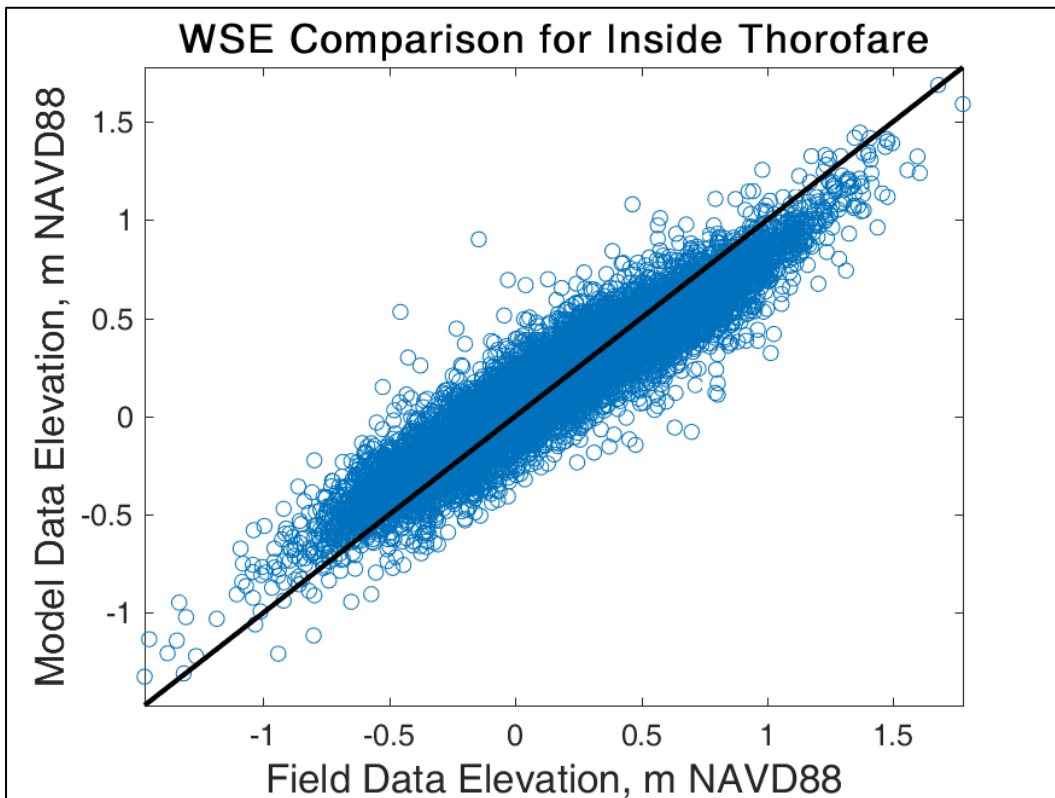


Figure 26. Water surface elevation comparisons over time for Ingram Thorofare.

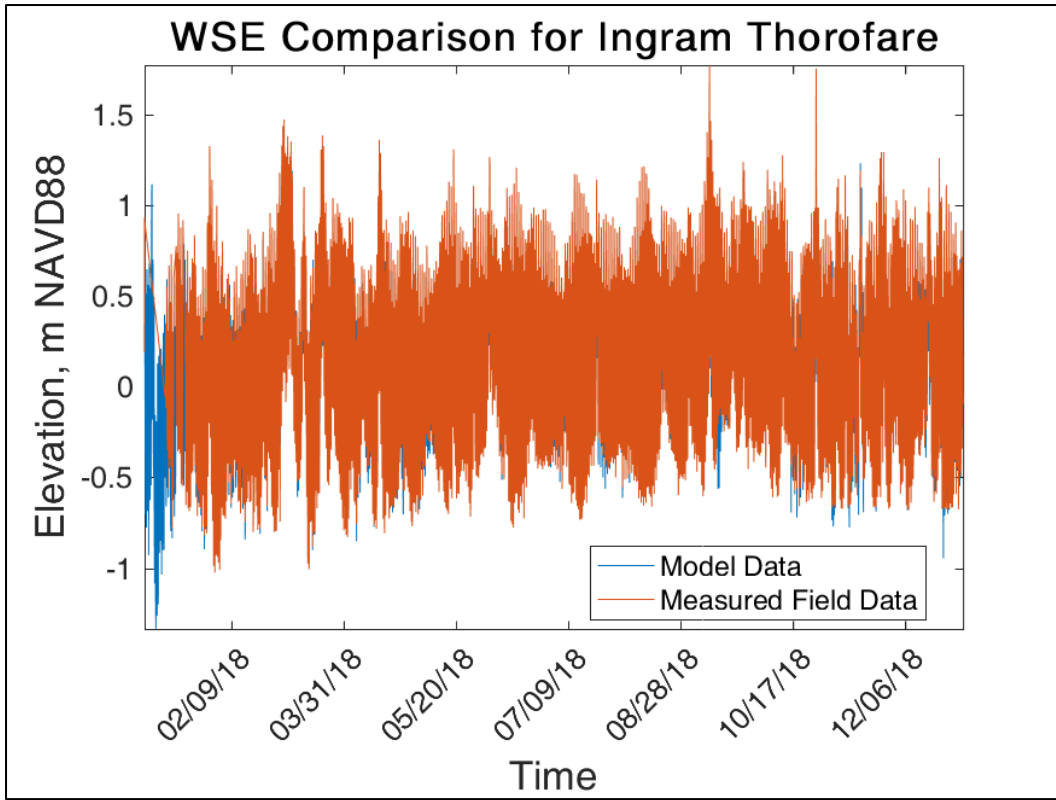
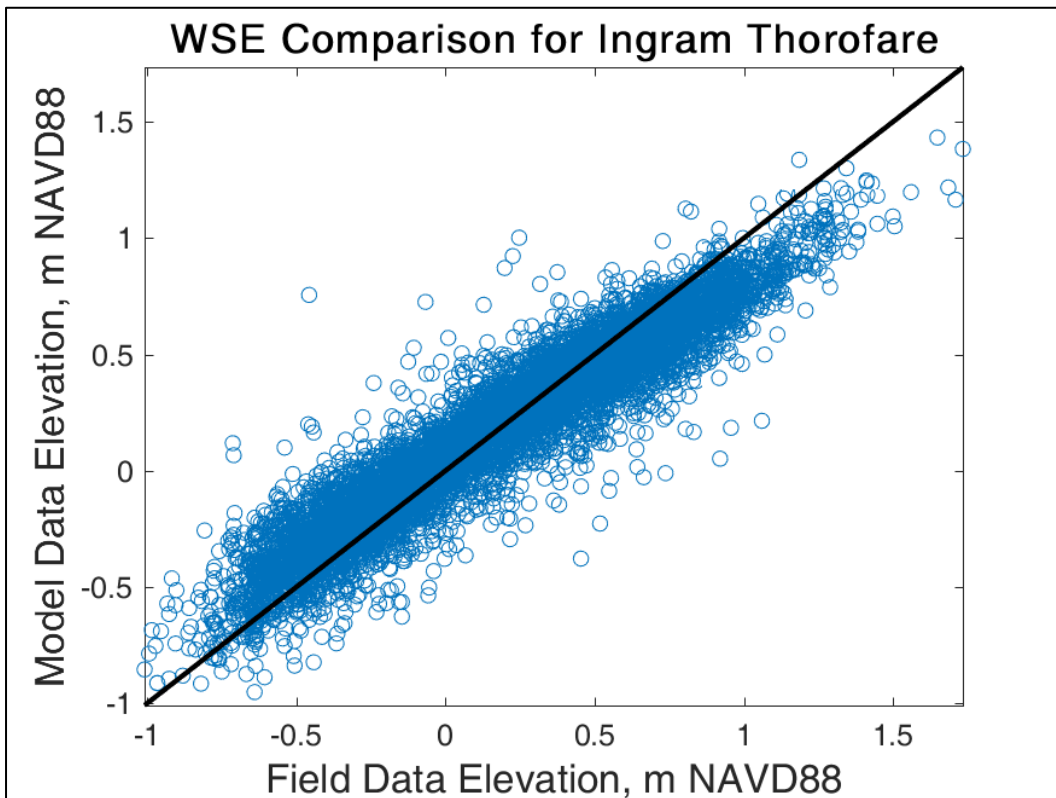


Figure 27. Water surface elevation calibration comparison box plot for Ingram Thorofare.



Harmonic Analysis

A harmonic analysis was performed for all water surface elevation model/field comparison locations (Figure 19) using the `t_tides` utility in Matlab. This analysis determines the field and model harmonic constituents' tidal amplitude and phase over the year-long simulation but does not remove any non-harmonic portion of the water surface elevation since that is not known definitively. Figure 28 through Figure 35 show the model/field comparison for the tidal amplitude and phase for the largest 10 amplitudes at each of the circled locations in Figure 19. The plotted results will show different components for each location depending on which ones are the largest. Results for all locations are provided in Appendix C.

The harmonic components compare well overall. There are some locations and component amplitudes that differ by a few centimeters. There are also some locations and components with several degrees of phase difference but this value is always less than 50 degrees (much less for most comparisons). The largest difference is found at Ludlum Thorofare in its MKS2 component (M2+K2-S2) which is made up of solar and lunar semi-diurnal components. In addition, a large amplitude difference is observed at Absecon Creek in the M2 (semi-diurnal lunar) component. It is possible that wind events that influence the water surface elevation can skew the harmonic analysis unless the non-harmonic signal is removed from the data – which it is not in this analysis.

Figure 28. Harmonic constituent amplitude comparison for Barnegat Bay at Mantoloking (largest 10 component amplitudes).

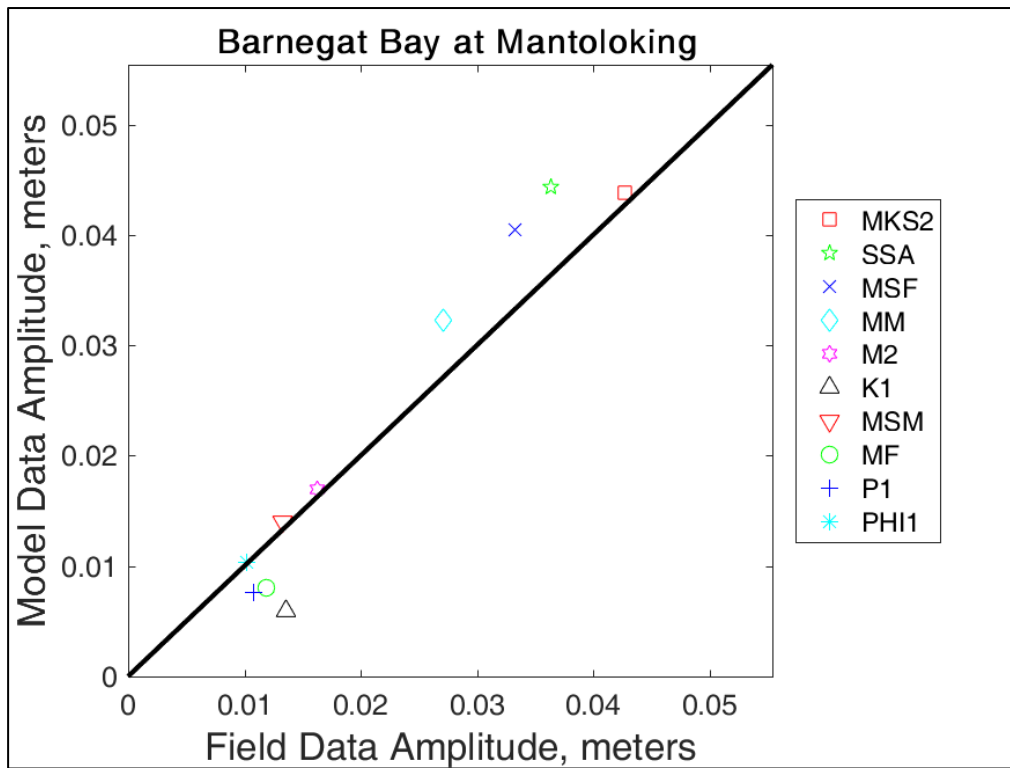


Figure 29. Harmonic constituent phase comparison for Barnegat Bay at Mantoloking (largest 10 component amplitudes).

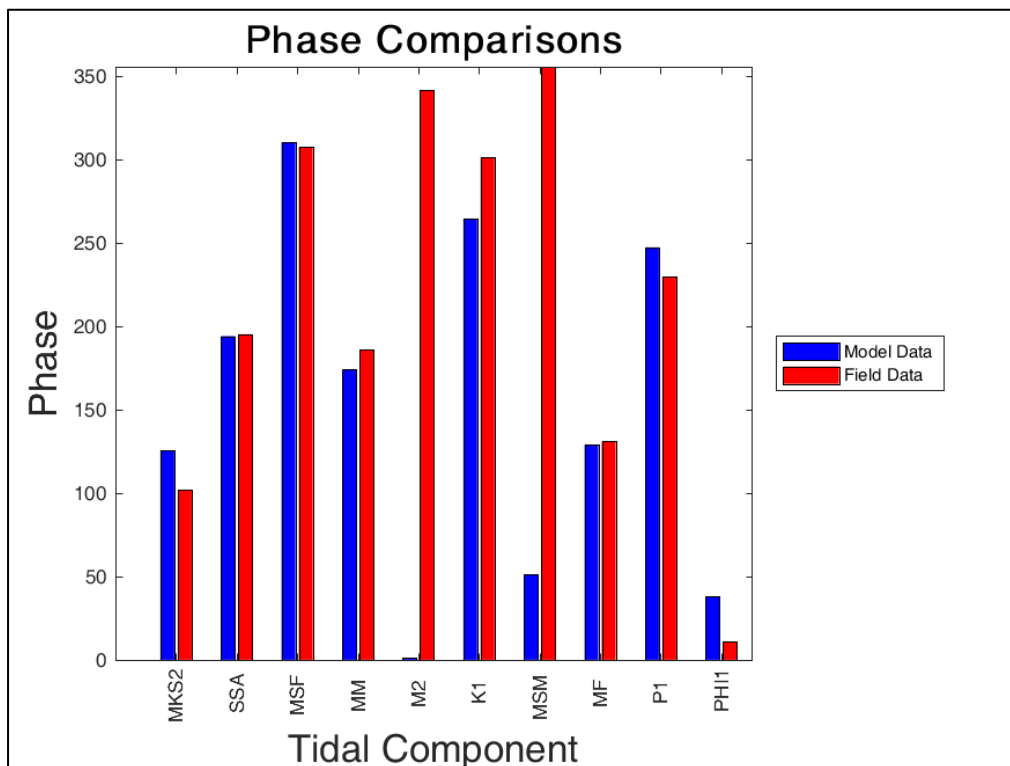


Figure 30. Harmonic constituent amplitude comparison for Barnegat Bay at Barnegat Light (largest 10 component amplitudes).

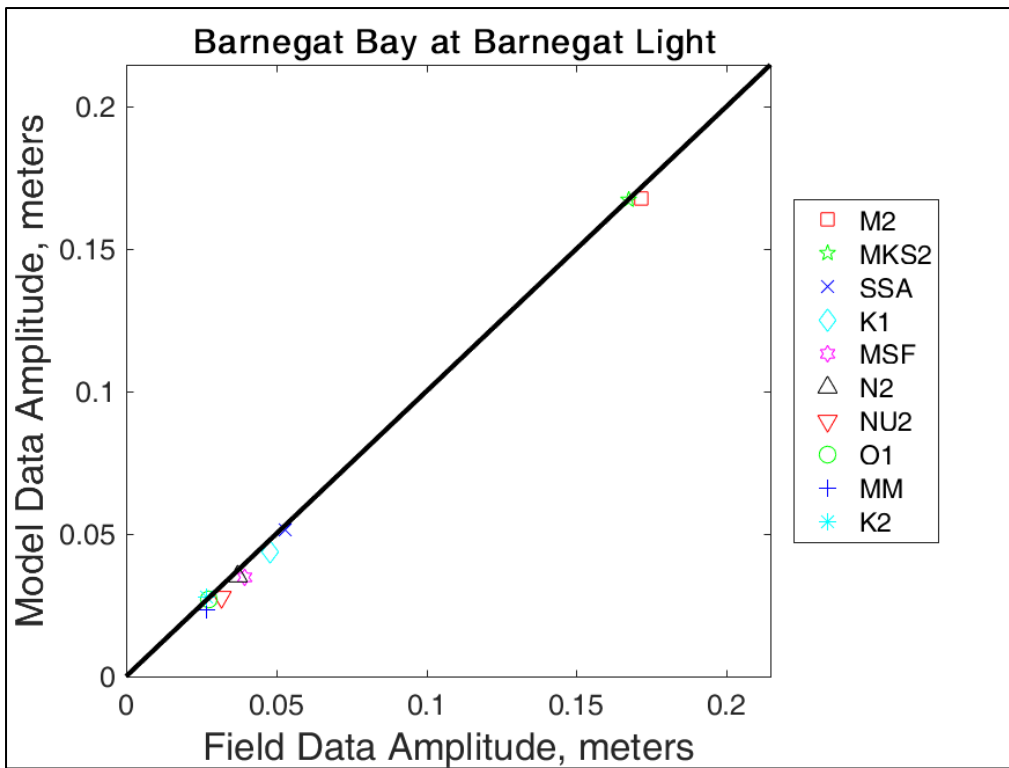


Figure 31. Harmonic constituent phase comparison for Barnegat Bay at Barnegat Light (largest 10 component amplitudes).

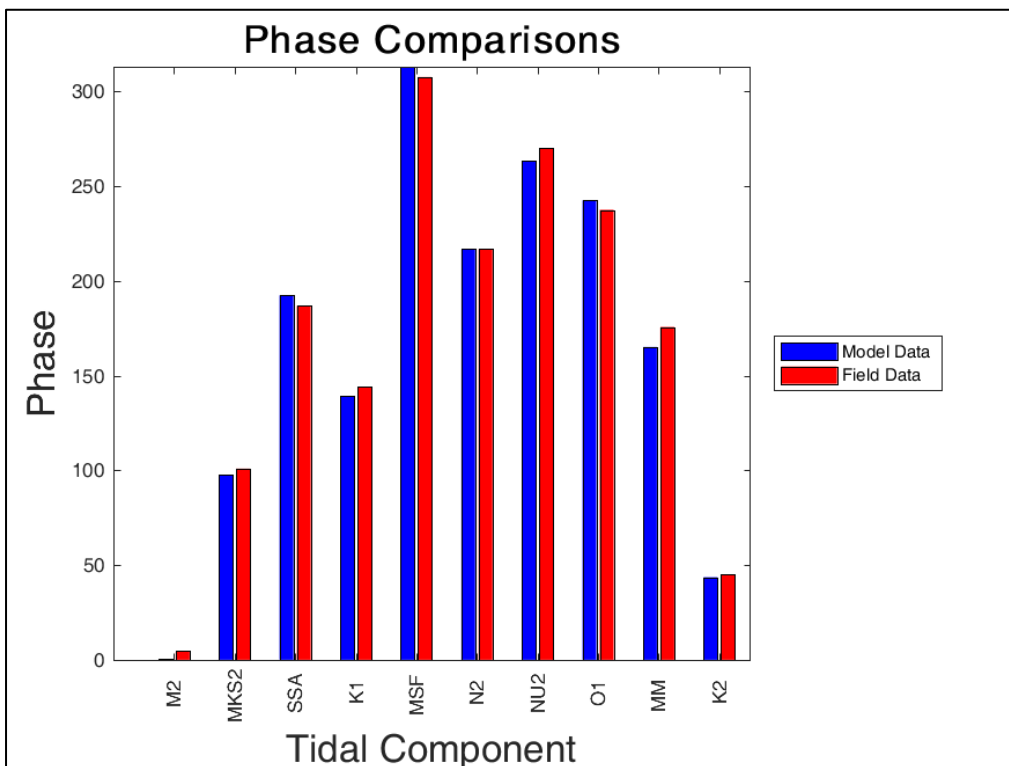


Figure 32. Harmonic constituent amplitude comparison for Inside Thorofare (largest 10 component amplitudes).

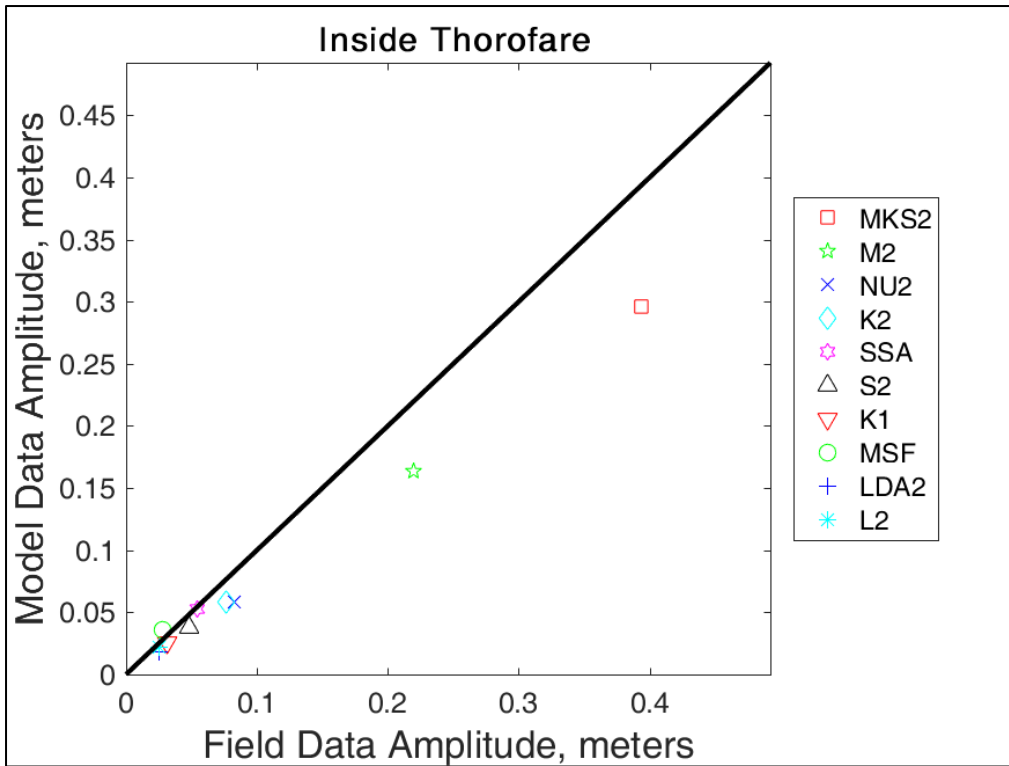


Figure 33. Harmonic constituent phase comparison for Inside Thorofare (largest 10 component amplitudes).

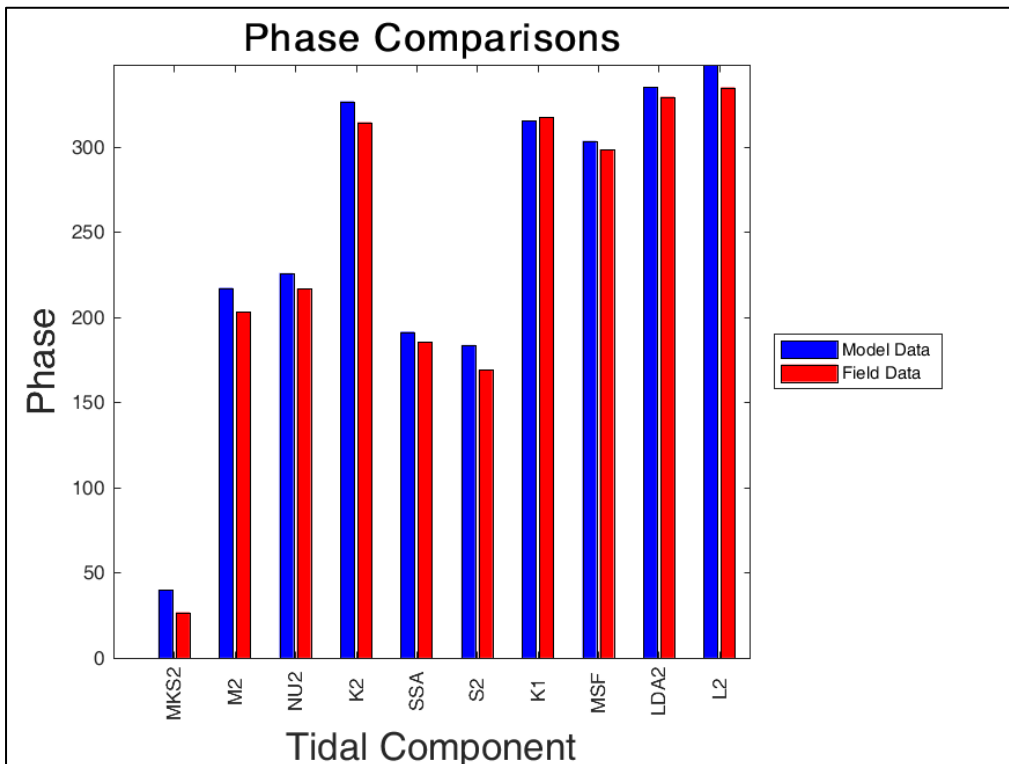


Figure 34. Harmonic constituent amplitude comparison for Ingram Thorofare (largest 10 component amplitudes).

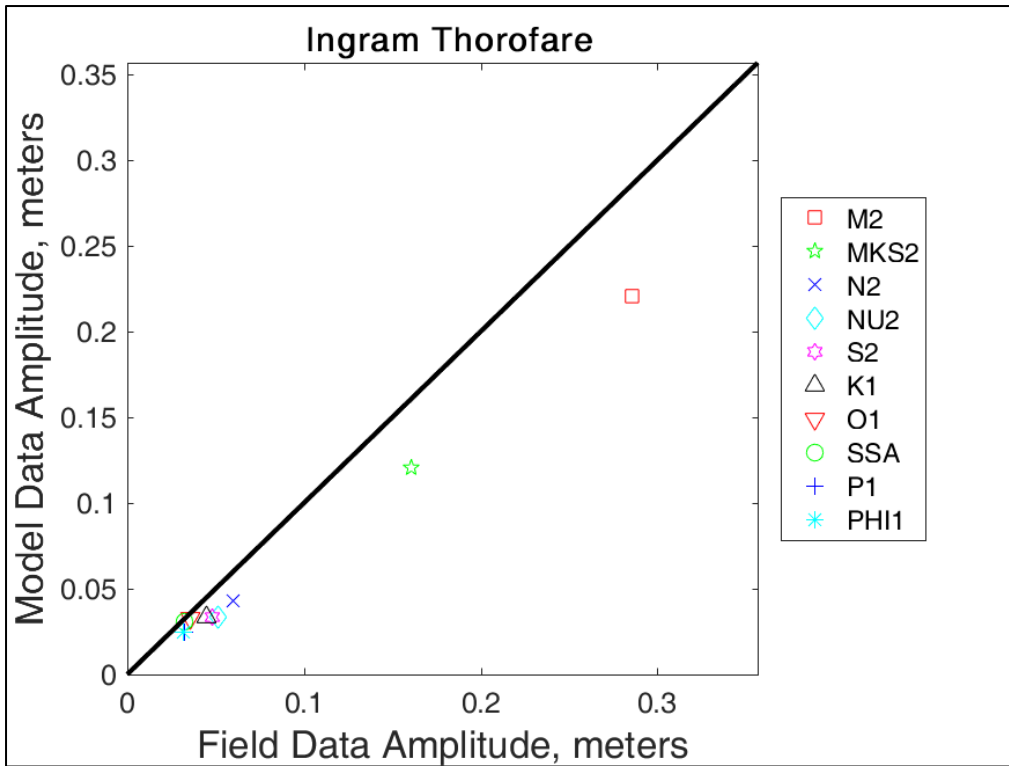
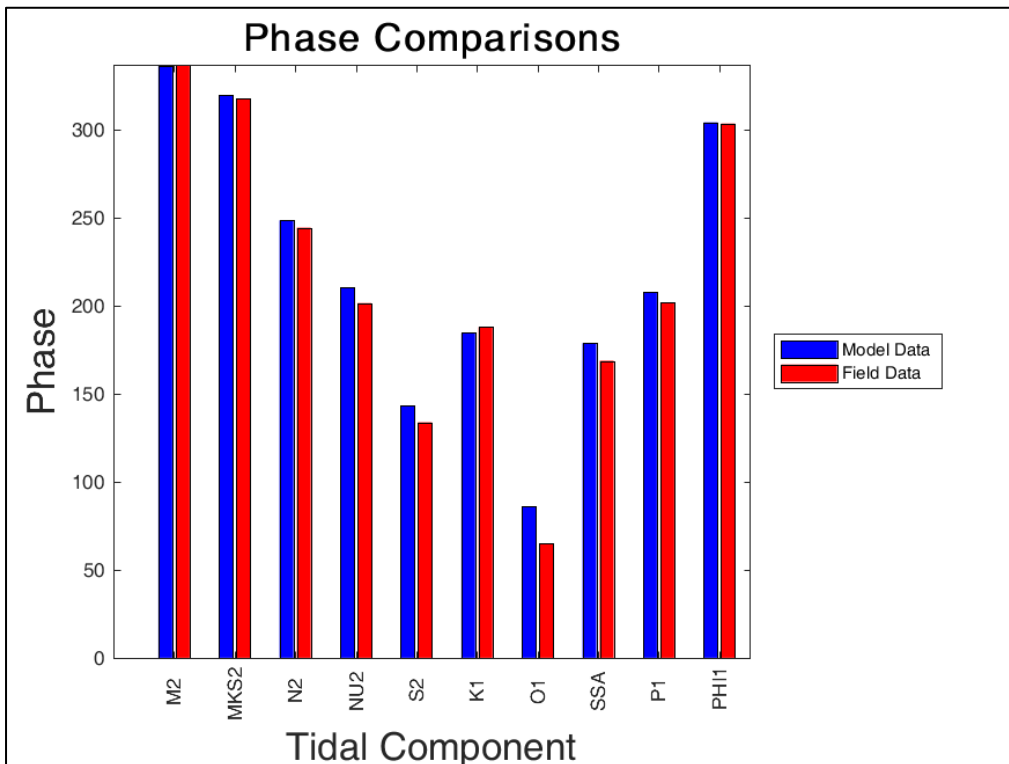


Figure 35. Harmonic constituent phase comparison for Ingram Thorofare (largest 10 component amplitudes).



Discharge

Discharge calibration comparisons are made at all of the transects that were included in the CHL field data collection – Barnegat Inlet, Great Egg Inlet, and Little Egg Inlet. Location figures and plot comparisons are provided for each inlet in the sections below.

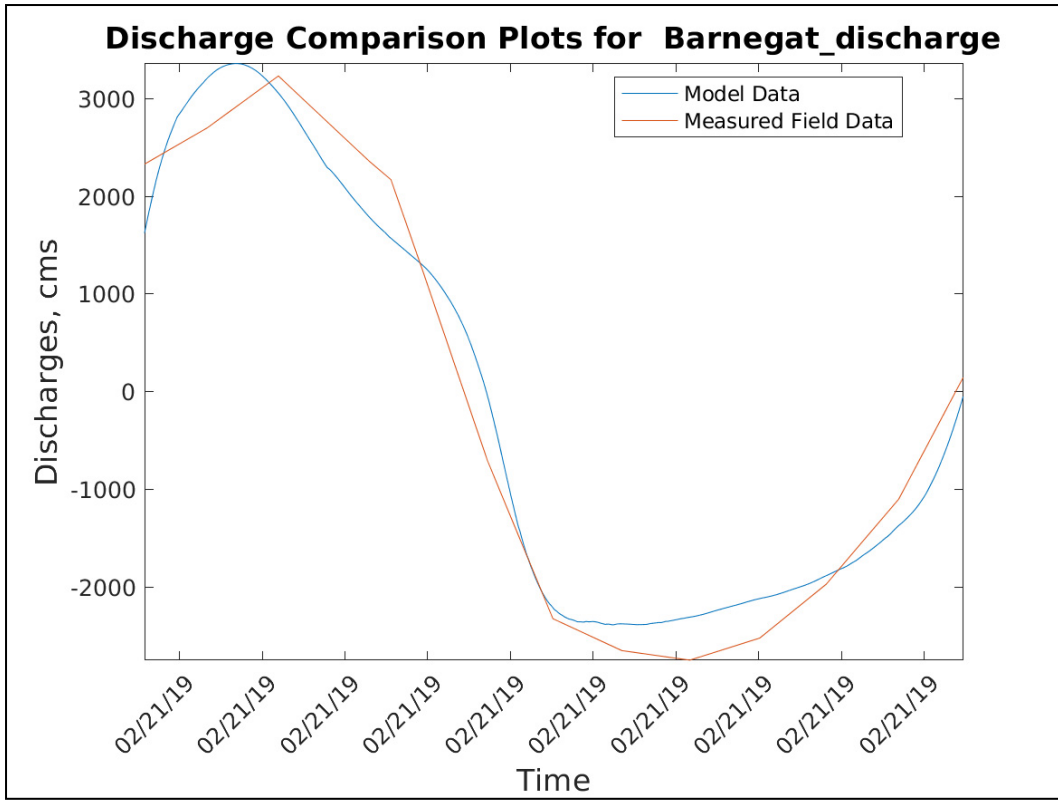
Figure 36 through Figure 47 show the time history discharge (positive: flood; negative: ebb) and the transect locations. The overall pattern of the discharge signal is reproduced by the model, and the comparison of the magnitude is also good. Adjustments to bed roughness parameters were made to get the best match to the field data discharge.

Barnegat Inlet

Figure 36. Barnegat Inlet discharge transect.



Figure 37. Barnegat Inlet discharge comparison.



Little Egg Inlet

Figure 38. Little Egg Inlet discharge transects.

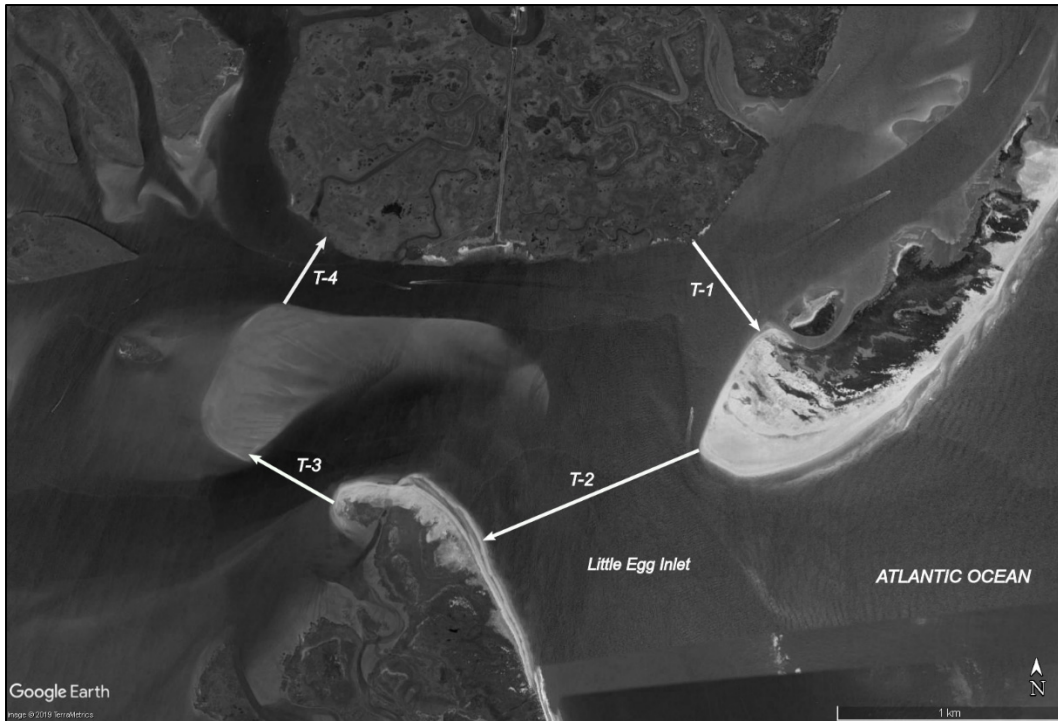


Figure 39. Little Egg Inlet discharge comparison at Transect 1.

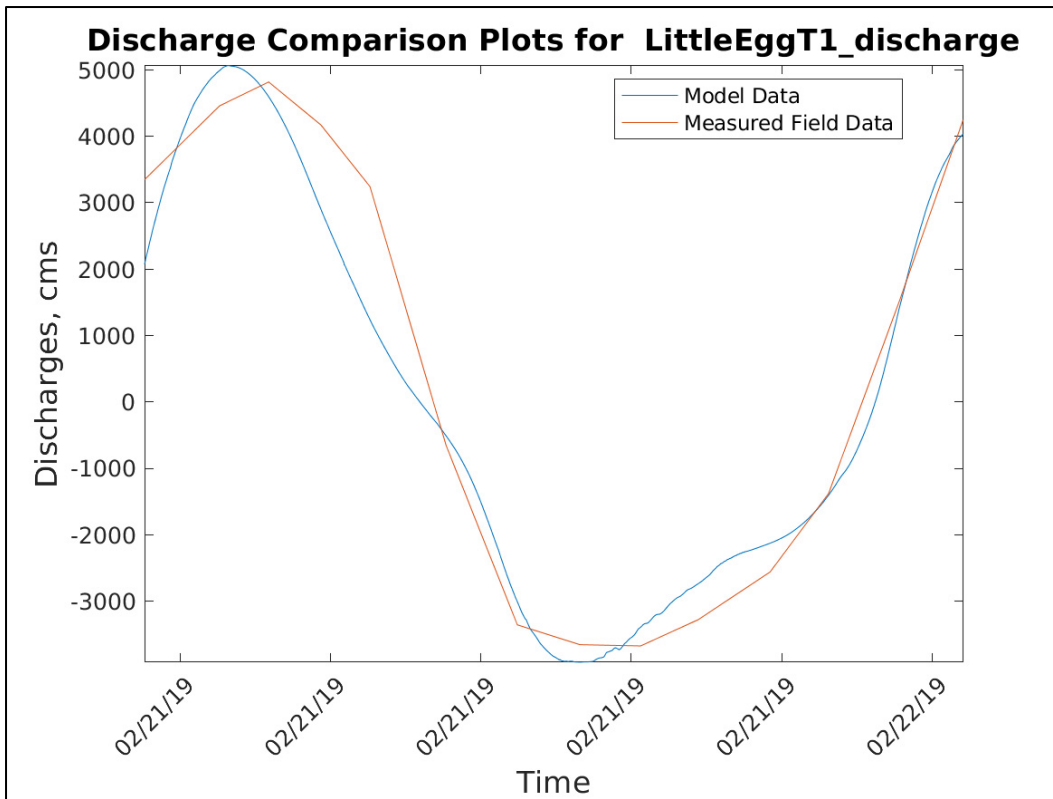


Figure 40. Little Egg Inlet discharge comparison at Transect 2.

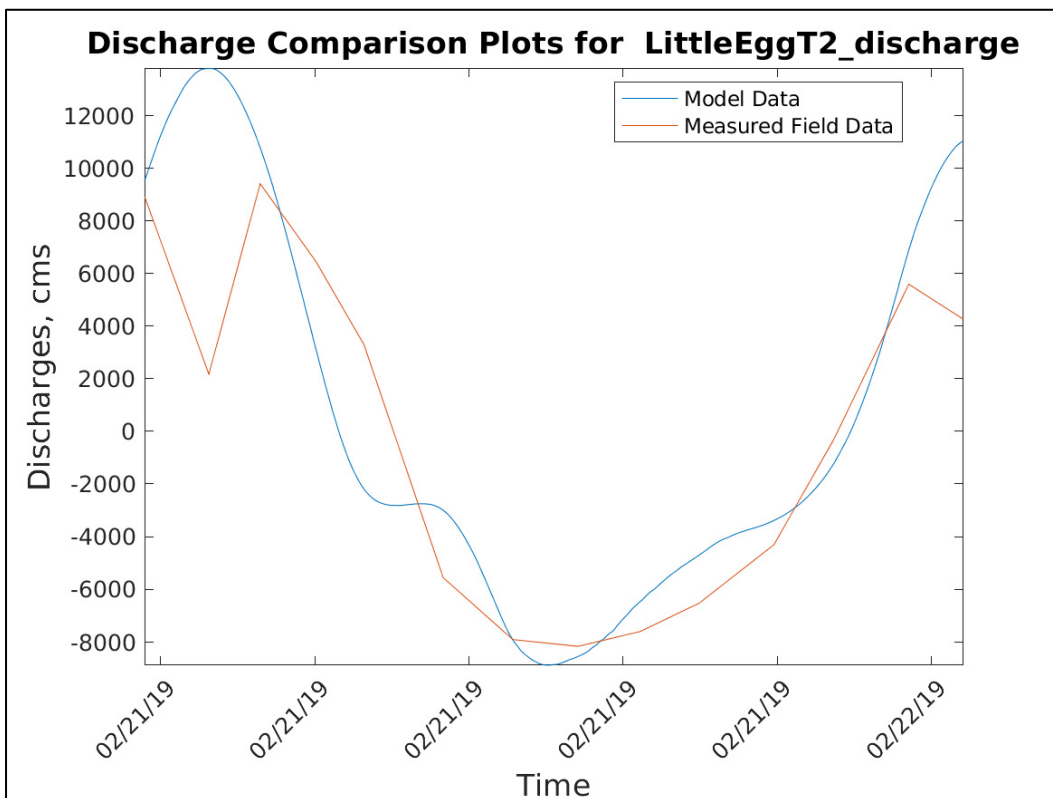


Figure 41. Little Egg Inlet discharge comparison at Transect 3.

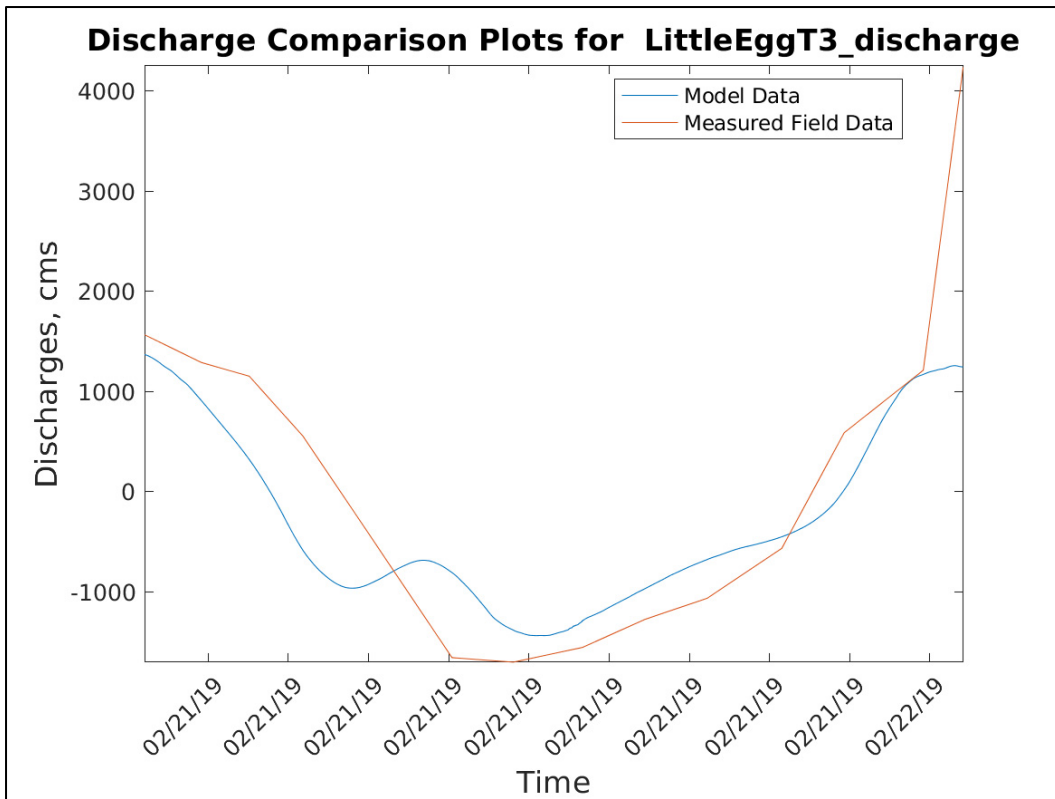
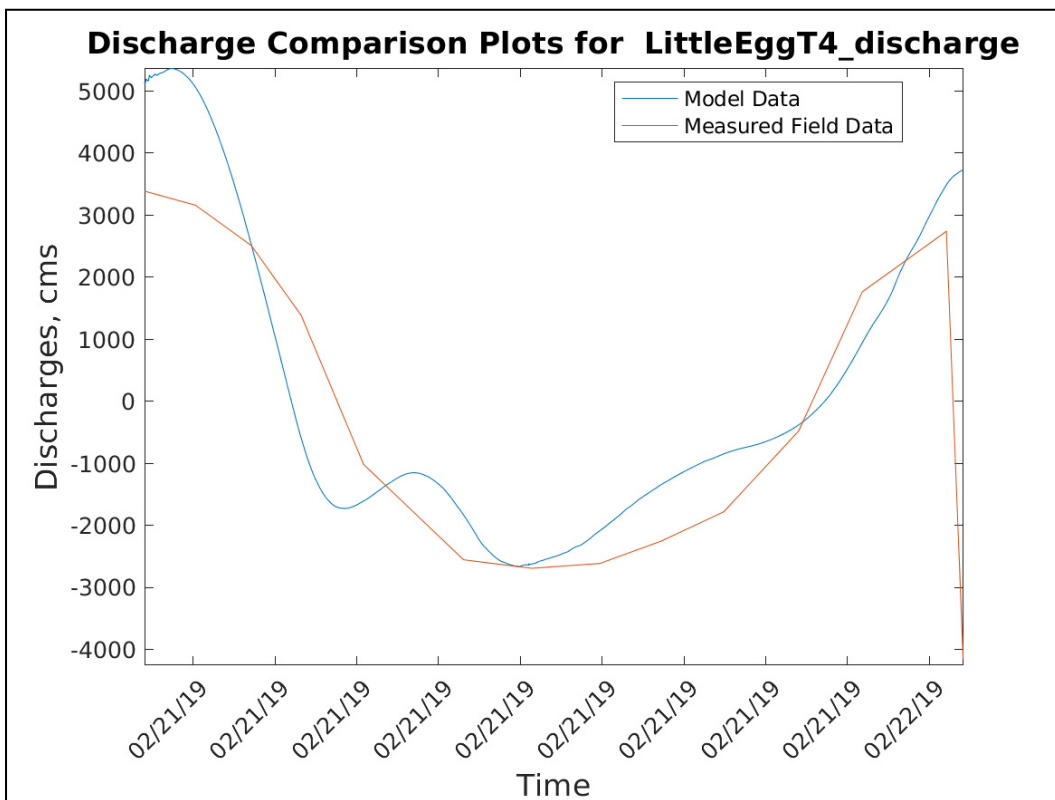


Figure 42. Little Egg Inlet discharge comparison at Transect 4.



Great Egg Inlet

Figure 43. Great Egg Inlet discharge transects.



Figure 44. Great Egg Inlet discharge comparison at Transect 41.

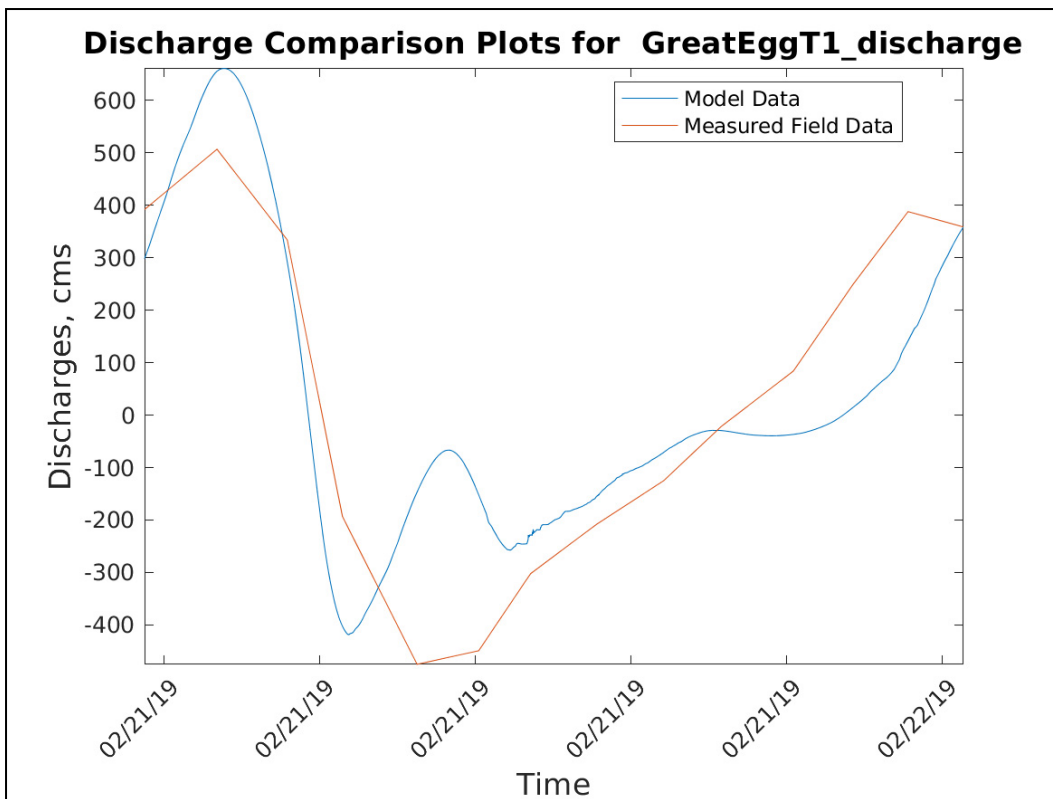


Figure 45. Great Egg Inlet discharge comparison at Transect 2.

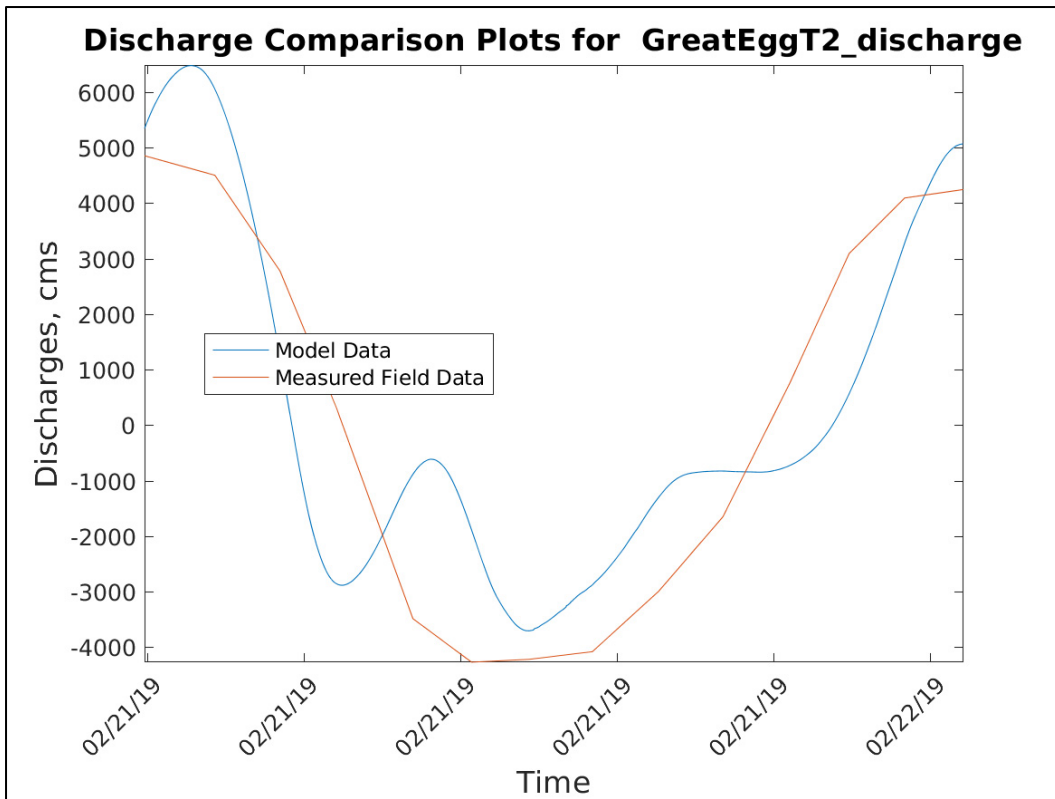


Figure 46. Great Egg Inlet discharge comparison at Transect 3.

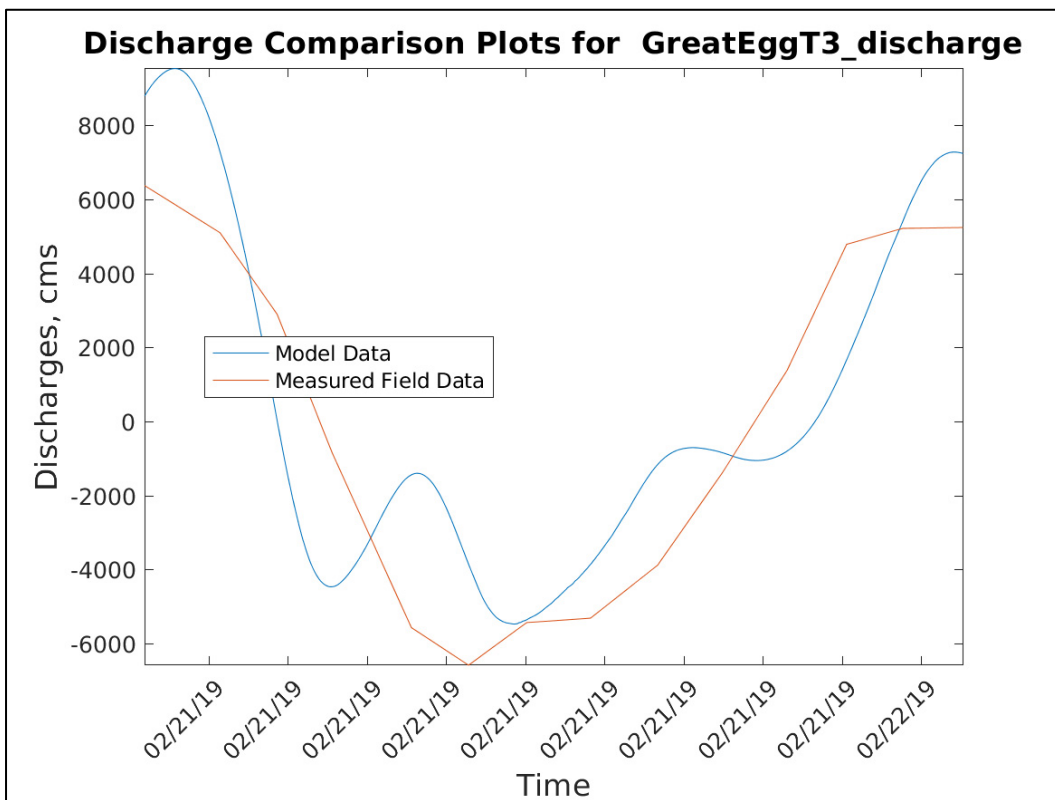
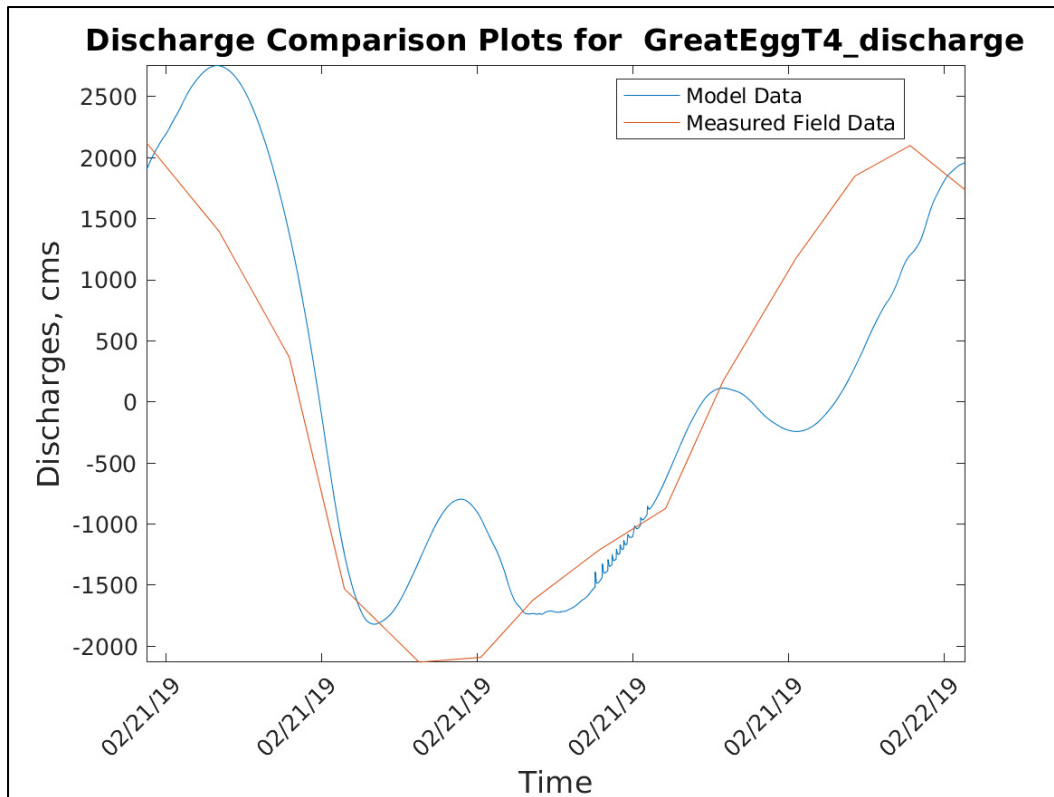


Figure 47. Great Egg Inlet discharge comparison at Transect 4.



Salinity comparisons

The field salinity data for model calibration were obtained from USGS, NERRS, and NJDEP (Figure 48). There are 12 total salinity calibration sites throughout the NJBB for 2018; however, the southern bay, south of Little Egg Inlet, as no available data for 2018. Historic data will be used to compare salinity ranges for this lower bay area.

Time-history comparisons at selected locations (those circled in red in Figure 48) are shown in Figure 50 through Figure 53. The field data are represented by the red line whereas the model data are shown in blue for depth averaged salinity. This area is generally well mixed, i.e. the surface and bottom salinity values are approximately equal. The field-measured salinity is typically measured at the surface, but it is not specified for all data. The full set of salinity comparisons is provided in Appendix C.

Figure 48. Salinity comparison locations.

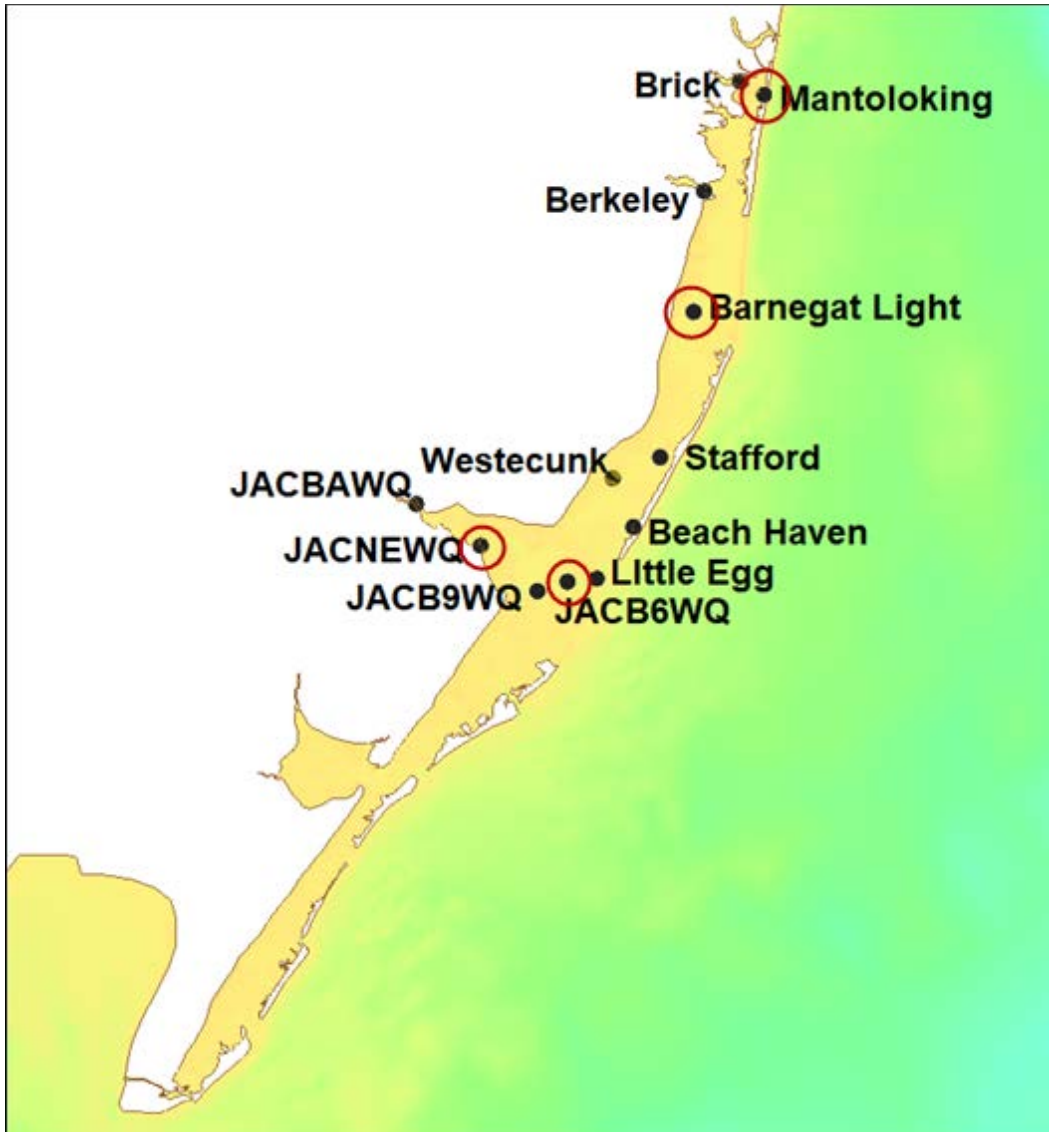


Figure 49. Historic salinity comparison locations.

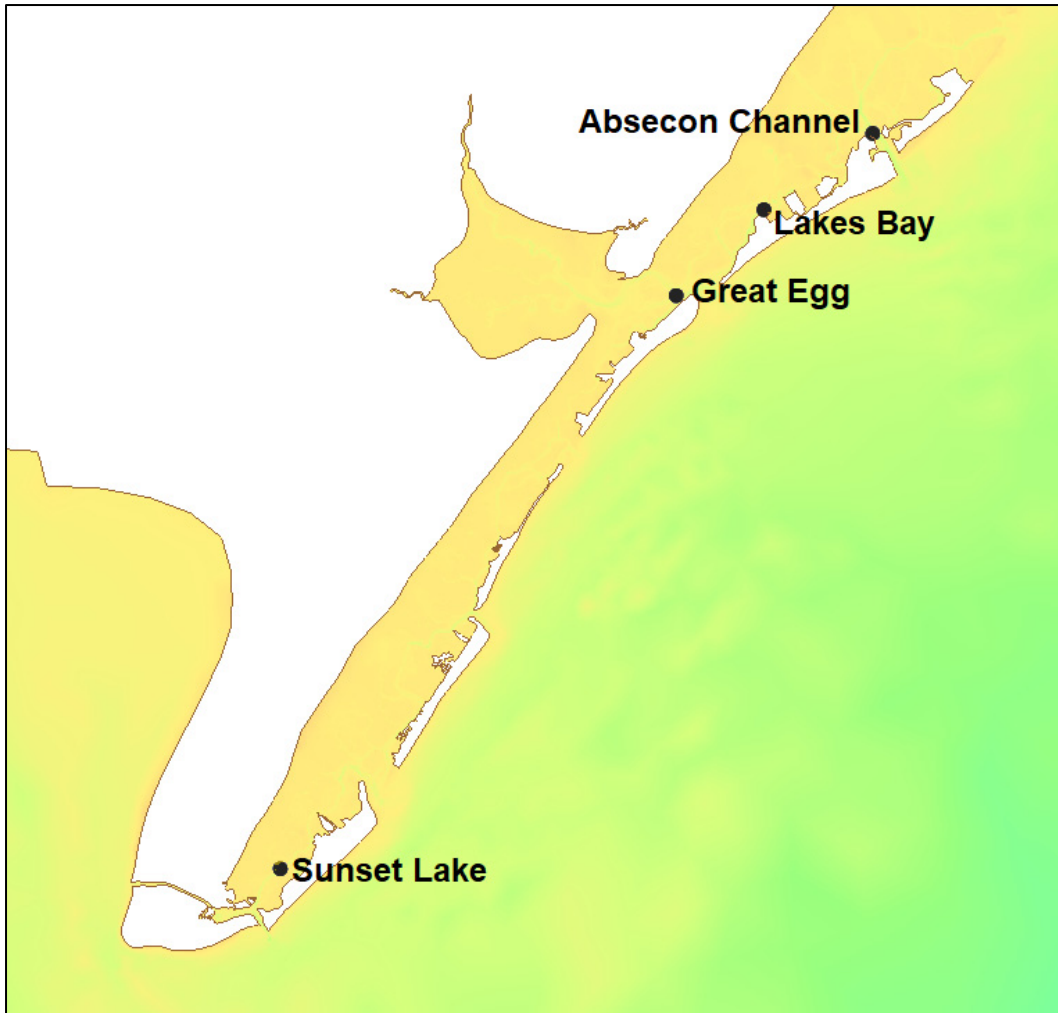


Figure 50. Mantoloking salinity comparison.

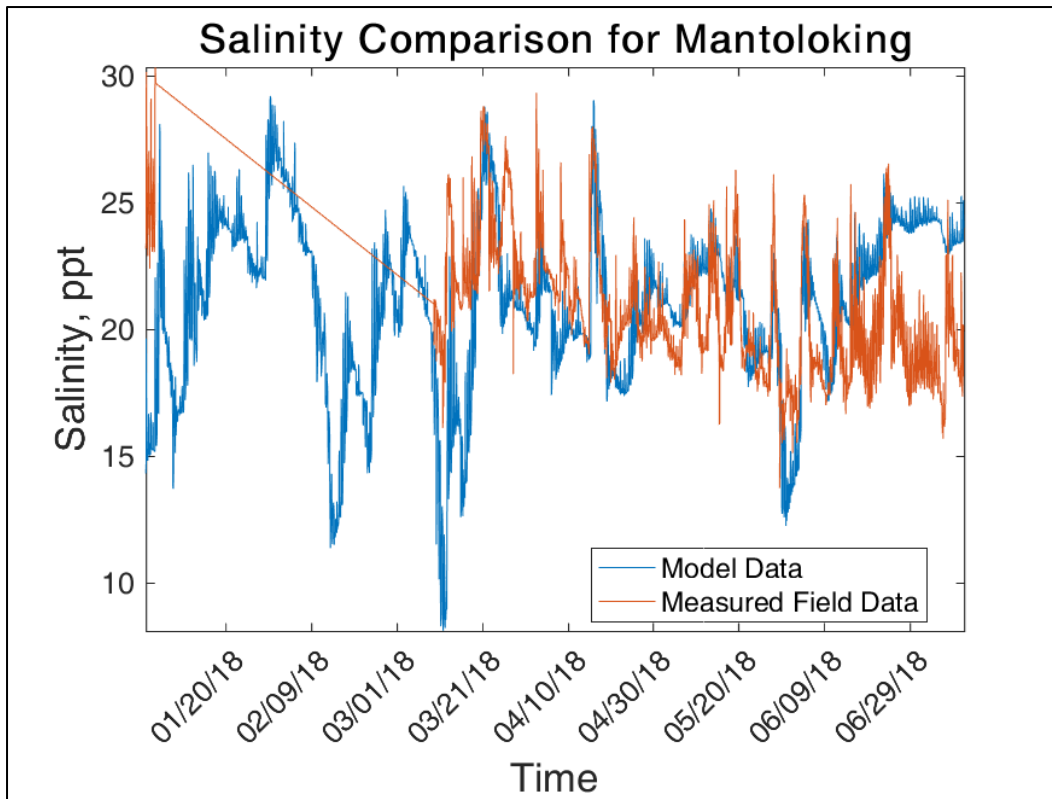


Figure 51. Barnegat Light salinity comparison.

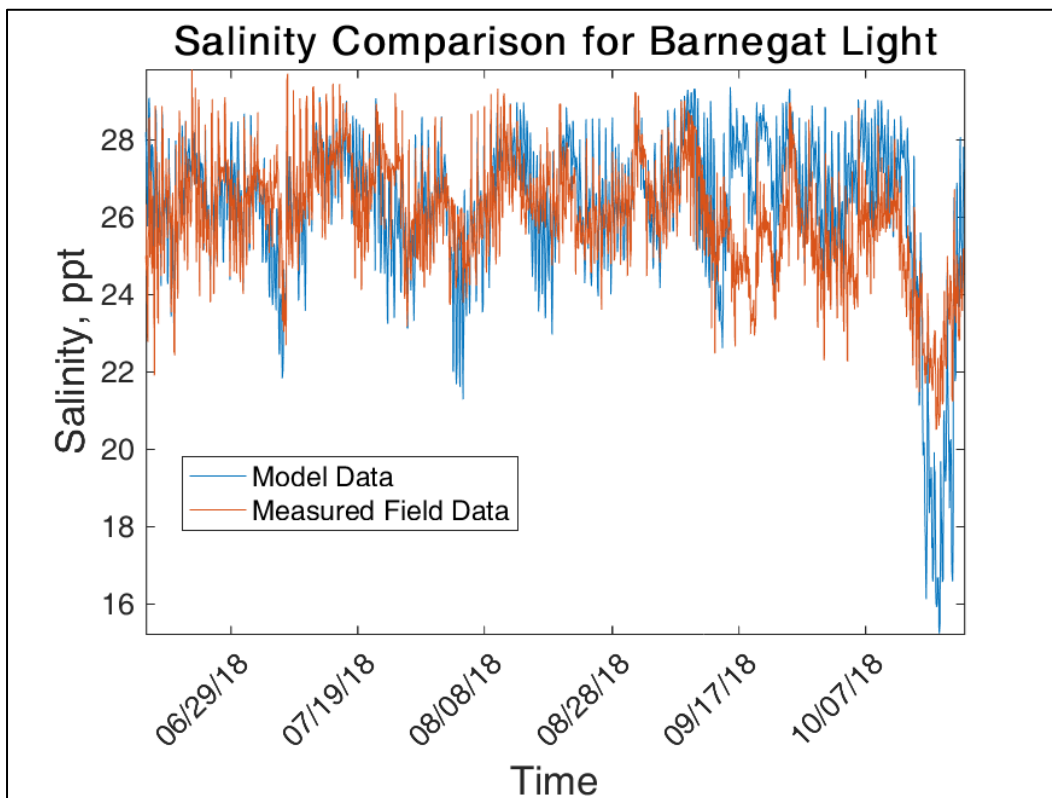


Figure 52. JACB6WQ salinity comparison.

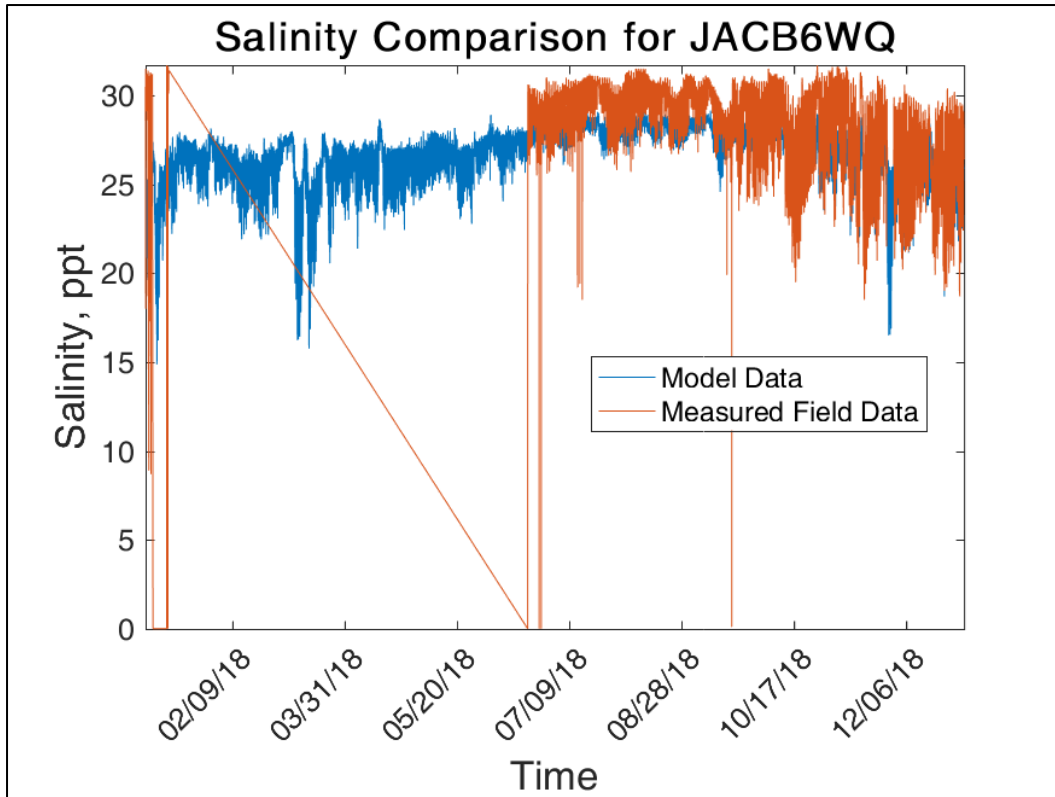
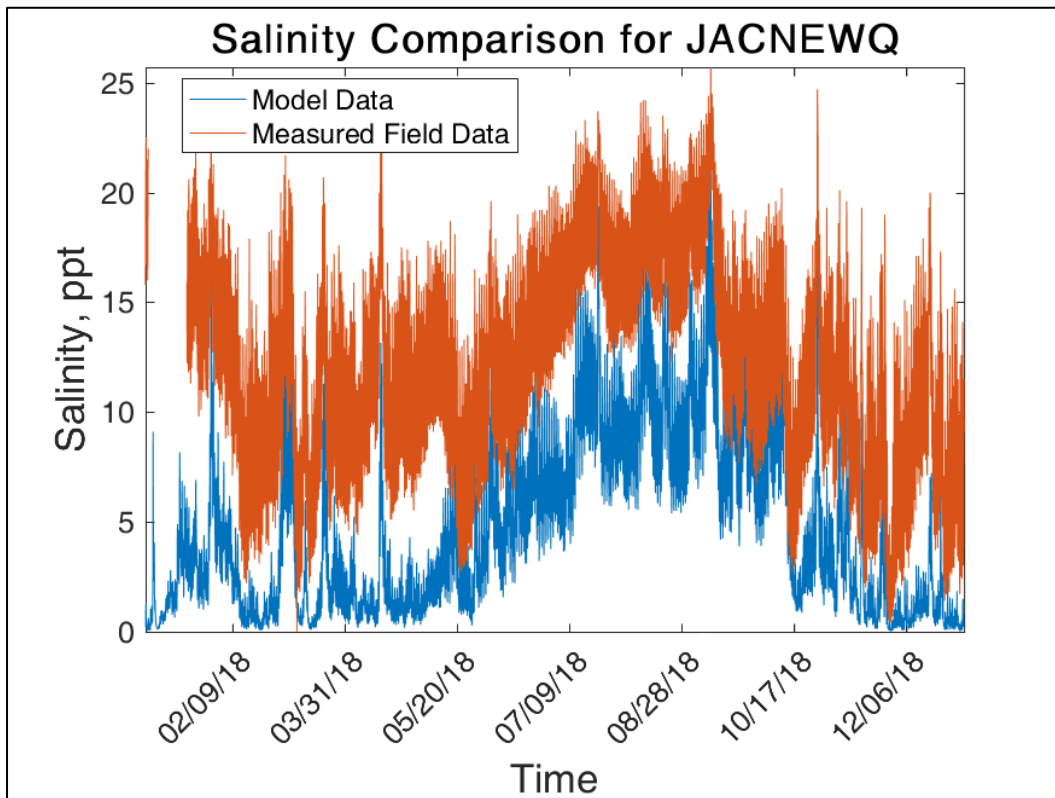


Figure 53. JACNEWQ salinity comparison.



Overall, the salinity patterns are replicated in the model. However, some locations compare better in magnitude than others. Locations closest to the inlets generally reproduce the magnitude with larger differences coming at locations further up the small, back bay channels. These channels and the conveyance of salt are limited in the model by the available bathymetry data and resolution. Time could be invested into perfecting these comparisons but was not due to the good representation of the salinity pattern over time. For relative changes in salinity due to storm protection structures at the inlets, these model results are adequate.

4 Inlet Area of Influence

A sensitivity test was performed to determine the area of influence of a particular inlet on the salinity at particular locations. Each inlet in the system was closed individually (one inlet was closed while all others remained open) and the salinity was compared at the validation locations. These simulations were performed over a six day period simply to see the variation in the salinity with each inlet closed.

Figure 54. Inlet labels.

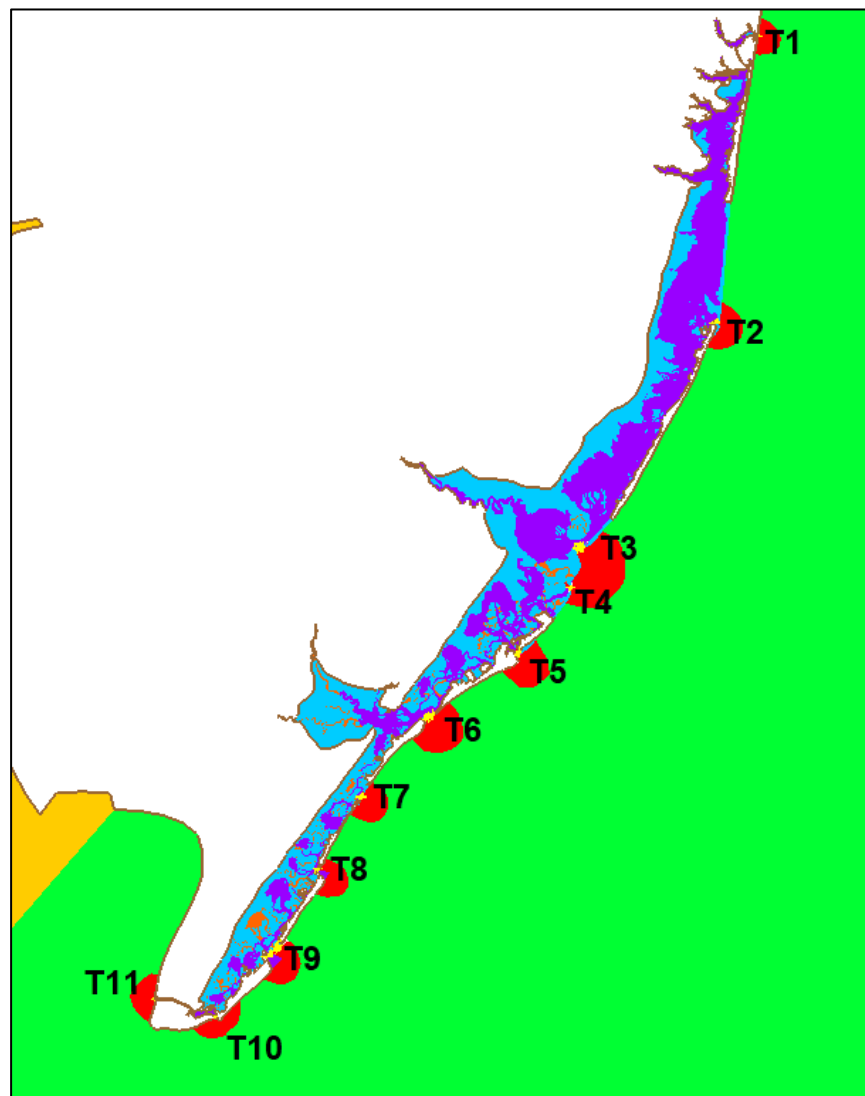


Figure 55. Salinity comparison locations. JACBAWQ will not be compared.



Figure 56 through Figure 66 show the salinity under various inlet closures for each analysis location. The base condition is run with all inlets open. Each labeled alternative indicates the inlet that was closed. If the salinity matches the base condition then that inlet is not influencing the salinity at the given location. If the lines deviate, the inlet does influence that location.

Closing T2, Barnegat inlet, impacts the salinity from Brick to the north, down to Little Egg to the south. The T1 closure at Manasquan impacts salinity at Brink and Mantoloking but nothing further south. The closure at Little Egg Inlet, T3, influences salinity as far north at all comparison locations. Unfortunately, comparisons were not made at locations south of Little Egg, because it is known that many of these closures would influence that area. Closures at Great Egg and further south, T6 – T11, do not show an influence at any of the comparison locations.

Figure 56. Inlet influence comparison at Brick.

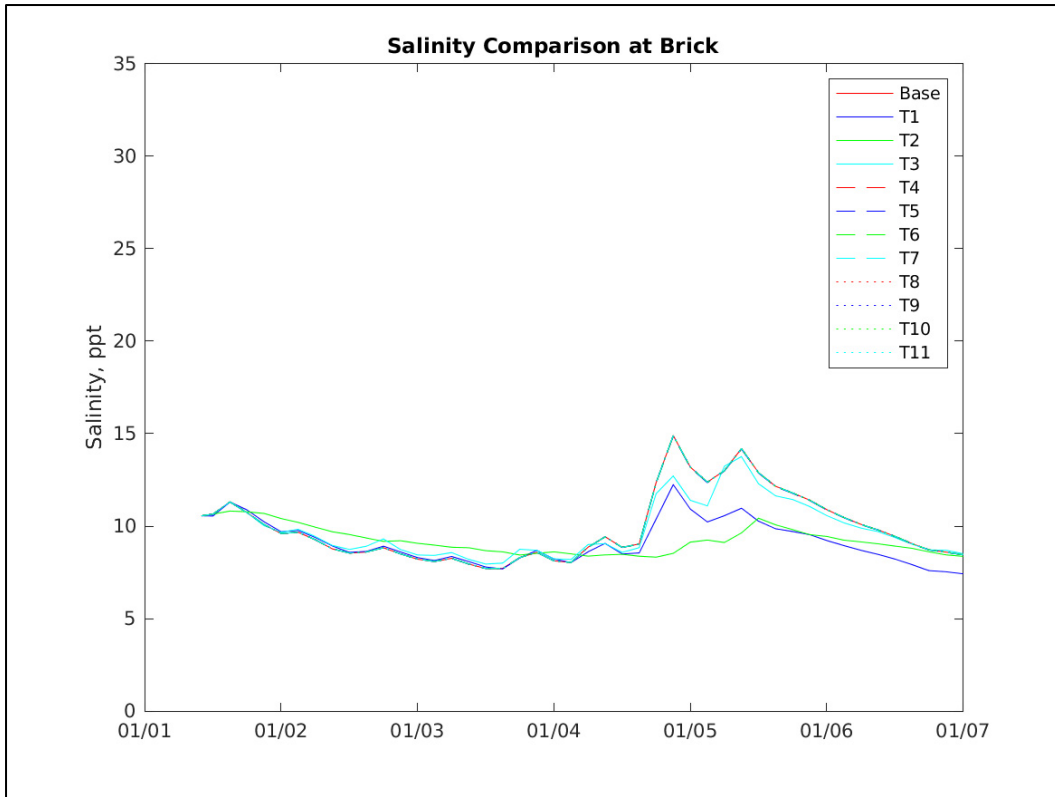


Figure 57. Inlet influence comparison at Barnegat Bay at Mantoloking.

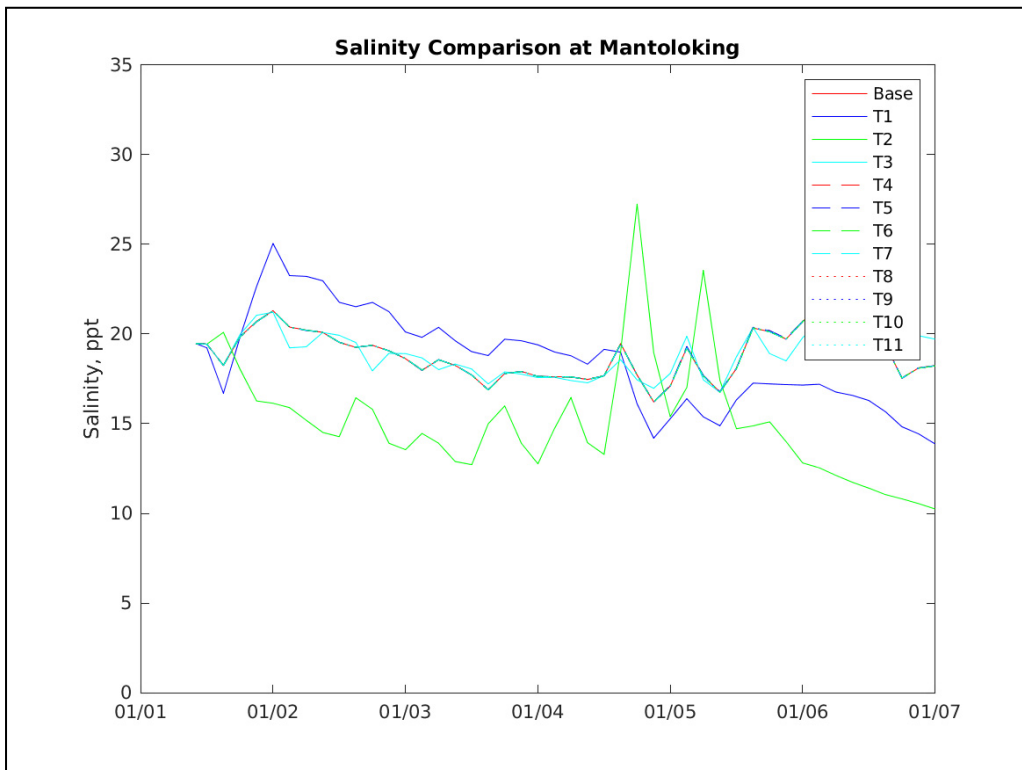


Figure 58. Inlet influence comparison at Berkeley.

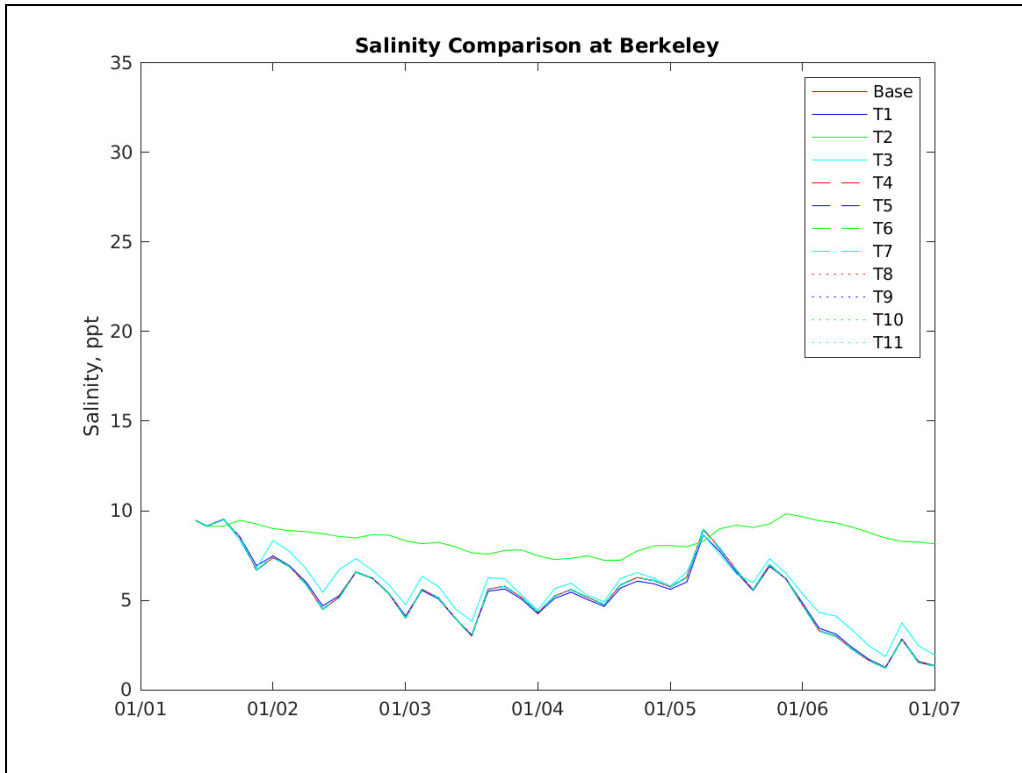


Figure 59. Inlet influence comparison at Barnegat Light.

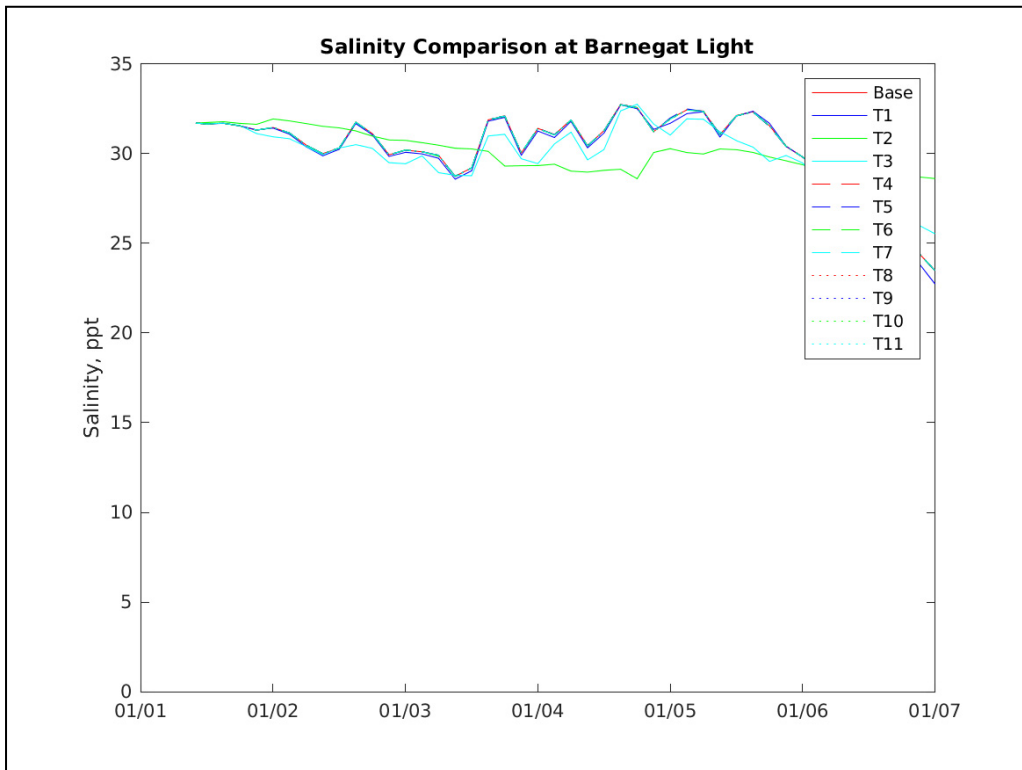


Figure 60. Inlet influence comparison at Stafford.

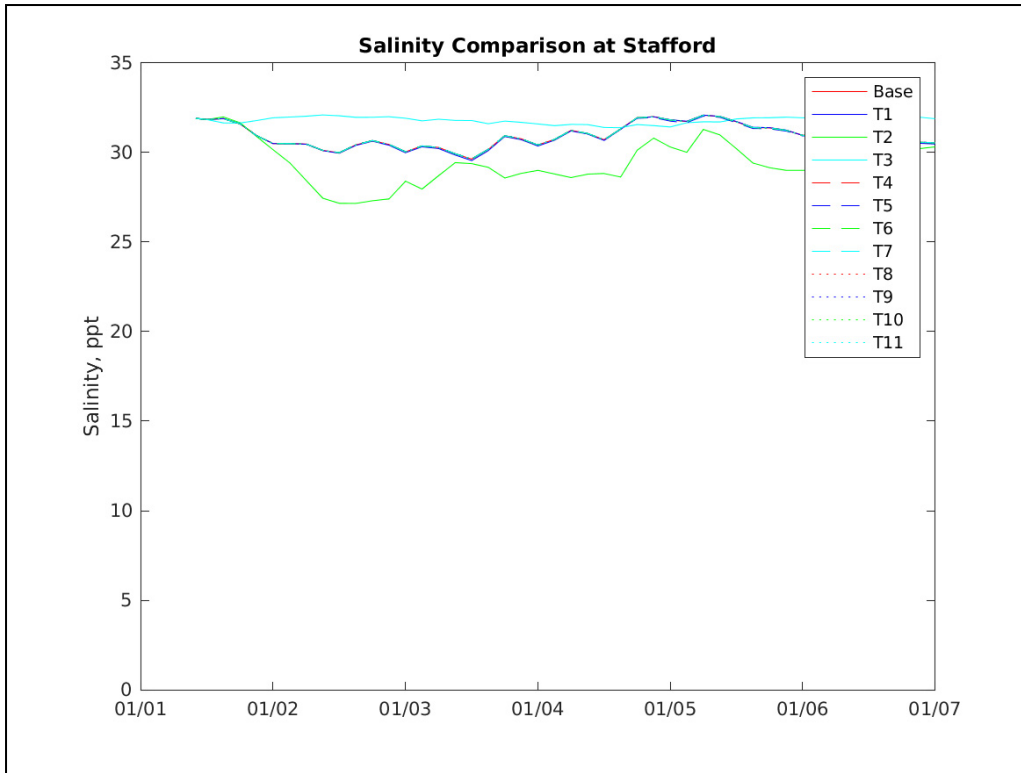


Figure 61. Inlet influence comparison at Westecunk.

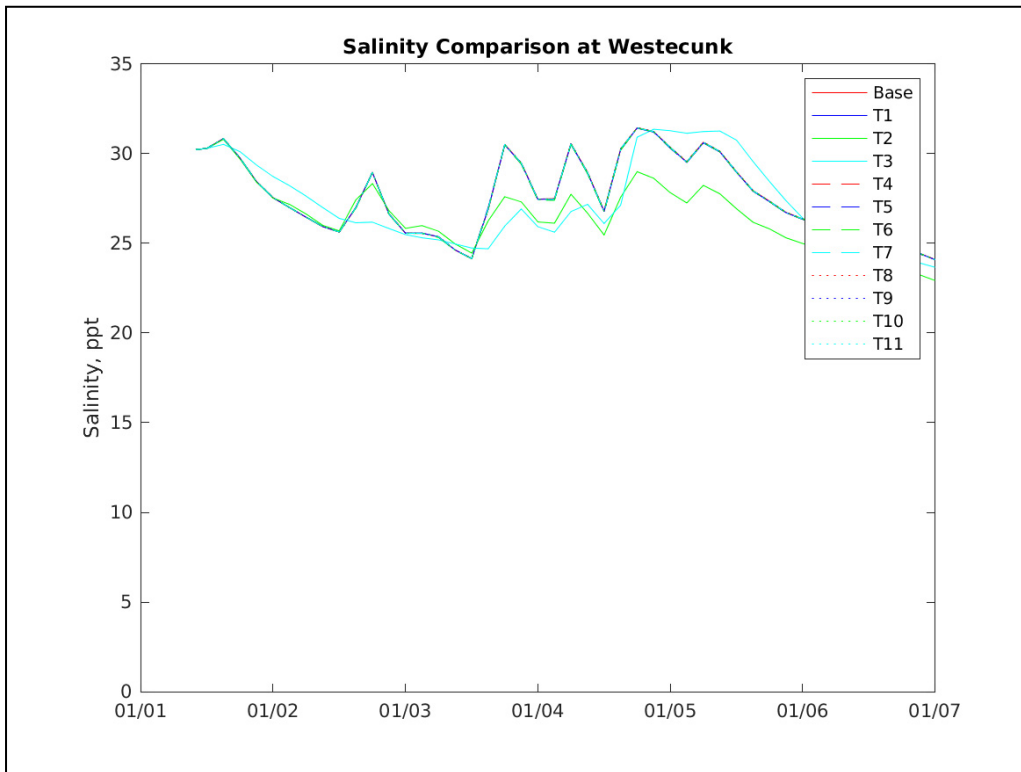


Figure 64. Inlet influence comparison at JACB6WQ.

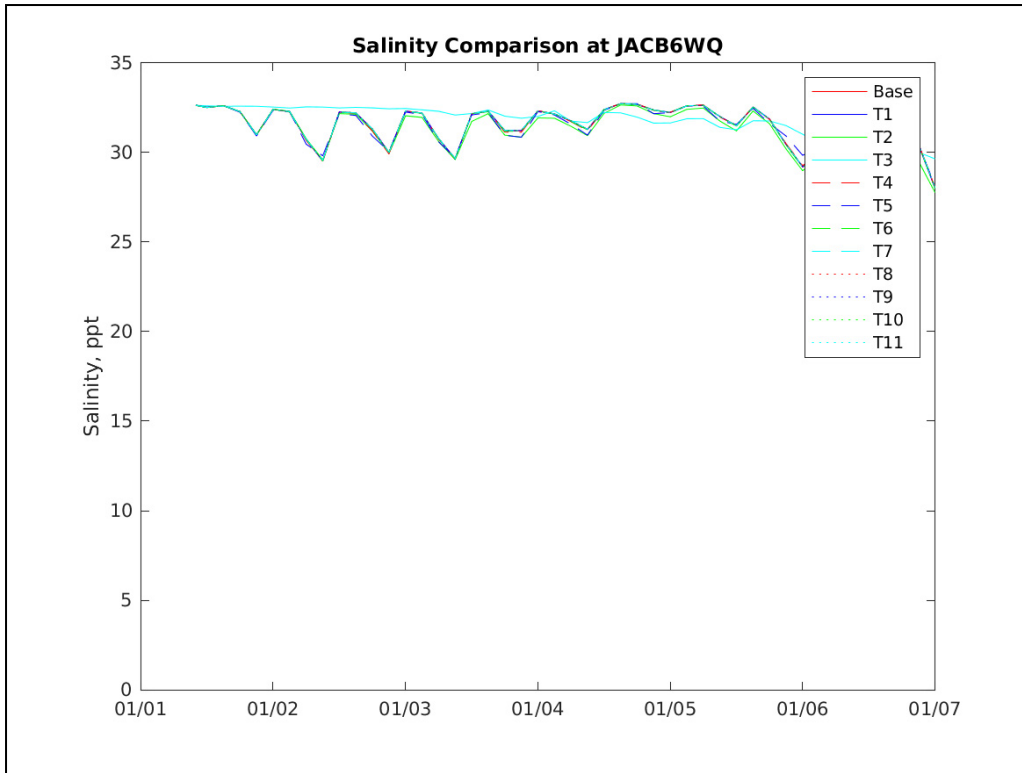
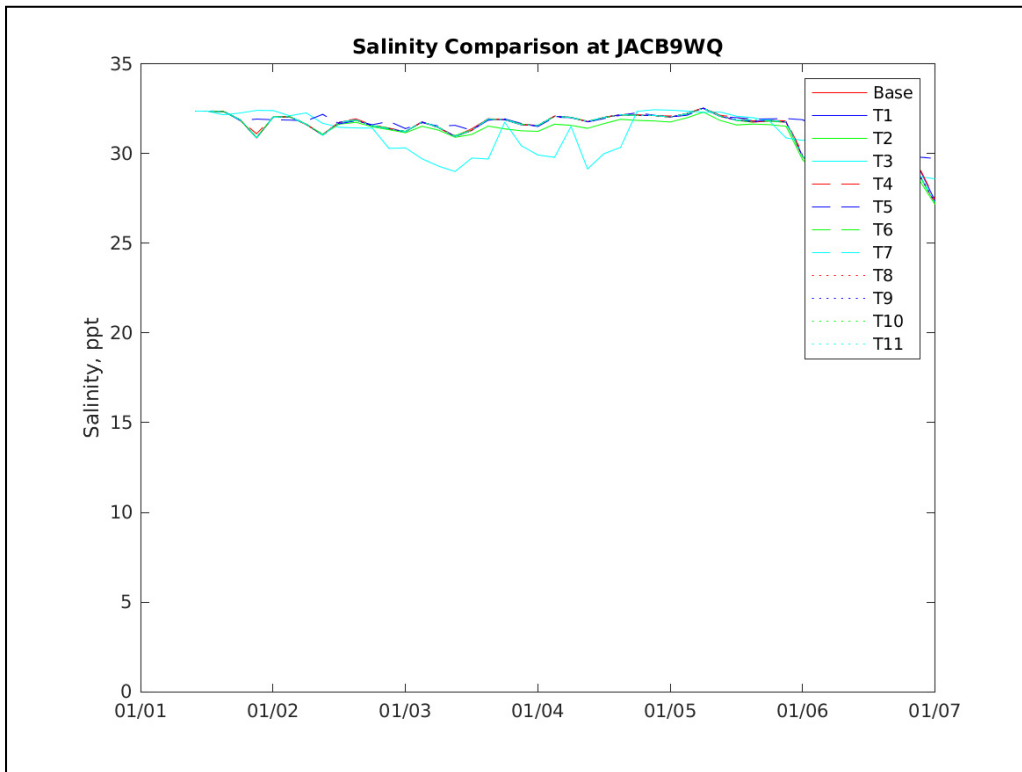


Figure 65. Inlet influence comparison at JACB9WQ.



5 Plan Alternatives

A matrix of alternatives was established by NAP to test a range of storm surge protection structures at several inlets as well as various combinations of structures. A total of 9 alternatives were simulated along with a Base condition. Three of these simulations include sea level rise.

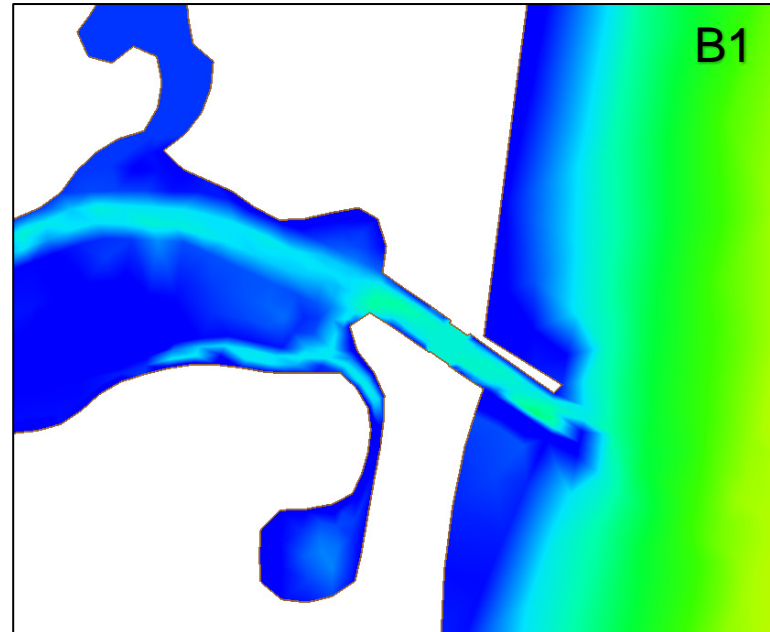
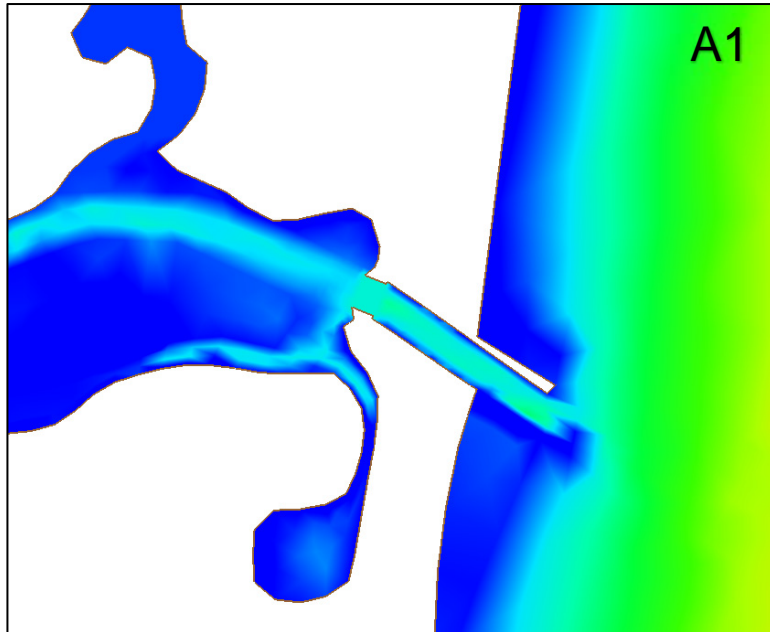
The structure definitions for each location are provided in Figure 67 through Figure 73. These structures are grouped into six with project alternatives as shown in Table 4. The final three alternatives include sea level rise for the Base, alternative 1, and alternative 5.

An elevation shift of 0.445 m was added to the water surface elevation at the tide boundary. The USACE Sea Level Rise guidance in EC 1165-2-212 was used to determine the necessary shift based on the intermediate sea level rise curve (NRCI). The NAVD88 elevation of the NOAA gage at Atlantic City was used as the controlling tide gage. Year zero is considered 2018 since this is the year of the data used to drive the model. The target year is 2080 (specified by NAP). The historic observed rate of sea level rise for the controlling gage is 0.00409 m/yr. The equation yields a shift in the water surface elevation of 0.445m from the 2018 measured elevation.

The mesh domain was not expanded to account for potential wetted area with rising sea level. However, the ADCIRC NACCS domain was used to determine how much would possibly be inundated under this additional water level and that area was extremely small, as seen in Figure 74.

Additionally, vegetated areas were not raised in the sea level rise simulations. Oftentimes the assumption that vegetated marsh will keep up with the projected sea level rise is used but it was not in these simulations. This assumption should be considered when reviewing the results of the sea level rise alternatives. The sea level rise alternatives will only be compared with each other and will not be compared to alternatives without sea level rise.

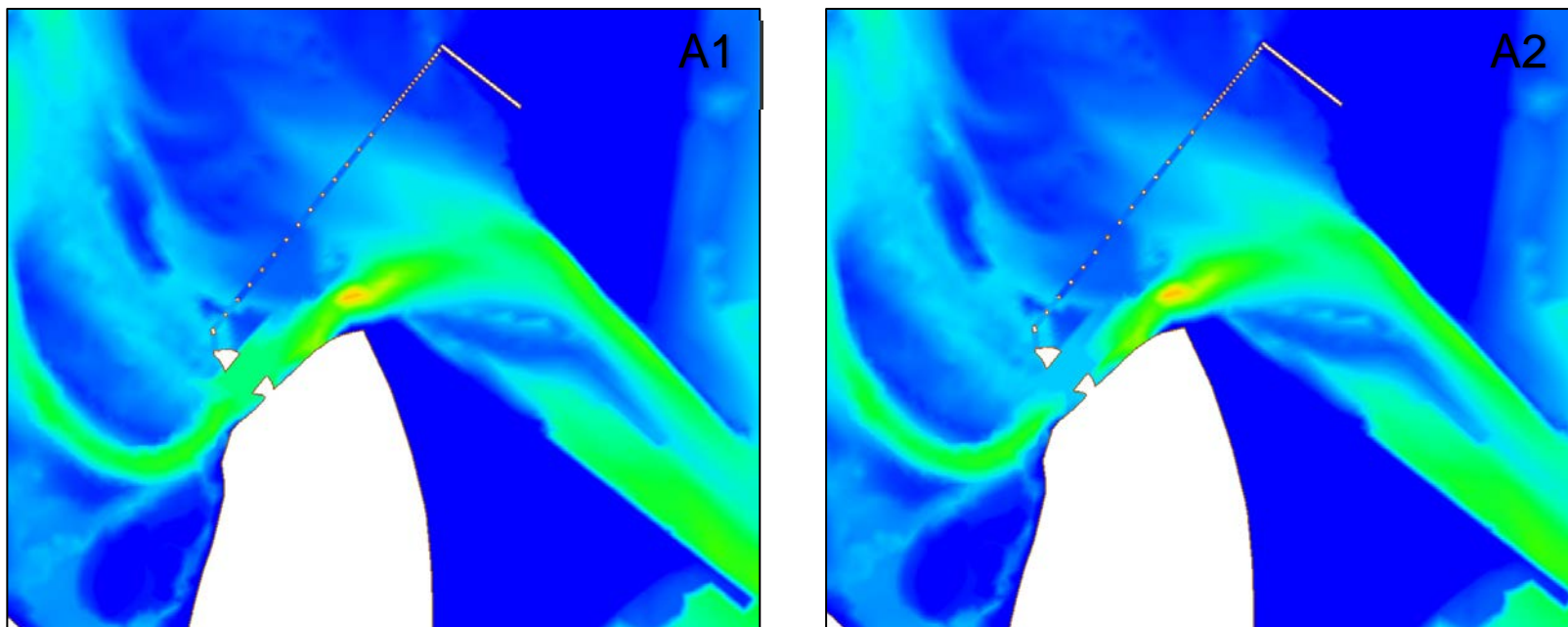
Figure 67. Manasquan structure A1 and A2.



Gate Type	Opening Size	Sill Elevation (NAVD88)
2 horizontal sector gates	340 ft	-18.25 ft

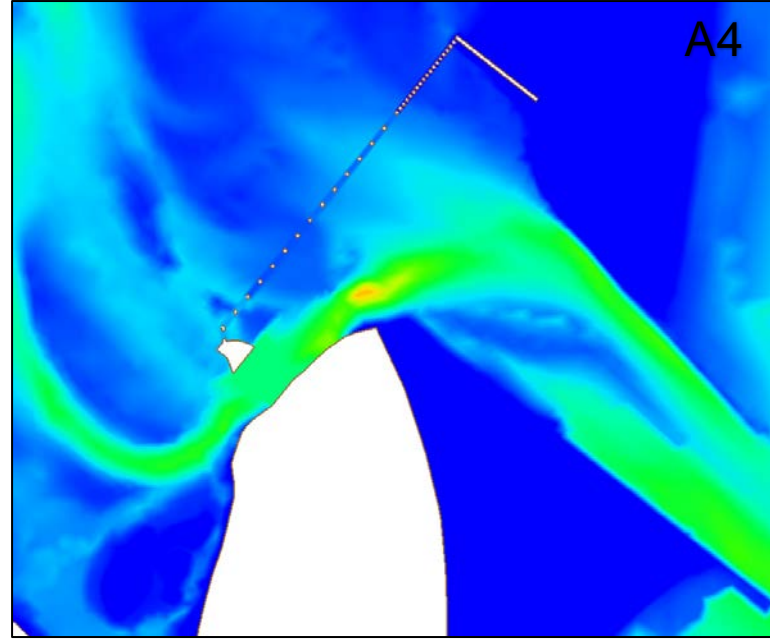
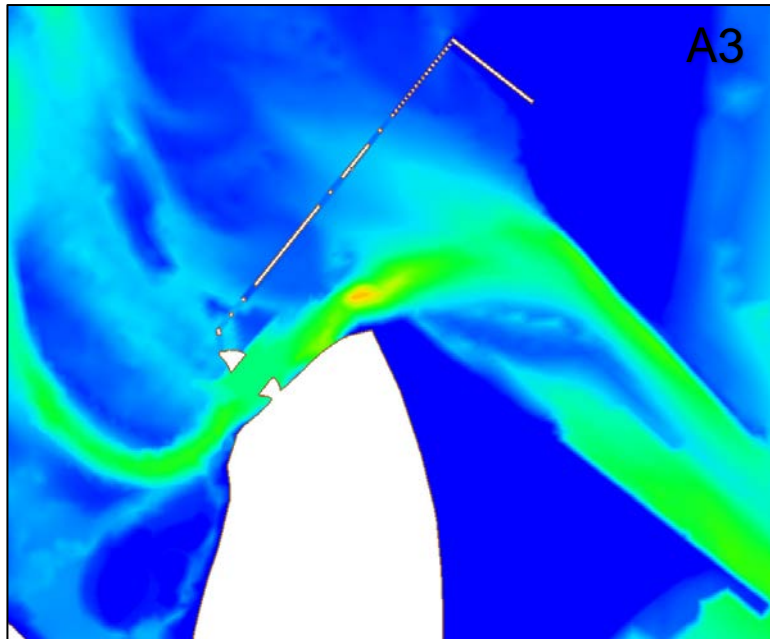
Gate Type	Opening Size	Sill Elevation (NAVD88)
2 horizontal sector gates	340 ft	-18.25 ft

Figure 68. Barnegat structure A1 and A2.



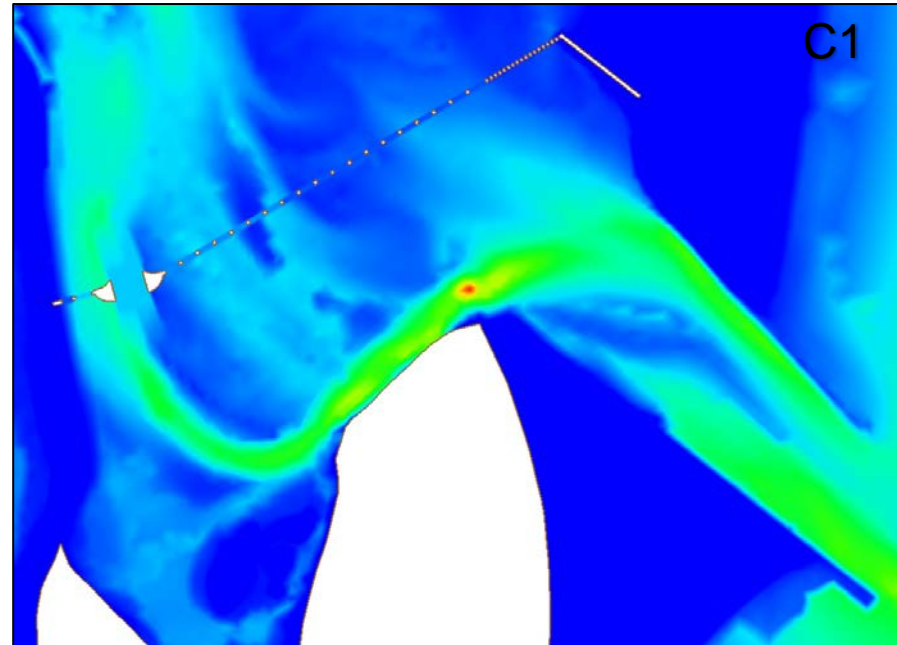
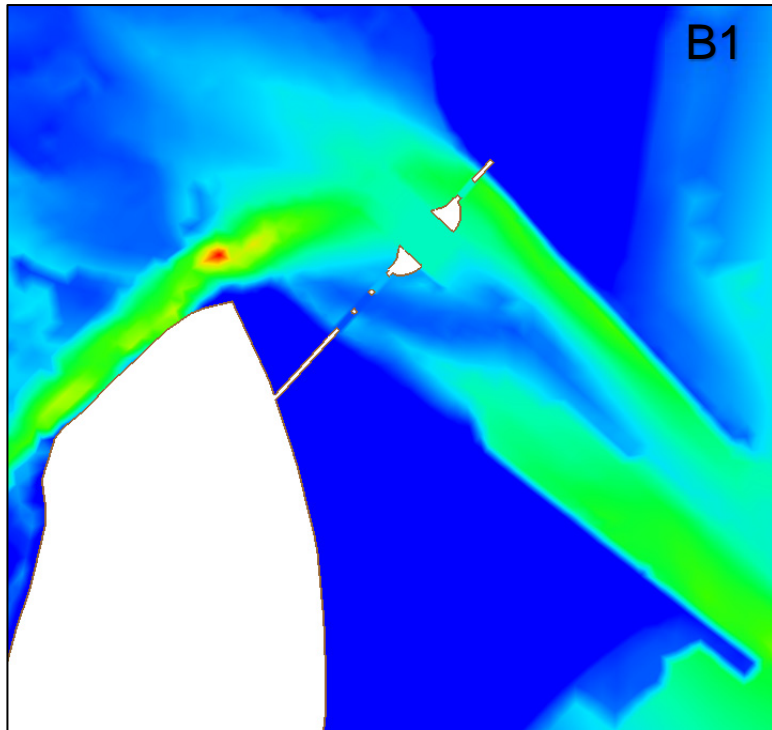
Gate Type	Opening Size	Sill Elevation (NAVD88)
2 horizontal sector gates	320 ft	-25 ft (A2); -13 ft (A1)
15 vertical lift gates	150 ft	-11 to -7 ft
18 culverts	24 x 8 ft	-2 ft

Figure 69. Barnegat structure A3 and A4



Gate Type	Opening Size	Sill Elevation (NAVD88)
2 horizontal sector gates	320 ft	-25 ft
8 vertical lift gates	150 ft	-11 to -7 ft
18 culverts	24 x 8 ft	-2 ft

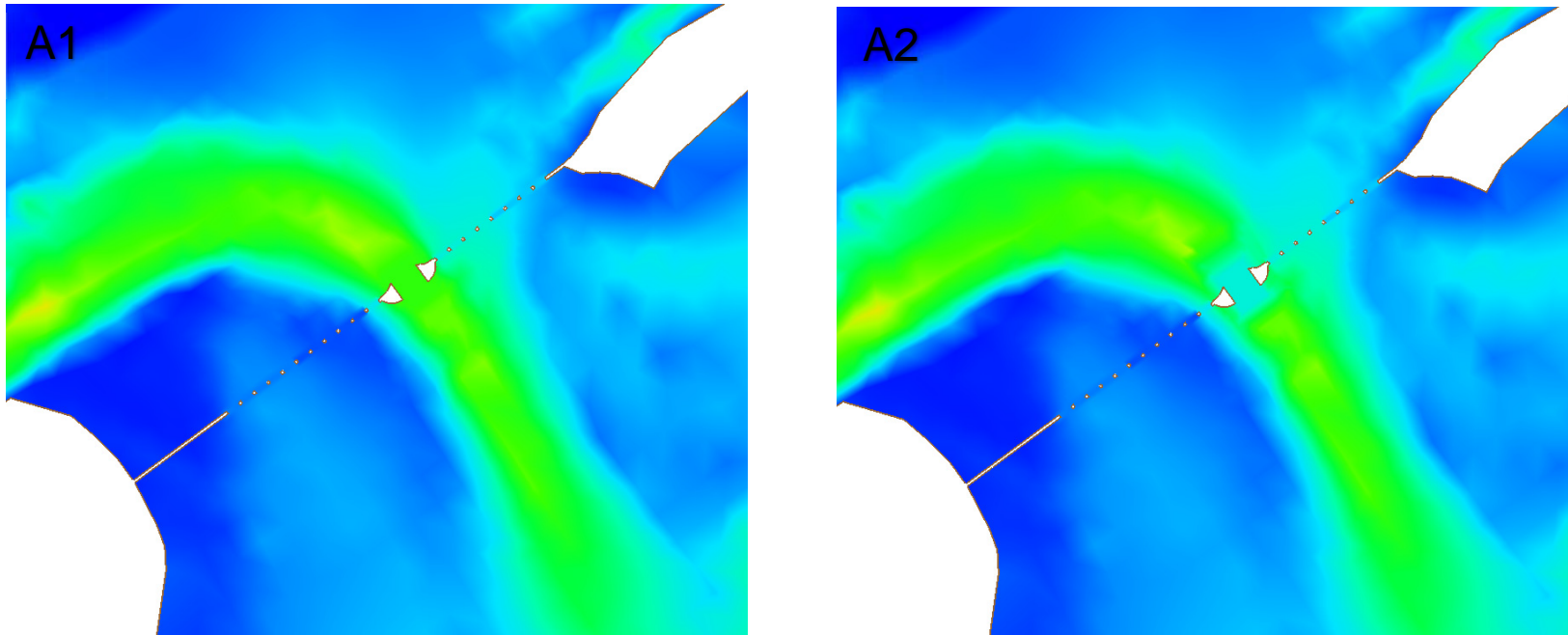
Gate Type	Opening Size	Sill Elevation (NAVD88)
2 horizontal sector gates	460 ft	-25 ft
15 vertical lift gates	150 ft	-11 to -7 ft
18 culverts	24 x 8 ft	-2 ft



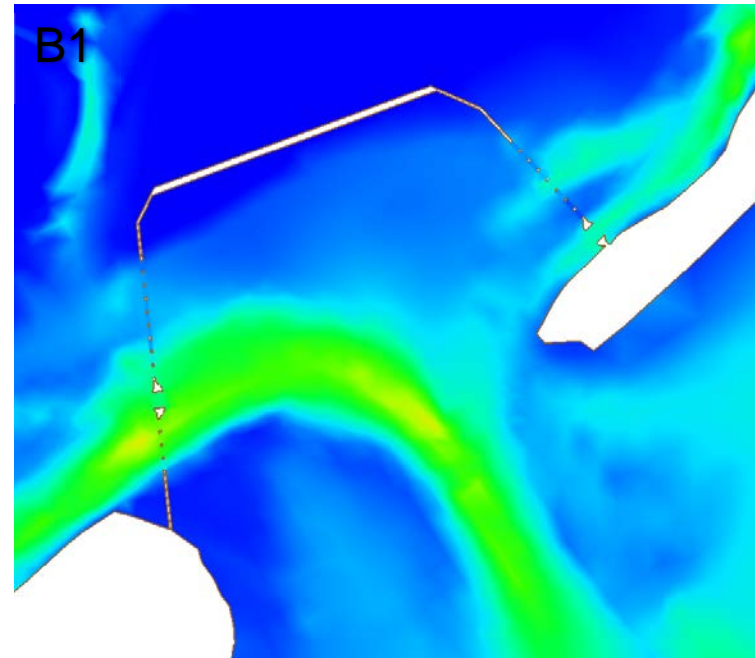
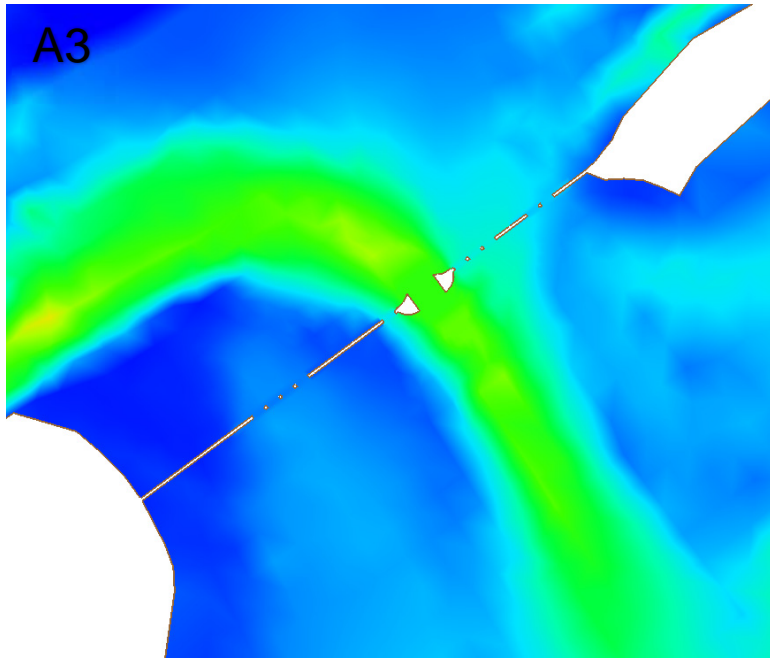
Gate Type	Opening Size	Sill Elevation (NAVD88)
2 horizontal sector gates	320 ft	-13 ft
3 vertical lift gates	150 ft	-20 to -5 ft

Gate Type	Opening Size	Sill Elevation (NAVD88)
2 horizontal sector gates	306 ft	-13 ft
2 vertical lift gates	150 ft	-9 to -5 ft
17 box culverts	24 x 8 ft	-2 ft

Figure 70. Great Egg structures A1 and A2.



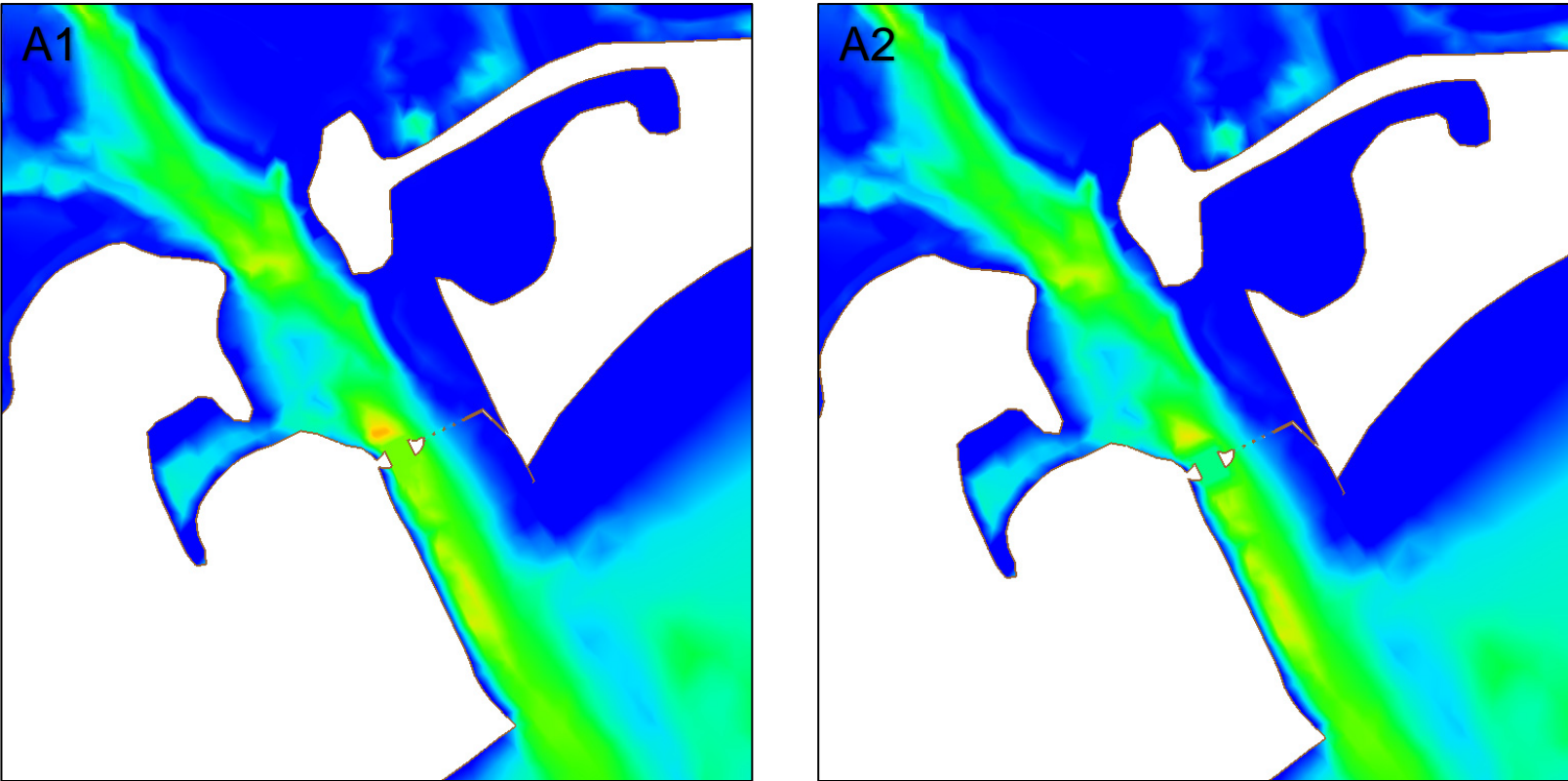
Gate Type	Opening Size	Sill Elevation (NAVD88)
2 horizontal sector gates	320 ft	-35 ft (A1); -18 ft (A2)
19 vertical lift gates	150 ft	-18 to -5 ft



Gate Type	Opening Size	Sill Elevation (NAVD88)
2 horizontal sector gates	320 ft	-35 ft
10 vertical lift gates	150 ft	-18 to -8 ft

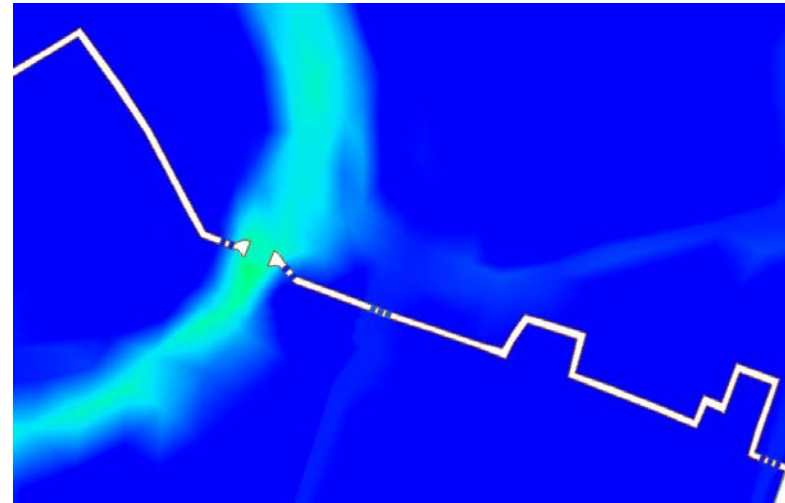
Gate Type	Opening Size	Sill Elevation (NAVD88)
4 horizontal sector gates	220 ft	-26 ft (left); -20 ft (right)
21 vertical lift gates	150 ft	-40 to -5 ft

Figure 71. Absecon structures A1 and A2.



Gate Type	Opening Size	Sill Elevation (NAVD88)
2 horizontal sector gates	420 ft	-40 ft (A1); -24.44 ft (A2)
4 vertical lift gates	150 ft	-22 to -6 ft

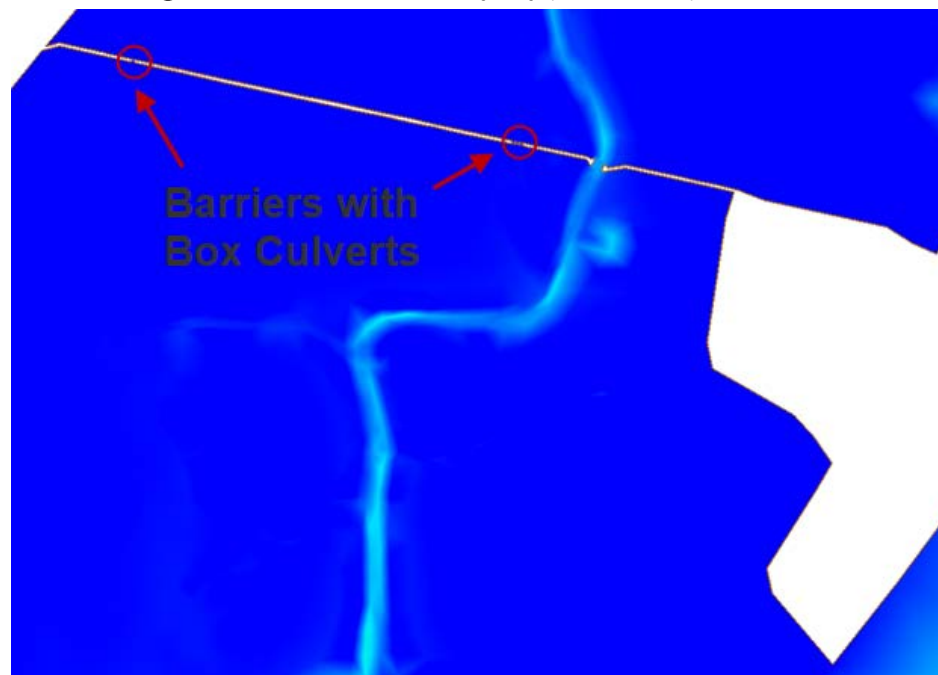
Figure 72. Absecon Bay Boulevard structures.



Gate Type	Opening Size	Sill Elevation (NAVD88)
10 box culverts	24 x 8 ft to 24 x 6 ft	-2 to 0 ft

Gate Type	Opening Size	Sill Elevation (NAVD88)
2 horizontal sector gates	120 ft	-20 ft
10 box culverts	24 x 8 ft to 24 x 12 ft	-6 to -2 ft

Figure 73. Southern Ocean City Bay (72nd Street) structures.

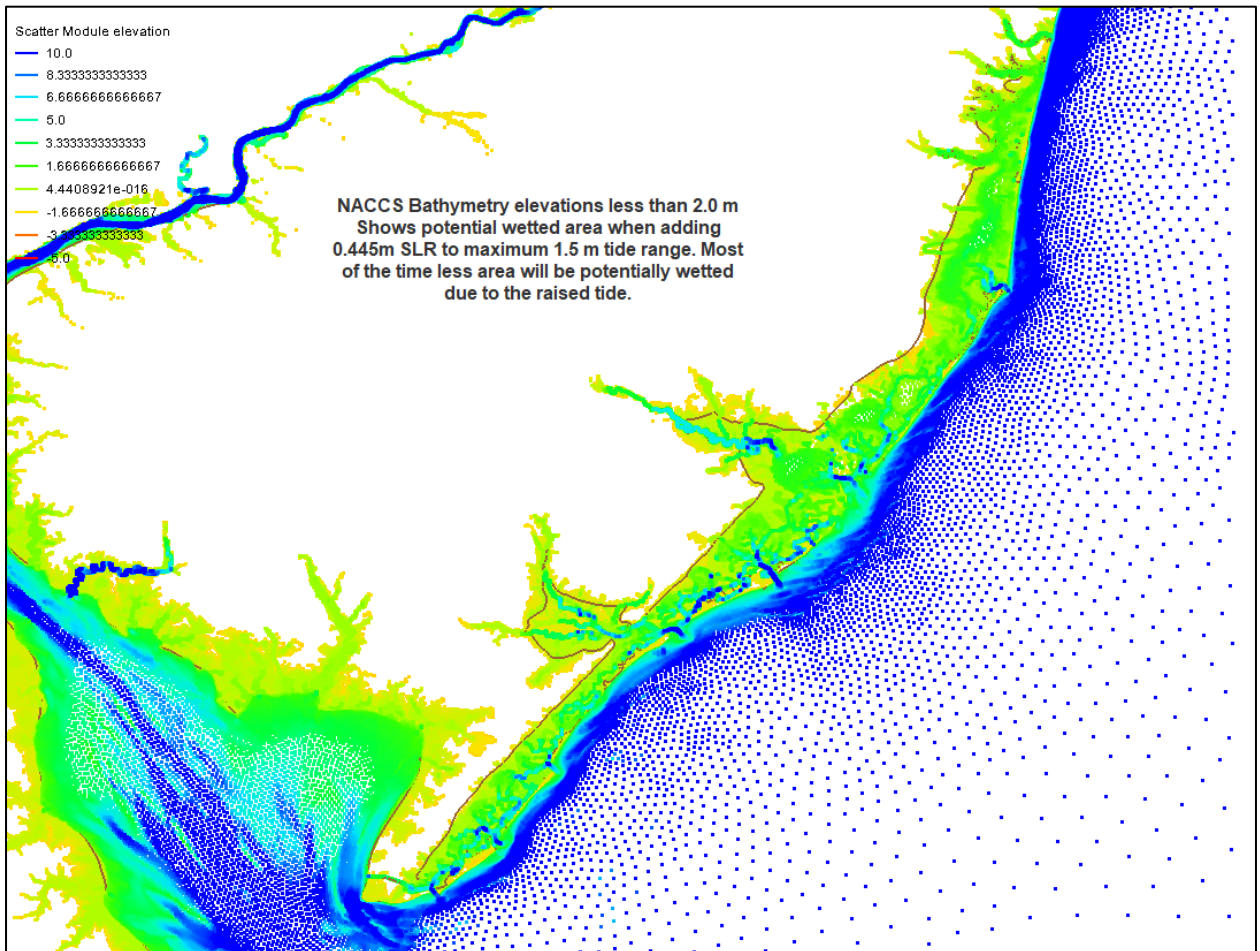


Gate Type	Opening Size	Sill Elevation (NAVD88)
2 horizontal sector gates	120 ft	-10 ft
4 box culverts	24 x 8 ft	-1 to 1 ft

Table 4. With project alternative combinations.

	1	2	3	4	5	6
Manasquan	A1	A1	A1	A1	B1	A1
Barnegat	A1	A2	A3	A4	B1	C1
Absecon					A1	A2
Great Egg	A1	A2	A3	B1	A1	A1
Absecon Bay Blvd	A1	A1	A1	A1		
Ocean City Bay	A1	A1	A1	A1		

Figure 74. NACCS bathymetry showing area that could wet under the 0.445m sea level rise. Points are the NACCS data and the brown line is the AdH model domain.



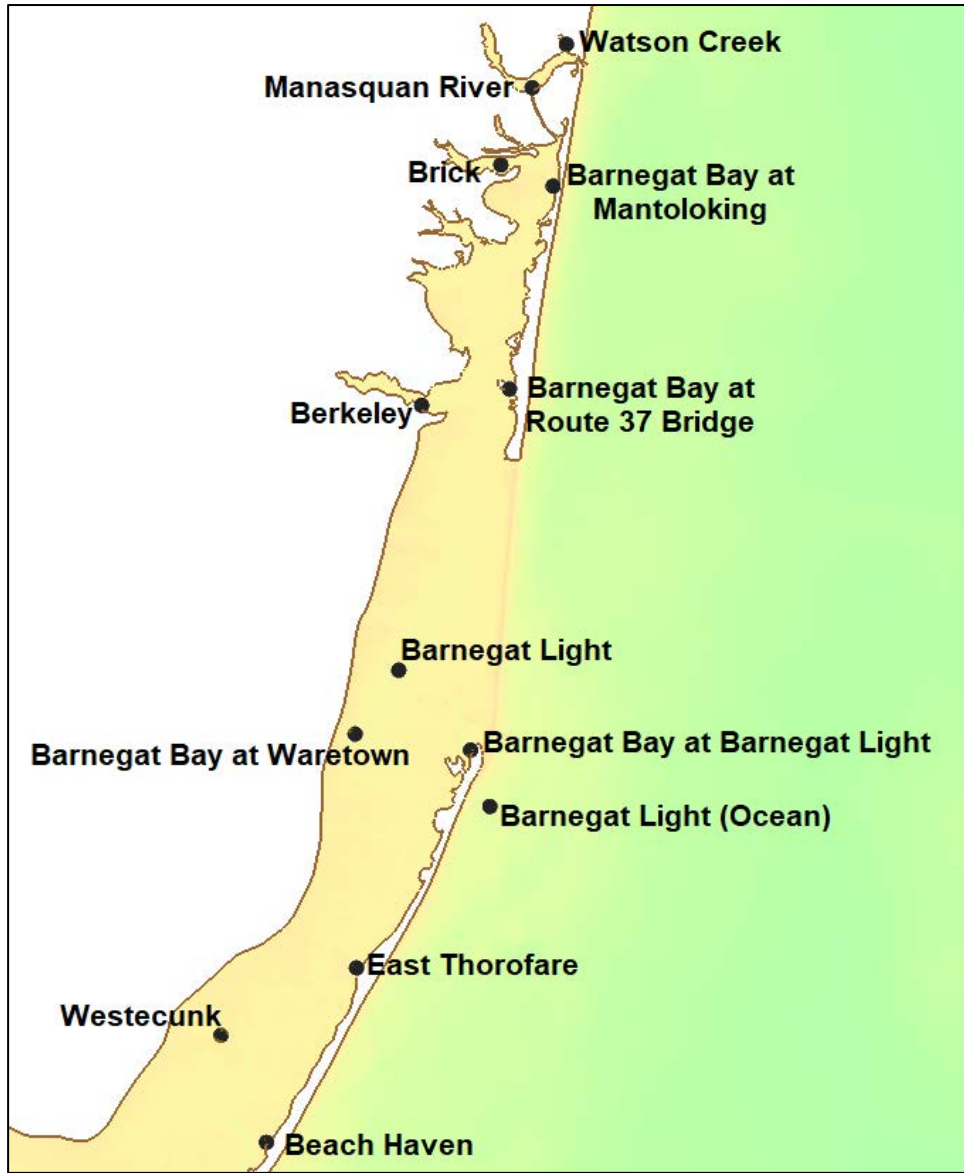
6 Alternative Result Analysis

The 10 alternatives — Base, WP1 through WP6, Base-SLR, WP1SLR, and WP5SLR — were simulated using 2D AdH as stated in the previous chapters. Present is year 2018, and sea level rise is projected for year 2080. The results include changes in salinity, velocity, and water level throughout the model domain under the various alternative conditions. Analysis are computed on the one-year simulation results. Comparison of with and without project should be done on the present conditions and the sea level rise conditions separately to isolate impacts due to the project alone.

Analysis Locations

NAP identified 30 locations for specific analysis such as time history, percent-less-than, and maximum/minimum/average computations of salinity and velocity magnitude. These locations will also be used to analyze tidal amplitude throughout the system. The domain is separated into three regions — north, central, and south. There are 13 locations in the northern region, 13 locations in the central region, and 4 locations in the southern region. These locations are shown in Figure 75 through Figure 77. Analysis plots and images for all locations will be included in the appendices.

Figure 75. Northern Region Analysis Locations



Name	UTM zone 18 meters	
	X	Y
Watson Creek	581410.1	4440588.9
Manasquan River	579521.1	4438187.9
Brick	577789.5	4433927.1
Barnegat Bay at Mantoloking	580677.0	4432757.0
Barnegat Bay at Route 37 Bridge	578266.0	4421554.0
Berkeley	573421.8	4420662.1
Barnegat Light	572158.3	4406042.5

Name	UTM zone 18 meters	
	X	Y
Barnegat Bay at Waretown	569741.0	4402521.0
Barnegat Bay at Barnegat Light	576121.0	4401631.0
Barnegat Light (Ocean)	577186.2	4398519.1
East Thorofare	569820.1	4389612.6
Westecunk	562340.1	4385892.9
Beach Haven	564763.4	4380002.7

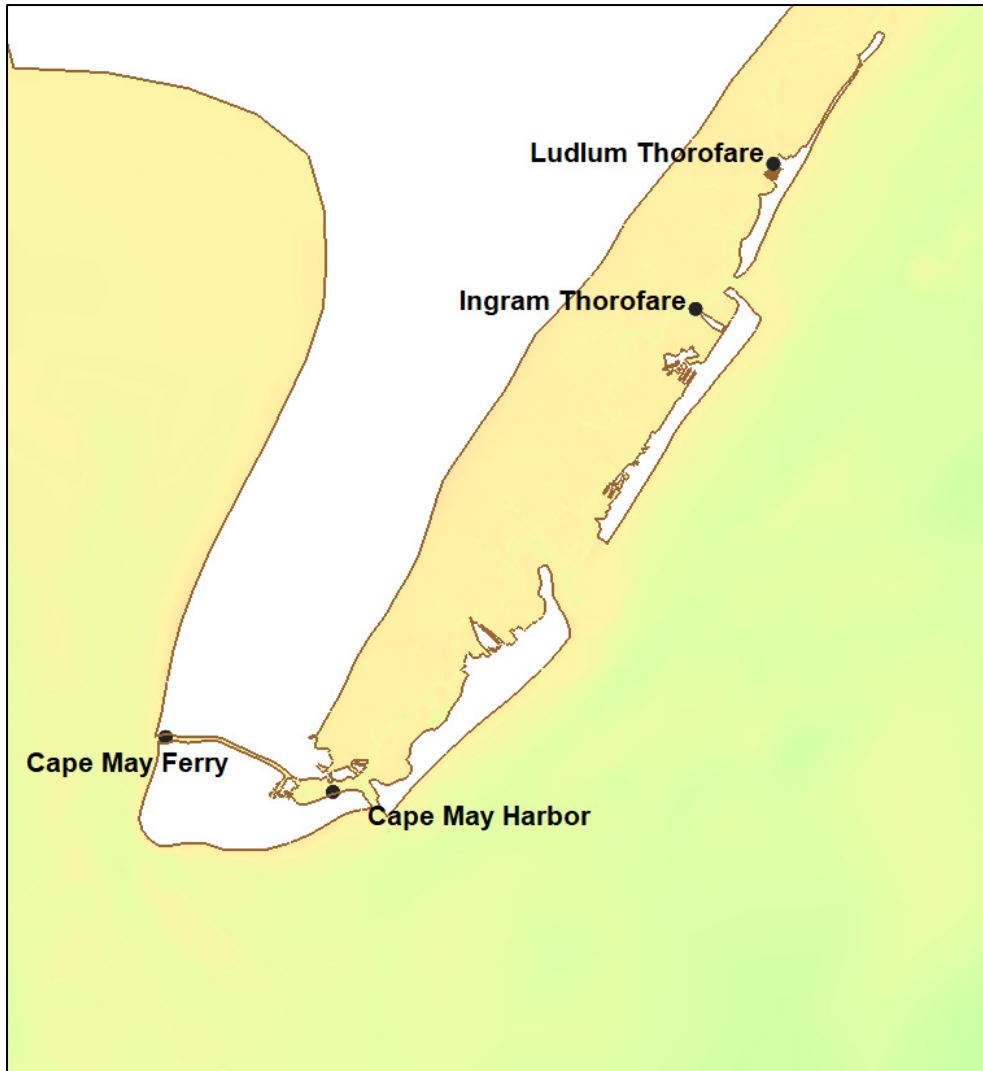
Figure 76. Central Region Analysis Locations



Name	UTM zone 18 meters	
	X	Y
JACNEWQ	546439.5	4377816.6
Little Egg Inlet	558054.0	4373310.0
Absecon Creek	544316.0	4364000.0
Brigantine	554174.9	4363951.5
Absecon Channel	549422.1	4359936.4
Atlantic City (Ocean)	551315.0	4356953.0
Inside Thorofare	546789.7	4356158.9

Name	UTM zone 18 meters	
	X	Y
Beach Thorofare	541921.0	4354360.0
Scull Bay	538625.6	4354325.3
Great Egg Harbor River	528124.5	4353109.2
Great Egg Harbor Bay	536548.0	4348645.0
Ocean City 39th St	532280.7	4344580.2
Corson Sound	529794.9	4340924.7

Figure 77. Southern Region Analysis Locations



Name	UTM zone 18 meters	
	X	Y
Ludlum Thorofare	525984.0	4334401.0
Ingram Thorofare	523102.0	4329037.0

Name	UTM zone 18 meters	
	X	Y
Cape May Ferry	503468.9	4313179.9
Cape May Harbor	509668.9	4311150.0

Model Results

The AdH model results are analyzed numerous ways to determine how various parameters are impacted by the geometric changes introduced in the alternative conditions. The analysis and results provided are:

- Mean tables and contour plots

- Percent change from base tables
- Maximum, minimum, and mean plots
- Percent less than plots
- Time history plots
- Residual velocity plots

These analyses are computed on the one-year simulation results. The results will be presented by location from north to south and grouped regionally where applicable. In some instances only the northern and central regions will be provided.

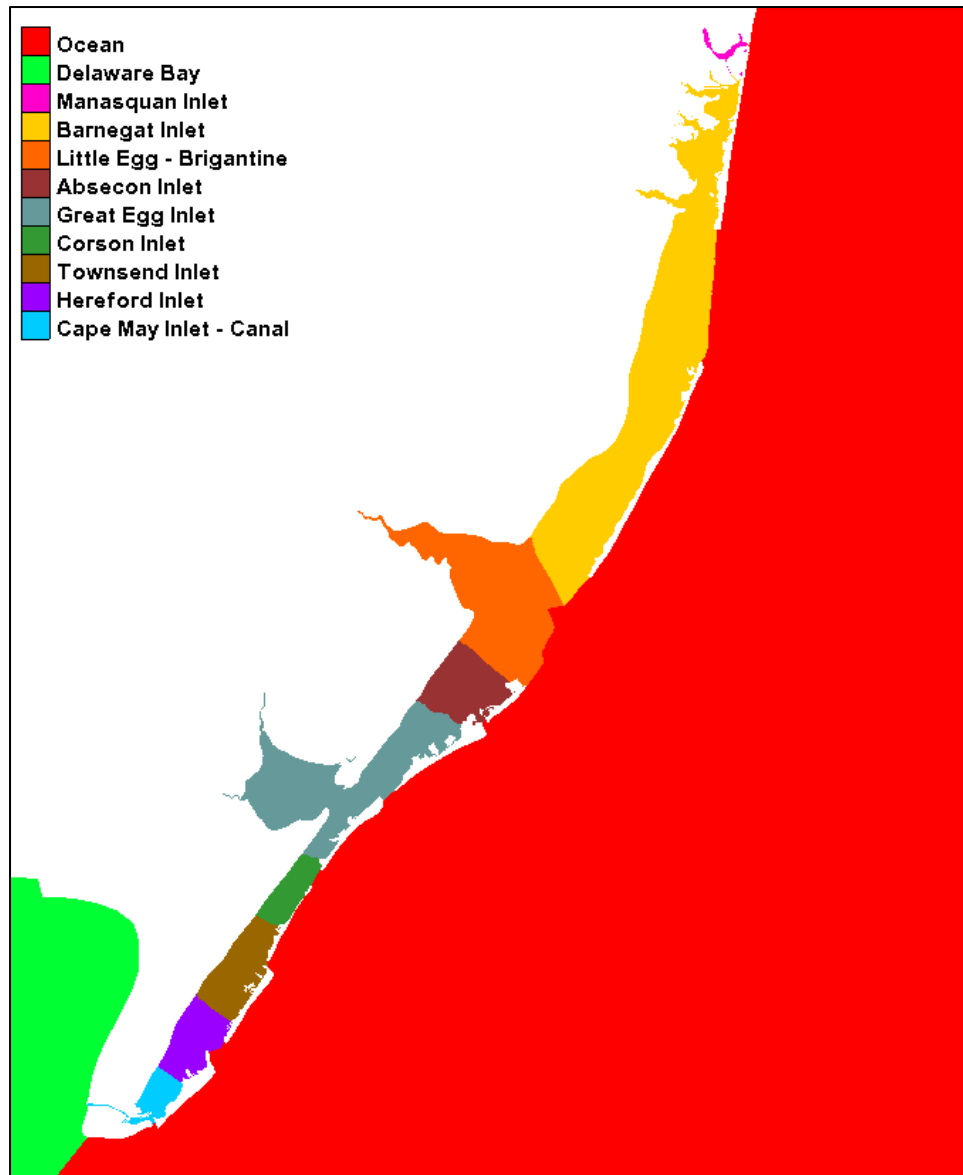
Percentile Analysis

Percent less than computations are made to show how the velocity magnitude, salinity, and tidal amplitude vary over the year-long analysis period. The maximum value for a parameter is given at 100% and the minimum value at 0%. The 50% value indicates that the parameter value is less than this value for 50% of the analysis time and greater than this value 50% of the time. These results are shown for the Base and all alternatives (with and without sea level rise) at each of the analysis locations in the appropriate appendix – Appendix D for tidal amplitude and tidal prism, Appendix E for salinity, and Appendix F for velocity.

Tidal Prism

Changes to the system geometry can impact the tidal exchange into a bay environment such as the New Jersey Back Bays. The alternatives greatly impact the cross sectional area of the entrances into the bays which will allow for changes in the volume of flow being exchanged through the inlets. The tidal prism is a calculation of the volume of water that enters and leaves through the inlets with each tide. This volume was computed for all tides over the analysis year and the average tidal prism was computed for various regions of the model domain. Nine regions are defined for the bay portion of the model domain as shown in Figure 78.

Figure 78. Tidal prism analysis regions.



Tidal prism is computed on the nine regions defined previously. Only the bay portions of the domain are included in the analysis results. Table 5 shows the Base mean tidal prism and the percent change from the Base for each alternative in the nine regions. Table 6 shows the comparison for the sea level rise alternatives. Negative values of change indicate that the alternative mean tidal prism is less than the base tidal prism. Percentile plots showing how the tidal prism varies over the one-year analysis period are provided in the appropriate appendices.

The change in the tidal prism is largest at locations and for alternatives where the greatest inlet restriction occurs. WP5 shows the largest change

at Manasquan but the smallest change at the southern regions. The largest changes overall occur at Great Egg for WP3 and Absecon for WP6. Given the structure design at these locations for each alternative, the large differences make sense. For the alternatives with sea level rise, the same reasoning can be applied. The largest impact is seen at Barnegat for WP5 and at Great Egg for WP1.

Table 5. Mean tidal prism comparison to base.

Location	Base Mean Prism (m ³)	% Change in Mean Tidal Prism from Base					
		WP1	WP2	WP3	WP4	WP5	WP6
Manasquan Inlet	2,392,363	0.13	-0.62	0.33	0.09	2.19	0.56
Barnegat Inlet	79,322,854	-2.43	-3.80	-4.89	-2.16	-6.53	-1.73
Little Egg - Brigantine	59,313,965	-0.44	-0.61	-0.60	-0.63	-0.71	-1.98
Absecon Inlet	27,489,518	-0.97	-1.12	-1.15	-1.08	-3.75	-8.70
Great Egg Inlet	51,041,642	-4.76	-6.75	-9.25	-3.20	-4.46	-5.11
Corson Inlet	8,307,946	-1.62	-1.95	-2.06	-1.42	-0.45	-0.82
Townsend Inlet	16,539,248	-1.02	-1.10	-2.37	-2.30	-0.03	-1.49
Hereford Inlet	13,290,585	-0.79	-0.95	-1.69	-1.65	-0.01	-1.11
Cape May Inlet - Canal	10,479,052	-0.33	-0.59	-0.73	-0.74	0.01	-0.63

Table 6. Mean tidal prism comparison to base sea level rise.

Location	Base Mean Prism (m ³)	% Change in Mean Tidal Prism from Base	
		WP1 SLR	WP5 SLR
Manasquan Inlet	3,275,140	1.37	3.29
Barnegat Inlet	105,599,678	-2.29	-8.19
Little Egg - Brigantine	84,856,949	-0.52	-1.26
Absecon Inlet	40,897,898	-0.49	-4.69
Great Egg Inlet	73,904,353	-6.07	-5.46
Corson Inlet	13,052,848	-1.98	-0.86
Townsend Inlet	27,276,078	-0.66	-0.12
Hereford Inlet	21,990,320	-0.71	-0.04
Cape May Inlet - Canal	15,765,271	-0.36	0.00

Tidal Amplitude

The tidal amplitude is the change in the water level from low tide to high tide and vice versa. The tidal prism gives an overall impact on the water exchange whereas the tidal amplitude may vary at locations depending on where the system modifications are made and changes in the flow patterns within the system. The mean tidal amplitude for each of the analysis locations is provided in the Table 7 and the comparison to the base condition in Table 8. The same results are provided for the sea level rise conditions in Table 9 and Table 10. Time history plots of tidal amplitude as well as plots of the mean tidal amplitude comparisons are provided in the appendices.

Table 7. Mean tidal amplitude.

	Mean Tidal Amplitude (m)						
	Base	WP1	WP2	WP3	WP4	WP5	WP6
Watson Creek	0.941	0.955	0.943	0.957	0.955	0.966	0.947
Manasquan River	0.604	0.593	0.591	0.596	0.593	0.618	0.607
Brick	0.103	0.098	0.095	0.092	0.098	0.084	0.096
Barnegat Bay at Mantoloking	0.162	0.154	0.149	0.145	0.155	0.133	0.153
Barnegat Bay at Route 37 Bridge	0.170	0.160	0.154	0.150	0.161	0.141	0.160
Berkeley	0.164	0.154	0.150	0.146	0.155	0.136	0.155
Barnegat Light	0.168	0.157	0.151	0.146	0.159	0.135	0.158
Barnegat Bay at Waretown	0.172	0.162	0.156	0.150	0.163	0.140	0.163
Barnegat Bay at Barnegat Light	0.404	0.153	0.337	0.332	0.381	0.280	0.401
Barnegat Light (Ocean)	0.708	0.692	0.687	0.681	0.693	0.664	0.687
East Thorofare	0.472	0.463	0.457	0.452	0.464	0.433	0.457
Westecunk	0.336	0.332	0.330	0.328	0.331	0.316	0.329
Beach Haven	0.505	0.492	0.490	0.487	0.493	0.478	0.493
JACNEWQ	0.428	0.414	0.410	0.408	0.412	0.402	0.414
Little Egg Inlet	0.570	0.558	0.553	0.551	0.558	0.535	0.554
Absecon Creek	0.586	0.567	0.565	0.562	0.571	0.535	0.545
Brigantine	0.530	0.514	0.512	0.506	0.513	0.491	0.494
Absecon Channel	0.681	0.677	0.674	0.676	0.677	0.650	0.611
Atlantic City (Ocean)	0.739	0.738	0.740	0.739	0.740	0.739	0.739
Inside Thorofare	0.686	0.670	0.663	0.658	0.677	0.669	0.663
Beach Thorofare	0.710	0.682	0.673	0.663	0.692	0.680	0.681

Scull Bay	0.560	0.543	0.537	0.526	0.550	0.542	0.540
Great Egg Harbor River	0.600	0.586	0.581	0.581	0.596	0.585	0.588
Great Egg Harbor Bay	0.713	0.689	0.668	0.656	0.697	0.689	0.690
Ocean City 39th St	0.622	0.608	0.599	0.592	0.608	0.608	0.610
Corson Sound	0.566	0.554	0.549	0.543	0.551	0.559	0.557
Ludlum Thorofare	0.573	0.563	0.557	0.555	0.558	0.567	0.565
Ingram Thorofare	0.641	0.635	0.634	0.627	0.627	0.637	0.635
Cape May Ferry	1.022	1.018	1.017	1.011	1.012	1.018	1.018
Cape May Harbor	0.909	0.906	0.903	0.898	0.899	0.905	0.903

Table 8. Mean tidal amplitude comparison to base.

Location	Mean Base Amplitude (m)	% Change in Mean Tidal Amplitude from Base					
		WP1	WP2	WP3	WP4	WP5	WP6
Watson Creek	0.941	1.51	0.13	1.65	1.51	2.65	0.61
Manasquan River	0.604	-1.82	-2.28	-1.38	-1.85	2.22	0.44
Brick	0.103	-5.31	-7.95	-10.89	-4.82	-18.11	-6.63
Barnegat Bay at Mantoloking	0.162	-4.99	-7.99	-10.82	-4.50	-18.37	-6.07
Barnegat Bay at Route 37 Bridge	0.170	-5.85	-9.01	-11.63	-5.22	-17.02	-5.60
Berkeley	0.164	-5.85	-8.59	-11.09	-5.31	-16.75	-5.37
Barnegat Light	0.168	-6.31	-9.91	-13.01	-5.50	-19.37	-5.80
Barnegat Bay at Waretown	0.172	-6.14	-9.66	-12.82	-5.39	-18.89	-5.74
Barnegat Bay at Barnegat Light	0.404	-8.34	-16.58	-17.72	-5.59	-30.57	-0.67
Barnegat Light (Ocean)	0.708	-2.27	-3.03	-3.78	-2.15	-6.29	-2.95
East Thorofare	0.472	-1.89	-3.13	-4.21	-1.85	-8.33	-3.32
Westecunk	0.336	-1.34	-1.97	-2.57	-1.66	-5.89	-2.21
Beach Haven	0.505	-2.60	-2.98	-3.74	-2.50	-5.42	-2.51
JACNEWQ	0.428	-3.20	-4.11	-4.61	-3.59	-5.99	-3.28
Little Egg Inlet	0.570	-2.05	-2.92	-3.29	-2.00	-6.08	-2.80
Absecon Creek	0.586	-3.09	-3.48	-4.02	-2.54	-8.62	-6.97
Brigantine	0.530	-3.03	-3.40	-4.48	-3.16	-7.31	-6.71
Absecon Channel	0.681	-0.69	-1.04	-0.80	-0.69	-4.67	-10.36

Atlantic City (Ocean)	0.739	-0.11	0.09	-0.01	0.13	0.02	-0.07
Inside Thorofare	0.686	-2.25	-3.26	-4.02	-1.31	-2.45	-3.31
Beach Thorofare	0.710	-4.02	-5.30	-6.71	-2.51	-4.25	-4.17
Scull Bay	0.560	-3.13	-4.26	-6.18	-1.95	-3.23	-3.70
Great Egg Harbor River	0.600	-2.30	-3.16	-3.13	-0.64	-2.39	-1.92
Great Egg Harbor Bay	0.713	-3.39	-6.40	-8.04	-2.25	-3.41	-3.30
Ocean City 39th St	0.622	-2.22	-3.73	-4.81	-2.22	-2.23	-2.04
Corson Sound	0.566	-2.07	-3.02	-4.06	-2.58	-1.16	-1.53
Ludlum Thorofare	0.573	-1.89	-2.83	-3.20	-2.76	-1.05	-1.48
Ingram Thorofare	0.641	-0.92	-1.06	-2.09	-2.04	-0.56	-0.88
Cape May Ferry	1.022	-0.41	-0.55	-1.10	-0.96	-0.37	-0.46
Cape May Harbor	0.909	-0.36	-0.62	-1.24	-1.07	-0.40	-0.62

Table 9. Mean tidal amplitude for sea level rise alternatives.

	Mean Tidal Amplitude (m)		
	Base SLR	WP1 SLR	WP5 SLR
Watson Creek	0.88	0.87	0.82
Manasquan River	0.74	0.67	0.58
Brick	0.22	0.21	0.19
Barnegat Bay at Mantoloking	0.23	0.22	0.20
Barnegat Bay at Route 37 Bridge	0.25	0.23	0.23
Berkeley	0.24	0.23	0.23
Barnegat Light	0.20	0.19	0.20
Barnegat Bay at Waretown	0.20	0.19	0.17
Barnegat Bay at Barnegat Light	0.46	0.40	0.29
Barnegat Light (Ocean)	1.02	1.02	1.02
East Thorofare	0.38	0.37	0.33
Westecunk	0.32	0.31	0.29
Beach Haven	0.53	0.48	0.43
JACNEWQ	0.39	0.38	0.35
Little Egg Inlet	0.75	0.68	0.57
Absecon Creek	0.63	0.62	0.52
Brigantine	0.65	0.61	0.61
Absecon Channel	0.91	0.82	0.62

Atlantic City (Ocean)	1.04	1.04	1.04
Inside Thorofare	0.70	0.66	0.57
Beach Thorofare	0.75	0.70	0.60
Scull Bay	0.75	0.60	0.52
Great Egg Harbor River	0.50	0.47	0.42
Great Egg Harbor Bay	0.95	0.78	0.65
Ocean City 39th St	0.72	0.57	0.53
Corson Sound	0.49	0.48	0.45
Ludlum Thorofare	0.47	0.47	0.42
Ingram Thorofare	0.74	0.68	0.57
Cape May Ferry	1.28	1.28	1.28
Cape May Harbor	1.10	1.10	0.94

Table 10. Mean tidal amplitude comparison to base for sea level rise alternatives.

Location	Mean Base Amplitude (m)	% Change in Mean Tidal Amplitude from Base	
		WP1 SLR	WP5 SLR
Watson Creek	0.881	-1.32	-6.73
Manasquan River	0.736	-8.87	-21.56
Brick	0.218	-5.60	-14.81
Barnegat Bay at Mantoloking	0.235	-5.23	-15.55
Barnegat Bay at Route 37 Bridge	0.249	-5.95	-7.48
Berkeley	0.243	-6.38	-4.50
Barnegat Light	0.198	-3.55	3.42
Barnegat Bay at Waretown	0.203	-5.34	-13.98
Barnegat Bay at Barnegat Light	0.463	-13.42	-38.04
Barnegat Light (Ocean)	1.018	0.16	0.05
East Thorofare	0.382	-3.07	-13.81
Westecunk	0.319	-1.87	-8.80
Beach Haven	0.531	-9.43	-18.59
JACNEWQ	0.389	-3.31	-10.73
Little Egg Inlet	0.748	-9.43	-23.98
Absecon Creek	0.633	-1.51	-18.00
Brigantine	0.645	-4.76	-5.56
Absecon Channel	0.905	-9.48	-31.42
Atlantic City (Ocean)	1.037	0.04	0.10

Inside Thorofare	0.701	-6.42	-19.36
Beach Thorofare	0.749	-6.90	-19.61
Scull Bay	0.746	-19.79	-29.73
Great Egg Harbor River	0.498	-6.66	-15.76
Great Egg Harbor Bay	0.947	-17.63	-31.86
Ocean City 39th St	0.721	-20.66	-26.20
Corson Sound	0.494	-2.38	-8.76
Ludlum Thorofare	0.473	-0.74	-10.74
Ingram Thorofare	0.744	-8.90	-23.01
Cape May Ferry	1.283	0.05	0.07
Cape May Harbor	1.096	0.00	-14.22

Salinity

The maximum, minimum, and mean salinity is computed for the year-long analysis period at each point in the model domain. Table 11 and Table 12 give the mean salinity for all of the analysis locations for without and with sea level rise, respectively. Appendix E includes the spatial contour plots of the mean salinity are provided for the Base and each alternative for the northern region (two sections) – Manasquan and Barnegat – and the central region (one section) – Great Egg and Absecon. Also included in Appendix E are the time history of salinity at each of the 30 analysis locations and the percentile analysis results.

Table 11. Mean salinity.

	Mean Salinity (ppt)						
	Base	WP1	WP2	WP3	WP4	WP5	WP6
Watson Creek	23.44	23.50	23.71	23.51	23.51	23.74	23.90
Manasquan River	24.03	24.14	24.36	24.18	24.15	24.45	24.52
Brick	5.14	5.20	5.14	5.00	5.22	4.68	5.12
Barnegat Bay at Mantoloking	20.87	21.00	21.16	21.05	21.02	21.54	21.37
Barnegat Bay at Route 37 Bridge	12.48	12.38	12.44	12.46	12.43	13.71	12.95
Berkeley	1.91	1.92	1.87	1.86	1.94	1.86	1.93
Barnegat Light	25.10	24.86	24.79	24.48	24.90	24.26	24.89
Barnegat Bay at Waretown	25.29	25.06	25.02	24.79	25.10	24.56	25.10
Barnegat Bay at Barnegat Light	27.10	21.37	27.02	27.20	27.48	26.57	26.87

Barnegat Light (Ocean)	28.38	28.42	28.42	28.37	28.42	28.25	28.37
East Thorofare	25.77	25.92	25.88	25.96	25.95	26.20	25.95
Westecunk	21.78	21.96	21.94	21.98	21.98	21.90	21.87
Beach Haven	27.28	27.37	27.36	27.39	27.39	27.43	27.37
JACNEWQ	4.80	5.14	5.14	5.16	5.15	4.75	4.75
Little Egg Inlet	26.89	27.04	27.08	27.06	27.05	26.94	26.97
Absecon Creek	27.52	27.60	27.61	27.63	27.60	27.37	27.08
Brigantine	27.67	27.71	27.73	27.74	27.72	27.42	27.01
Absecon Channel	28.44	28.50	28.52	28.54	28.50	28.38	28.26
Atlantic City (Ocean)	28.65	28.70	28.74	28.73	28.71	28.61	28.54
Inside Thorofare	27.60	27.25	27.15	27.22	27.56	27.44	27.61
Beach Thorofare	28.25	28.18	28.13	28.05	28.37	28.16	28.20
Scull Bay	27.77	27.75	27.71	27.67	27.89	27.68	27.71
Great Egg Harbor River	18.99	18.73	18.38	18.08	18.75	18.28	18.14
Great Egg Harbor Bay	27.34	27.21	27.08	27.30	27.33	27.06	27.06
Ocean City 39th St	25.75	25.45	25.22	25.28	25.57	25.27	25.25
Corson Sound	28.05	28.17	28.24	28.31	28.14	28.09	28.13
Ludlum Thorofare	27.74	27.80	27.84	27.83	27.78	27.75	27.78
Ingram Thorofare	28.34	28.38	28.42	28.35	28.34	28.34	28.34
Cape May Ferry	27.33	27.35	27.41	27.36	27.33	27.33	27.41
Cape May Harbor	28.64	28.67	28.68	28.67	28.66	28.64	28.65

Table 12. Mean salinity for sea level rise alternatives.

	Mean Salinity (ppt)		
	Base SLR	WP1 SLR	WP5 SLR
Watson Creek	24.87	24.74	24.97
Manasquan River	25.46	25.29	25.66
Brick	7.96	8.31	7.04
Barnegat Bay at Mantoloking	21.79	21.26	22.26
Barnegat Bay at Route 37 Bridge	13.65	12.55	13.68
Berkeley	2.64	2.62	2.29
Barnegat Light	26.74	26.67	25.95
Barnegat Bay at Waretown	26.20	26.27	25.33
Barnegat Bay at Barnegat Light	27.69	27.95	27.40

Barnegat Light (Ocean)	28.73	28.71	28.57
East Thorofare	26.61	26.52	26.92
Westecunk	24.34	24.41	24.43
Beach Haven	27.90	27.83	27.97
JACNEWQ	10.01	9.90	9.89
Little Egg Inlet	27.31	27.29	27.32
Absecon Creek	27.77	27.81	27.57
Brigantine	27.93	27.92	27.80
Absecon Channel	28.51	28.52	28.44
Atlantic City (Ocean)	28.61	28.62	28.55
Inside Thorofare	27.89	27.57	27.74
Beach Thorofare	28.46	28.33	28.38
Scull Bay	27.81	27.68	27.71
Great Egg Harbor River	21.79	20.97	21.16
Great Egg Harbor Bay	27.43	27.06	27.08
Ocean City 39th St	25.79	25.18	25.26
Corson Sound	27.97	28.12	28.07
Ludlum Thorofare	27.95	27.97	27.99
Ingram Thorofare	28.57	28.58	28.57
Cape May Ferry	27.33	27.28	27.34
Cape May Harbor	28.64	28.66	28.64

Velocity Magnitude

The maximum, minimum, and mean velocity magnitude is computed for the year-long analysis period at each point in the model domain. The direction of the flow is removed for these computations such that only the magnitude of the flow is considered. Table 13 and Table 14 give the mean velocity for all of the analysis locations for without and with sea level rise, respectively. Appendix F includes the spatial contour plots of the mean velocity magnitude for the Base and each alternative for the northern region (two sections) – Manasquan and Barnegat – and the central region (one section) – Great Egg and Absecon. Time history of velocity at each of the 30 analysis locations as well as percentile analysis results are also provided in Appendix F.

Table 13. Mean velocity magnitude.

	Mean Velocity Magnitude (m/s)						
	Base	WP1	WP2	WP3	WP4	WP5	WP6
Watson Creek	0.028	0.029	0.029	0.029	0.029	0.029	0.028
Manasquan River	0.262	0.259	0.257	0.258	0.259	0.264	0.264
Brick	0.013	0.013	0.013	0.012	0.013	0.012	0.013
Barnegat Bay at Mantoloking	0.101	0.104	0.102	0.101	0.104	0.097	0.100
Barnegat Bay at Route 37 Bridge	0.080	0.075	0.073	0.070	0.076	0.066	0.076
Berkeley	0.034	0.034	0.033	0.032	0.034	0.031	0.033
Barnegat Light	0.095	0.091	0.089	0.087	0.092	0.084	0.093
Barnegat Bay at Waretown	0.034	0.033	0.033	0.032	0.033	0.031	0.033
Barnegat Bay at Barnegat Light	0.132	0.100	0.067	0.090	0.170	0.101	0.134
Barnegat Light (Ocean)	0.052	0.052	0.052	0.052	0.052	0.052	0.052
East Thorofare	0.072	0.071	0.072	0.073	0.071	0.077	0.073
Westecunk	0.070	0.069	0.069	0.069	0.069	0.070	0.069
Beach Haven	0.159	0.154	0.154	0.154	0.154	0.158	0.158
JACNEWQ	0.258	0.253	0.252	0.253	0.253	0.258	0.257
Little Egg Inlet	0.339	0.336	0.335	0.336	0.335	0.339	0.337
Absecon Creek	0.011	0.011	0.011	0.011	0.011	0.011	0.010
Brigantine	0.065	0.064	0.064	0.064	0.064	0.066	0.067
Absecon Channel	0.412	0.409	0.408	0.408	0.408	0.397	0.371
Atlantic City (Ocean)	0.131	0.129	0.127	0.129	0.129	0.126	0.119
Inside Thorofare	0.027	0.027	0.028	0.030	0.027	0.026	0.027
Beach Thorofare	0.301	0.281	0.273	0.262	0.289	0.282	0.283

Scull Bay	0.071	0.068	0.067	0.064	0.069	0.068	0.067
Great Egg Harbor River	0.149	0.140	0.138	0.130	0.138	0.144	0.139
Great Egg Harbor Bay	0.276	0.261	0.255	0.247	0.268	0.262	0.261
Ocean City 39th St	0.012	0.011	0.011	0.011	0.012	0.011	0.012
Corson Sound	0.089	0.086	0.086	0.087	0.087	0.089	0.089
Ludlum Thorofare	0.453	0.441	0.441	0.446	0.447	0.453	0.457
Ingram Thorofare	0.459	0.454	0.454	0.431	0.431	0.459	0.437
Cape May Ferry	0.012	0.012	0.013	0.012	0.012	0.012	0.012
Cape May Harbor	0.027	0.027	0.027	0.027	0.027	0.027	0.027

Table 14. Mean velocity magnitude for sea level rise alternatives.

	Mean Velocity Magnitude (m/s)		
	Base SLR	WP1 SLR	WP5 SLR
Watson Creek	0.02	0.02	0.02
Manasquan River	0.29	0.29	0.29
Brick	0.02	0.02	0.01
Barnegat Bay at Mantoloking	0.11	0.11	0.11
Barnegat Bay at Route 37 Bridge	0.12	0.11	0.10
Berkeley	0.03	0.03	0.03
Barnegat Light	0.10	0.10	0.09
Barnegat Bay at Waretown	0.04	0.04	0.04
Barnegat Bay at Barnegat Light	0.10	0.07	0.10
Barnegat Light (Ocean)	0.05	0.05	0.05
East Thorofare	0.13	0.13	0.14
Westecunk	0.07	0.07	0.07
Beach Haven	0.18	0.17	0.18
JACNEWQ	0.38	0.37	0.38
Little Egg Inlet	0.47	0.46	0.47
Absecon Creek	0.01	0.01	0.01
Brigantine	0.07	0.07	0.08
Absecon Channel	0.58	0.58	0.55
Atlantic City (Ocean)	0.19	0.19	0.19
Inside Thorofare	0.04	0.04	0.03
Beach Thorofare	0.44	0.40	0.41

Scull Bay	0.09	0.08	0.08
Great Egg Harbor River	0.20	0.19	0.19
Great Egg Harbor Bay	0.37	0.34	0.34
Ocean City 39th St	0.02	0.02	0.02
Corson Sound	0.17	0.16	0.17
Ludlum Thorofare	0.44	0.41	0.44
Ingram Thorofare	0.60	0.60	0.60
Cape May Ferry	0.01	0.01	0.01
Cape May Harbor	0.03	0.03	0.03

Residual Velocity

Residual velocity is the velocity that remains when the tidally varying velocity has been averaged out. The direction of the velocity at each point is important in this computation. This vector defines the predominant flow direction and speed of a particle of water. Although the tide will cause the particle to move back and forth, there is generally a flow direction that is a little stronger than the other, allowing for a particle to migrate along a certain path. These results are contoured to show the difference between the Base and alternative condition speed with vectors displayed to show the change in residual flow direction. These plots for all alternatives (with and without sea level rise) are provided in Appendix F.

7 Discussion of Alternatives

A total of ten alternatives were simulated with the validated 2D AdH model – Base, 6 with project structure combinations (WP1 – WP6), Base with sea level rise (Base SLR), and 2 with project structure combinations with sea level rise (WP1 SLR and WP5 SLR). Some of the structure alternatives differ only by a sill elevation; others differ drastically in the number of gate openings and width. Chapter 5 details the alternatives.

Tidal Prism

The change in the tidal prism is largest at locations and for alternatives where the greatest inlet restriction occurs. The tidal prism change is largest for the Great Egg Inlet region and the Barnegat Inlet region. At Great Egg there is a 9.25% reduction from the Base for WP3 and a 6.75% reduction for WP2. All of the project alternatives generate a reduction in the tidal prism for the Great Egg region by more than 3% but less than 10%. At the Barnegat Inlet region, the reduction from the Base condition is between 1.73% and 8.19%. The other region with a large reduction in tidal prism is the Absecon region but only for WP5, WP5 SLR, and WP6. The other alternatives are bay obstructions and those do not reduce the tidal prism in the Absecon region by more than 1.15%. The Manasquan region shows an increase – by as much as 3.29% - in the tidal prism for all alternatives except WP2. Changes in the tidal prism are generally small – less than 4% - for most regions and alternatives other than for Barnegat and Great Egg.

Water Surface Elevation and Tidal Amplitude

The changes to the water surface elevation and tidal amplitude are very small among the alternatives. The sea level rise alternatives show a larger variation in mean tidal amplitude than those without sea level rise. The absolute change in elevation or amplitude may be relatively small whereas the percentage change may be large depending on the magnitude of the value; a 10% change at Absecon Channel is equal to 0.07m. The largest percent change in tidal amplitude is a 38% reduction at Barnegat Light for WP5 SLR. This same location for WP5 shows a 30% reduction in mean tidal amplitude. This is the largest percentage change by far. All others are less than 22% with most less than 10%.

Salinity

Overall, the with project alternatives do not impact the salinity in the back bay region. The mean salinity does not vary by more than 2 ppt for any given location and alternative. There is a slightly larger range in the salinity variation among the sea level rise alternatives but this is still generally less than 2 ppt. The variation at specific times may be larger but overall the impact is small. Given the well mixed nature of the inlets, ocean salinity is pushed into the

back bay areas and allowed to move easily throughout the area. The restrictions created by the alternative structures and the reduction in tidal prism are not large enough to significantly impact the salinity at the analysis locations.

Velocity

There are variations in the velocity magnitudes and directions, especially near the location of the alternative structures. Reducing the cross sectional area generates an increase in the flow magnitude and typically creates a streamlined flow pattern through the opening. The location of eddies often changes when the opening is restricted as well as the extent of any flow jets through the opening. The mean velocity magnitude at locations in the back bay region is generally unchanged from the Base condition. The variation at specific times may be larger but overall the impact is small (less than 0.02 m/s) at locations away from the inlet changes.

Understanding maximum velocity magnitudes are critical to maintaining safe navigation. The maximum velocity is reduced for most of the point analysis locations as these do not lie in the structure openings. The flood/ebb velocity images and the residual velocity comparisons provided in Appendix F are useful to understand how the maximum velocity, and navigation, may be impacted with the structures.

In General

Overall the impact of the storm protection measures placed at the inlets as defined in these alternatives is small. The salinity is not modified greatly and the velocity remains fairly consistent. The critical pieces to selecting one alternative over another would be the impacts to navigation and ensuring that the velocity through a navigation structure remains within the safe limit for the vessels using the channels as well as the impacts of tidal exchange on water quality measures and environmental stability. The hydrodynamics do not indicate large changes in the back bay marsh regions but the tidal prism is reduced in most of the regions under most of the alternatives. It must be determined that this change is within safe limits for vegetation and species survival over the project life span.

8 Conclusions

The 2D AdH model of the New Jersey inlets and back bays presented in this report has been developed based on the available data and known primary influences on the physics within the system. The model includes freshwater inflows, tides, salinity, and wind in an effort to reproduce the field for water surface elevation, velocity magnitude and direction, and salinity over a wide range of conditions. The model was compared to field data for 2018 due to the availability of various data sets during this time.

Based on the AdH model definition as stated in Chapter 2 and the model/field comparisons for water surface elevation, velocity, and salinity, as presented in Chapter 3, this model is available to simulate present and proposed future conditions, with and without project. Water surface elevation comparisons show good agreement between the model and the field over the simulation year. The discharge comparisons are good at the inlets but no data comparisons were performed at any of the smaller back bay channels. The model reproduces the salinity patterns over time but is better at reproducing the magnitude of the salinity in the inlet areas and less accurate further into the back bay channels. These channels are small and interconnected among the marsh terrain making replication in the model difficult without more detailed bathymetry collection in these shallow back bay regions.

The project alternatives do not impact the salinity in the area by more than 1-2 ppt at most. The tidal prism analysis does show change on the order of a 6-8% reduction for bays with large structural impacts due to the reduction in cross sectional area of the inlets. The velocity patterns and magnitudes at the proposed structure locations are greatly changed, as expected, but the impact to velocity magnitudes away from the structures is very little. The velocity at the inlets and structures should be reviewed for impacts to navigation as well as potential sedimentation impacts. However, the changes produced by modifying the flow at the inlets is fairly localized.

Although proven to match field conditions over a range of conditions, this model is intended to be used to reasonably forecast behavior assuming events do not occur that change the physics of the system. Hurricanes, severe storms, and anthropogenic influences (among other forces) over time can generate changes to the system that will require model updates or re-validation. The model is best used for determining trends and impacts in a percentage change and range of results type of analyses. Note that this model should not be used to predict actual values for any future parameters as the future is unknown, and it is extremely unlikely that the future will mimic exactly what is modeled.

References

- <https://www.metoffice.gov.uk/hadobs/en4/download-en-4-2-1.html>, EN 4.2.1, monthly average salinity, accessed 25 March 2019.
- Good, S. A., M. J. Martin, and N. A. Rayner, 2013. EN4: quality controlled ocean temperature and salinity profiles and monthly objective analyses with uncertainty estimates, *Journal of Geophysical Research: Oceans*, 188, 6704-6716, doi:10.1002/2013JC009067
- Cialone, Mary A., Alison S. Grzegorzewski, David J. Mark, Mary A. Bryant, and Thomas C. Massey. 2017. *Coastal-Storm Model Development and Water-Level Validation for the North Atlantic Coast Comprehensive Study*. *Journal of Waterway, Port, Coastal, and Ocean Engineering*, Volume 143 Issue 5. September 2017.
- U.S. Army Corps of Engineers. 2015. *North Atlantic Coast Comprehensive Study: Resilient Adaptation to Increasing Risk*.
- Bell, Gary L., N. D. Clifton, and D. D. Abraham. 2017. *Hydrodynamics in the Morganza Floodway Report 1: Phase 1 – Model Development and Calibration*. Mississippi River Geomorphology and Potamology Program Report No. 13. Vicksburg, MS: U.S. Army Engineer Research and Development Center.
- Clifton, N., D. Abraham, and D. Pridal. 2017. *Upper and Lower Hamburg Bend 2011 Flood Evaluation on the Missouri River near Hamburg, Iowa*. ERDC/CHL TR-17-1. Vicksburg, MS: U.S. Army Engineer Research and Development Center.
- Heath, R. E., G. L. Brown, C. D. Little, T. C. Pratt, J. J. Ratcliff, D. Abraham, D. W. Perkey, N. B. Ganesh, S. K. Martin, and D. P. May. 2015. *Old River Control Complex Sedimentation Investigation*. ERDC/CHL TR-15-8. Vicksburg, MS: U.S. Army Engineer Research and Development Center.
- Letter, J. V., G. L. Brown, R. T. McAdory, and T. C. Pratt. 2015. *Numerical Modeling of Trinity River Shoaling below Wallisville, Texas*. ERDC/CHL TR-15-1. Vicksburg, MS: U.S. Army Engineer Research and Development Center.
- McAlpin, T. O., G. Savant, G. L. Brown, S. J. Smith, and R. S. Chapman. 2013. "Hydrodynamics of Knik Arm: Modeling Study." *Journal of Waterway, Port, Coastal, and Ocean Engineering* 139(3).
- Savant, G., R. C. Berger, T. O. McAlpin, and C. J. Trahan. 2014. *Three-Dimensional Shallow Water Adaptive Hydraulics (AdH-SW3): Hydrodynamic Verification and Validation*. ERDC/CHL TR-14-7. Vicksburg, MS: U.S. Army Engineer Research and Development Center.
- Savant, G., and R. C. Berger. 2015. *Three-Dimensional Shallow Water Adaptive Hydraulics (AdH-SW3) Validation: Galveston Bay Hydrodynamics and Salinity Transport*. ERDC/CHL TR-15-3. Vicksburg, MS: U.S. Army Engineer Research and Development Center.
- Sharp, J. A., C. D. Little, G. L. Brown, T. C. Pratt, R. E. Heath, L. C. Hubbard, F. Pinkard, S. K. Martin, N. D. Clifton, D. W. Perkey, and N. B. Ganesh. 2013. *West Bay Sediment Diversion Effects*. ERDC/CHL TR-13-15. Vicksburg, MS: U.S. Army Engineer Research and Development Center.

- Tate, J. N., J. P. McKinney, T. C. Pratt, F. C. Carson, M. W. Tubman, G. L. Brown, K. M. Barry, R. T. McAdory, and M. J. Briggs. 2009. *Salinas de San Pedro (Cabrillo) Wetland Restoration Project. Volume 1, Main Text*. ERDC/CHL TR-09-14. Vicksburg, MS: U.S. Army Engineer Research and Development Center.
- Teeter, A. Michael. 2002. *Sediment Transport in Wind-Exposed Shallow, Vegetated Aquatic Systems*. A Dissertation. Louisiana State University.
- Wu, J. 1982. "Wind-Stress Coefficients Over Sea Surface from Breeze to Hurricane." *Journal of Geophysical Research* 87(C12). 9704–9706.

Appendix A: Model Bathymetry Development

The bathymetry data used in the 2D AdH model was generated by combining several data sources. The model uses the NAVD88 vertical datum and the UTM zone 18 horizontal datum. The model is run in metric units.

NAP district surveys were provided for several New Jersey inlets and the intercoastal waterway. The inlet data spanned 2015 to 2019 and the intercoastal waterway data spanned 2015 to 2018. Most data sets were in a vertical datum of Mean Lower Low Water (MLLW) and a few were in NAVD88 with units of feet. The MLLW data sets were merged initially. NOAA's VDatum software was used to get a conversion from MLLW to NAVD88 for all points in the merged data set since this conversion varies spatially (Figure 79). VDatum was unable to provide a conversion for a few sections of the survey data, indicated by the dark blue areas in the figure. These sections were provided a conversion that matched the average of the VDATUM conversion values on each side of the unknown reach and was consistent over the unknown reach, as these were not very large spans. Figure 80 shows the converted survey data in feet.

Figure 79. VDatum computed conversion from MLLW to NAVD88 (ft)

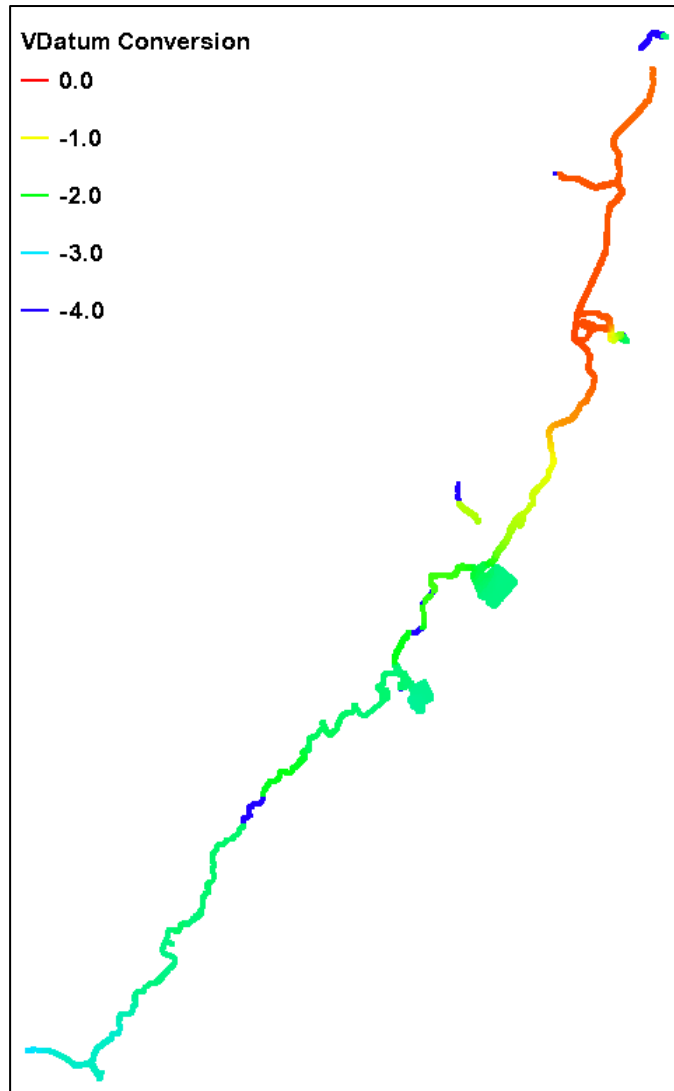
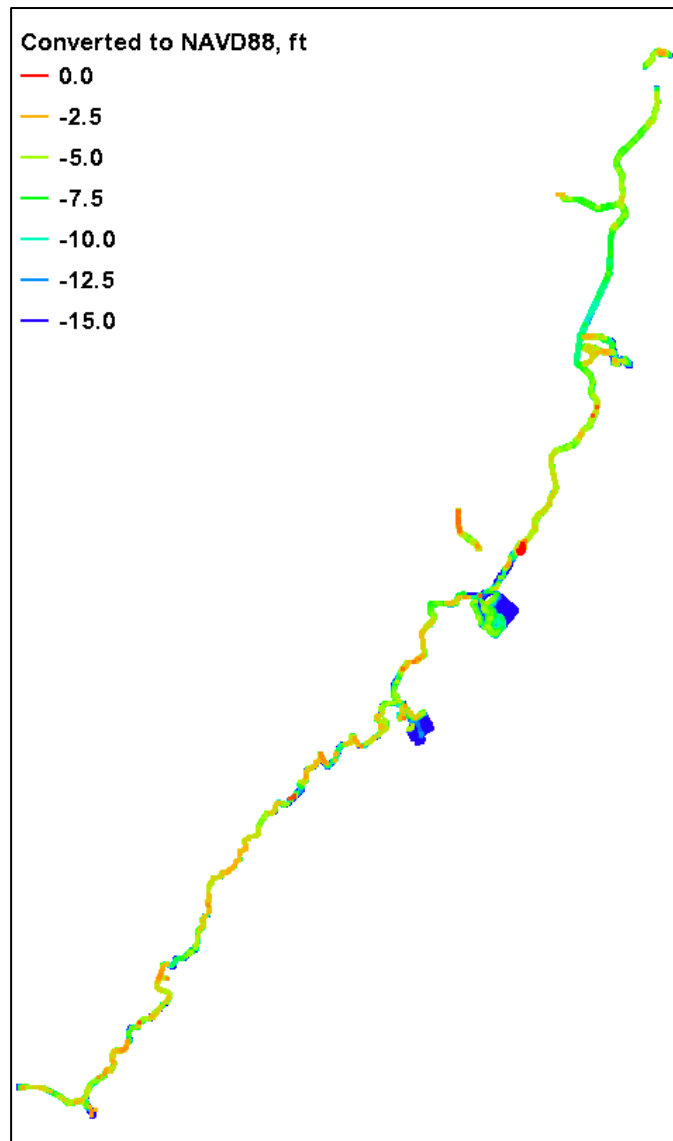
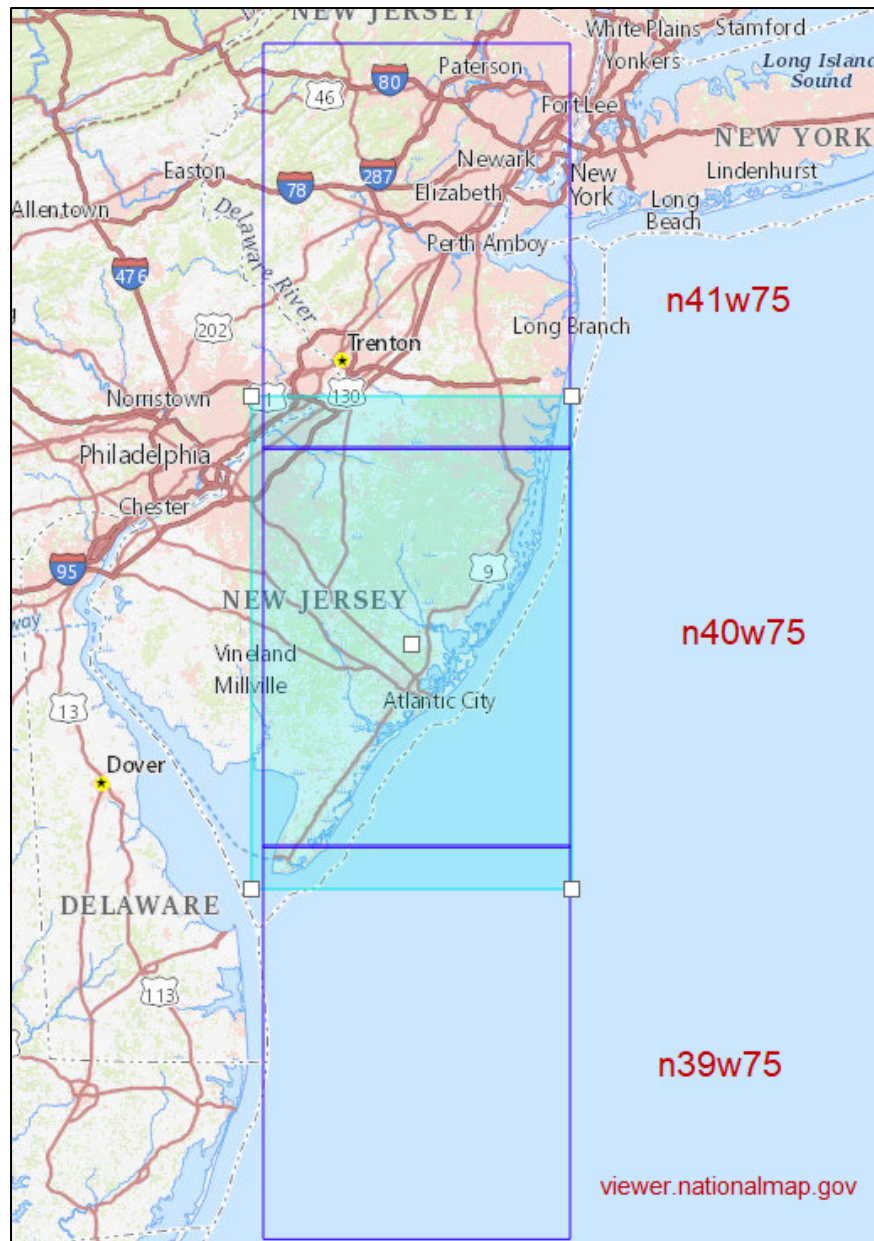


Figure 80. Converted survey data



The National Elevation Dataset (NED) 1 arc-sec (~30 m) was pulled for the regions overlapping the model domain (Figure 81). This dataset provides mostly topography with hard zeroes in water areas. The NED is NAD83 geographic coordinates horizontally and NAVD88 meters vertically. This region, other than the southern tip at Cape May, was surveyed in 2015. The southern dataset includes surveys between 1999 and 2013. The NED dataset is used in all areas where its data are nonzero.

Figure 81. NED dataset quadrants.



The Coastal Relief Model (CRM) 90 m grid developed by the National Geophysical Data Center, NOAA, was used for all other areas. These data are a mix of MLLW and NAVD88 and the datasets were obtained from 1999 to present. The shift between datums, according to the source agency, is within the vertical accuracy of the data (1 m), and therefore no datum shifts were incorporated when combining the various data sets into the CRM.

For the model domain mesh, the NAP surveyed channel regions are applied for all nodes where this set has data. Then the NED dataset is applied where non-zero followed by the CRM dataset in all areas where the NED is zero. Therefore, the topography/bathymetry priority is

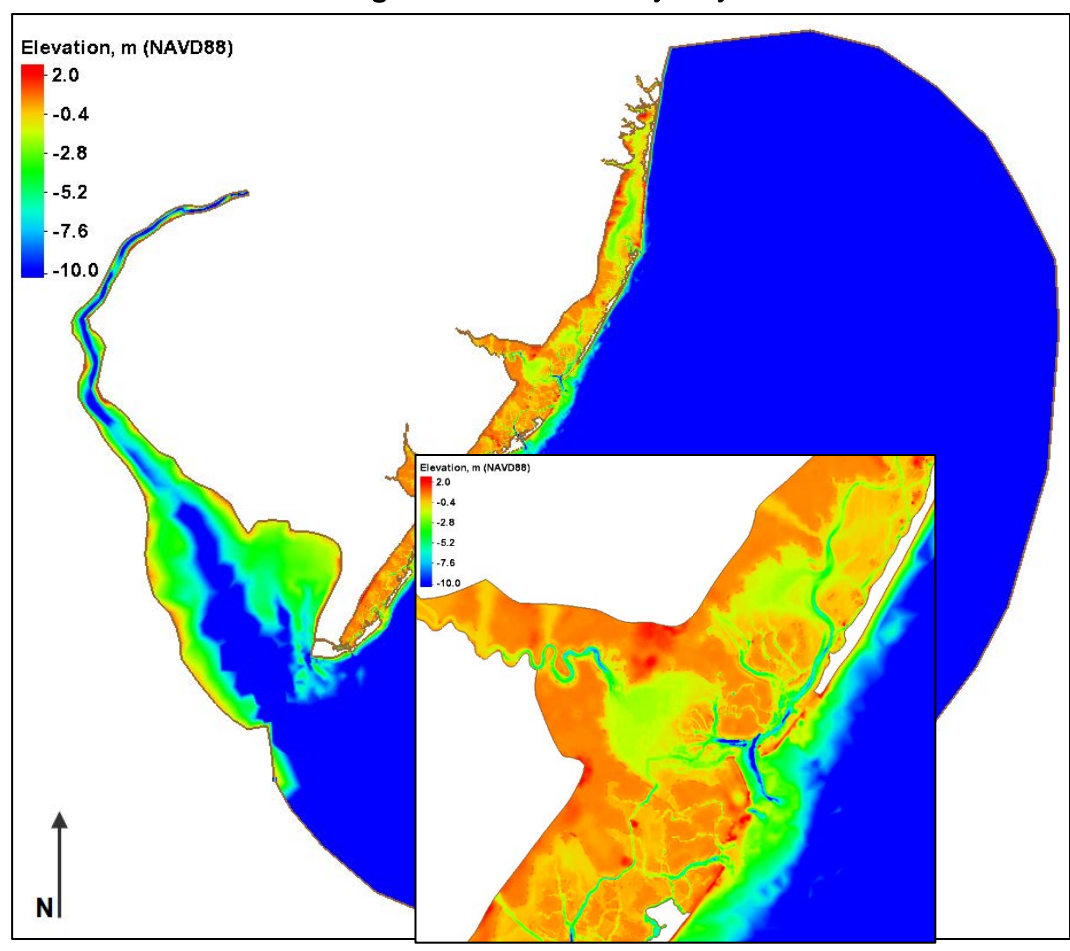
NAP survey, NED, then CRM. All data are applied to the mesh as NAVD88 meters and converted to UTM zone 18 meters.

Additional bathymetry datasets were available and investigated for potential use in the model development. The Barnegat Bay Continuous Terrain Model was determined to provide no advantage over the previous sources. Although its data sets are finer in resolution, the AdH mesh resolution is approximately 80 m in the bays and cannot take advantage of the finer data. In addition, the data sets are older (1934-2012). The National Centers for Environmental Information (NCEI) also provides DEM data (30 m) for the model domain area. However, these data are many decades old. Barnegat Bay data were surveyed 1934 to 1936; New Jersey Inland Bays data were surveyed 1935 to 1940; Delaware Bay data were surveyed 1945 to 1993. Again, these data are much older than the data provided in the CRM and NED datasets.

So that river inflows could enter the domain appropriately, the bathymetry in a few areas was modified if the resolution of the mesh did not account for the needed detail or if the interpolation of the datasets required adjustment. Figure 82 shows the elevation contours of the AdH model for the full domain and a subset.

It is known that the inlets along the New Jersey coast are dynamic and change shape often. This AdH model is a fixed bed model and therefore requires a set inlet shape. The surveys and datasets discussed in this document will provide the inlet shape for the AdH model unless otherwise directed by NAP. It must also be understood that the dynamic nature of these inlets may impact the level of accuracy of the model validation depending on the date of the bathymetry survey and the date of the model validation.

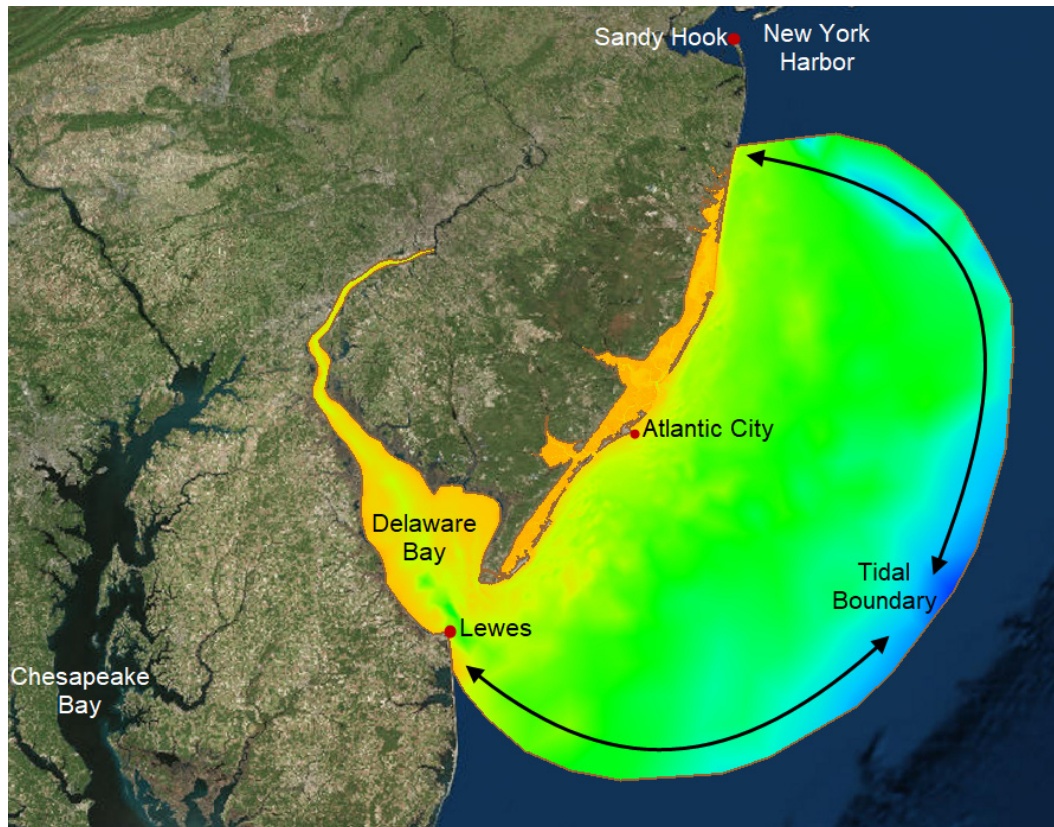
Figure 82. AdH model bathymetry



Appendix B: Tide Boundary Condition Development

The tidal boundary condition was created using harmonic and nonharmonic components from various sources in an effort to build the most representative condition for the AdH model boundary location. The semi-circular AdH model boundary lies approximately 70 miles offshore at its greatest distance (Figure 83).

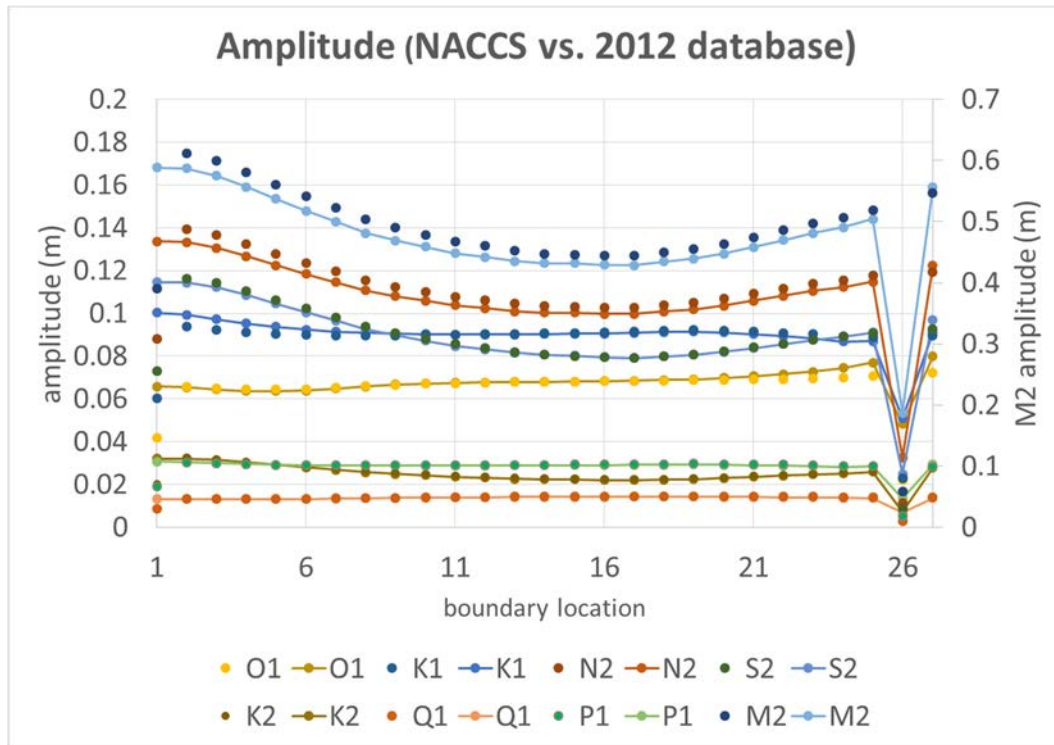
Figure 83. Model domain and tidal boundary location.



Constituents from the 2012 ADCIRC database and NOAA at Atlantic City, NJ were analyzed against each other and the tide-only model validation effort for the North Atlantic Coast Comprehensive Study (NACCS) to determine the appropriate combination of components and nonharmonic signals. Harmonic constituents from the 2012 ADCIRC database were pulled at 27 locations along the AdH model boundary edge. Harmonic constituents from the NACCS ADCIRC model validation results were also pulled at these same locations. Eight common constituents between the two sources were compared. The comparison of the constituent amplitude is shown in Figure 84, left to right defined as north to south along the model boundary. There are significant differences at locations near land boundaries. However, all other locations compare very well between the two data sources. The largest variation

between the NAACS model constituents and the ADCIRC database constituents that appears along the AdH model boundary is for M2 and N2.

Figure 84. Tidal constituent amplitude comparisons.



Additionally, the harmonic constituents from the 2012 ADCIRC database and those from the NACCS model were used to generate a harmonic tide at the approximate midpoint of the AdH model boundary. Figure 85 shows a section of this tide. The NACCS constituent tide is slightly larger in amplitude than that produced by the 2012 ADCIRC database constituents. When comparing the harmonic tides at all of the locations along the AdH model boundary (Figure 86), the variation can be as much as 0.35 m. The largest differences are at the same locations that produced large variations in the constituent amplitudes – those nearest land – as expected. However, the typical variation during a tidal cycle is nearly 0.04 m.

Figure 85. NACCS and ADCIRC database harmonic tide comparison.

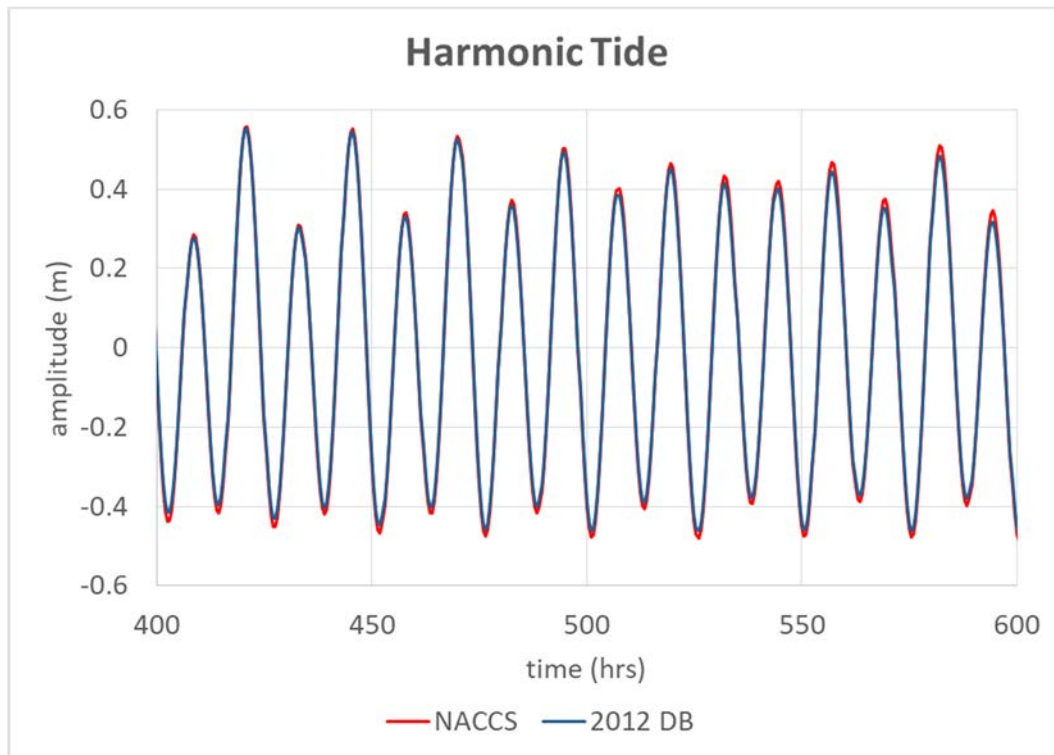
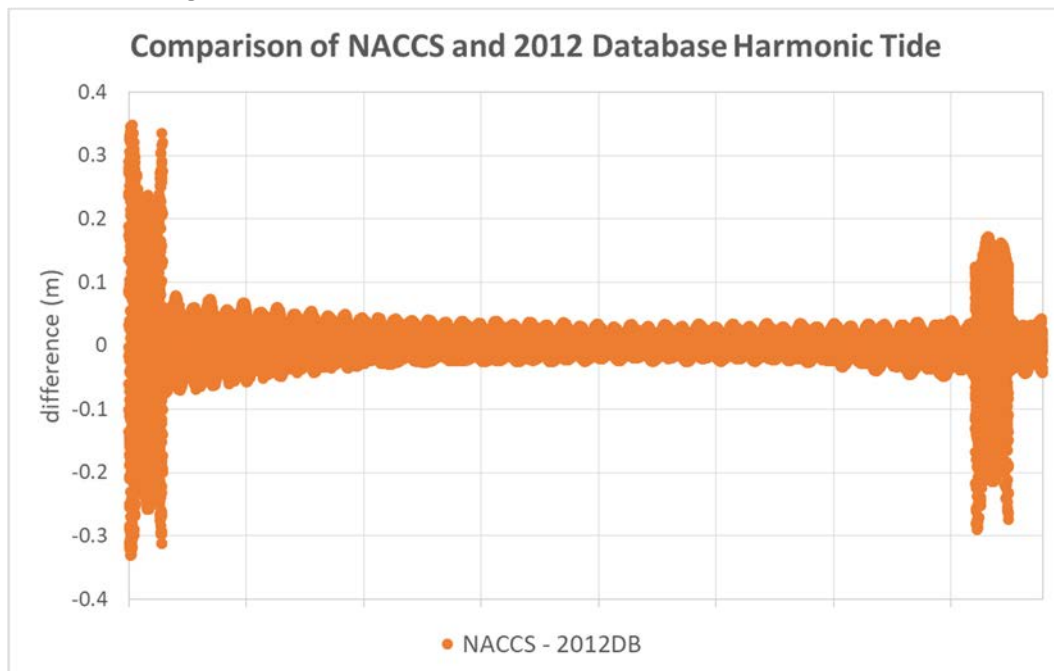


Figure 86. NACCS and ADCIRC database harmonic tide difference.



A final comparison of the 2012 ADCIRC database constituents were made to those for the NOAA gage at Atlantic City, NJ, to determine if all harmonic constituents should be taken from the 2012 ADCIRC database (Figure 87). The NOAA harmonic signal for Atlantic City is

plotted for a short period of time with the 2012 ADCIRC database harmonic signal in the figure below. The differences in the amplitudes are also provided. The NOAA gage harmonics produce a larger tidal amplitude at Atlantic City than do the 2012 ADCIRC database constituents. The variation is as much as 0.07 m. This variation indicates that the 2012 ADCIRC database may not be the best option for all of the harmonic constituents.

Figure 87. ADCIRC database and Atlantic City harmonic tide comparison.

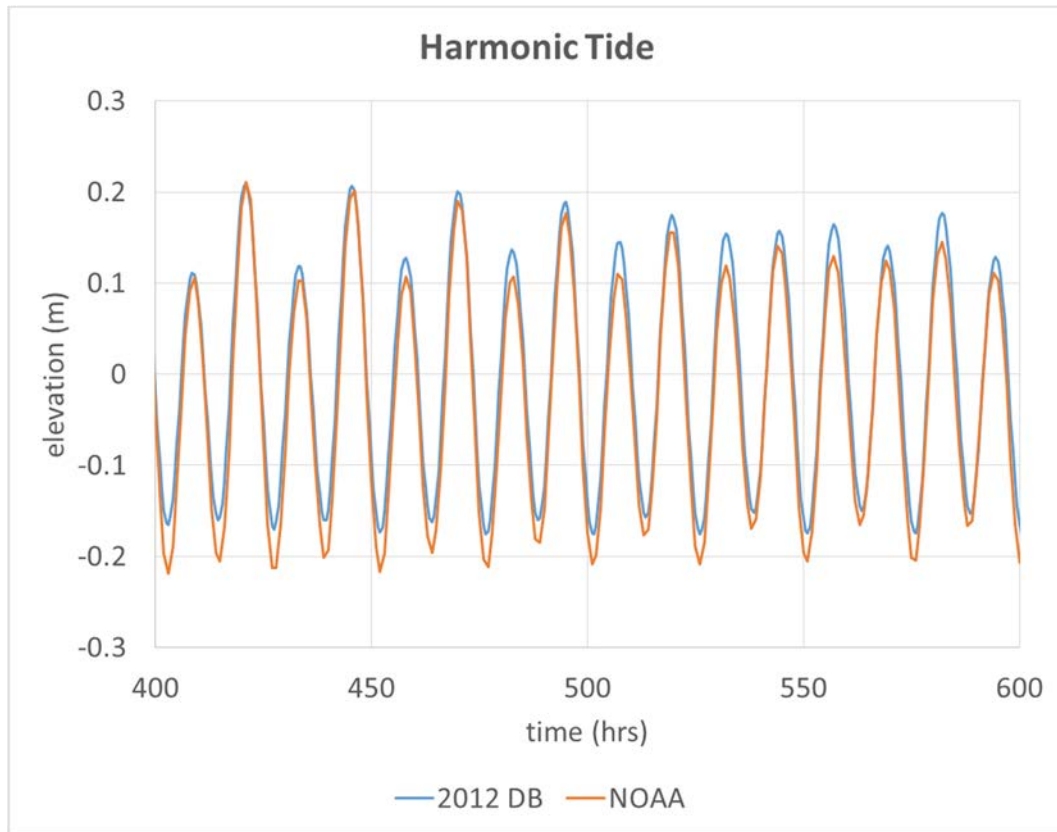
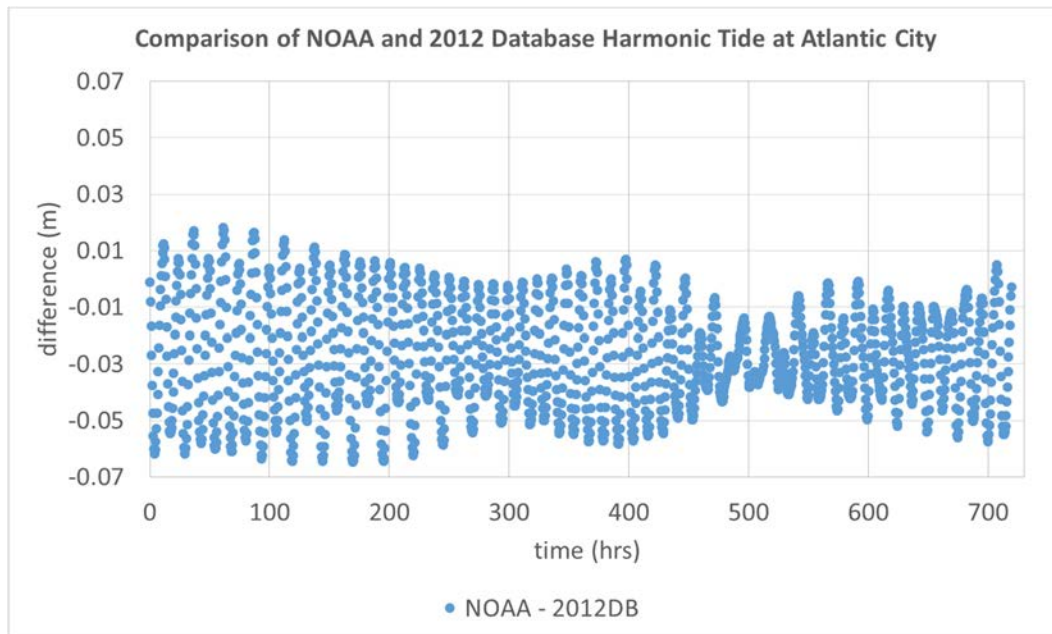


Figure 88. ADCIRC database and Atlantic City harmonic tide difference.



It was determined that since NOAA uses a much longer time history of data than the ADCIRC database to determine the harmonic constituents, the NOAA constituents should be used as the base values. Then, based on the previous comparisons, it was determined that the ADCIRC database constituents are best for the major 8 that are compared to the NACCS results in the previous section – M2, S2, N2, K2, K1, O1, Q1, P1 – since they can be obtained for each edge along the AdH model boundary.

In the area of the AdH model domain, NOAA data are available at Lewes, DE, Atlantic City, NJ, and Sandy Hook, NY. The tide signal generated by these 27 secondary harmonic constituents were compared to determine if large variations occur between them. If there is large variation then some type of interpolation is necessary when including these constituents along the tidal boundary. However, if the signals are similar, the Atlantic City constituents can be used uniformly along the AdH tidal boundary. A section of the secondary harmonic tide signals is shown in Figure 89. The differences between Sandy Hook and Atlantic City as well as that between Lewes and Atlantic City are shown in Figure 90. The signals are fairly similar, especially between Atlantic City and Lewes which are within the AdH model domain. The differences between the magnitudes, though, can be large at times – nearly 0.1 m.

Although there are measureable differences in the tide generated by the secondary NOAA constituents, it was determined that initial simulations would utilize only the Atlantic City constituents rather than attempt an interpolation of these constituents along the AdH model boundary, especially since the closest gage to the north is approximately 25 miles away from the AdH model boundary. If the model calibration process indicates a need for more detailed

signals along the AdH model boundary, these variable constituents will be included. Therefore, the harmonic signal along the AdH model boundary will include variable amplitudes and phases for the eight constituents noted and constant amplitudes and phases for the other 27 constituents.

Figure 89. NOAA gage secondary harmonic constituent tide comparison.

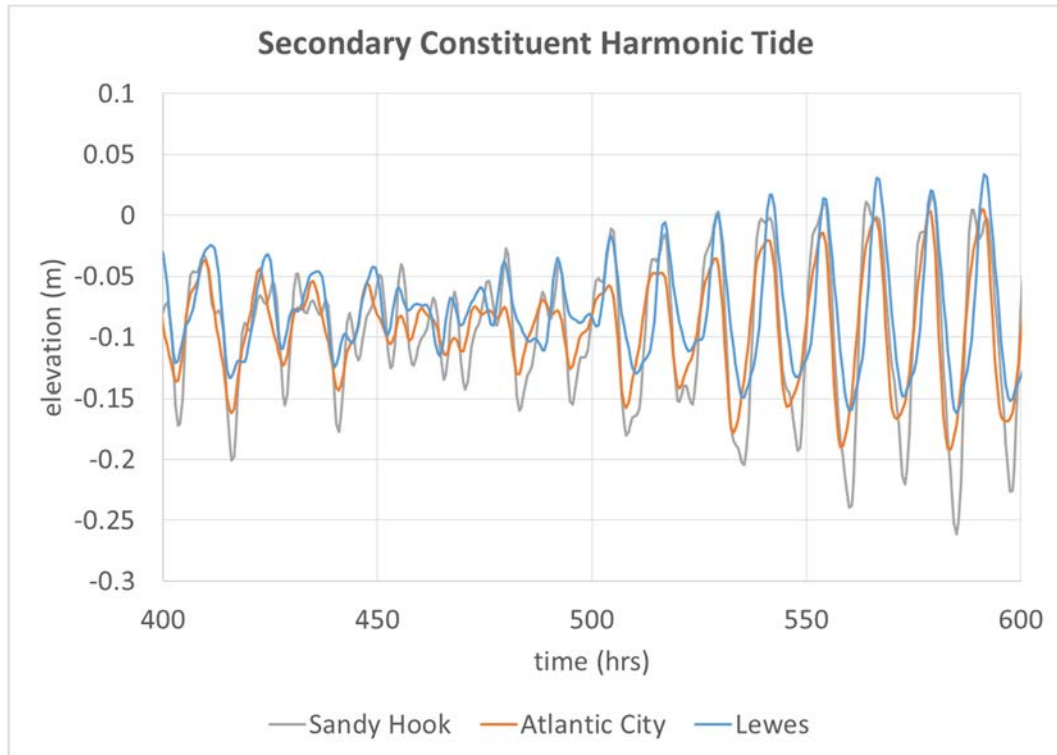
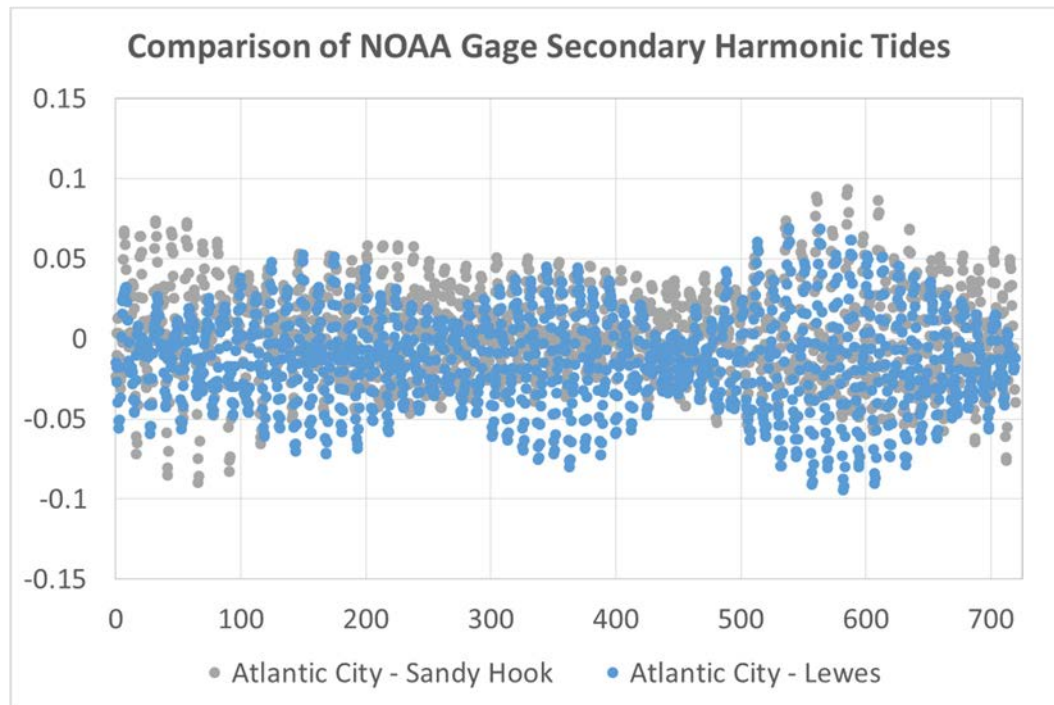
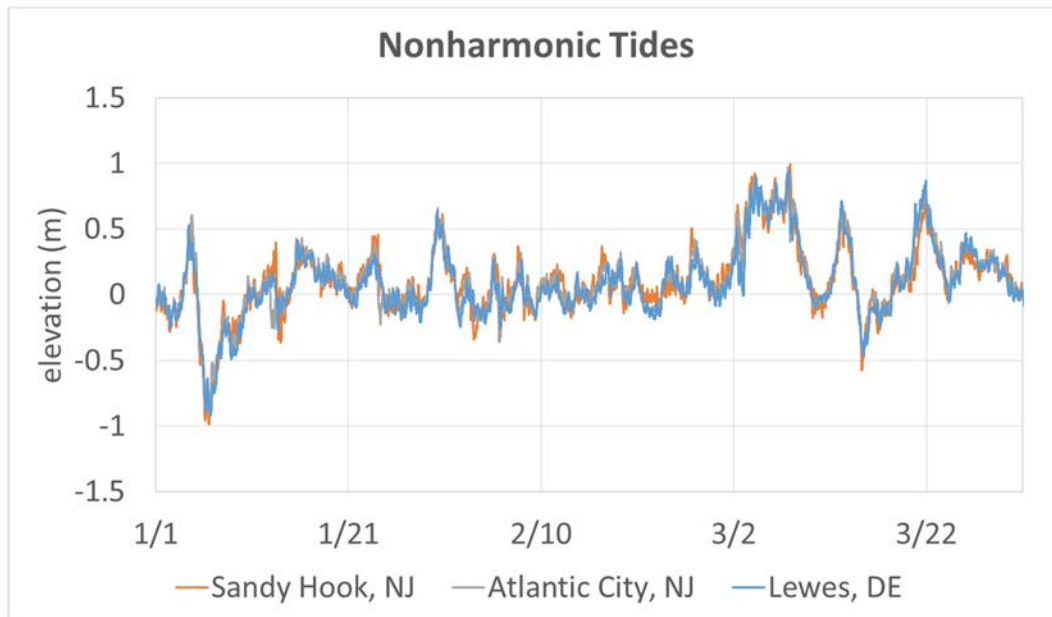


Figure 90. NOAA gage secondary harmonic constituent tide difference.



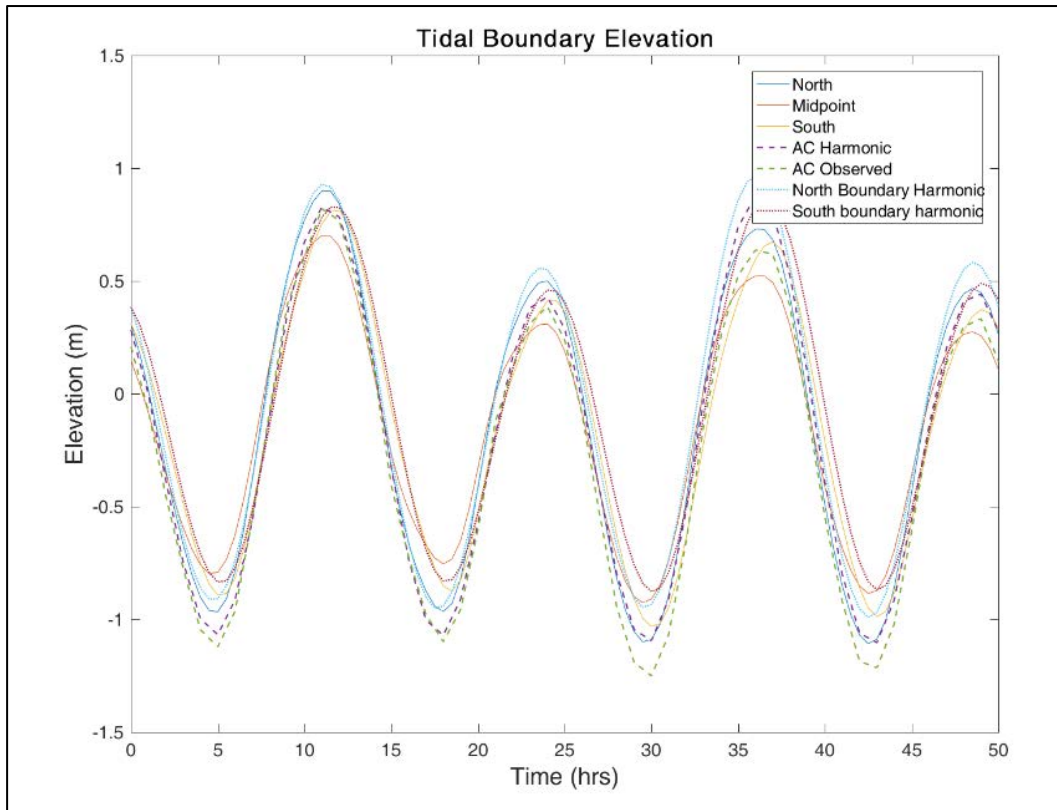
The nonharmonic signal must also be included in the AdH model tidal boundary condition to account for storms and other nonharmonic events. This information is determined from measured (observed) values and must come from the NOAA gages (observed – predicted). In the area of the AdH model domain, NOAA data are available at Lewes, DE, Atlantic City, NJ, and Sandy Hook, NY. These locations were compared to determine if large variations occur between them in the nonharmonic signal. If they do occur then some type of interpolation is necessary along the AdH model boundary to account for the variation. However, if the nonharmonic signals are similar then there is justification to utilize only the nonharmonic signal from Atlantic City at all AdH model boundary locations. Given the similar signals of the nonharmonic signals seen in Figure 91, the nonharmonic component of the AdH model boundary tide condition will be applied from Atlantic City and applied equally along the model boundary.

Figure 91. NOAA gage nonharmonic tide comparison.



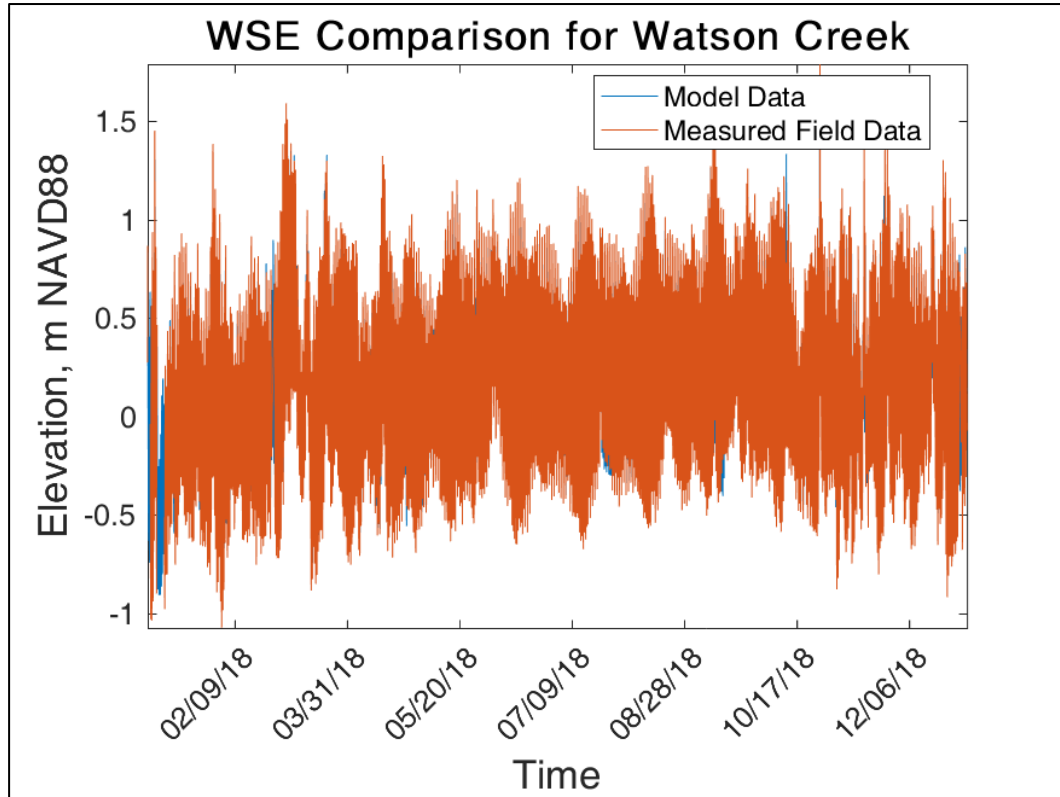
The AdH model boundary consists of 30 edges that will each have a time-varying elevation boundary condition. As determined from the previous analysis, the harmonic signal along the AdH model boundary will include variable amplitudes and phases for the eight constituents noted and constant amplitudes and phases from NOAA's Atlantic City gage for the other 29 harmonic constituents and the nonharmonic signal. Figure 92 shows a section of the generated tidal signal at the AdH northernmost boundary edge, a midpoint edge, and the southernmost boundary edge. Also included on the plot is the harmonic (predicted) tide and the observed tide at Atlantic City. Finally, the harmonic only generated tide signal (mix of NOAA and 2012 ADCIRC database constituents) is shown for the northernmost and southernmost AdH model boundary. These are plotted together to show that the measured and generated tide signals make sense and lie in a reasonable position relative to each other.

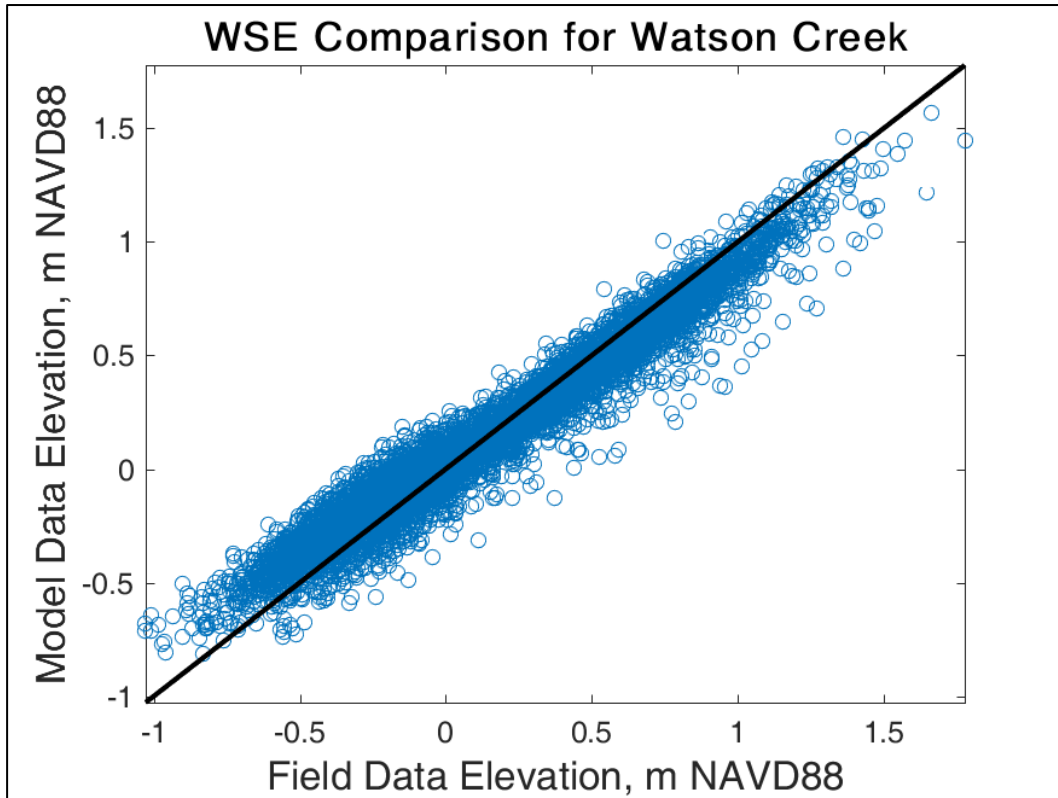
Figure 92. AdH model boundary tide at select locations and comparison to other components.

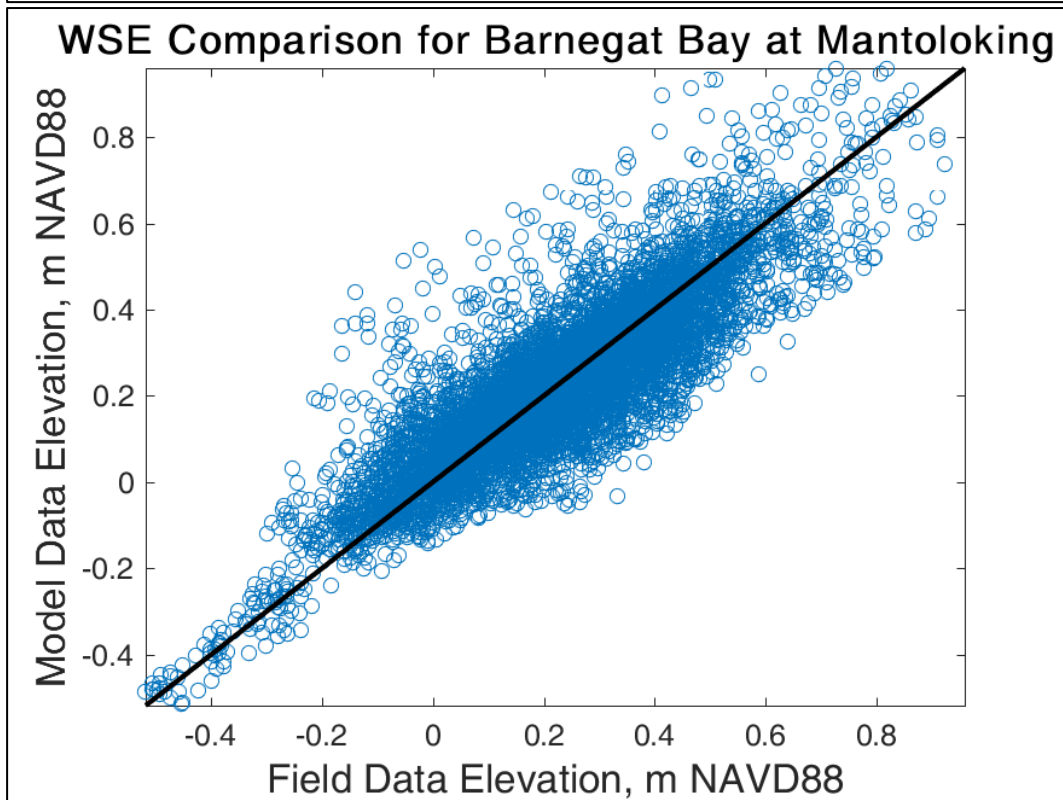
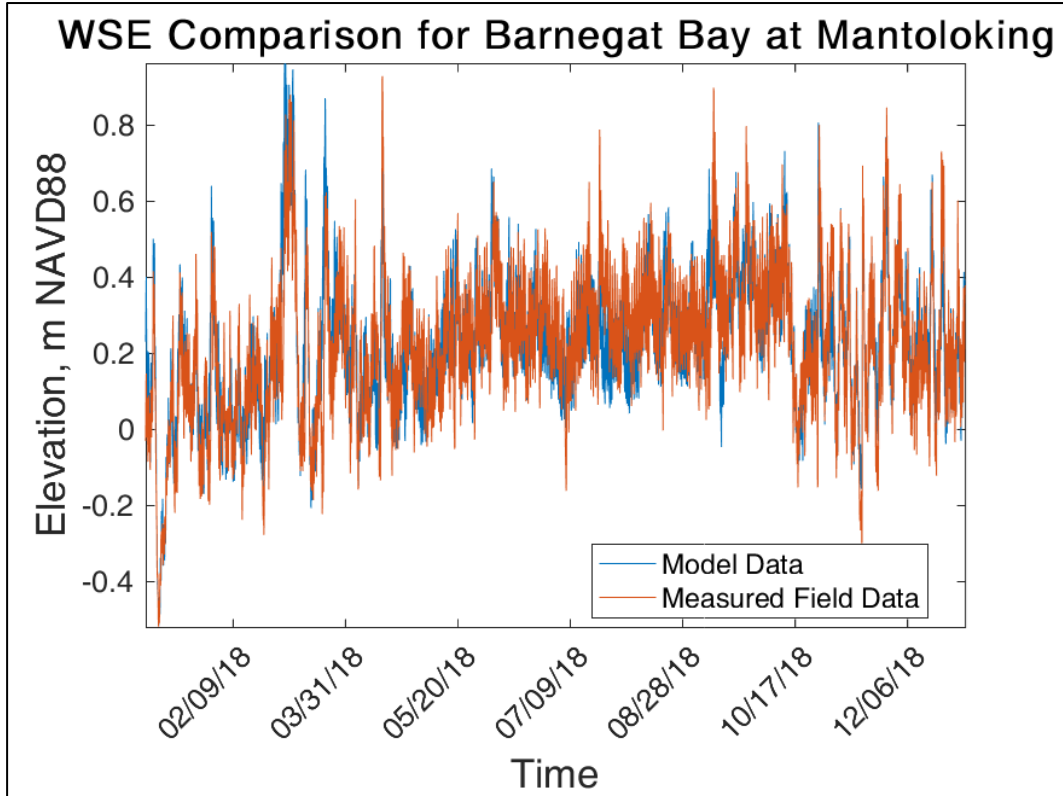


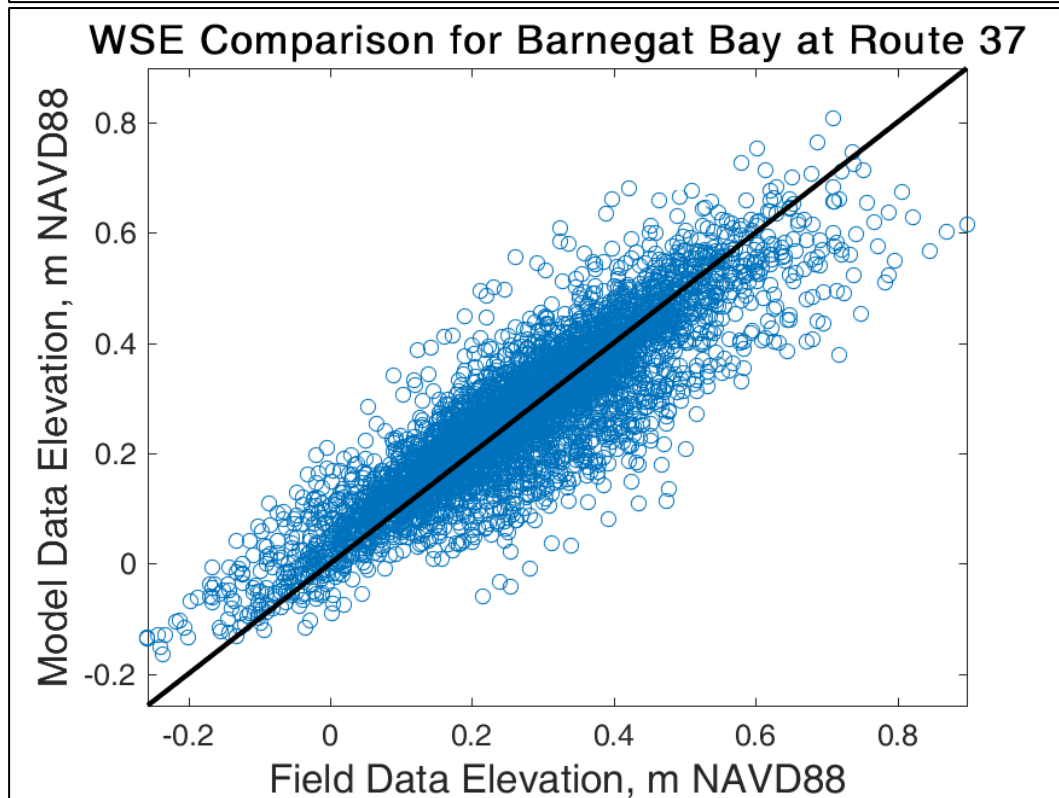
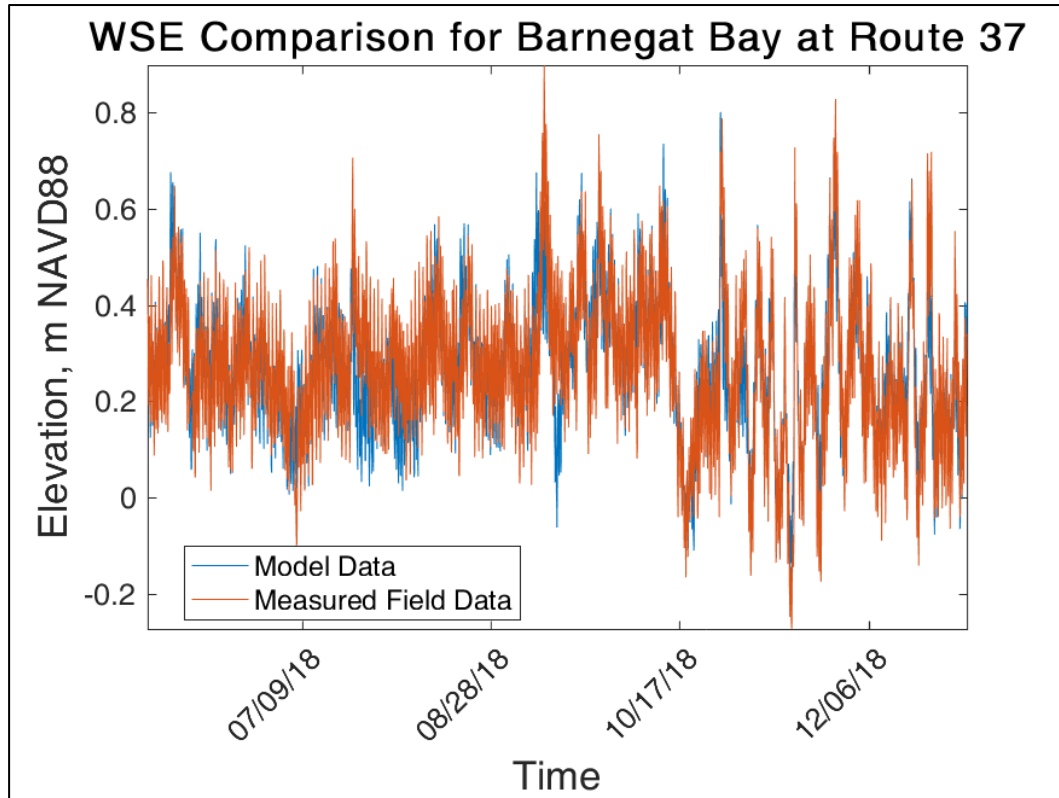
Appendix C: Model/Field Comparisons

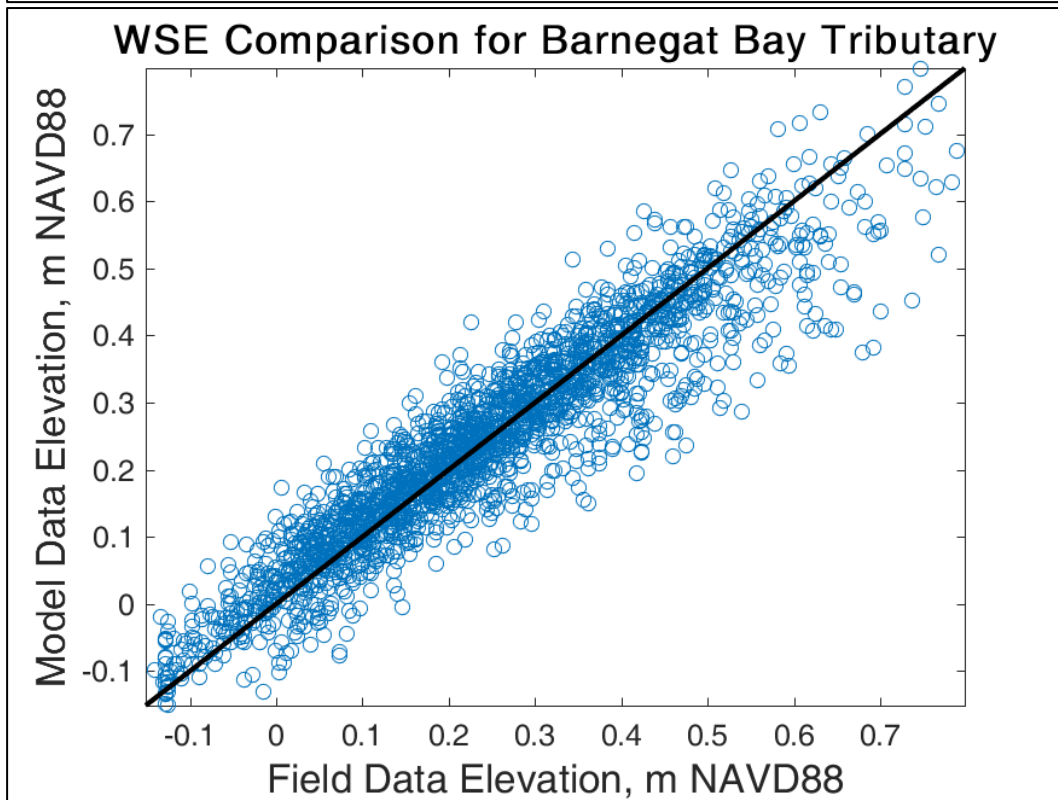
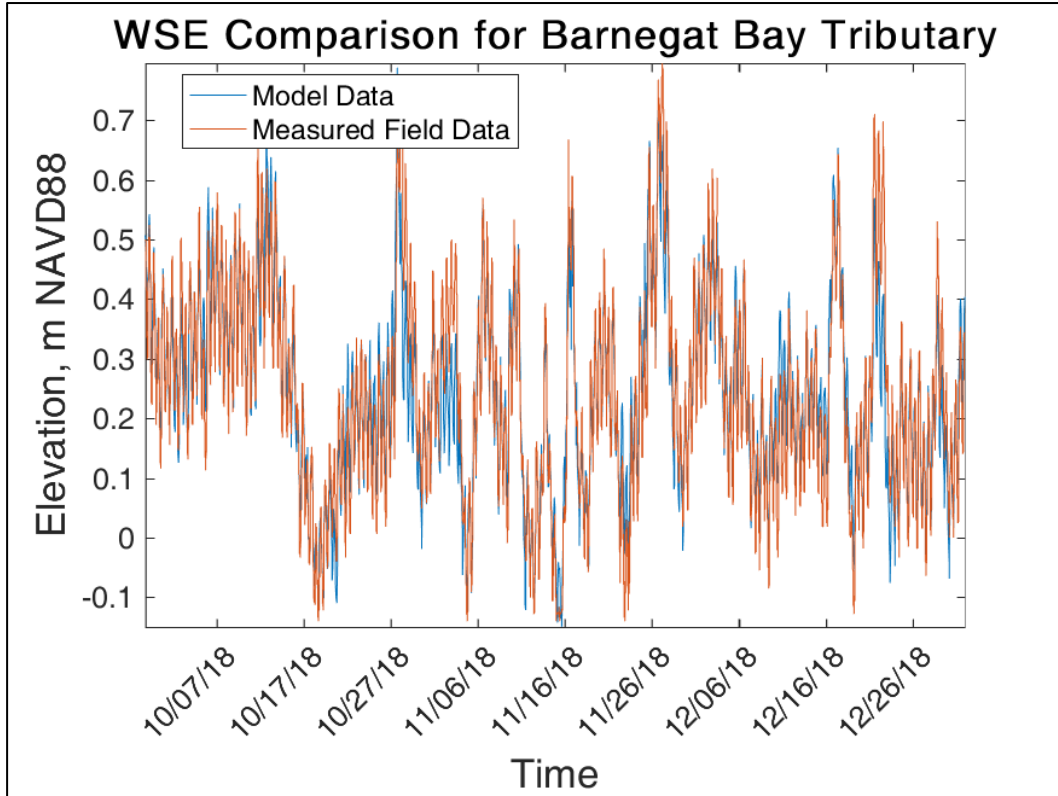
Water Surface Elevation

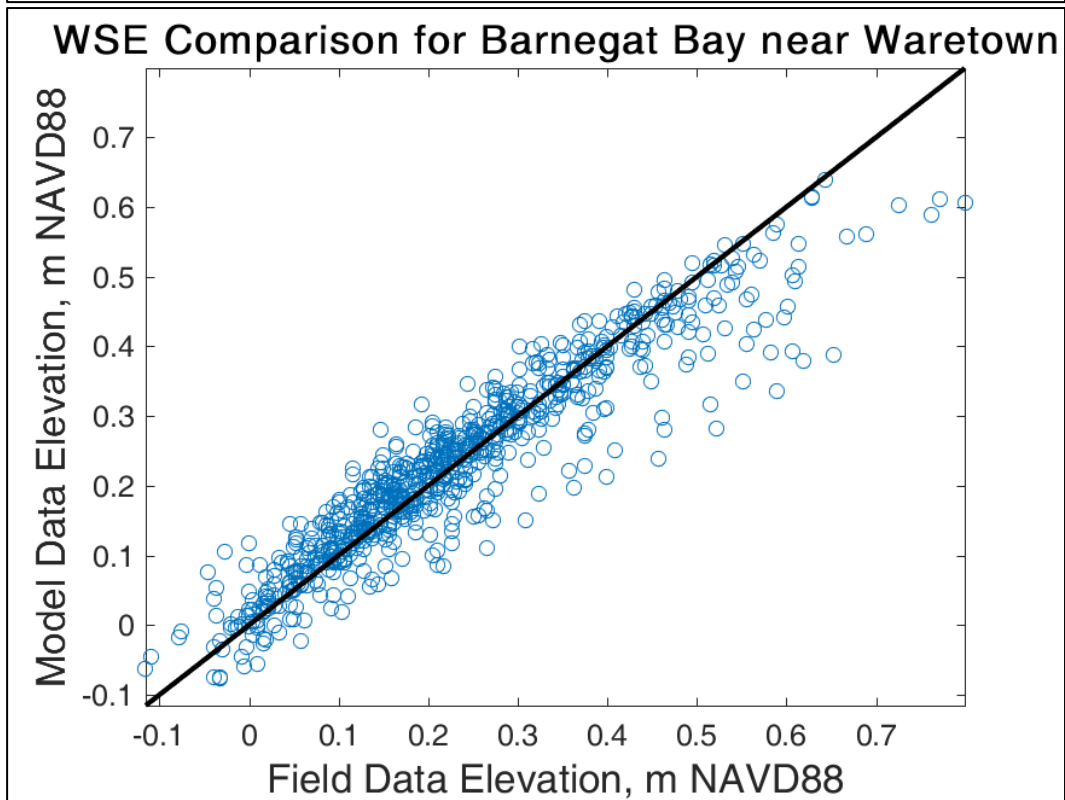
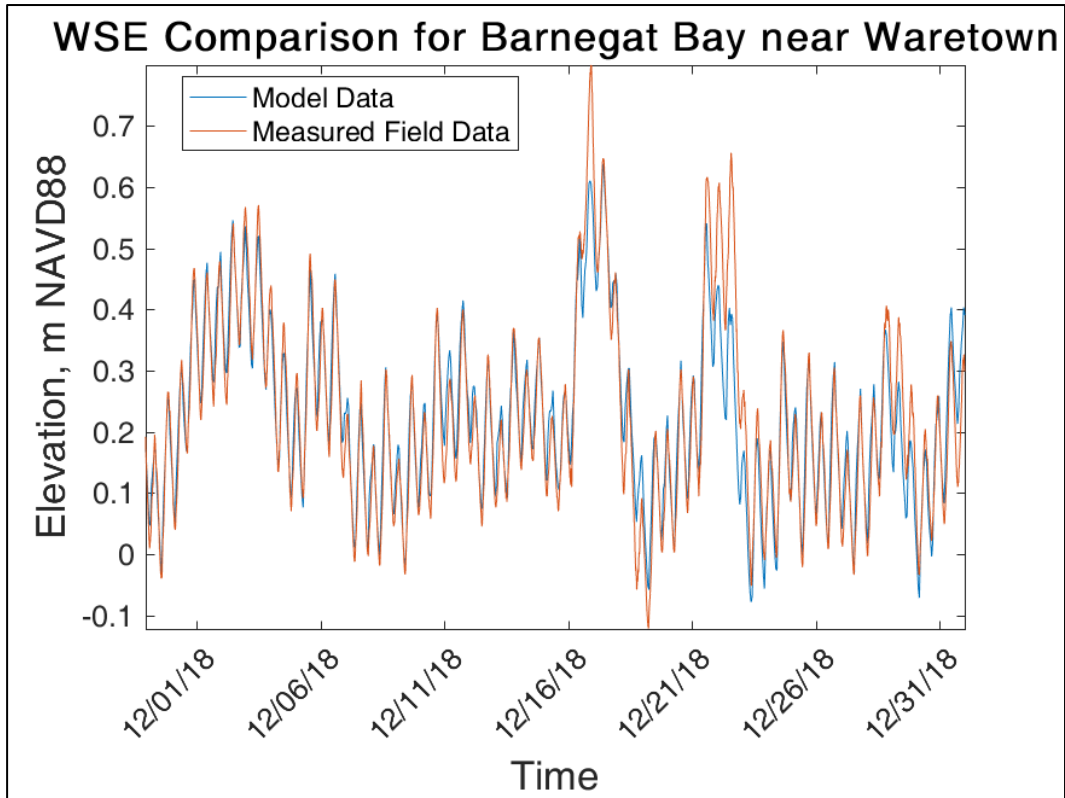


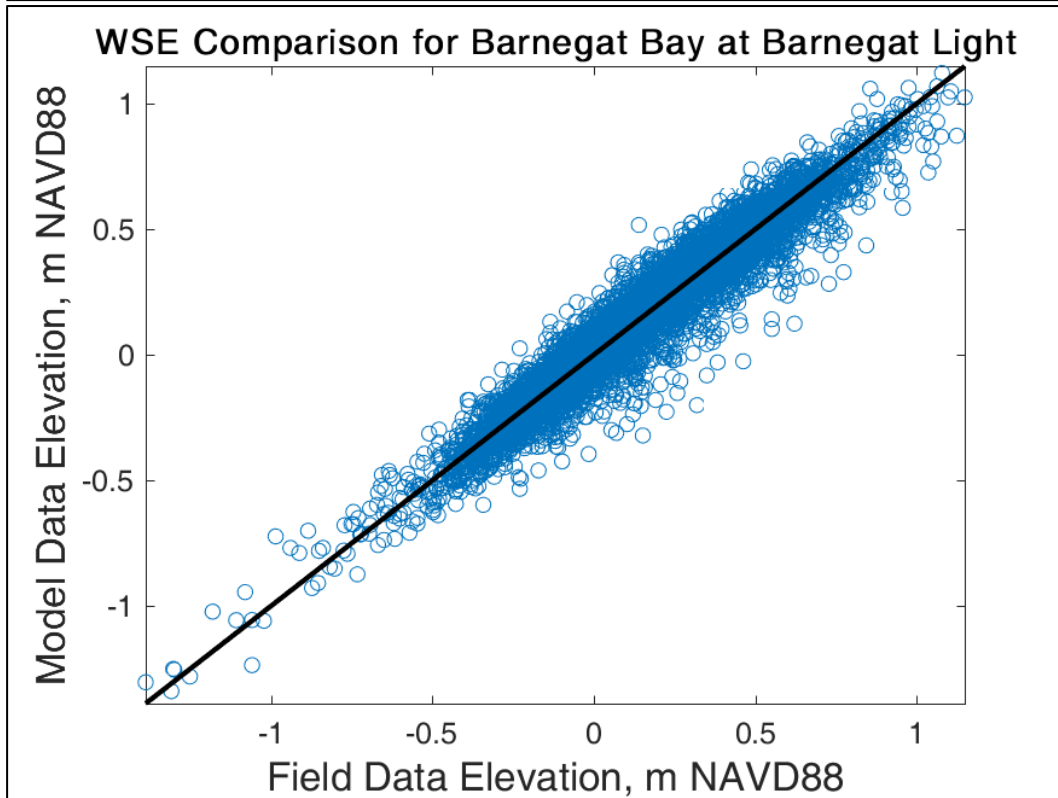
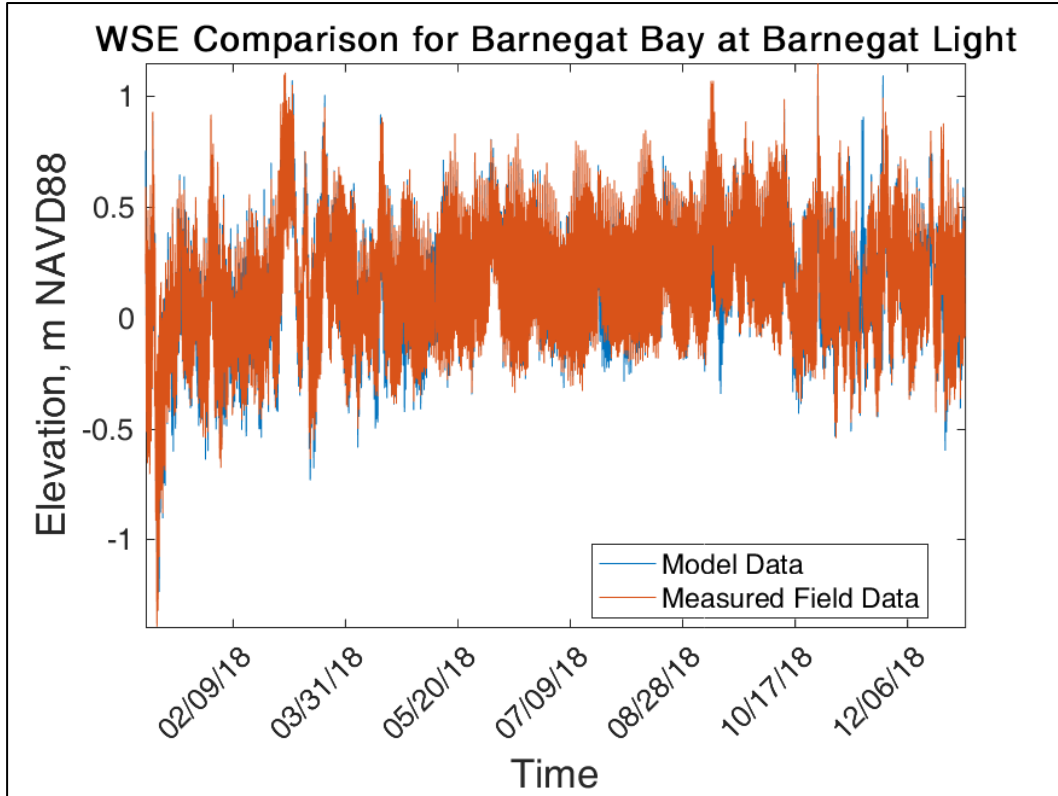


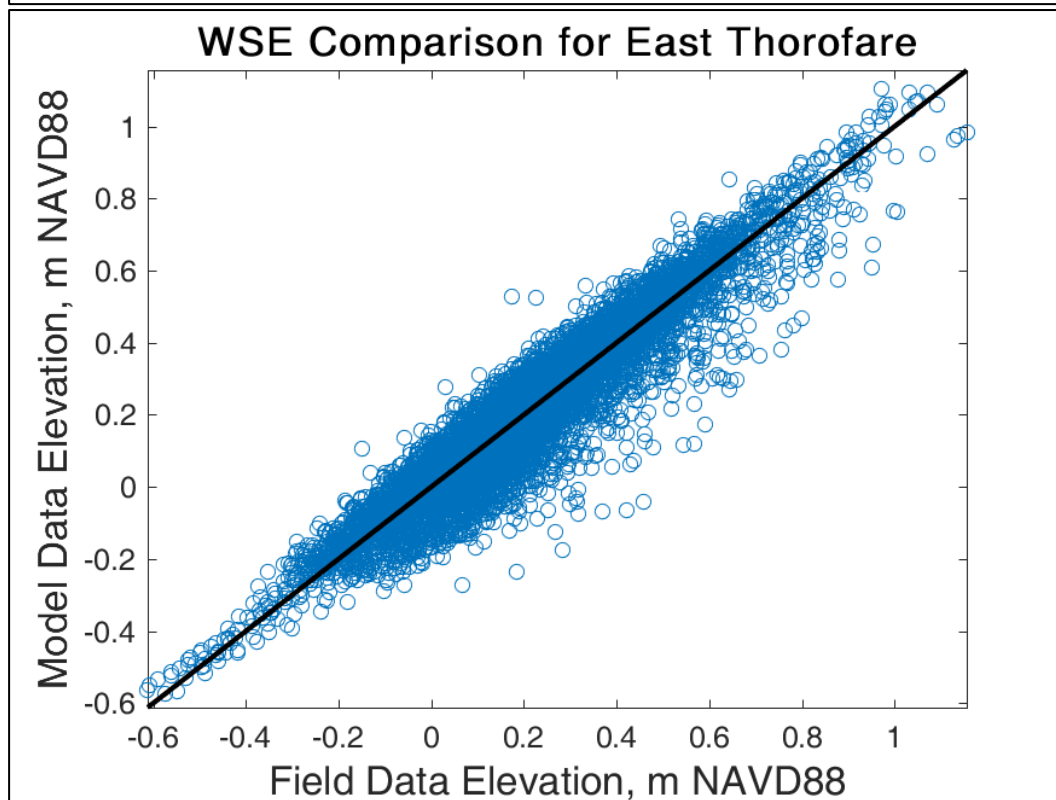
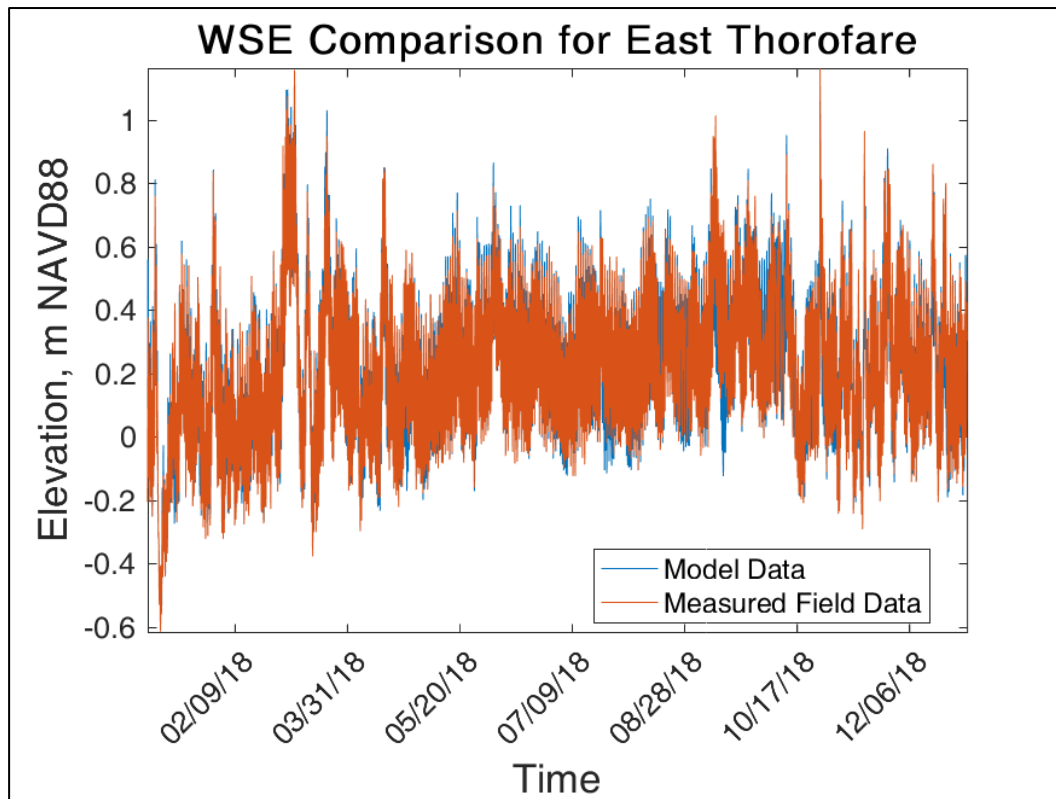


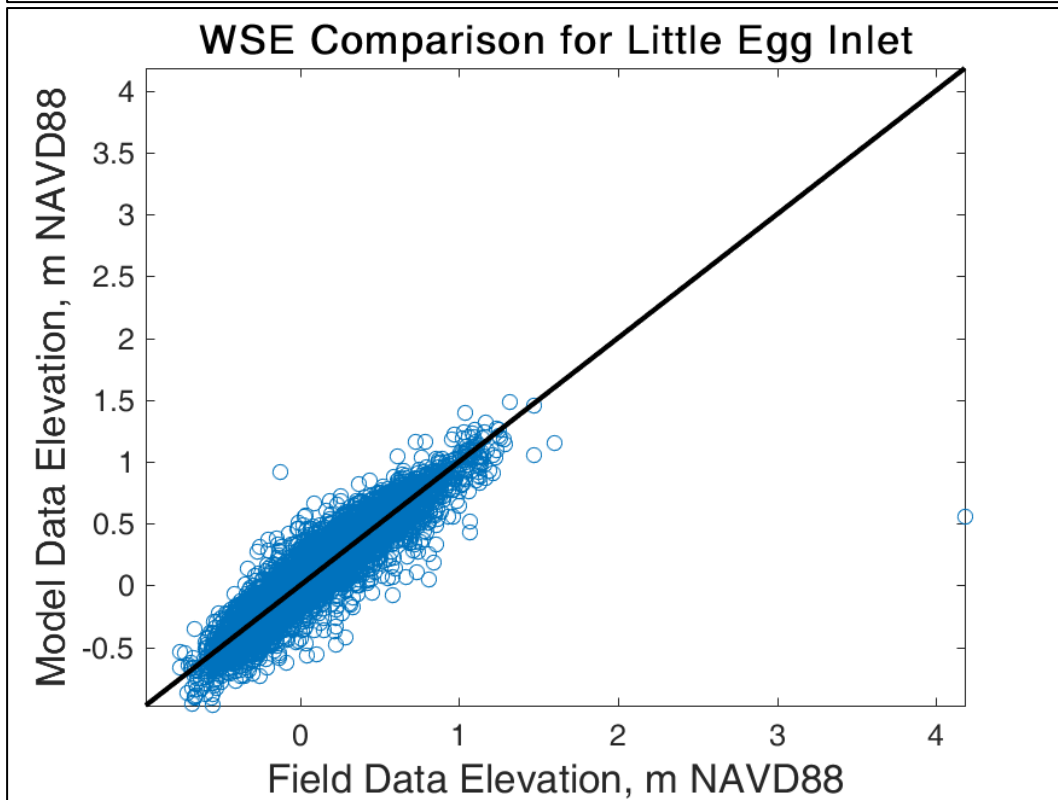
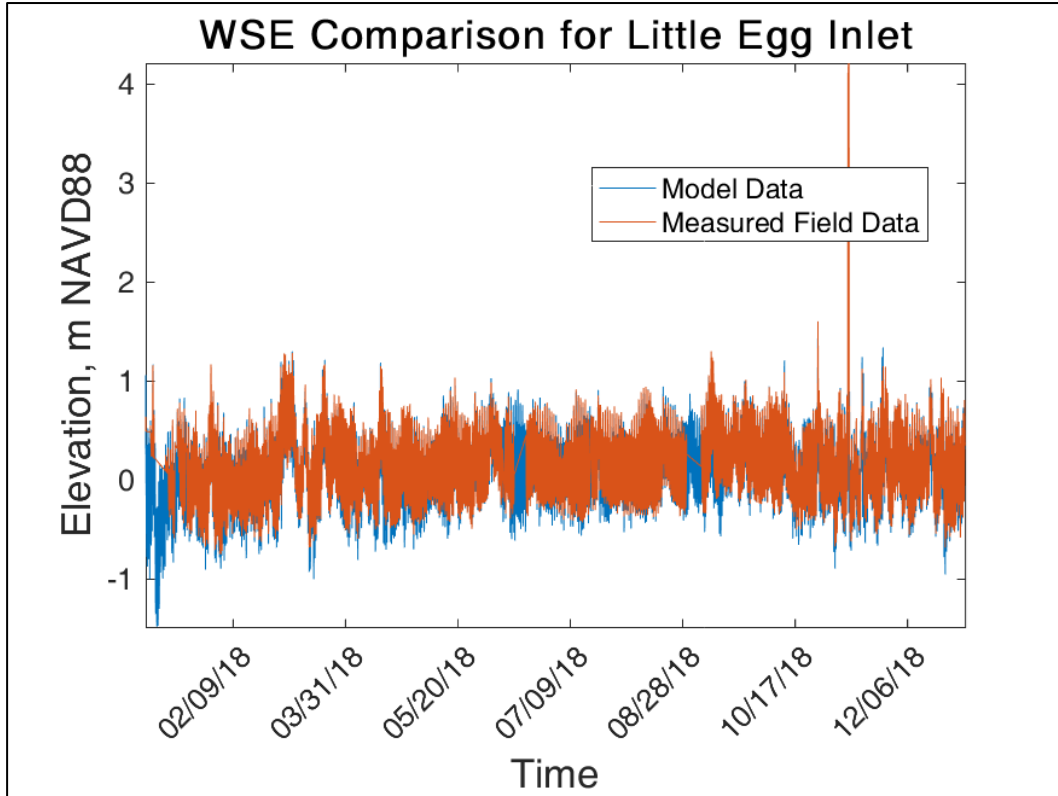


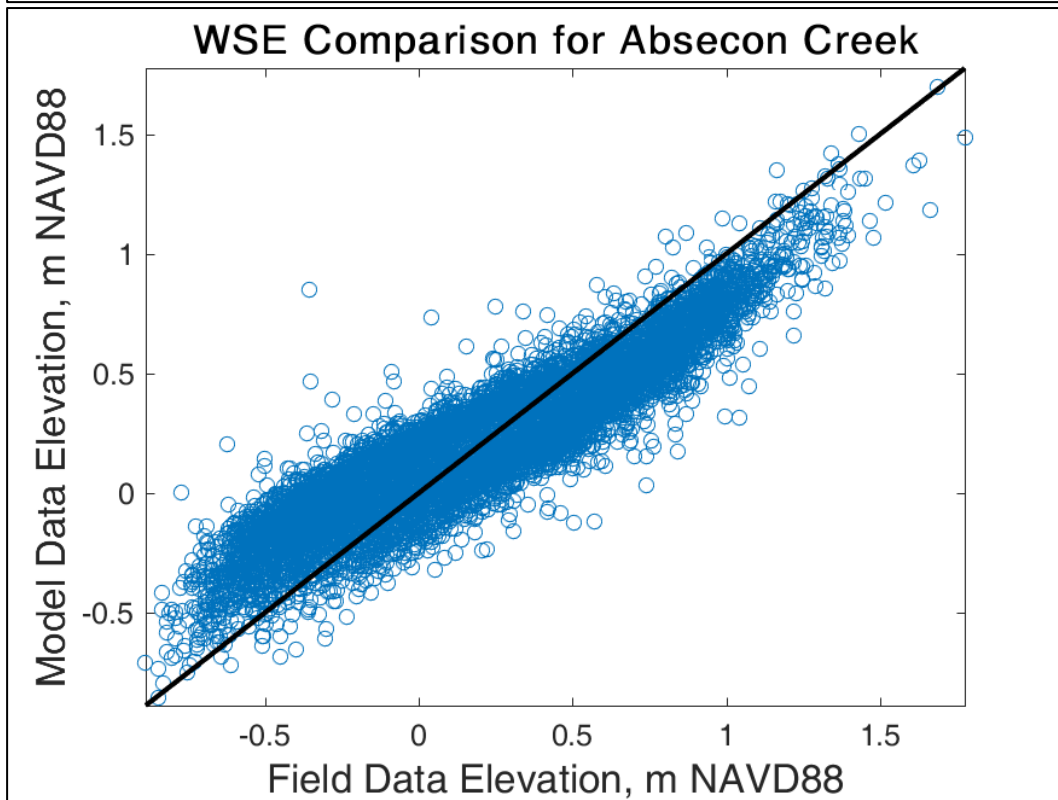
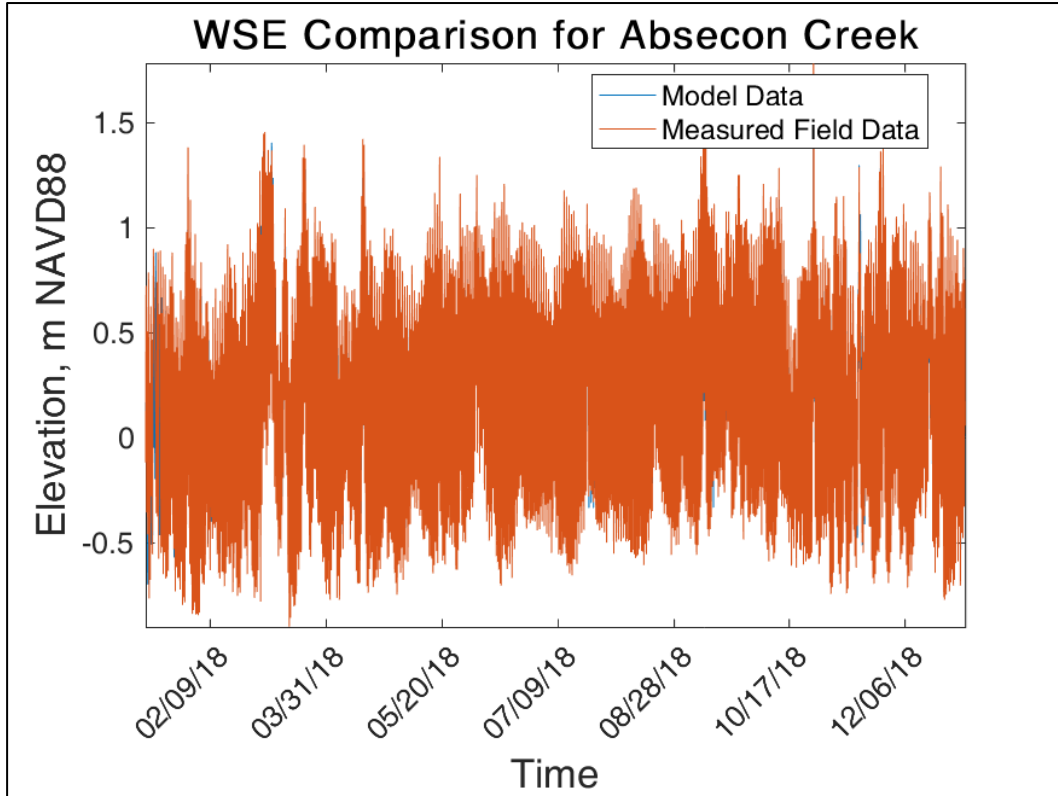


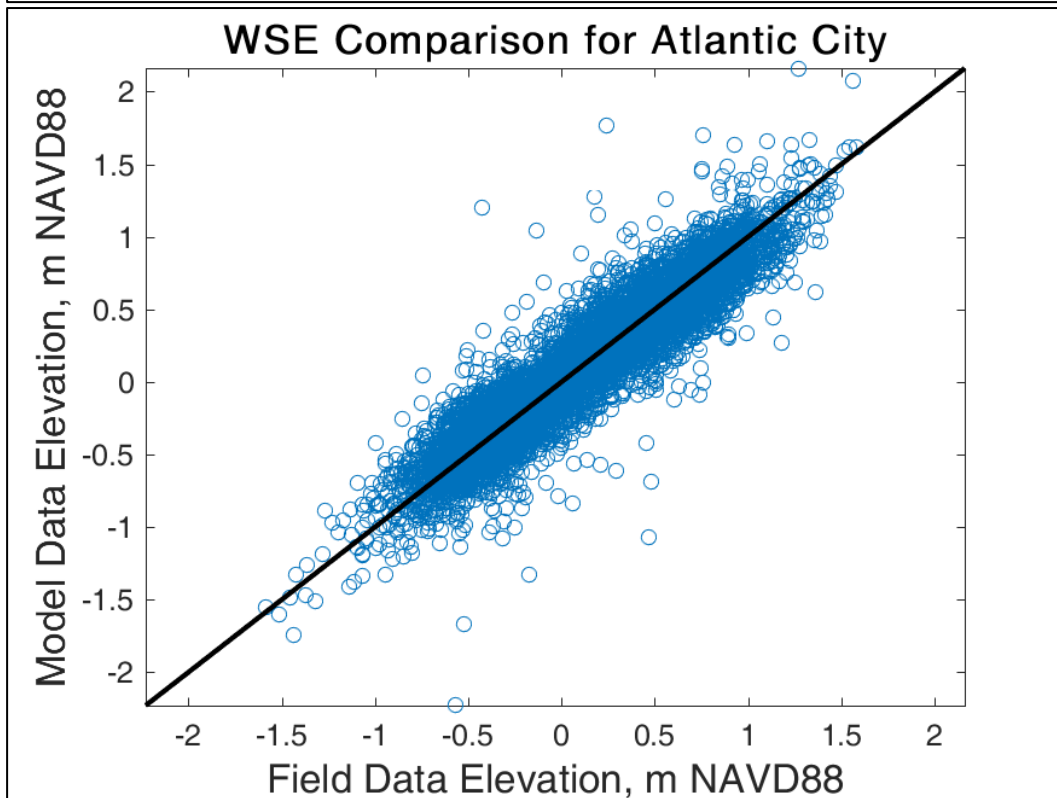
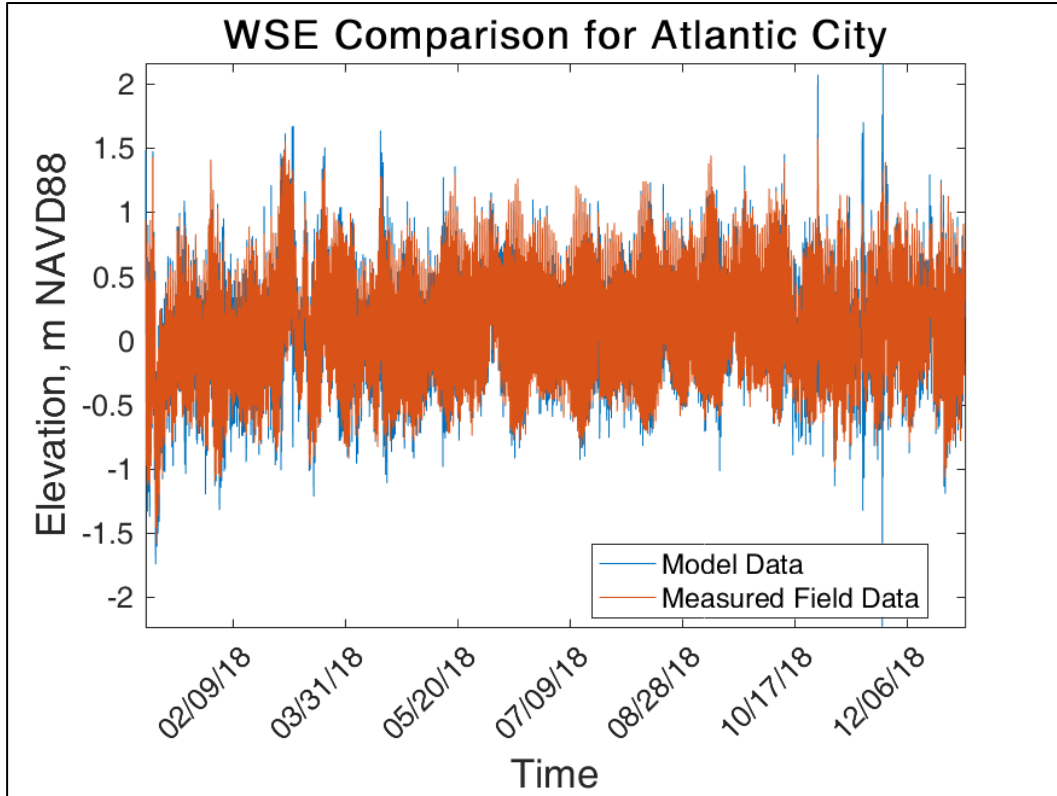


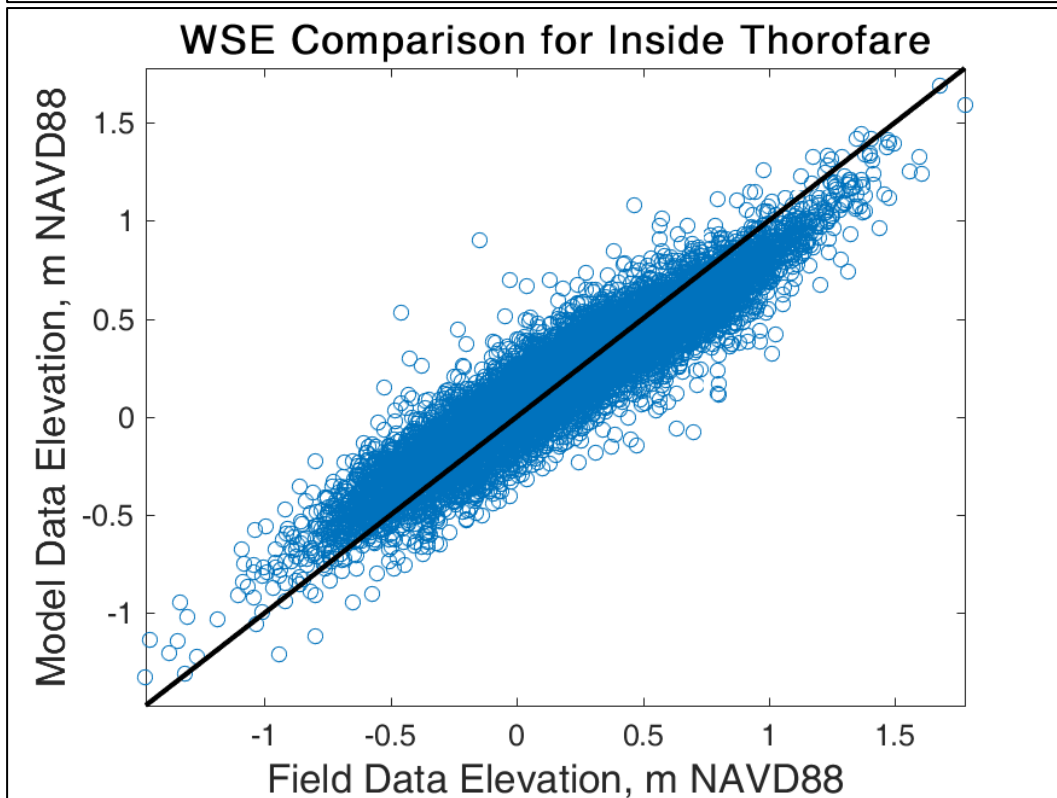
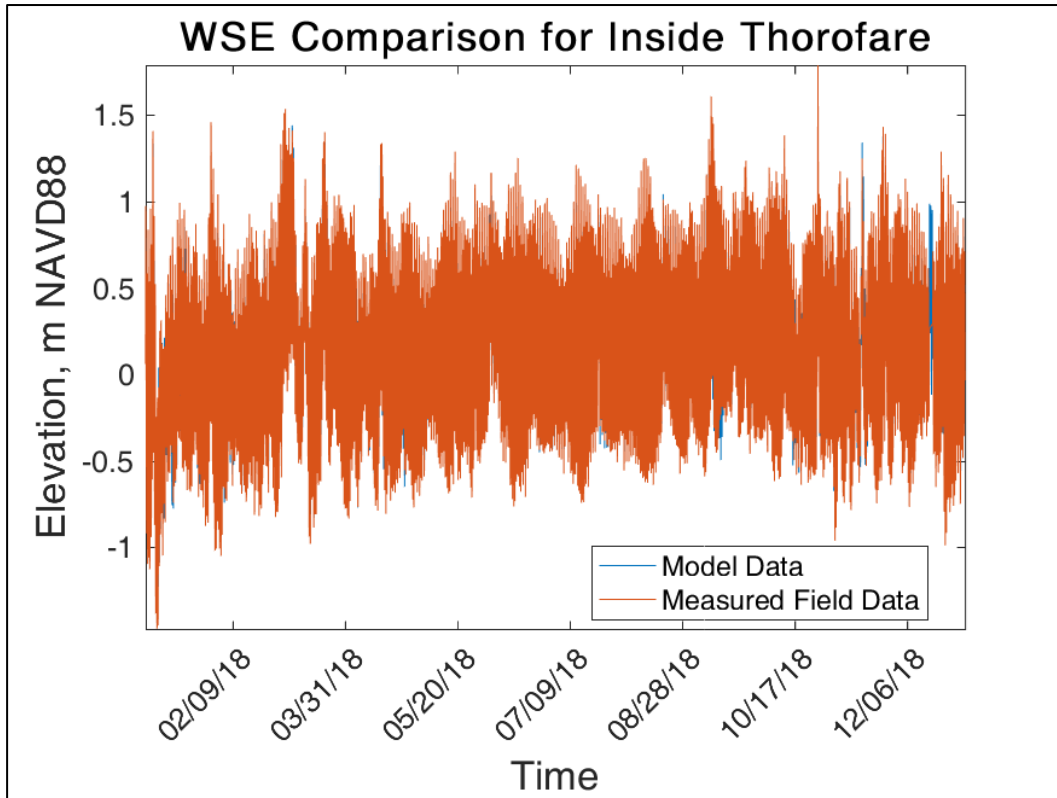


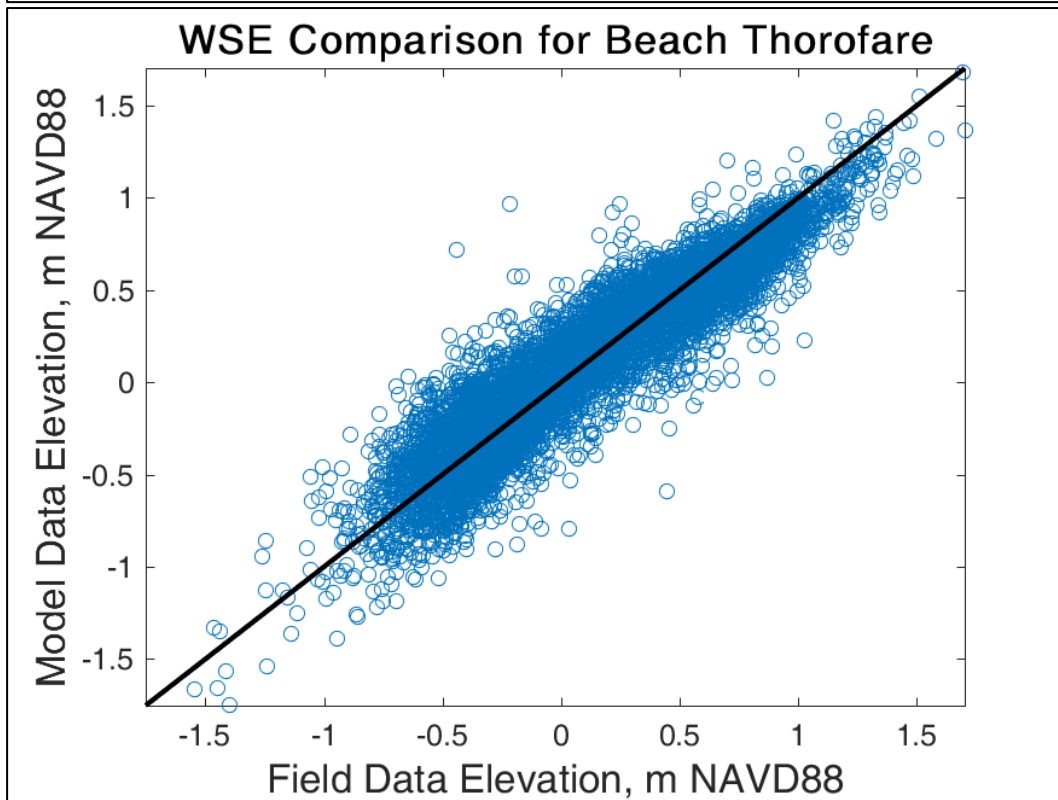
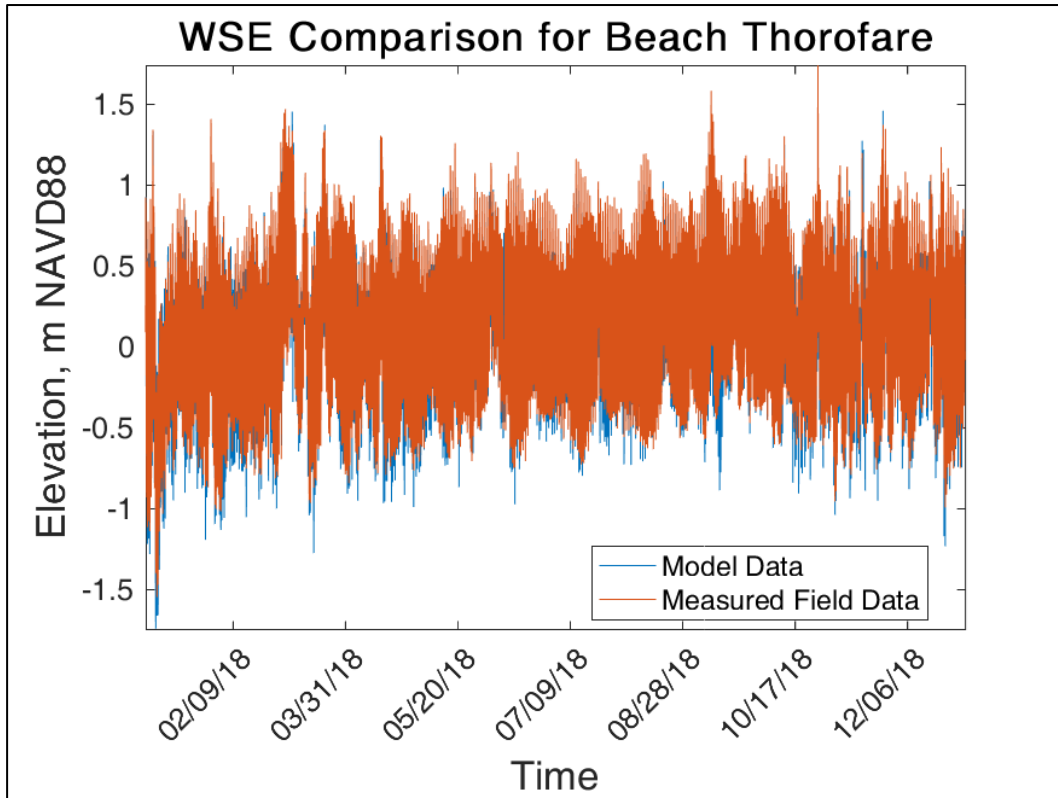


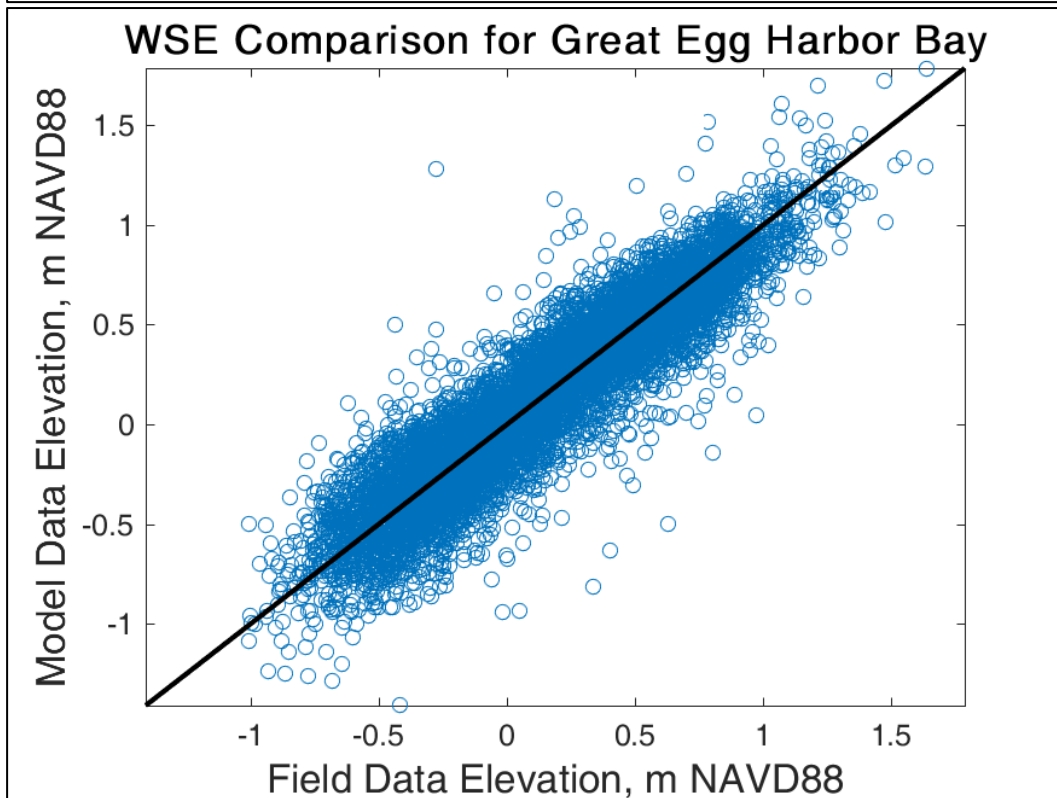
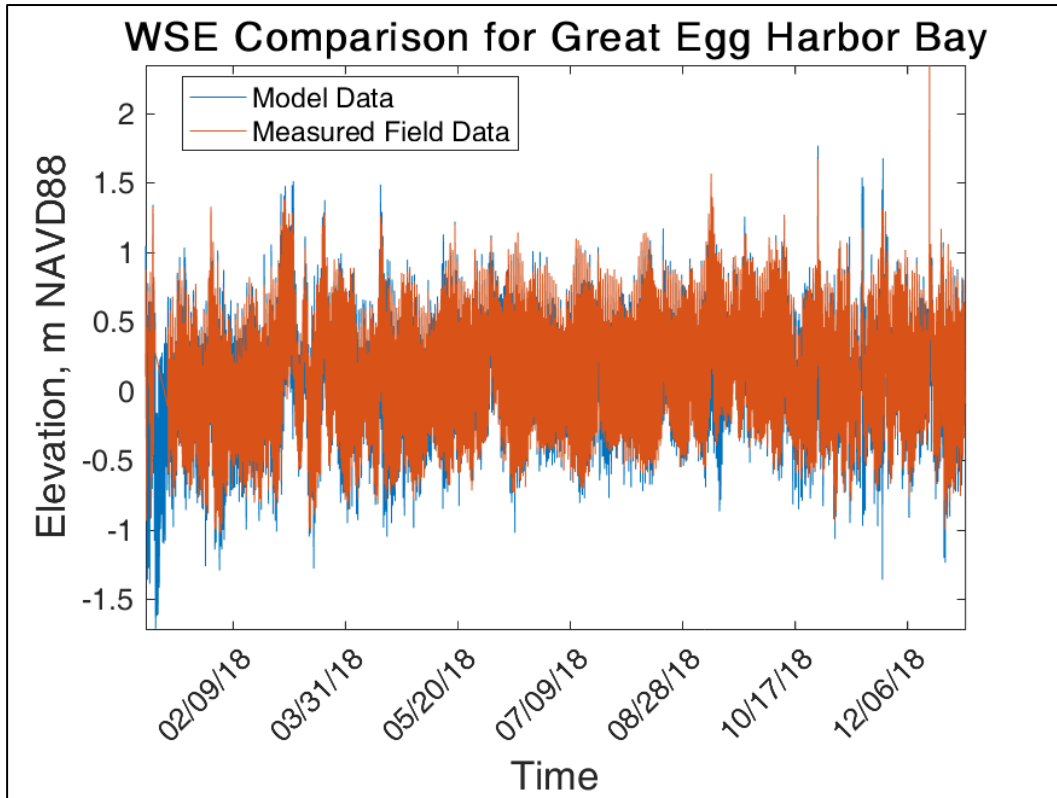


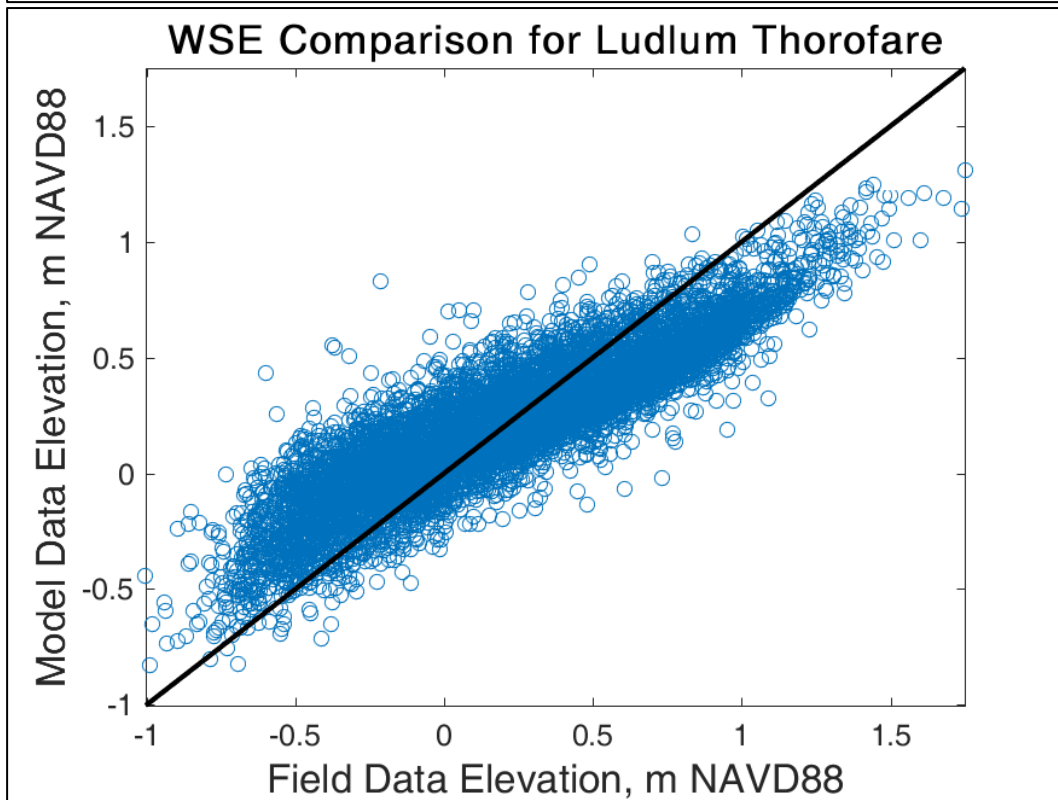
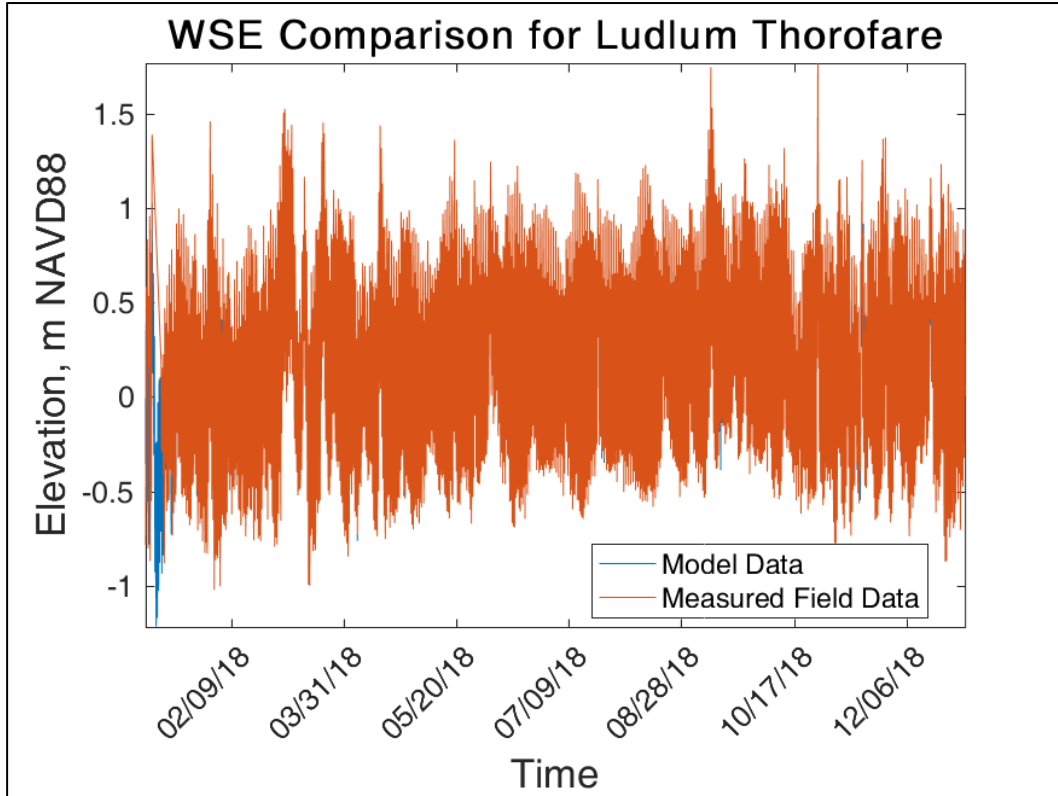


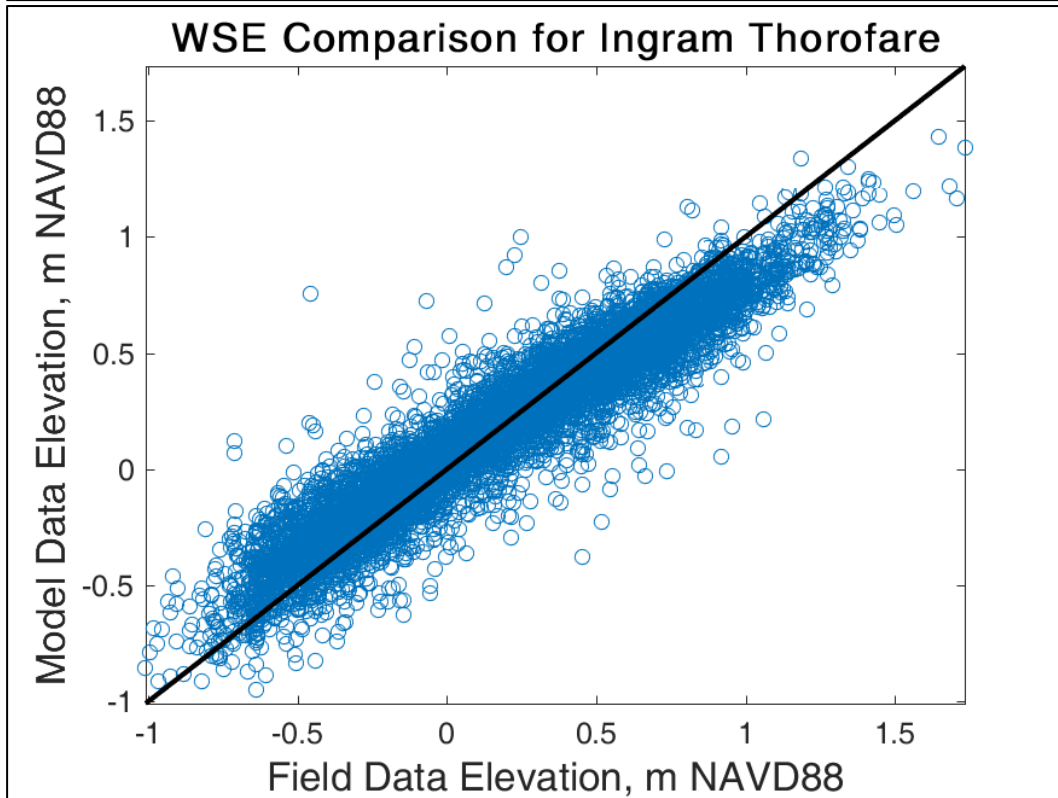
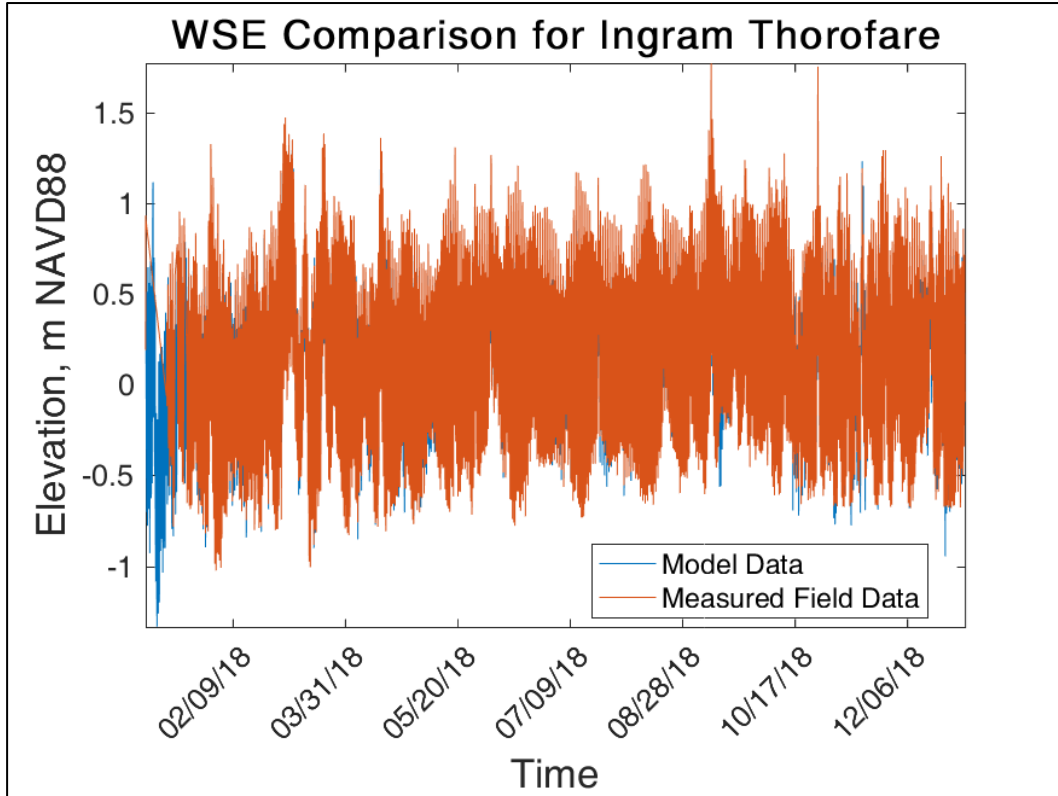


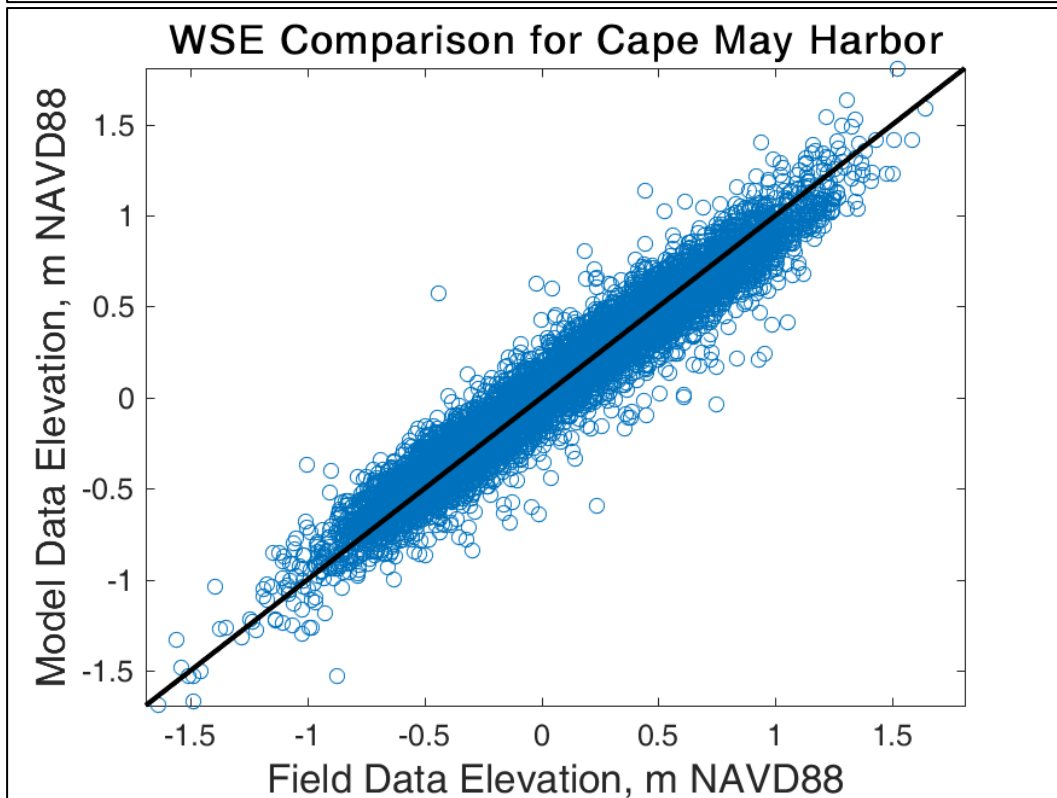
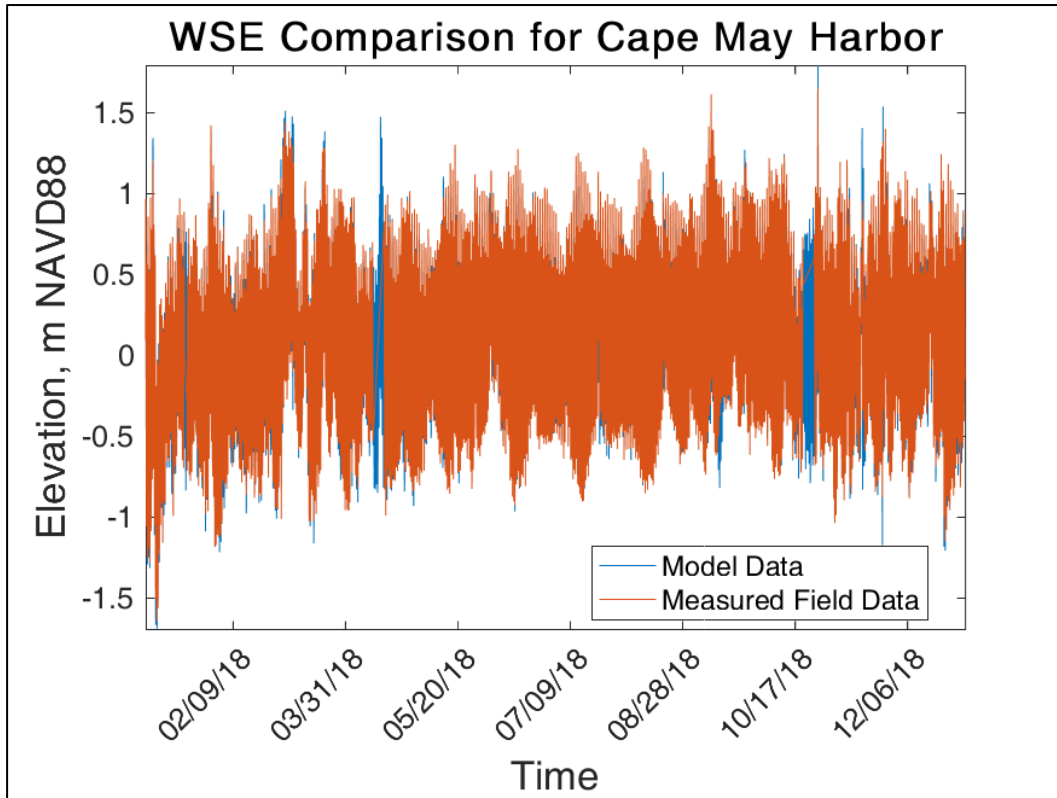




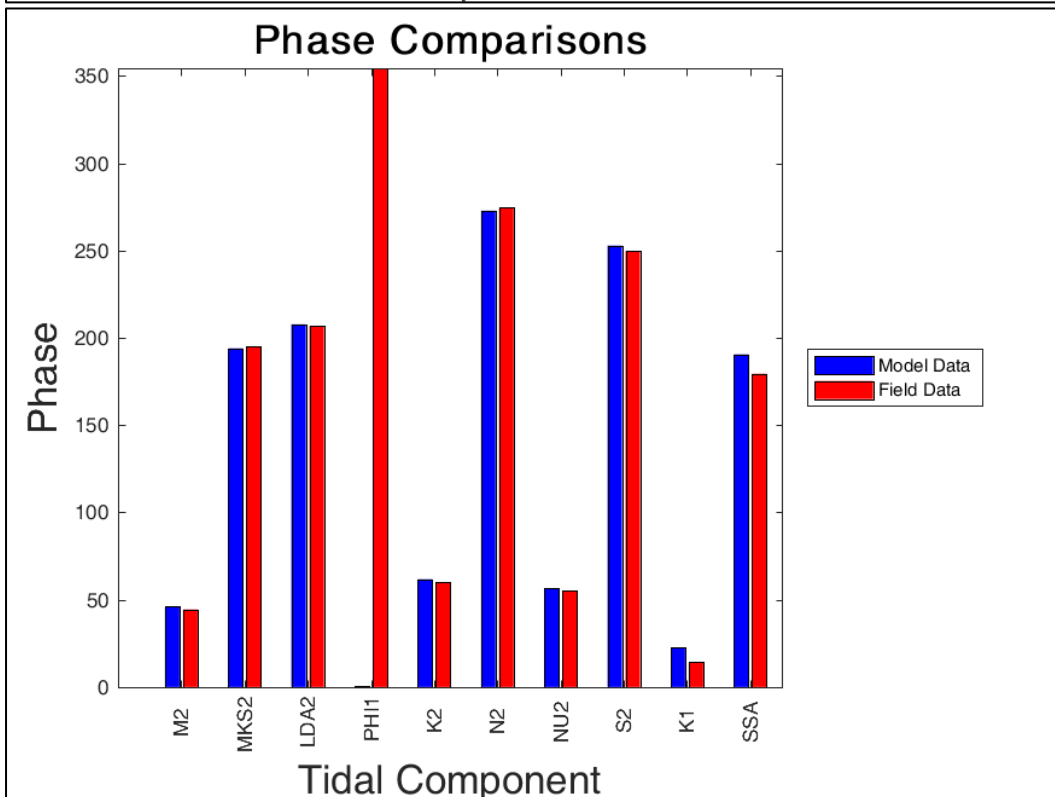
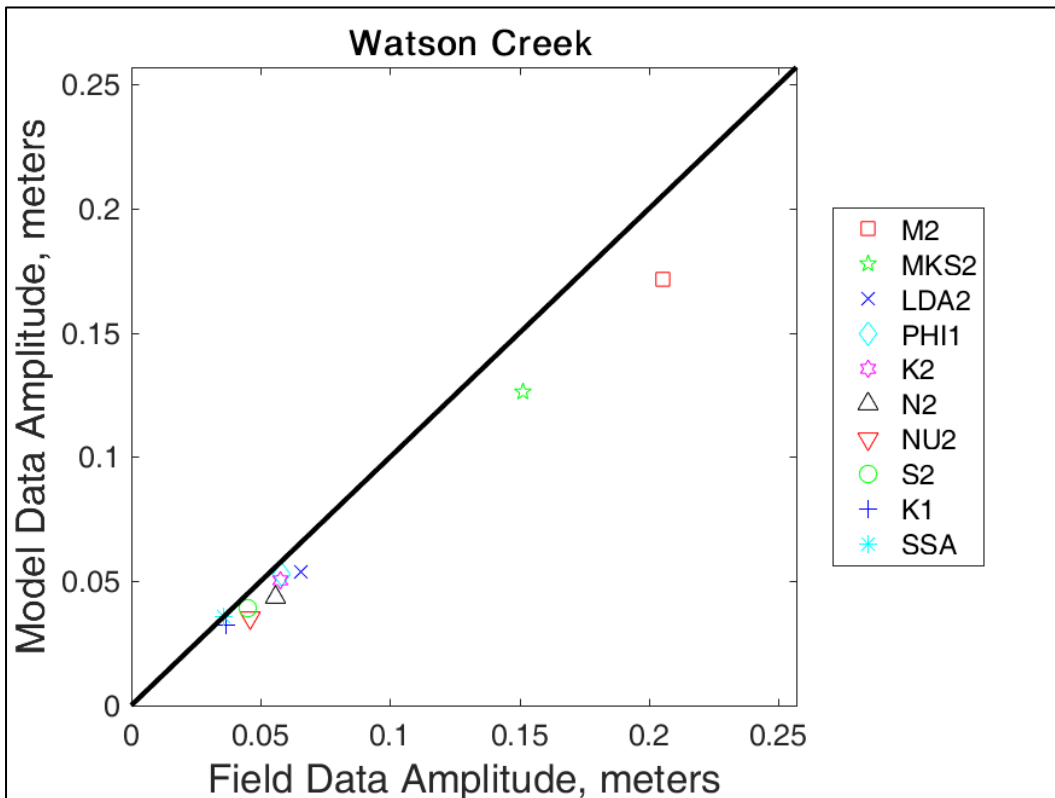


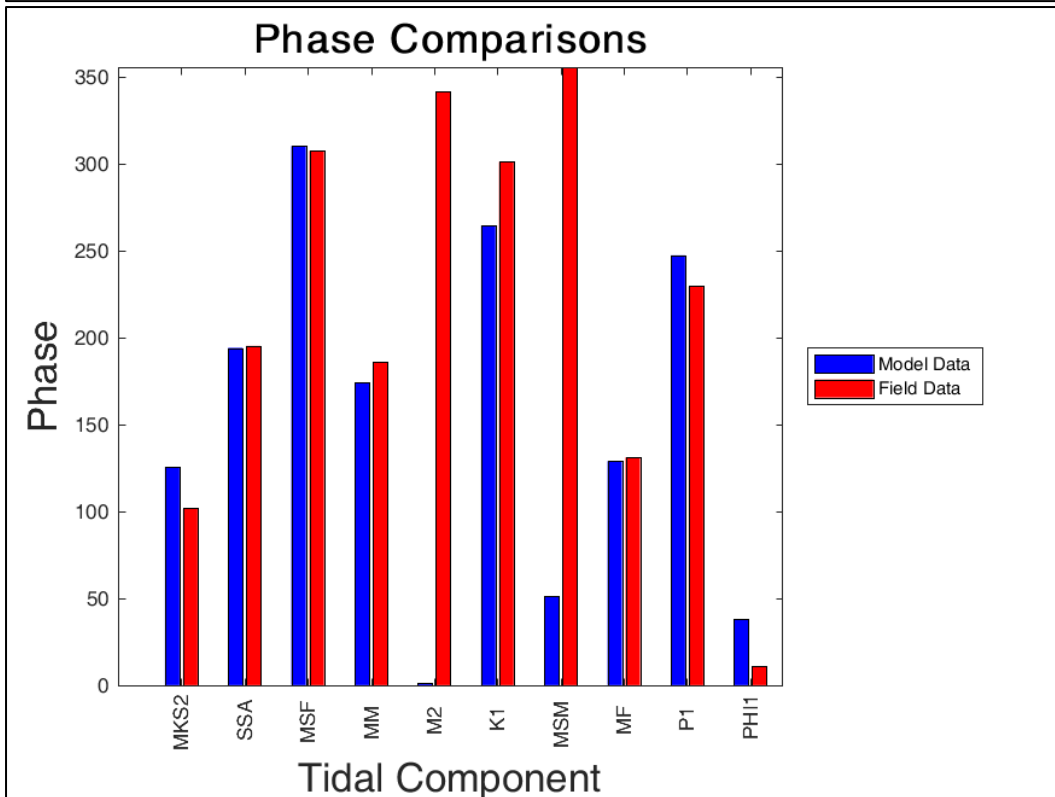
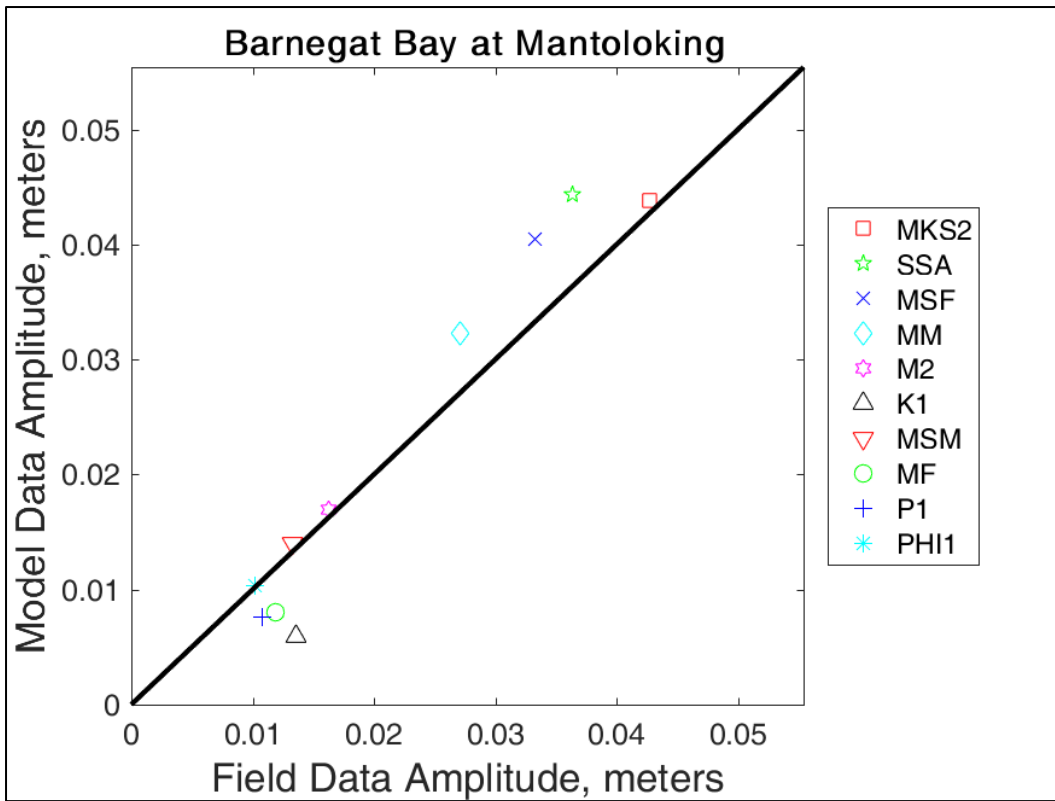


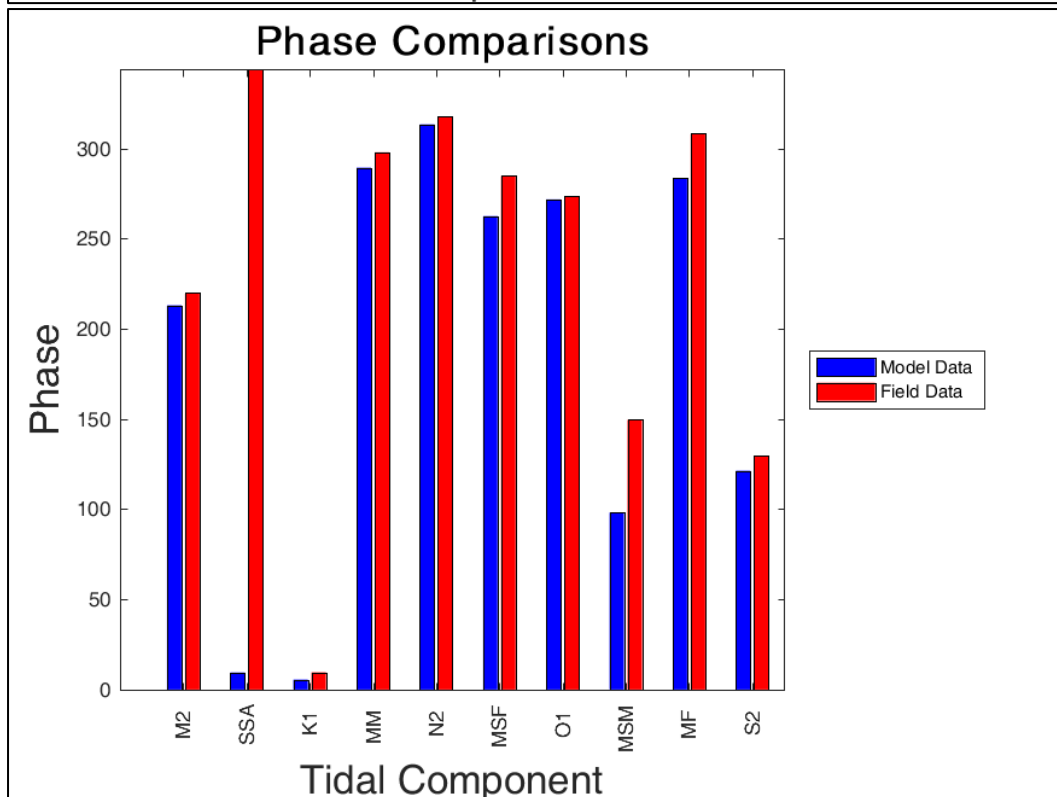
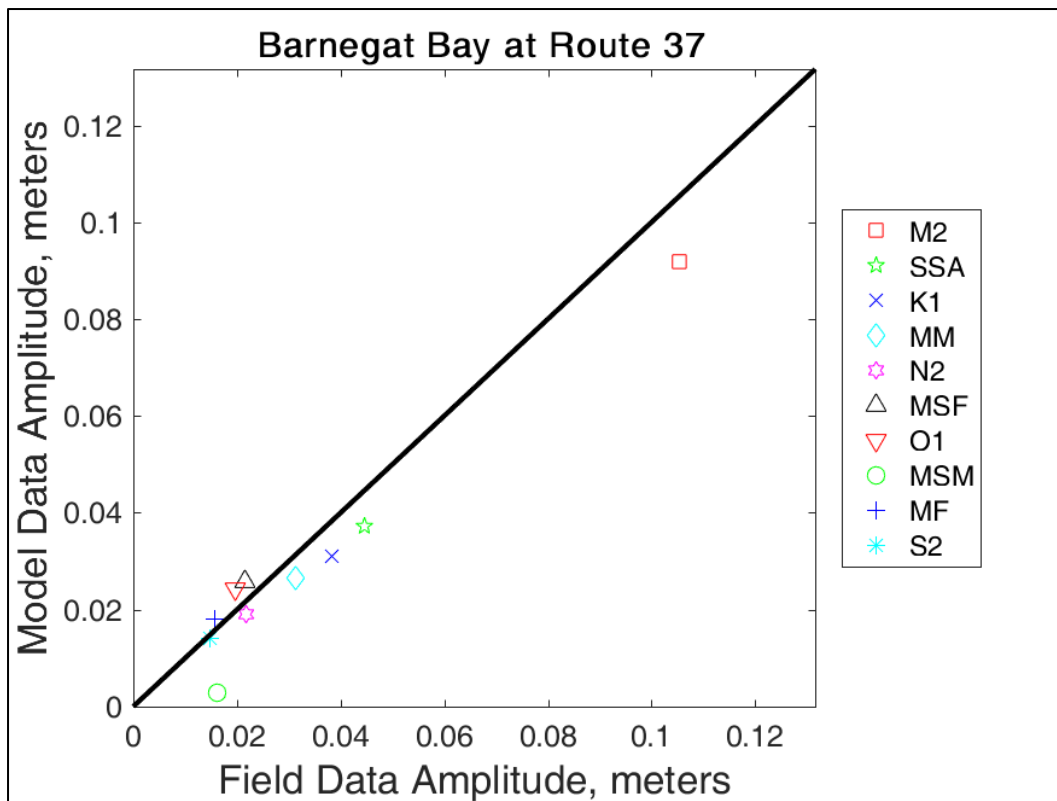


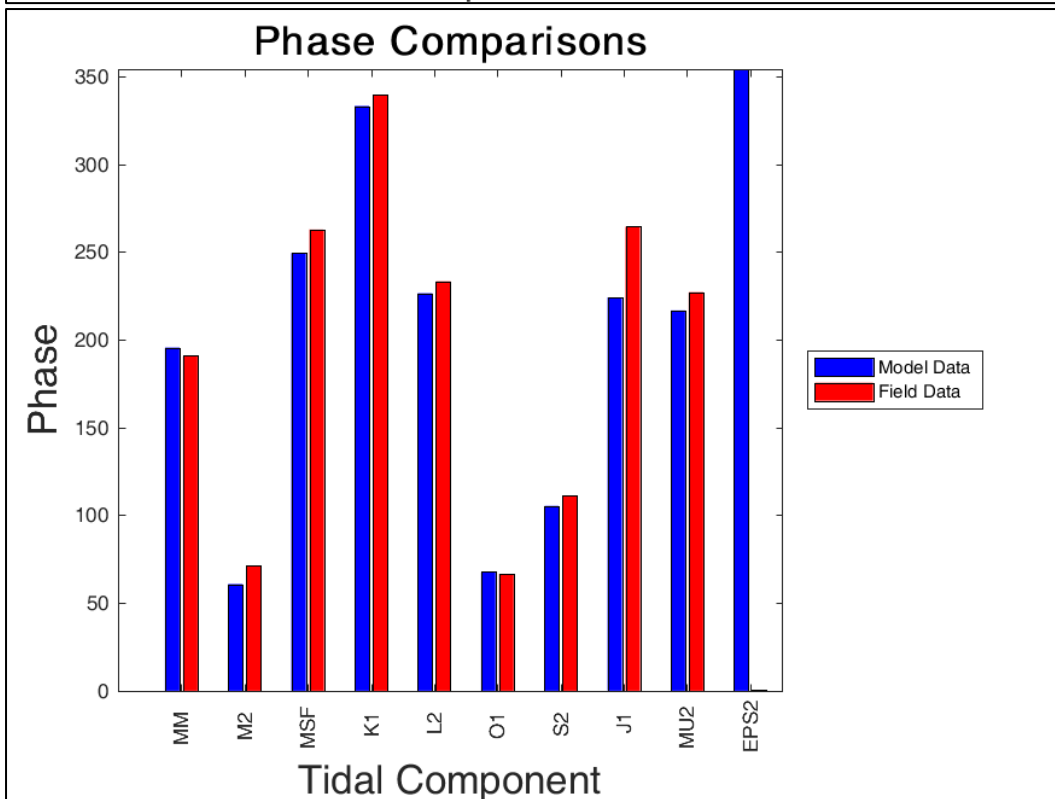
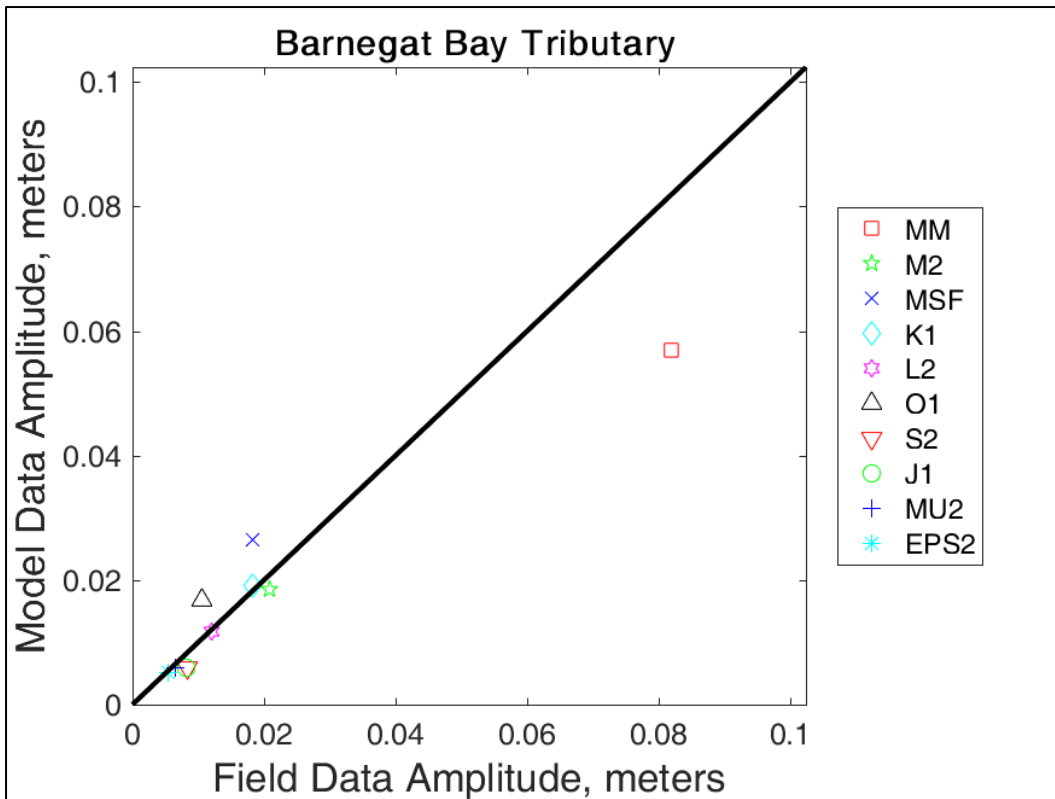


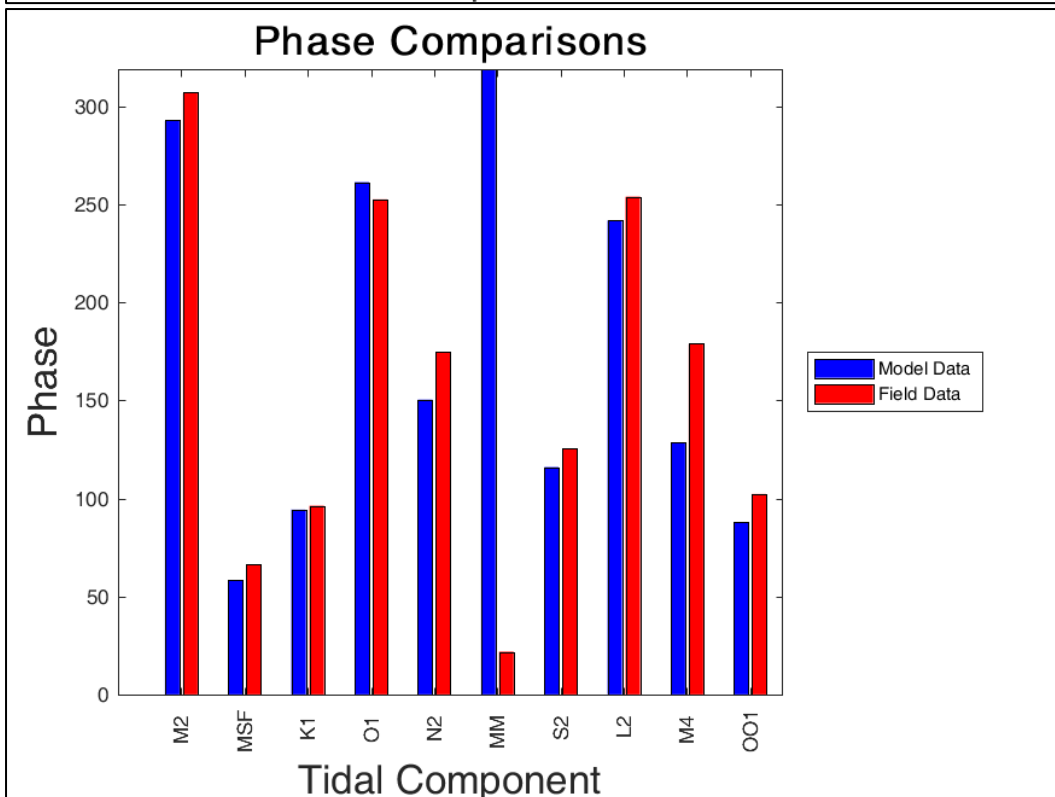
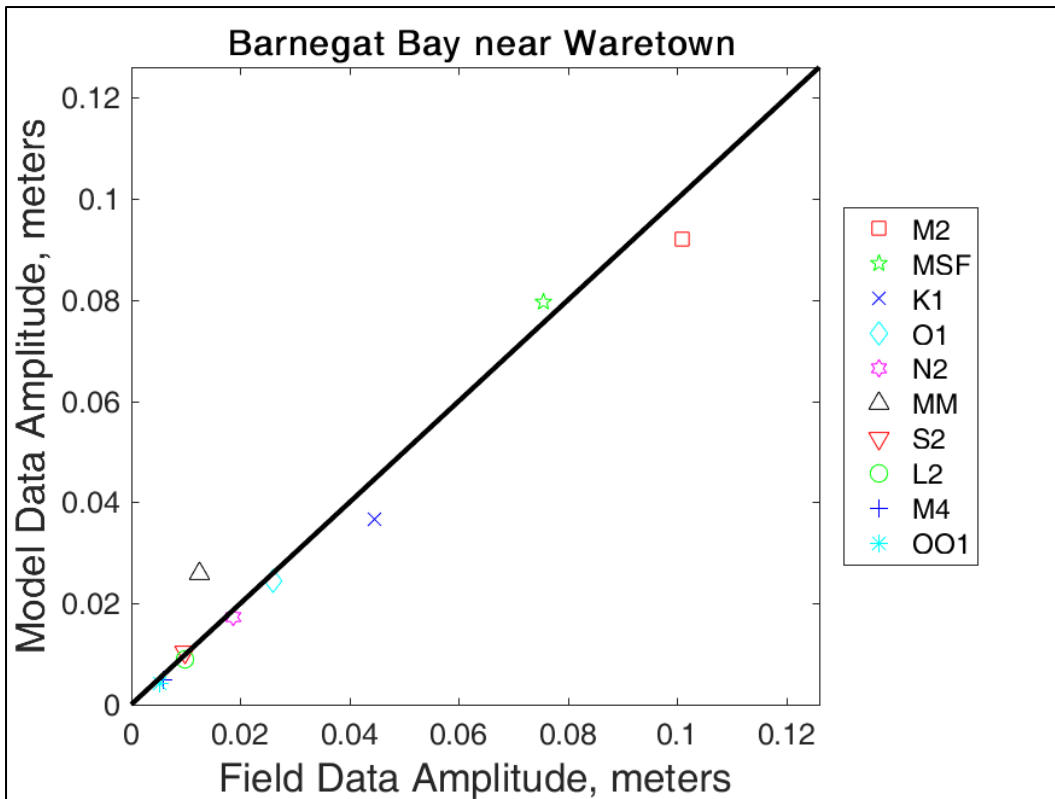
Harmonic Analysis

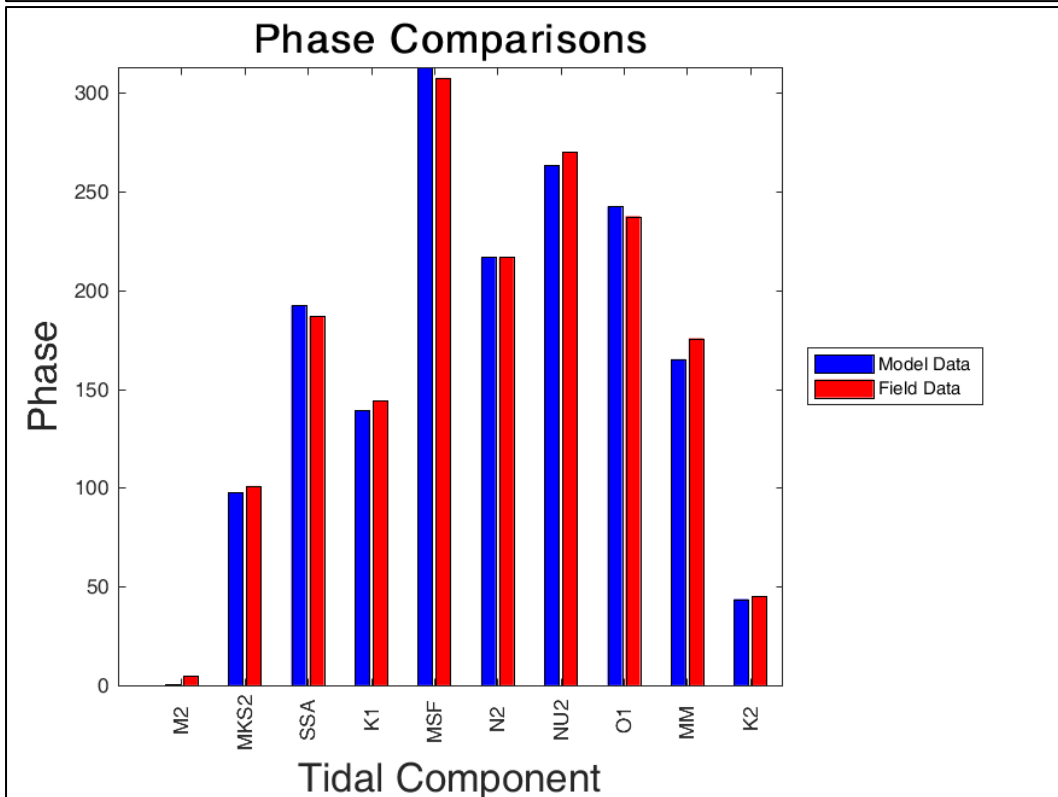
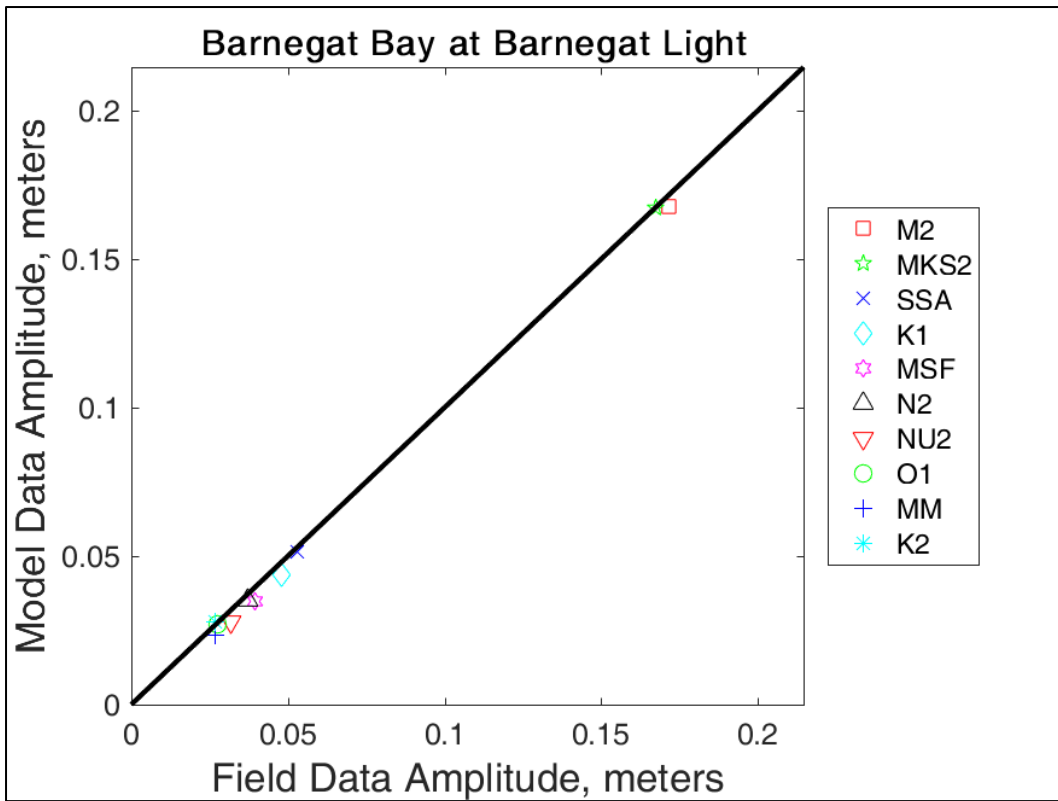


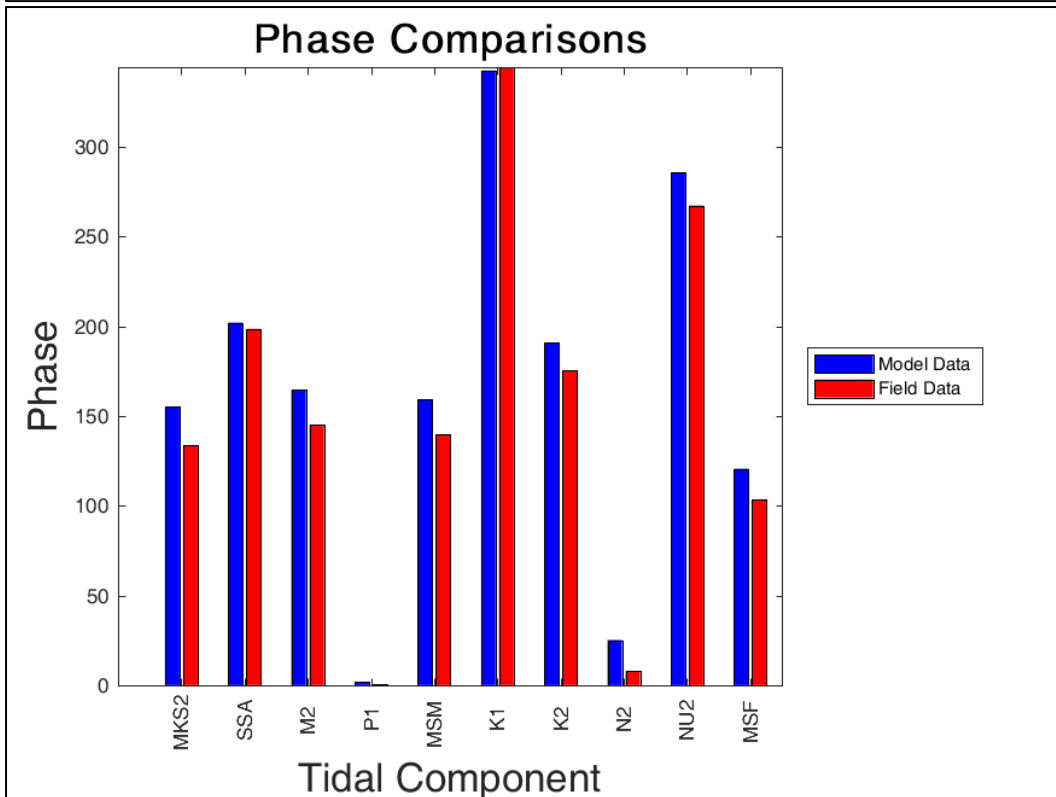
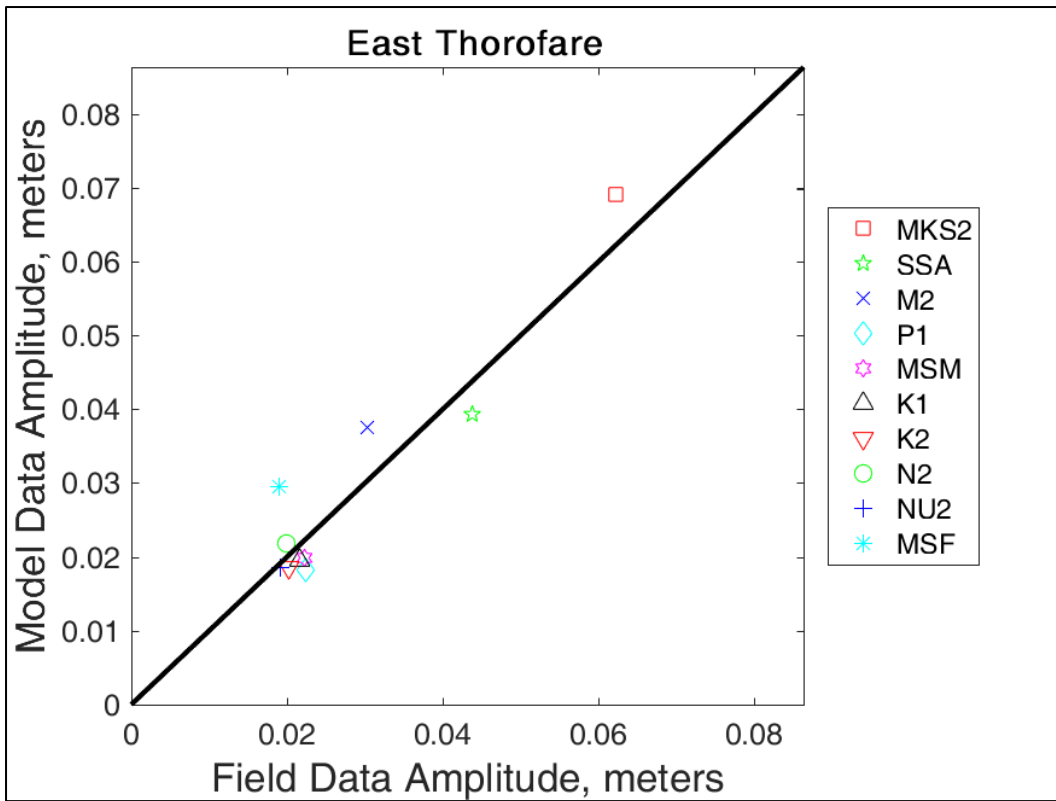


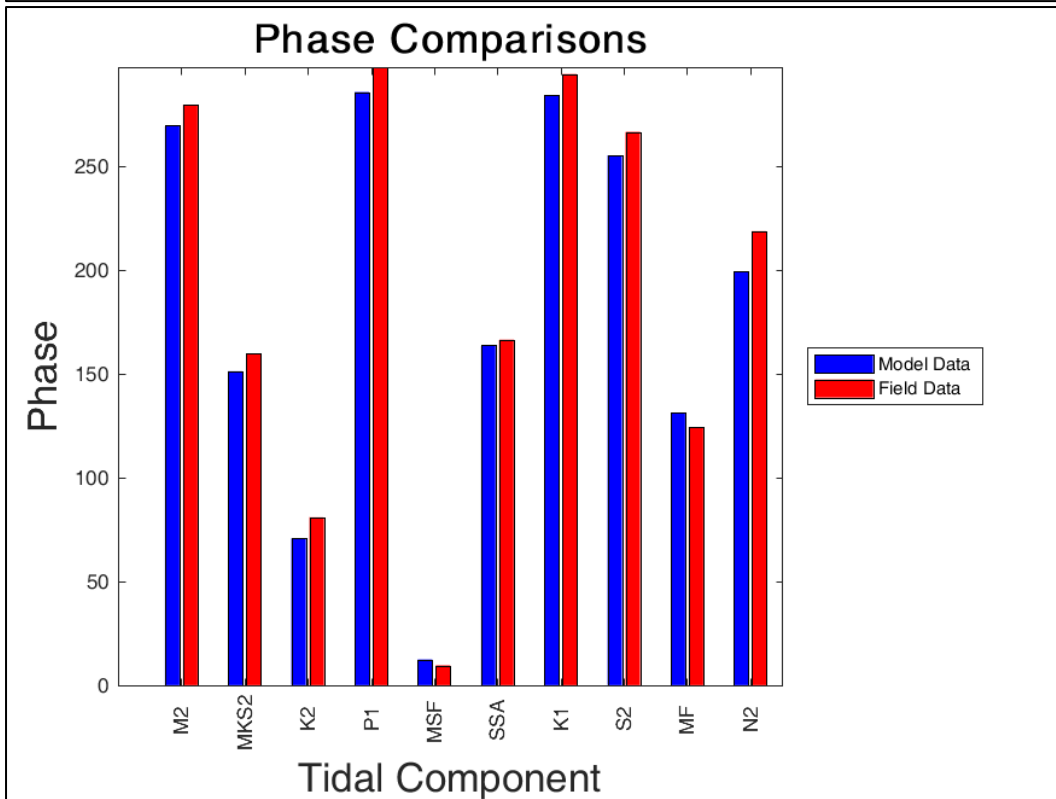
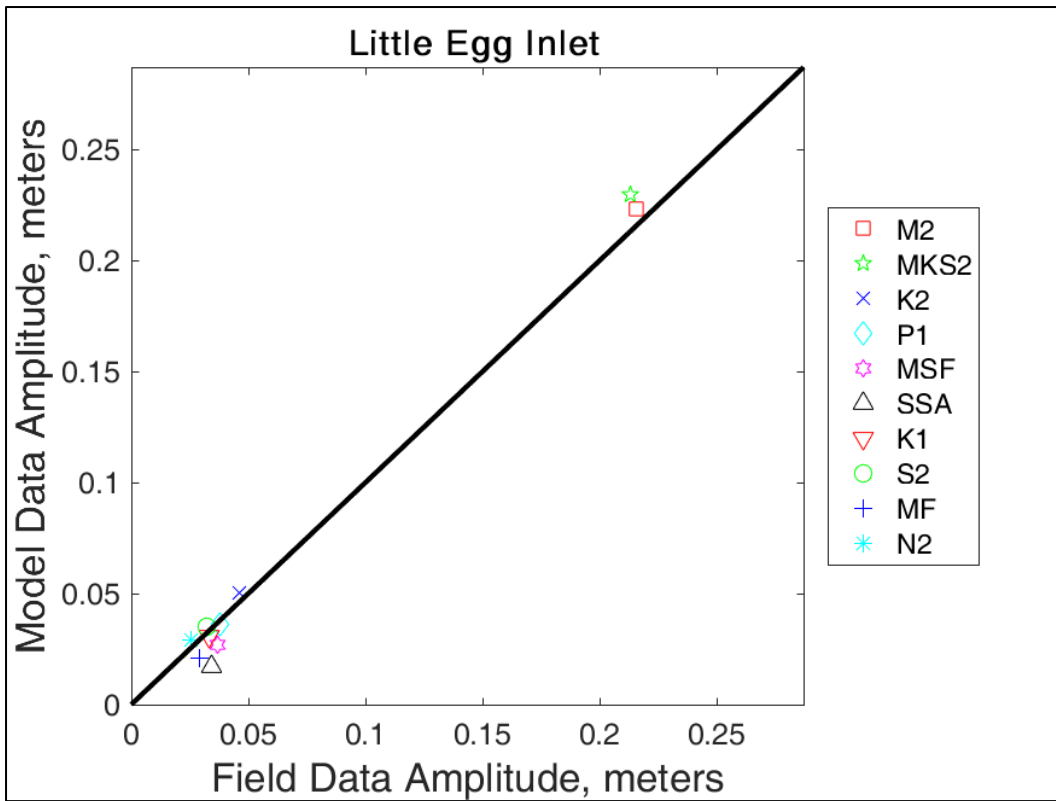


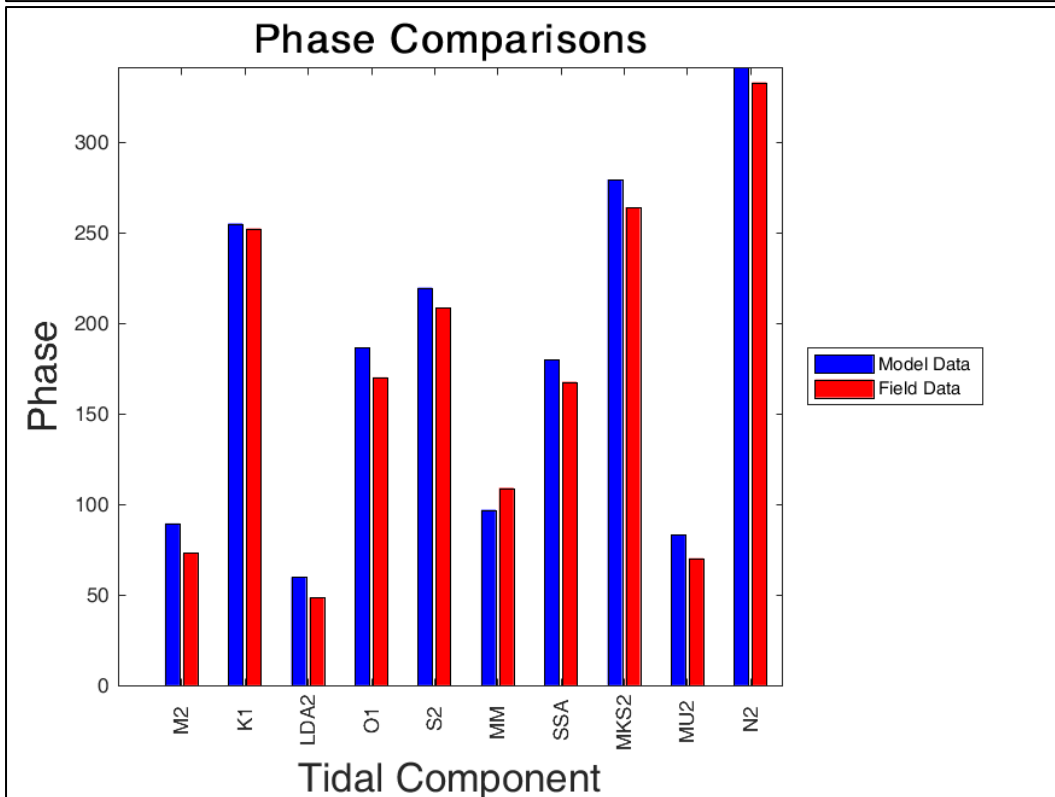
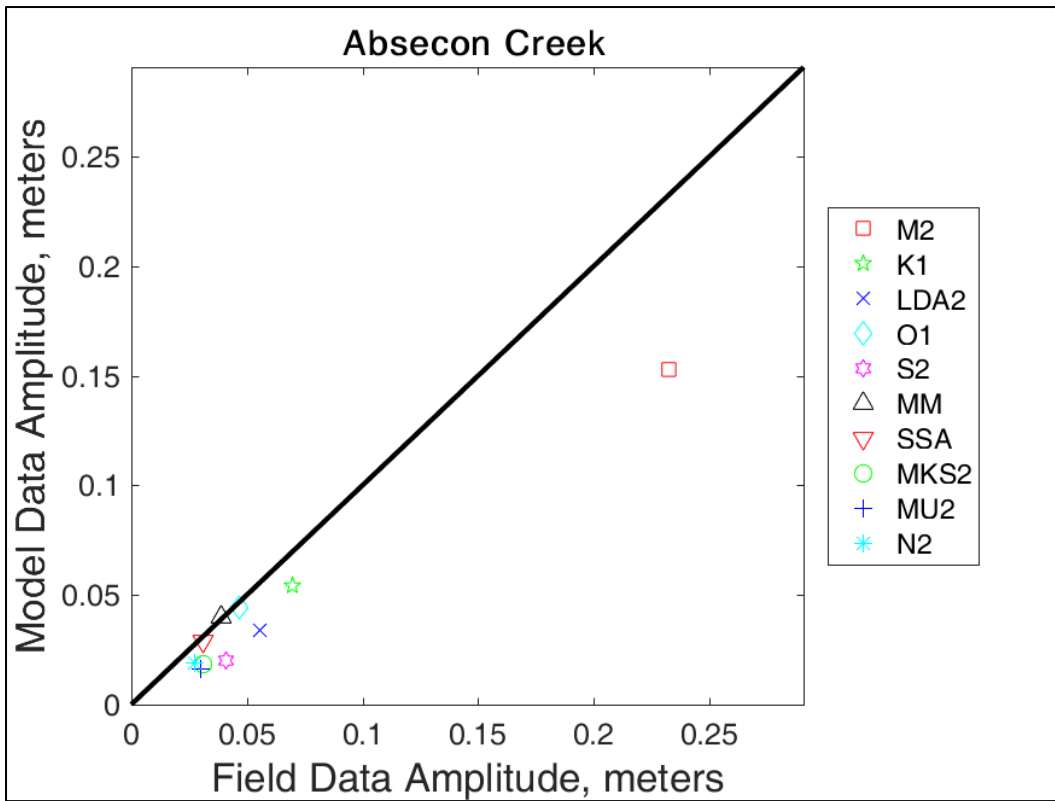


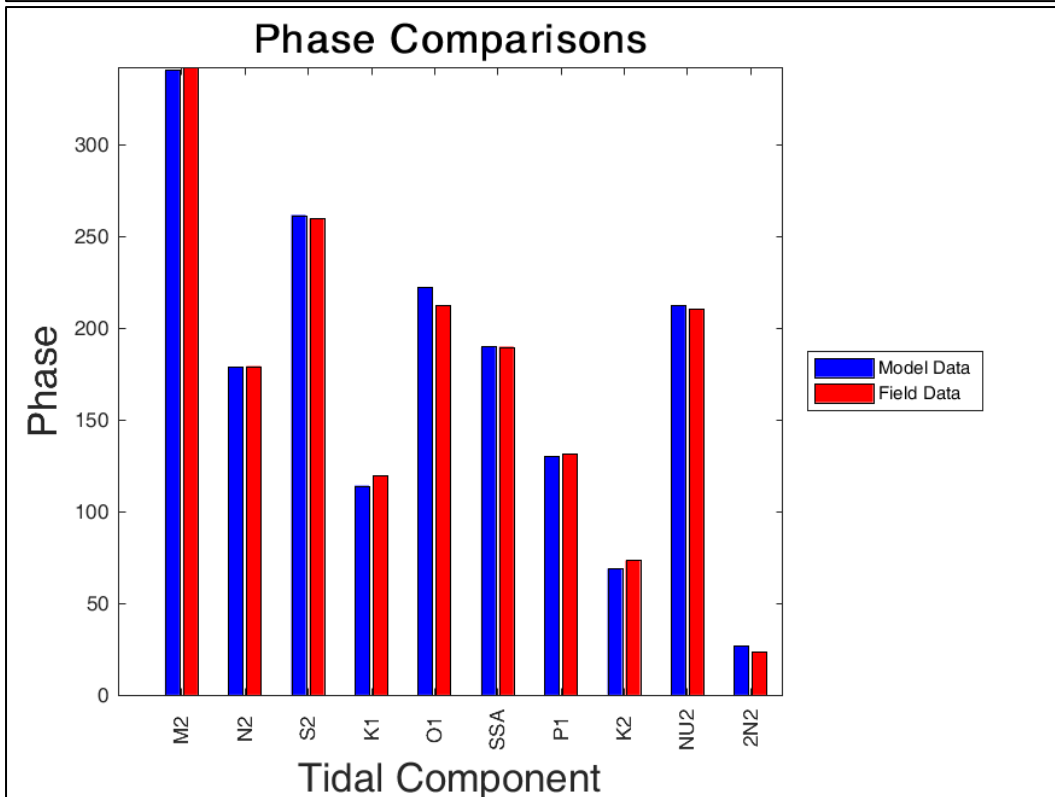
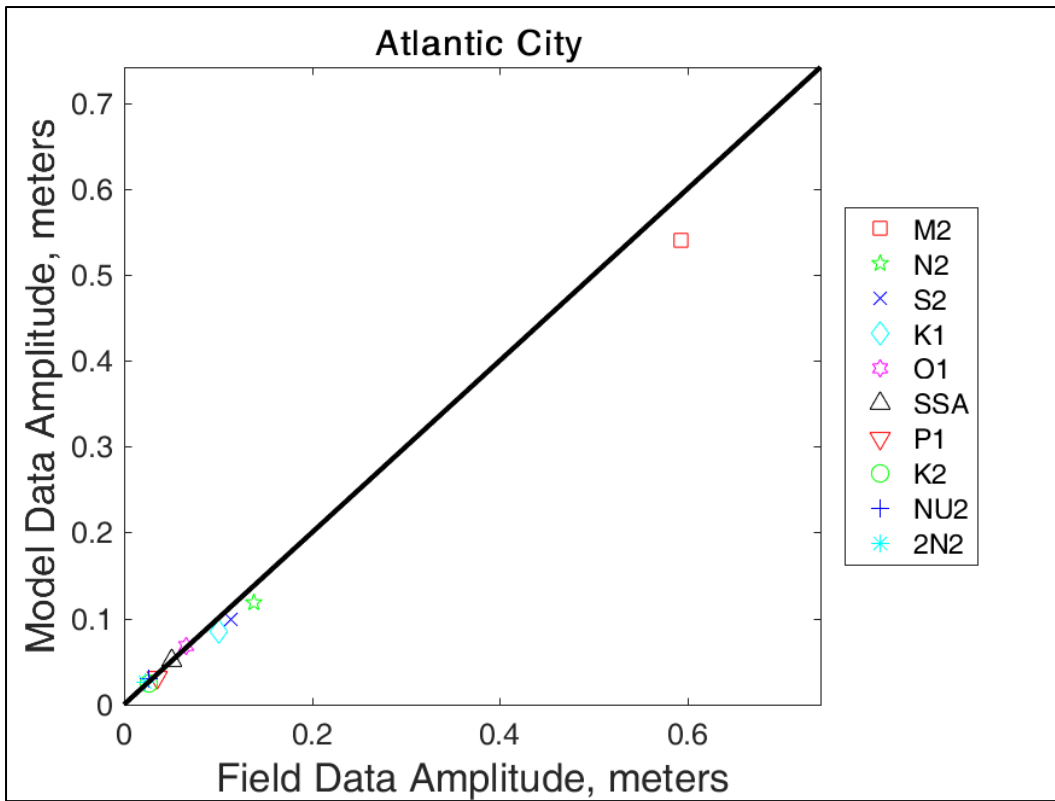


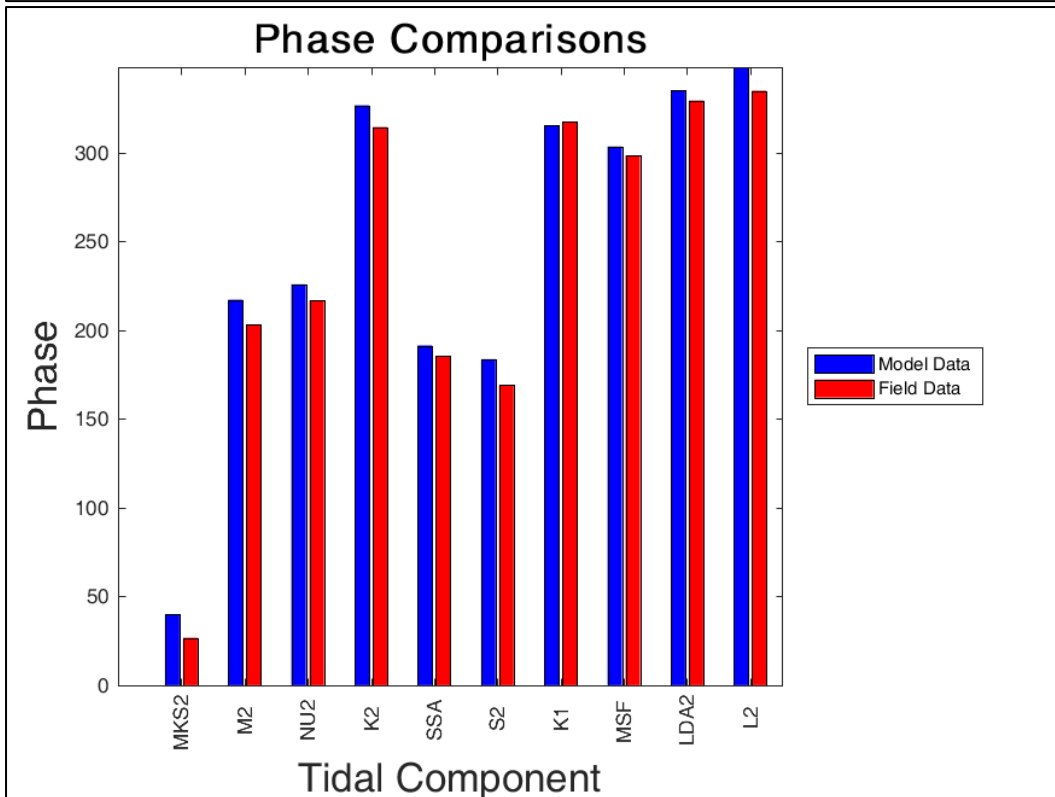
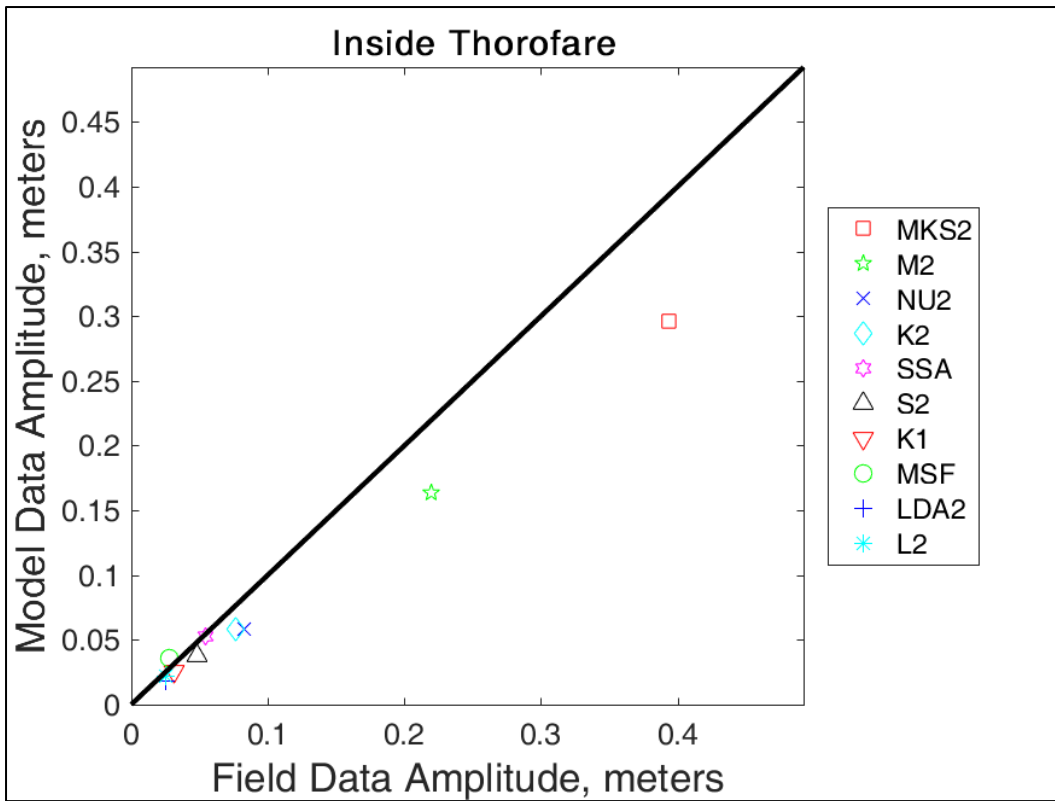


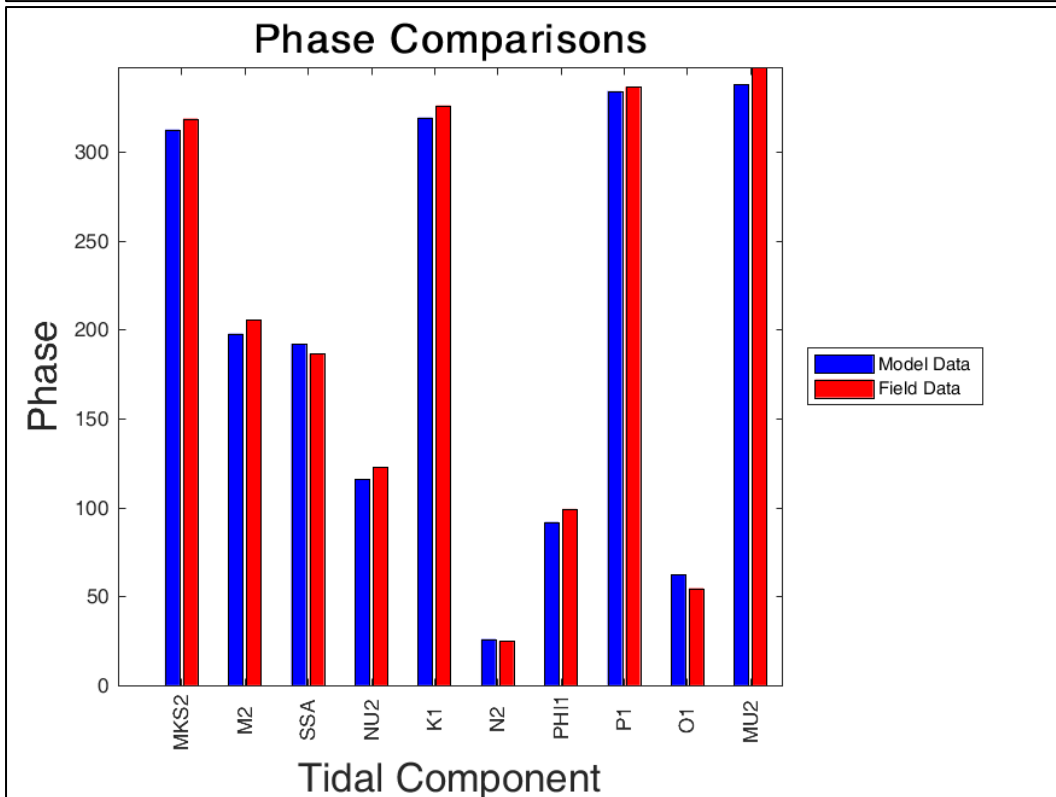
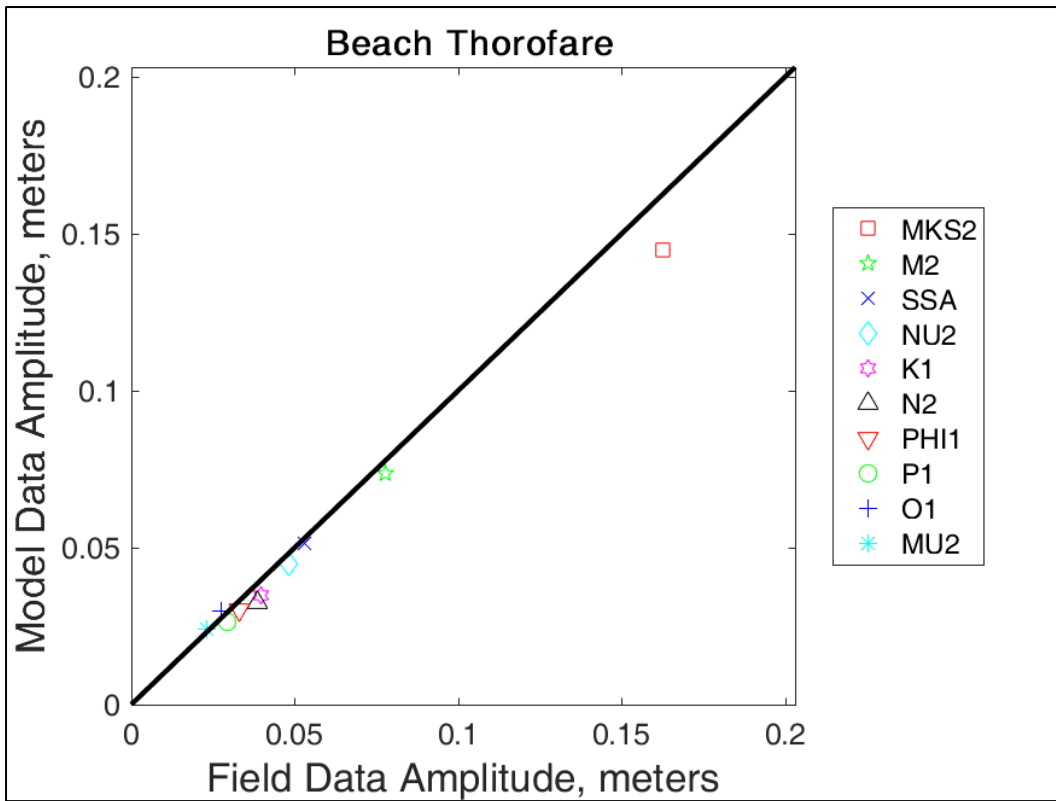


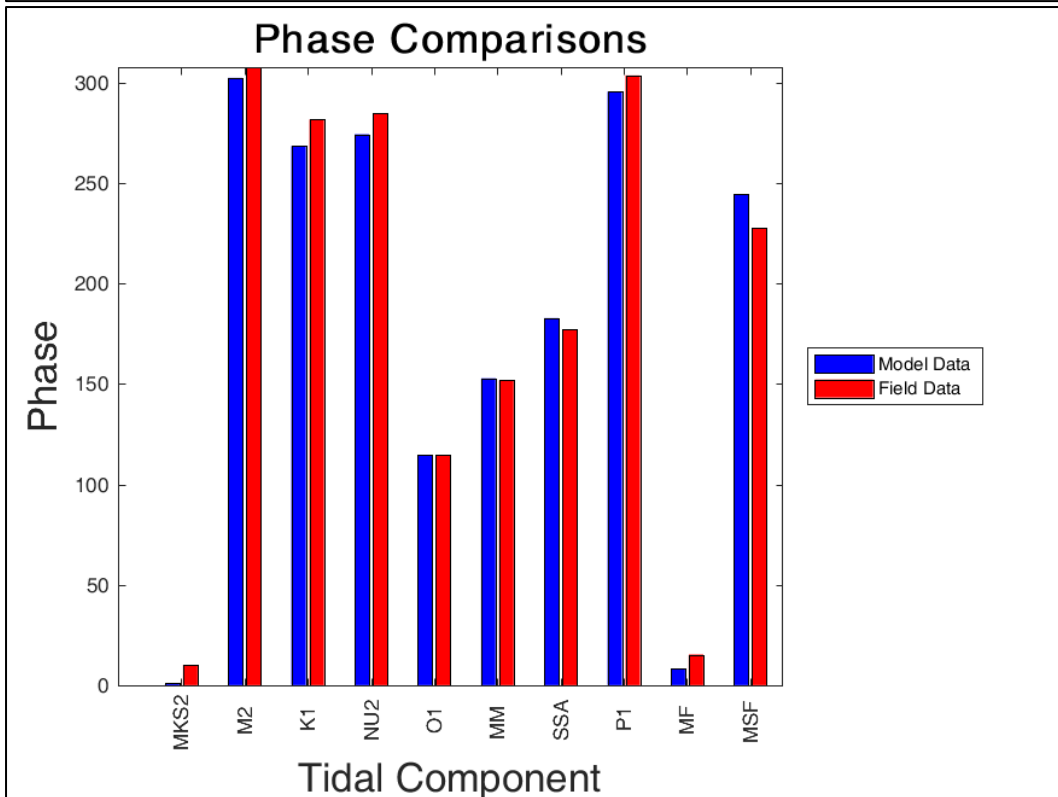
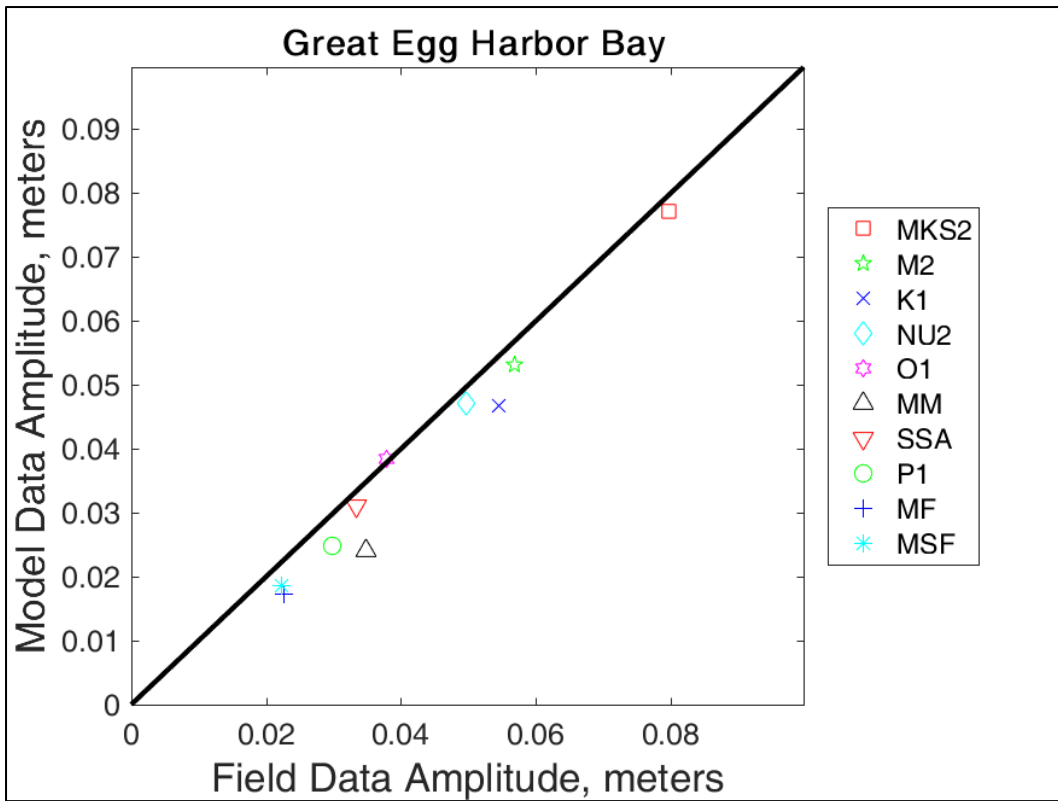


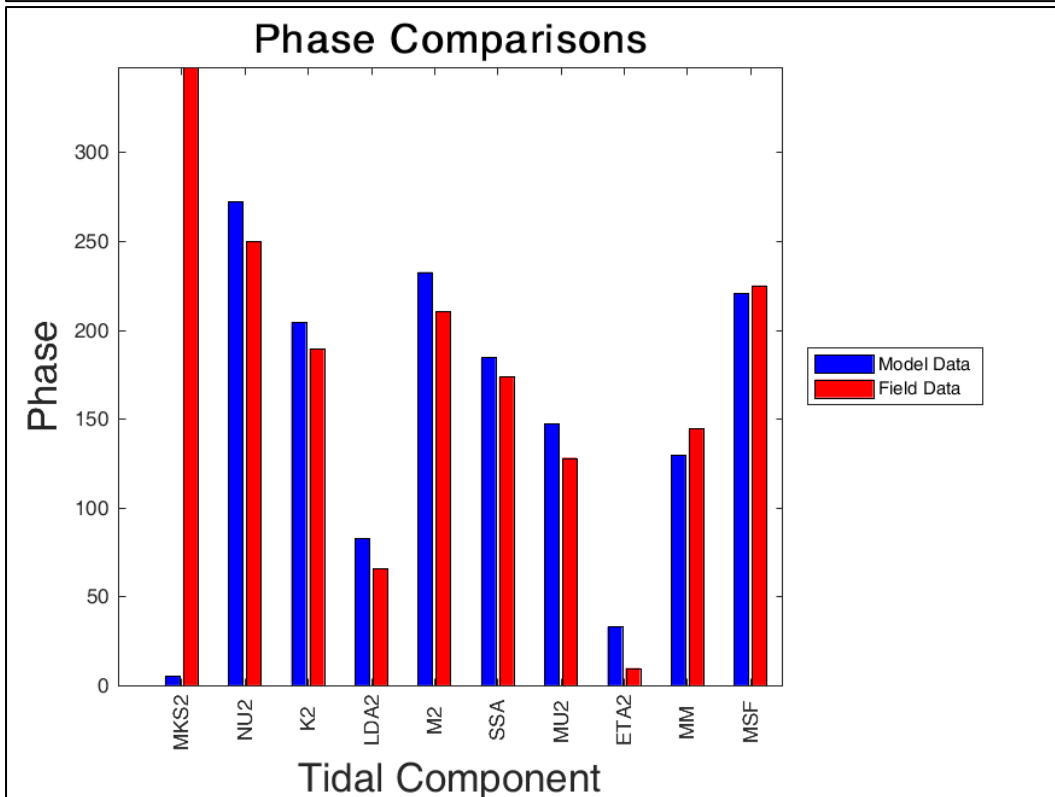
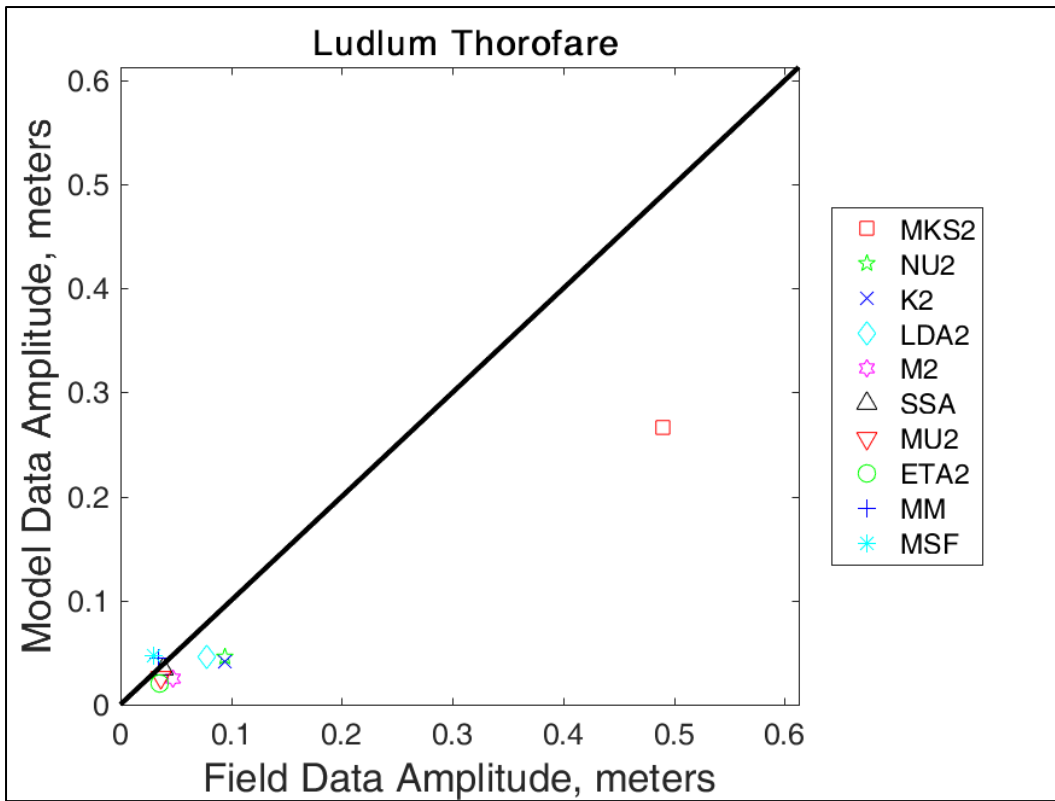


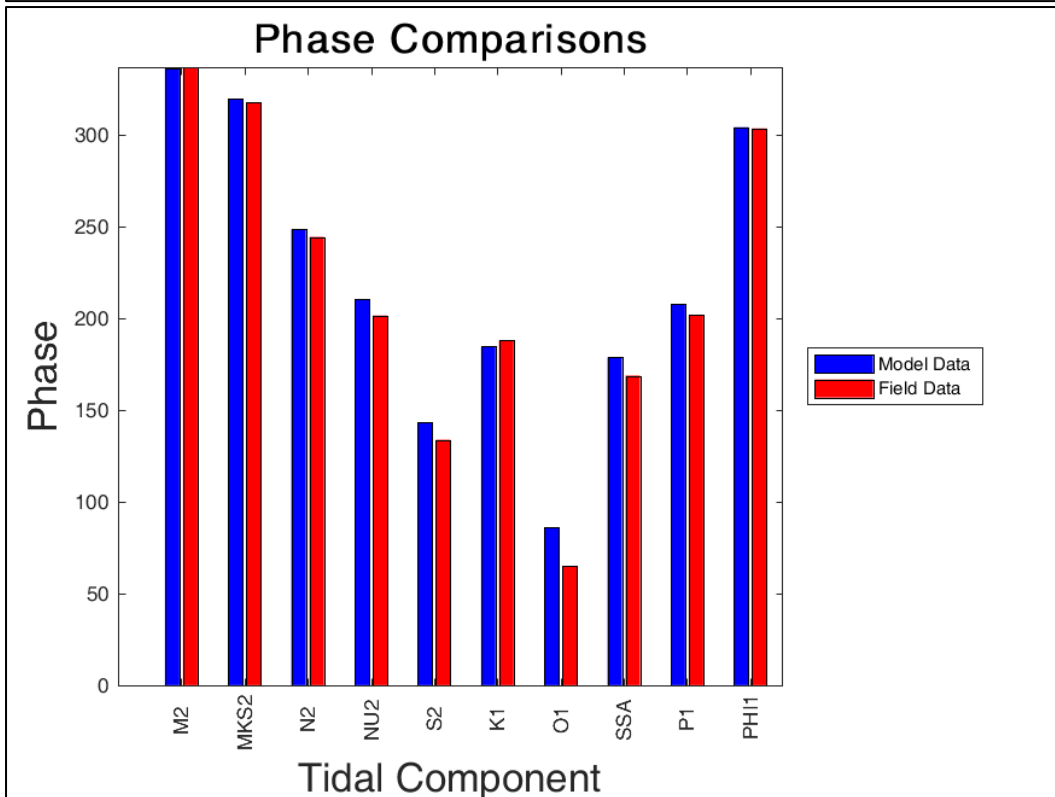
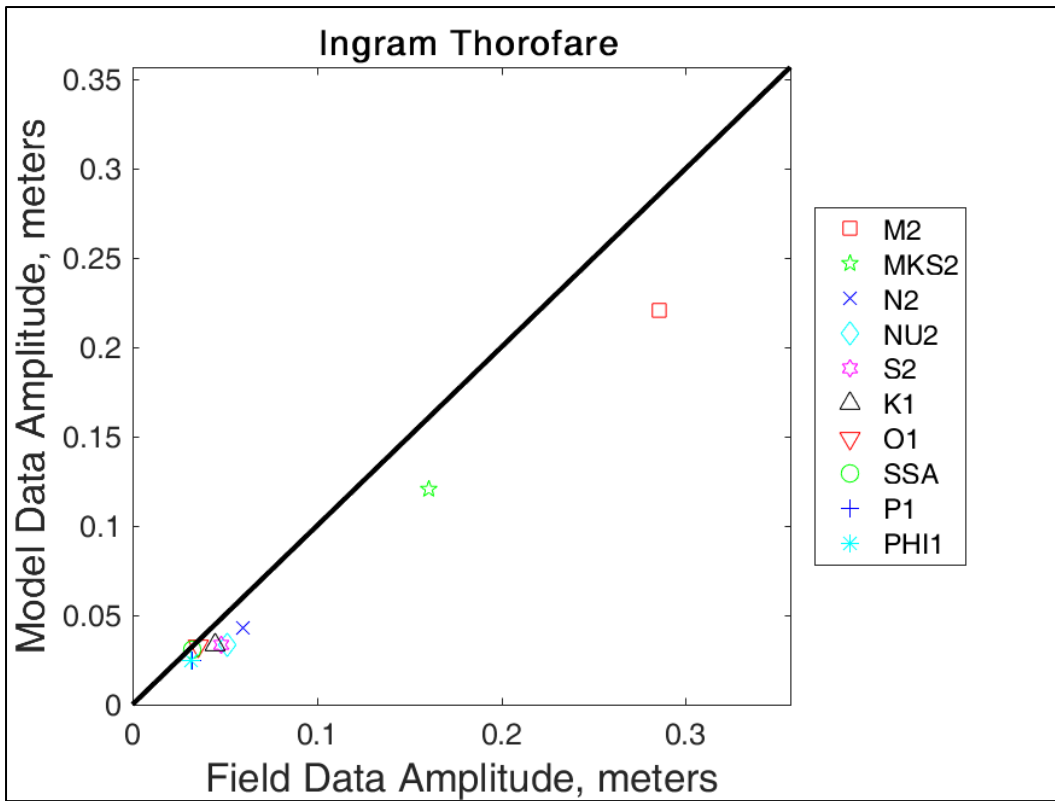


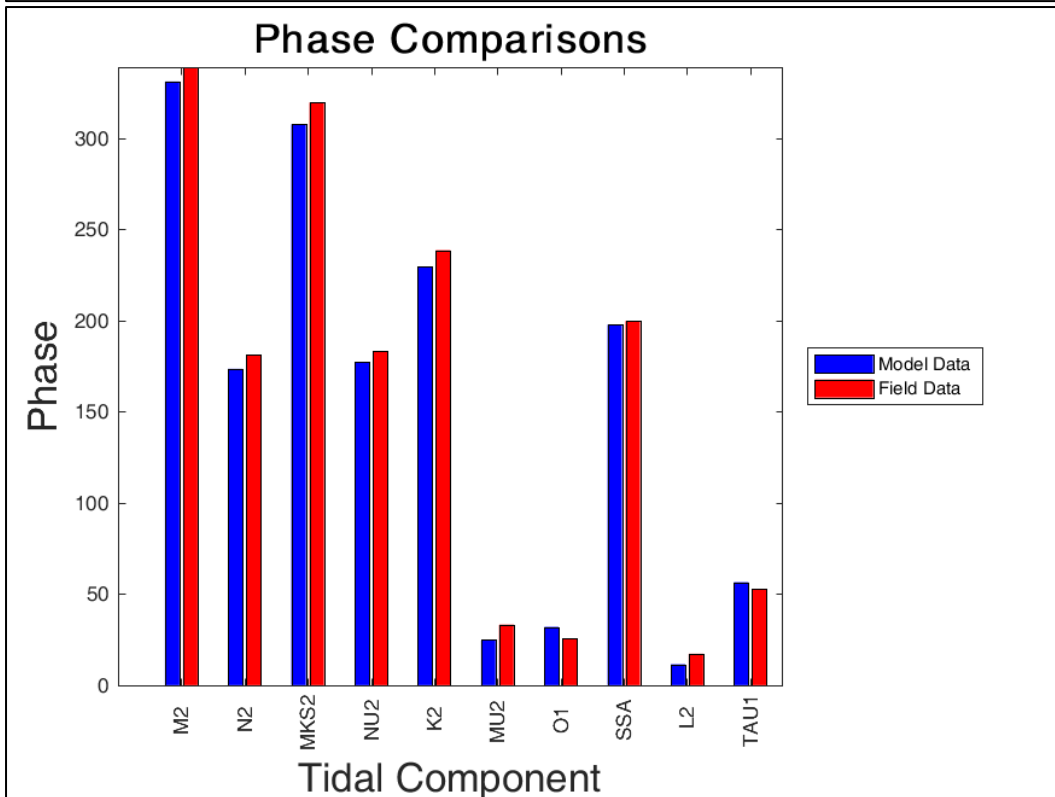
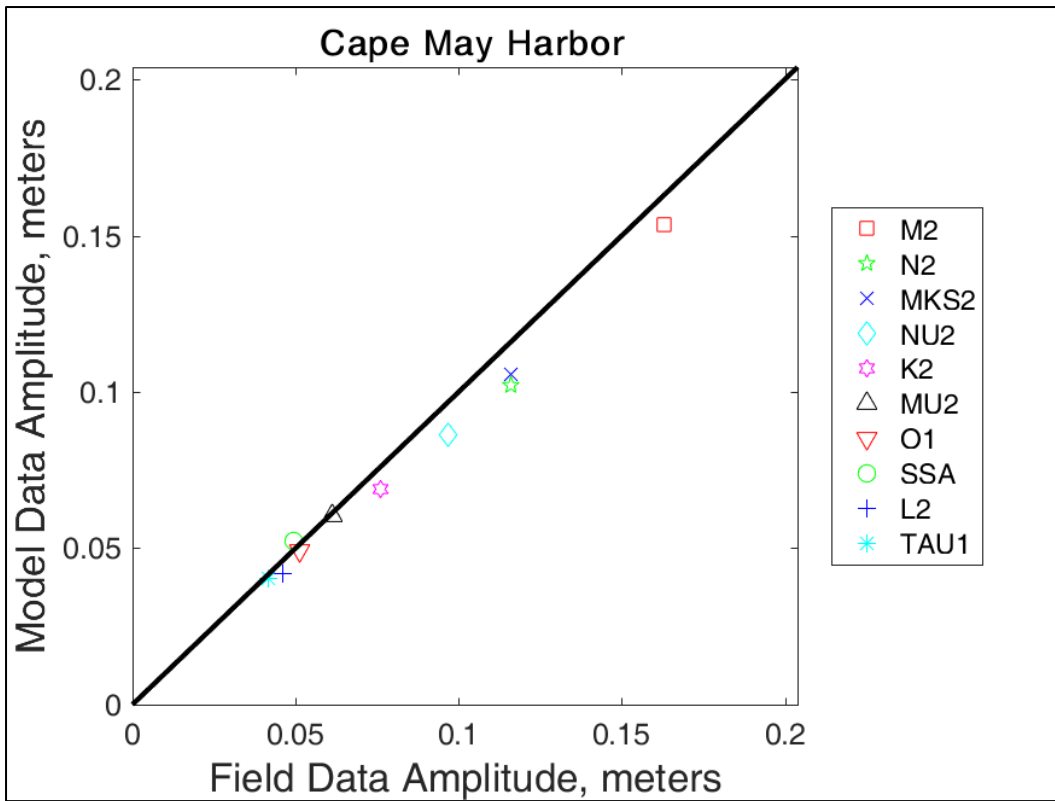




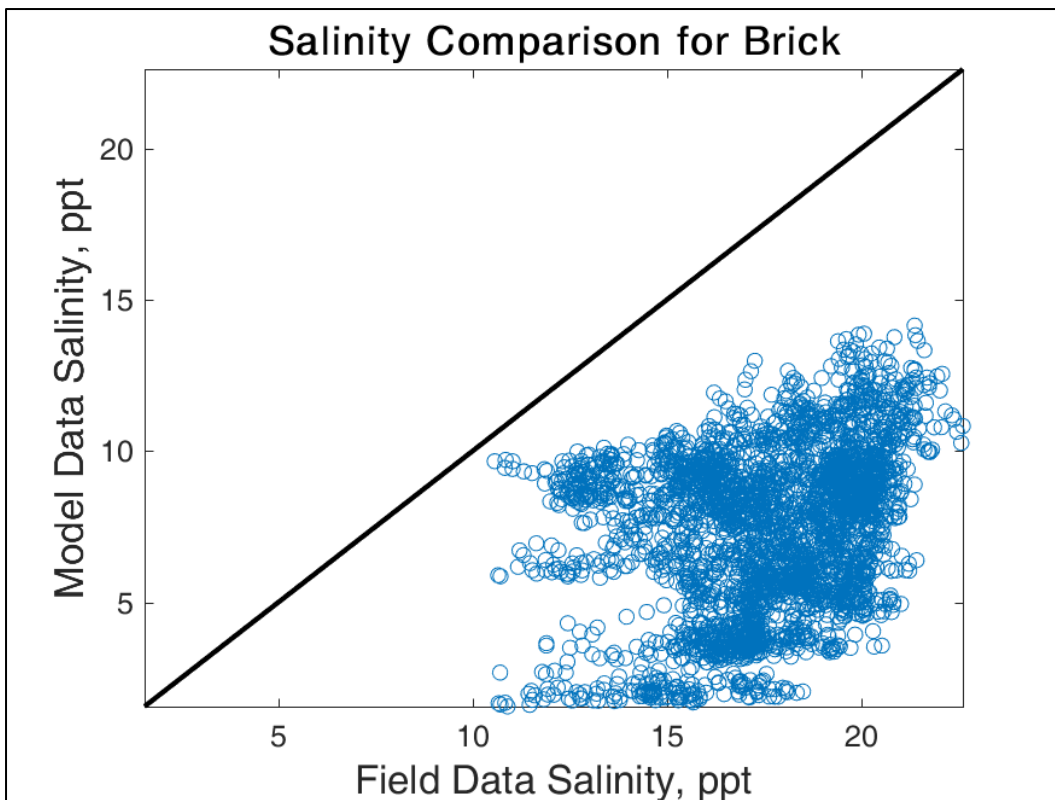
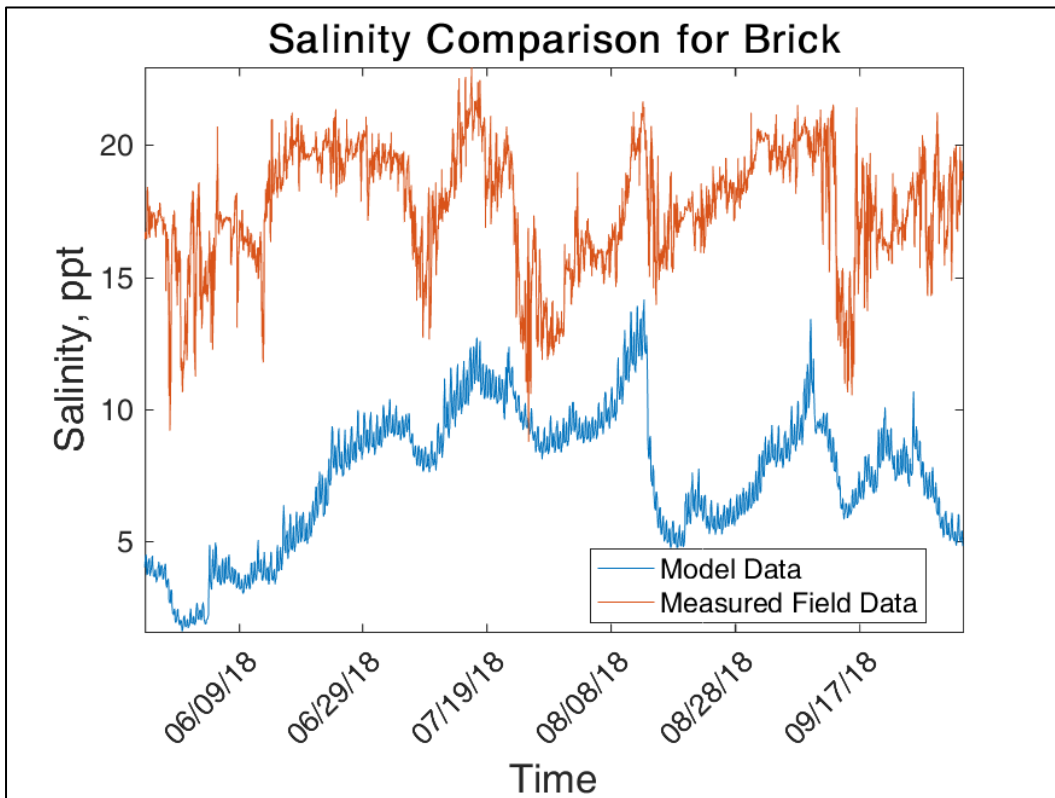


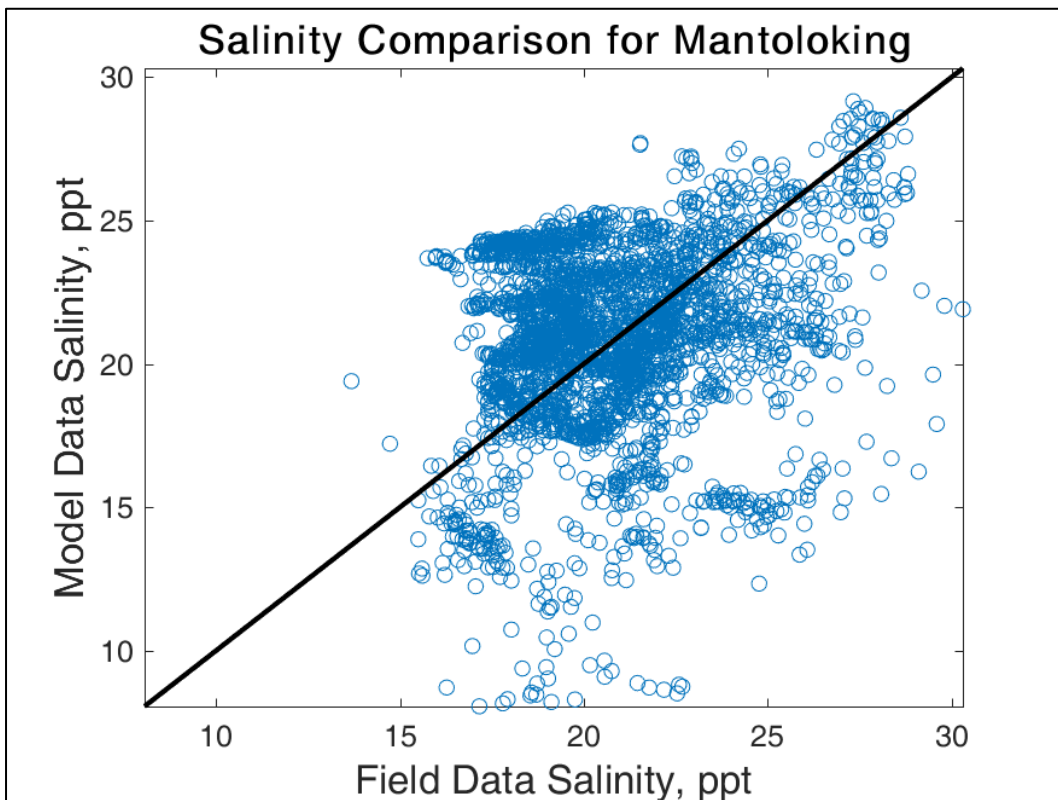
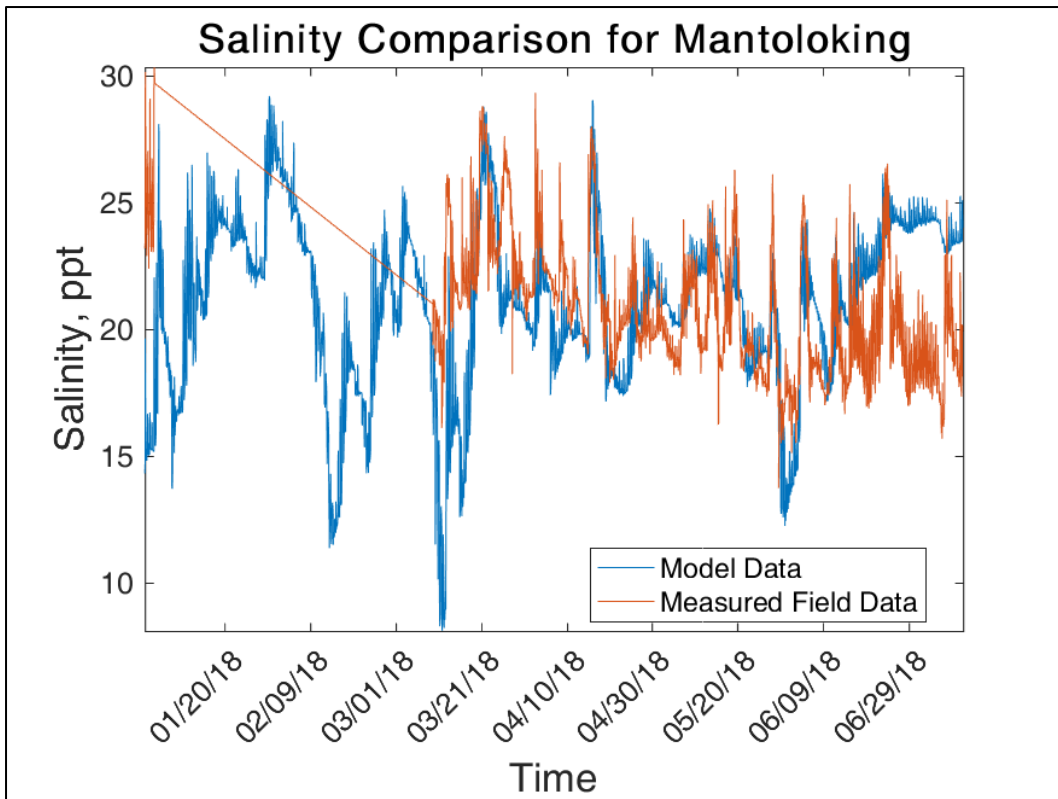


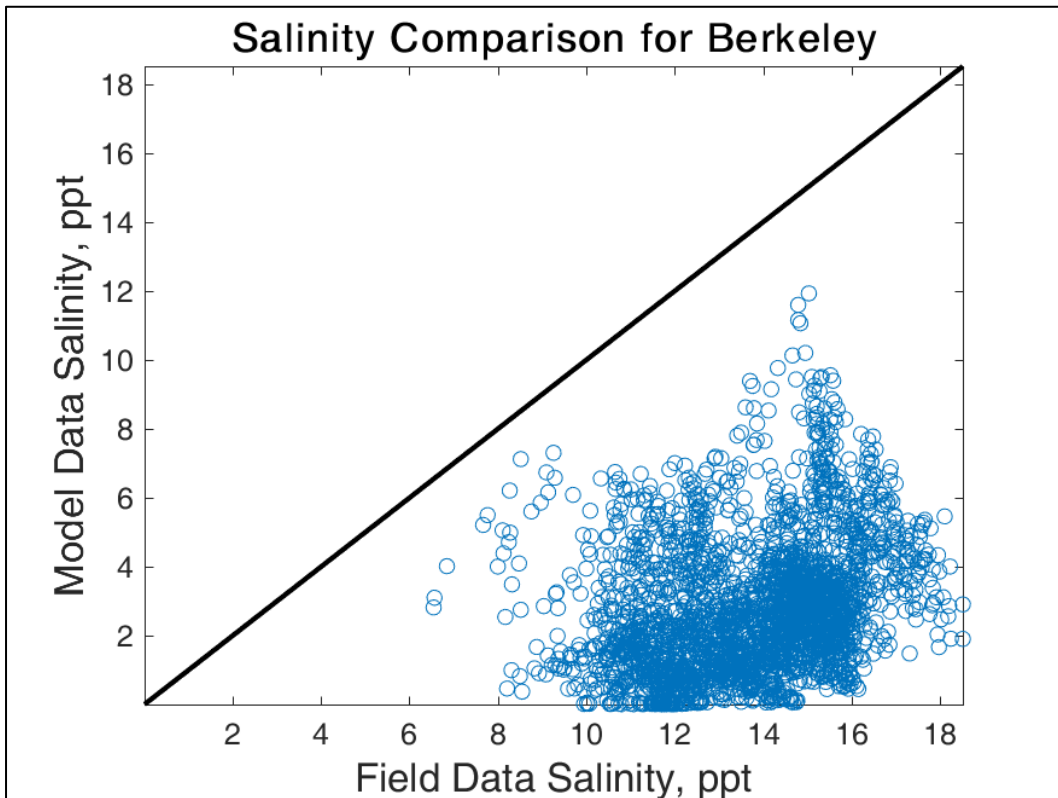
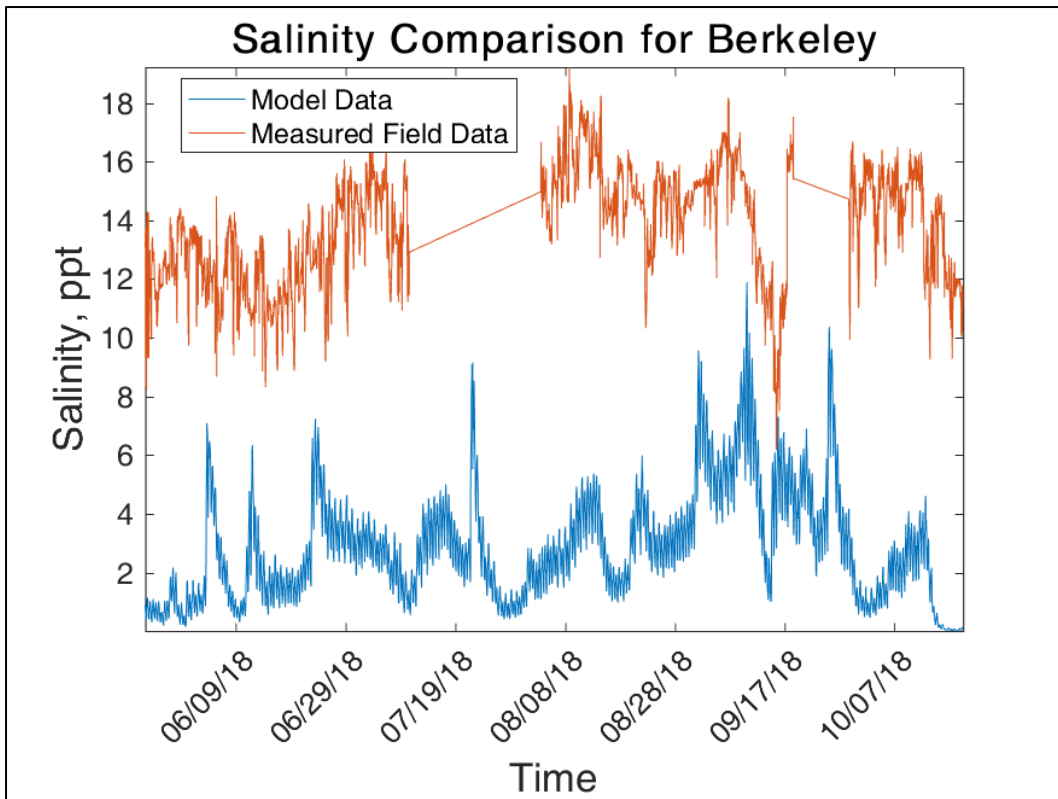


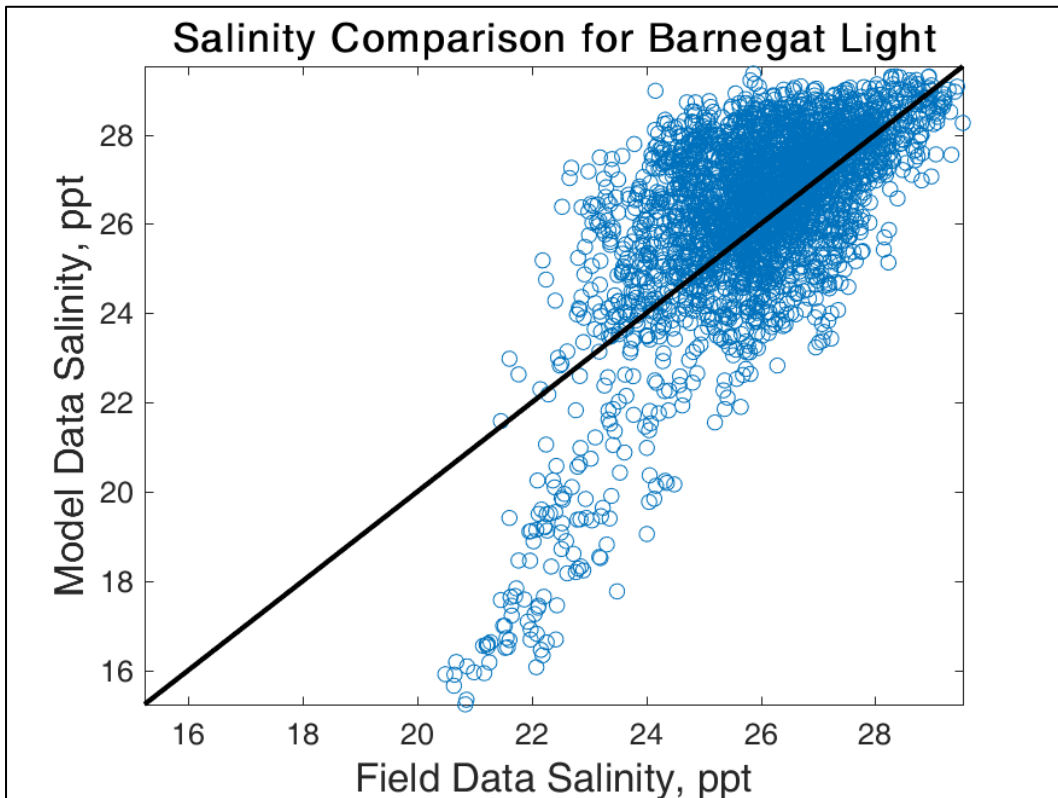
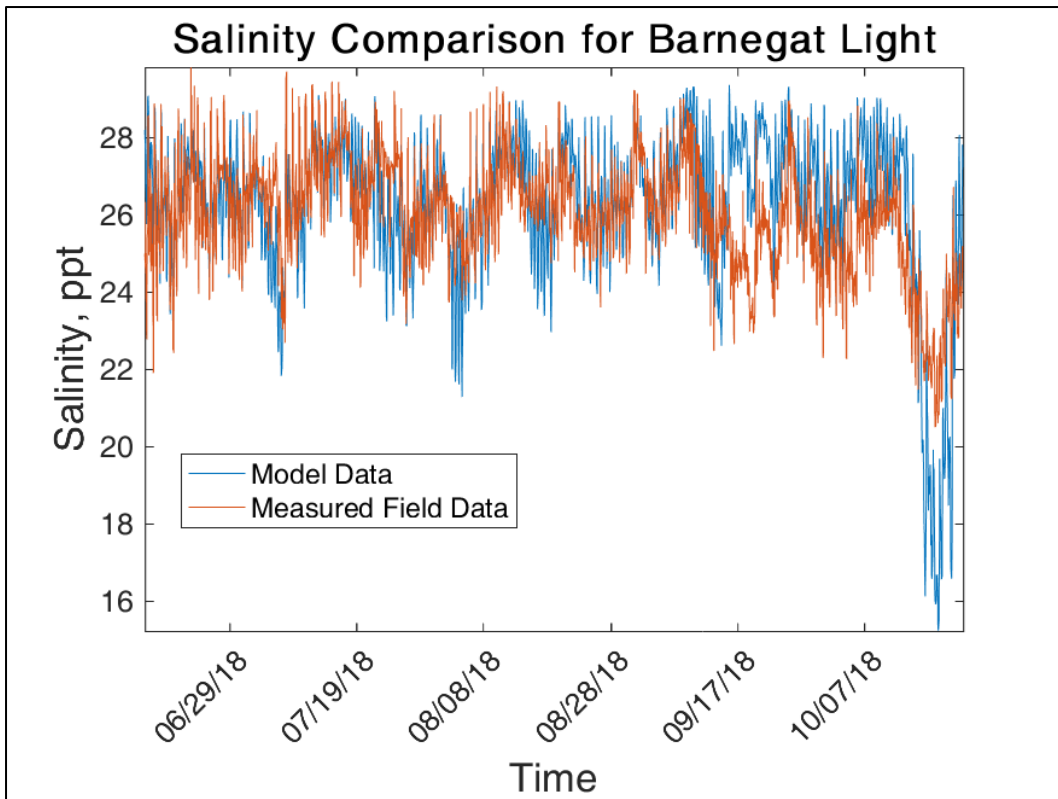


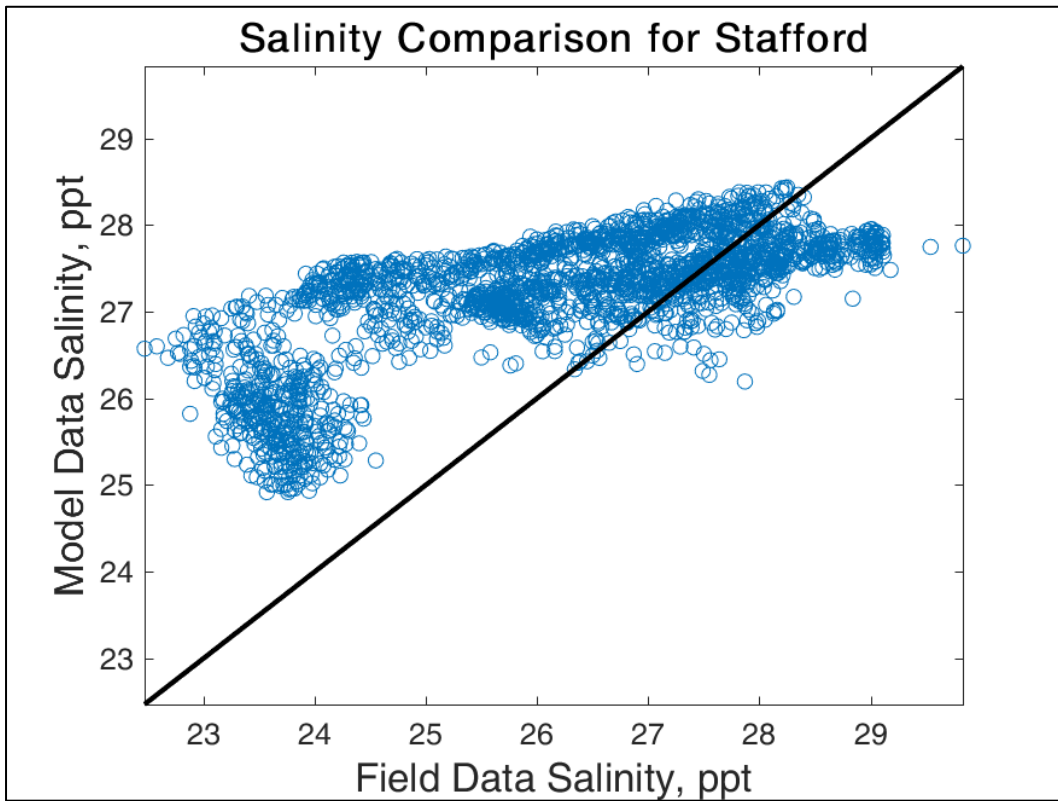
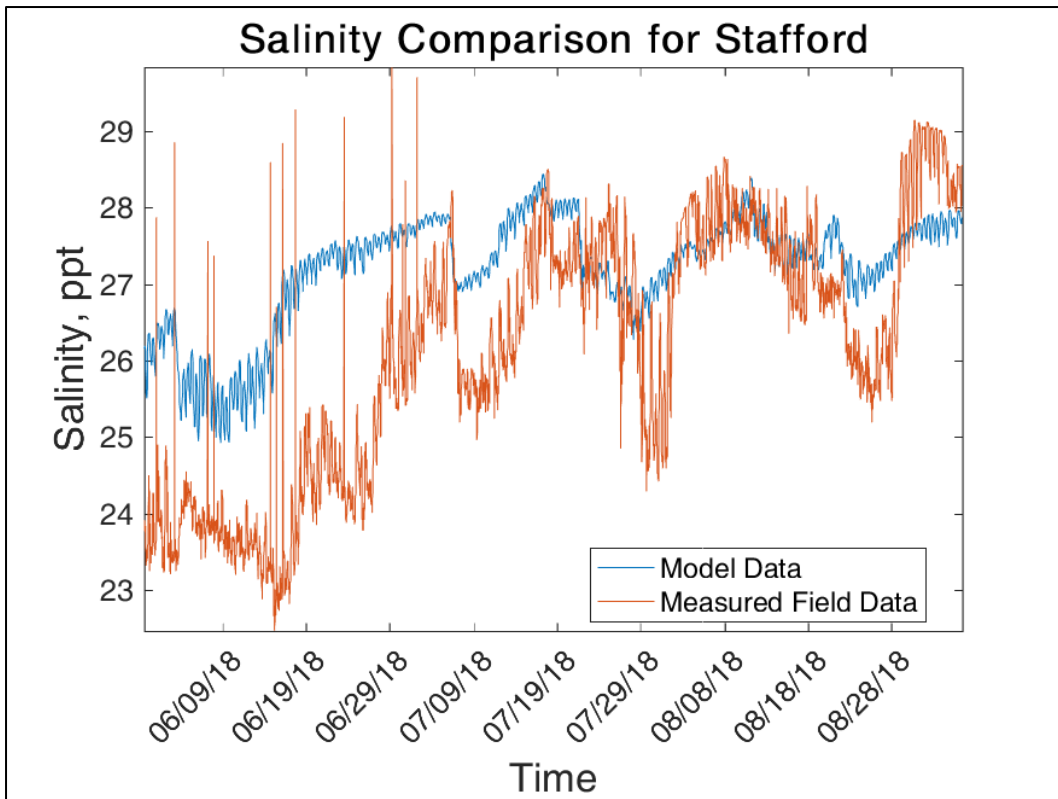
Salinity

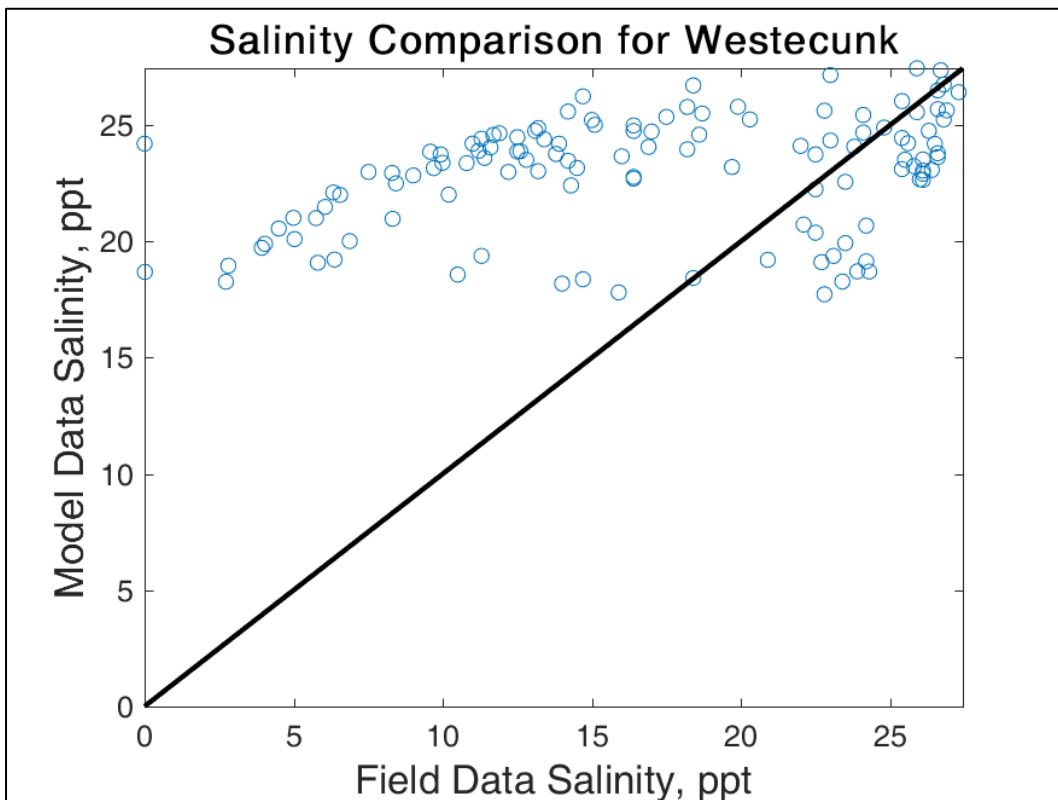
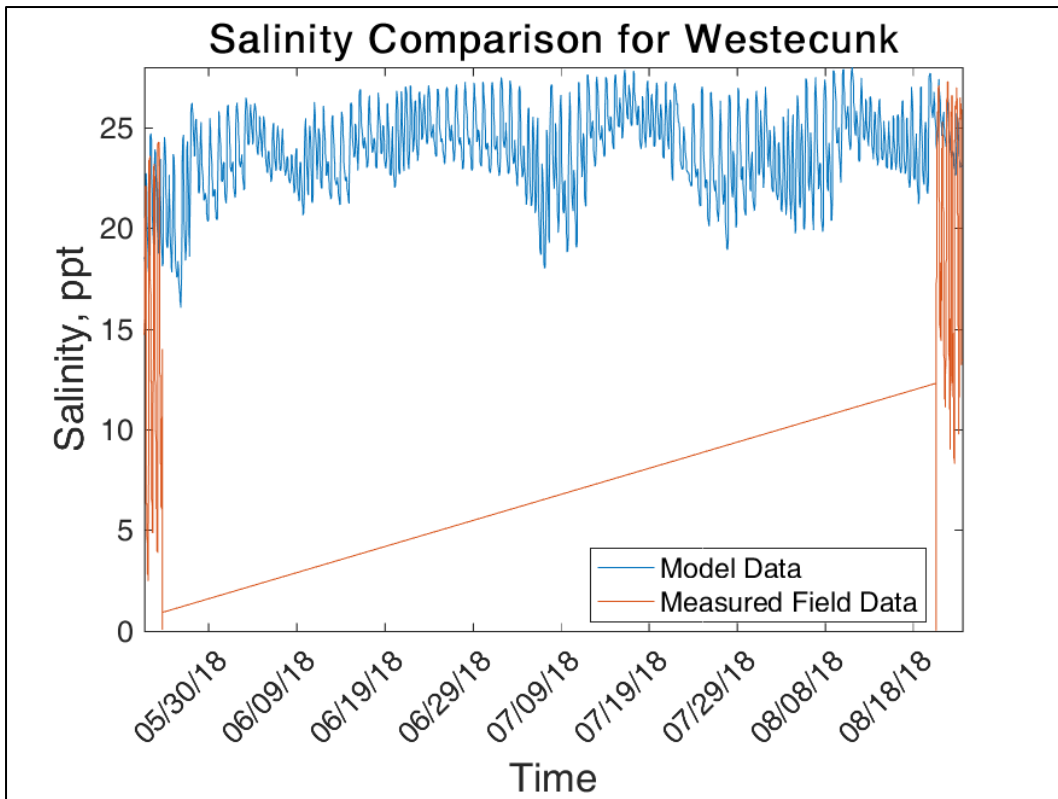


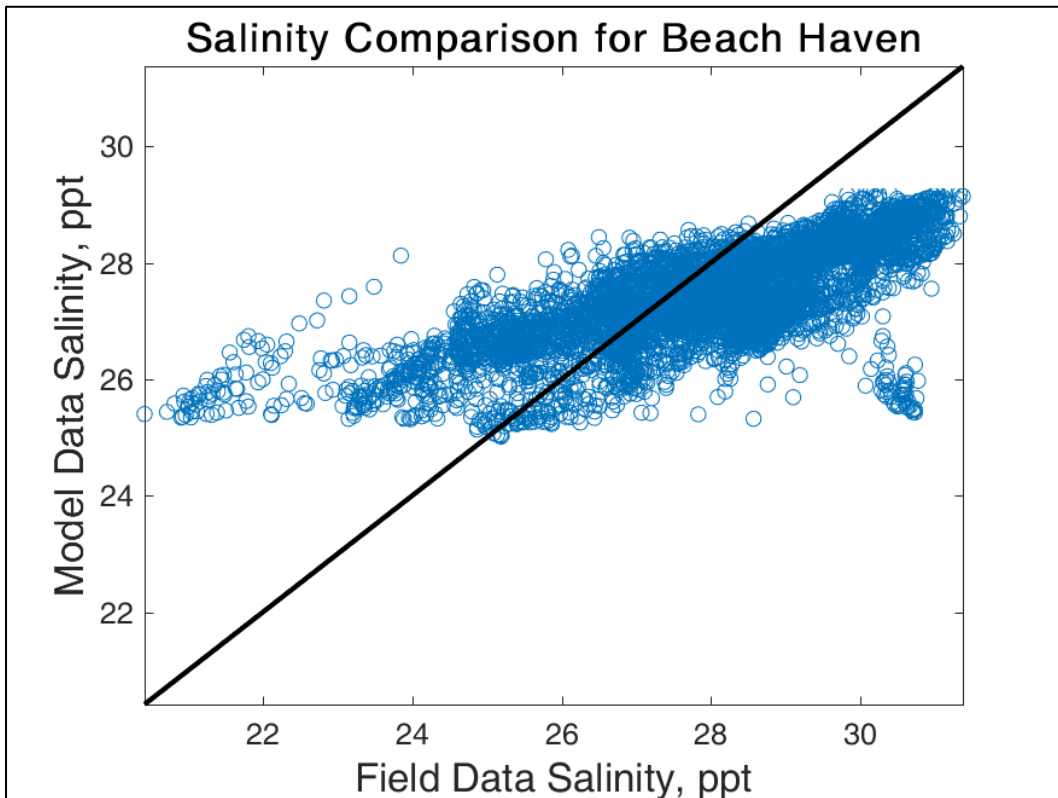
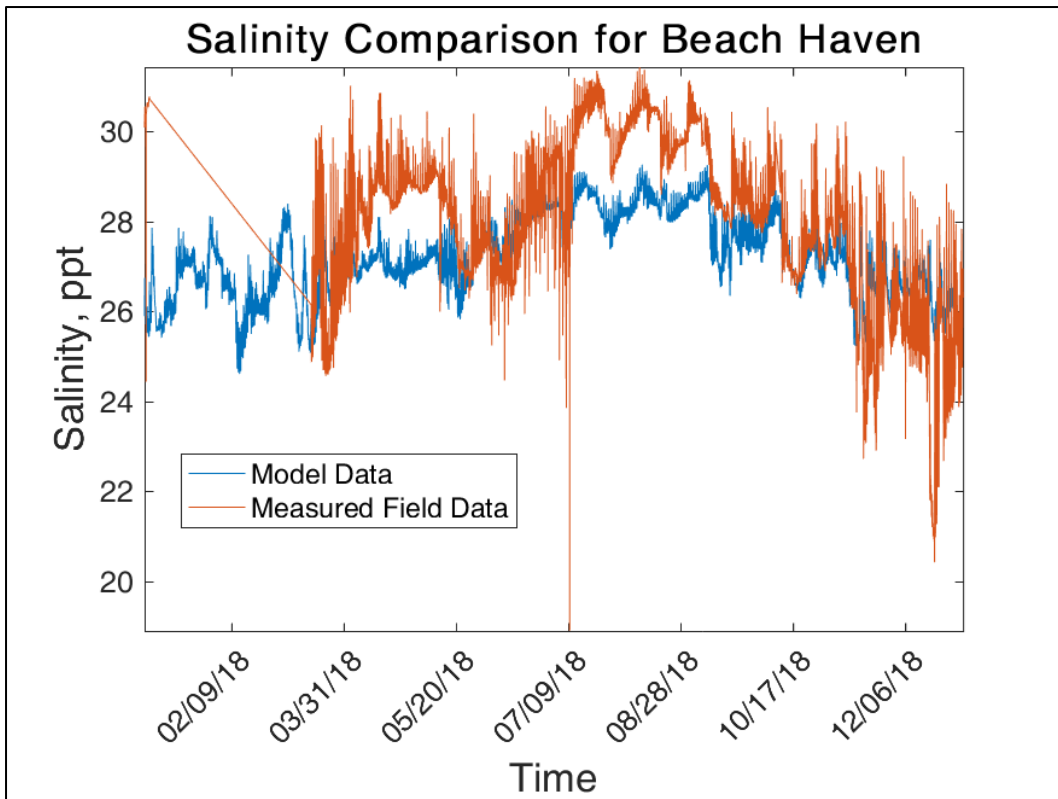


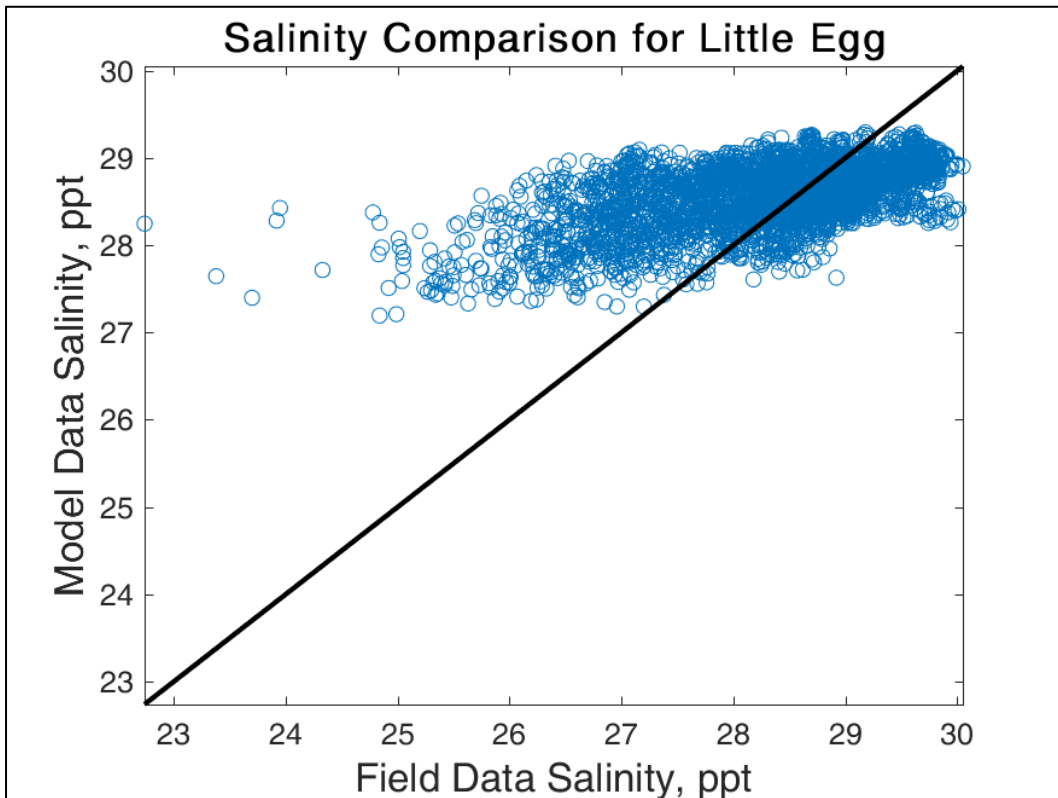
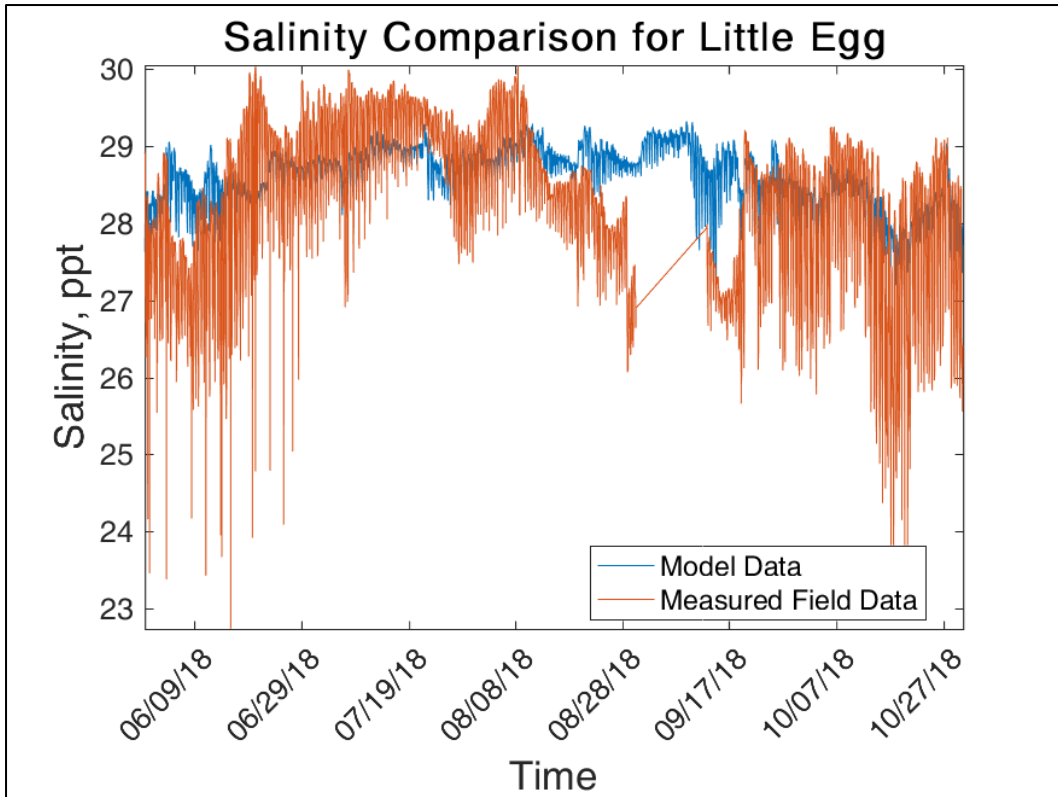


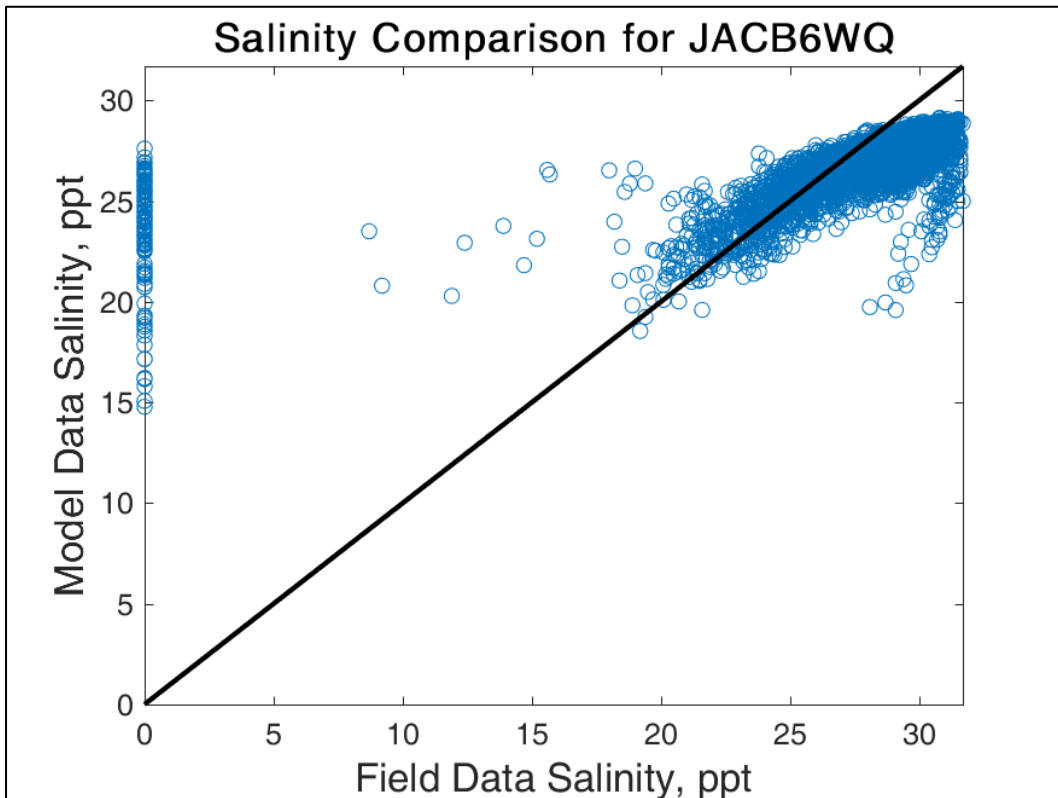
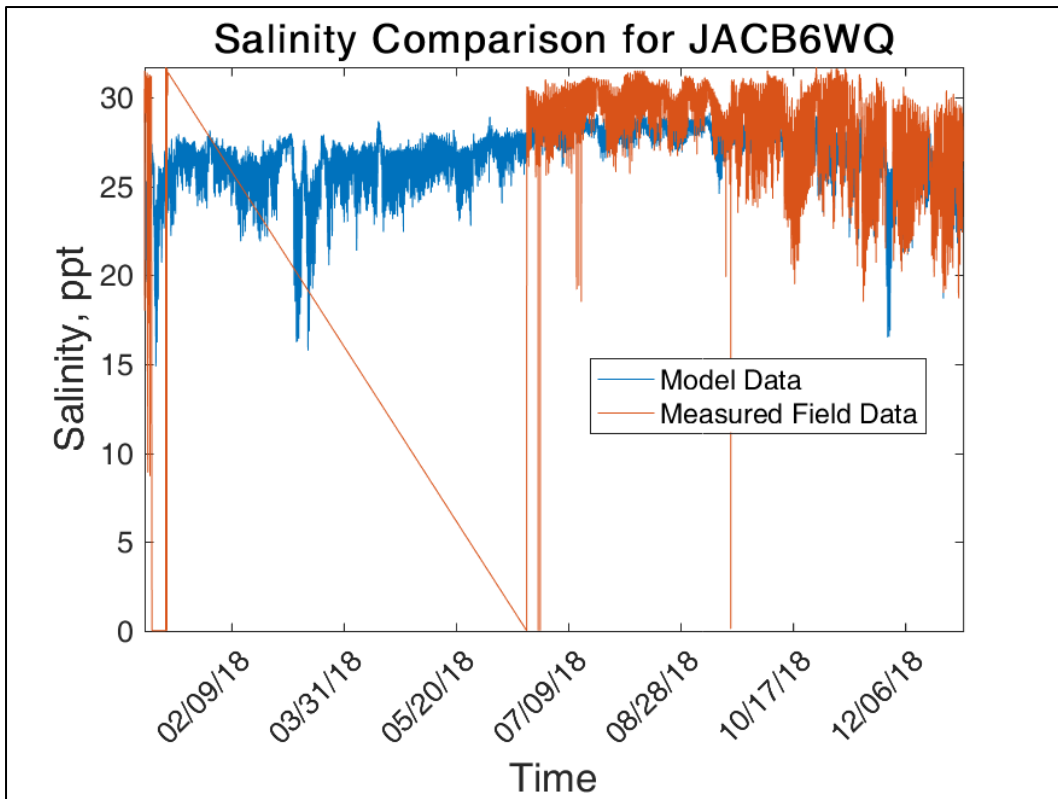


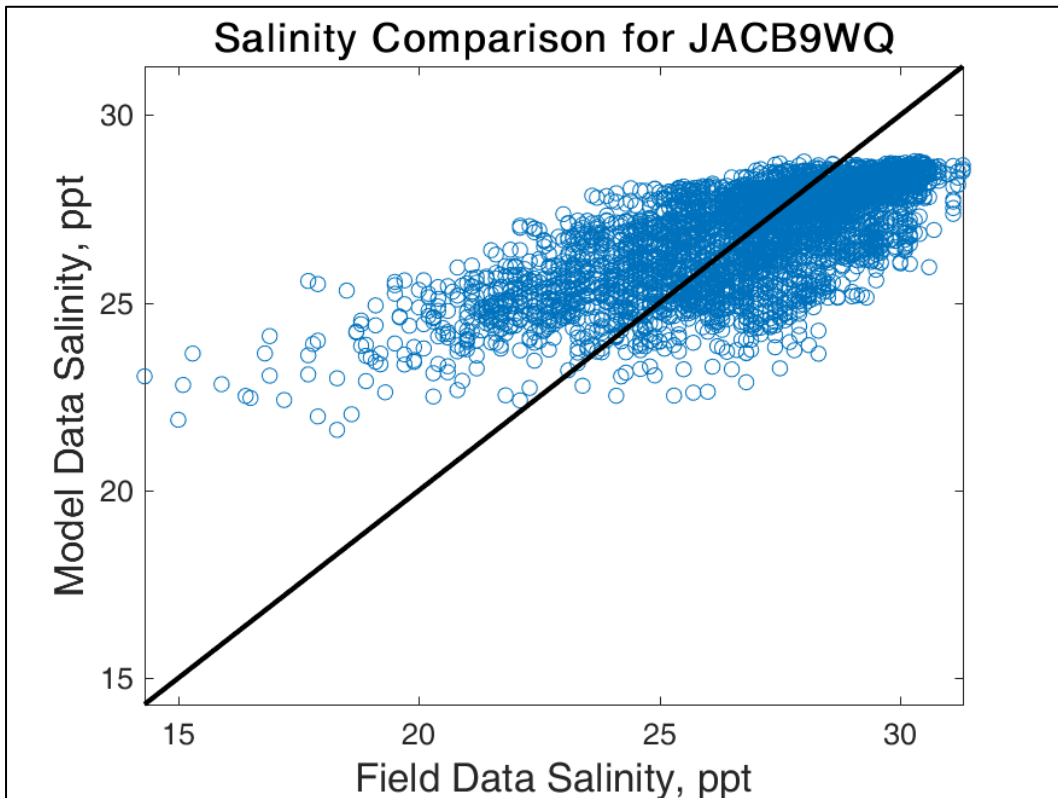
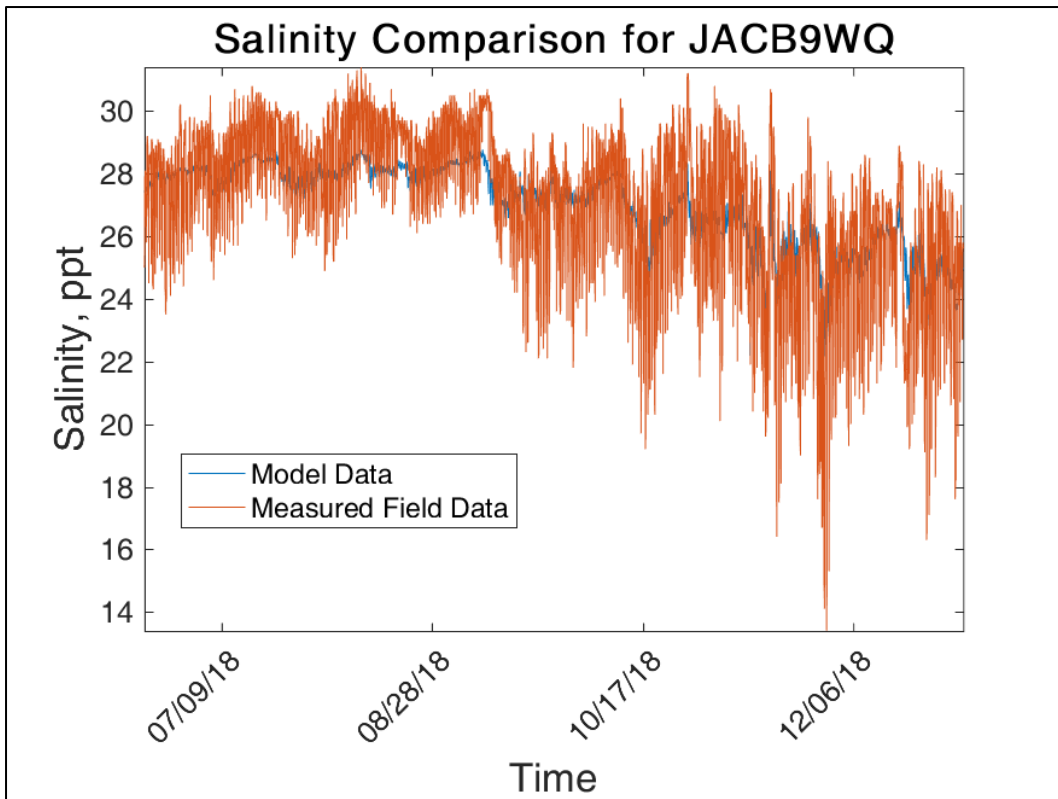


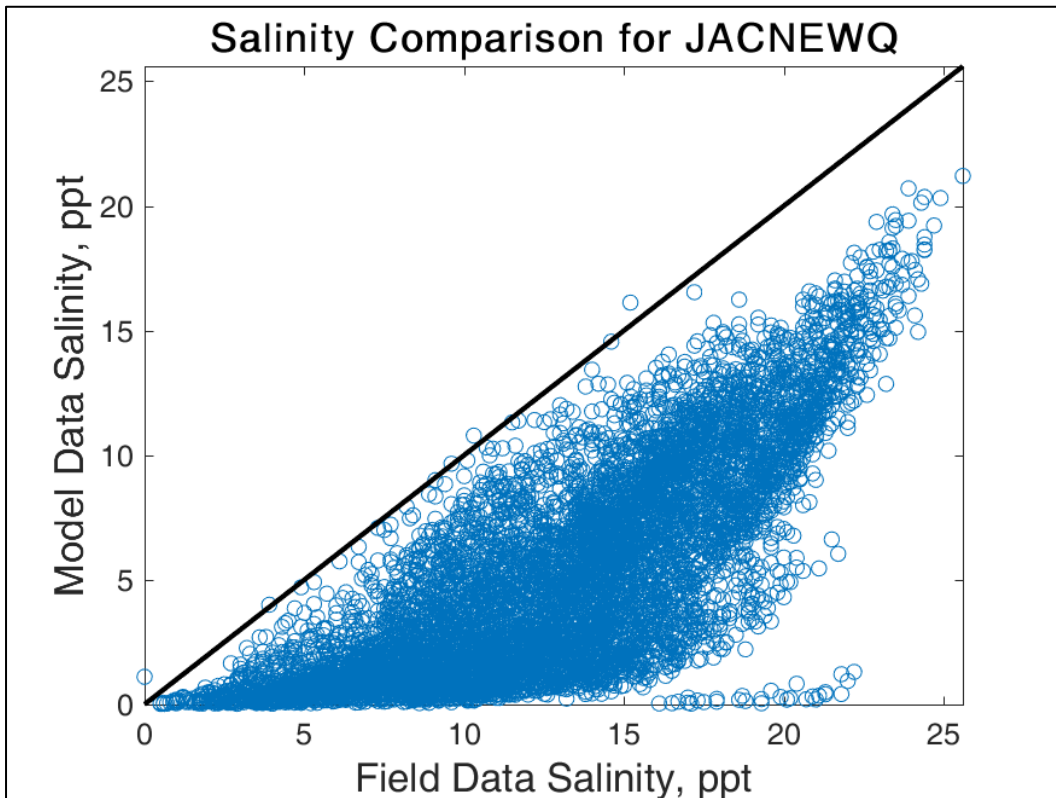
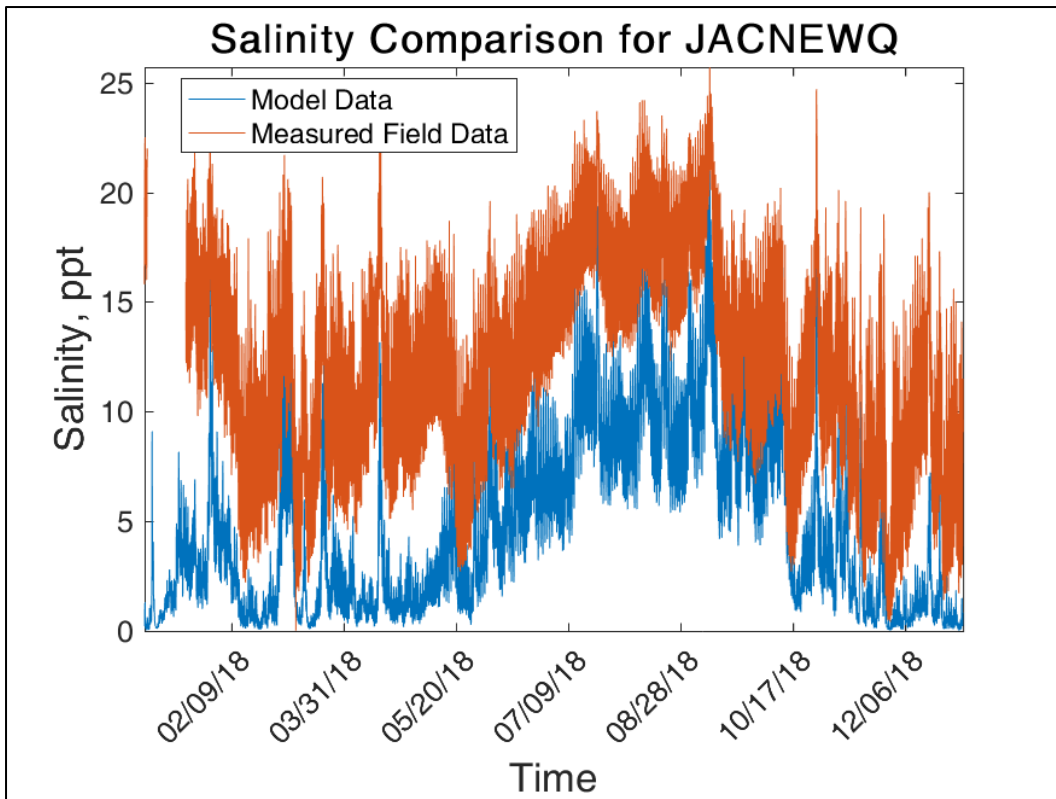


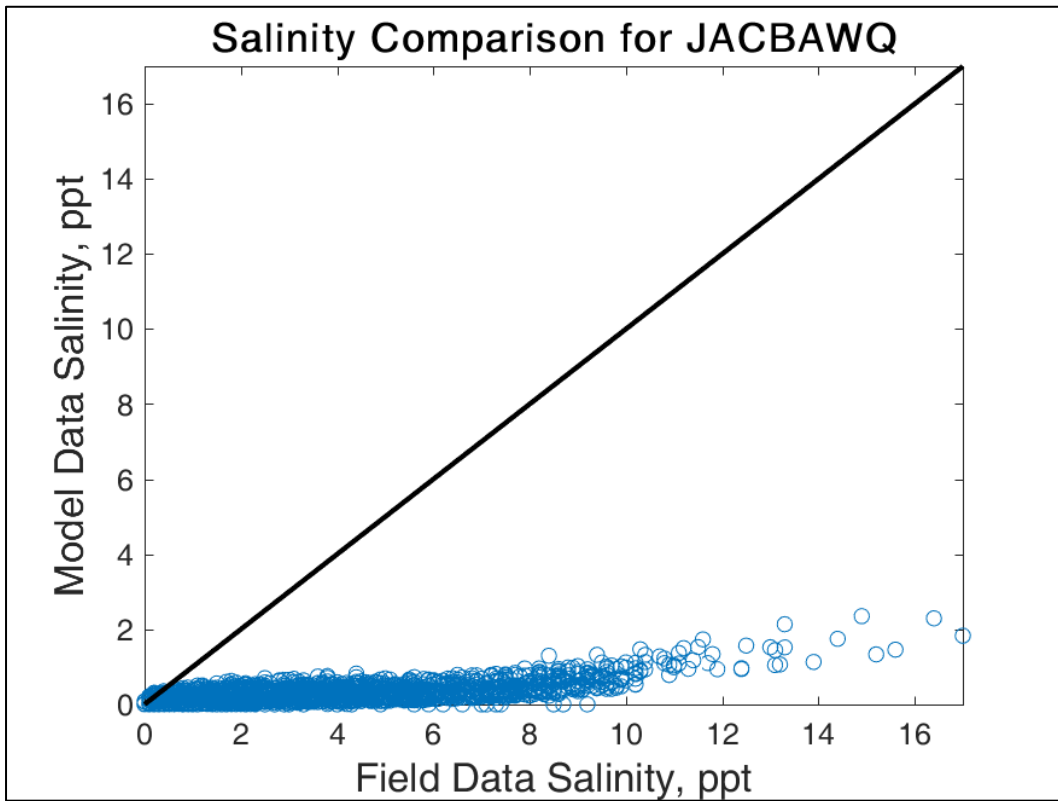
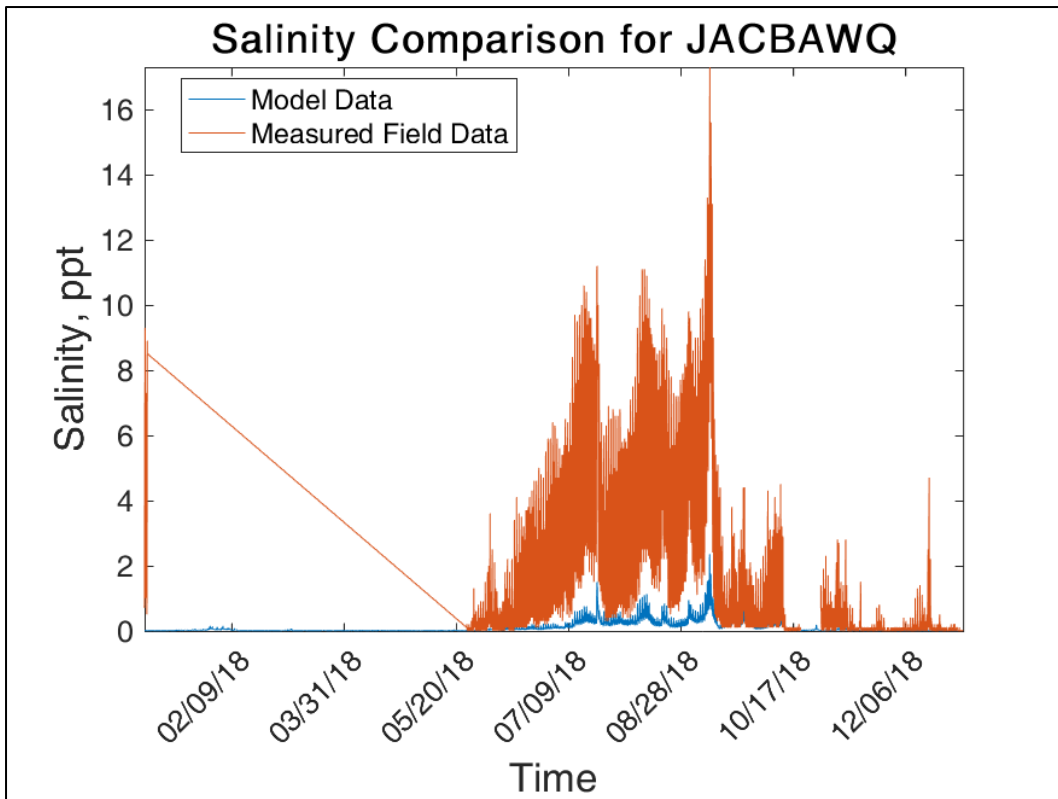


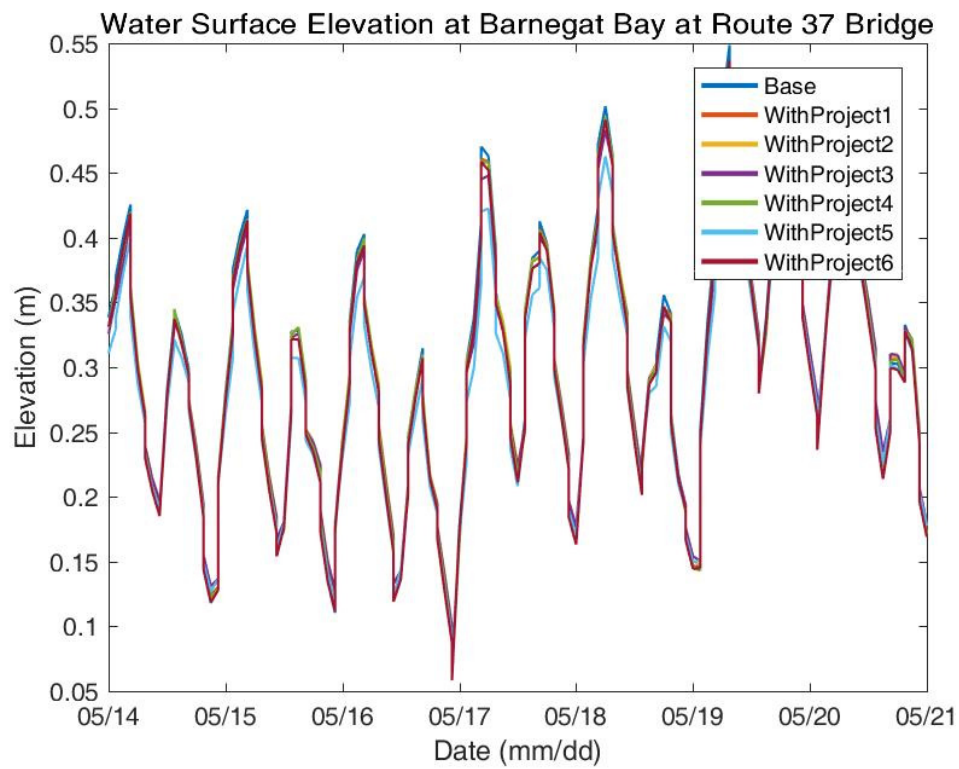
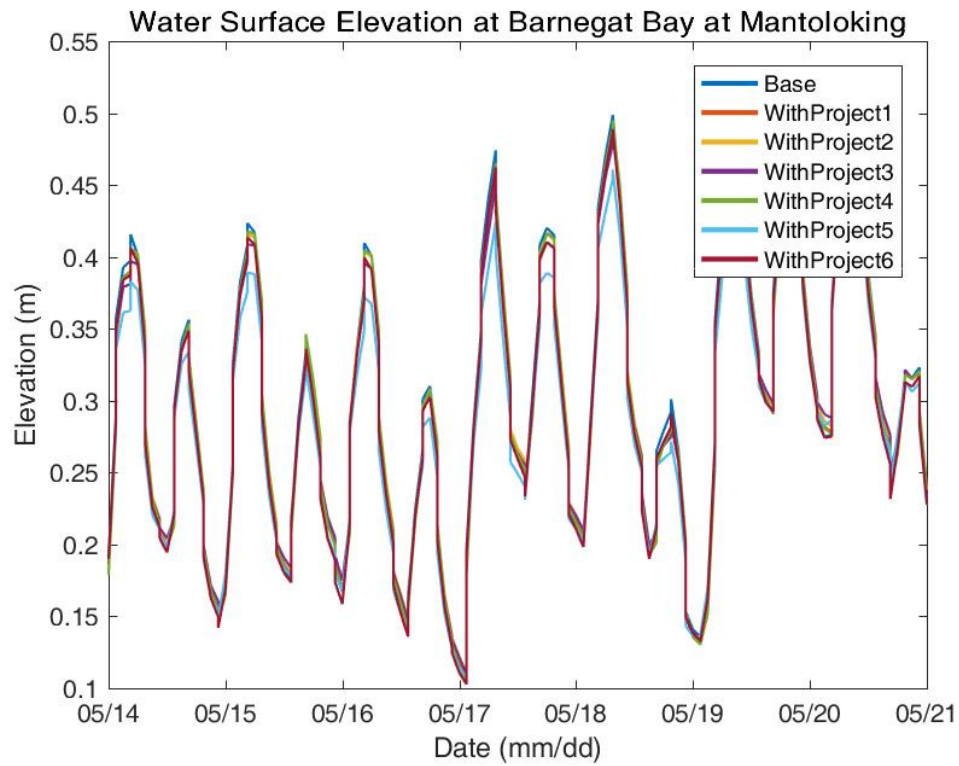


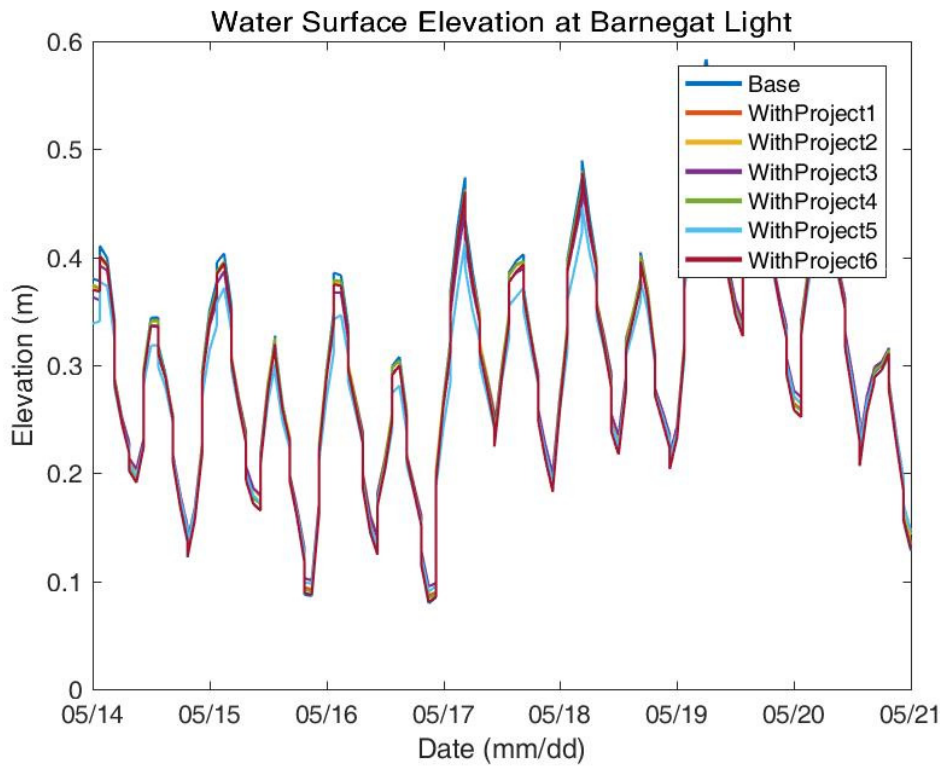
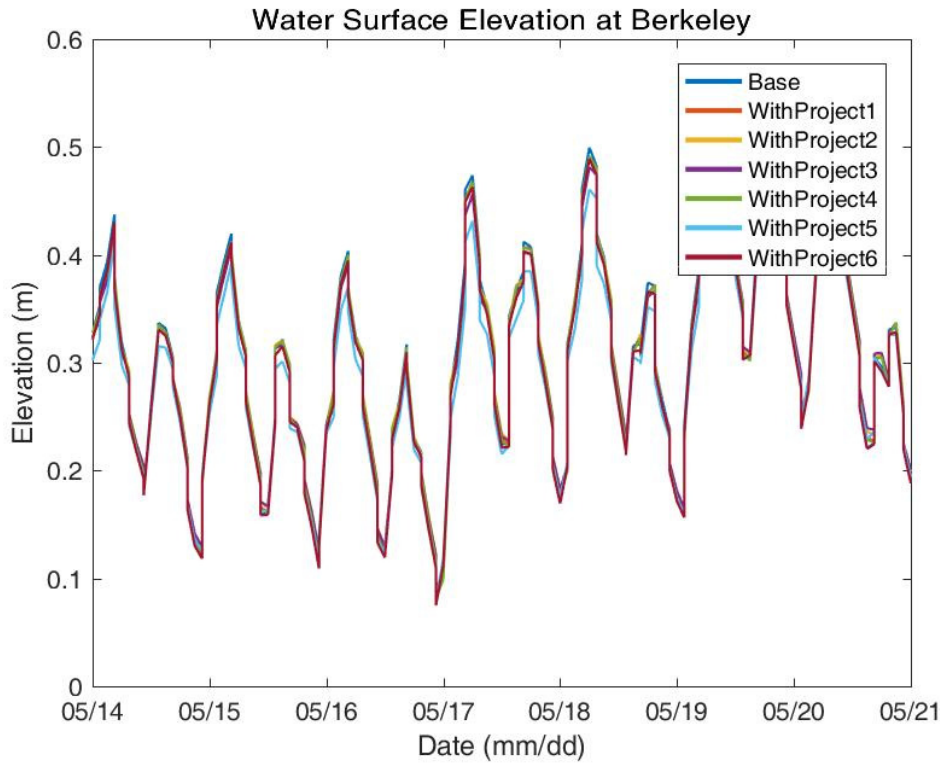


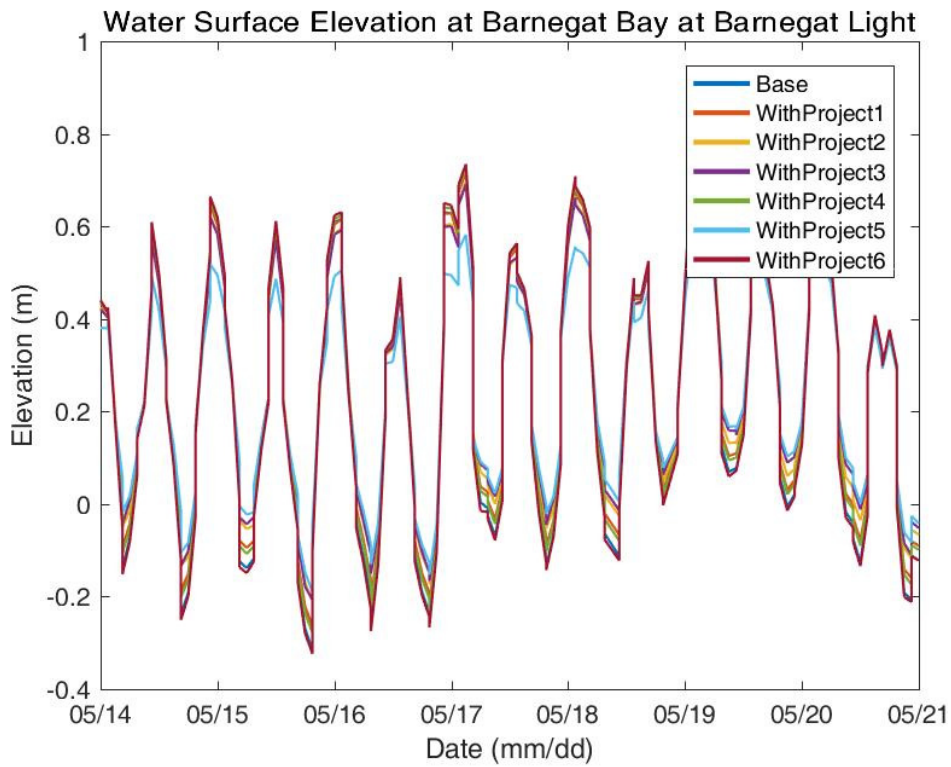
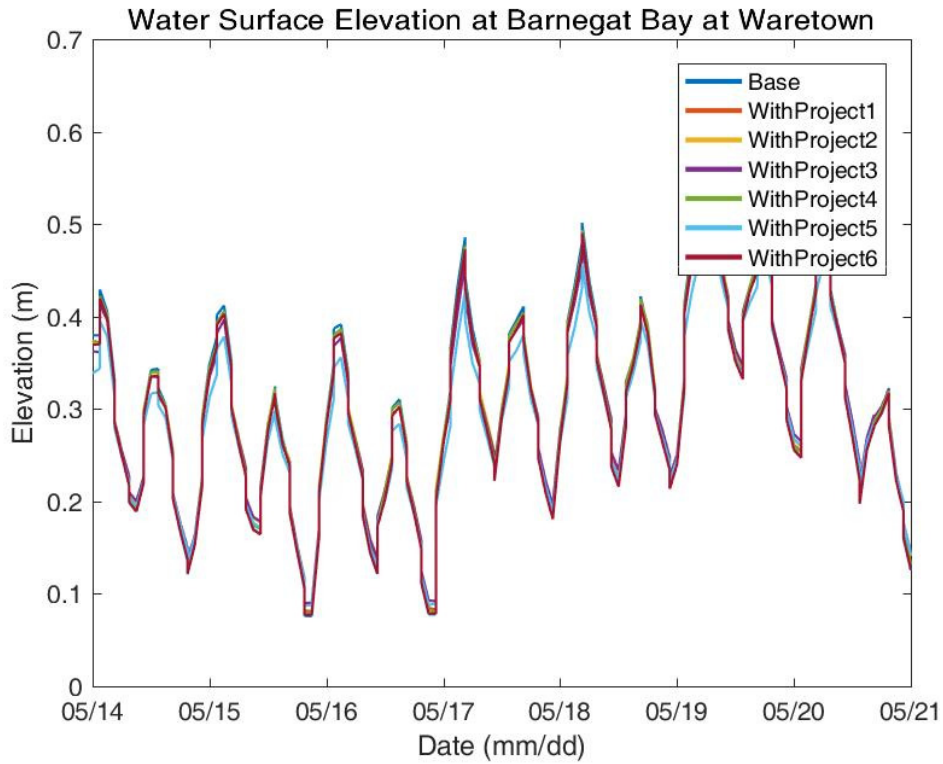


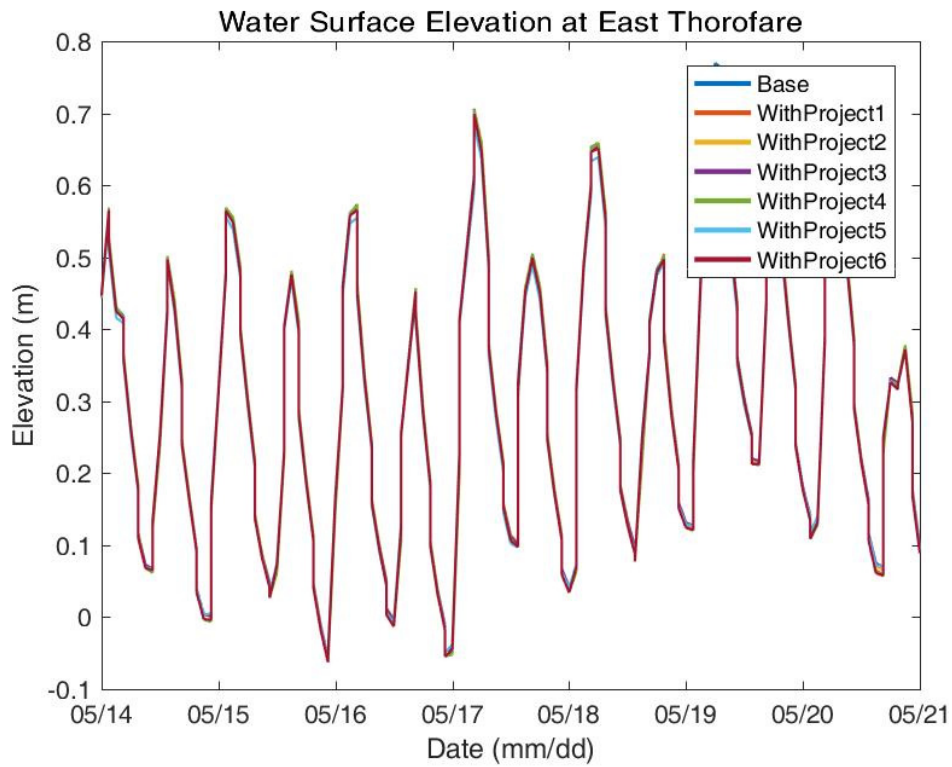
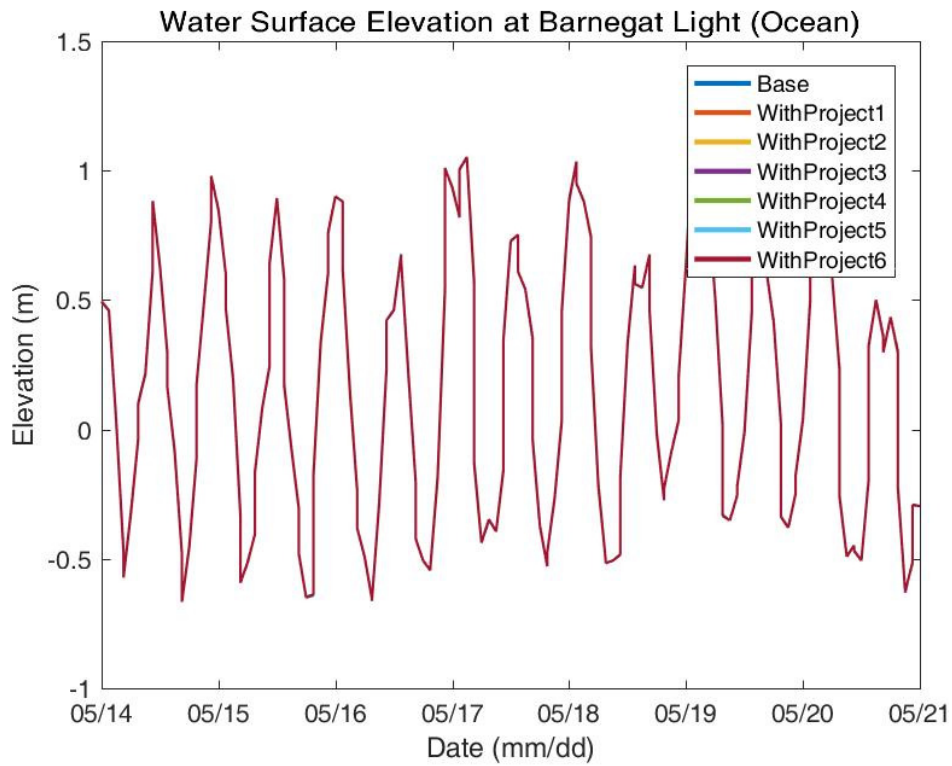


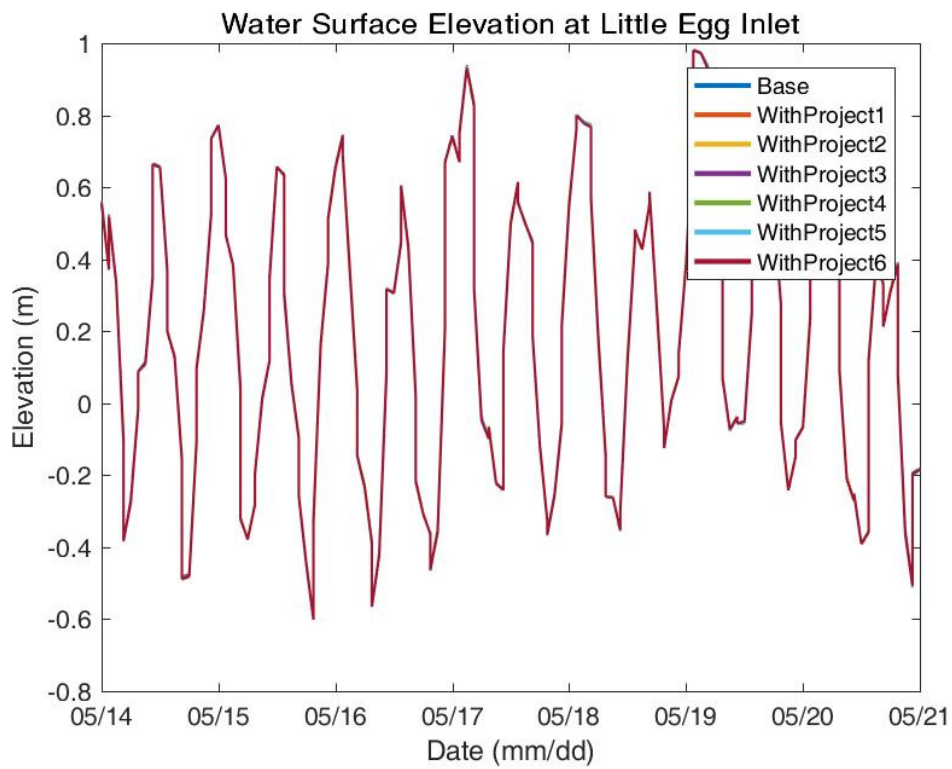
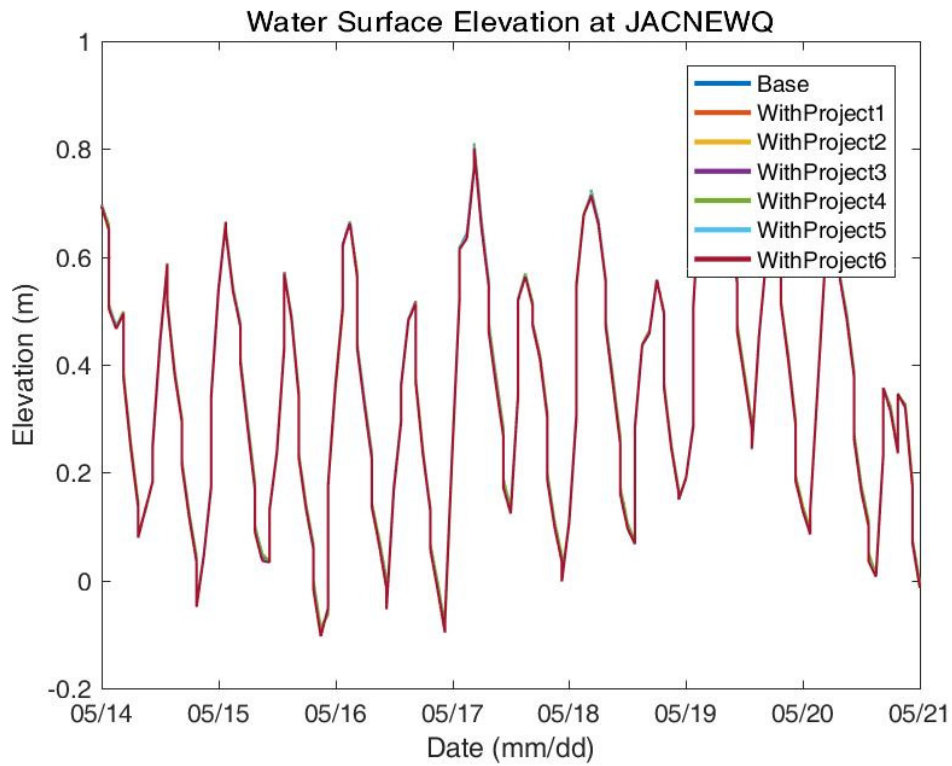


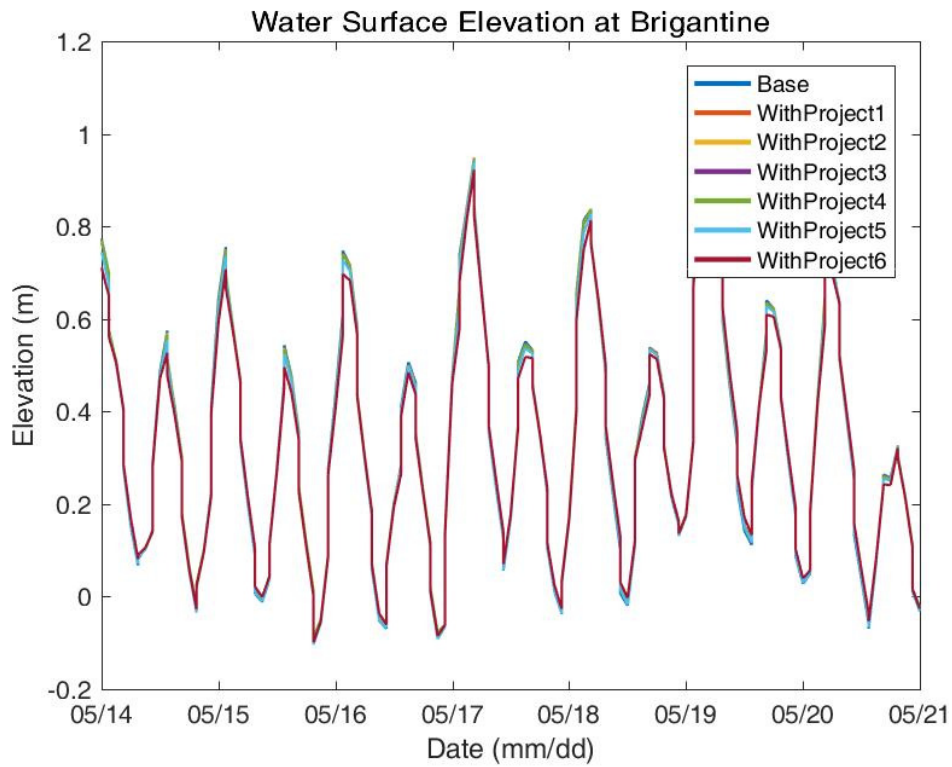
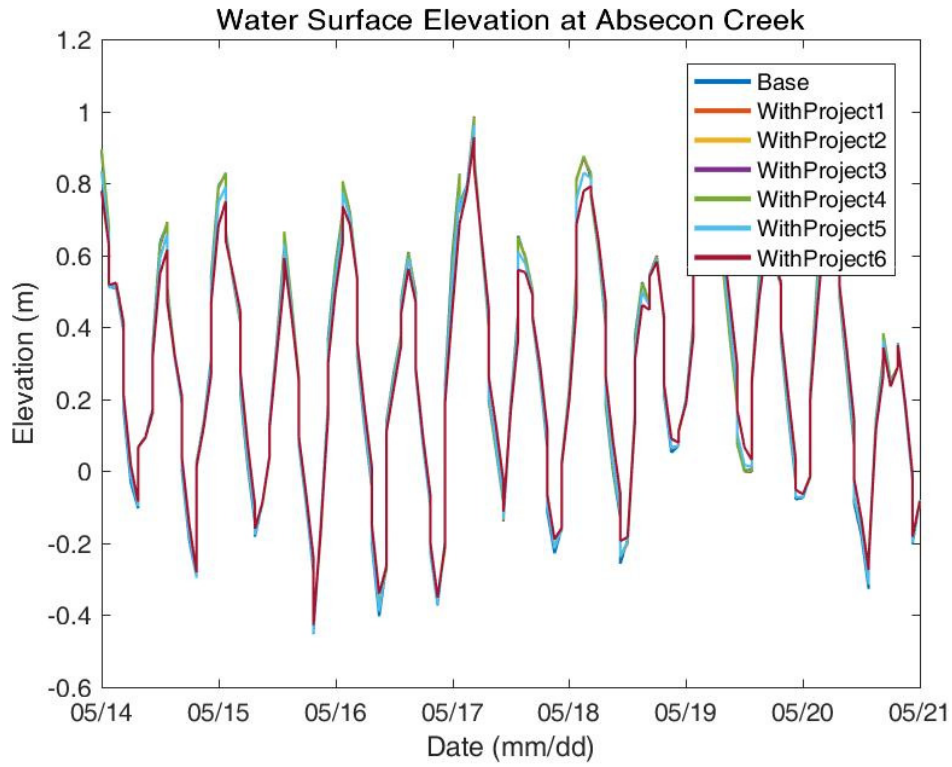


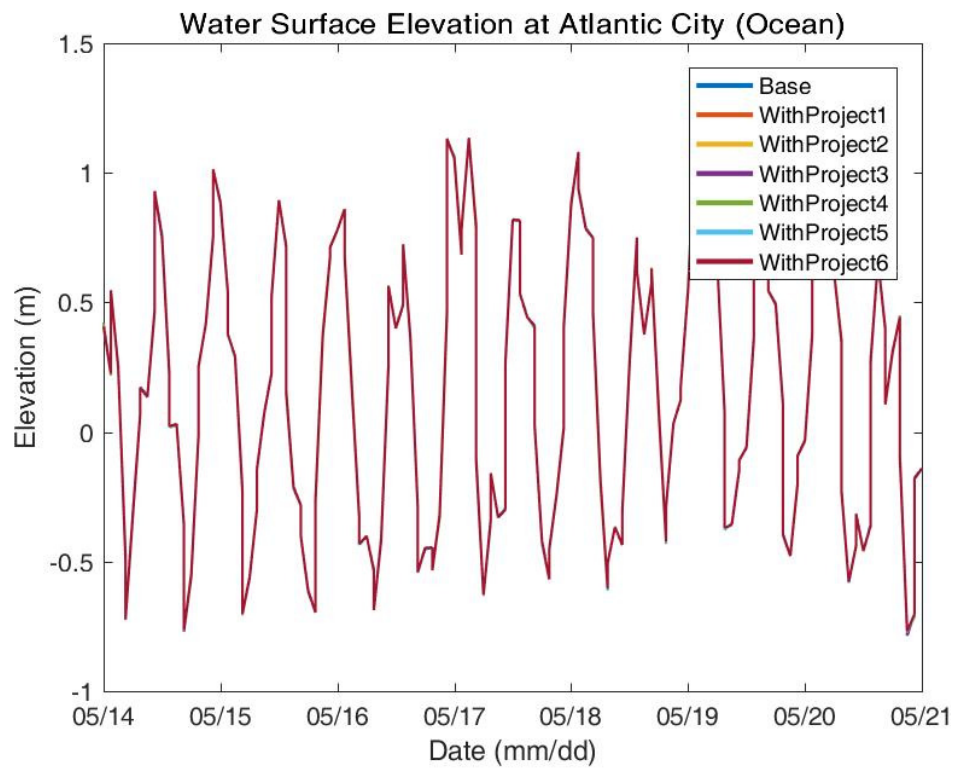
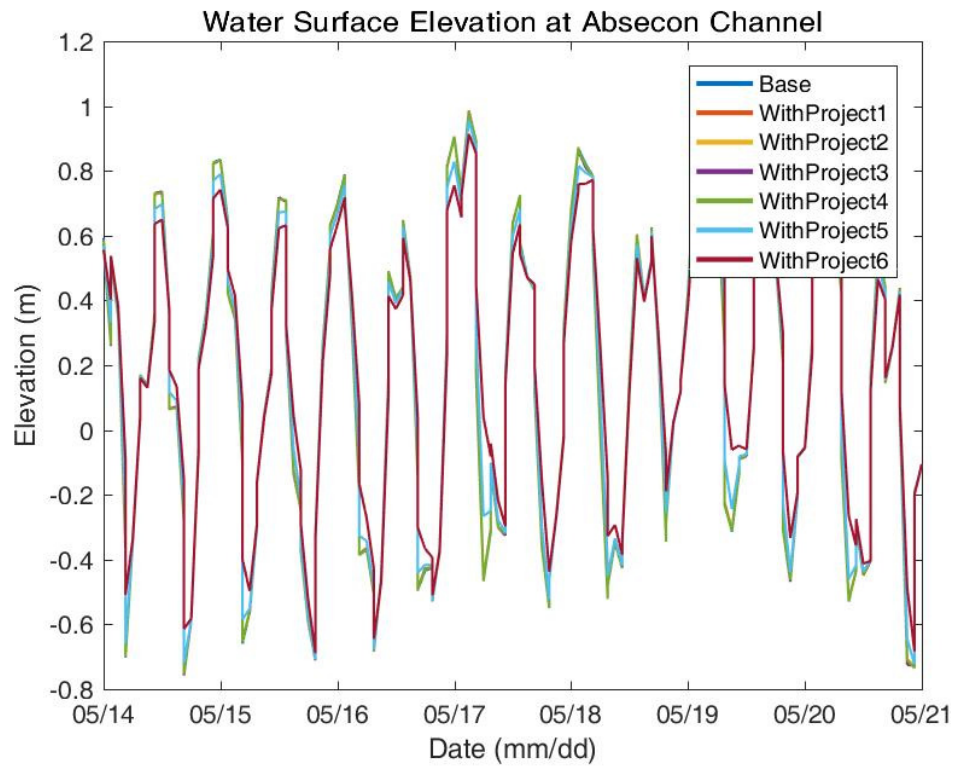


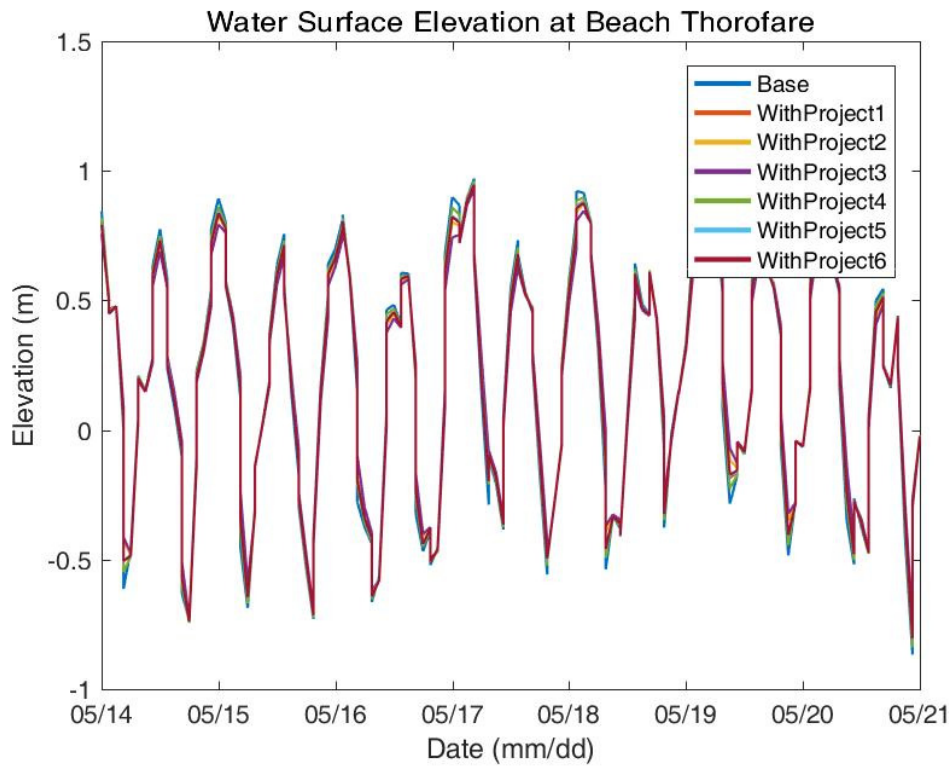
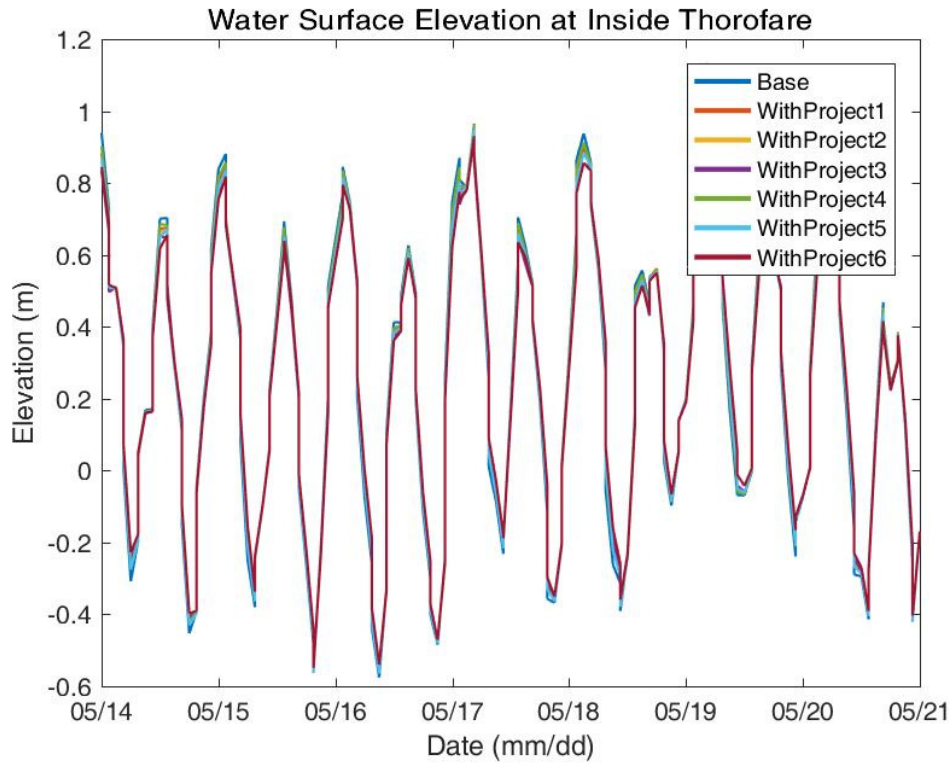


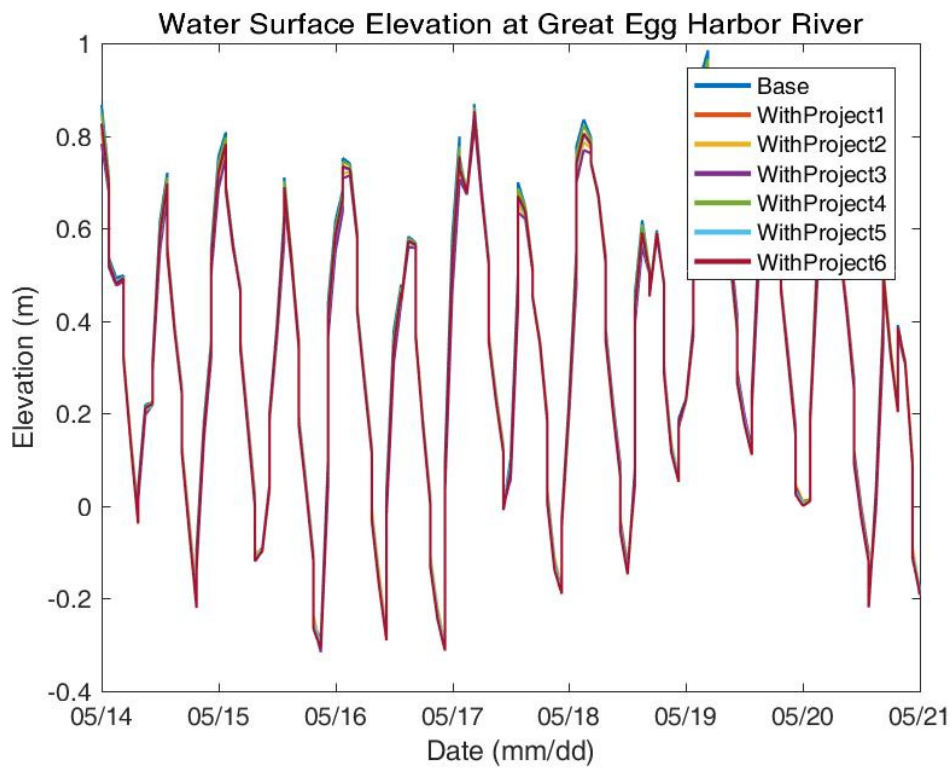
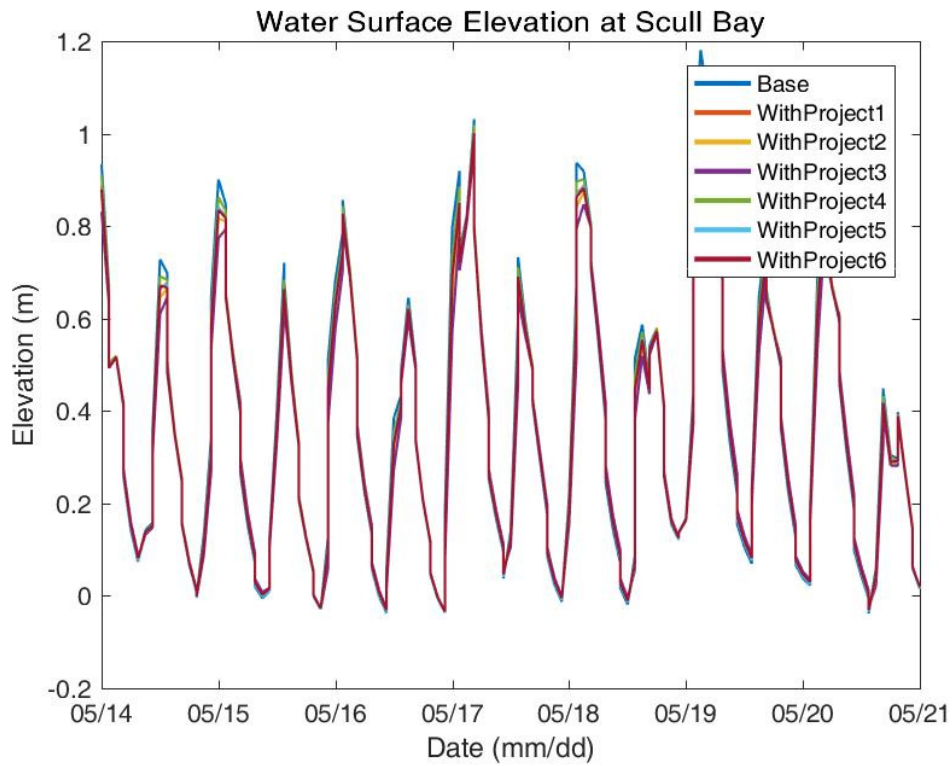


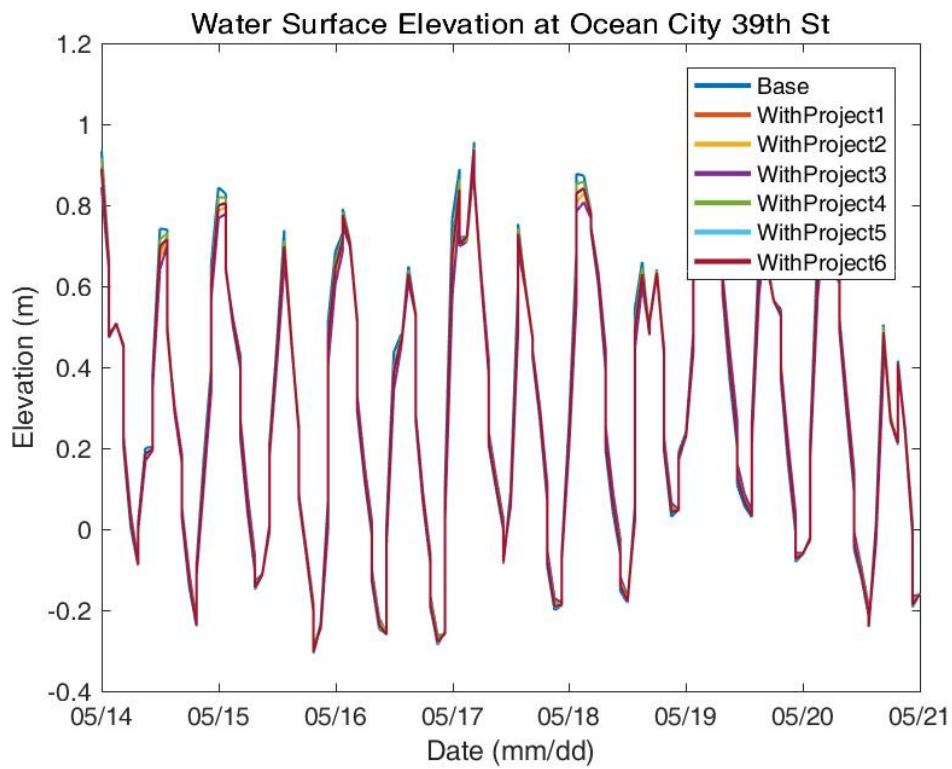
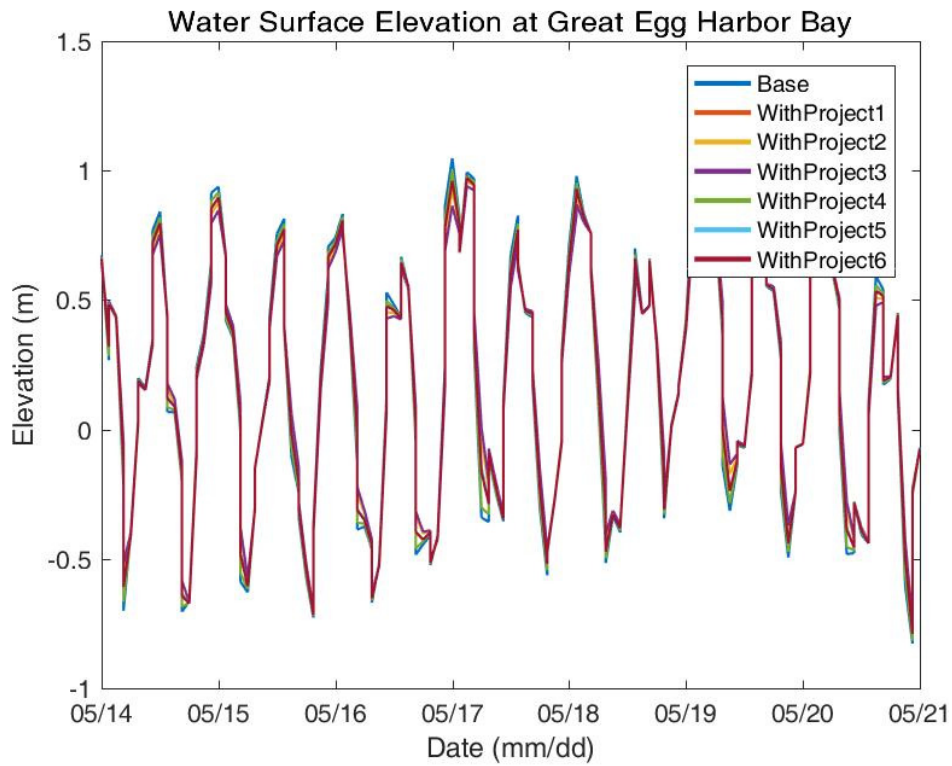


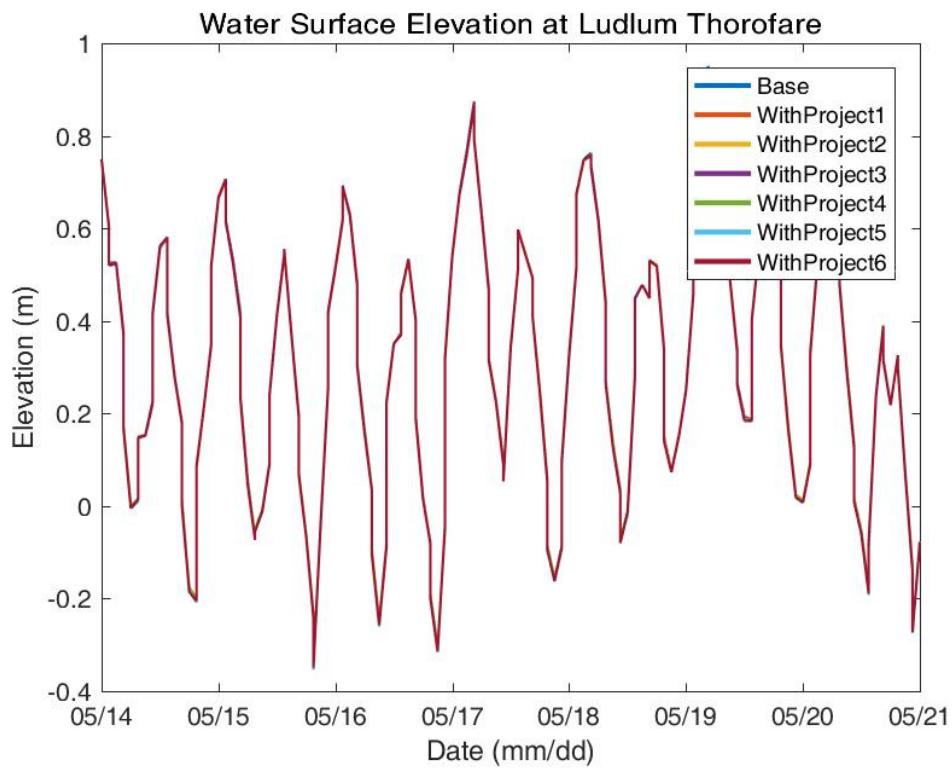
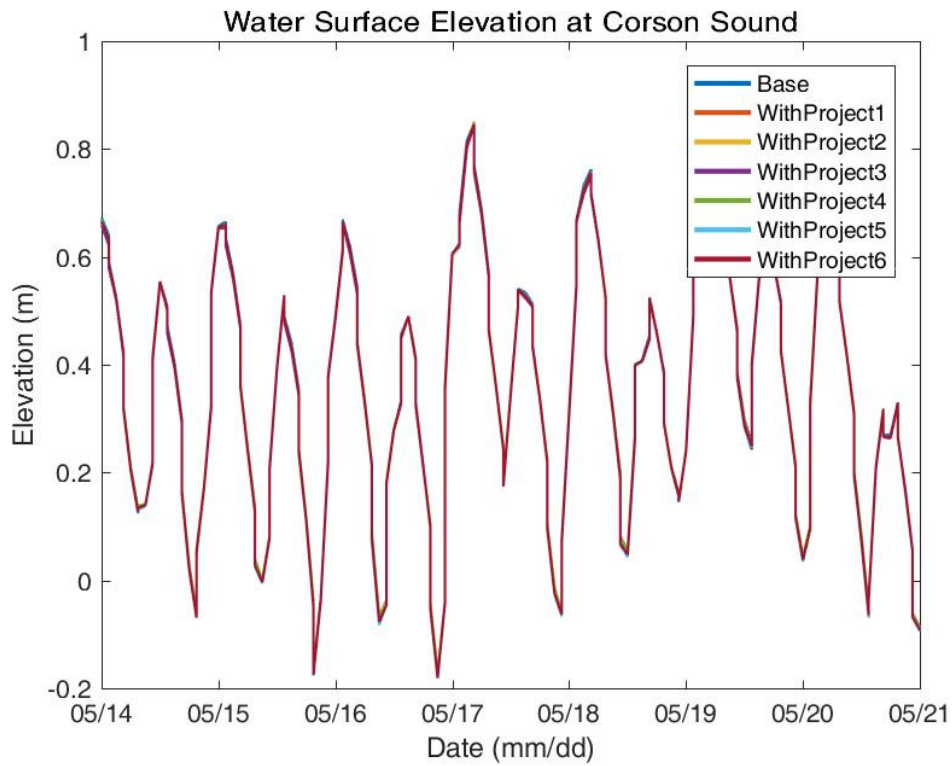


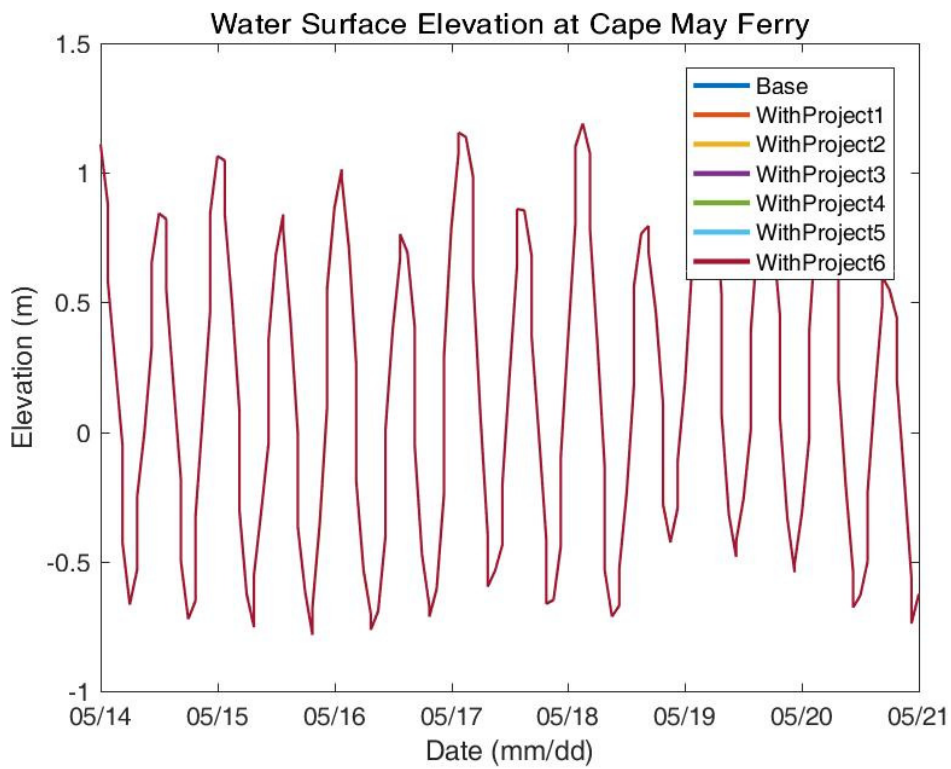
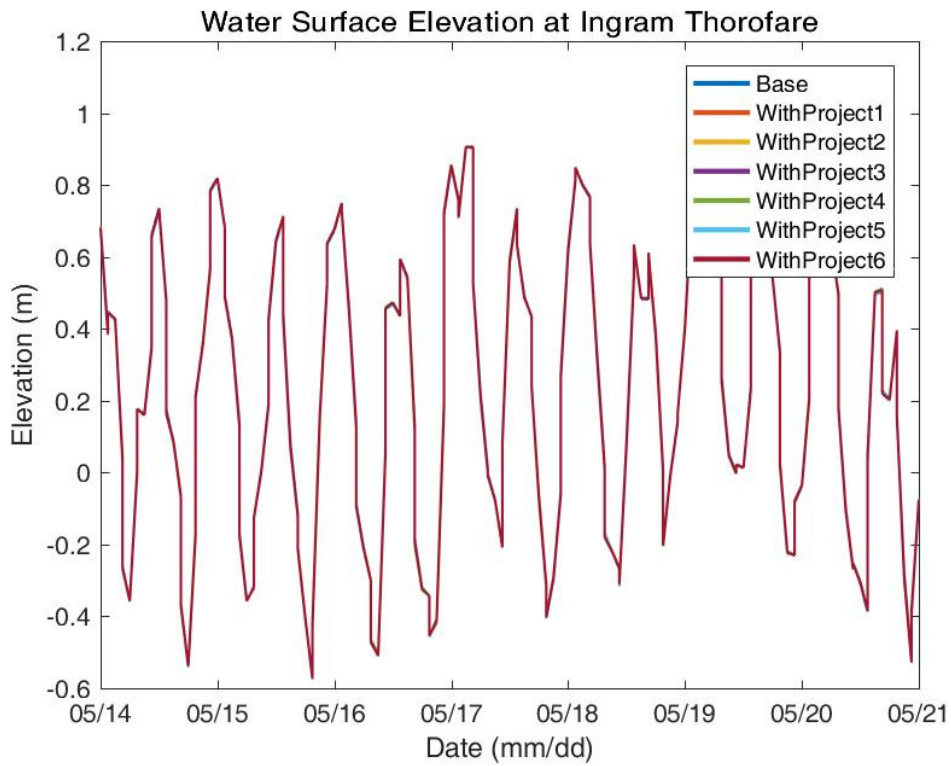


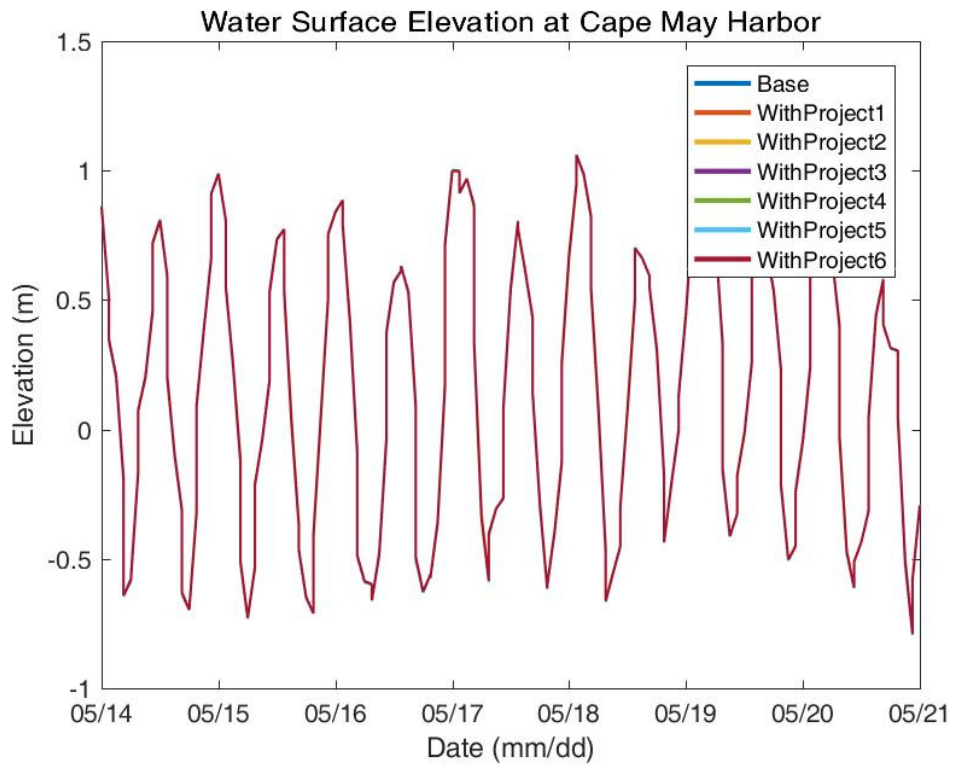


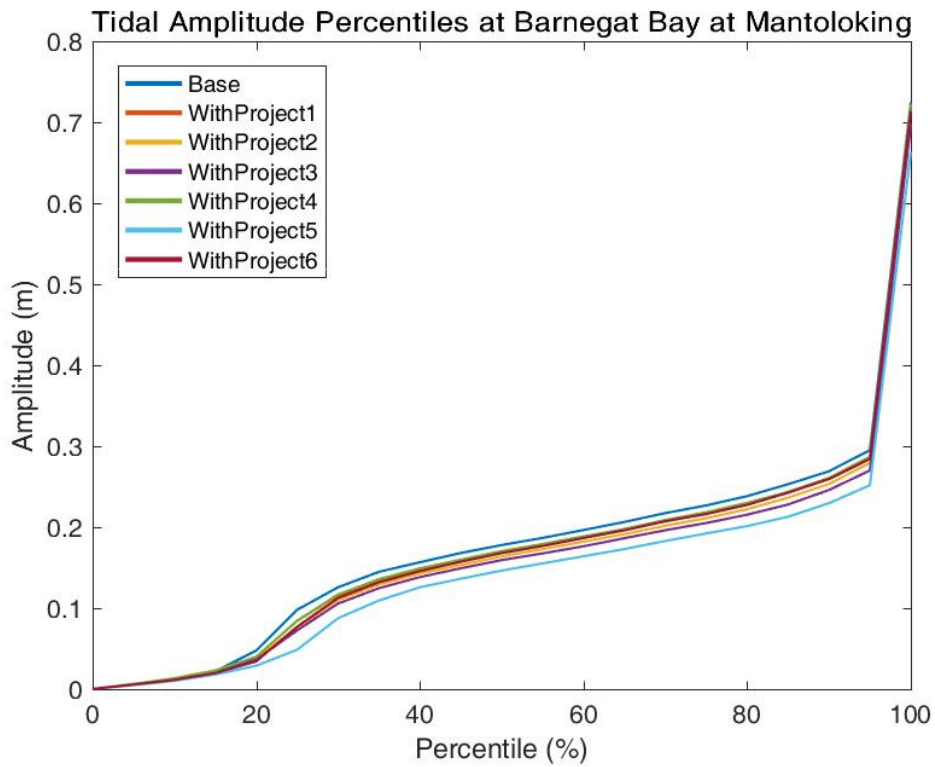
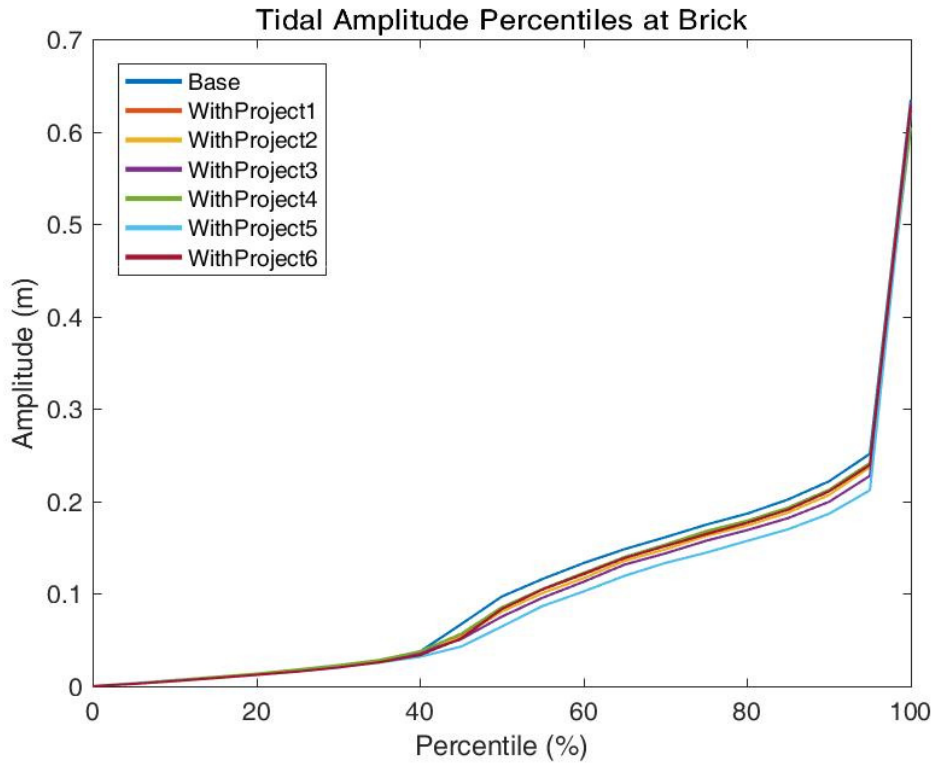


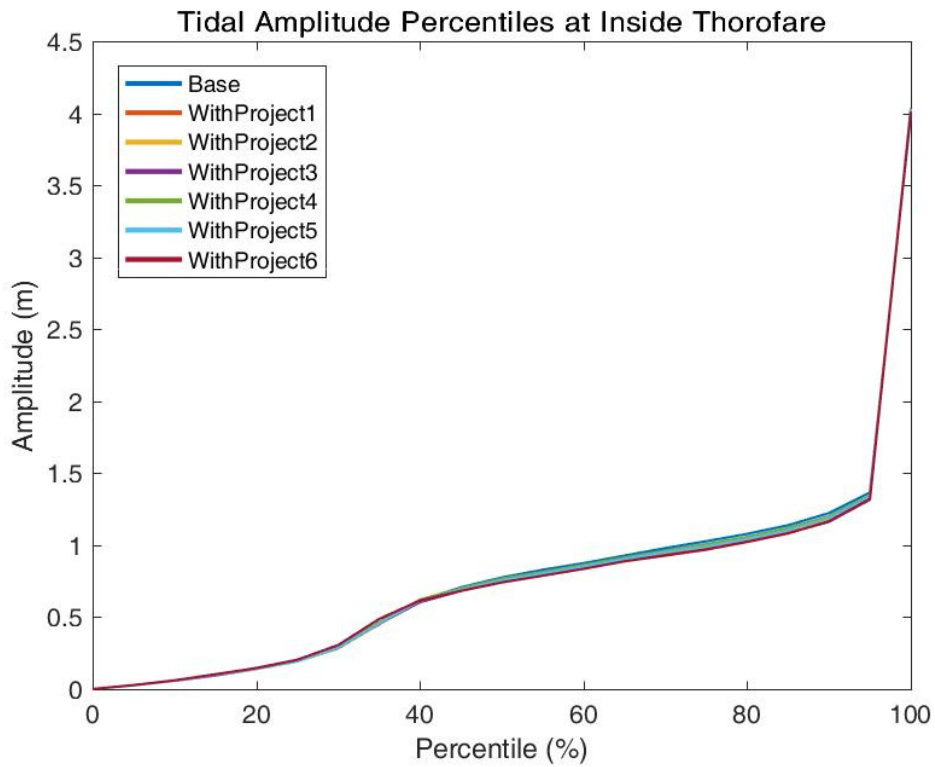
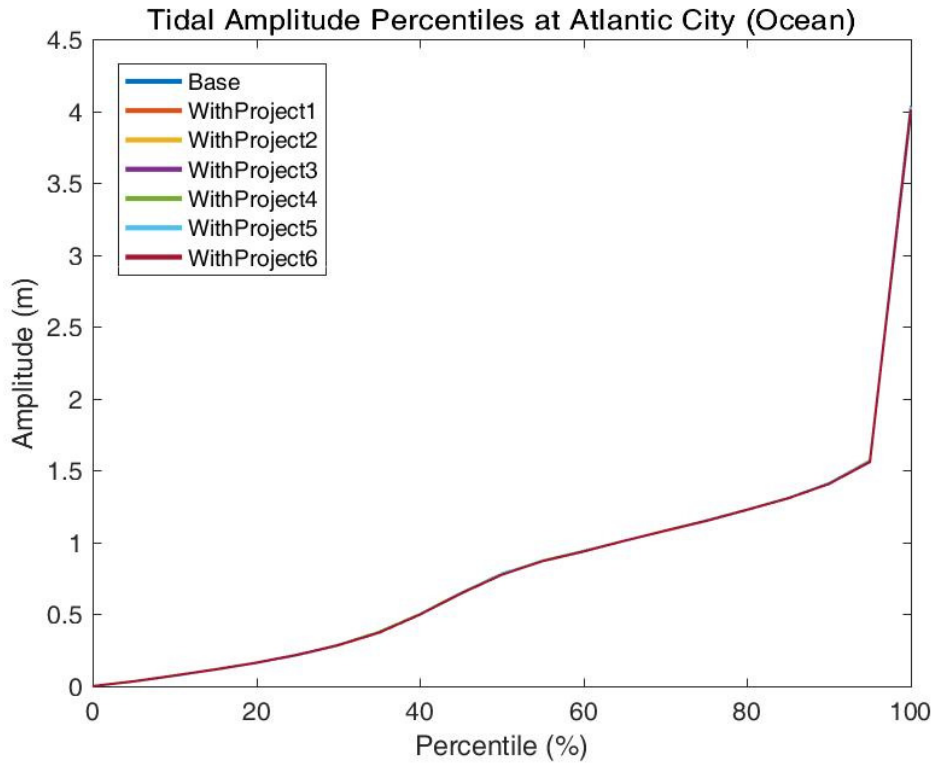


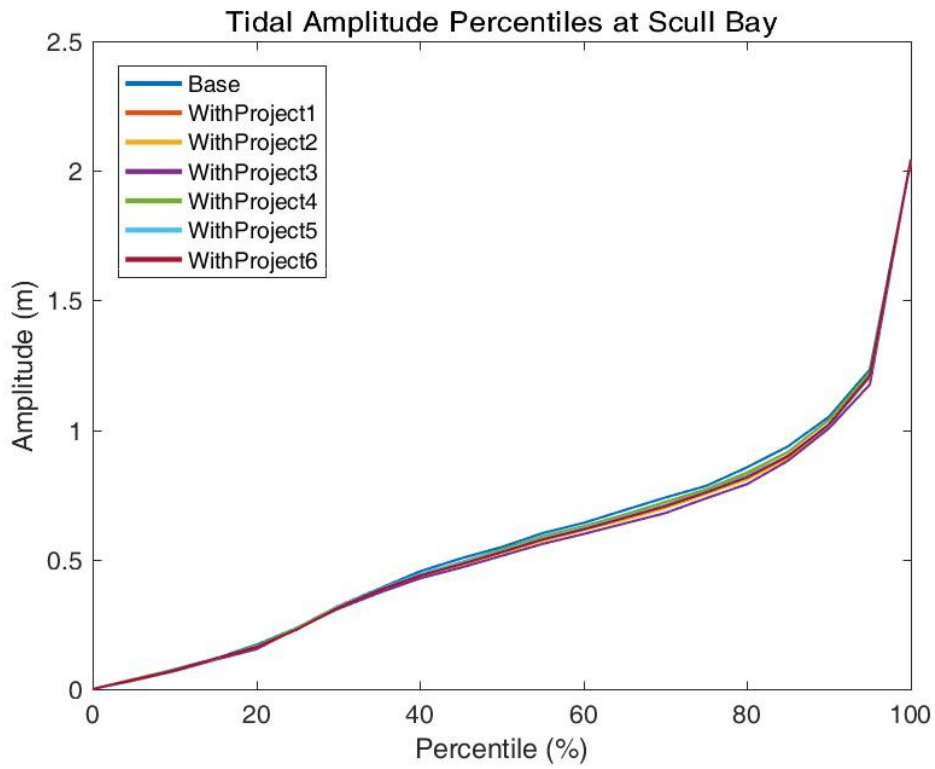
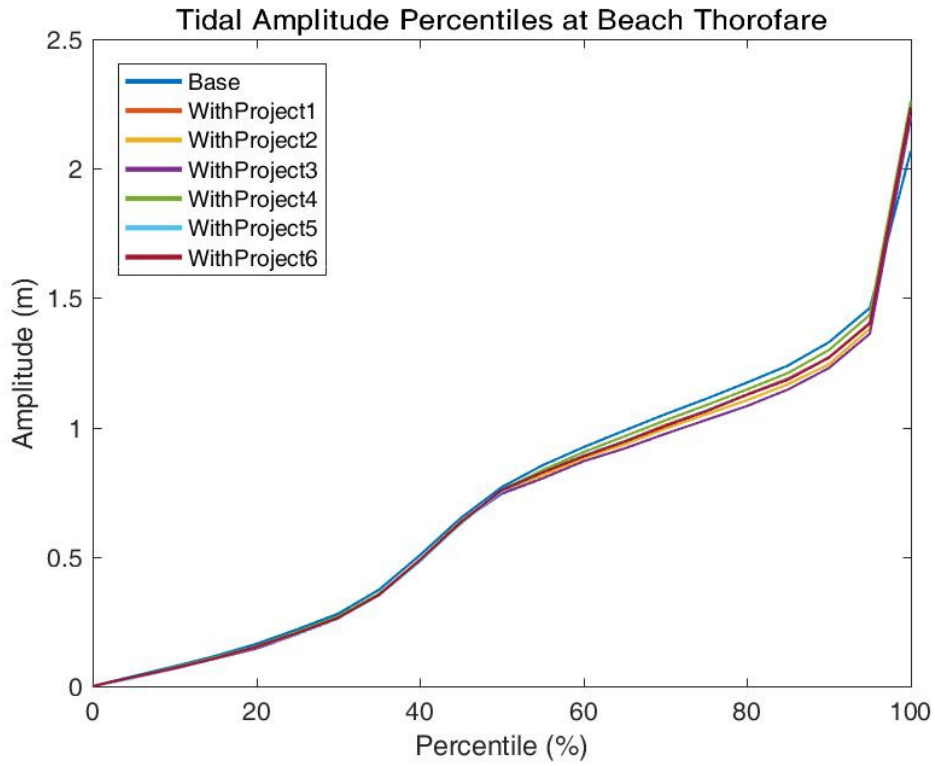


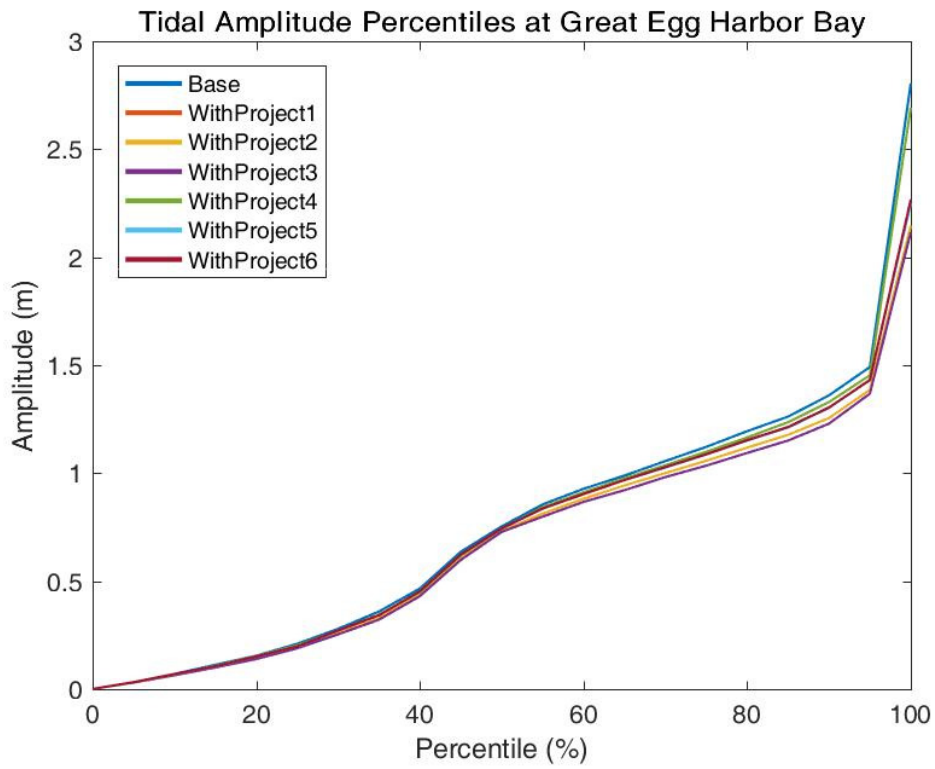
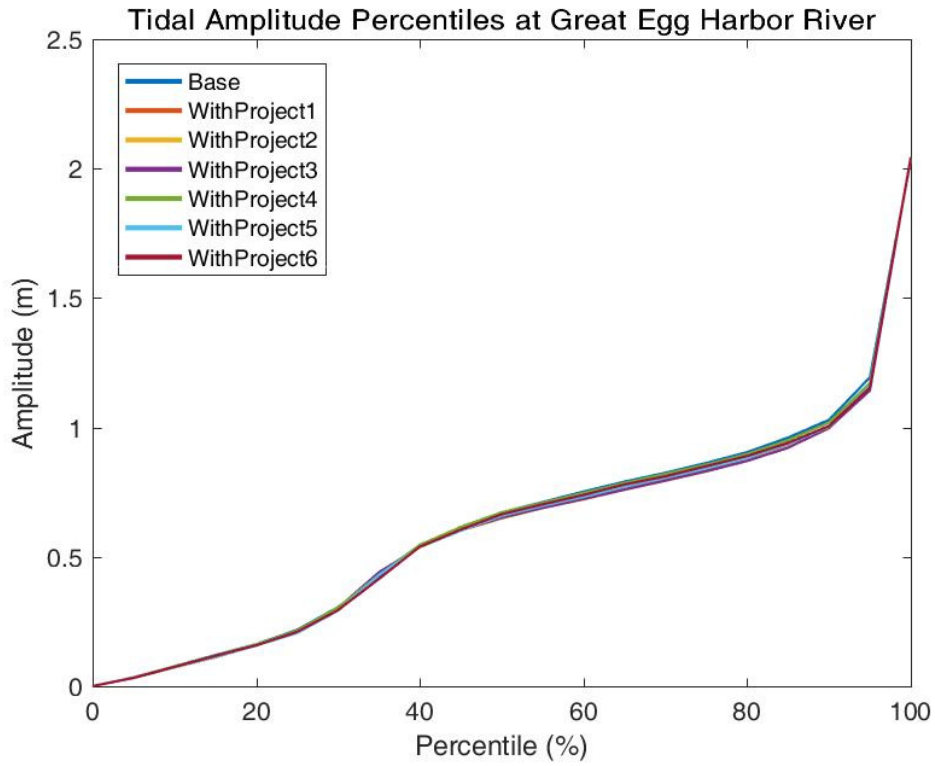


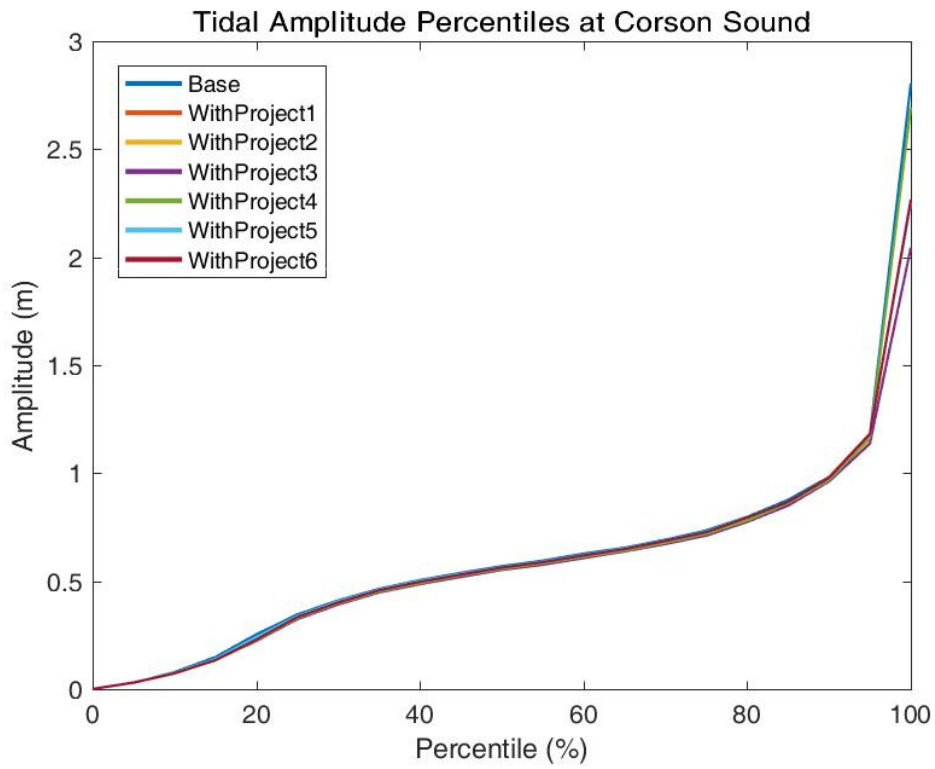
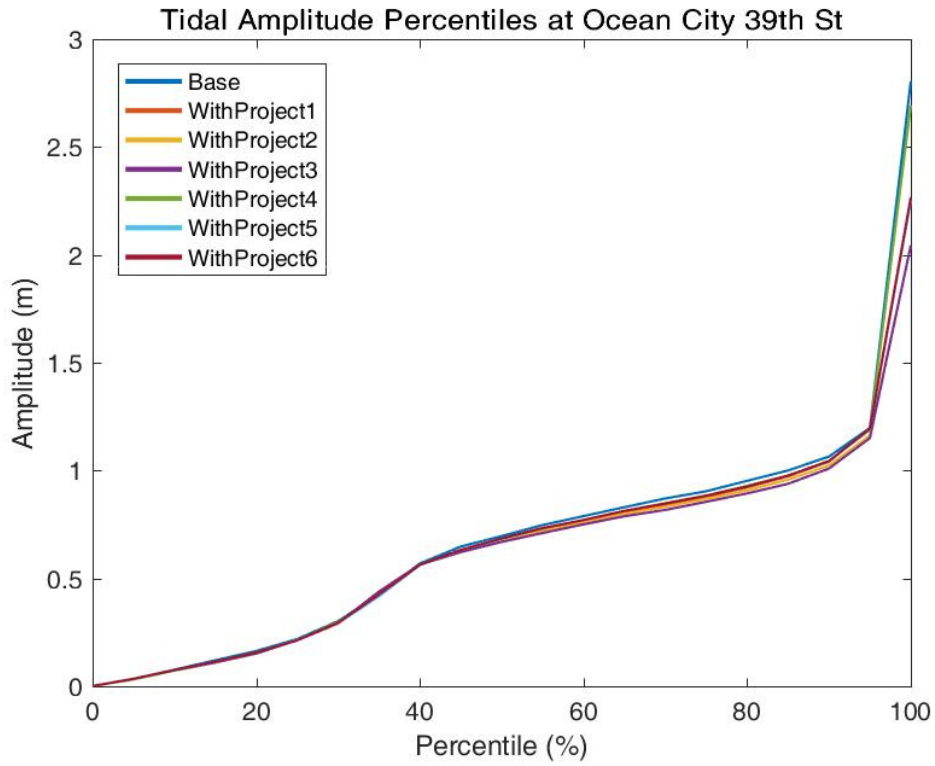


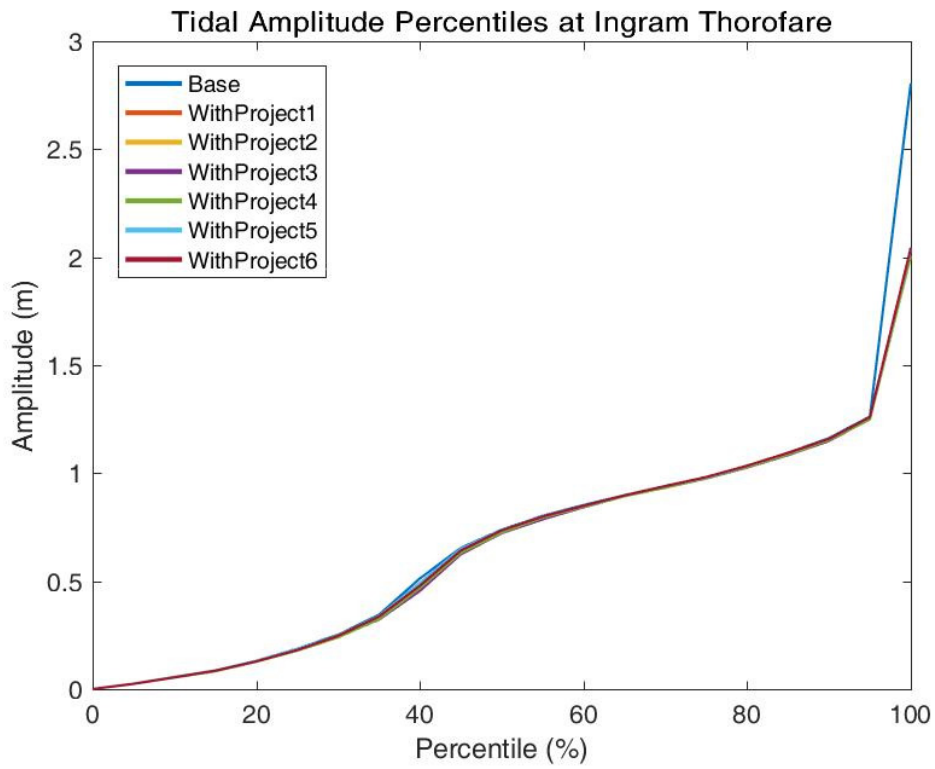
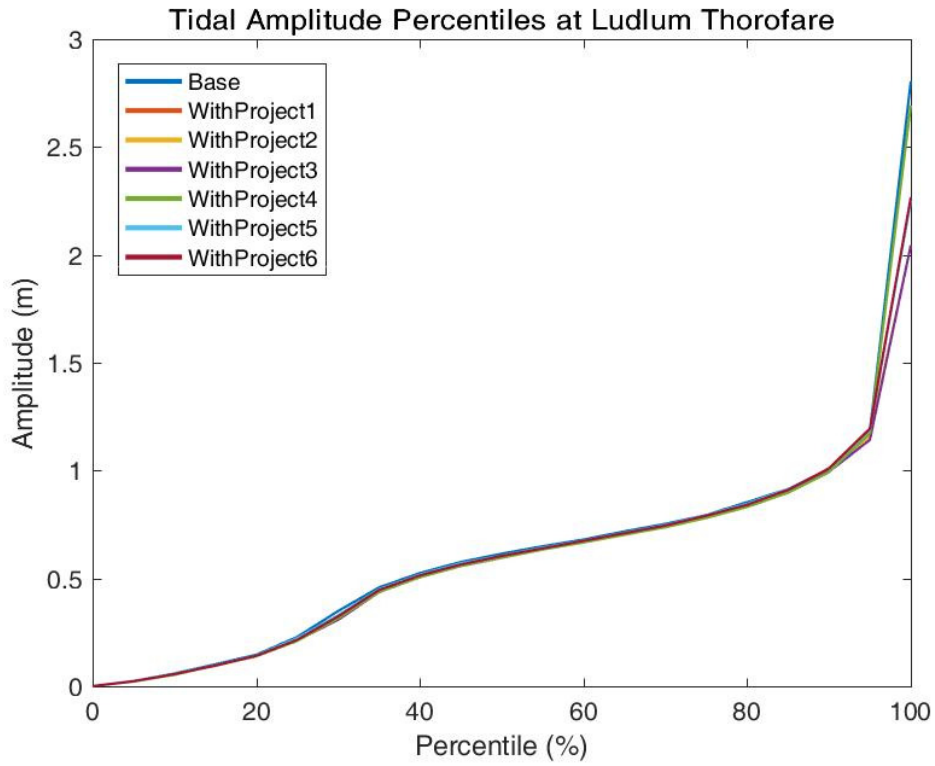


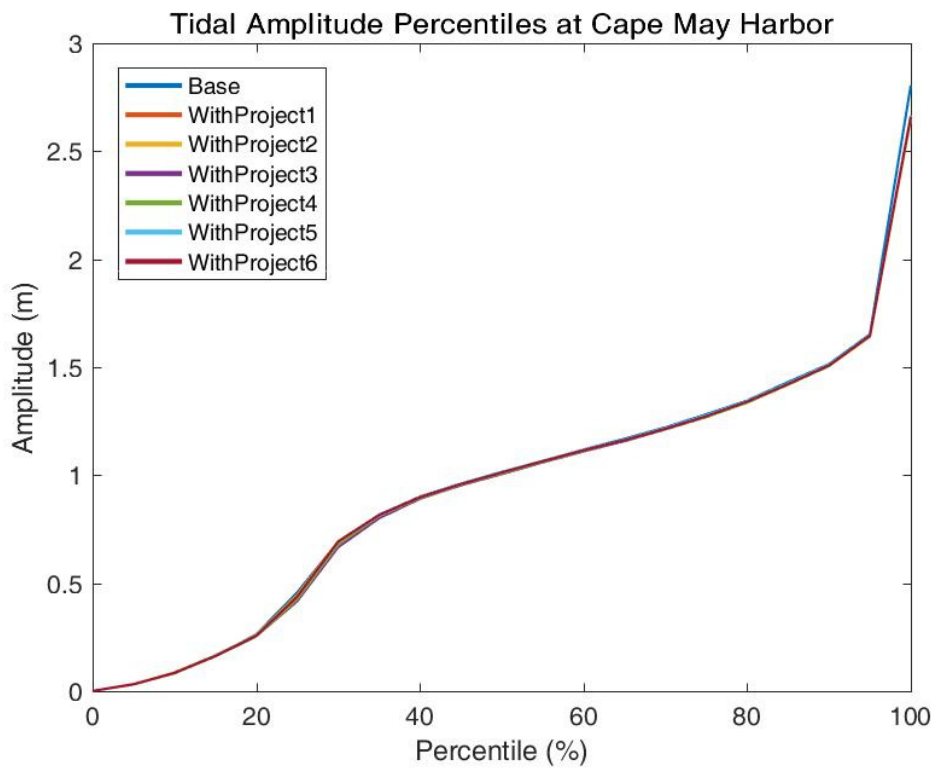
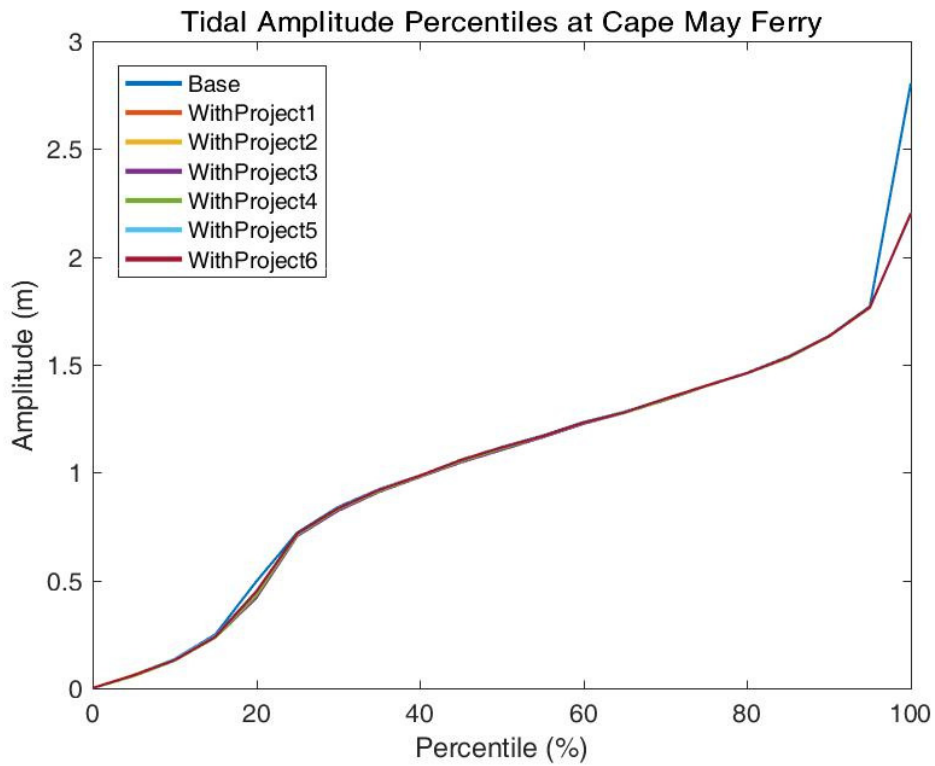




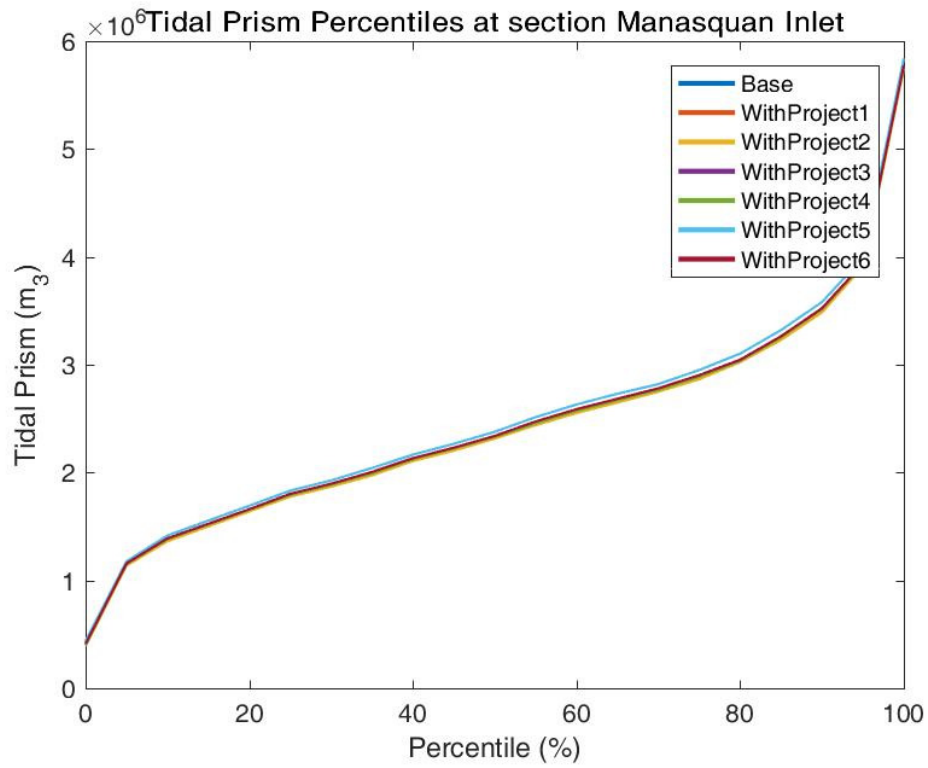
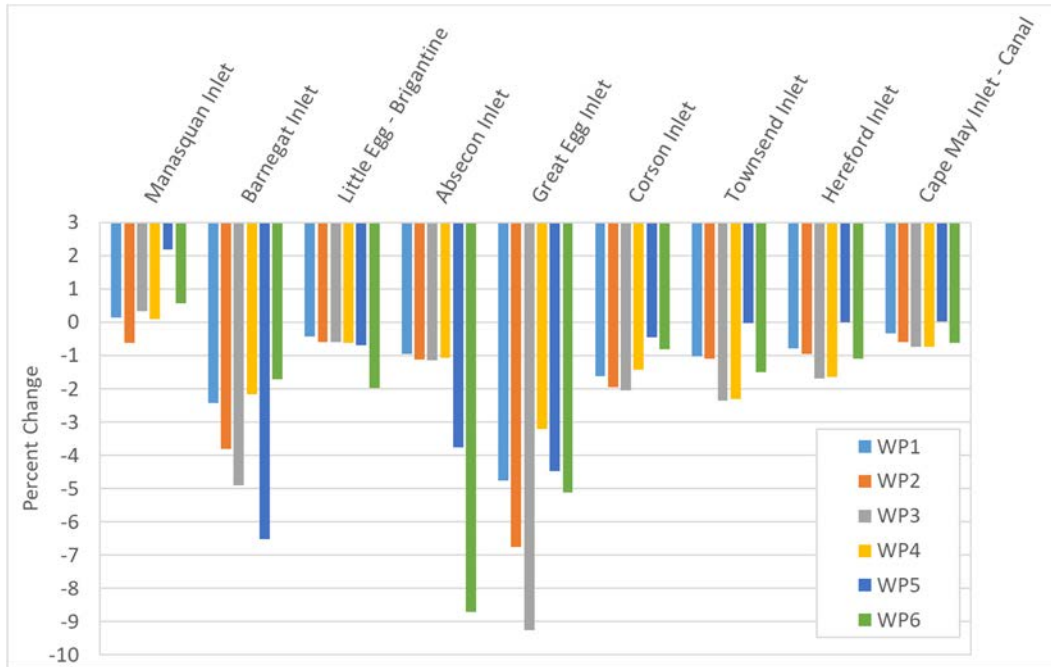


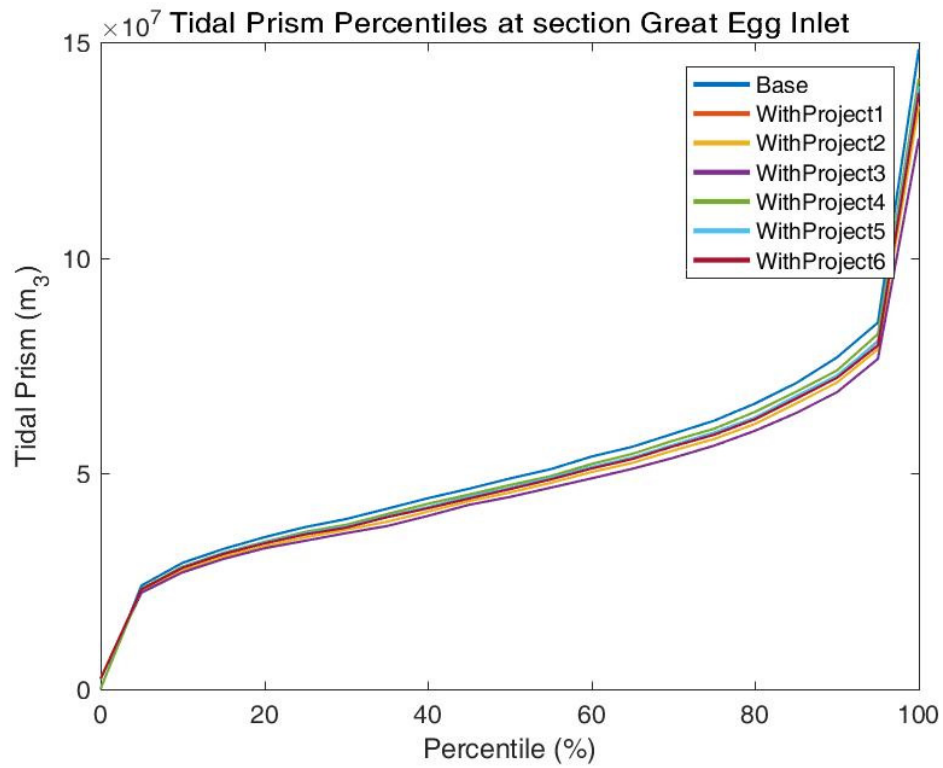
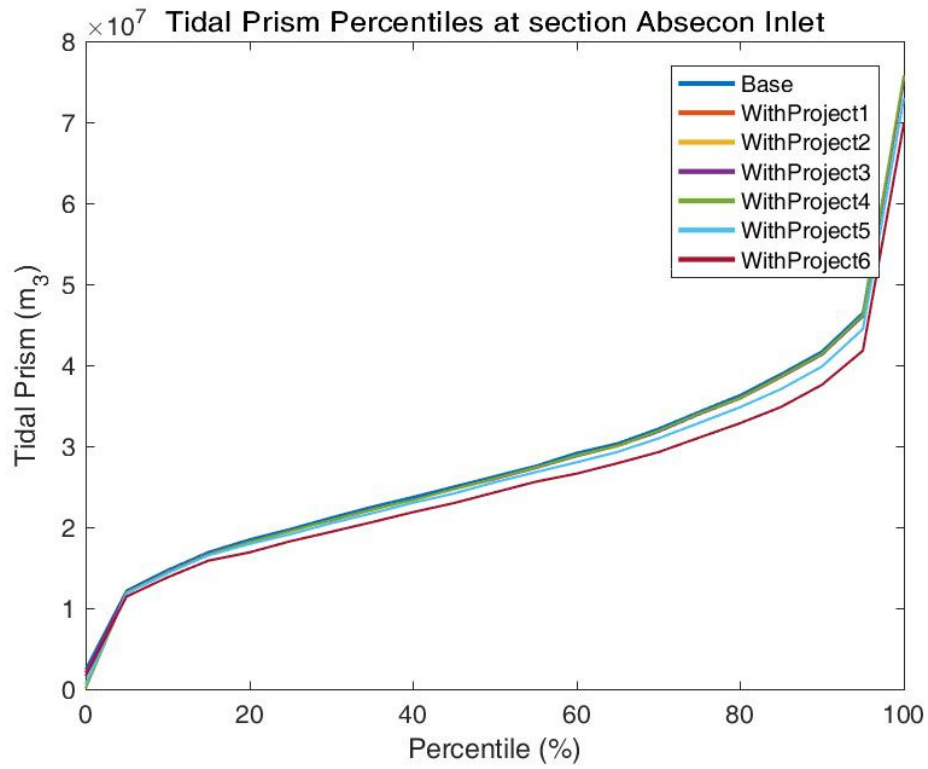


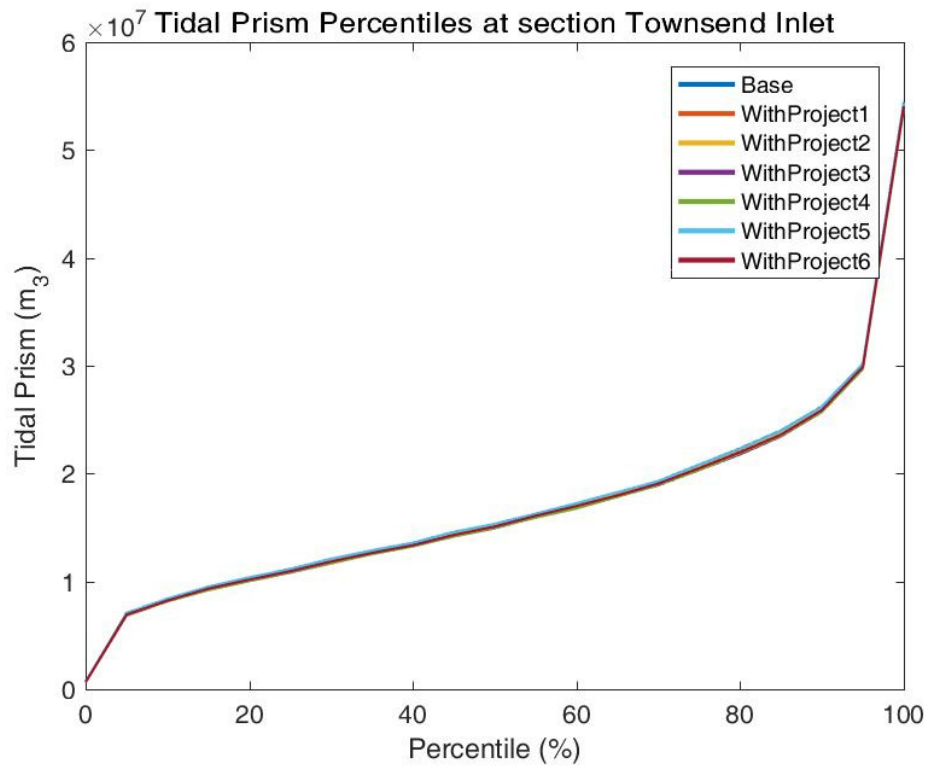
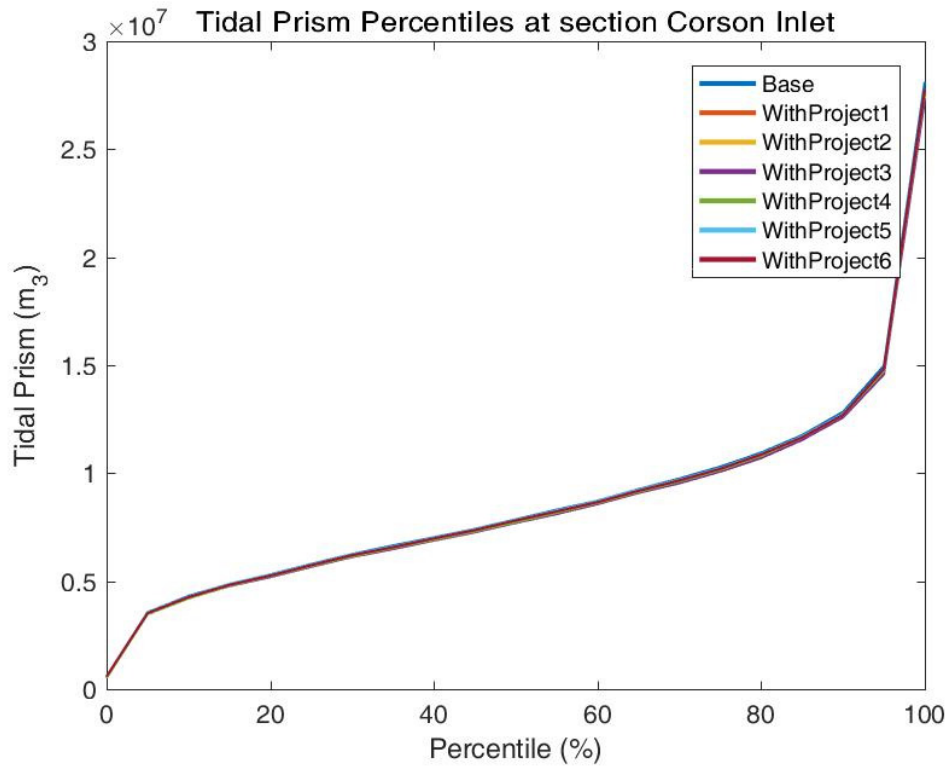


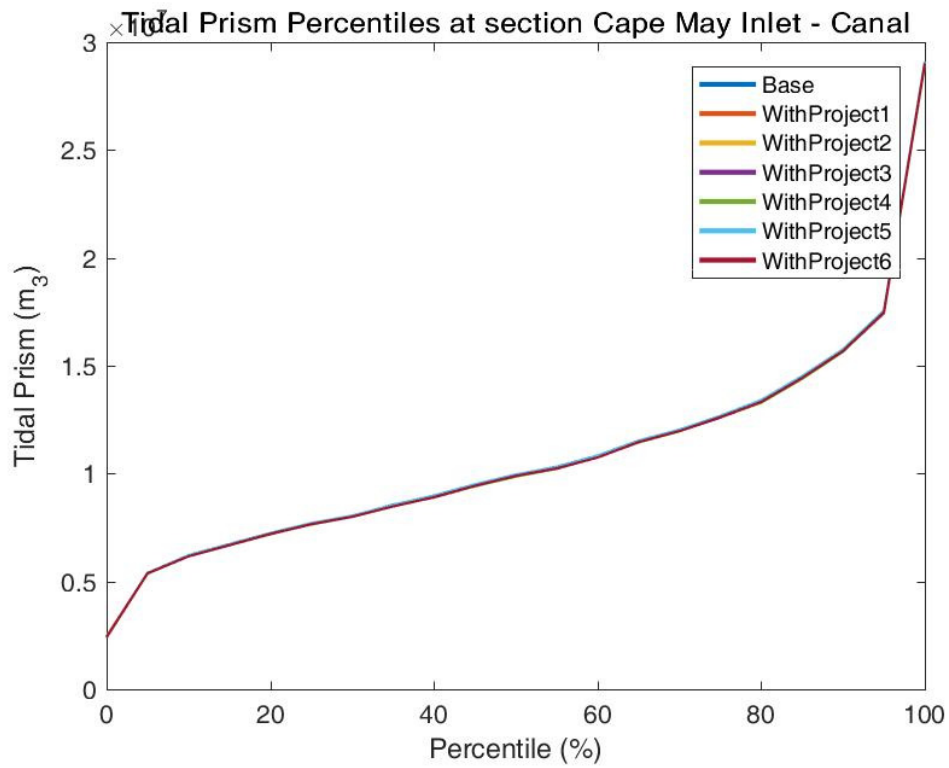
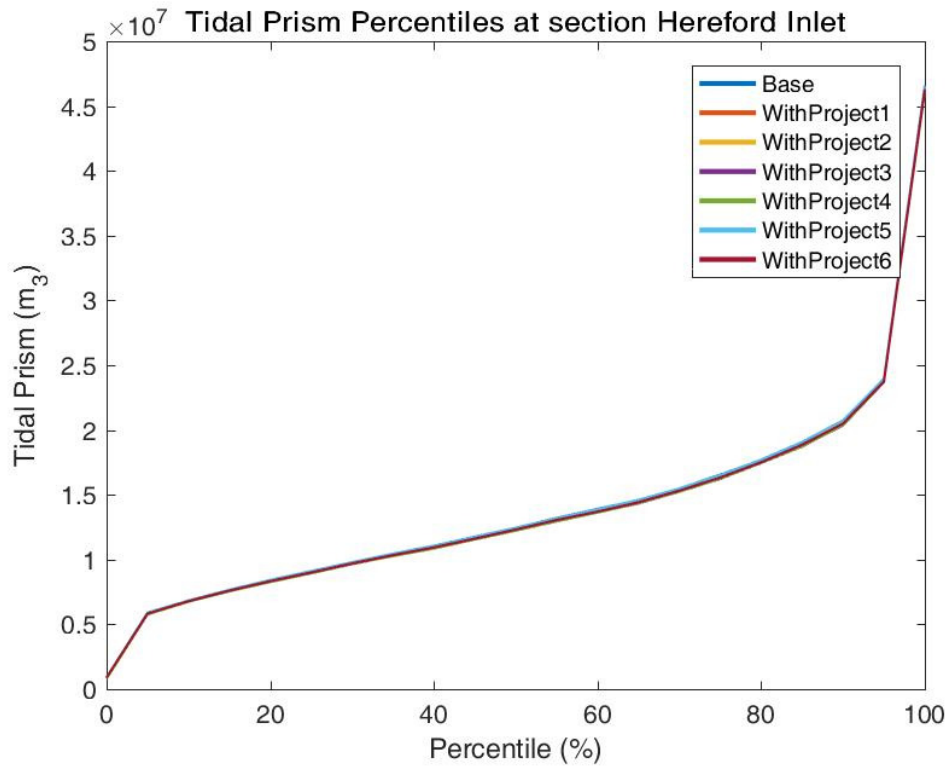


Tidal Prism Plots



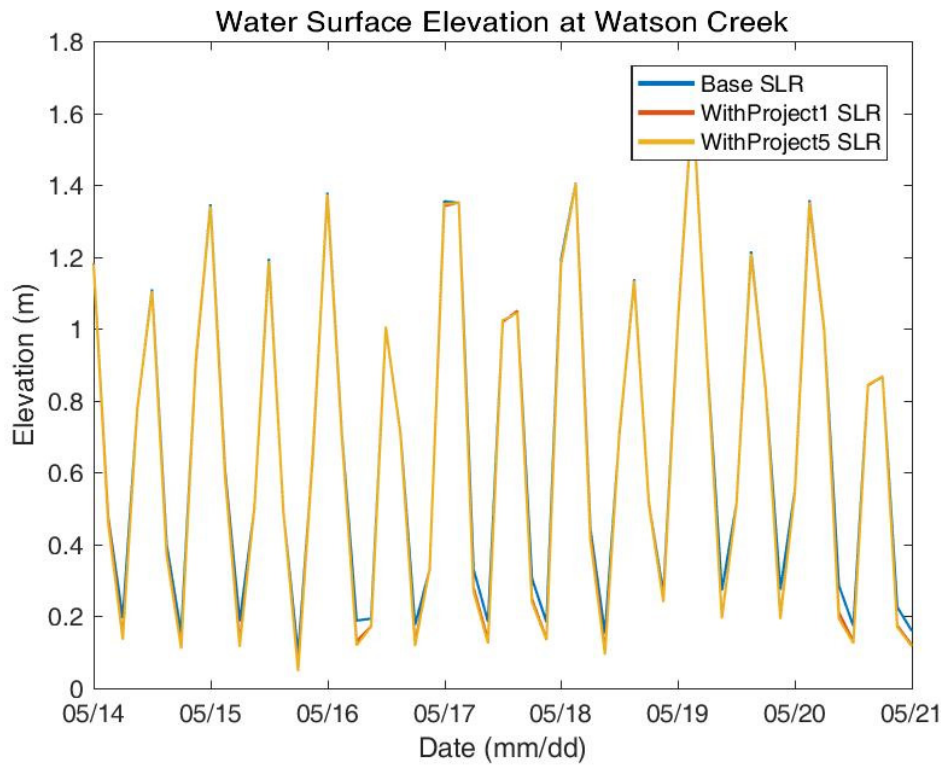


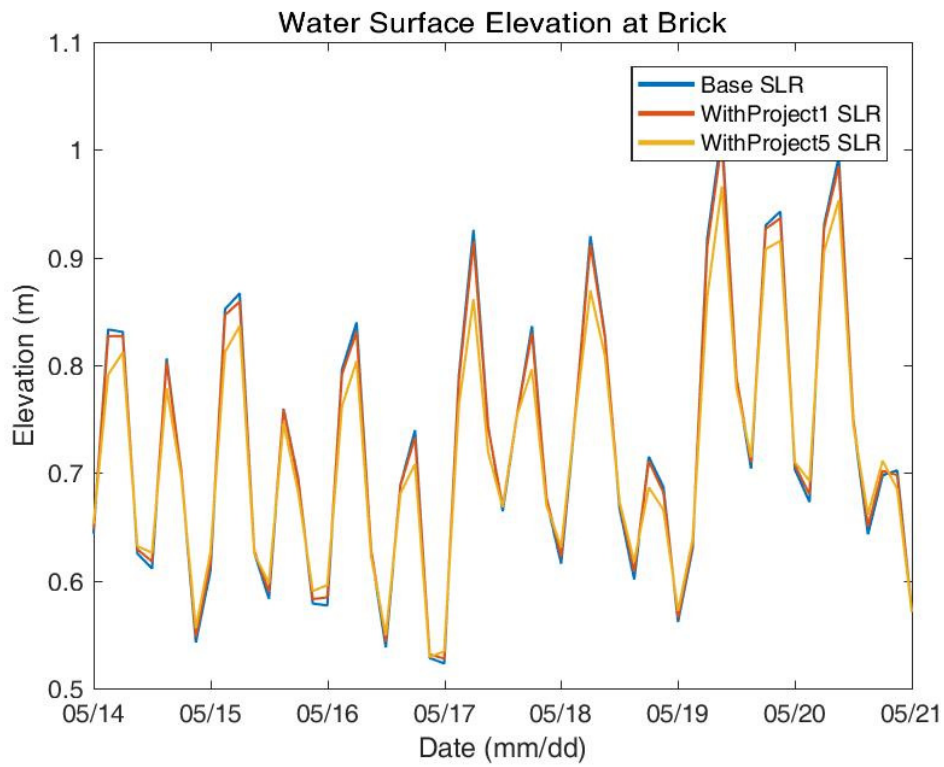
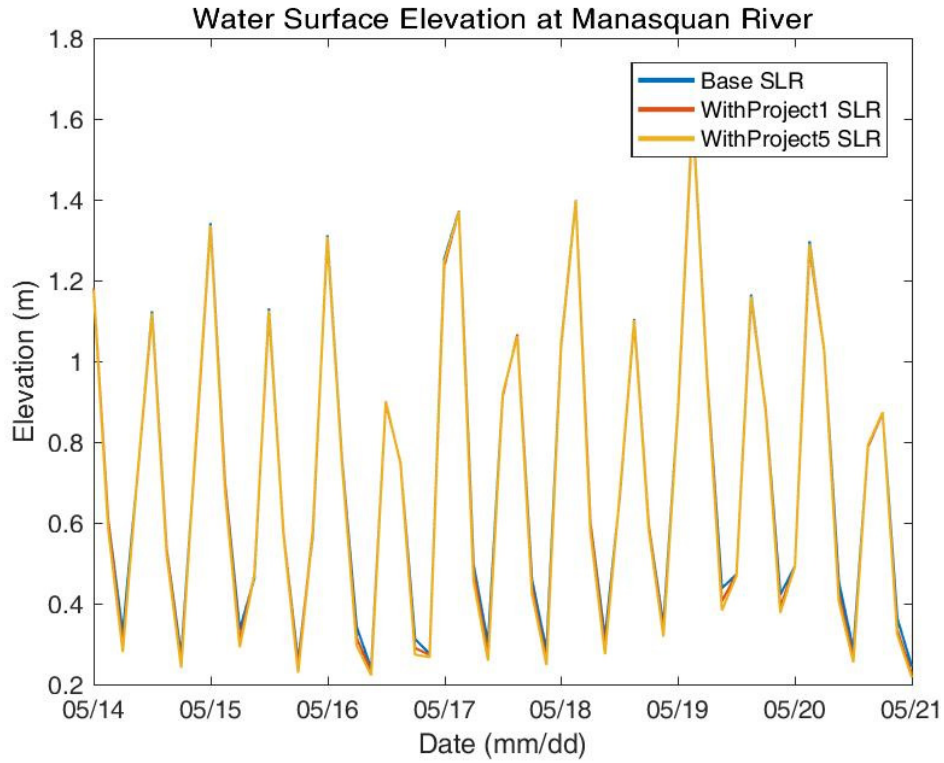


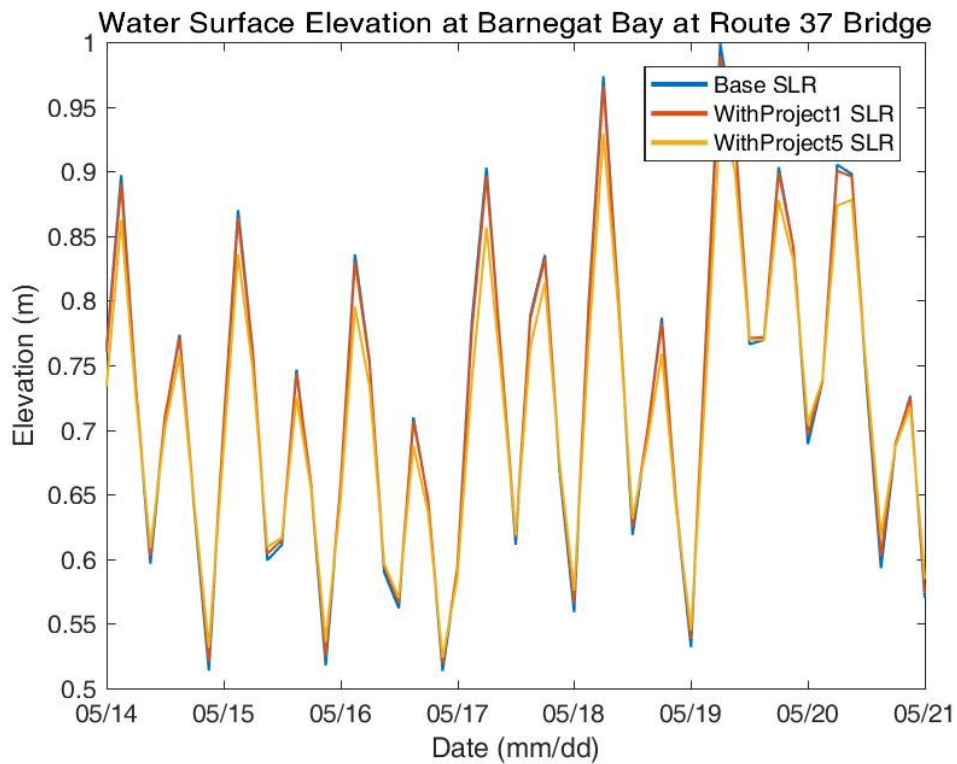
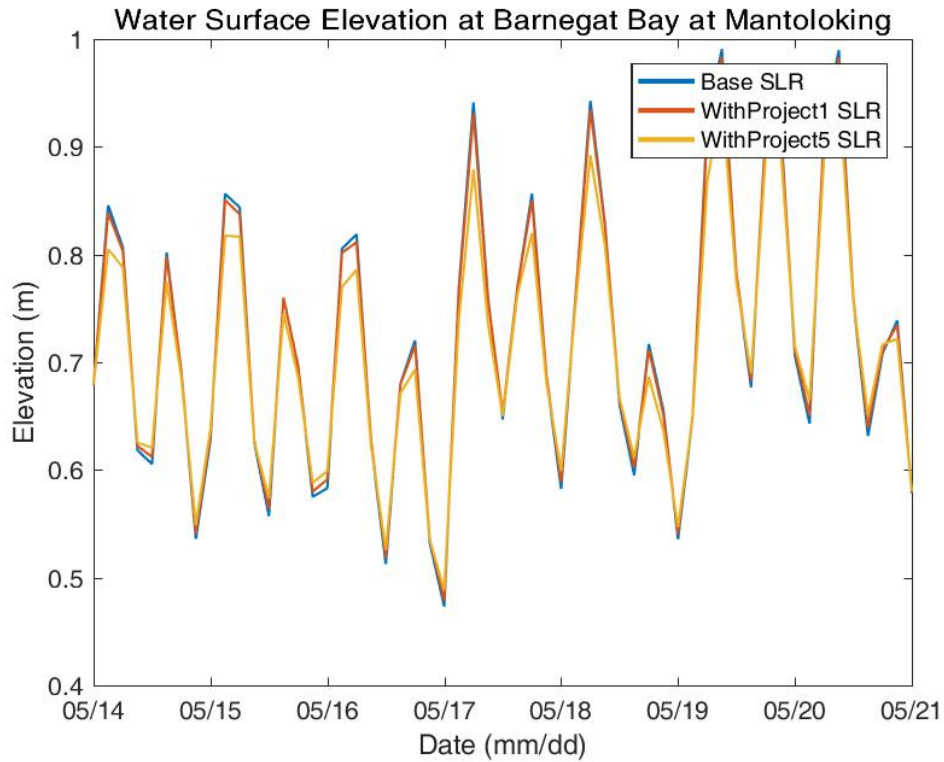


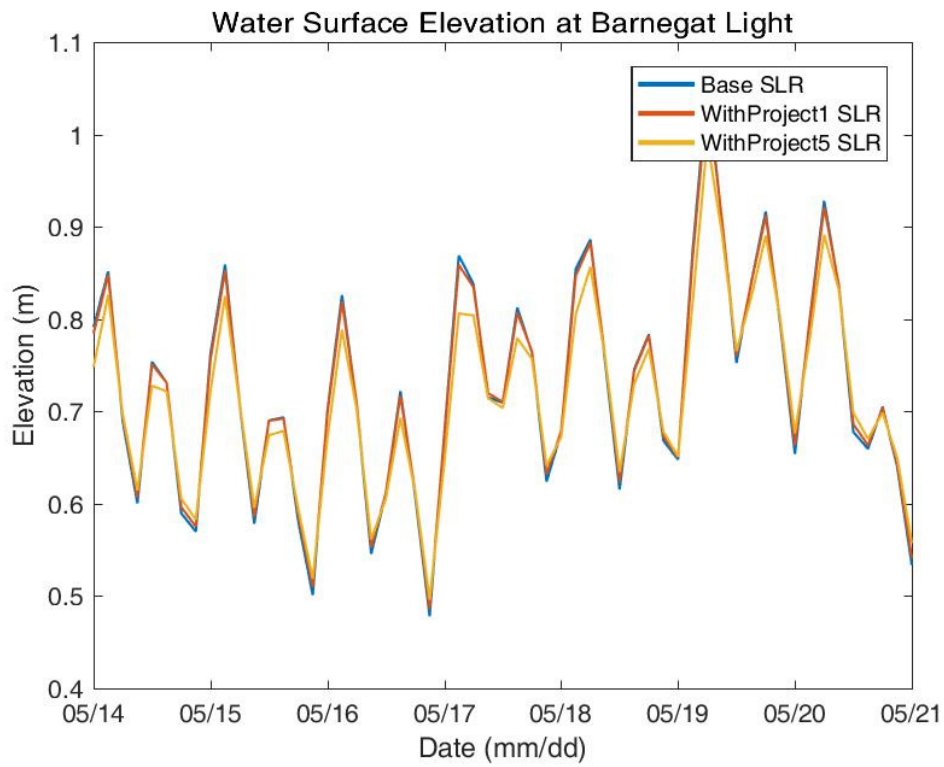
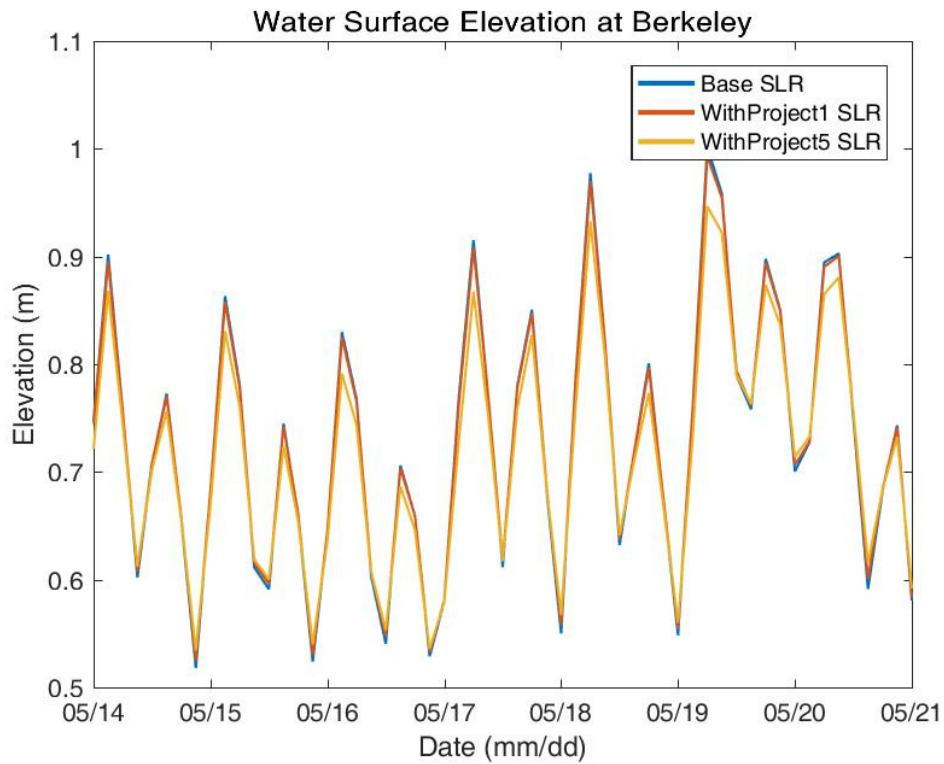
Comparisons to Base with Sea Level Rise

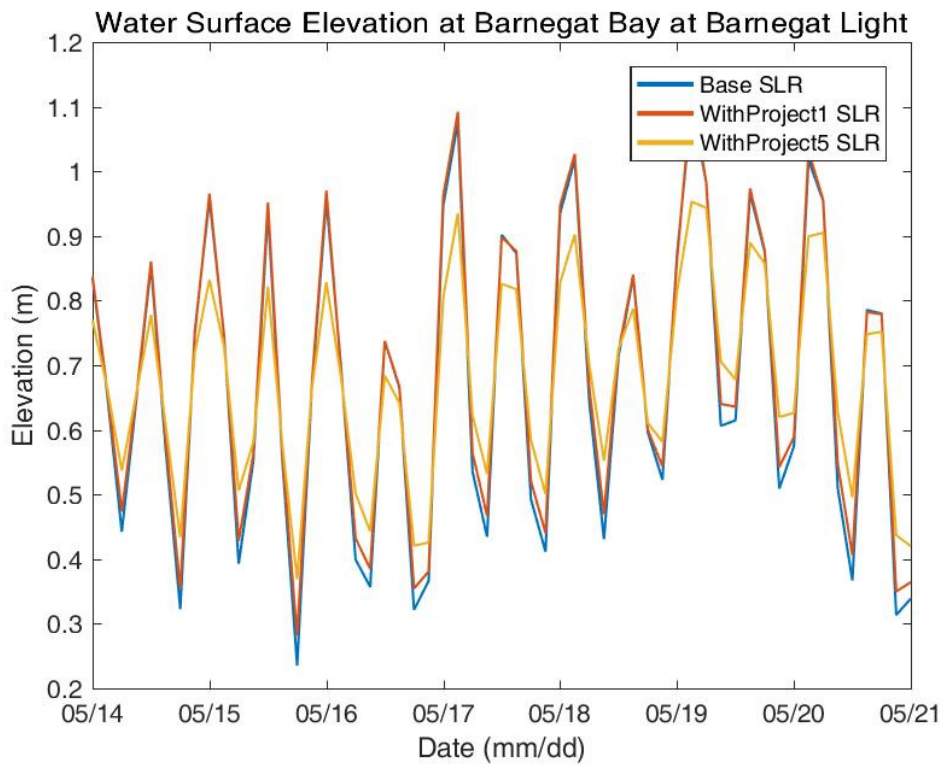
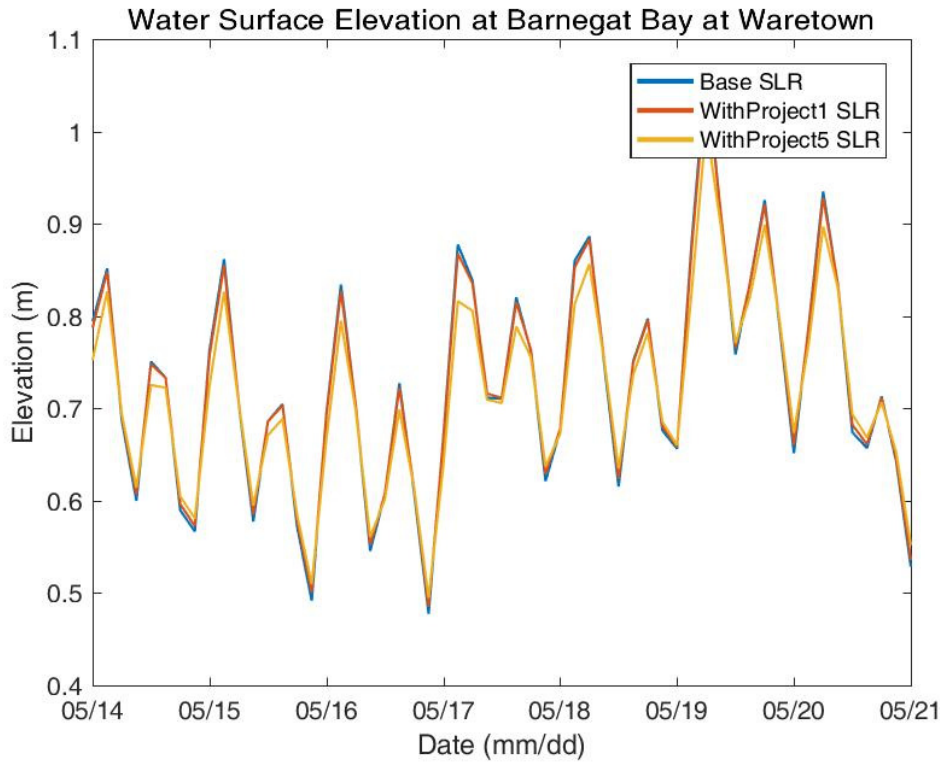
Water Surface Elevation Plots

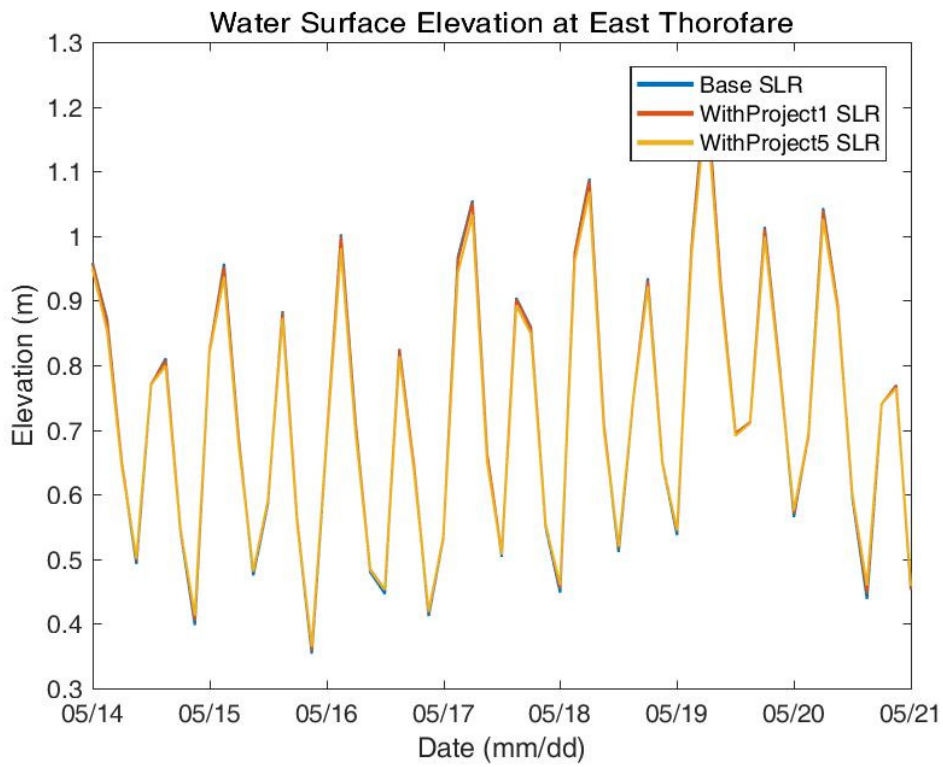
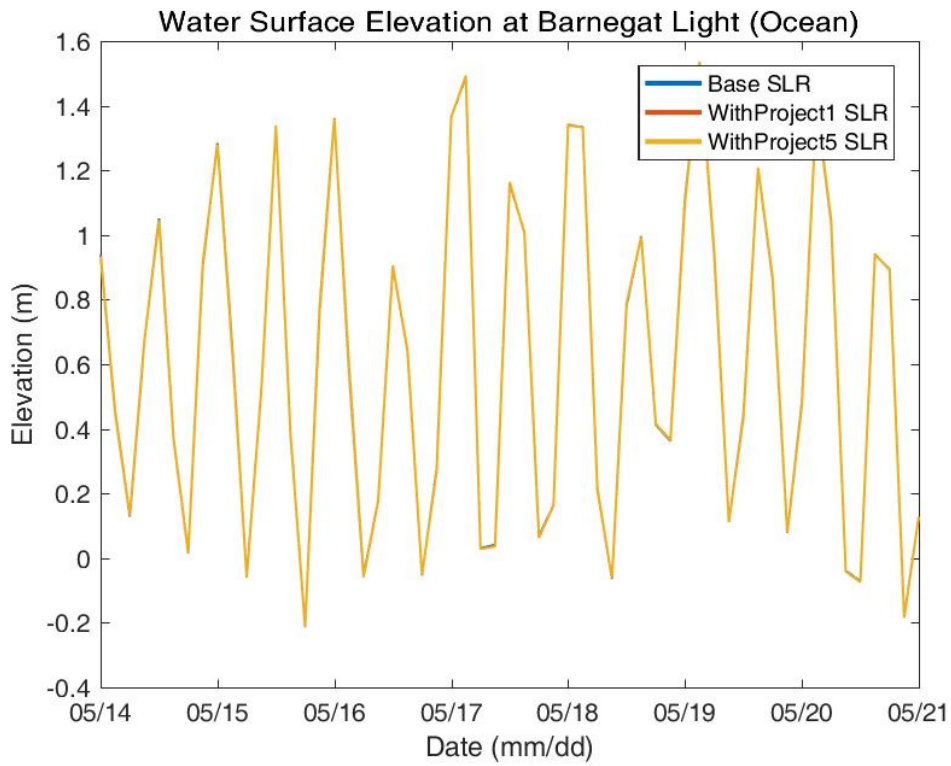


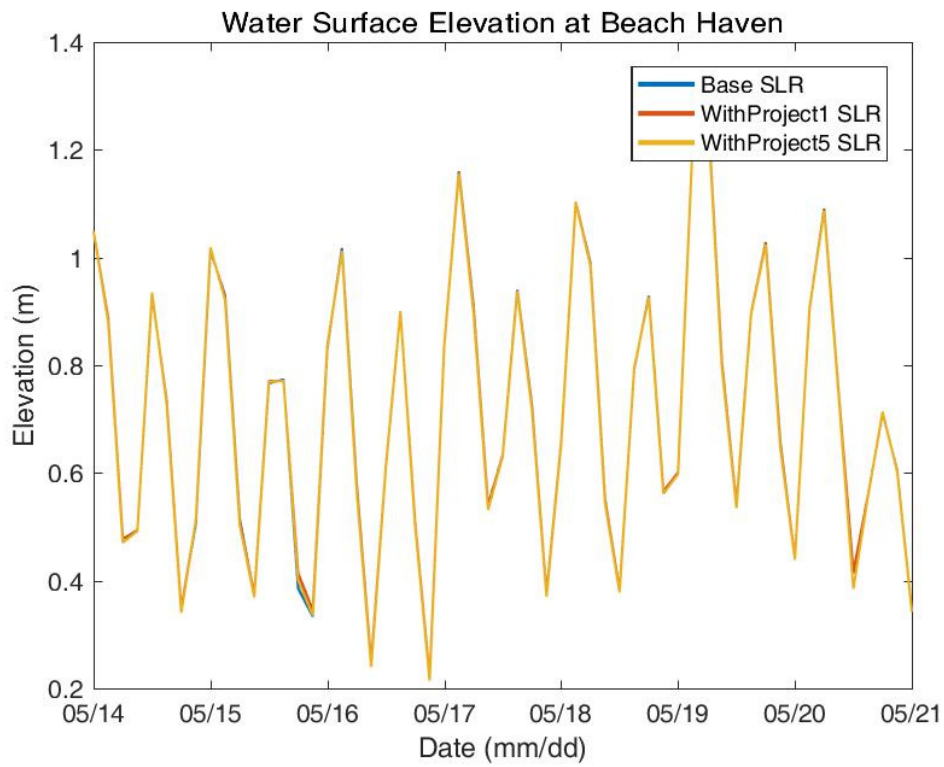
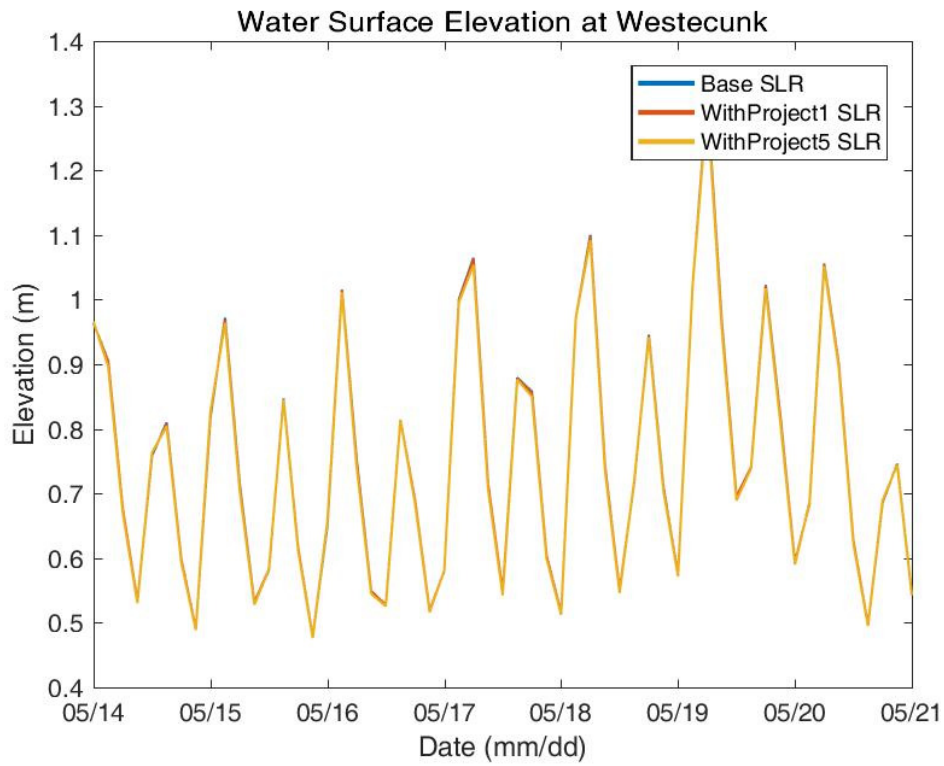


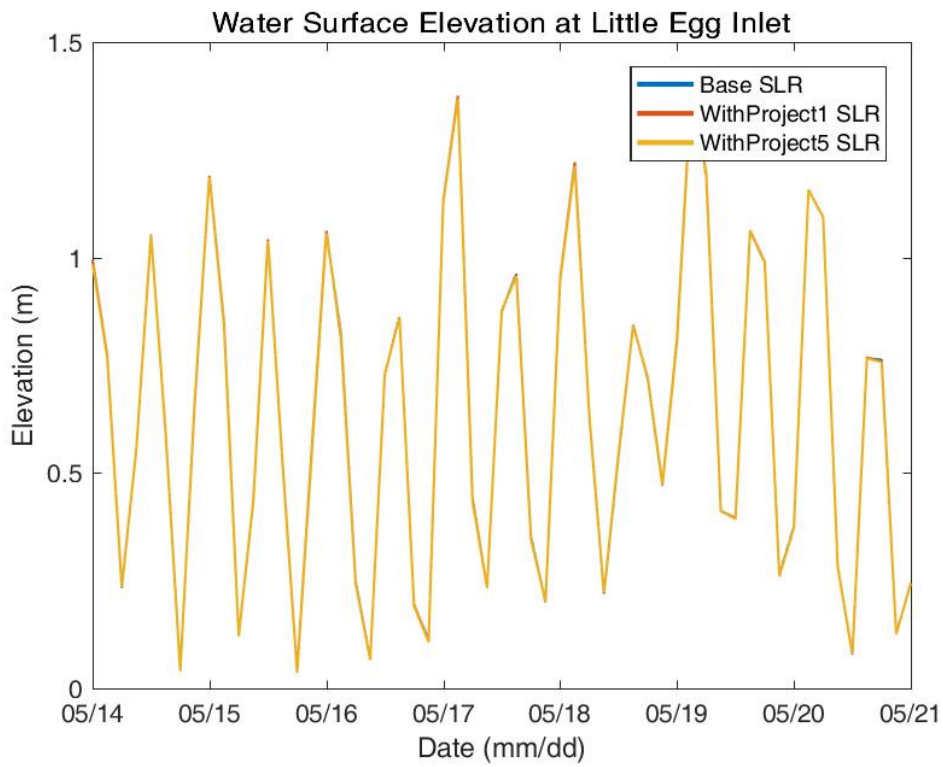
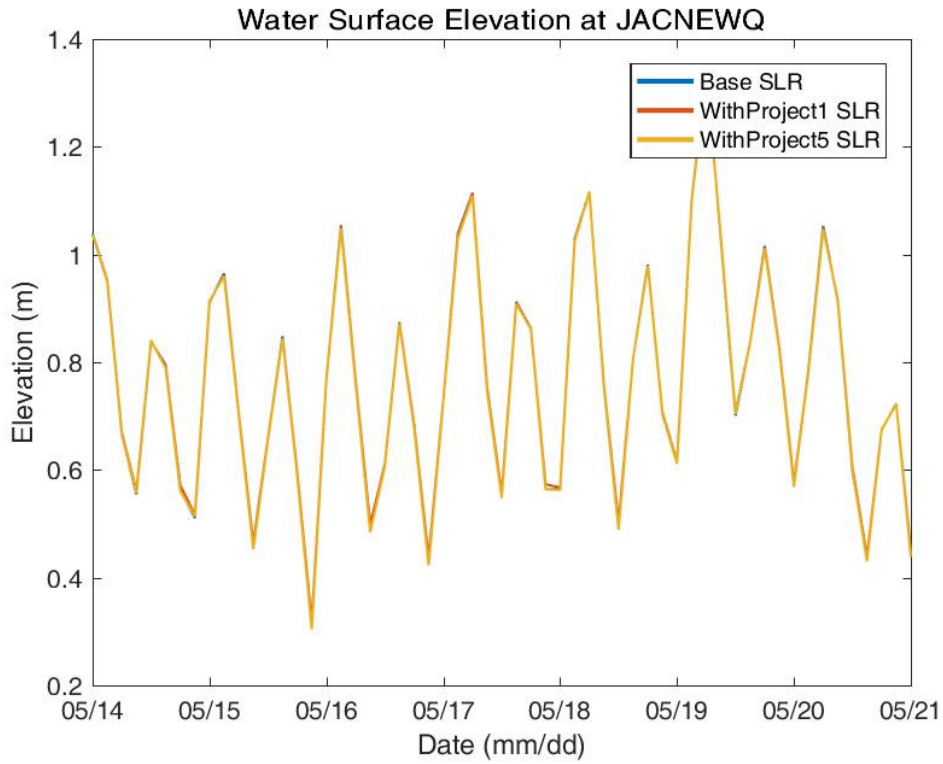


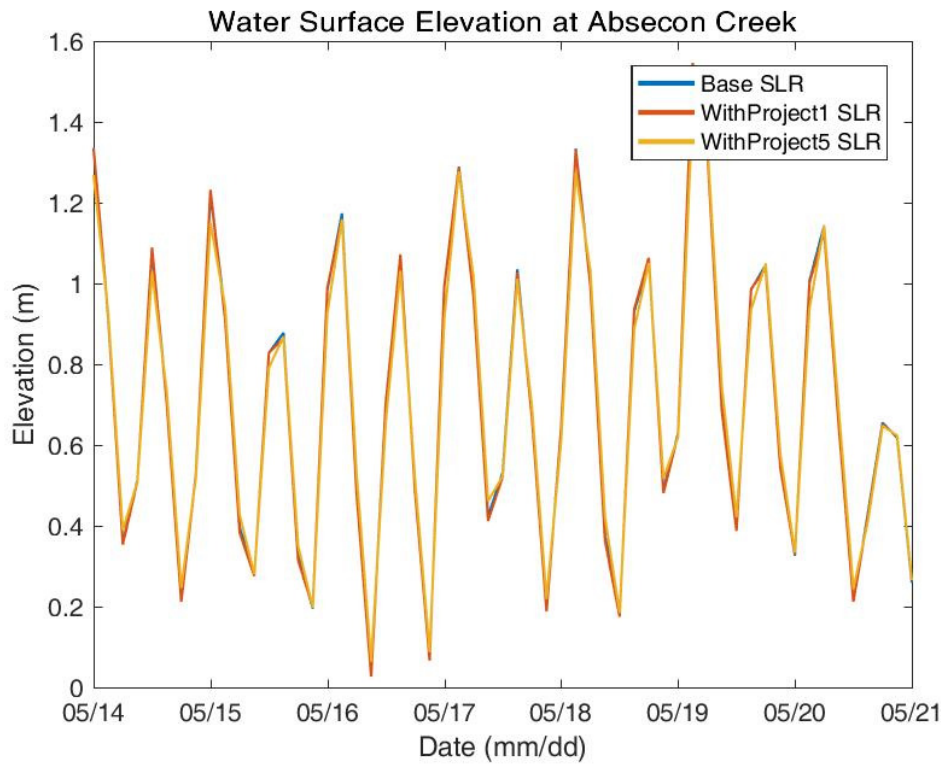


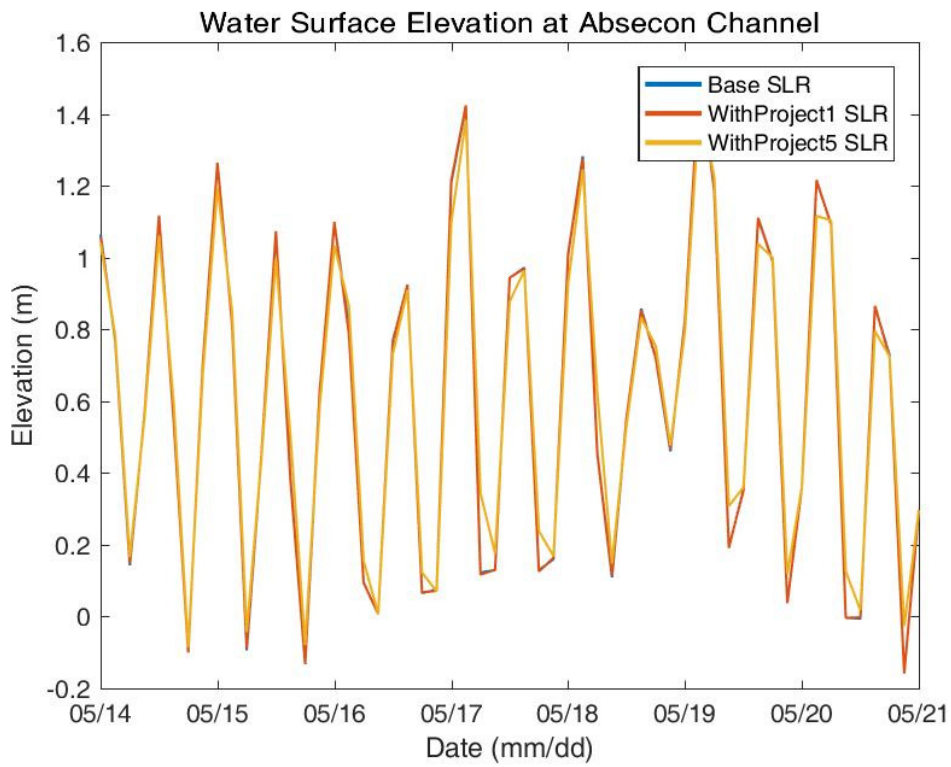
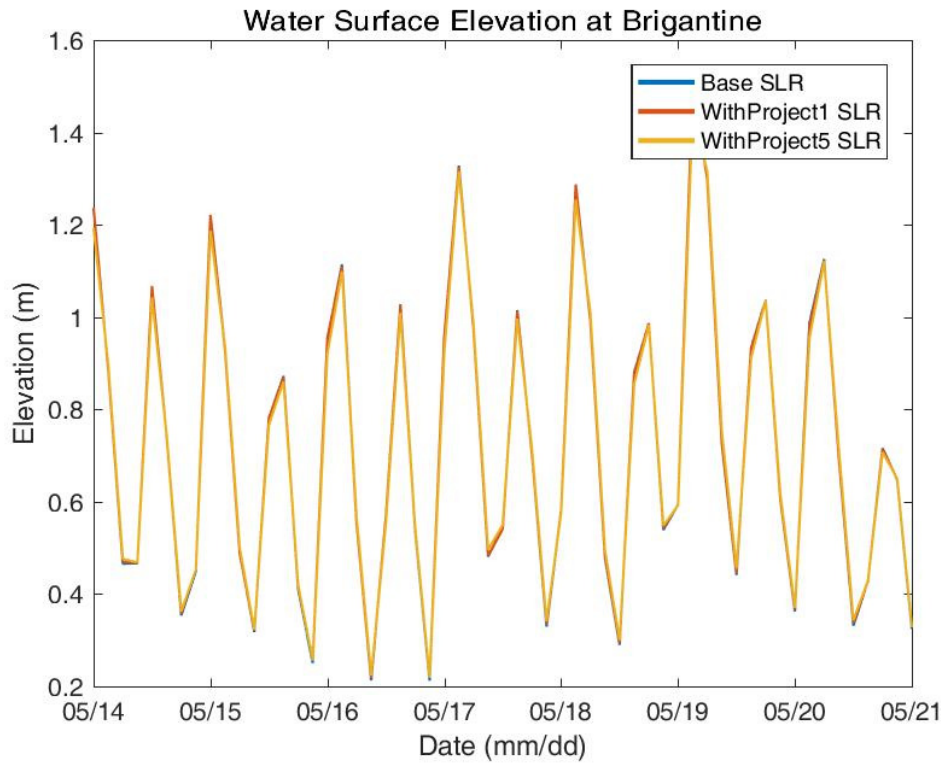


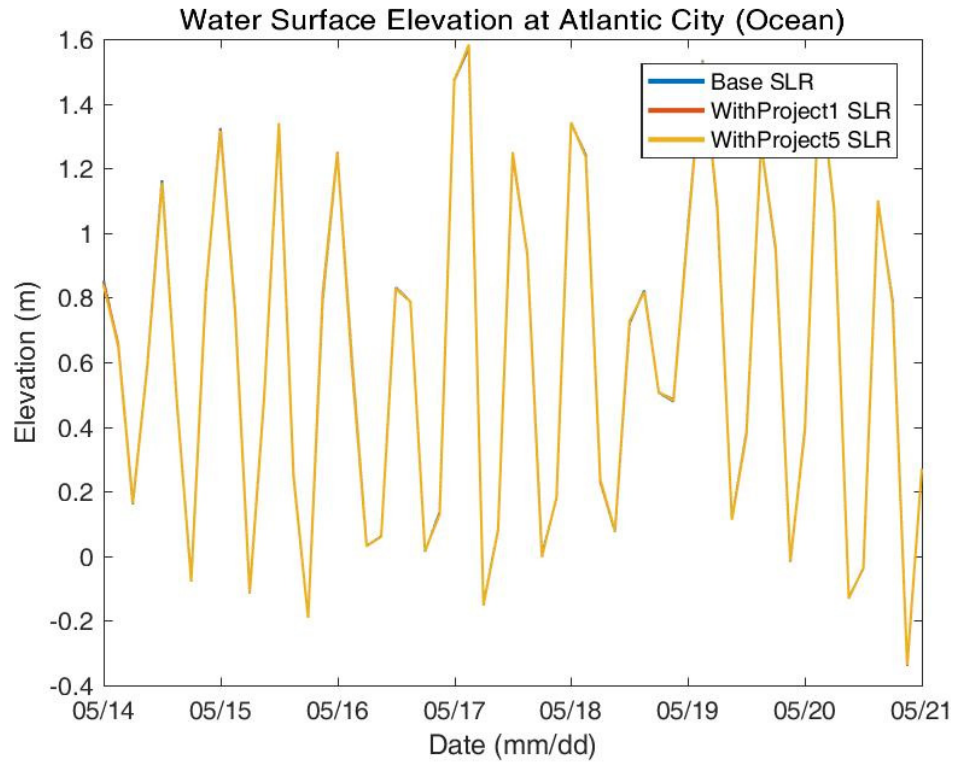


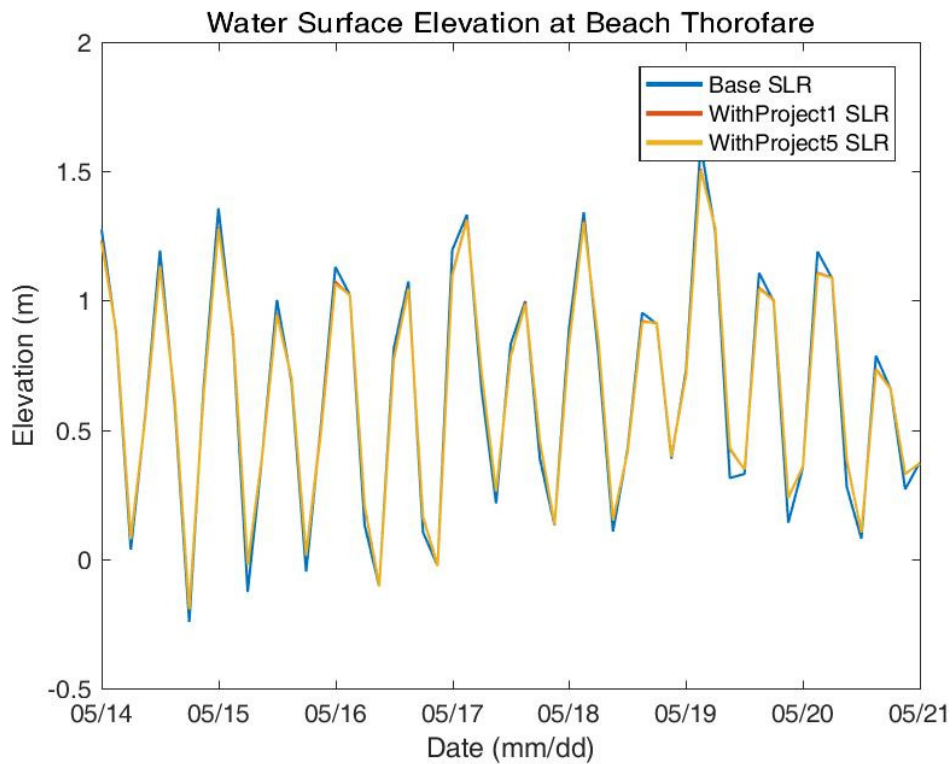
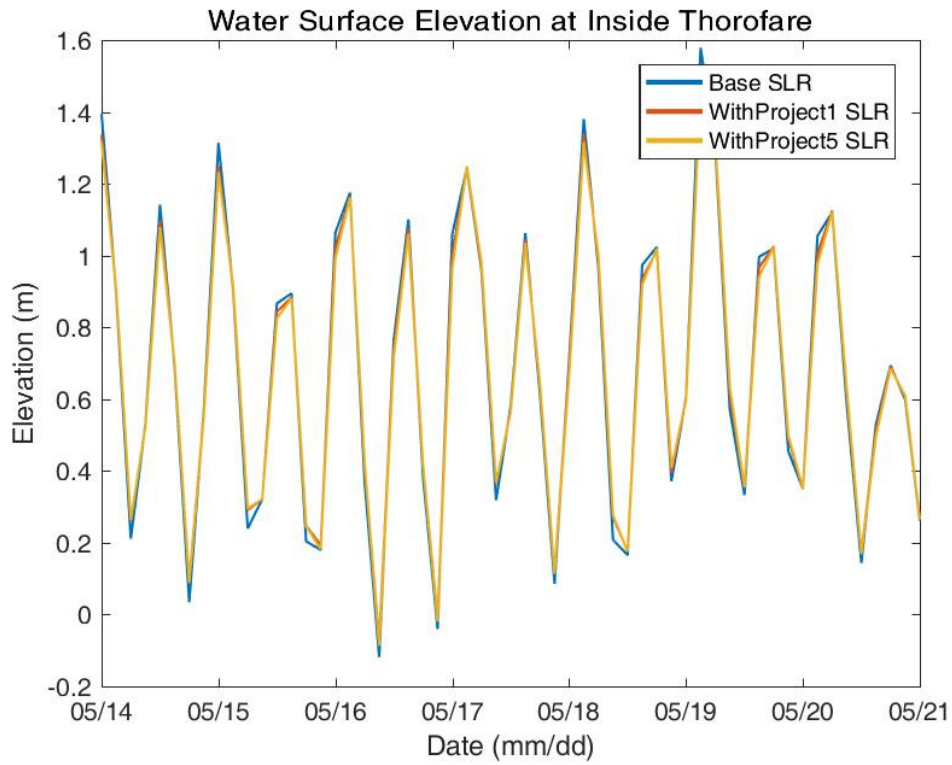


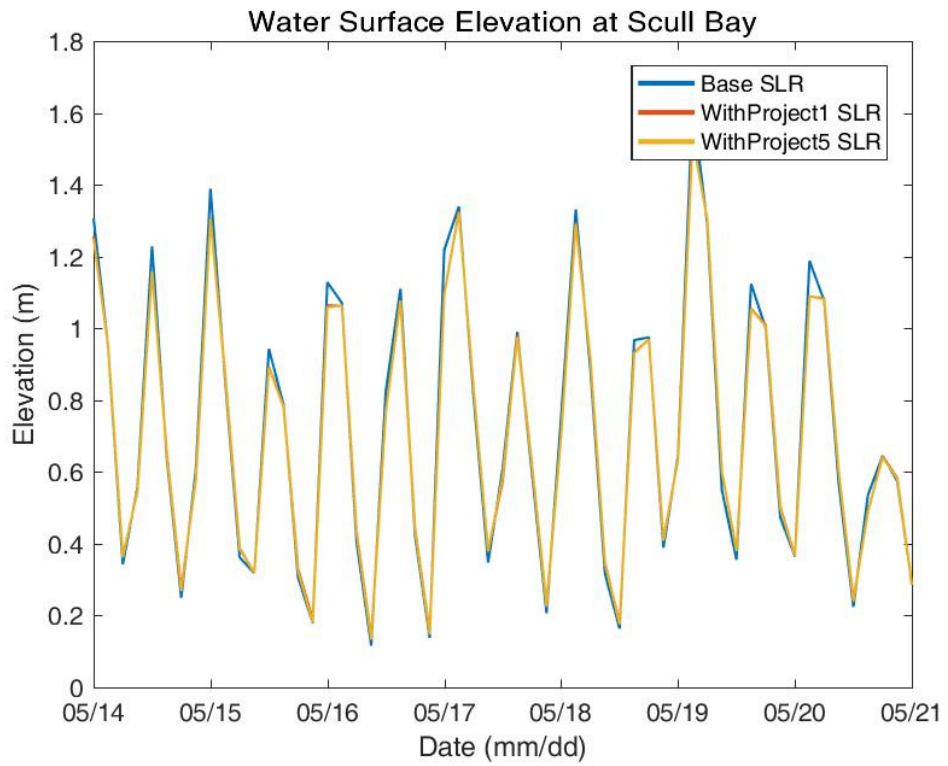


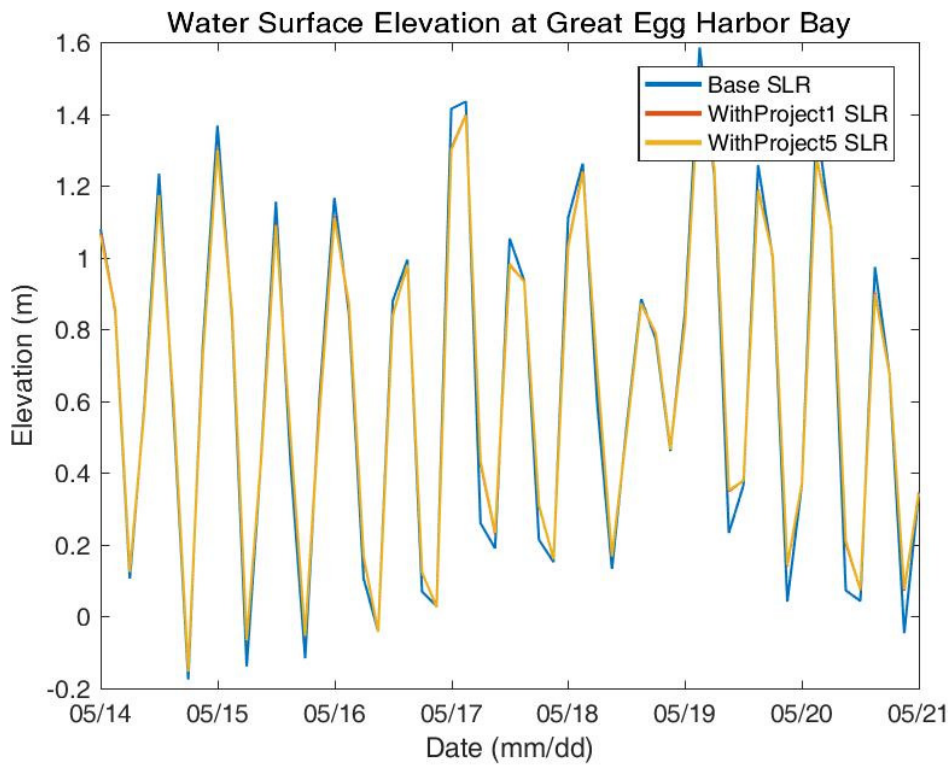
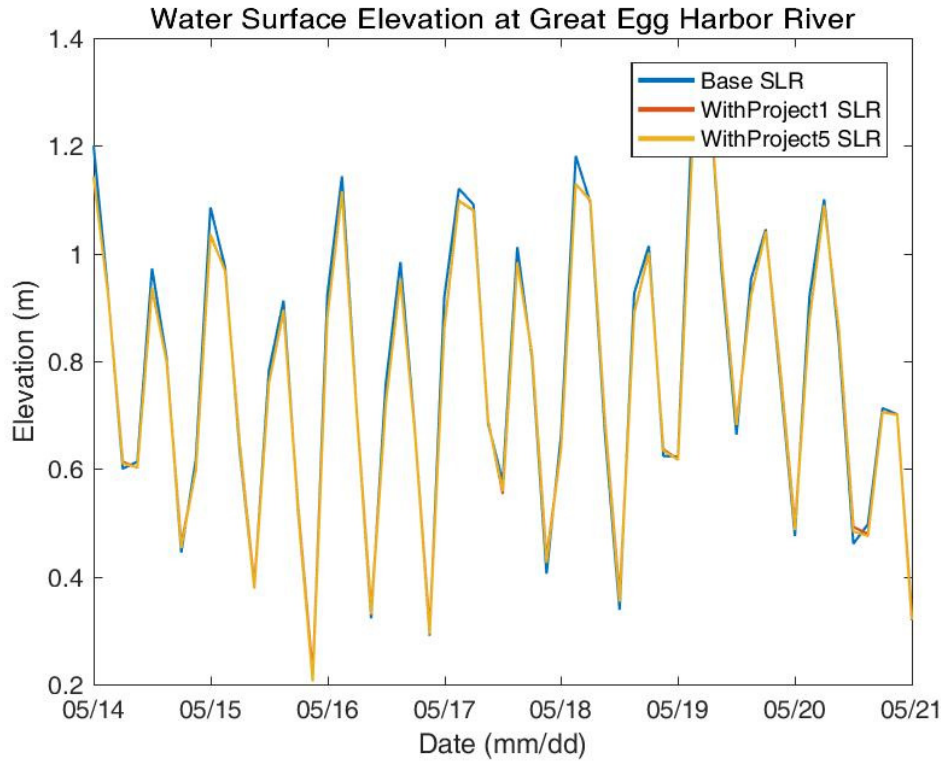


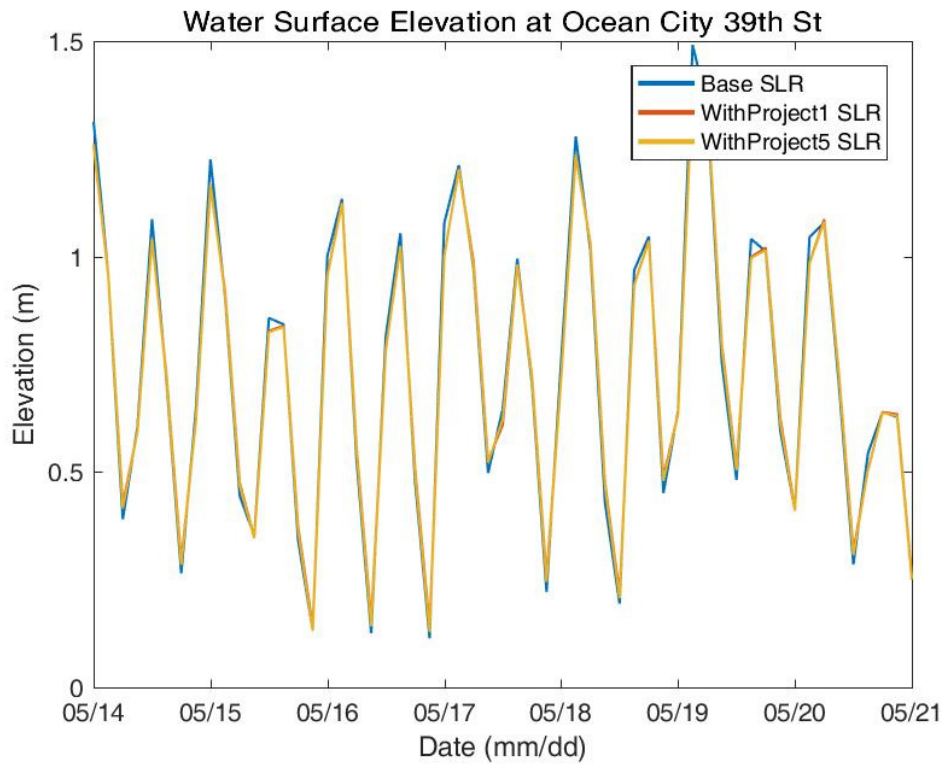


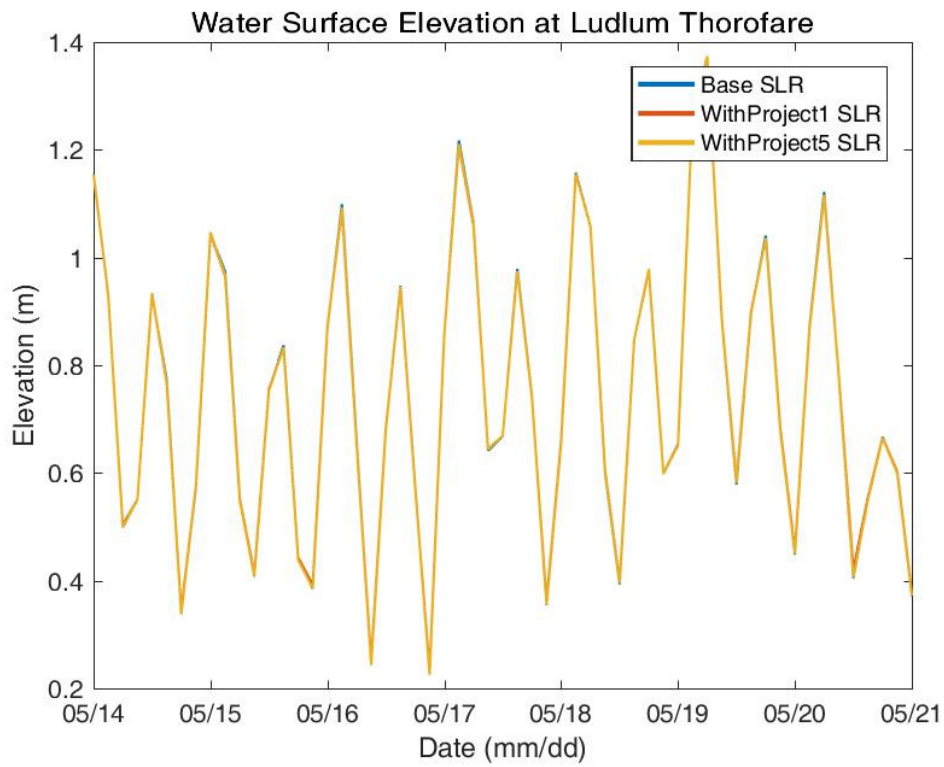
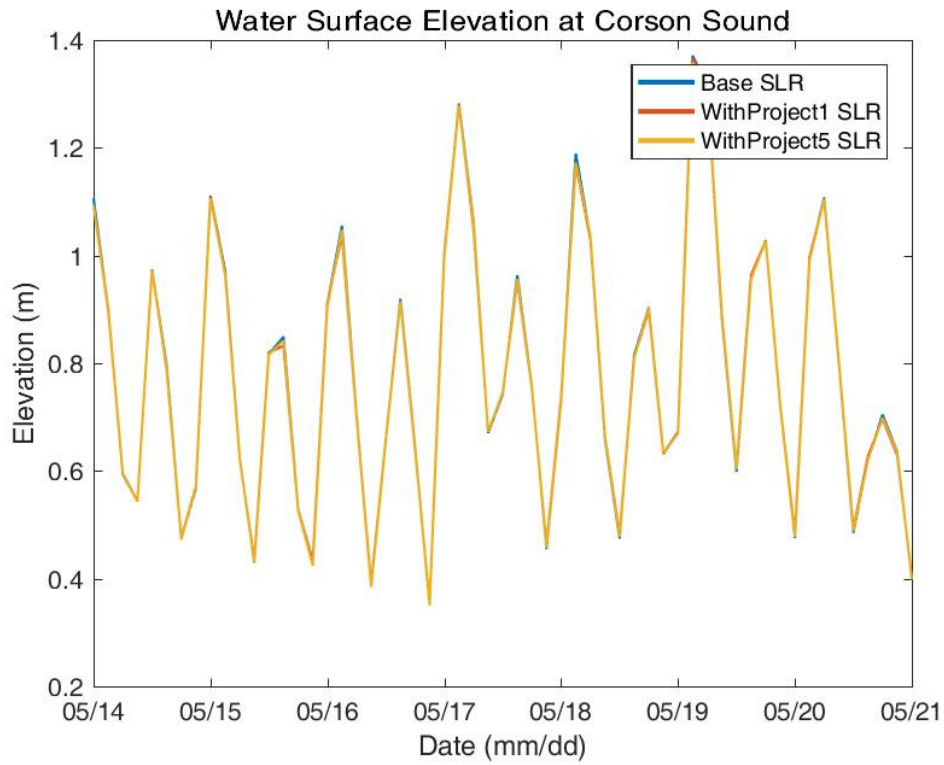


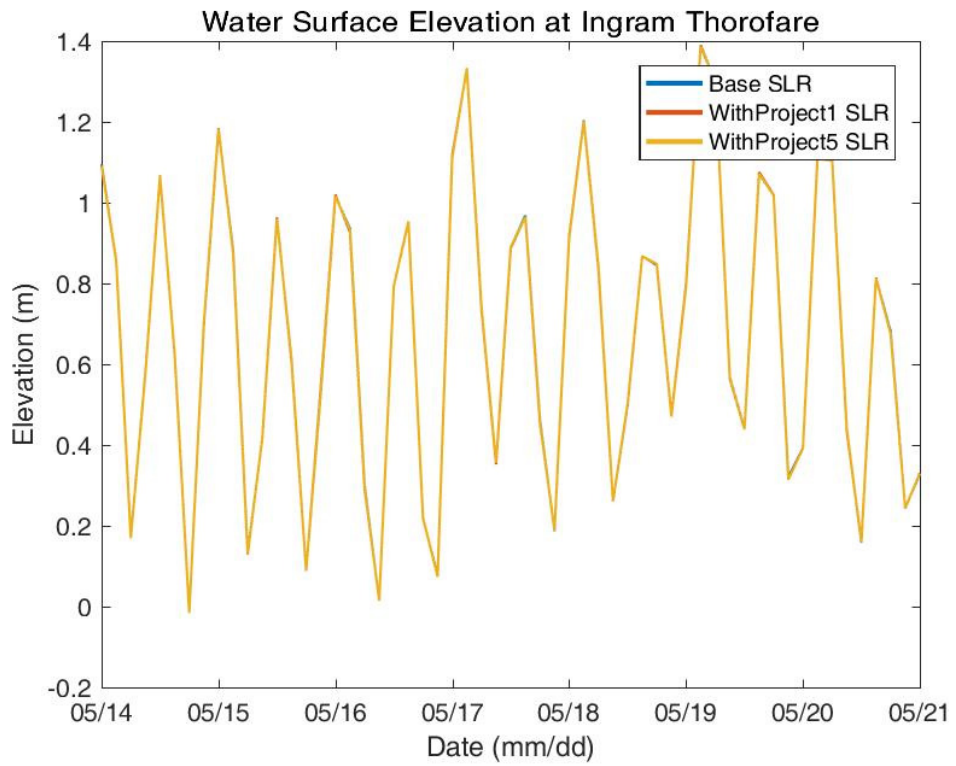


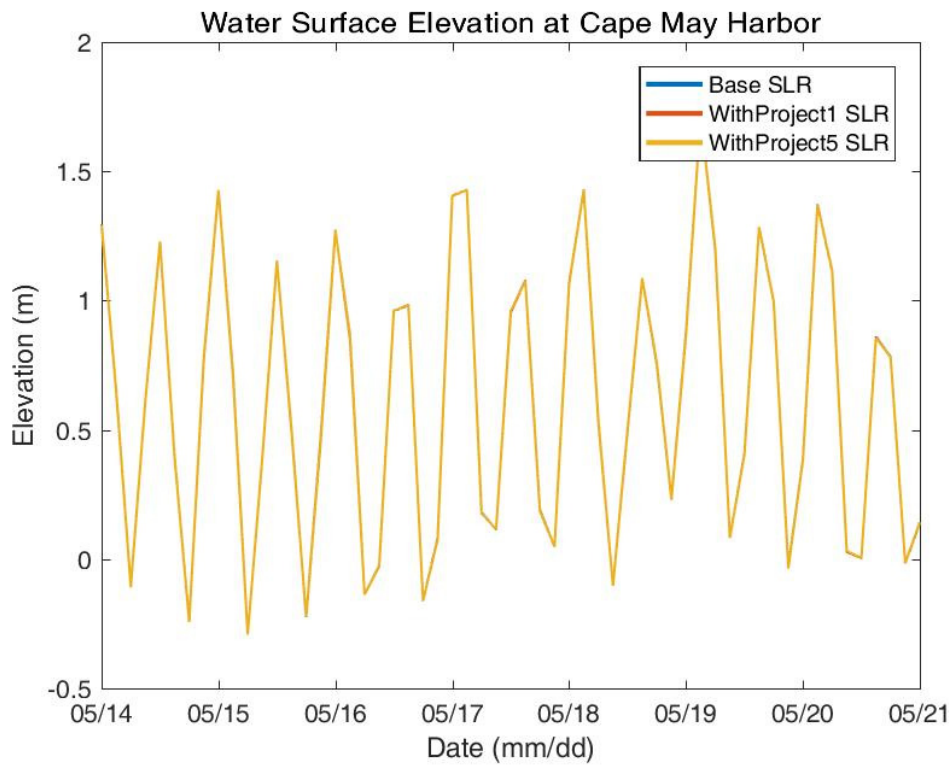
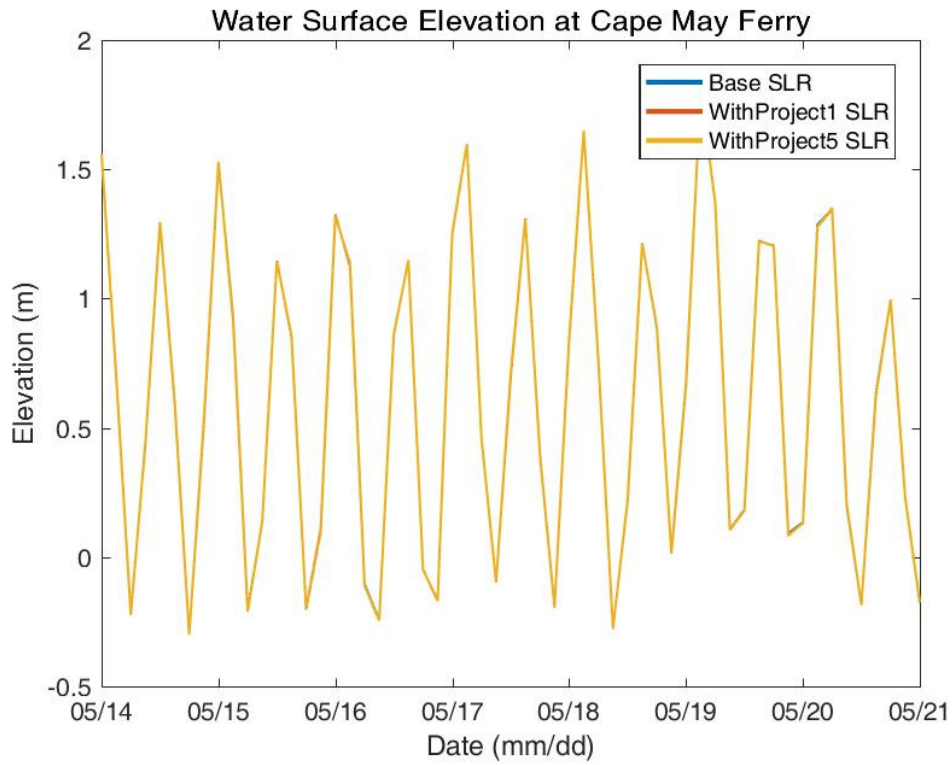




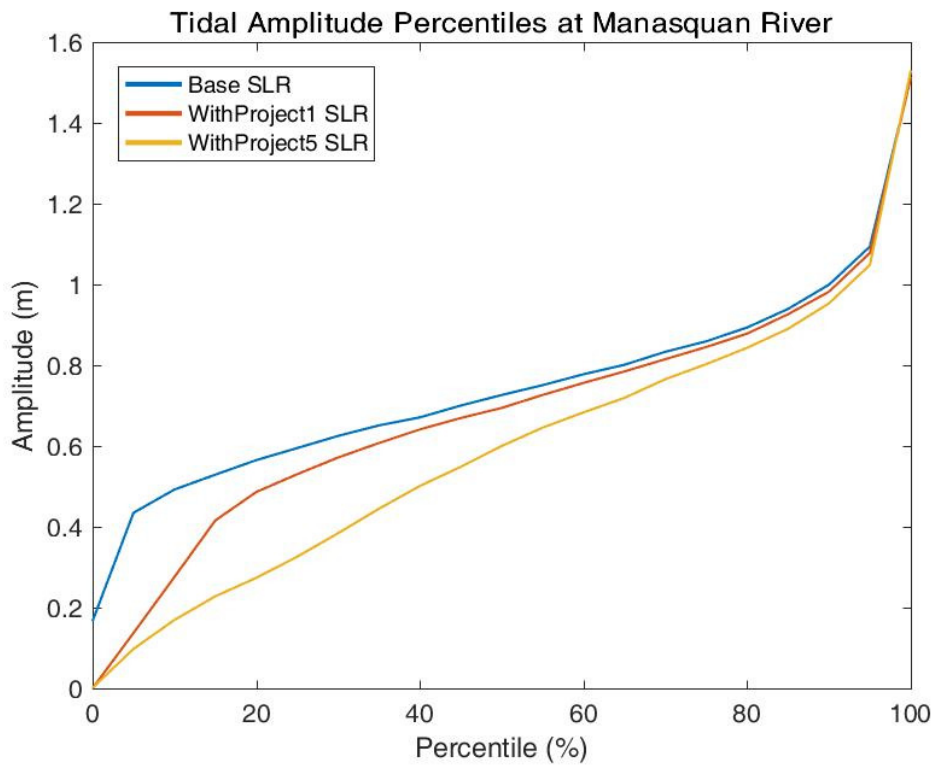
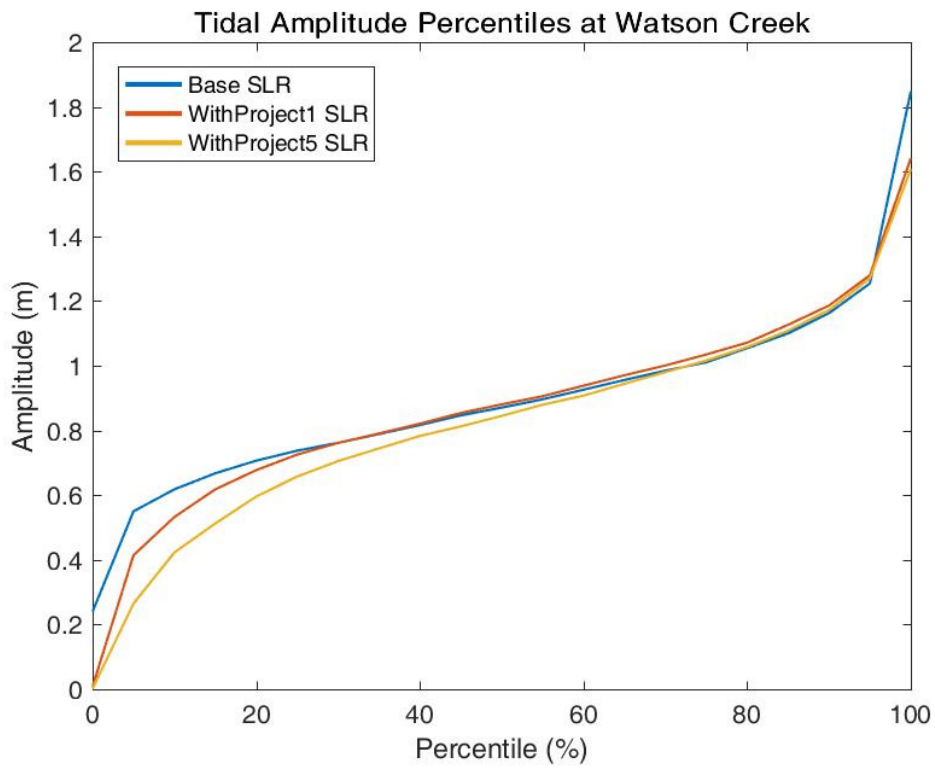


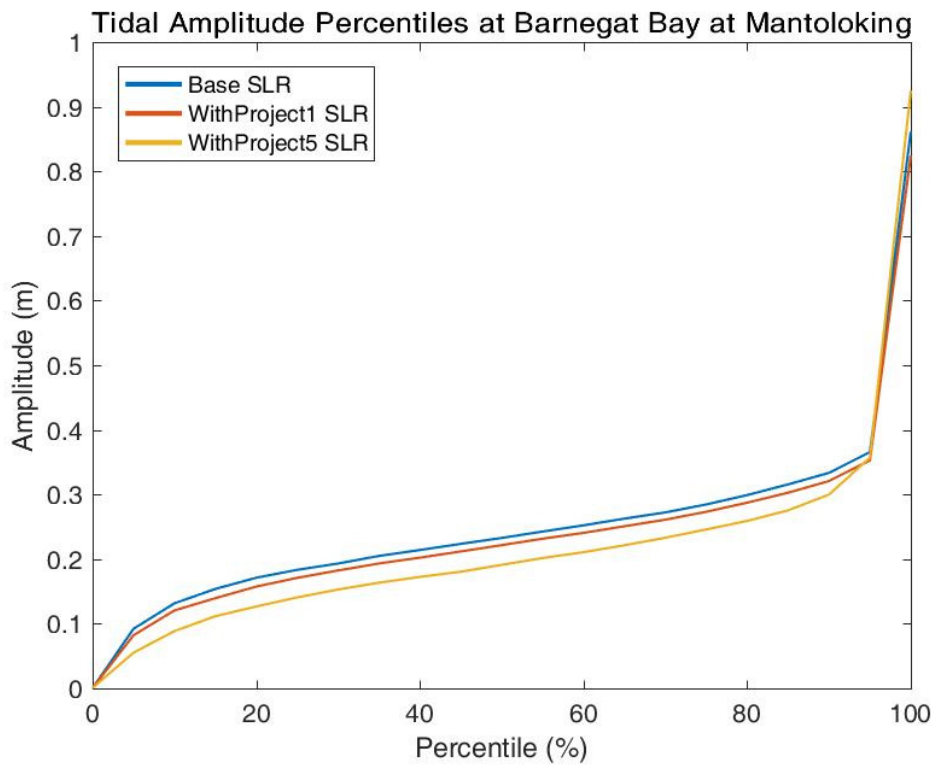
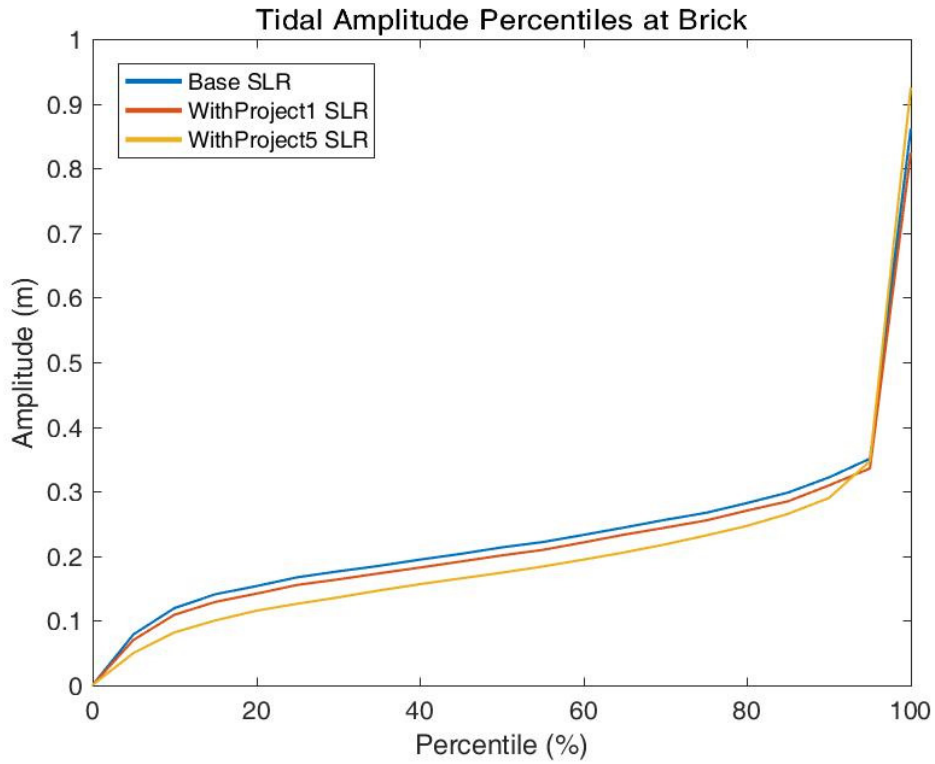


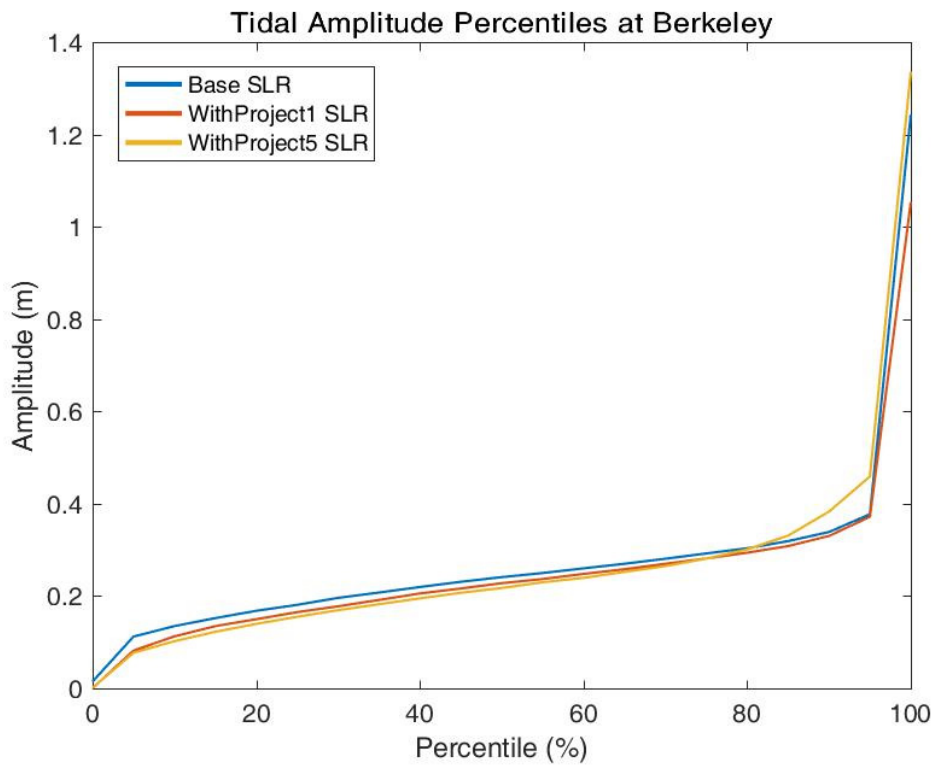
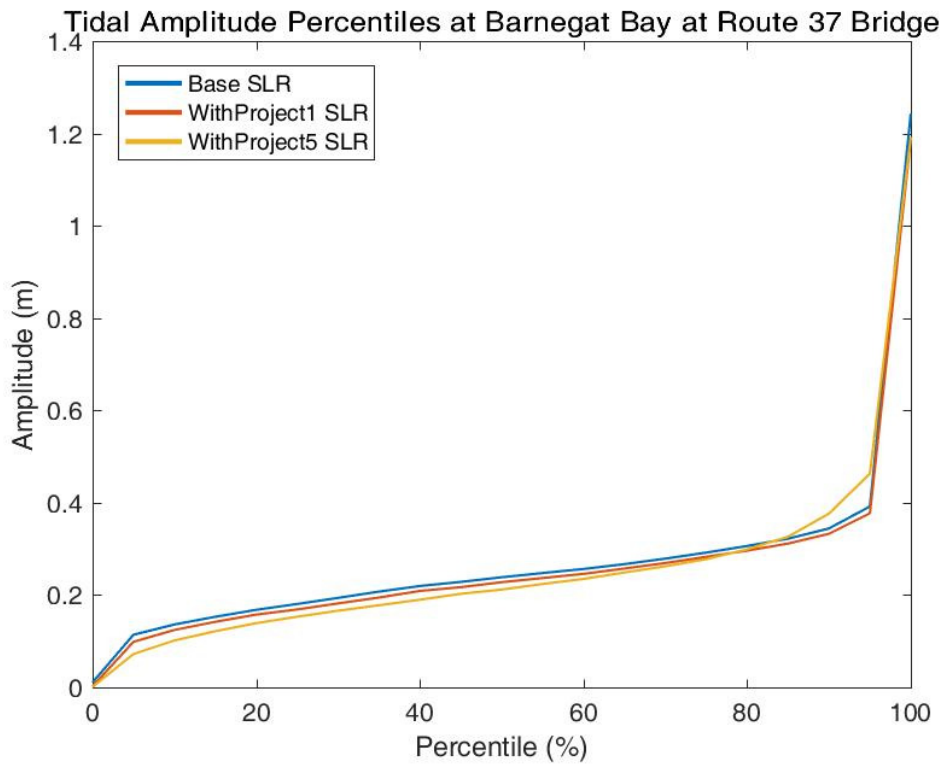


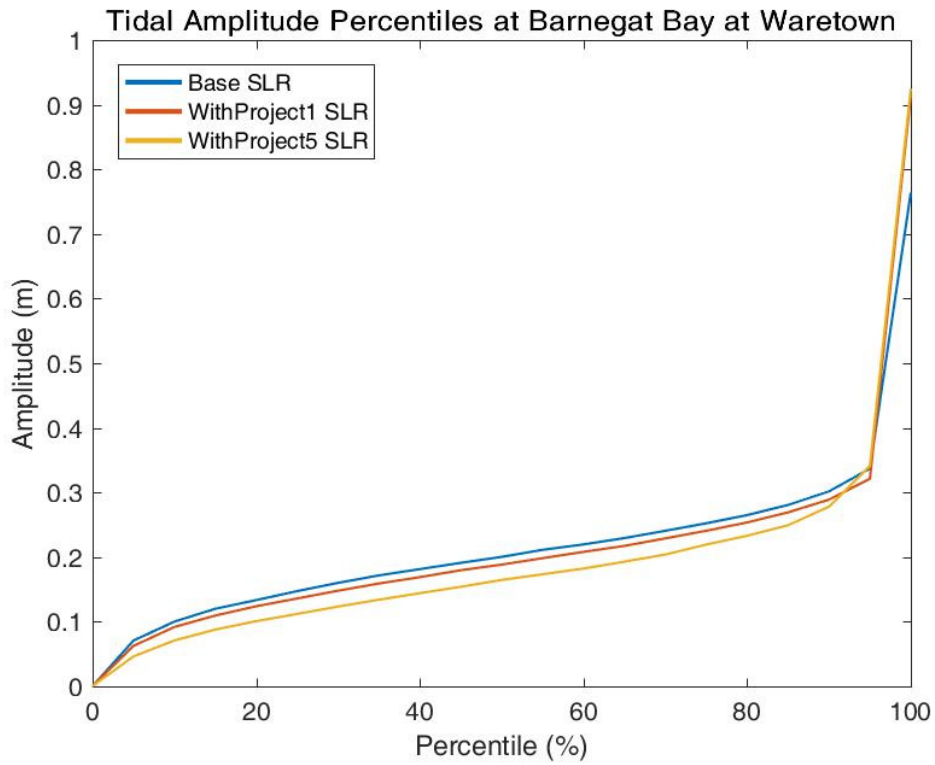
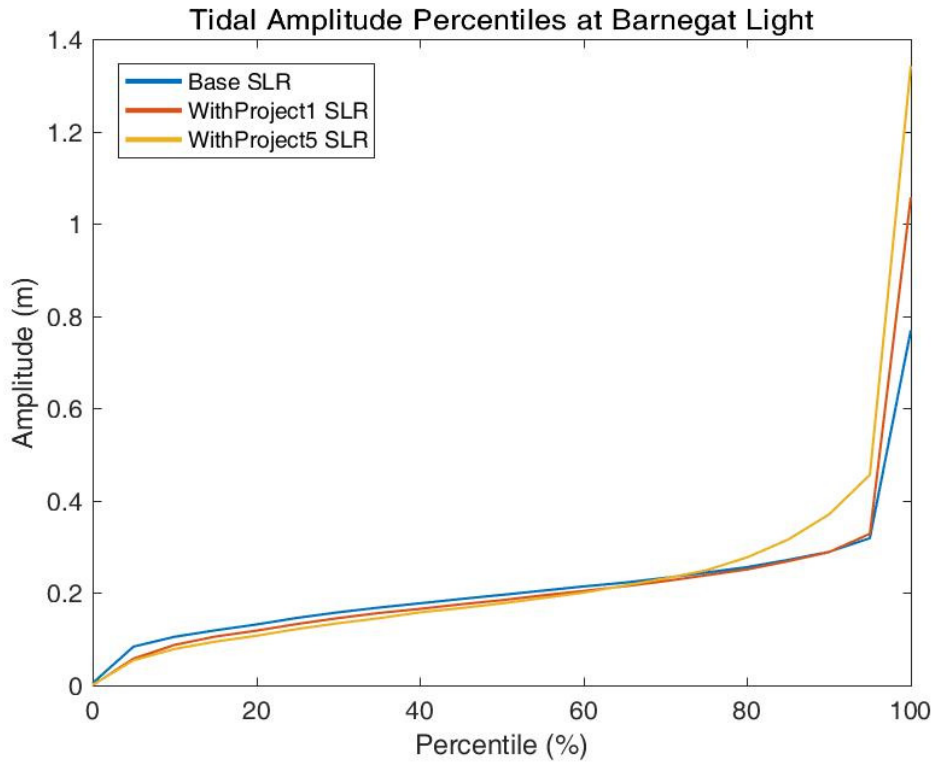


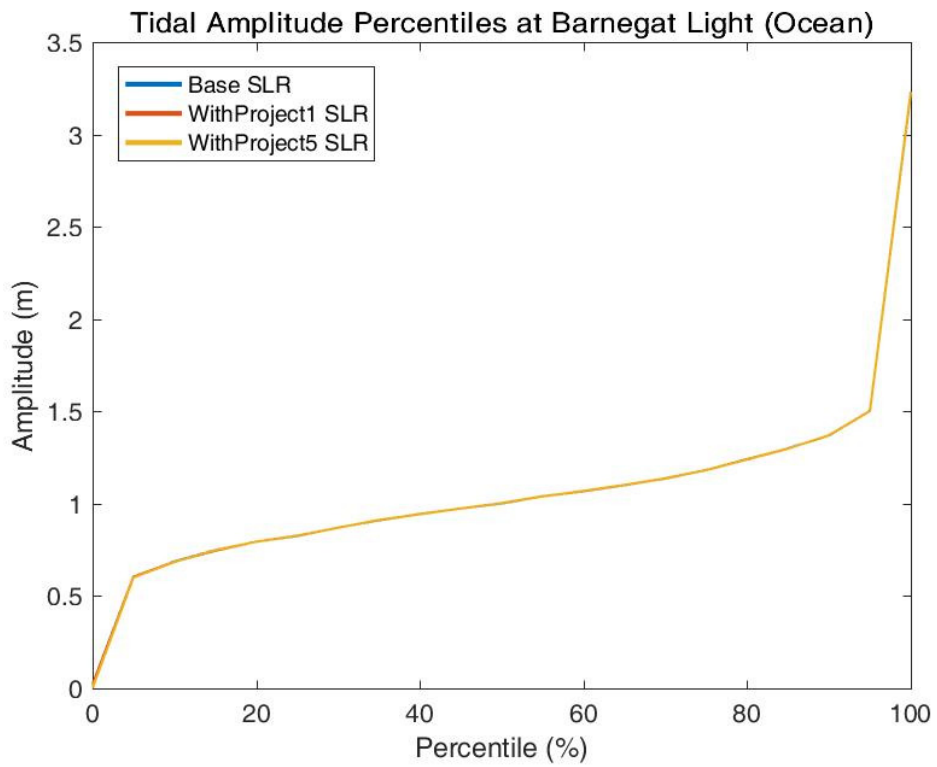
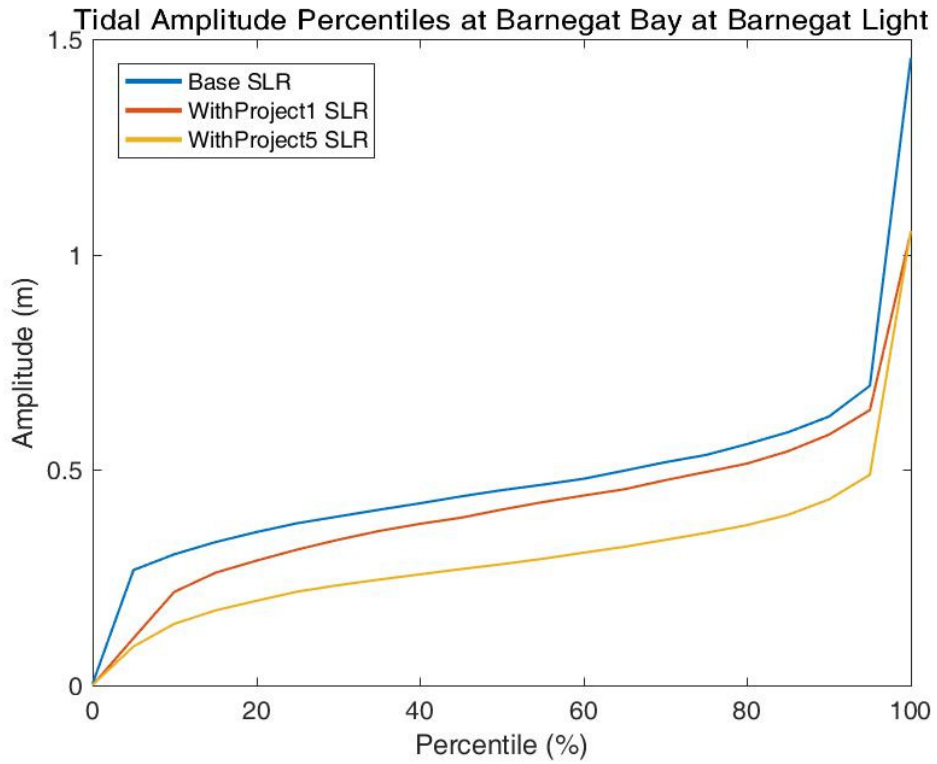
Tidal Amplitude Plots

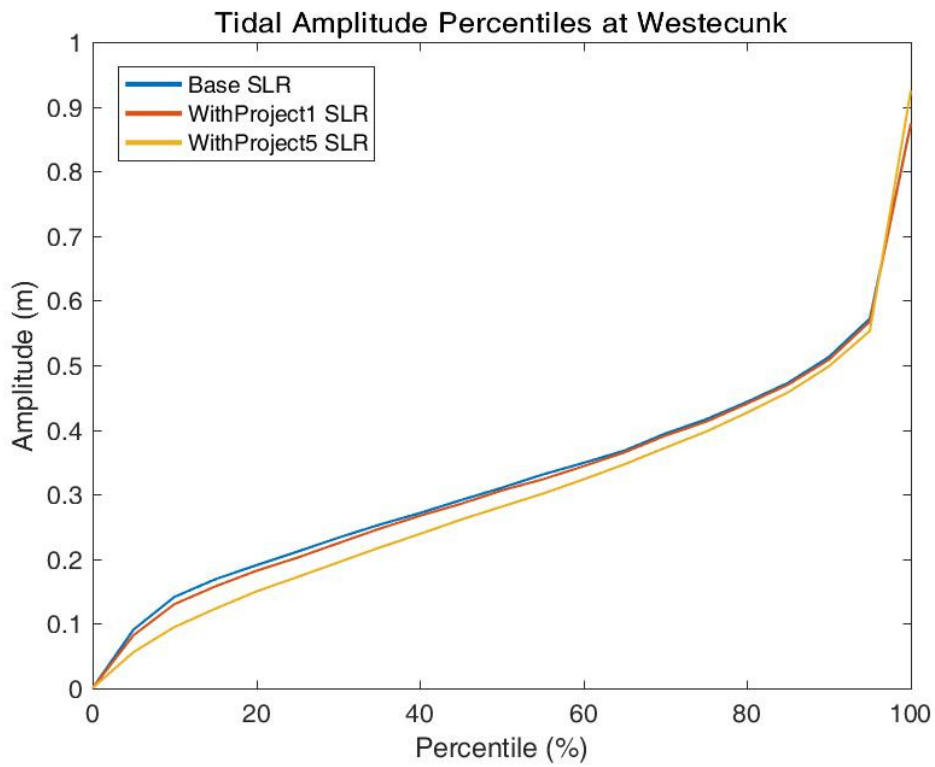
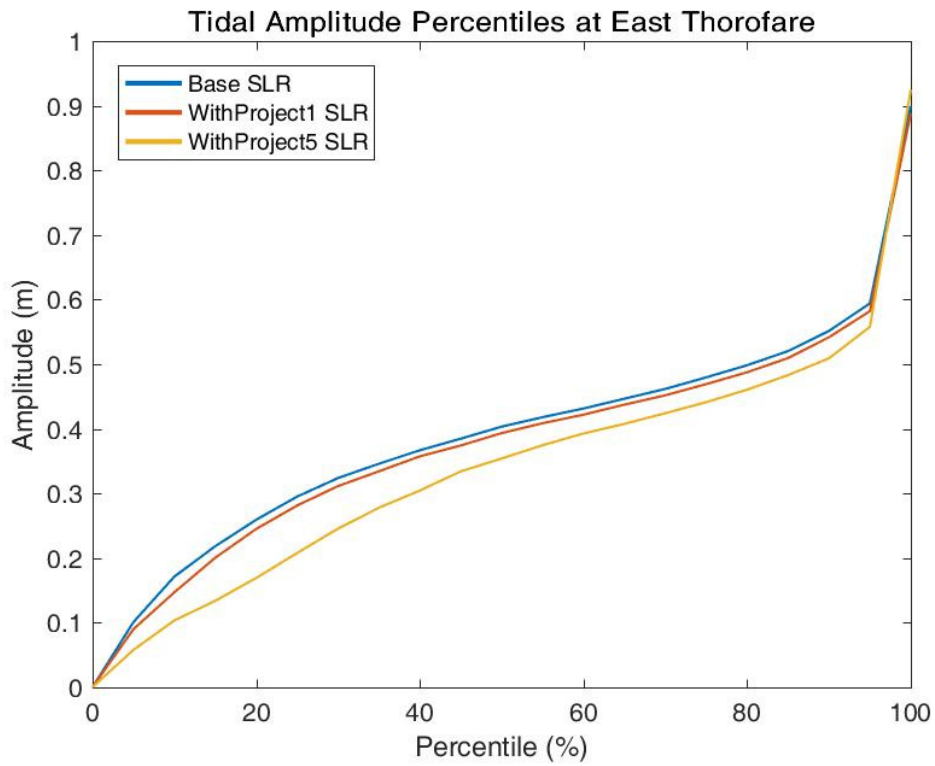


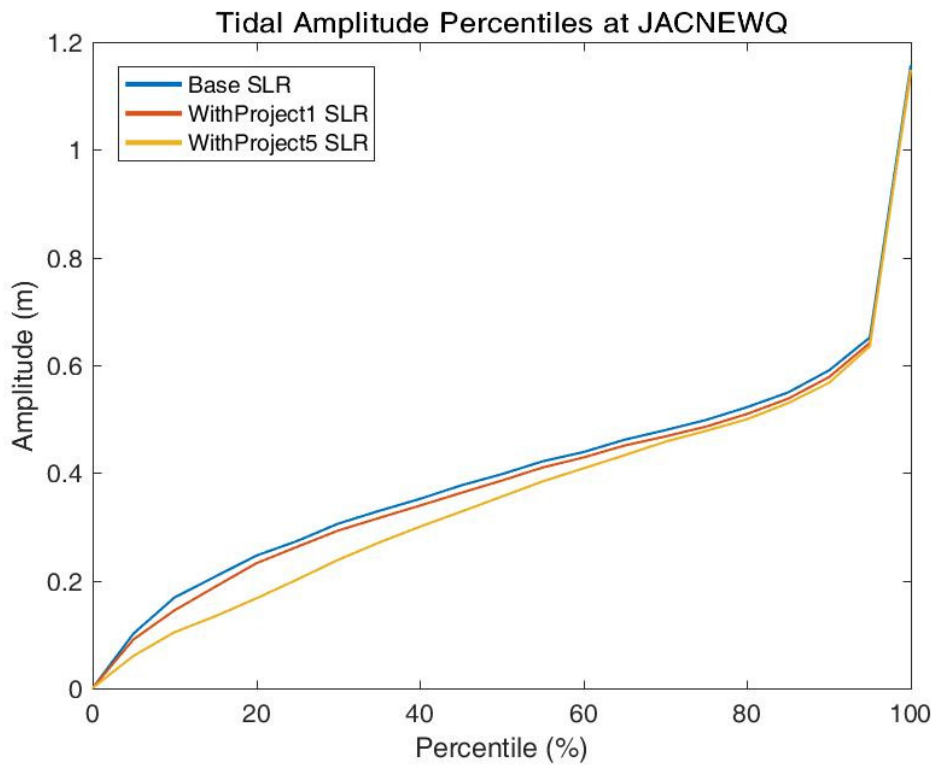
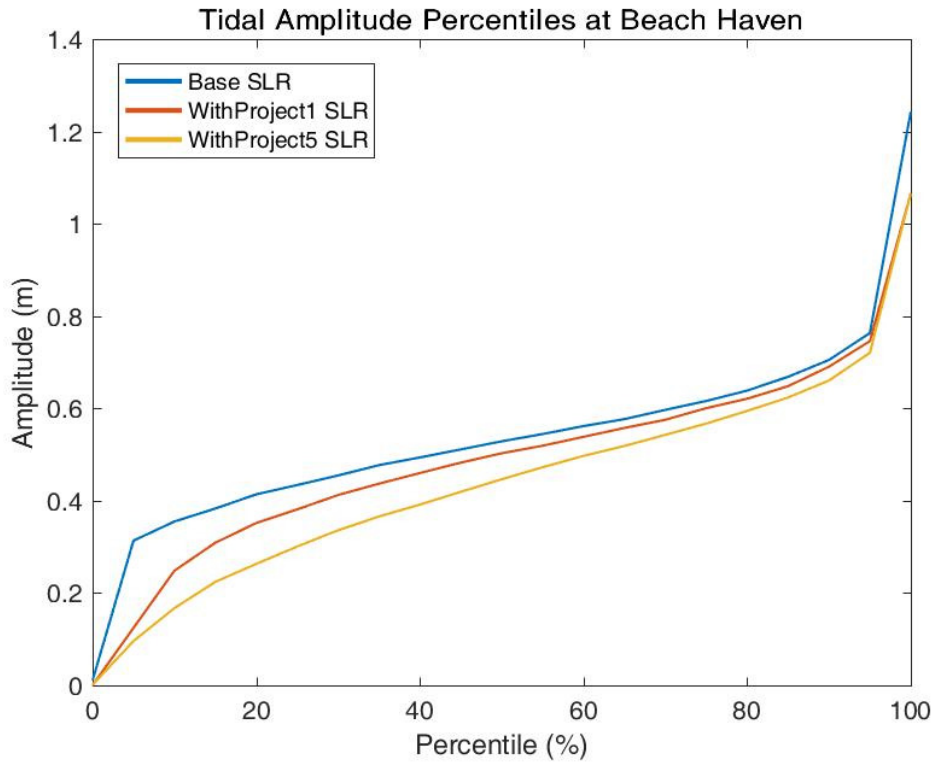


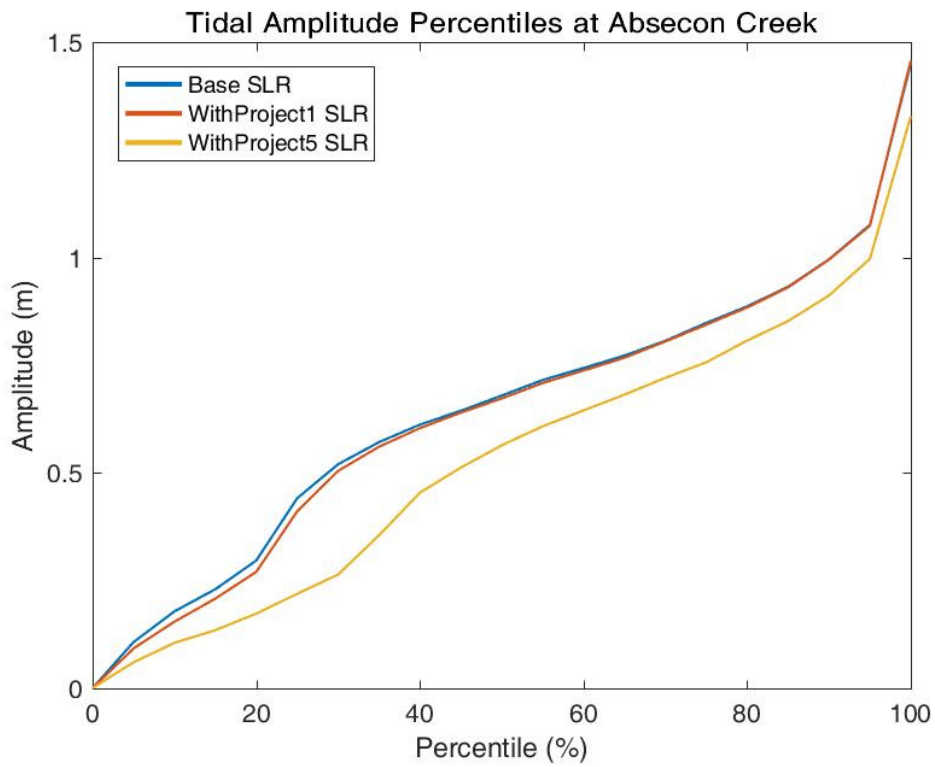
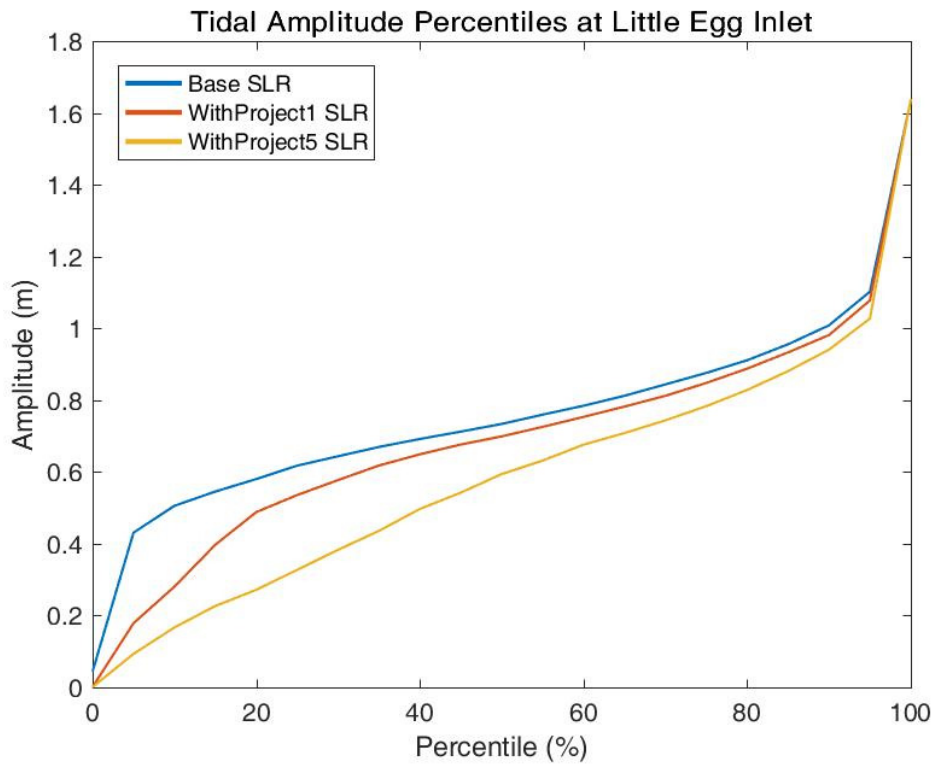


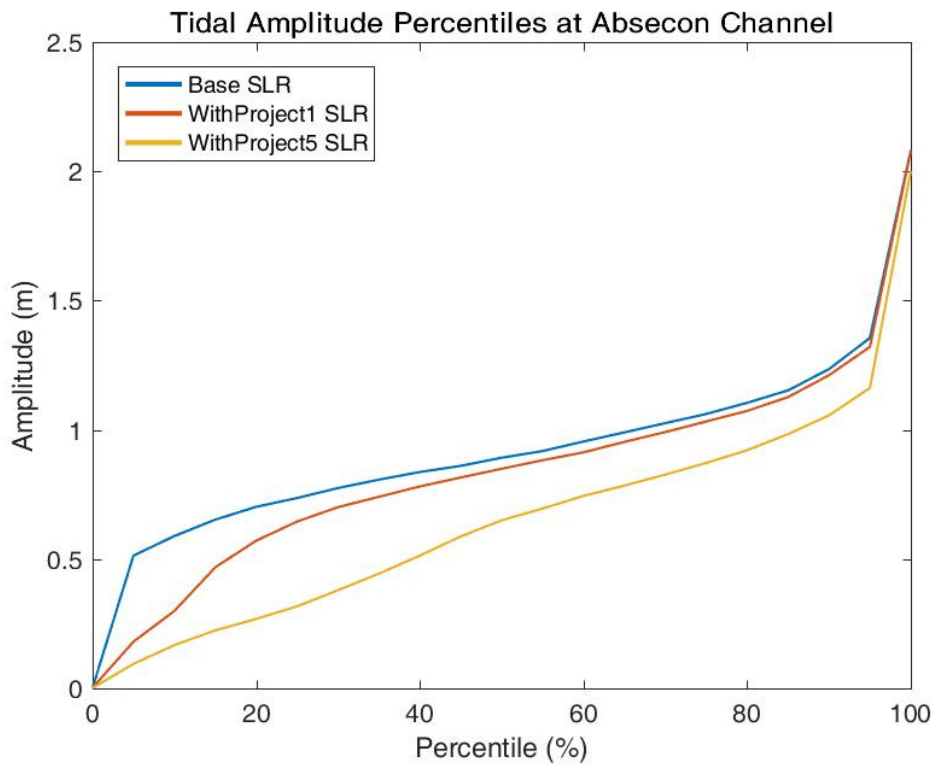
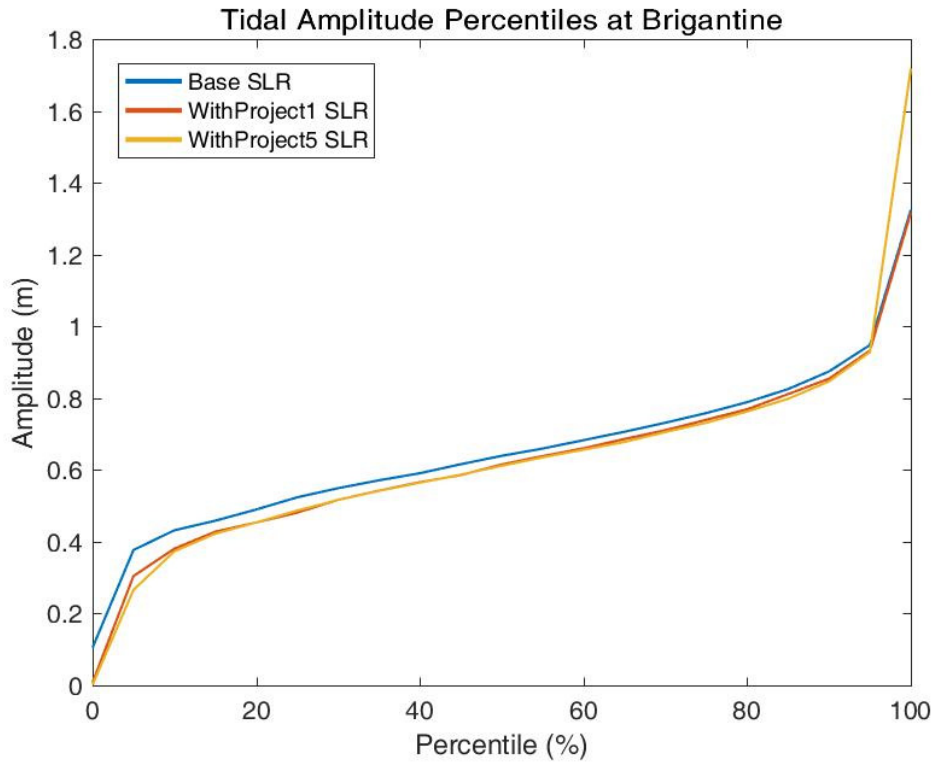


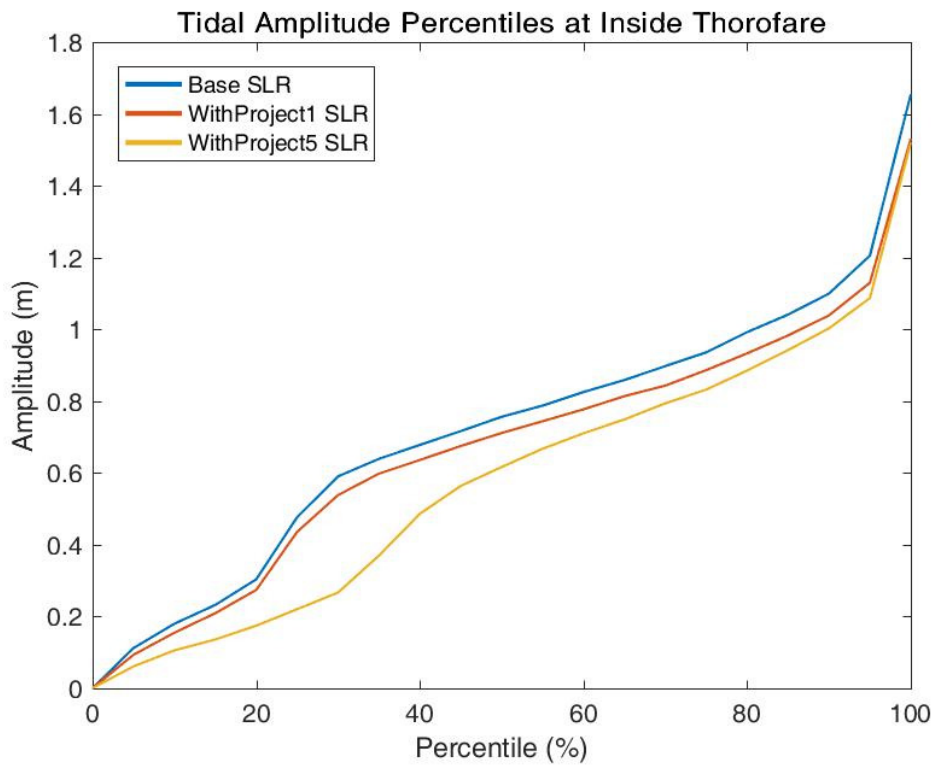
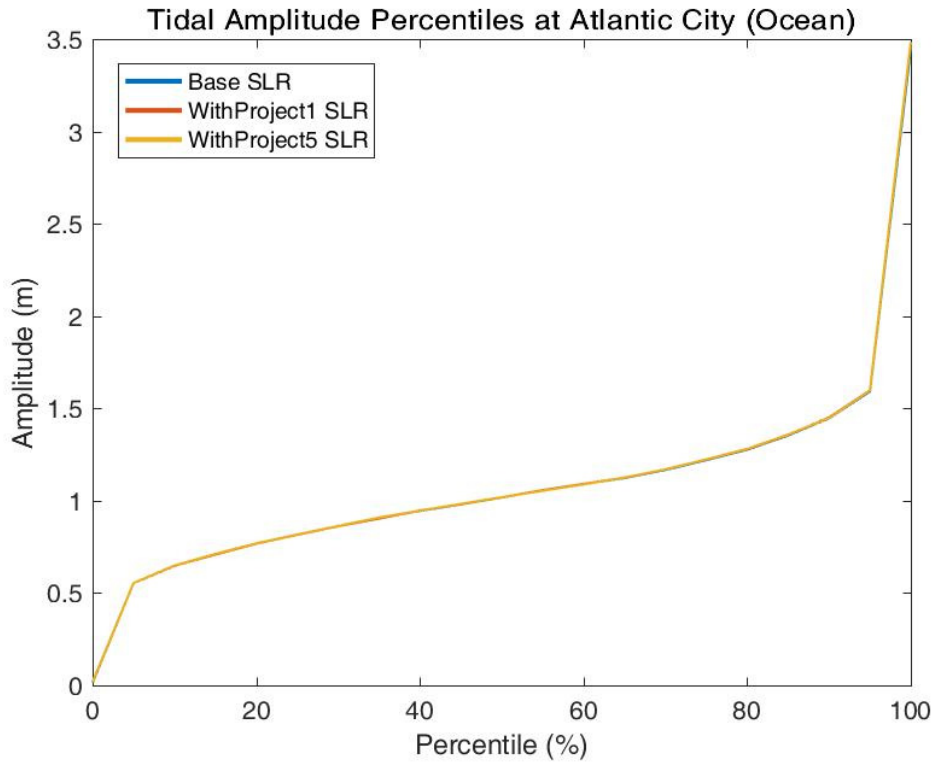


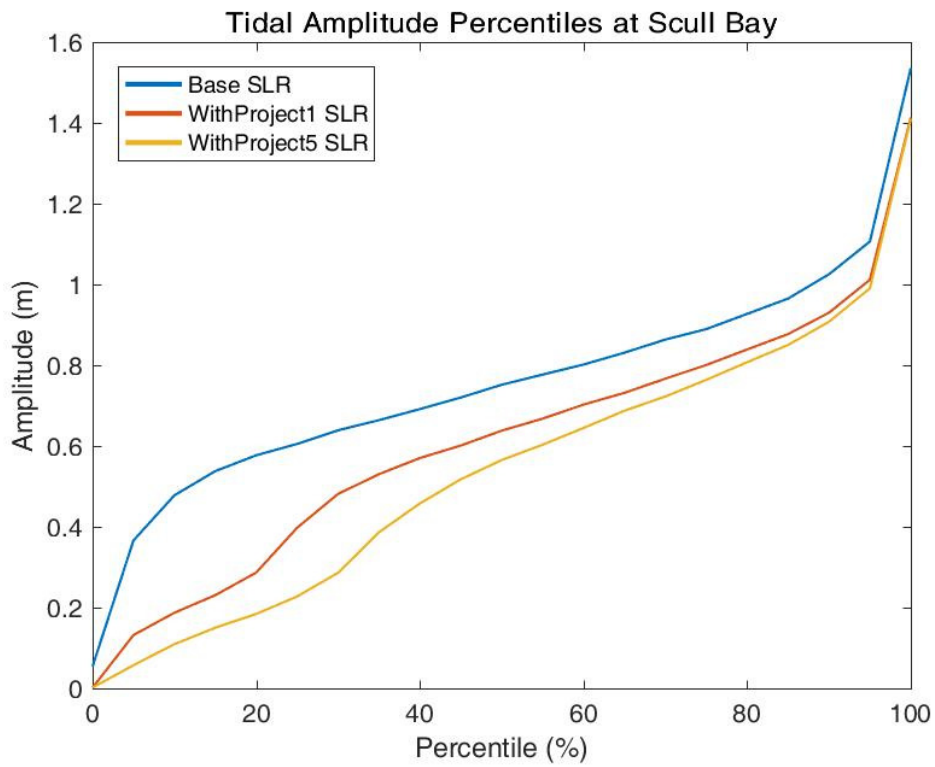
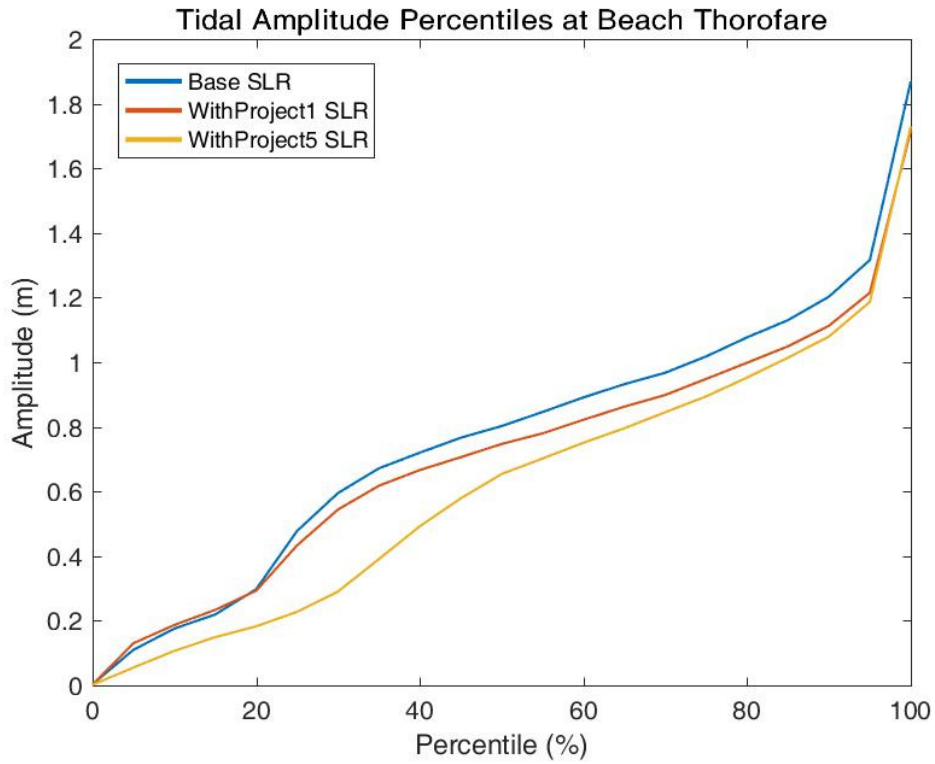


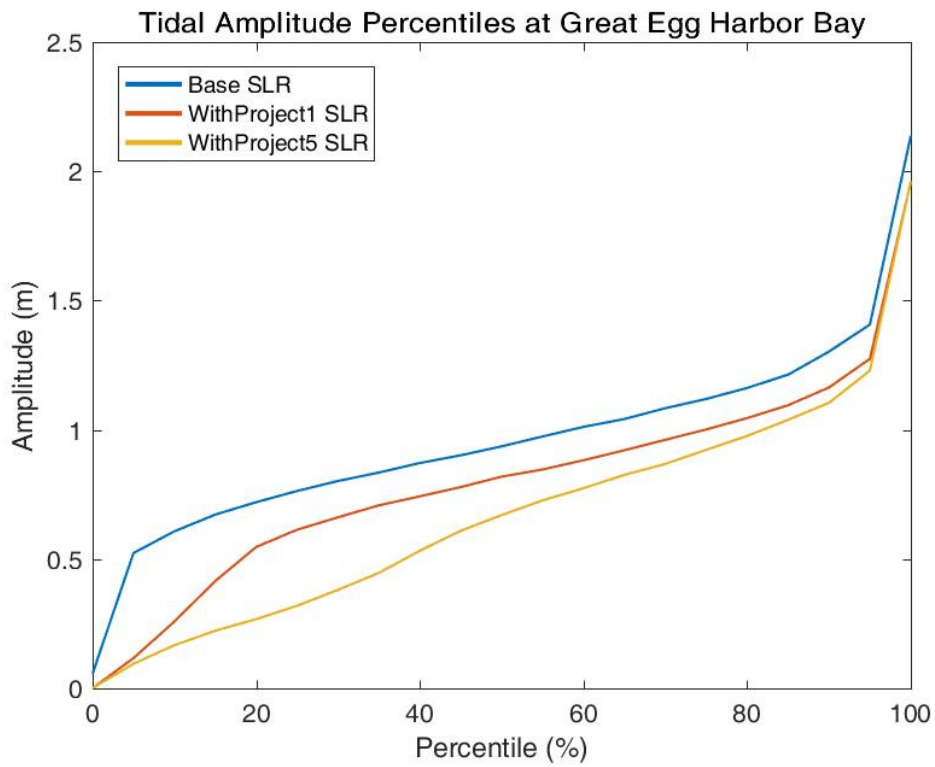
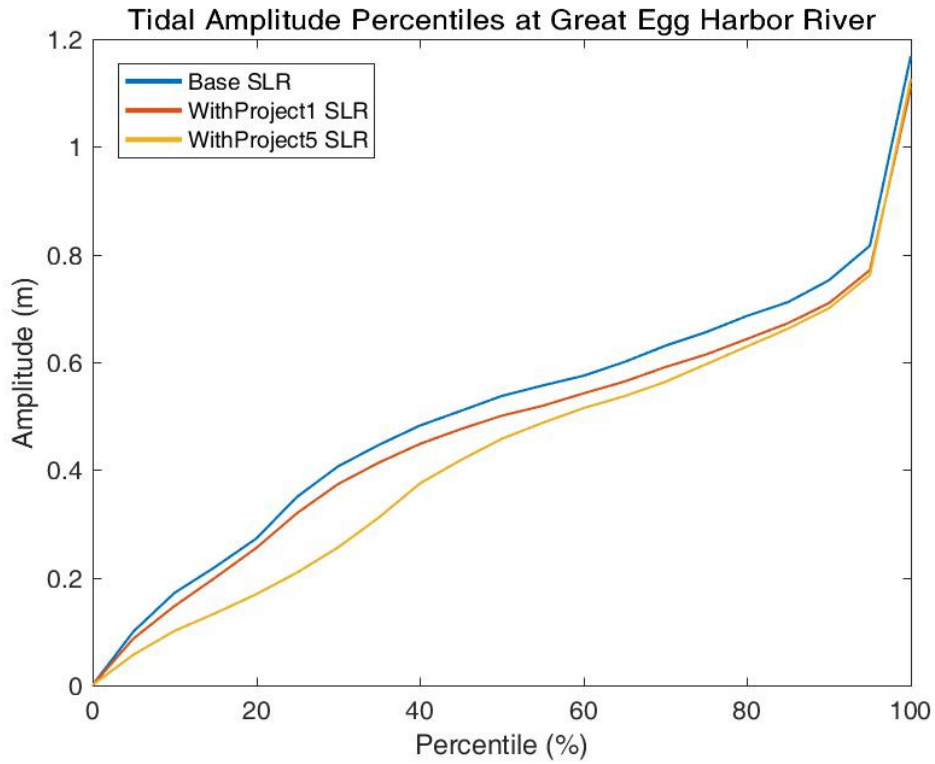


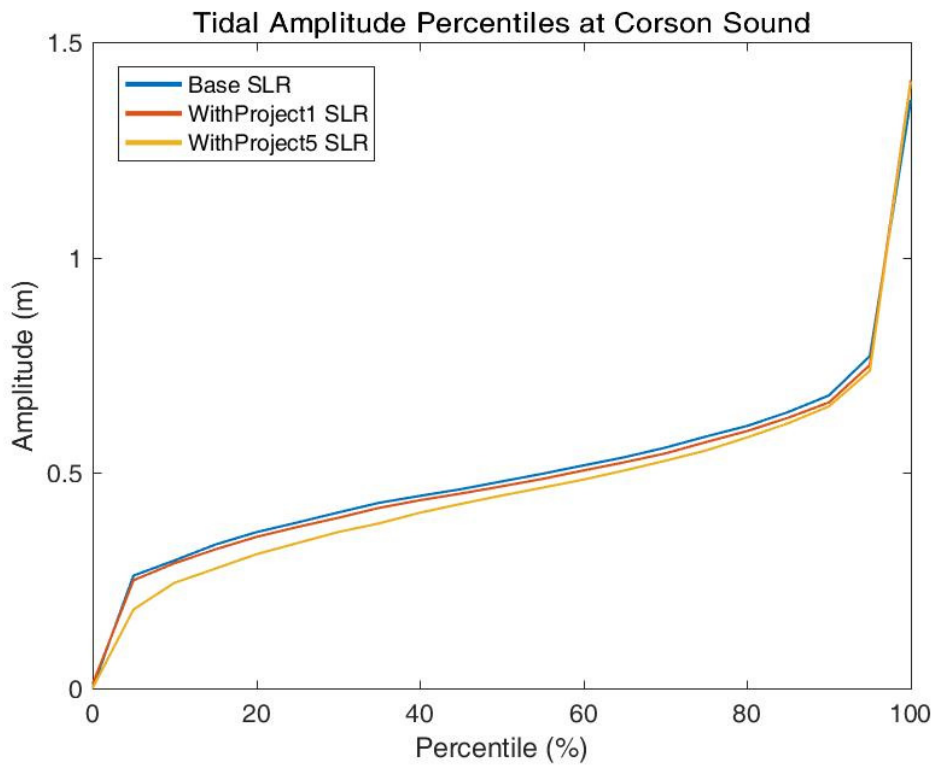
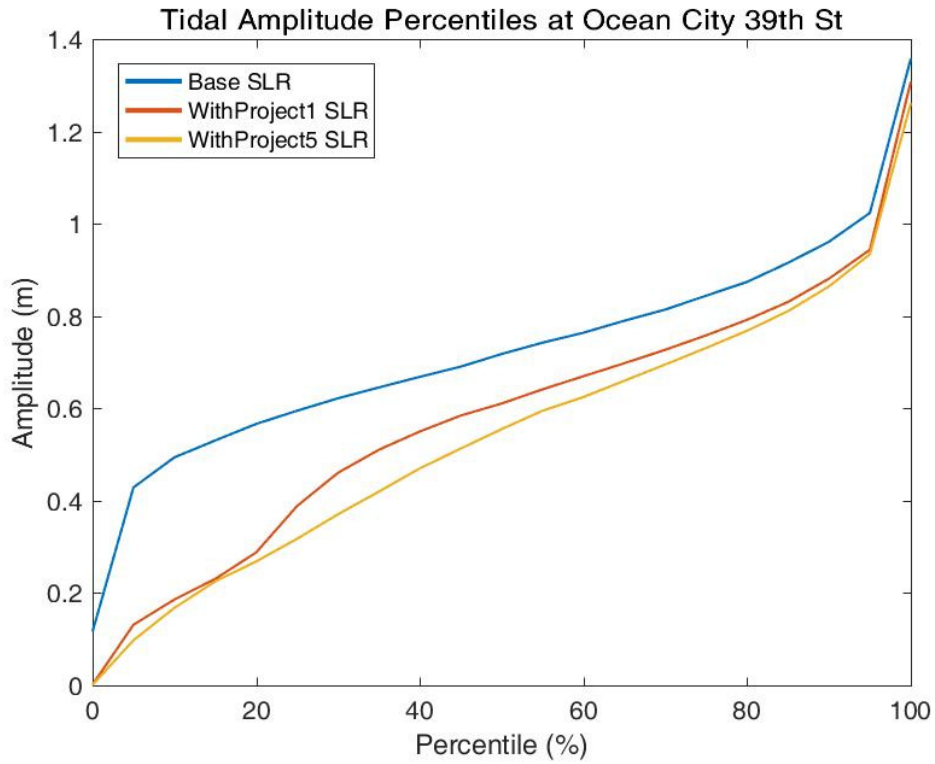


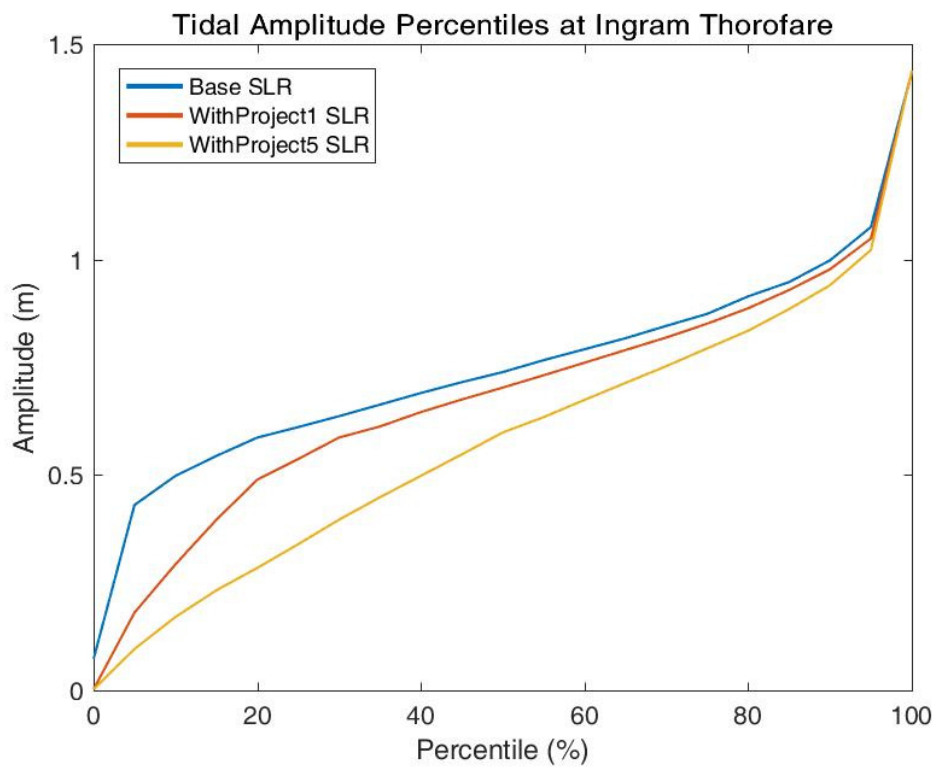
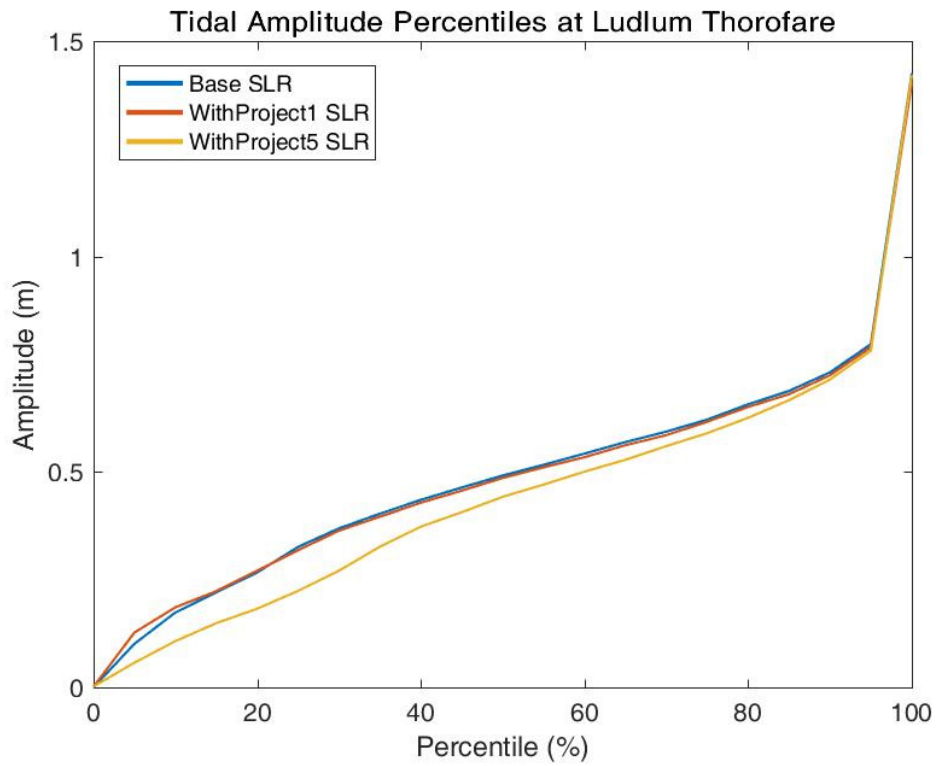


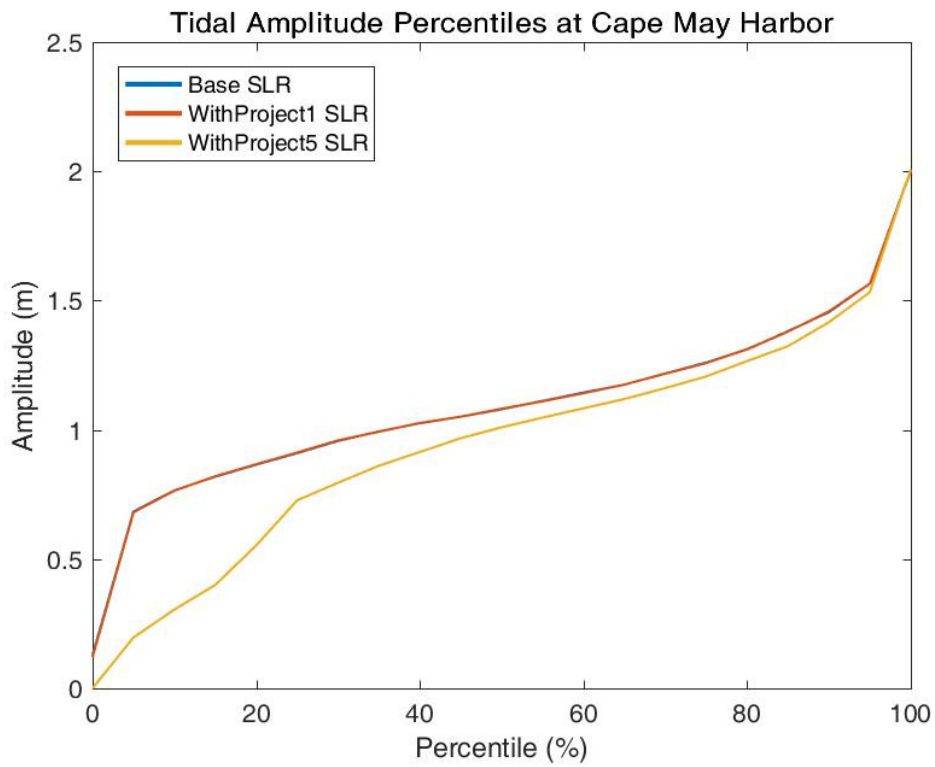
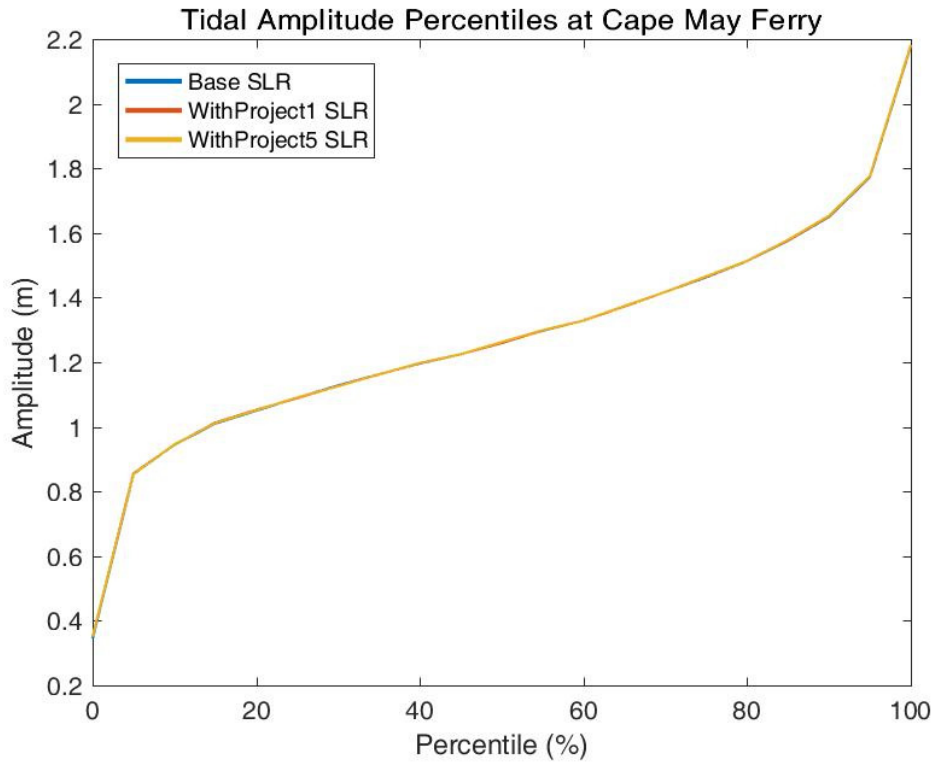


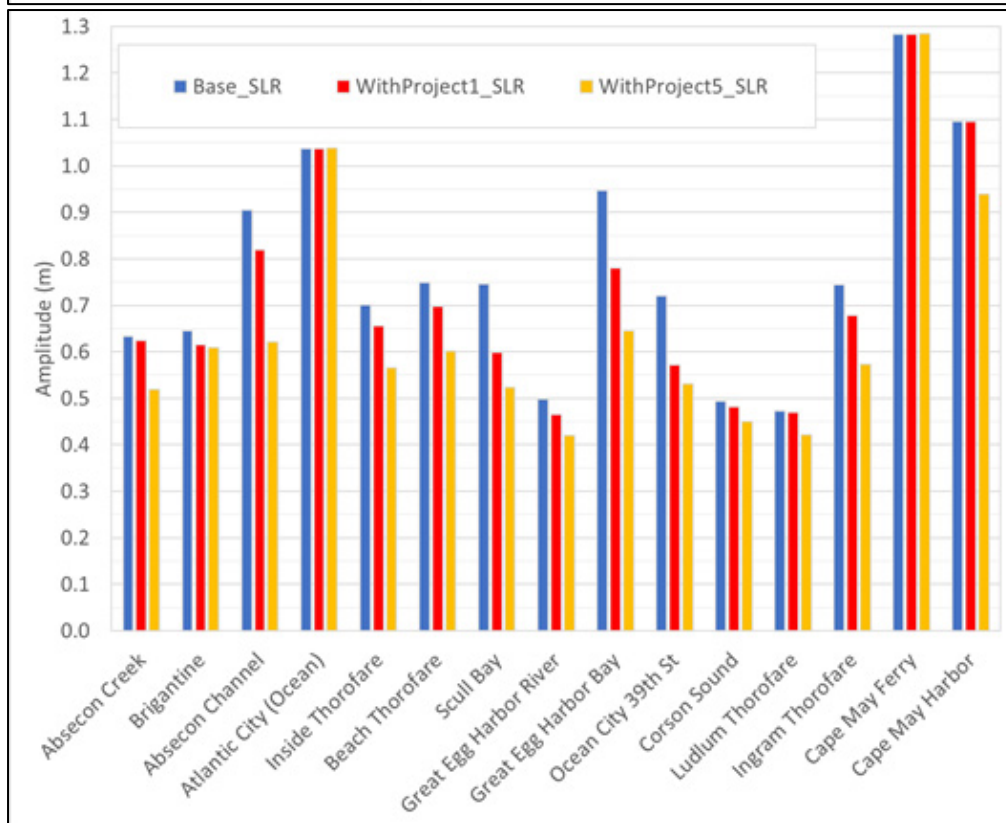
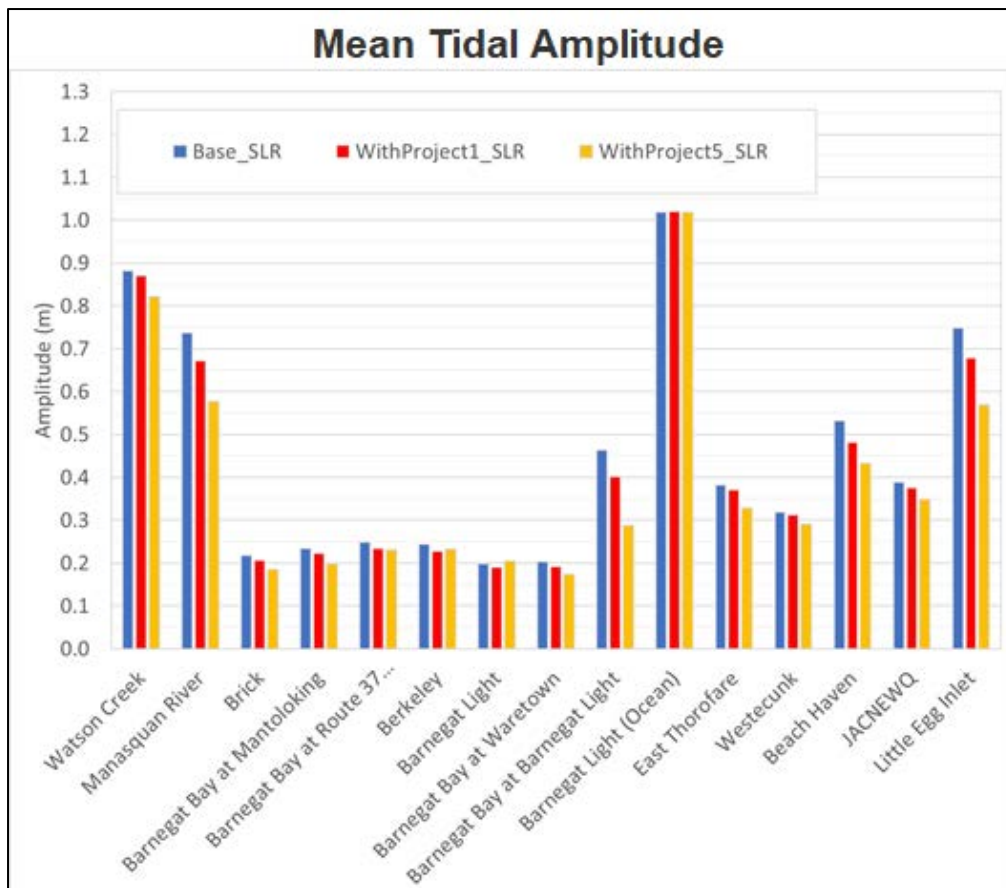




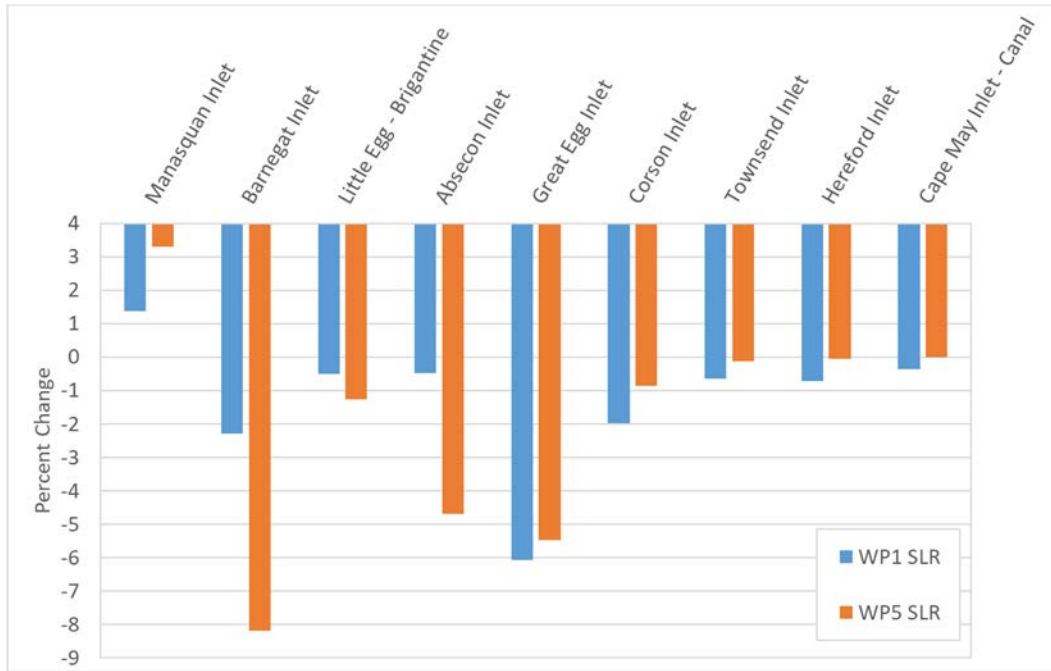




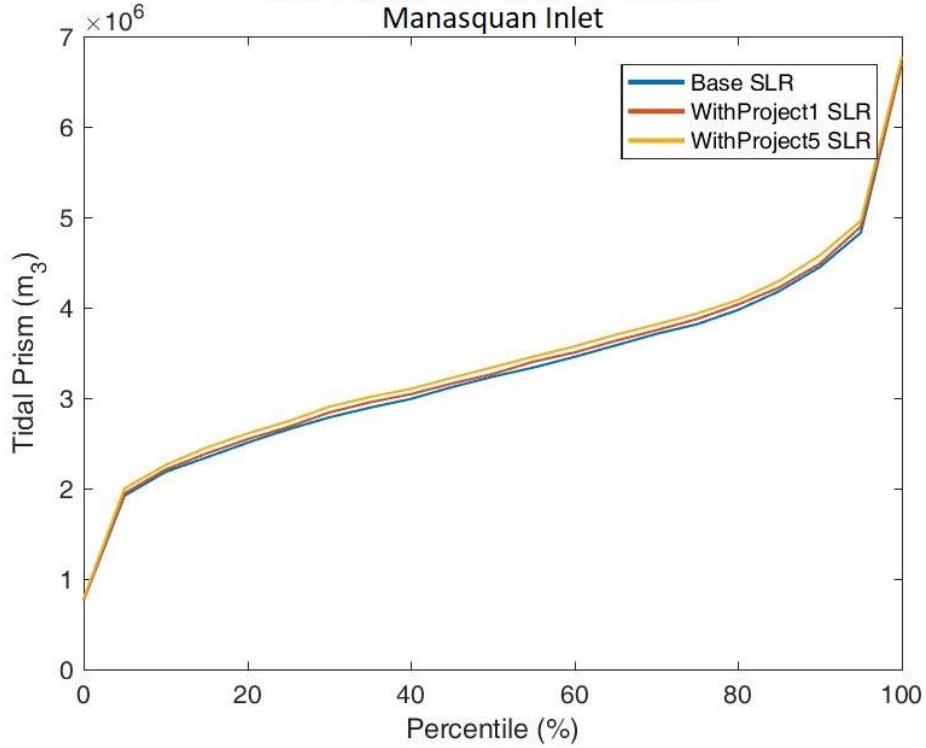


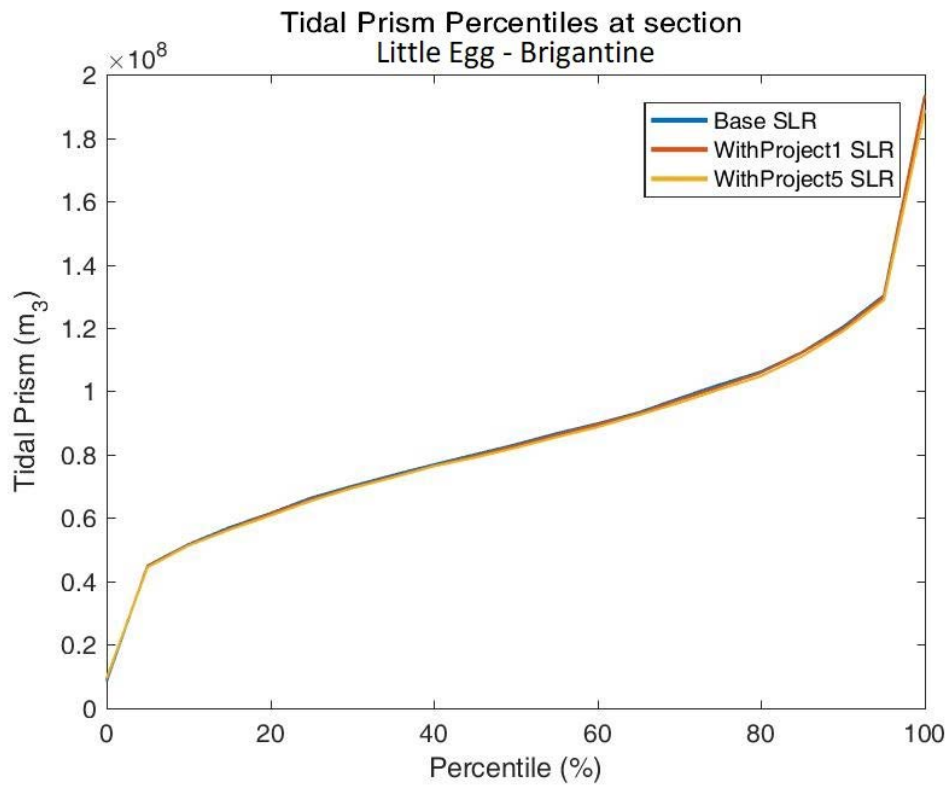
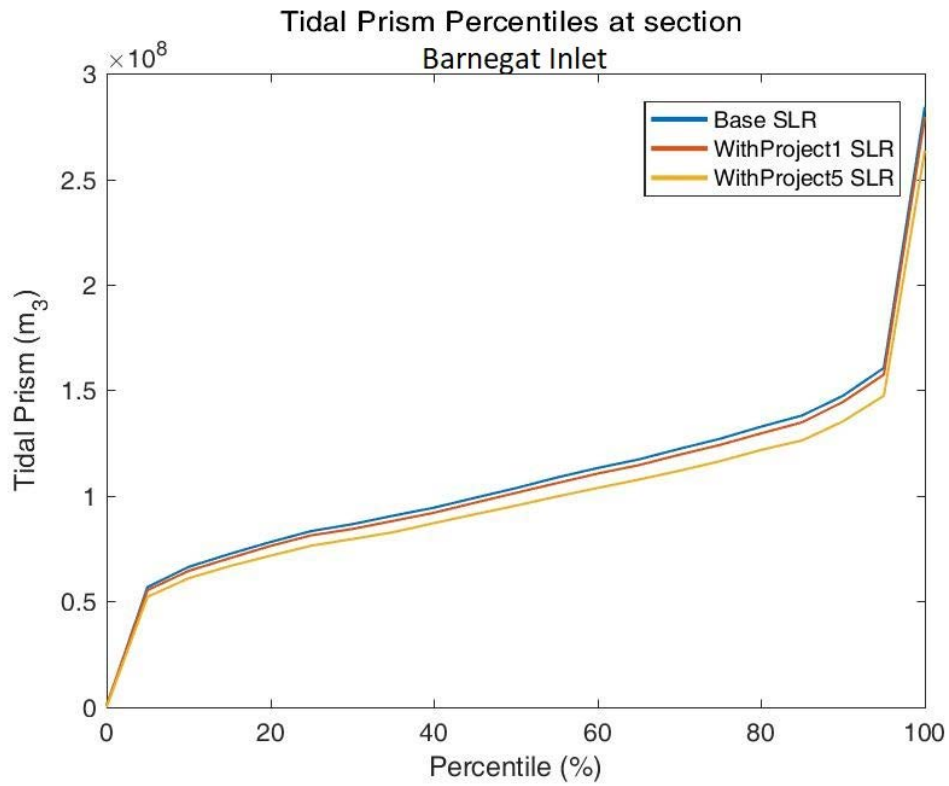


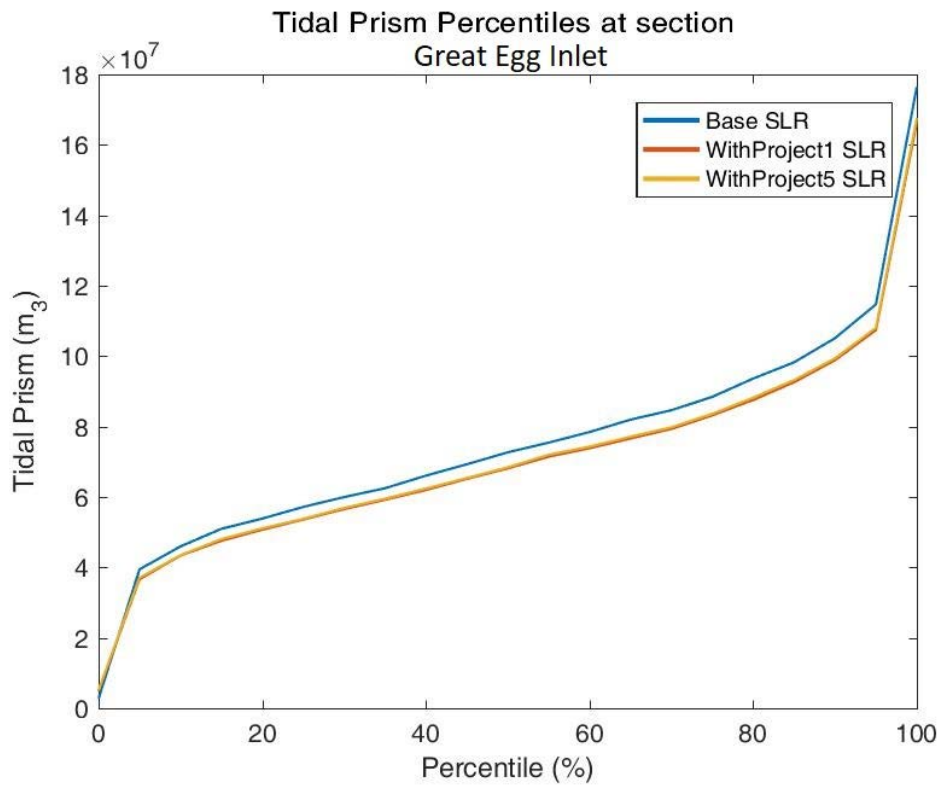
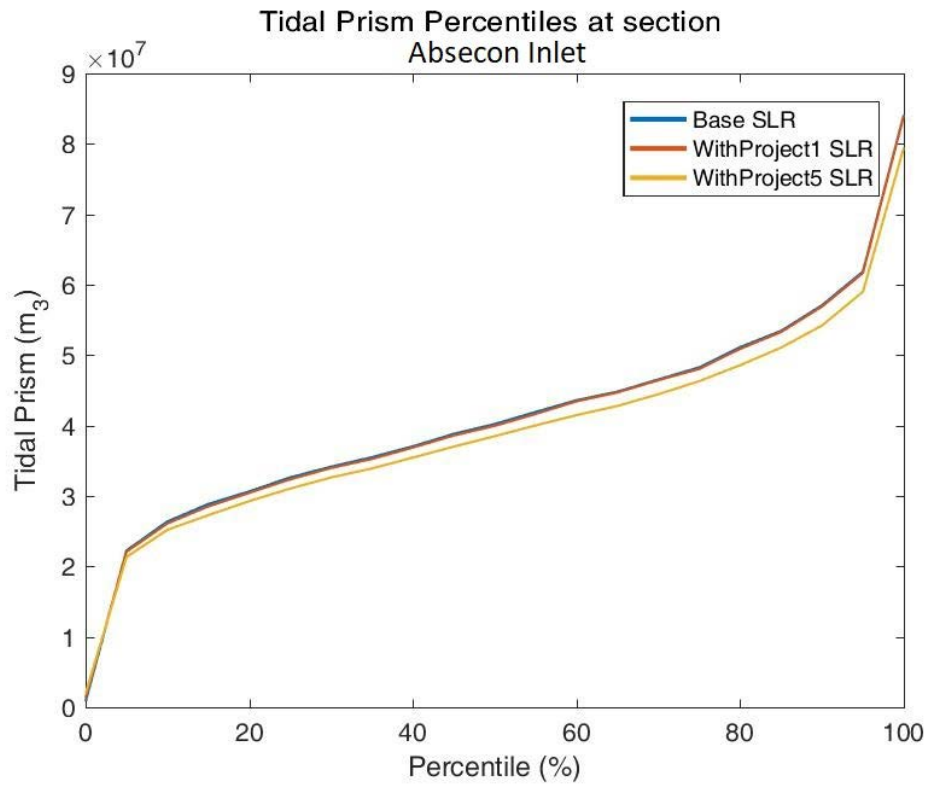
Tidal Prism Plots

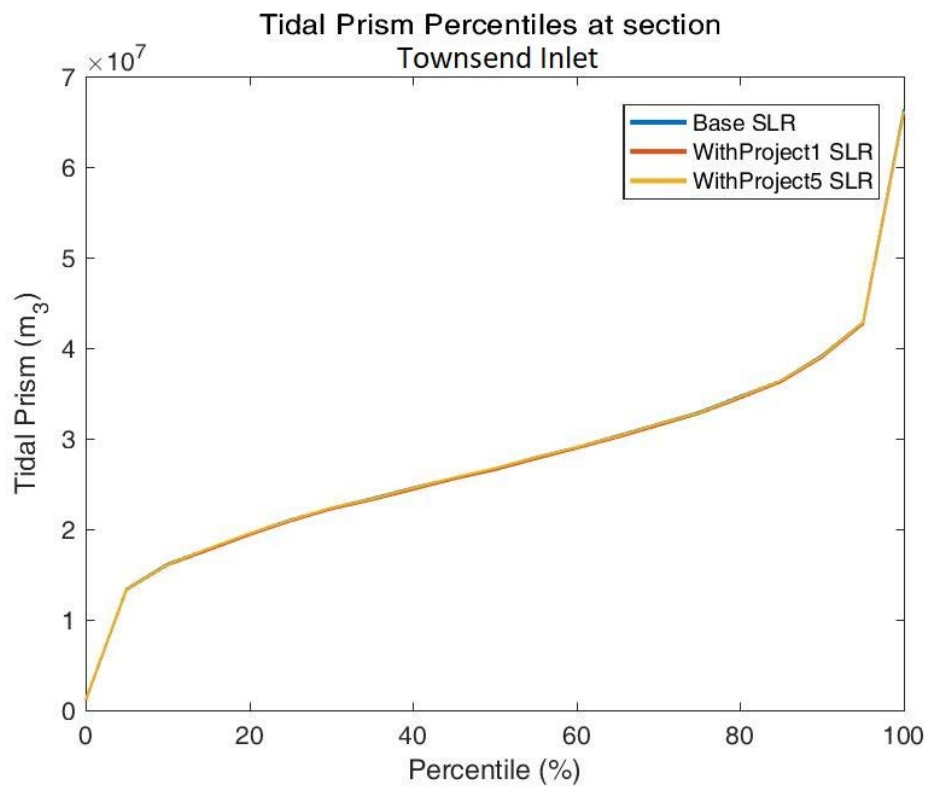
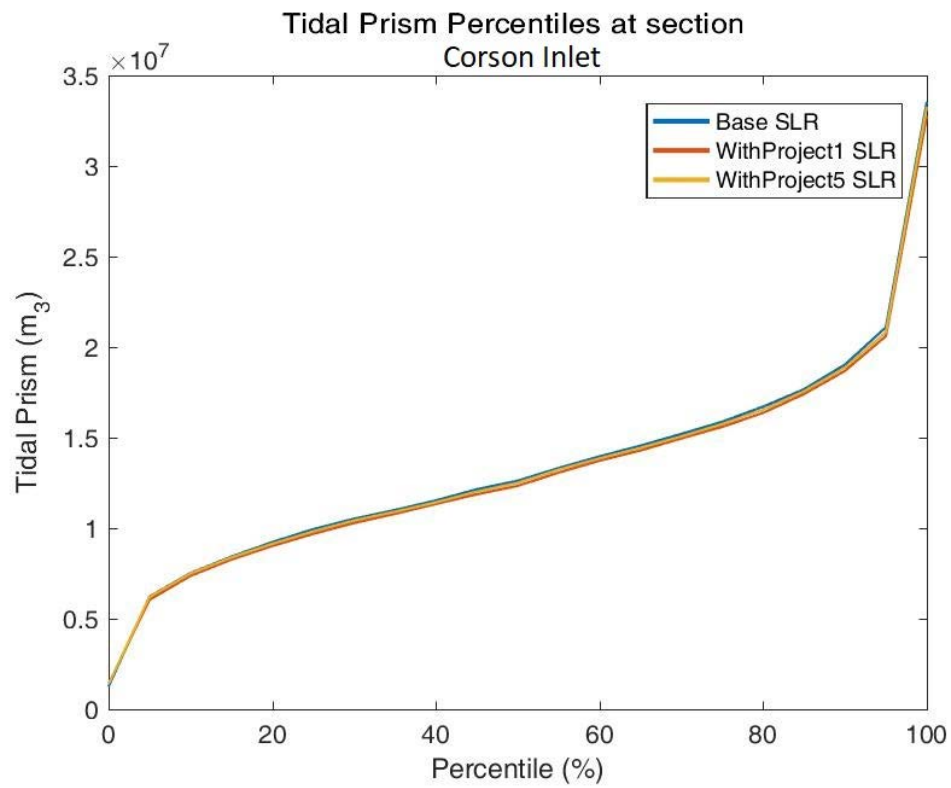


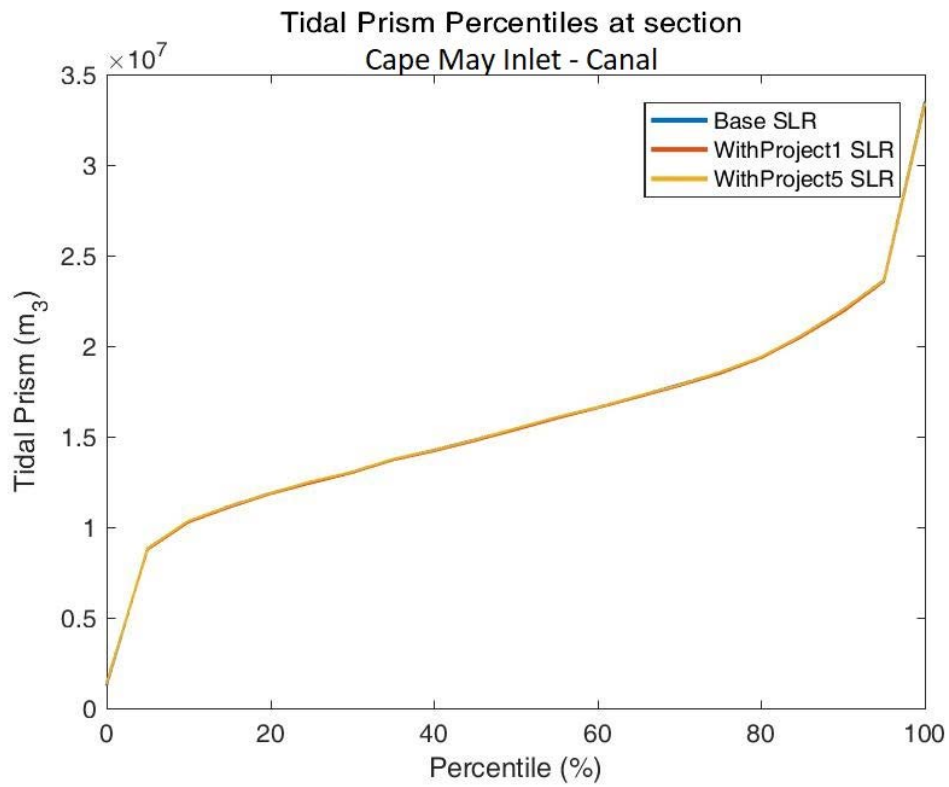
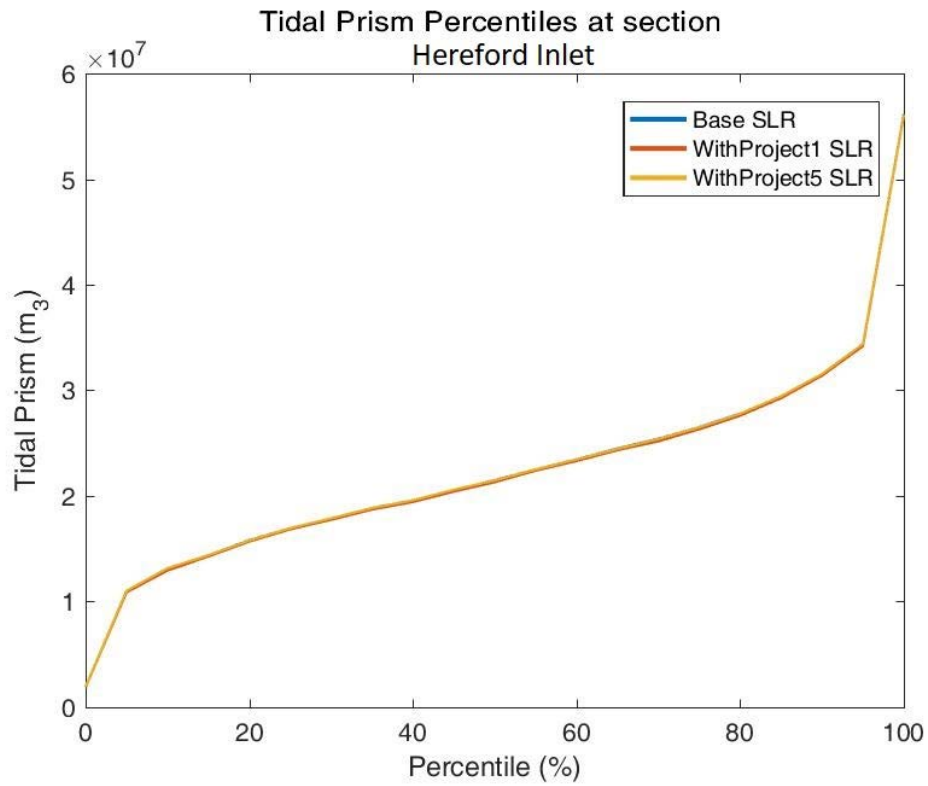
Tidal Prism Percentiles at section Manasquan Inlet











Appendix E: Alternative Salinity Comparisons

The following plots include all of the model/field comparisons for the available field data during 2018. Figure 48 in the main text shows the locations of all salinity comparison sites. The red line represents the measured field data. The model-computed depth-averaged salinity is given by the blue line.

Comparisons to Base

Maximum, Mean, Minimum

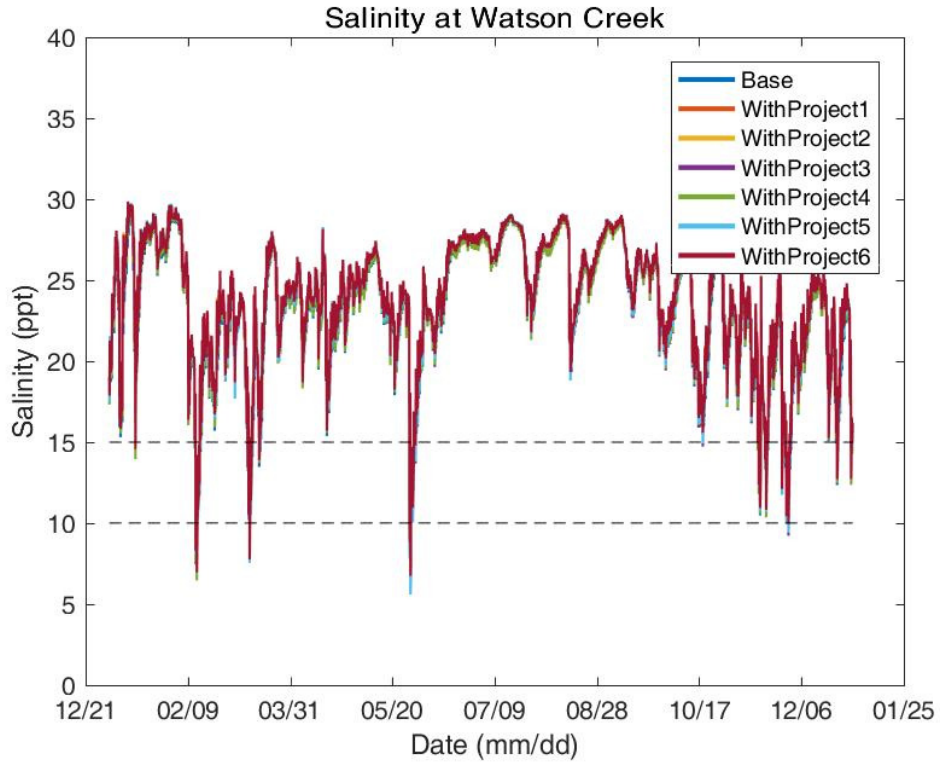
		Base	WP1	WP2	WP3	WP4	WP5	WP6
Watson Creek	Max	29.50	29.76	29.88	29.84	29.74	29.88	29.85
	Mean	23.44	23.50	23.71	23.51	23.51	23.74	23.90
	Min	6.76	6.26	6.36	5.90	6.27	5.59	6.74
Manasquan River	Max	30.57	30.59	30.60	30.59	30.58	30.62	30.60
	Mean	24.03	24.14	24.36	24.18	24.15	24.45	24.52
	Min	0.18	0.17	0.17	0.17	0.17	0.15	0.17
Brick	Max	13.91	13.73	13.60	13.25	13.77	12.71	13.77
	Mean	5.14	5.20	5.14	5.00	5.22	4.68	5.12
	Min	0.25	0.26	0.26	0.24	0.26	0.20	0.24
Barnegat Bay at Mantoloking	Max	29.14	29.29	29.40	29.49	29.28	29.81	29.43
	Mean	20.87	21.00	21.16	21.05	21.02	21.54	21.37
	Min	6.35	6.57	6.55	6.41	6.60	6.15	6.59
Barnegat Bay at Route 37 Bridge	Max	18.74	18.53	18.64	18.66	18.59	20.20	19.13
	Mean	12.48	12.38	12.44	12.46	12.43	13.71	12.95
	Min	8.56	8.40	8.44	8.39	8.44	9.13	8.82
Berkeley	Max	11.24	10.96	10.87	10.77	11.05	11.64	11.42
	Mean	1.91	1.92	1.87	1.86	1.94	1.86	1.93
	Min	0.00	0.00	0.00	0.00	0.00	0.00	0.00
Barnegat Light	Max	29.57	29.58	29.56	29.47	29.57	29.33	29.52
	Mean	25.10	24.86	24.79	24.48	24.90	24.26	24.89
	Min	7.28	7.46	7.46	7.42	7.50	7.57	7.45
	Max	27.60	27.53	27.50	27.31	27.54	27.00	27.49

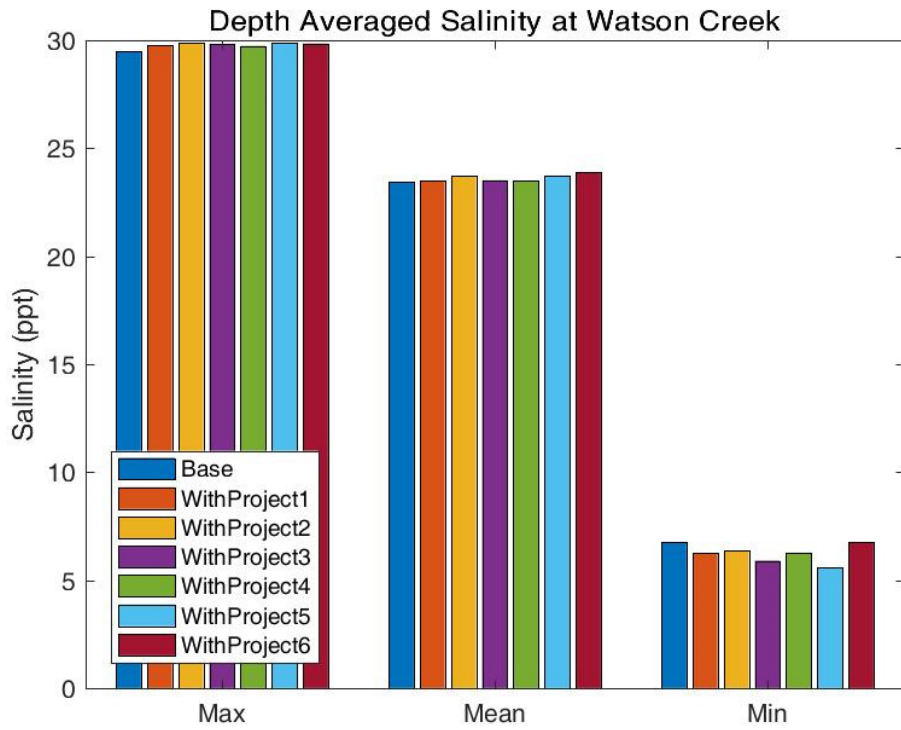
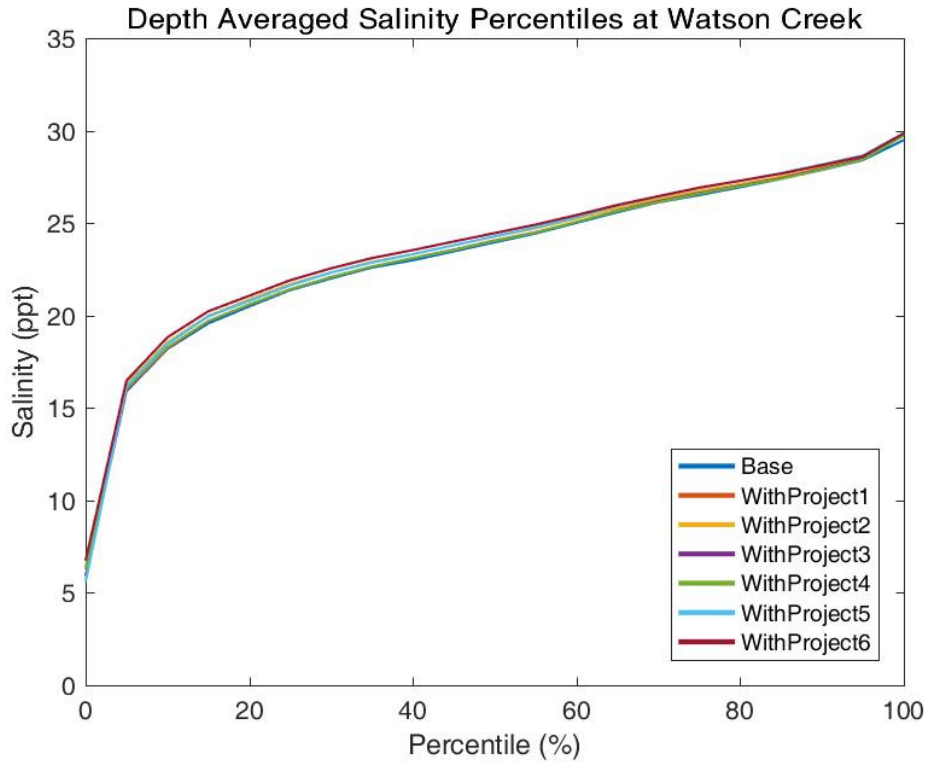
Barnegat Bay at Waretown	Mean	25.29	25.06	25.02	24.79	25.10	24.56	25.10
	Min	19.05	19.08	18.92	18.98	19.15	18.49	18.76
Barnegat Bay at Barnegat Light	Max	29.50	29.50	29.49	31.28	29.65	29.55	29.35
	Mean	27.10	27.27	27.02	27.20	27.48	26.57	26.87
	Min	15.35	15.97	16.74	15.65	13.84	16.66	16.01
Barnegat Light (Ocean)	Max	29.49	29.52	29.53	29.54	29.52	29.51	29.47
	Mean	28.38	28.42	28.42	28.37	28.42	28.25	28.37
	Min	22.73	23.02	22.93	22.73	22.82	22.43	23.12
East Thorofare	Max	28.26	28.39	28.38	28.43	28.41	28.50	28.38
	Mean	25.77	25.92	25.88	25.96	25.95	26.20	25.95
	Min	22.86	23.04	22.97	23.09	23.06	23.35	23.06
Westecunk	Max	28.02	28.10	28.10	28.11	28.11	28.09	28.05
	Mean	21.78	21.96	21.94	21.98	21.98	21.90	21.87
	Min	8.92	9.05	9.04	9.06	9.06	8.95	9.27
Beach Haven	Max	29.25	29.29	29.32	29.31	29.31	29.28	29.27
	Mean	27.28	27.37	27.36	27.39	27.39	27.43	27.37
	Min	24.68	24.81	24.82	24.85	24.84	24.84	24.76
JACNEWQ	Max	21.22	21.77	21.81	21.83	21.79	21.12	20.99
	Mean	4.80	5.14	5.14	5.16	5.15	4.75	4.75
	Min	0.02	0.02	0.02	0.02	0.02	0.02	0.02
Little Egg Inlet	Max	29.20	29.23	29.24	29.25	29.26	29.22	29.23
	Mean	26.89	27.04	27.08	27.06	27.05	26.94	26.97
	Min	18.03	18.52	18.58	18.57	18.55	17.89	17.74
Absecon Creek	Max	29.33	29.38	29.39	29.40	29.39	29.27	29.12
	Mean	27.52	27.60	27.61	27.63	27.60	27.37	27.08
	Min	23.11	24.52	24.52	24.55	24.51	24.26	23.90
Brigantine	Max	29.28	29.31	29.32	29.33	29.32	29.13	28.87
	Mean	27.67	27.71	27.73	27.74	27.72	27.42	27.01
	Min	25.02	25.06	25.09	25.08	25.06	24.75	24.29
Absecon Channel	Max	29.56	29.59	29.61	29.62	29.61	29.55	29.51
	Mean	28.44	28.50	28.52	28.54	28.50	28.38	28.26
	Min	26.20	26.37	26.41	26.50	26.34	25.92	25.51
	Max	29.59	29.62	29.63	29.63	29.63	29.59	29.57

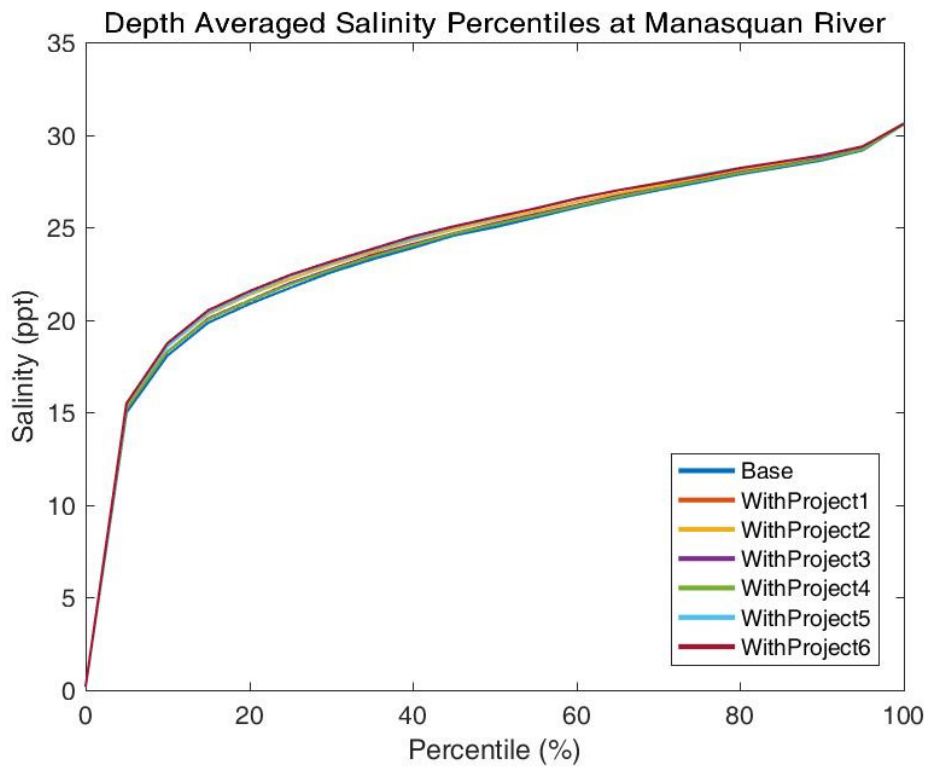
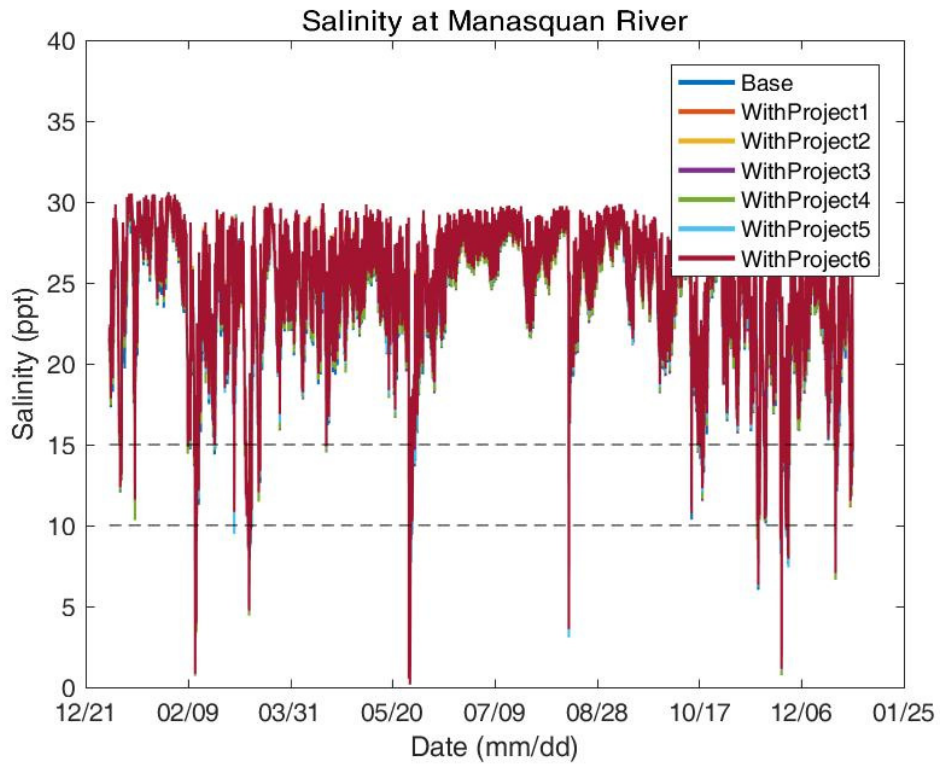
Atlantic City (Ocean)	Mean	28.65	28.70	28.74	28.73	28.71	28.61	28.54
	Min	27.27	27.37	27.41	27.43	27.38	27.10	26.80
Inside Thorofare	Max	29.04	28.85	28.77	28.84	29.07	28.98	29.09
	Mean	27.60	27.25	27.15	27.22	27.56	27.44	27.61
	Min	25.84	25.62	25.54	25.52	25.86	25.68	25.77
Beach Thorofare	Max	29.49	29.52	29.53	29.54	29.54	29.48	29.47
	Mean	28.25	28.18	28.13	28.05	28.37	28.16	28.20
	Min	26.31	26.23	26.15	26.09	26.41	26.20	26.27
Scull Bay	Max	29.30	29.34	29.35	29.35	29.43	29.30	29.30
	Mean	27.77	27.75	27.71	27.67	27.89	27.68	27.71
	Min	23.49	23.42	23.33	23.25	23.53	23.31	23.36
Great Egg Harbor River	Max	28.84	28.89	28.84	28.88	28.86	28.80	28.76
	Mean	18.99	18.73	18.38	18.08	18.75	18.28	18.14
	Min	2.79	2.40	2.24	1.93	2.48	2.32	2.30
Great Egg Harbor Bay	Max	29.33	29.35	29.36	29.40	29.36	29.31	29.30
	Mean	27.34	27.21	27.08	27.30	27.33	27.06	27.06
	Min	20.52	20.50	20.16	20.34	20.43	20.03	20.12
Ocean City 39th St	Max	28.65	28.58	28.51	28.57	28.62	28.48	28.45
	Mean	25.75	25.45	25.22	25.28	25.57	25.27	25.25
	Min	21.13	20.64	20.21	20.32	20.63	20.43	20.35
Corson Sound	Max	29.49	29.52	29.53	29.52	29.51	29.50	29.51
	Mean	28.05	28.17	28.24	28.31	28.14	28.09	28.13
	Min	24.64	24.86	24.84	25.16	24.85	24.50	24.54
Ludlum Thorofare	Max	29.40	29.43	29.43	29.42	29.41	29.41	29.41
	Mean	27.74	27.80	27.84	27.83	27.78	27.75	27.78
	Min	24.87	24.91	24.96	24.95	24.89	24.88	24.92
Ingram Thorofare	Max	29.48	29.51	29.51	29.50	29.50	29.48	29.48
	Mean	28.34	28.38	28.42	28.35	28.34	28.34	28.34
	Min	25.56	25.59	25.66	25.48	25.47	25.57	25.50
Cape May Ferry	Max	28.67	28.67	28.72	28.67	28.66	28.67	28.72
	Mean	27.33	27.35	27.41	27.36	27.33	27.33	27.41
	Min	25.27	25.32	25.41	25.34	25.28	25.27	25.38
Cape May Harbor	Max	29.56	29.57	29.57	29.57	29.57	29.56	29.56
	Mean	28.64	28.67	28.68	28.67	28.66	28.64	28.65

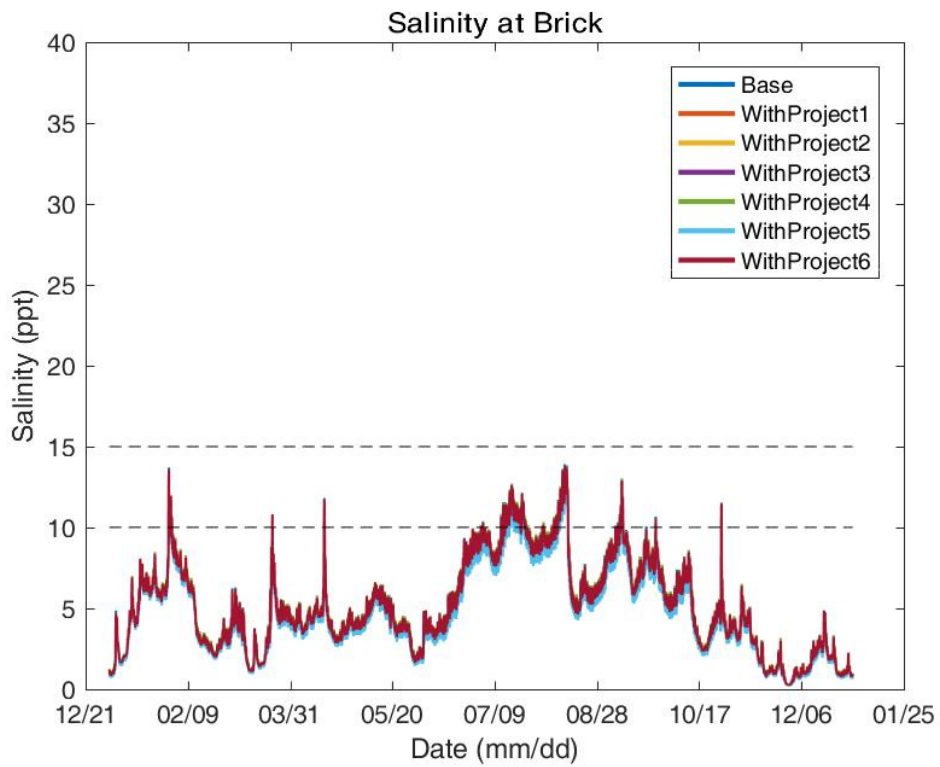
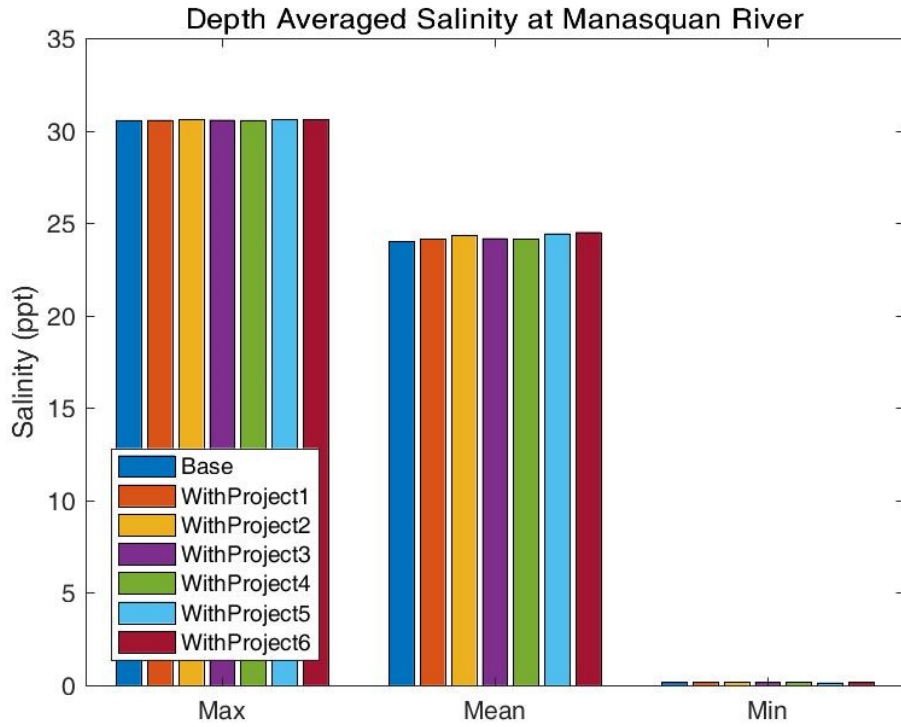
	Min	27.04	27.08	27.09	27.07	27.07	27.04	27.05
--	-----	-------	-------	-------	-------	-------	-------	-------

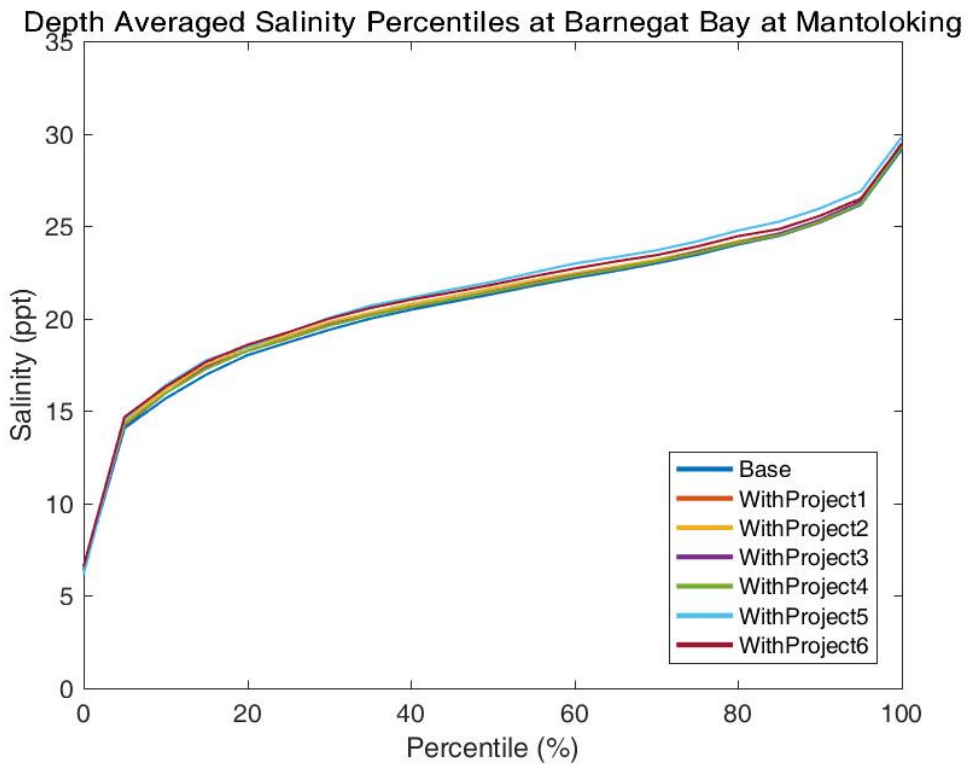
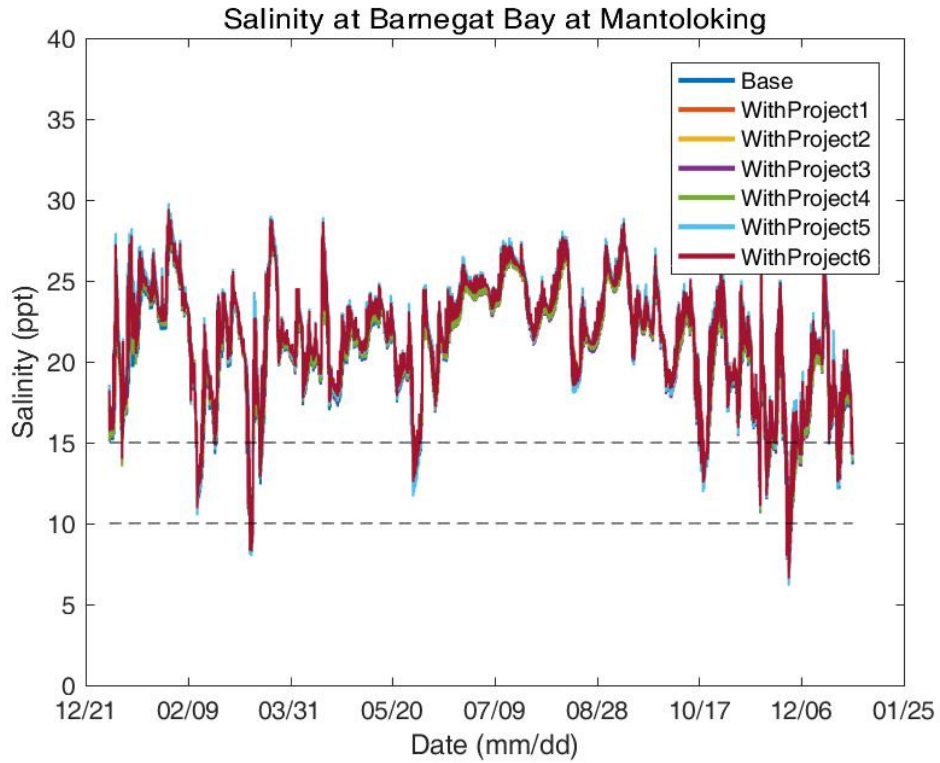
Point Comparisons



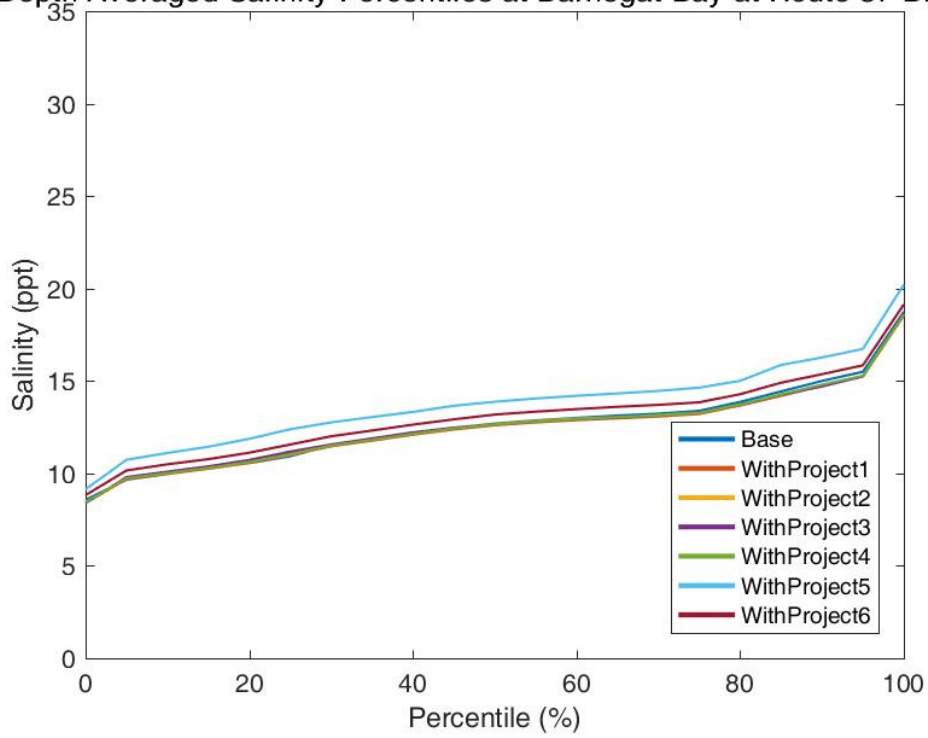




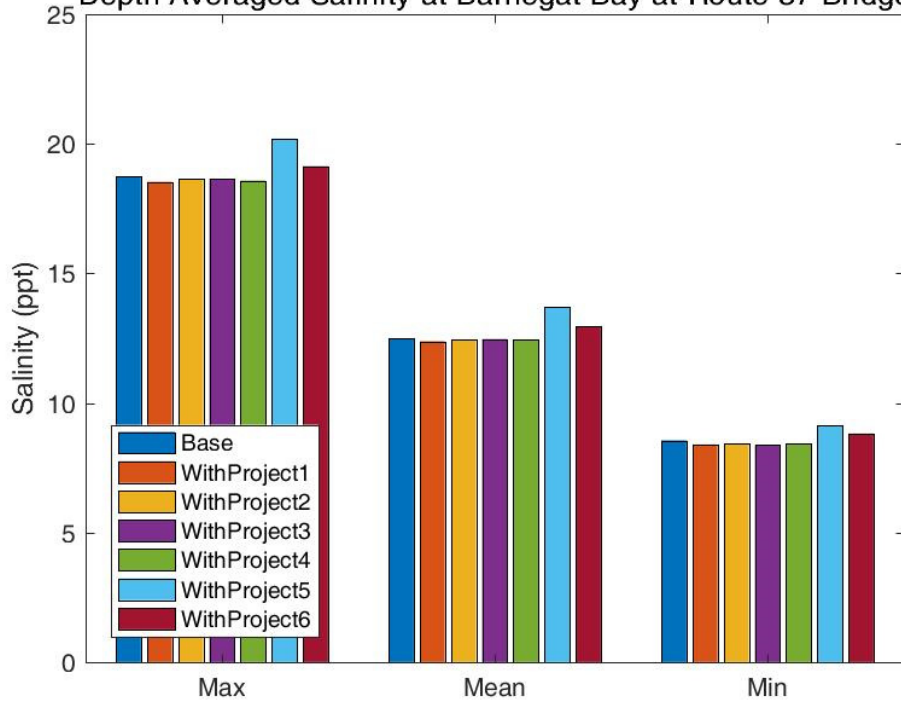


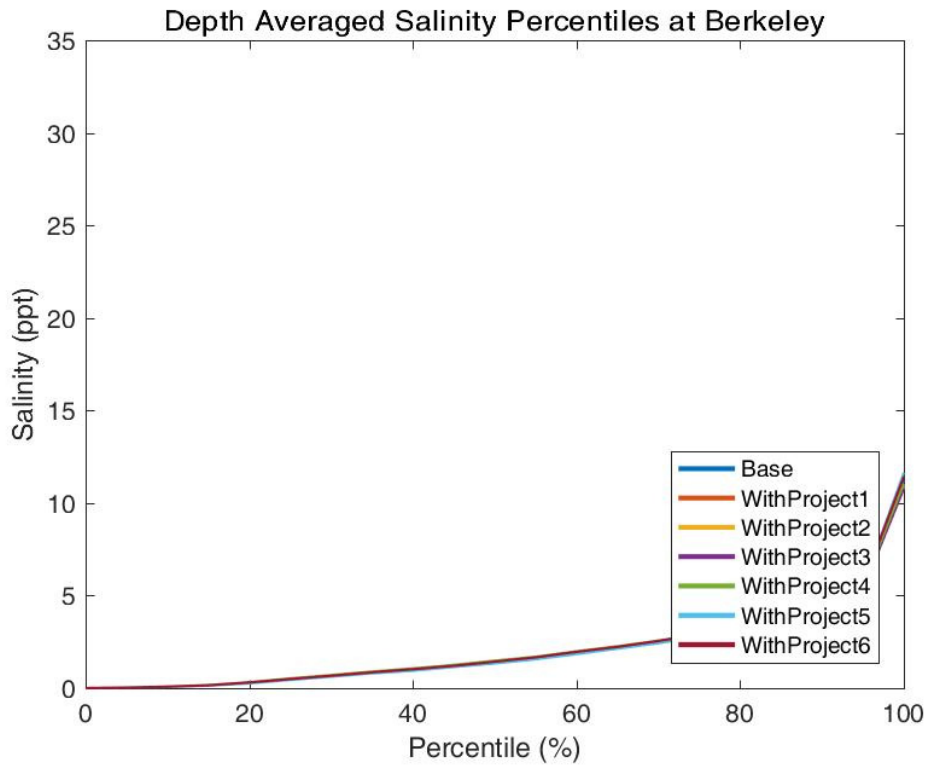
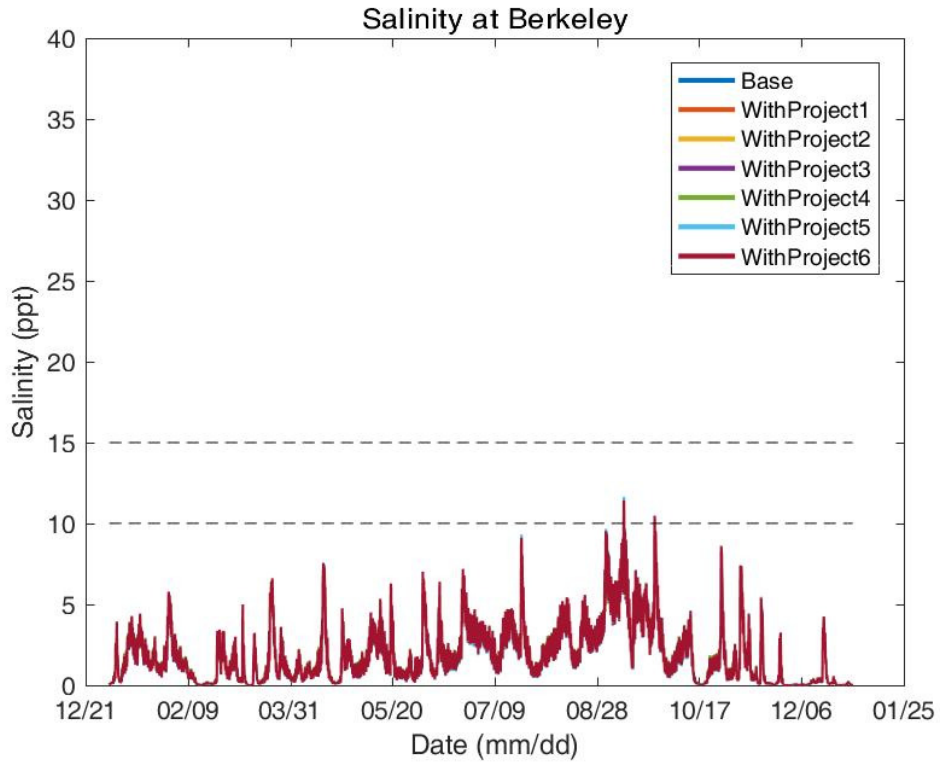


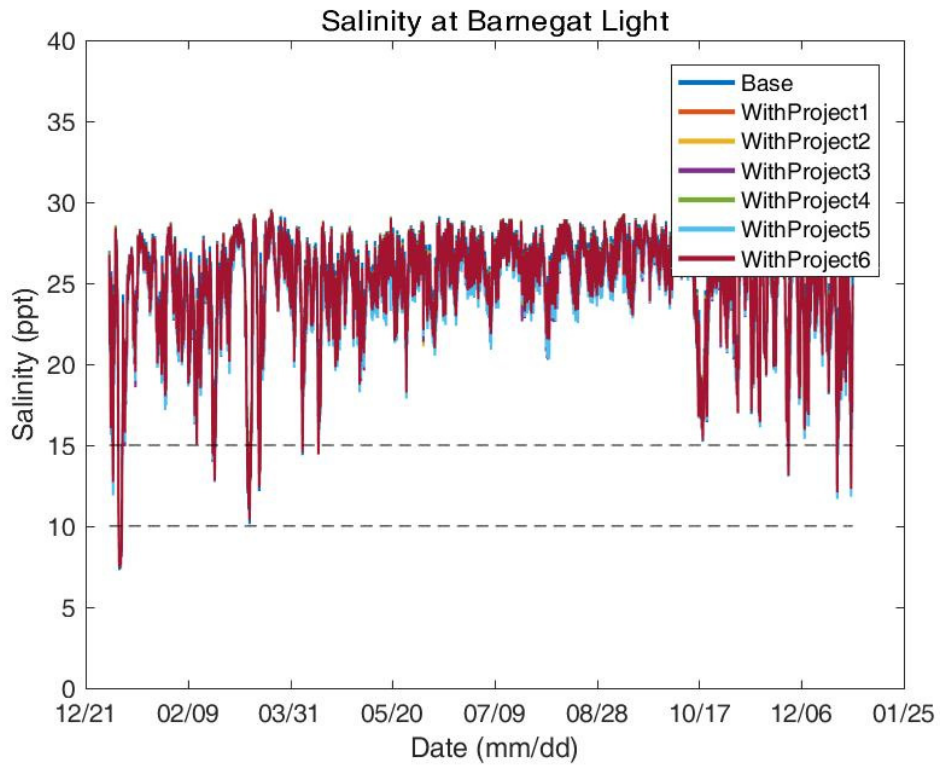
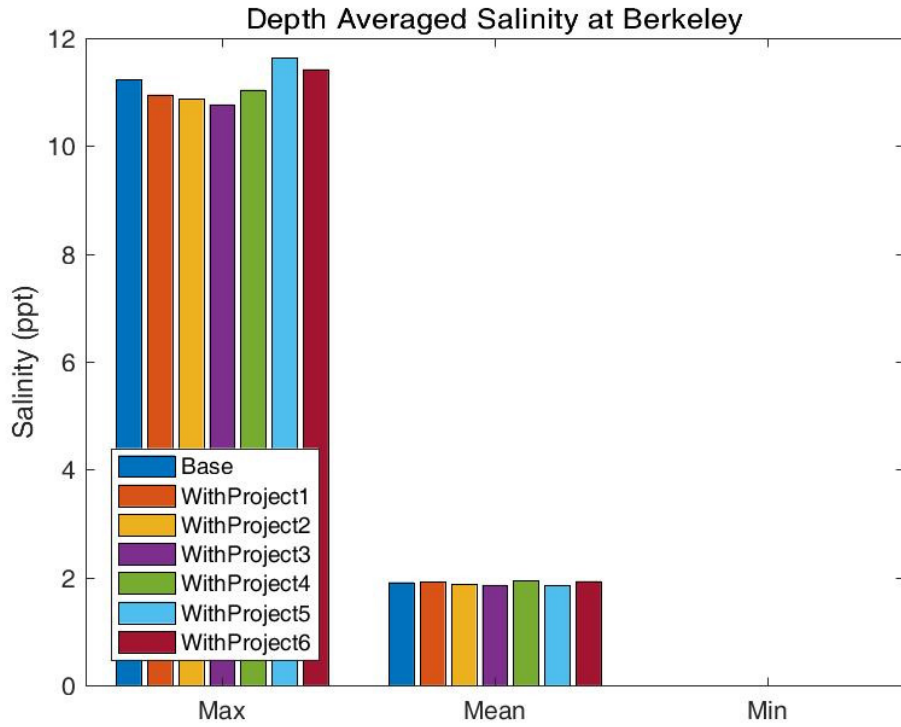
Depth Averaged Salinity Percentiles at Barnegat Bay at Route 37 Bridge

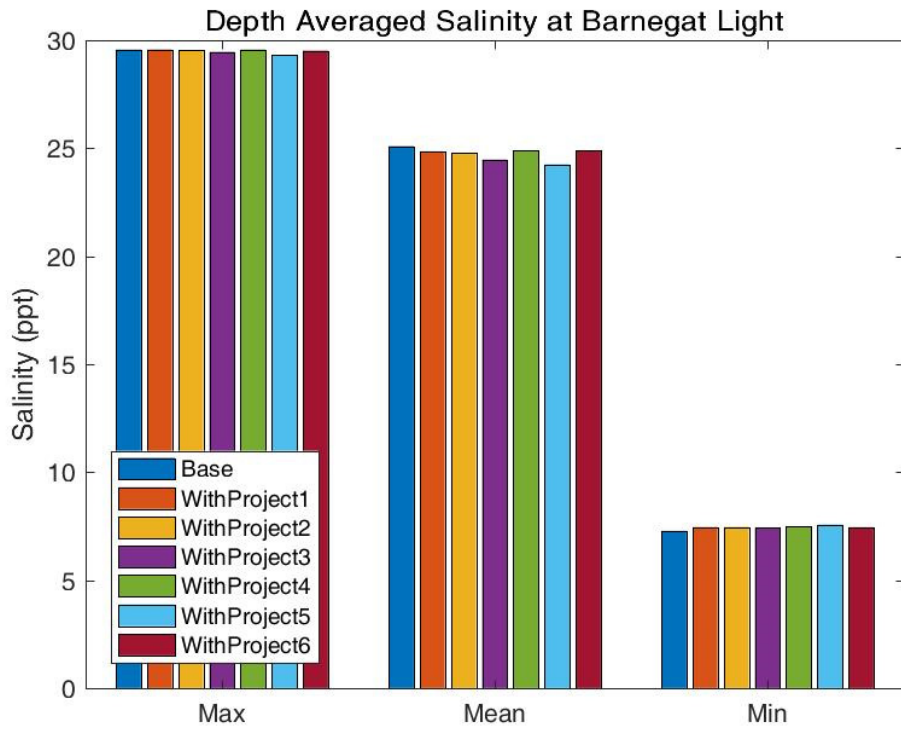
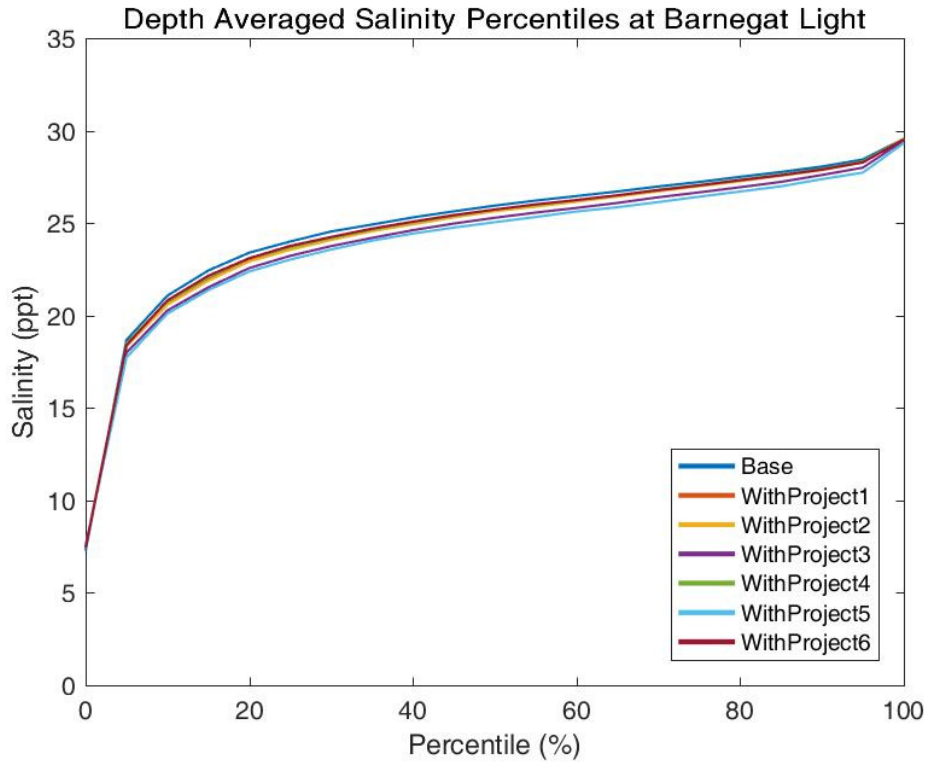


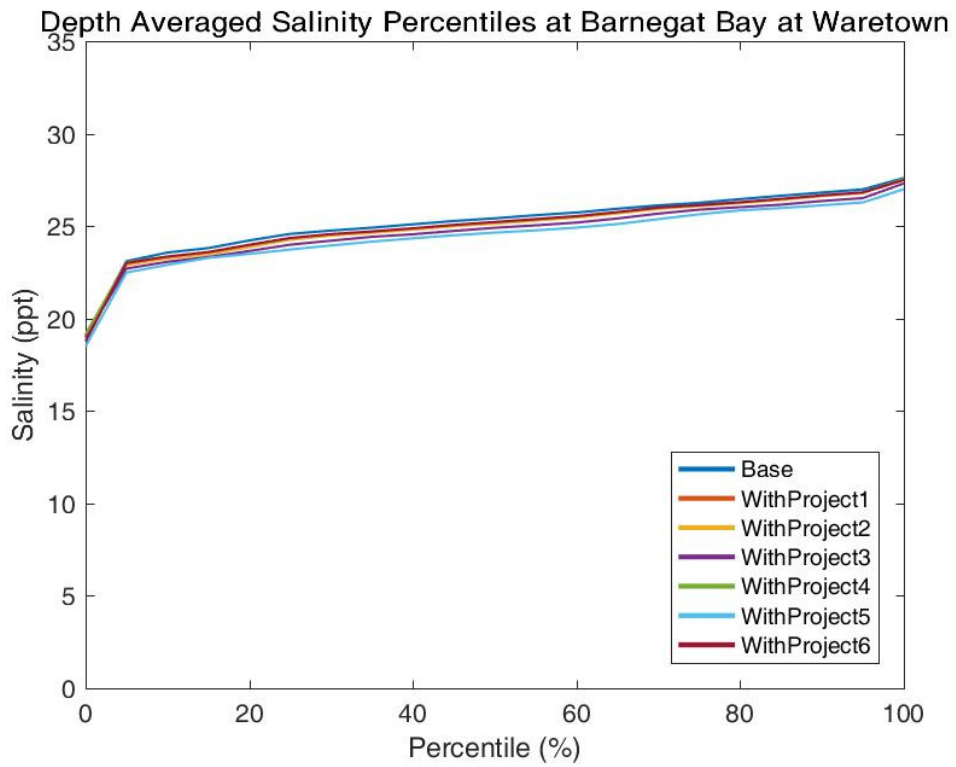
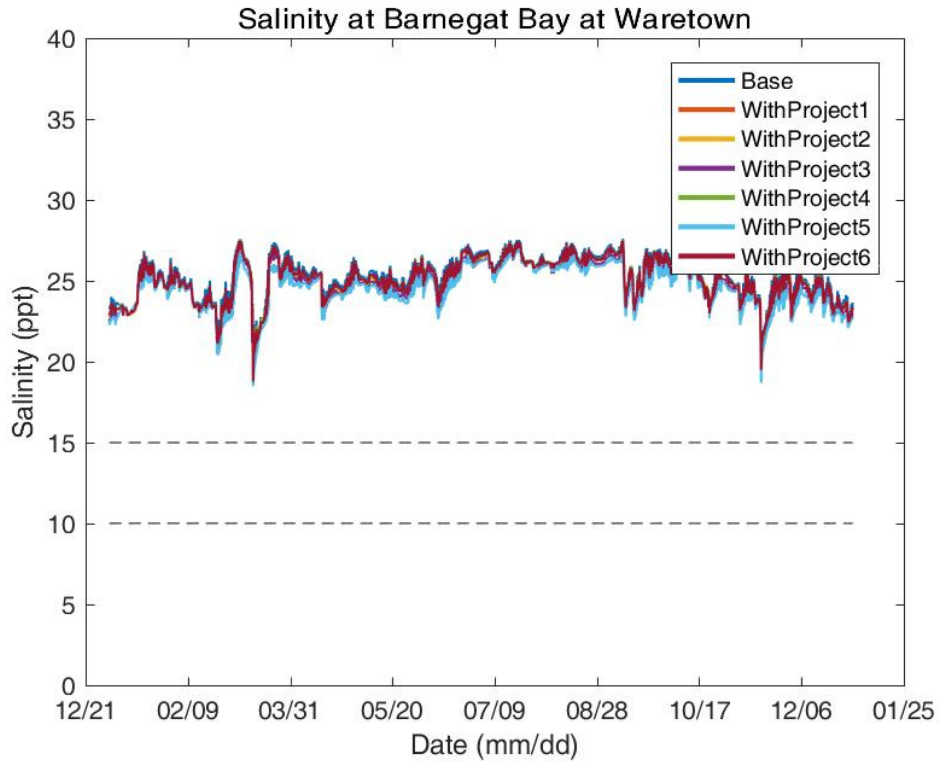
Depth Averaged Salinity at Barnegat Bay at Route 37 Bridge

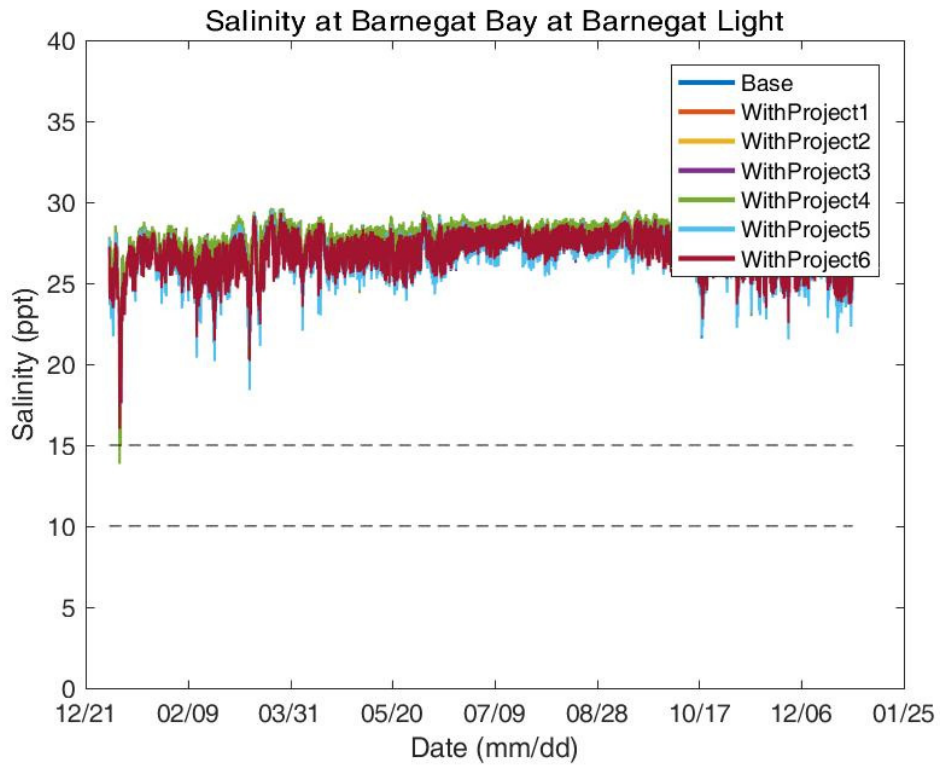
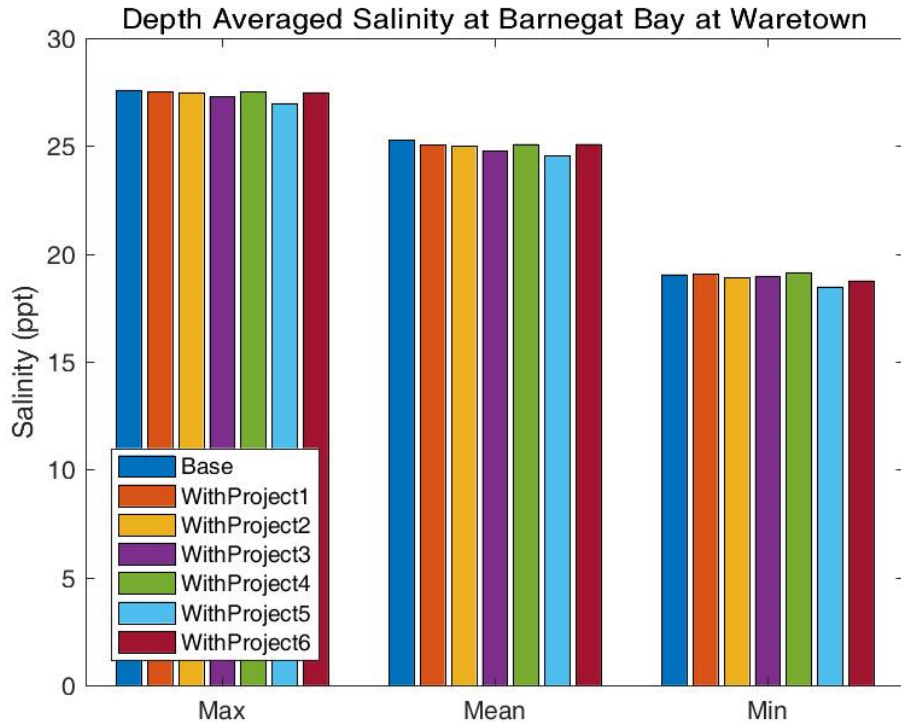




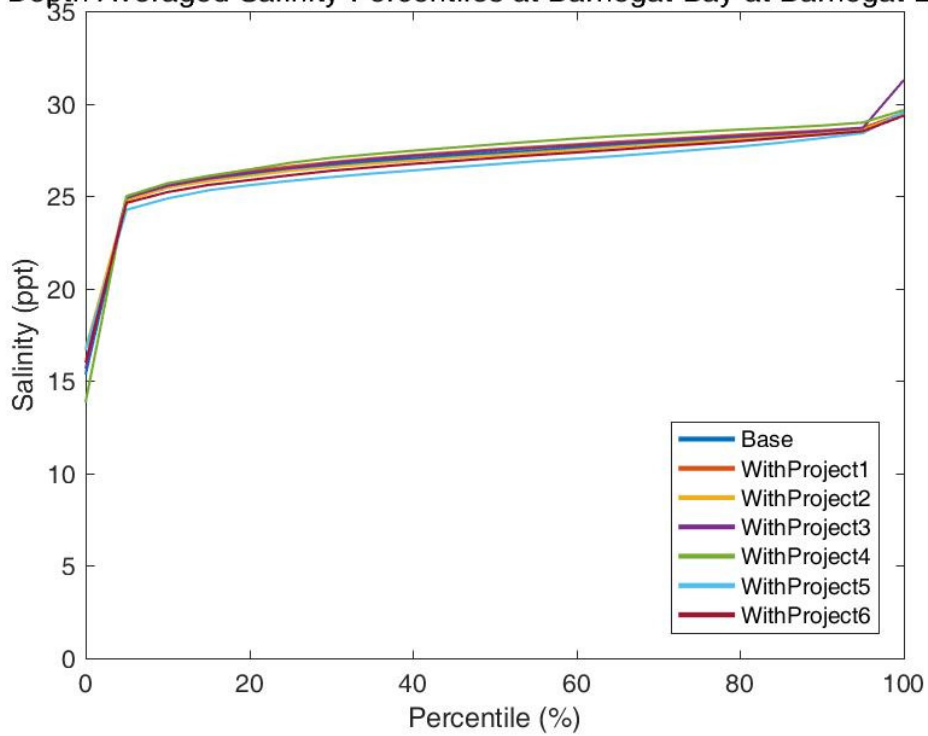




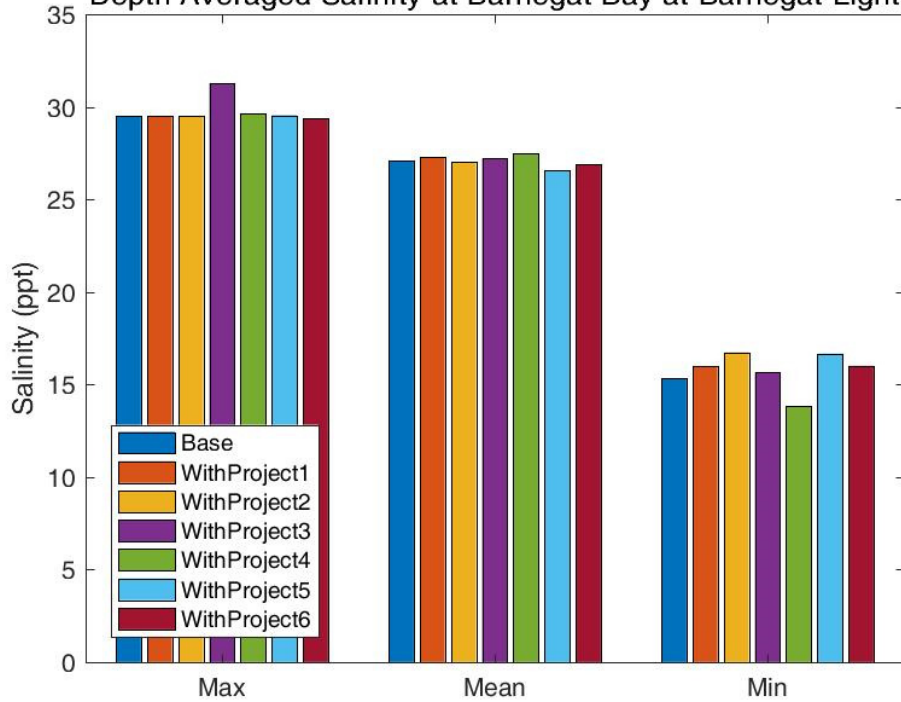


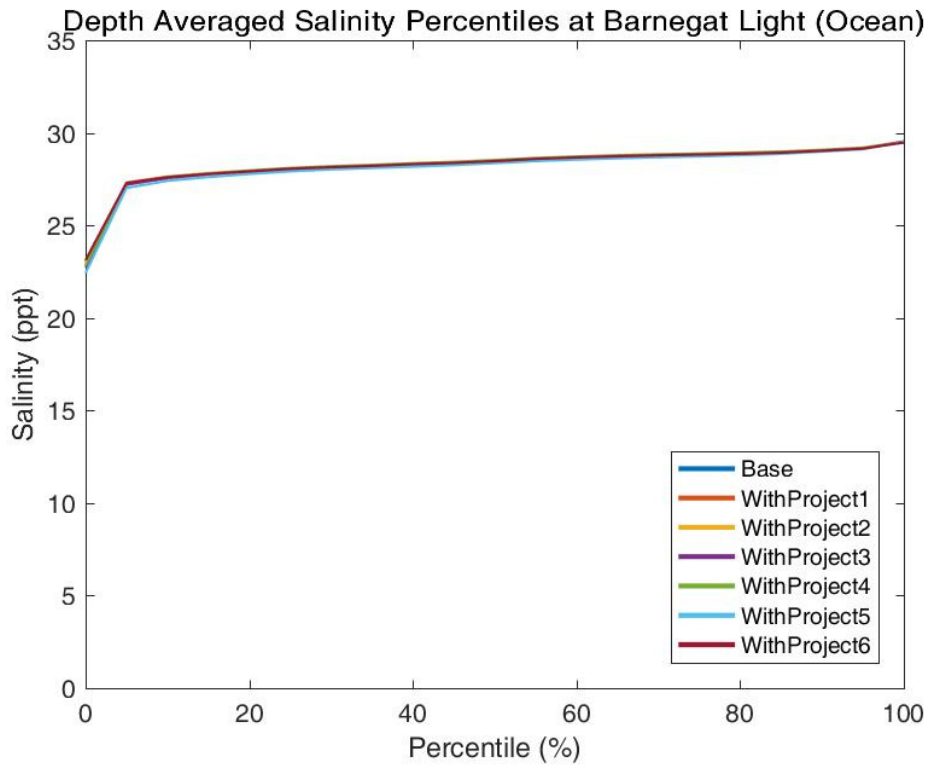
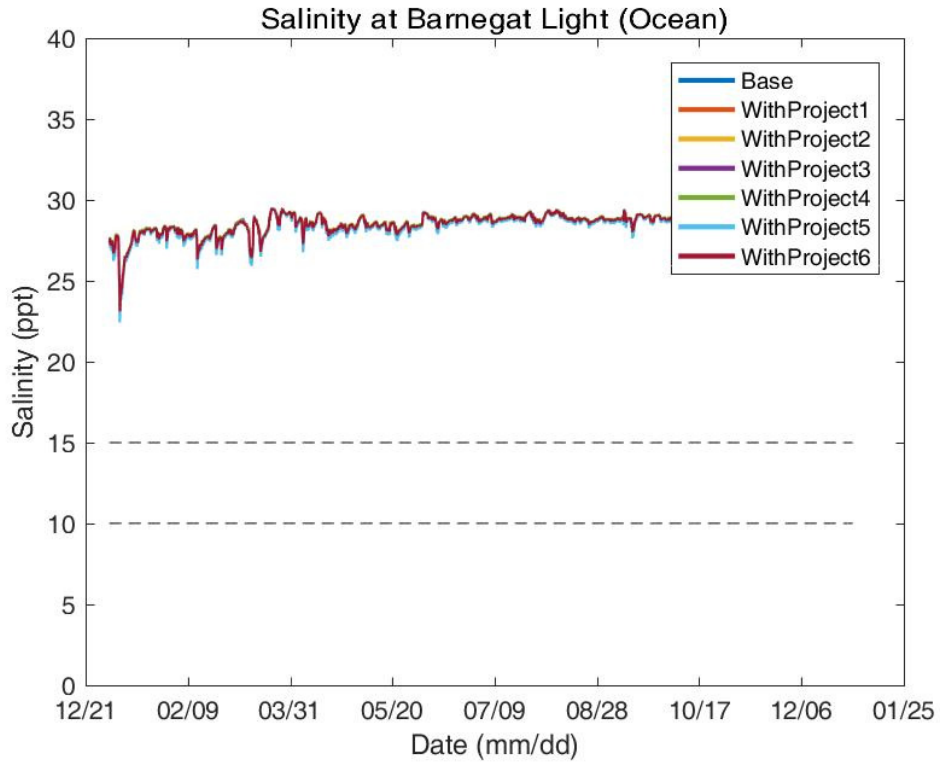


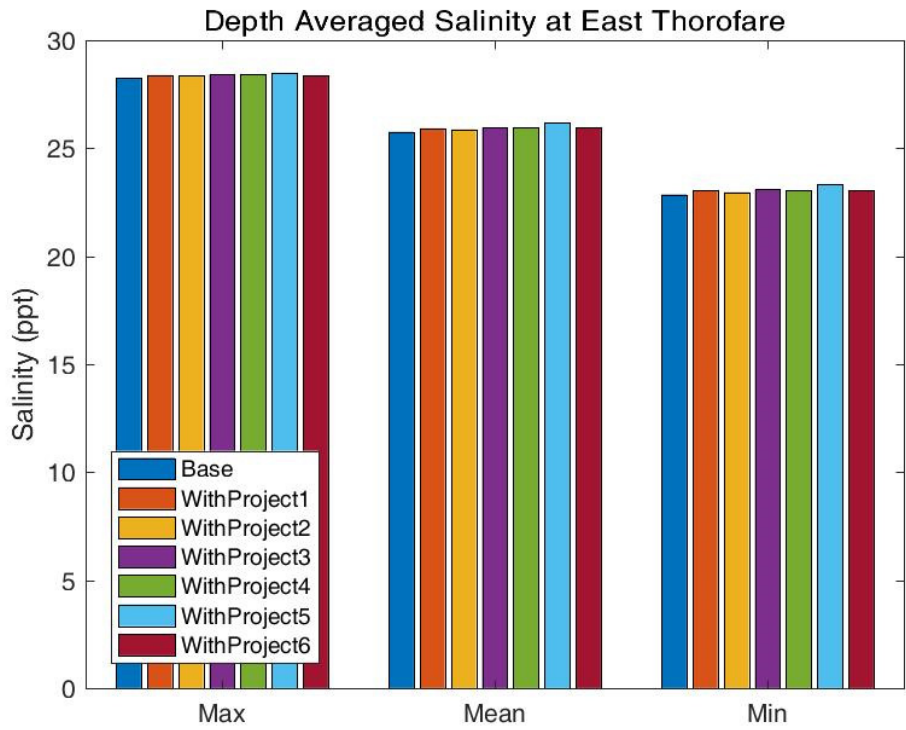
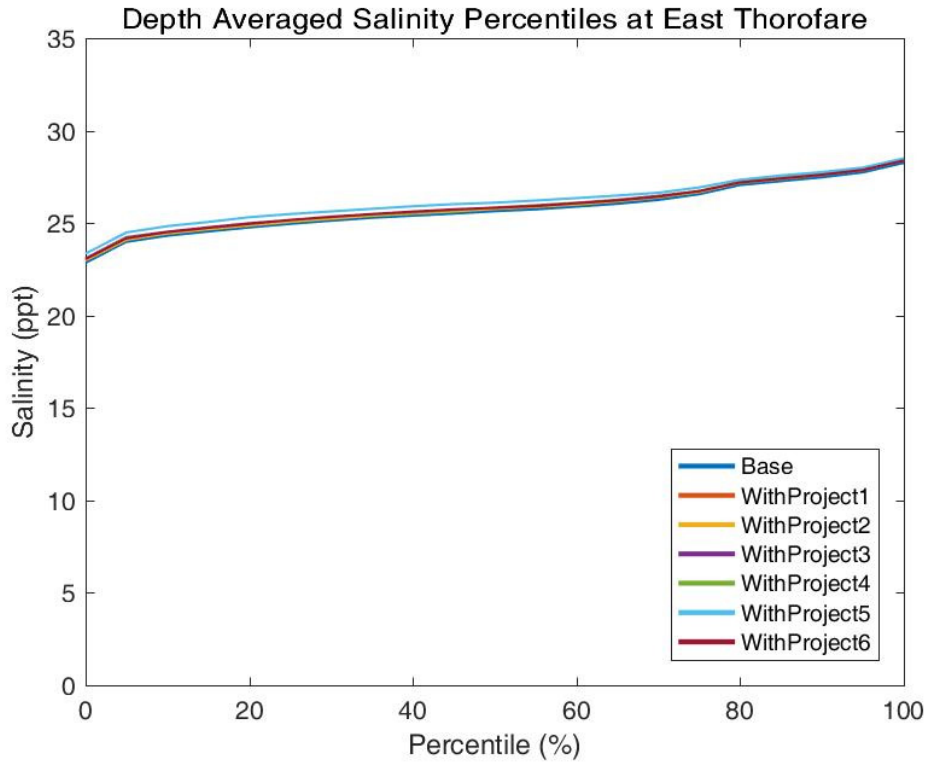
Depth Averaged Salinity Percentiles at Barnegat Bay at Barnegat Light

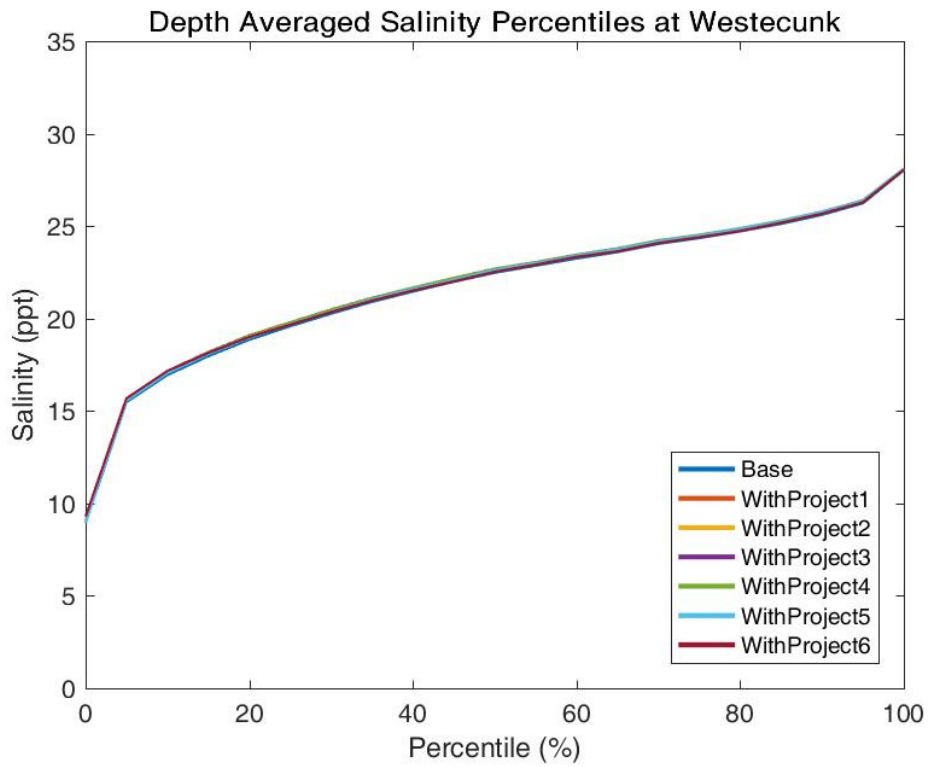
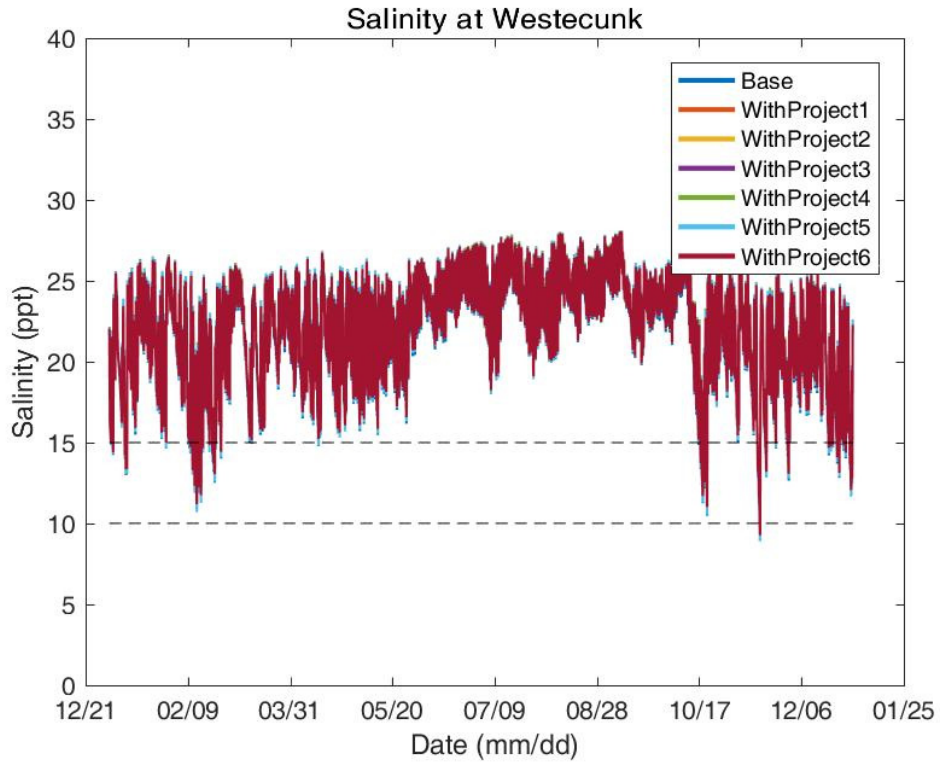


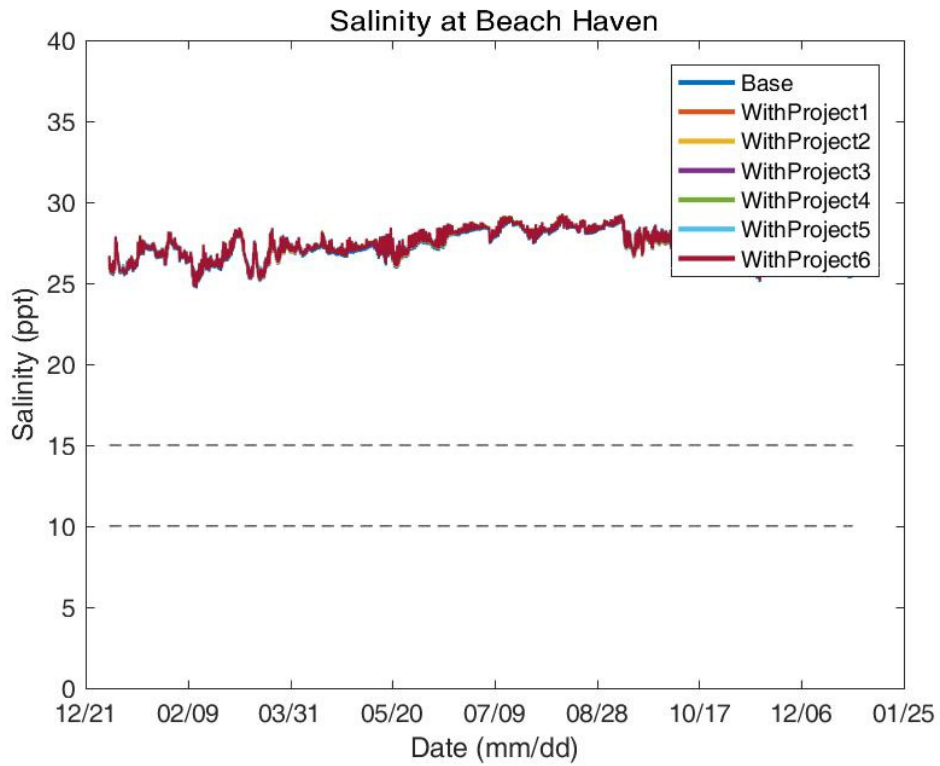
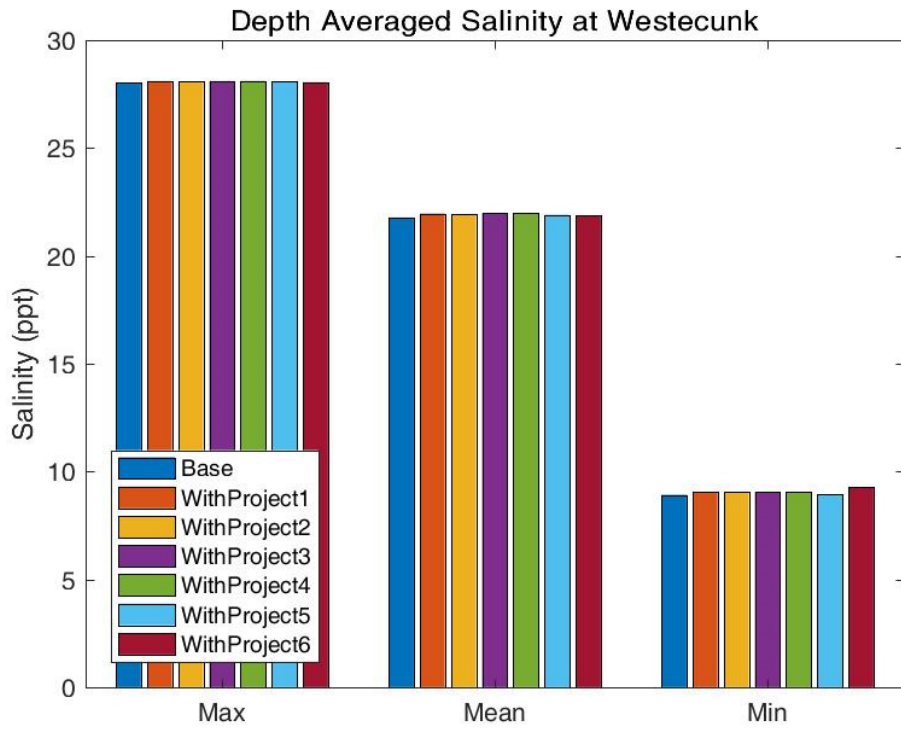
Depth Averaged Salinity at Barnegat Bay at Barnegat Light

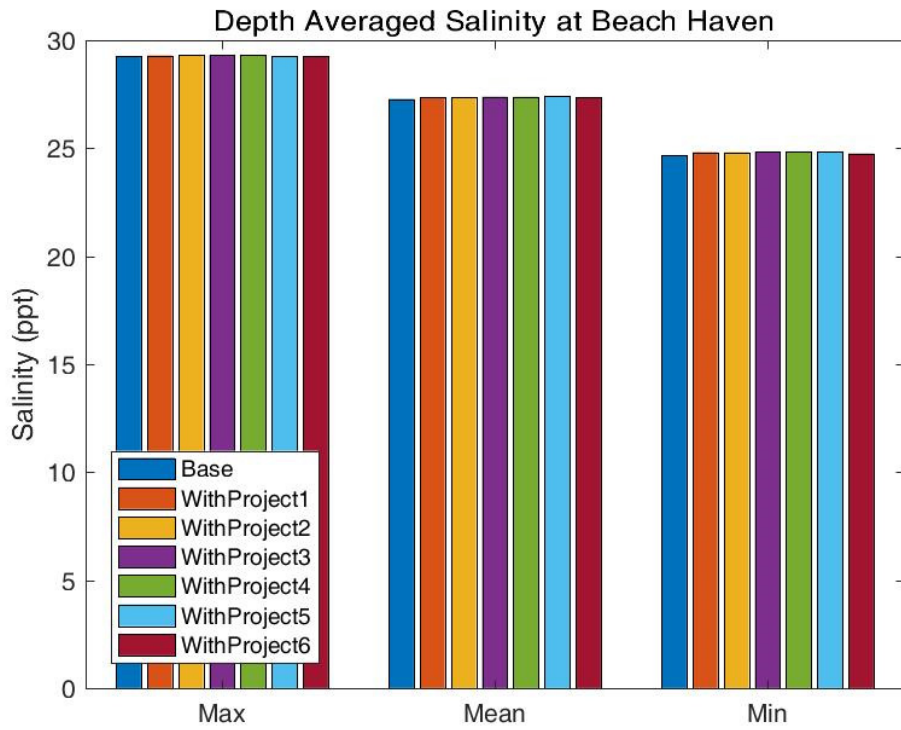
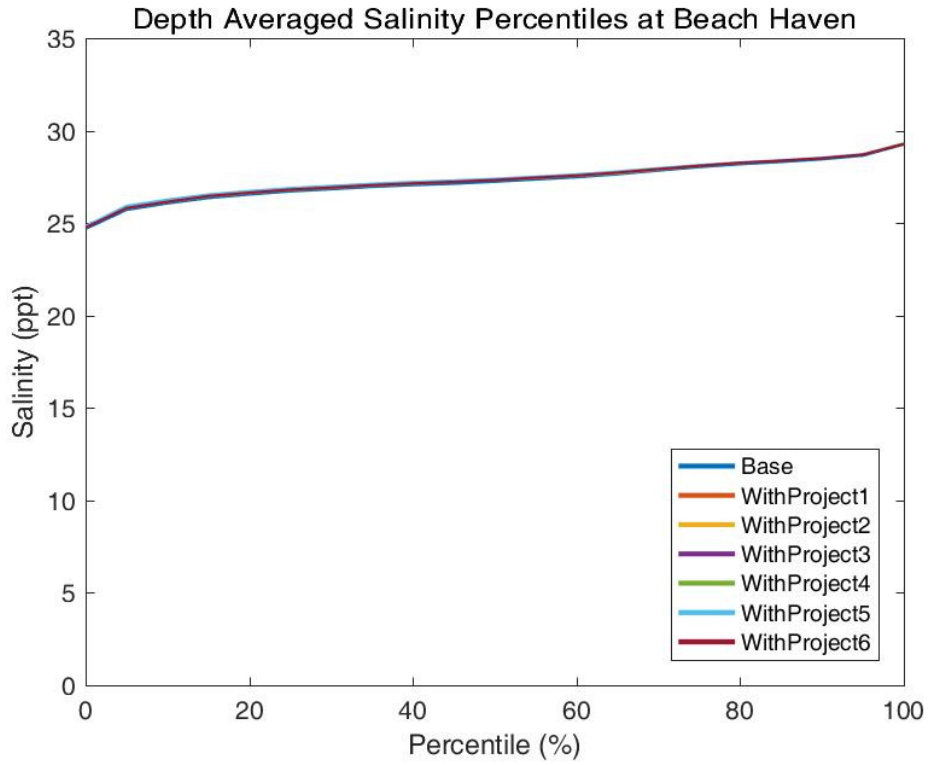


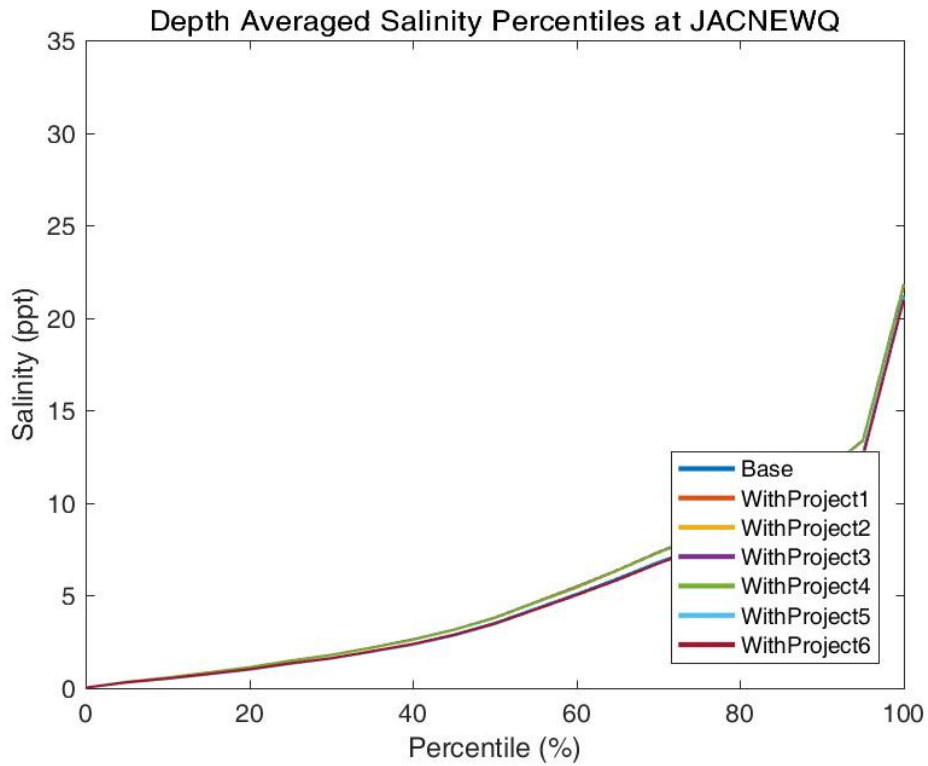
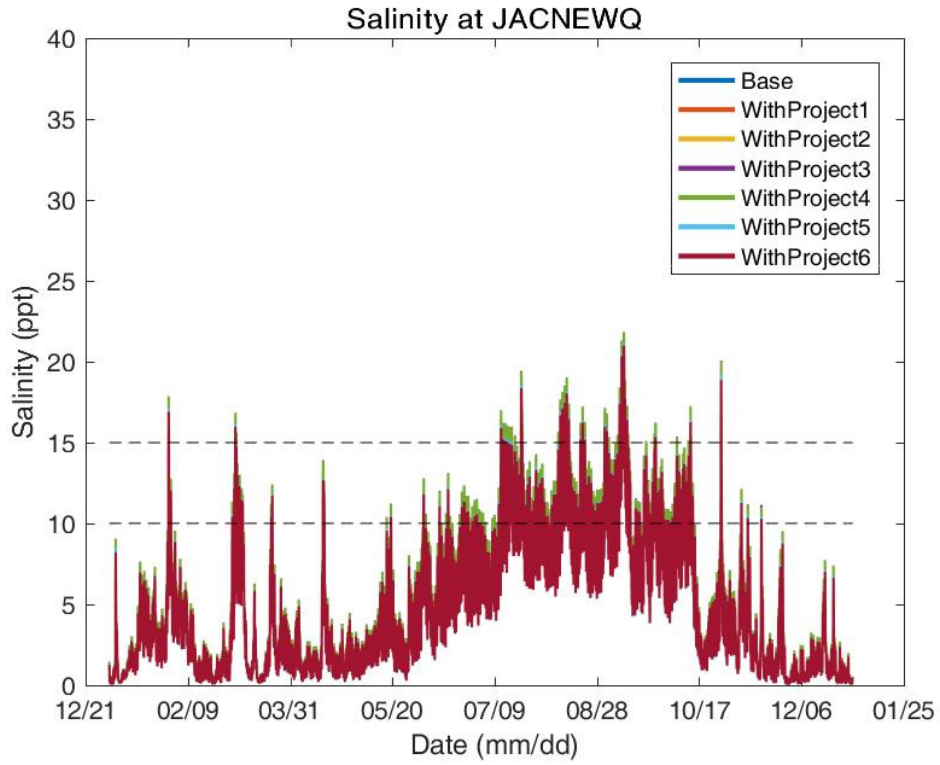


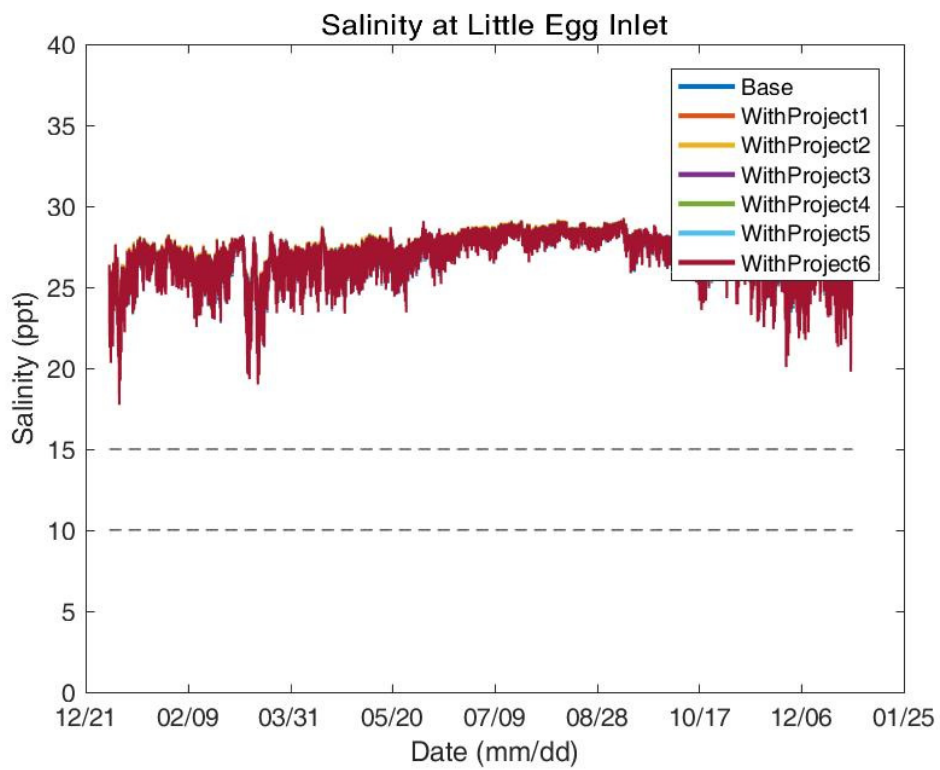
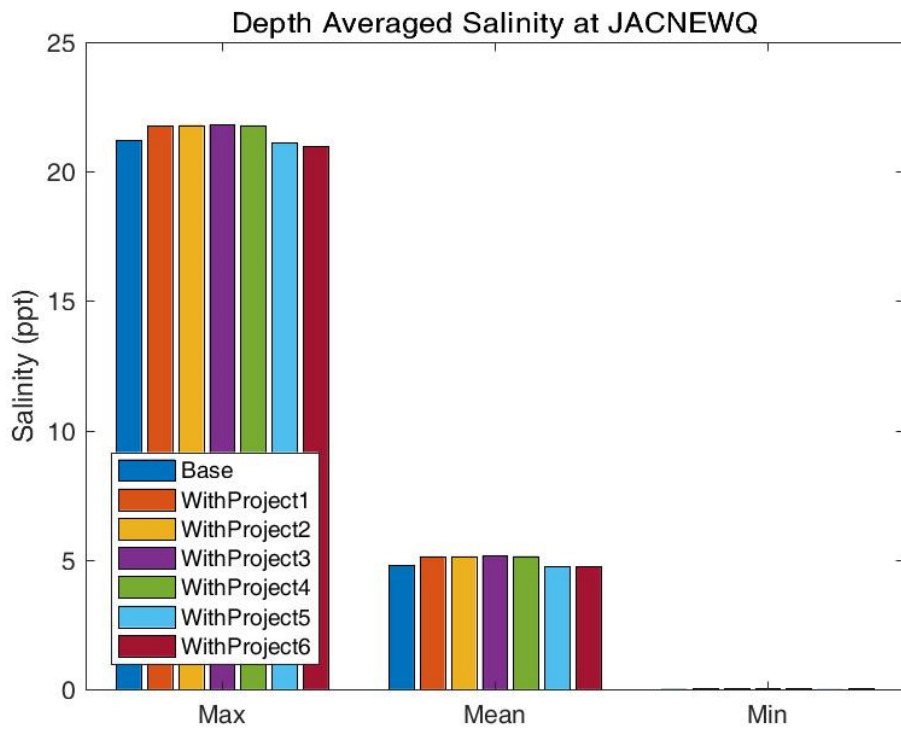


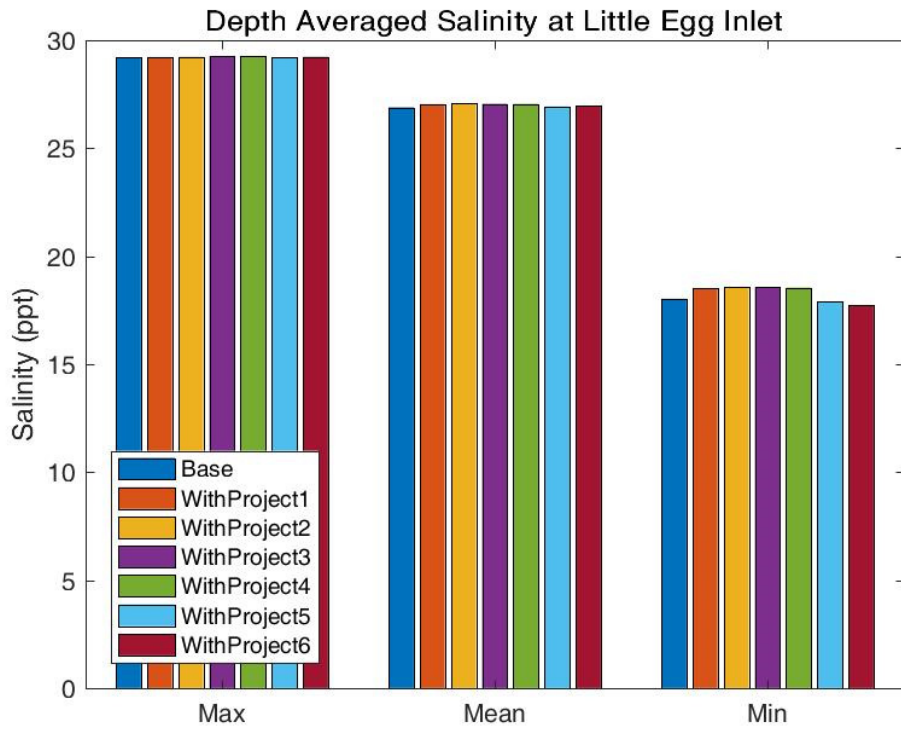
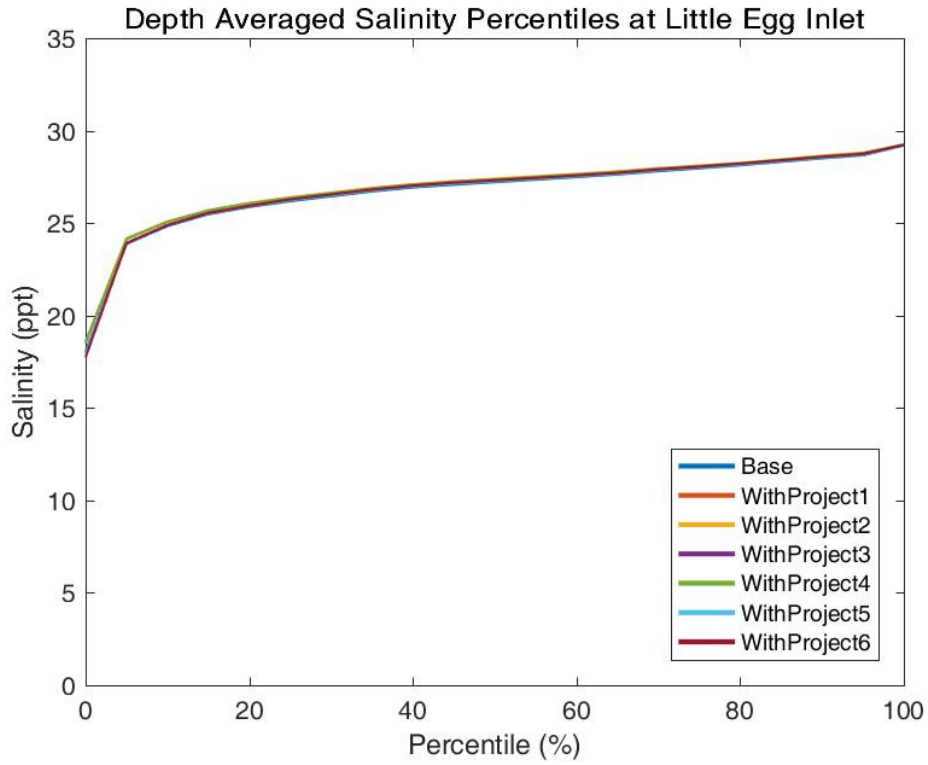


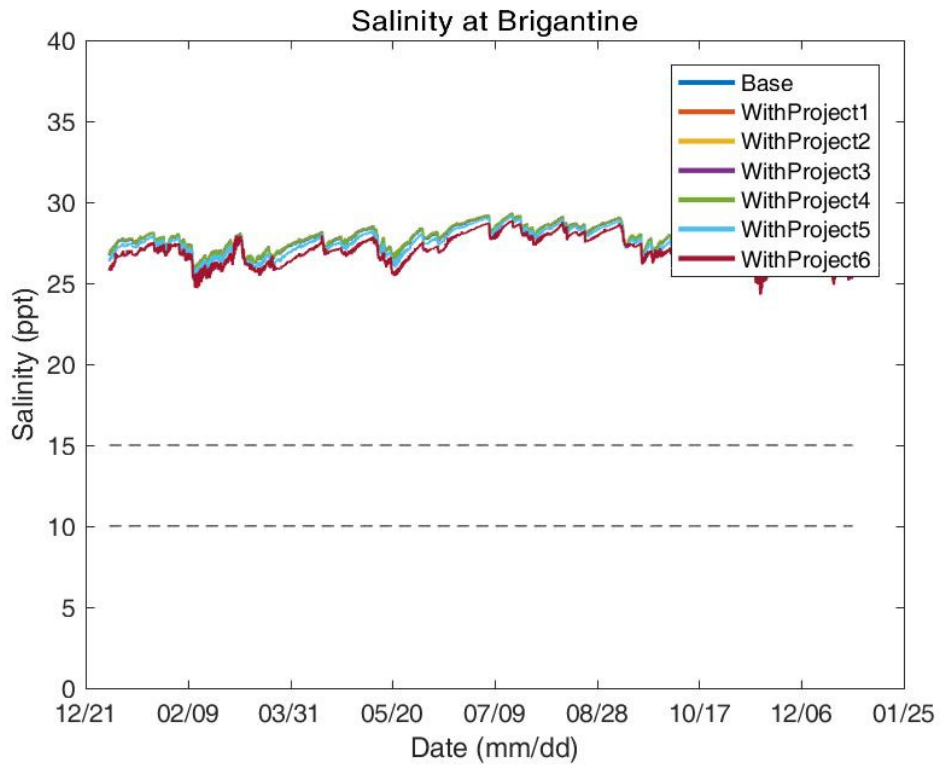
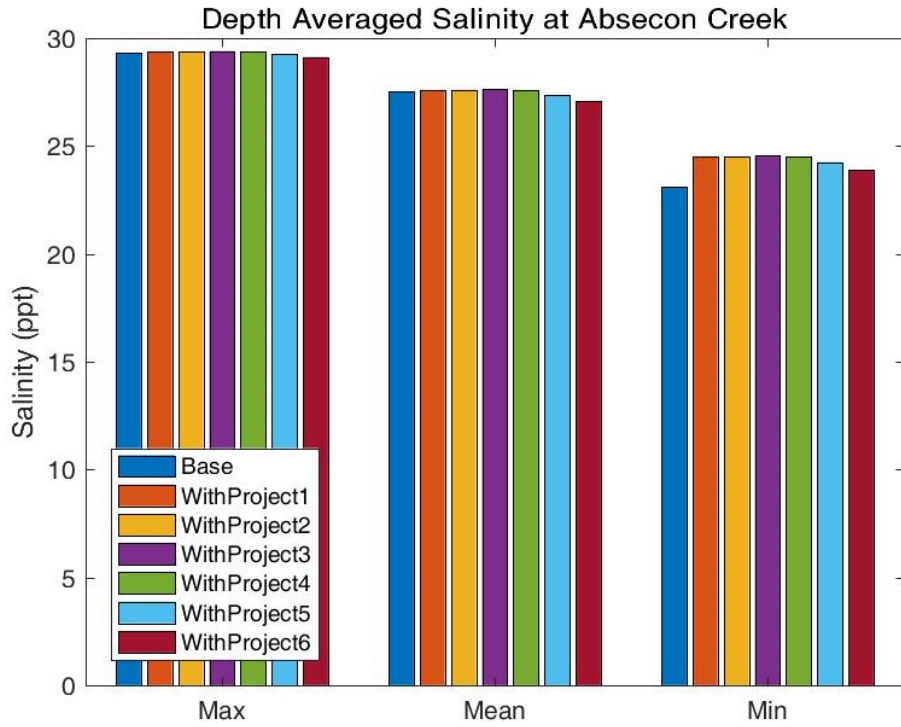


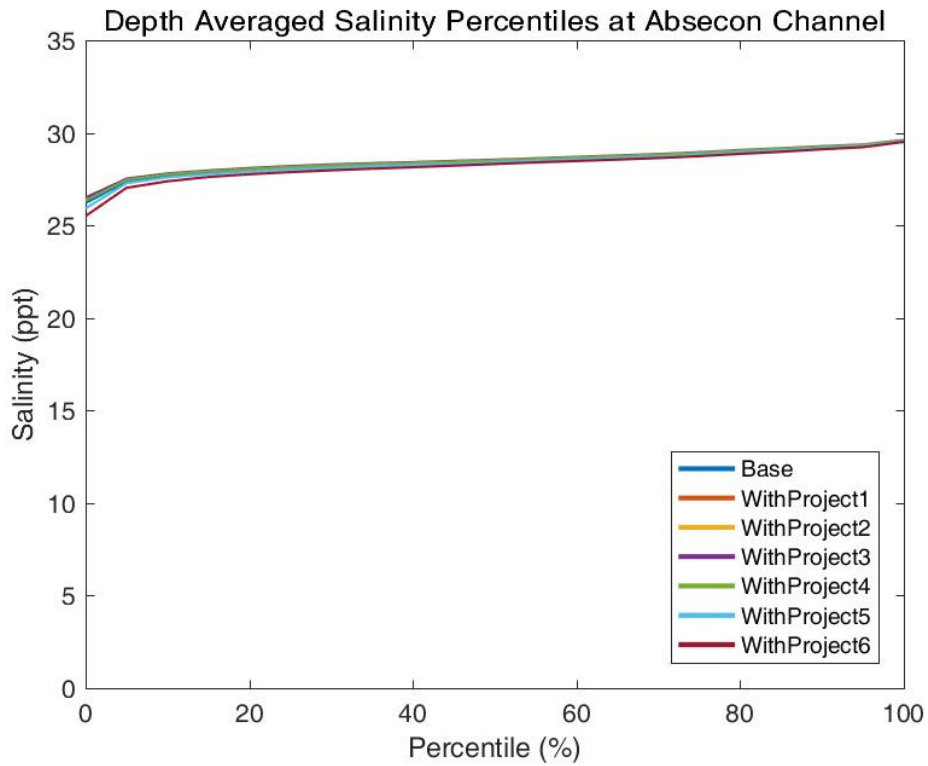
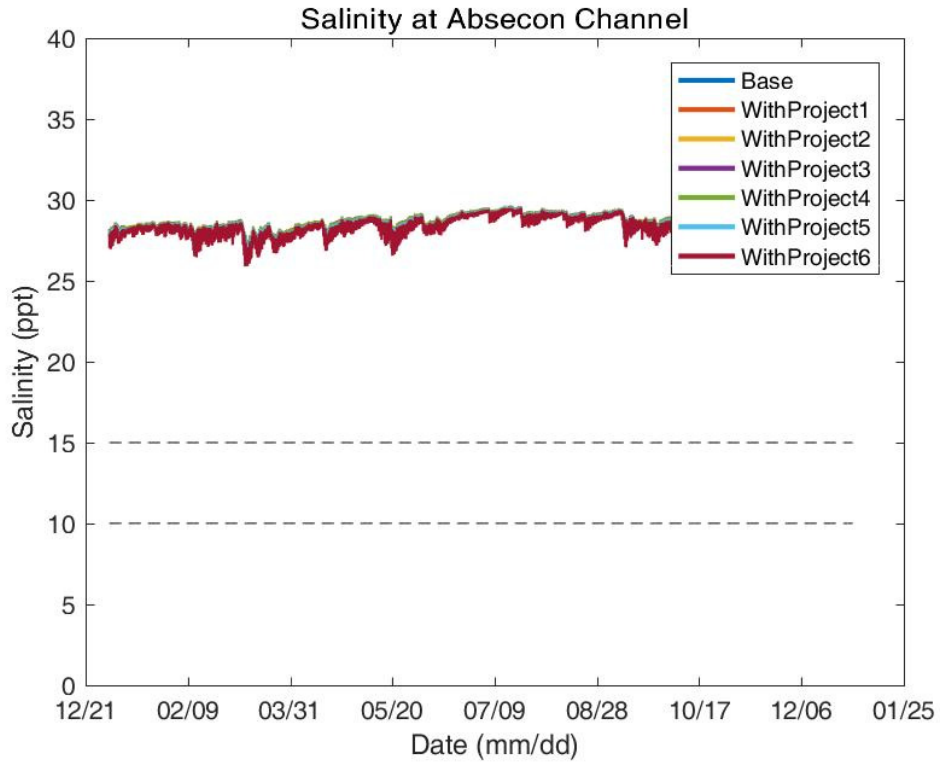


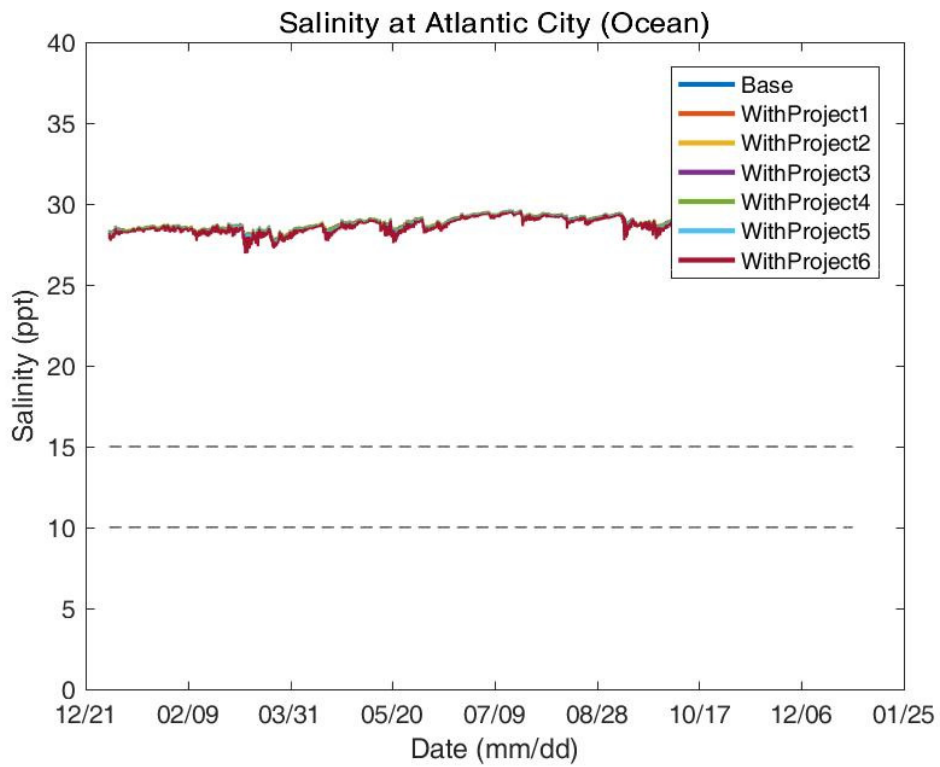
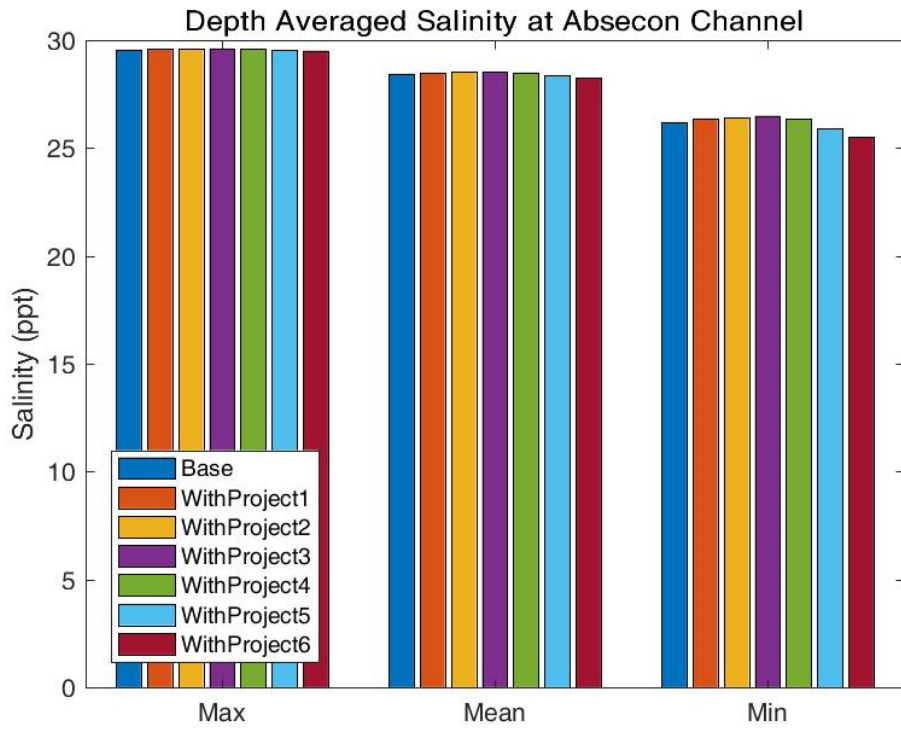


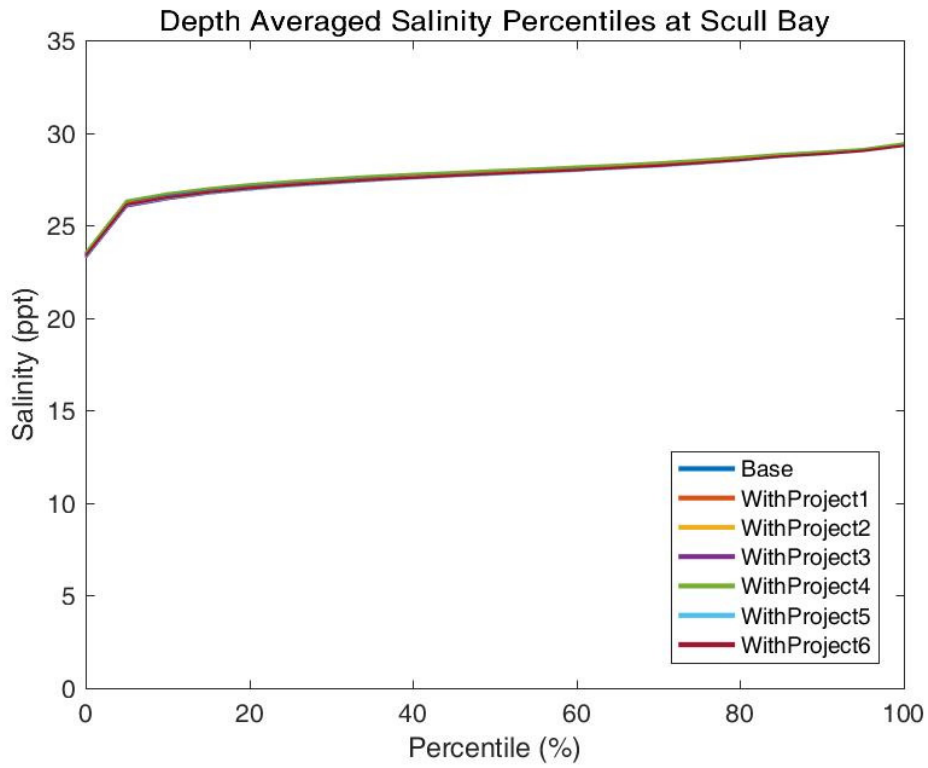
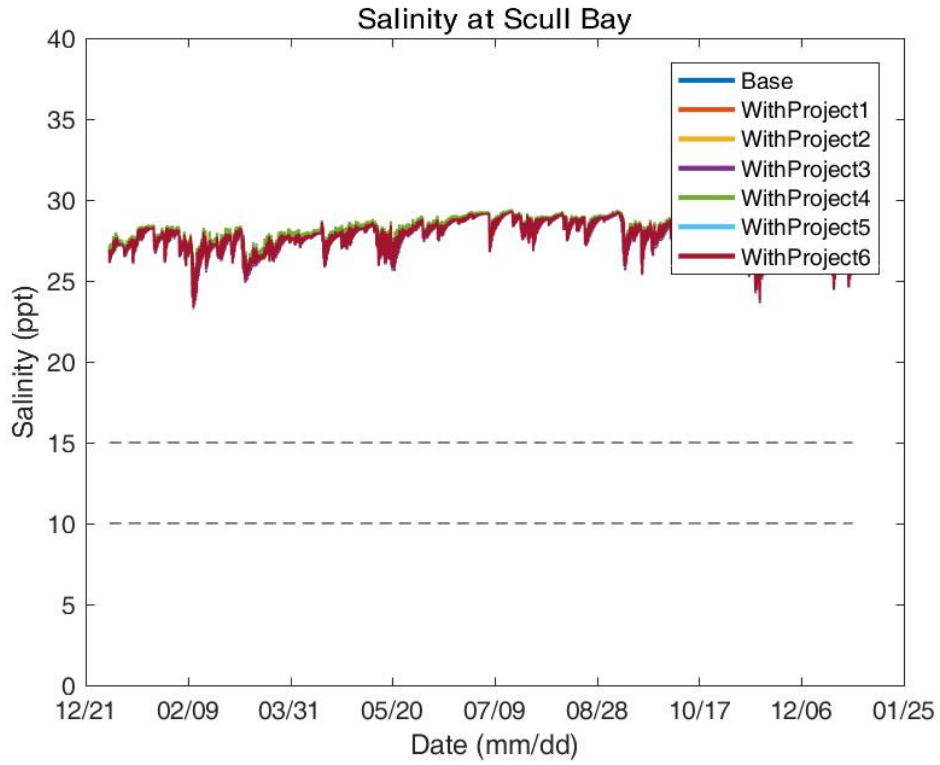


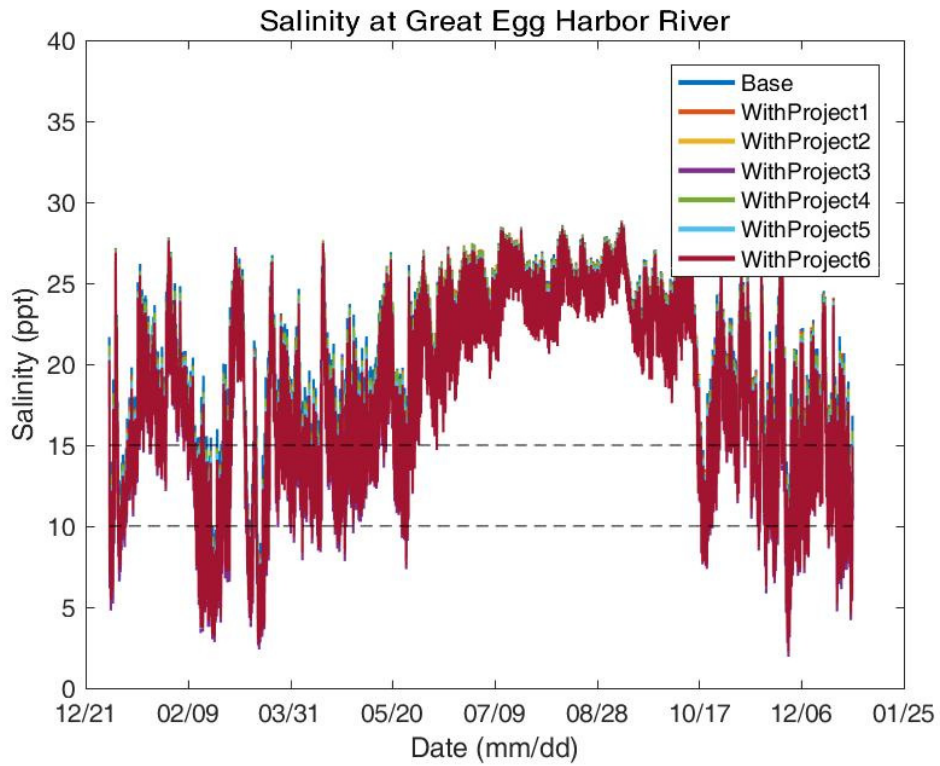
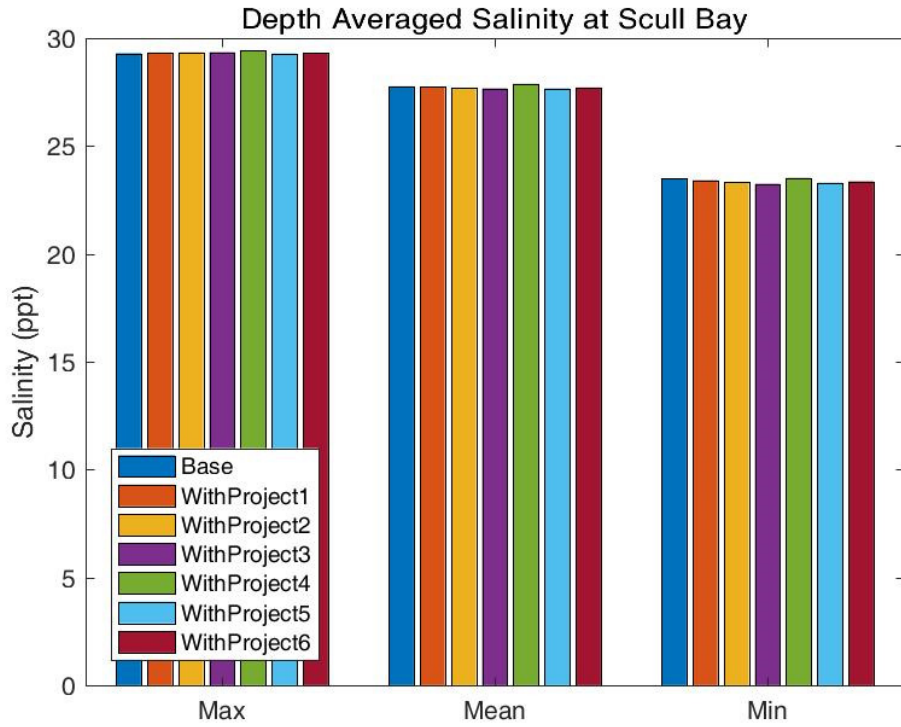


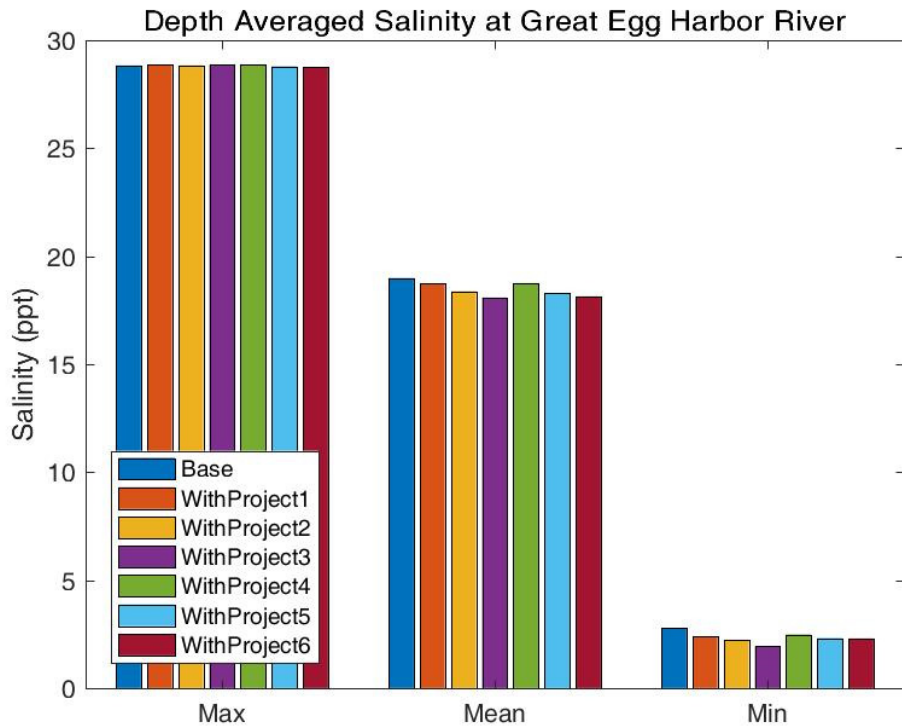
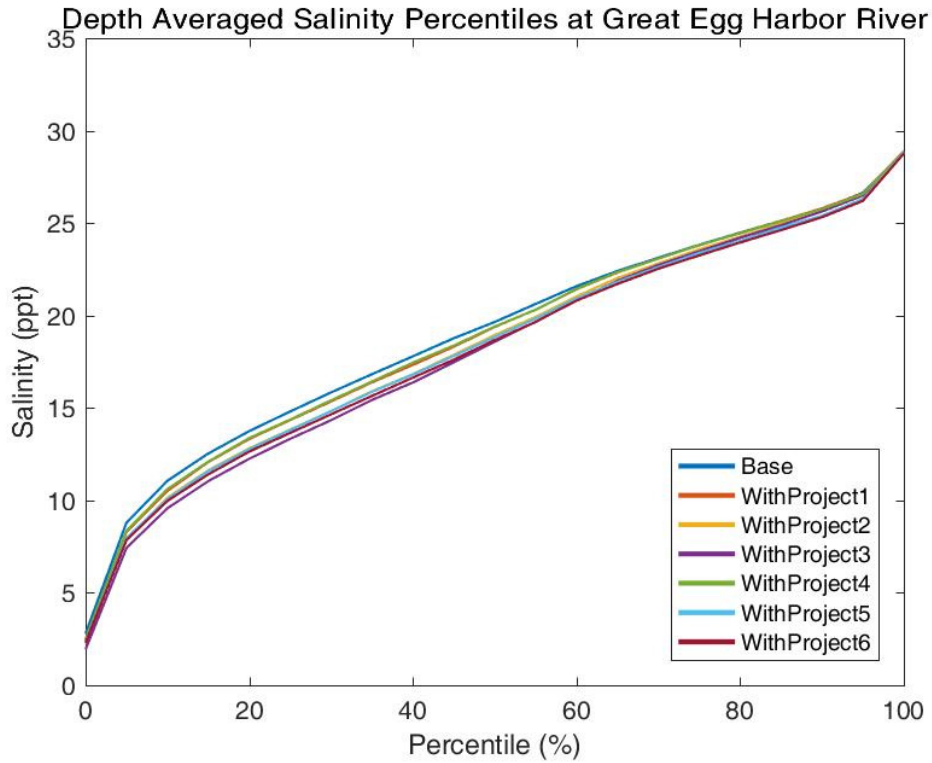


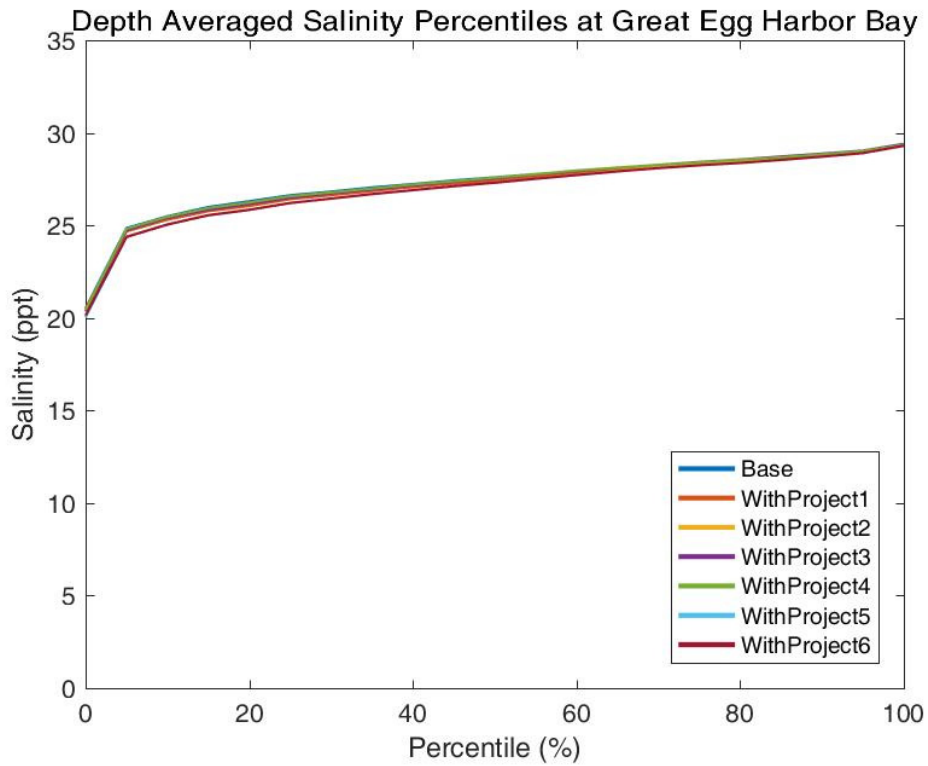
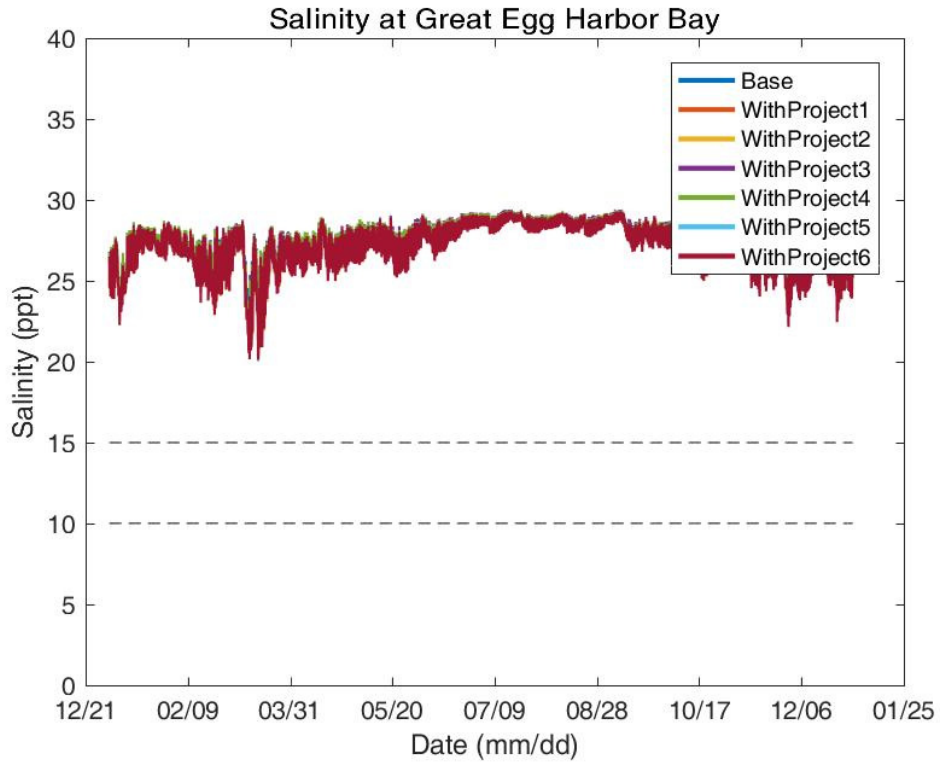


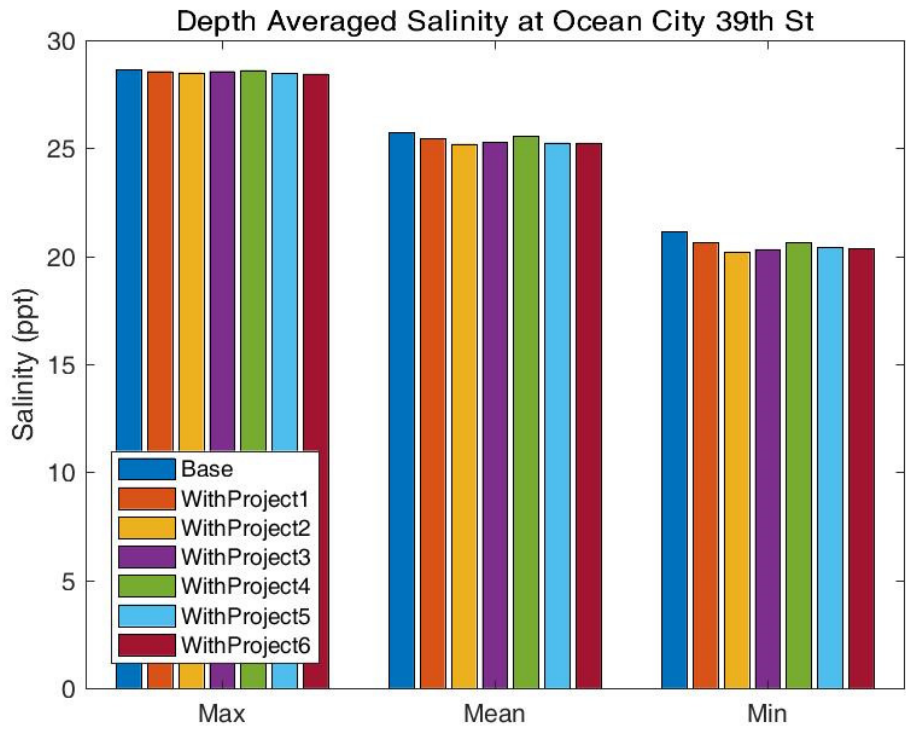
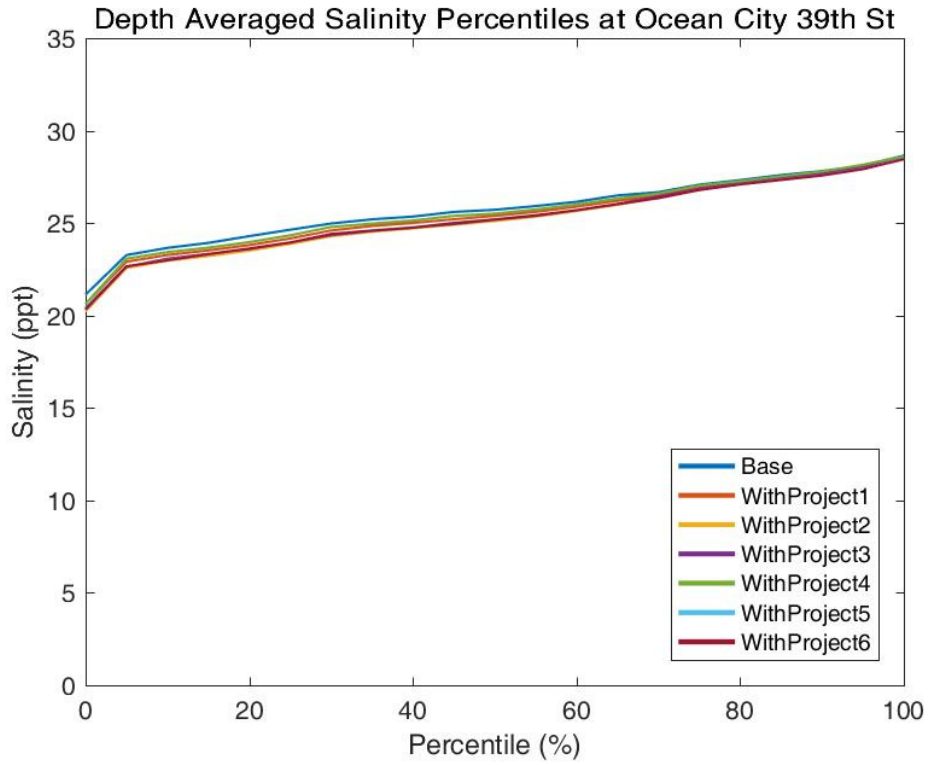


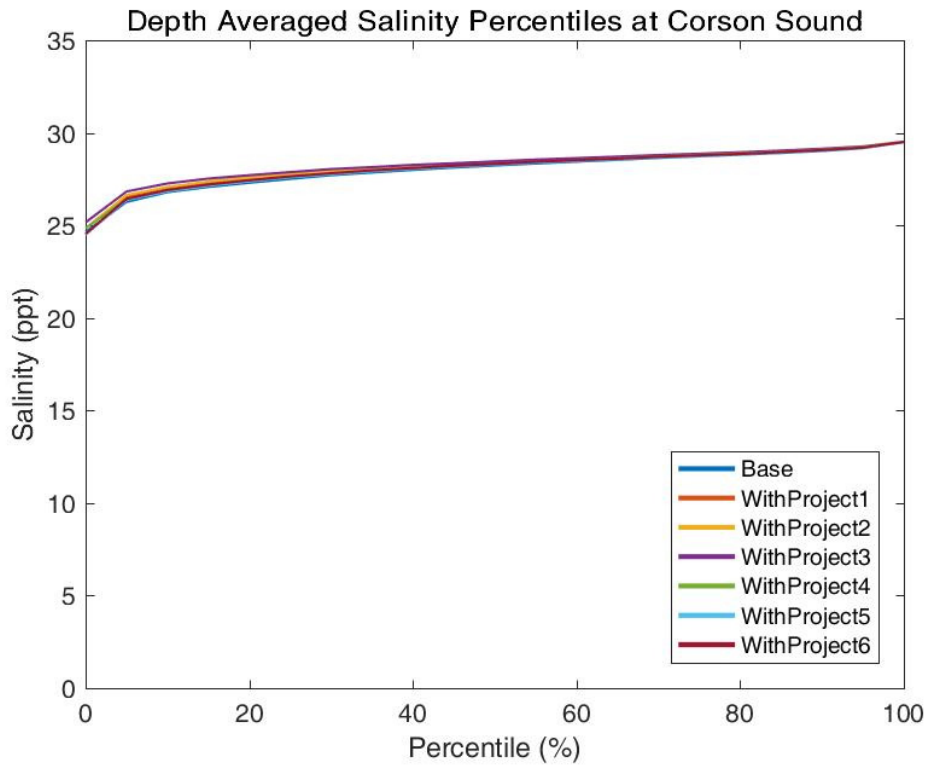
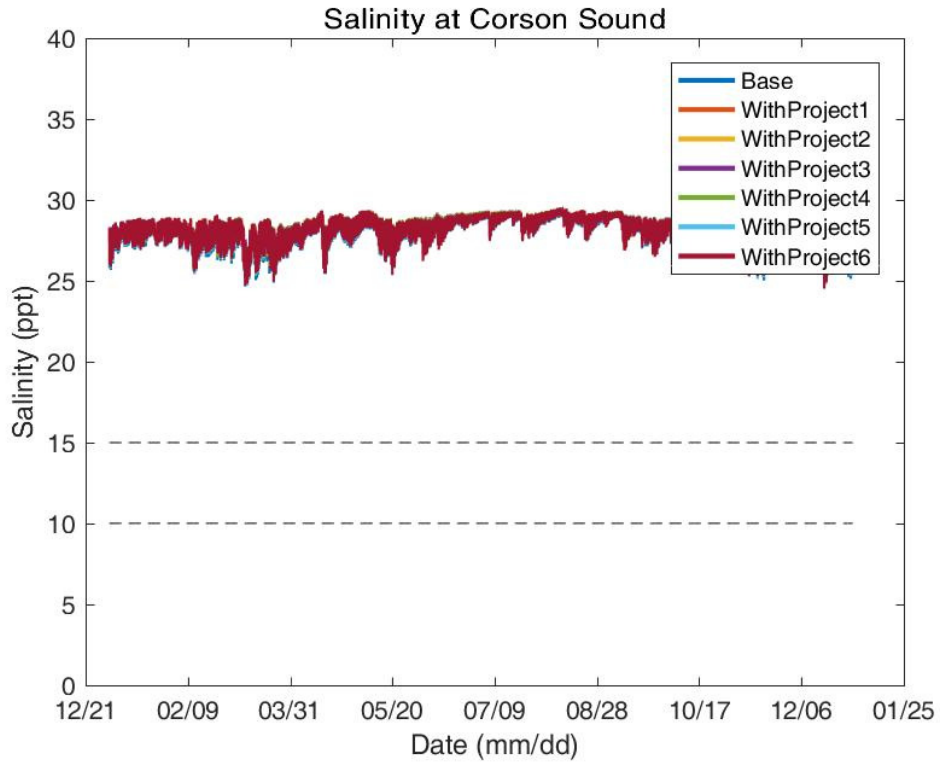


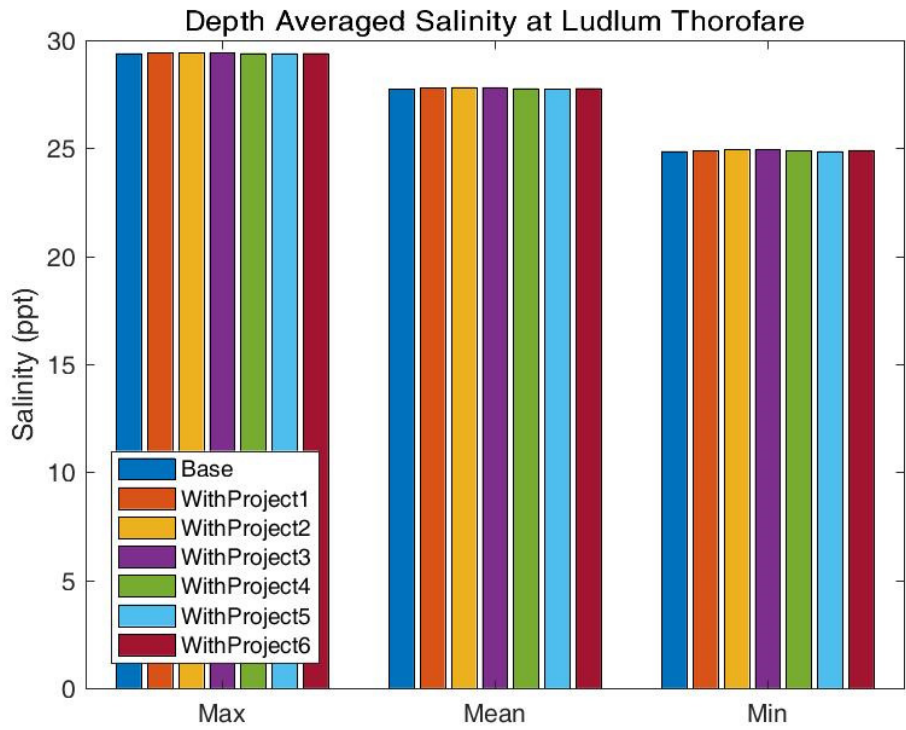
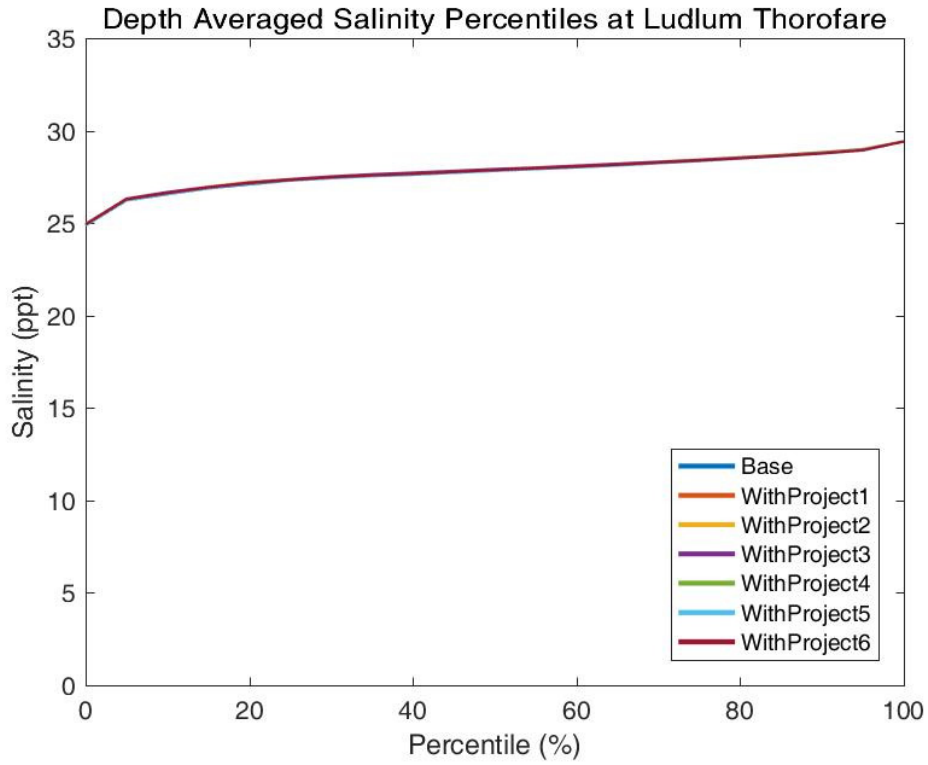


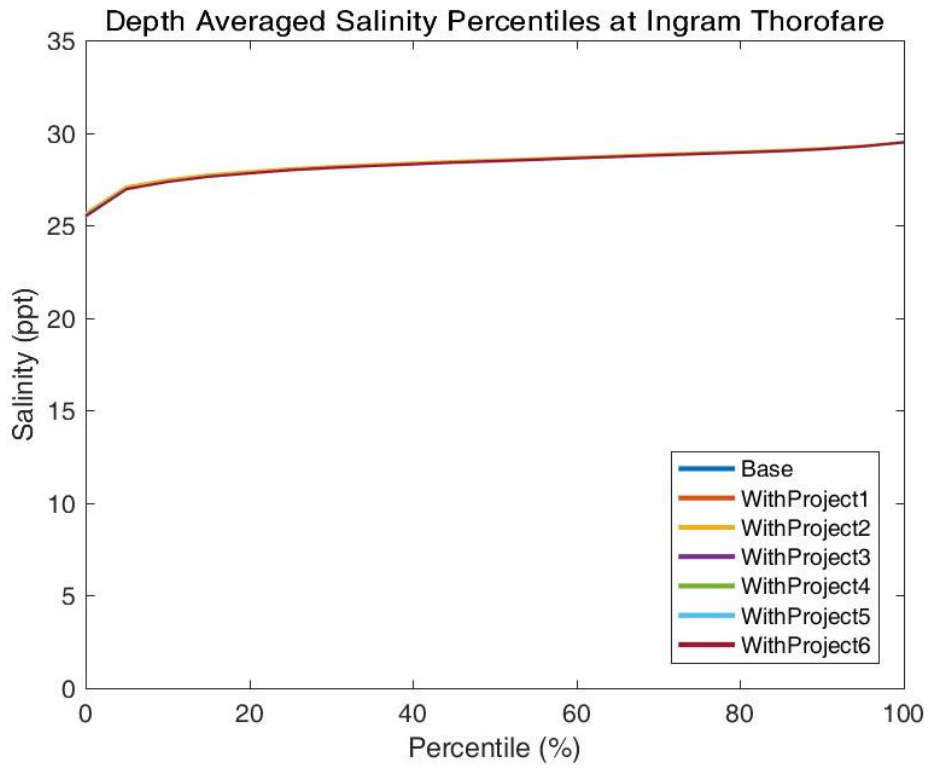
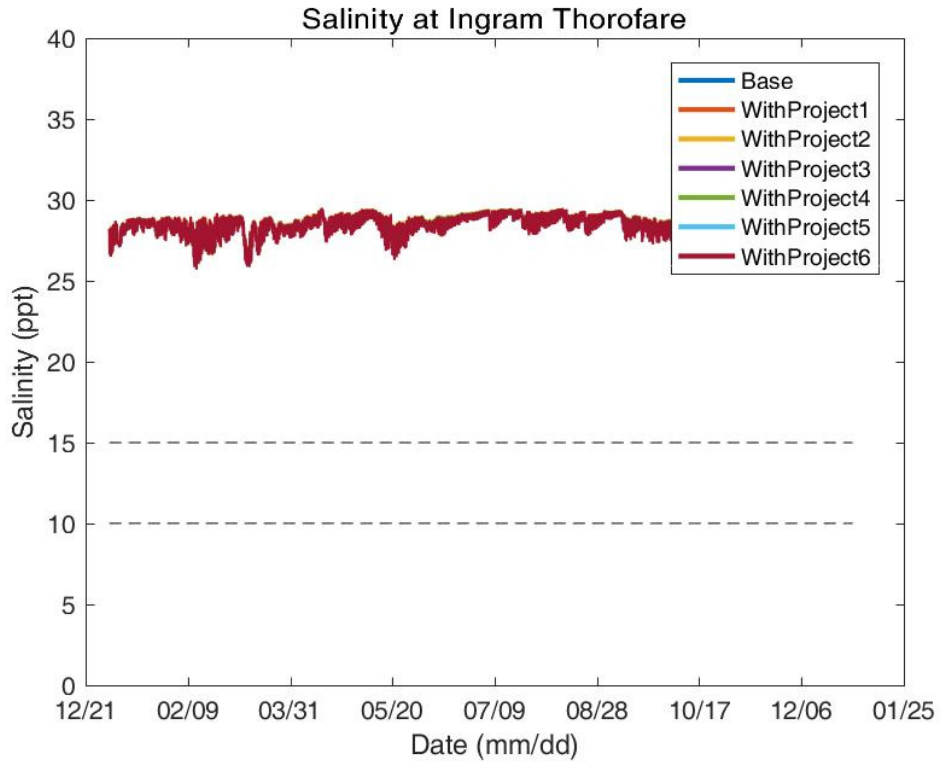


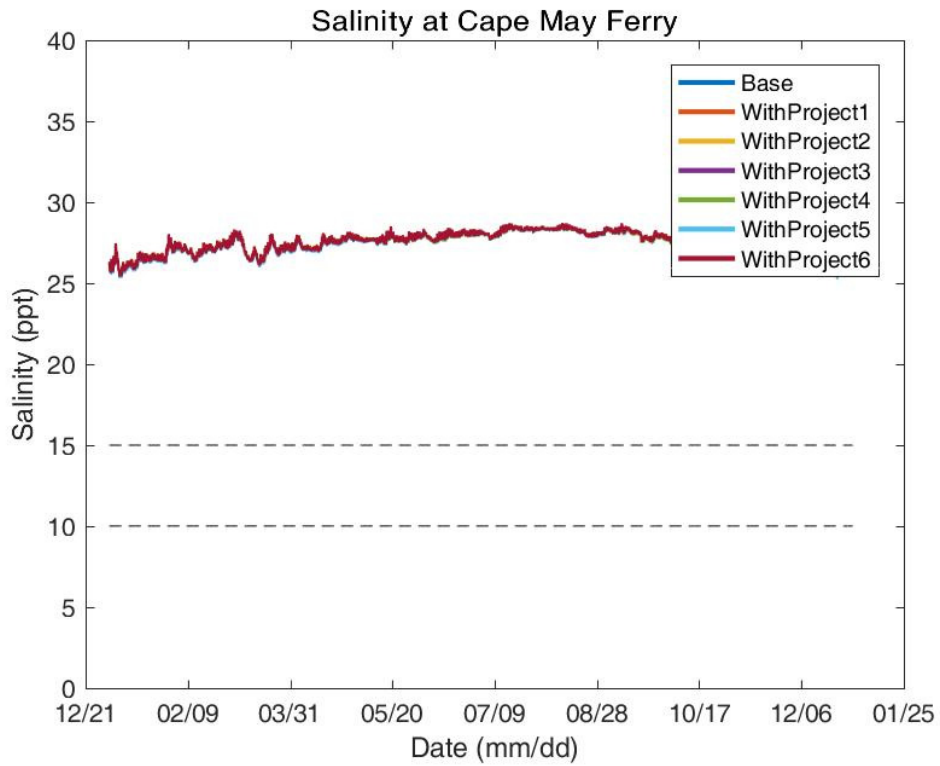
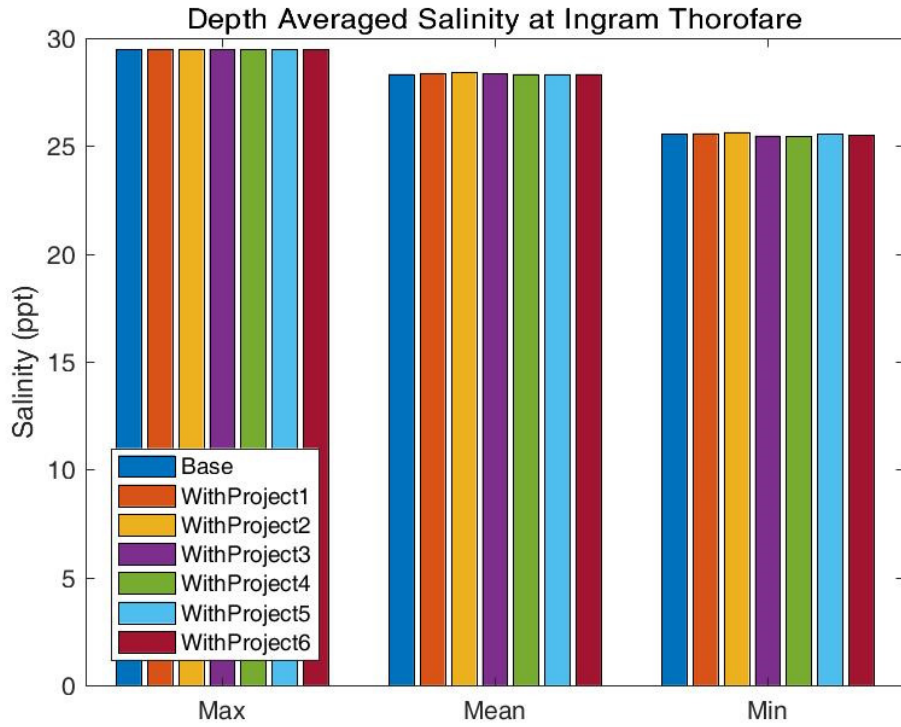


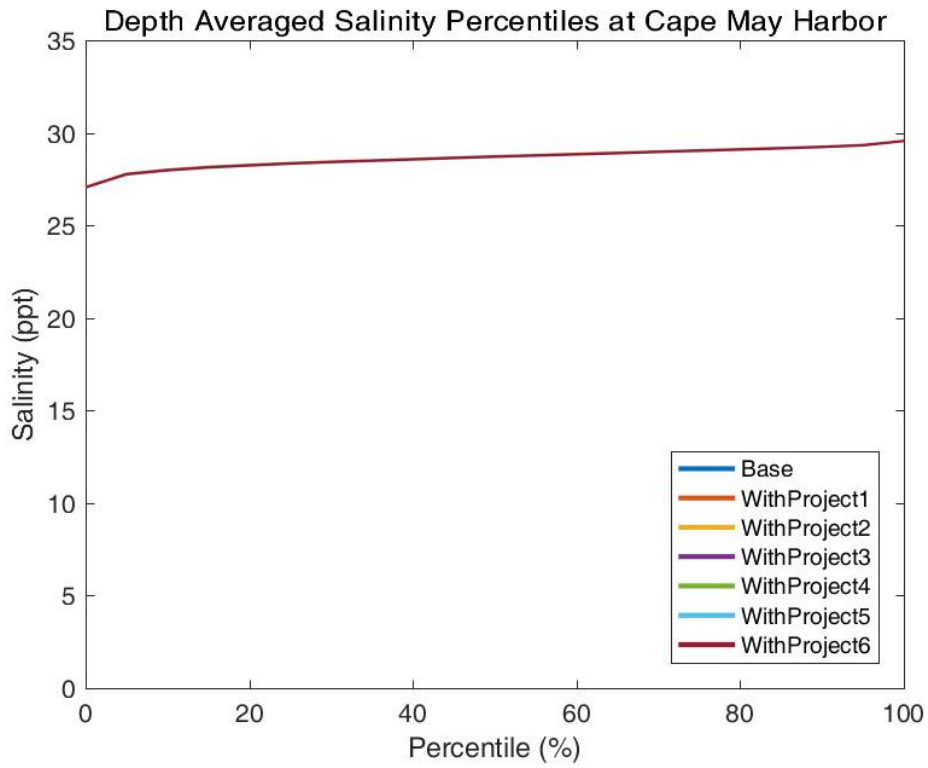
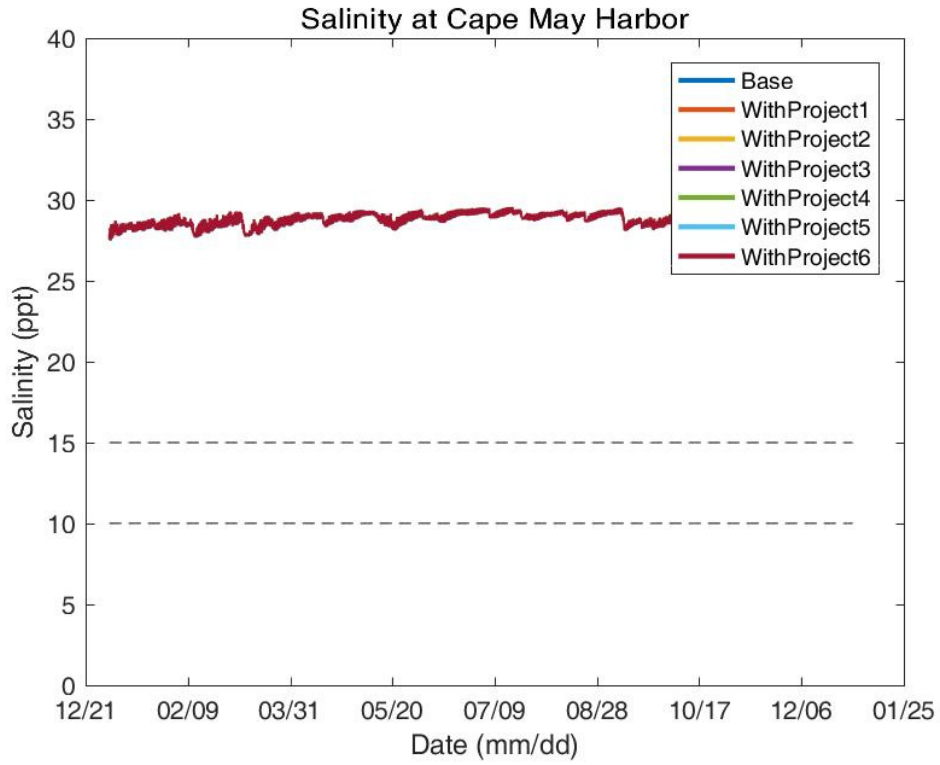












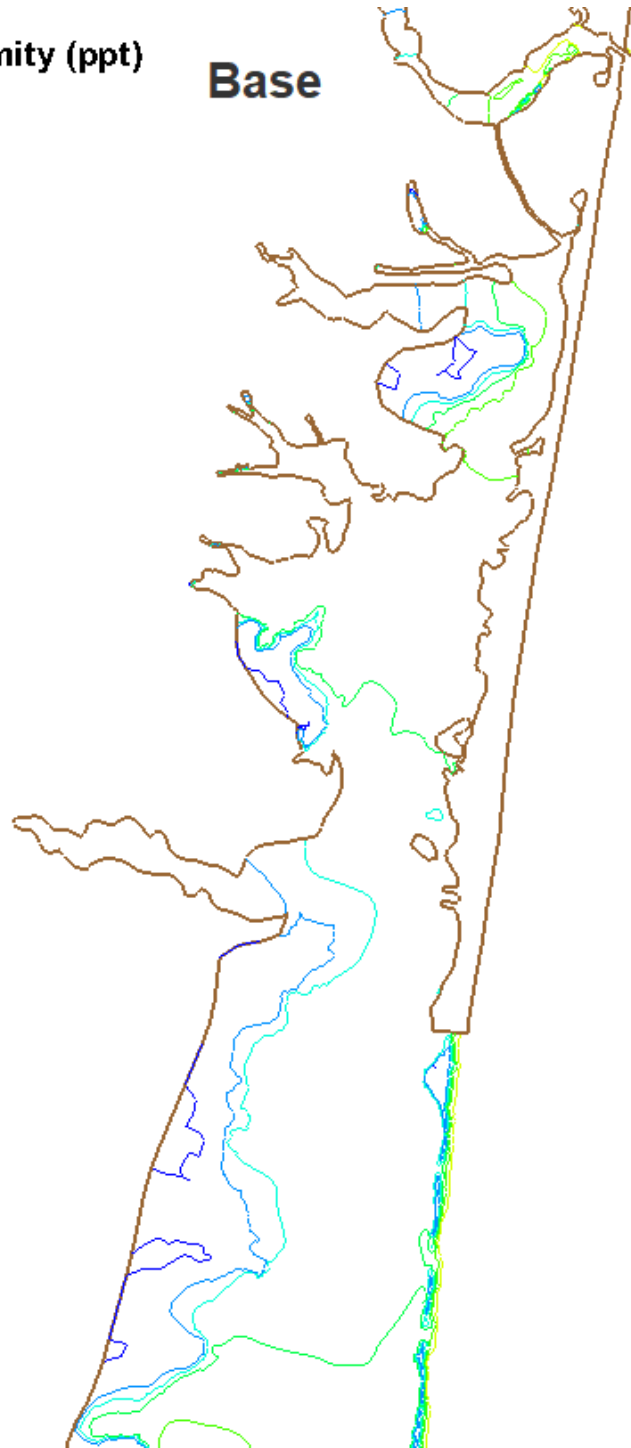
Regional Mean

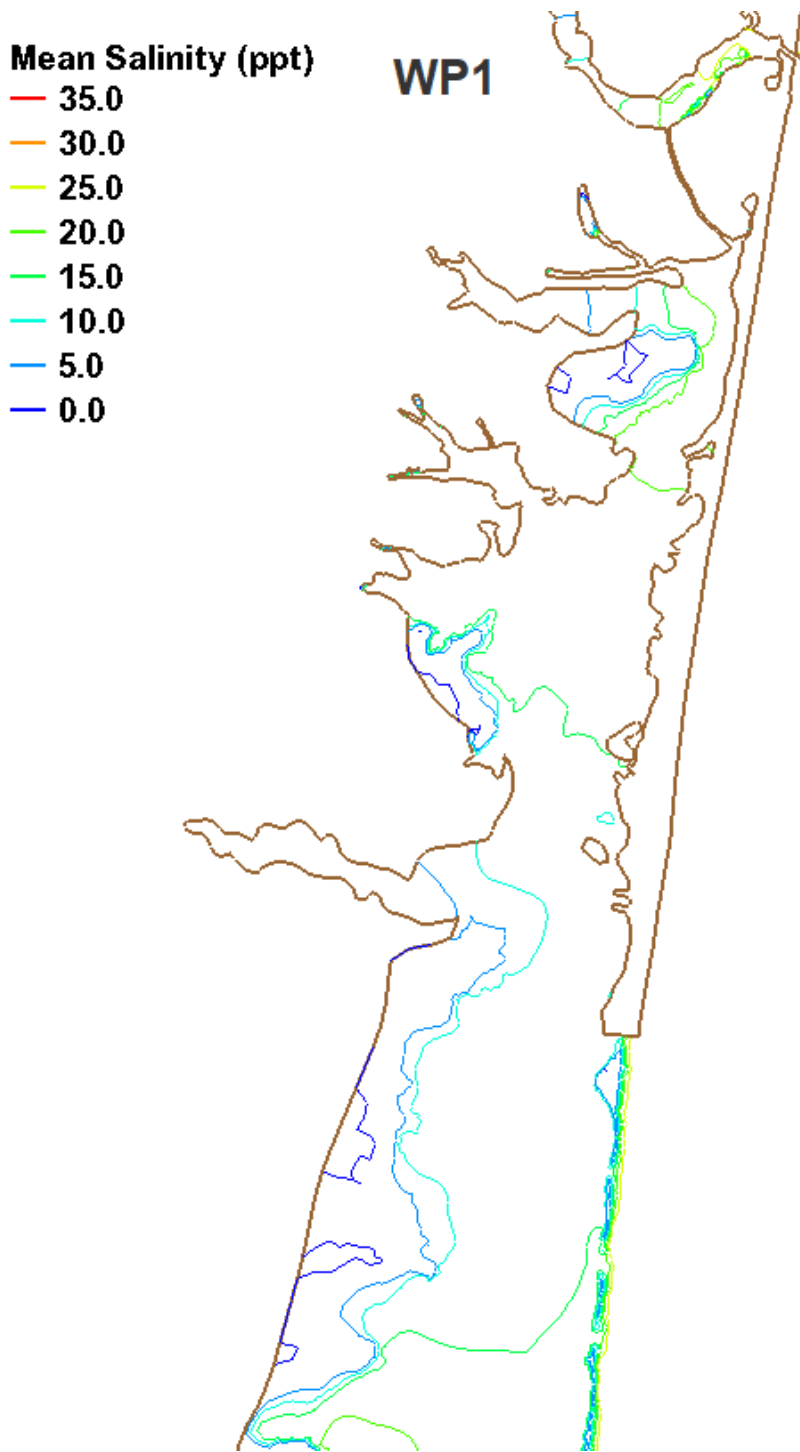
Northern Region (Manasquan and Barnegat)

Mean Salinity (ppt)

- 35.0
- 30.0
- 25.0
- 20.0
- 15.0
- 10.0
- 5.0
- 0.0

Base

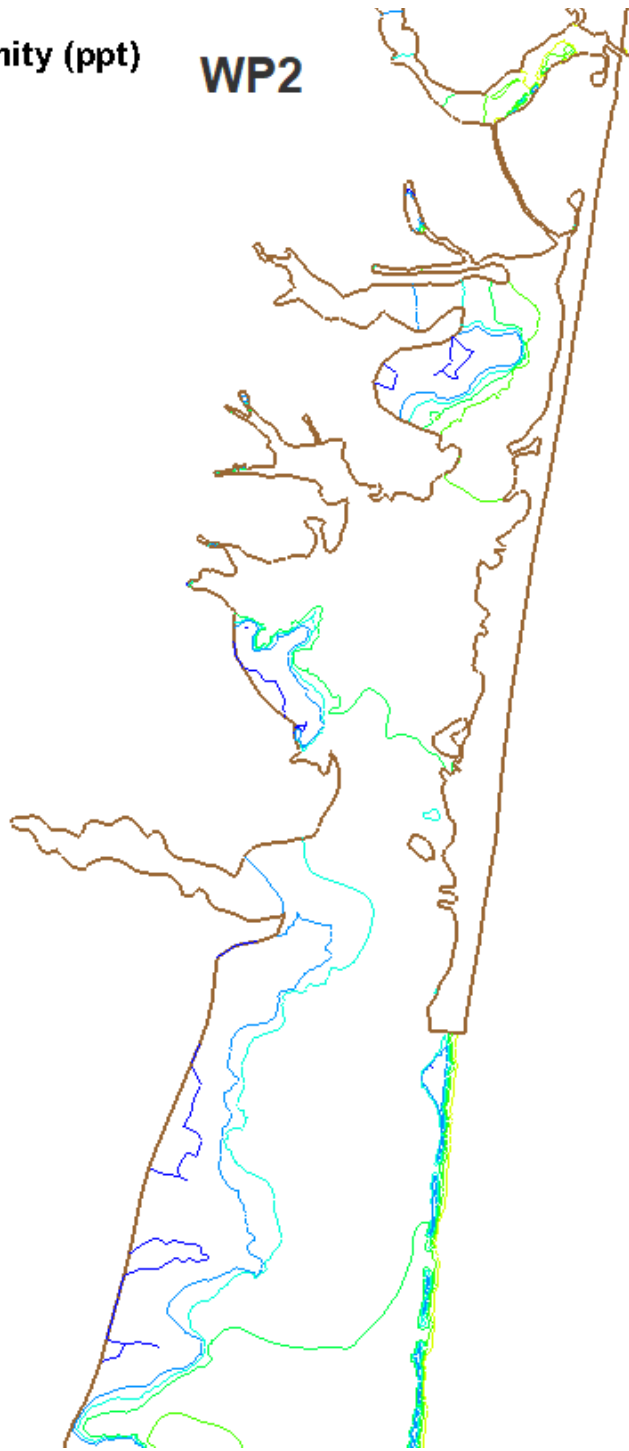




Mean Salinity (ppt)

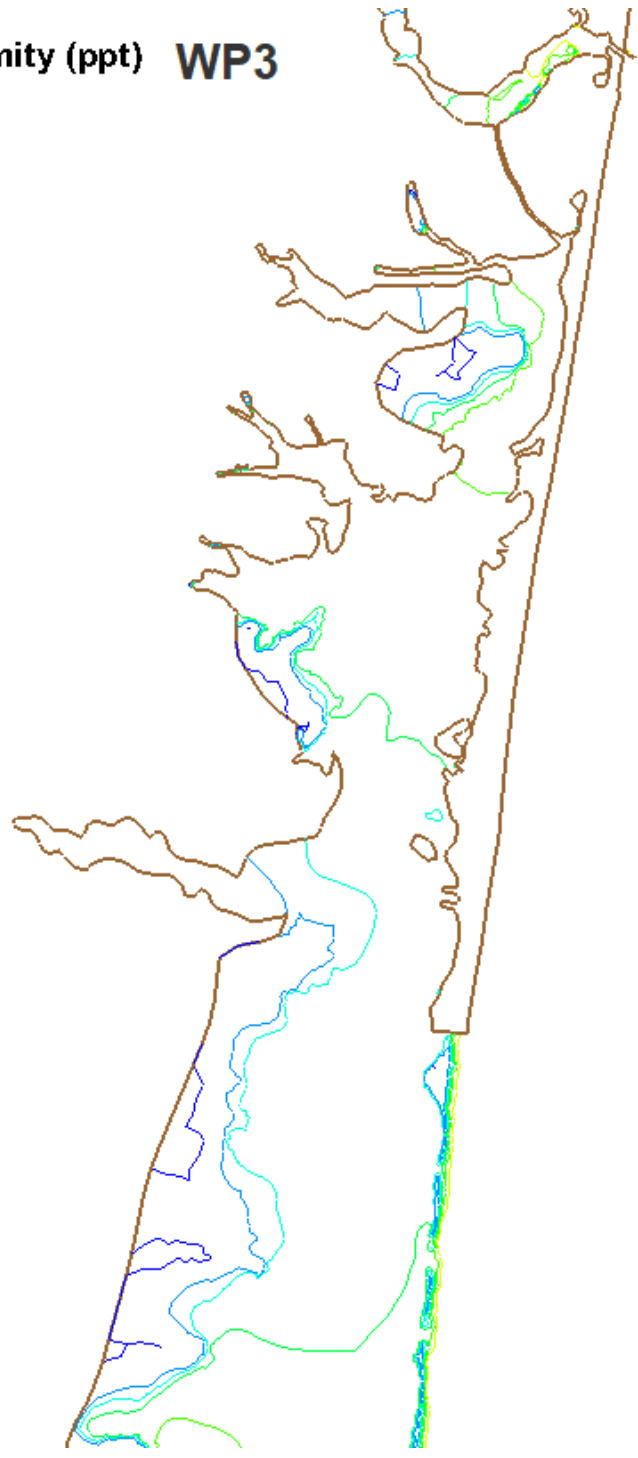
- 35.0
- 30.0
- 25.0
- 20.0
- 15.0
- 10.0
- 5.0
- 0.0

WP2



Mean Salinity (ppt) WP3

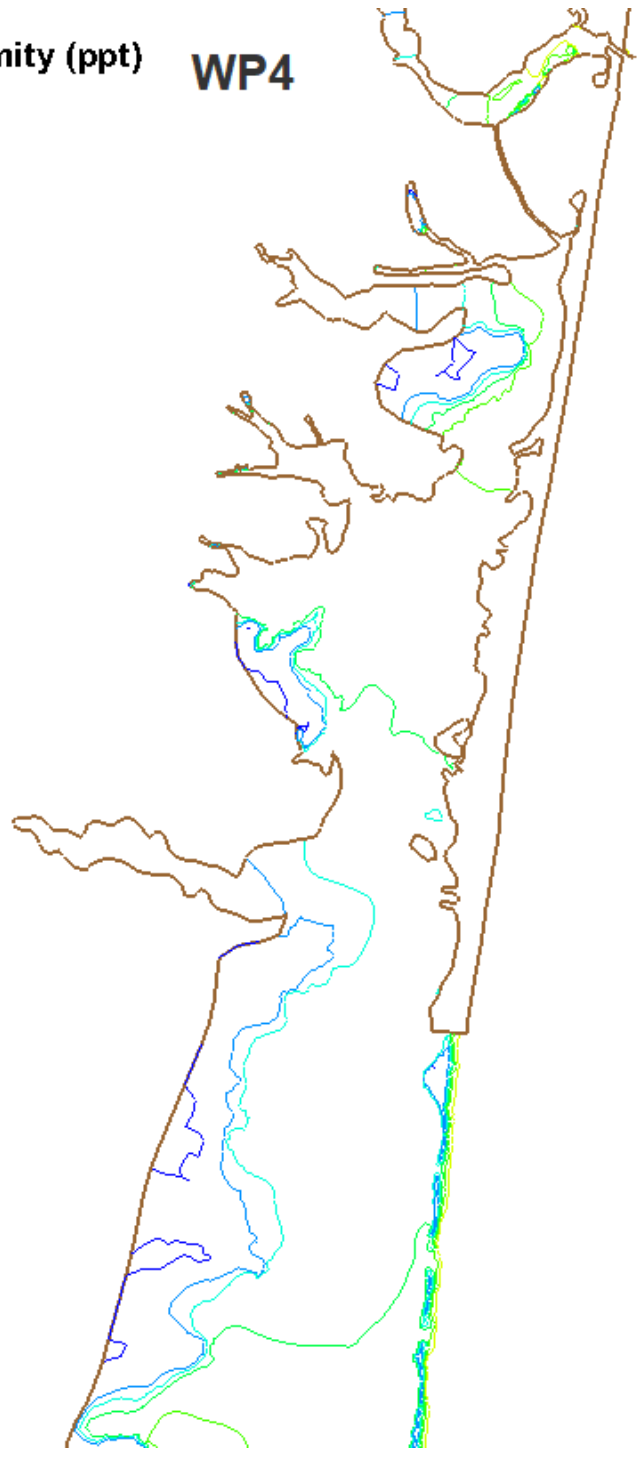
- 35.0
- 30.0
- 25.0
- 20.0
- 15.0
- 10.0
- 5.0
- 0.0

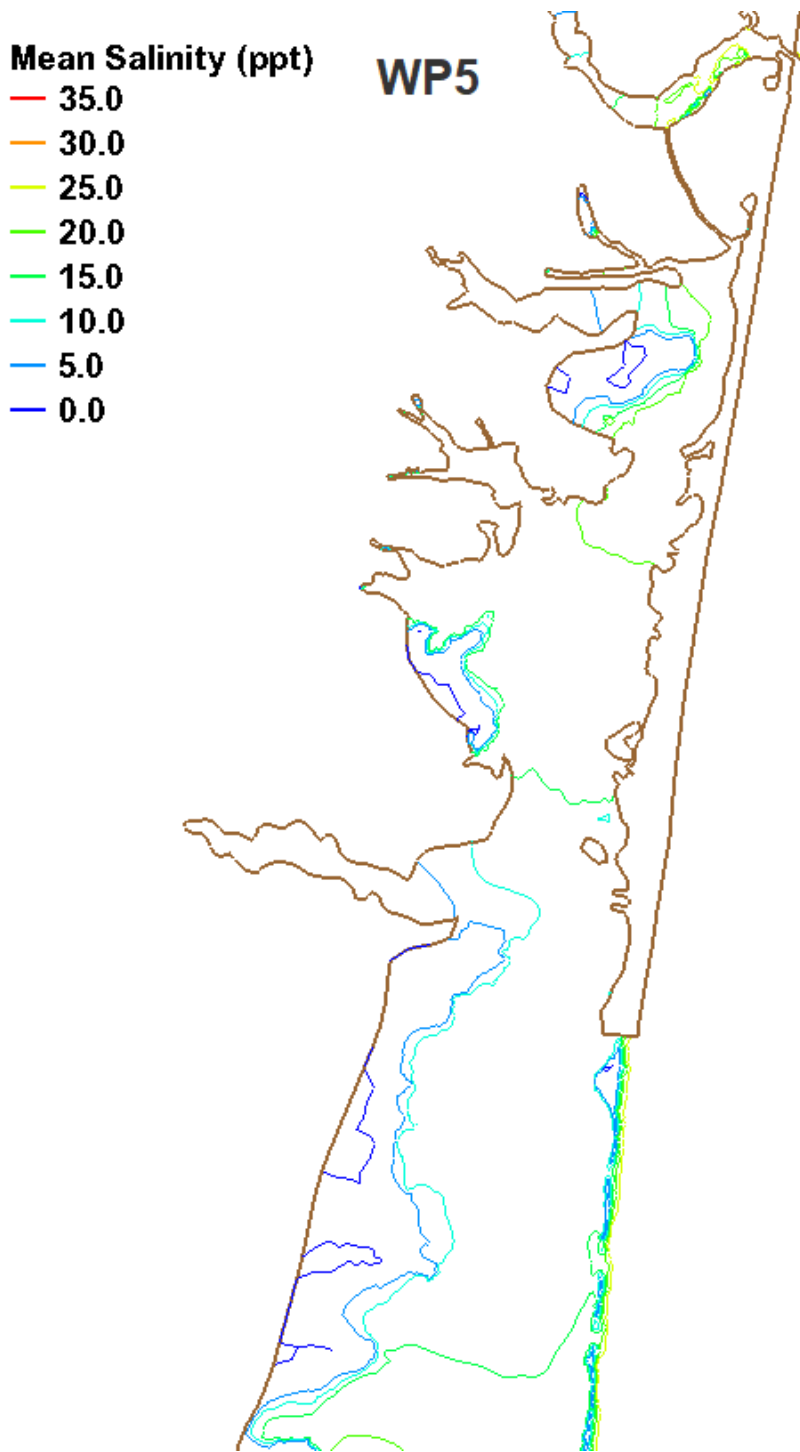


Mean Salinity (ppt)

- 35.0
- 30.0
- 25.0
- 20.0
- 15.0
- 10.0
- 5.0
- 0.0

WP4

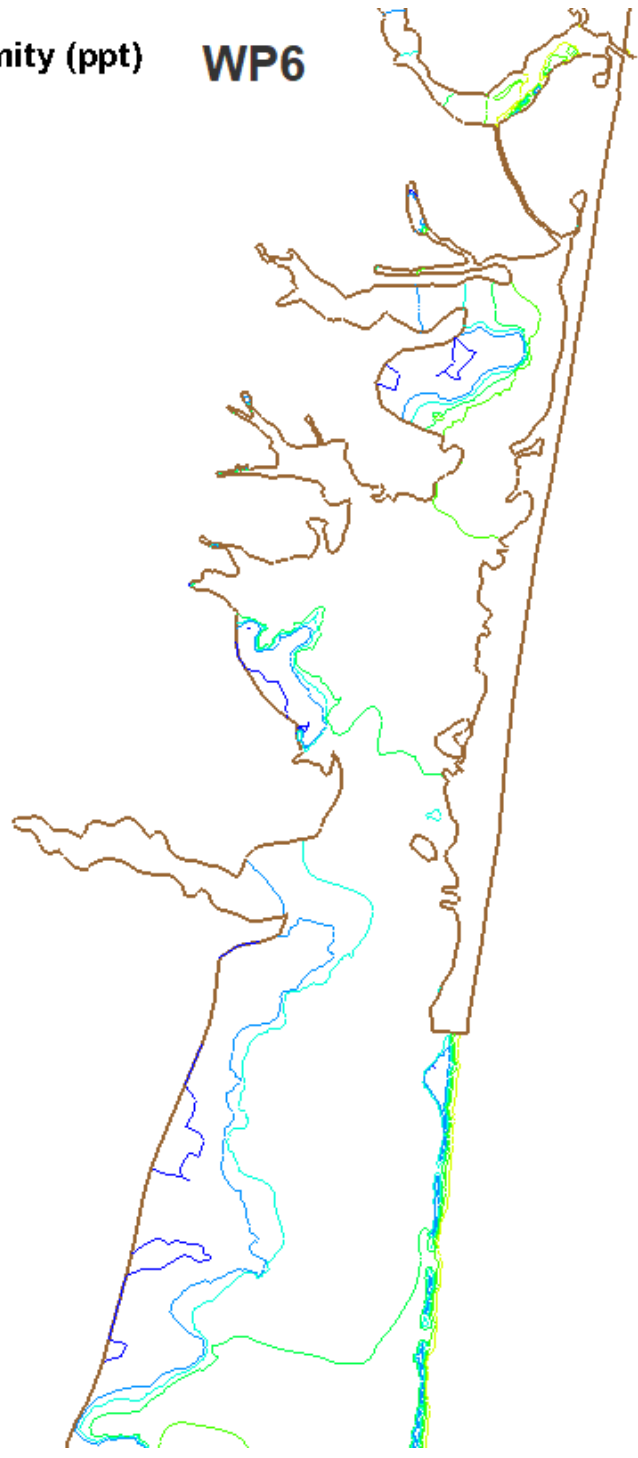


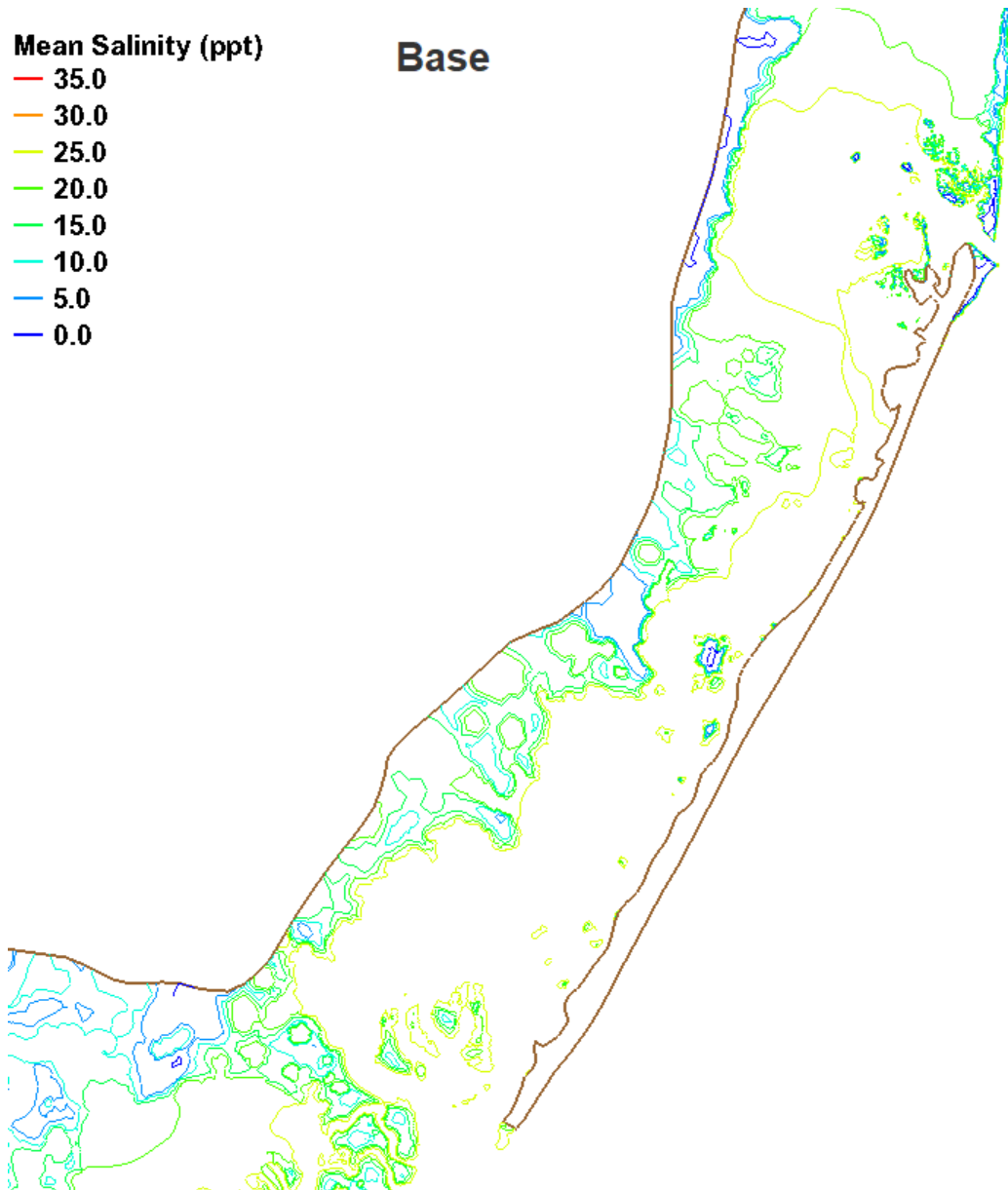


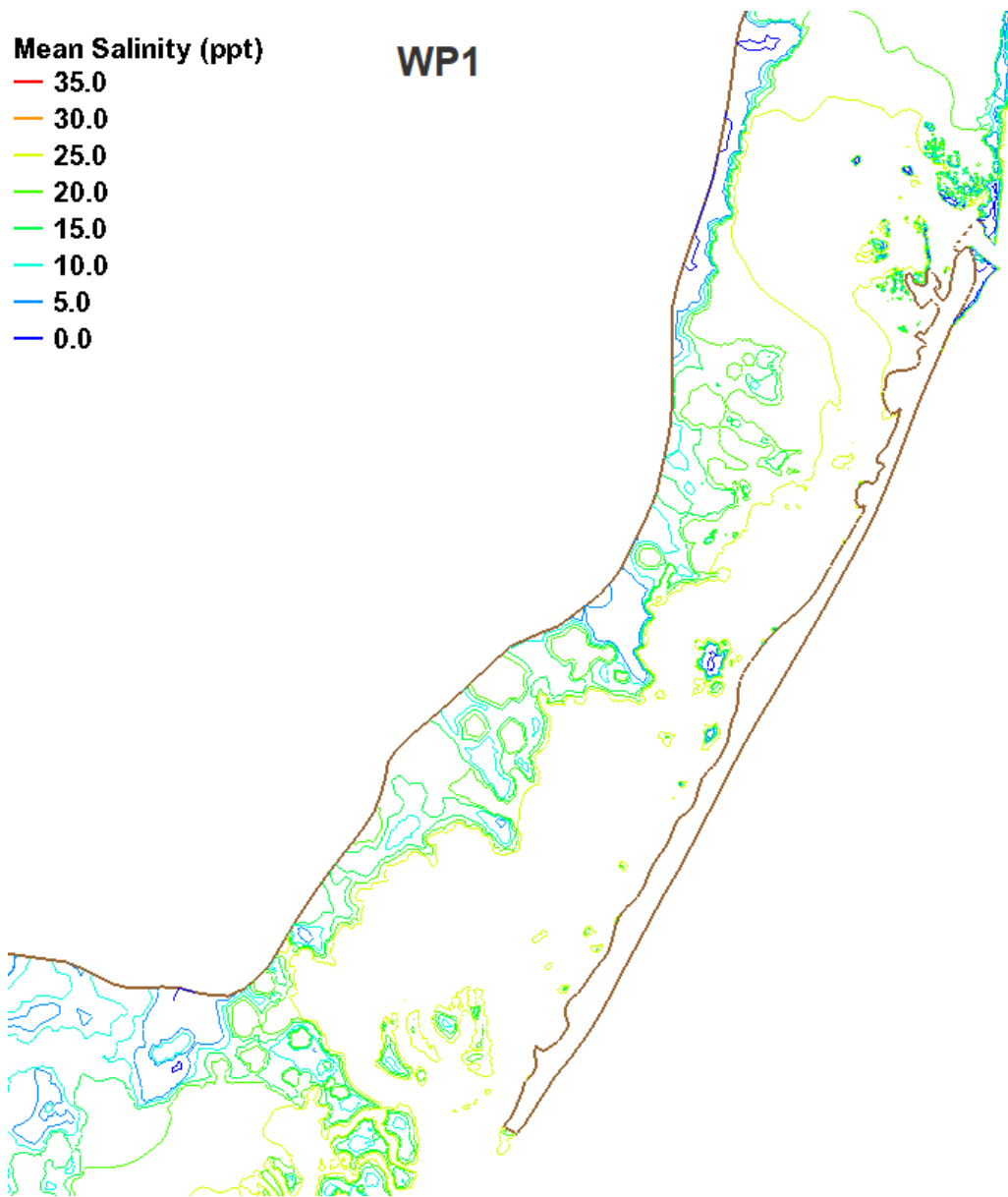
Mean Salinity (ppt)

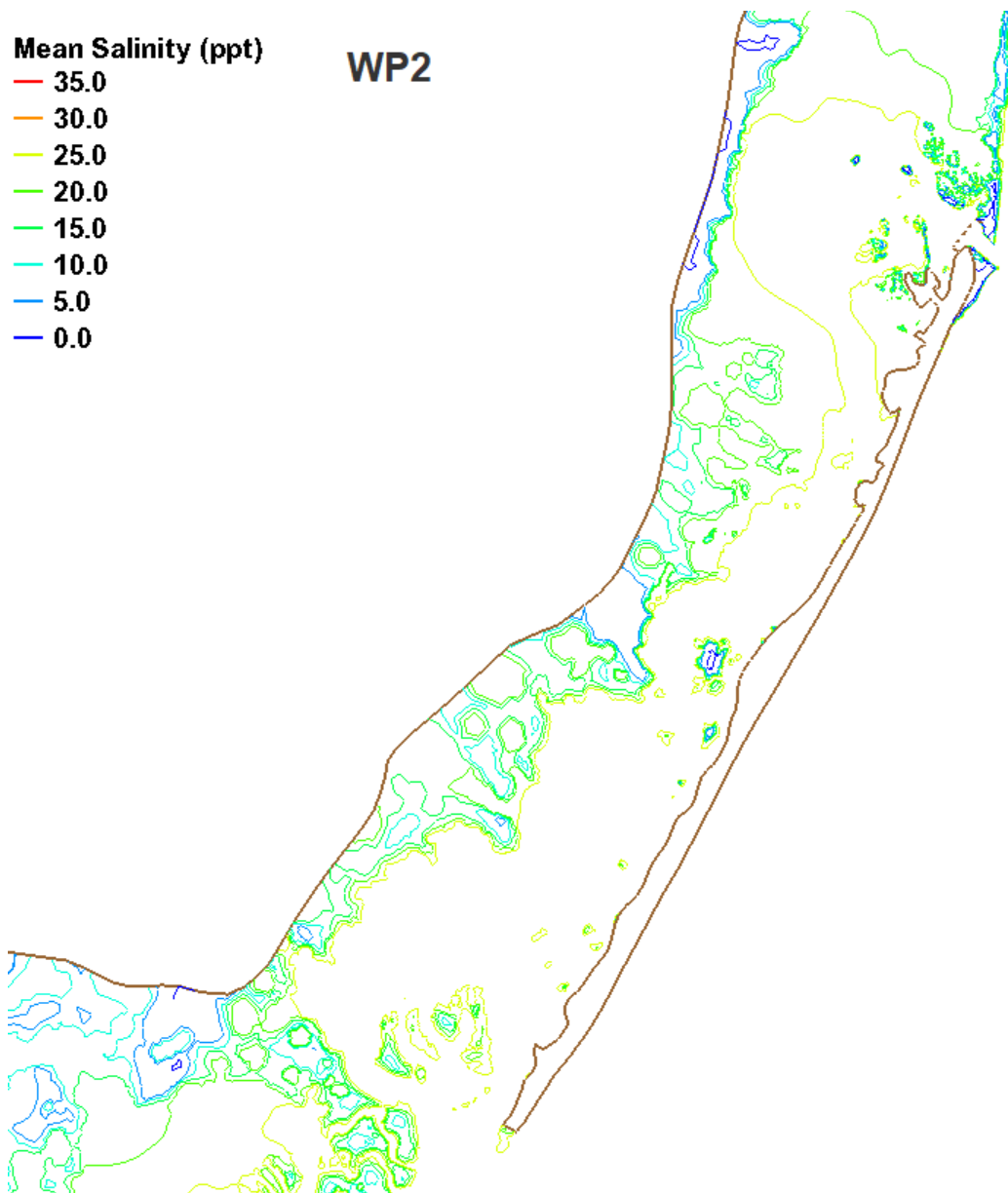
- 35.0
- 30.0
- 25.0
- 20.0
- 15.0
- 10.0
- 5.0
- 0.0

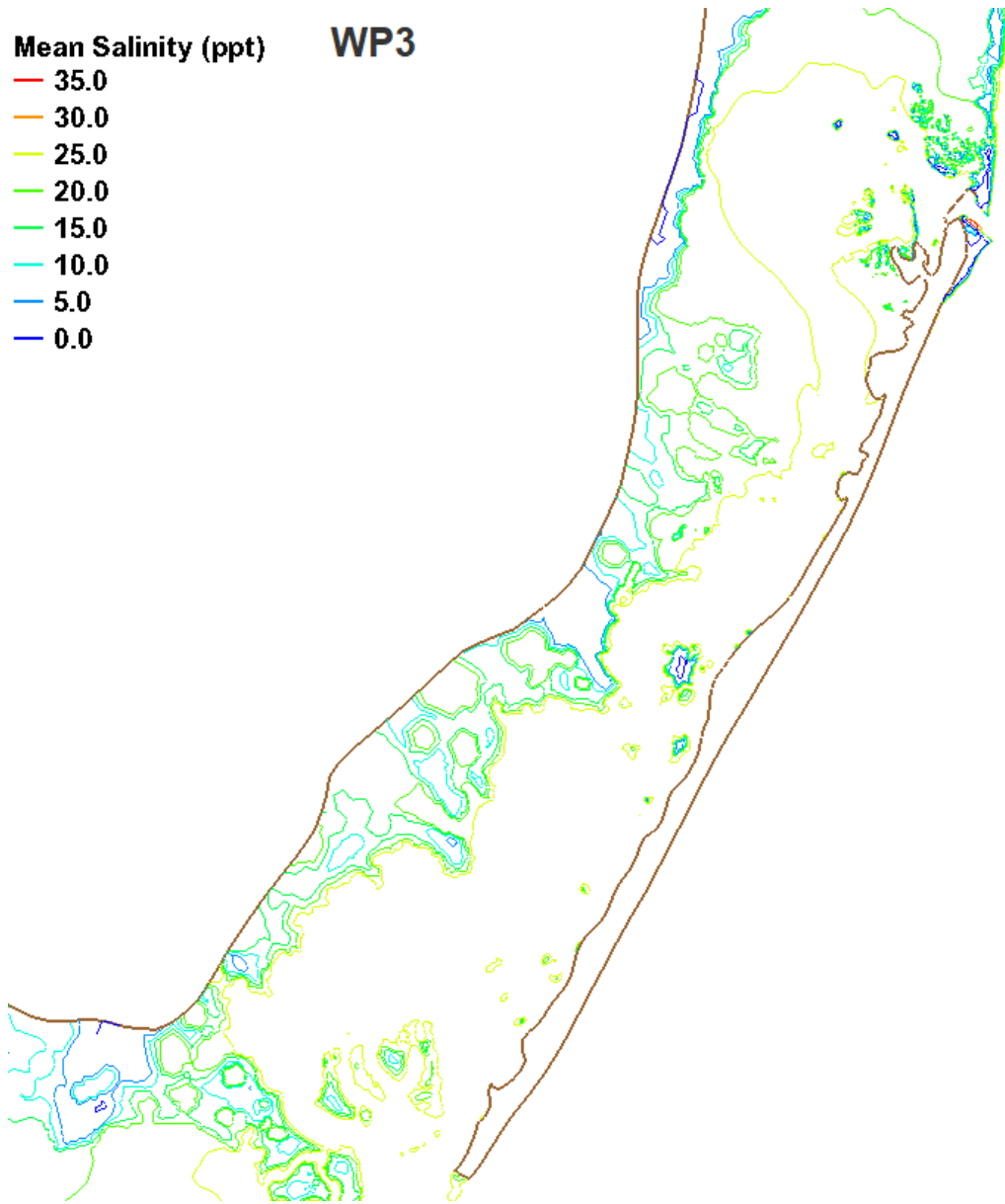
WP6

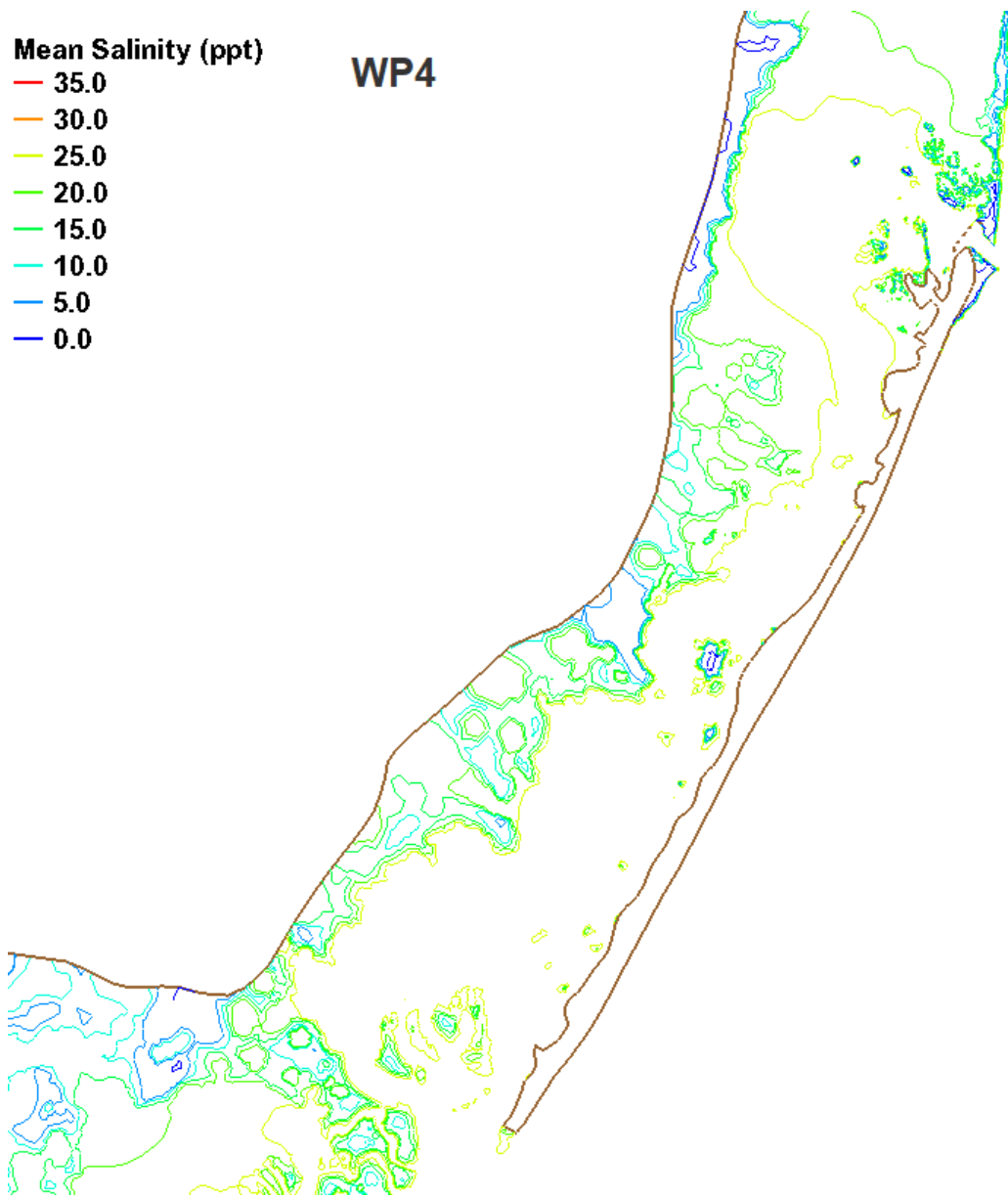


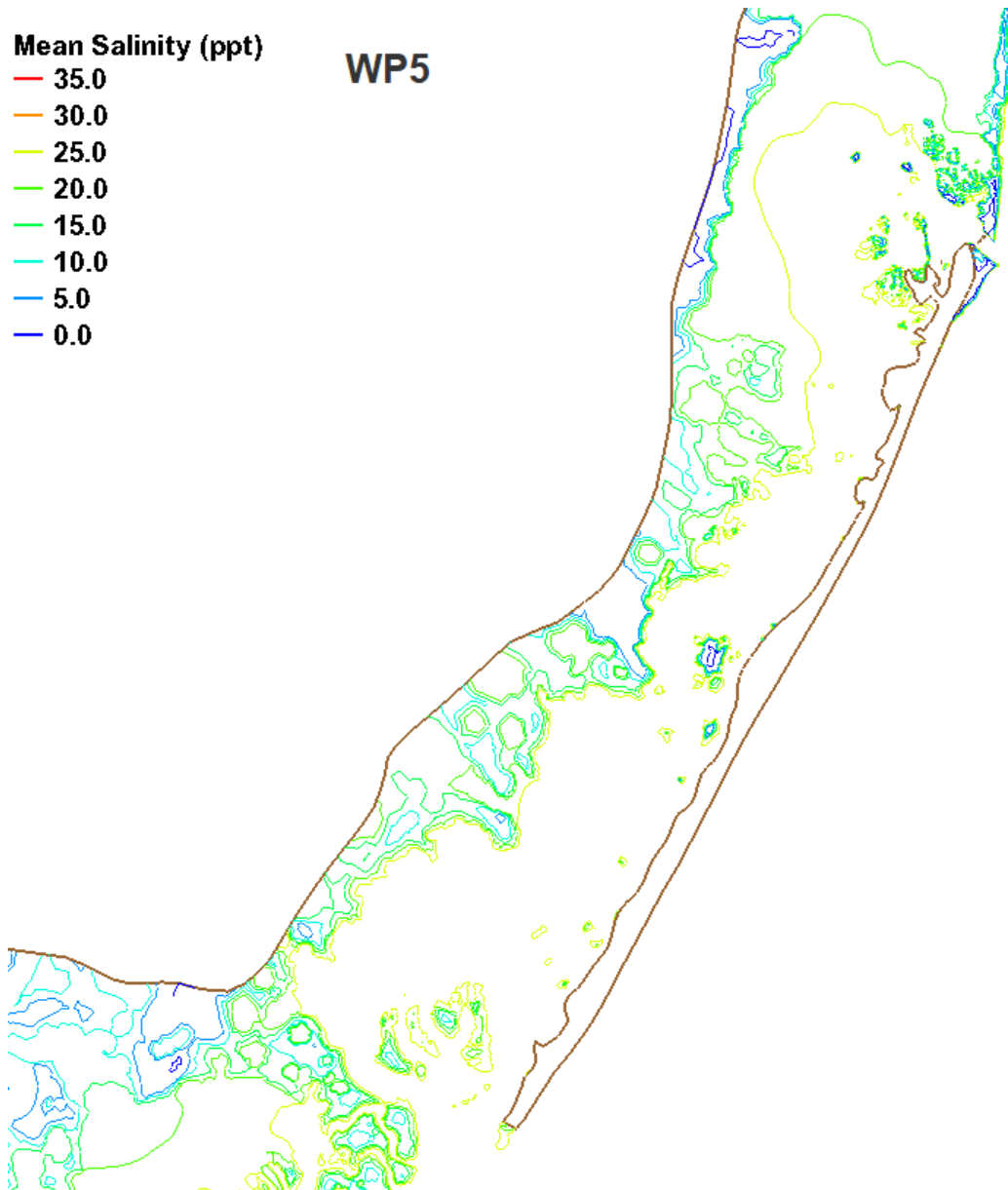


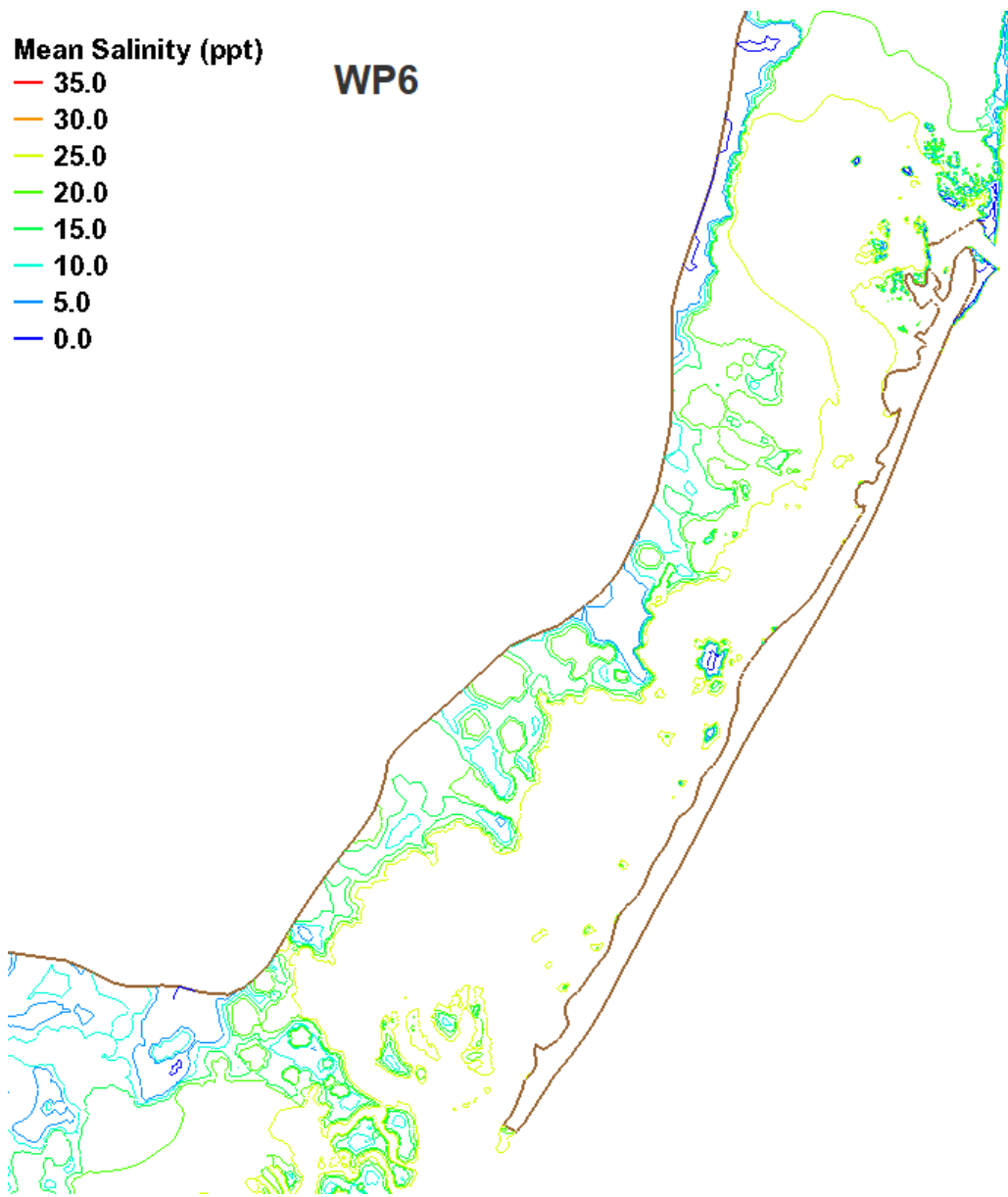




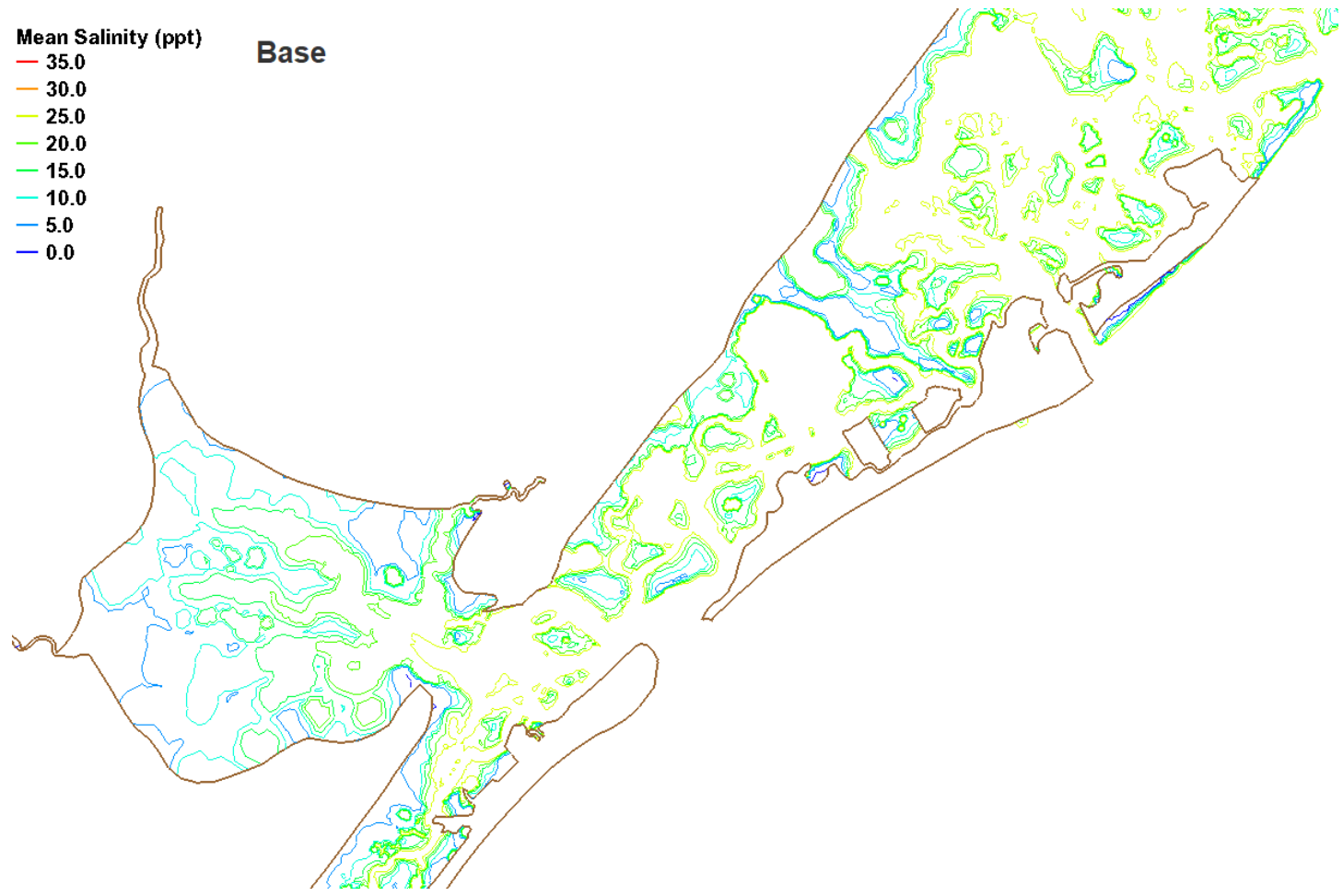


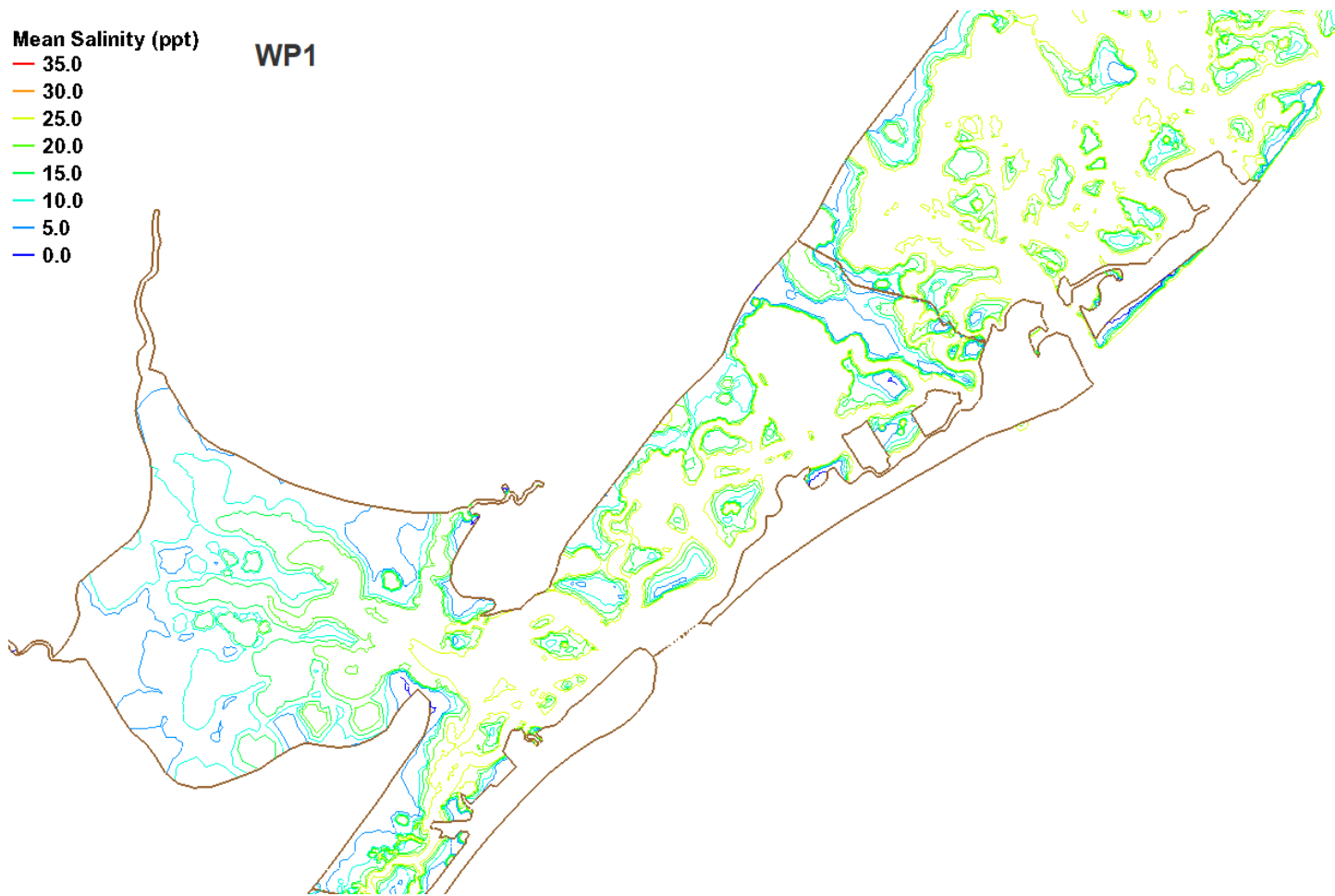


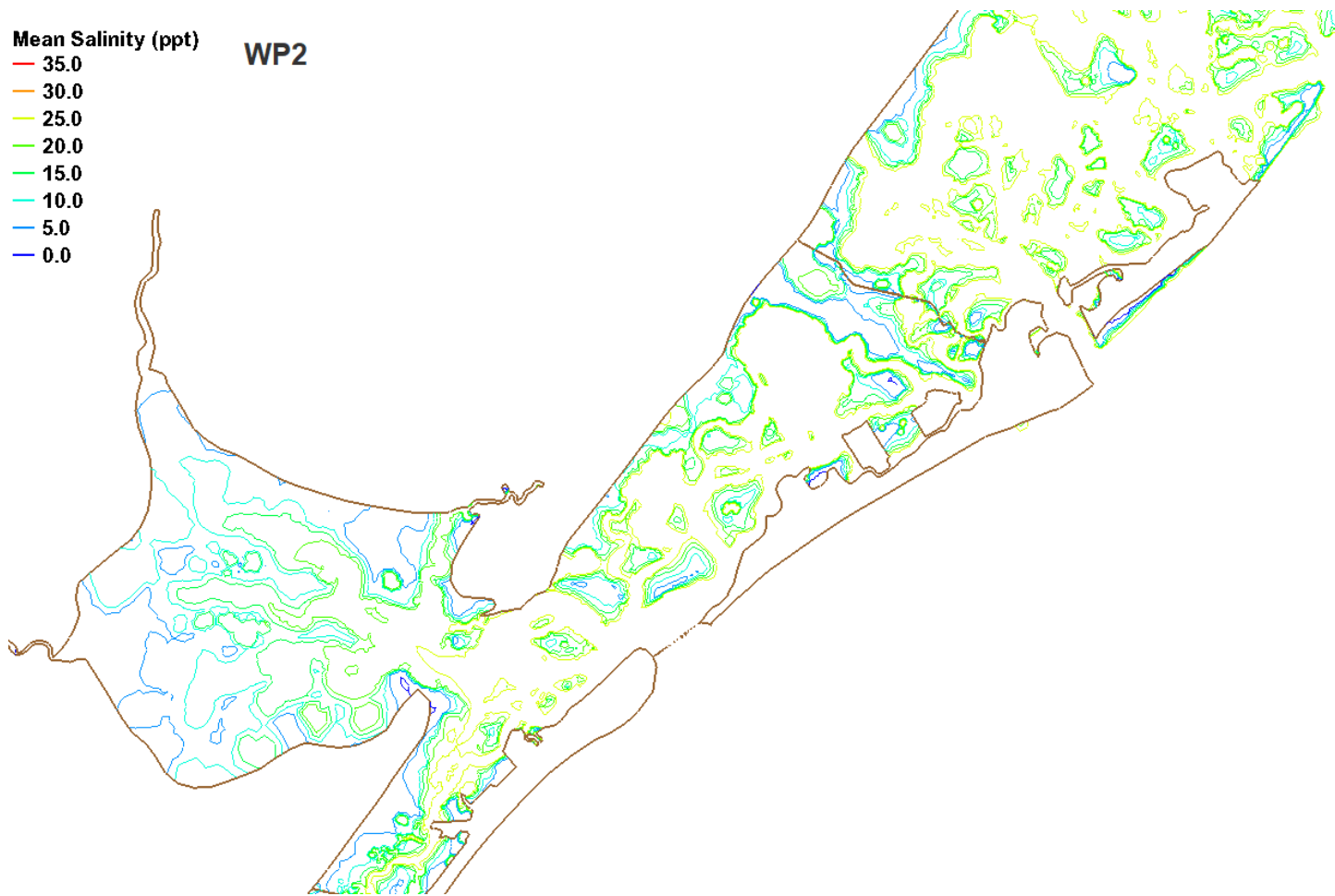


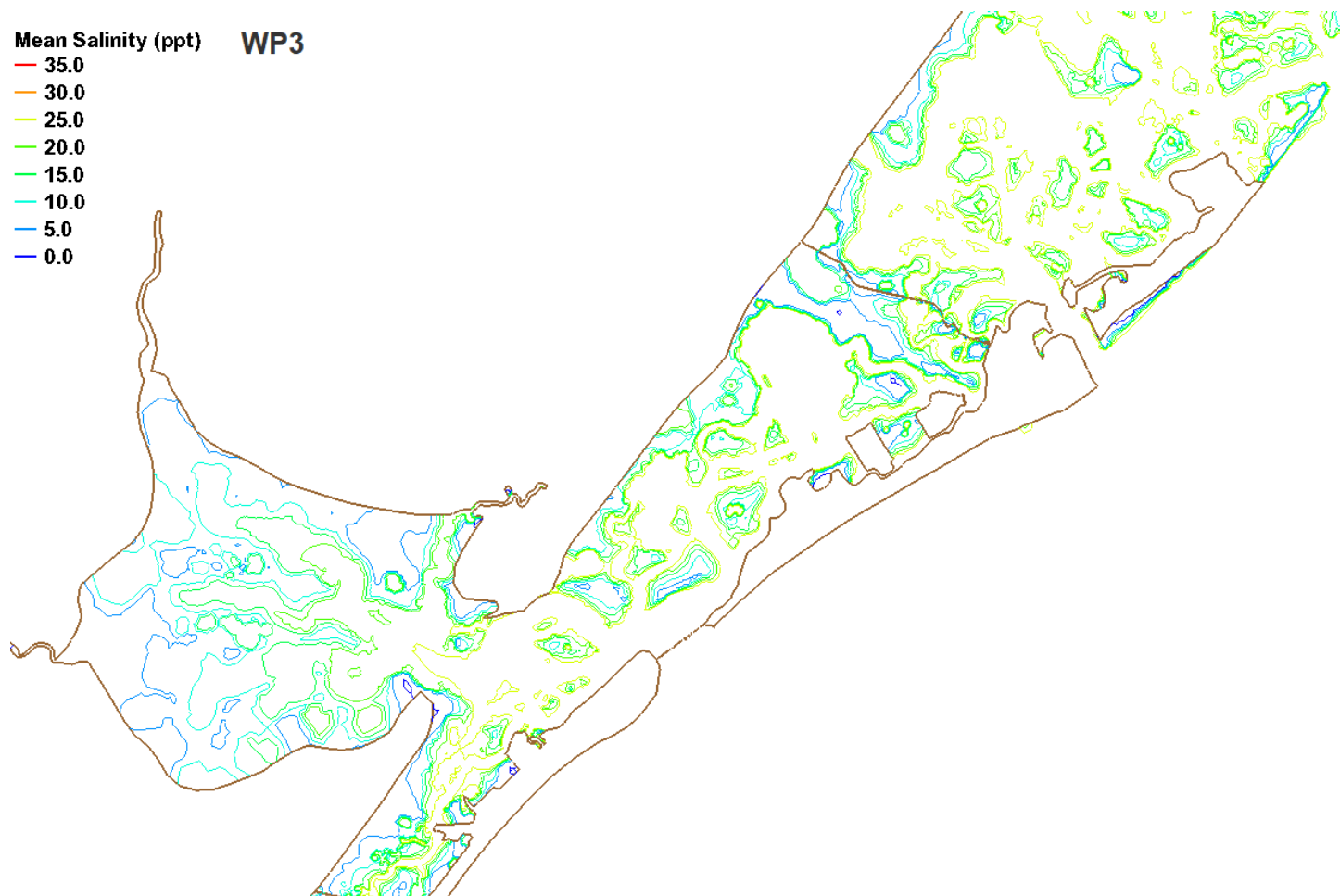


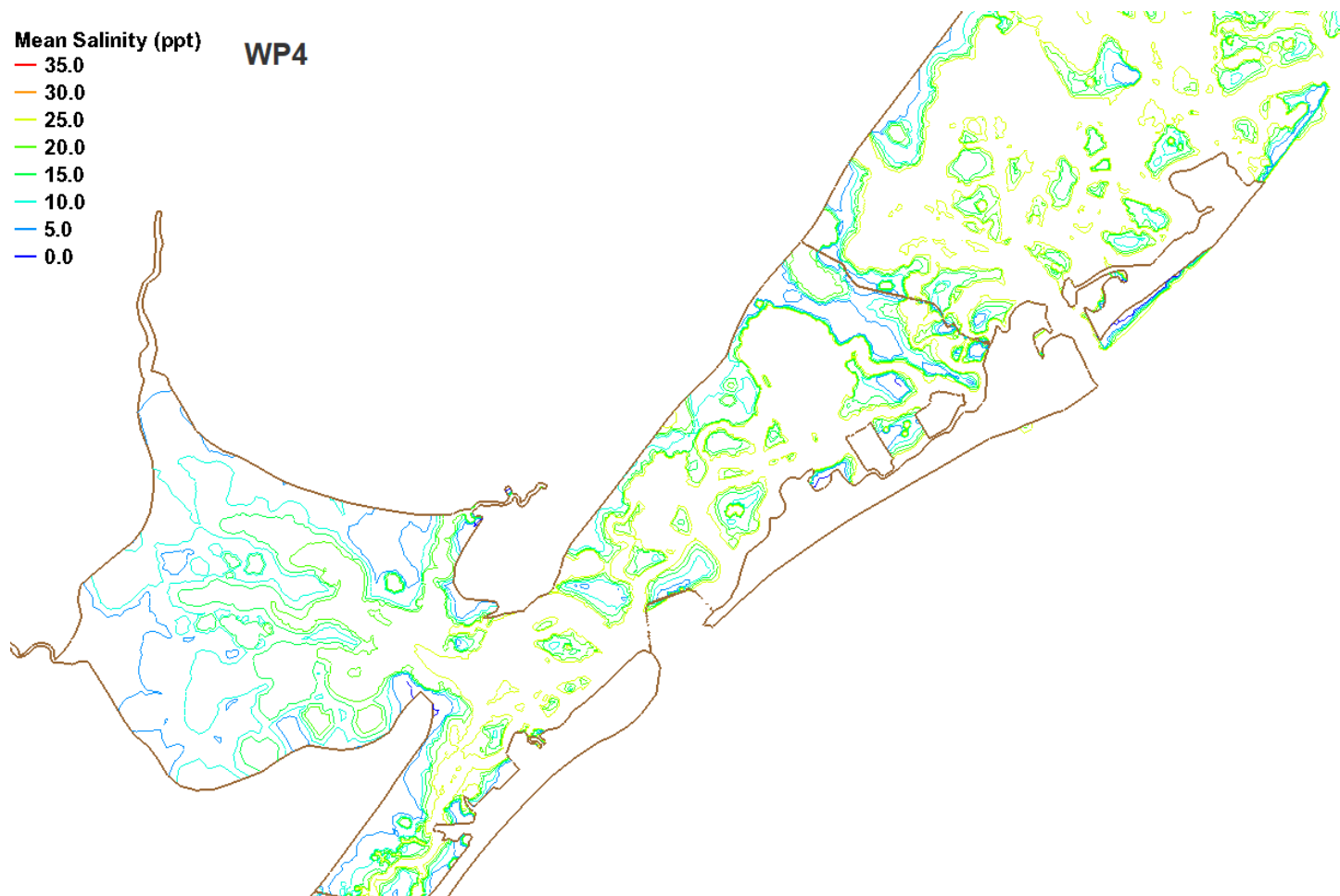
Central Region (Great Egg and Absecon)

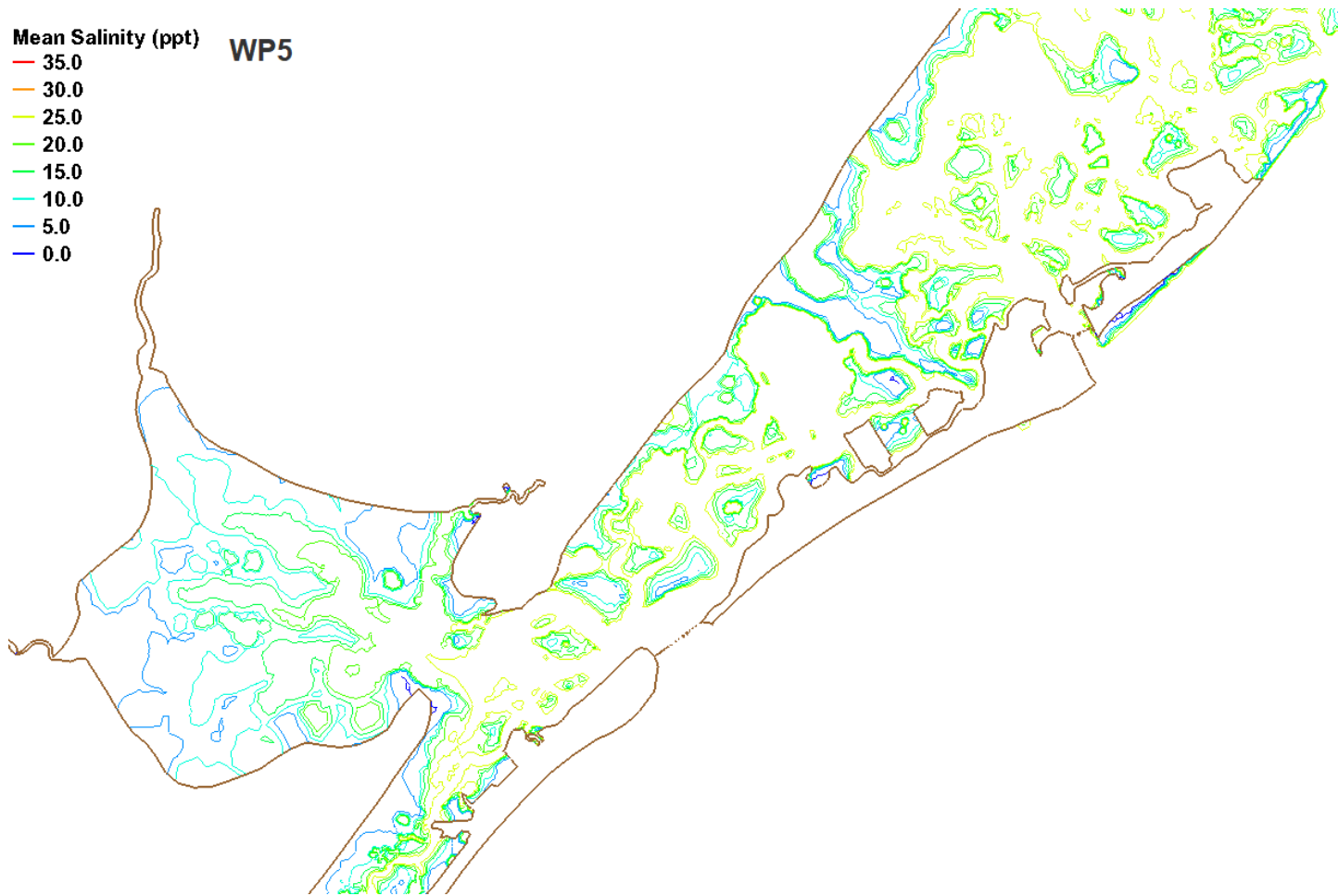


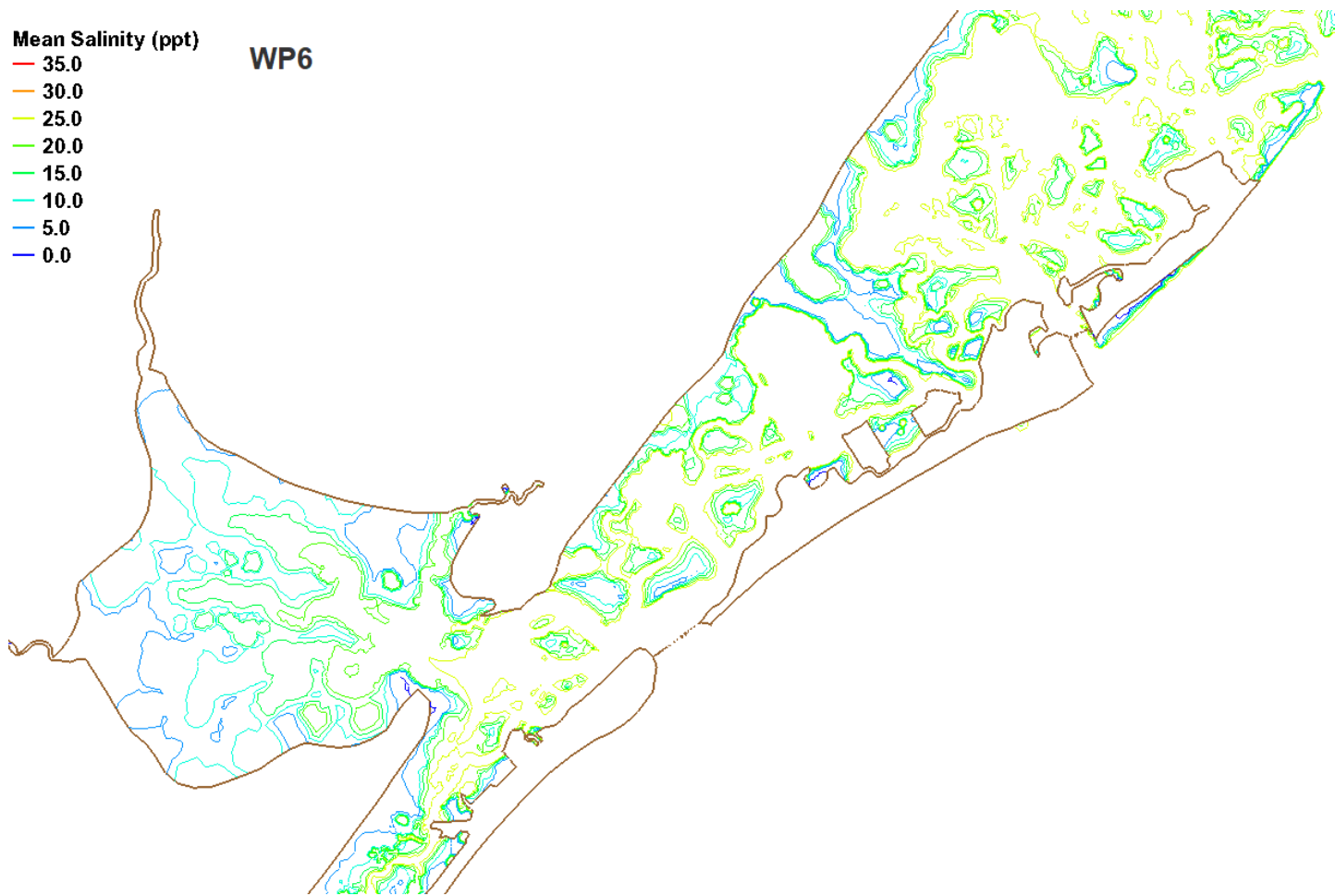












Comparisons to Base with Sea Level Rise

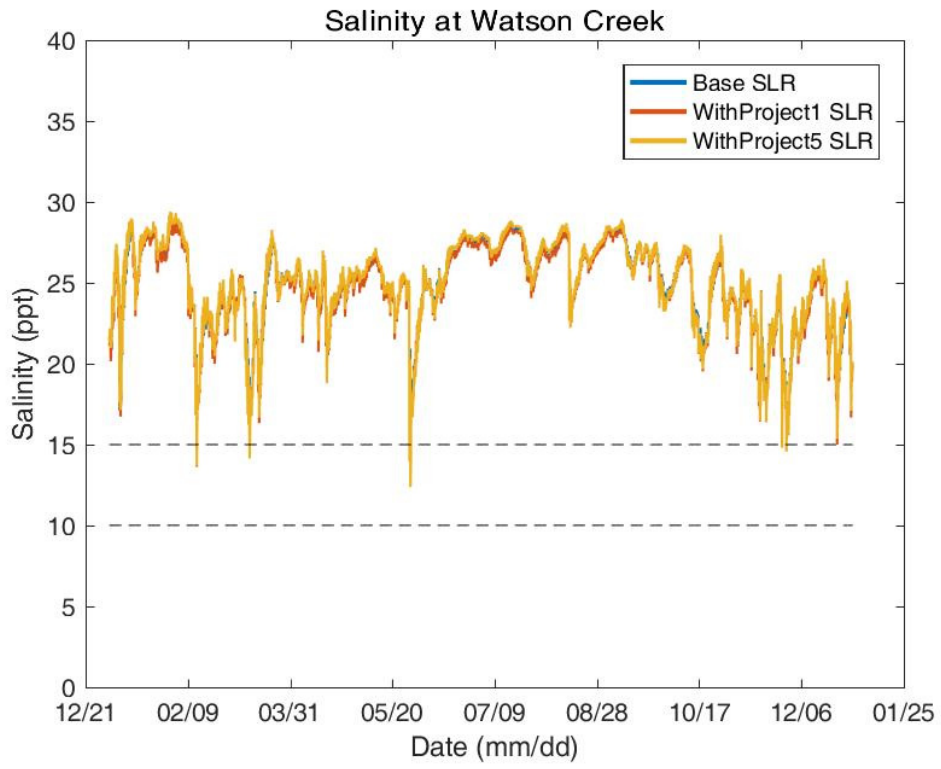
Maximum, Mean, Minimum

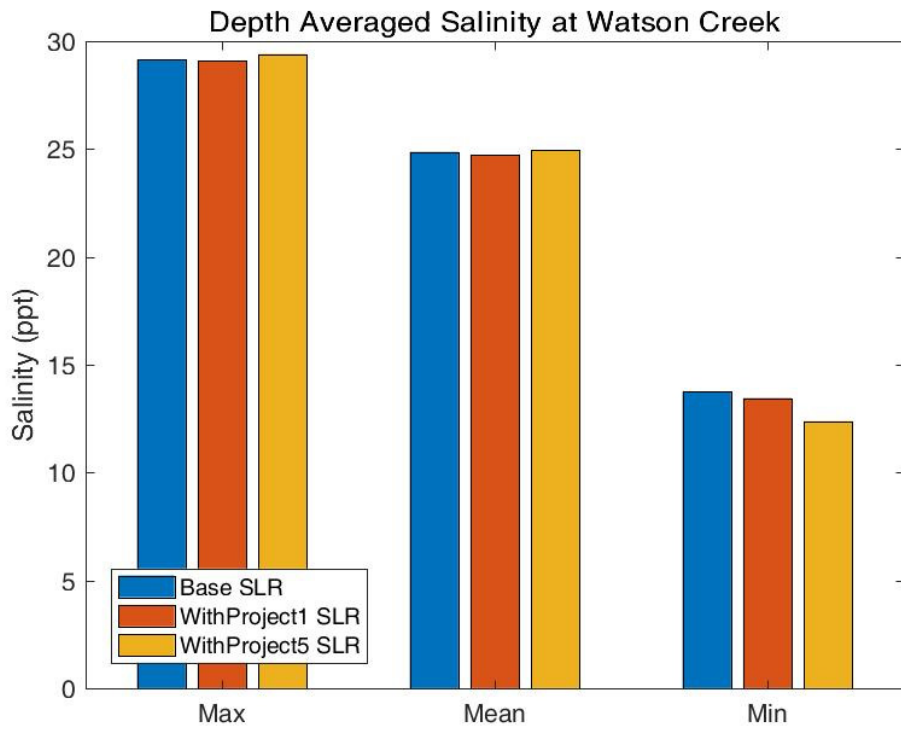
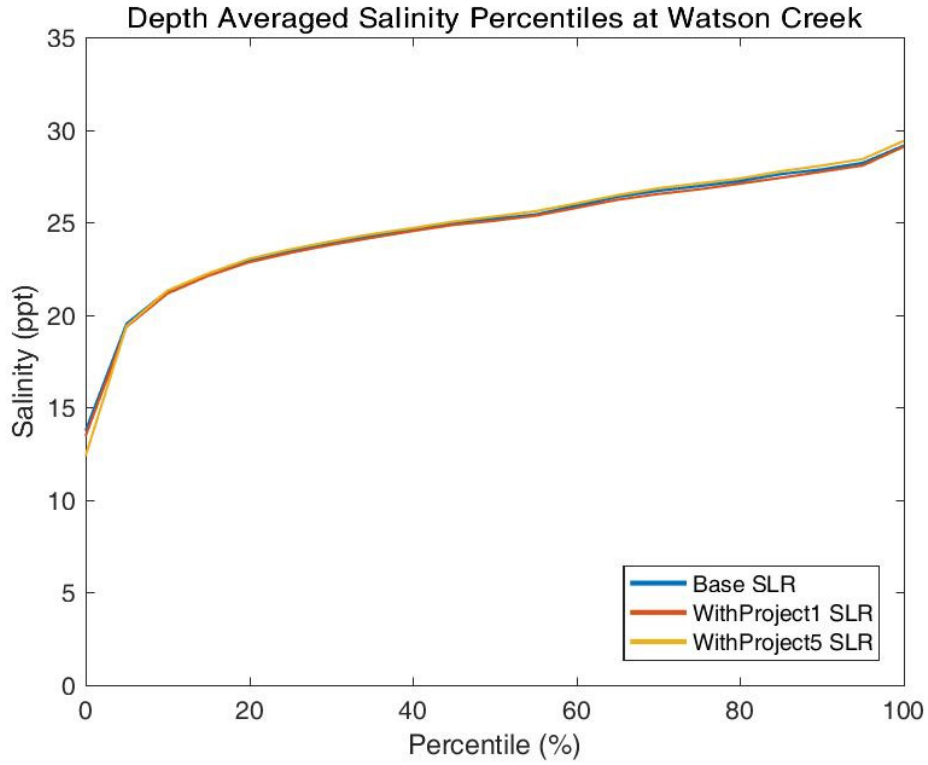
		Base SLR	WP1 SLR	WP5 SLR
Watson Creek	Max	29.15	29.09	29.41
	Mean	24.87	24.74	24.97
	Min	13.74	13.46	12.38
Manasquan River	Max	30.39	30.36	30.45
	Mean	25.46	25.29	25.66
	Min	1.24	1.61	1.62
Brick	Max	16.90	16.52	15.24
	Mean	7.96	8.31	7.04
	Min	0.82	1.01	0.64
Barnegat Bay at Mantoloking	Max	28.73	28.62	29.20
	Mean	21.79	21.26	22.26
	Min	11.15	11.22	11.16
Barnegat Bay at Route 37 Bridge	Max	17.90	16.28	18.79
	Mean	13.65	12.55	13.68
	Min	10.55	9.56	10.41
Berkeley	Max	11.35	10.73	10.22
	Mean	2.64	2.62	2.29
	Min	0.00	0.00	0.00
Barnegat Light	Max	29.42	29.34	29.22
	Mean	26.74	26.67	25.95
	Min	8.99	9.09	9.01
Barnegat Bay at Waretown	Max	28.13	28.20	27.58
	Mean	26.20	26.27	25.33
	Min	19.89	20.13	18.84
Barnegat Bay at Barnegat Light	Max	29.54	29.42	29.51
	Mean	27.69	27.95	27.40
	Min	15.61	16.62	15.61
Barnegat Light (Ocean)	Max	29.50	29.49	29.42
	Mean	28.73	28.71	28.57
	Min	24.92	24.94	24.56

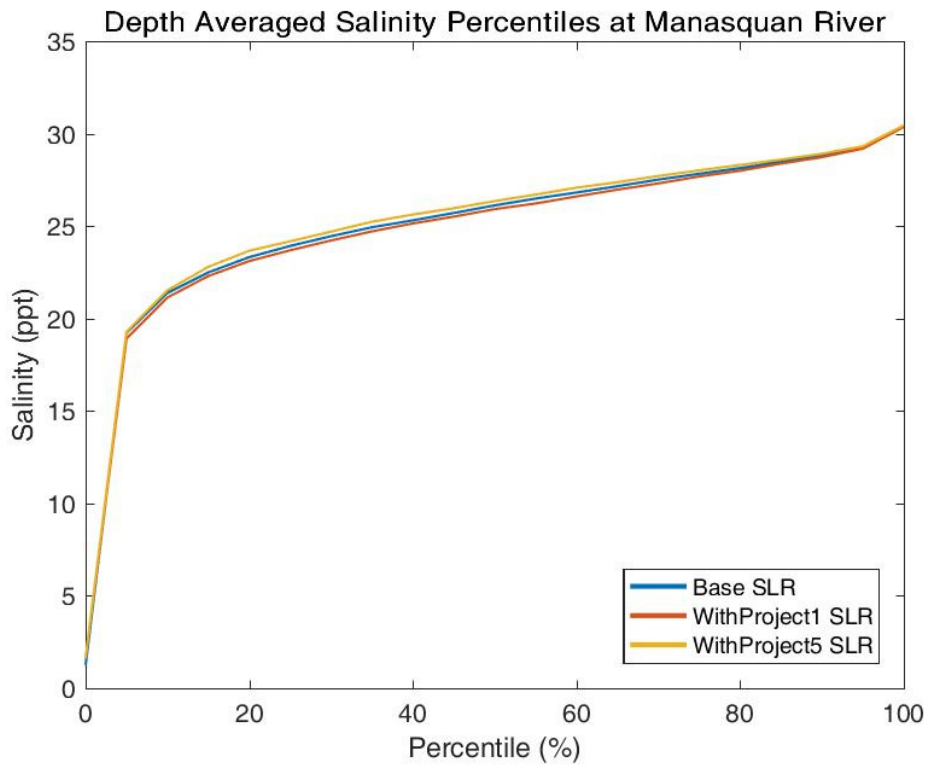
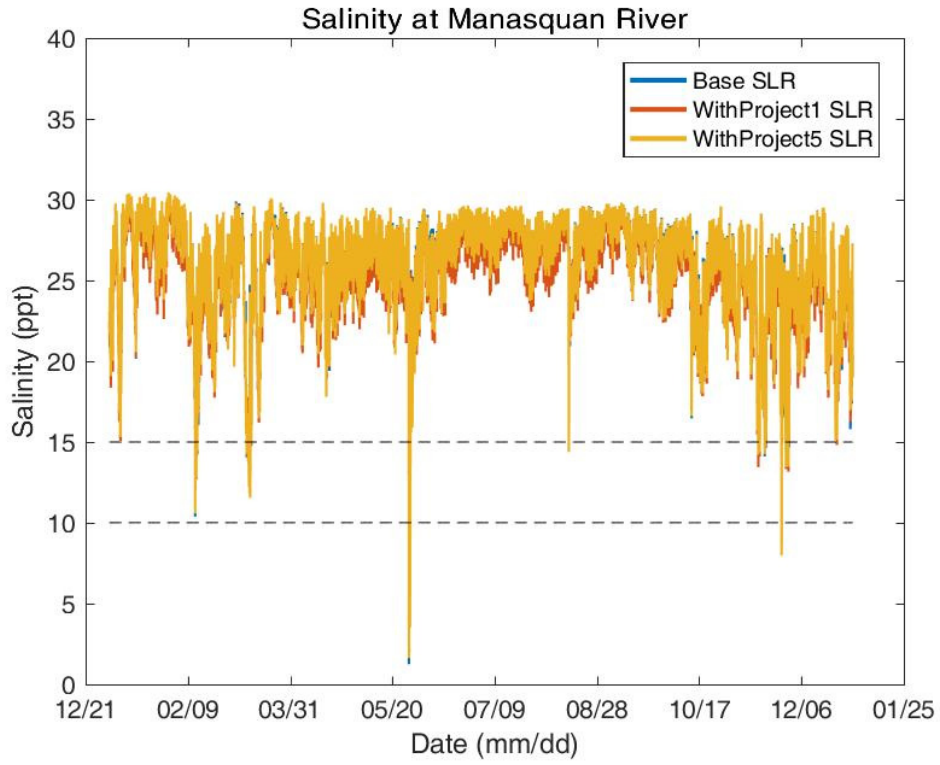
East Thorofare	Max	28.54	28.50	28.71
	Mean	26.61	26.52	26.92
	Min	24.04	23.97	24.39
Westecunk	Max	27.95	27.96	27.99
	Mean	24.34	24.41	24.43
	Min	17.34	17.45	17.44
Beach Haven	Max	29.27	29.26	29.29
	Mean	27.90	27.83	27.97
	Min	25.84	25.81	25.95
JACNEWQ	Max	22.27	22.11	22.08
	Mean	10.01	9.90	9.89
	Min	0.70	0.65	0.68
Little Egg Inlet	Max	29.18	29.18	29.19
	Mean	27.31	27.29	27.32
	Min	17.30	17.60	17.22
Absecon Creek	Max	29.32	29.38	29.24
	Mean	27.77	27.81	27.57
	Min	24.94	24.99	24.62
Brigantine	Max	29.29	29.29	29.23
	Mean	27.93	27.92	27.80
	Min	25.98	25.96	25.75
Absecon Channel	Max	29.52	29.53	29.51
	Mean	28.51	28.52	28.44
	Min	26.46	26.48	26.16
Atlantic City (Ocean)	Max	29.56	29.56	29.55
	Mean	28.61	28.62	28.55
	Min	27.04	27.04	26.85
Inside Thorofare	Max	29.09	28.93	29.02
	Mean	27.89	27.57	27.74
	Min	26.29	25.92	26.09
Beach Thorofare	Max	29.47	29.45	29.45
	Mean	28.46	28.33	28.38
	Min	26.64	26.38	26.50
Scull Bay	Max	29.19	29.11	29.12

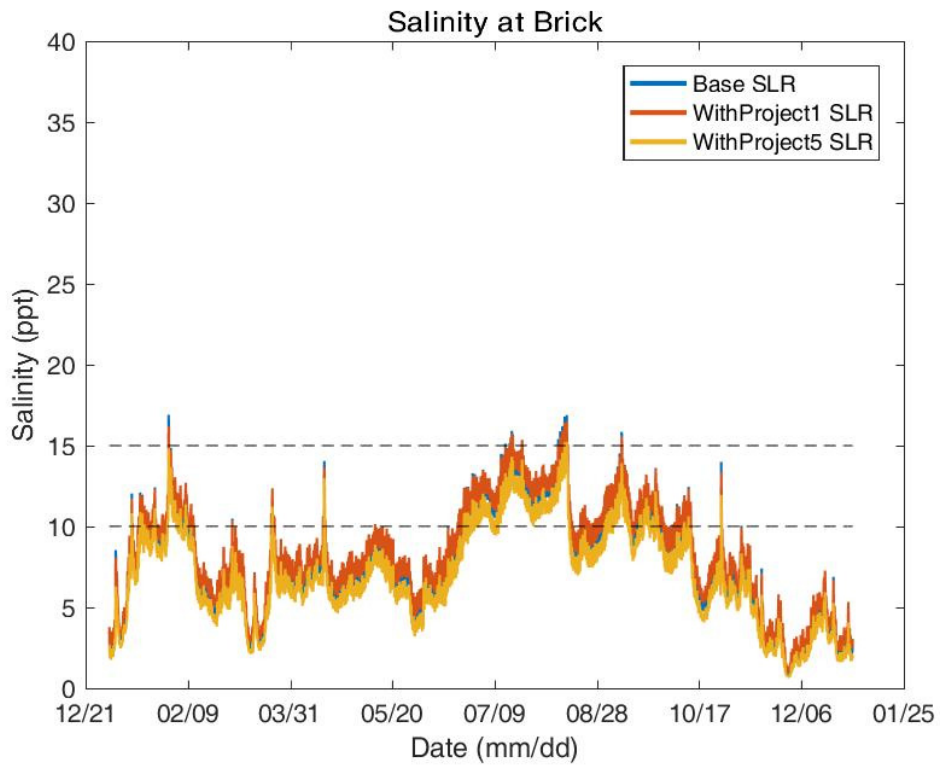
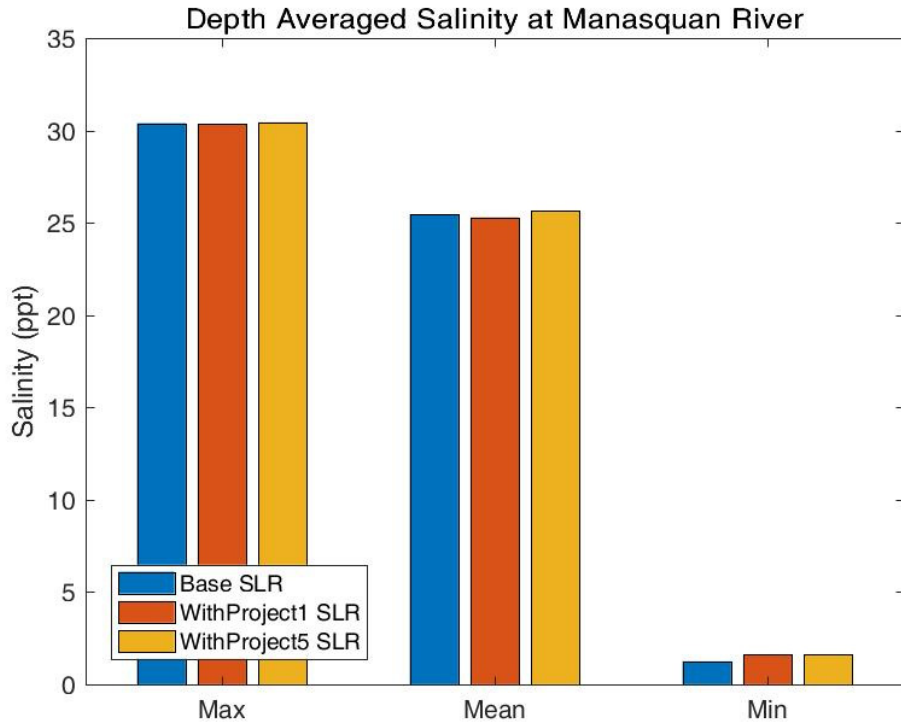
	Mean	27.81	27.68	27.71
	Min	24.97	24.88	24.88
Great Egg Harbor River	Max	28.82	28.63	28.69
	Mean	21.79	20.97	21.16
	Min	8.13	7.39	7.48
Great Egg Harbor Bay	Max	29.29	29.24	29.24
	Mean	27.43	27.06	27.08
	Min	21.20	20.49	20.57
Ocean City 39th St	Max	28.29	27.91	27.95
	Mean	25.79	25.18	25.26
	Min	22.29	21.67	21.65
Corson Sound	Max	29.45	29.46	29.45
	Mean	27.97	28.12	28.07
	Min	24.36	24.55	24.46
Ludlum Thorofare	Max	29.40	29.39	29.40
	Mean	27.95	27.97	27.99
	Min	25.21	25.18	25.24
Ingram Thorofare	Max	29.47	29.47	29.46
	Mean	28.57	28.58	28.57
	Min	25.89	25.88	25.89
Cape May Ferry	Max	28.68	28.65	28.69
	Mean	27.33	27.28	27.34
	Min	25.22	25.16	25.23
Cape May Harbor	Max	29.55	29.55	29.55
	Mean	28.64	28.66	28.64
	Min	27.00	27.03	27.00

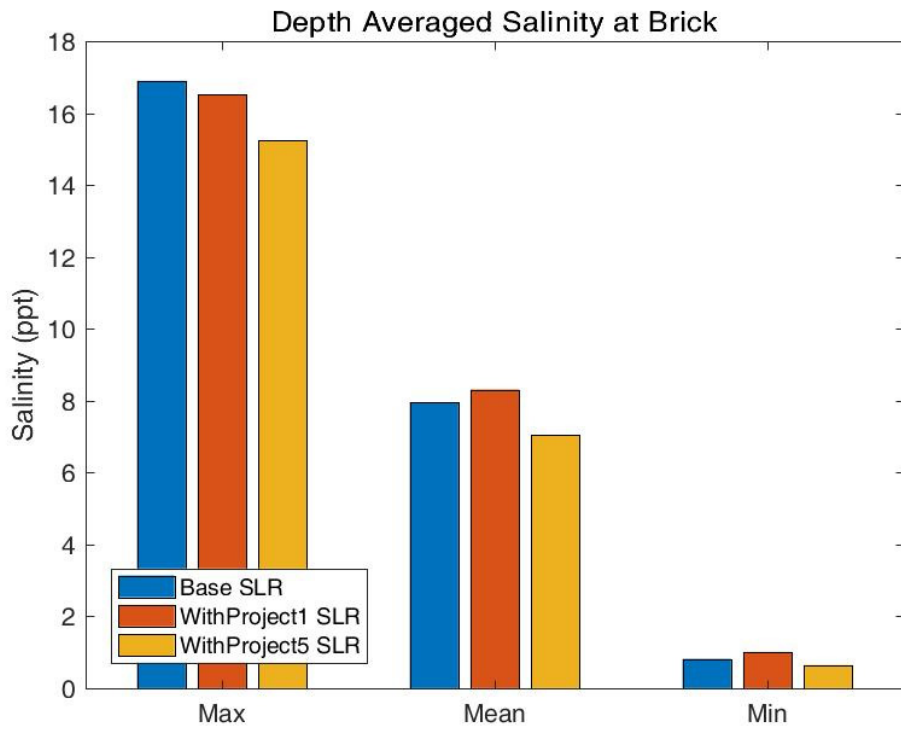
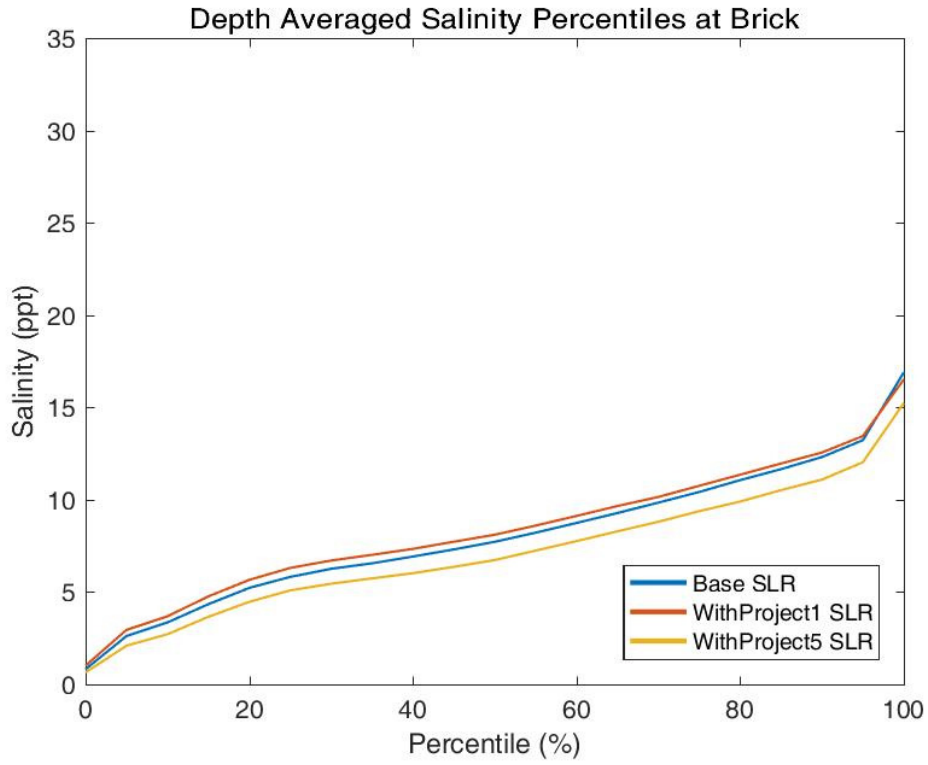
Point Comparisons

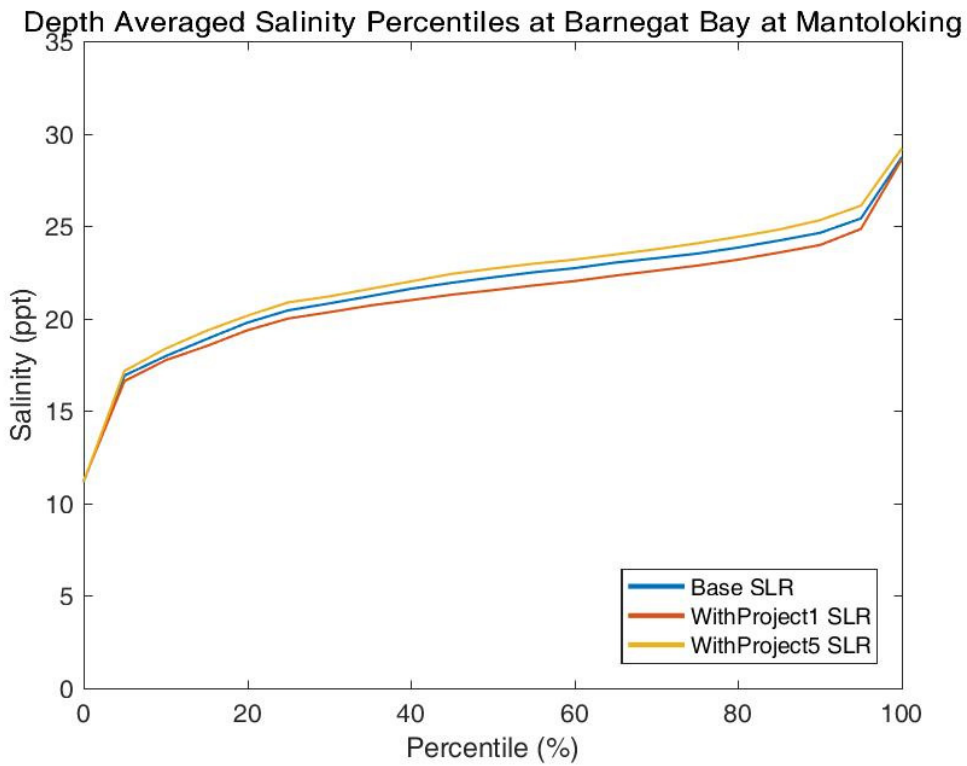
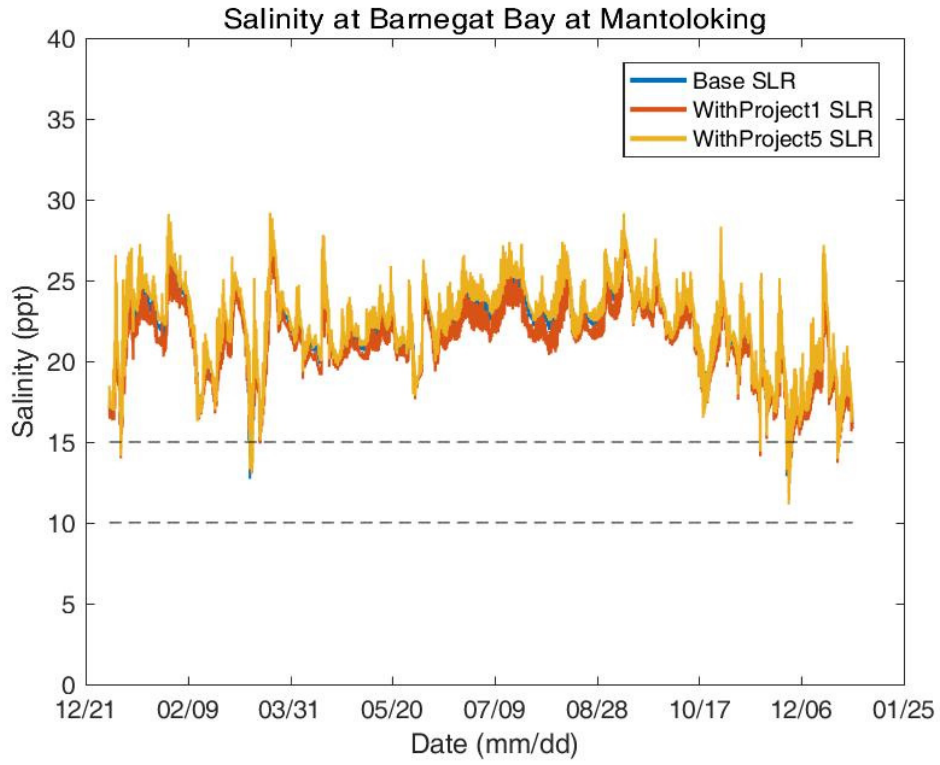


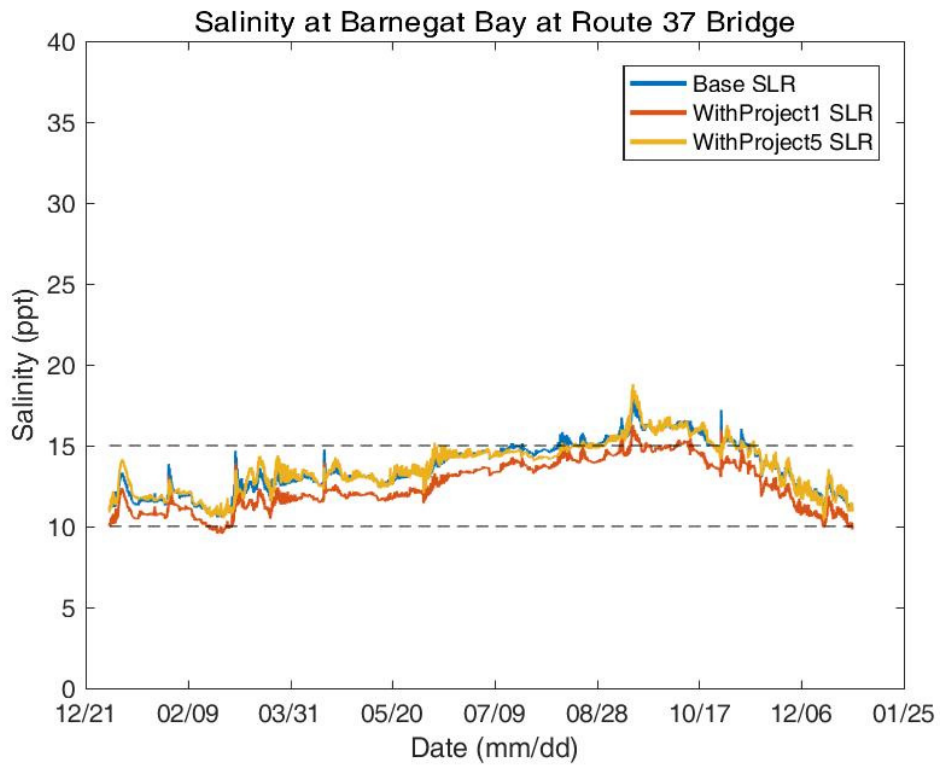
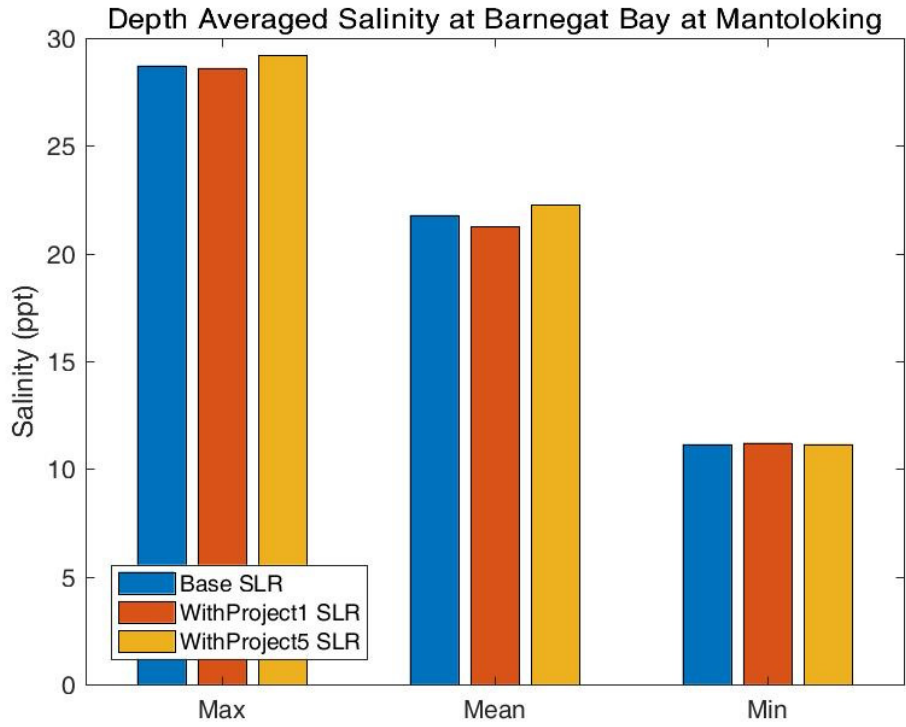




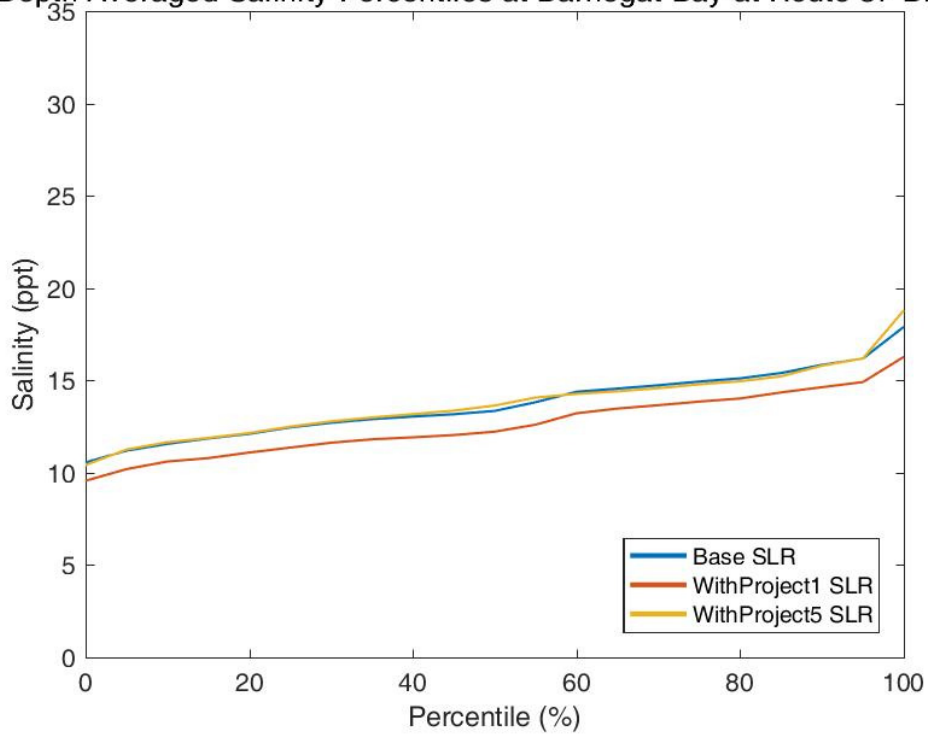




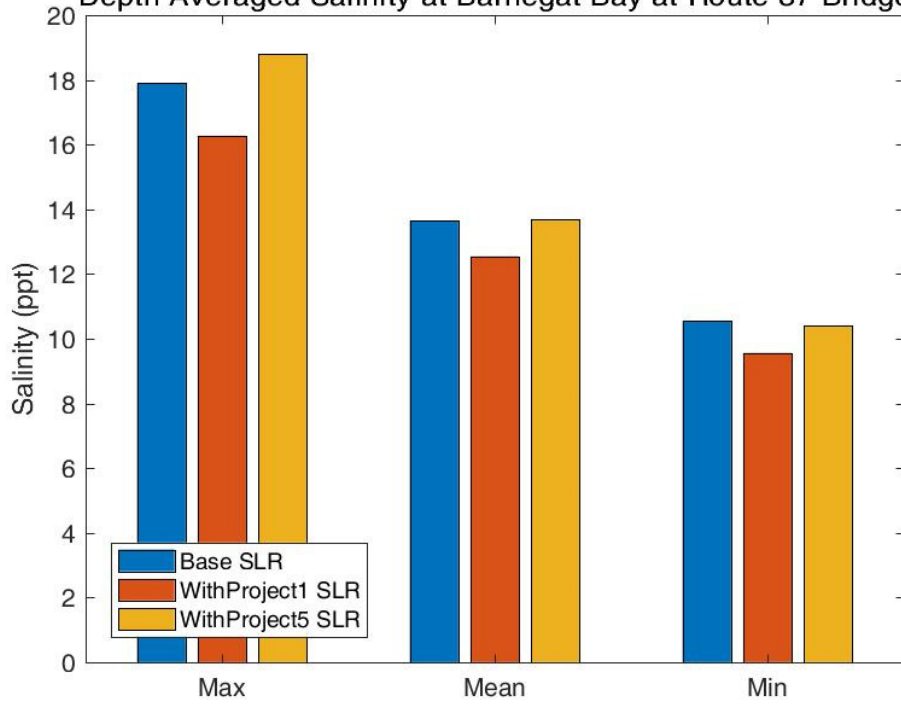


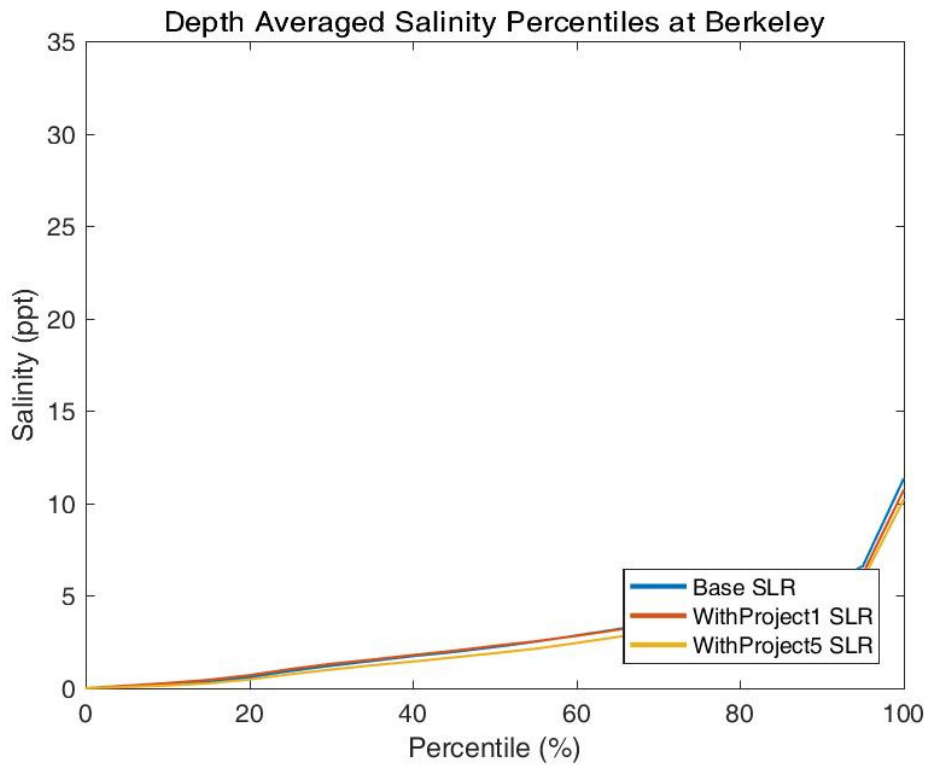
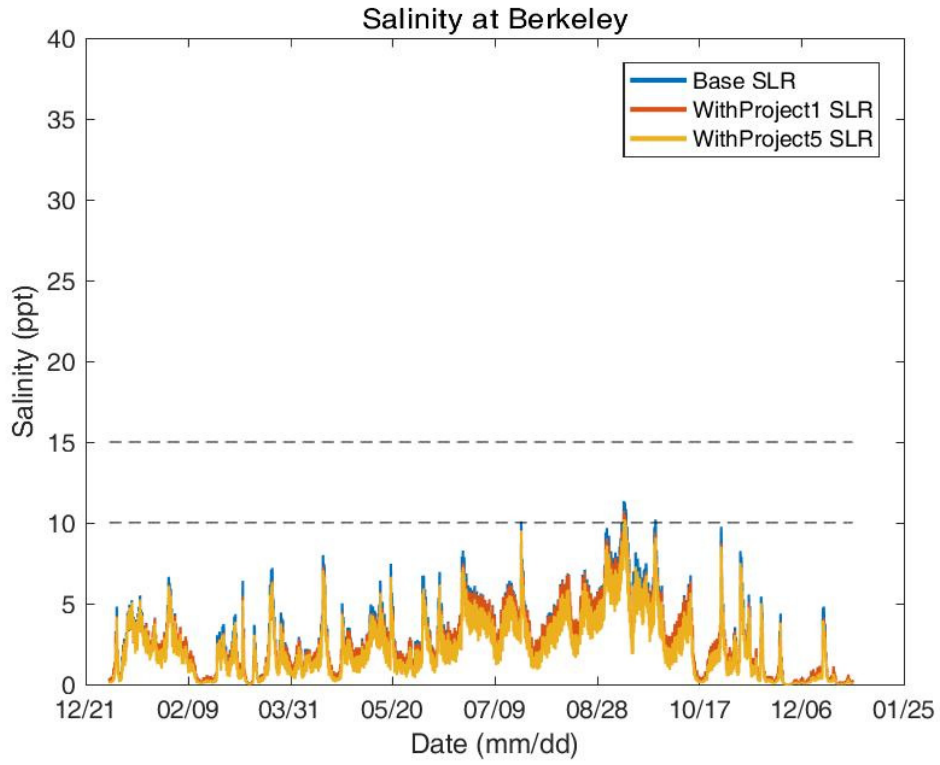


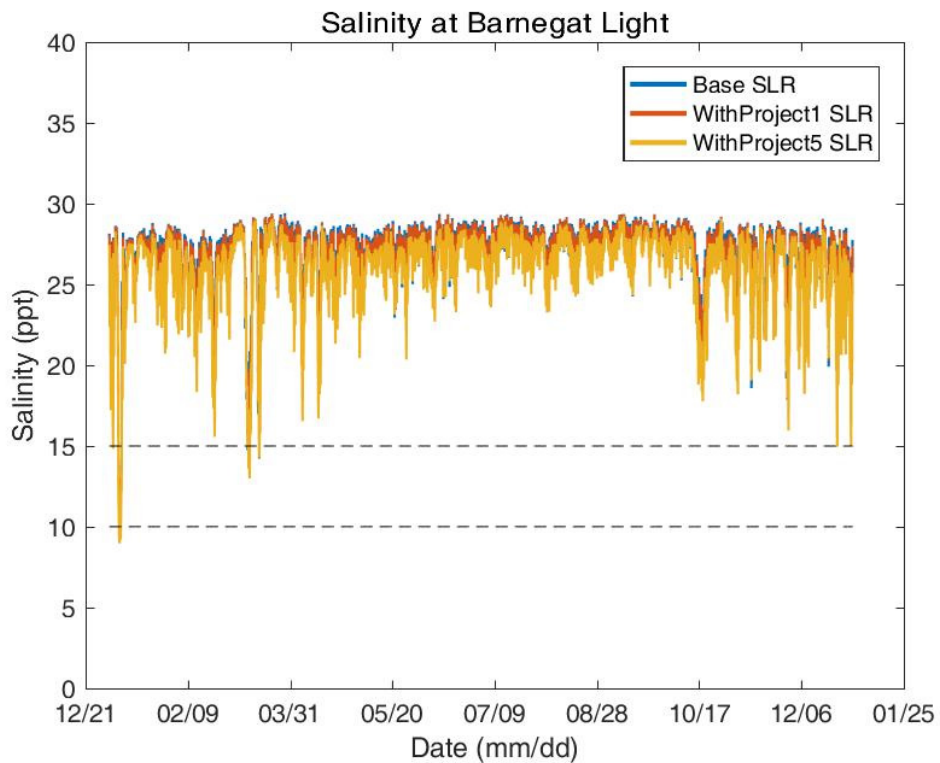
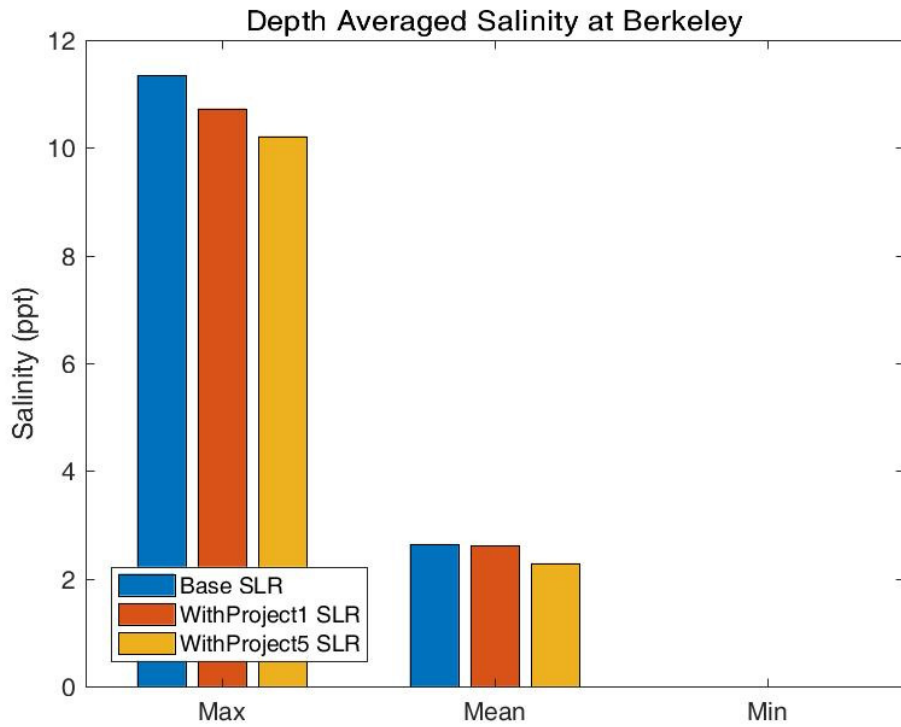
Depth Averaged Salinity Percentiles at Barnegat Bay at Route 37 Bridge

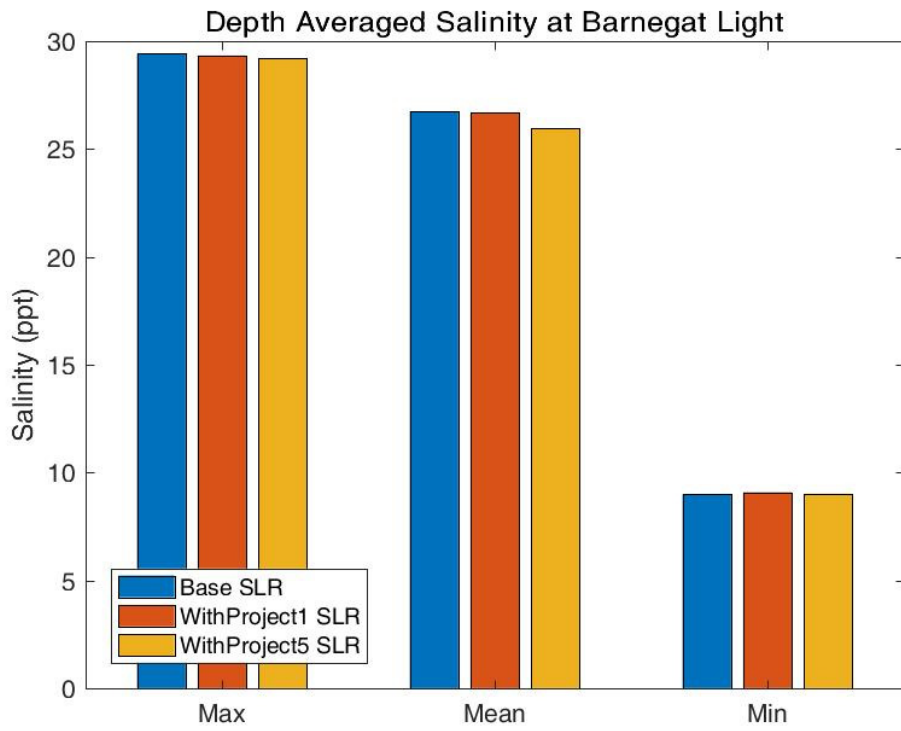
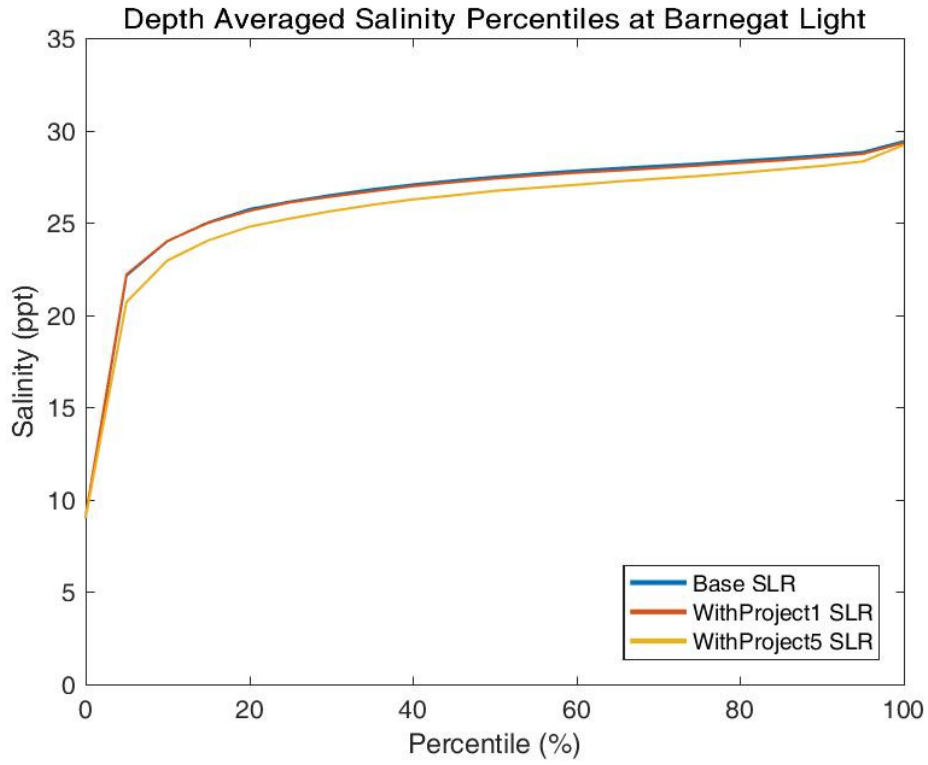


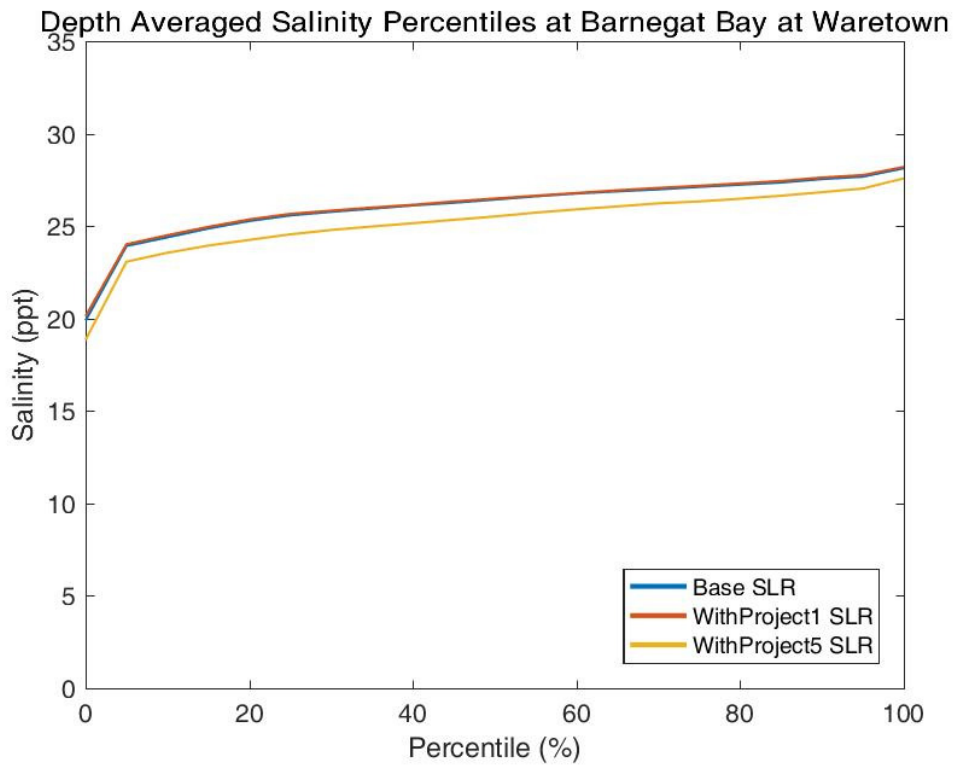
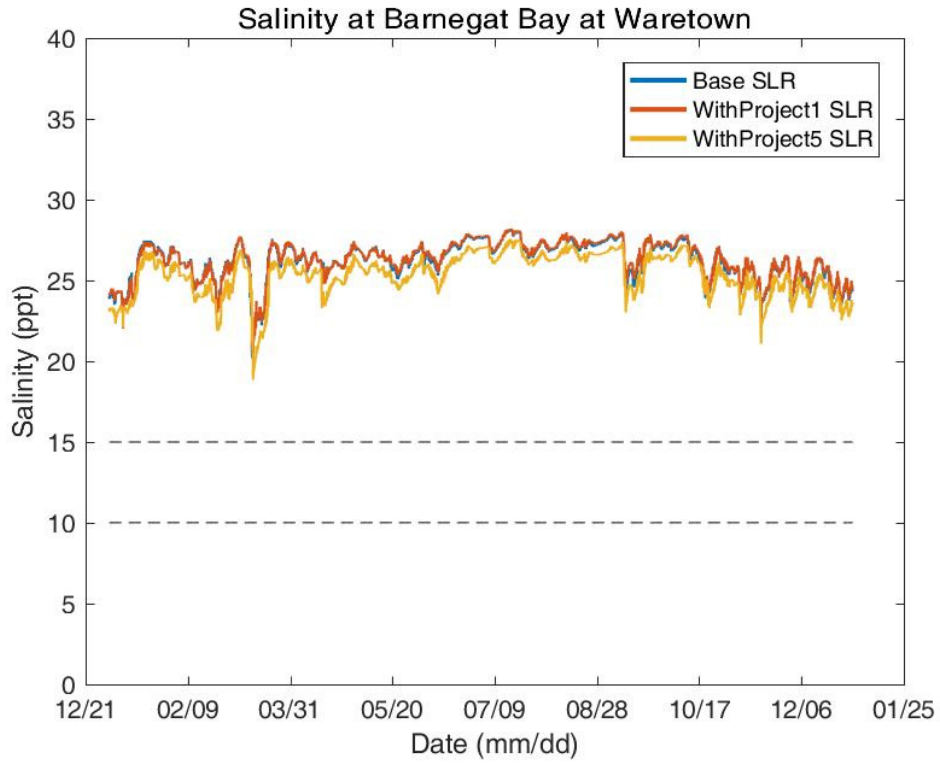
Depth Averaged Salinity at Barnegat Bay at Route 37 Bridge

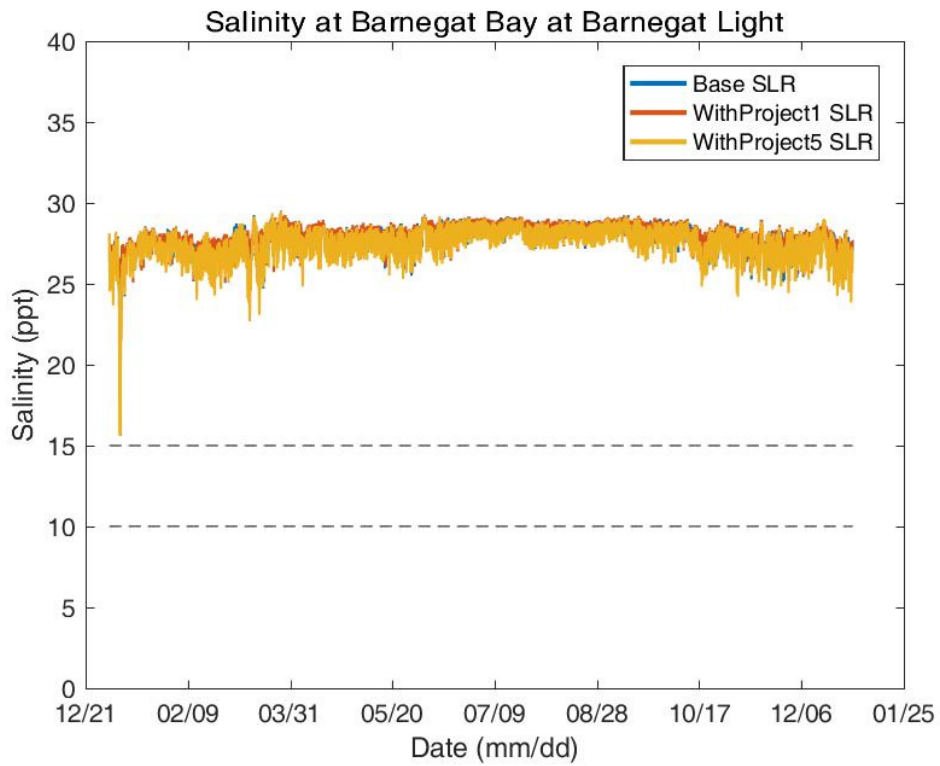
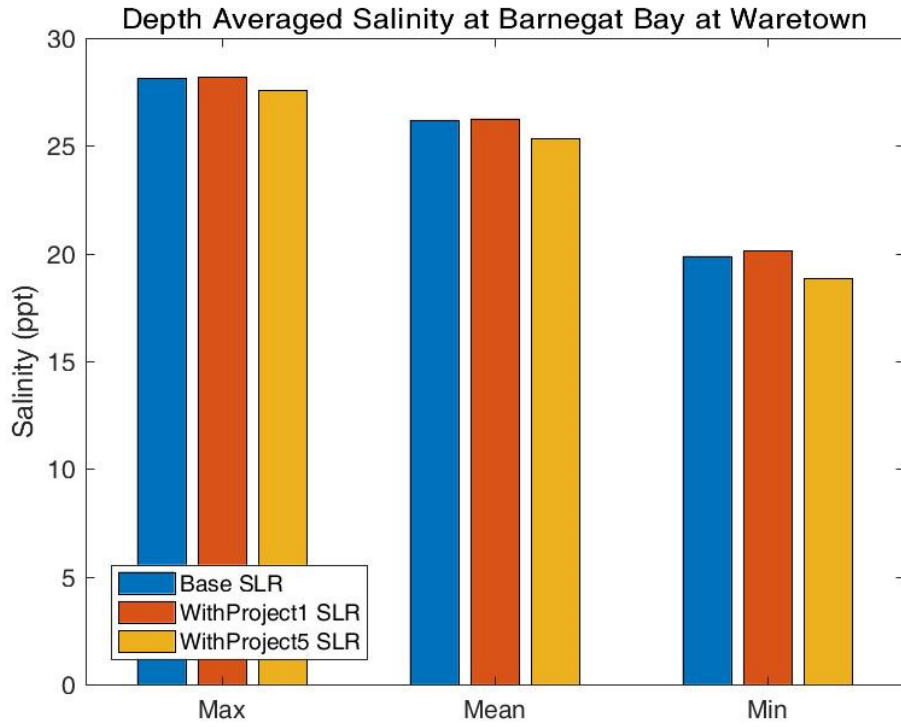




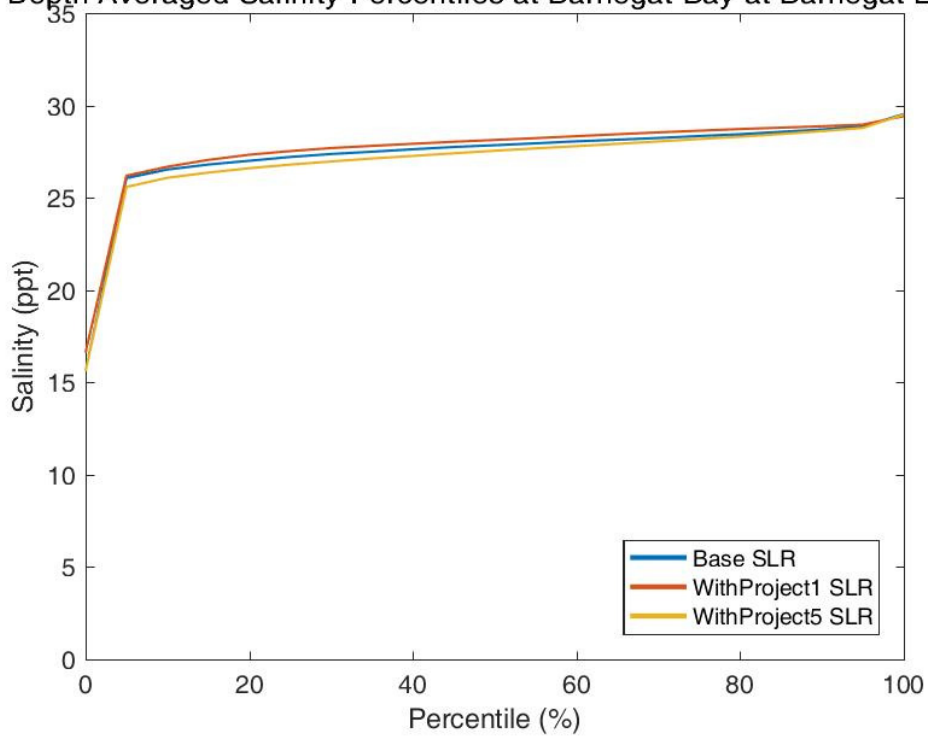




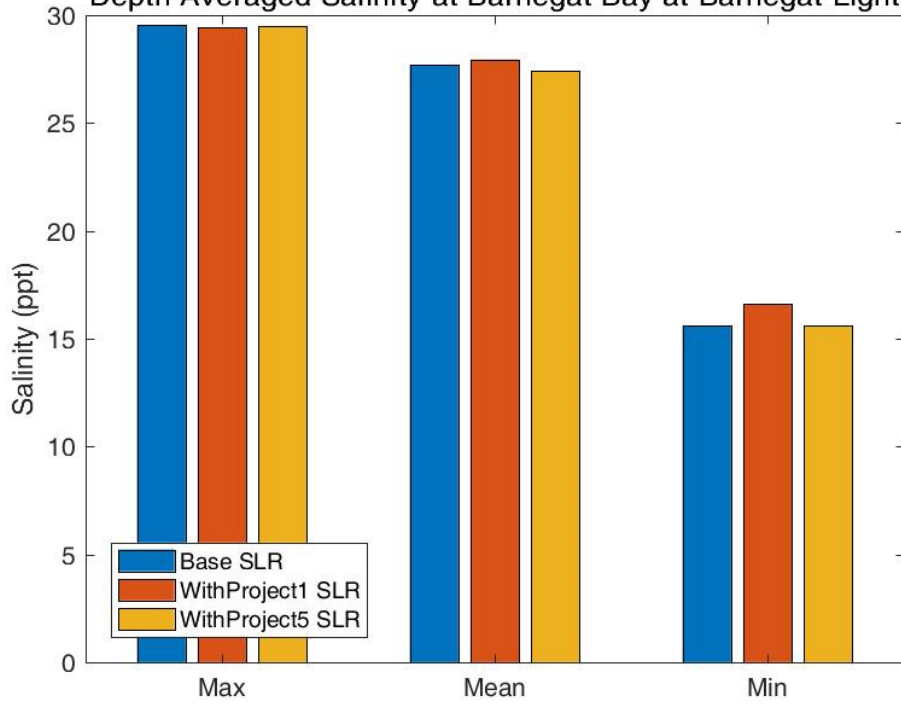


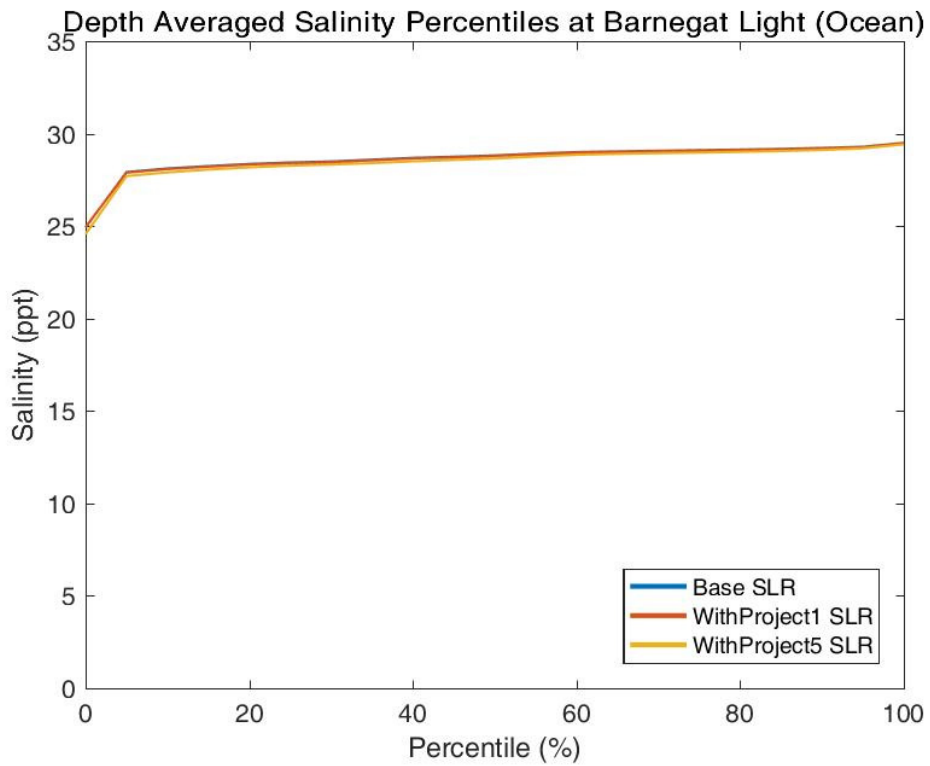
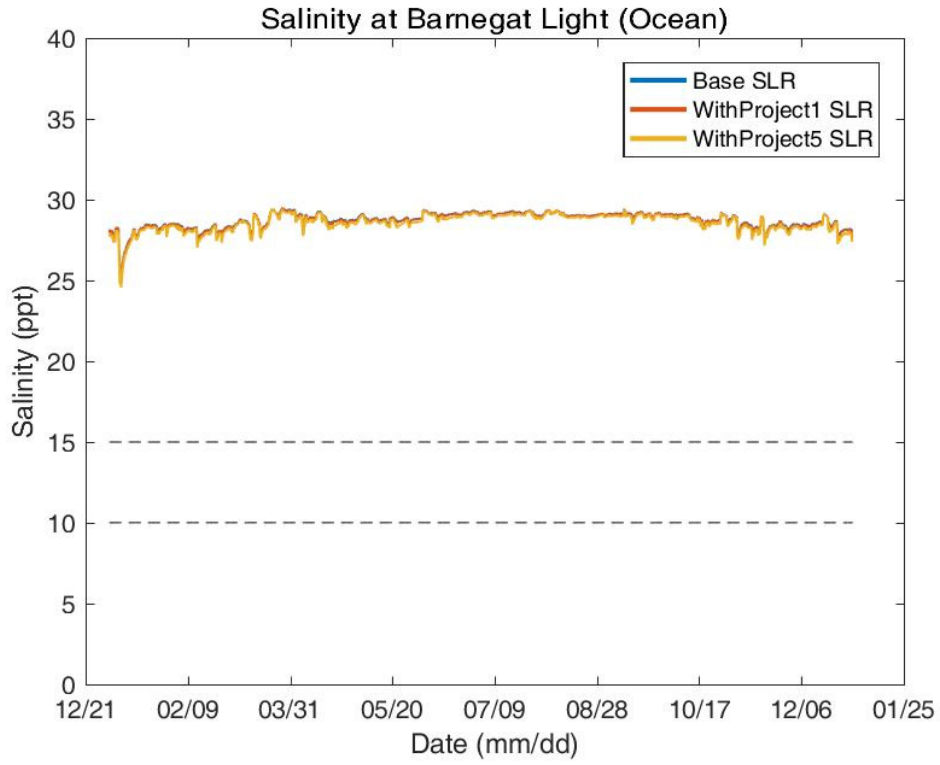


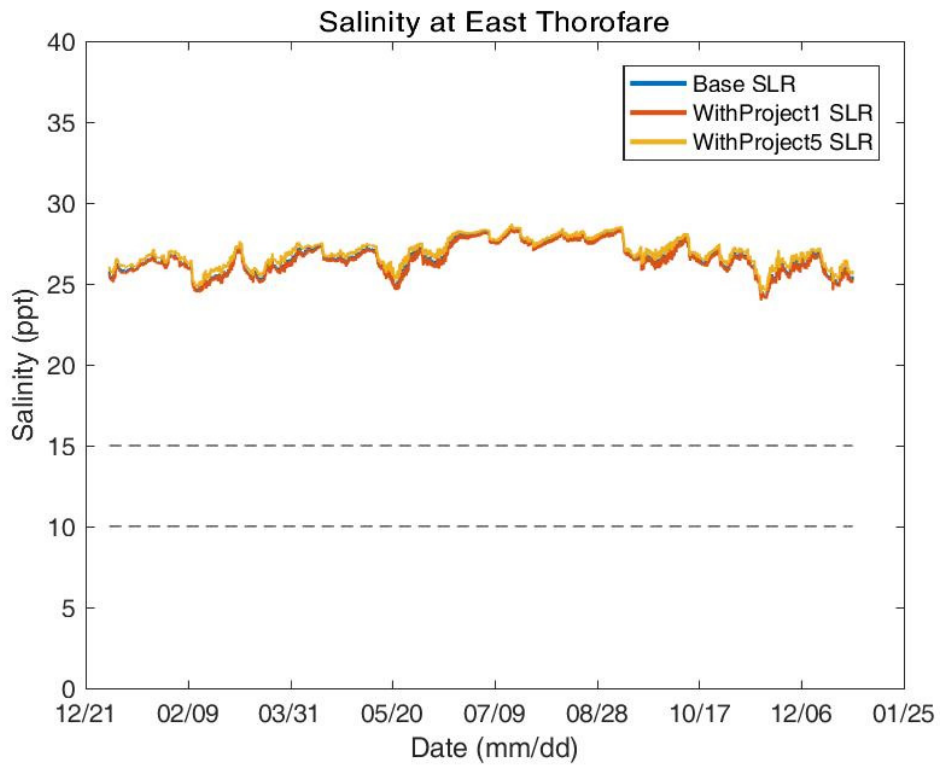
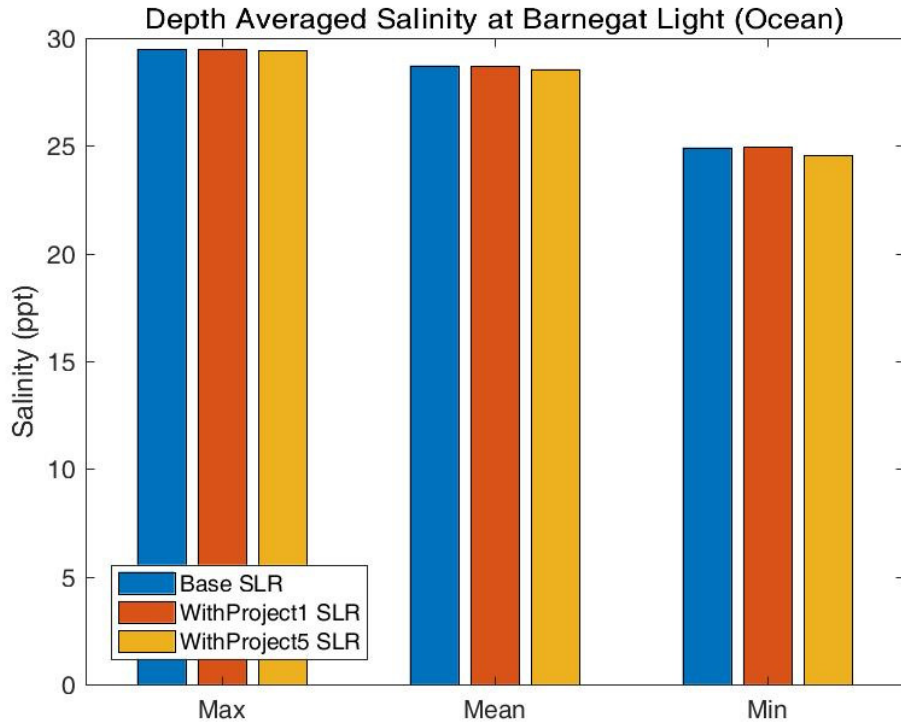
Depth Averaged Salinity Percentiles at Barnegat Bay at Barnegat Light

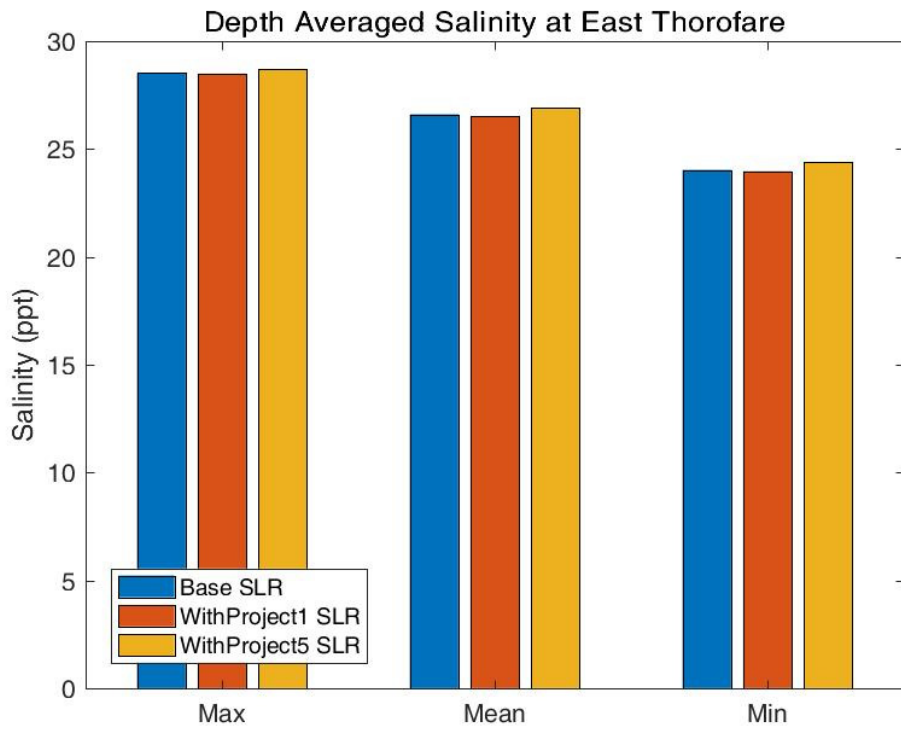
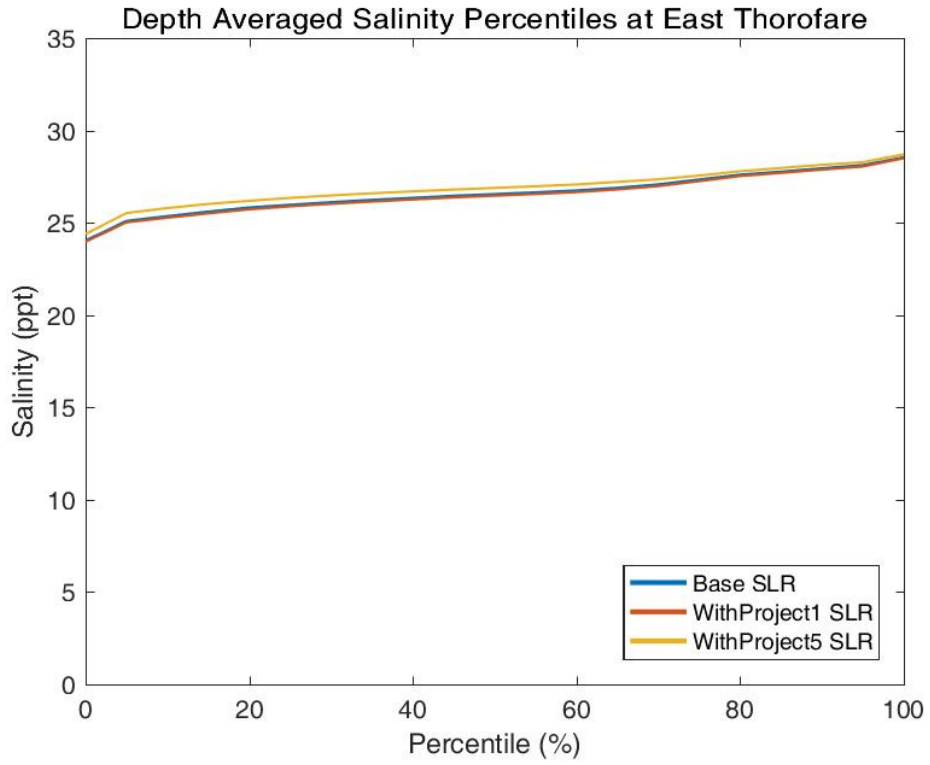


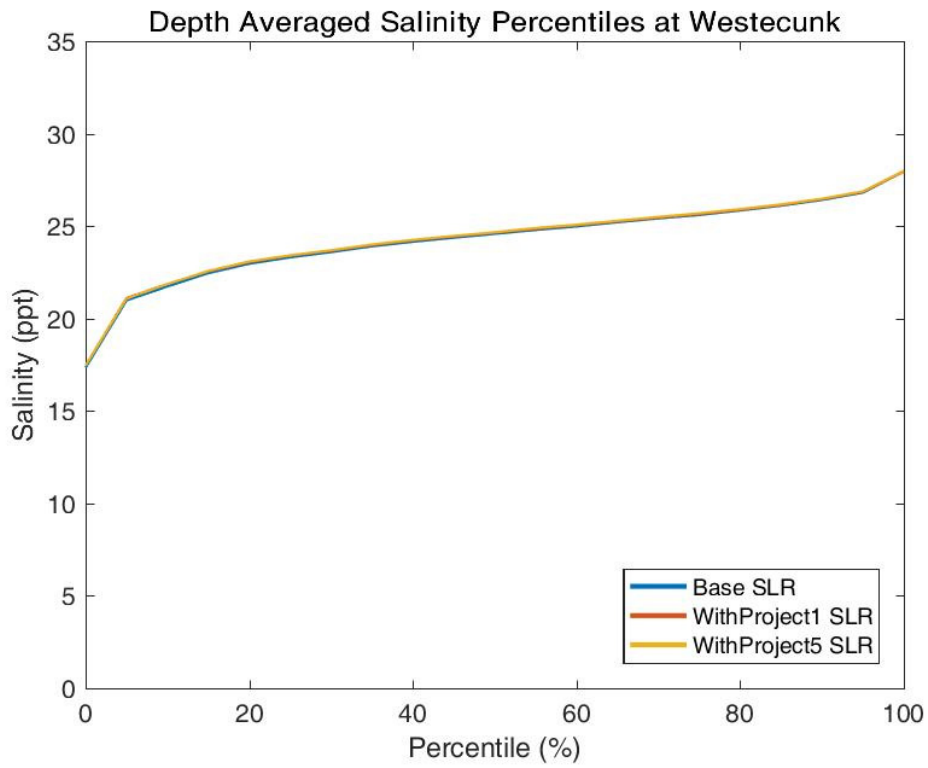
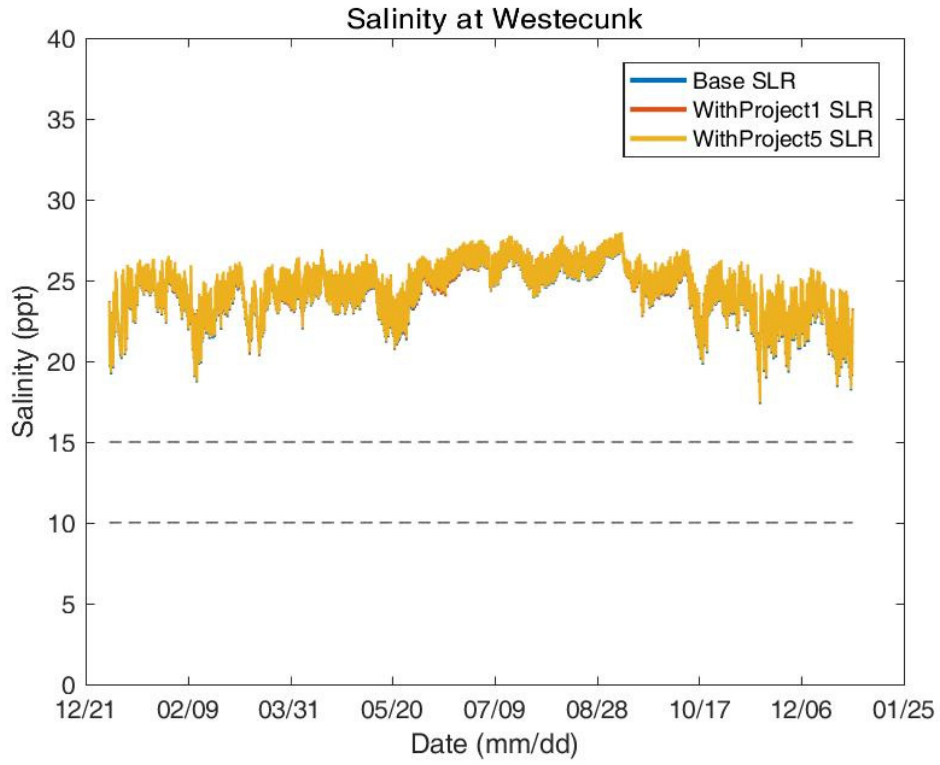
Depth Averaged Salinity at Barnegat Bay at Barnegat Light

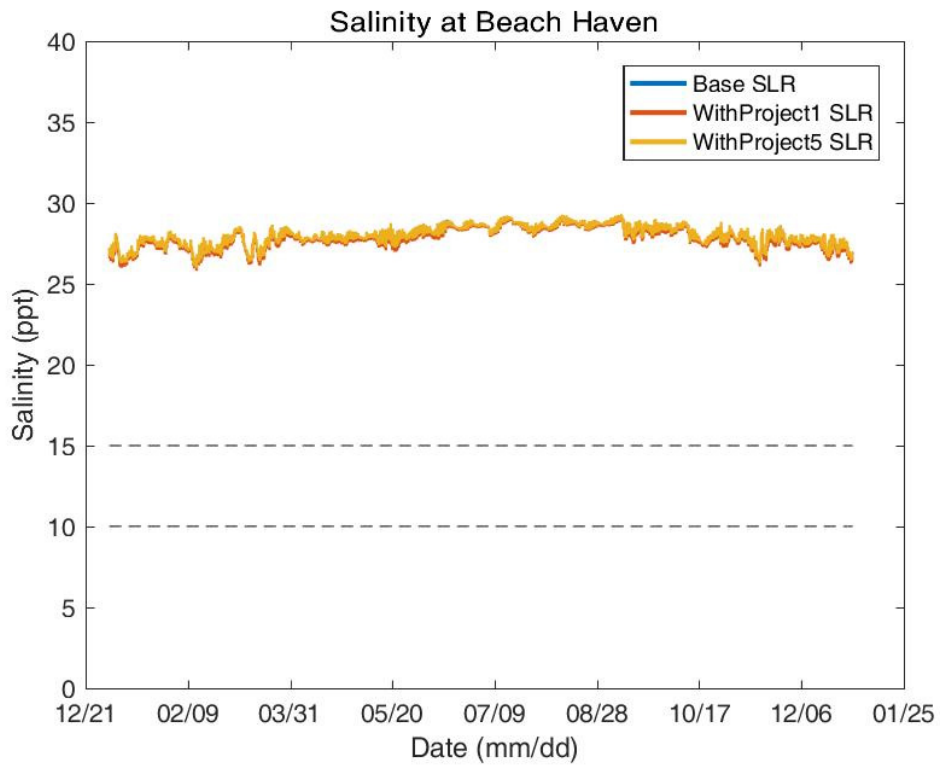
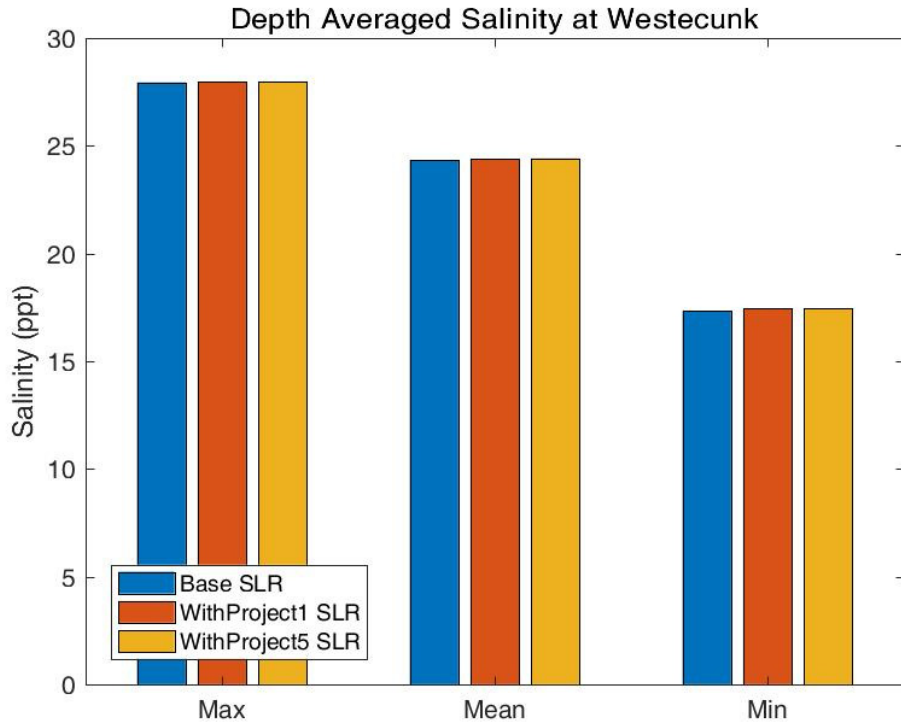


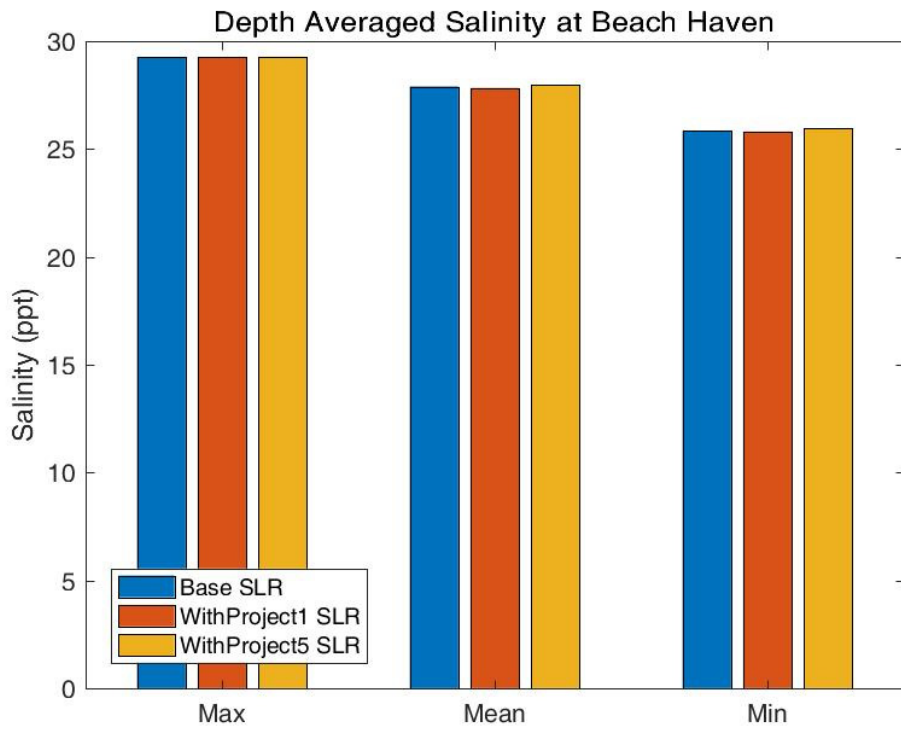
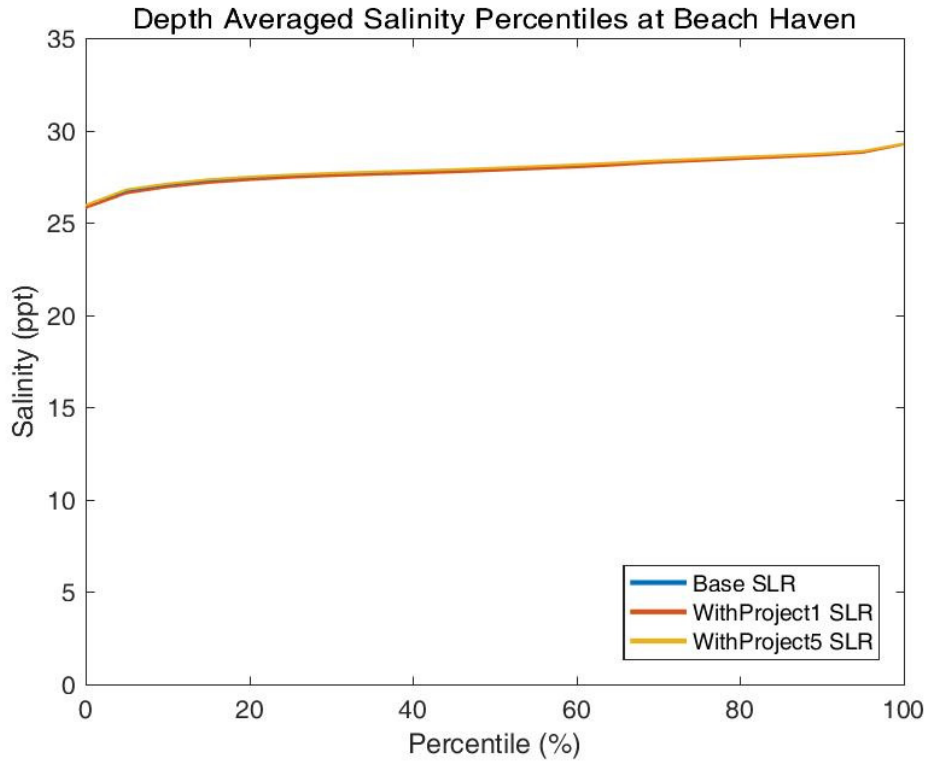


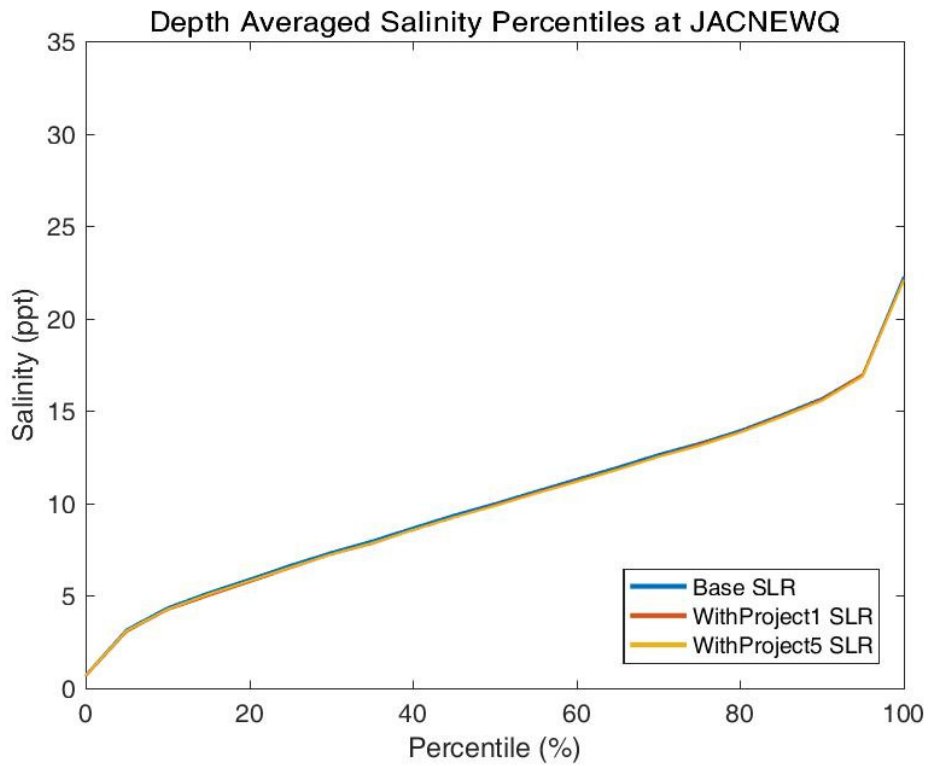
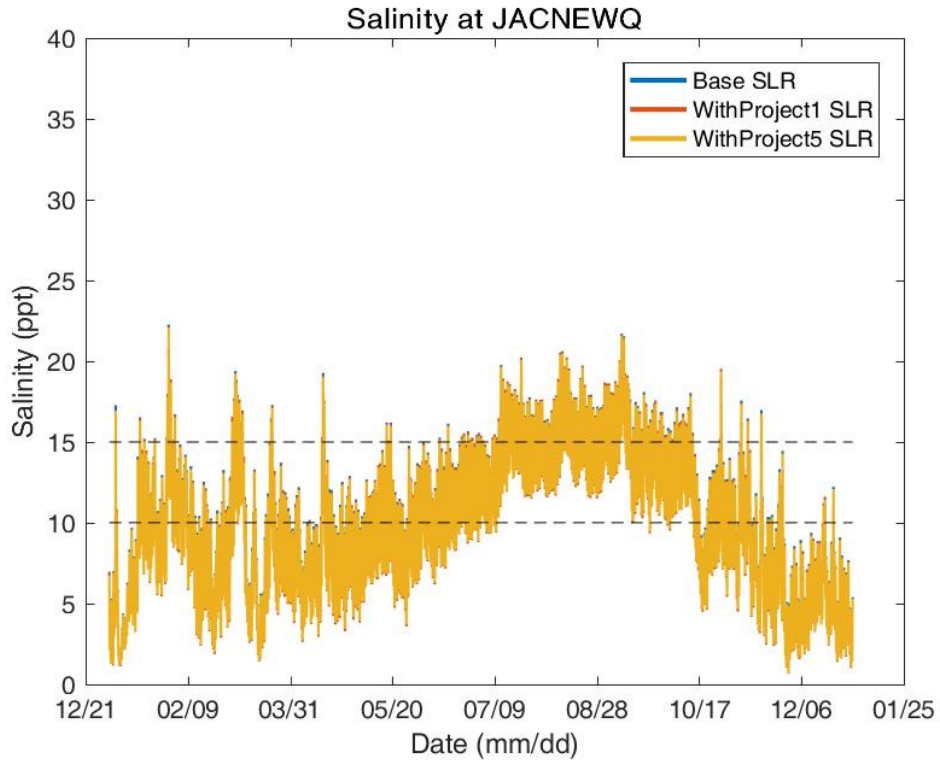


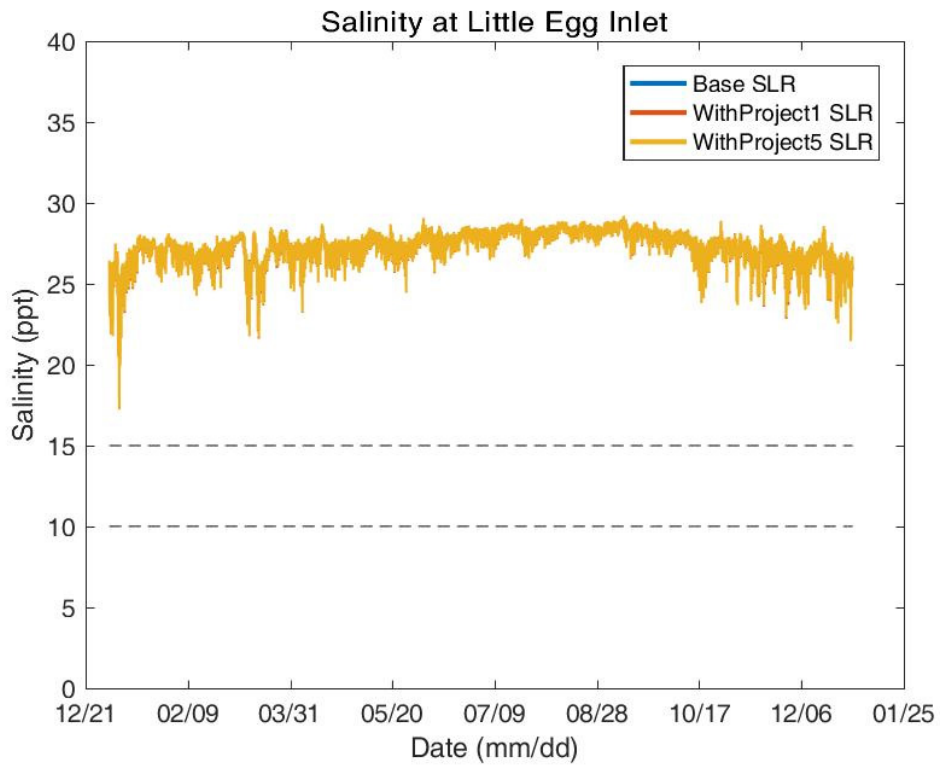
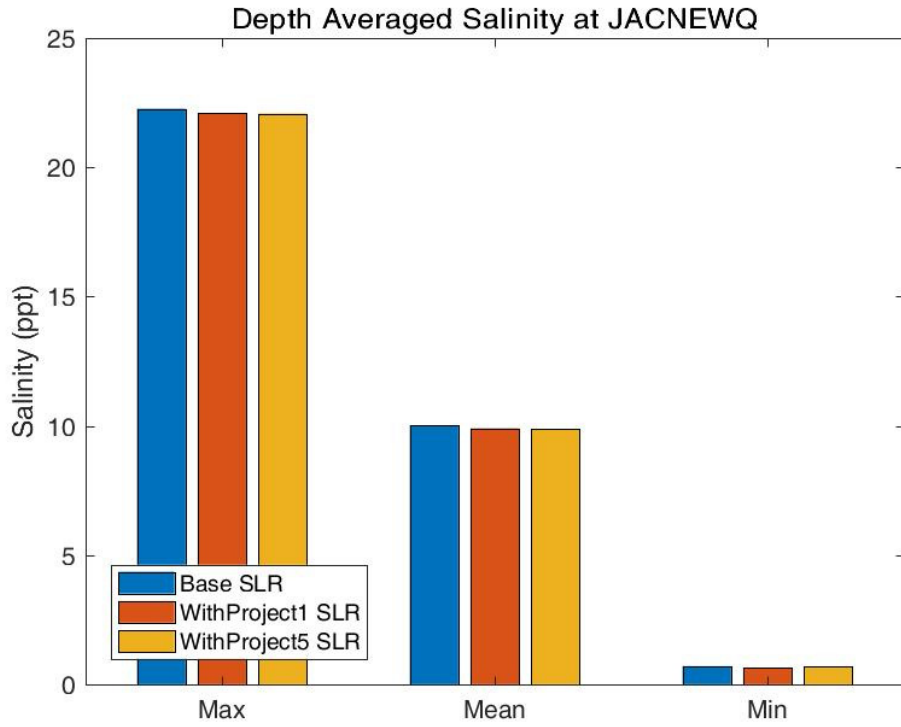


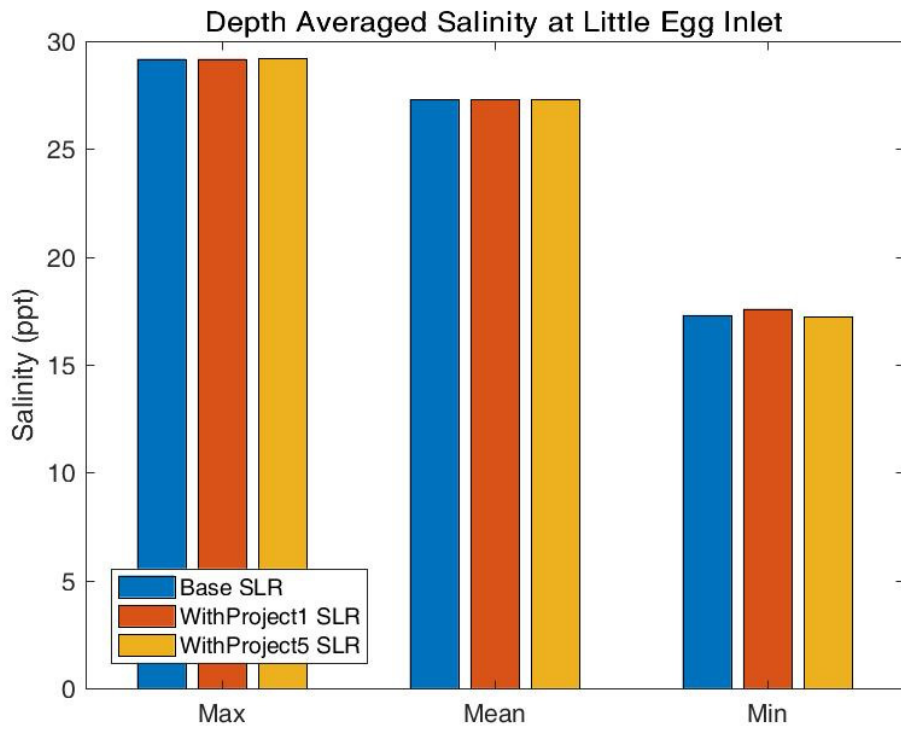
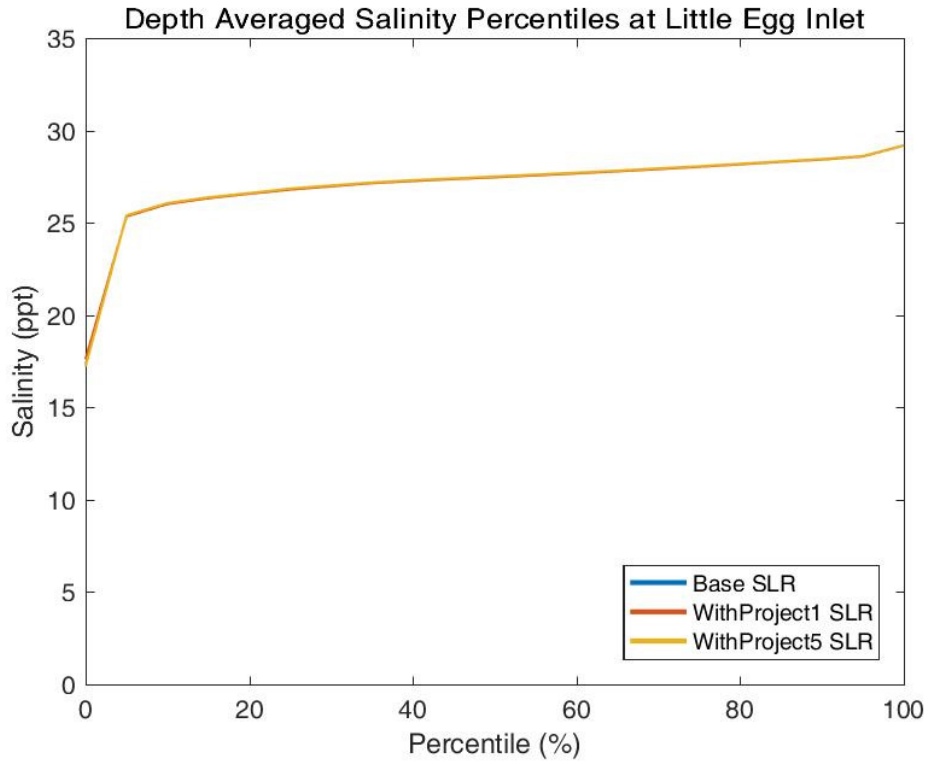


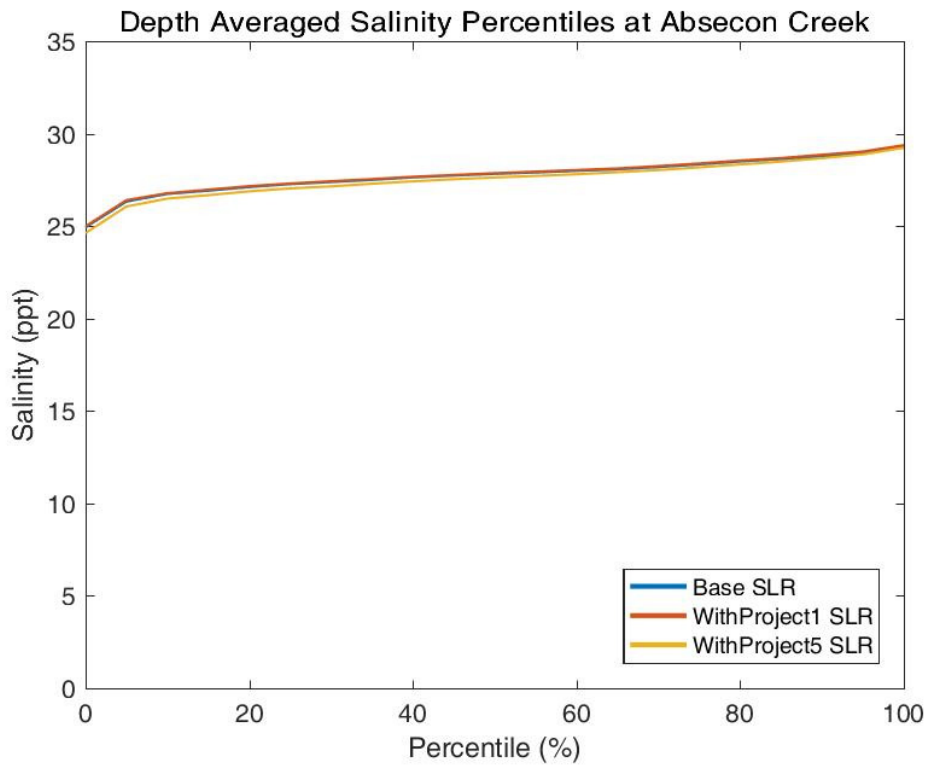
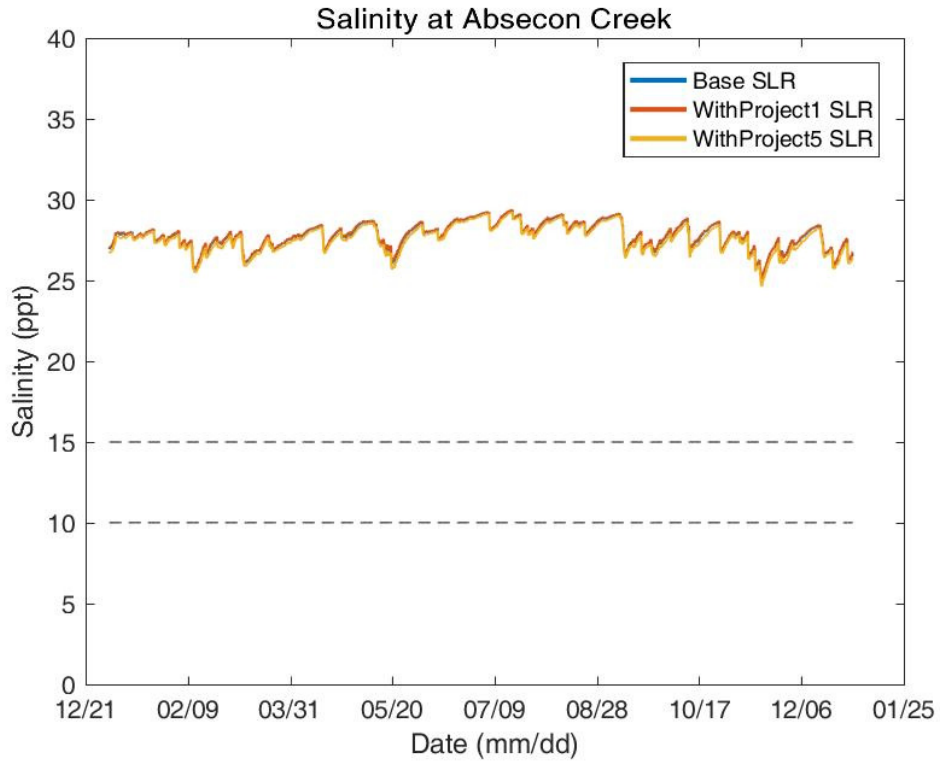


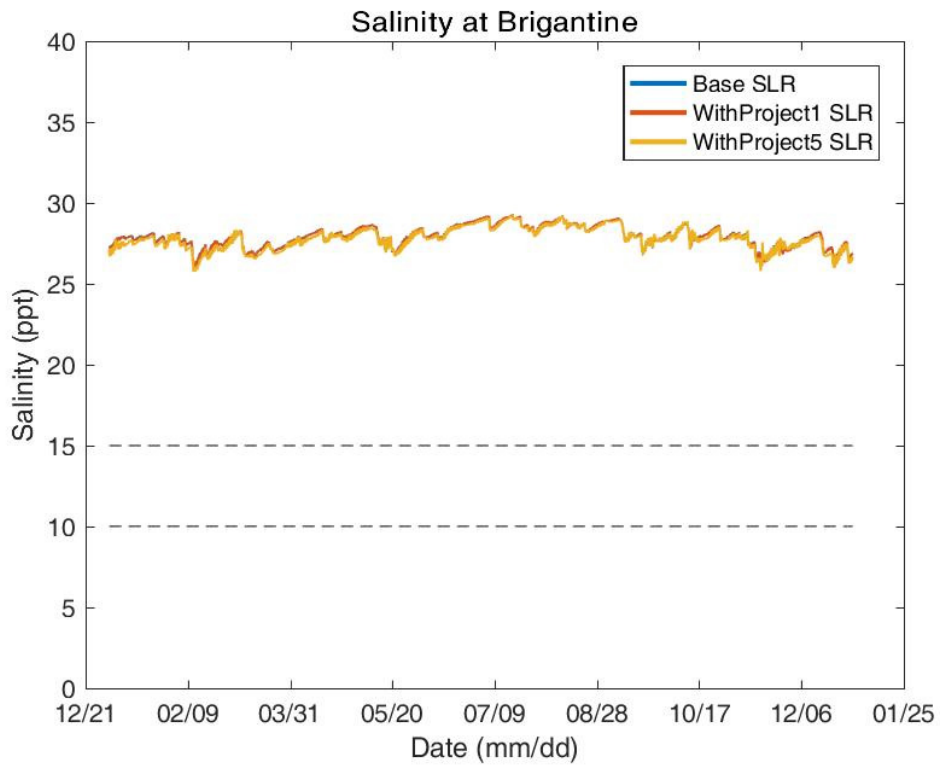
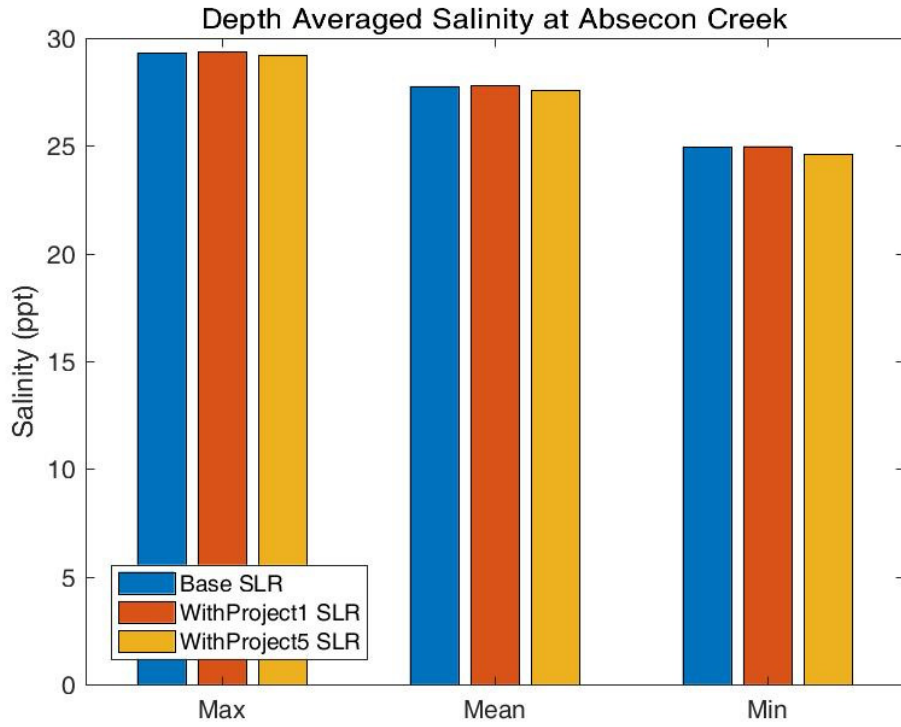


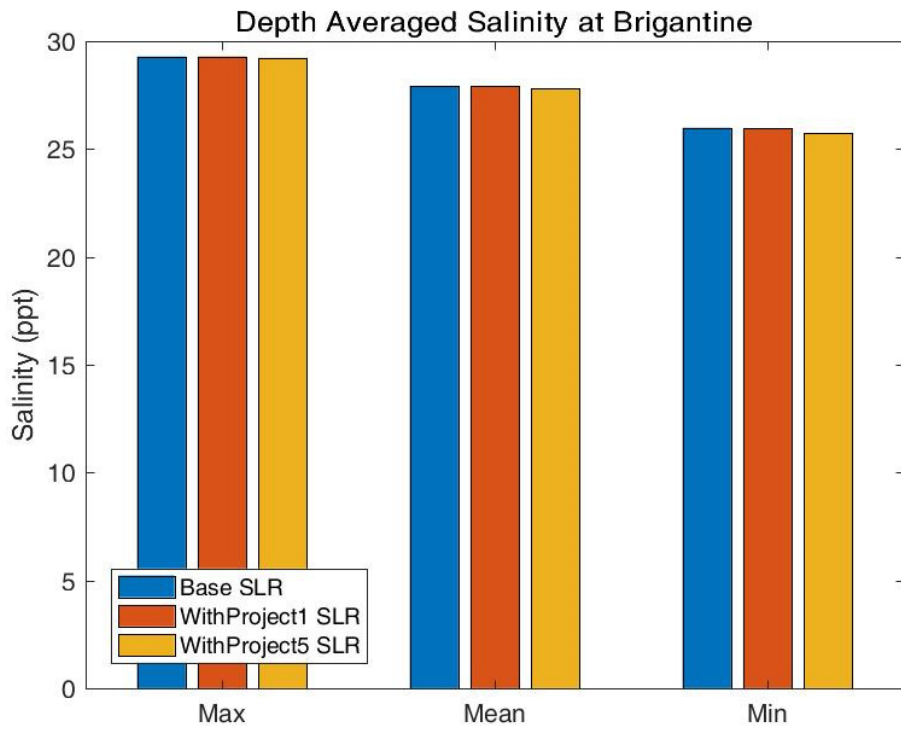
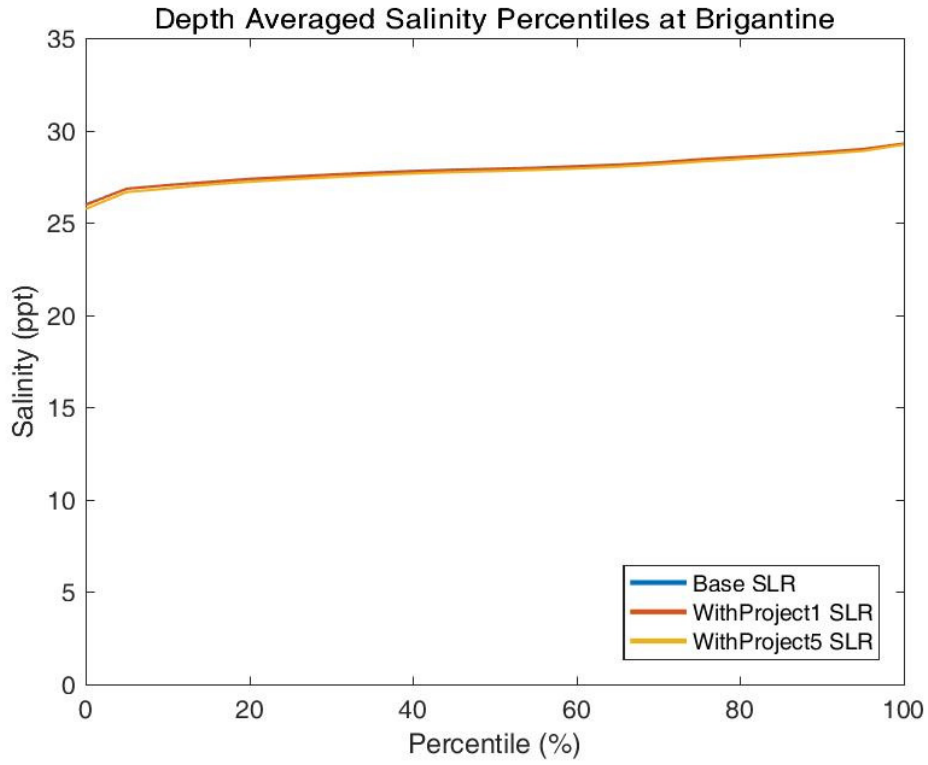


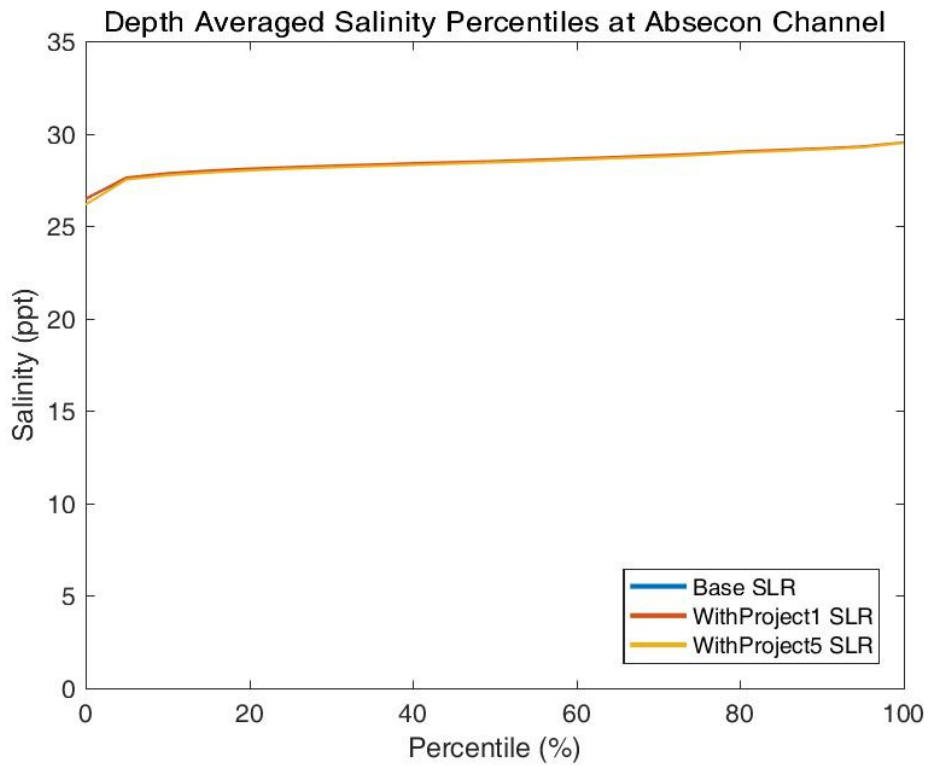
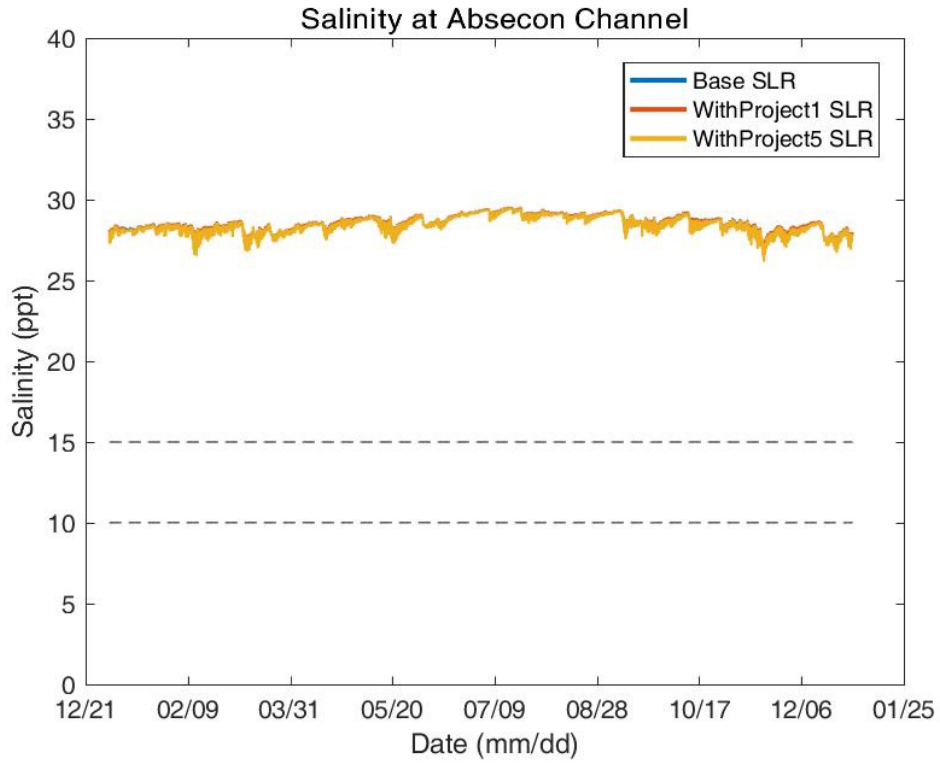


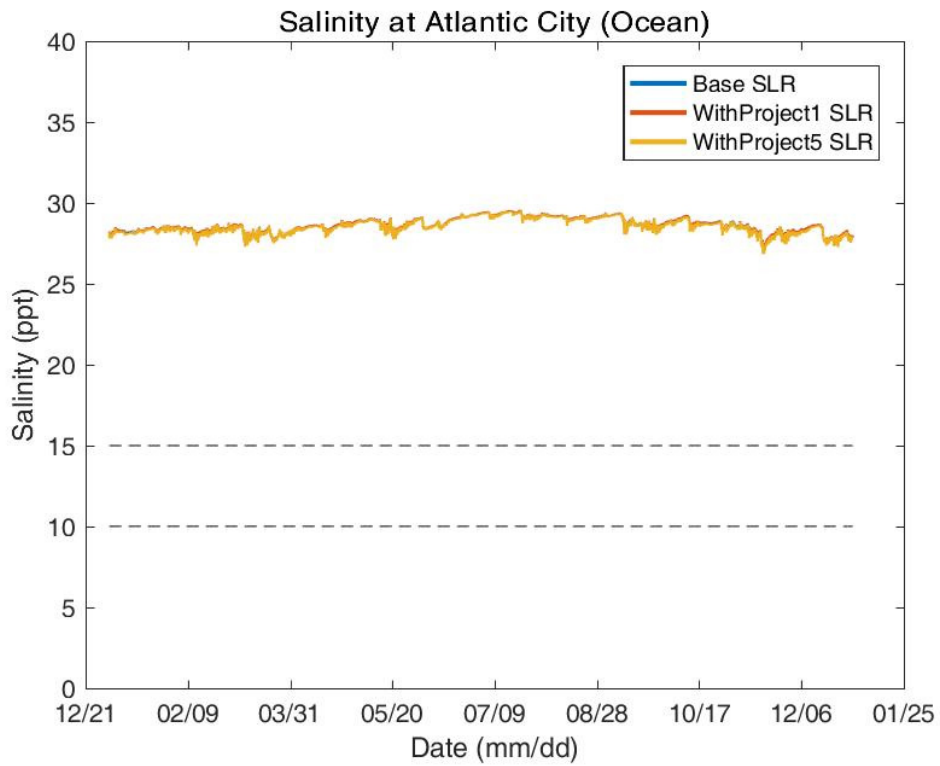
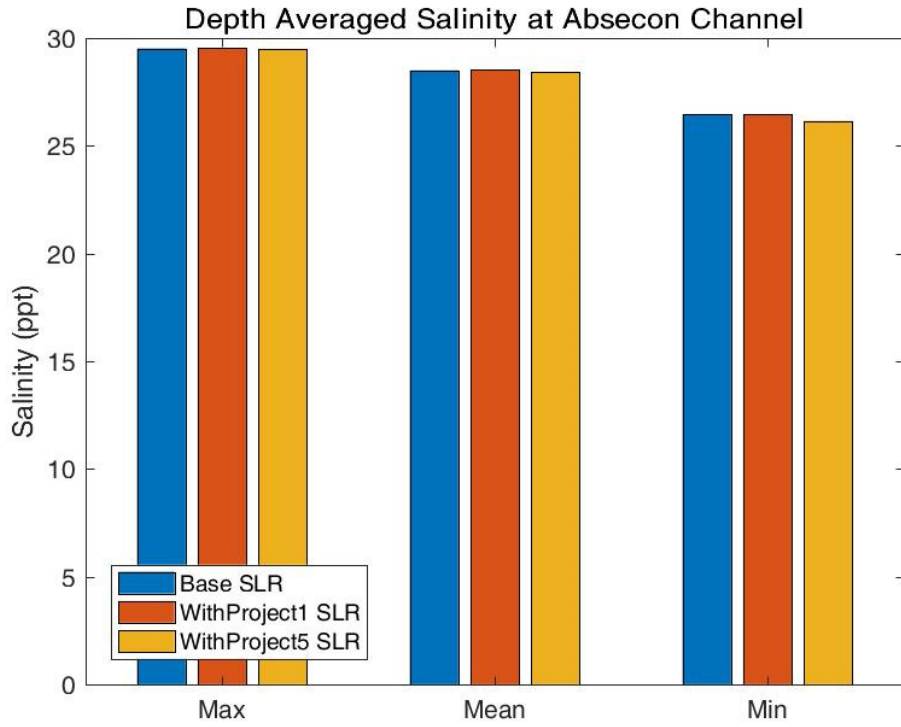


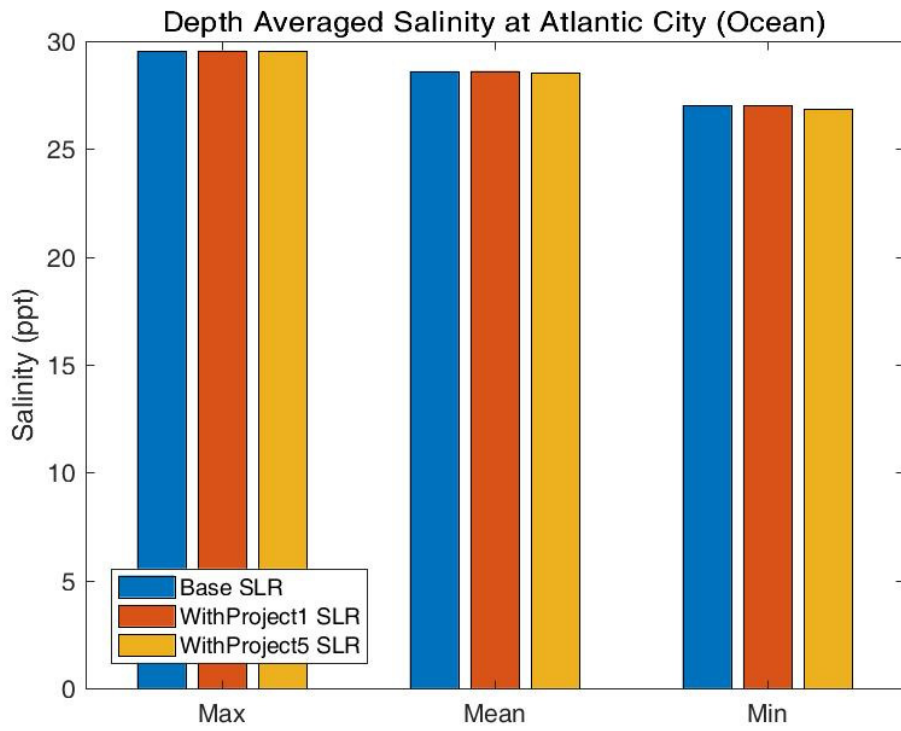
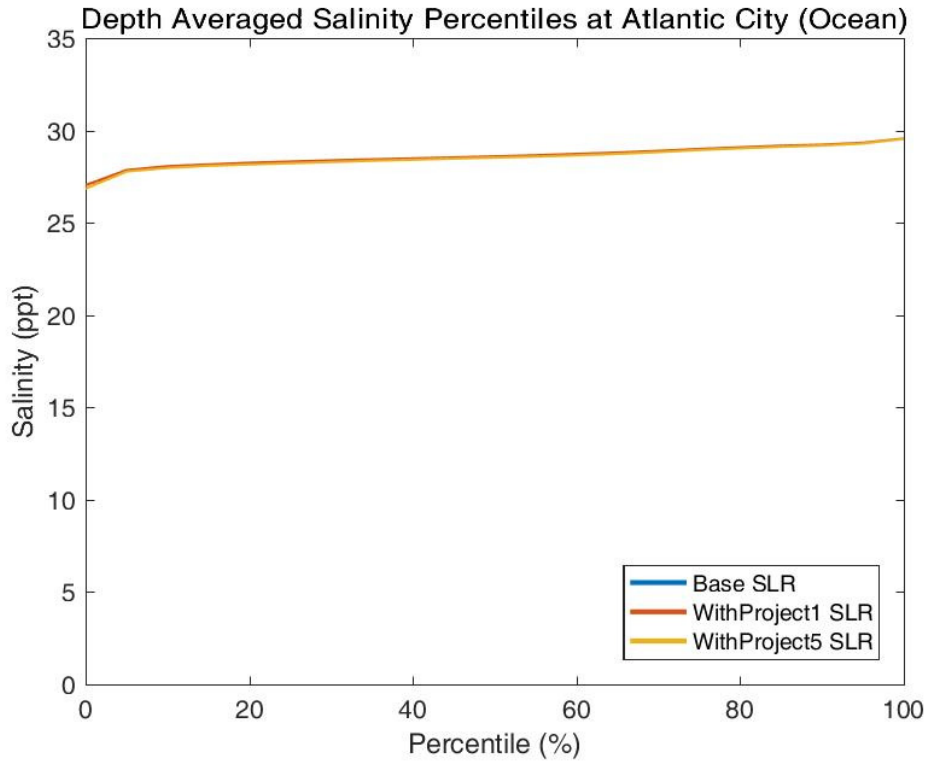


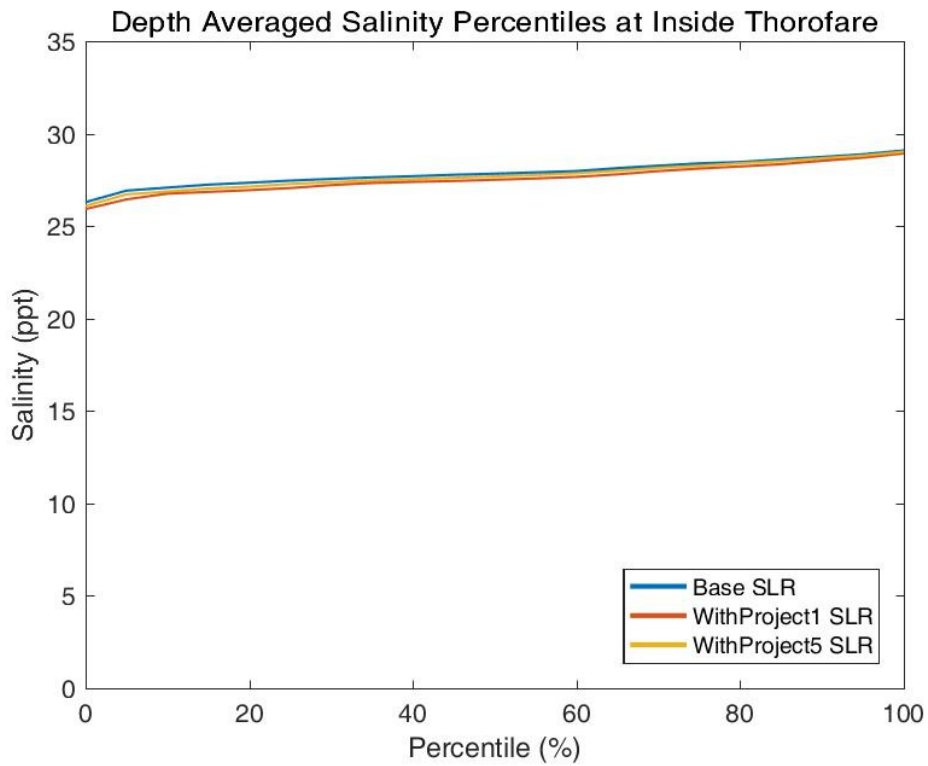
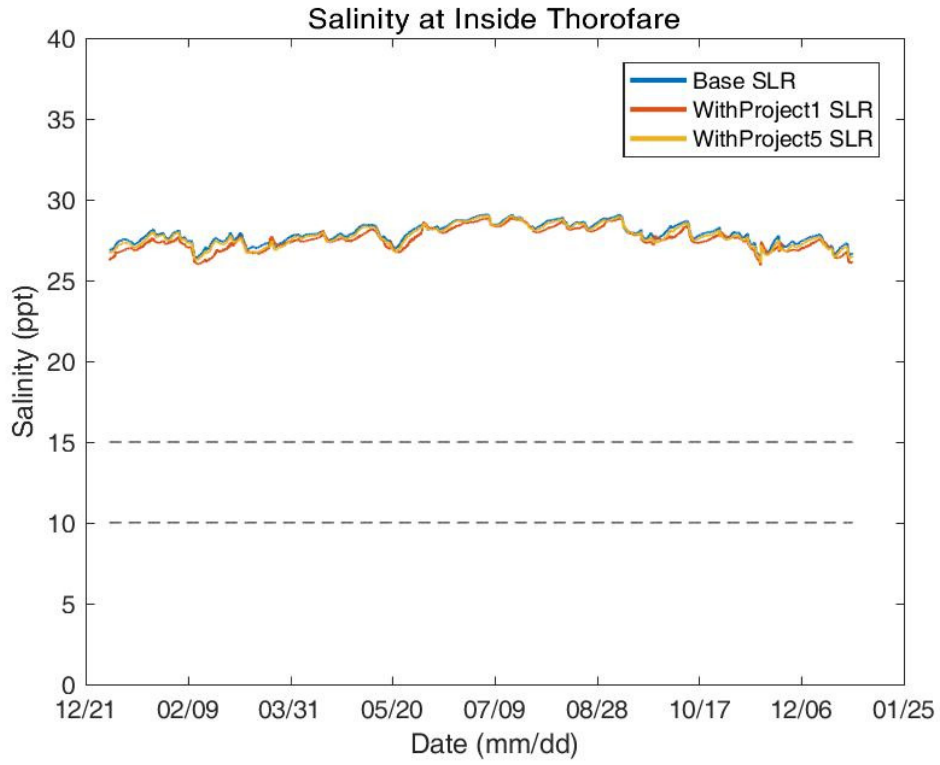


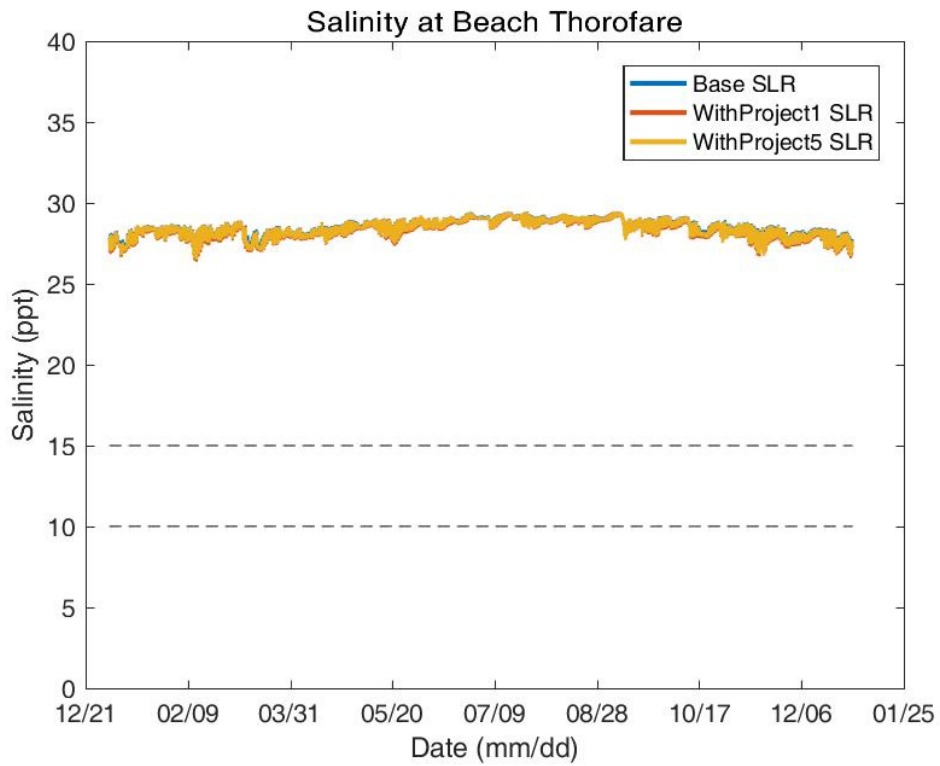
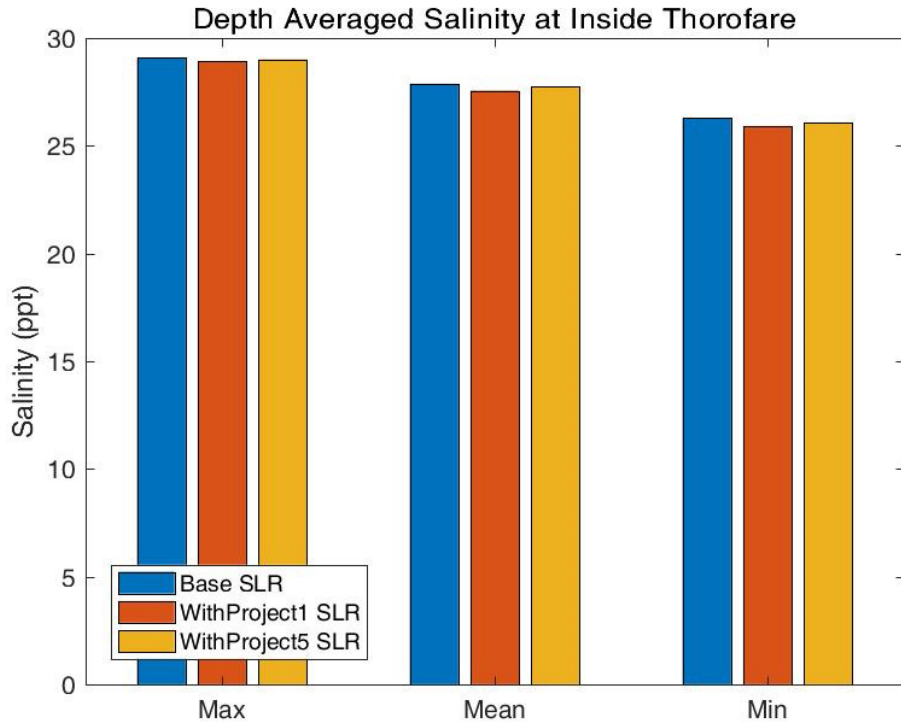


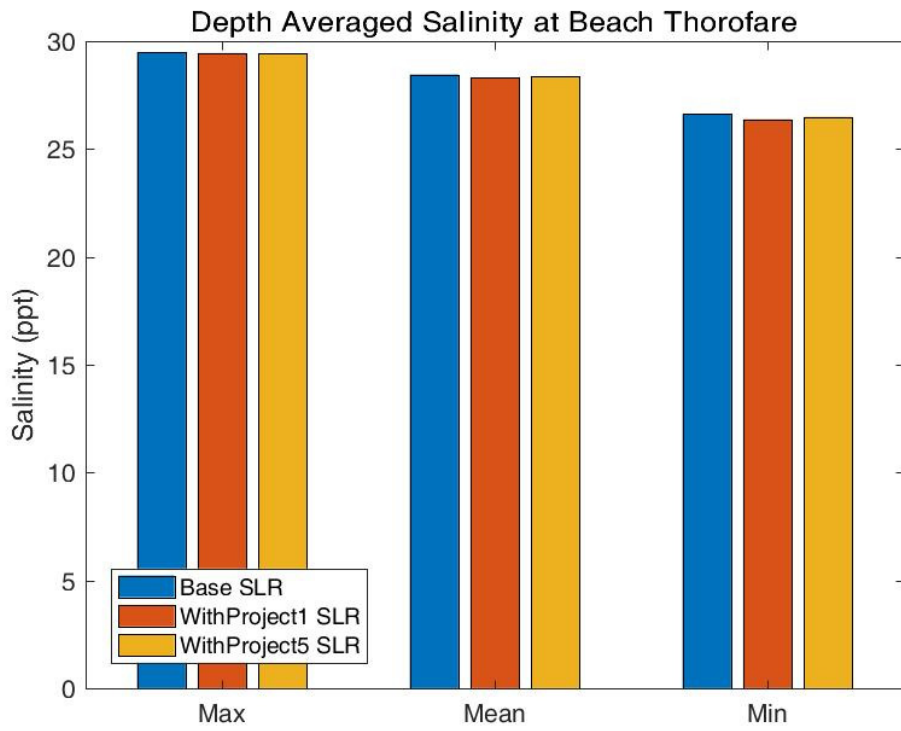
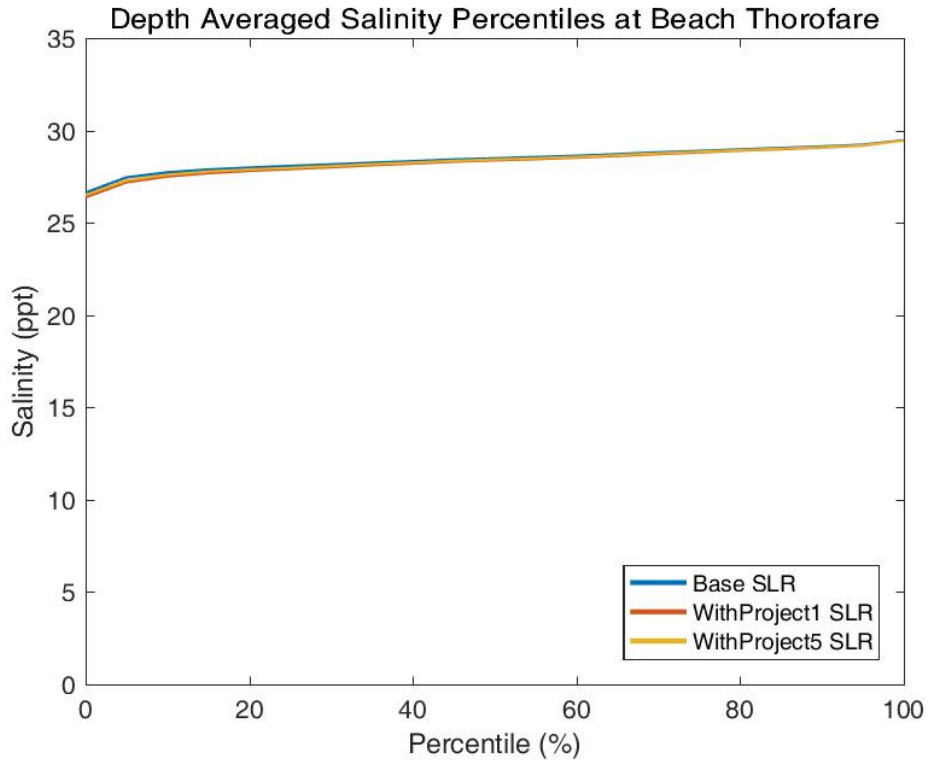


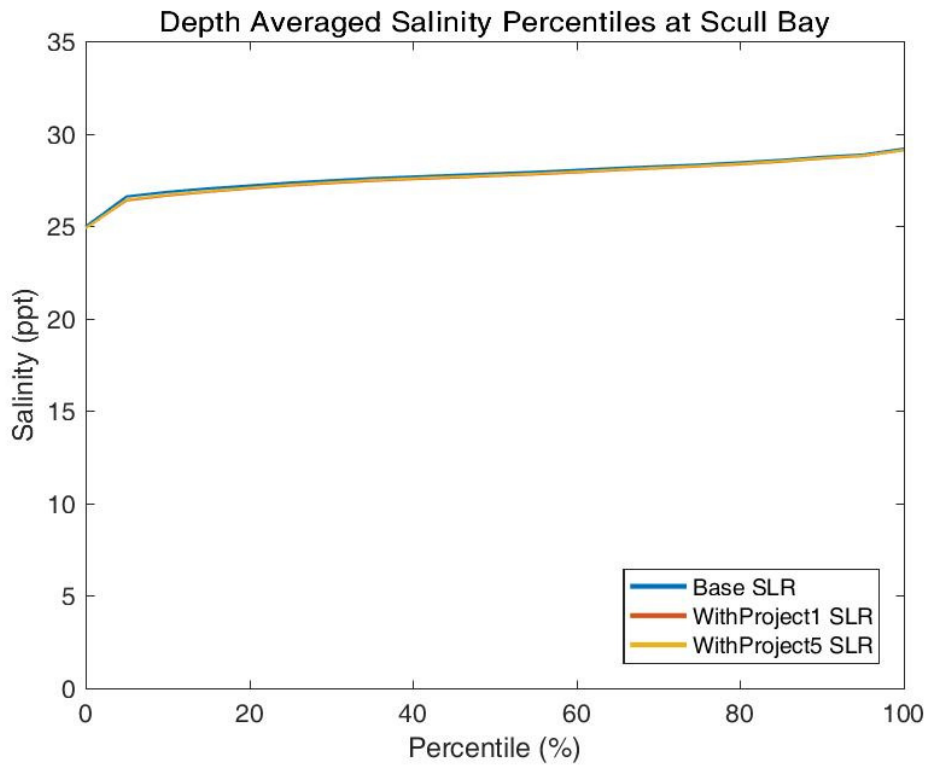
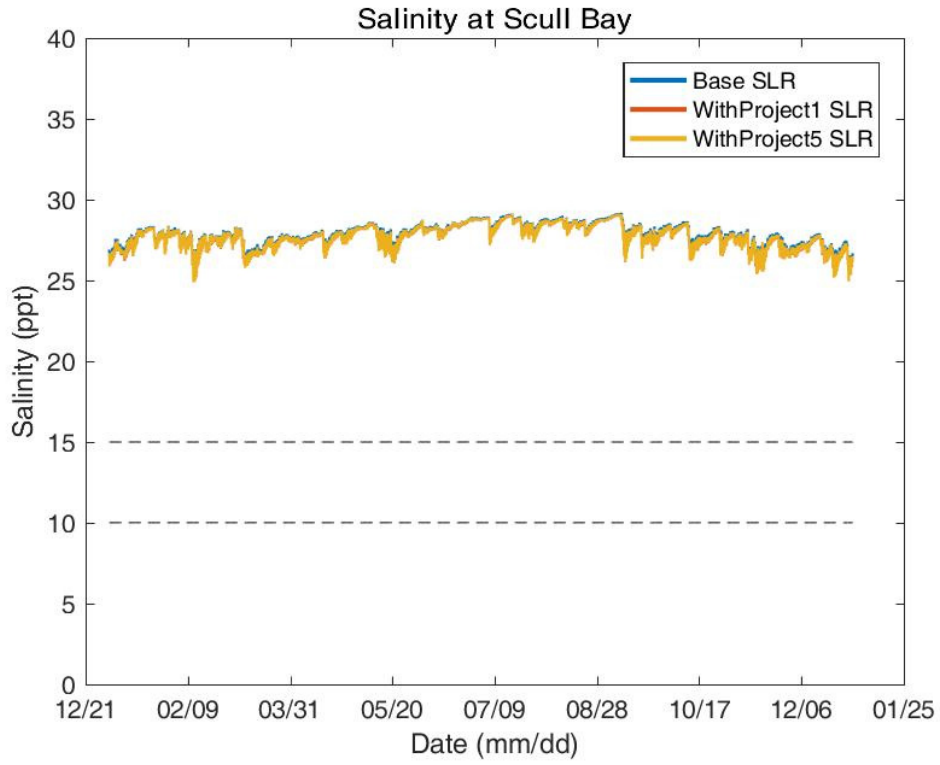


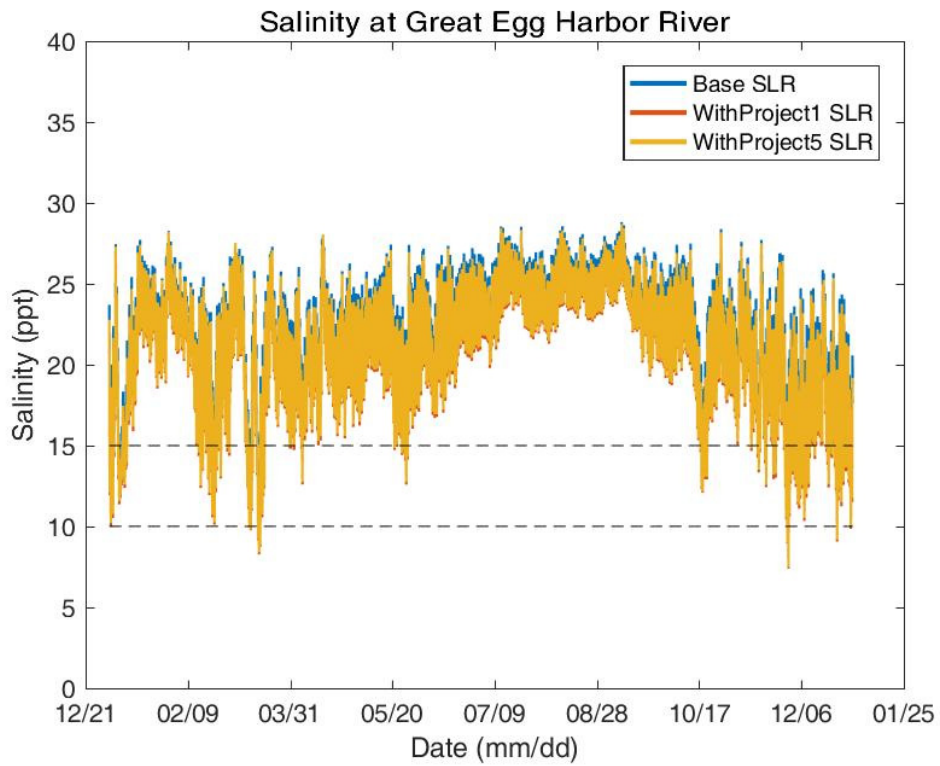
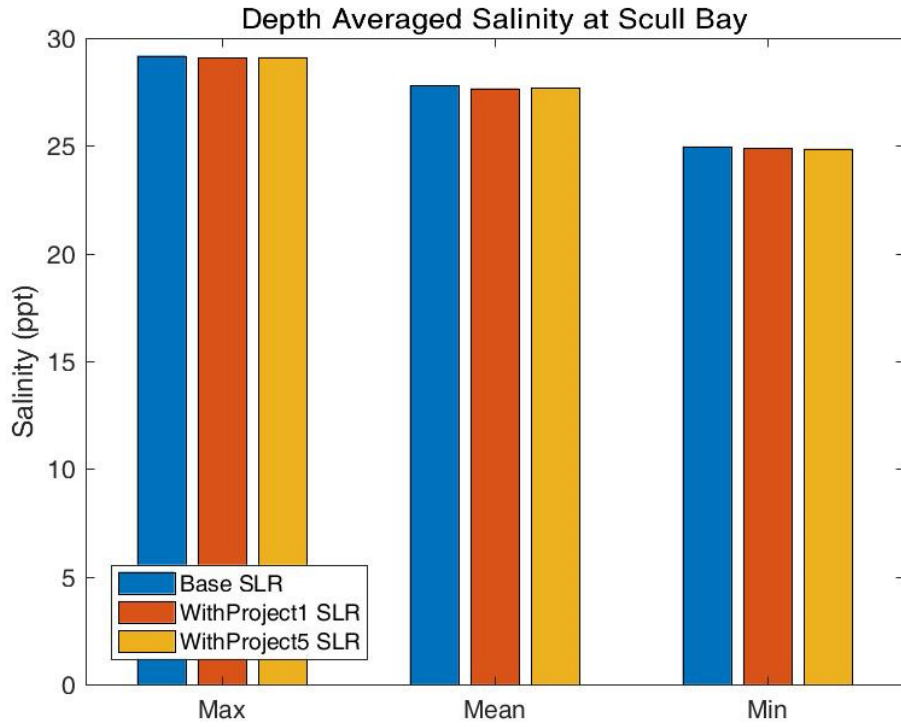


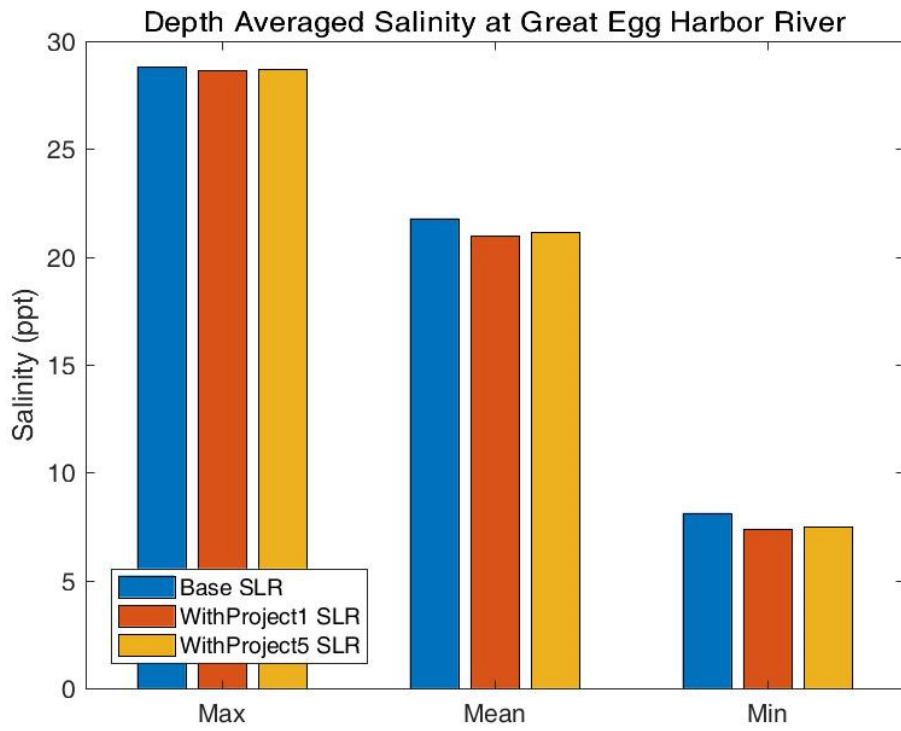
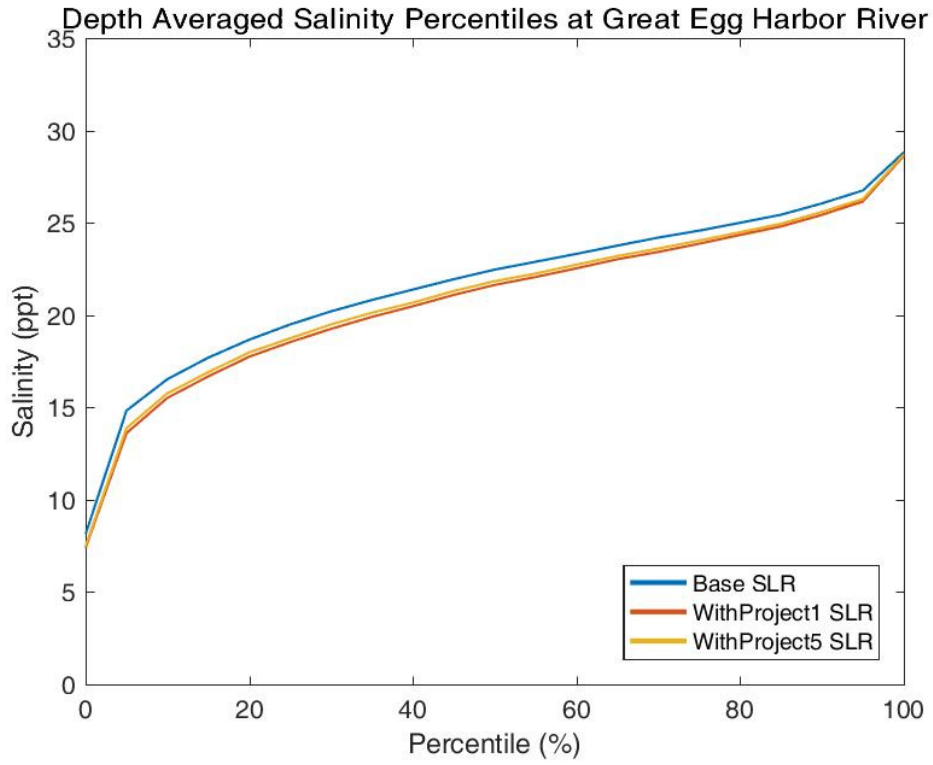


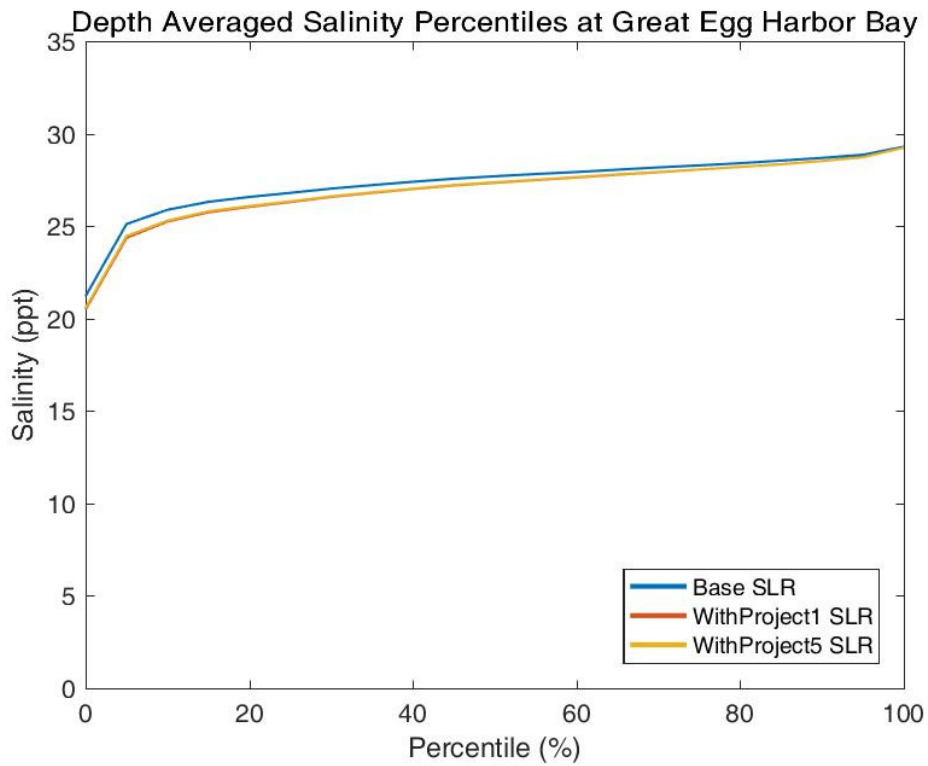
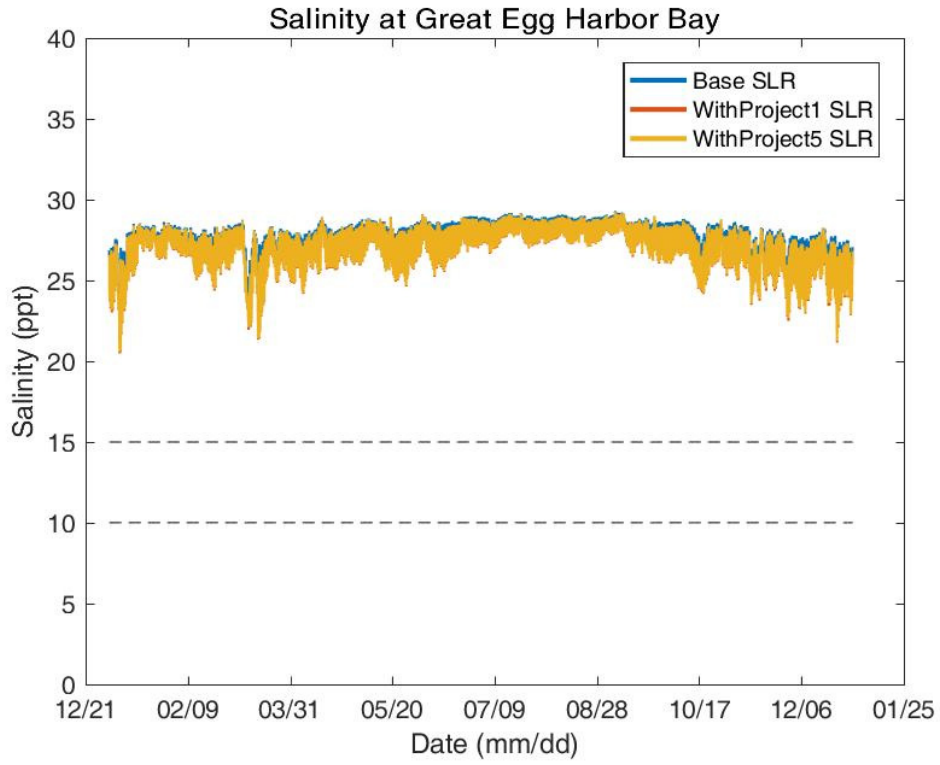


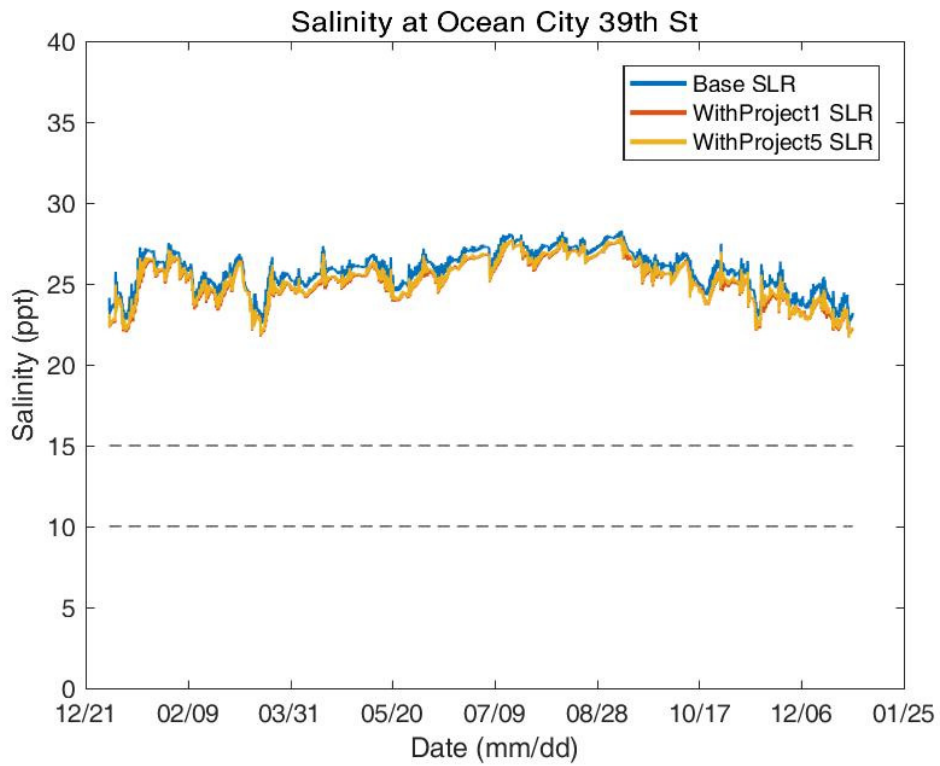
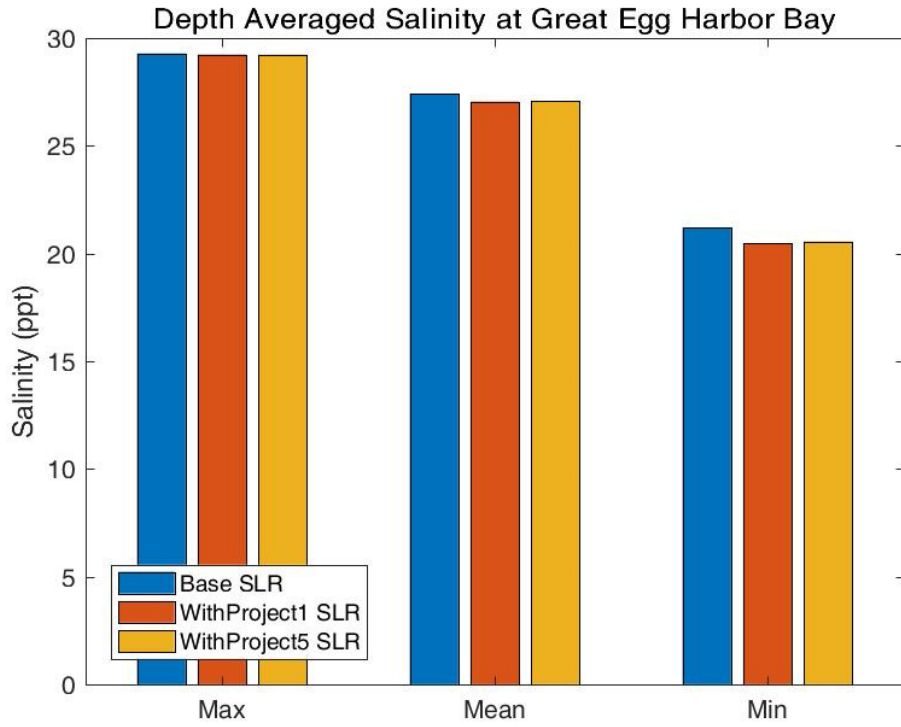


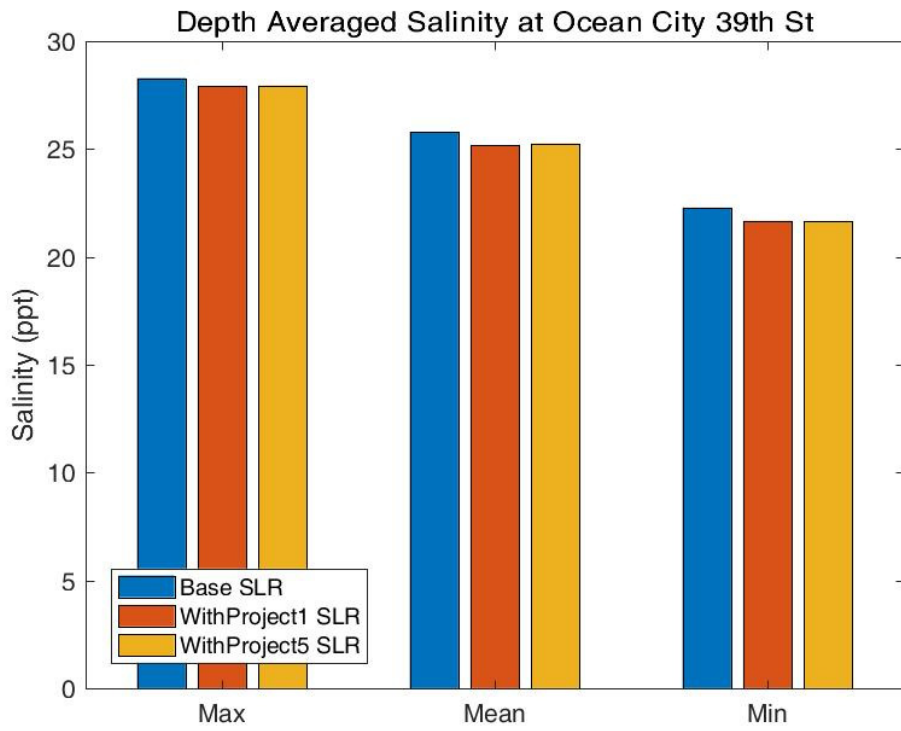
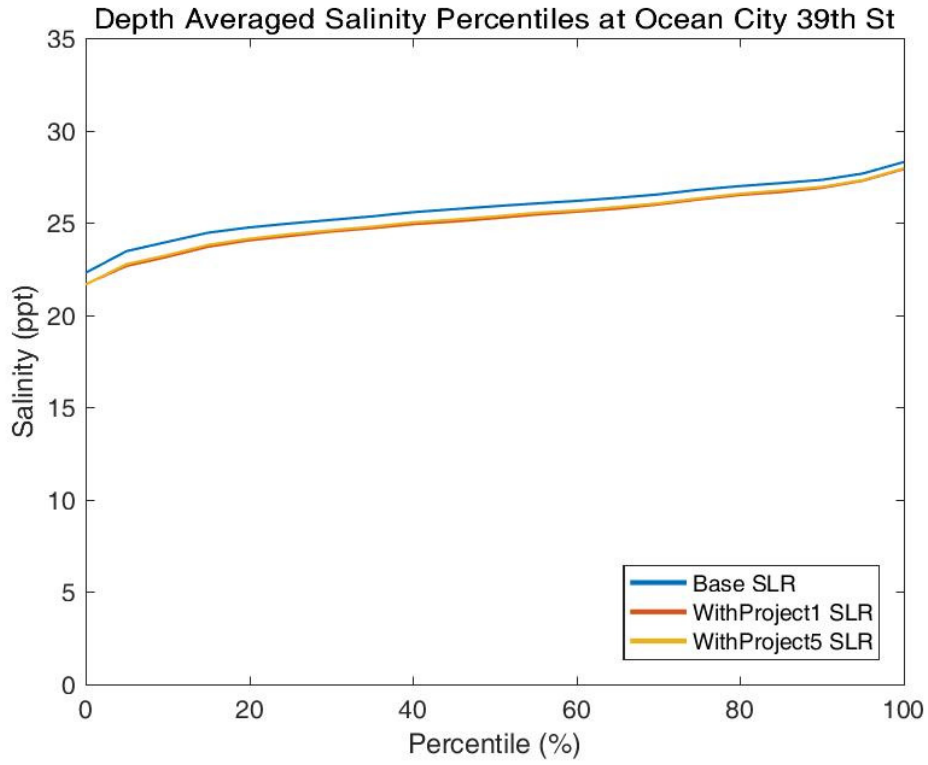


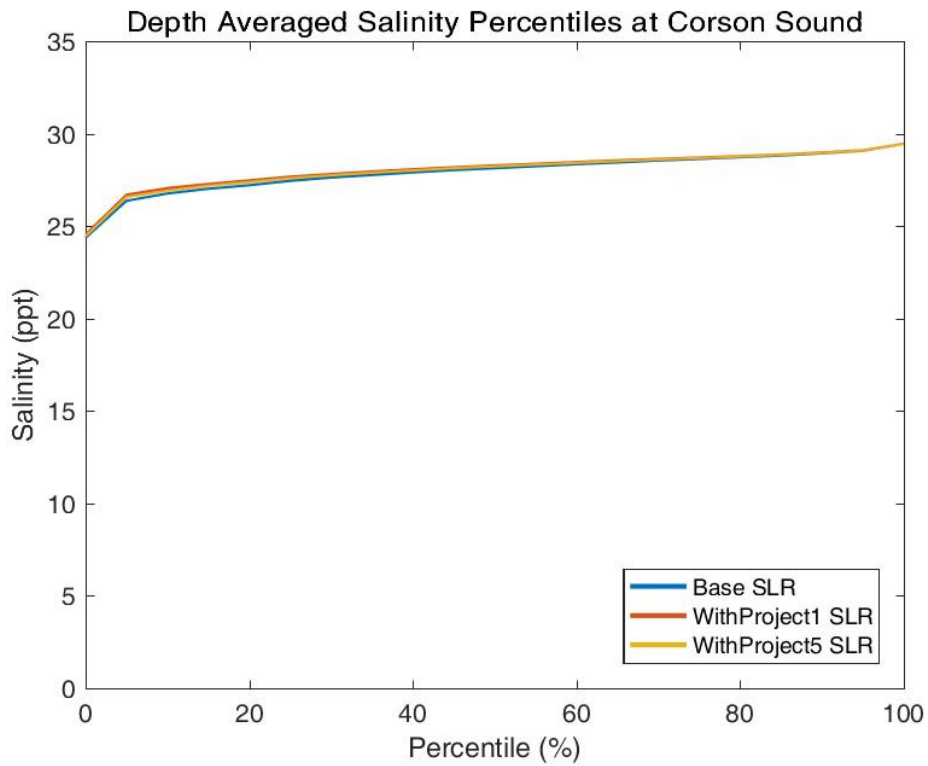
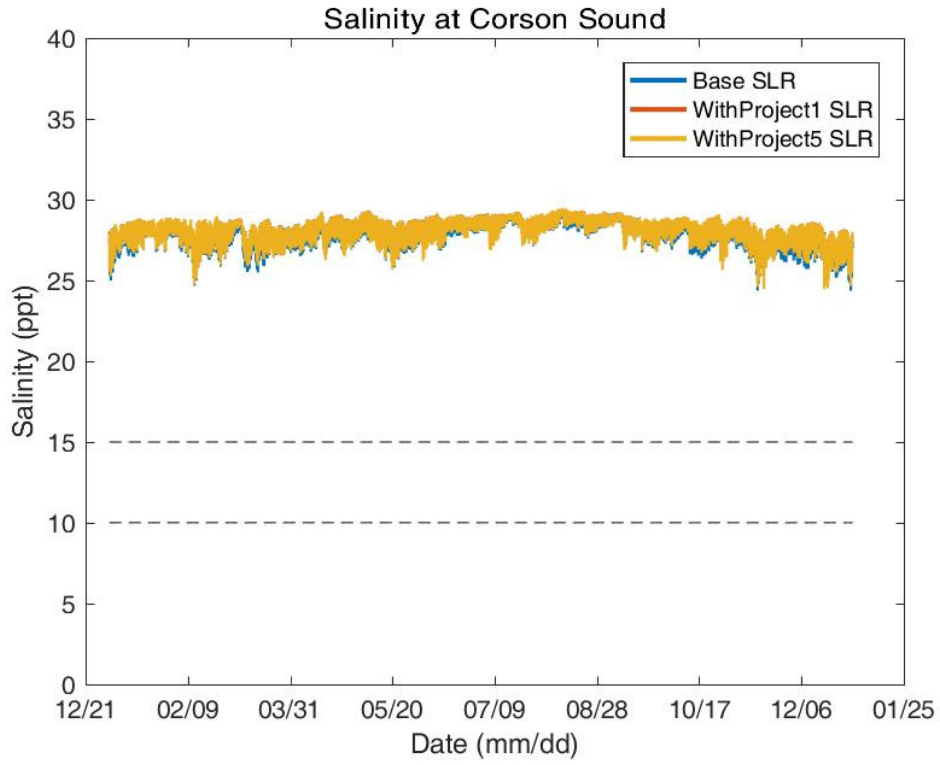


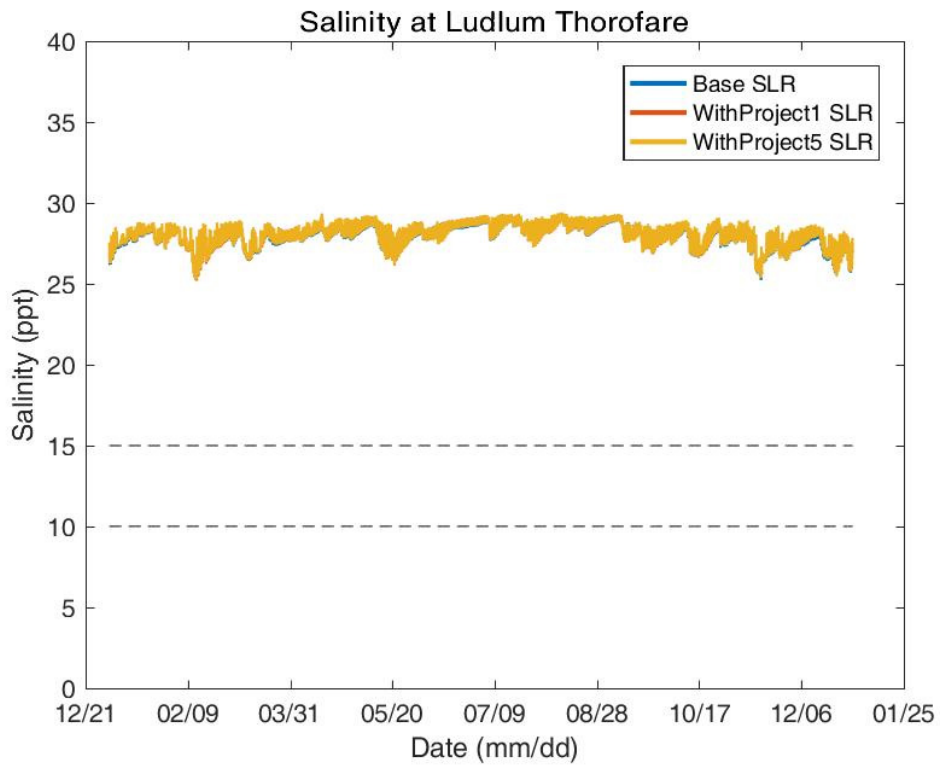
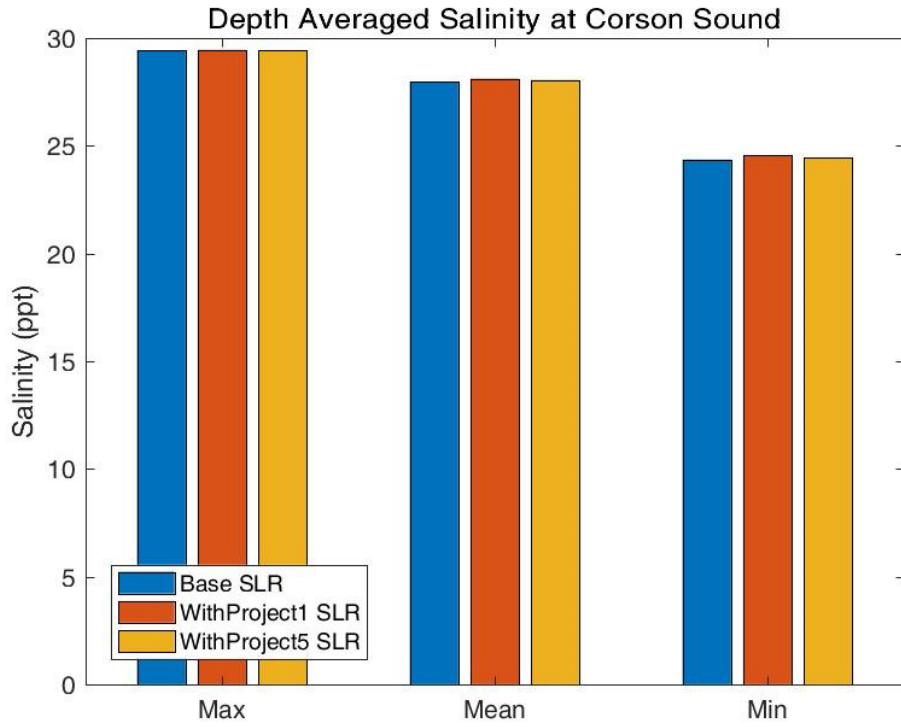


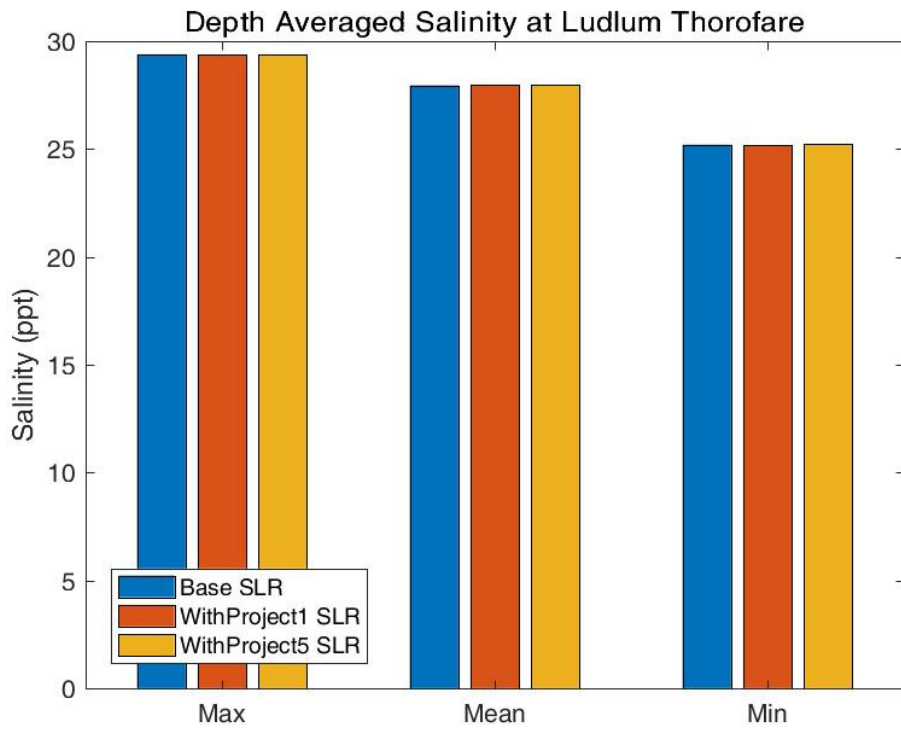
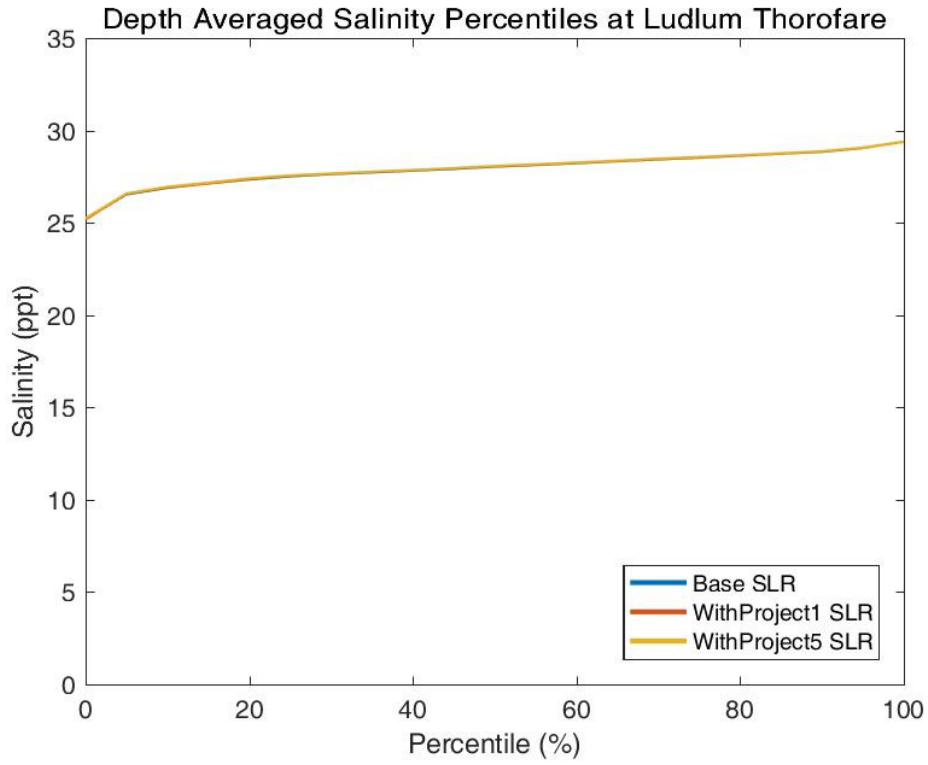


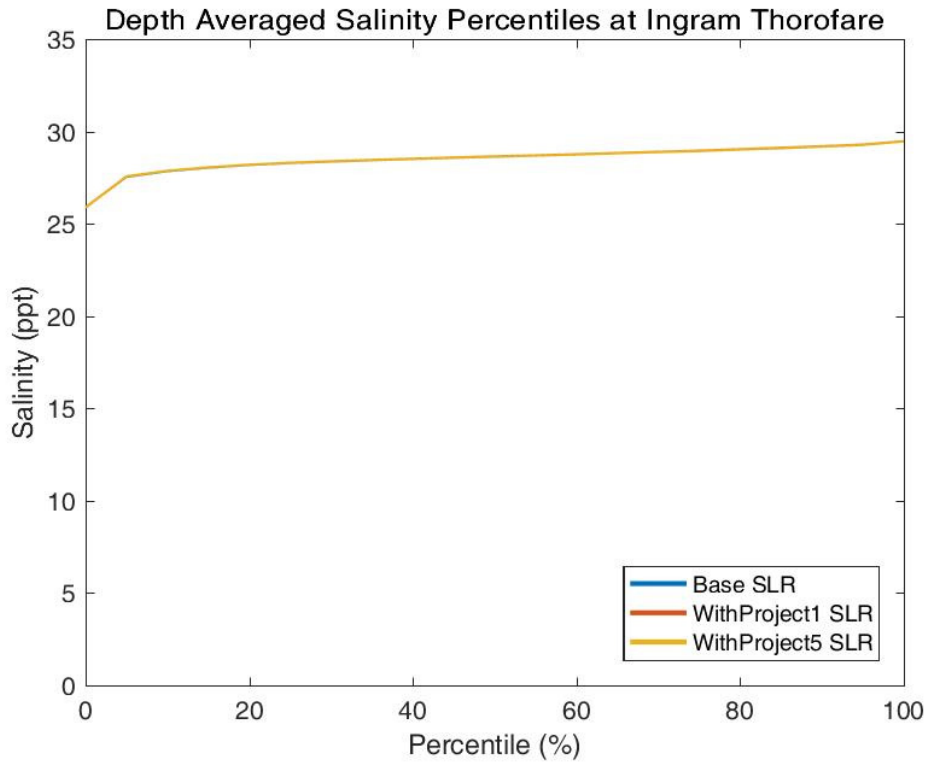
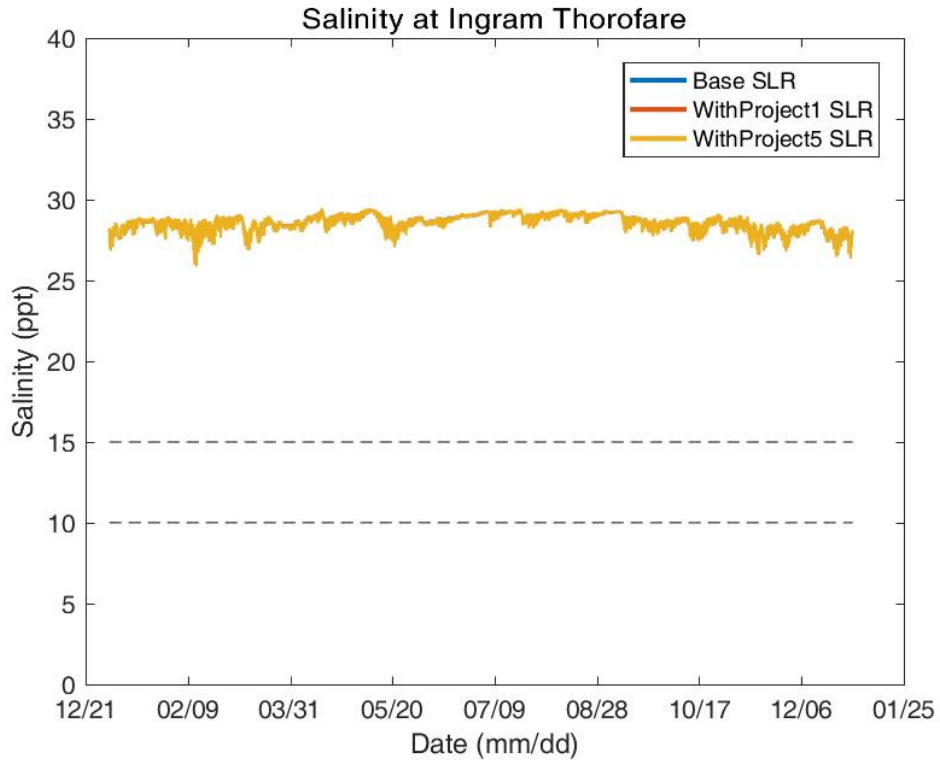


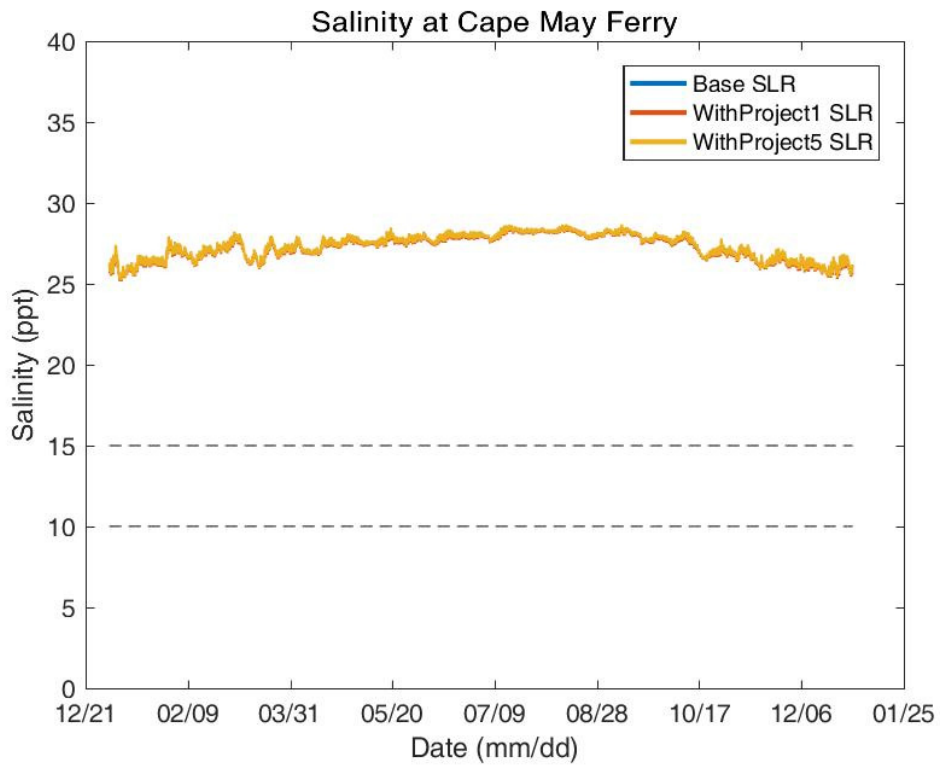
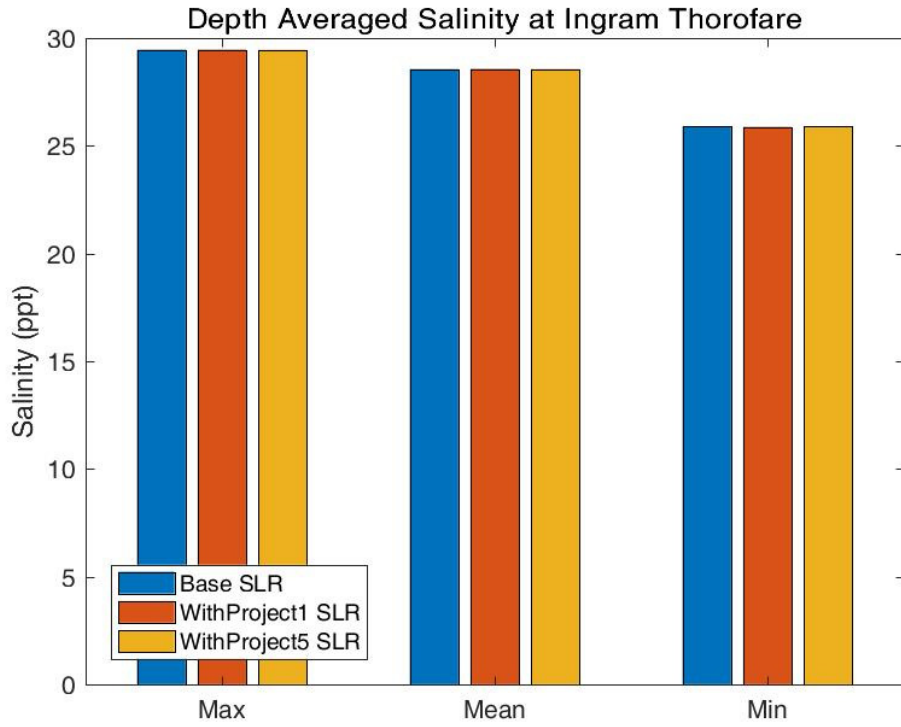


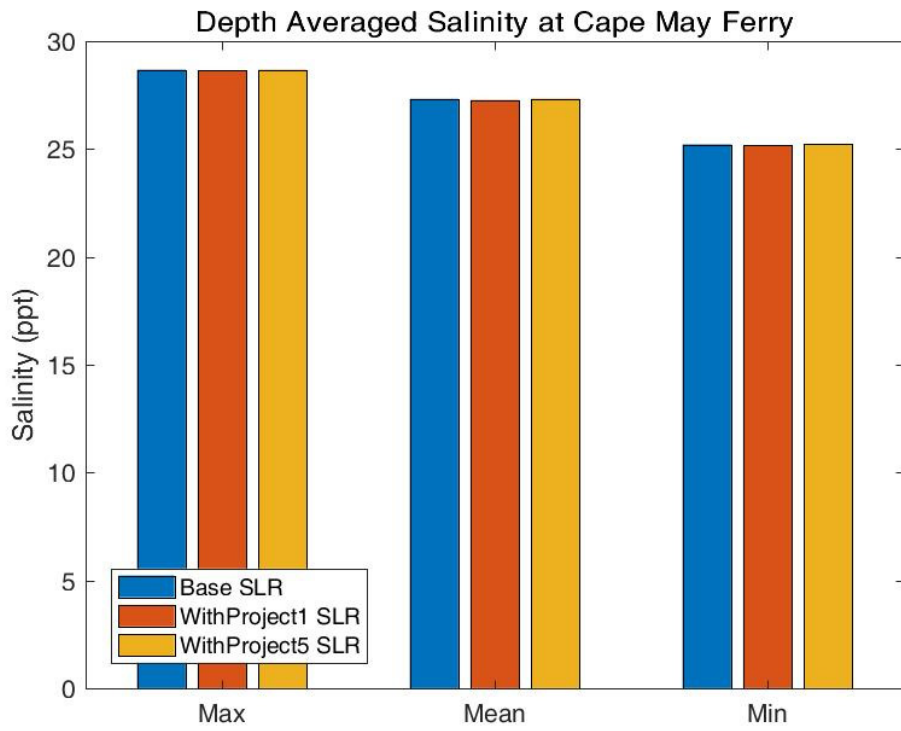
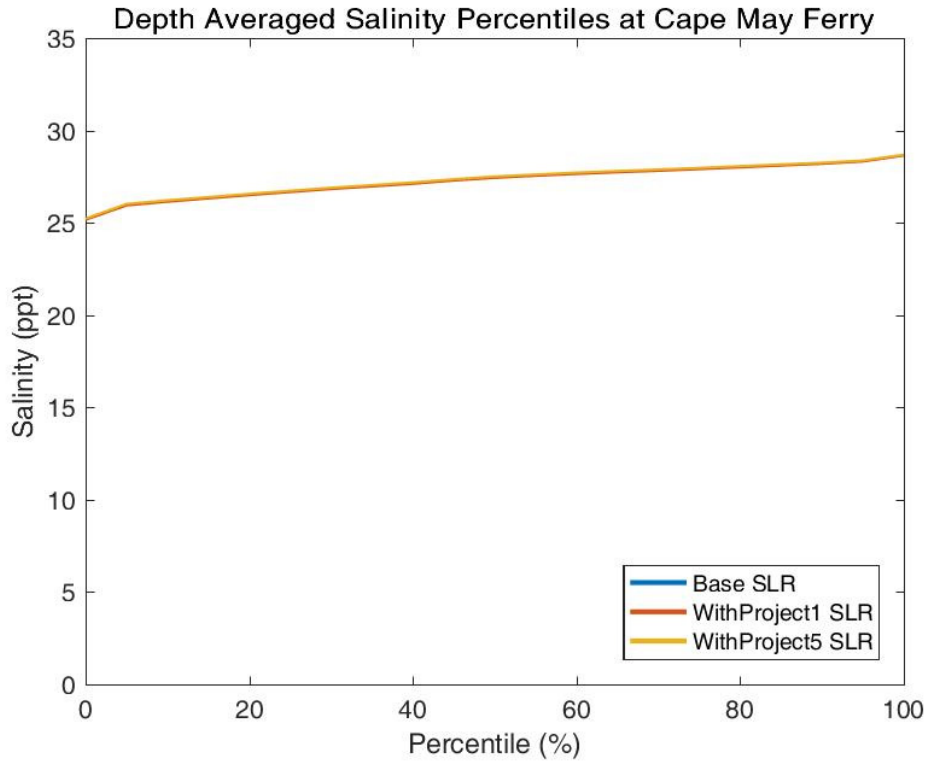


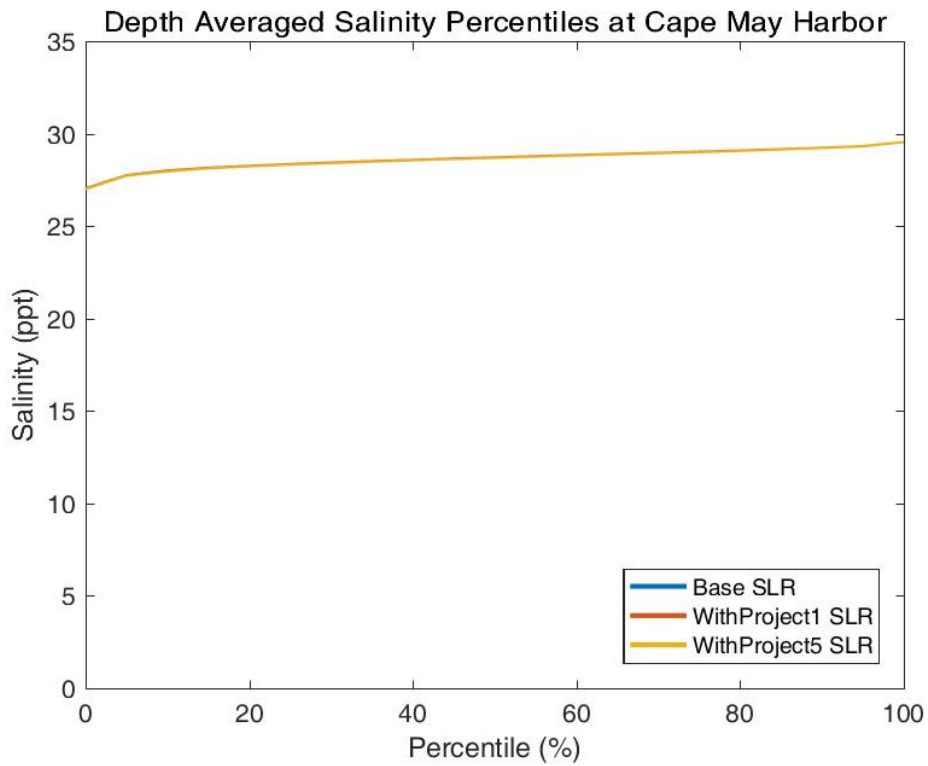
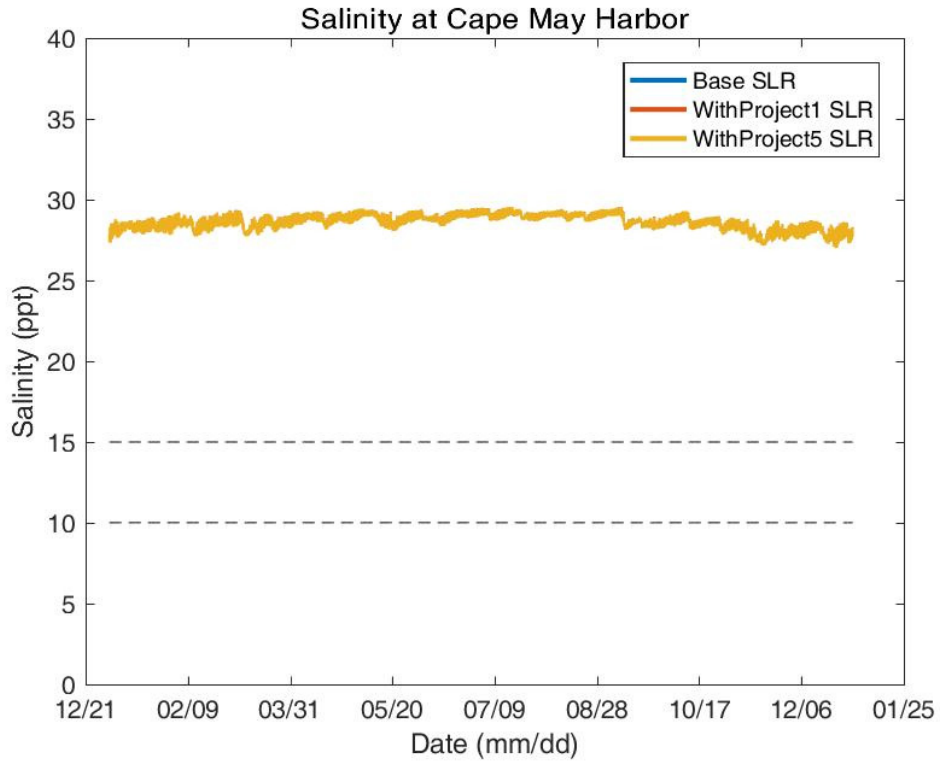


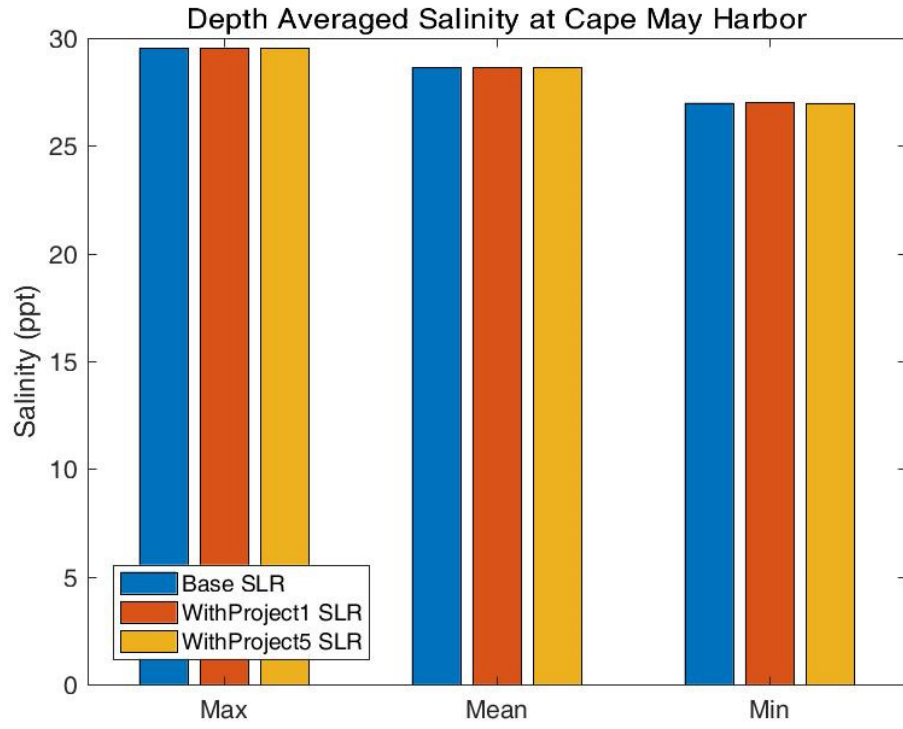












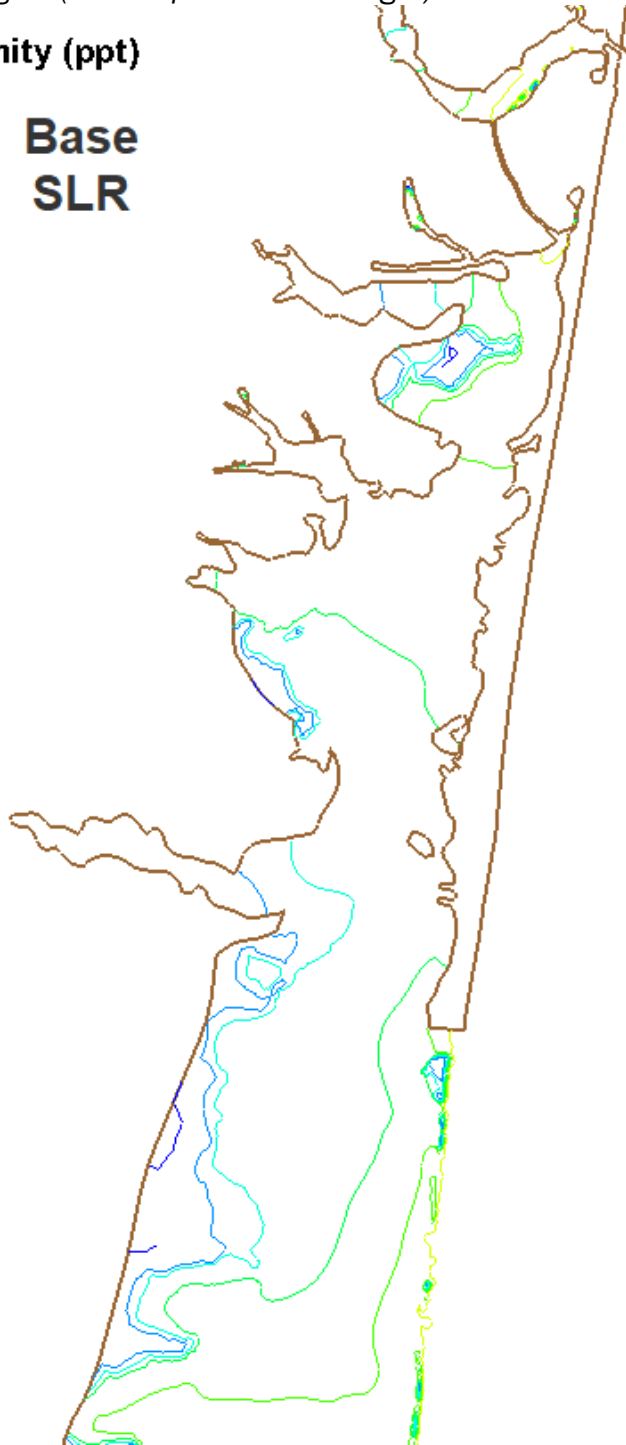
Regional Mean with Sea Level Rise

Northern Region (Manasquan and Barnegat)

Mean Salinity (ppt)

- 35.0
- 30.0
- 25.0
- 20.0
- 15.0
- 10.0
- 5.0
- 0.0

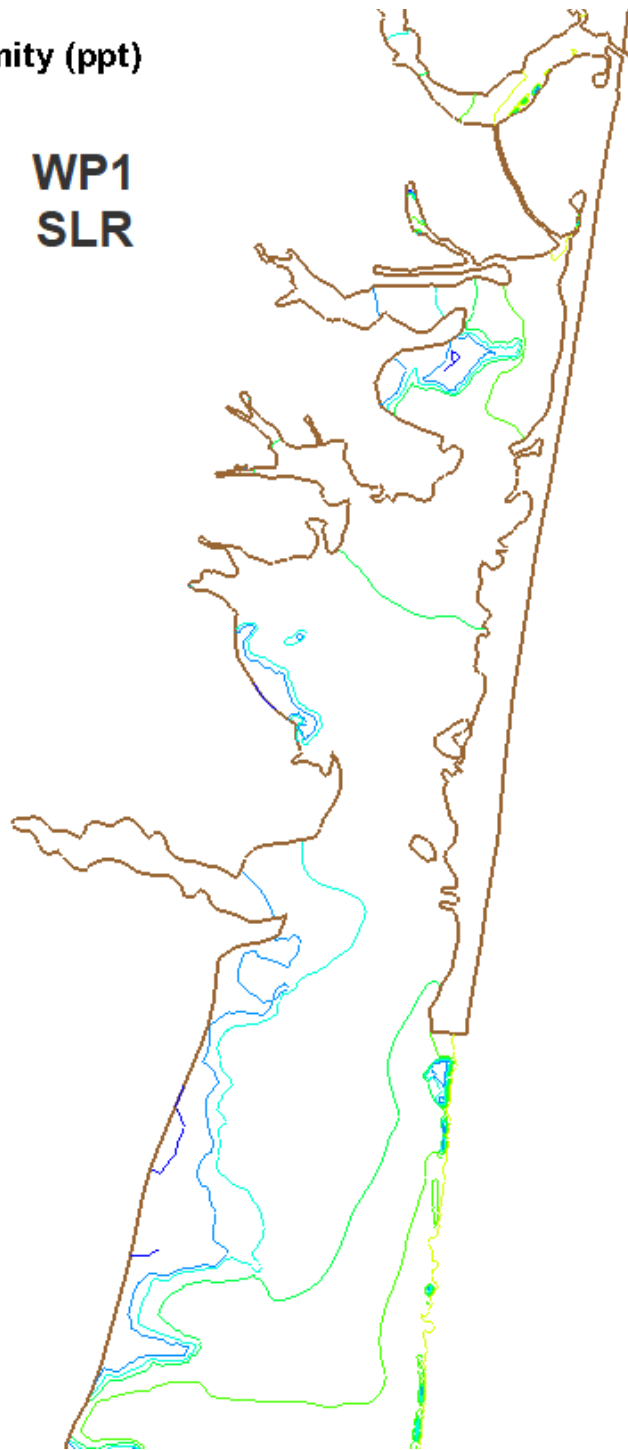
**Base
SLR**



Mean Salinity (ppt)

- 35.0
- 30.0
- 25.0
- 20.0
- 15.0
- 10.0
- 5.0
- 0.0

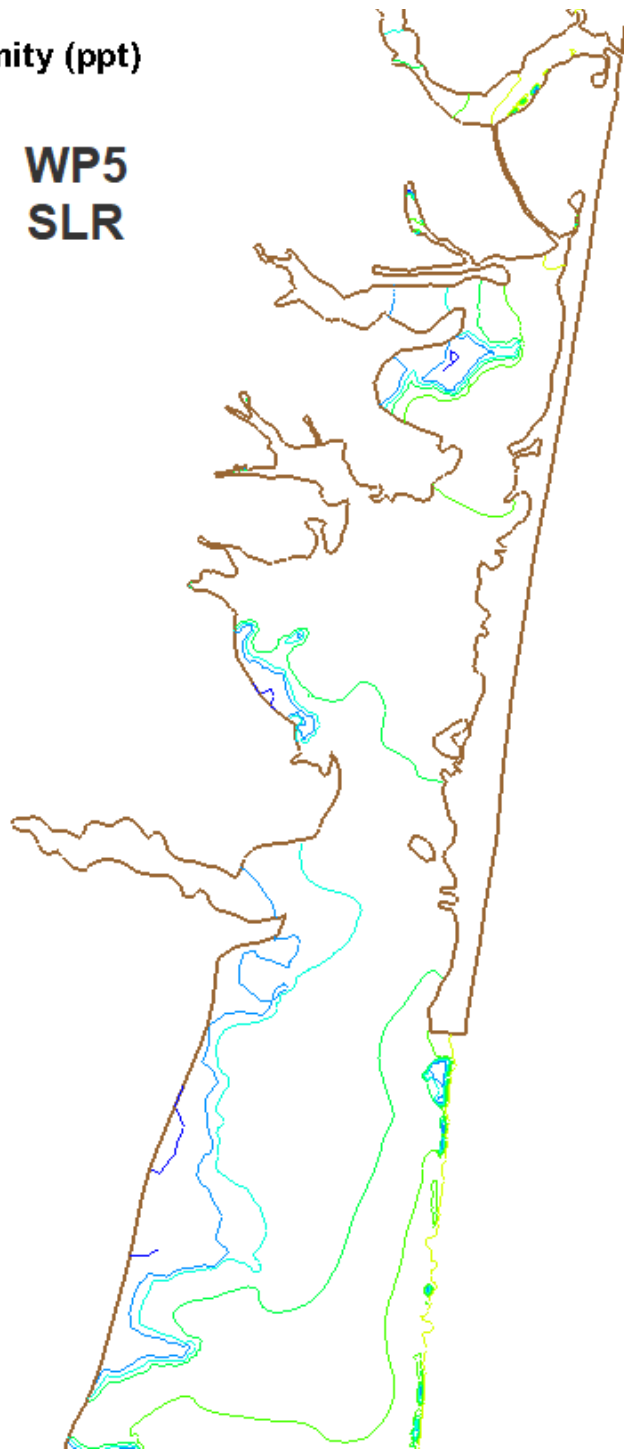
WP1
SLR



Mean Salinity (ppt)

- 35.0
- 30.0
- 25.0
- 20.0
- 15.0
- 10.0
- 5.0
- 0.0

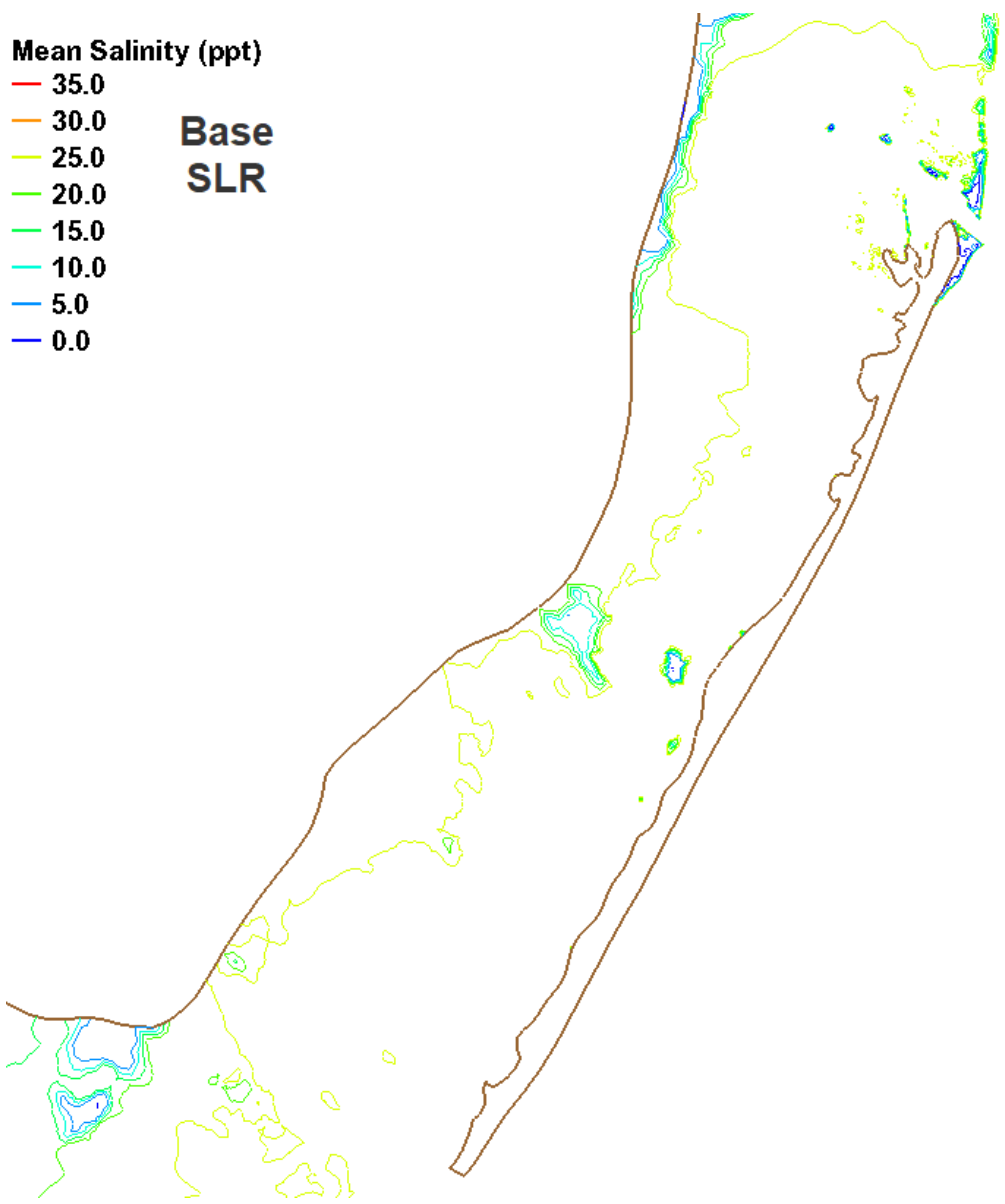
**WP5
SLR**



Mean Salinity (ppt)

- 35.0
- 30.0
- 25.0
- 20.0
- 15.0
- 10.0
- 5.0
- 0.0

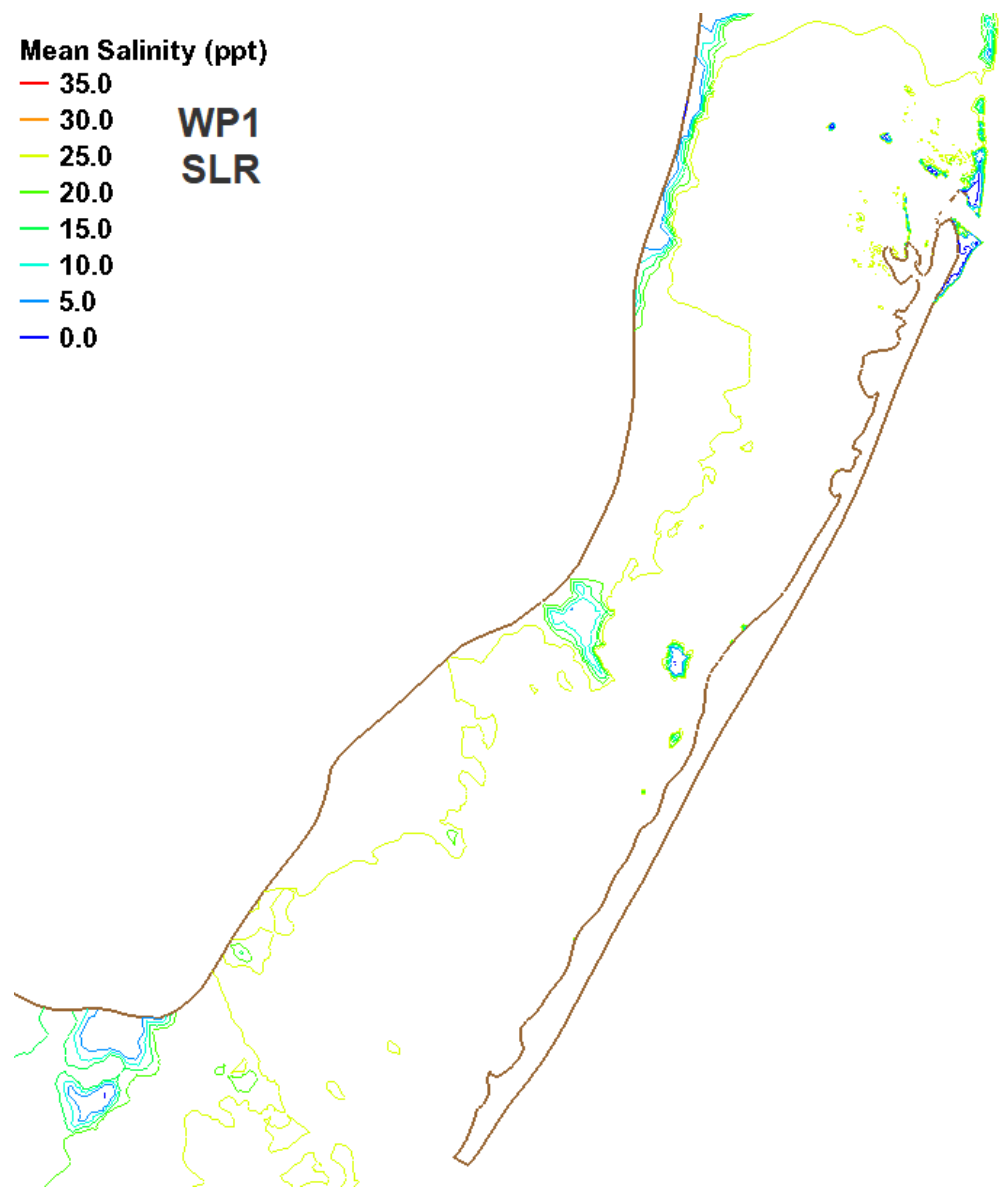
Base
SLR



Mean Salinity (ppt)

- 35.0
- 30.0
- 25.0
- 20.0
- 15.0
- 10.0
- 5.0
- 0.0

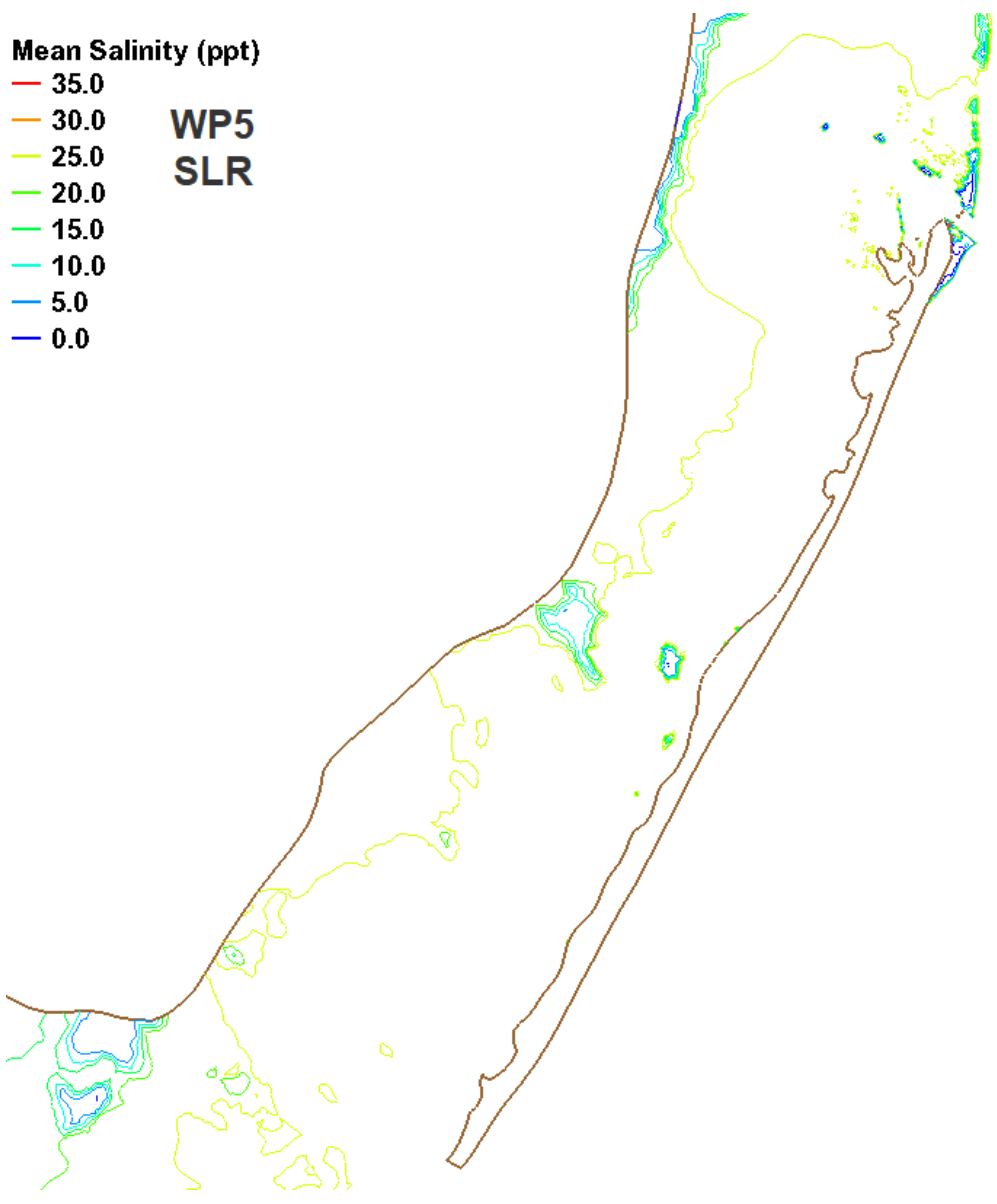
WP1
SLR



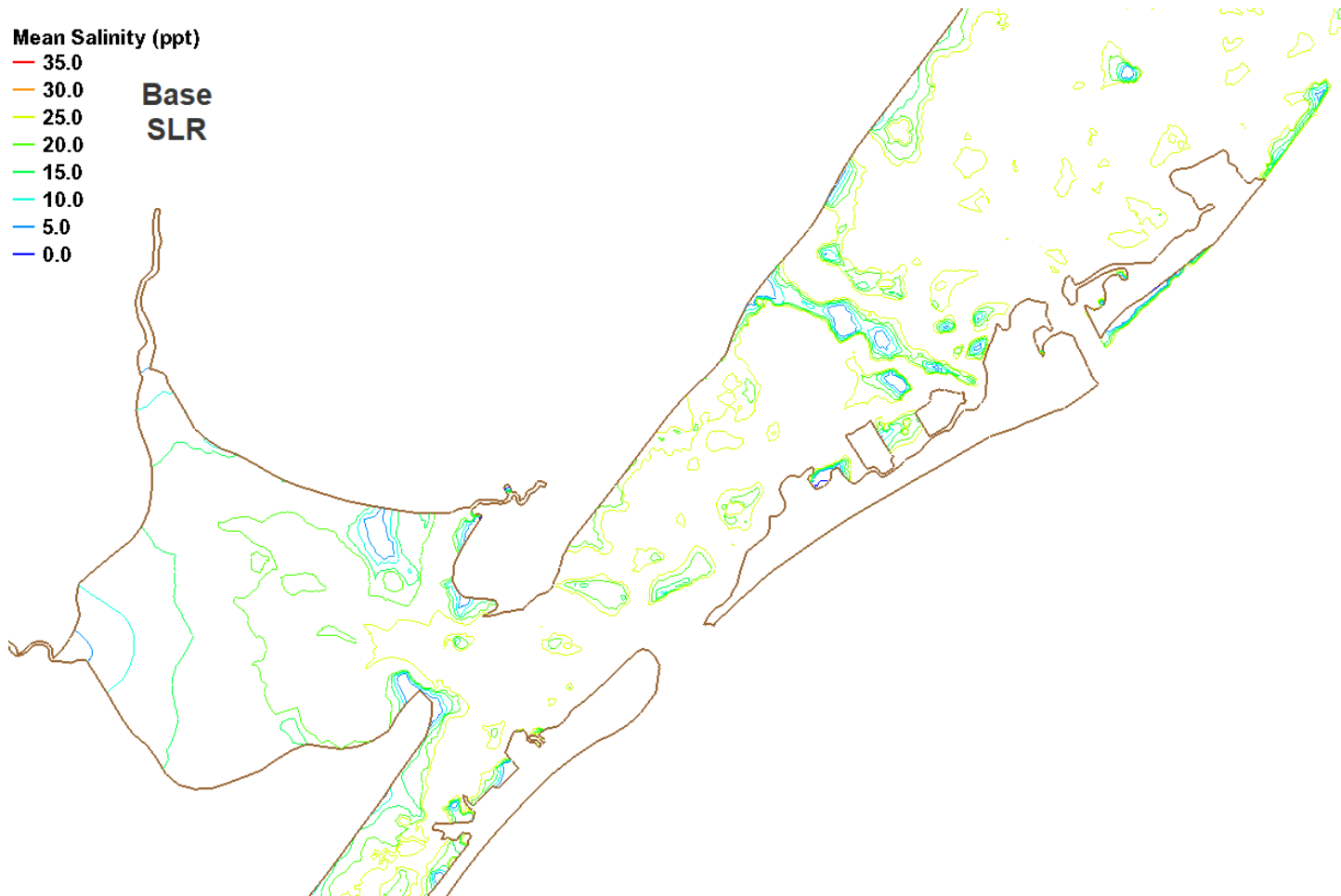
Mean Salinity (ppt)

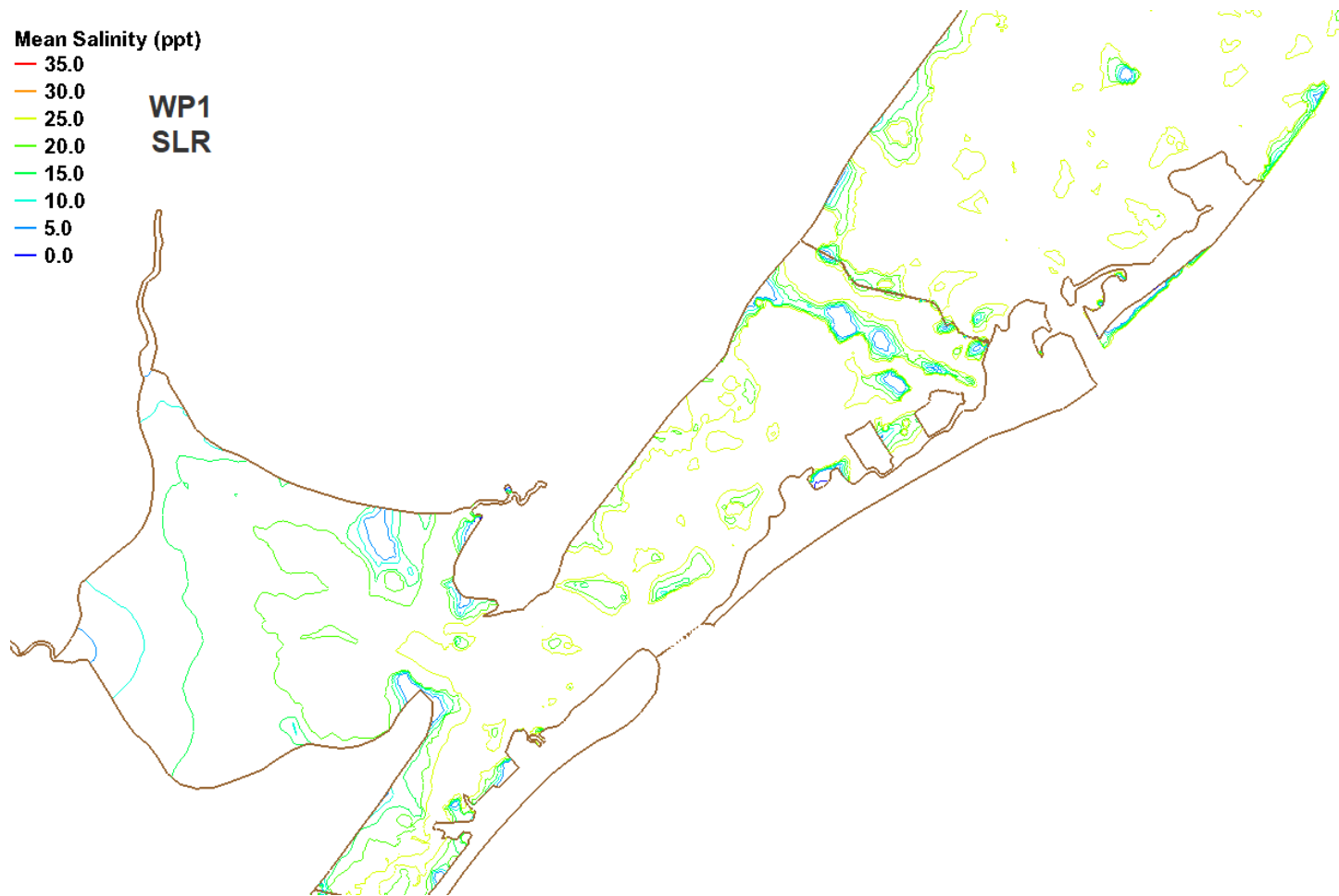
- 35.0
- 30.0
- 25.0
- 20.0
- 15.0
- 10.0
- 5.0
- 0.0

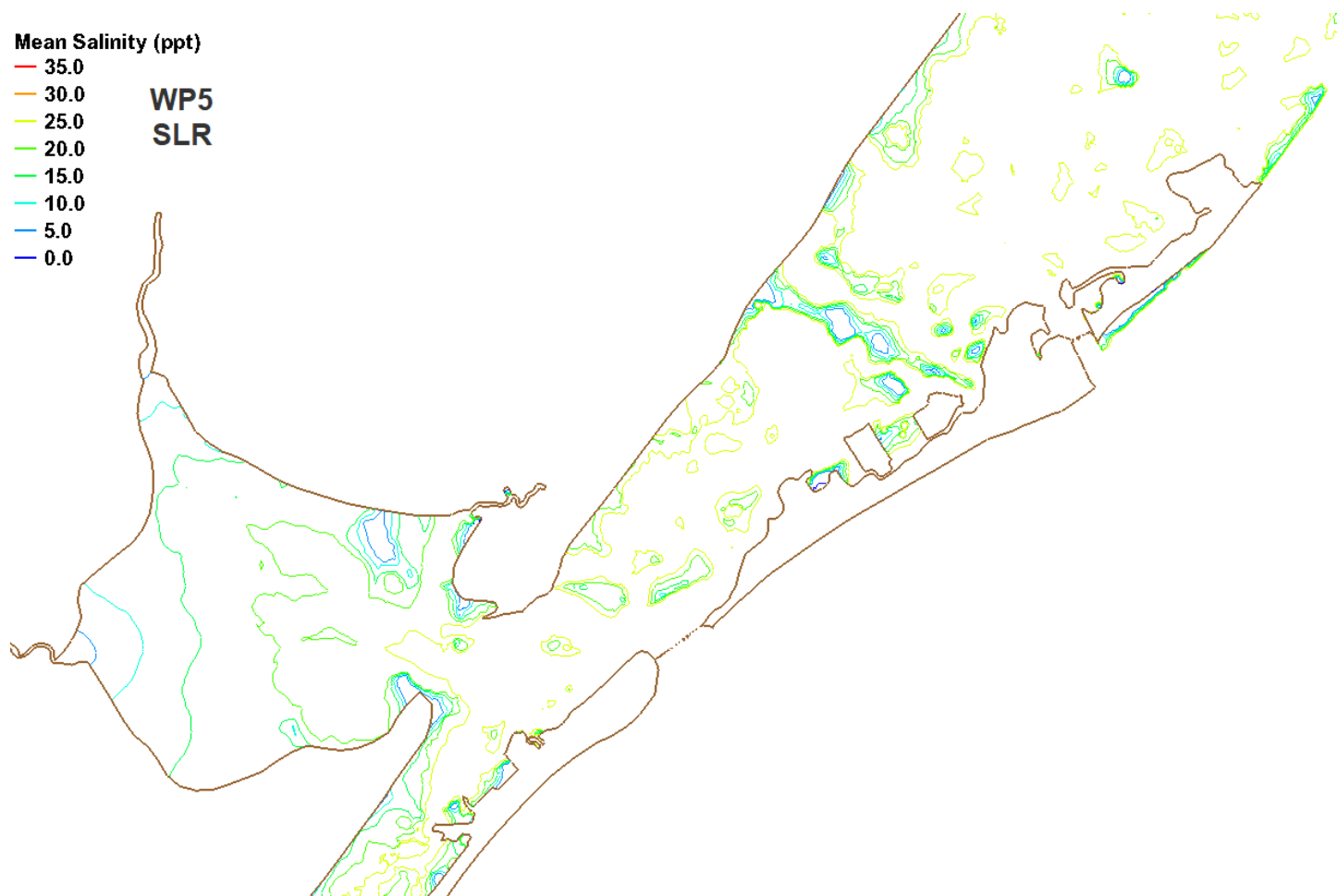
WP5
SLR



Central Region (Great Egg and Absecon)







Appendix F: Alternative Velocity Comparisons

The velocity magnitude and water surface elevation are shown for an arbitrary one-week time period (for visualization).

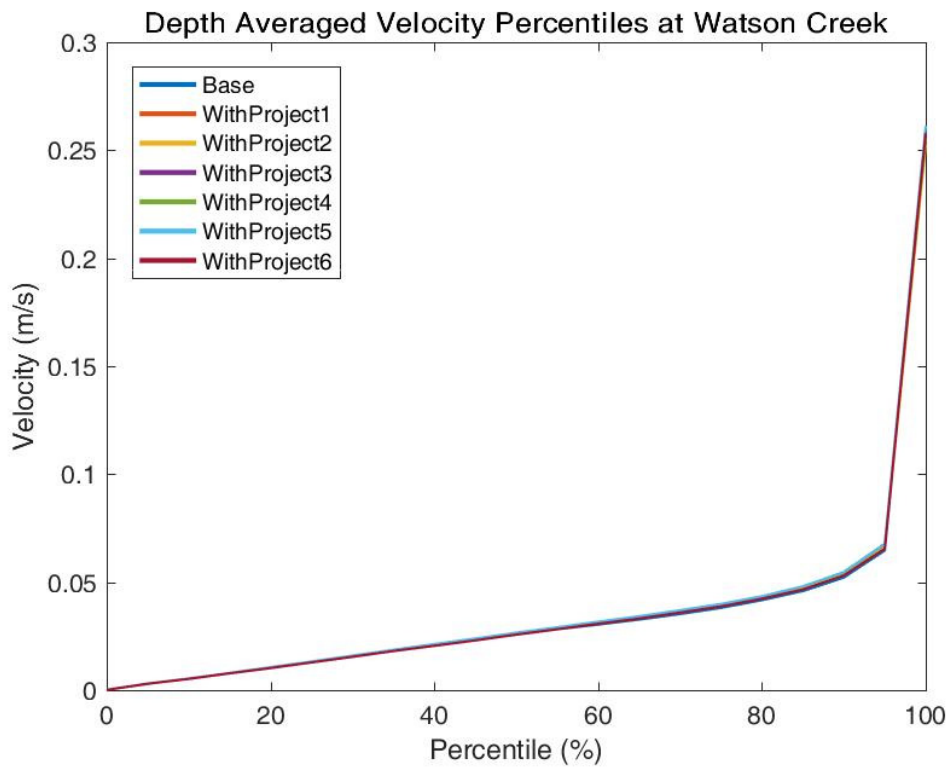
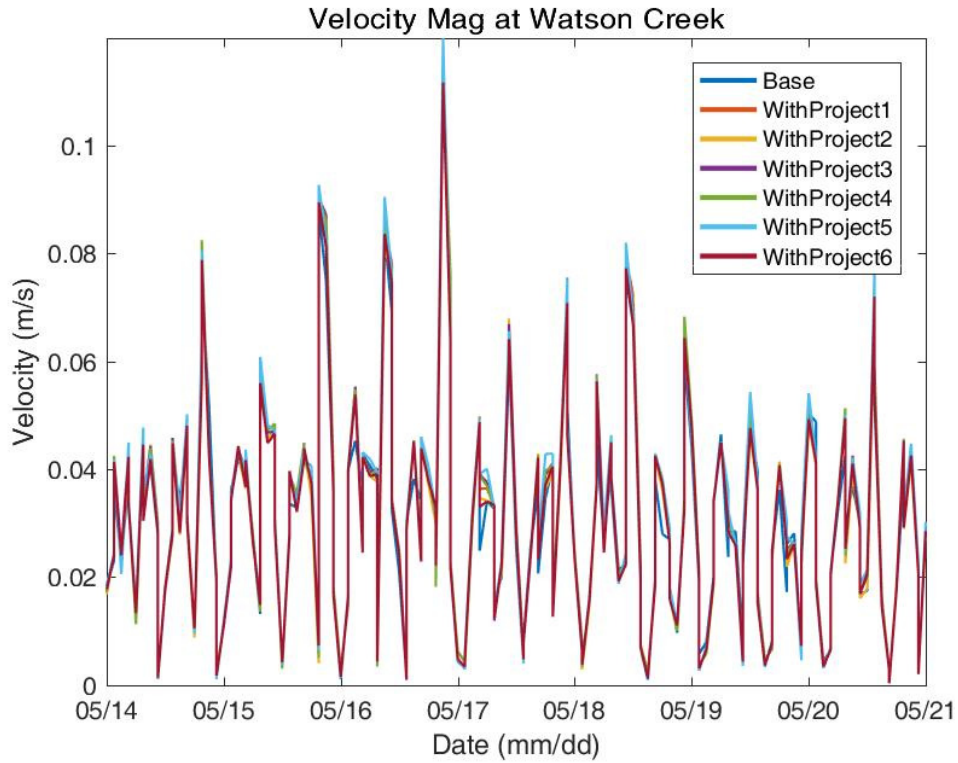
Comparisons to Base

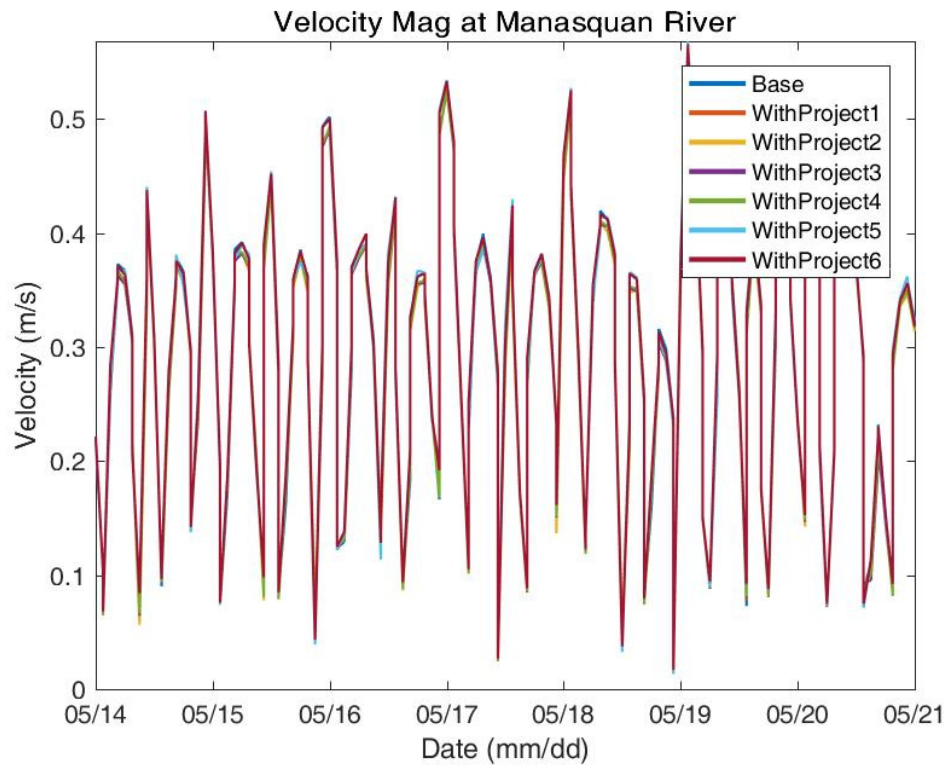
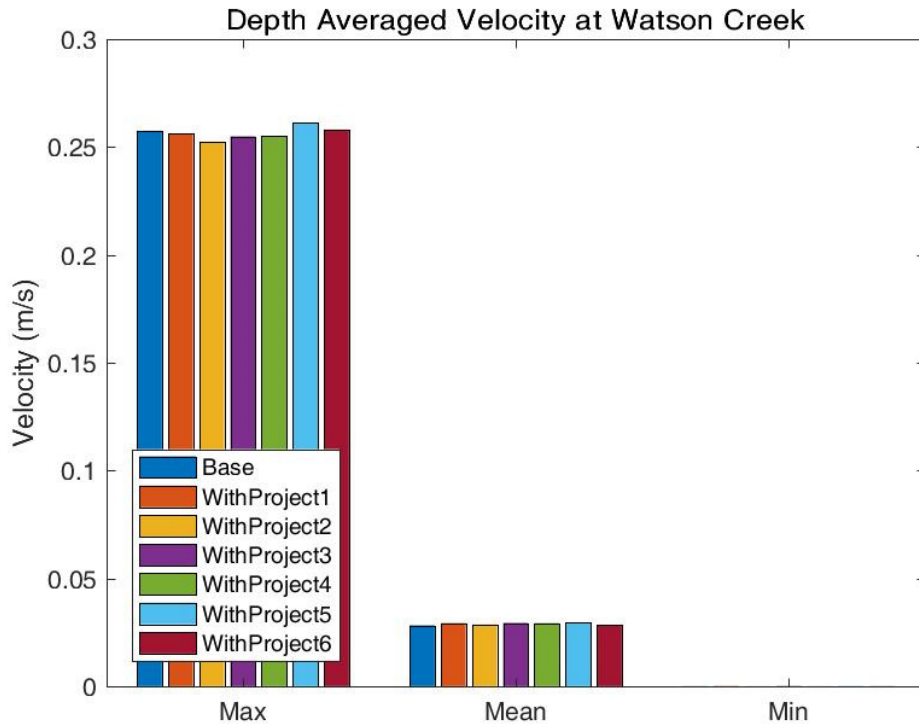
Maximum, Mean, Minimum

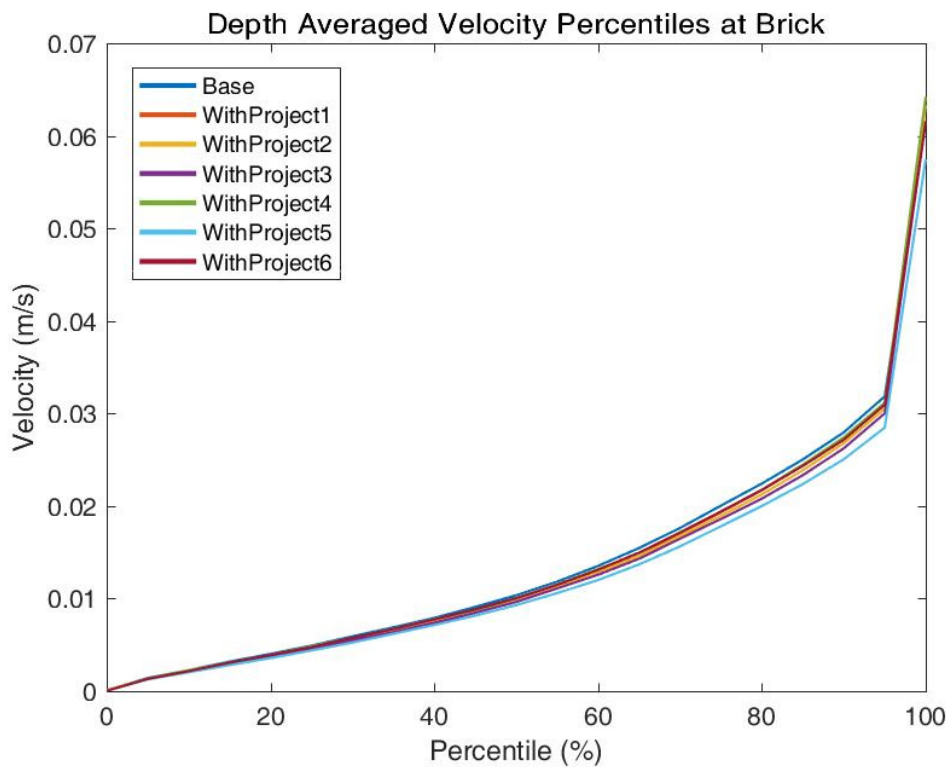
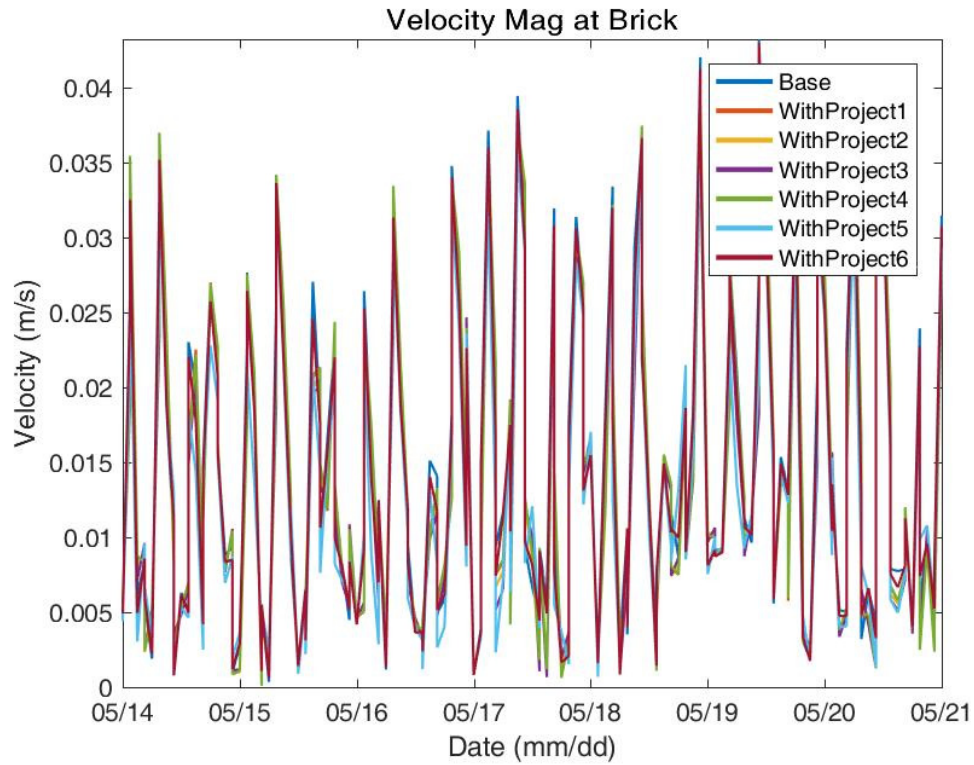
		Base	WP1	WP2	WP3	WP4	WP5	WP6
Watson Creek	Max	0.258	0.256	0.253	0.255	0.255	0.261	0.258
	Mean	0.028	0.029	0.029	0.029	0.029	0.029	0.028
	Min	0.000	0.000	0.000	0.000	0.000	0.000	0.000
Manasquan River	Max	0.661	0.649	0.649	0.649	0.648	0.660	0.655
	Mean	0.262	0.259	0.257	0.258	0.259	0.264	0.264
	Min	0.003	0.003	0.004	0.005	0.003	0.003	0.002
Brick	Max	0.061	0.064	0.063	0.062	0.064	0.057	0.062
	Mean	0.013	0.013	0.013	0.012	0.013	0.012	0.013
	Min	0.000	0.000	0.000	0.000	0.000	0.000	0.000
Barnegat Bay at Mantoloking	Max	0.453	0.447	0.445	0.438	0.447	0.433	0.453
	Mean	0.101	0.104	0.102	0.101	0.104	0.097	0.100
	Min	0.001	0.000	0.000	0.000	0.000	0.000	0.000
Barnegat Bay at Route 37 Bridge	Max	0.325	0.318	0.317	0.310	0.319	0.300	0.320
	Mean	0.080	0.075	0.073	0.070	0.076	0.066	0.076
	Min	0.000	0.000	0.001	0.001	0.000	0.000	0.000
Berkeley	Max	0.247	0.234	0.232	0.225	0.235	0.213	0.243
	Mean	0.034	0.034	0.033	0.032	0.034	0.031	0.033
	Min	0.000	0.000	0.000	0.000	0.000	0.000	0.000
Barnegat Light	Max	0.326	0.339	0.341	0.346	0.338	0.340	0.329
	Mean	0.095	0.091	0.089	0.087	0.092	0.084	0.093
	Min	0.002	0.003	0.002	0.004	0.004	0.003	0.002
Barnegat Bay at Waretown	Max	0.193	0.196	0.192	0.194	0.191	0.191	0.191
	Mean	0.034	0.033	0.033	0.032	0.033	0.031	0.033
	Min	0.000	0.000	0.000	0.000	0.000	0.000	0.000
	Max	0.817	0.483	0.362	0.483	0.639	0.582	0.739

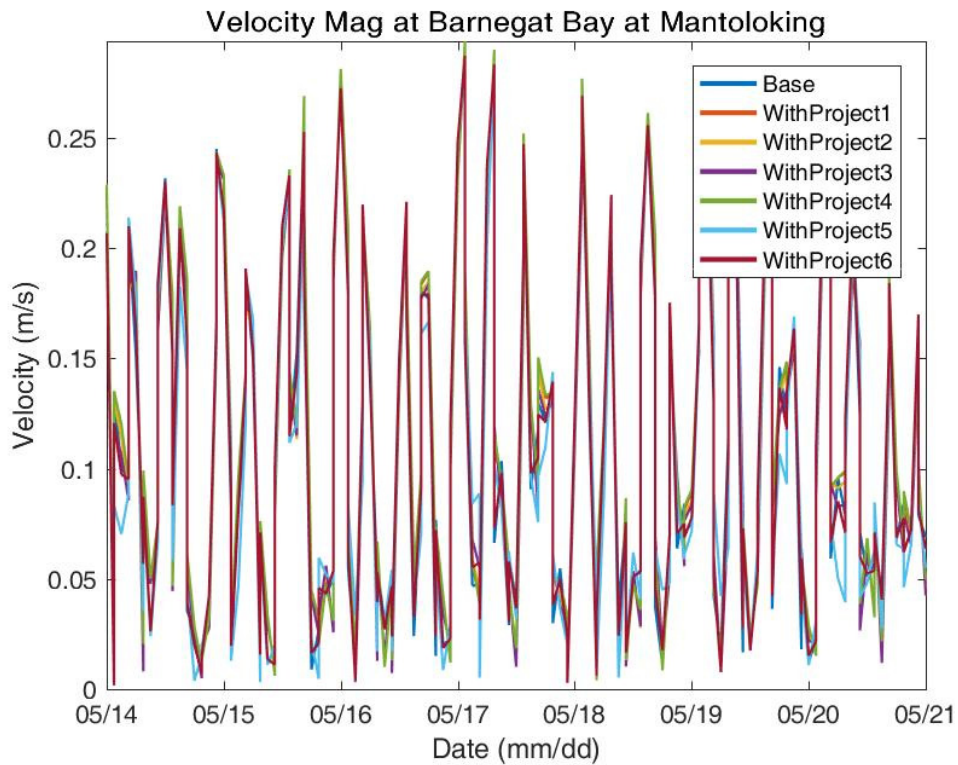
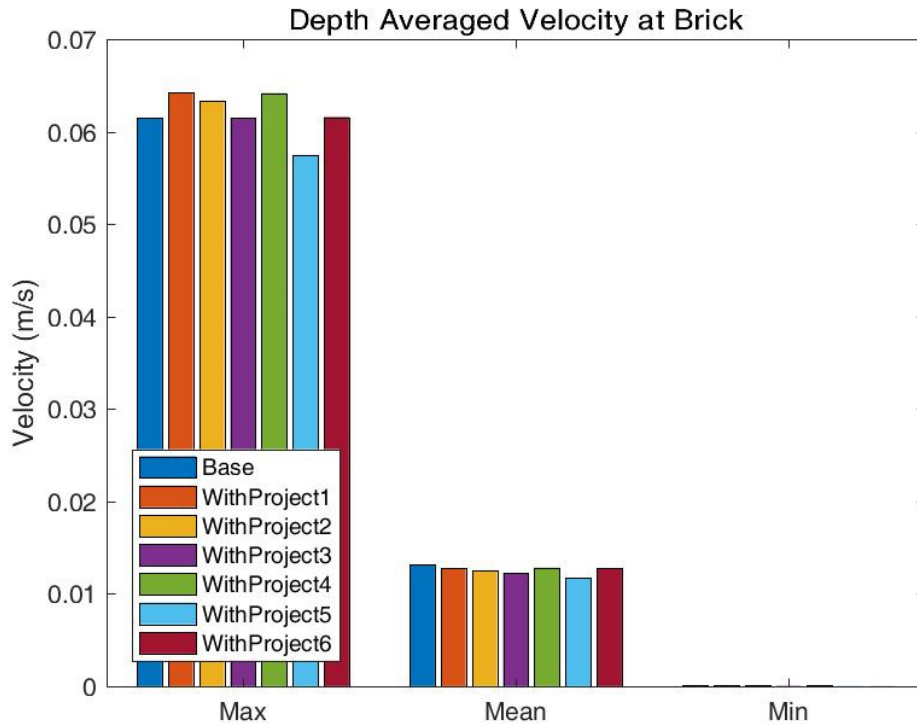
Barnegat Bay at Barnegat Light	Mean	0.132	0.086	0.067	0.090	0.170	0.101	0.134
	Min	0.001	0.002	0.001	0.002	0.000	0.000	0.000
Barnegat Light (Ocean)	Max	0.652	0.648	0.640	0.644	0.646	0.645	0.647
	Mean	0.052	0.052	0.052	0.052	0.052	0.052	0.052
	Min	0.000	0.000	0.000	0.000	0.001	0.000	0.000
East Thorofare	Max	0.363	0.365	0.366	0.373	0.366	0.377	0.366
	Mean	0.072	0.071	0.072	0.073	0.071	0.077	0.073
	Min	0.000	0.000	0.000	0.000	0.000	0.000	0.000
Westecunk	Max	0.141	0.142	0.142	0.142	0.142	0.141	0.141
	Mean	0.070	0.069	0.069	0.069	0.069	0.070	0.069
	Min	0.000	0.000	0.000	0.000	0.000	0.000	0.000
Beach Haven	Max	0.572	0.566	0.567	0.569	0.566	0.575	0.573
	Mean	0.159	0.154	0.154	0.154	0.154	0.158	0.158
	Min	0.001	0.000	0.000	0.001	0.000	0.000	0.000
JACNEWQ	Max	0.876	0.874	0.874	0.875	0.872	0.875	0.872
	Mean	0.258	0.253	0.252	0.253	0.253	0.258	0.257
	Min	0.001	0.000	0.000	0.000	0.000	0.000	0.000
Little Egg Inlet	Max	2.374	2.362	2.369	2.376	2.363	2.387	2.392
	Mean	0.339	0.336	0.335	0.336	0.335	0.339	0.337
	Min	0.000	0.001	0.000	0.001	0.001	0.000	0.000
Absecon Creek	Max	0.083	0.083	0.084	0.084	0.083	0.083	0.083
	Mean	0.011	0.011	0.011	0.011	0.011	0.011	0.010
	Min	0.000	0.000	0.000	0.000	0.000	0.000	0.000
Brigantine	Max	0.837	0.819	0.835	0.830	0.816	0.854	0.828
	Mean	0.065	0.064	0.064	0.064	0.064	0.066	0.067
	Min	0.000	0.000	0.000	0.000	0.000	0.000	0.000
Absecon Channel	Max	2.431	2.417	2.421	2.411	2.421	2.182	1.706
	Mean	0.412	0.409	0.408	0.408	0.408	0.397	0.371
	Min	0.000	0.001	0.001	0.001	0.001	0.000	0.001
Atlantic City (Ocean)	Max	1.099	1.078	1.096	1.072	1.078	1.067	0.997
	Mean	0.131	0.129	0.127	0.129	0.129	0.126	0.119
	Min	0.002	0.000	0.001	0.001	0.000	0.001	0.001
Inside Thorofare	Max	0.212	0.219	0.216	0.226	0.212	0.204	0.246
	Mean	0.027	0.027	0.028	0.030	0.027	0.026	0.027

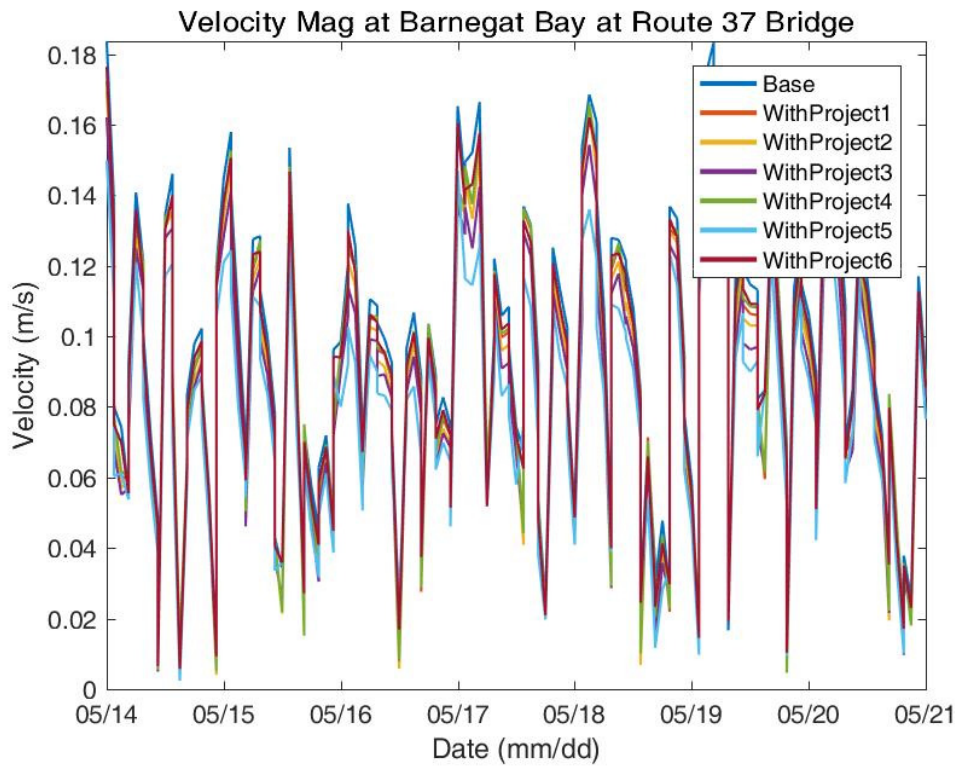
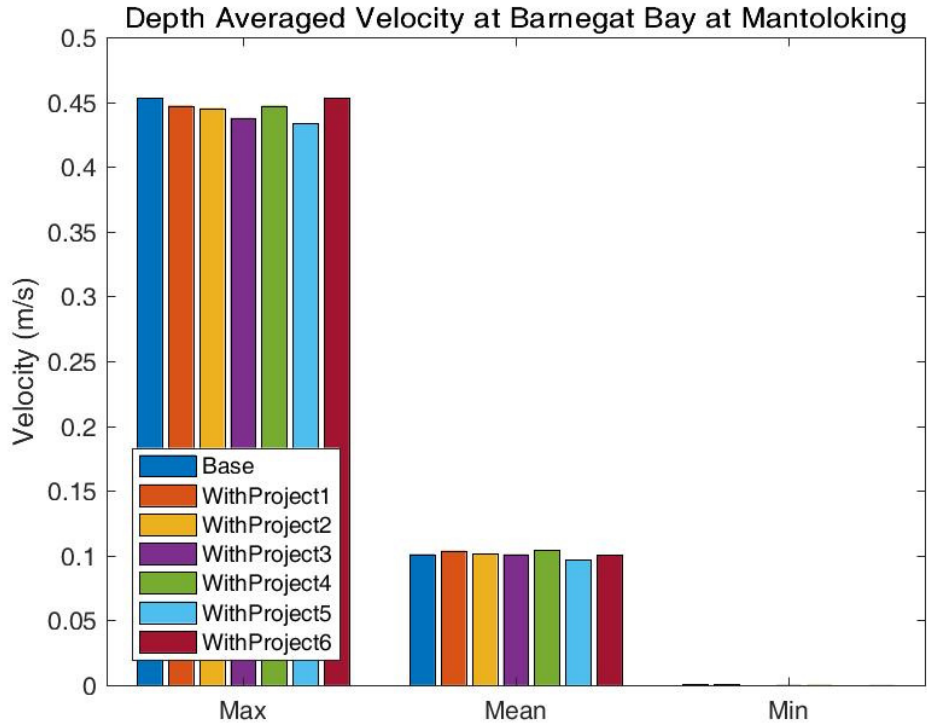
Point Comparisons

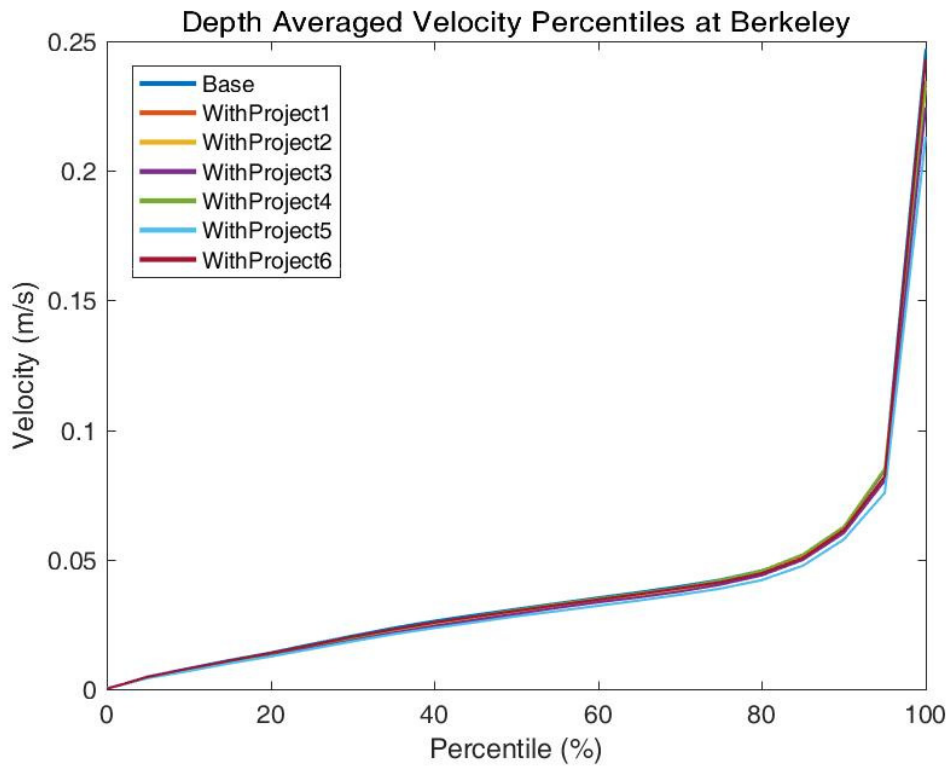
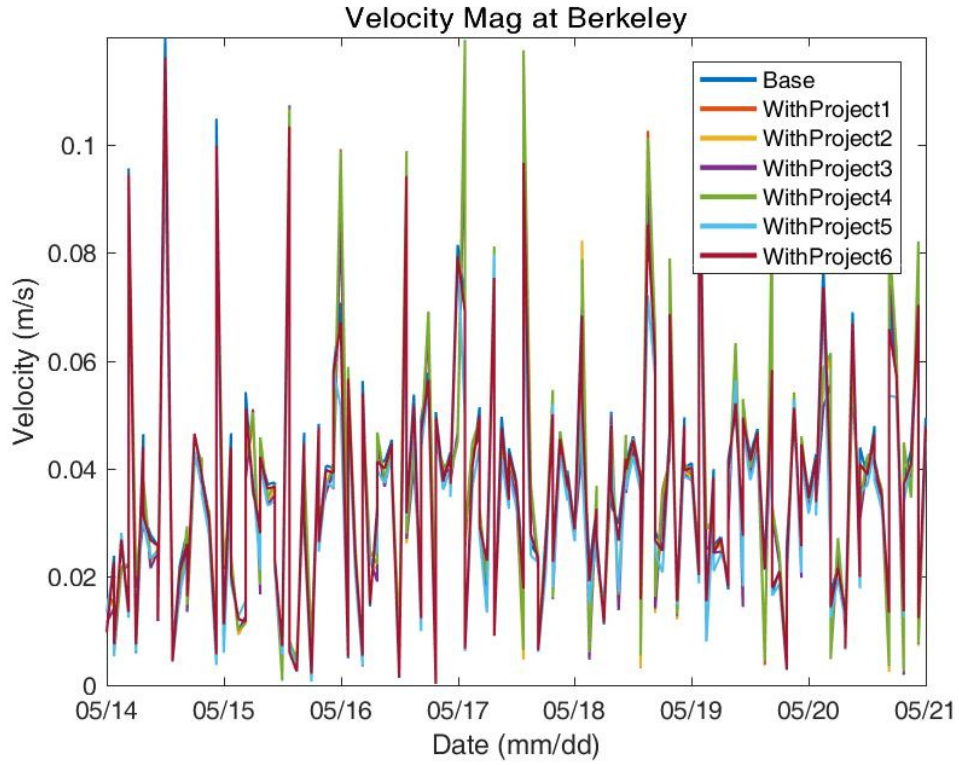


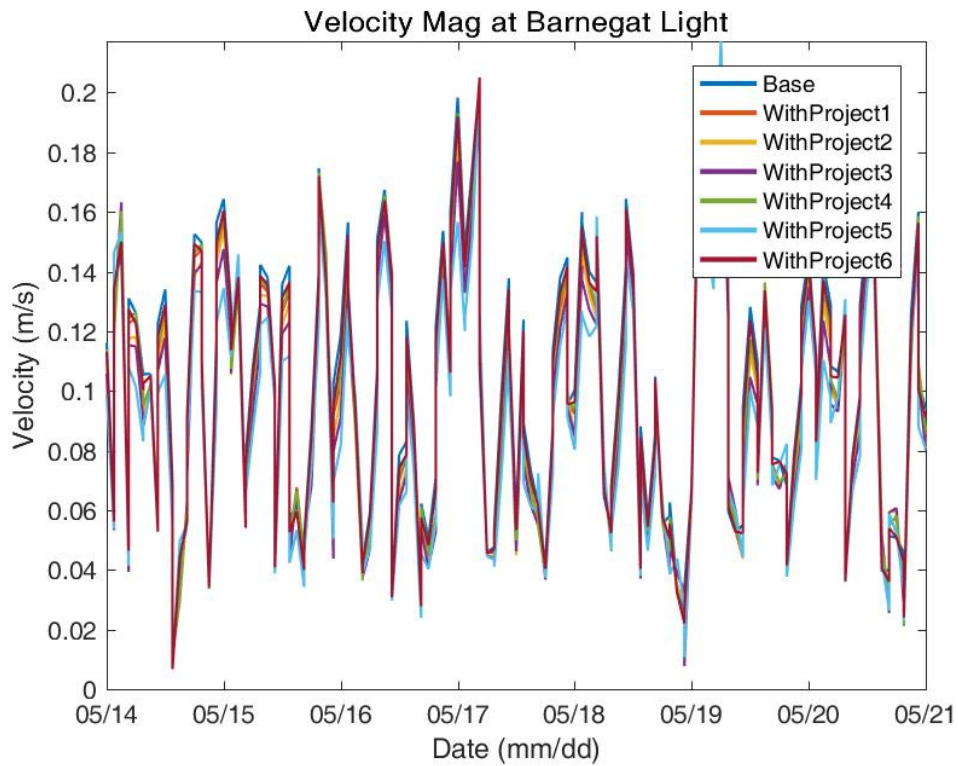
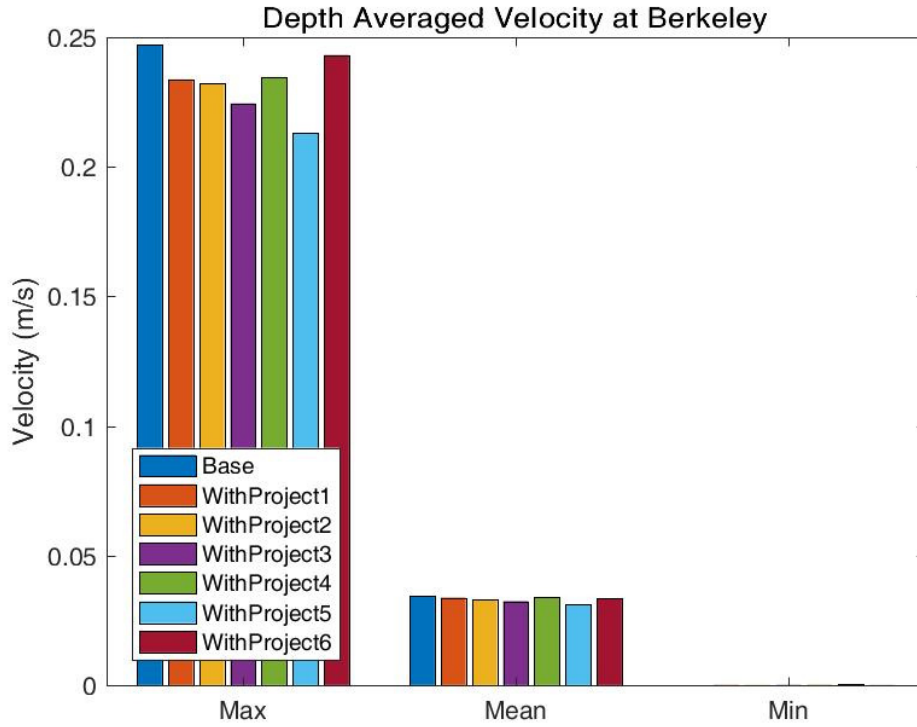


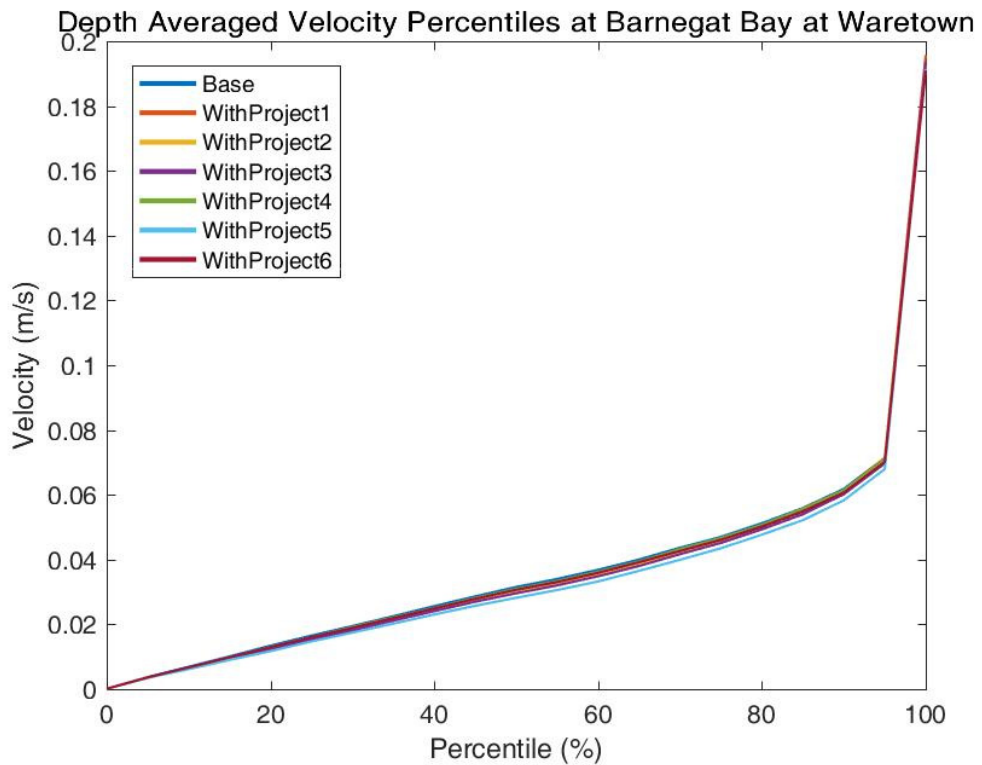
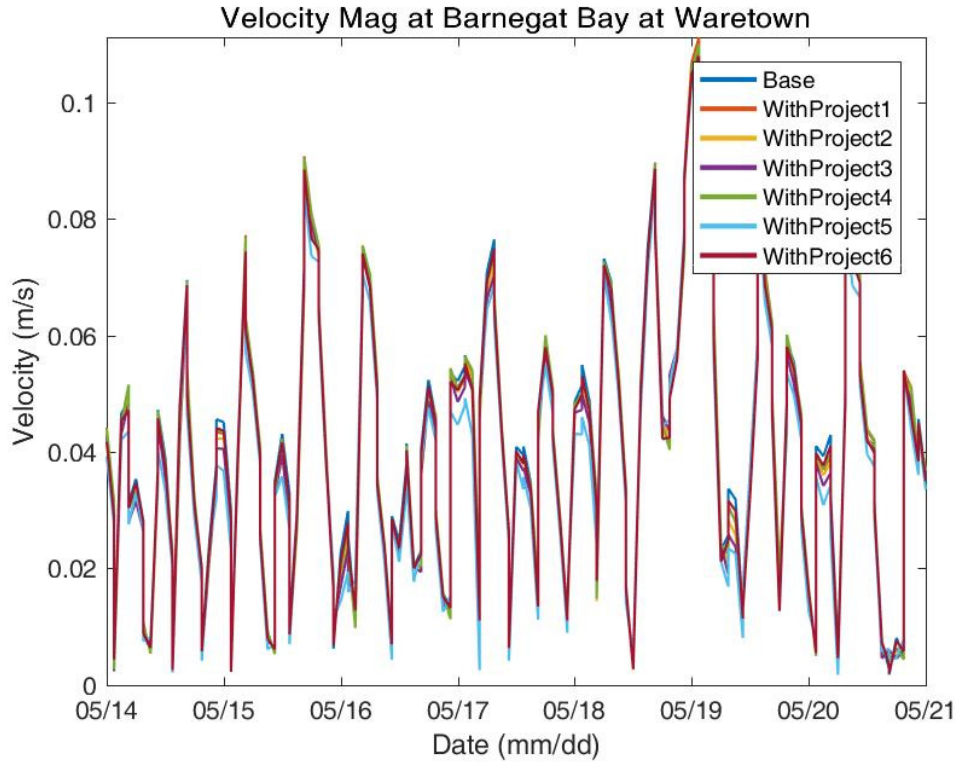


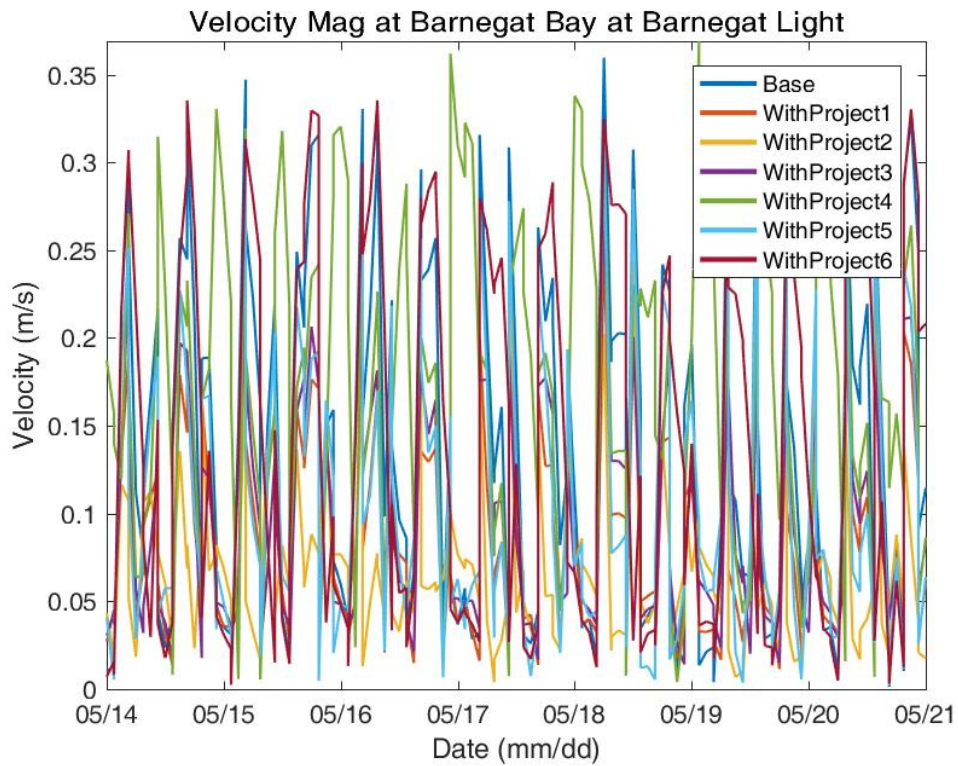
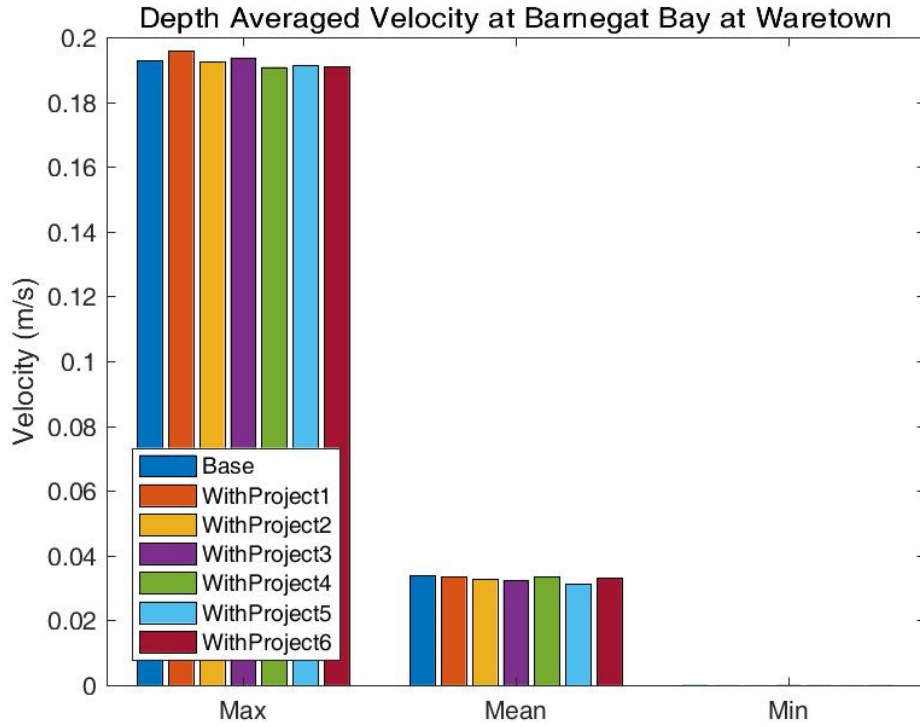


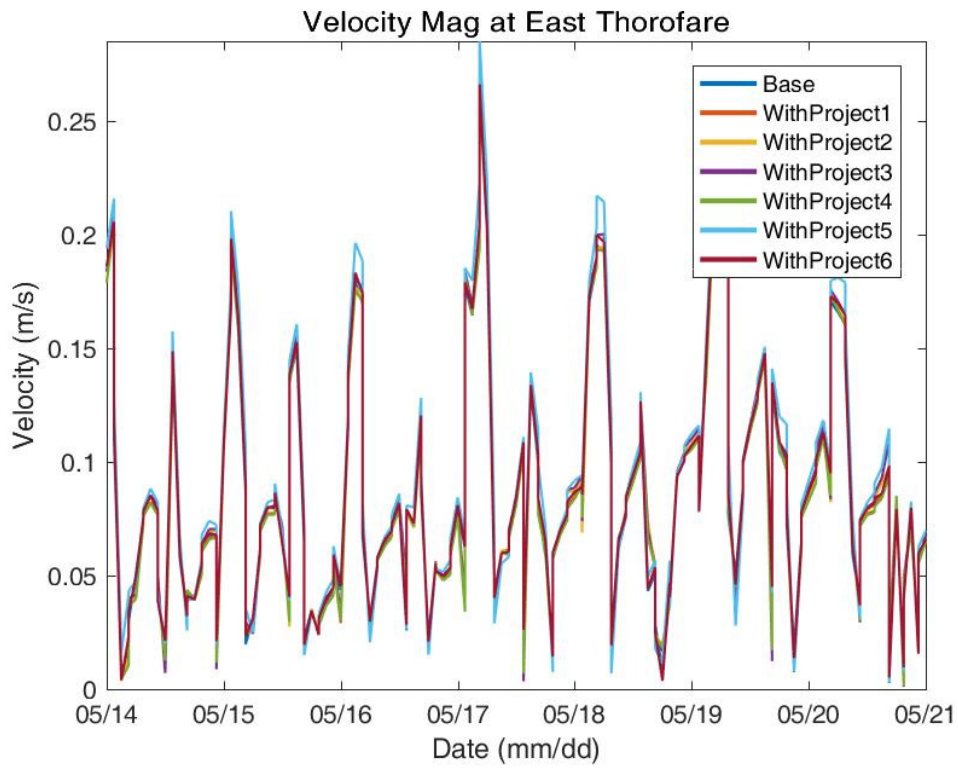
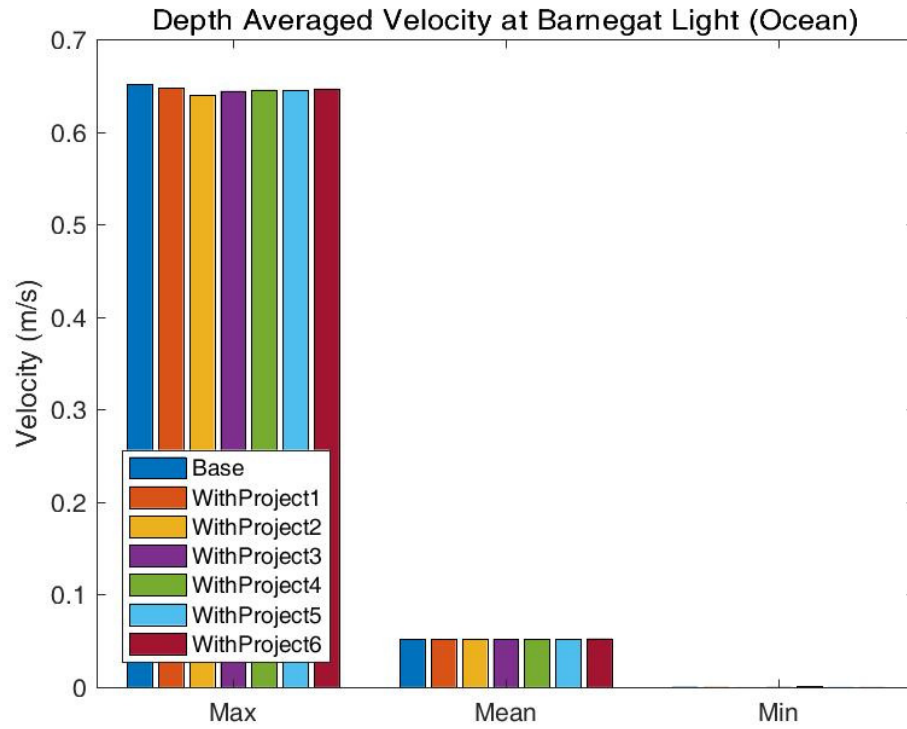


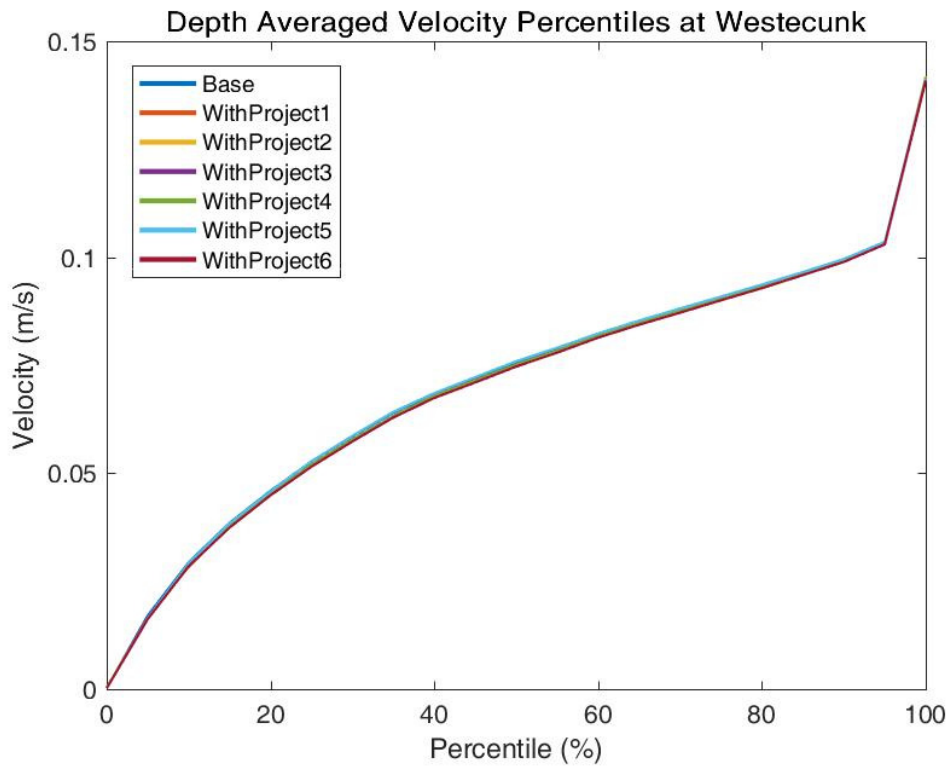
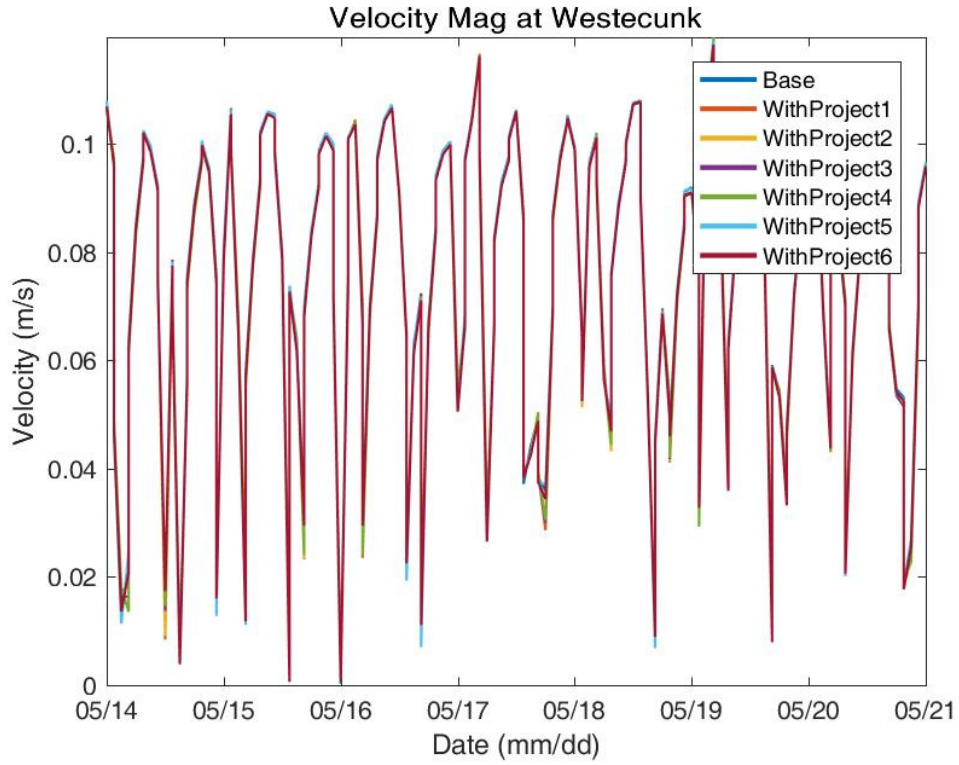


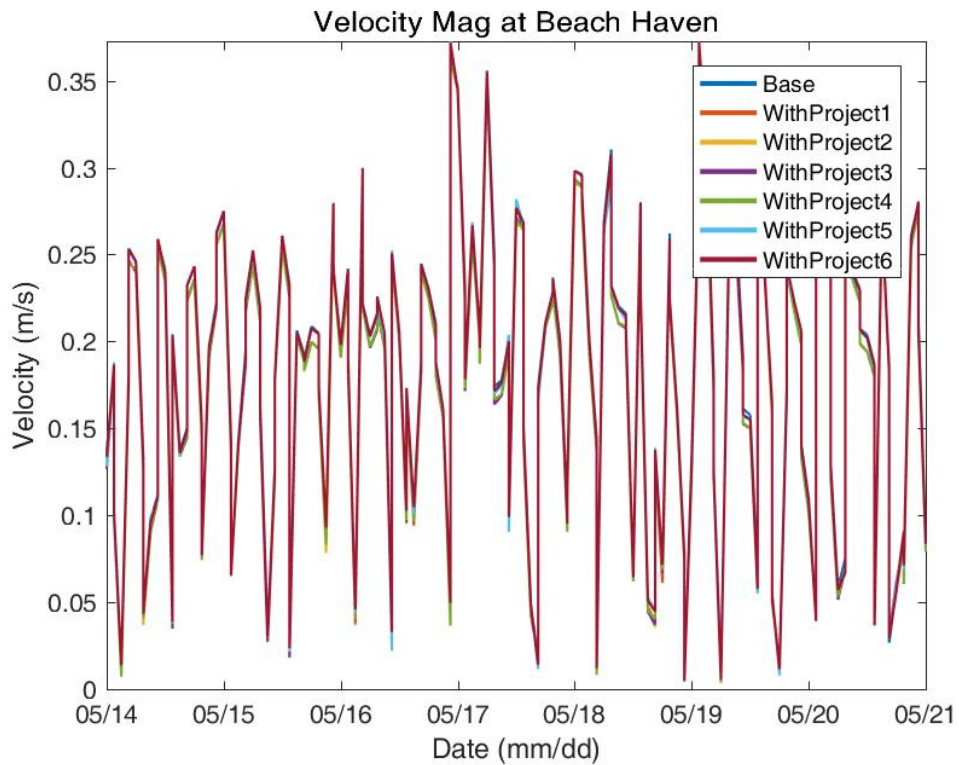
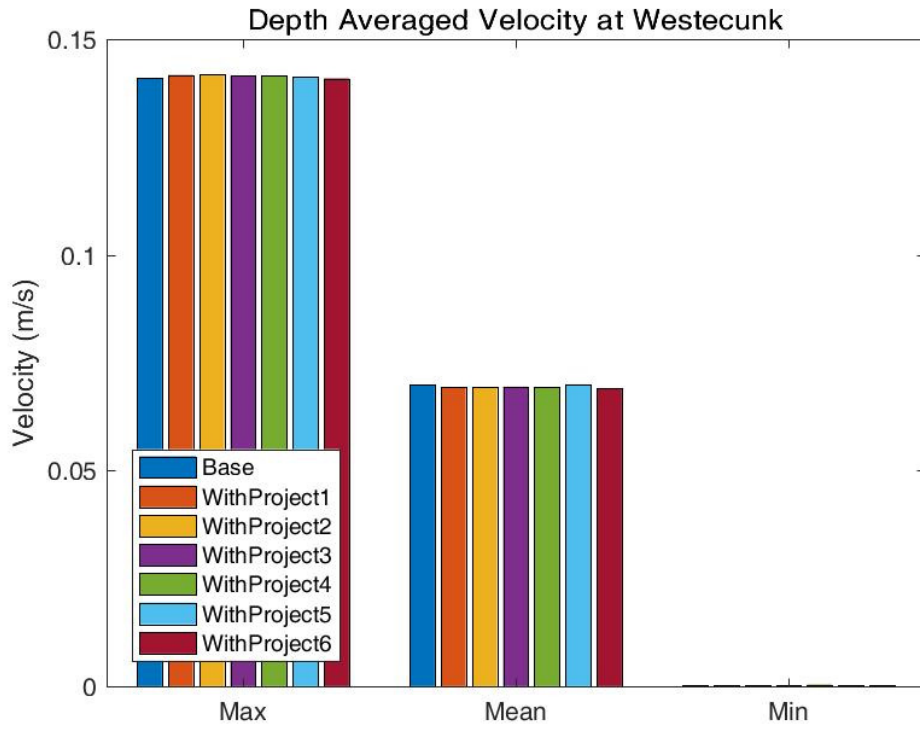


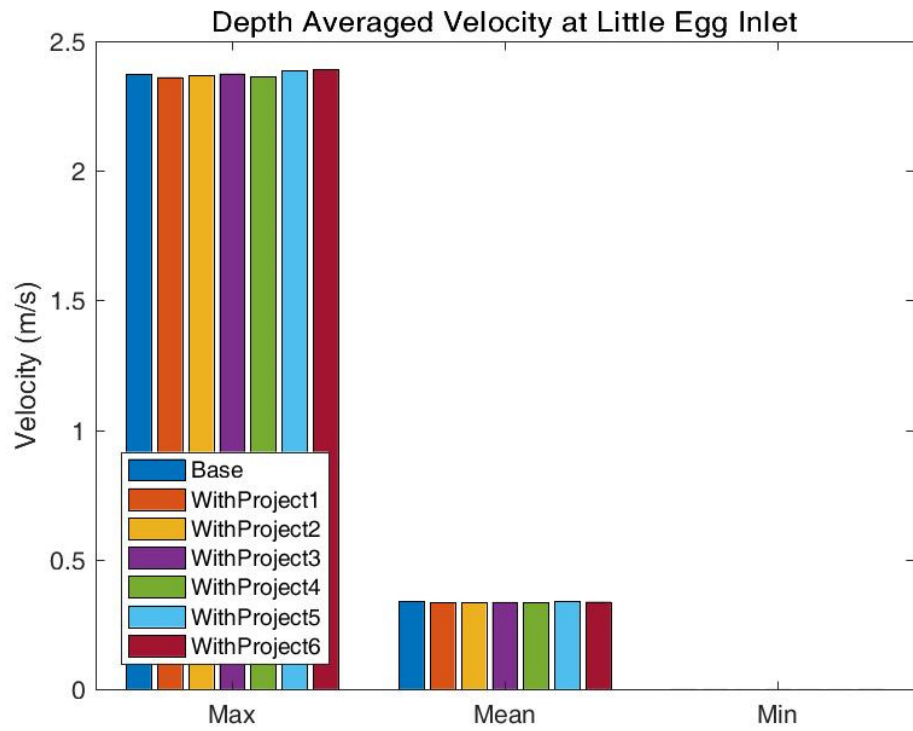
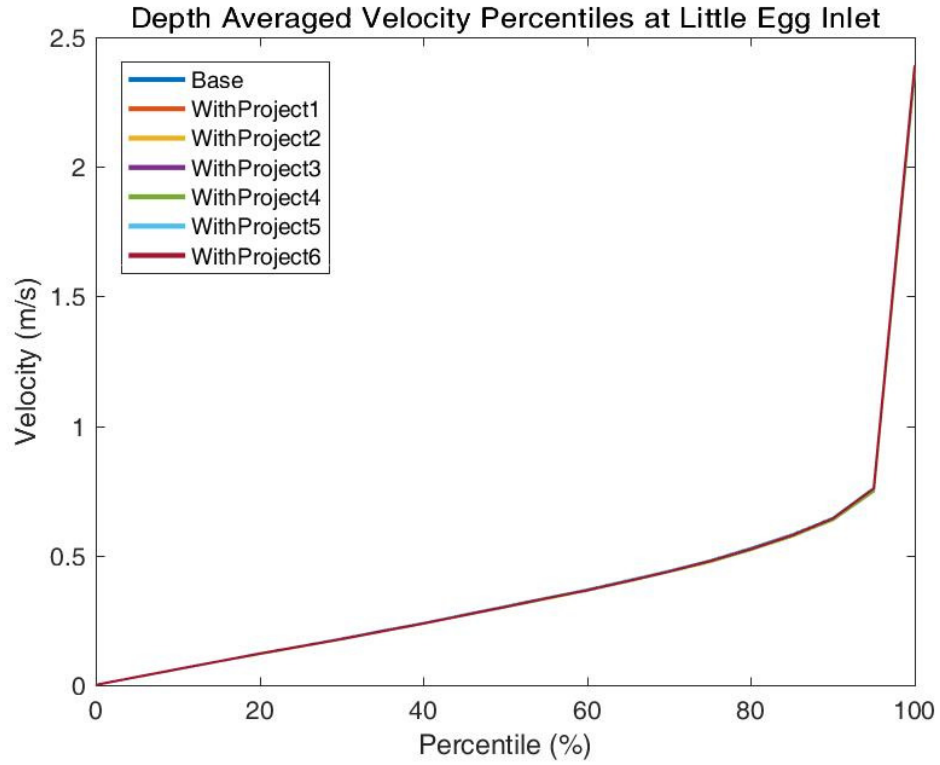


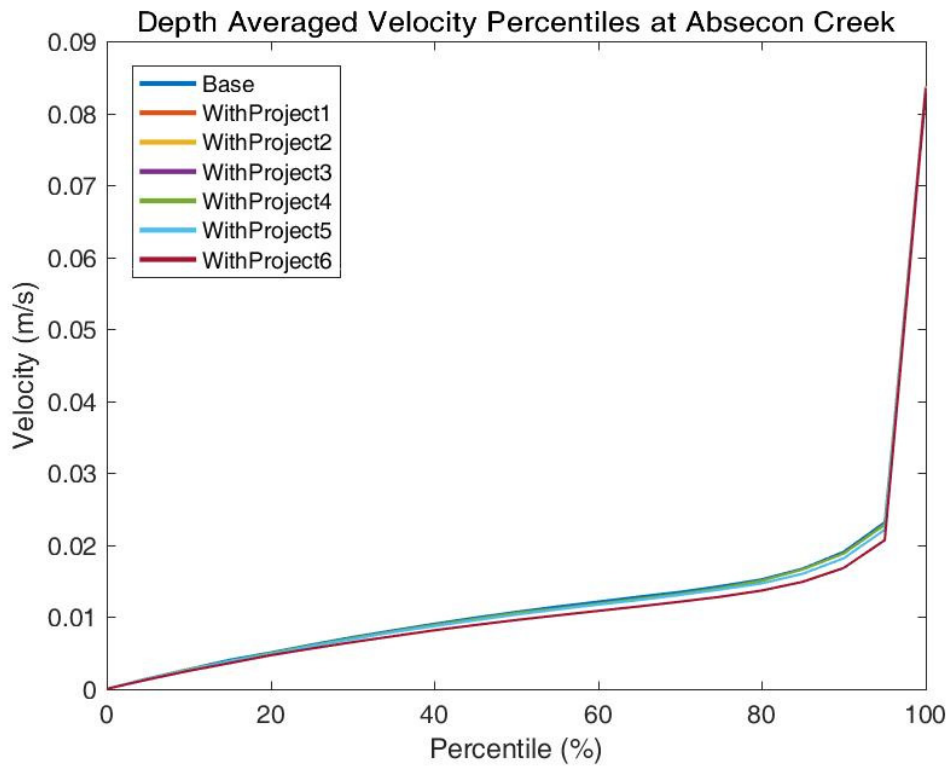
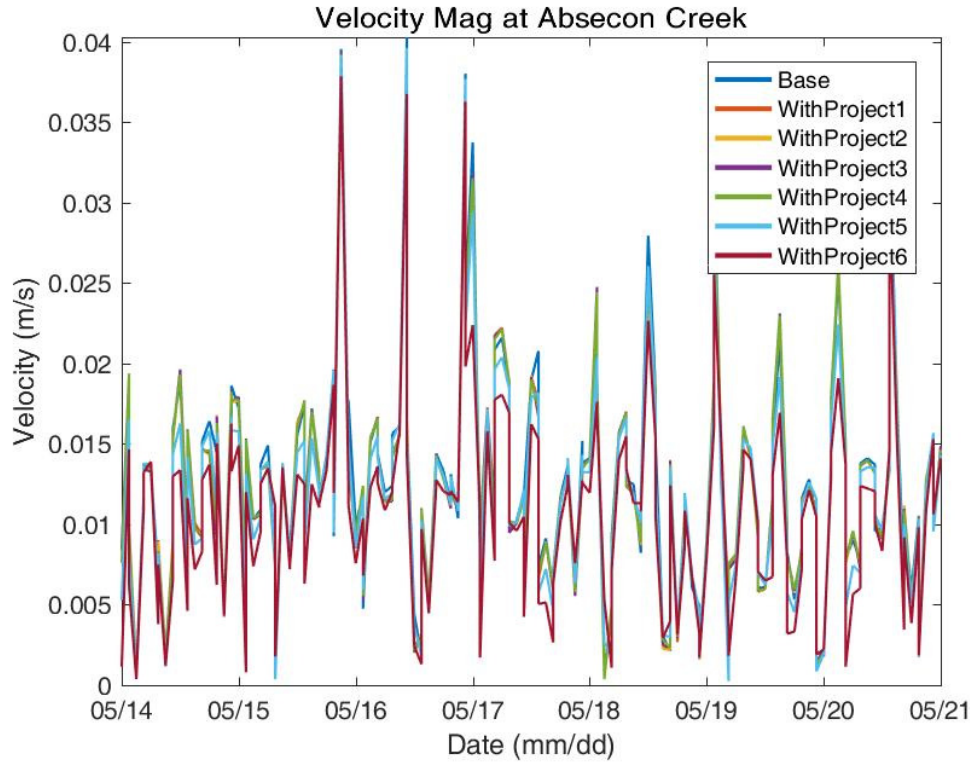


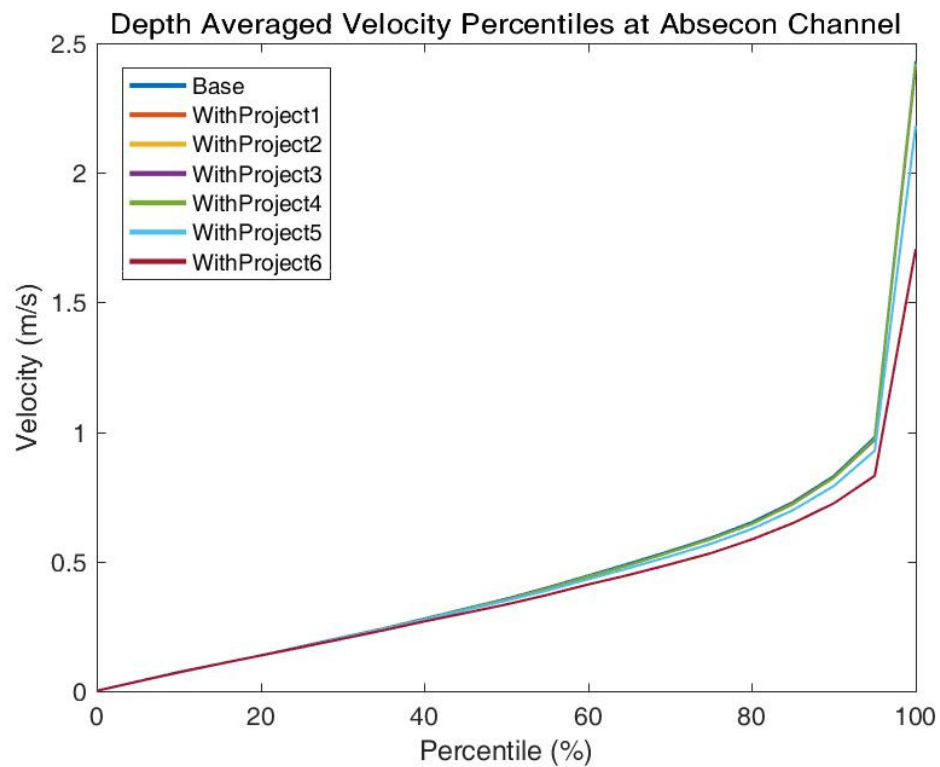
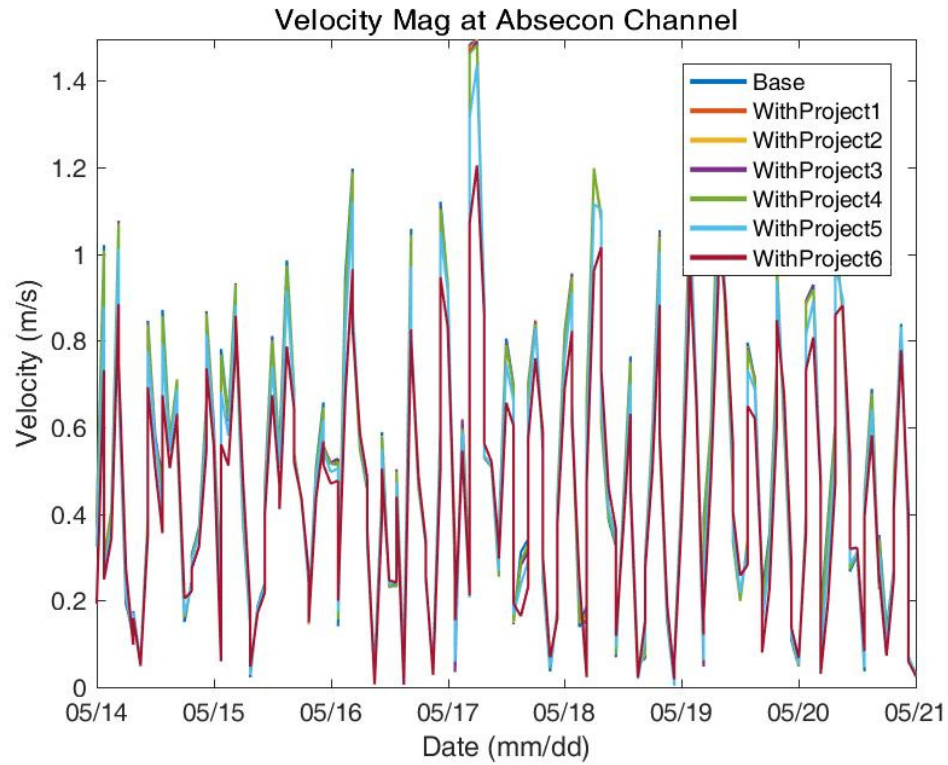


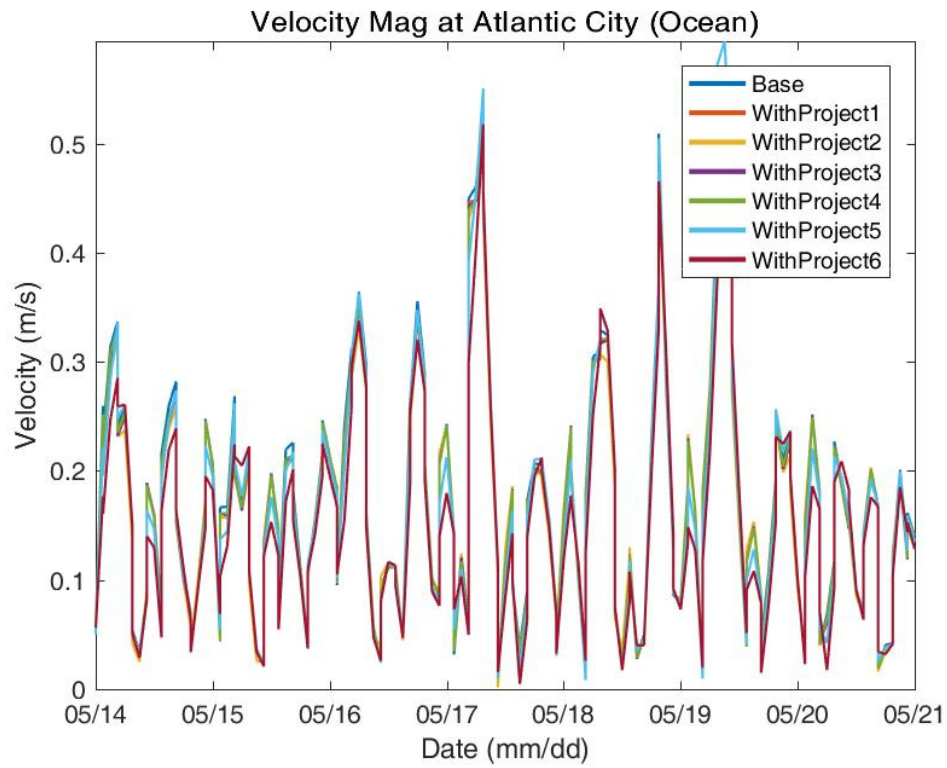
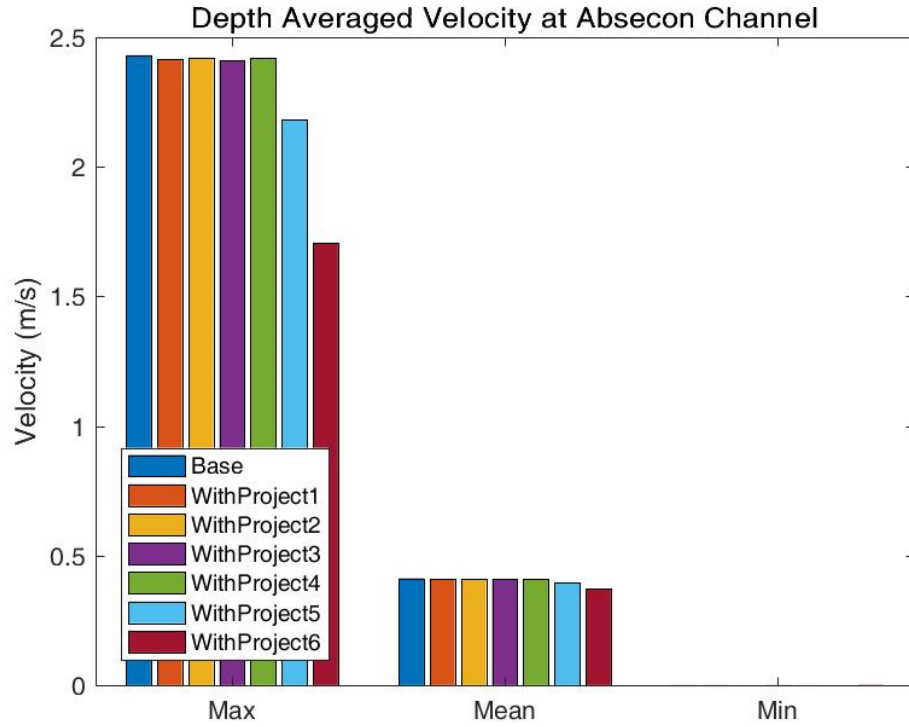


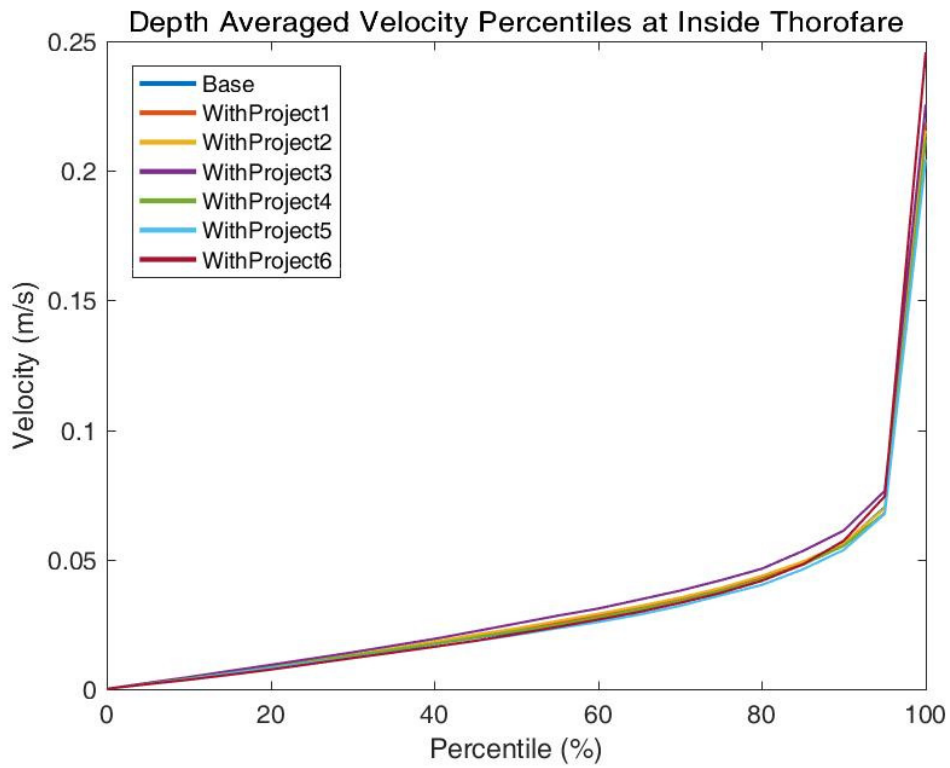
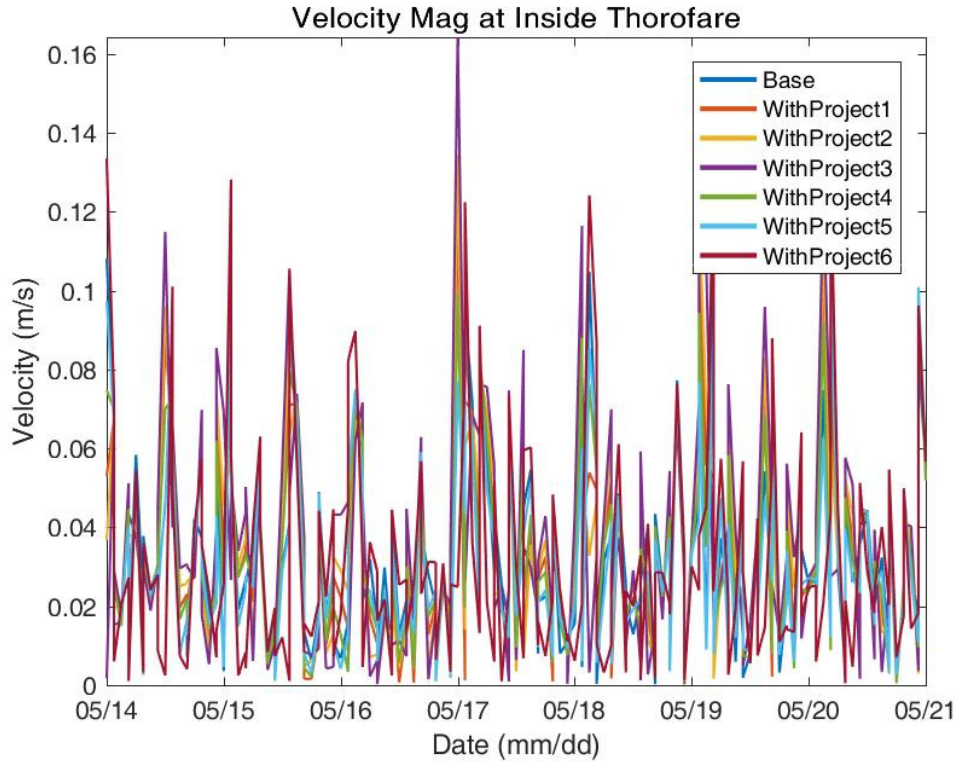


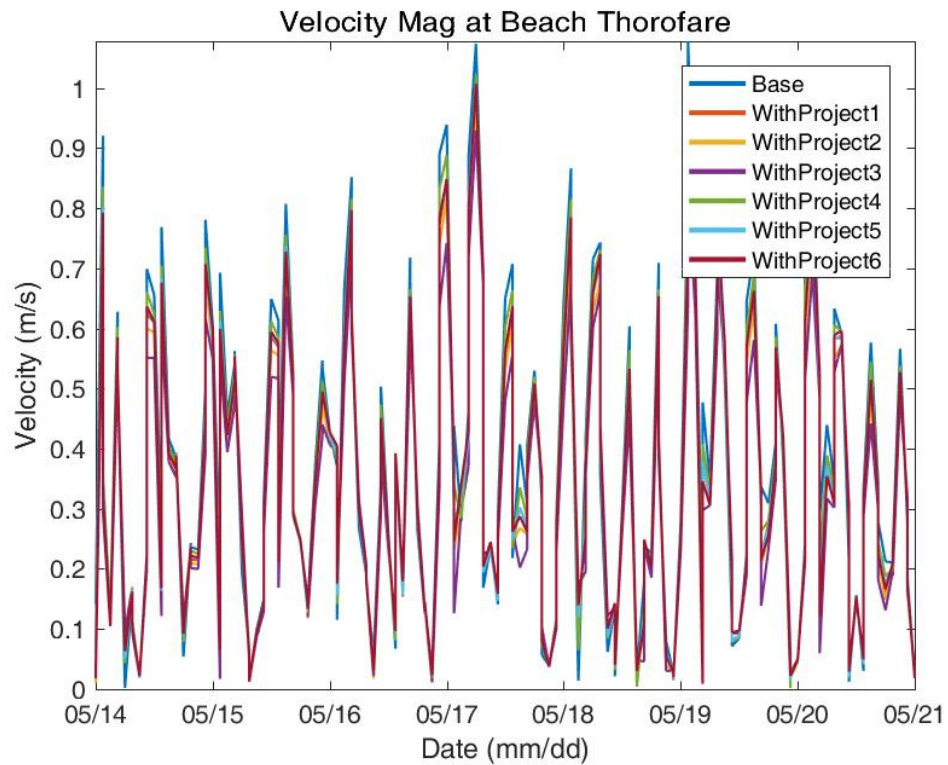
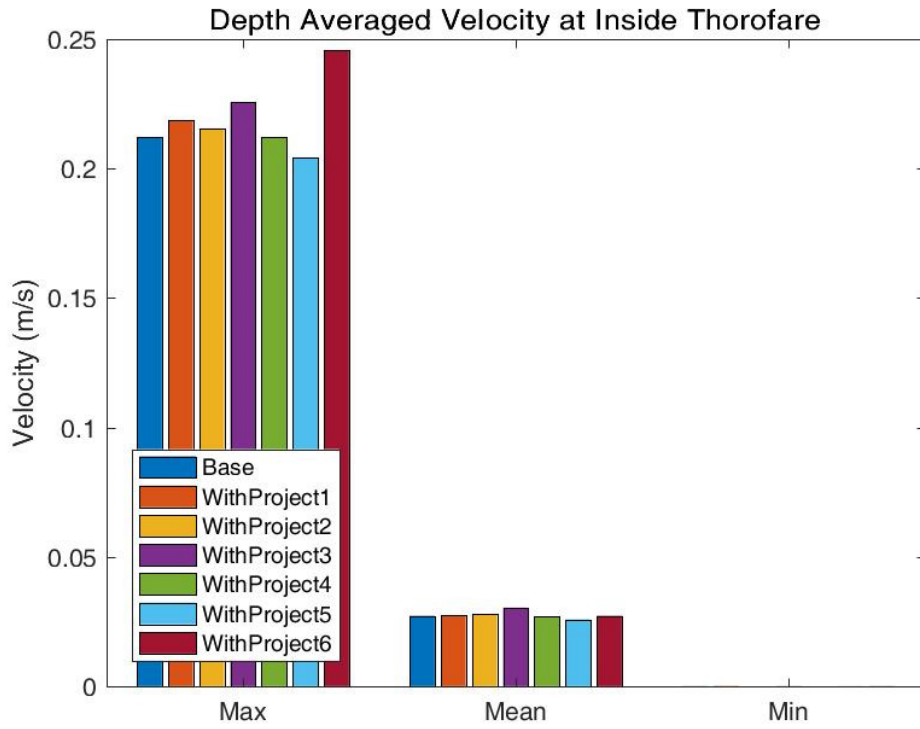


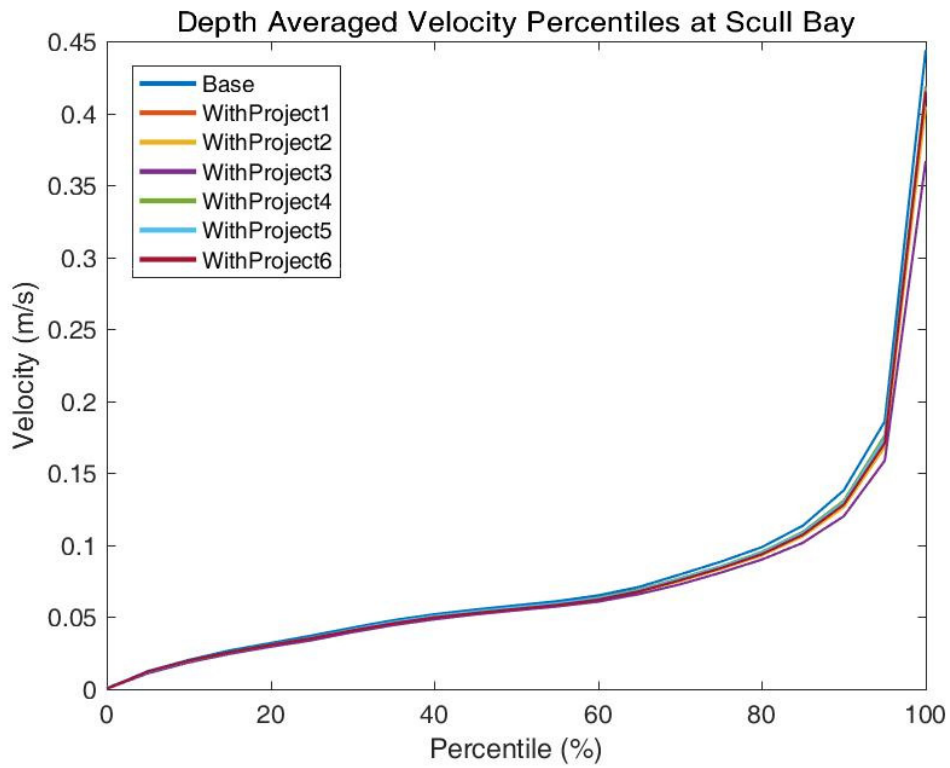
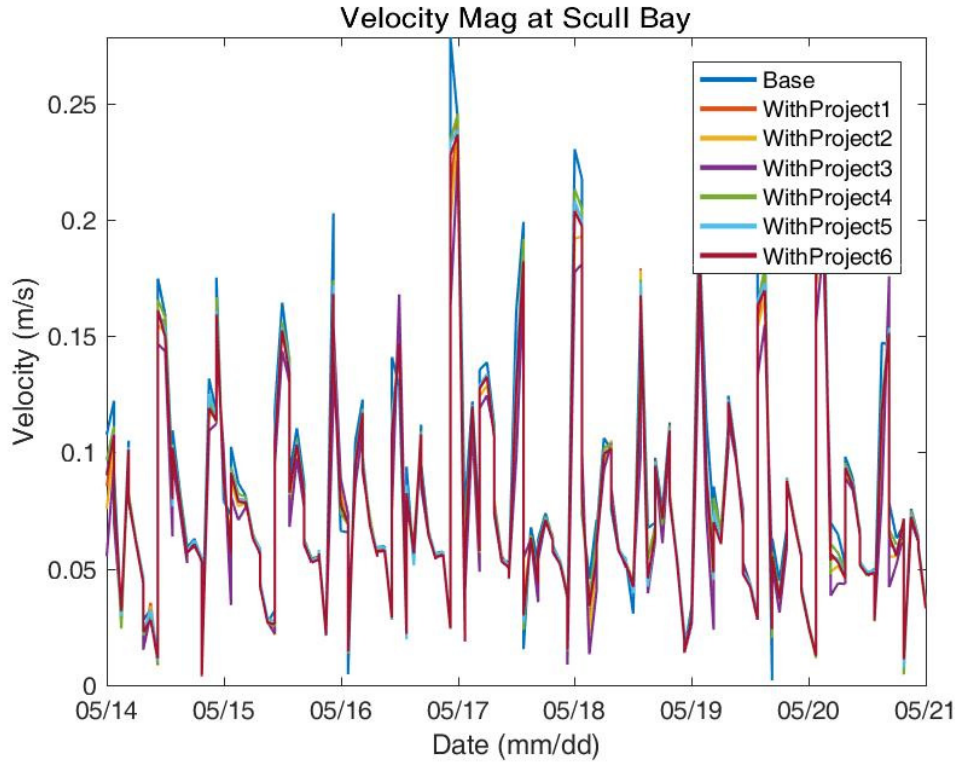


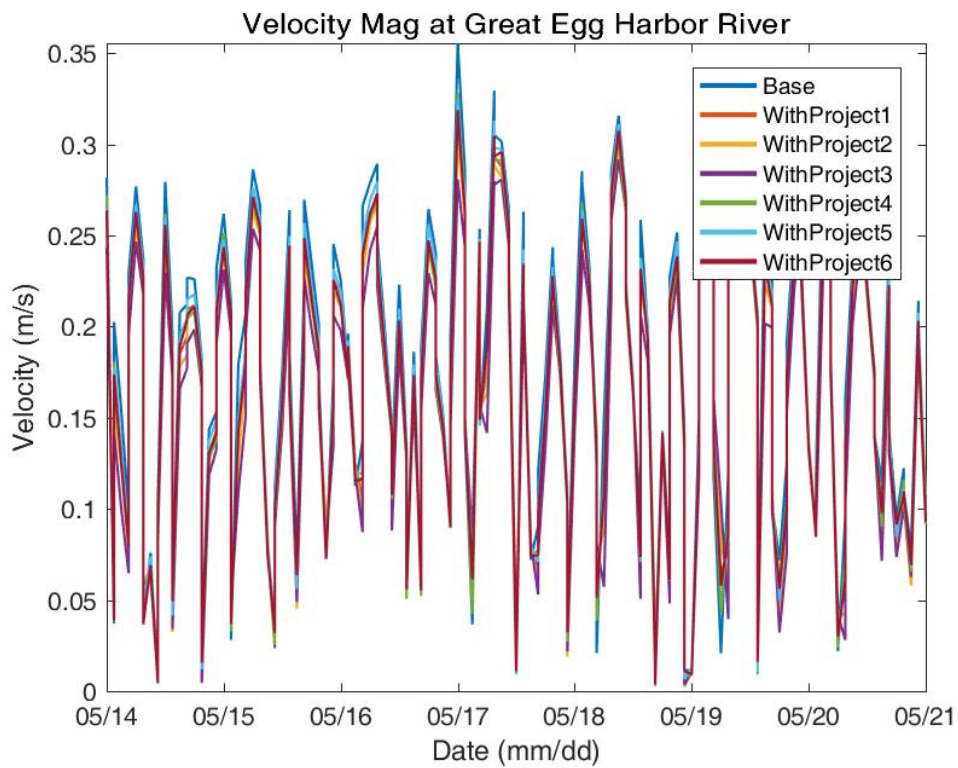
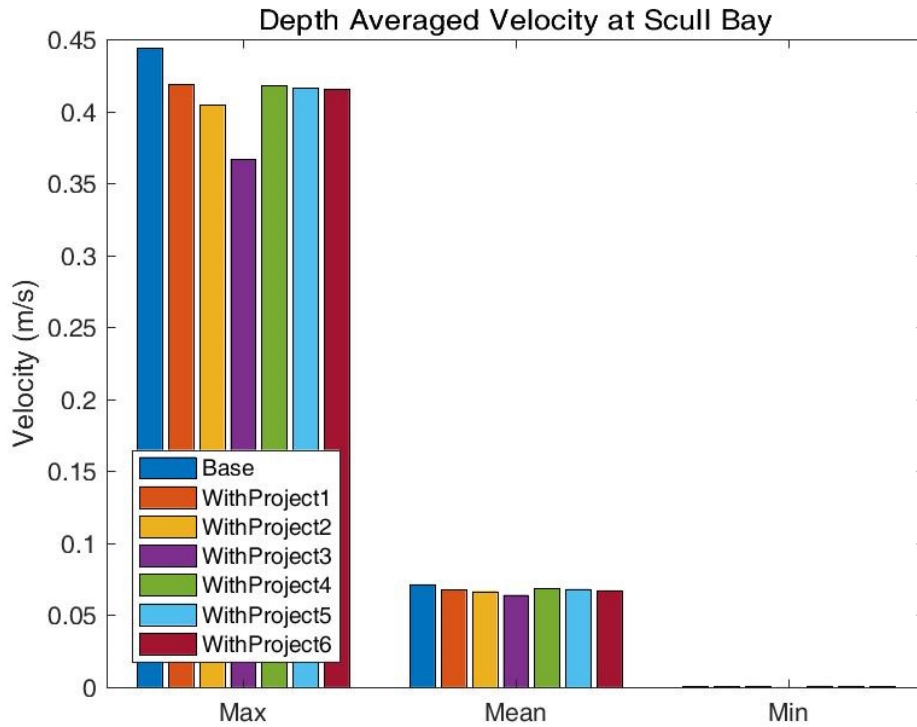


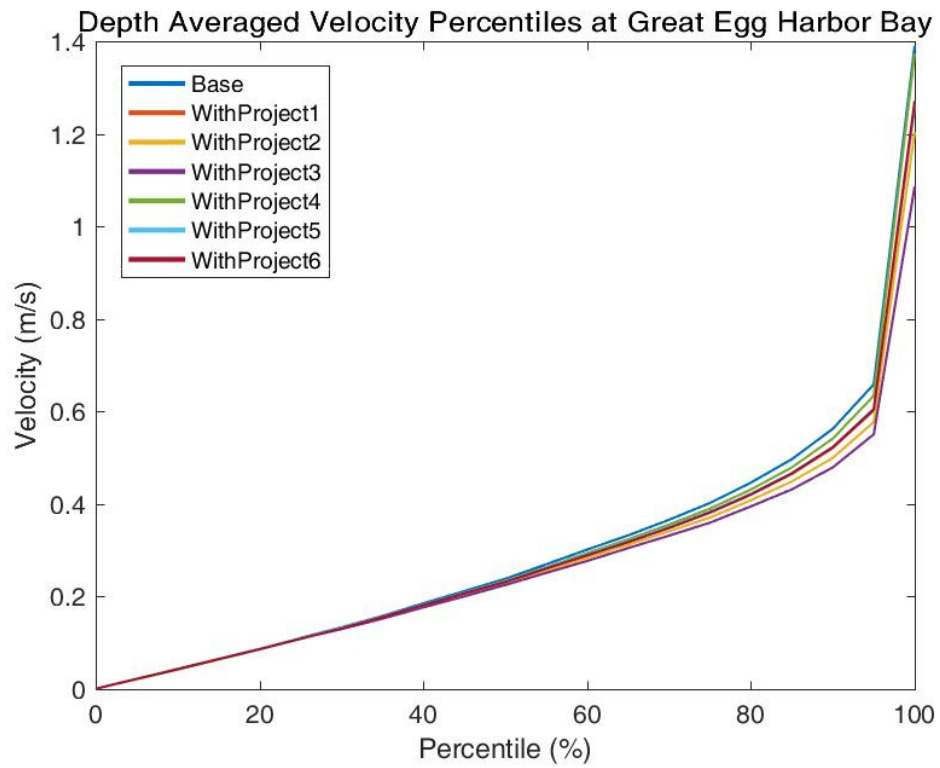
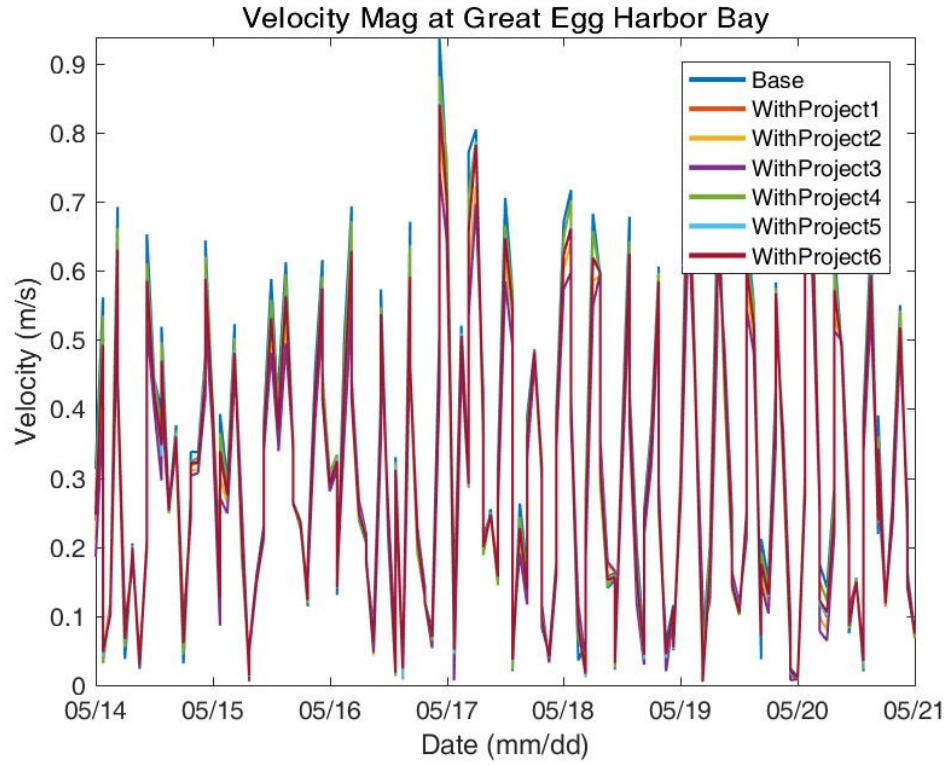


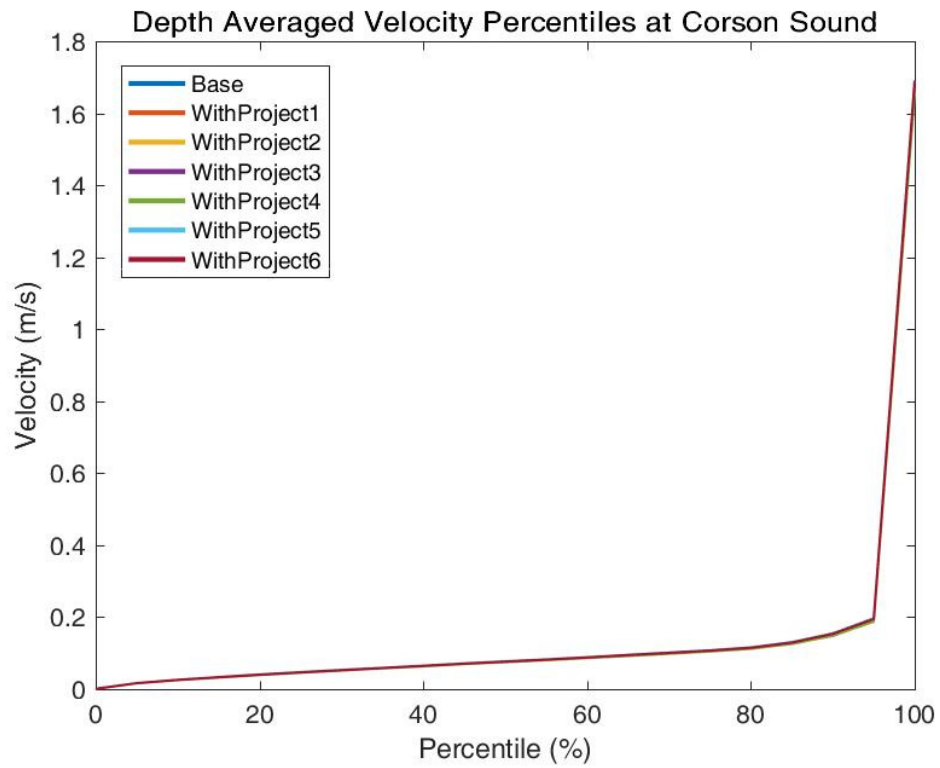
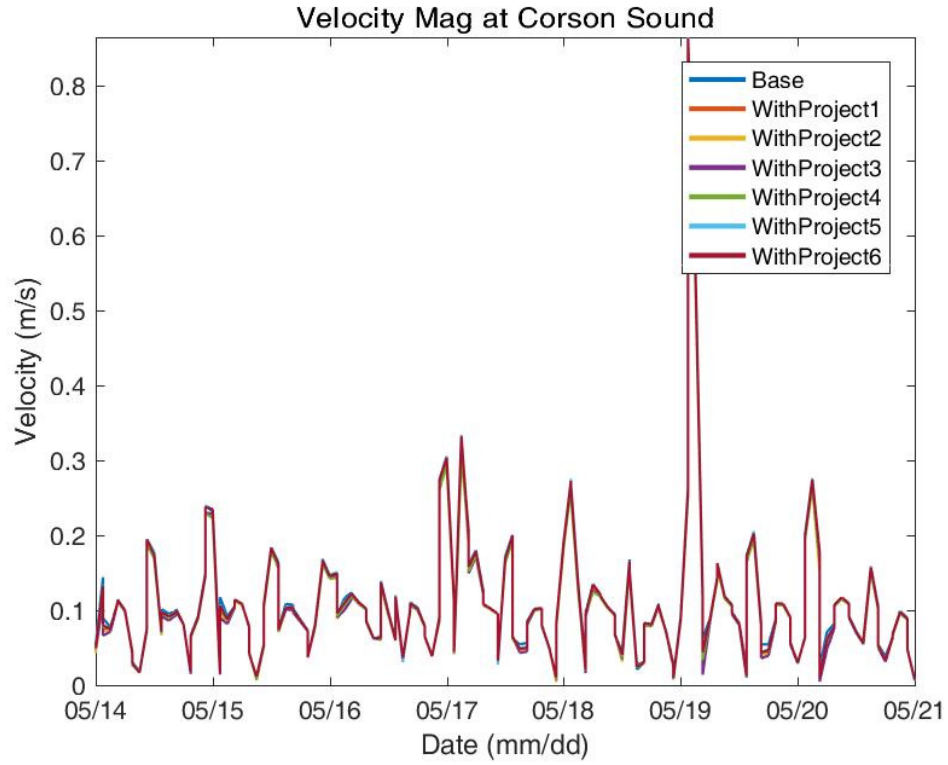


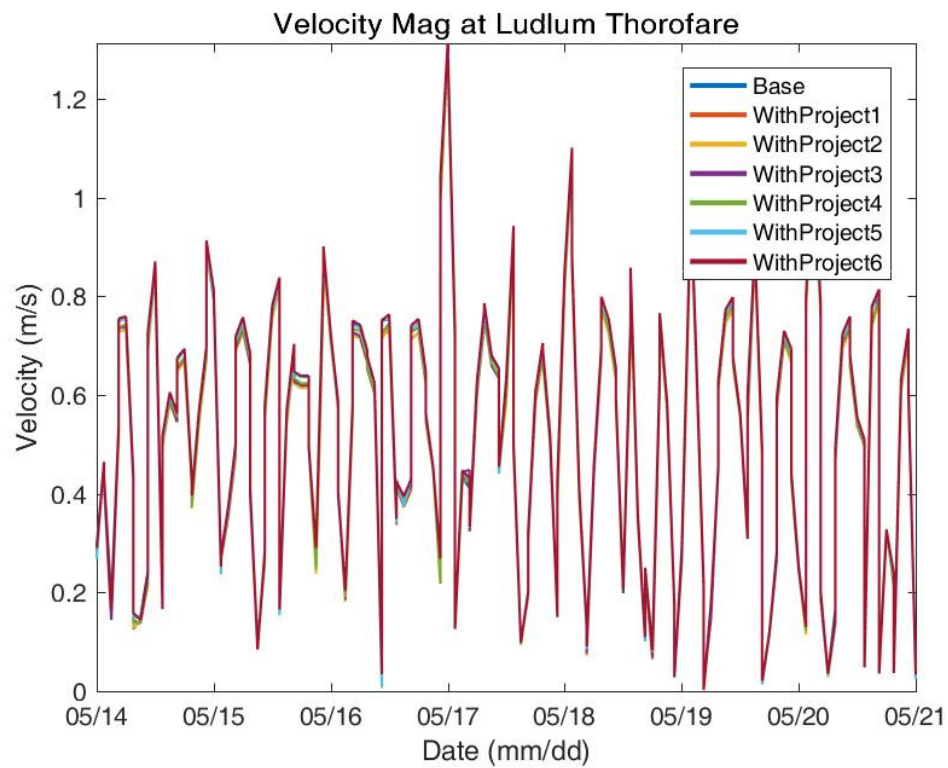
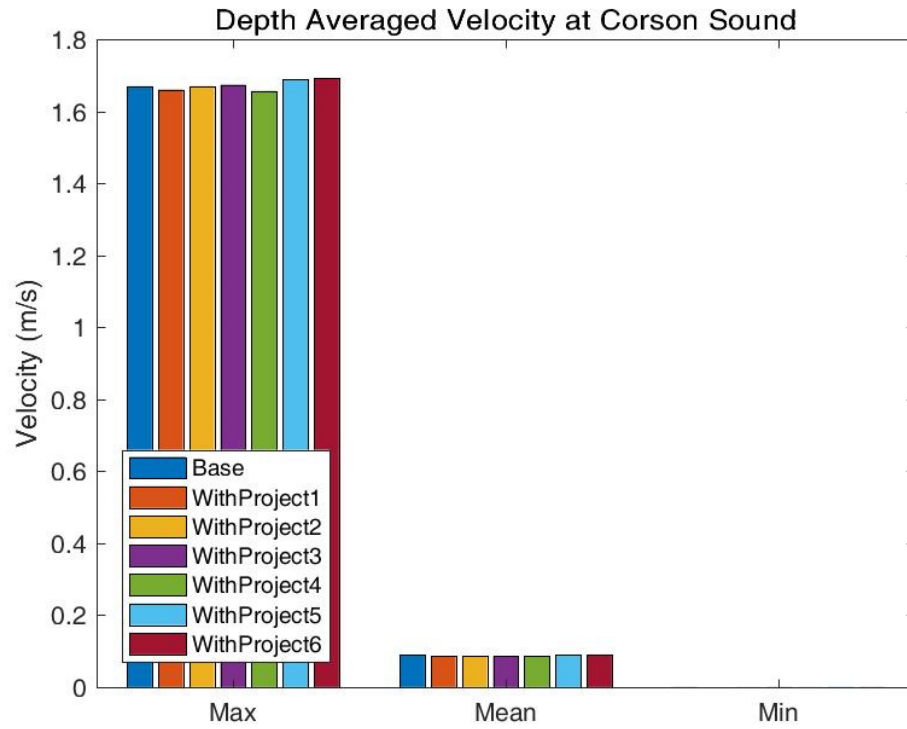


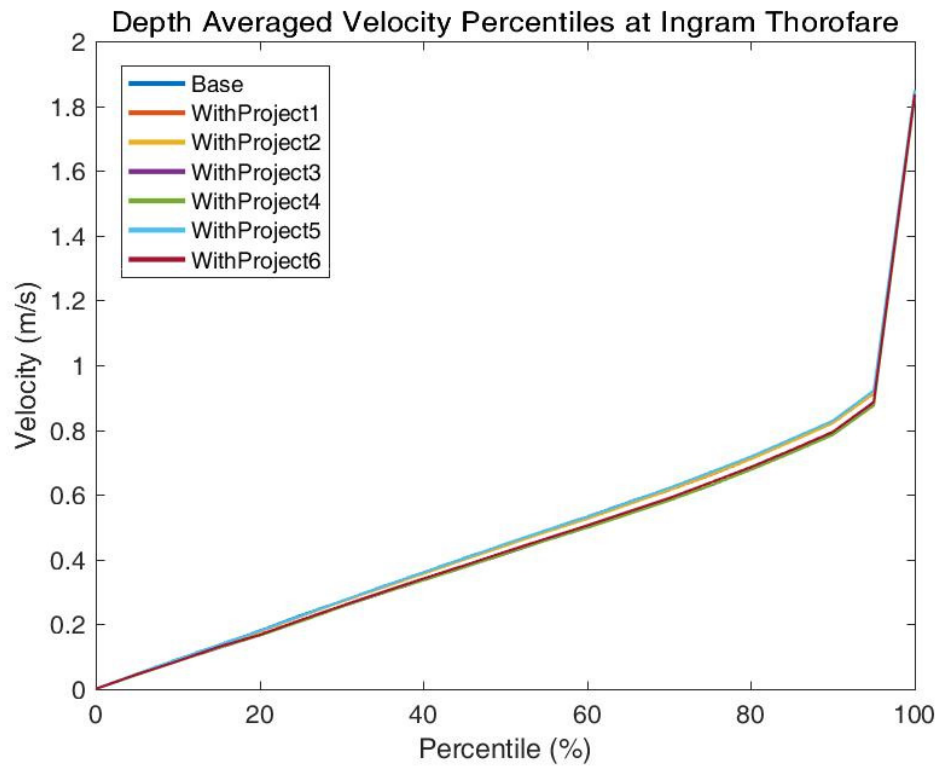
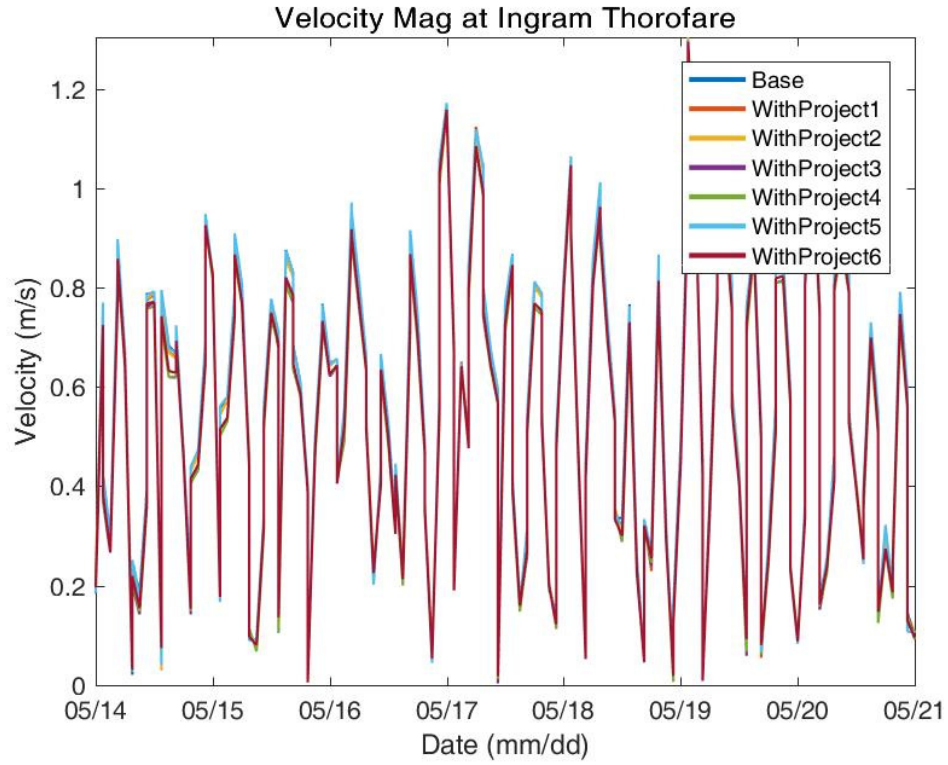


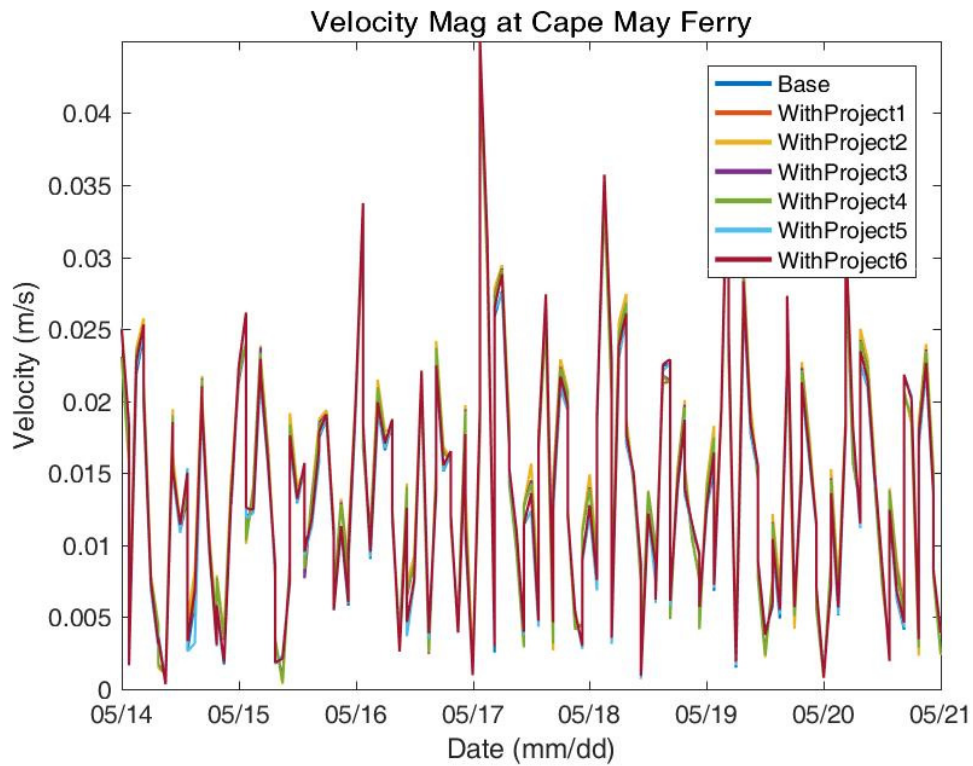
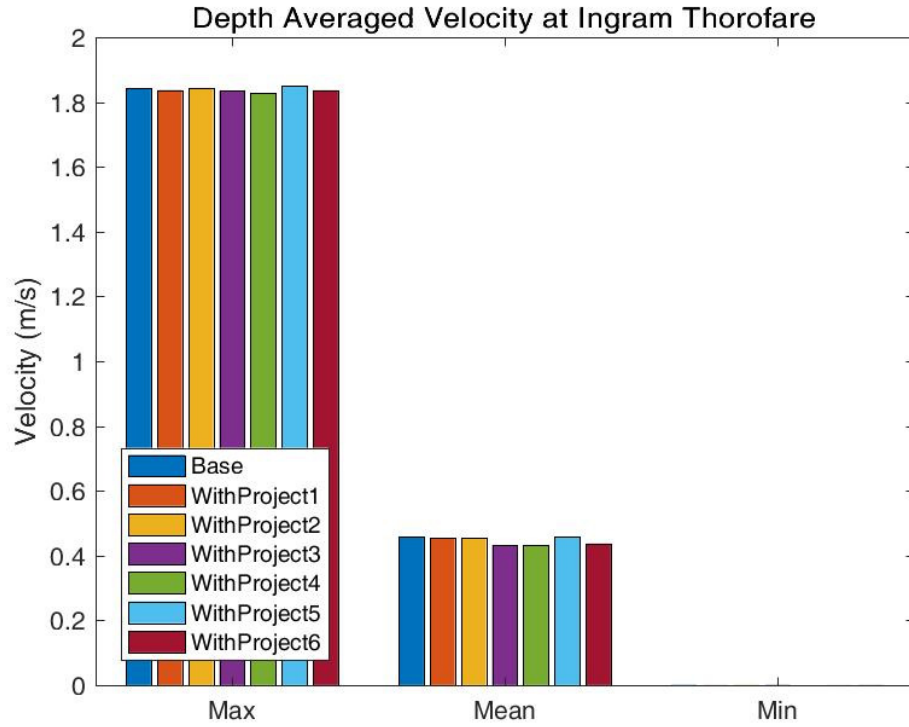


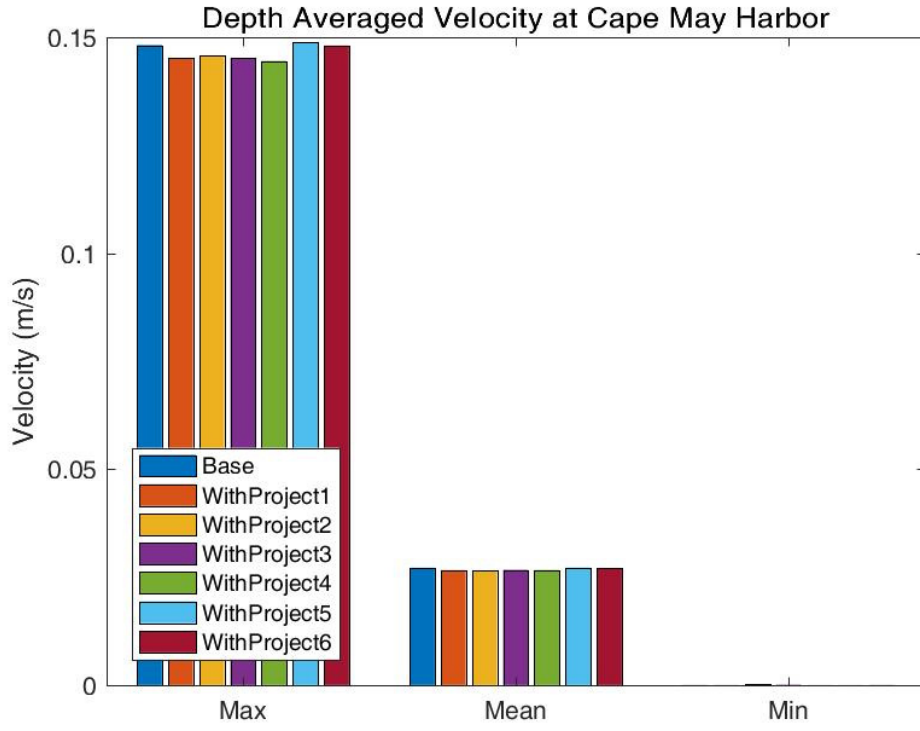








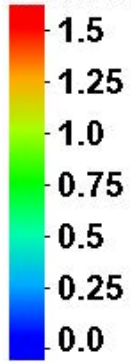




Regional Mean

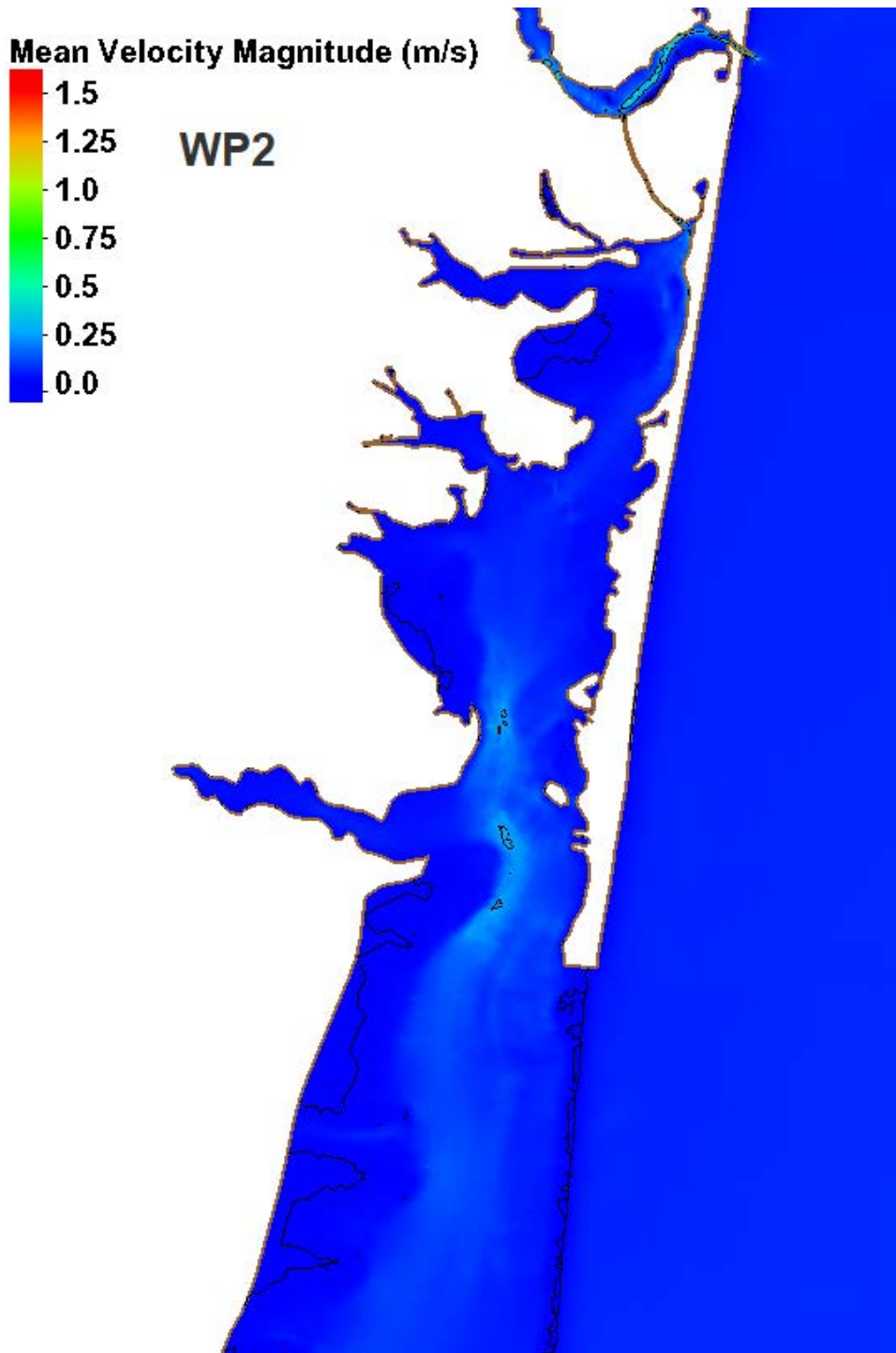
Northern Region (Manasquan and Barnegat)

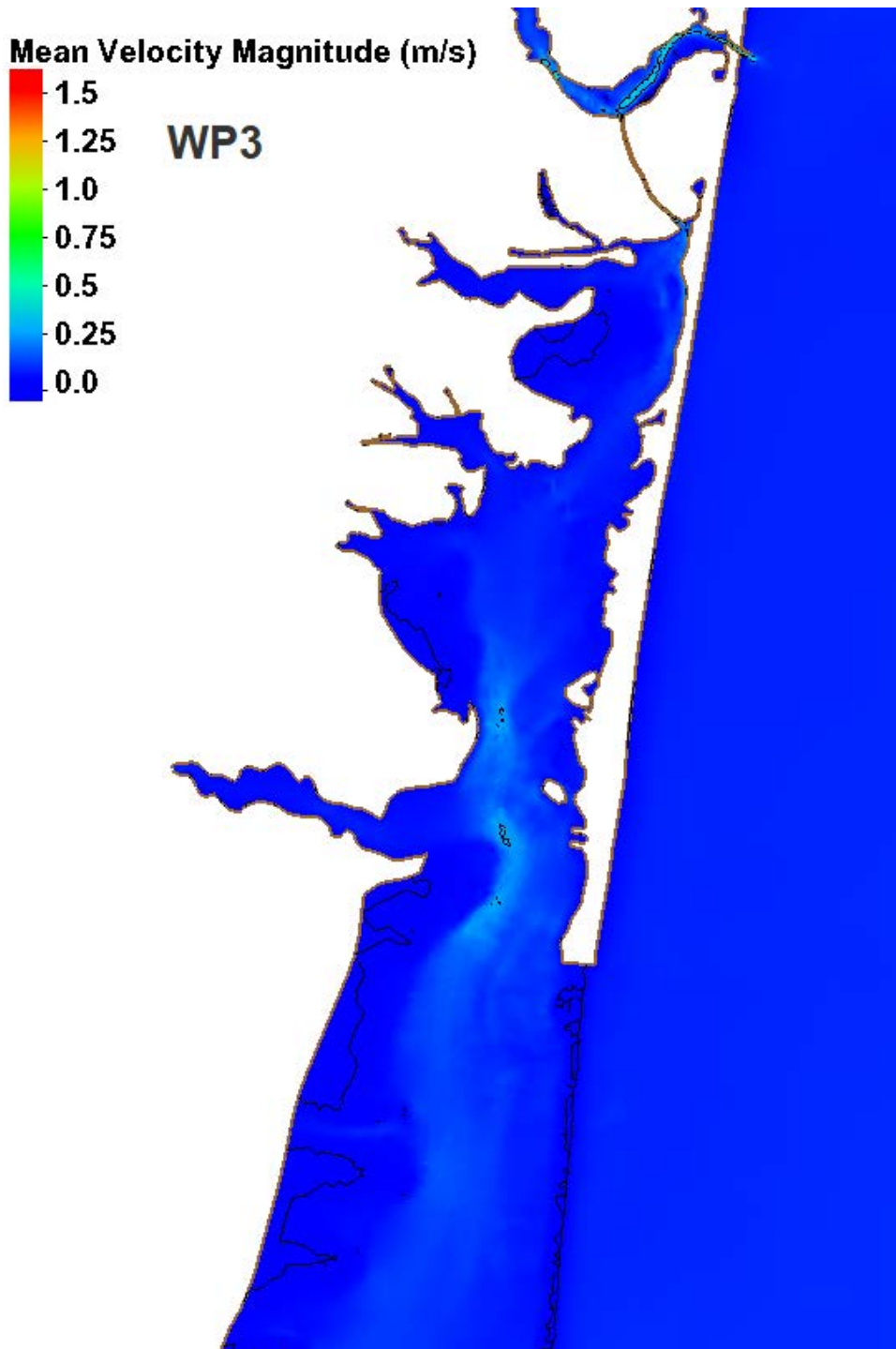
Mean Velocity Magnitude (m/s)

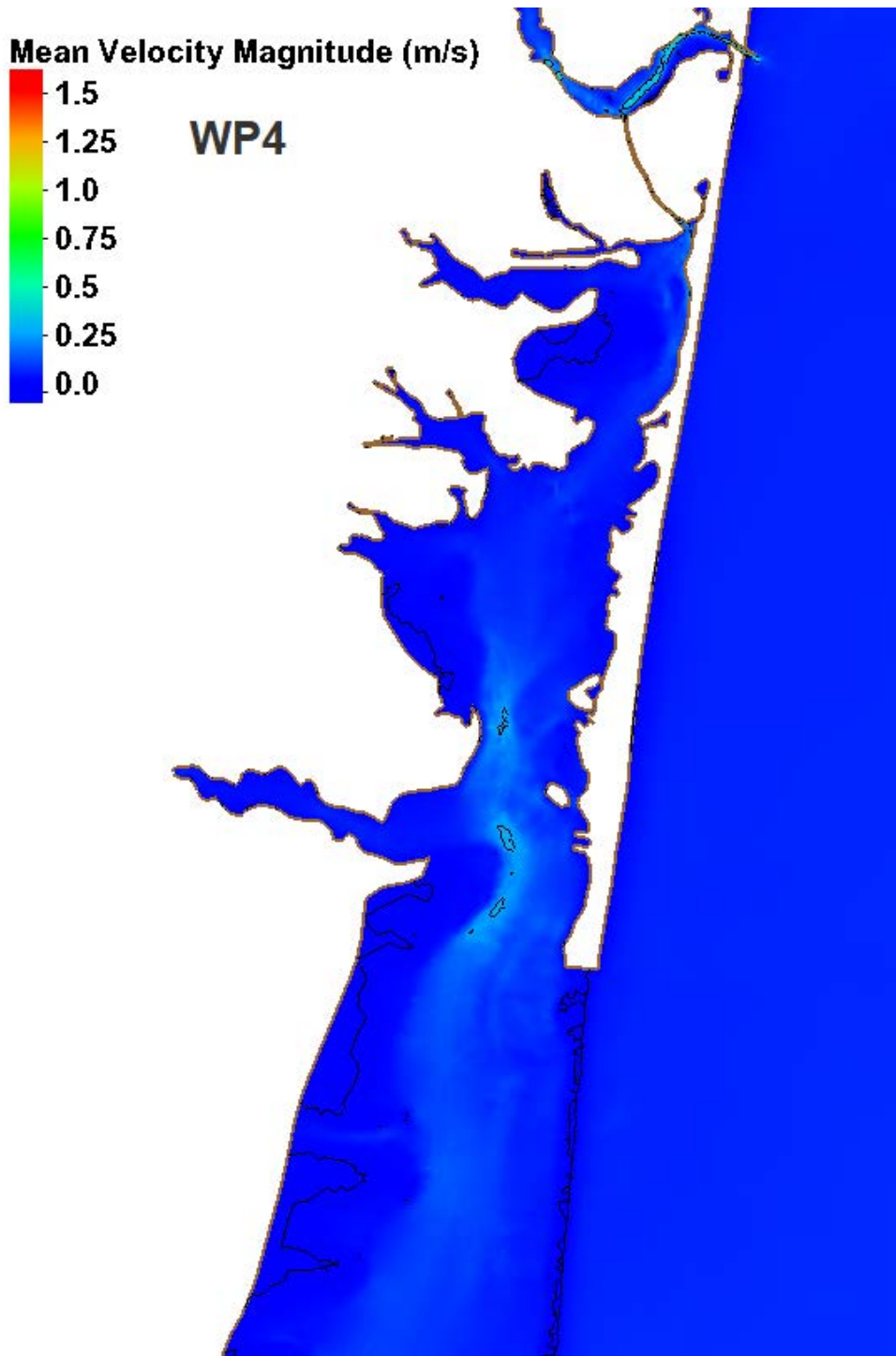


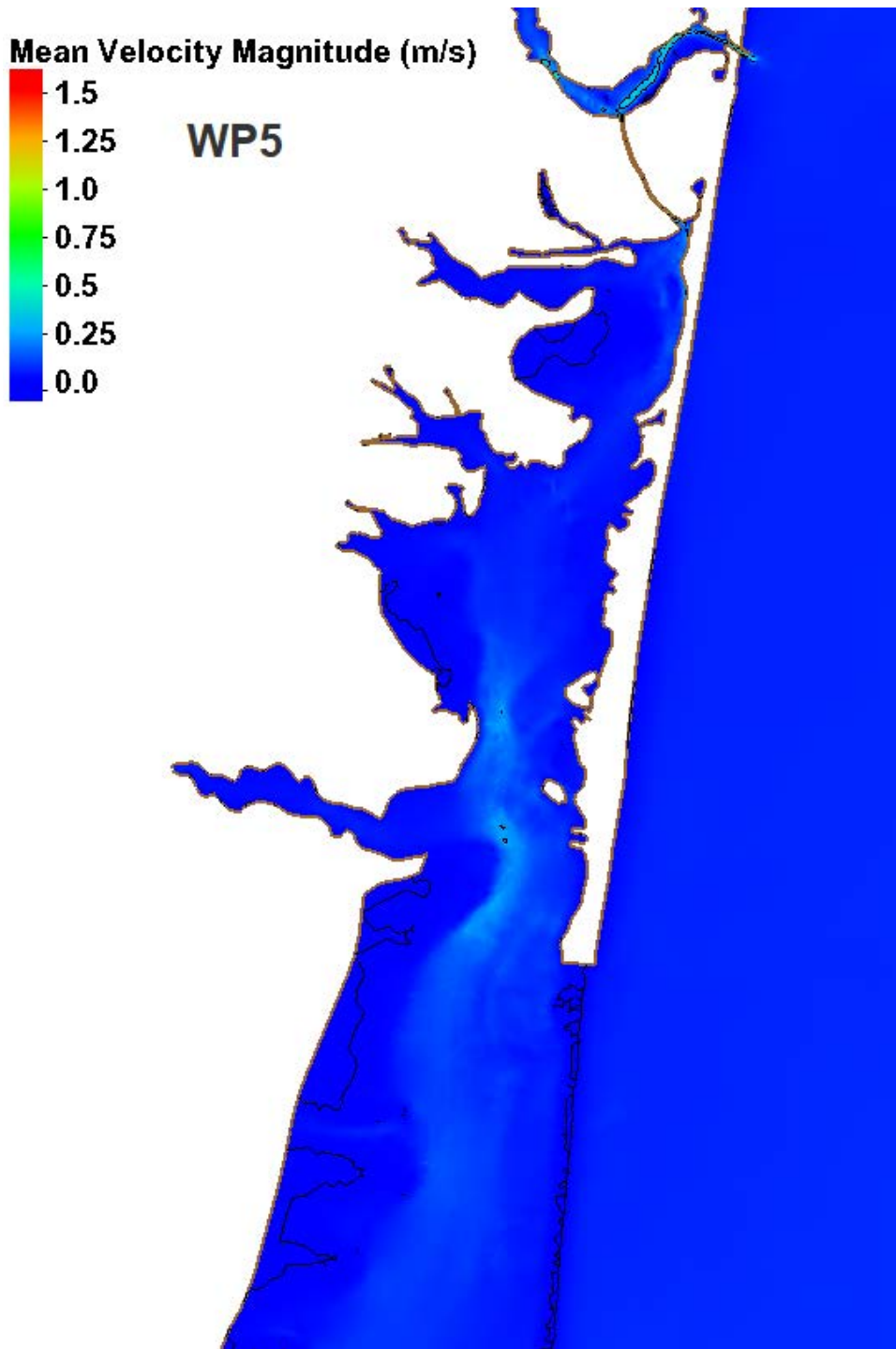
WP1

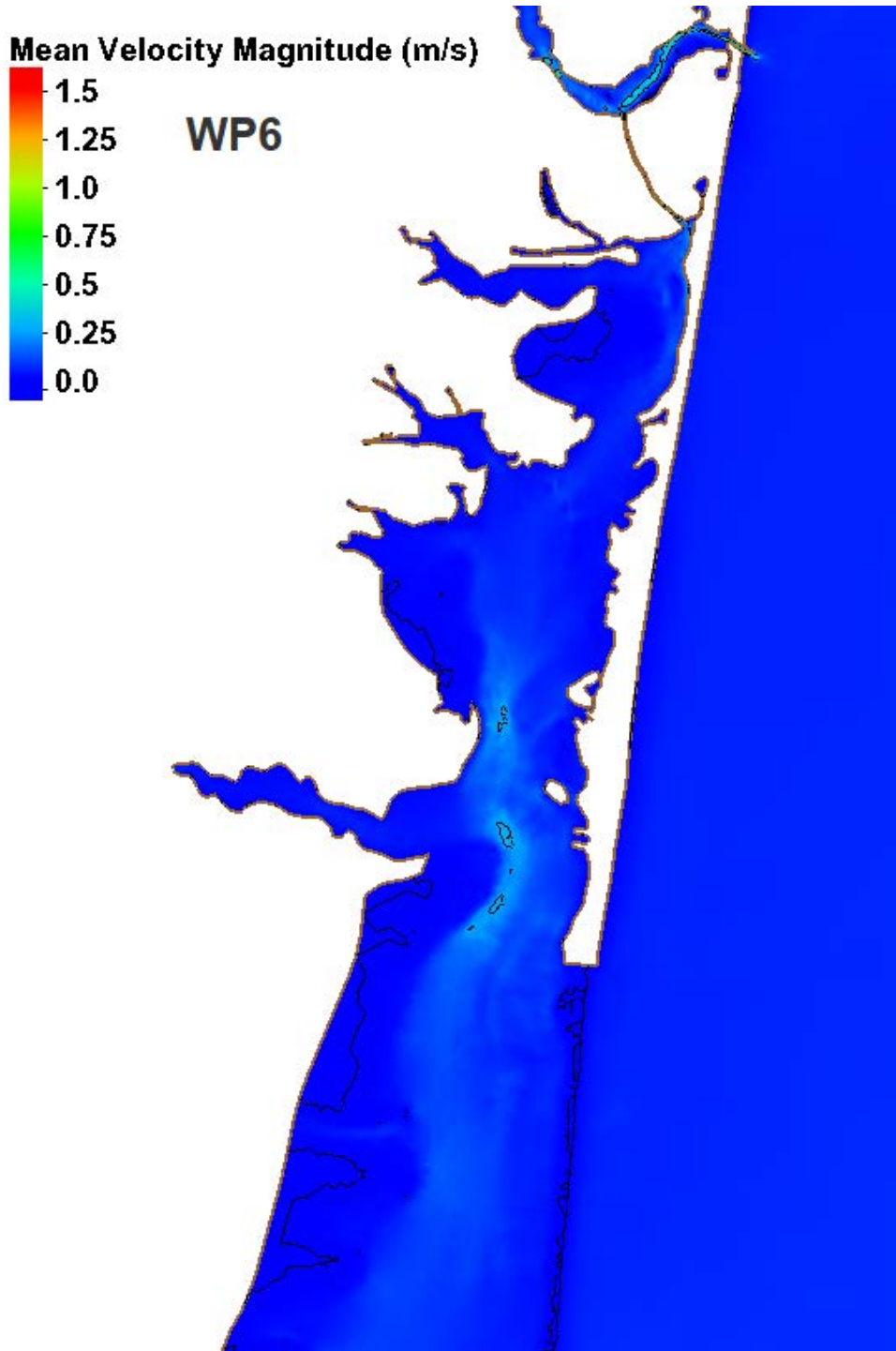


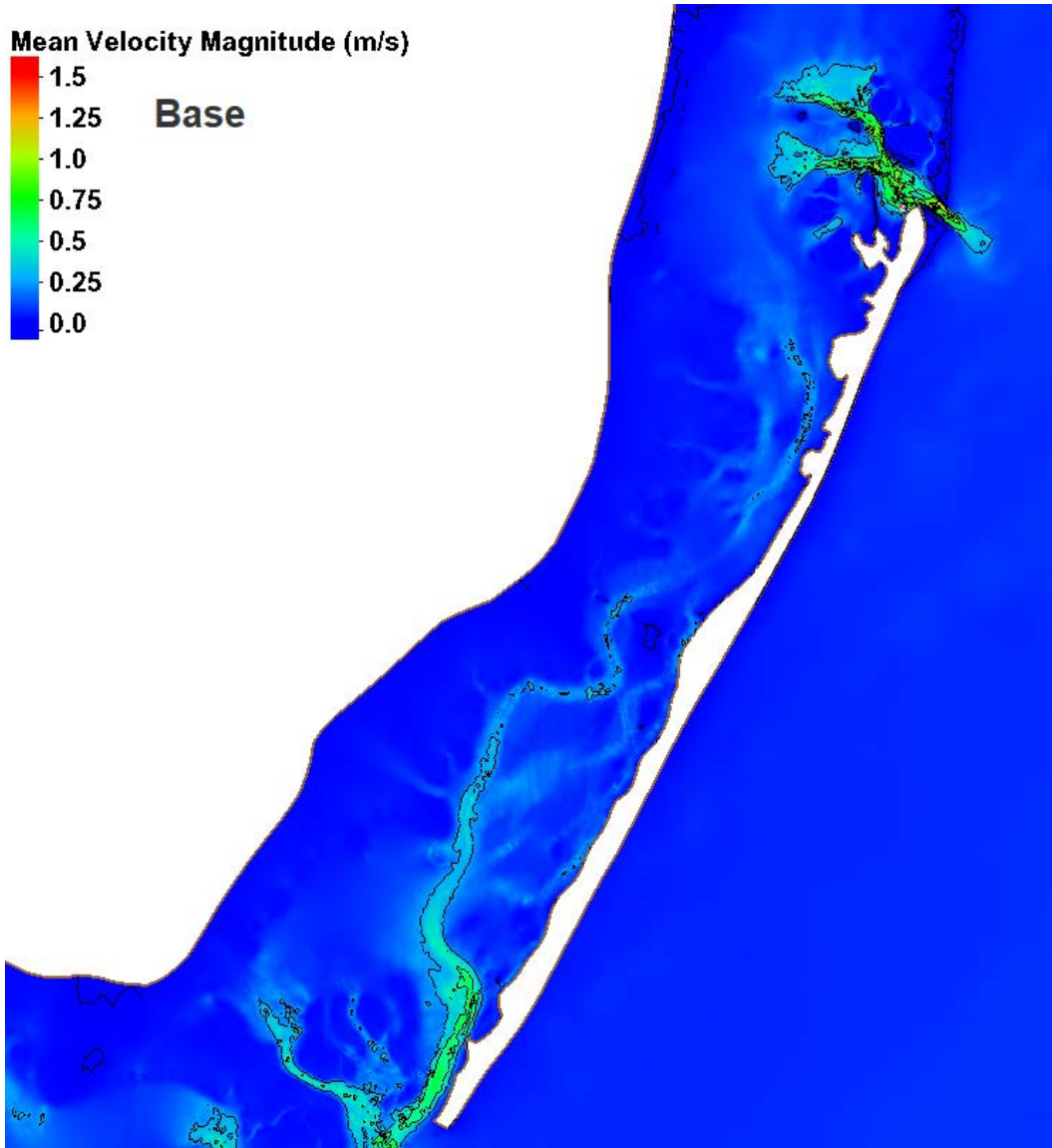


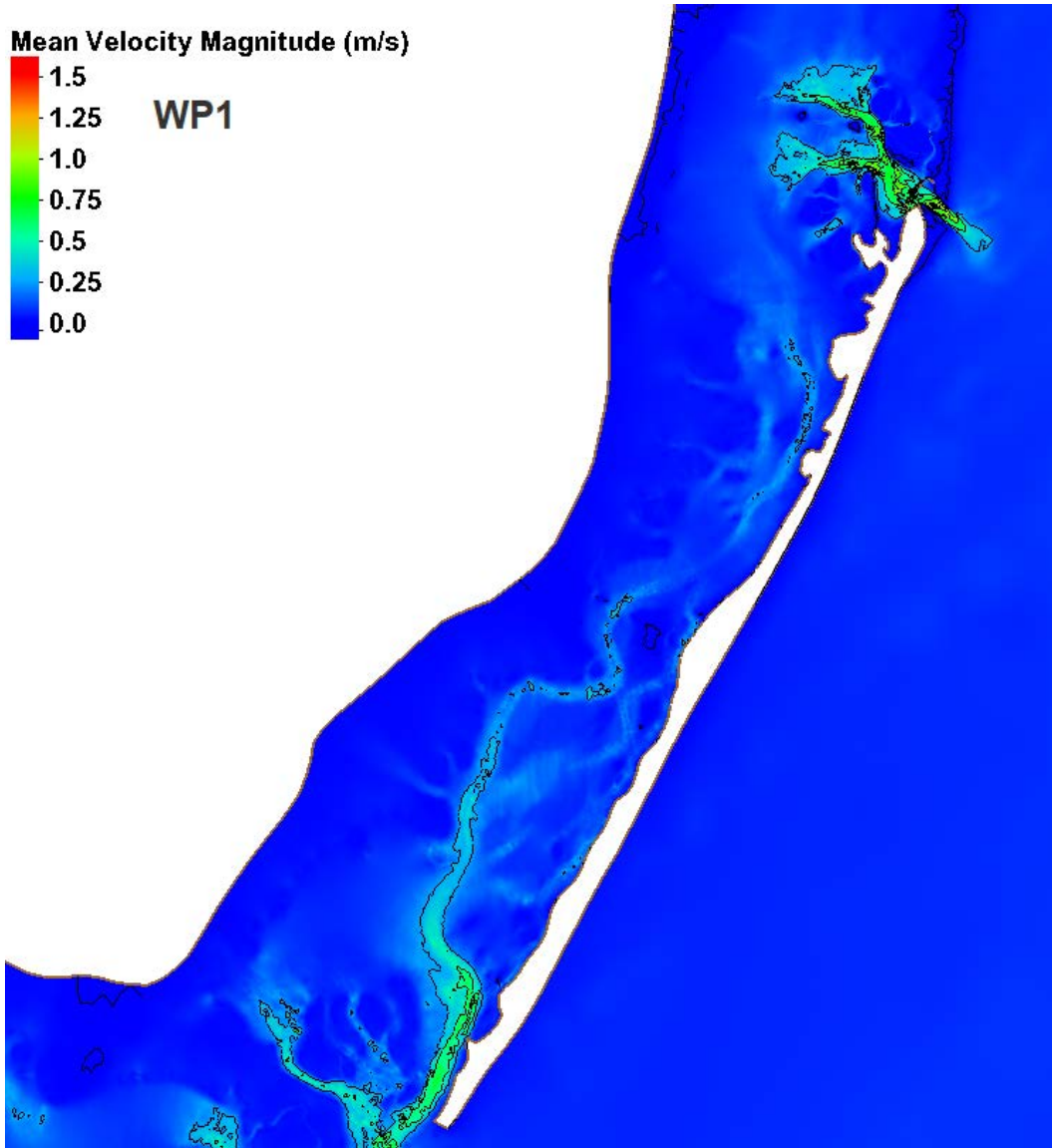


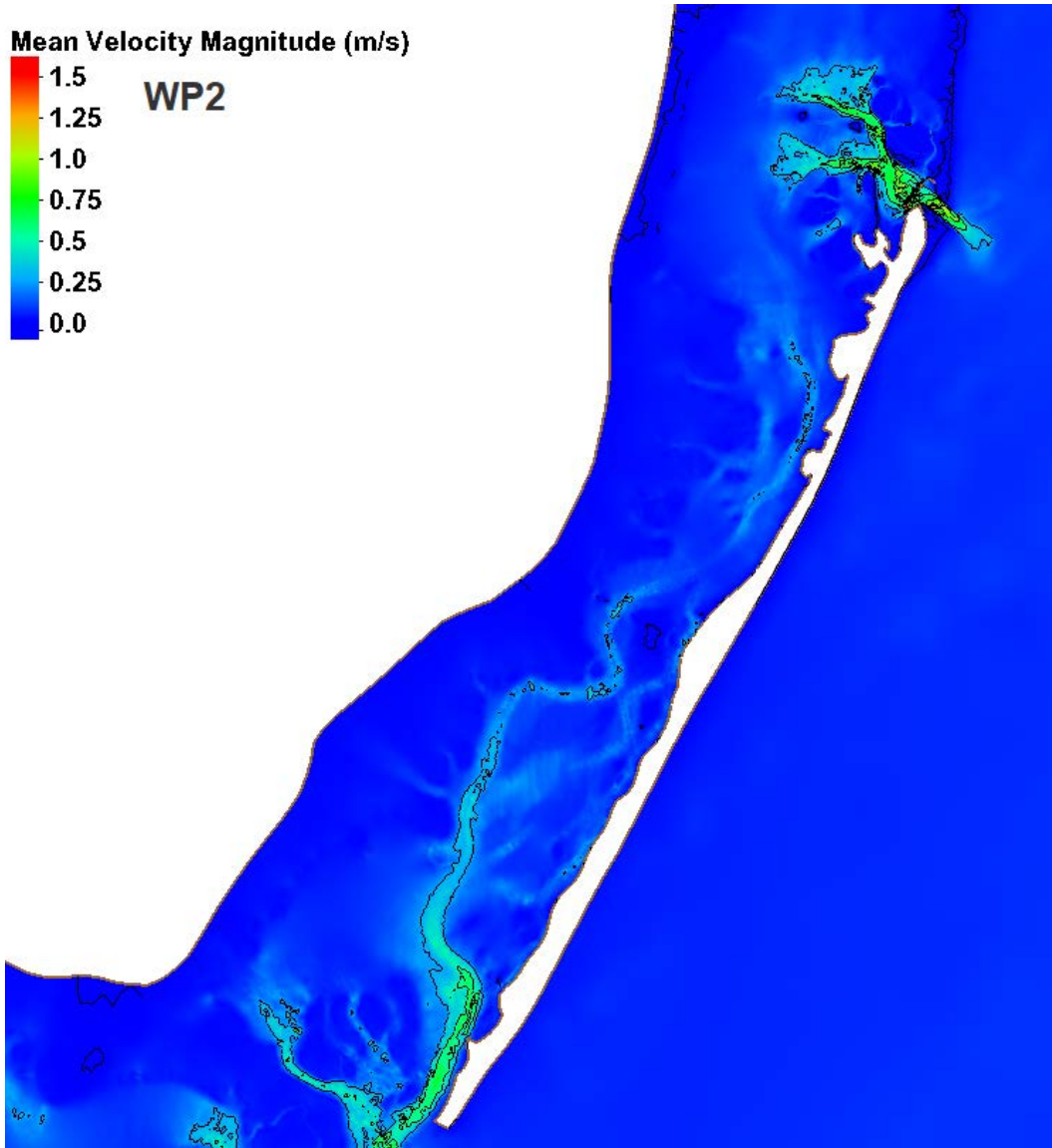


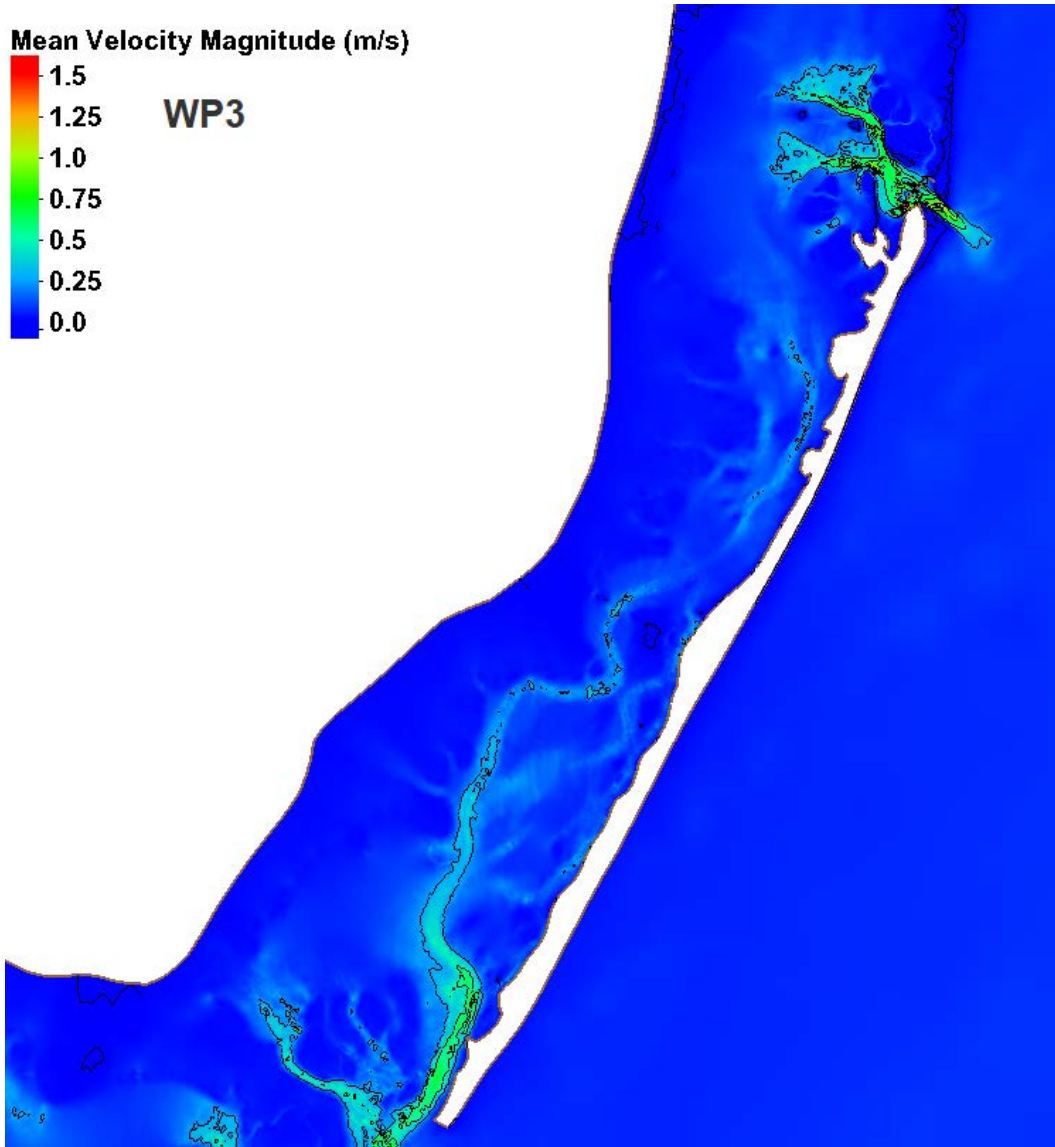


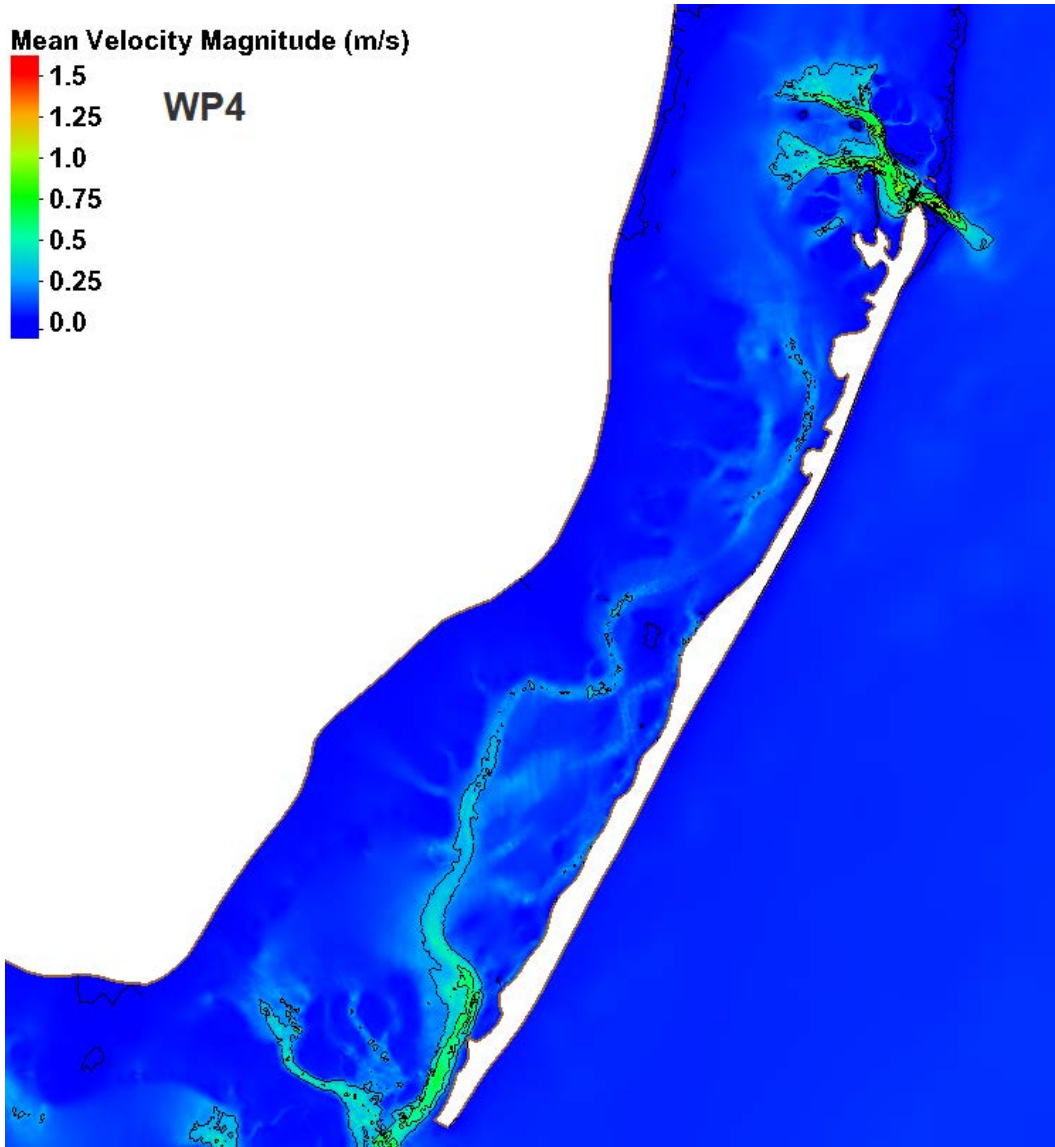


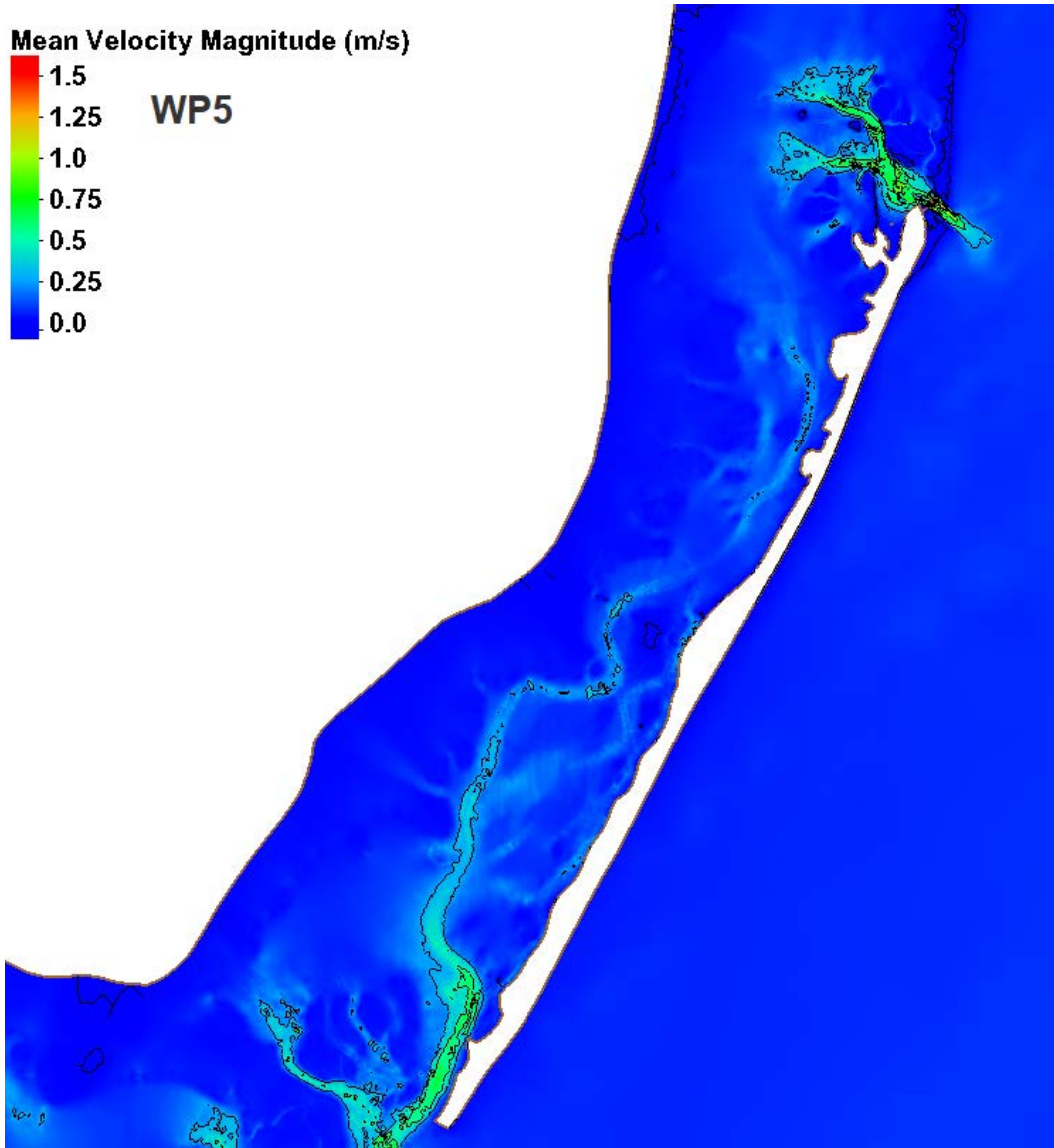


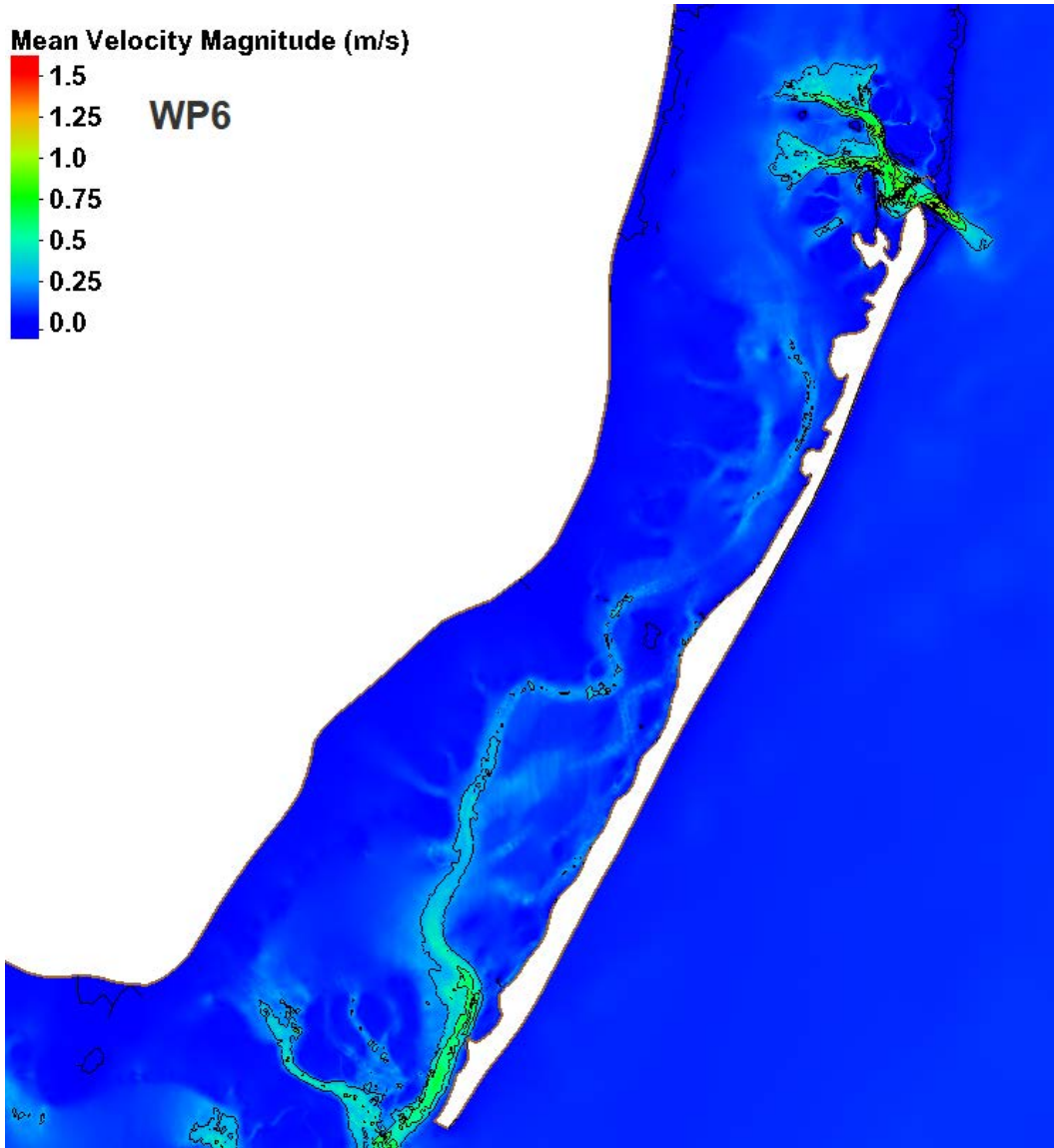




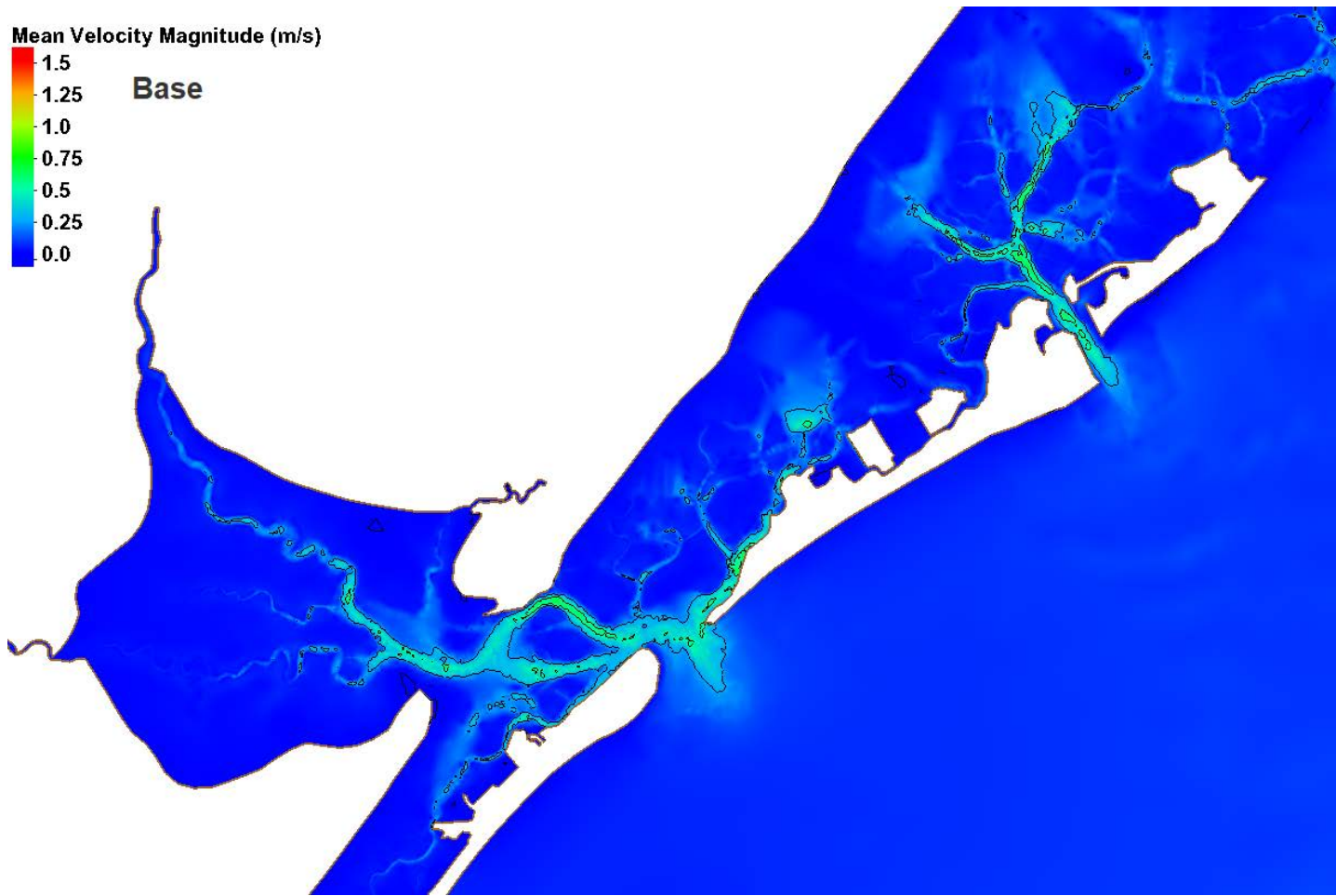


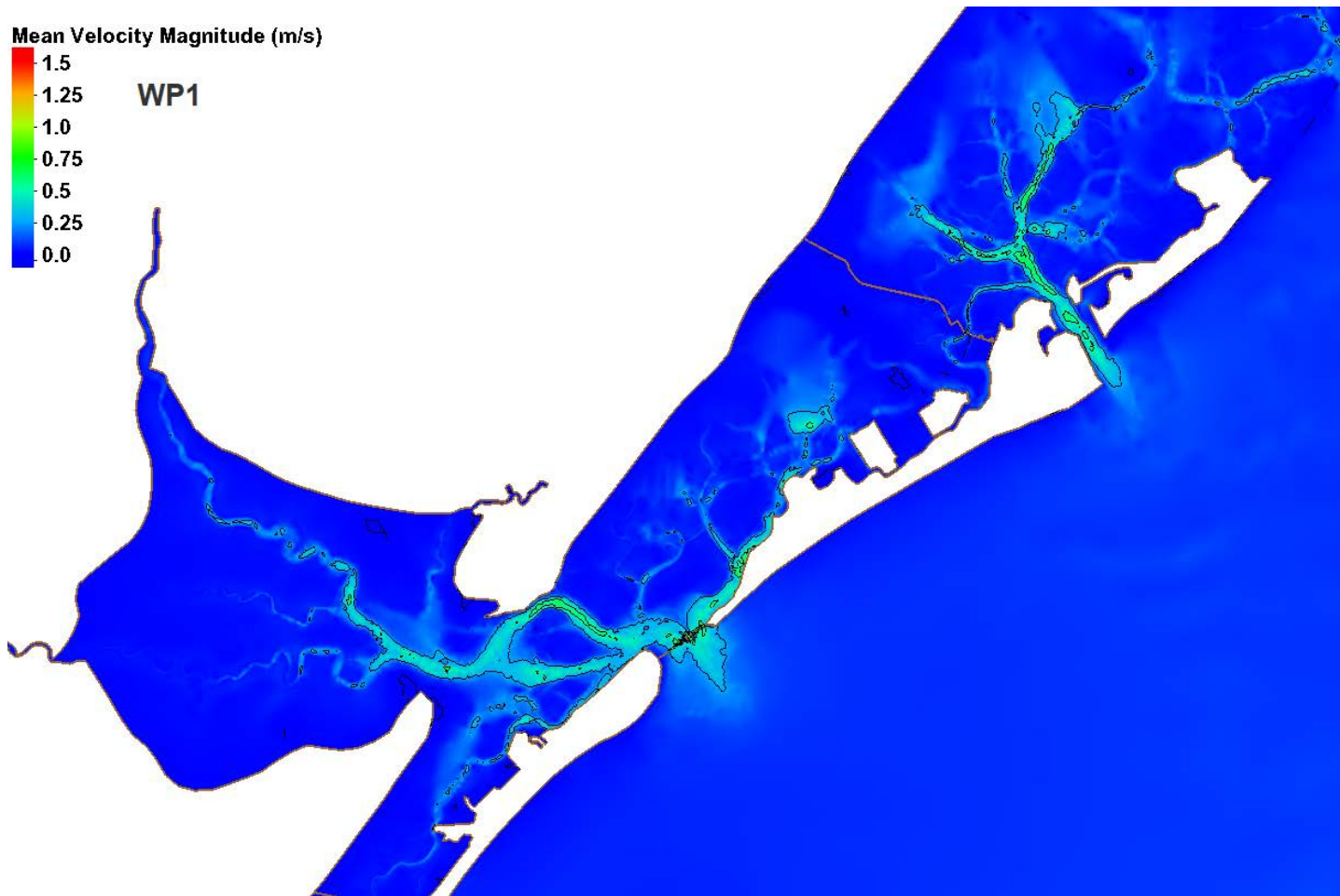


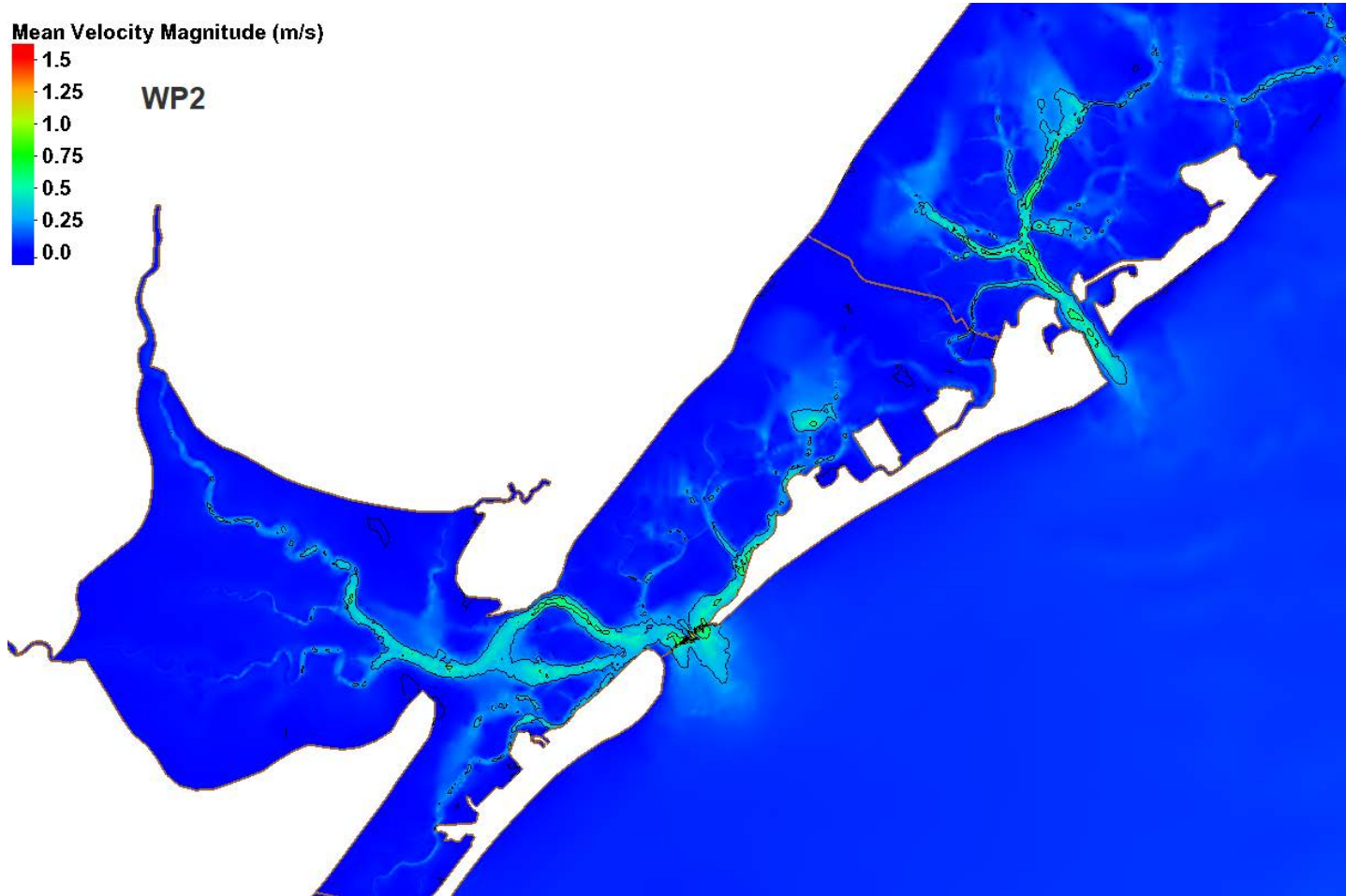


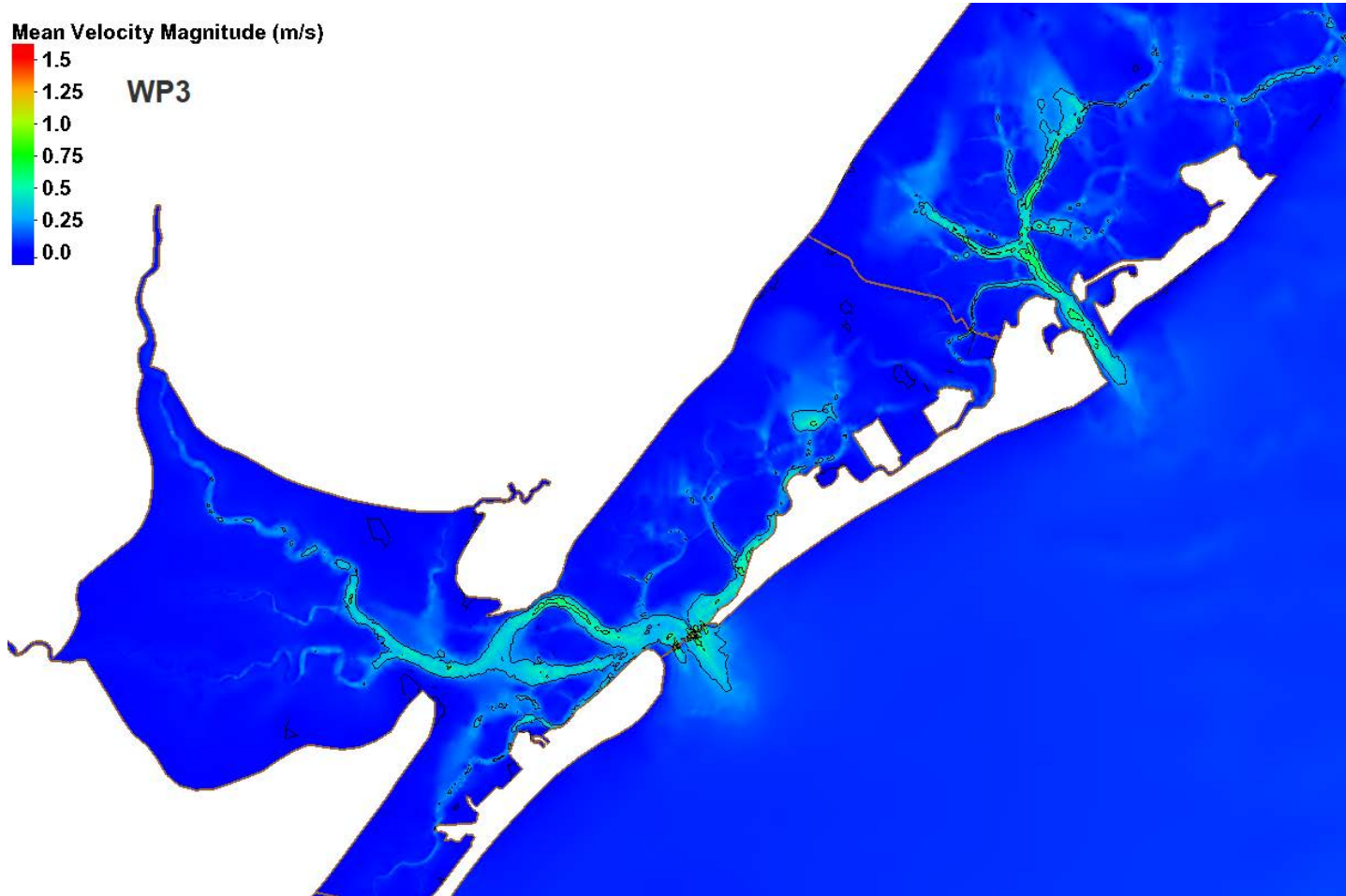


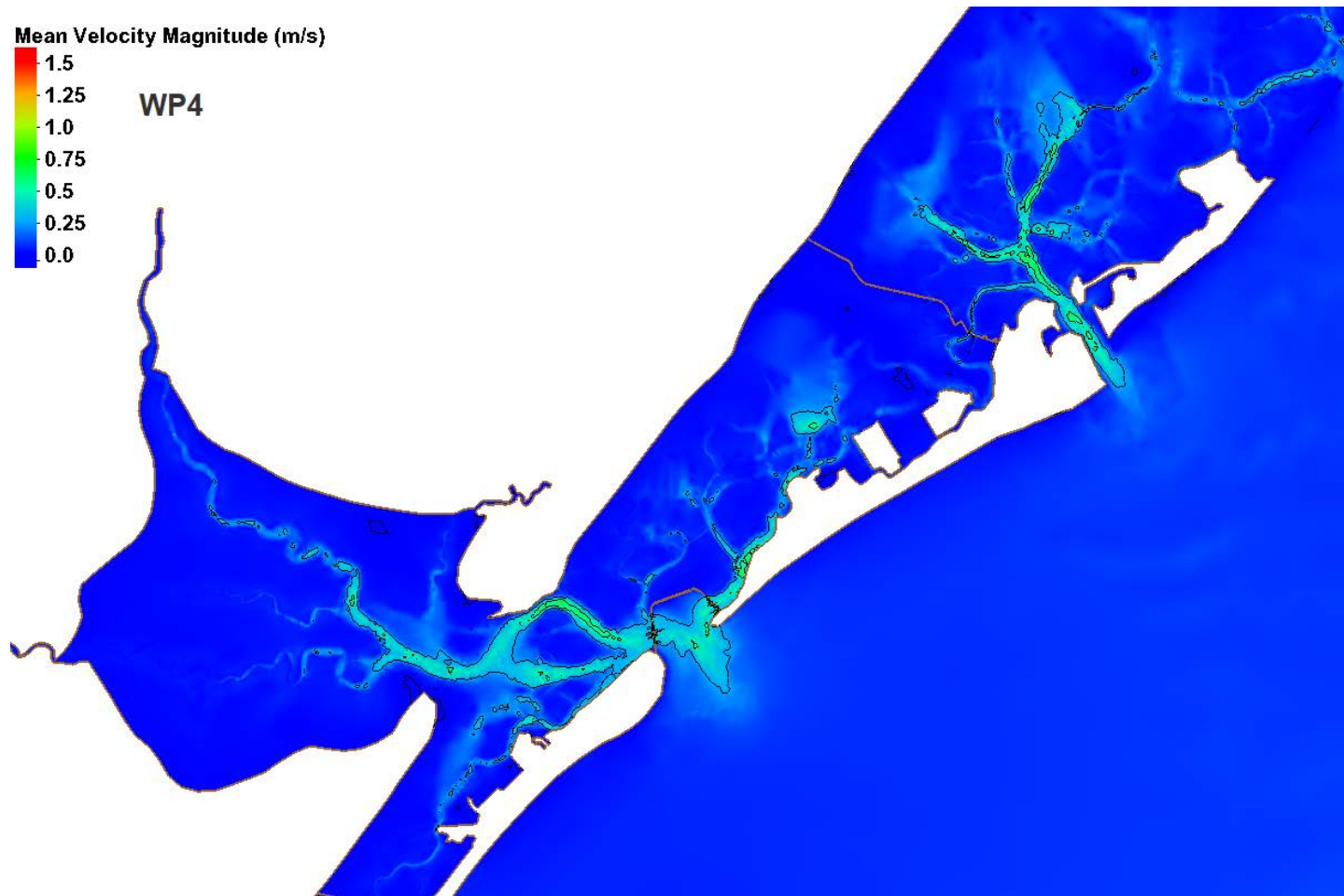
Central Region (Great Egg and Absecon)

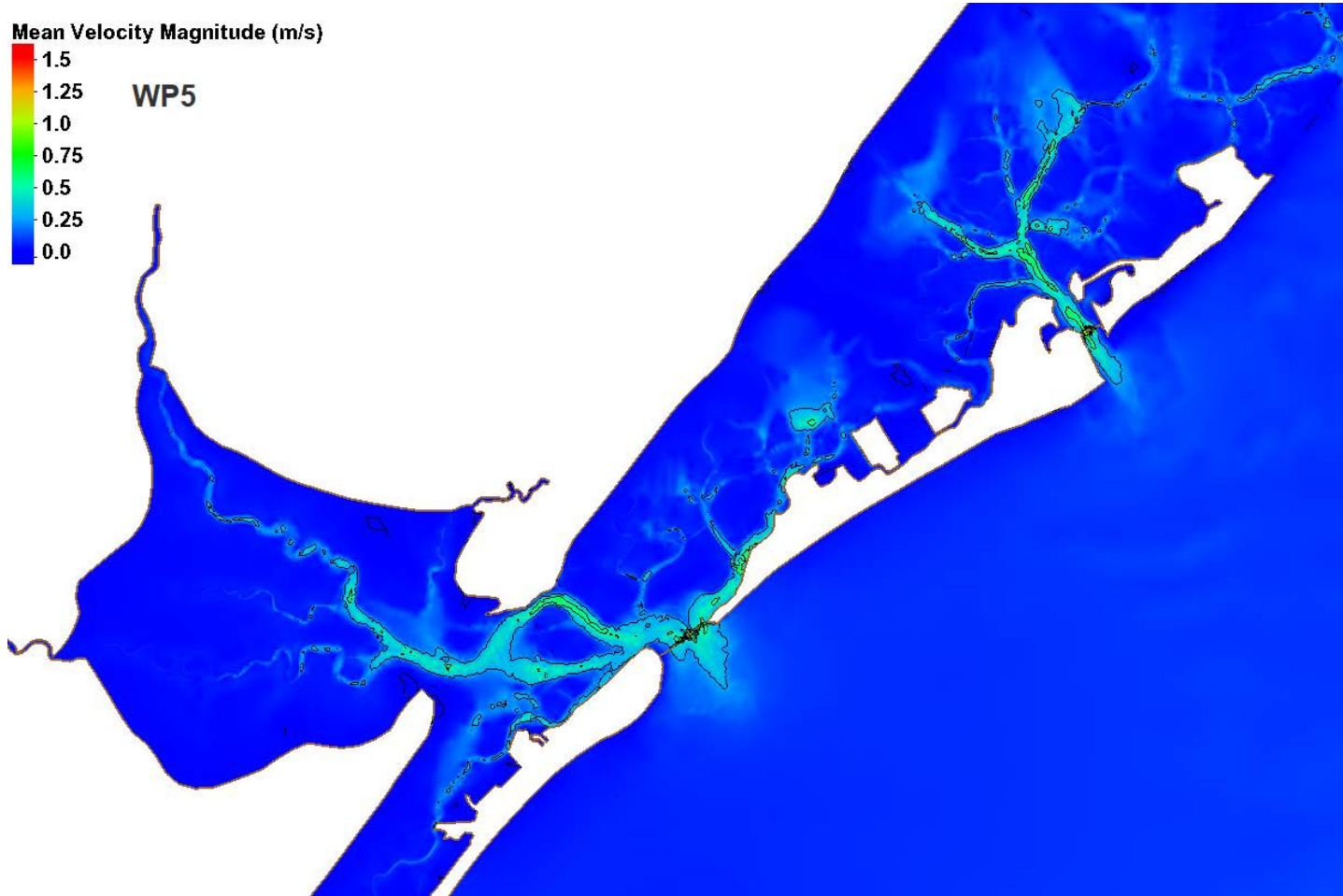


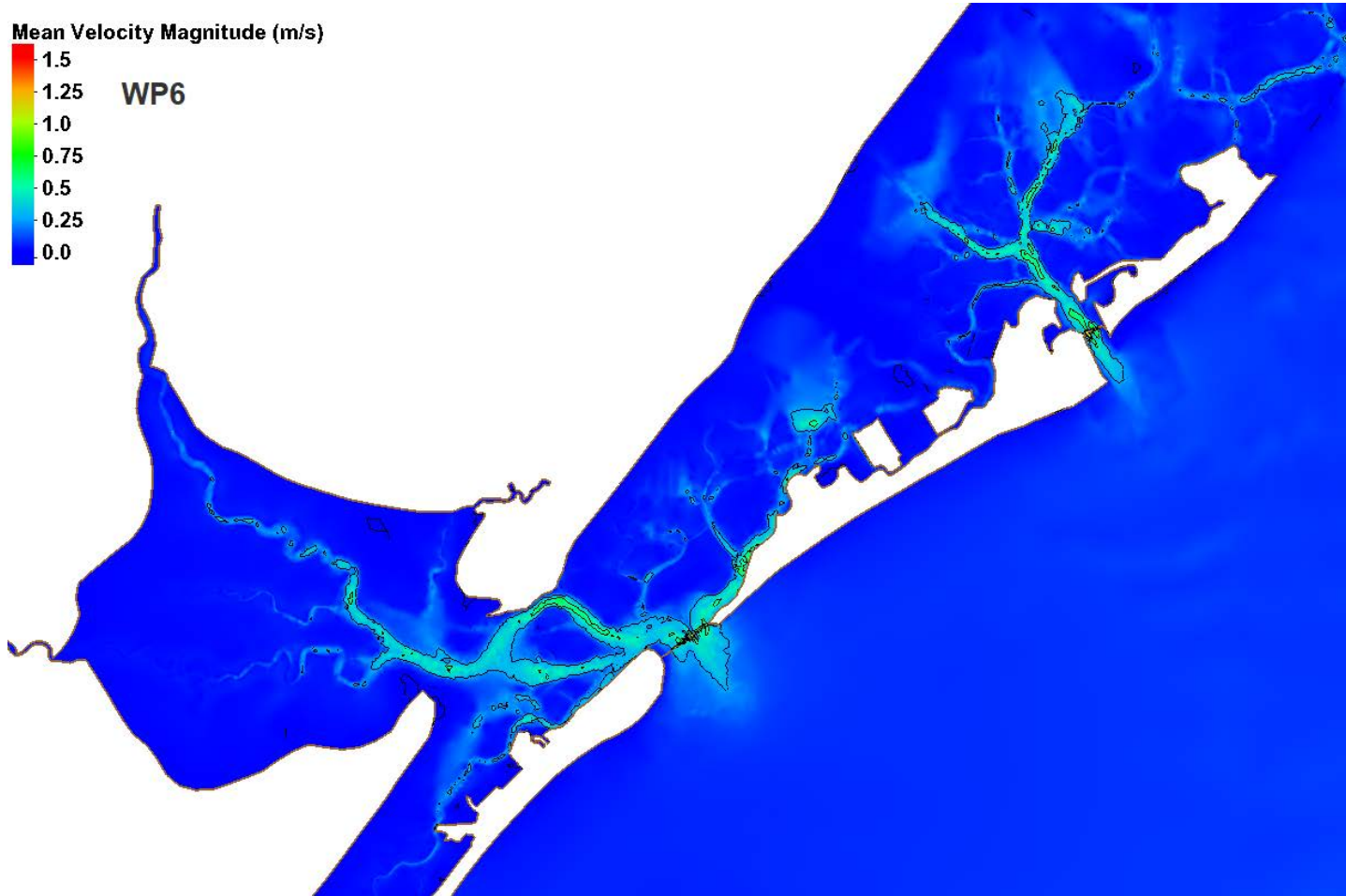








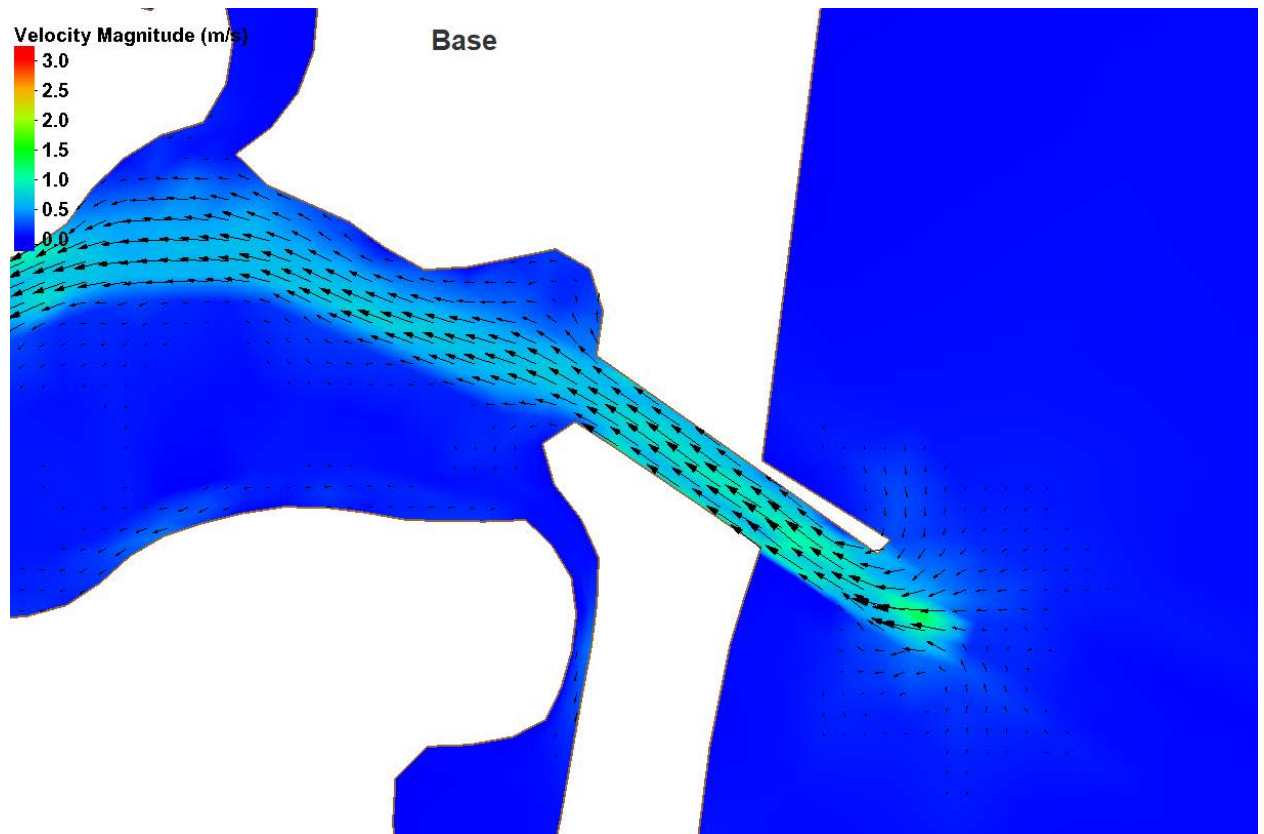


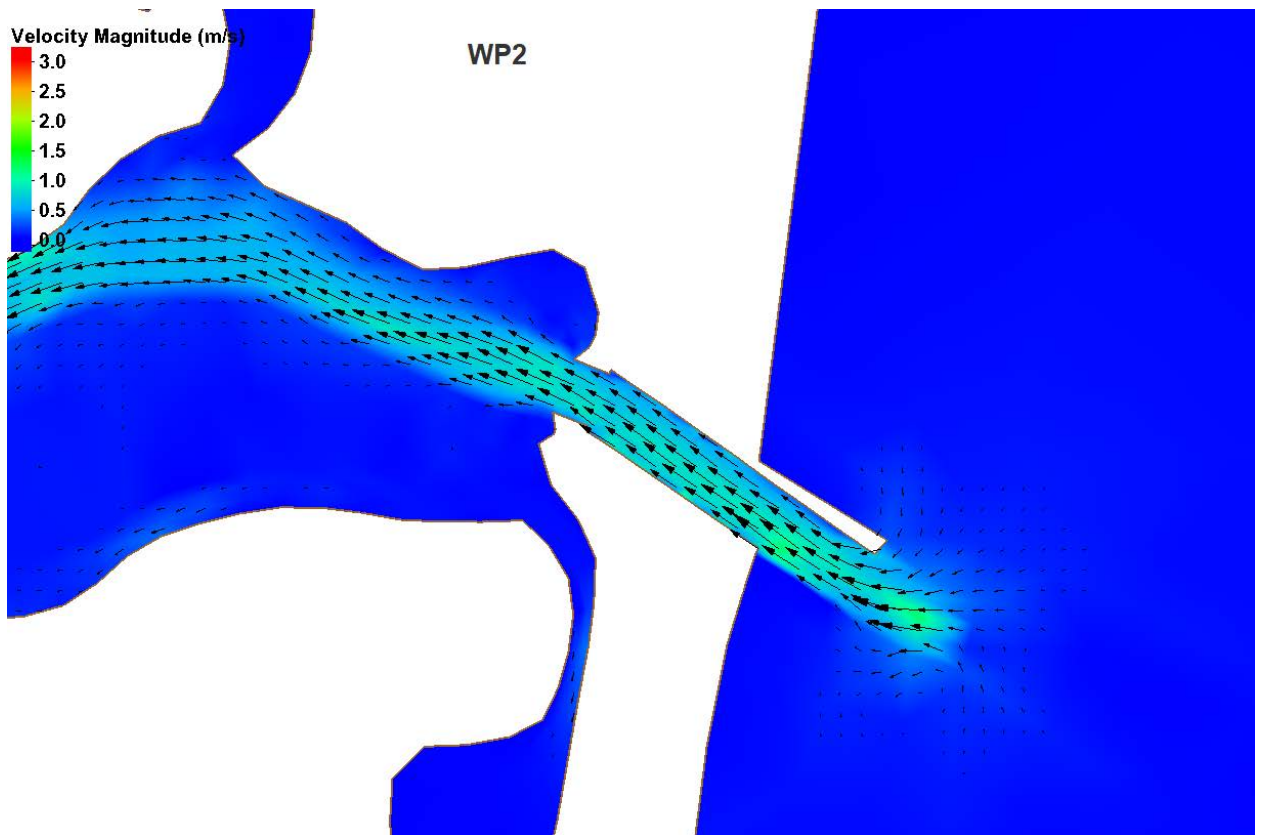
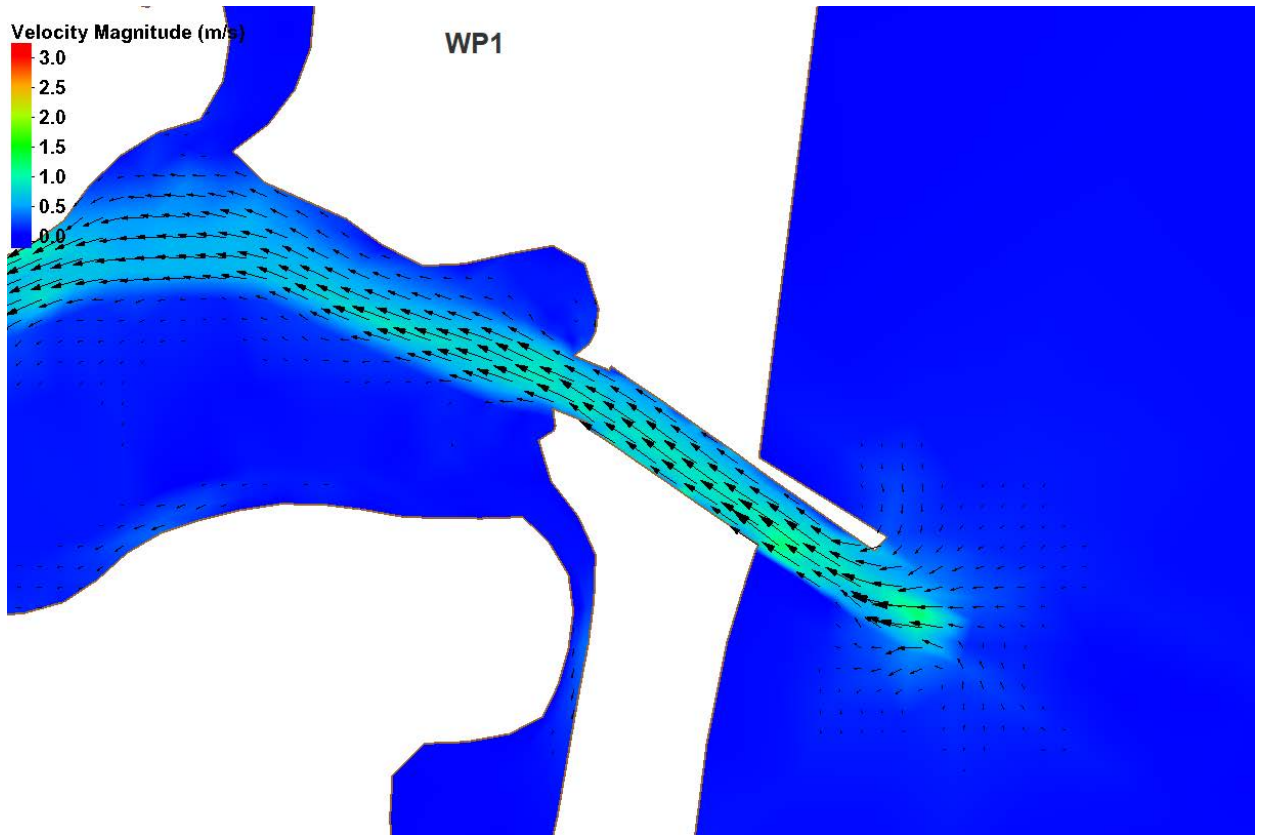


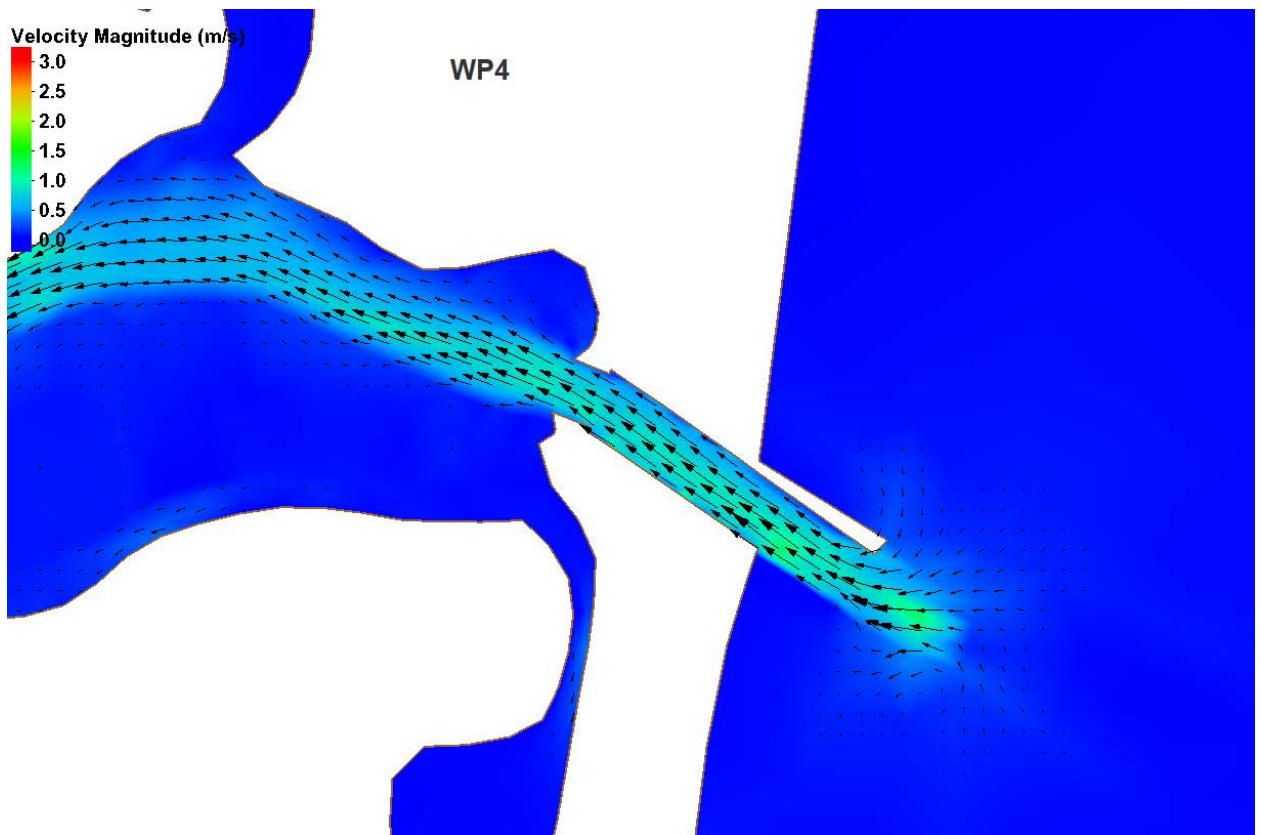
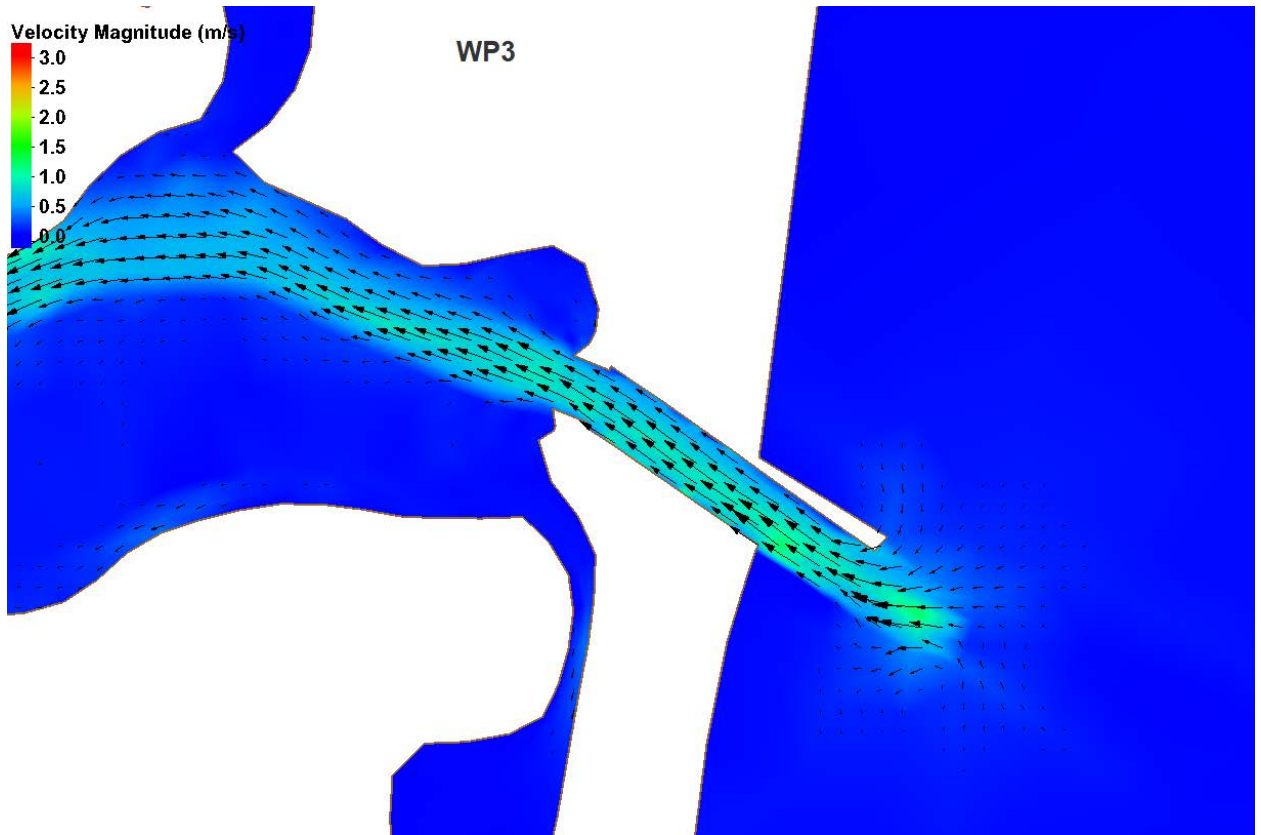
Flood/Ebb Velocity Comparison at Structures

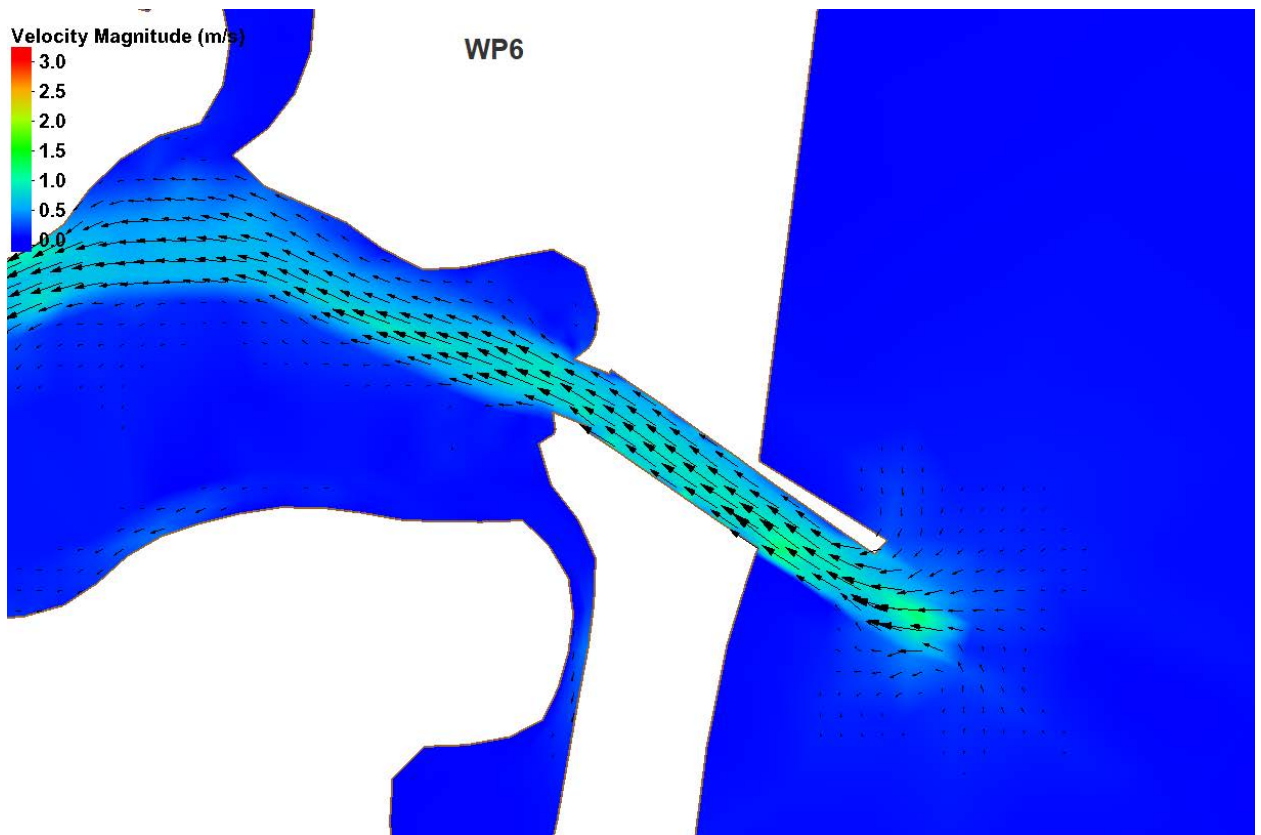
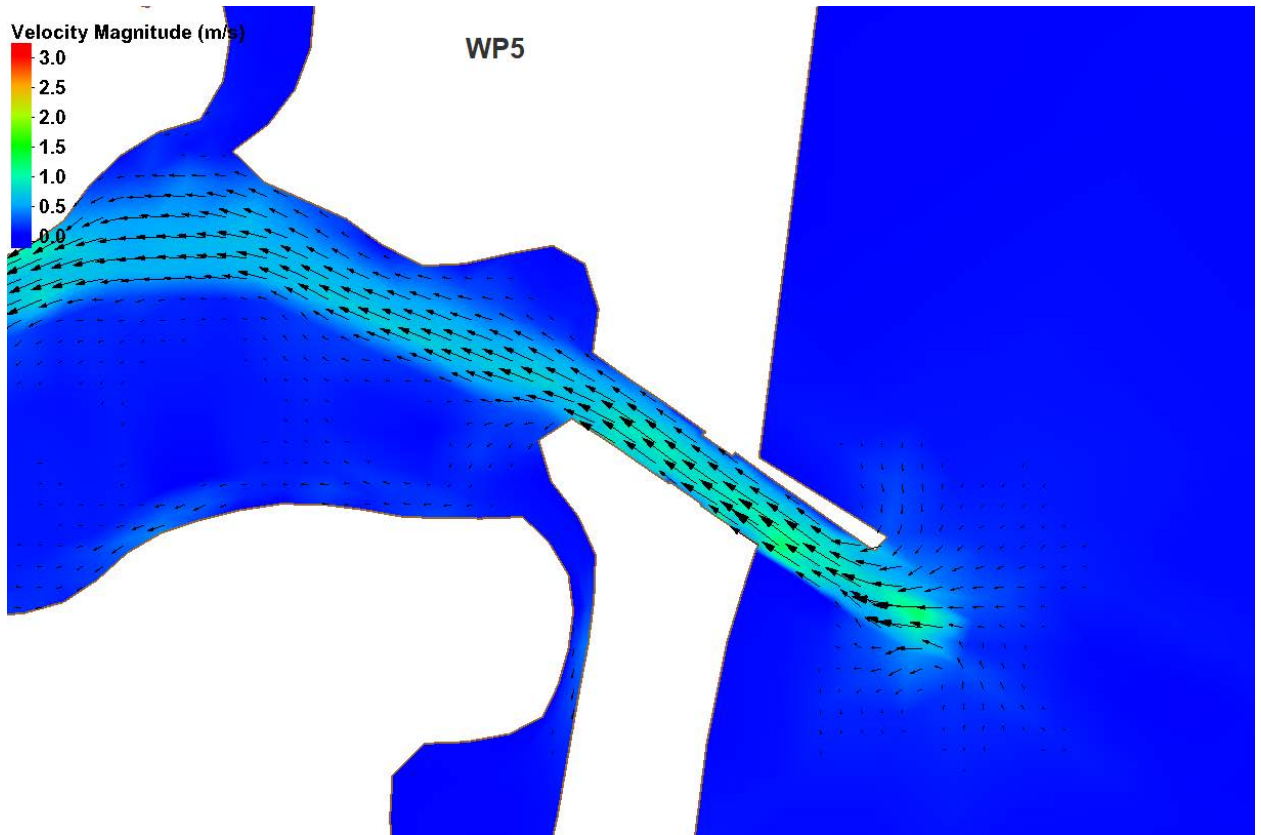
Flood directed flow is in toward the bays and ebb directed flow is out into the Atlantic Ocean. A representative maximum flood (16 April 12:00) and ebb time (16 April 18:00) is shown for all of the structure locations for velocity magnitude and direction comparison. These are contoured from 0 to 3 m/s with vectors scaled to the magnitude and shown on a grid.

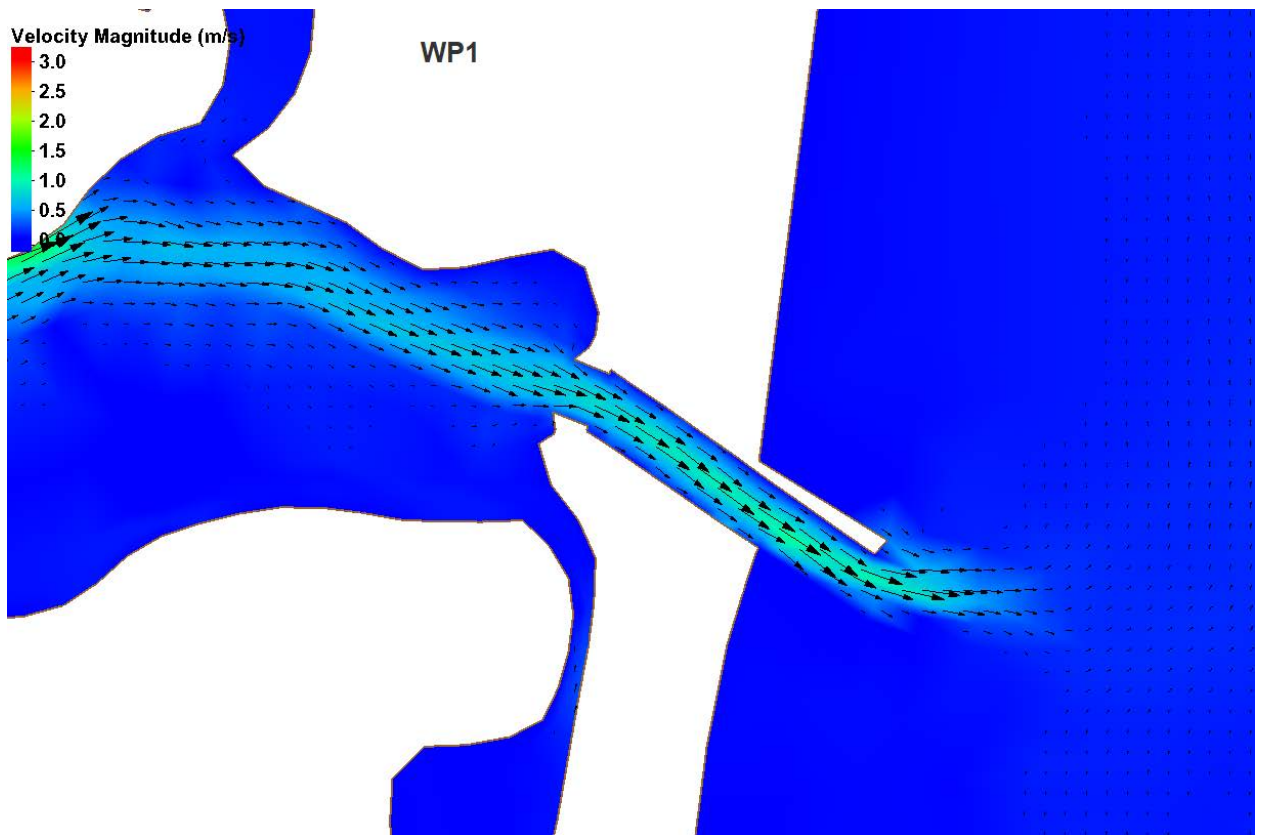
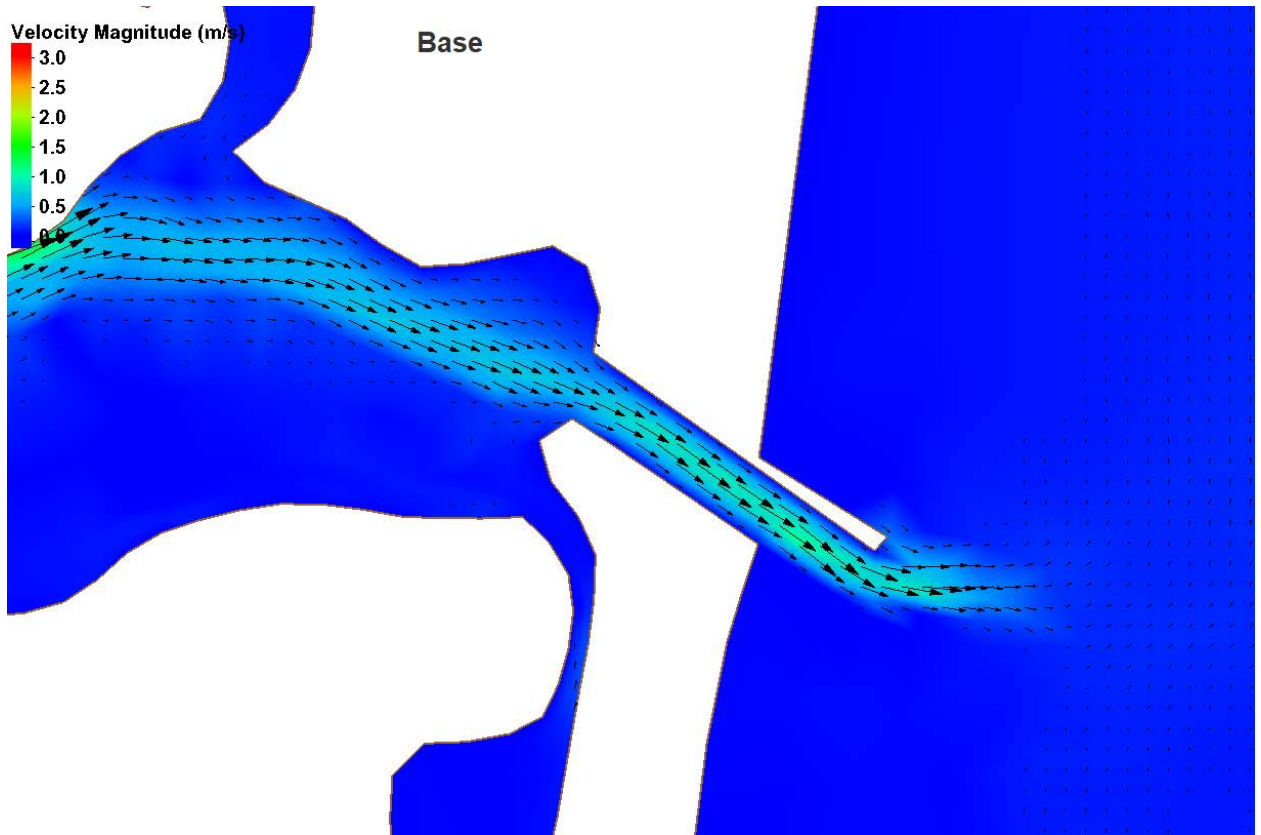
Manasquan

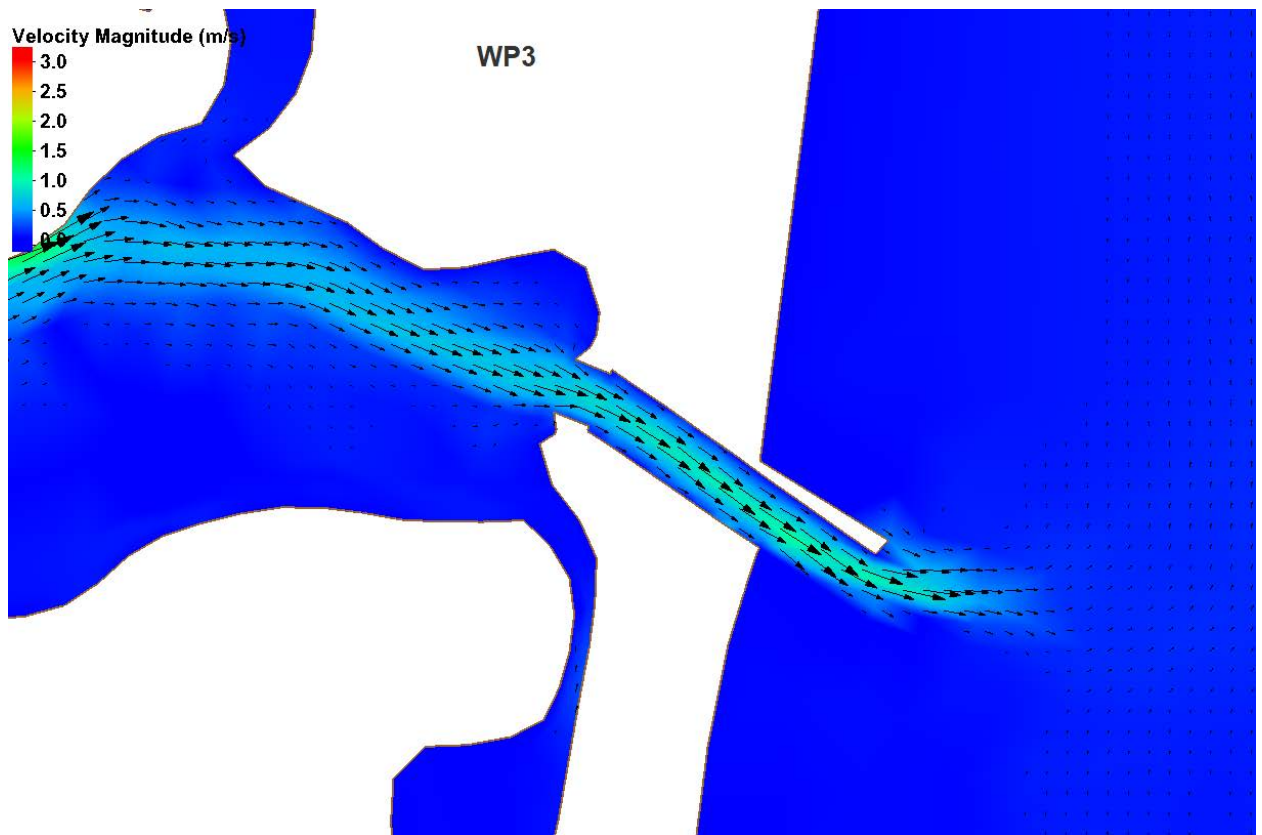
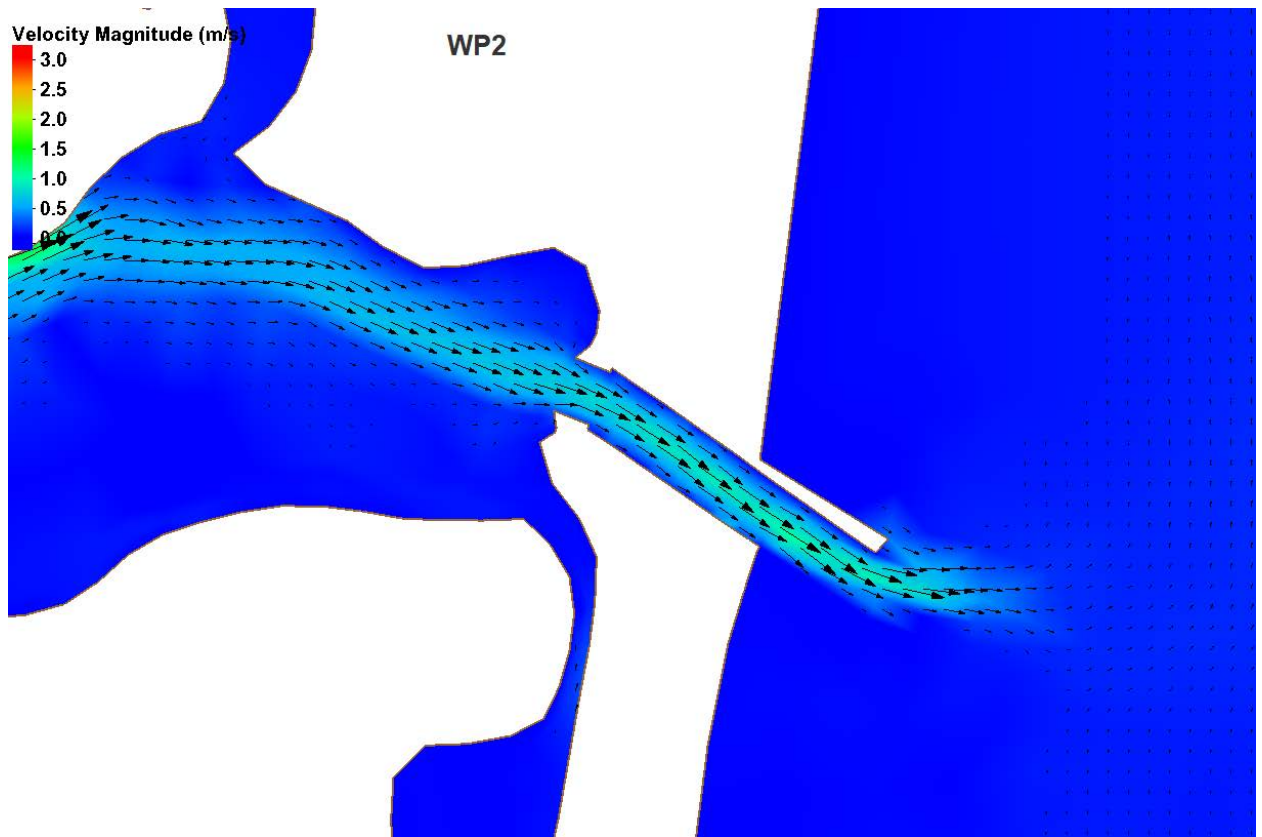


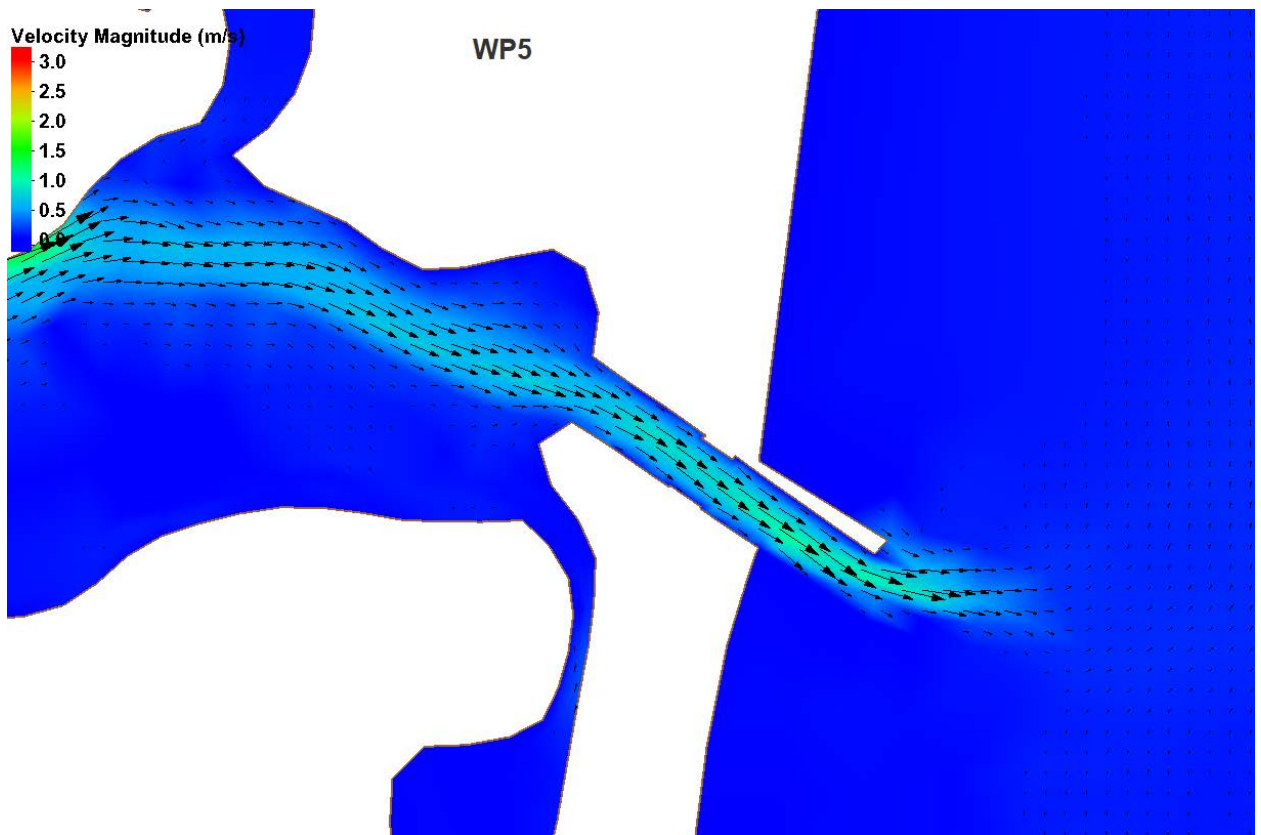
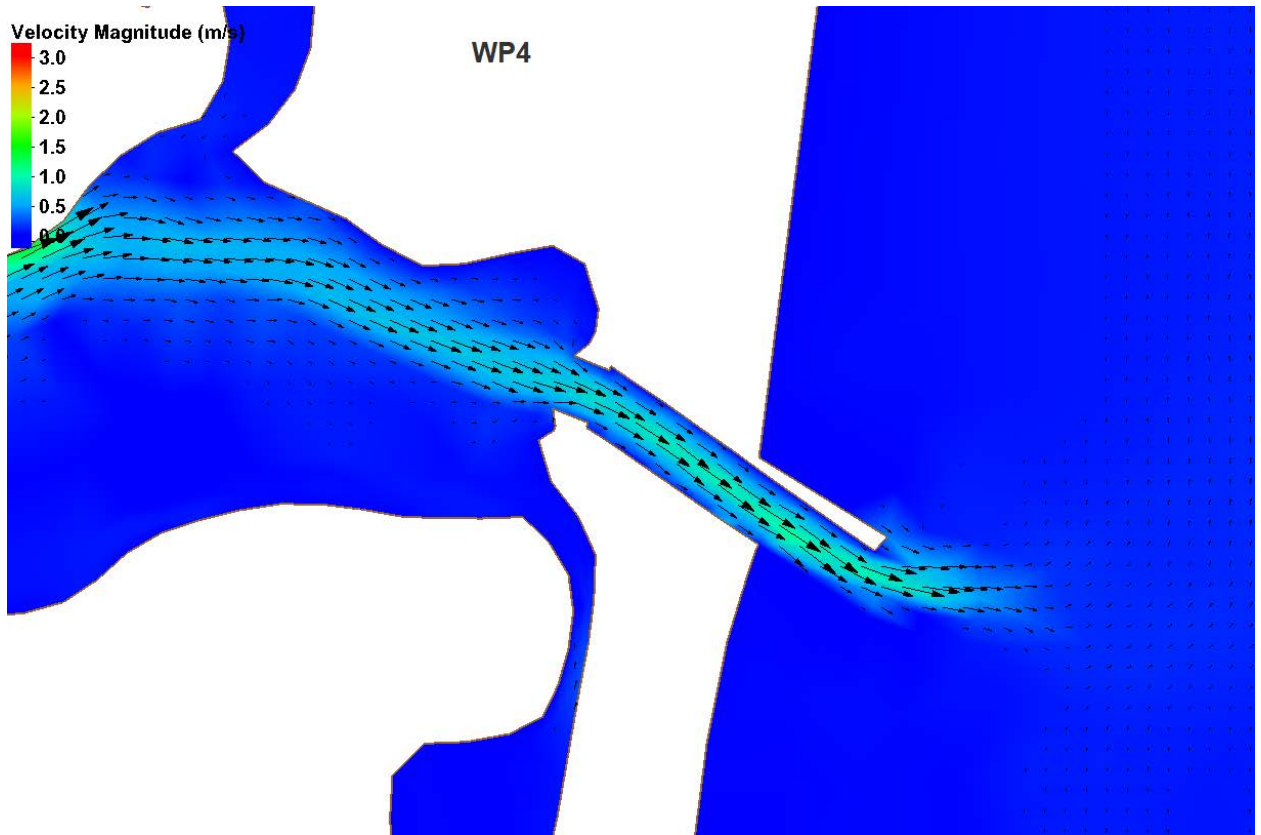


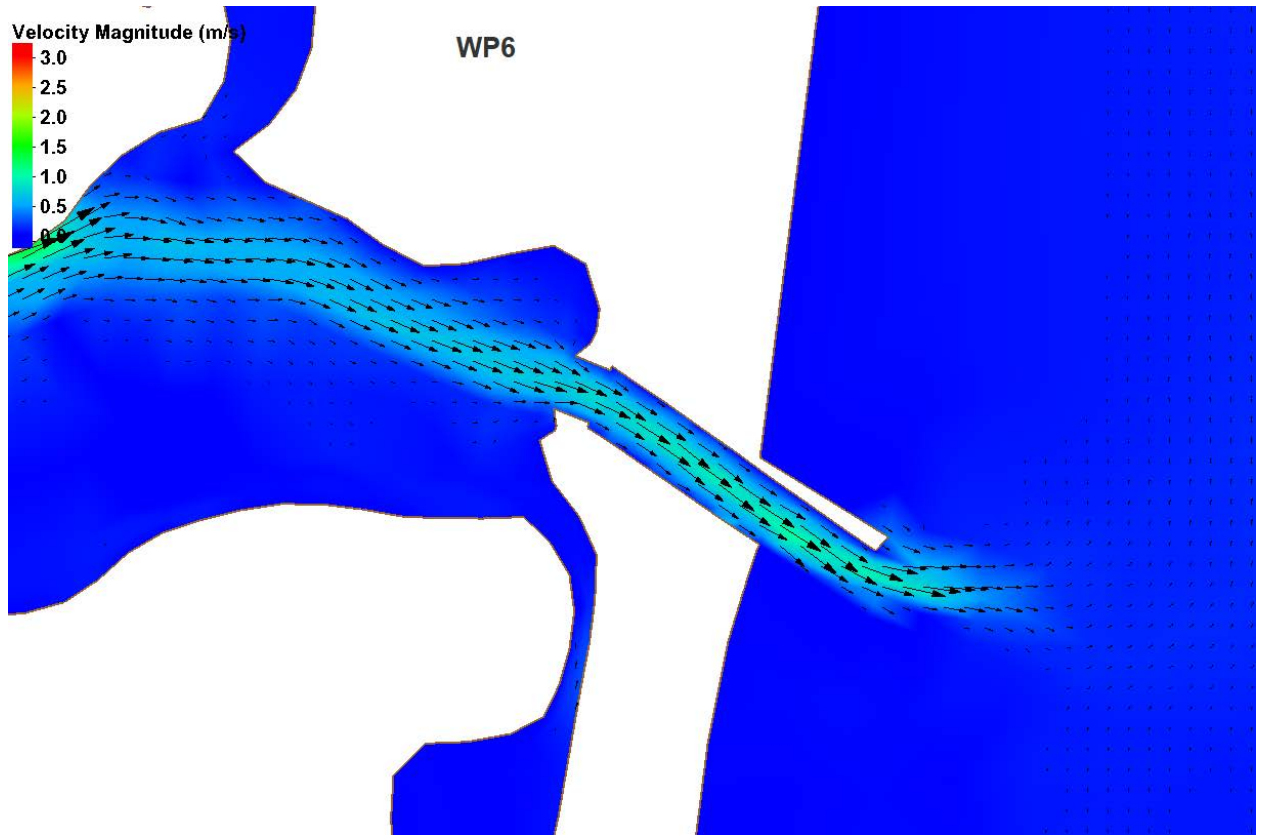




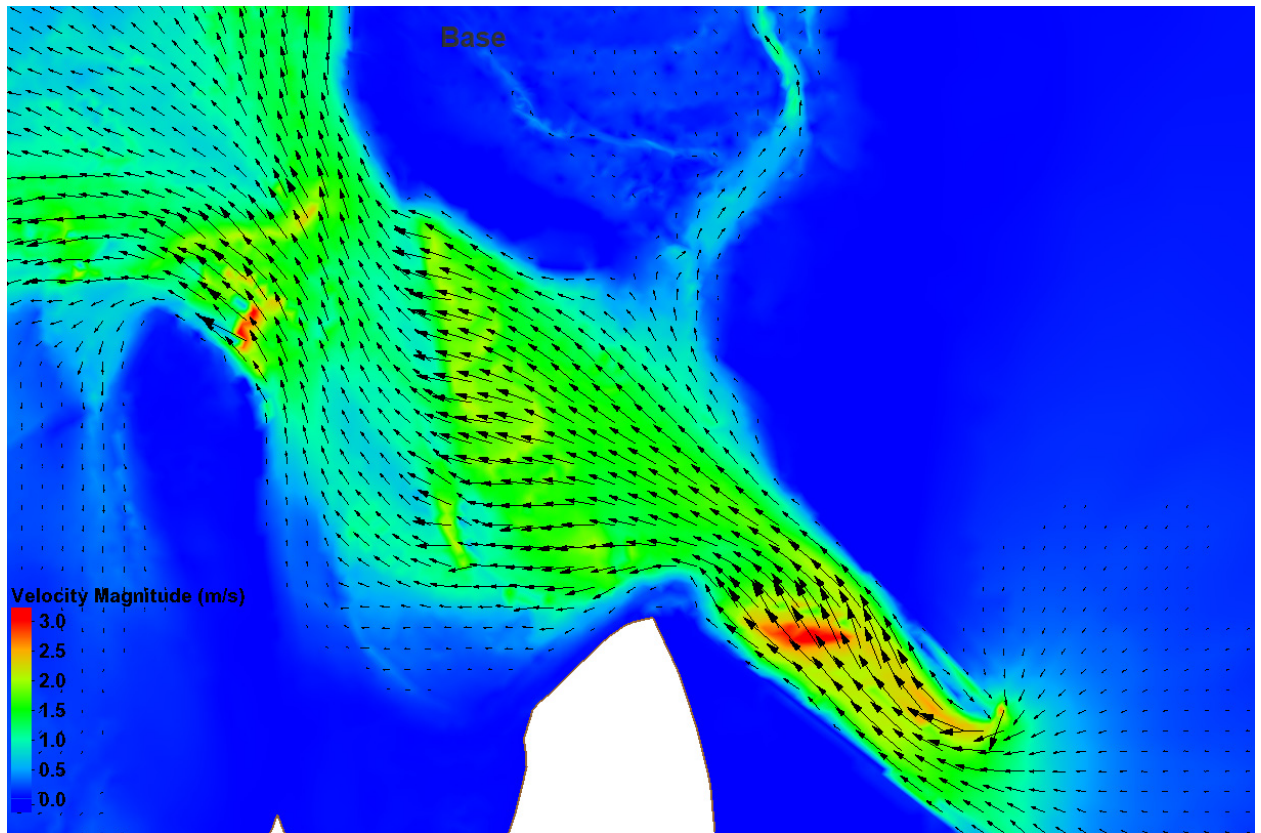


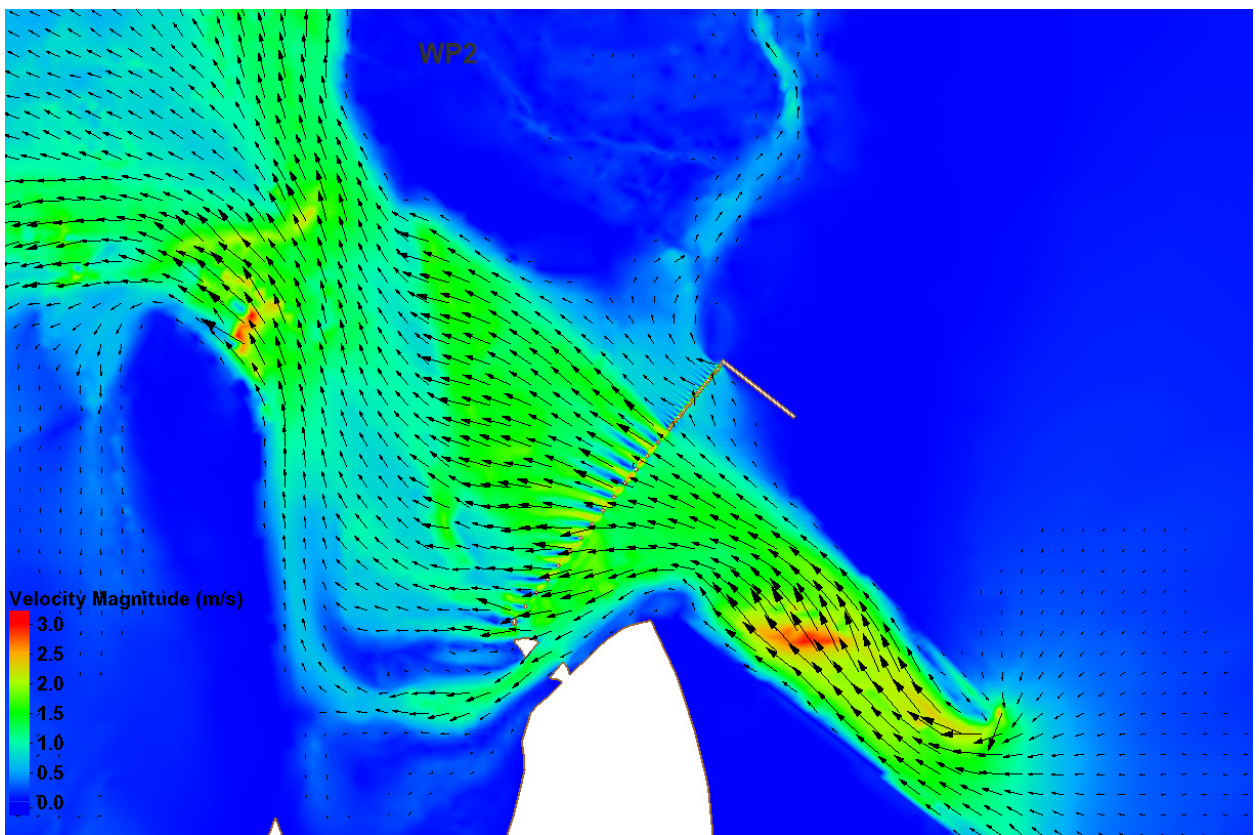
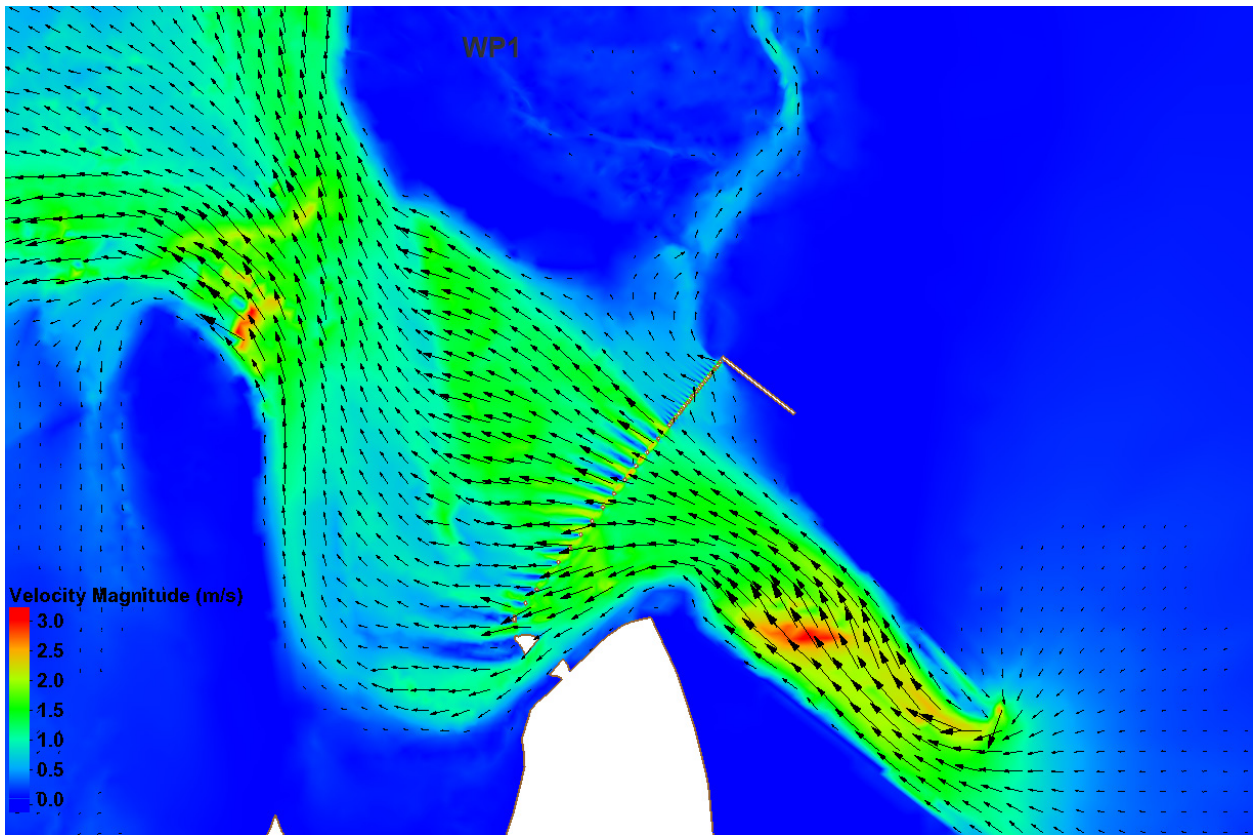


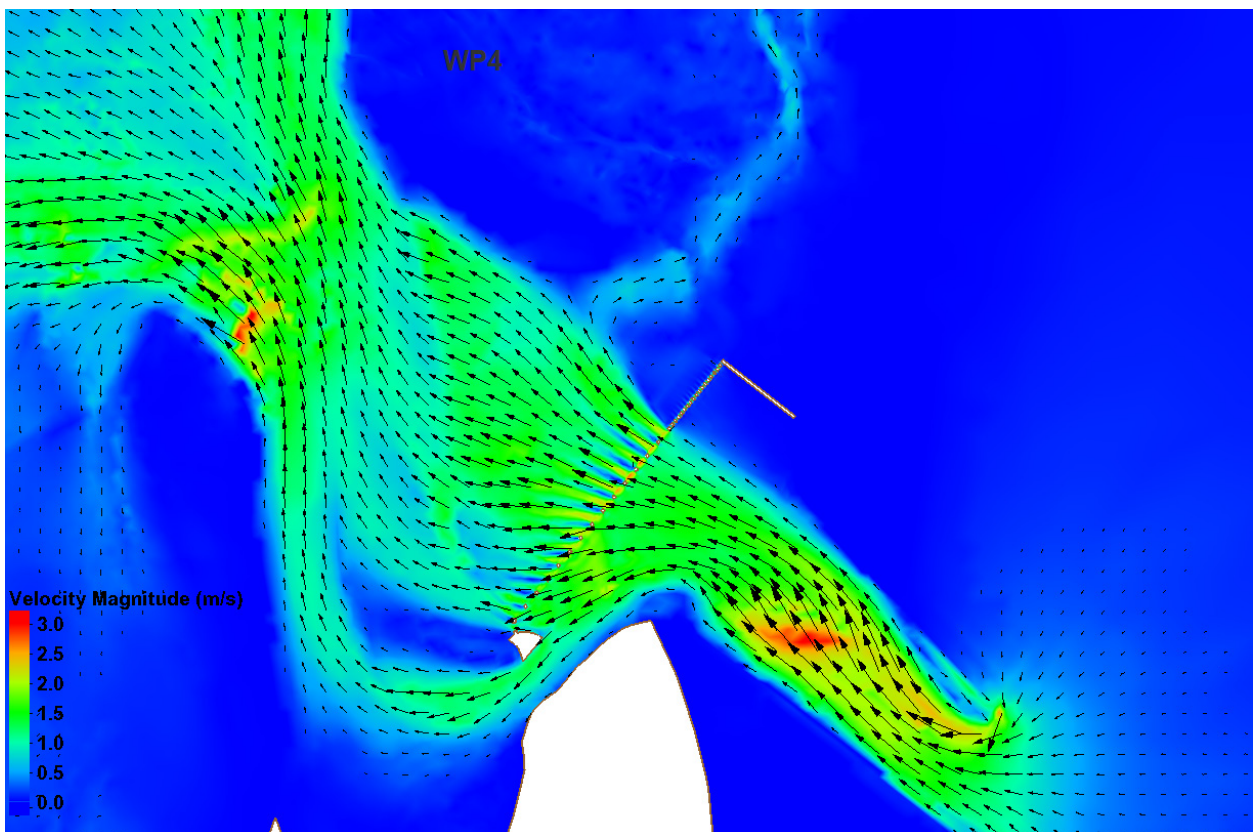
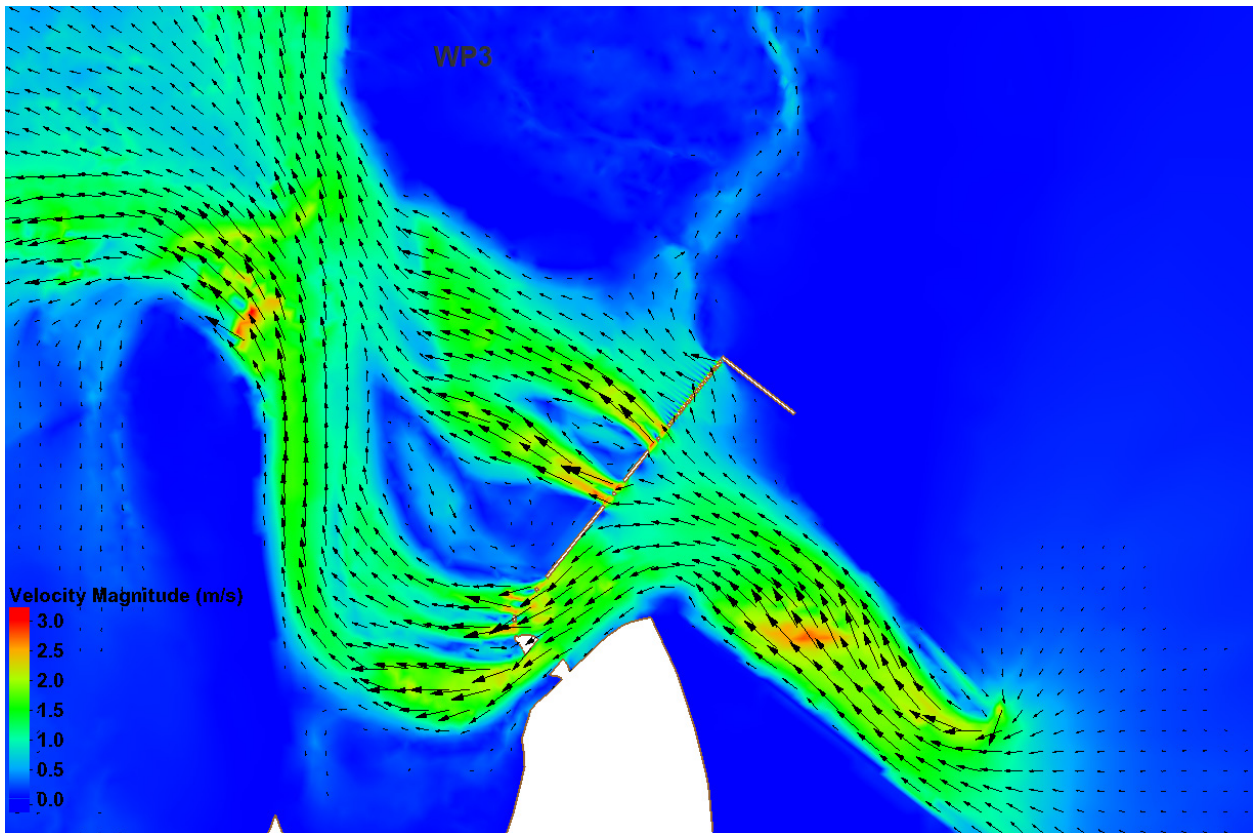


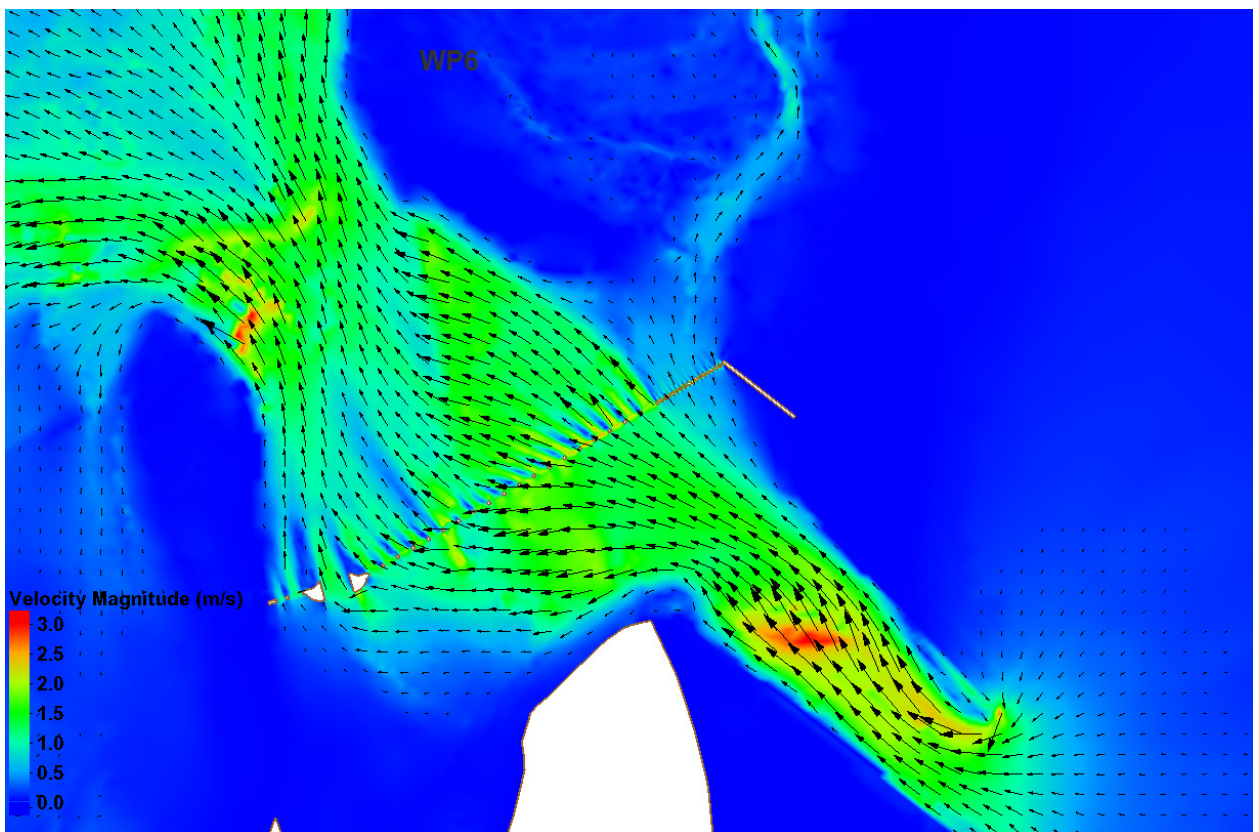
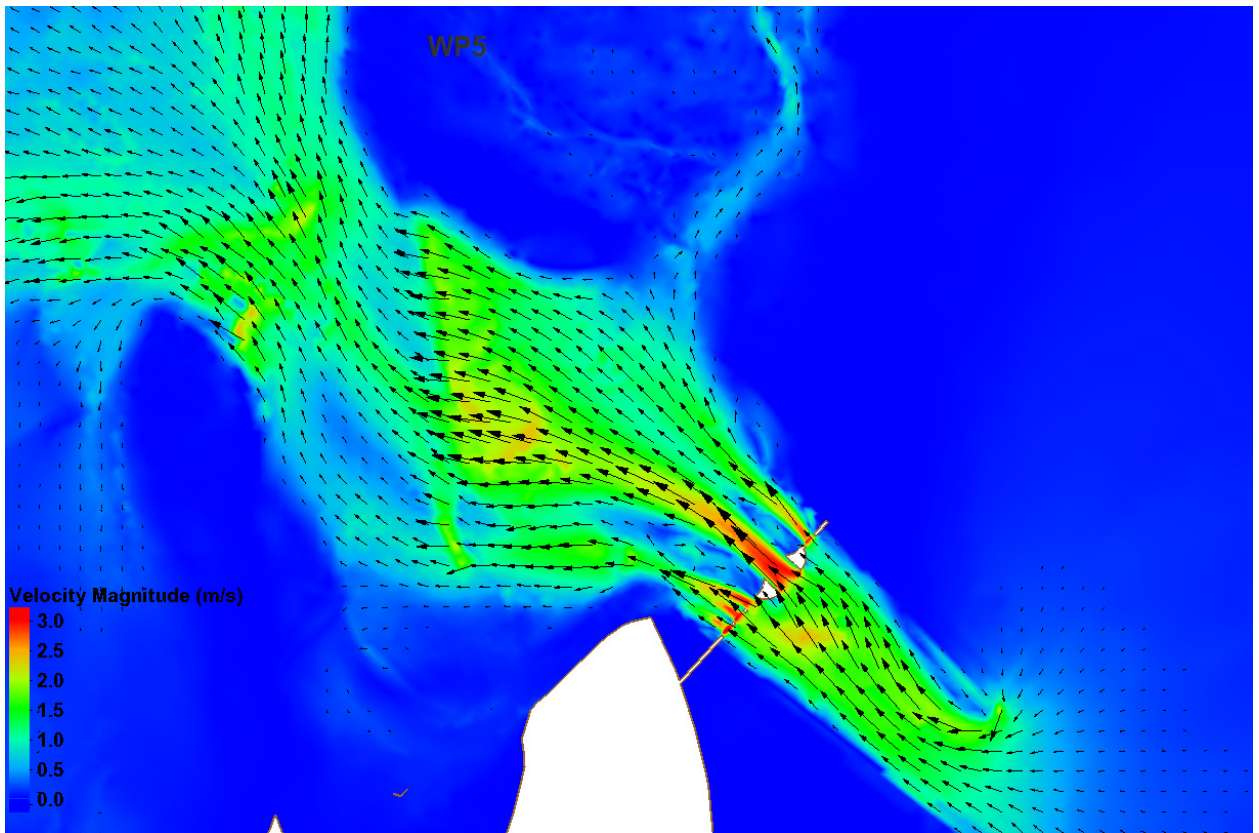


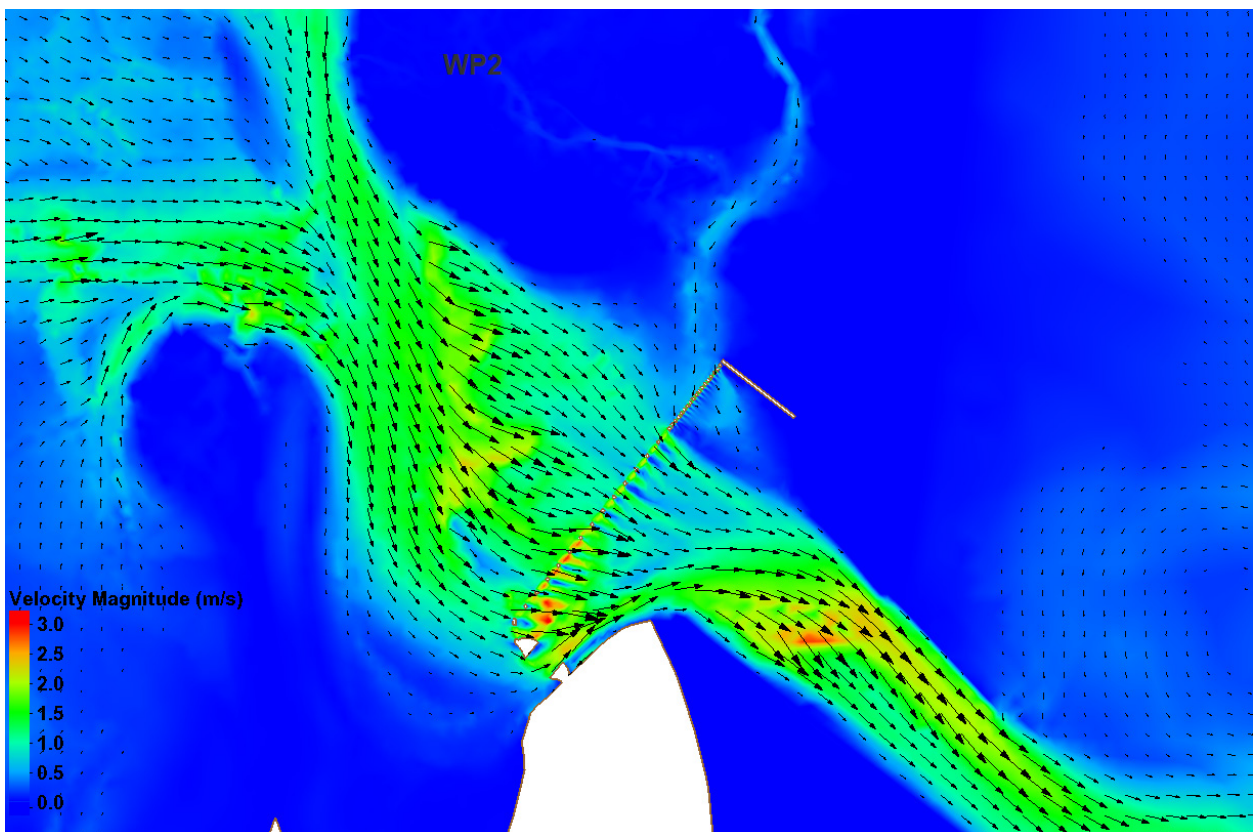
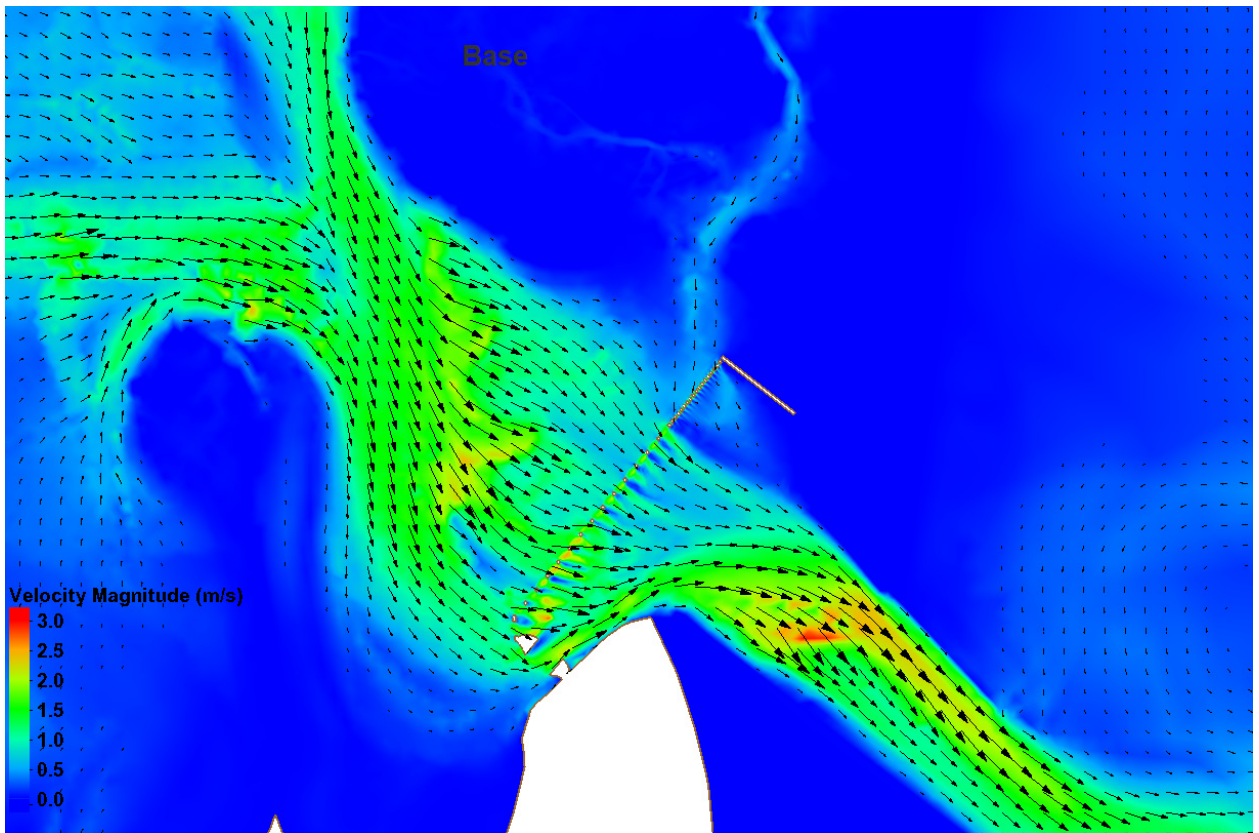
Barnegat

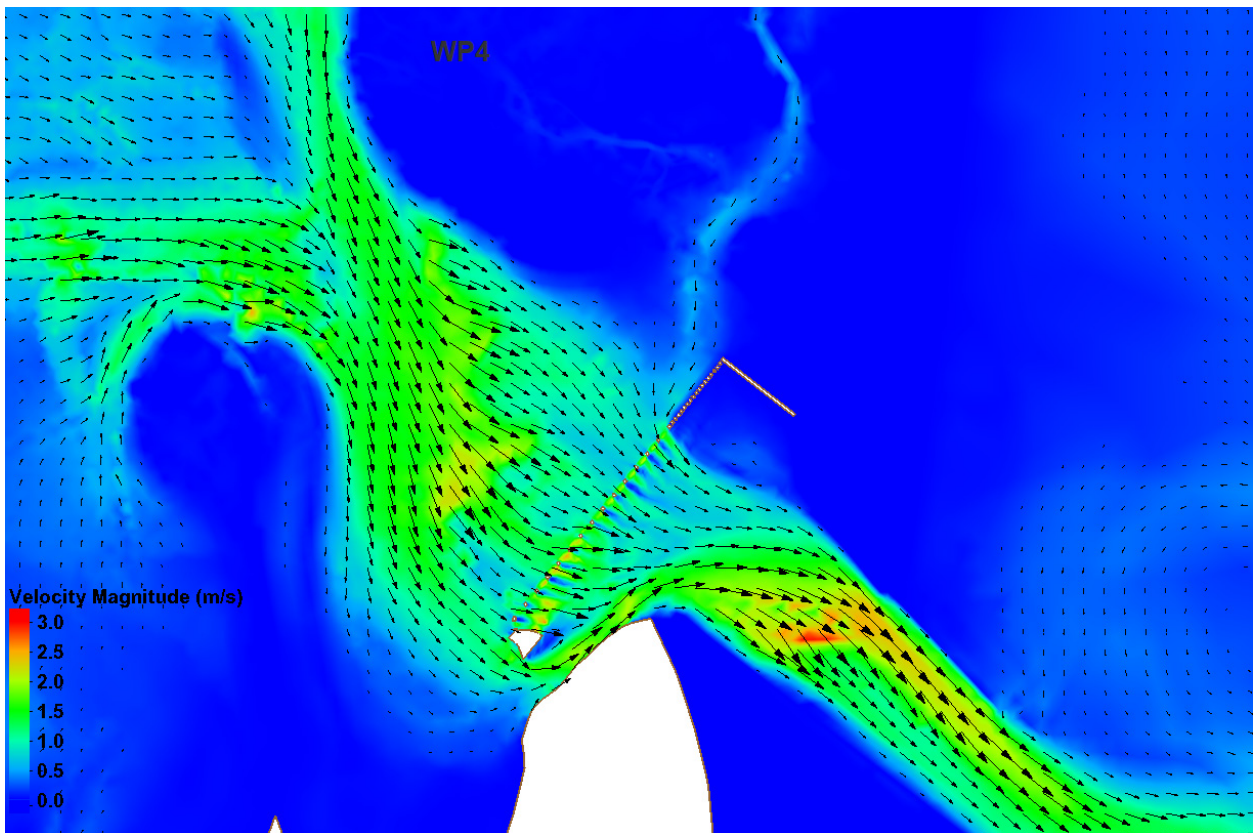
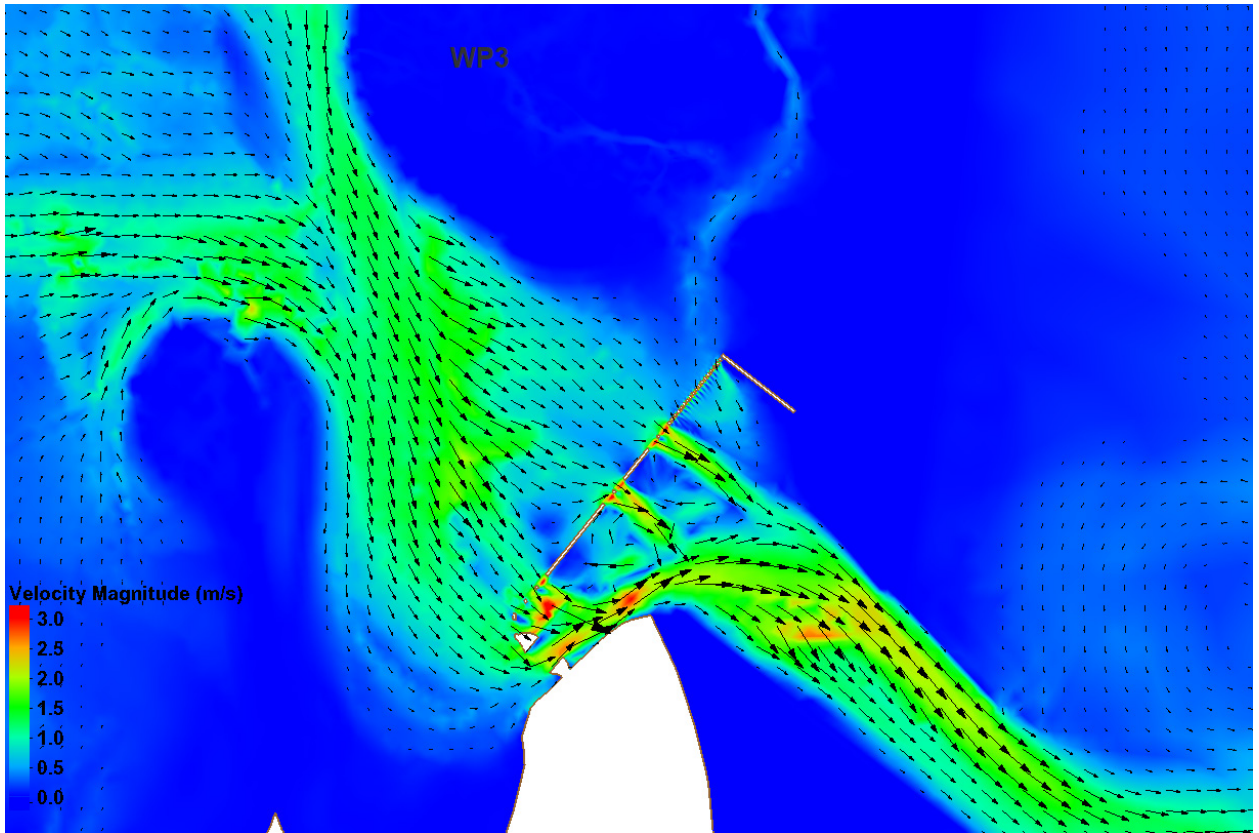


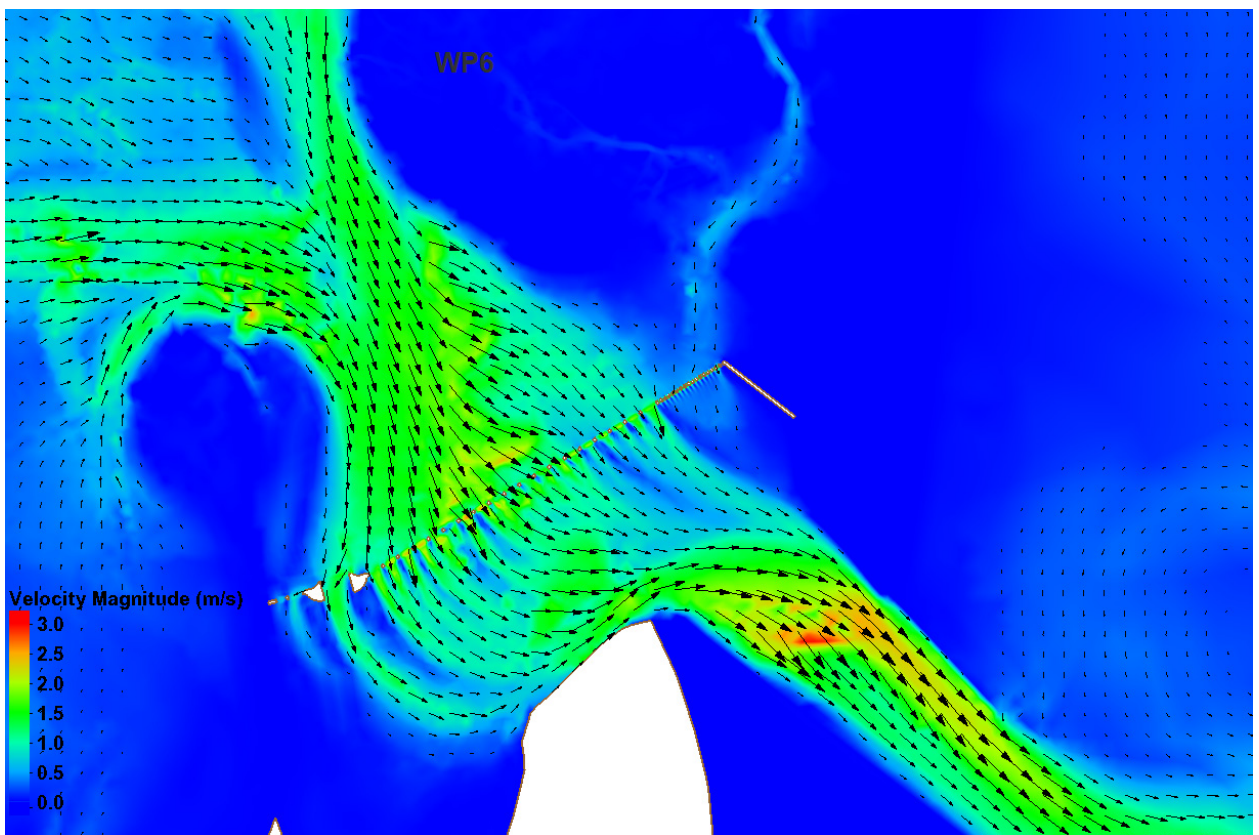
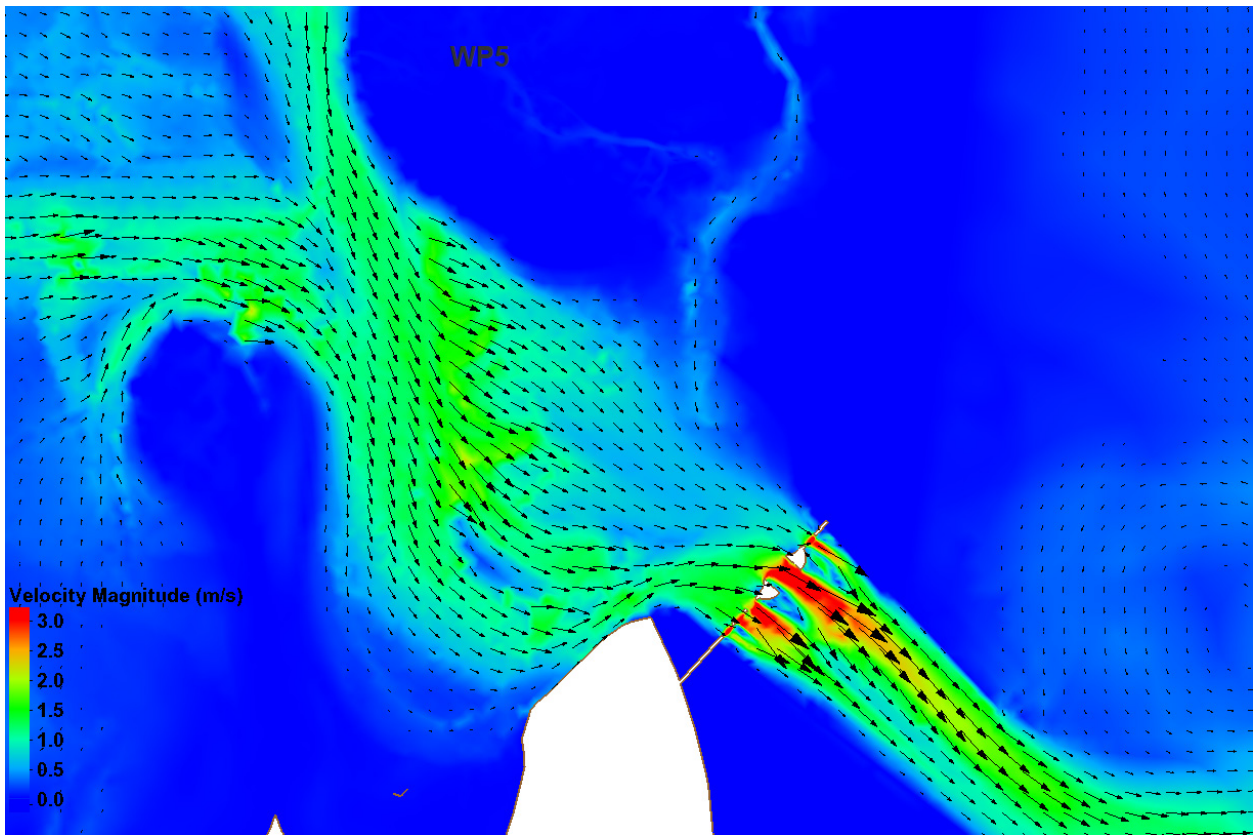




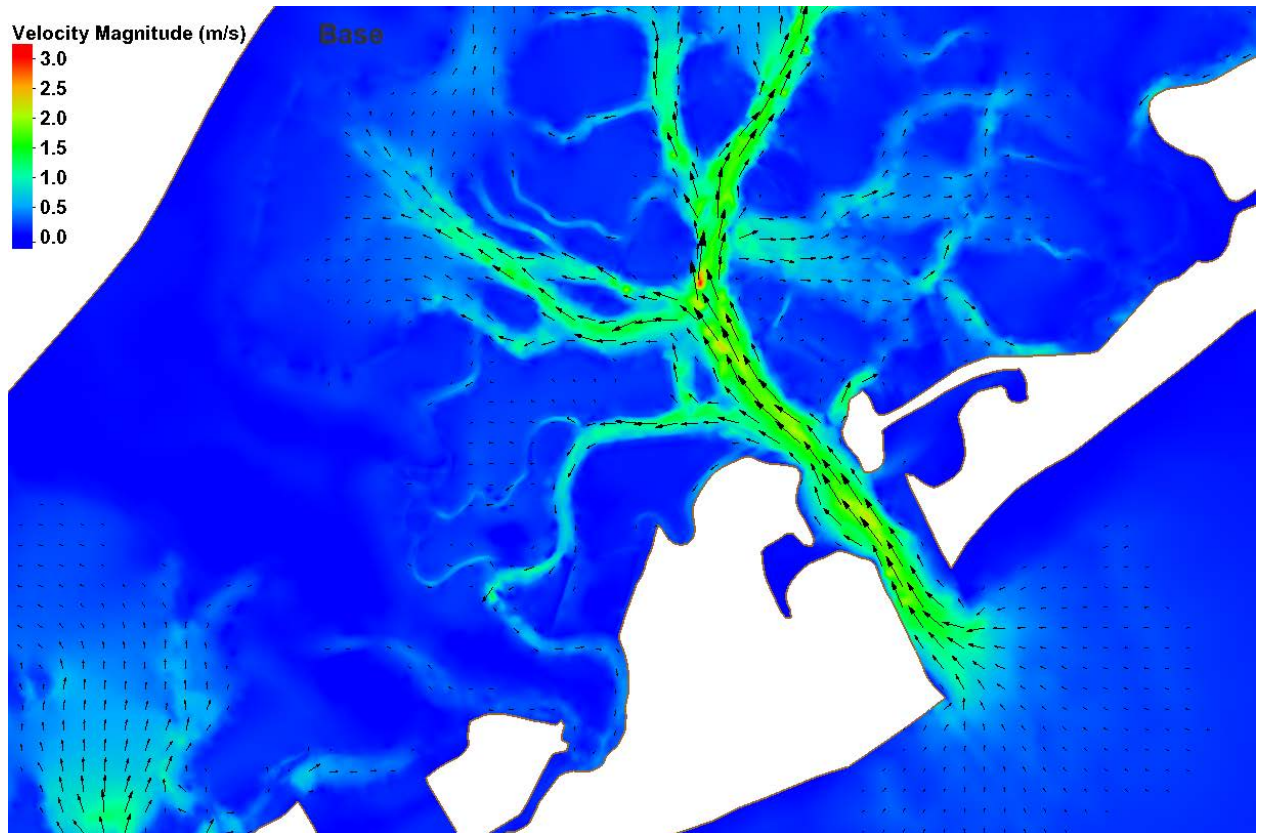


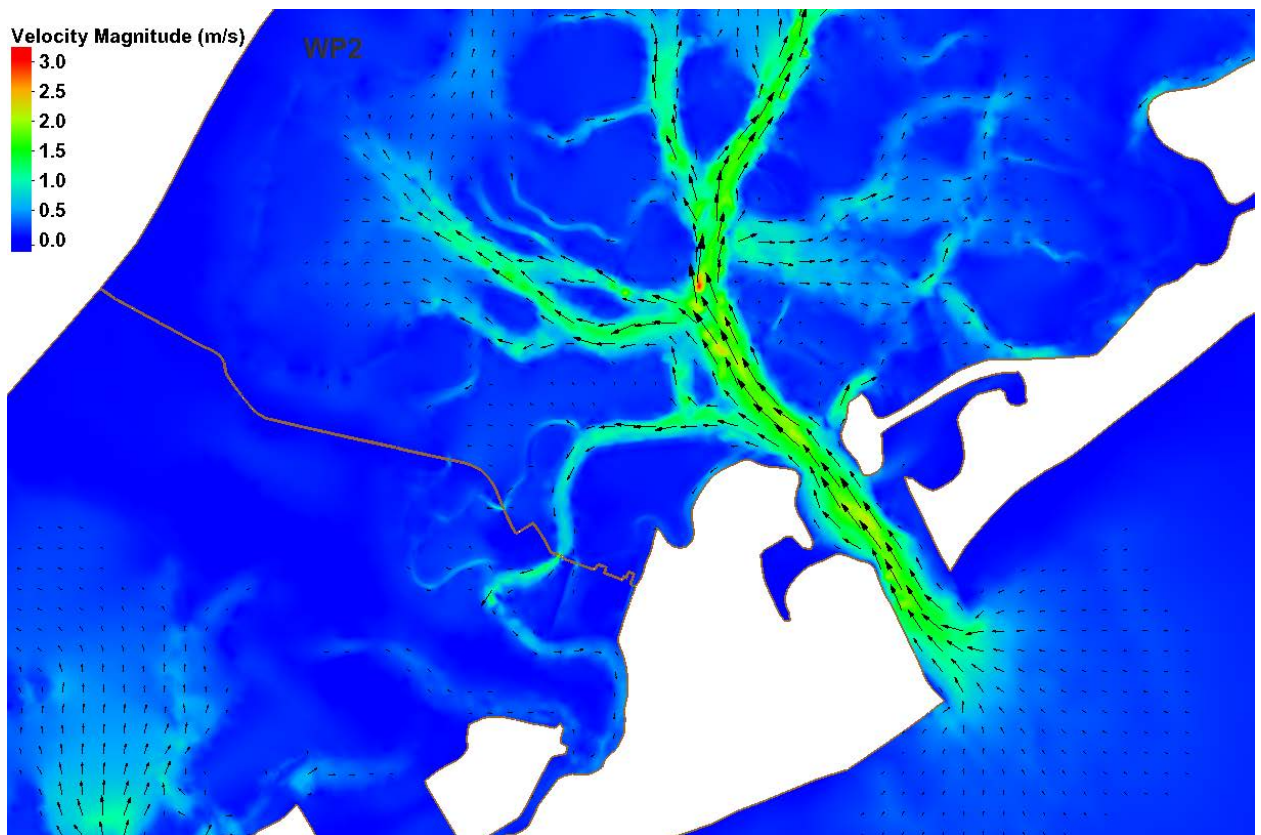
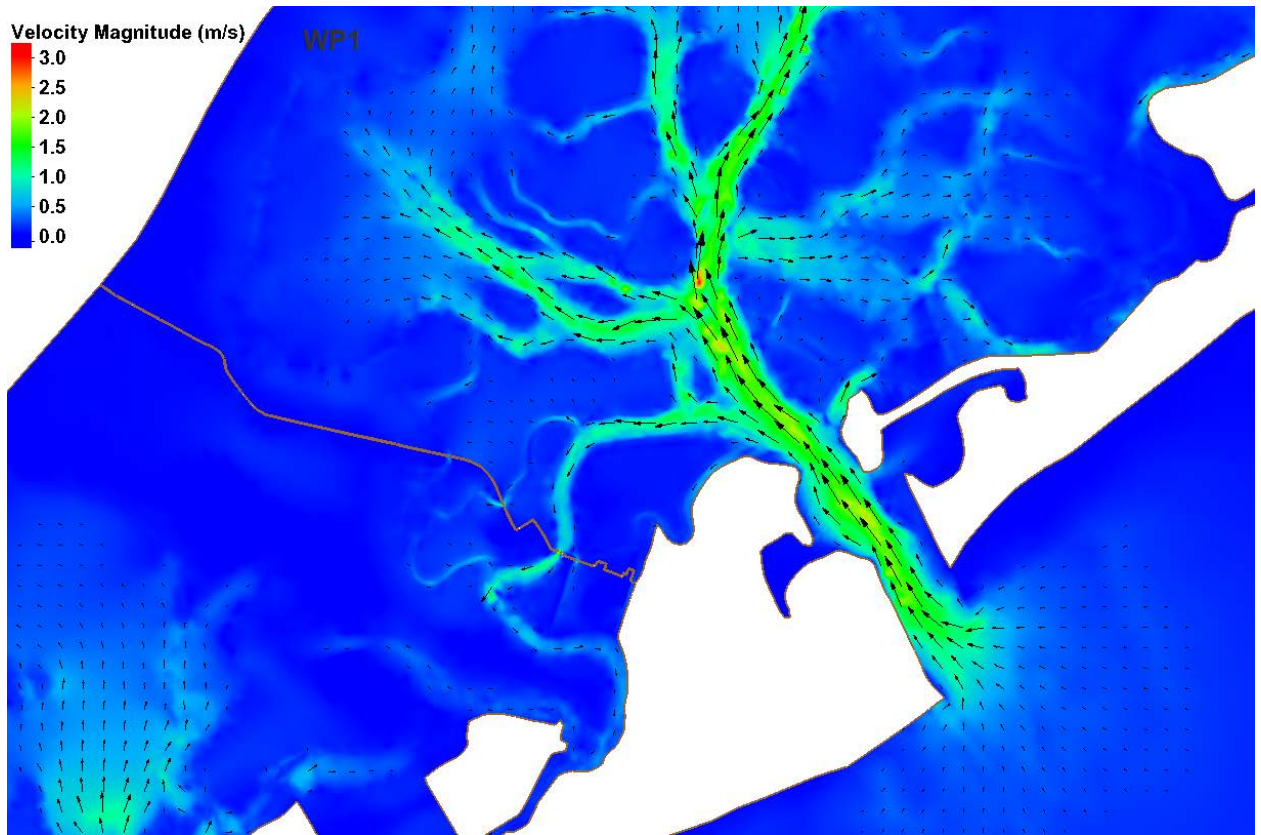


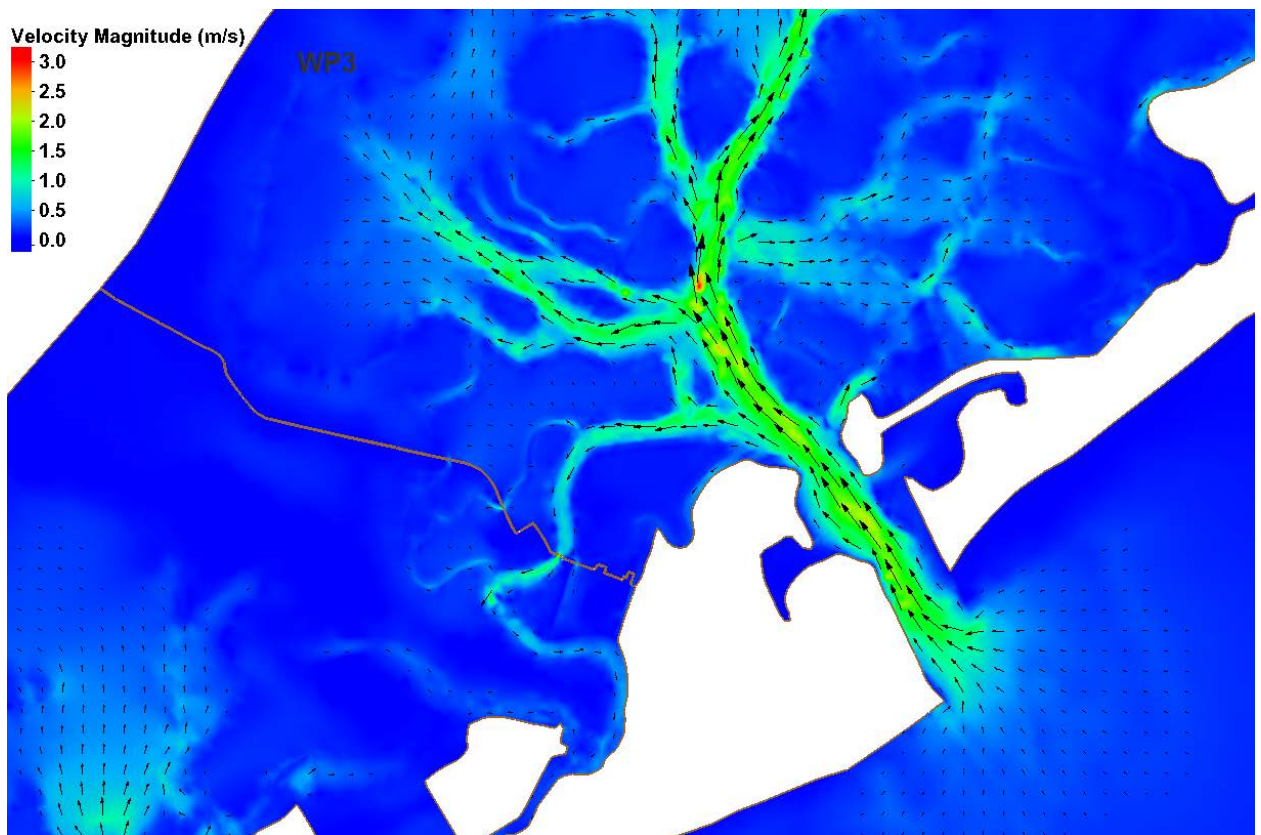
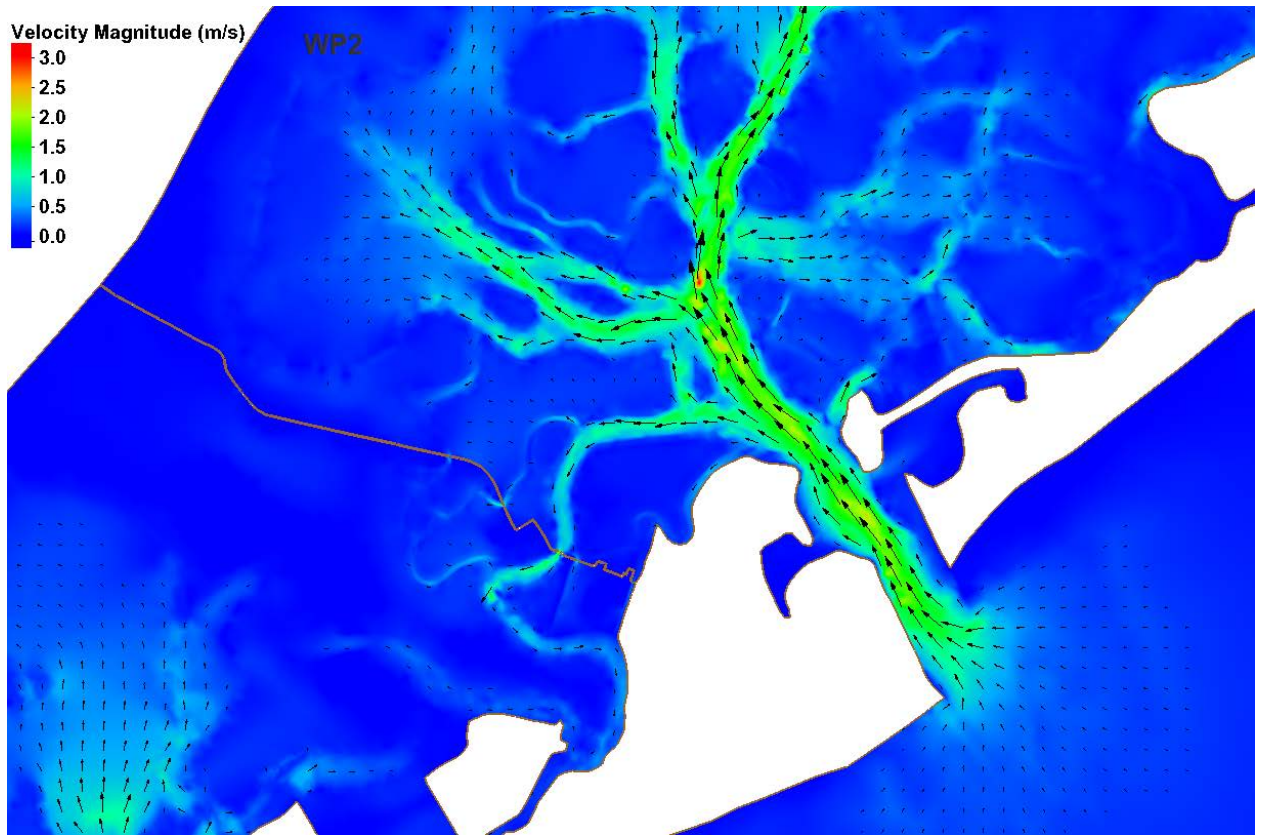


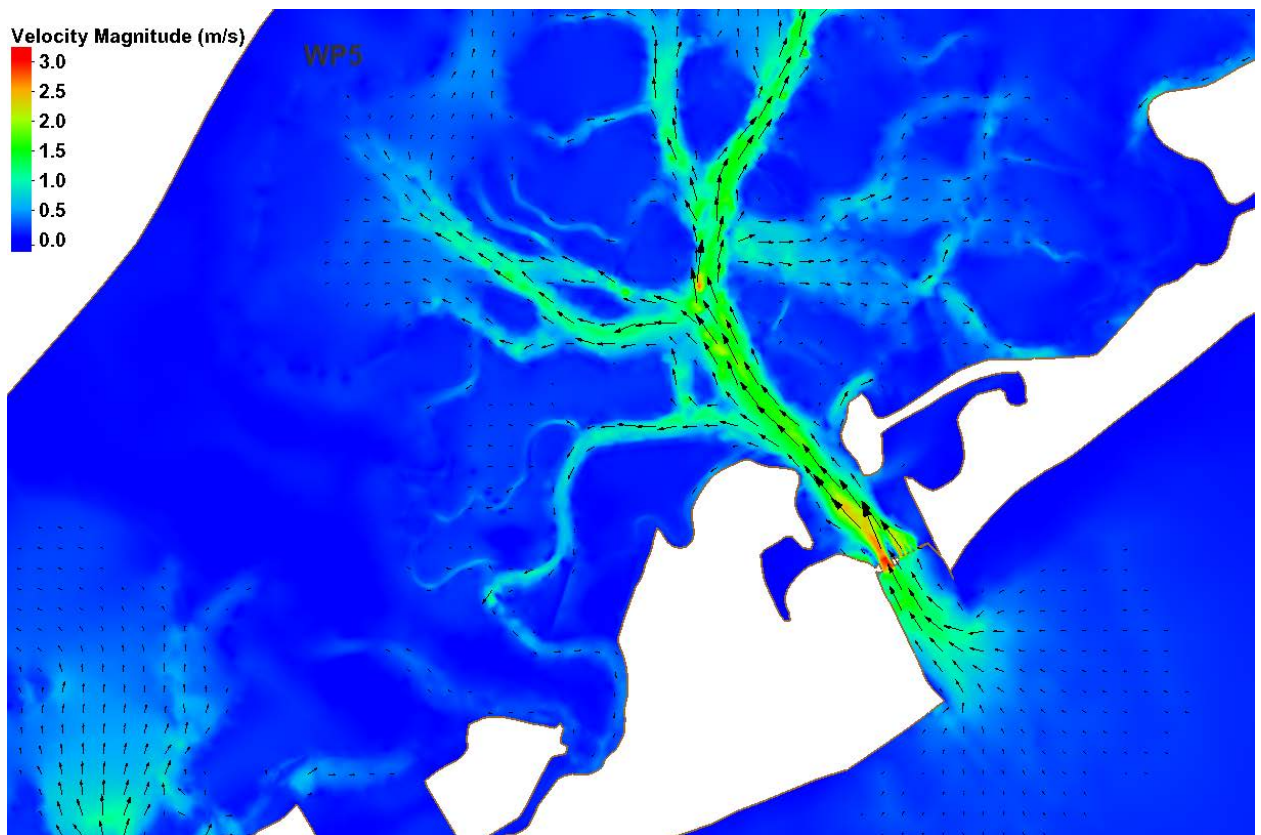
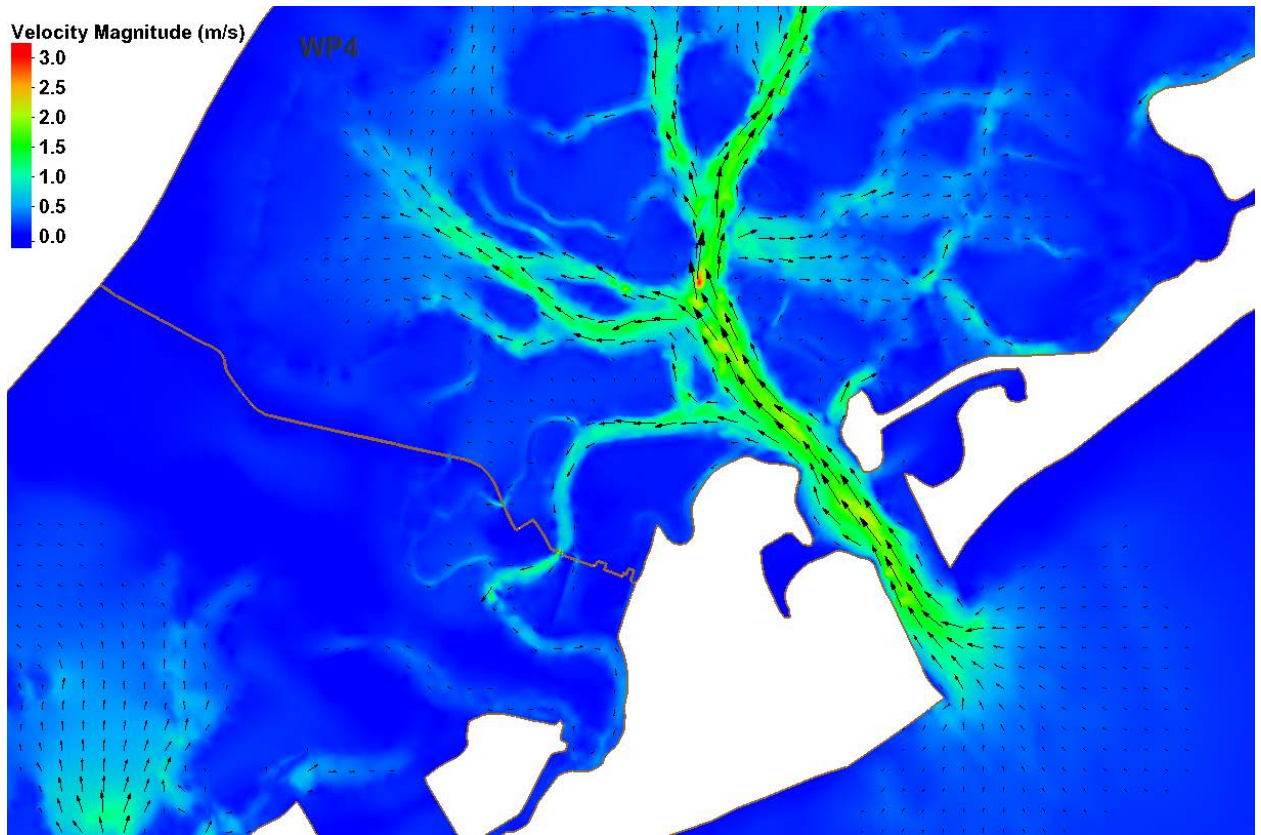


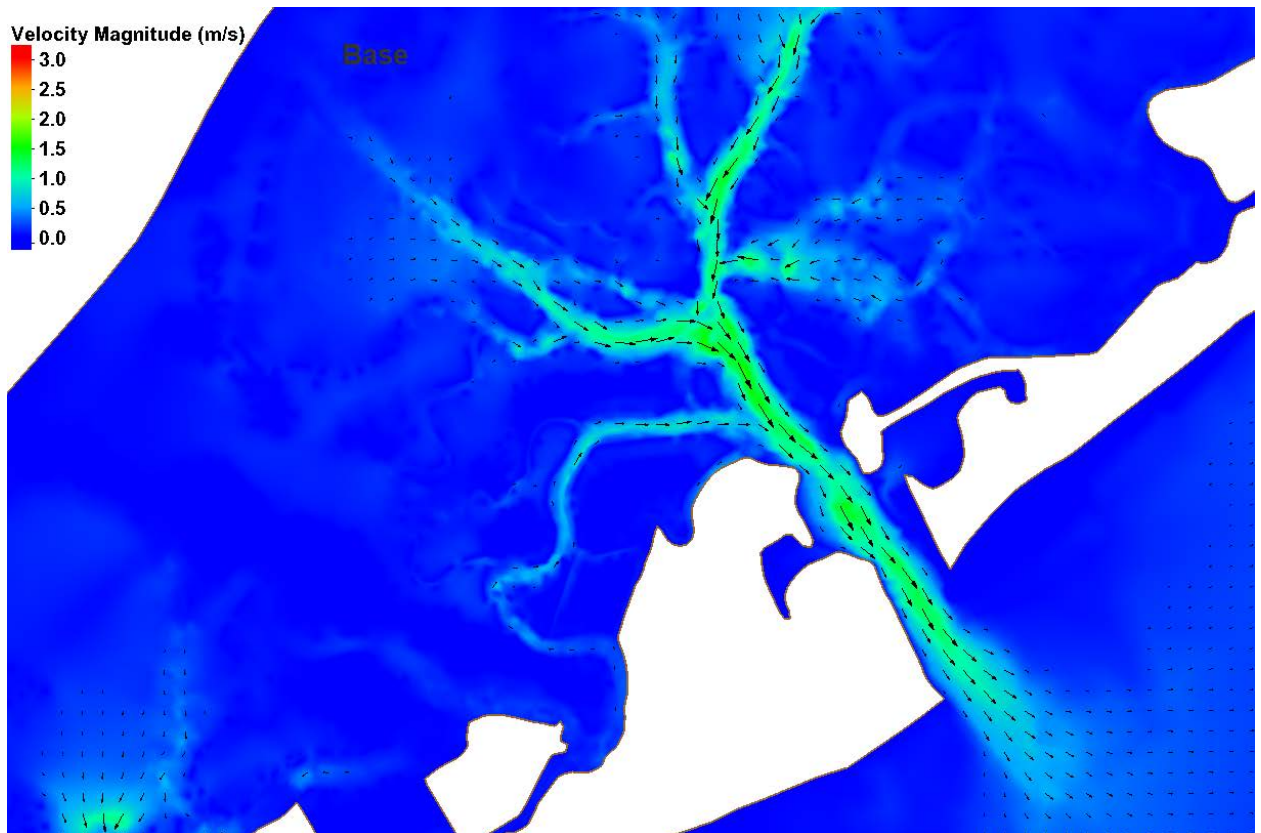
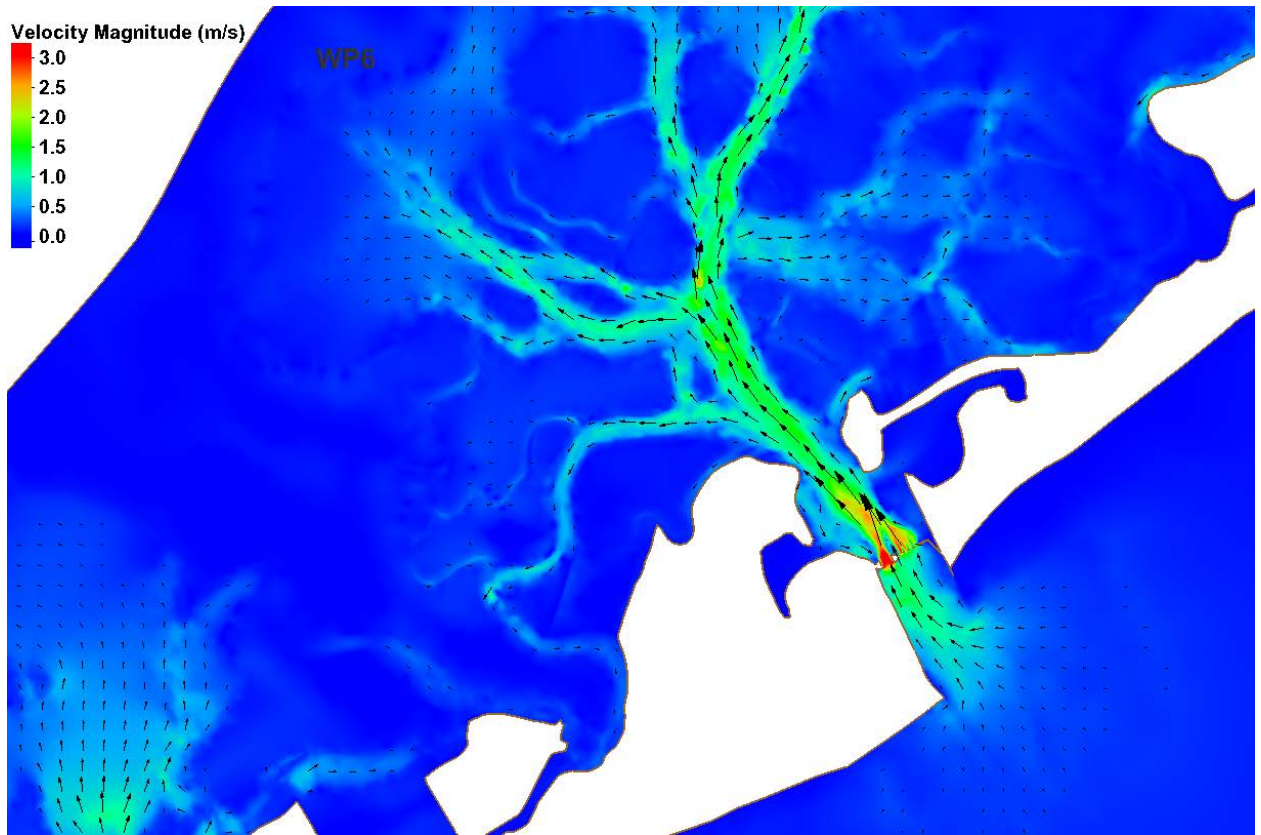
Absecon and Absecon Bay Blvd

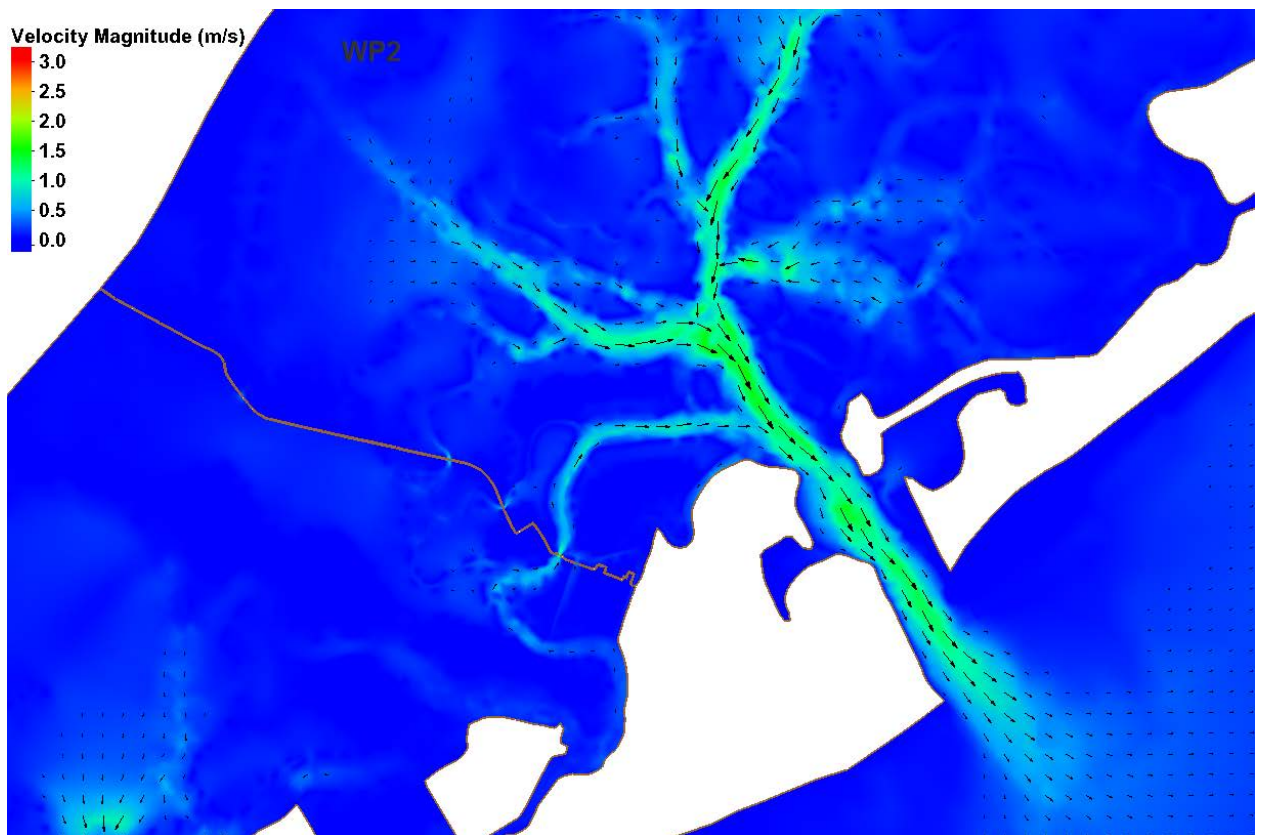
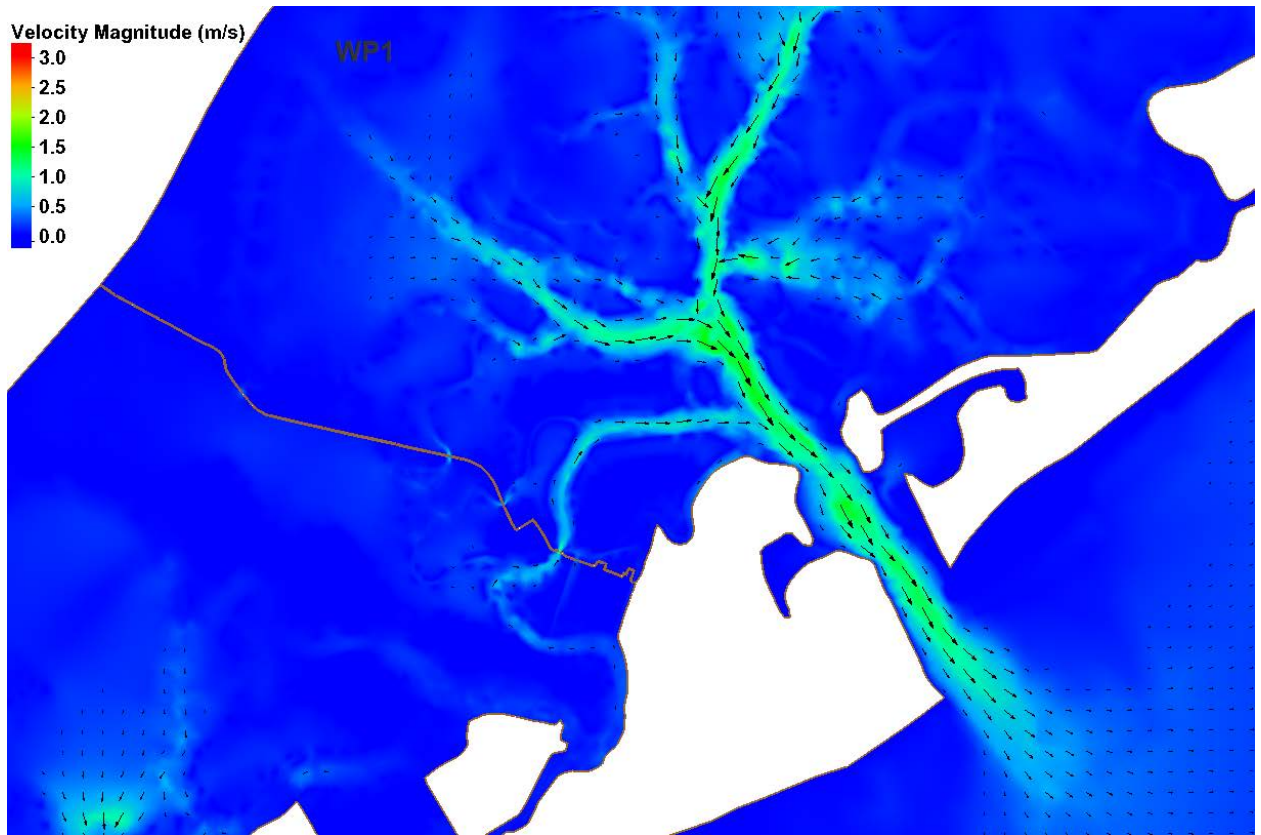


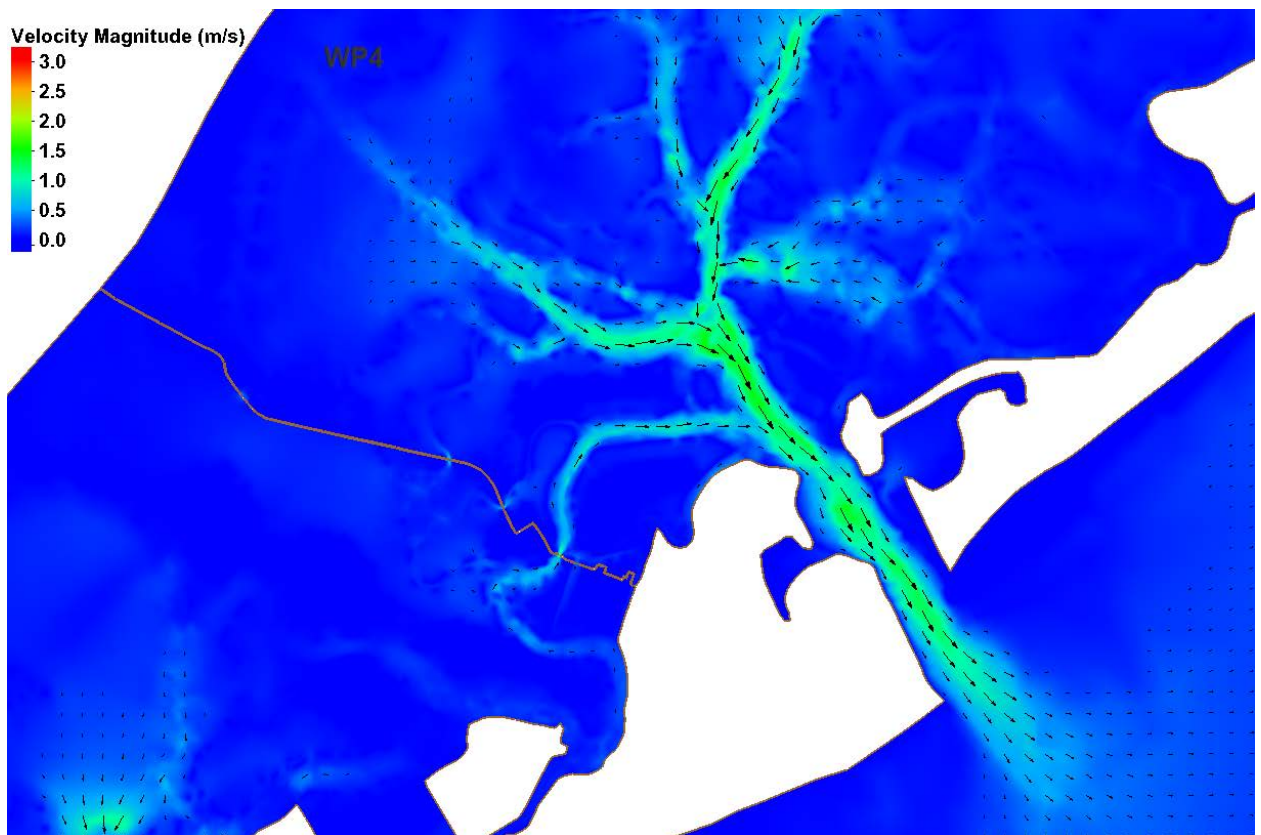
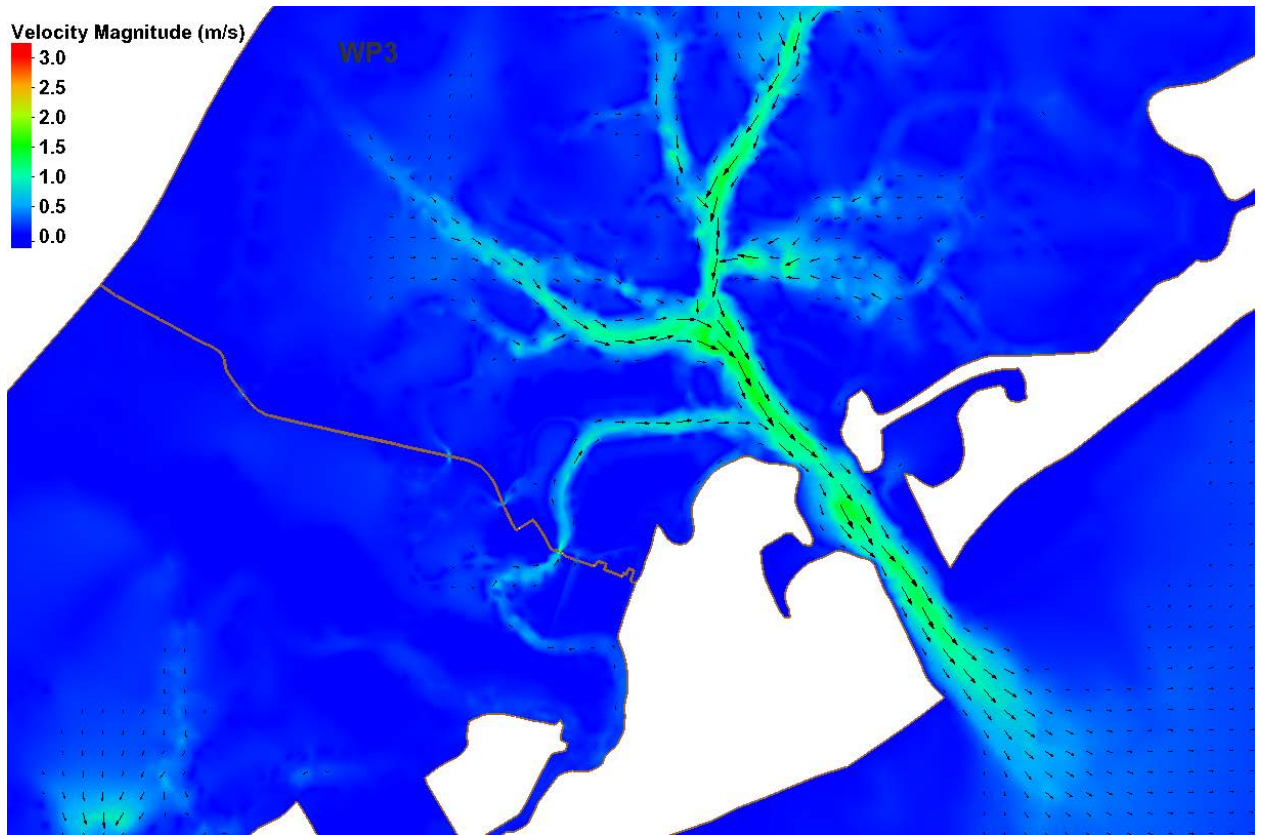


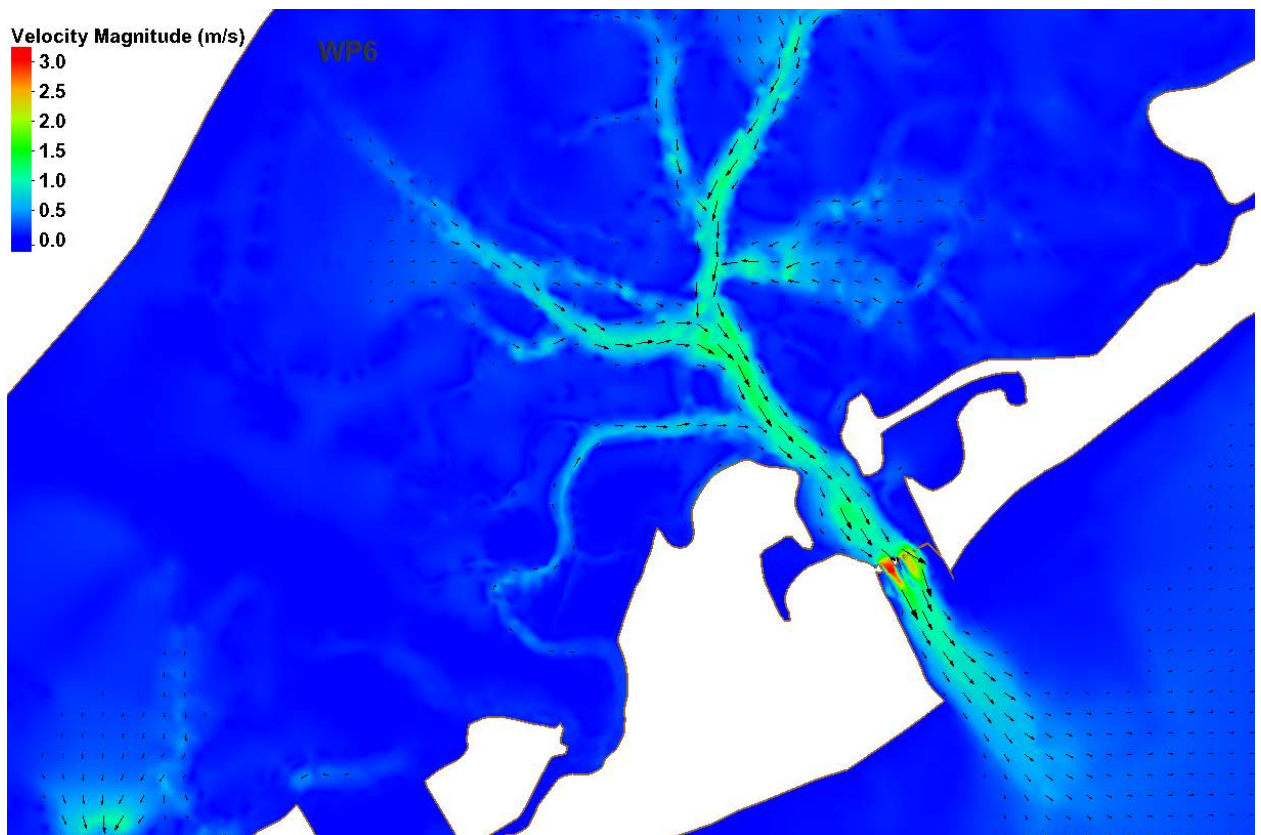
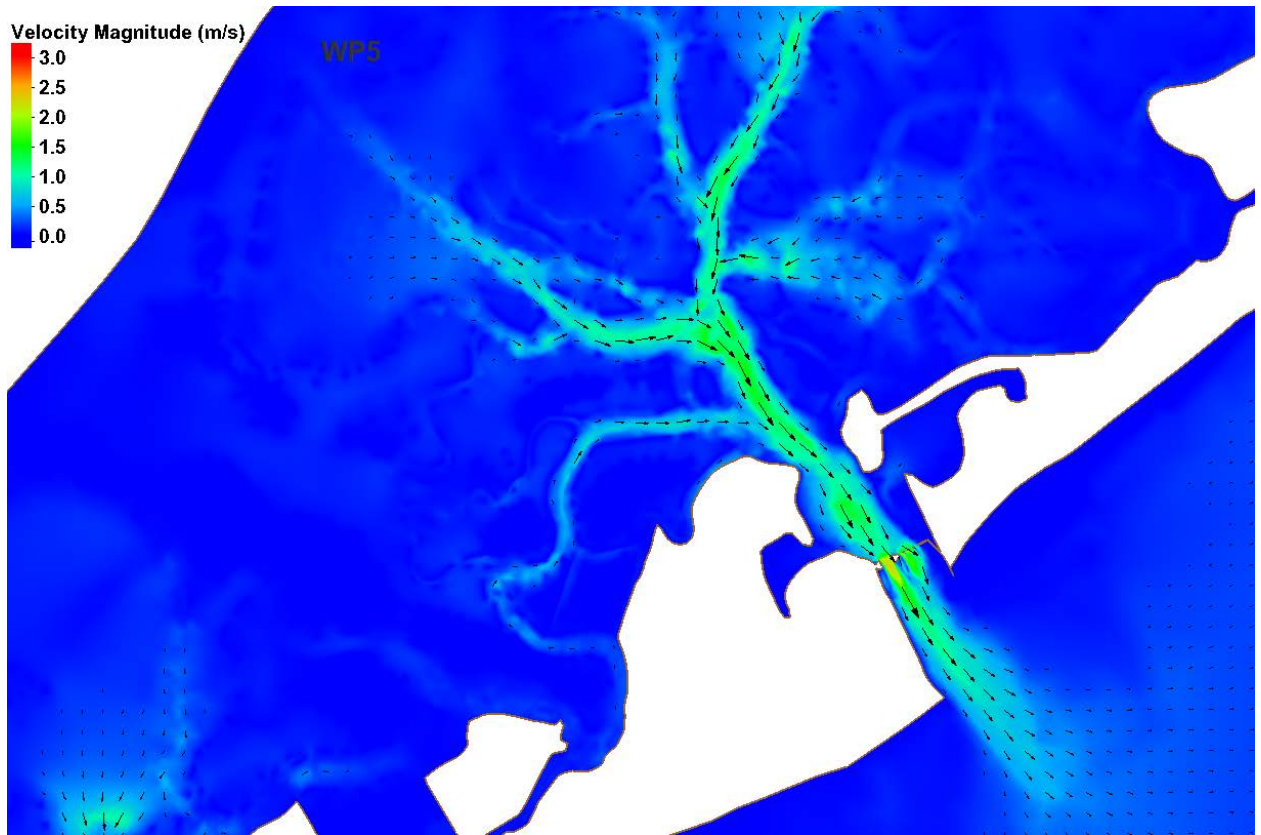




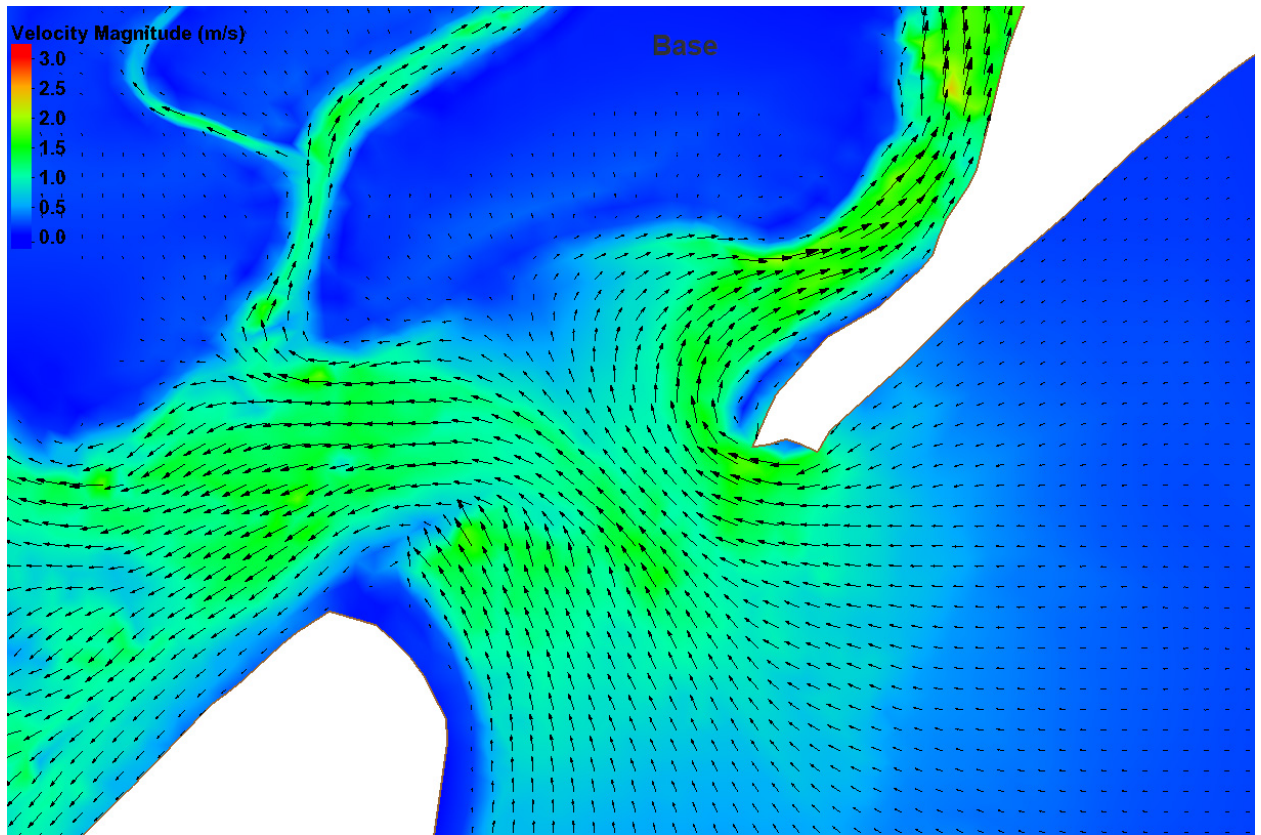


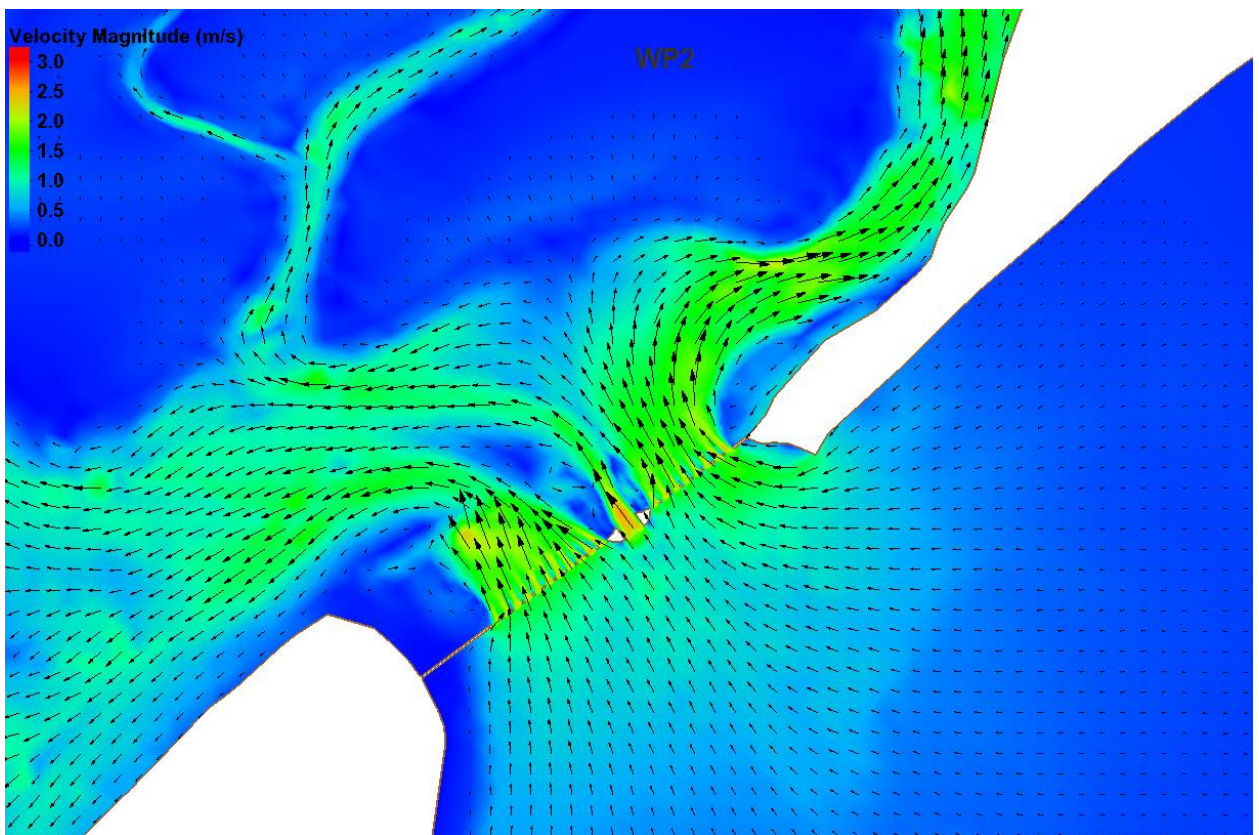
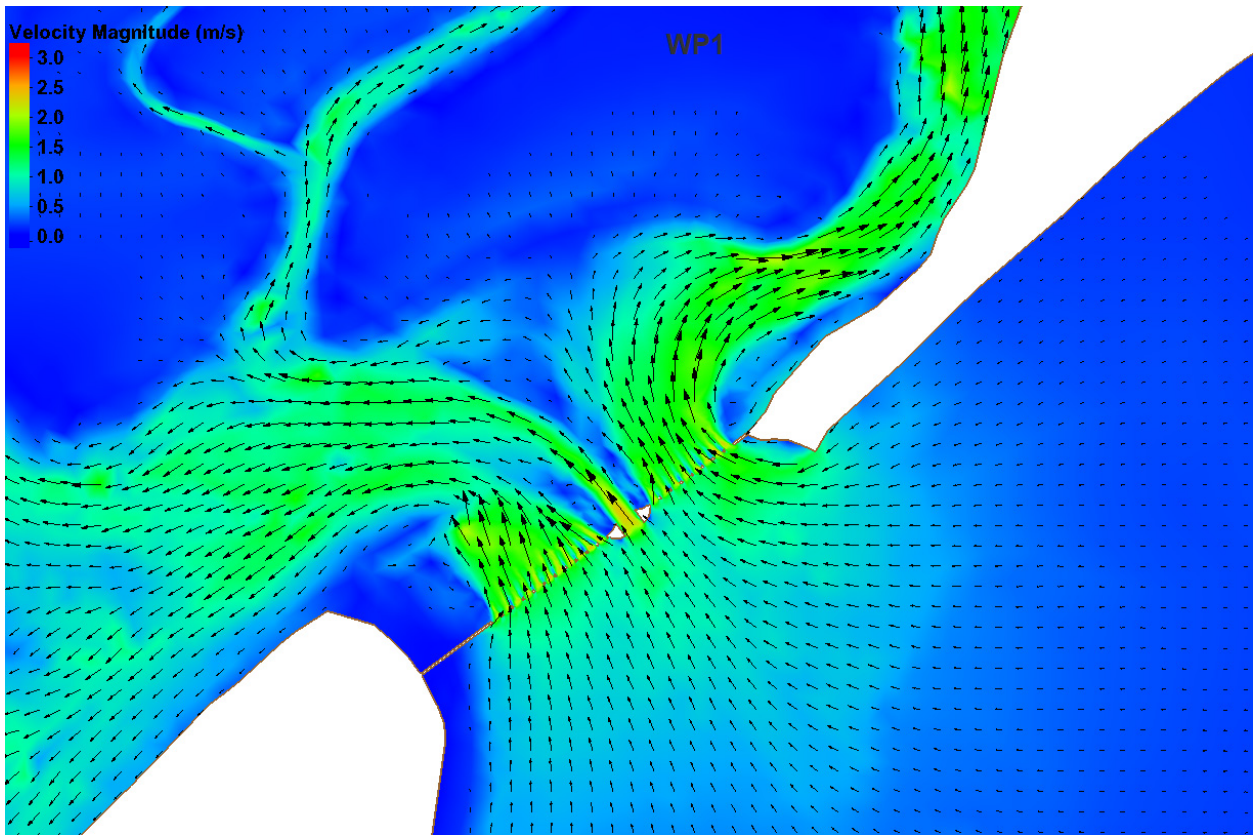


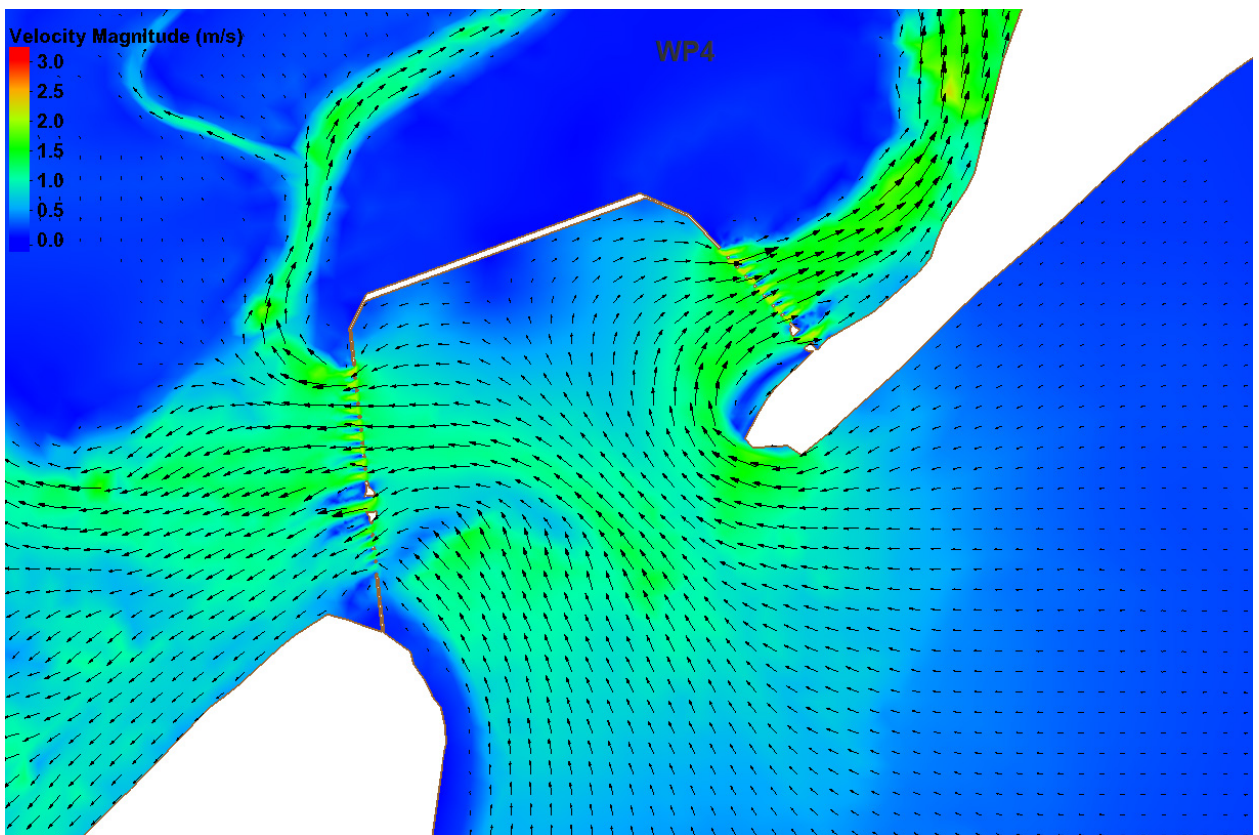
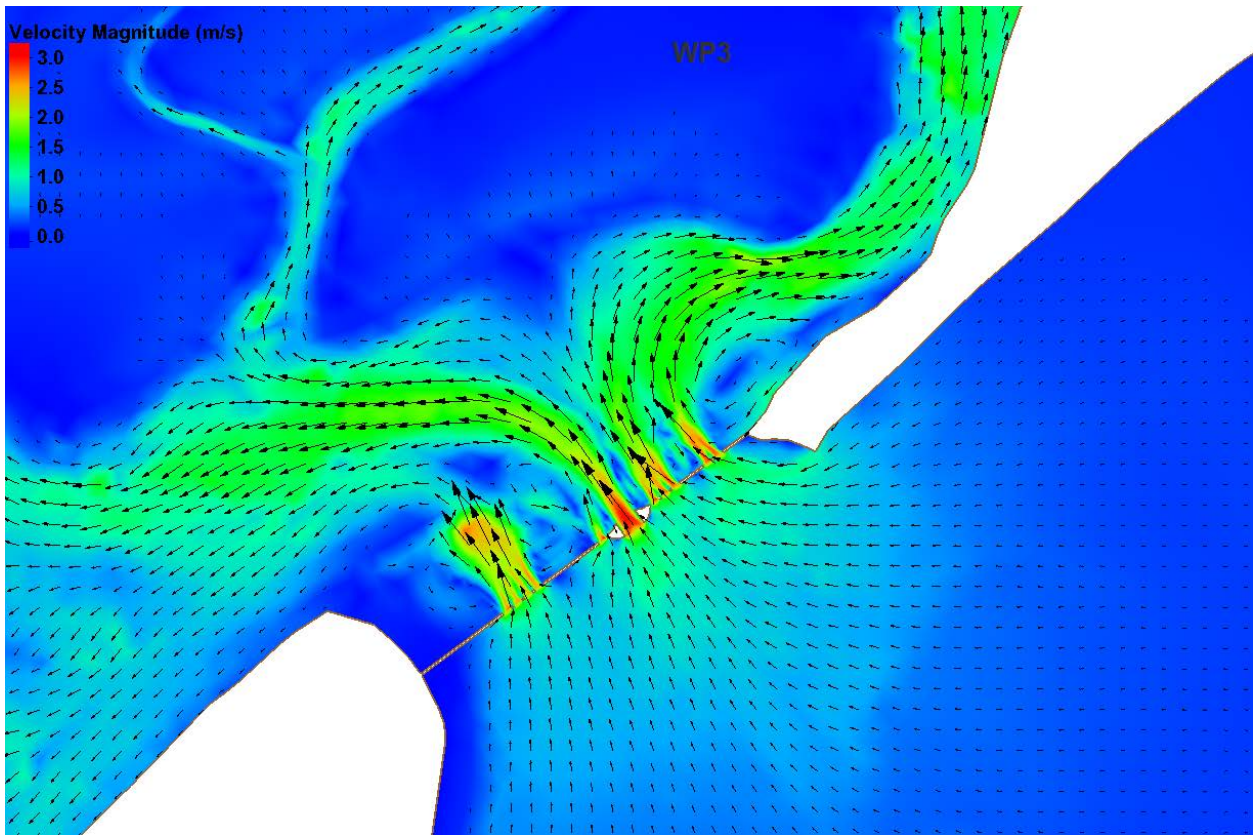


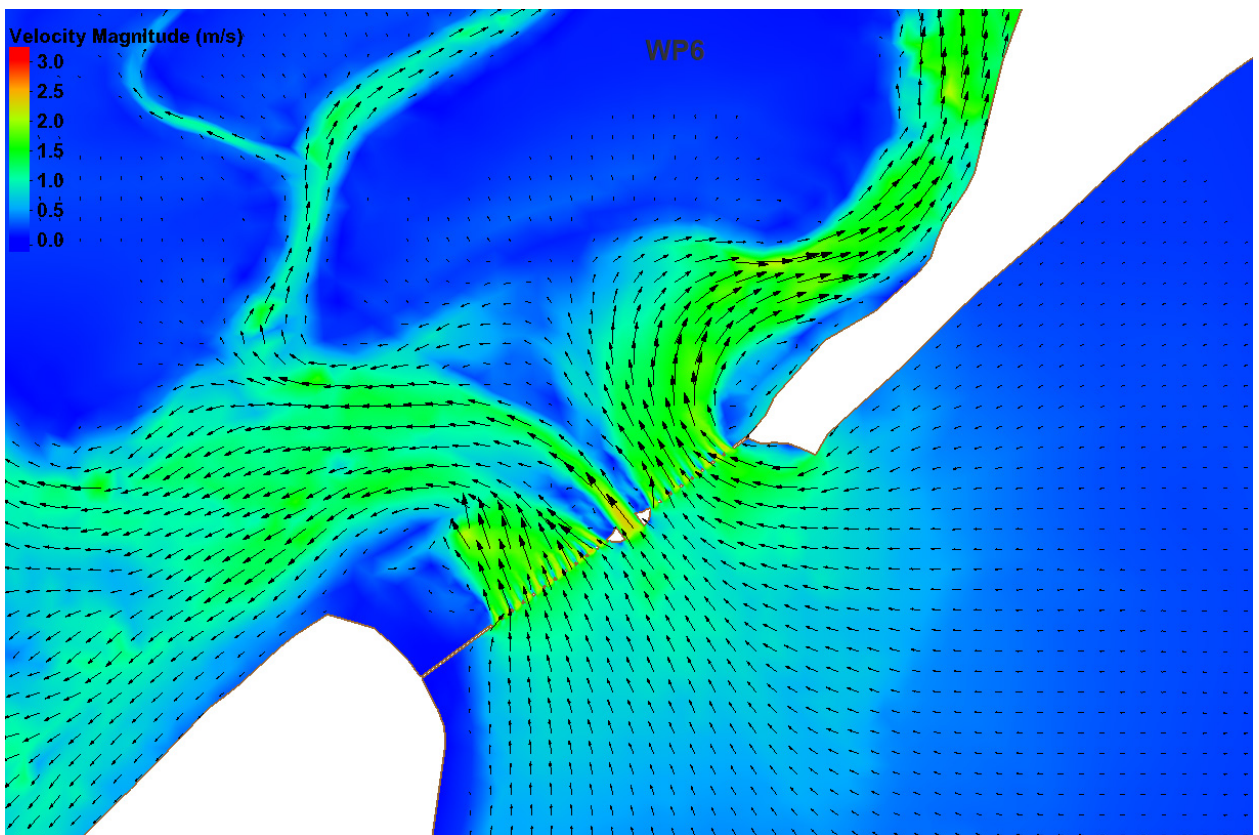
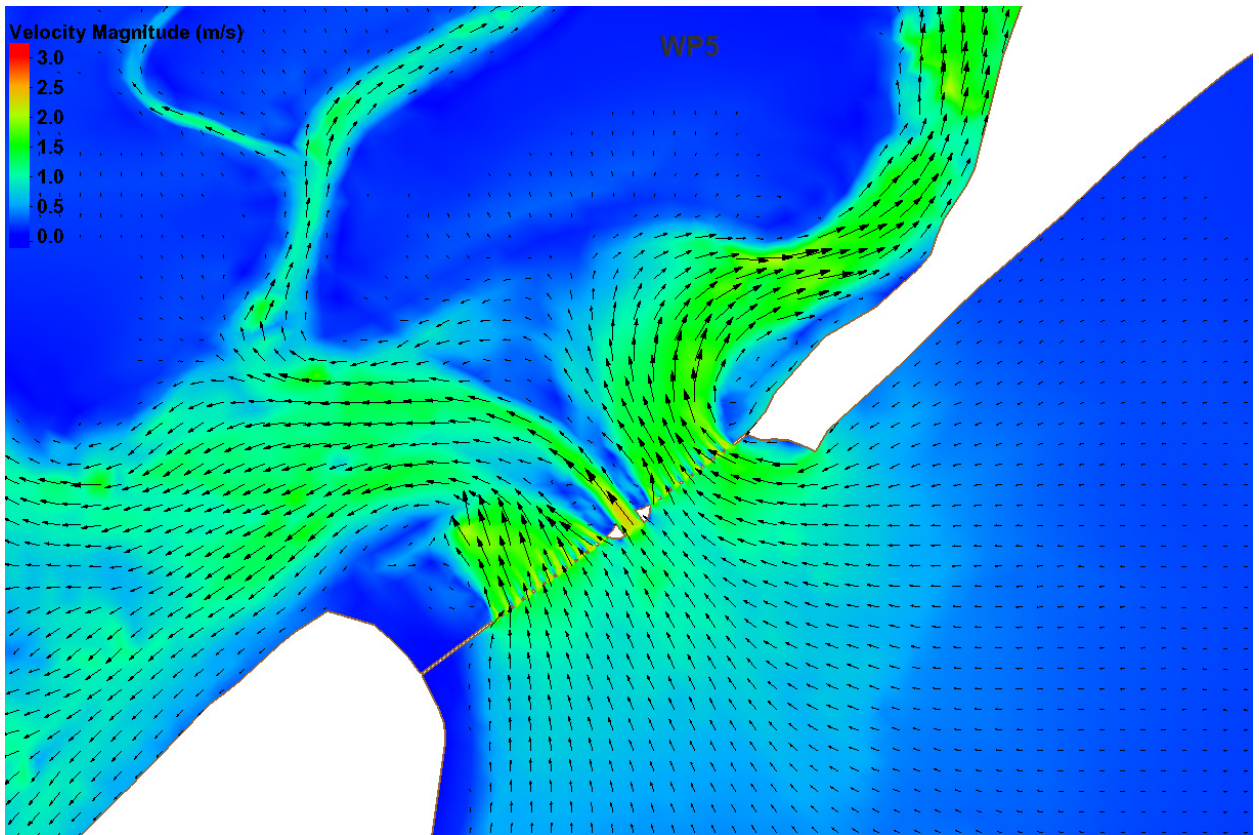


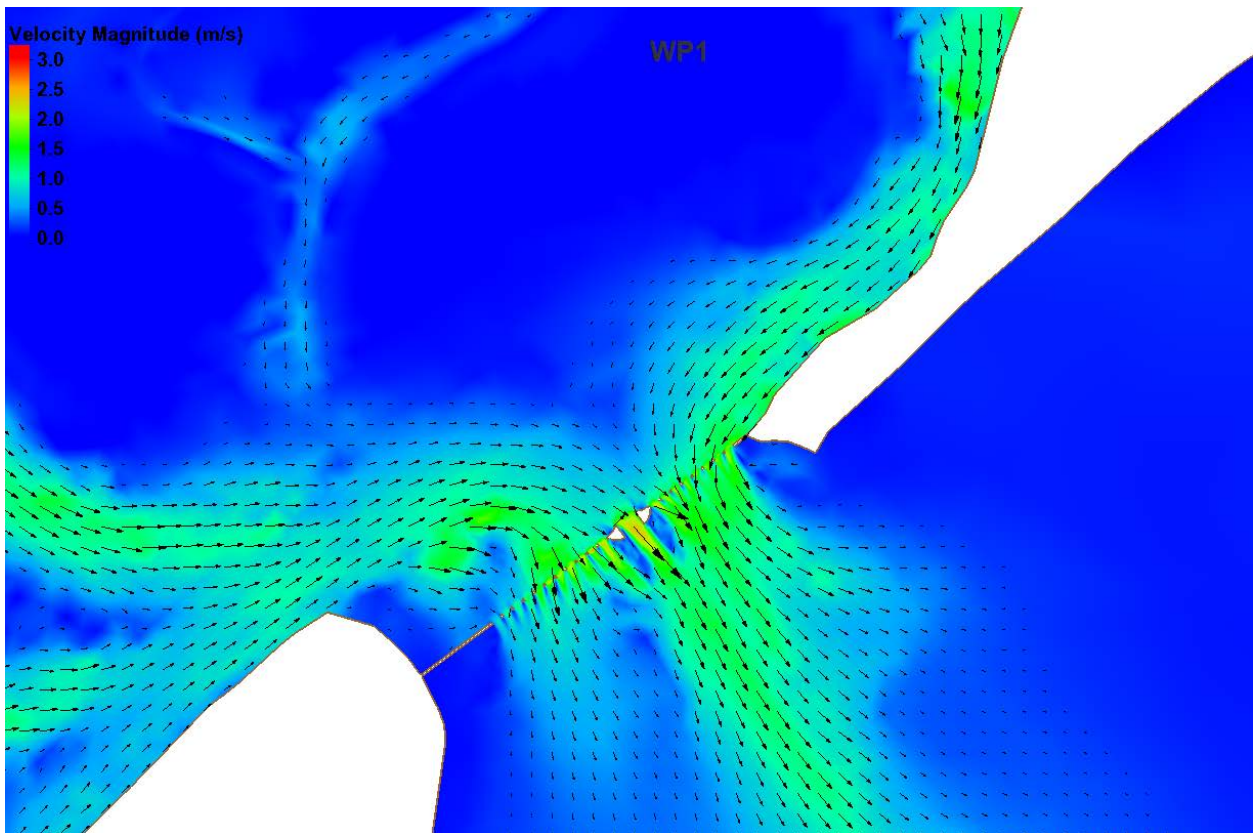
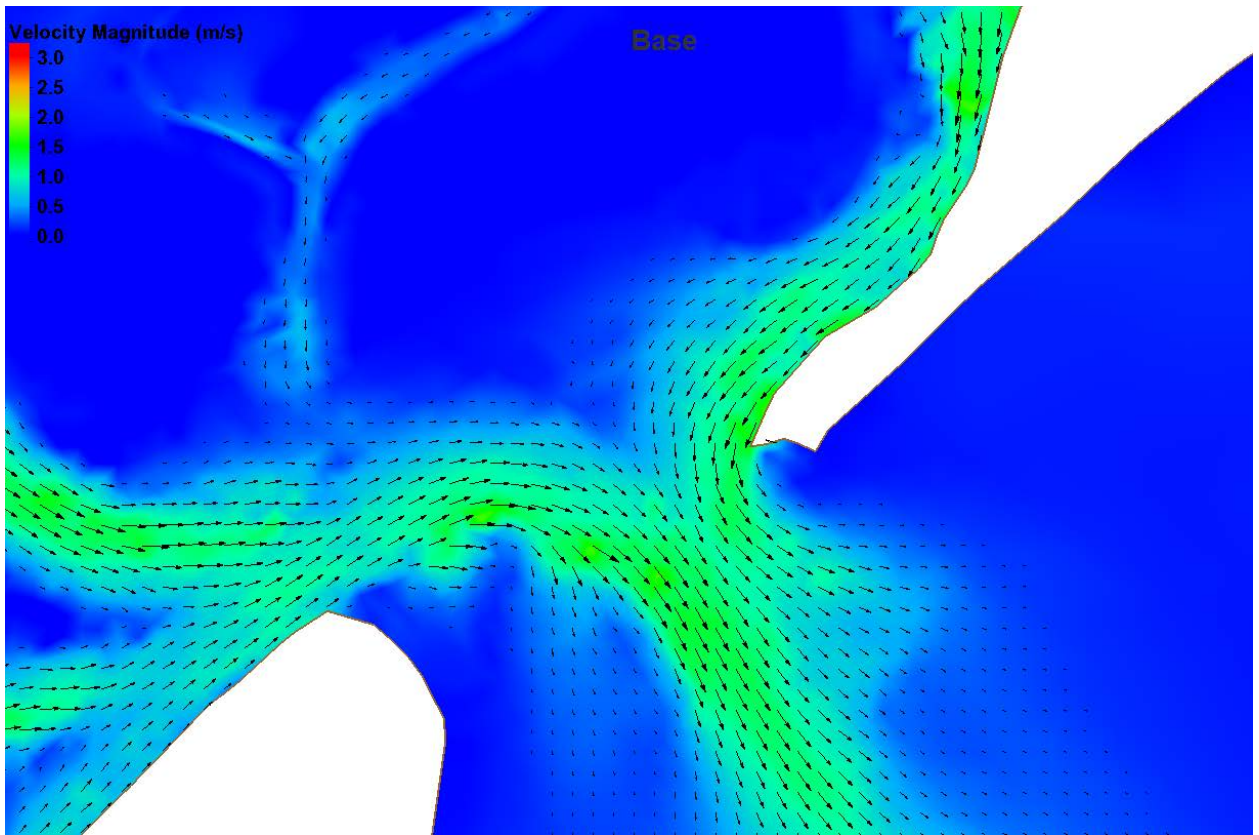
Great Egg

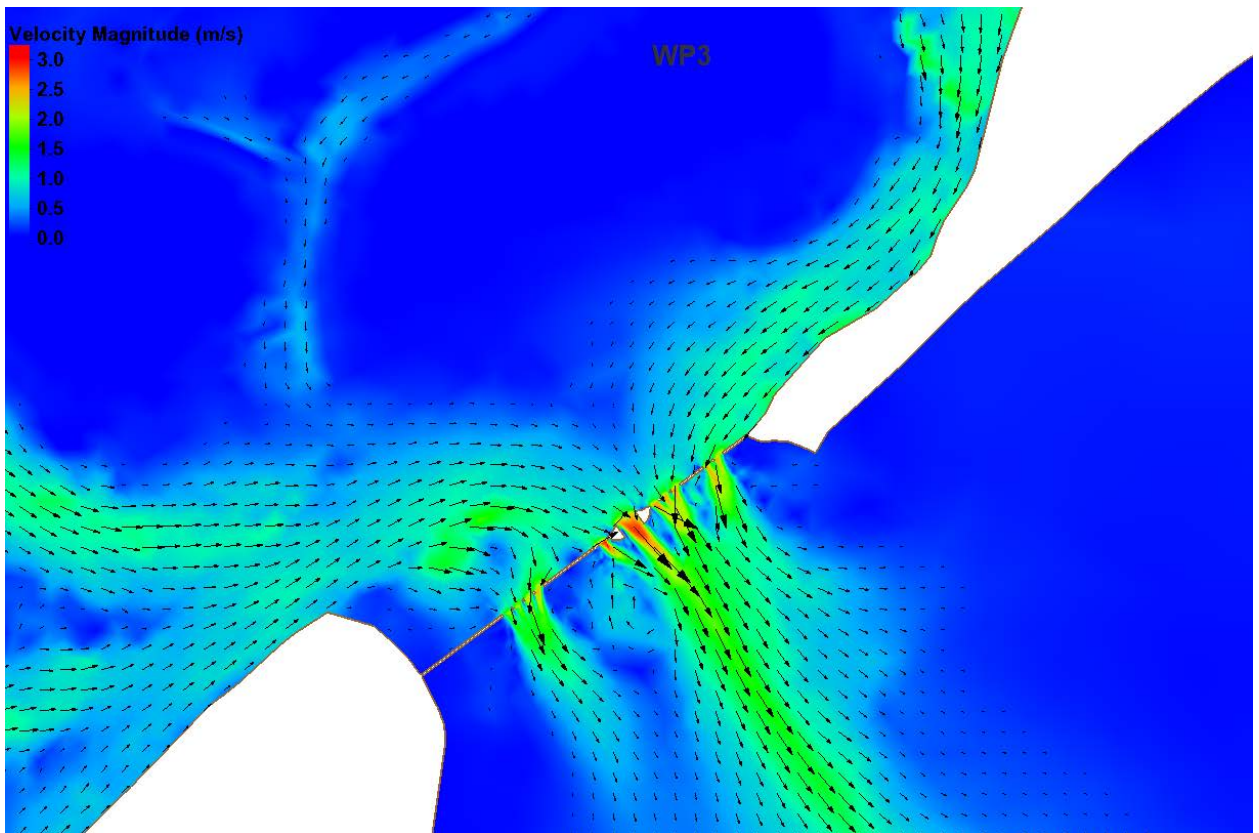
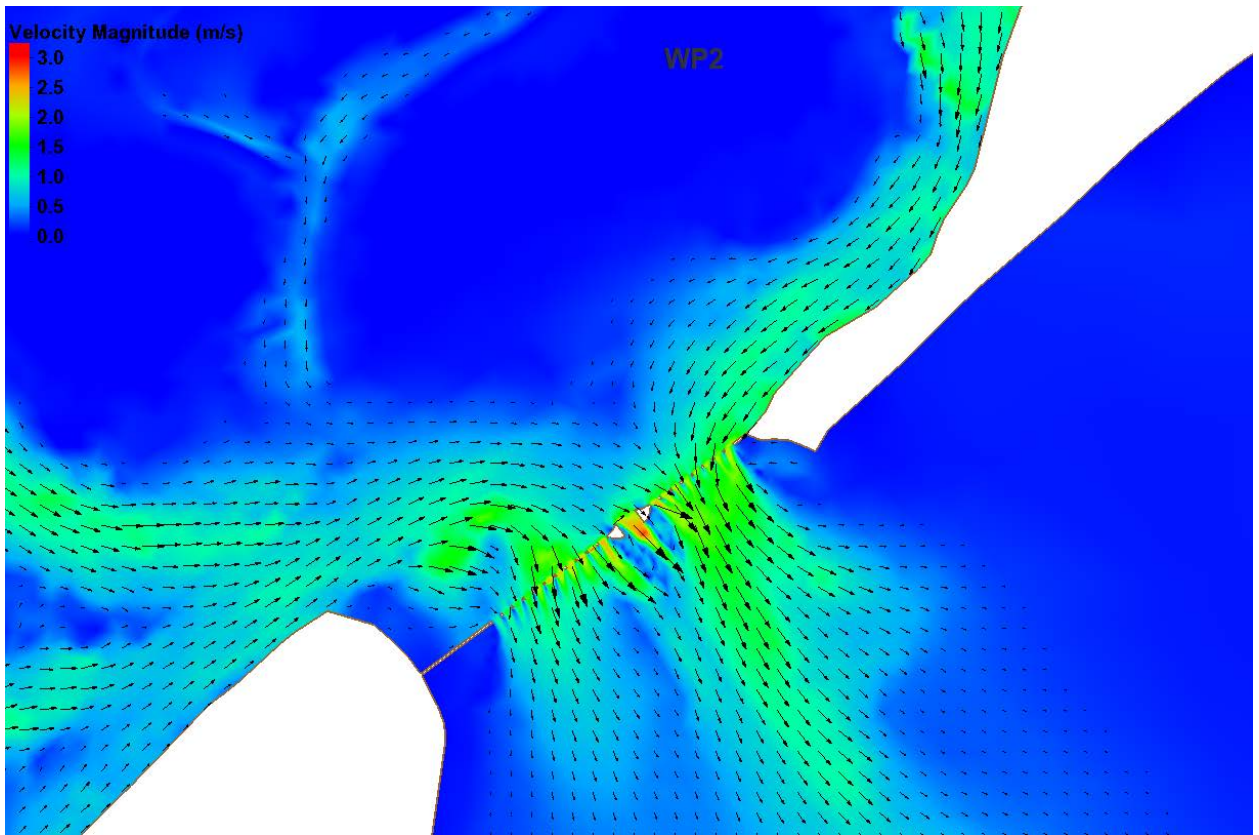


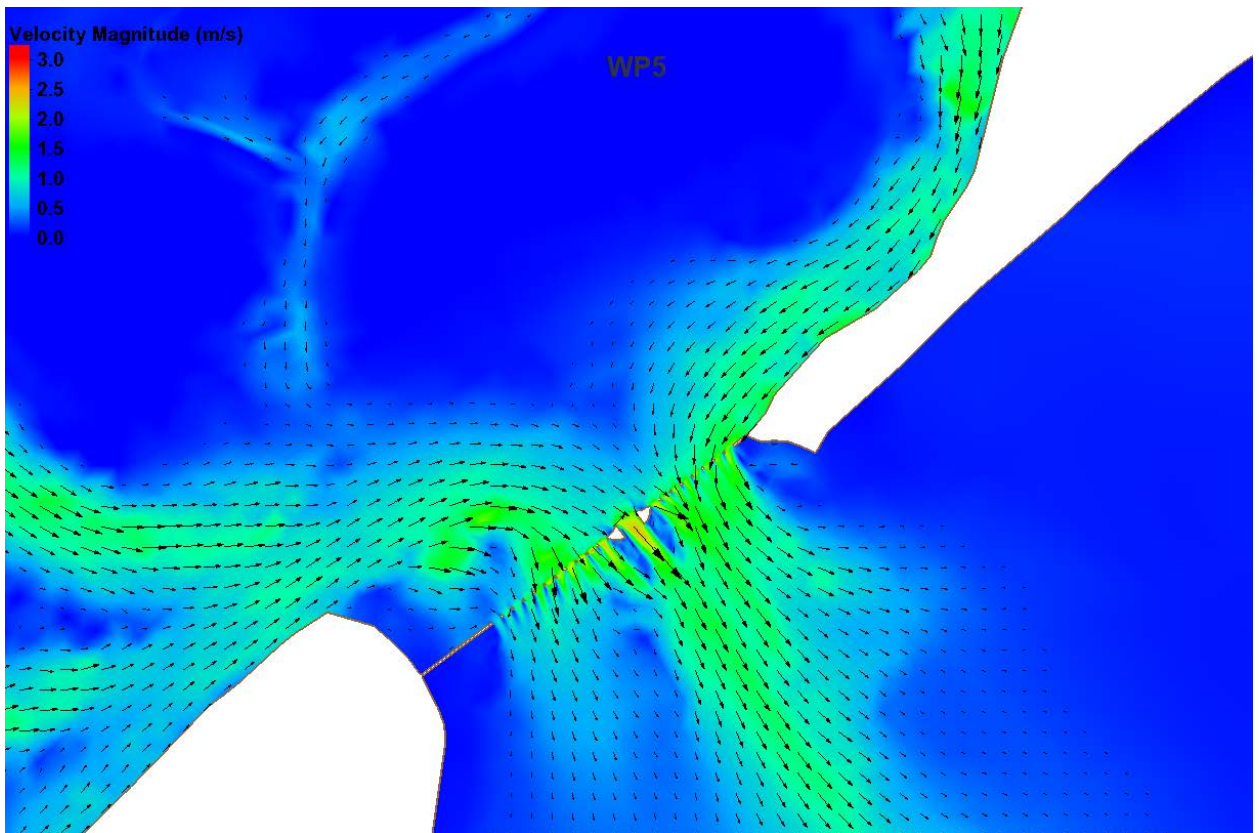
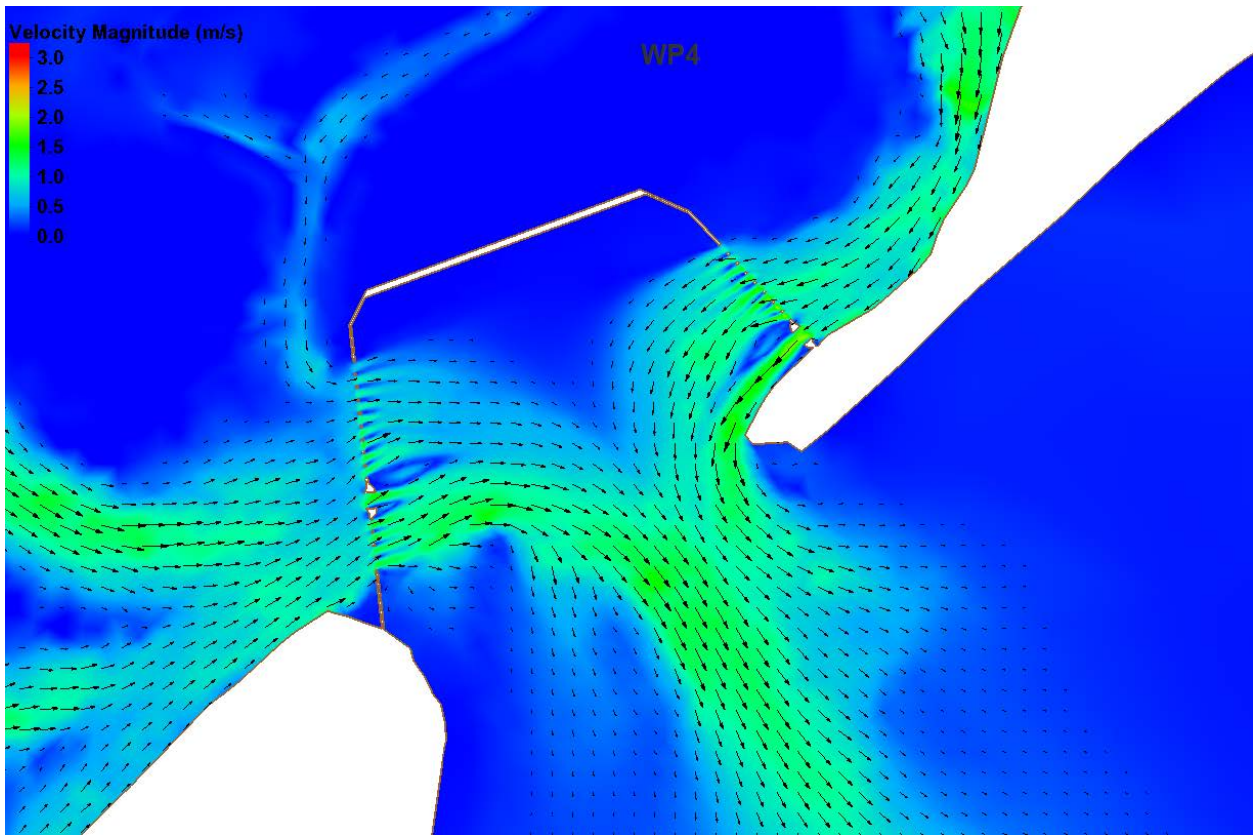


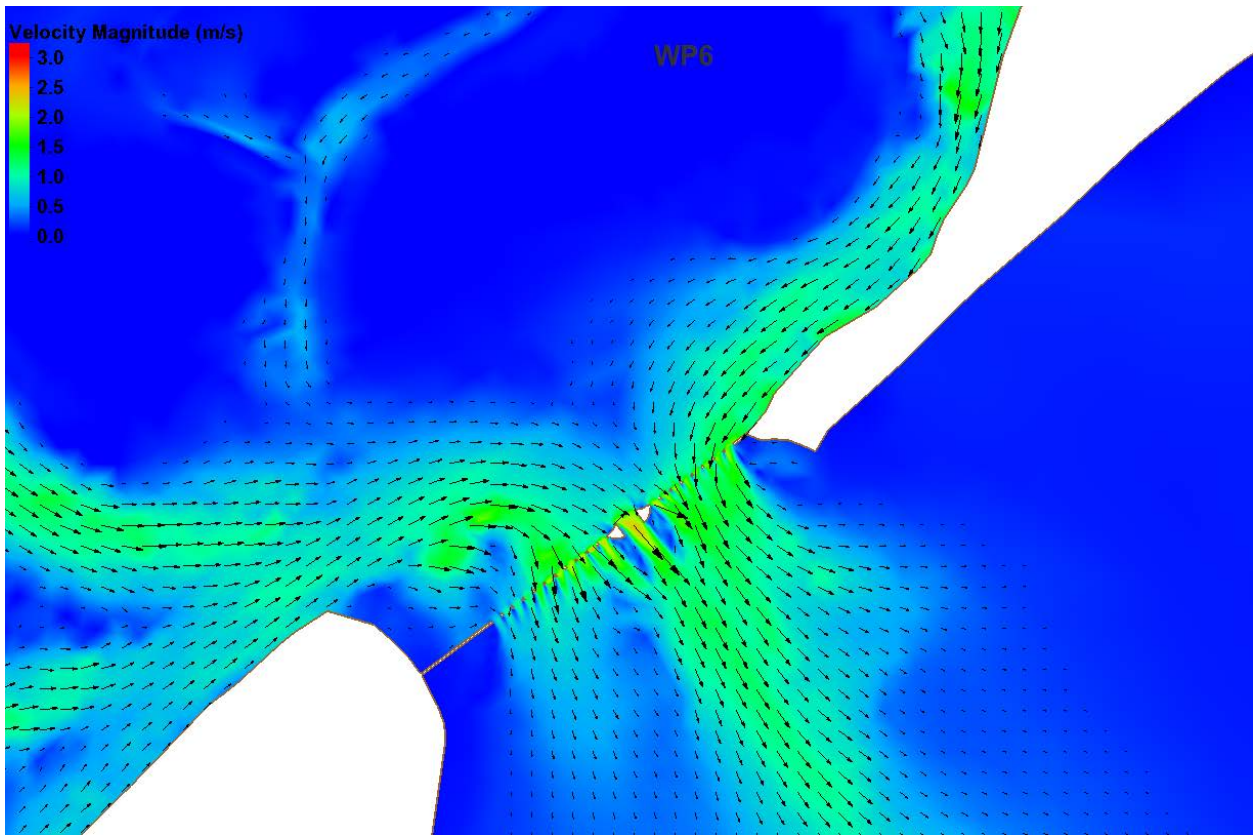




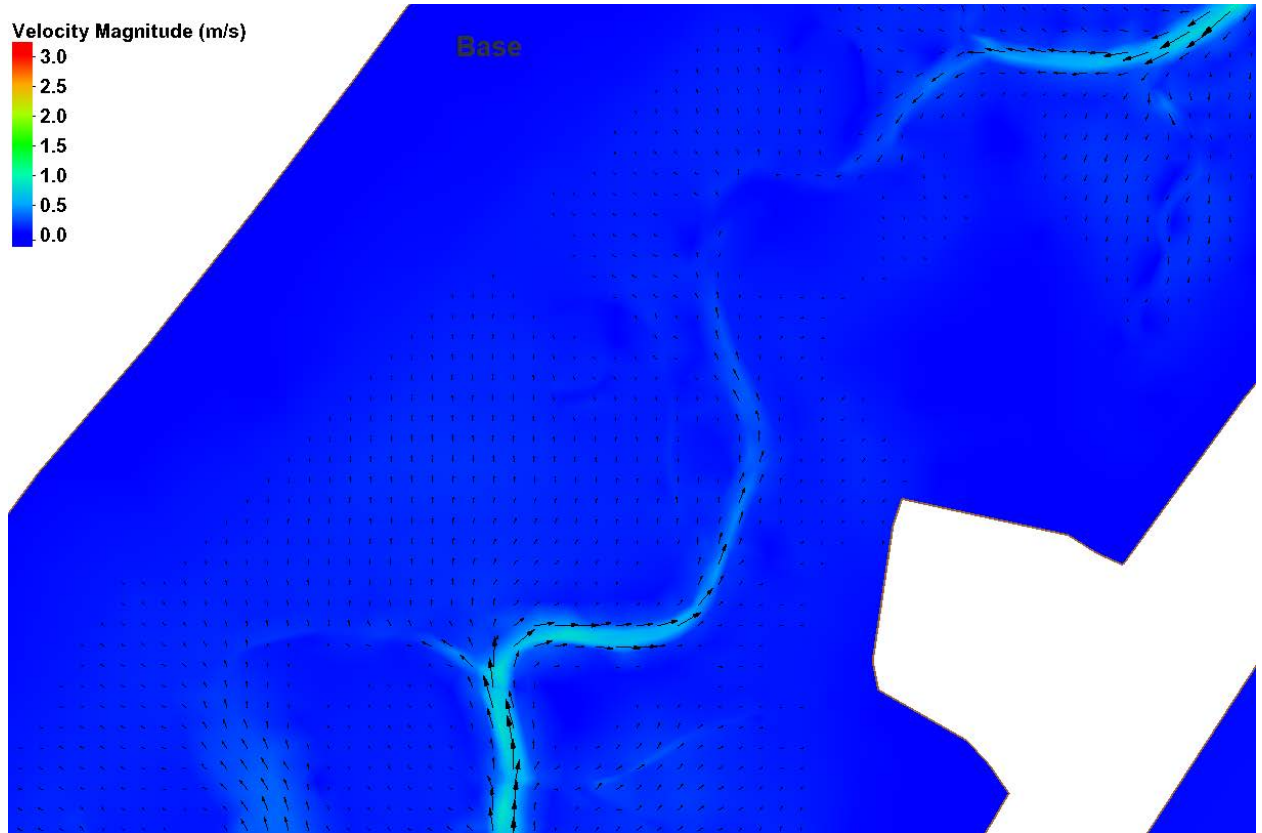


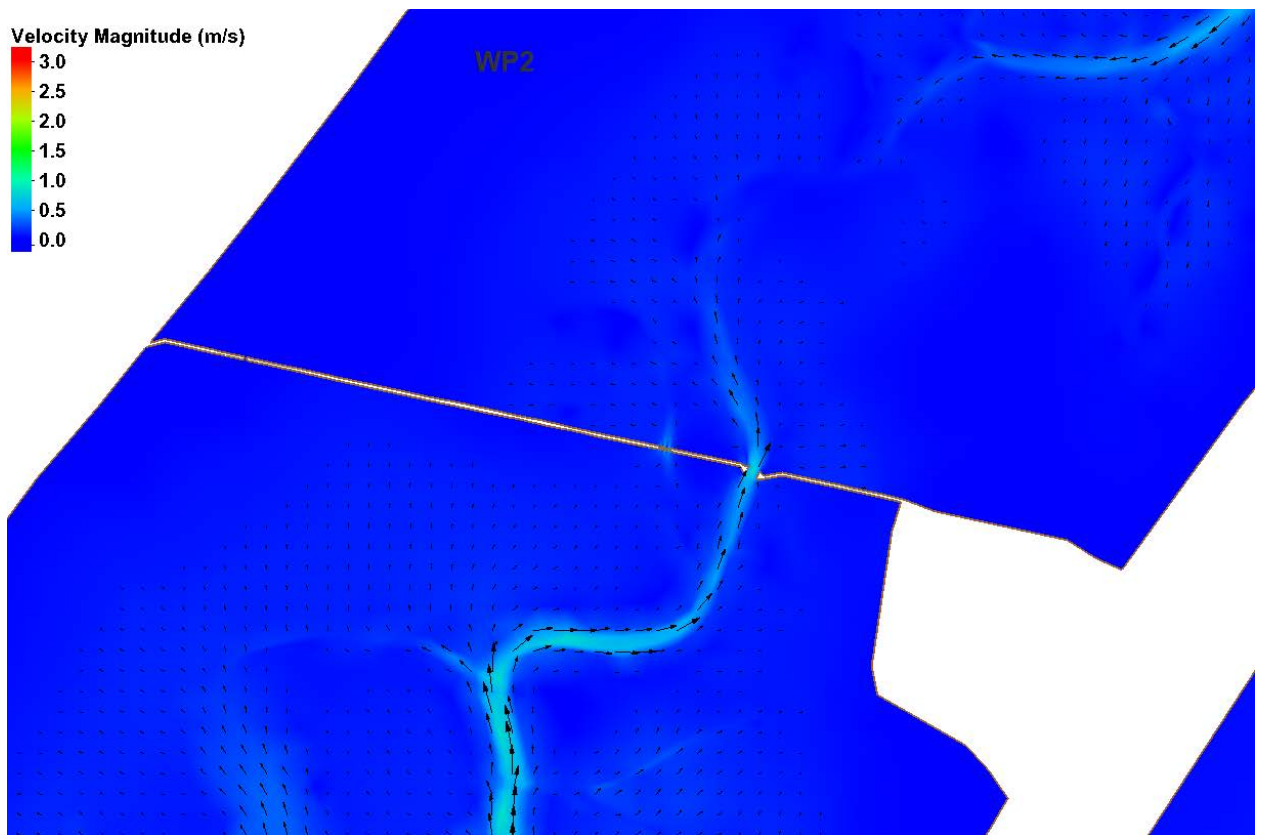
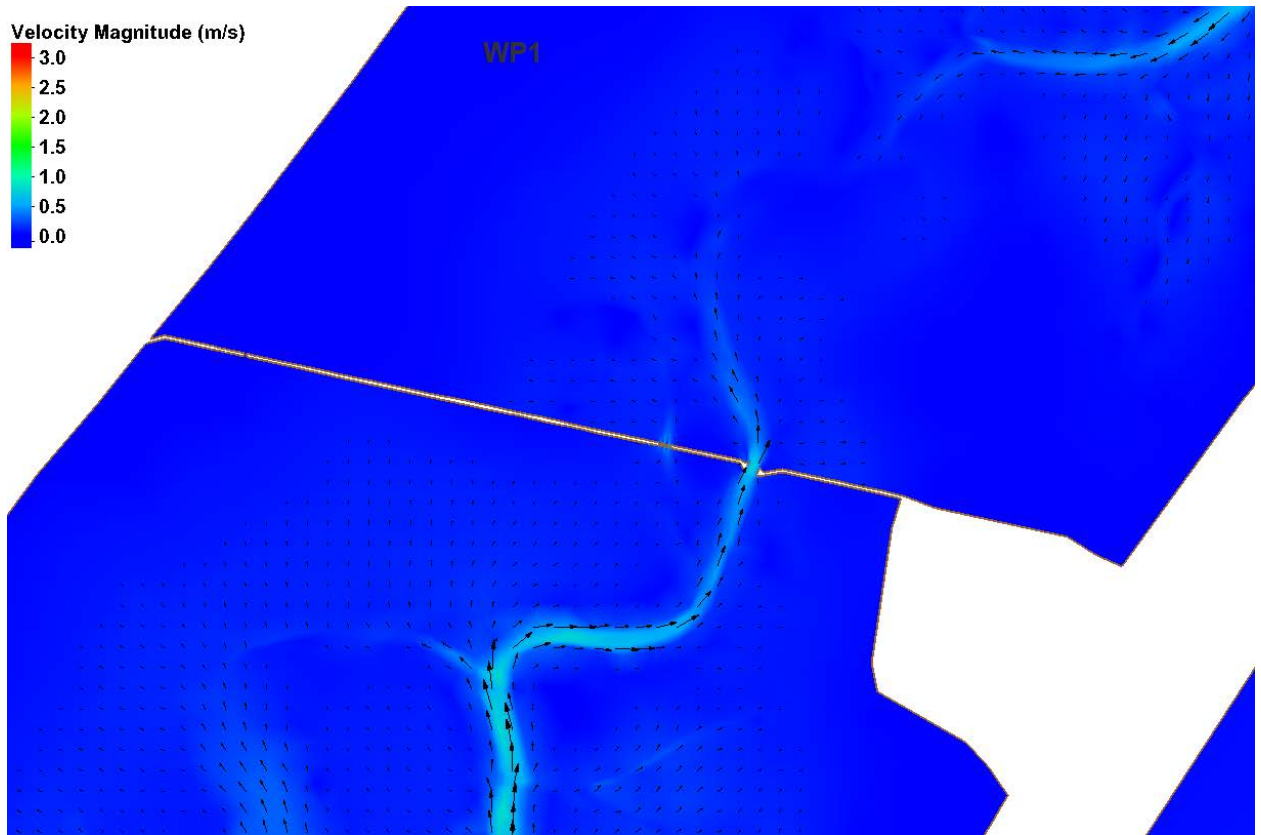


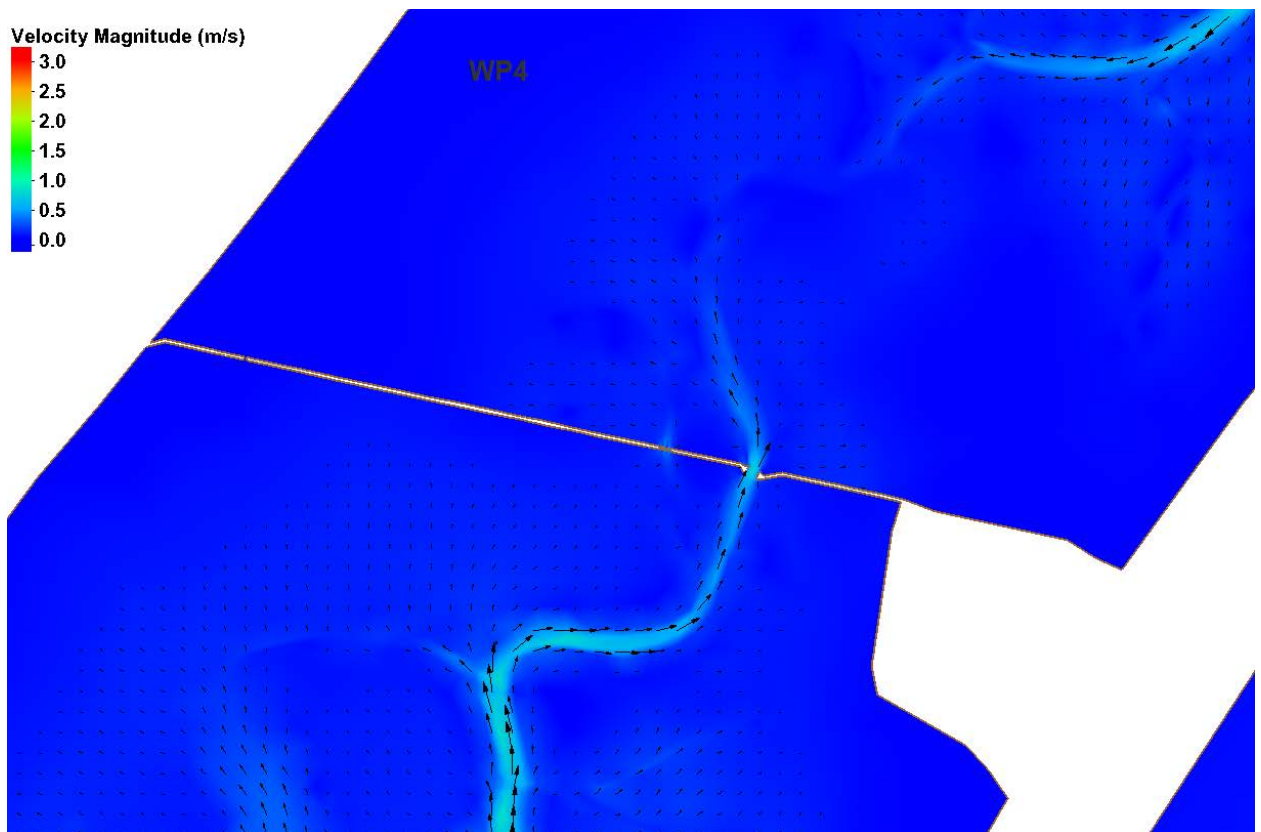
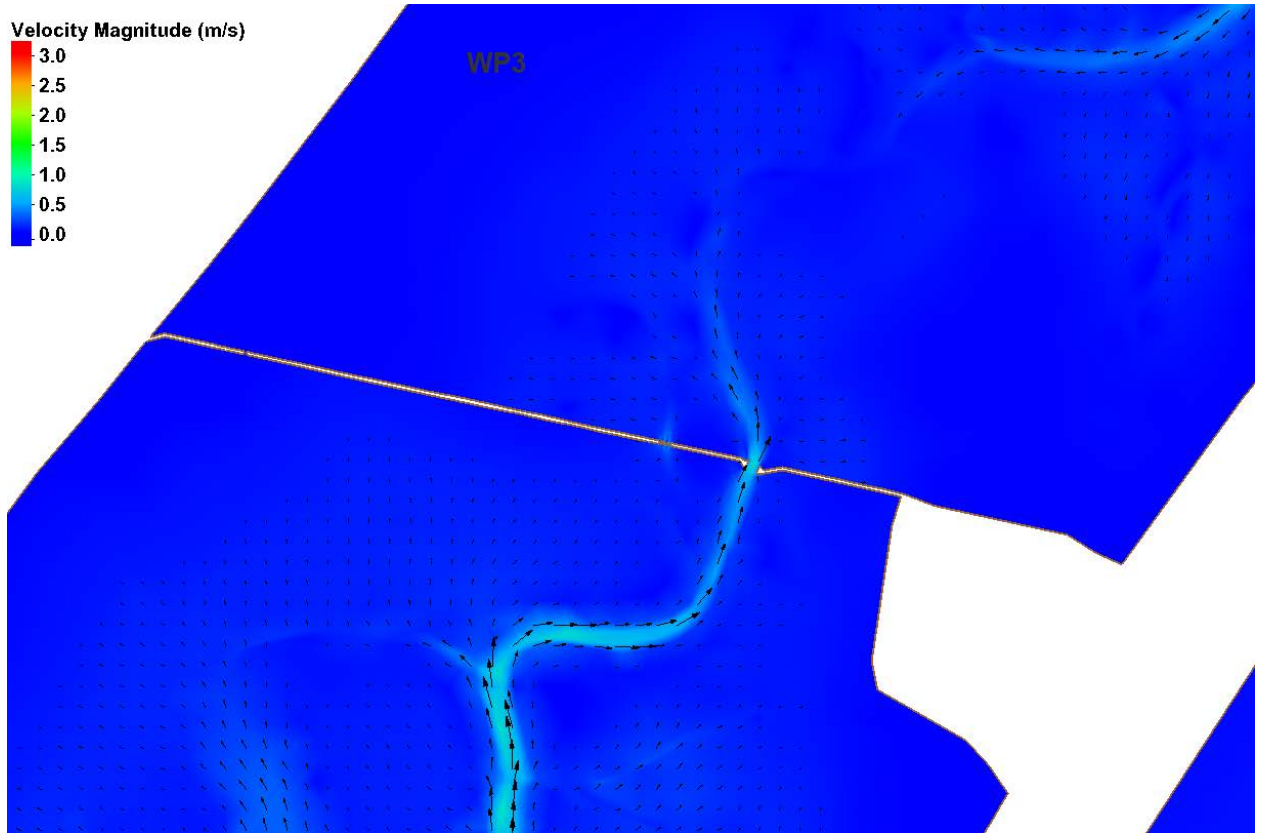


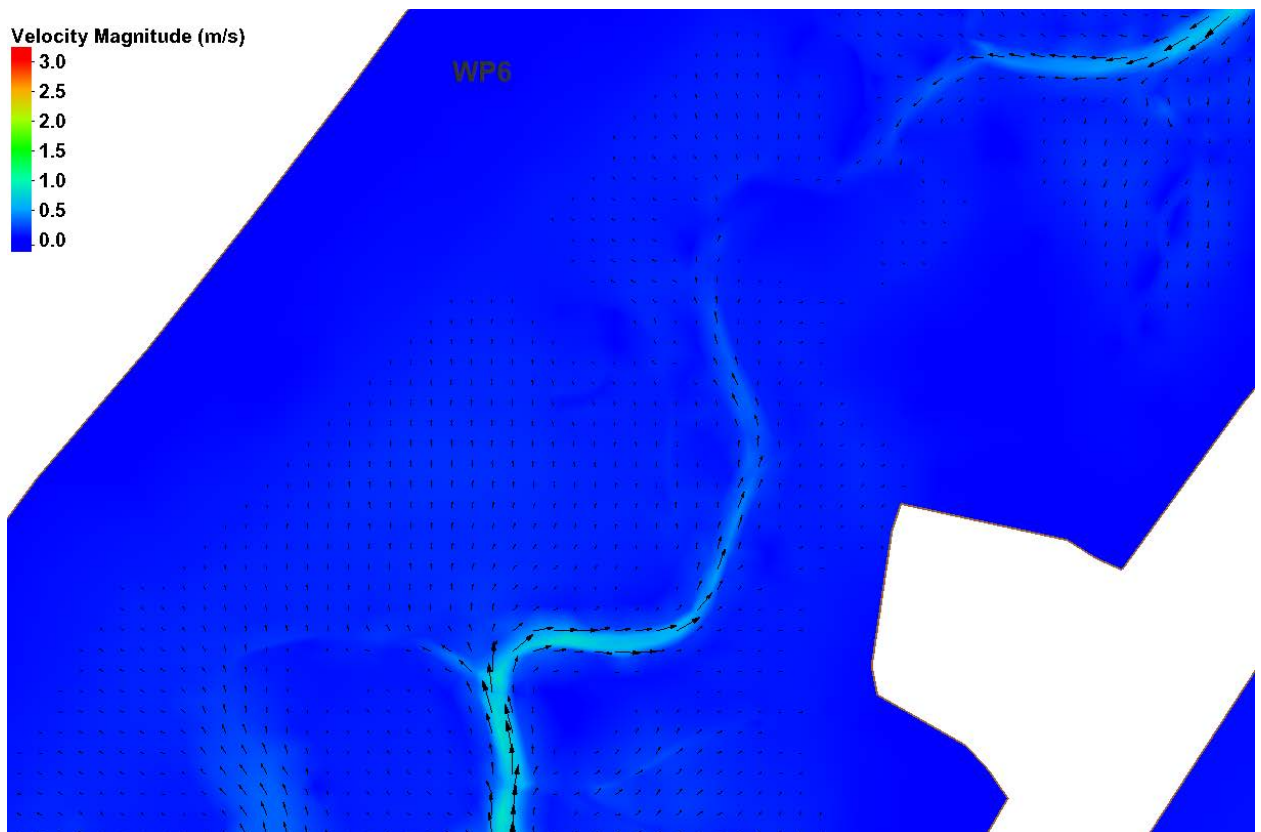
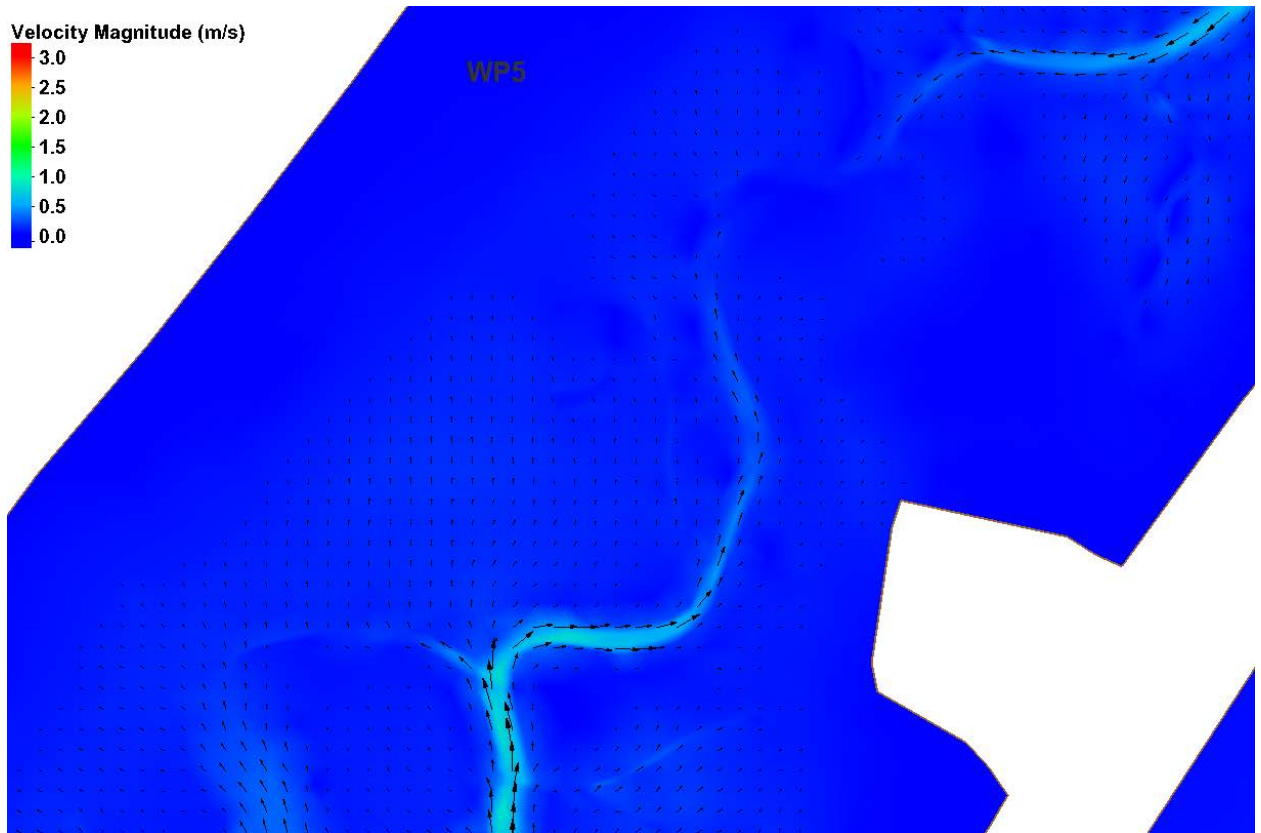


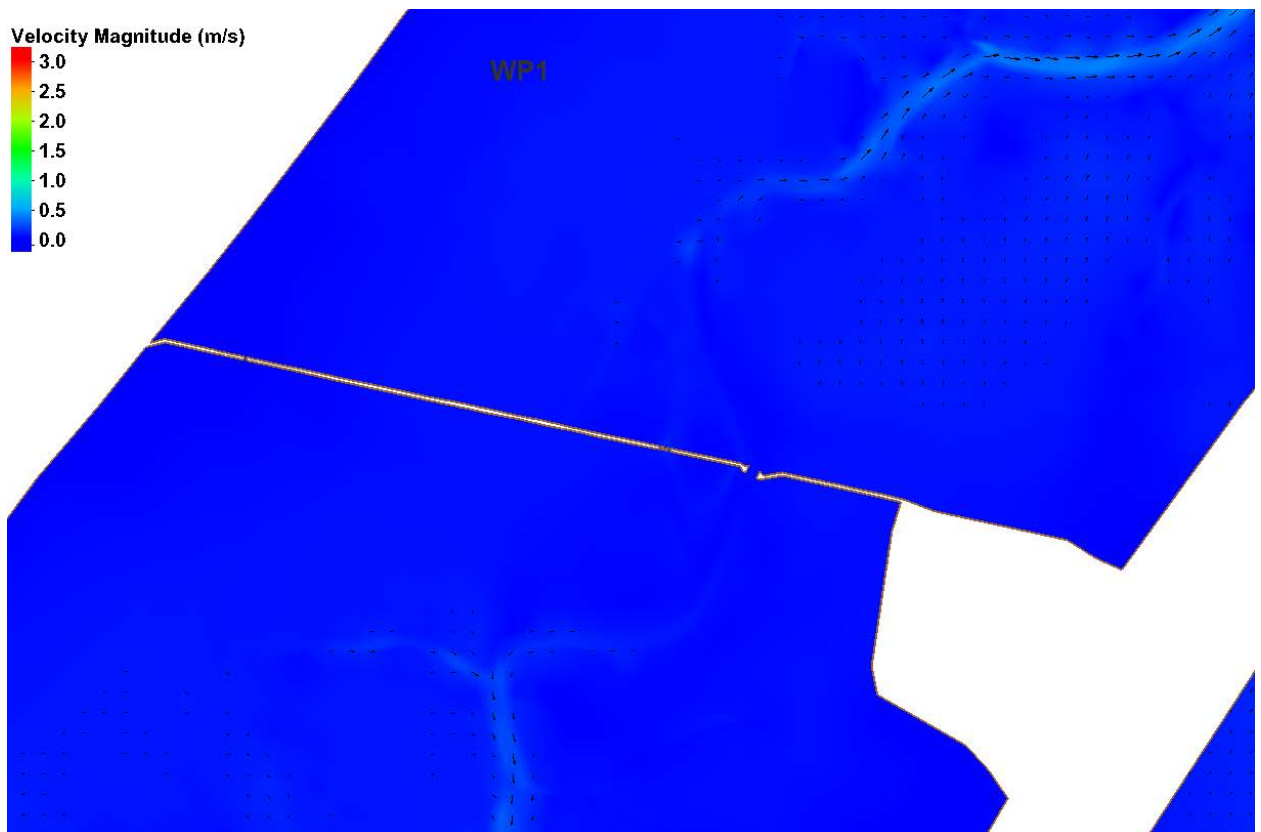
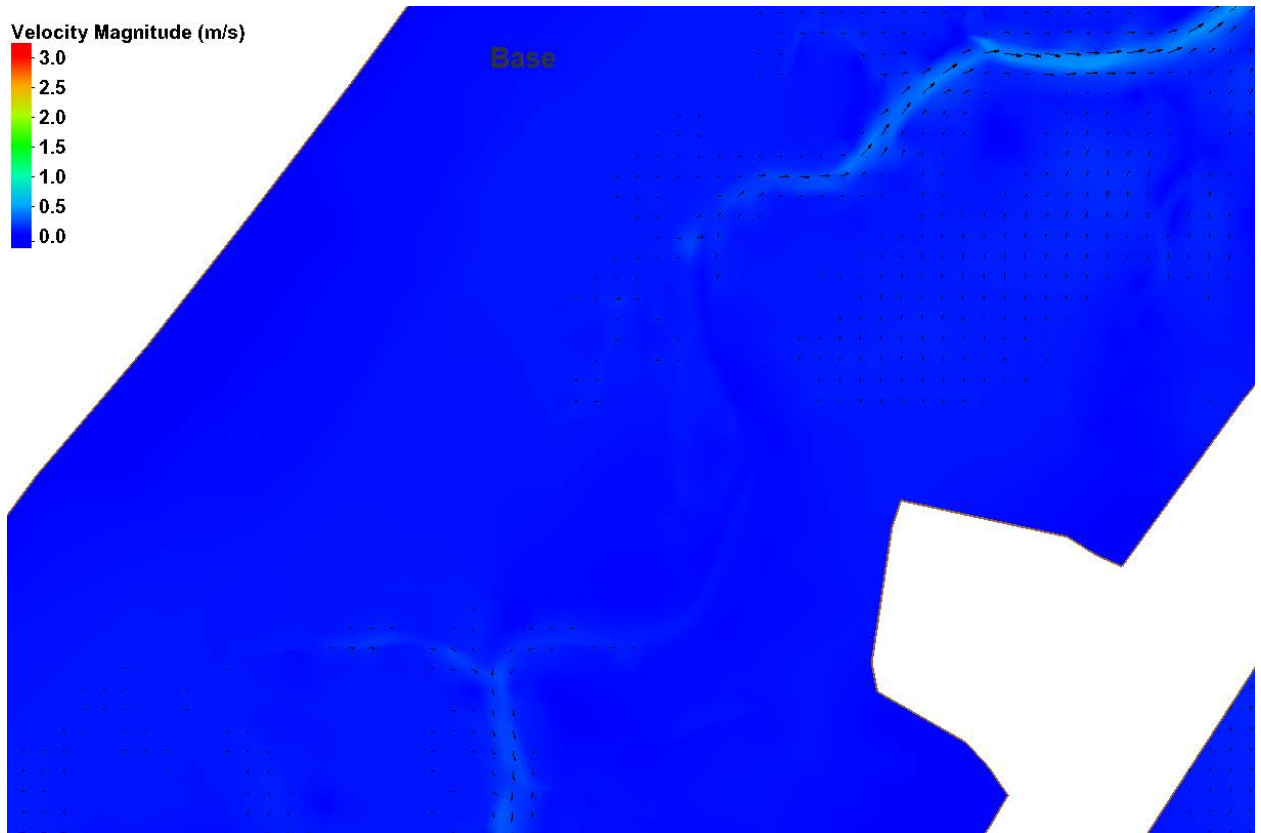
72nd Street

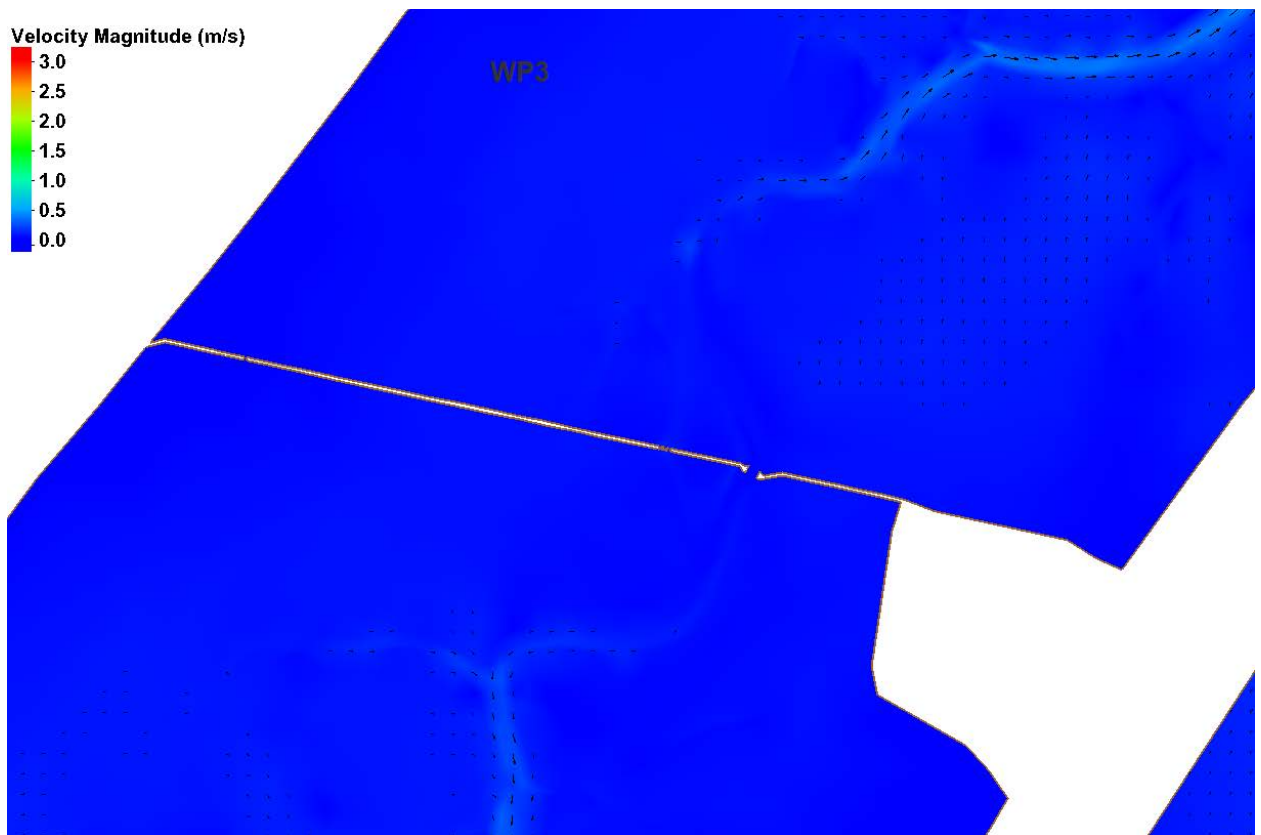
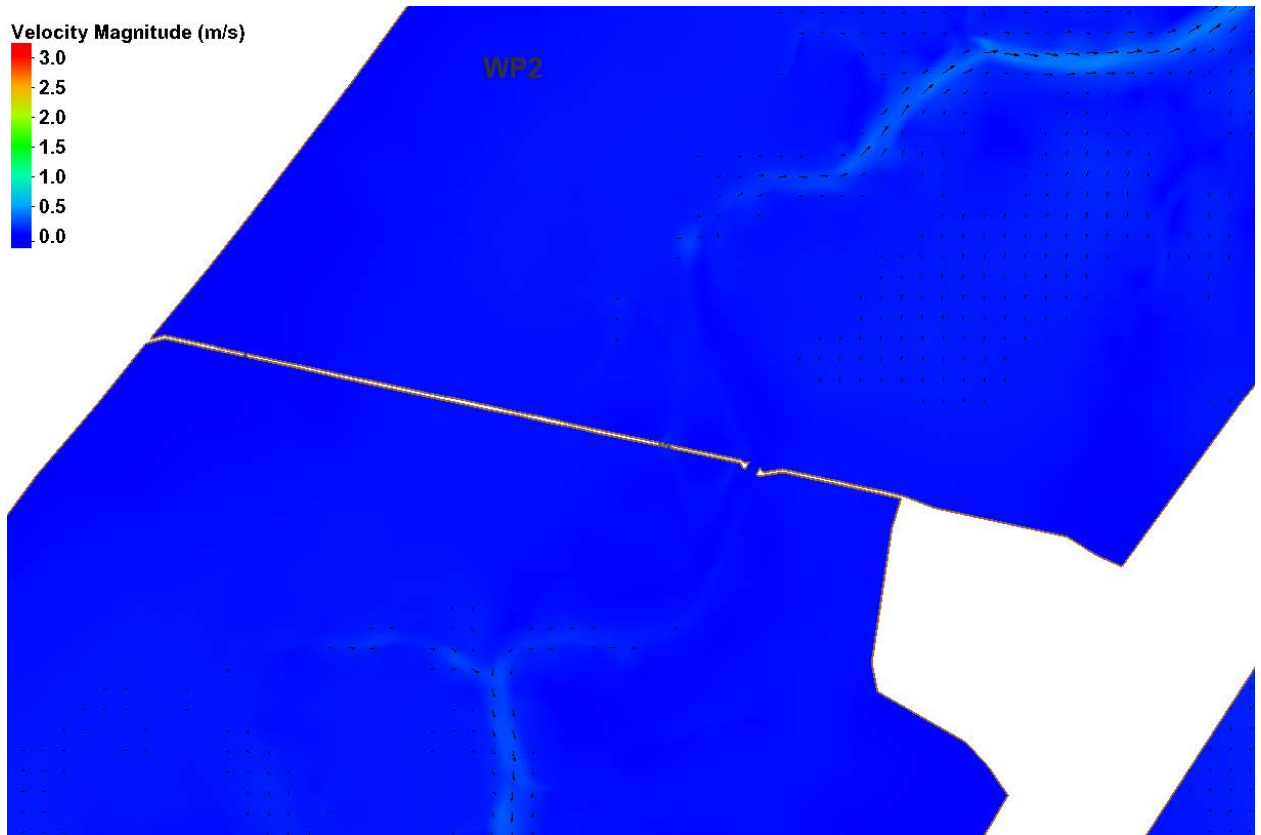


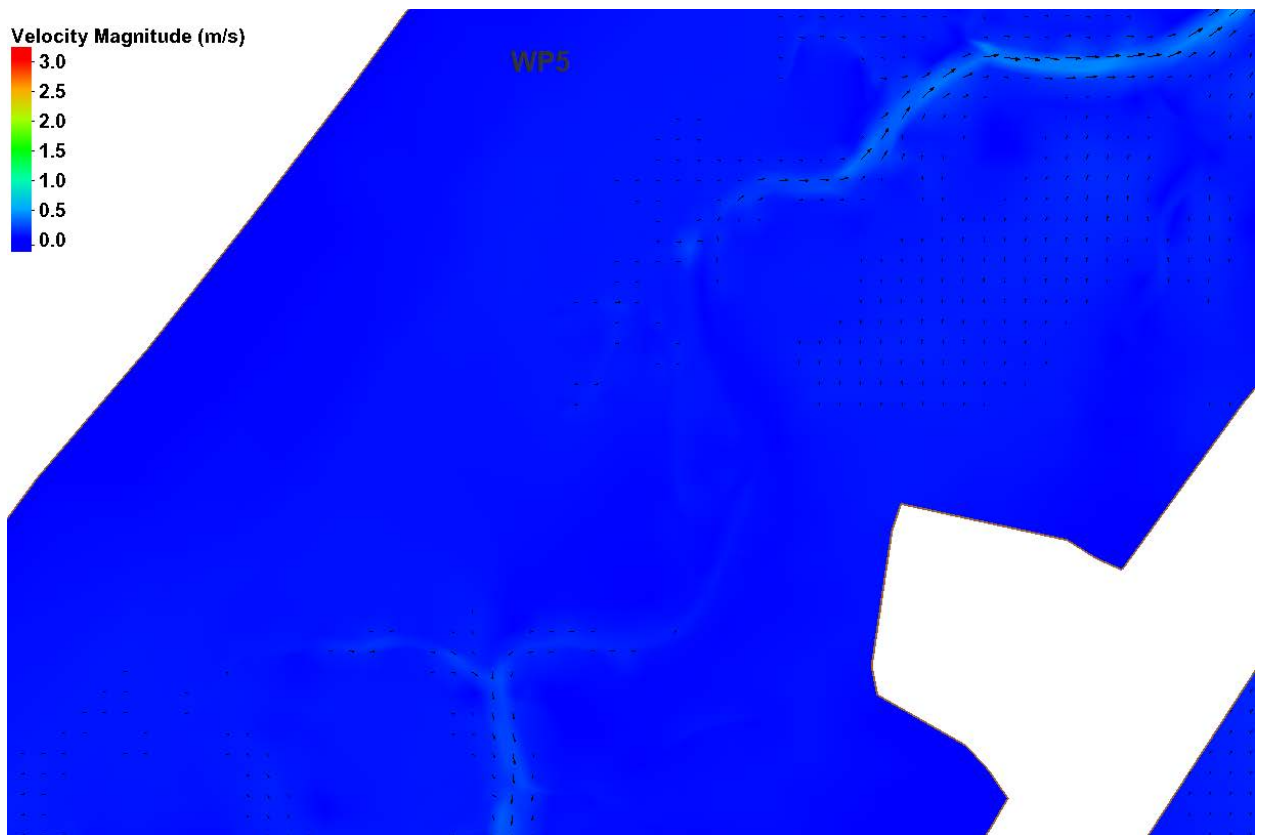
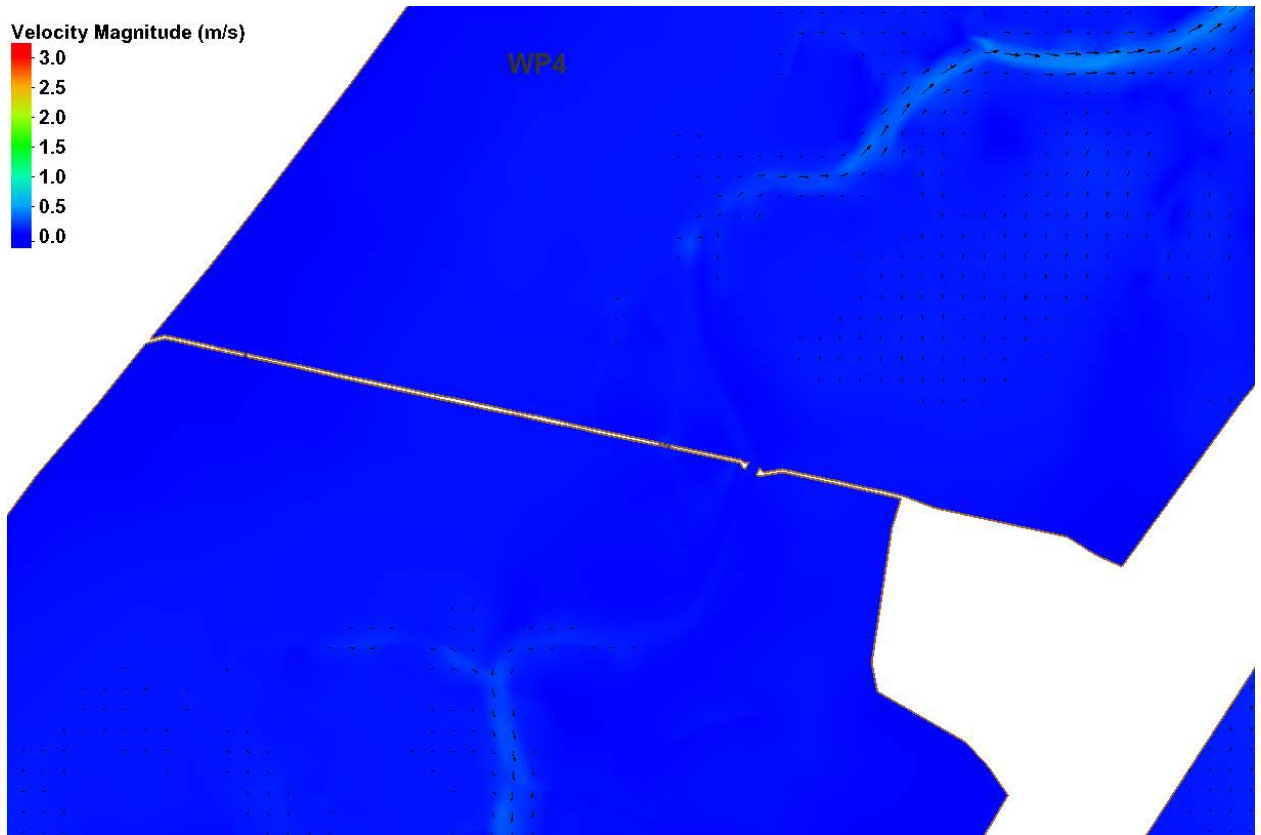


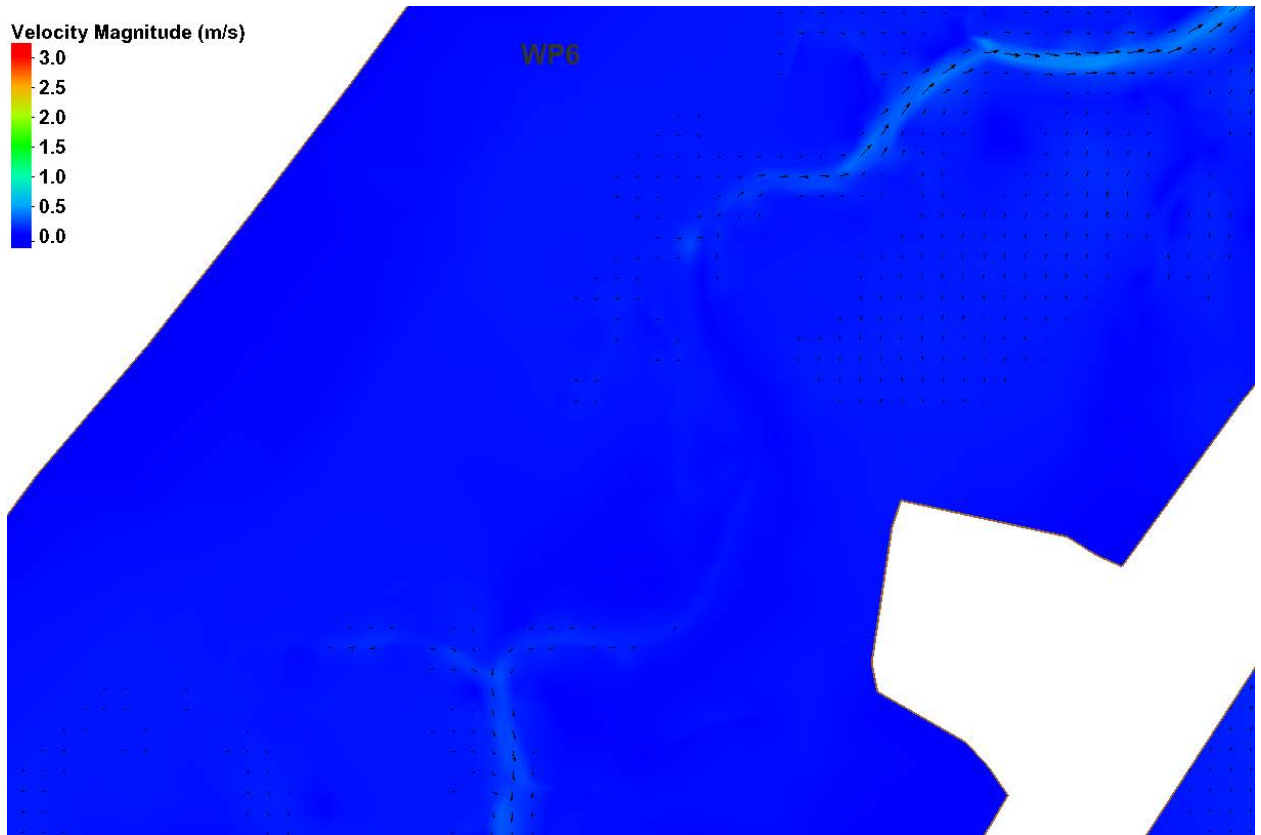










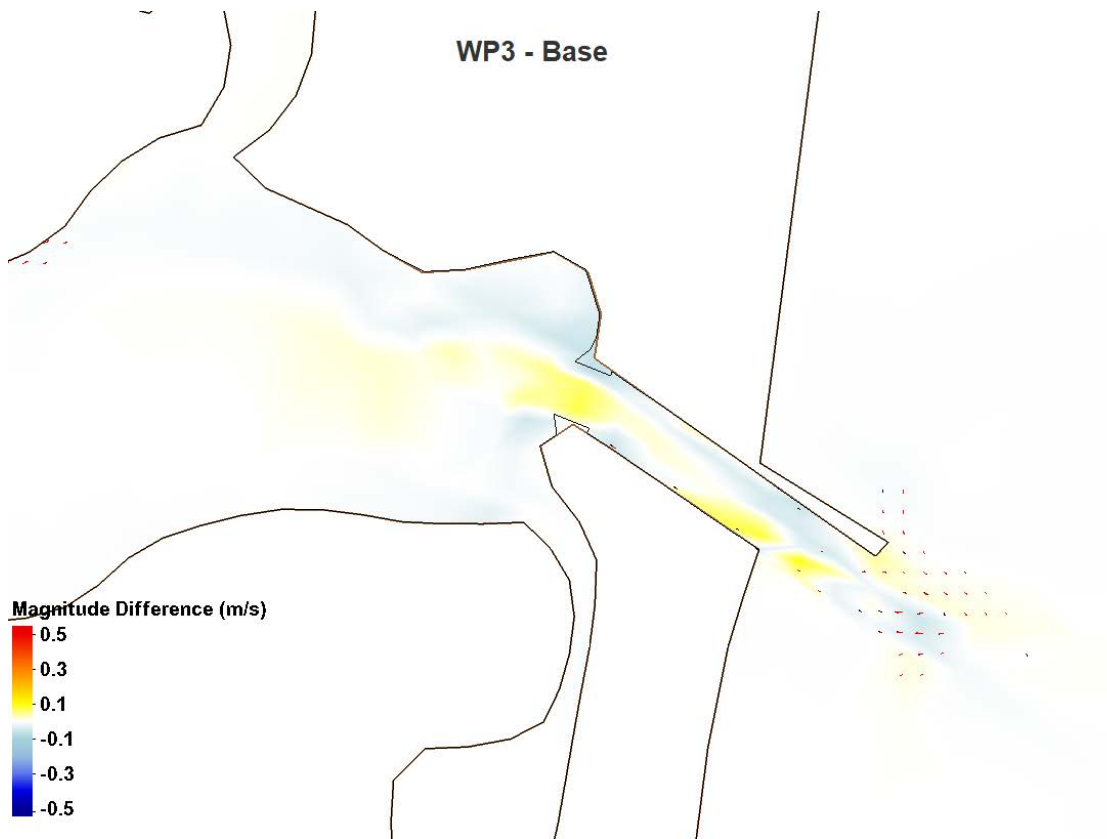
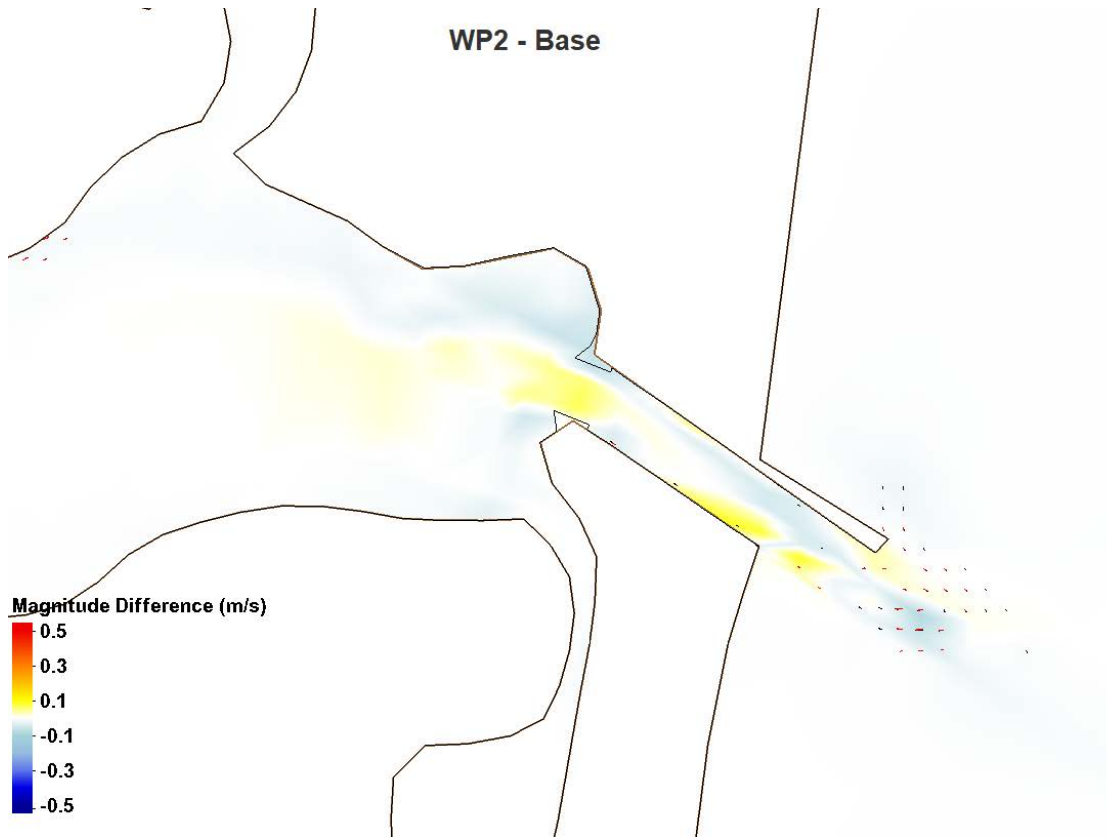


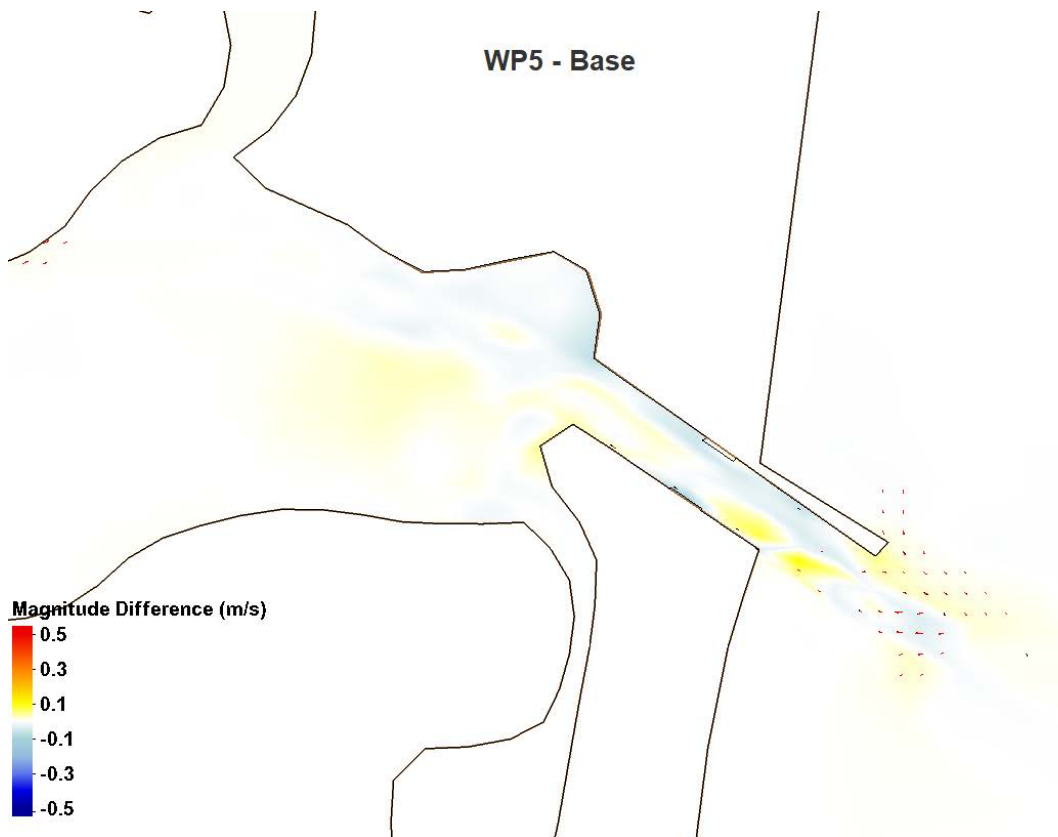
Residual Velocity at Structures

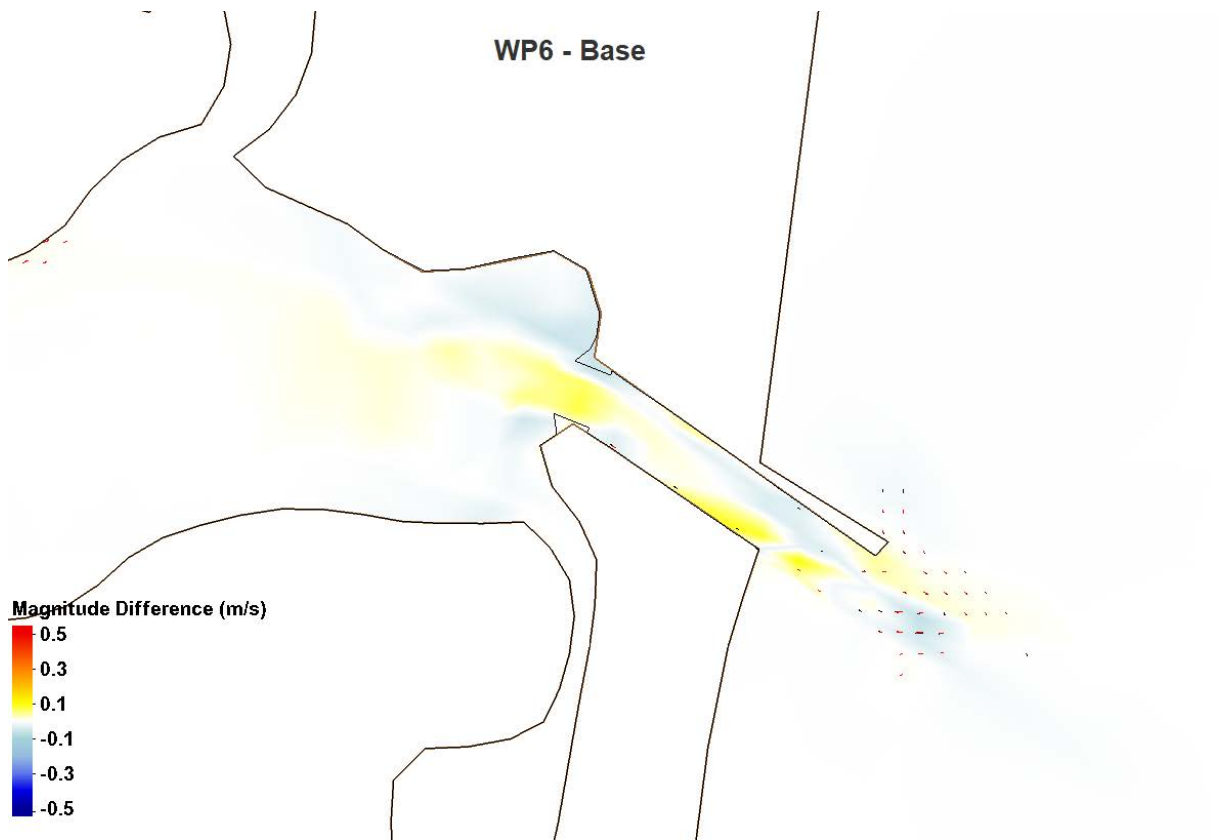
Residual velocity is the velocity that remains when the tidally varying velocity has been averaged out. This vector defines the predominant flow direction and speed of a particle of water. Although the tide will cause the particle to move back and forth, there is generally a flow direction that is a little stronger than the other, allowing for a particle to migrate along a certain path. The depth averaged velocity comparisons for Base and With Project alternatives are shown below. The red vectors indicate the direction of the alternative residual velocity and the black vectors, the Base. The contours represent the difference in the velocity magnitudes – alternative minus Base such that positive values (reds/yellows) indicate the alternative residual velocity magnitude is greater and negative values (blues) indicate that the Base residual velocity magnitude is greater. Residual velocity comparisons for the structure locations – Manasquan, Barnegat, Absecon, Great Egg, Absecon Bay Boulevard, and 72nd Street – are shown for all alternatives. Velocity vectors are scaled to be comparable.

Manasquan

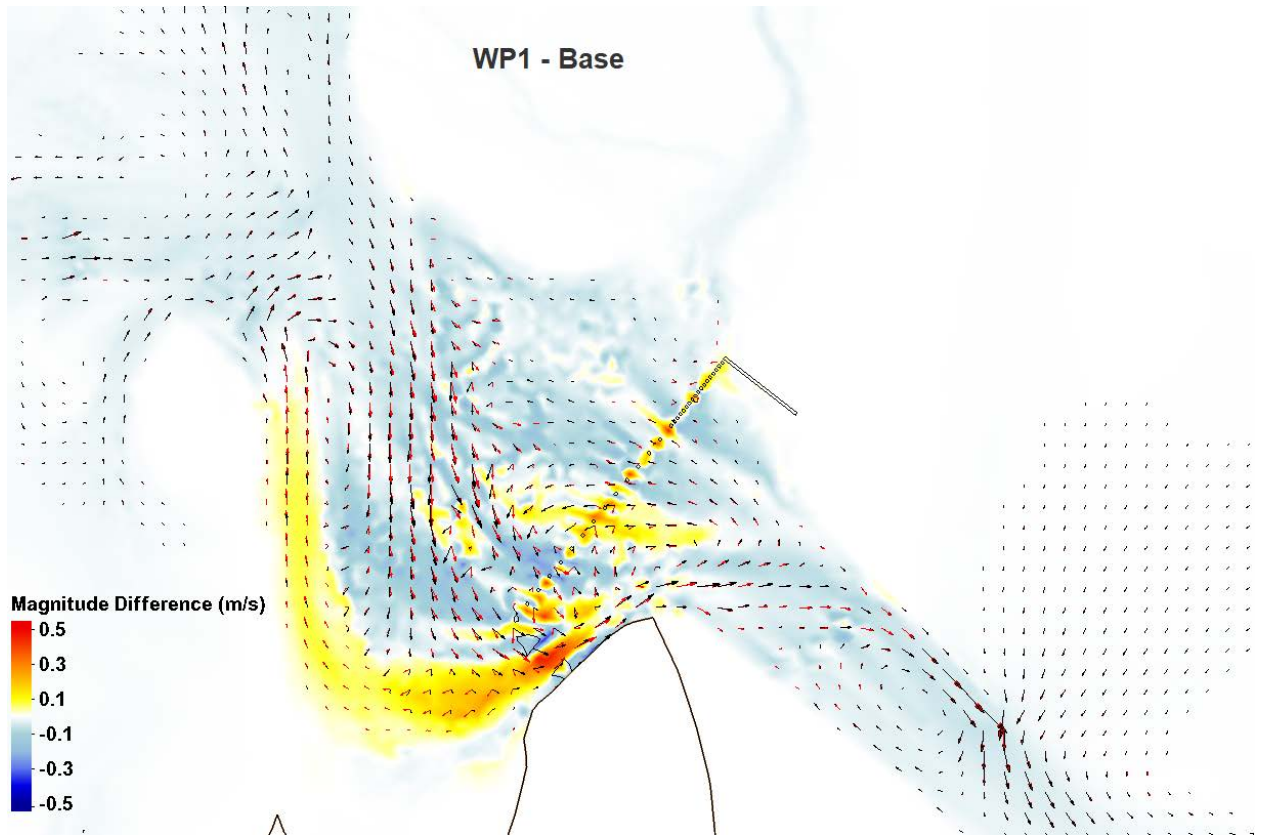


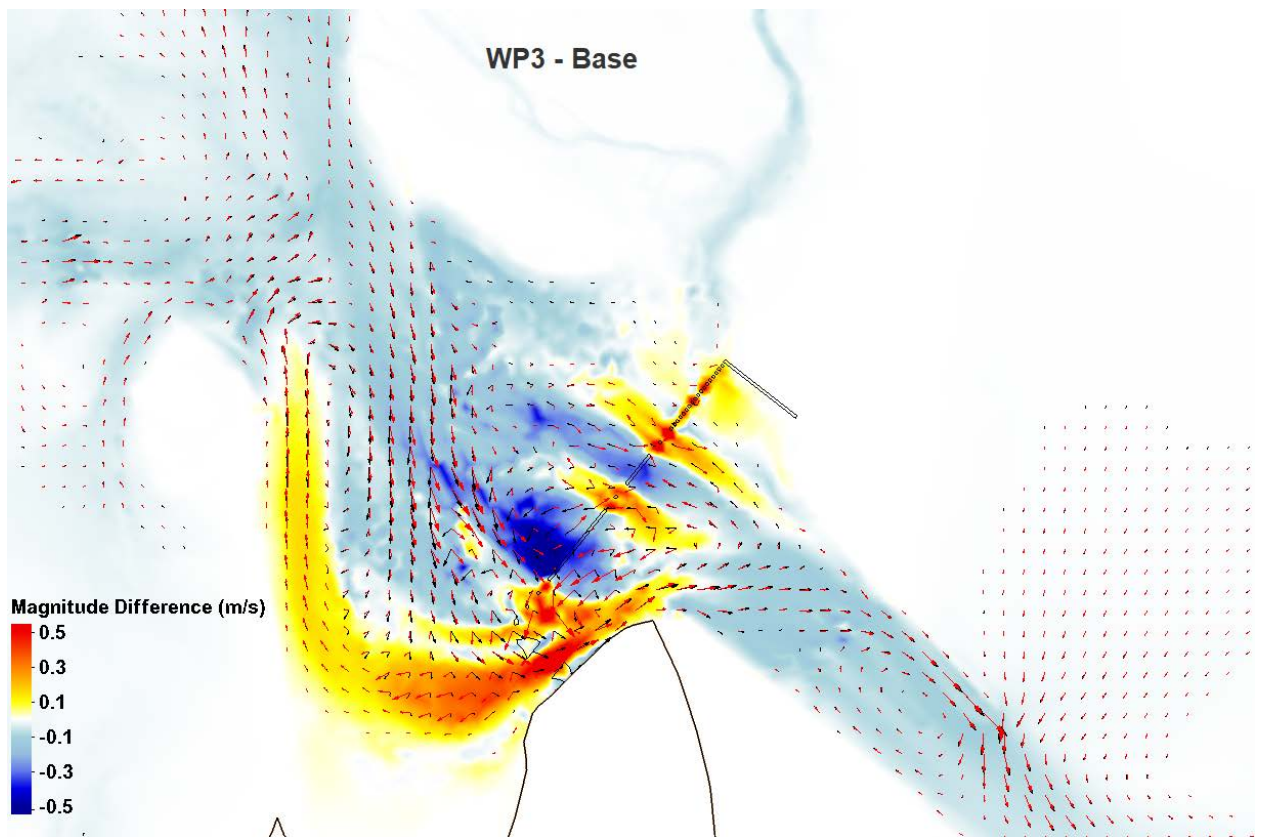
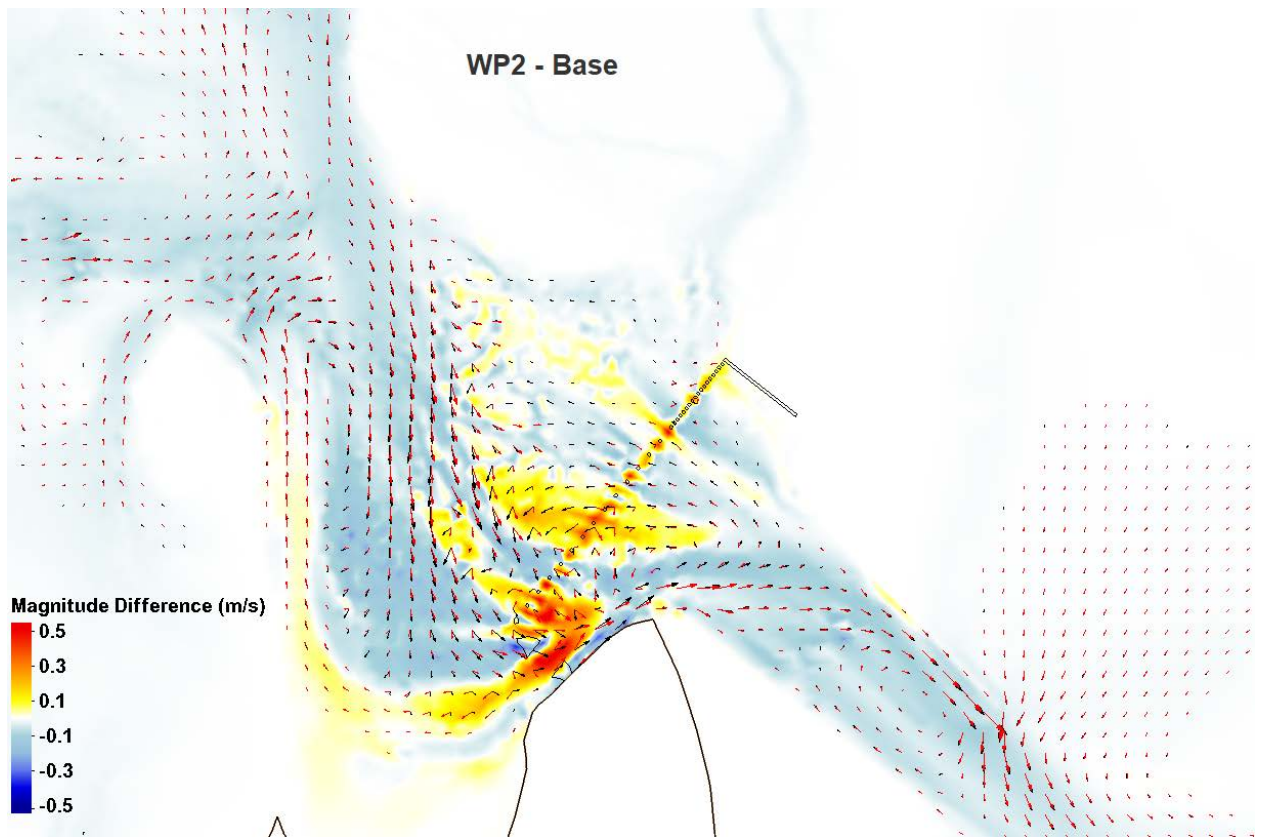


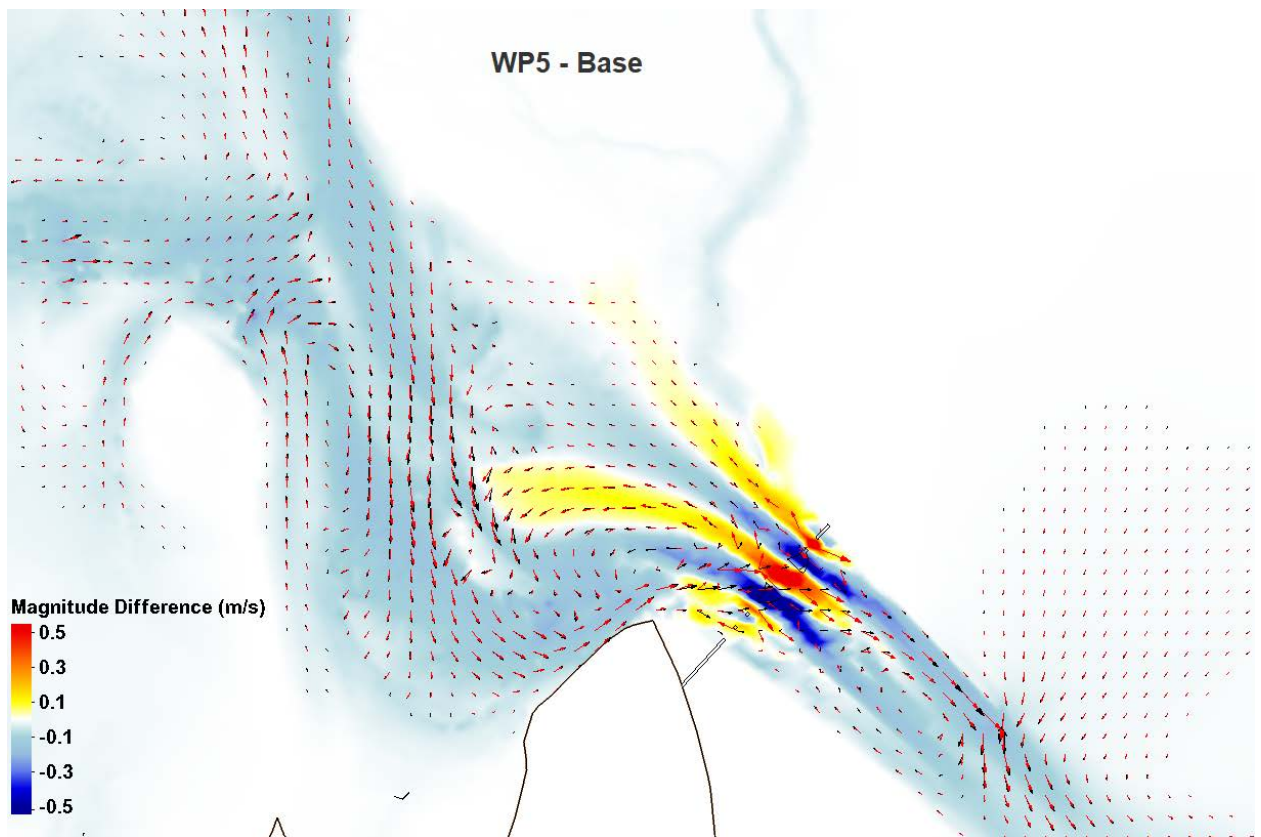
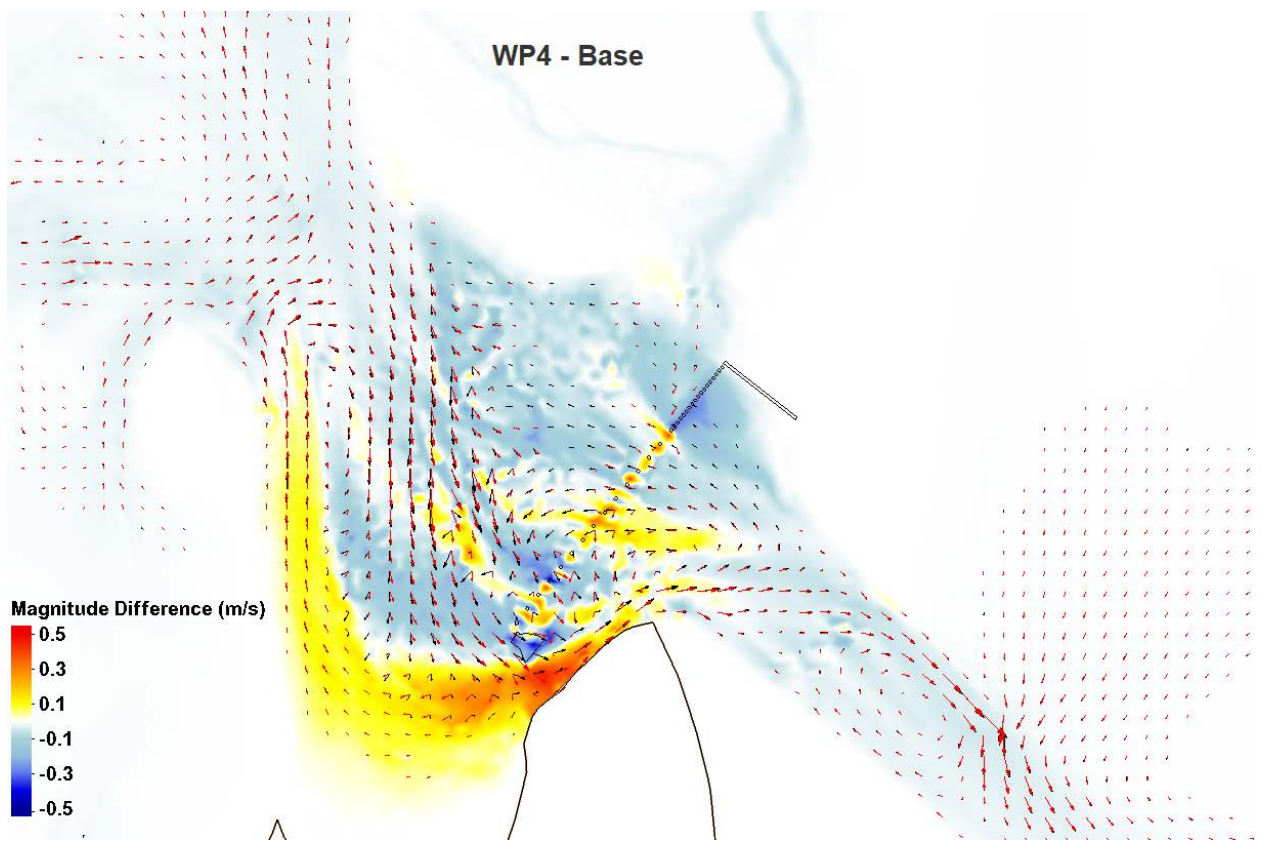


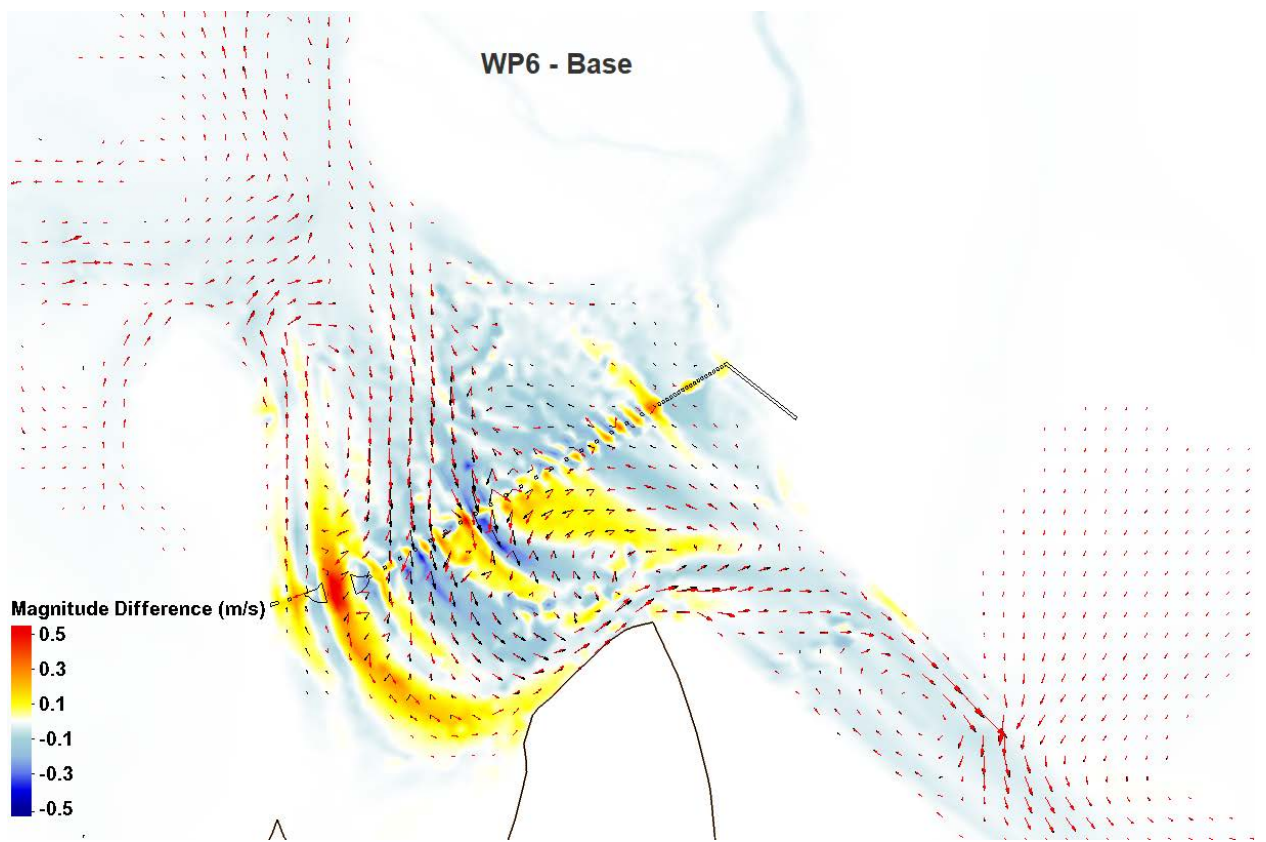


Barnegat

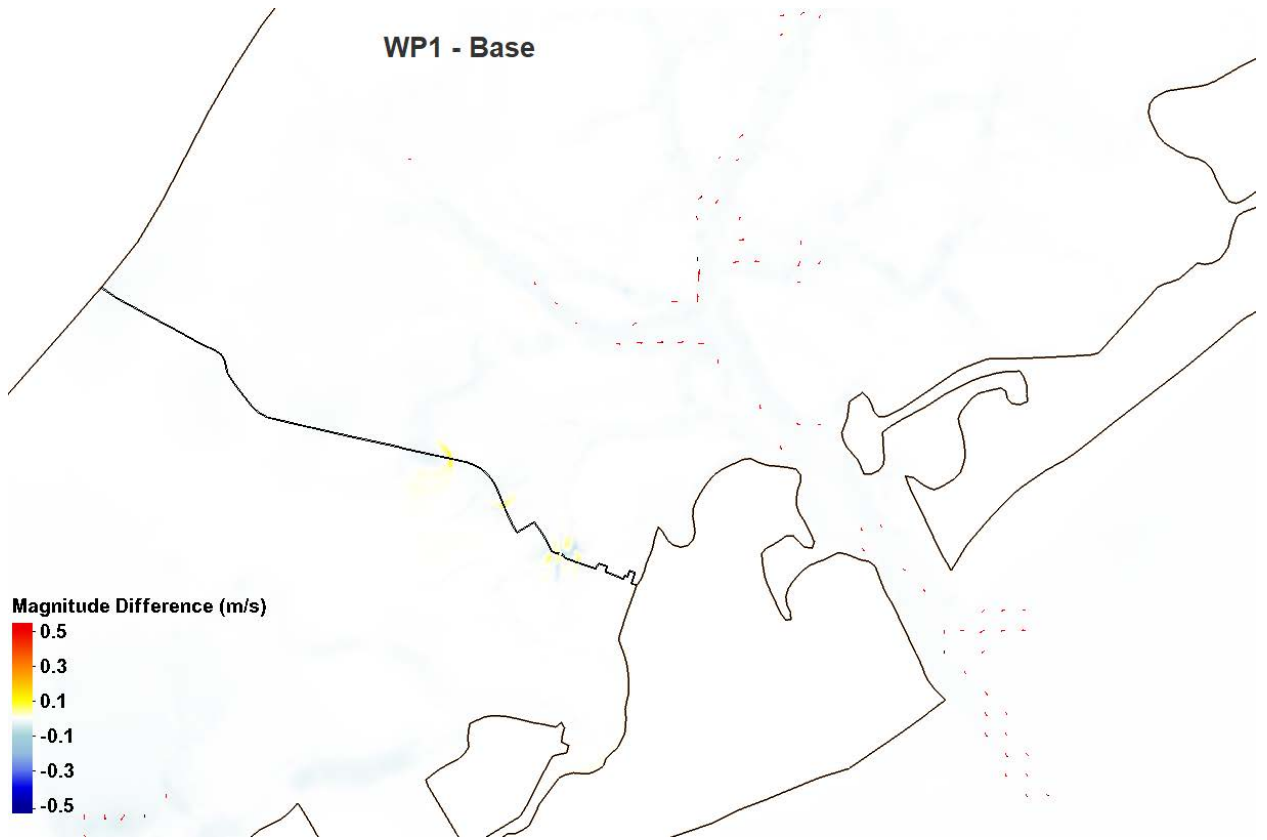


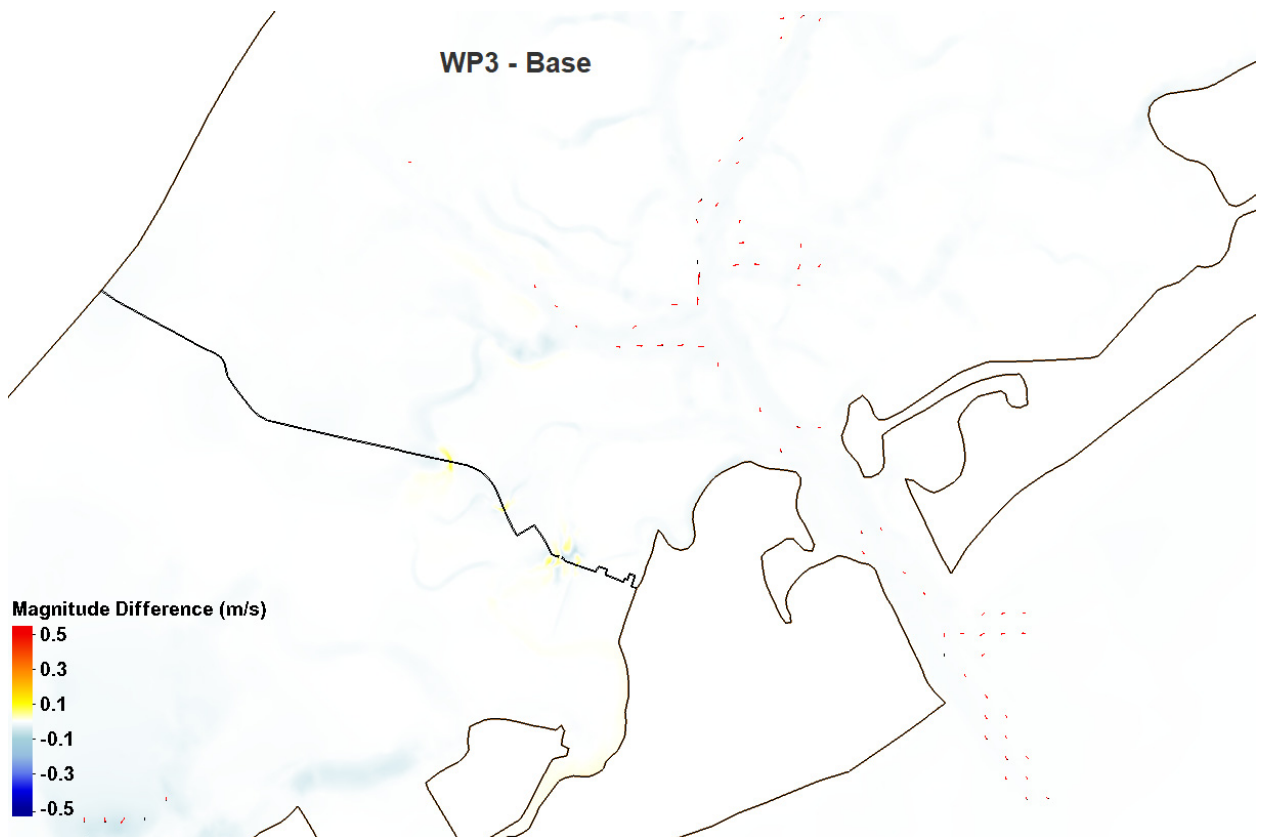
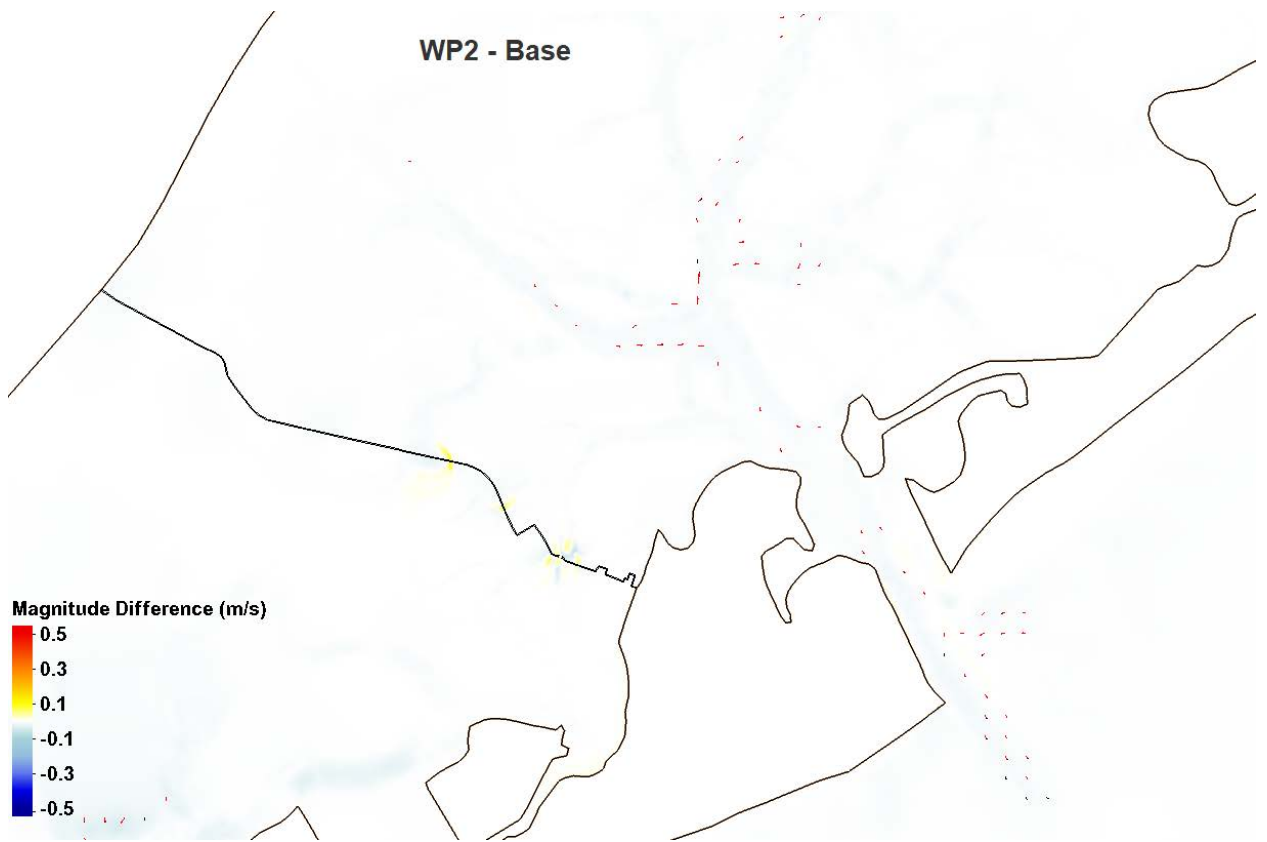


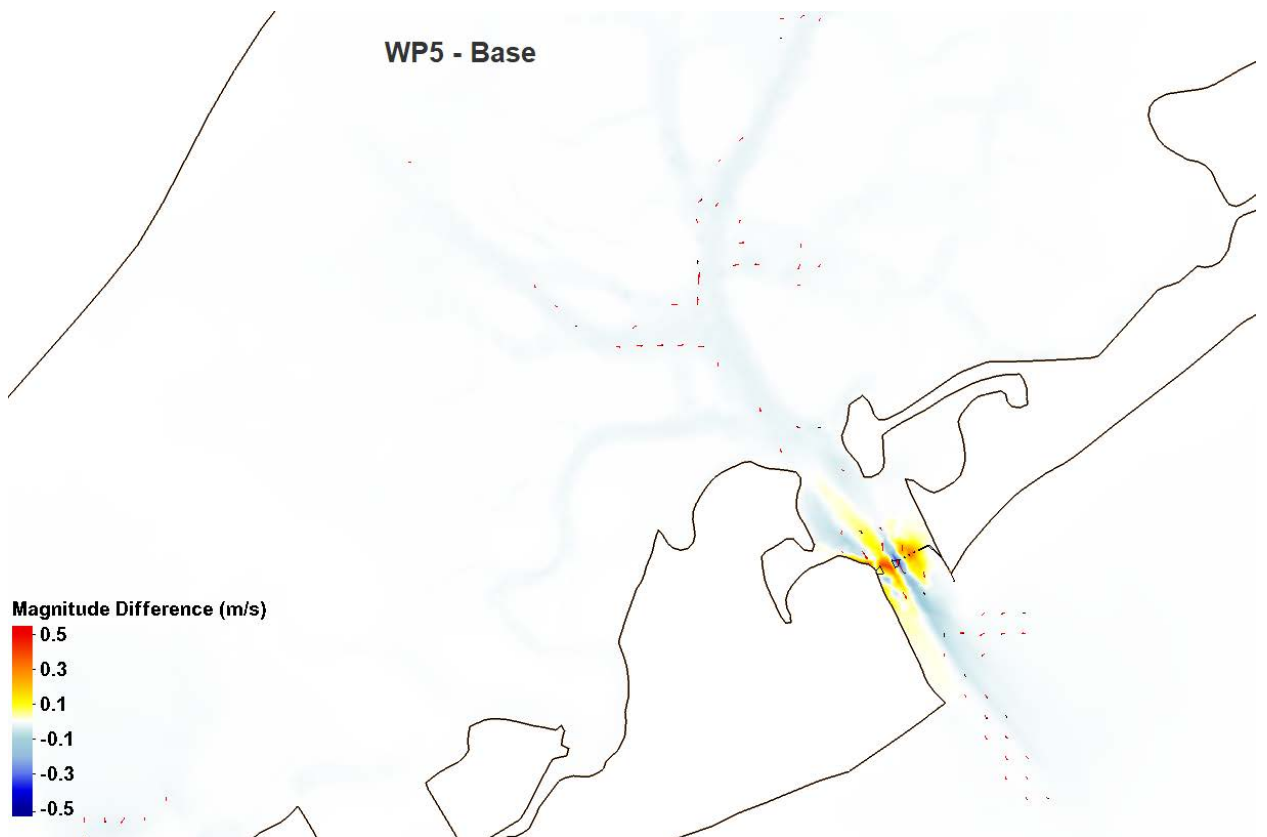
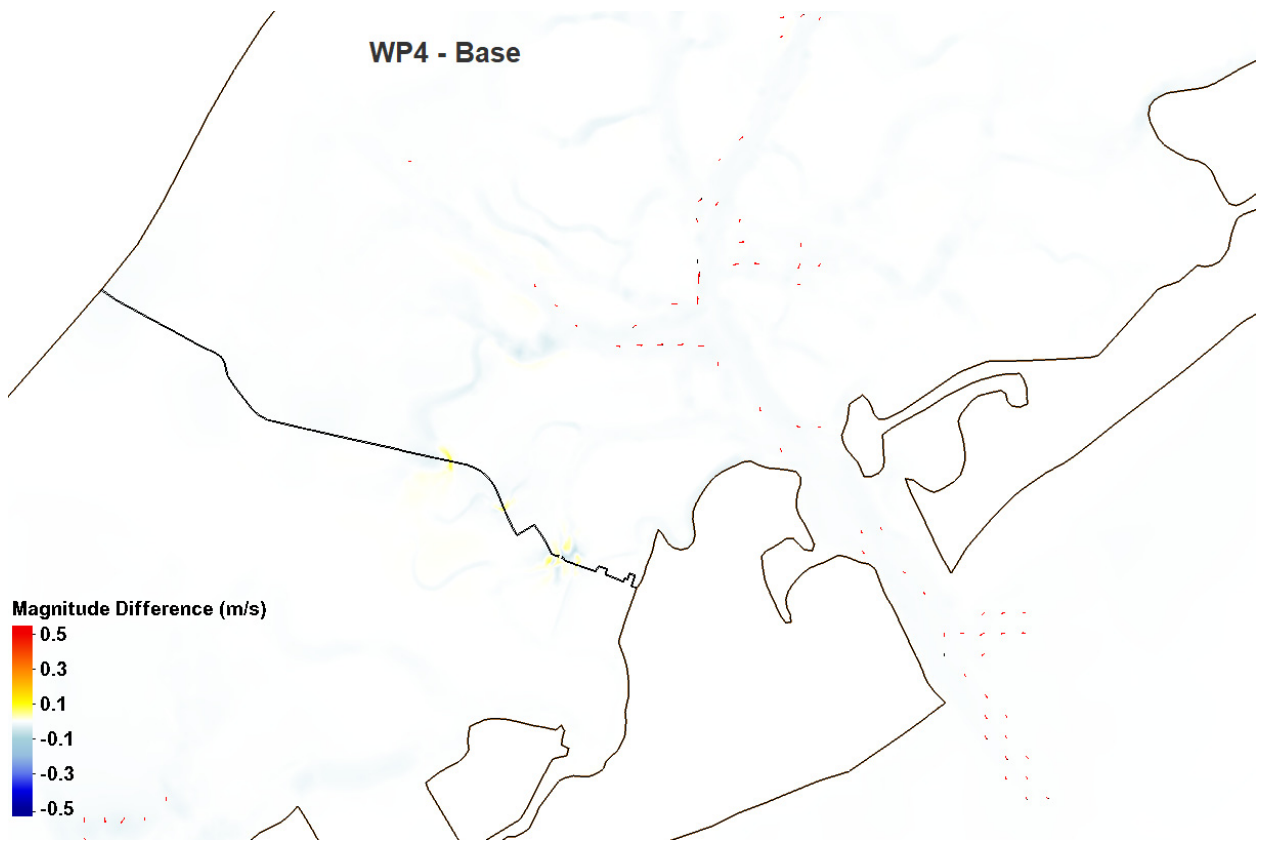


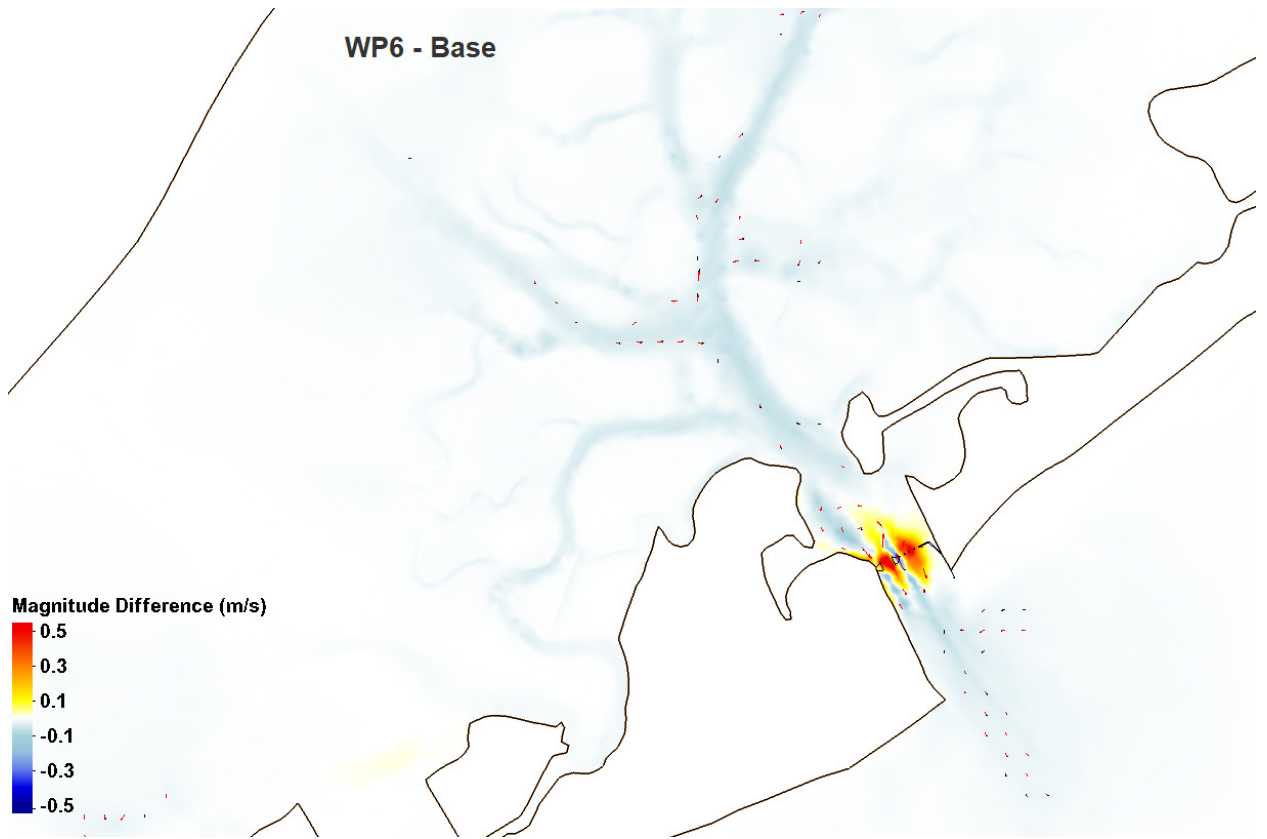


Absecon and Absecon Bay Blvd

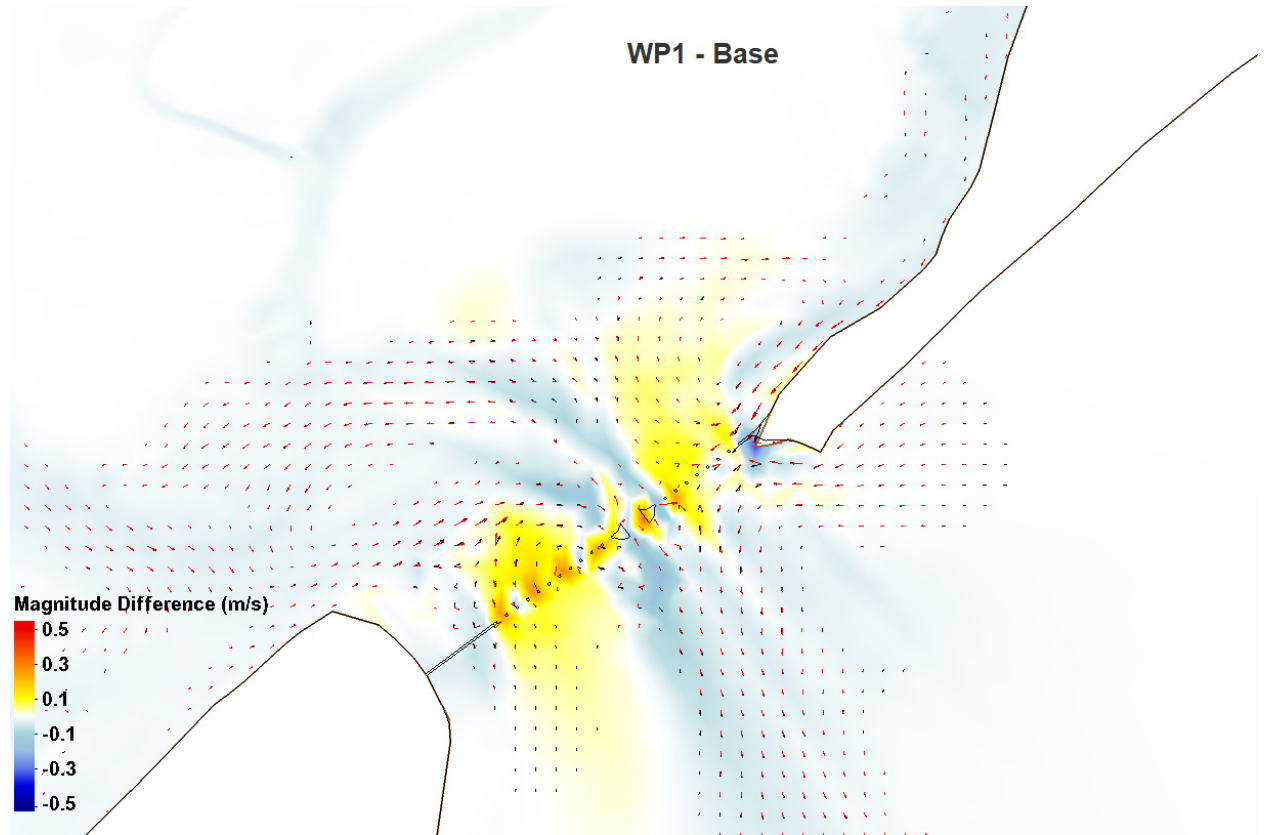


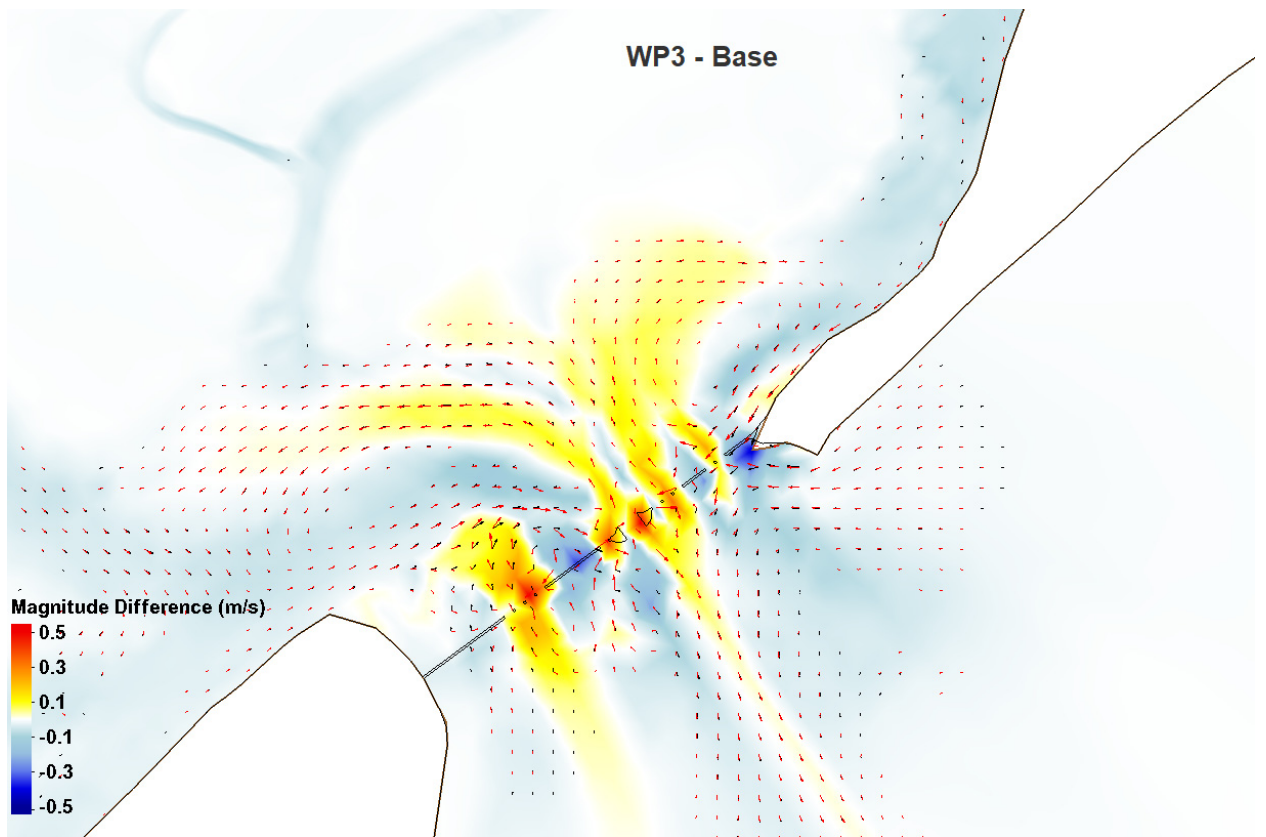
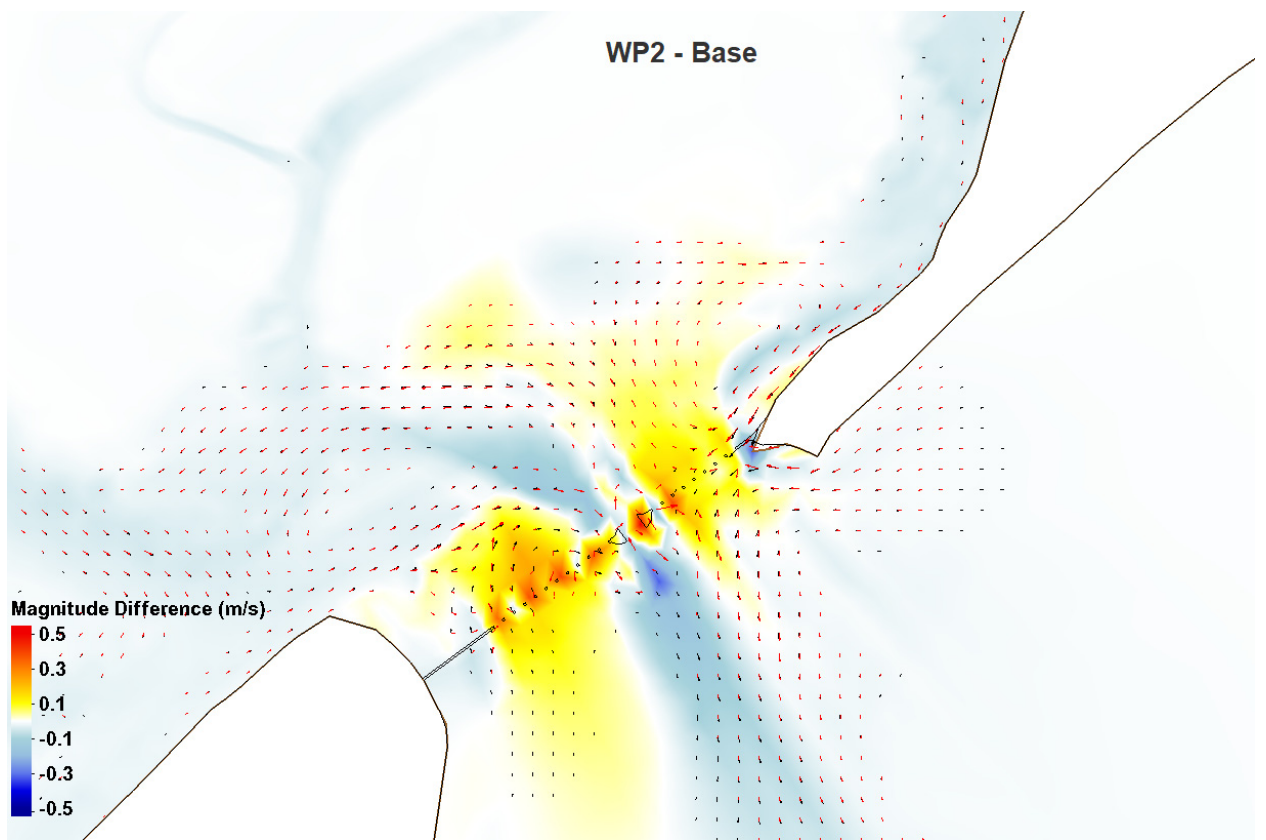


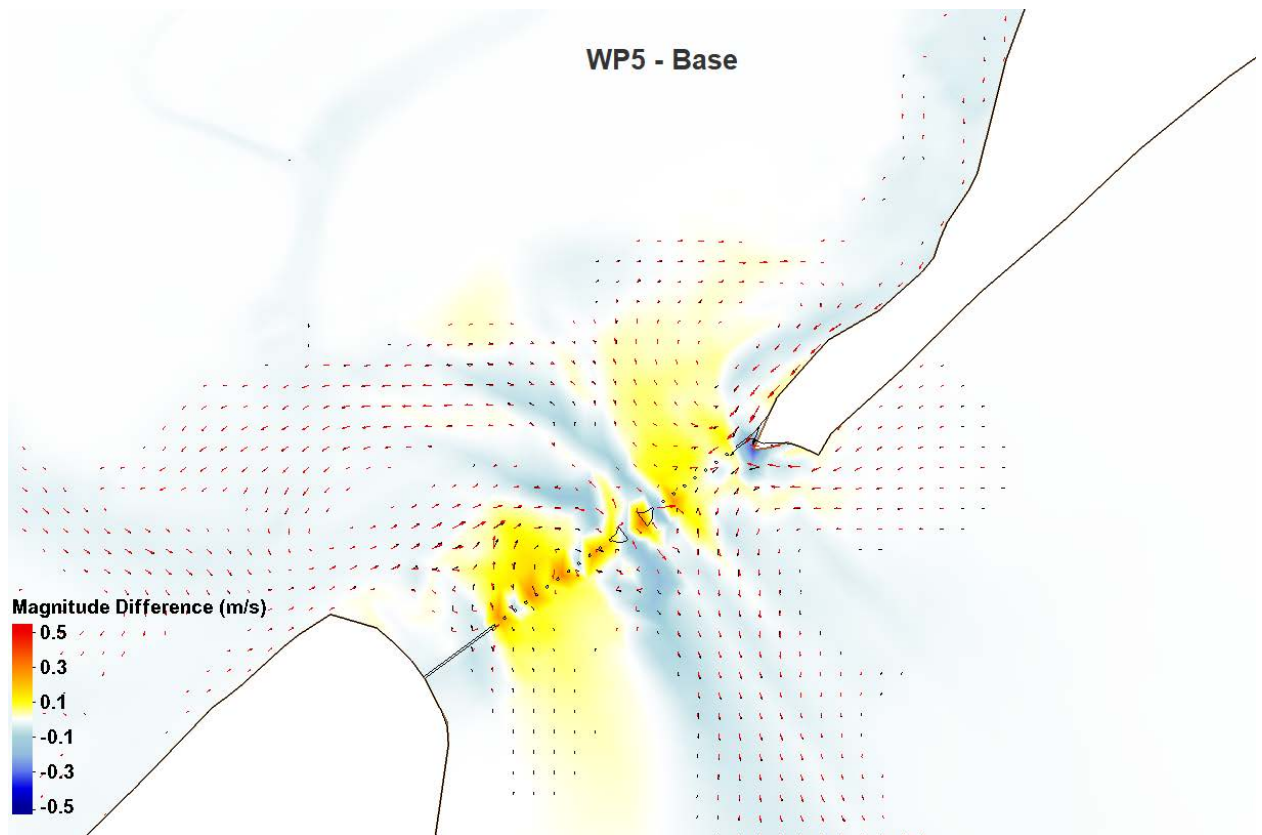
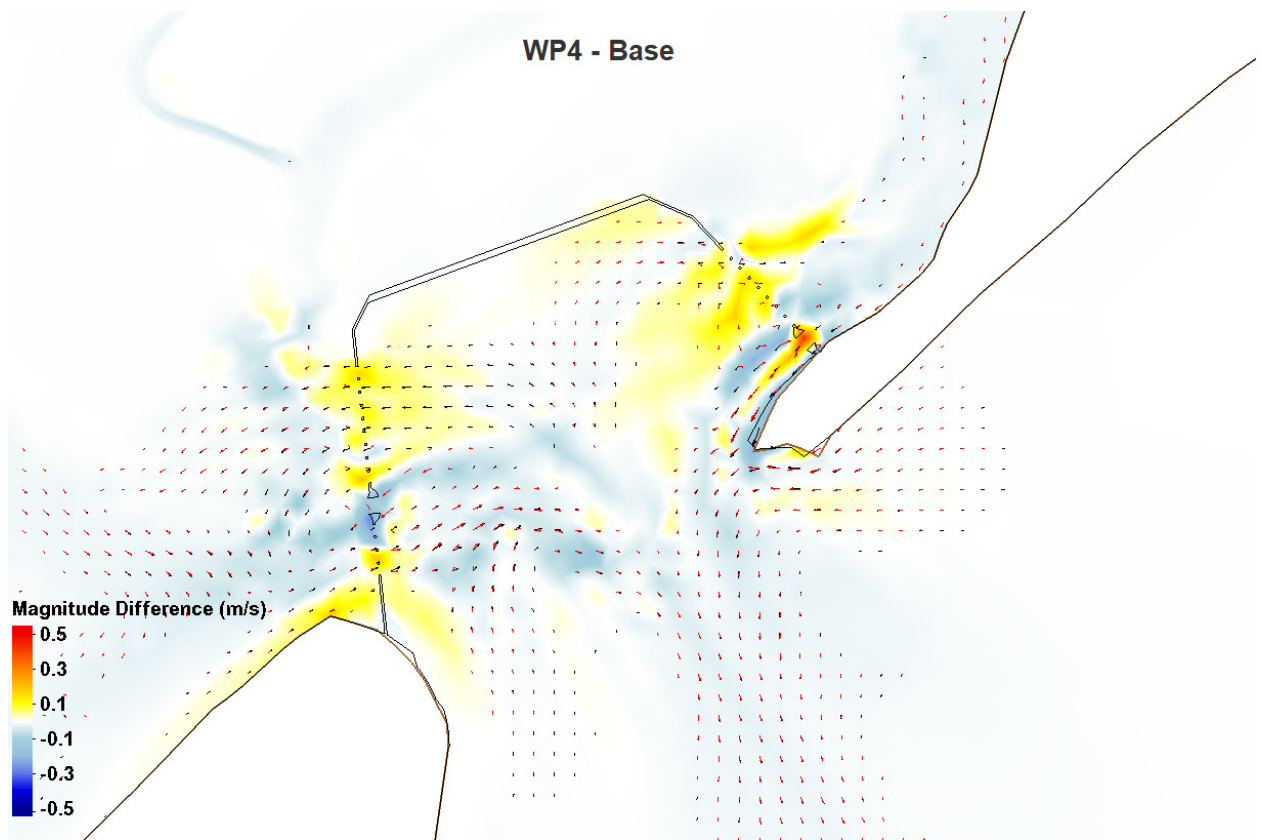


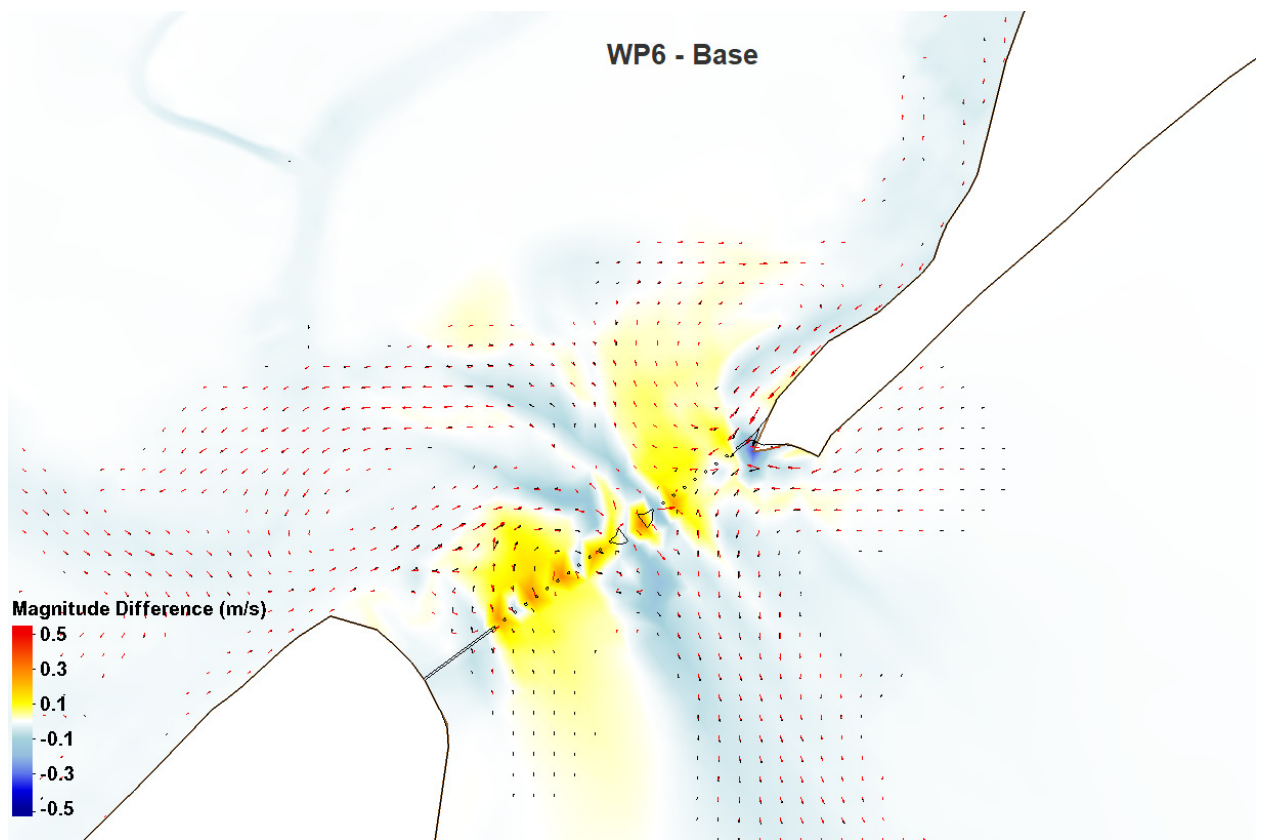


Great Egg









72nd Street

WP1 - Base









Comparisons to Base with Sea Level Rise

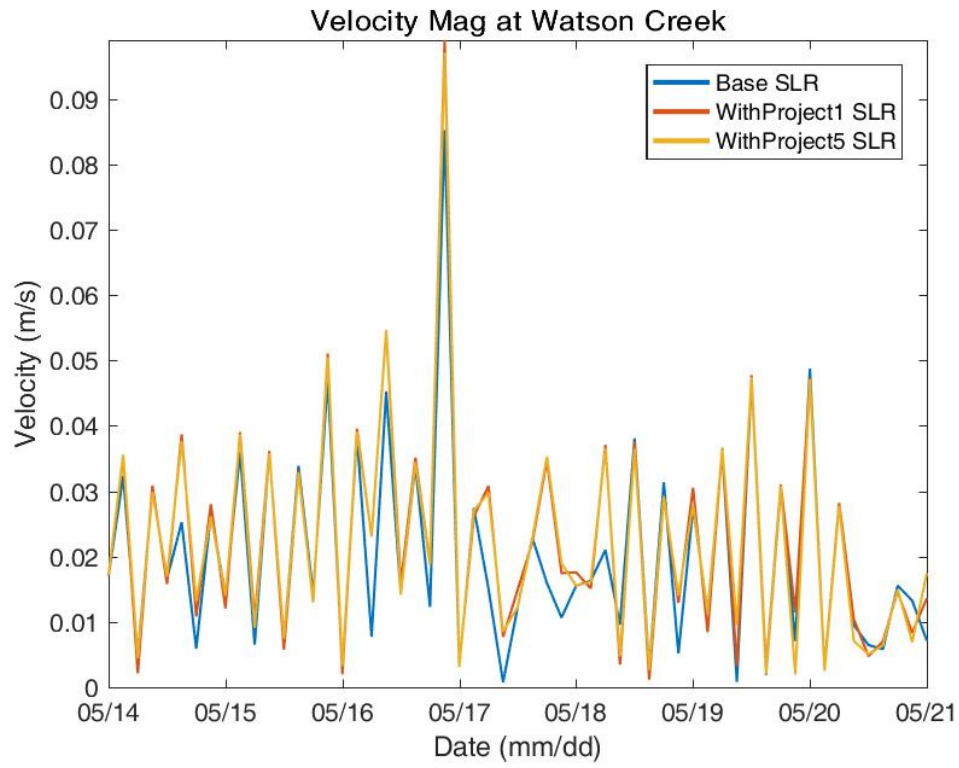
Maximum, Mean, Minimum

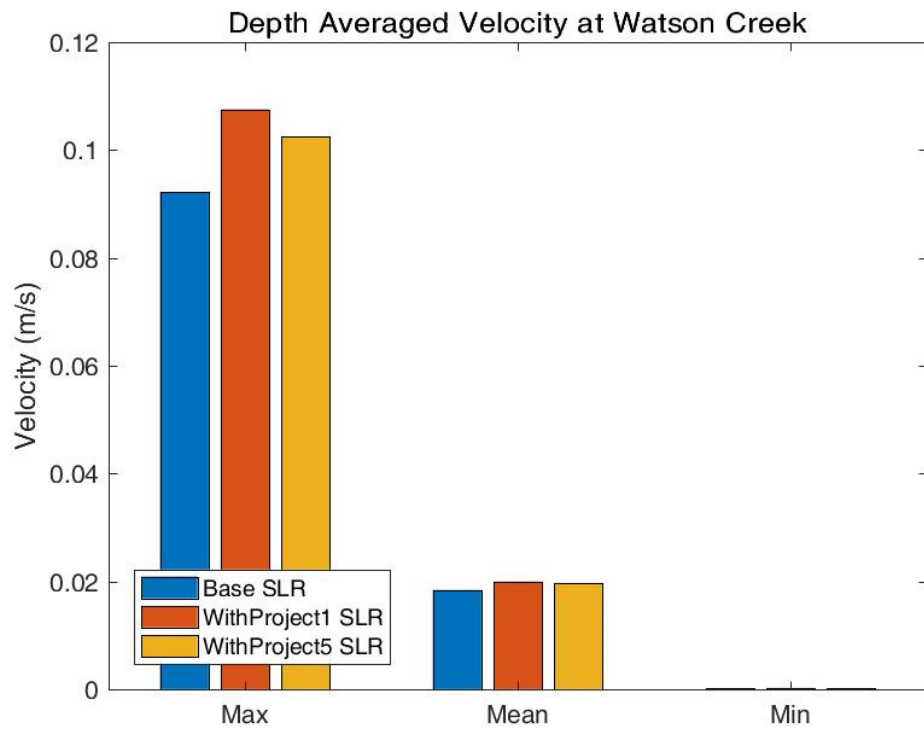
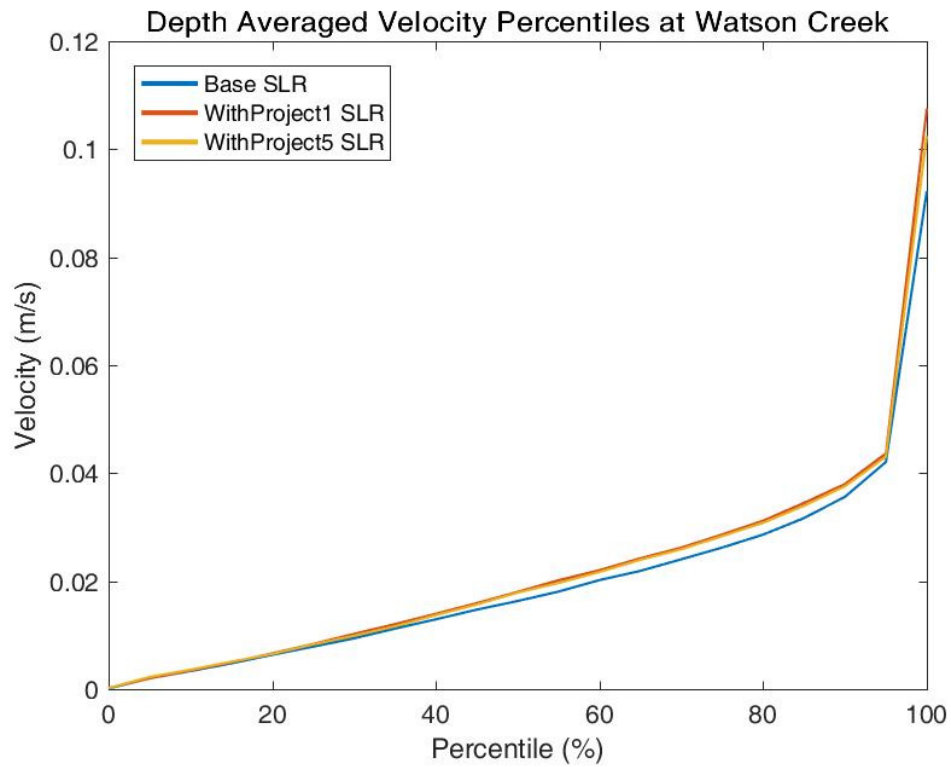
		Base SLR	WP1 SLR	WP5 SLR
Watson Creek	Max	0.09	0.11	0.10
	Mean	0.02	0.02	0.02
	Min	0.00	0.00	0.00
Manasquan River	Max	0.65	0.64	0.65
	Mean	0.29	0.29	0.29
	Min	0.01	0.01	0.01
Brick	Max	0.07	0.07	0.06
	Mean	0.02	0.02	0.01
	Min	0.00	0.00	0.00
Barnegat Bay at Mantoloking	Max	0.53	0.52	0.49
	Mean	0.11	0.11	0.11
	Min	0.00	0.00	0.00
Barnegat Bay at Route 37 Bridge	Max	0.34	0.33	0.32
	Mean	0.12	0.11	0.10
	Min	0.00	0.00	0.00
Berkeley	Max	0.18	0.17	0.16
	Mean	0.03	0.03	0.03
	Min	0.00	0.00	0.00
Barnegat Light	Max	0.25	0.26	0.26
	Mean	0.10	0.10	0.09
	Min	0.01	0.01	0.01
Barnegat Bay at Waretown	Max	0.20	0.19	0.19
	Mean	0.04	0.04	0.04
	Min	0.00	0.00	0.00
Barnegat Bay at Barnegat Light	Max	0.61	0.37	0.39
	Mean	0.10	0.07	0.10
	Min	0.00	0.00	0.00
Barnegat Light (Ocean)	Max	0.45	0.45	0.45
	Mean	0.05	0.05	0.05
	Min	0.00	0.00	0.00

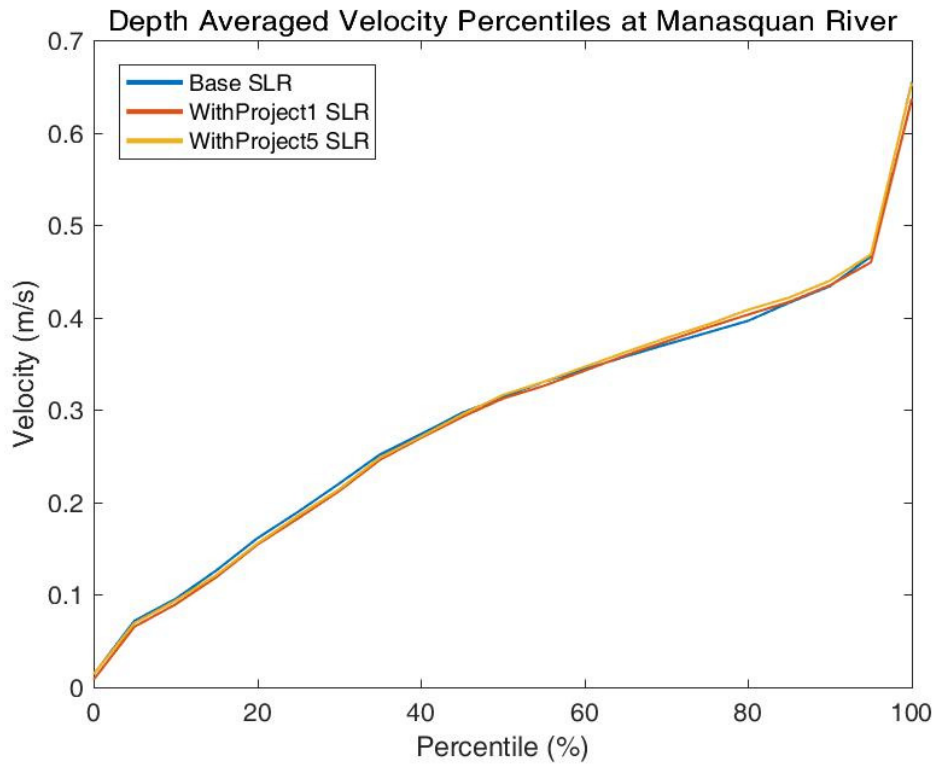
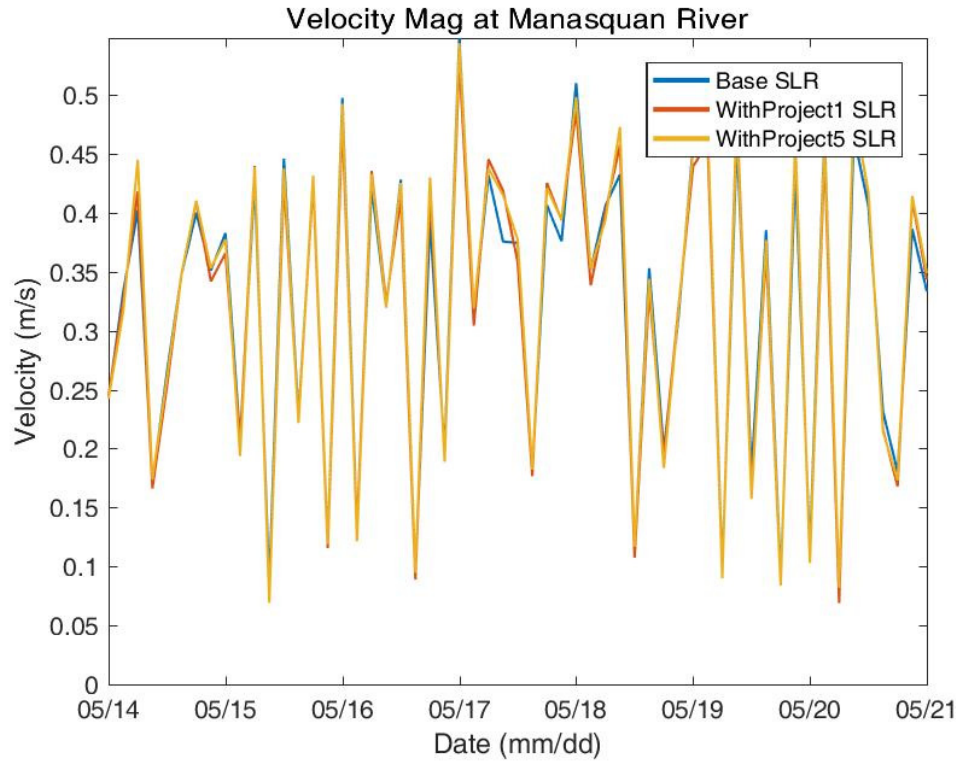
East Thorofare	Max	0.42	0.42	0.46
	Mean	0.13	0.13	0.14
	Min	0.00	0.00	0.00
Westecunk	Max	0.12	0.12	0.12
	Mean	0.07	0.07	0.07
	Min	0.00	0.00	0.00
Beach Haven	Max	0.48	0.47	0.48
	Mean	0.18	0.17	0.18
	Min	0.00	0.00	0.00
JACNEWQ	Max	0.86	0.84	0.85
	Mean	0.38	0.37	0.38
	Min	0.00	0.00	0.00
Little Egg Inlet	Max	1.73	1.73	1.73
	Mean	0.47	0.46	0.47
	Min	0.00	0.00	0.00
Absecon Creek	Max	0.04	0.04	0.04
	Mean	0.01	0.01	0.01
	Min	0.00	0.00	0.00
Brigantine	Max	0.50	0.51	0.54
	Mean	0.07	0.07	0.08
	Min	0.00	0.00	0.00
Absecon Channel	Max	3.02	3.00	2.46
	Mean	0.58	0.58	0.55
	Min	0.00	0.00	0.00
Atlantic City (Ocean)	Max	1.26	1.24	1.16
	Mean	0.19	0.19	0.19
	Min	0.00	0.00	0.00
Inside Thorofare	Max	0.21	0.19	0.20
	Mean	0.04	0.04	0.03
	Min	0.00	0.00	0.00
Beach Thorofare	Max	1.64	1.45	1.48
	Mean	0.44	0.40	0.41
	Min	0.00	0.00	0.00
Scull Bay	Max	0.36	0.32	0.32

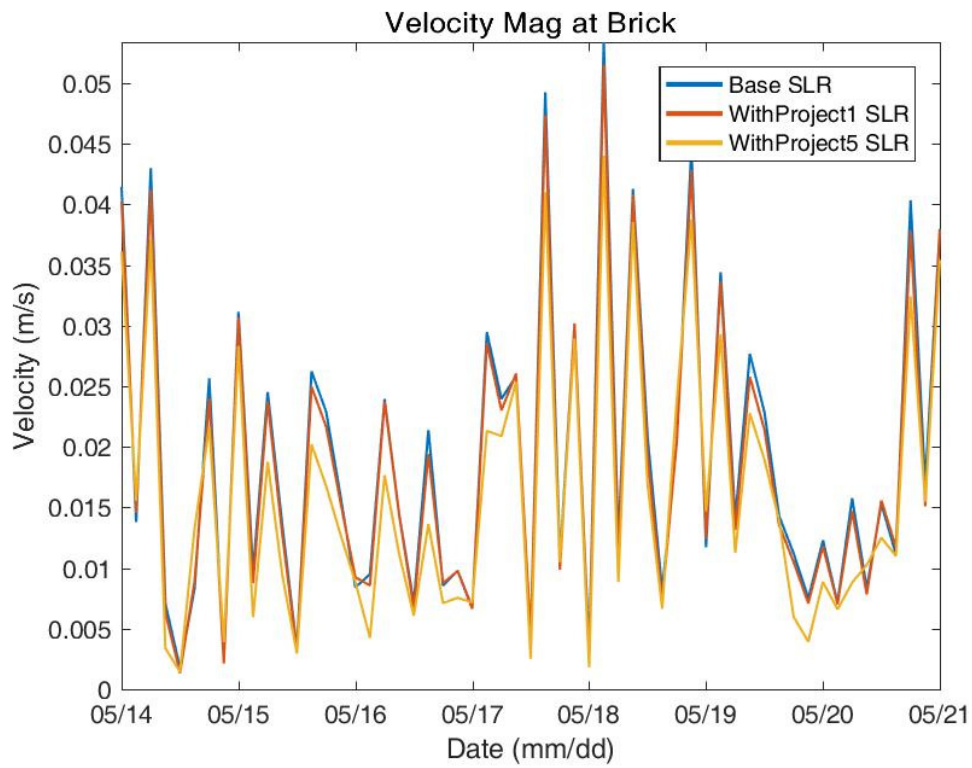
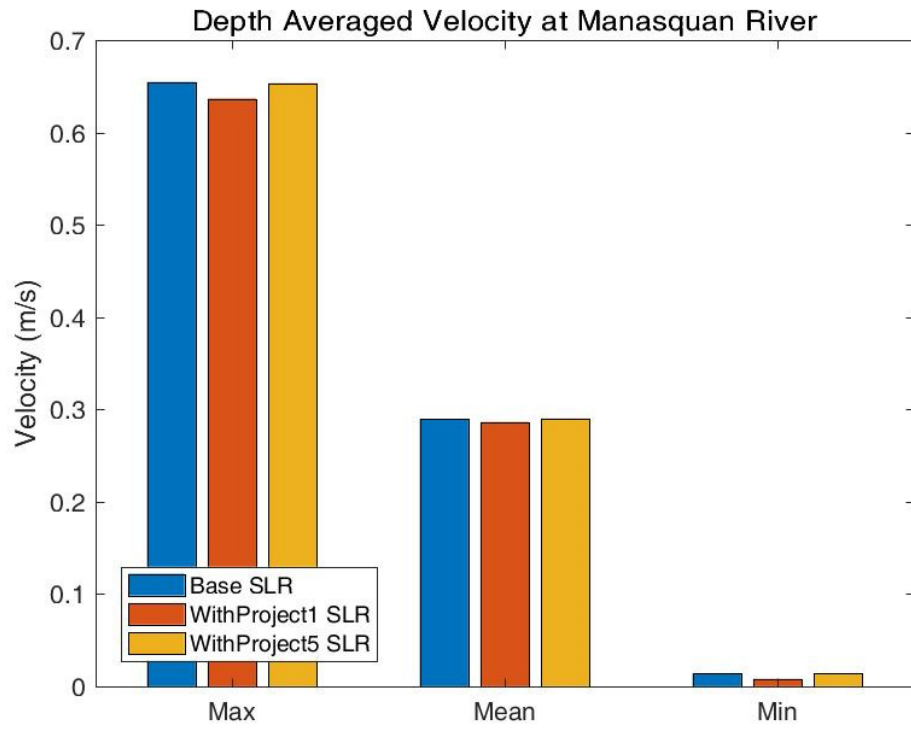
	Mean	0.09	0.08	0.08
	Min	0.00	0.00	0.00
Great Egg Harbor River	Max	0.45	0.42	0.43
	Mean	0.20	0.19	0.19
	Min	0.00	0.00	0.00
Great Egg Harbor Bay	Max	1.56	1.23	1.24
	Mean	0.37	0.34	0.34
	Min	0.00	0.00	0.00
Ocean City 39th St	Max	0.09	0.09	0.08
	Mean	0.02	0.02	0.02
	Min	0.00	0.00	0.00
Corson Sound	Max	1.16	1.12	1.16
	Mean	0.17	0.16	0.17
	Min	0.00	0.00	0.00
Ludlum Thorofare	Max	1.19	1.13	1.20
	Mean	0.44	0.41	0.44
	Min	0.00	0.00	0.00
Ingram Thorofare	Max	1.47	1.46	1.47
	Mean	0.60	0.60	0.60
	Min	0.00	0.00	0.00
Cape May Ferry	Max	0.08	0.07	0.08
	Mean	0.01	0.01	0.01
	Min	0.00	0.00	0.00
Cape May Harbor	Max	0.15	0.15	0.15
	Mean	0.03	0.03	0.03
	Min	0.00	0.00	0.00

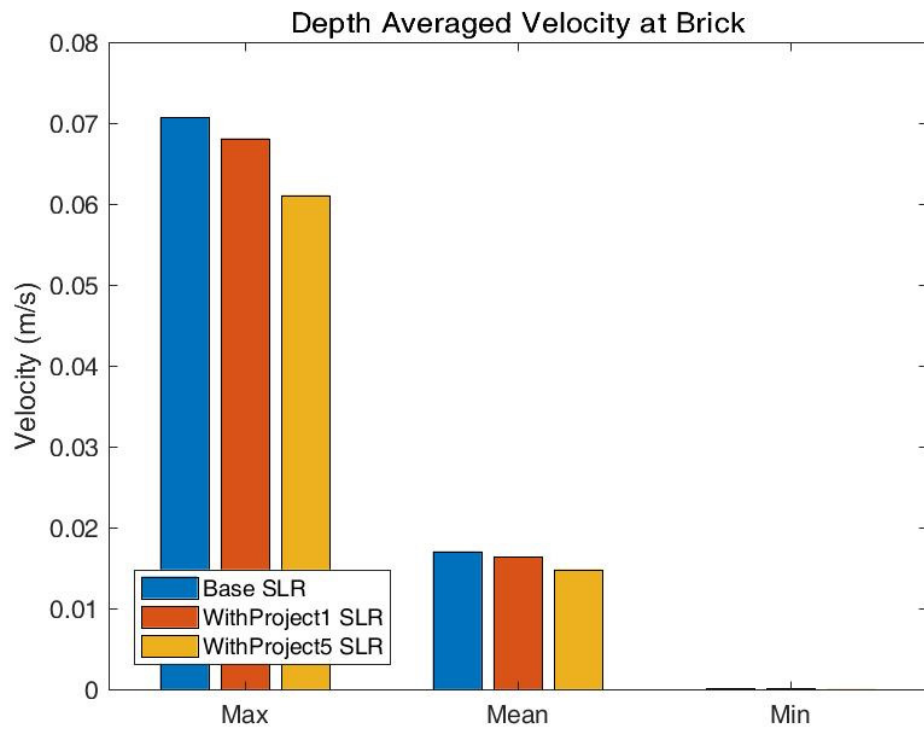
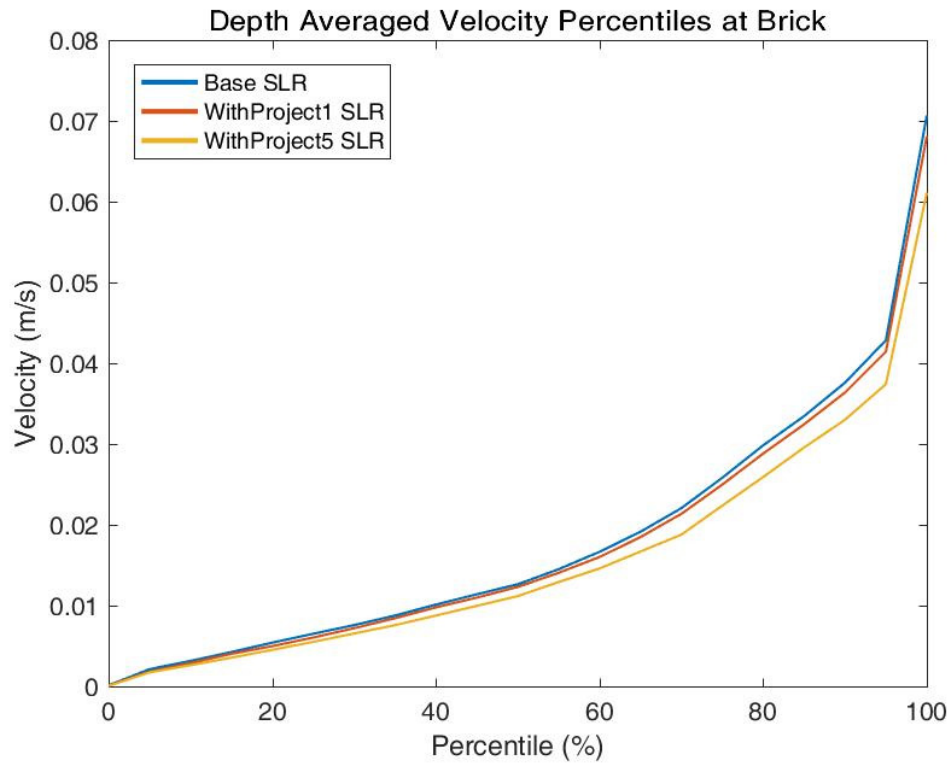
Point Comparisons

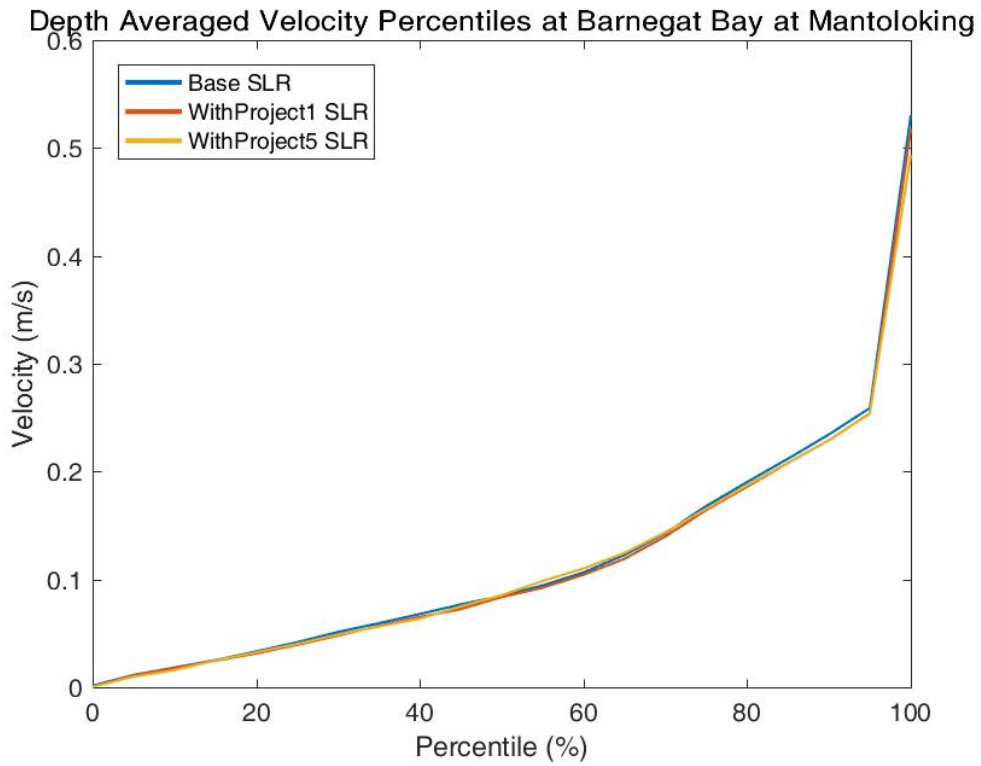
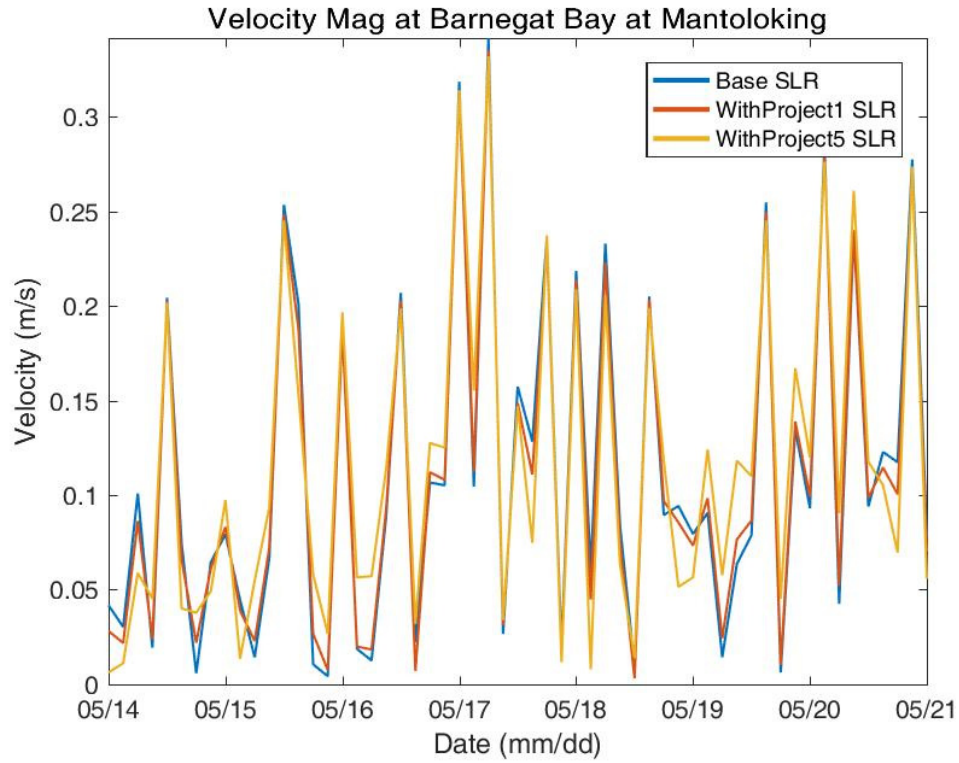


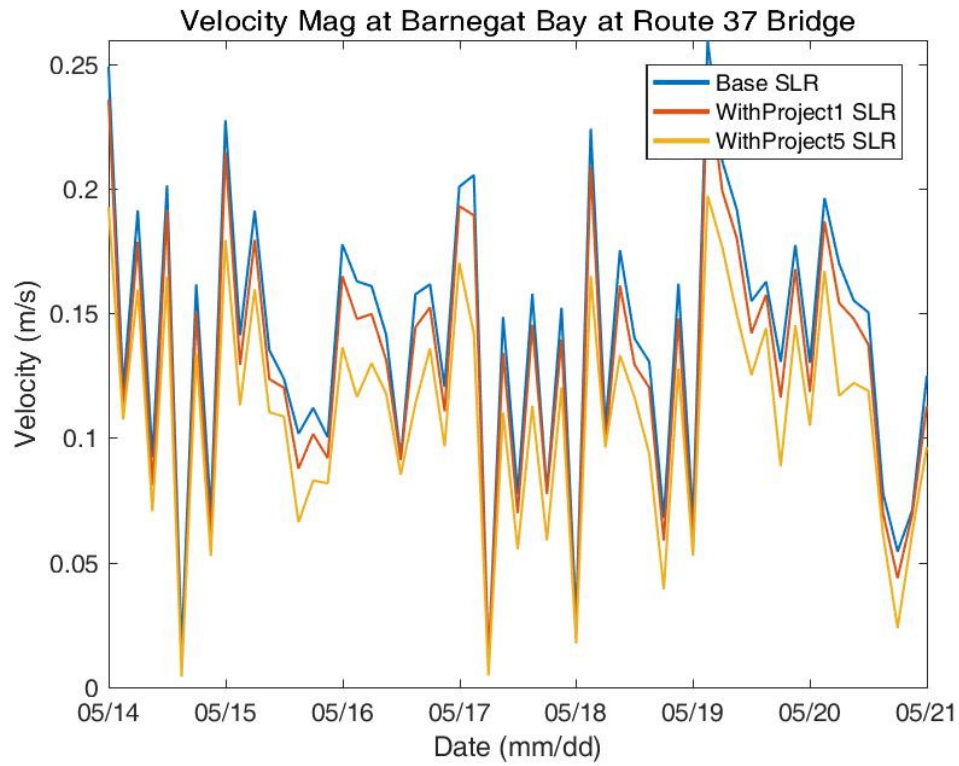
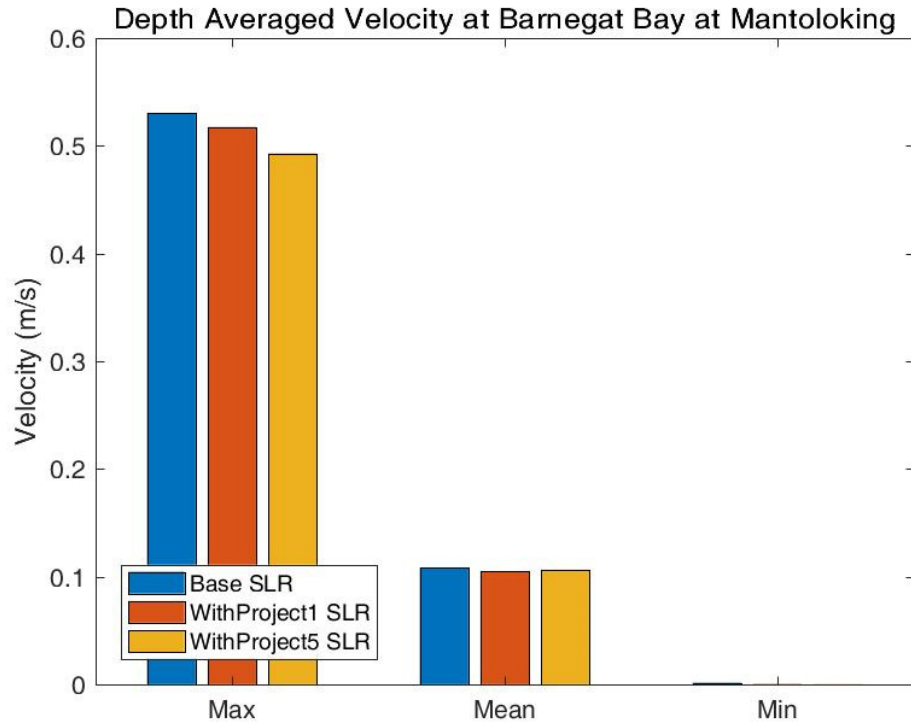




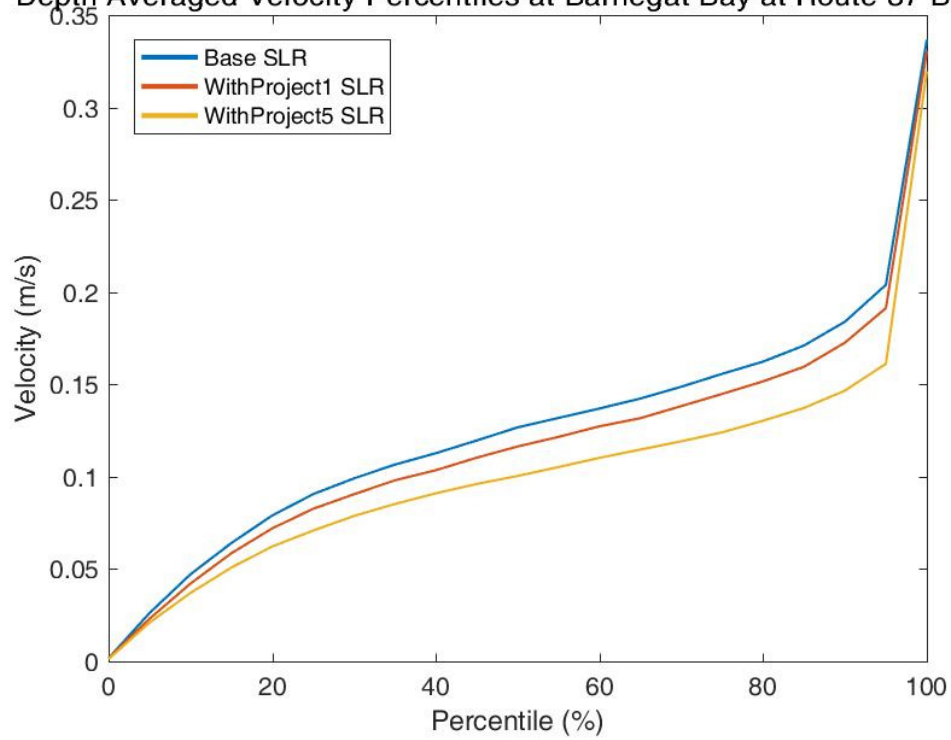




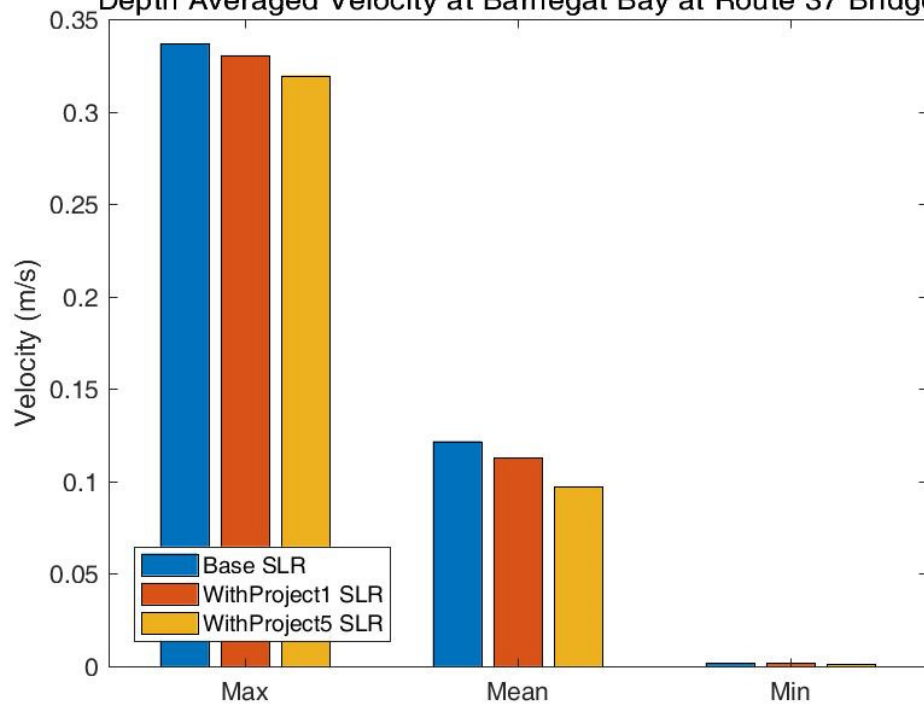


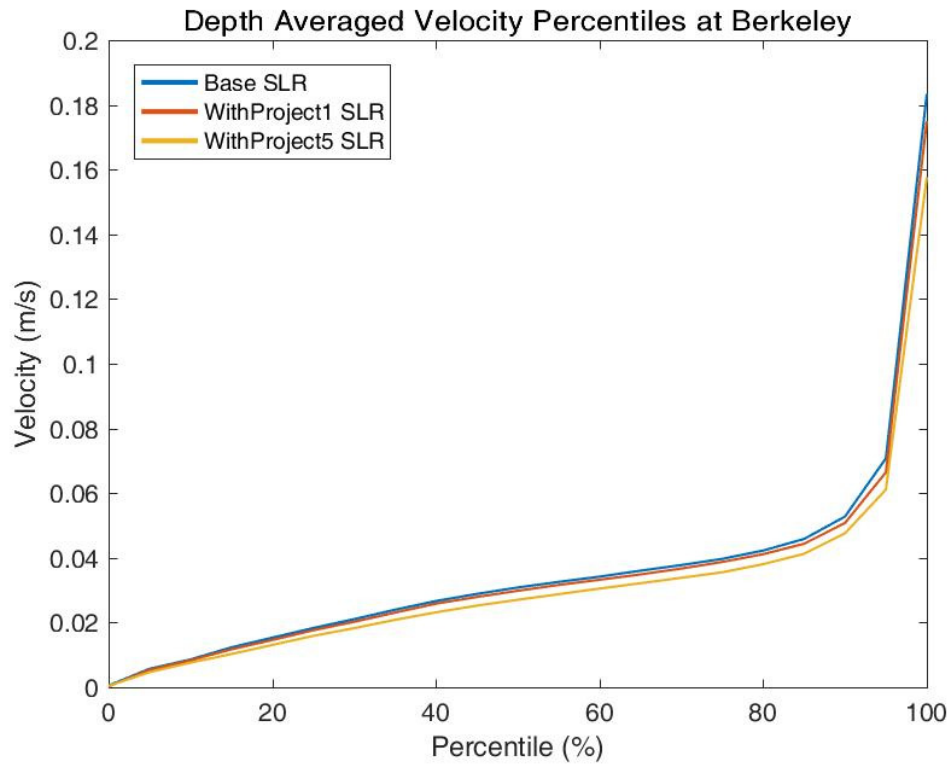
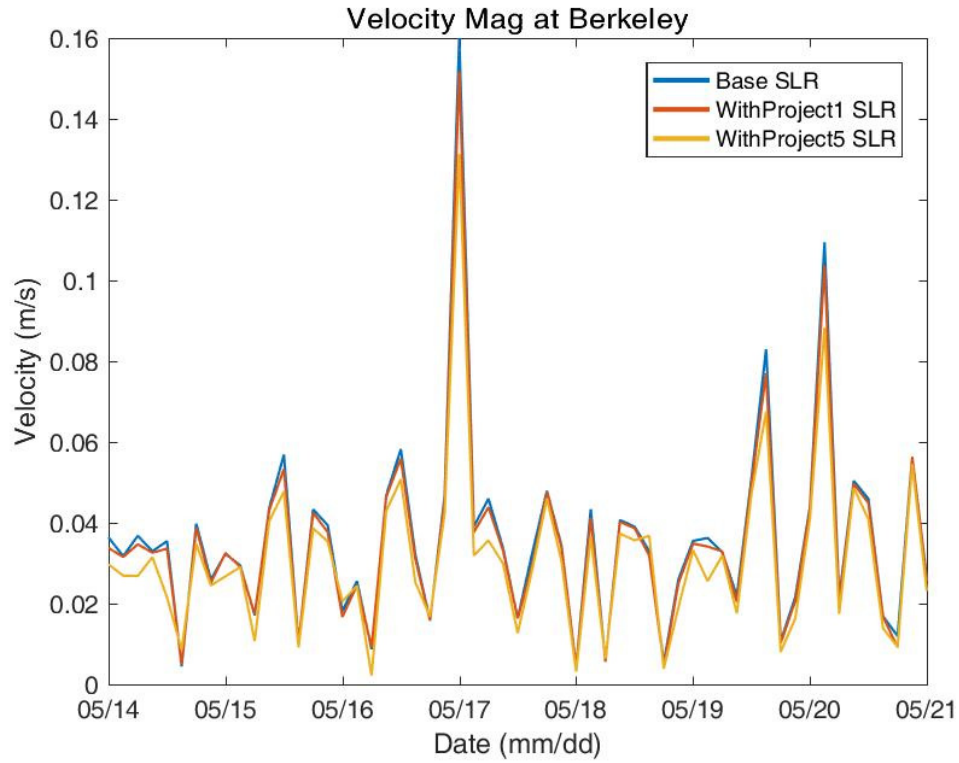


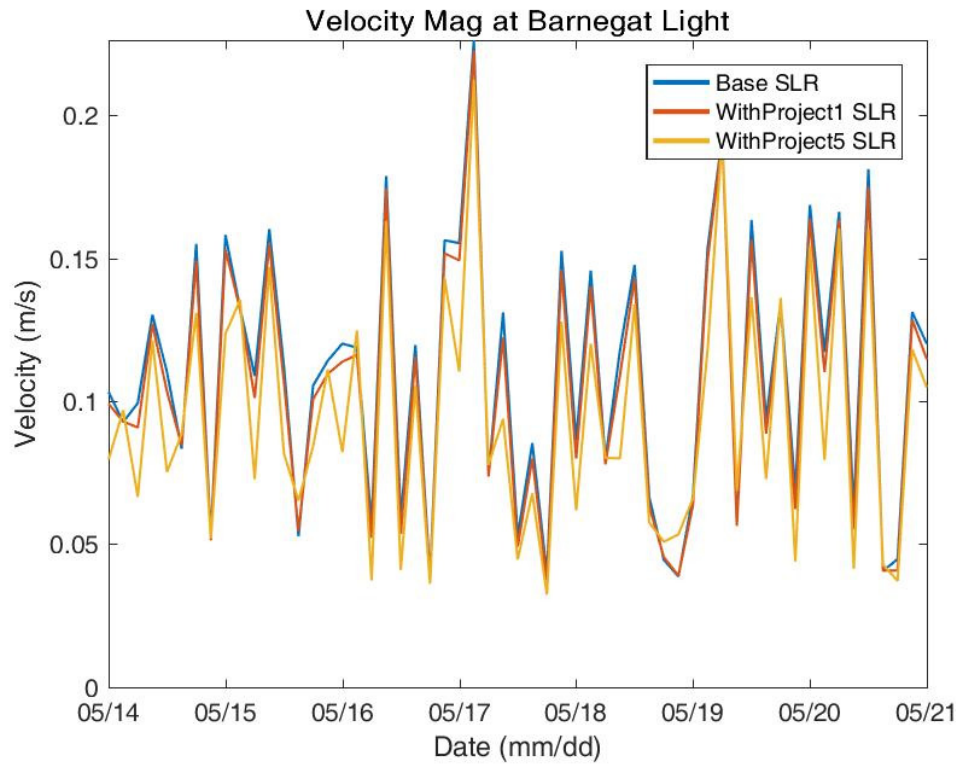
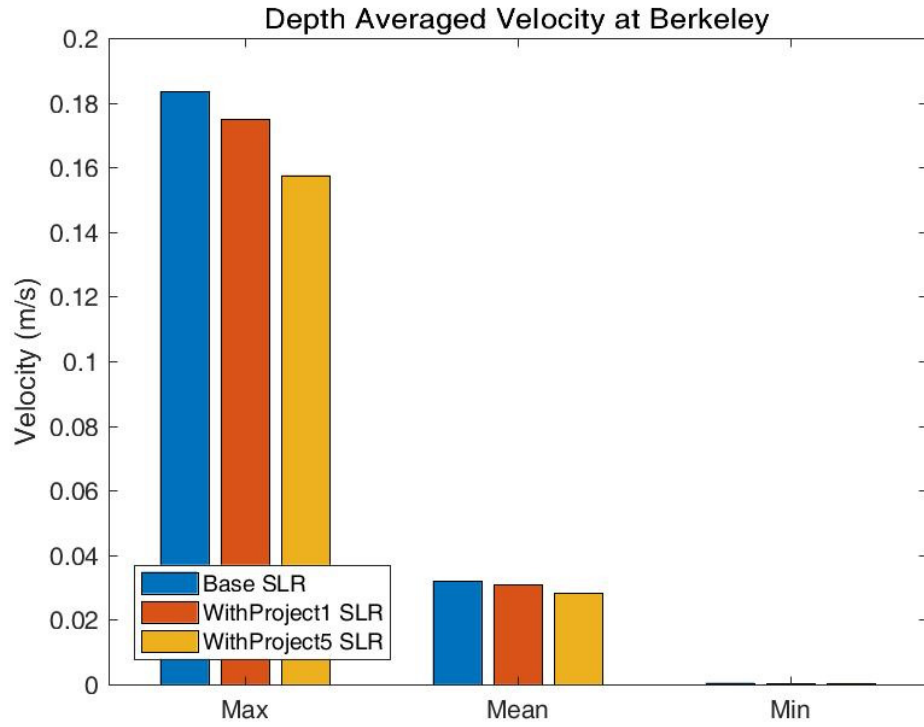
Depth Averaged Velocity Percentiles at Barnegat Bay at Route 37 Bridge

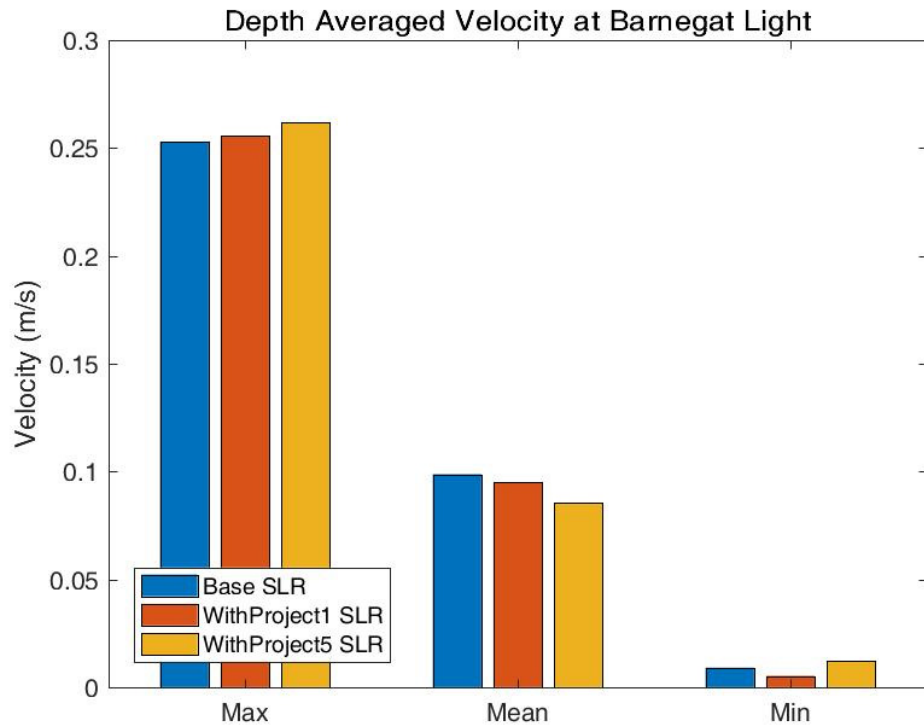
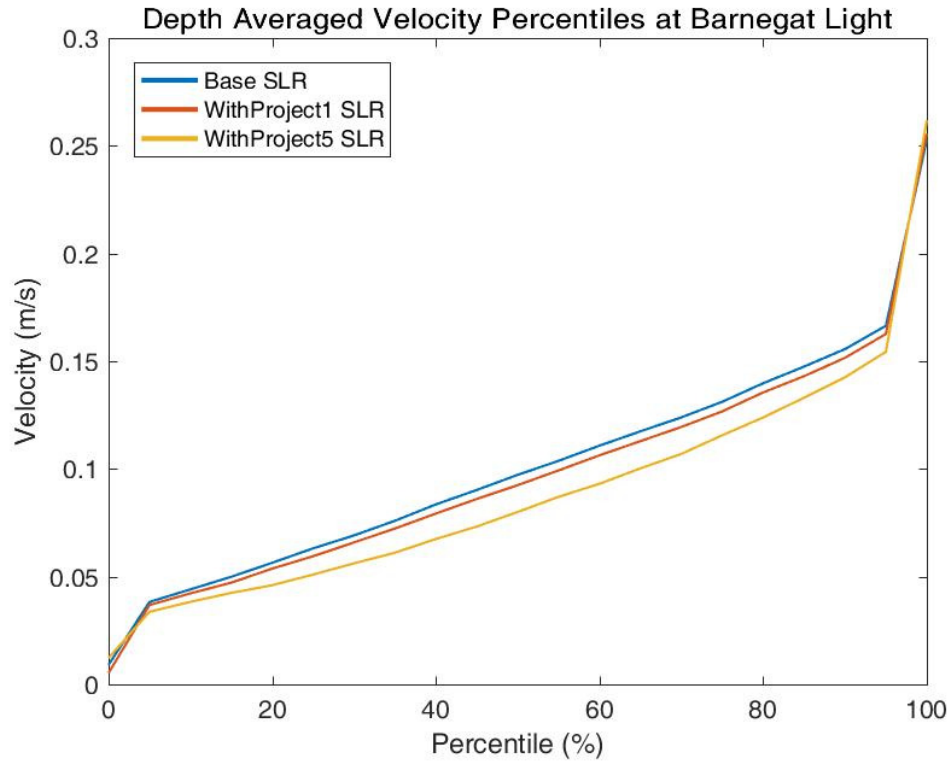


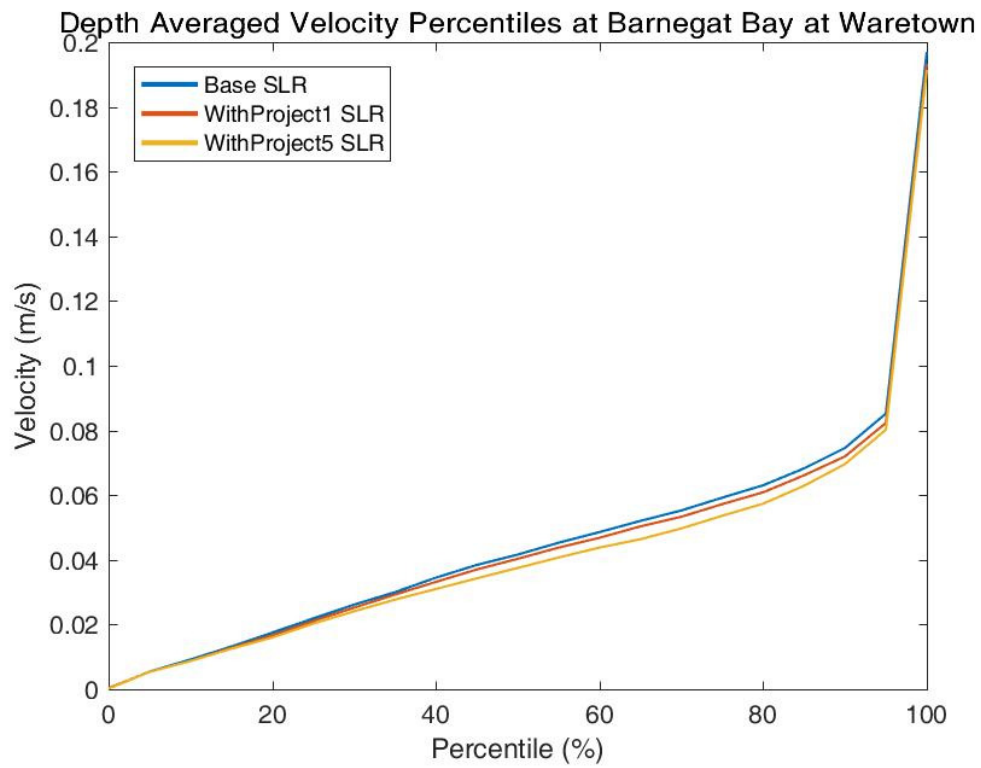
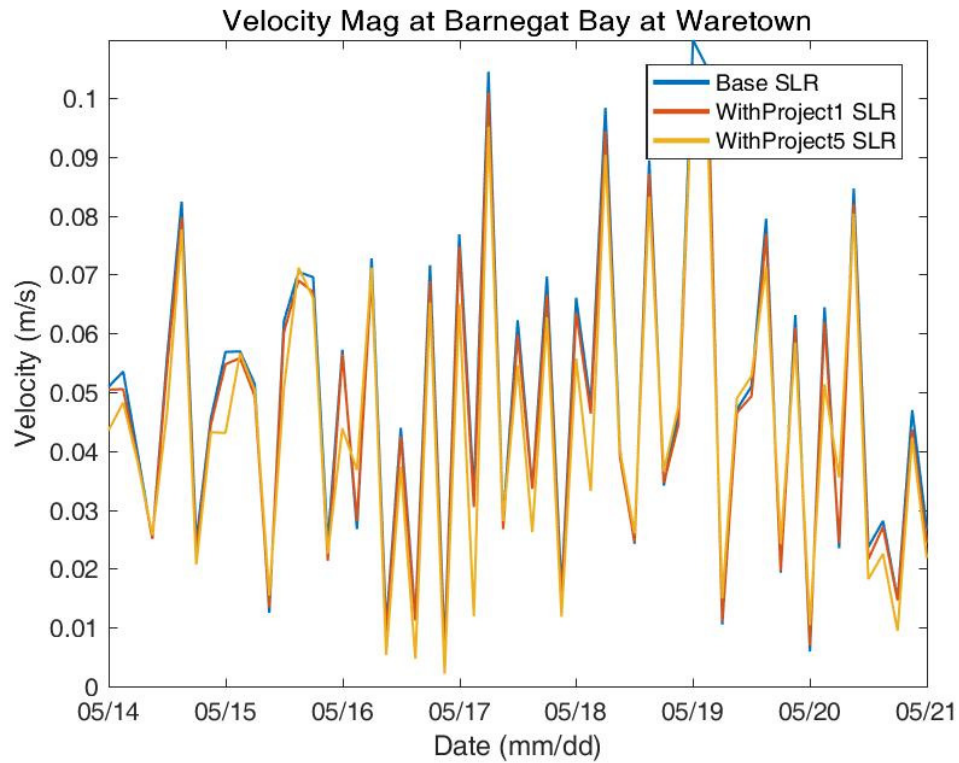
Depth Averaged Velocity at Barnegat Bay at Route 37 Bridge

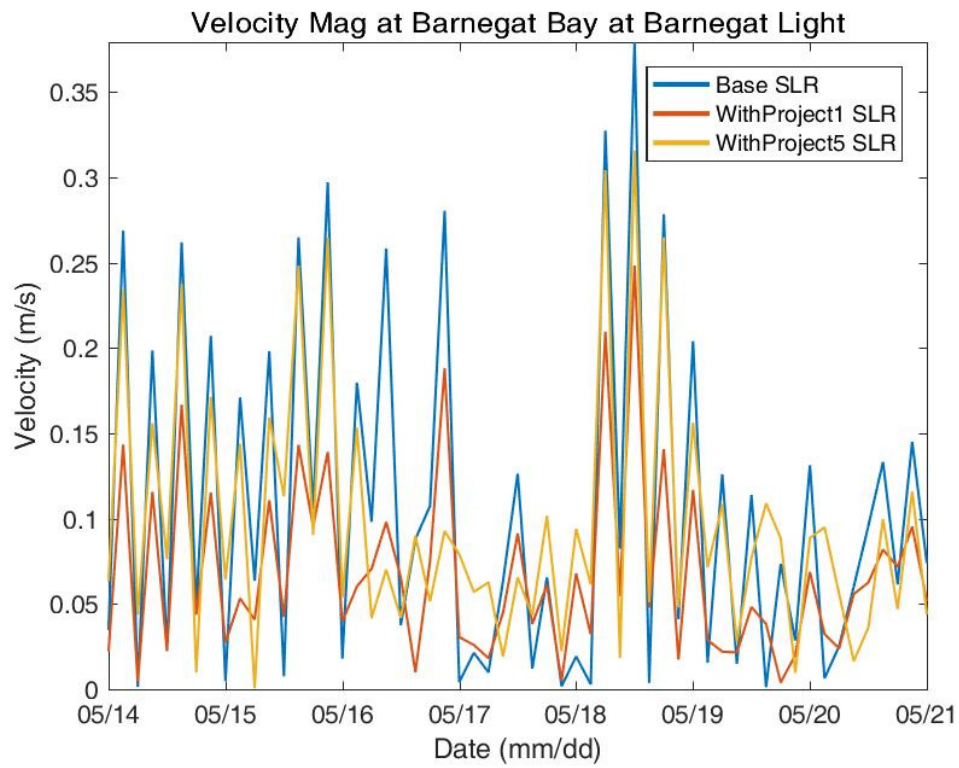
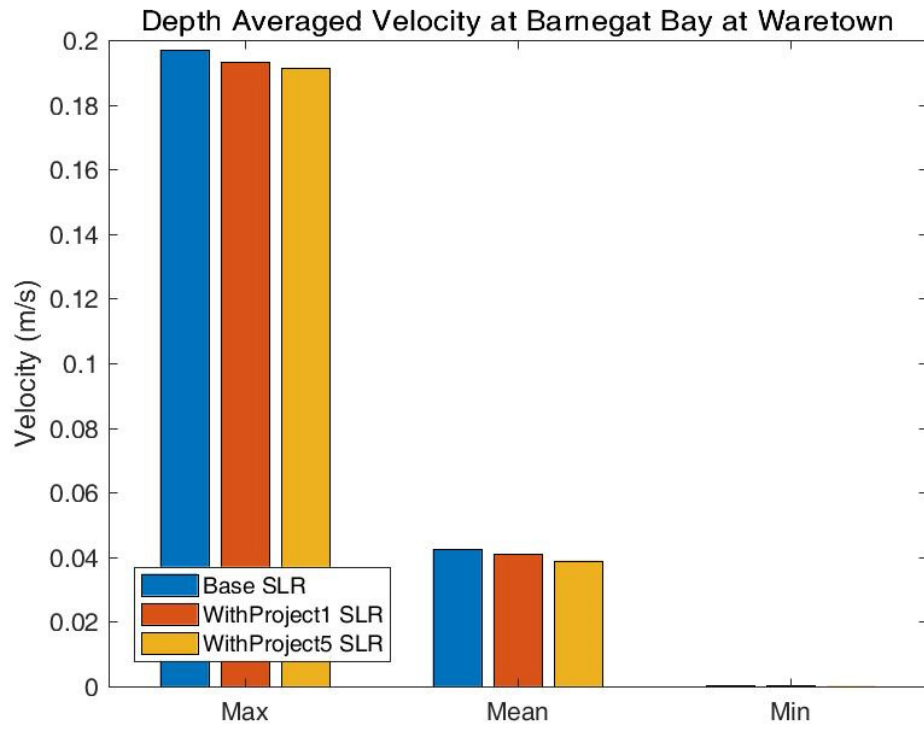




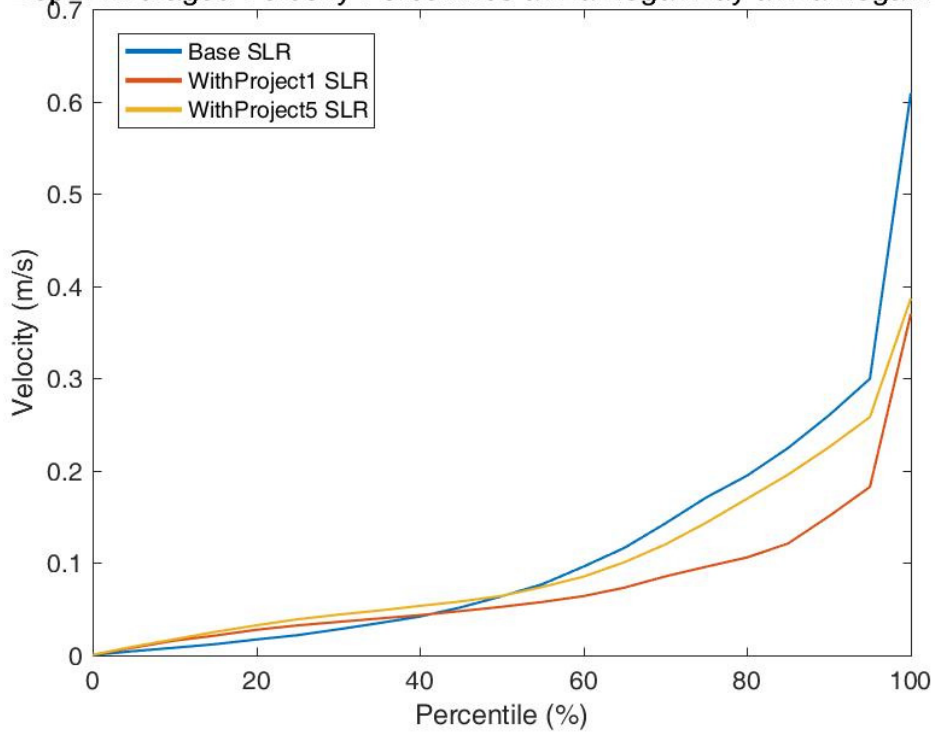




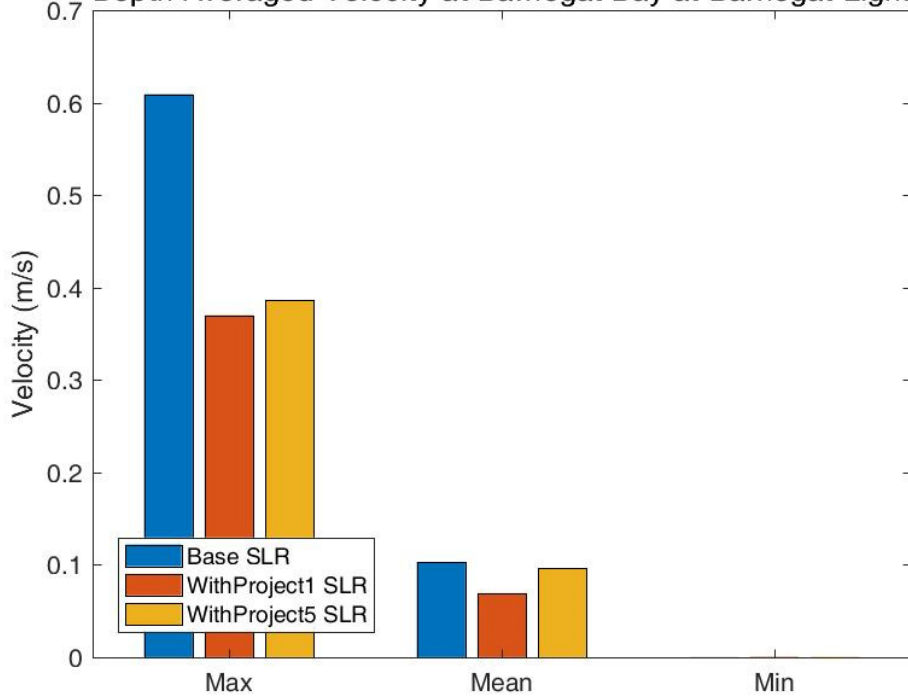


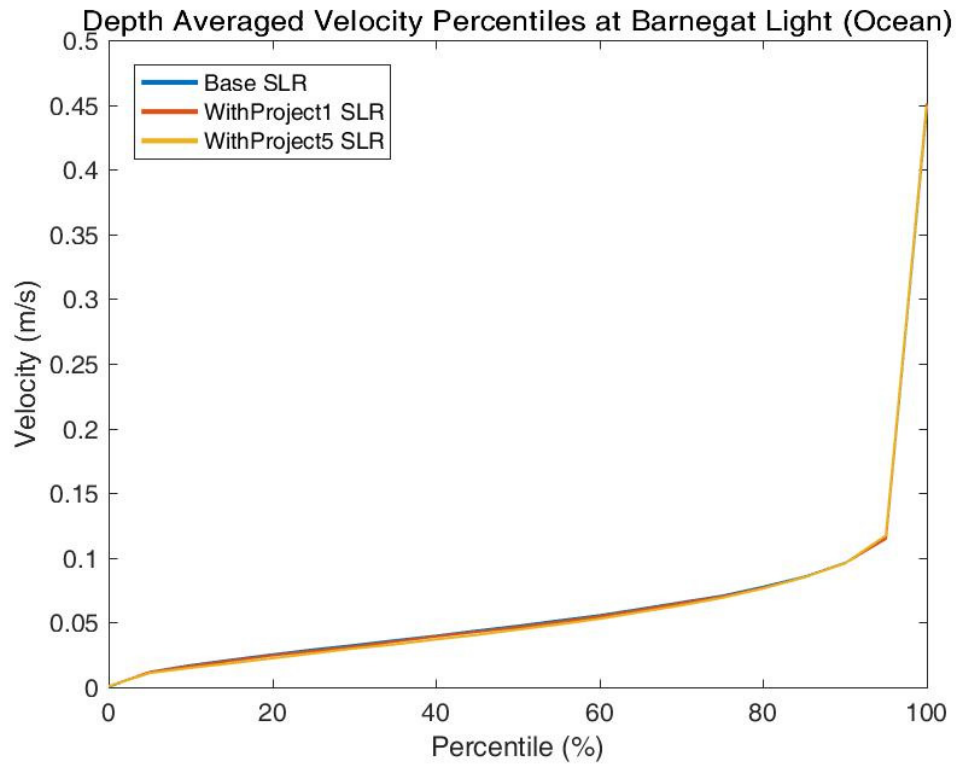
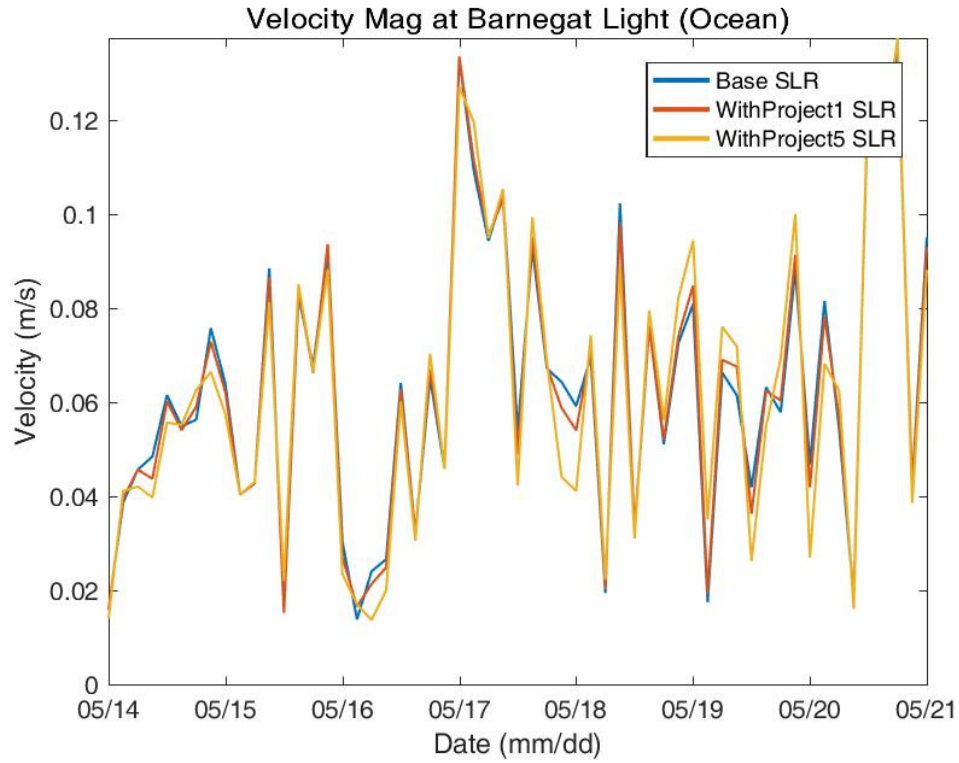


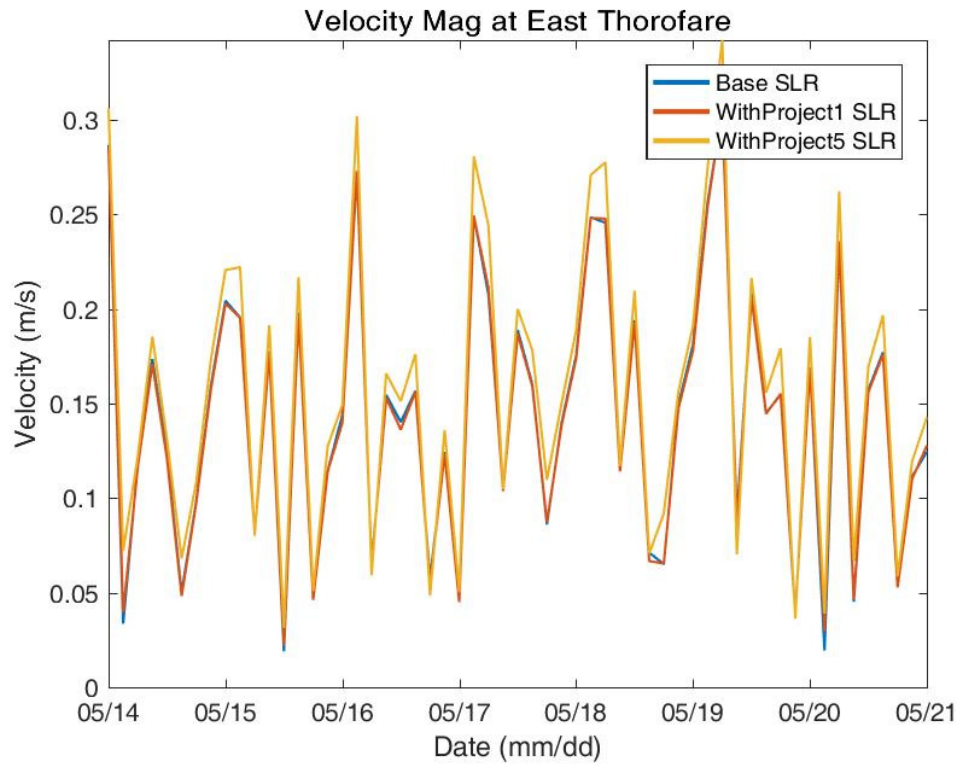
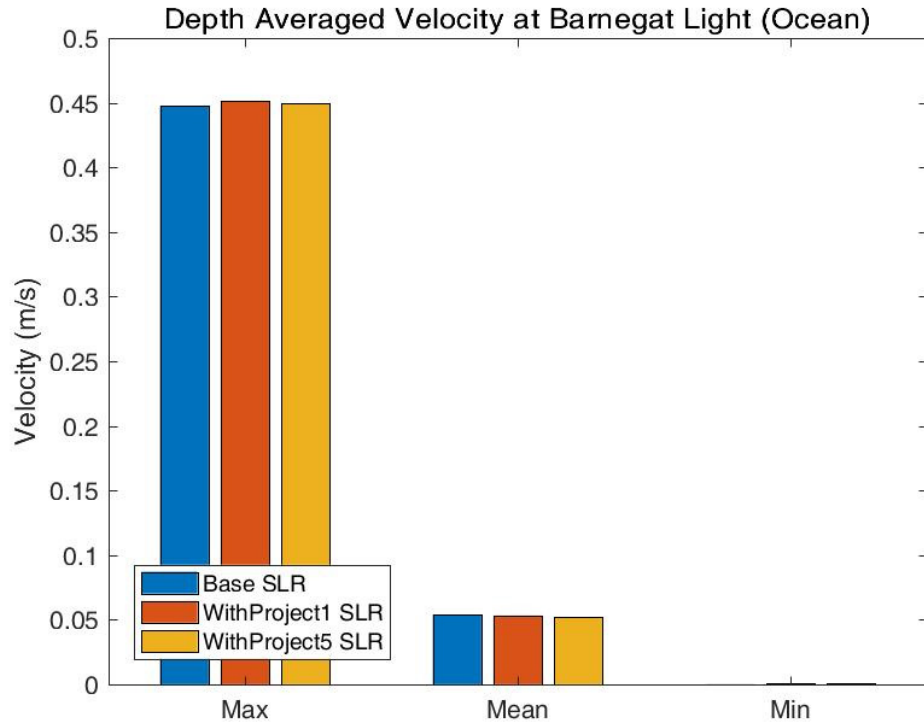
Depth Averaged Velocity Percentiles at Barnegat Bay at Barnegat Light

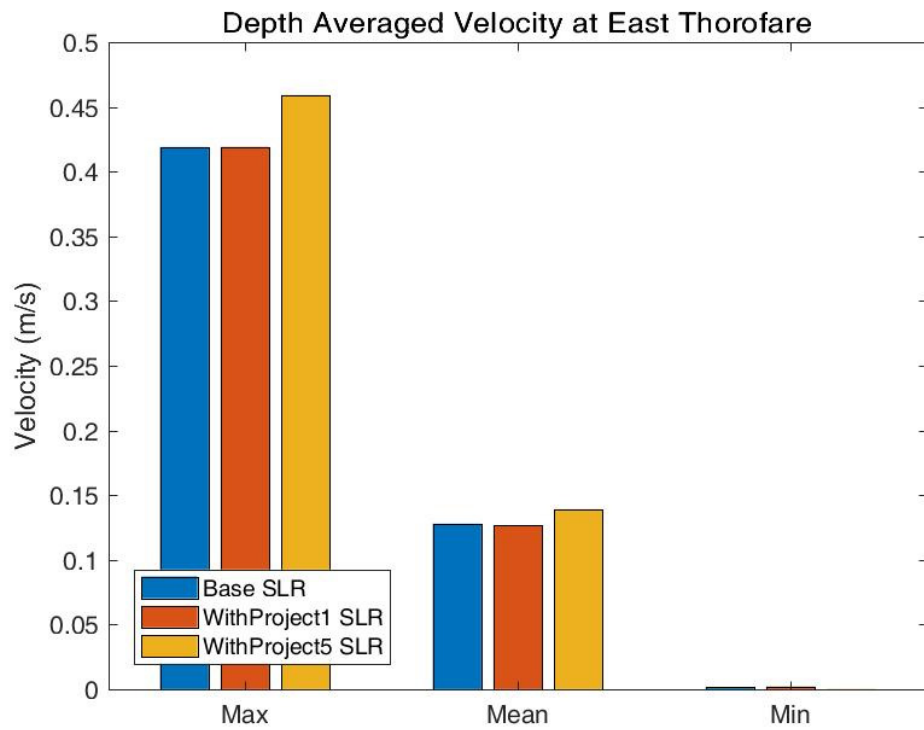
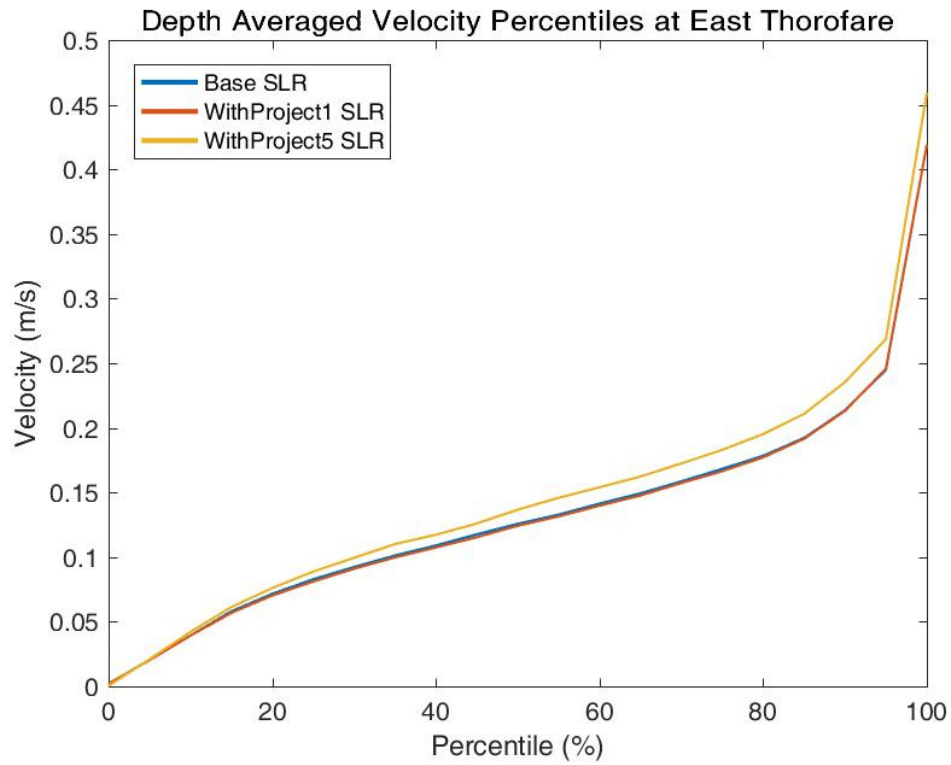


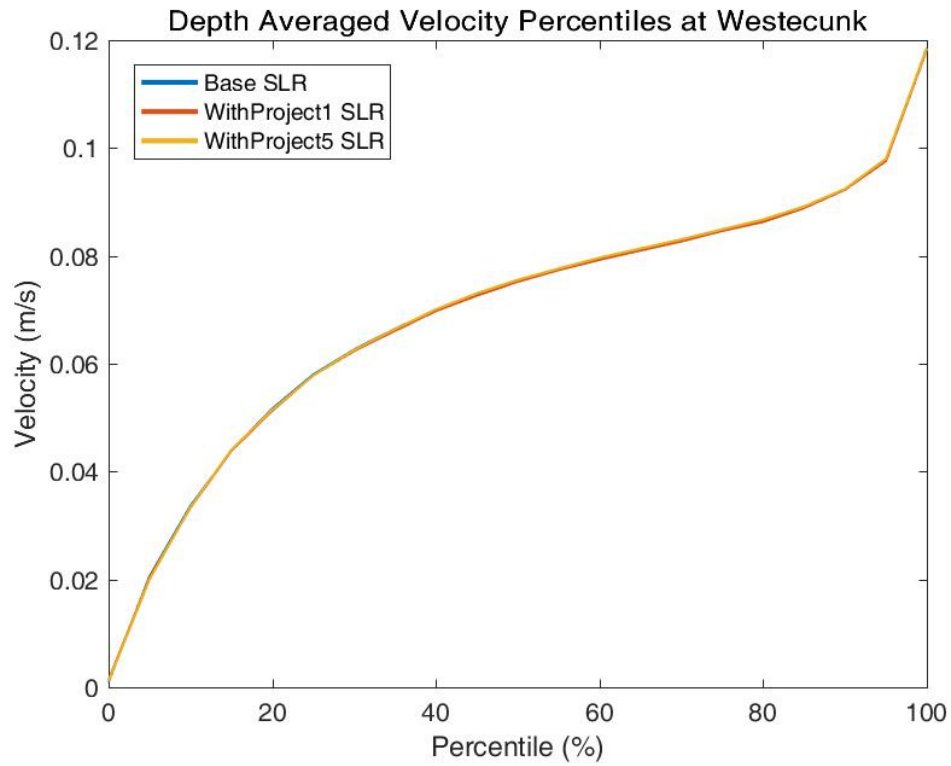
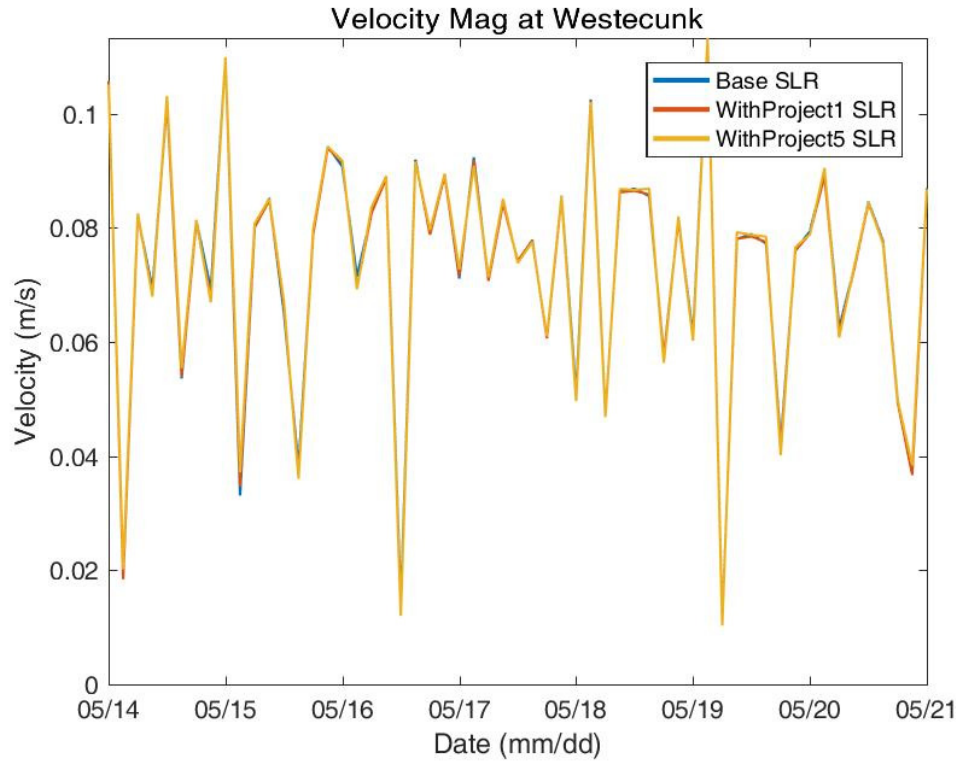
Depth Averaged Velocity at Barnegat Bay at Barnegat Light

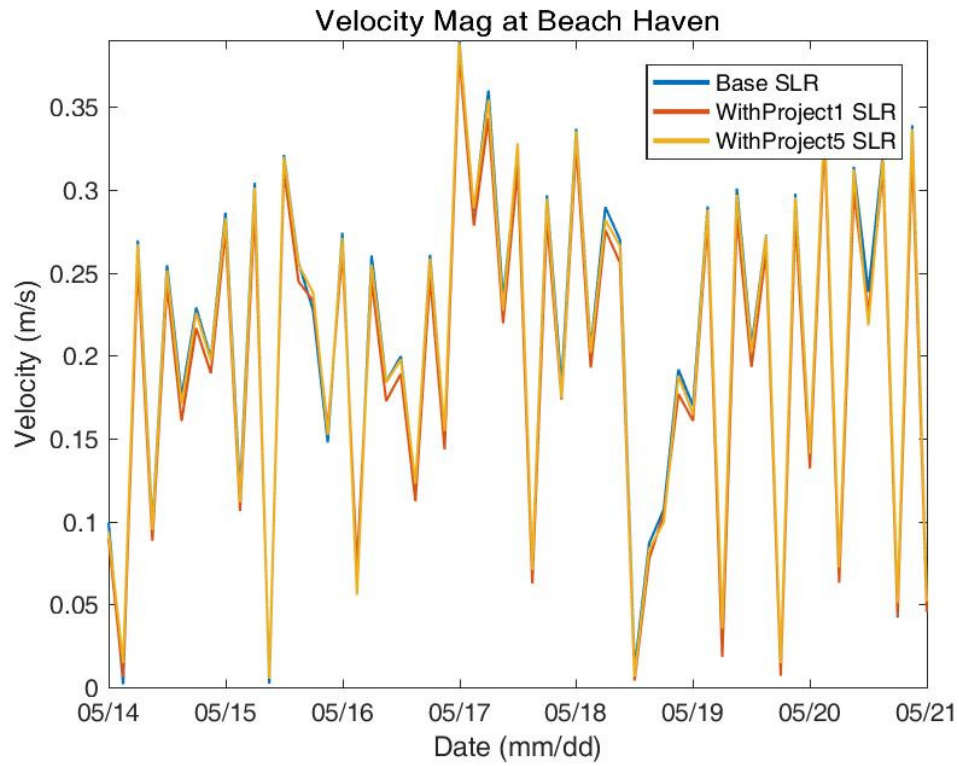
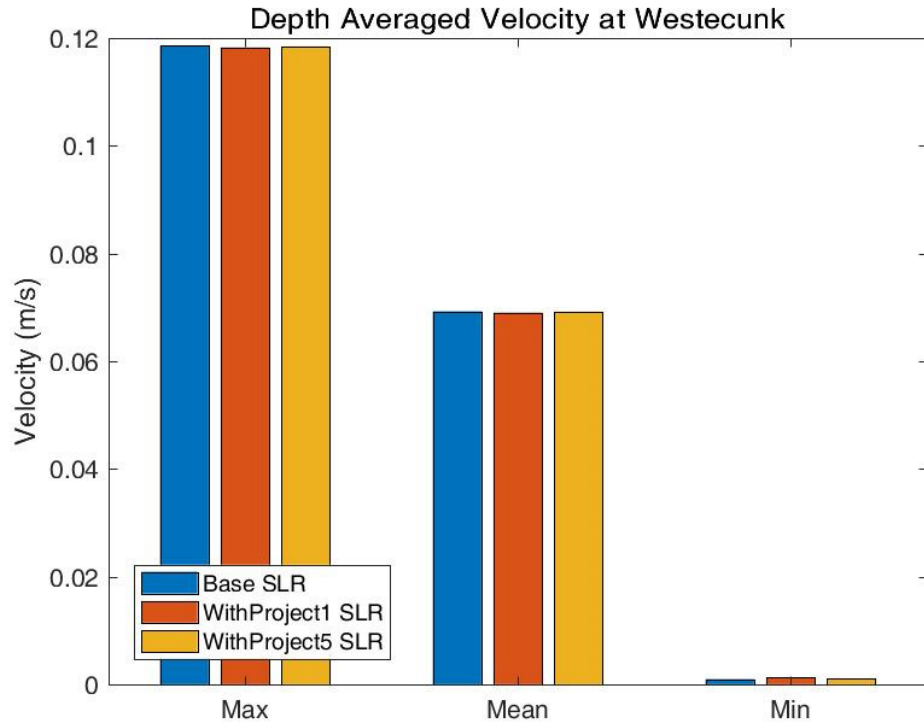


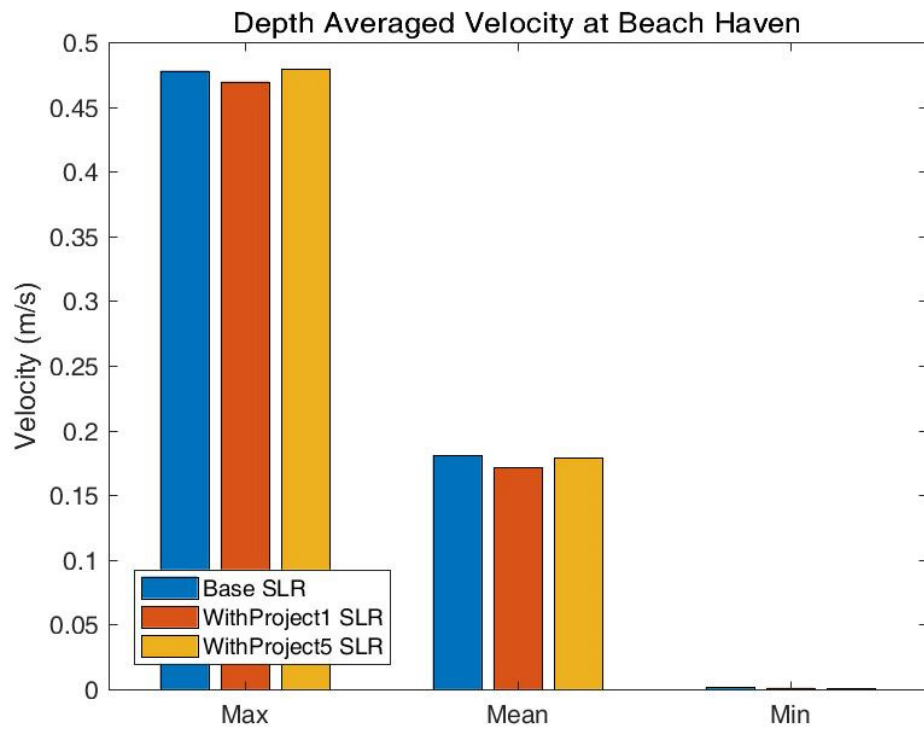
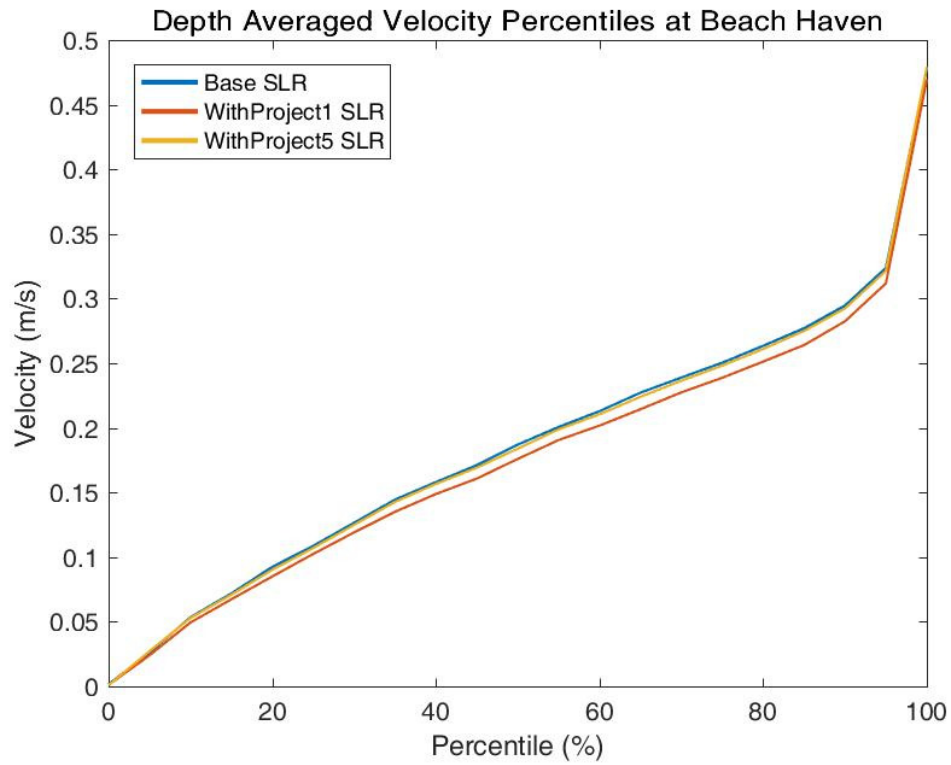


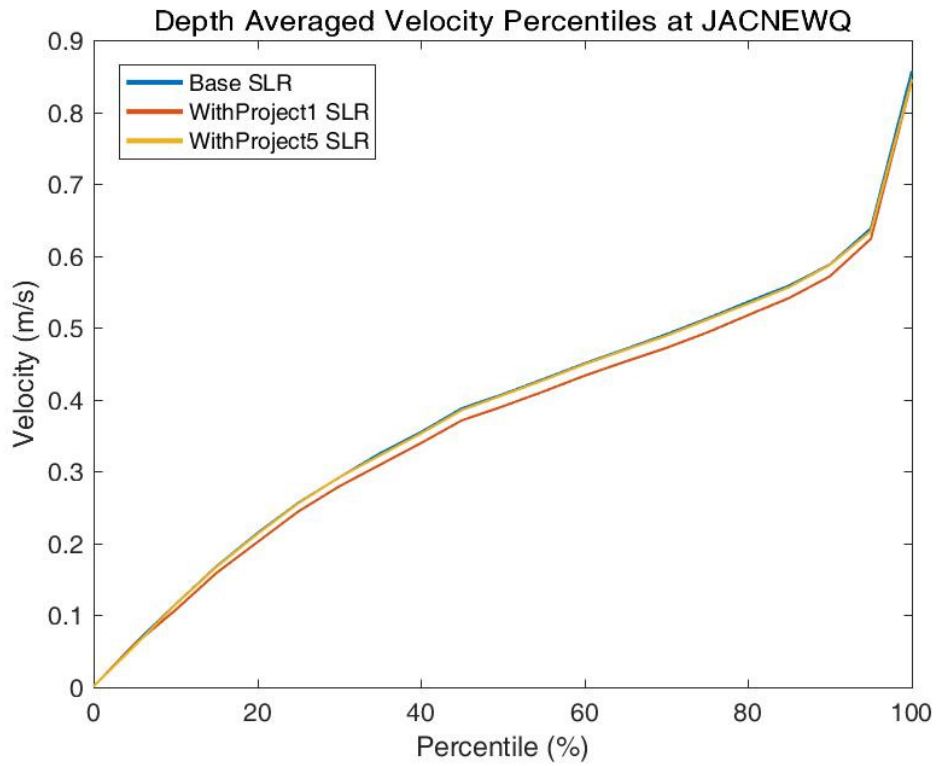
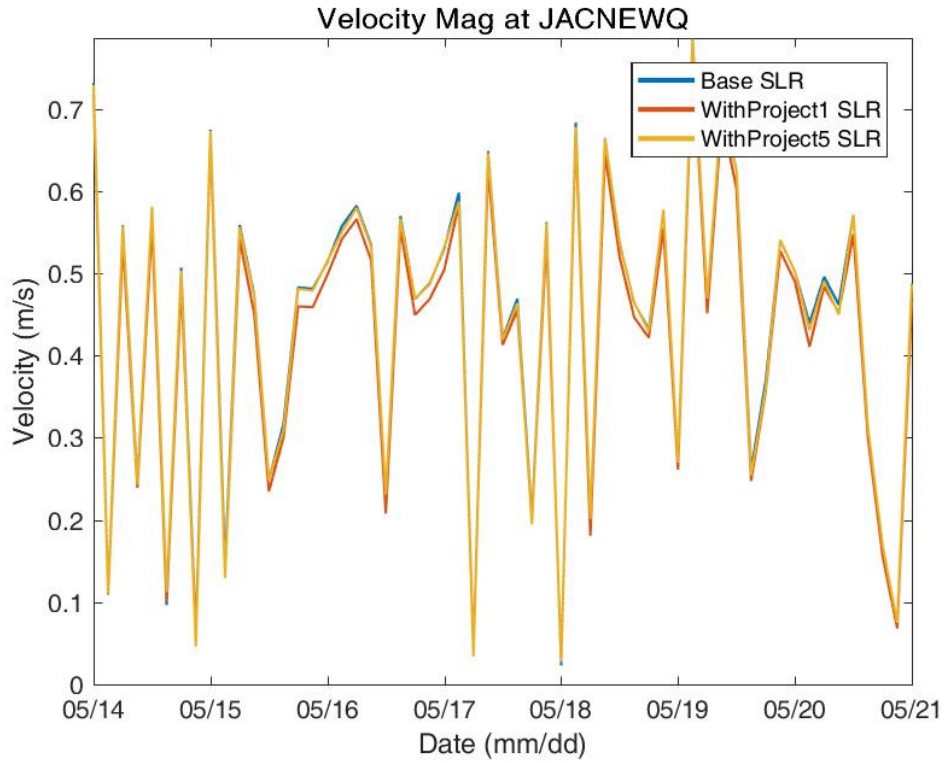


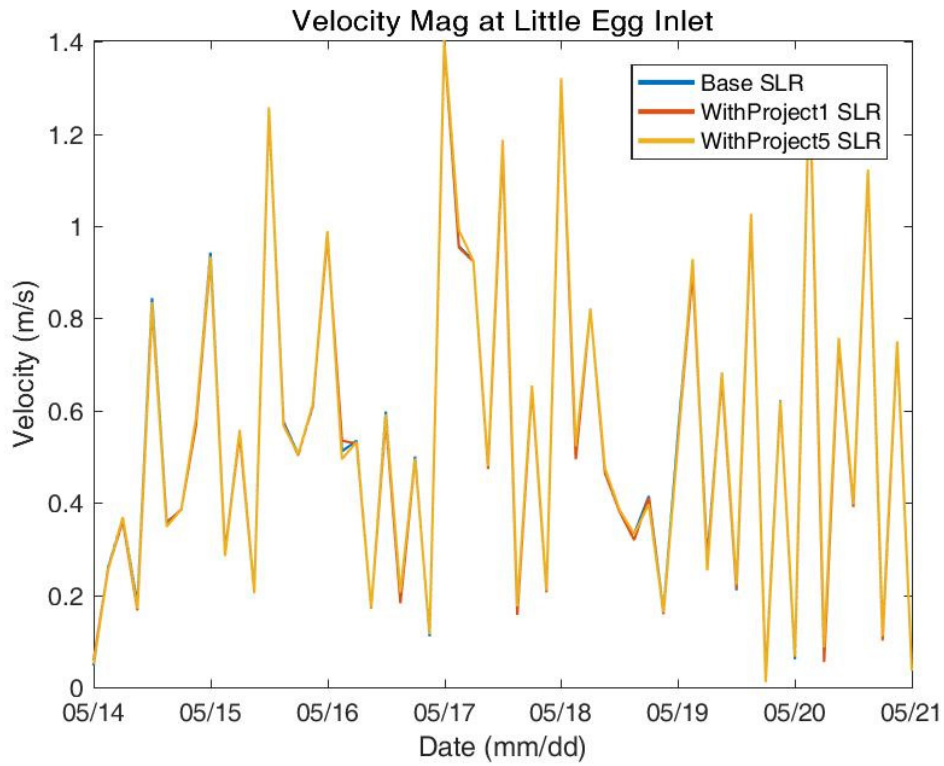
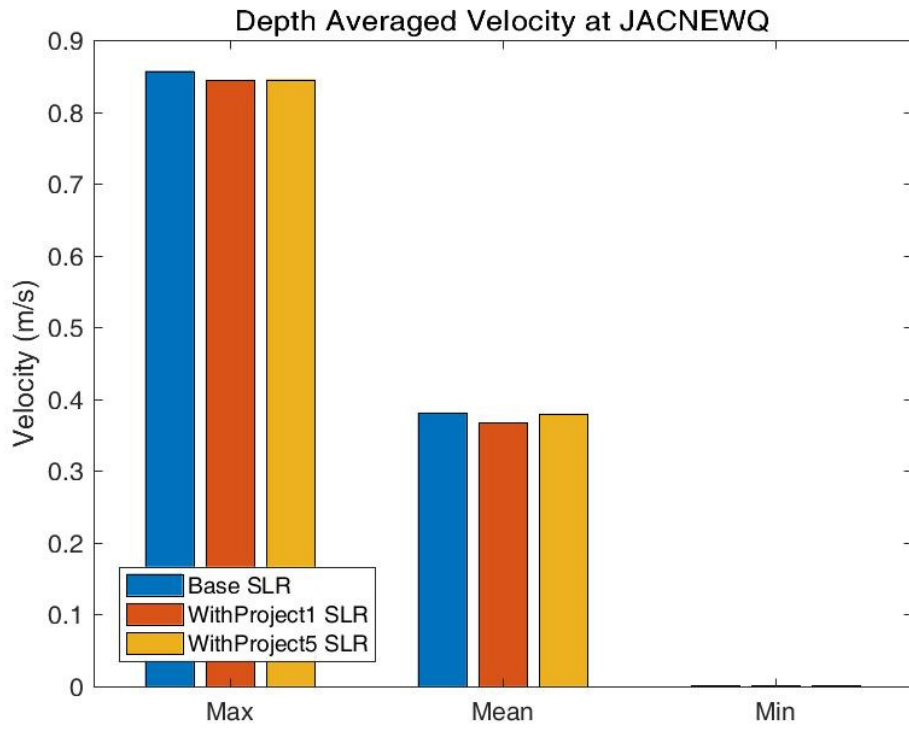


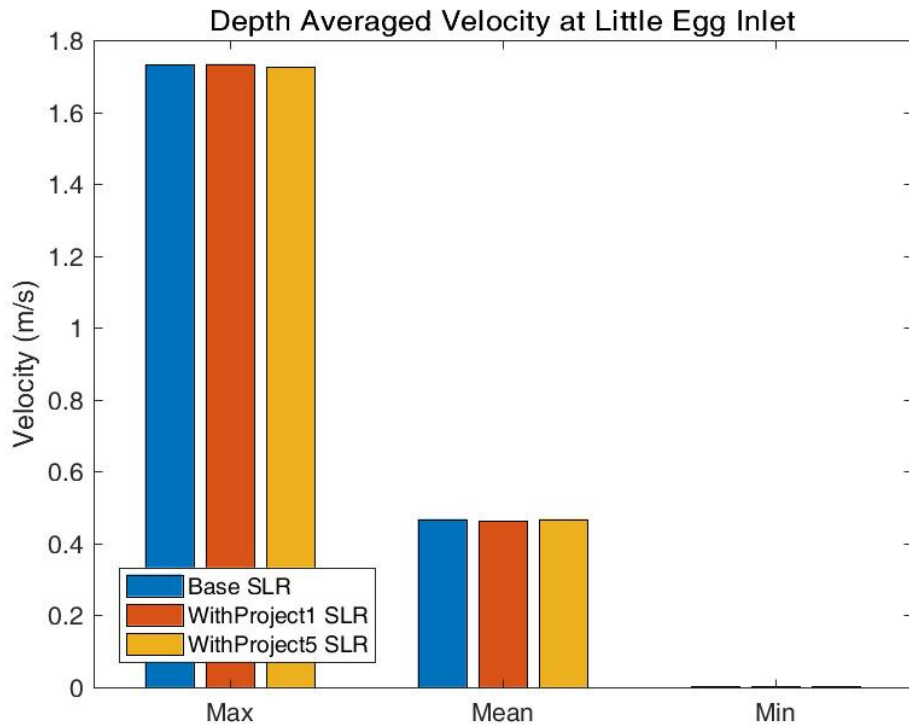
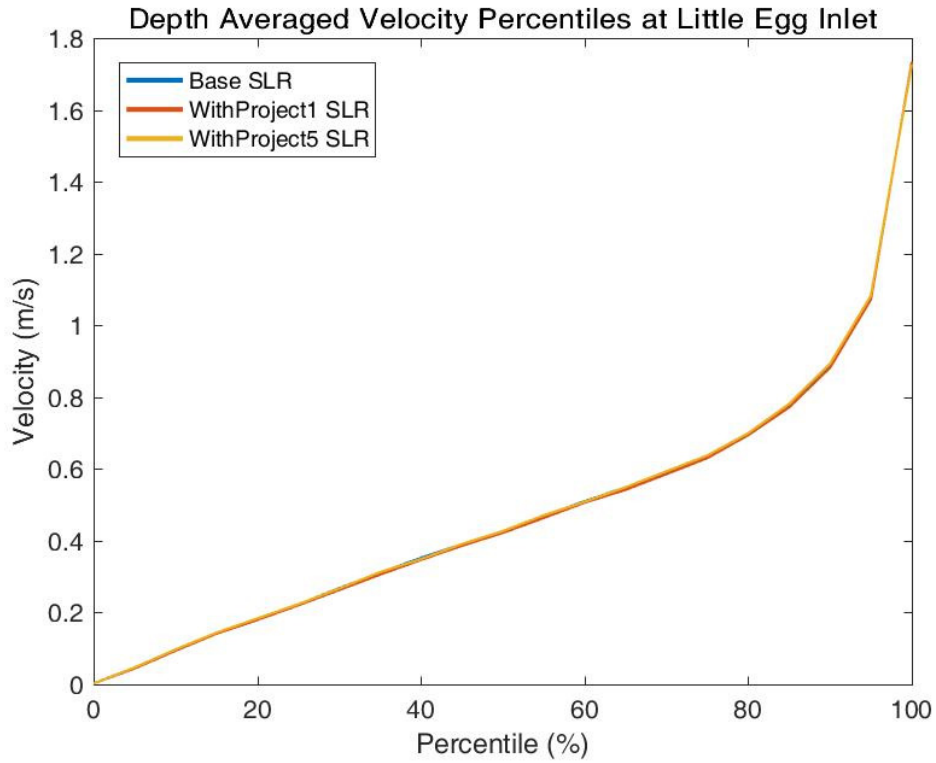


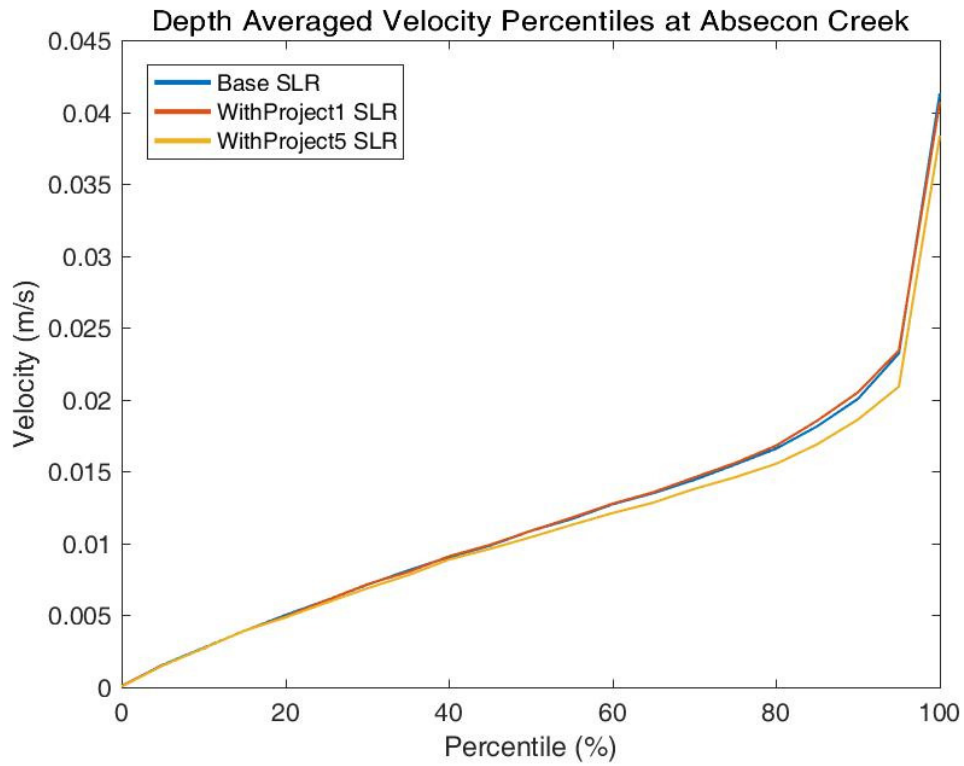
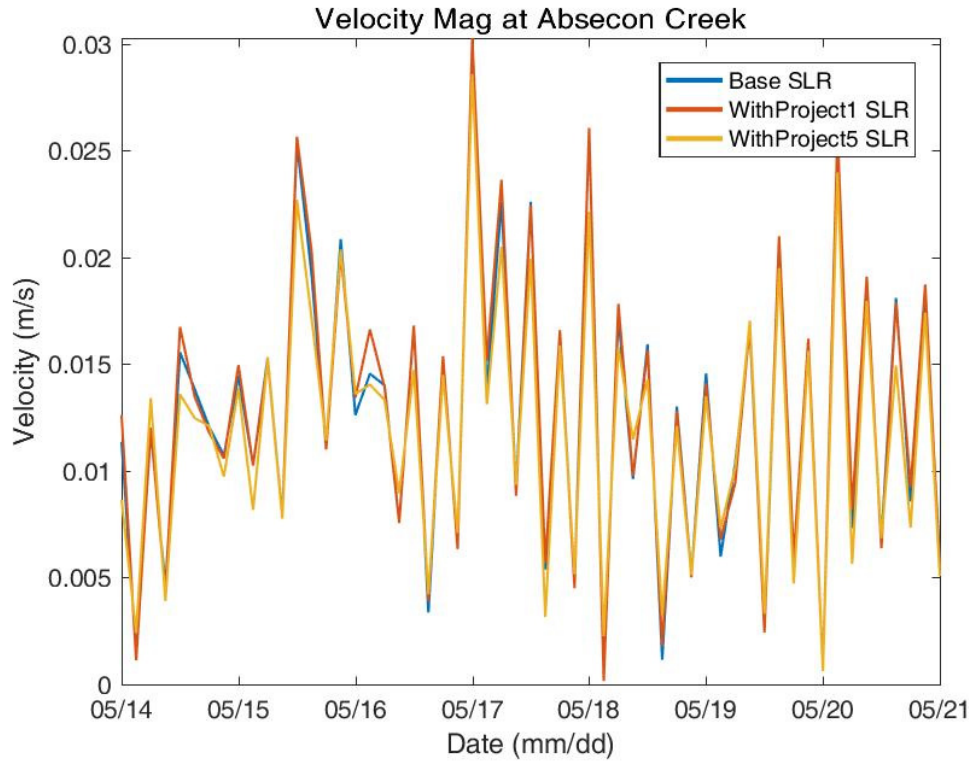


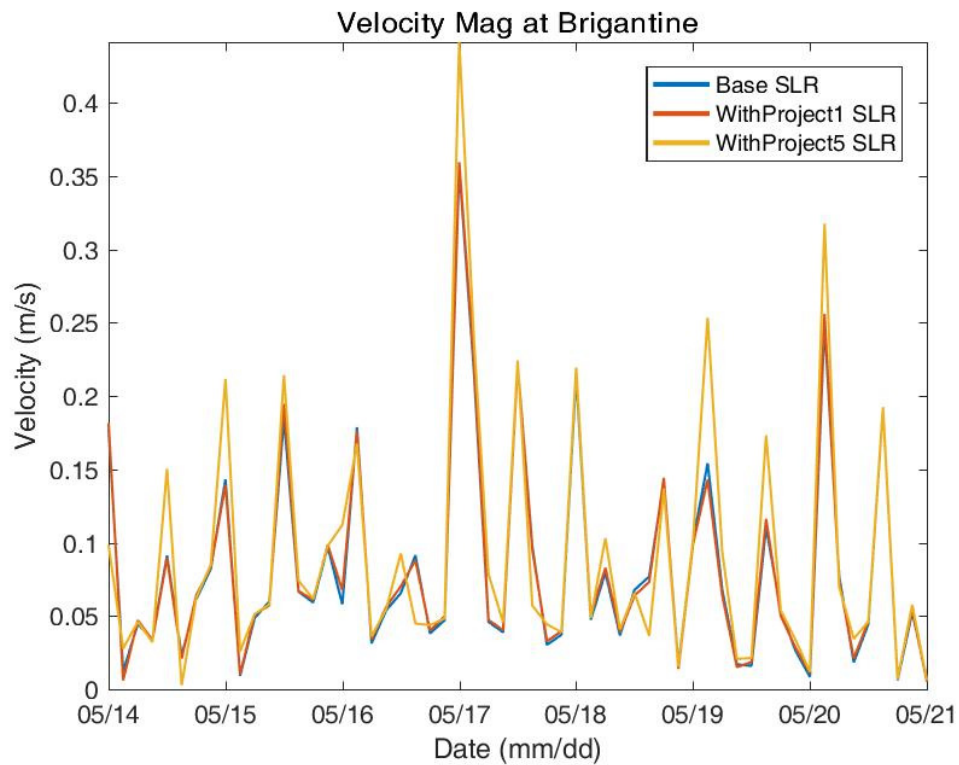
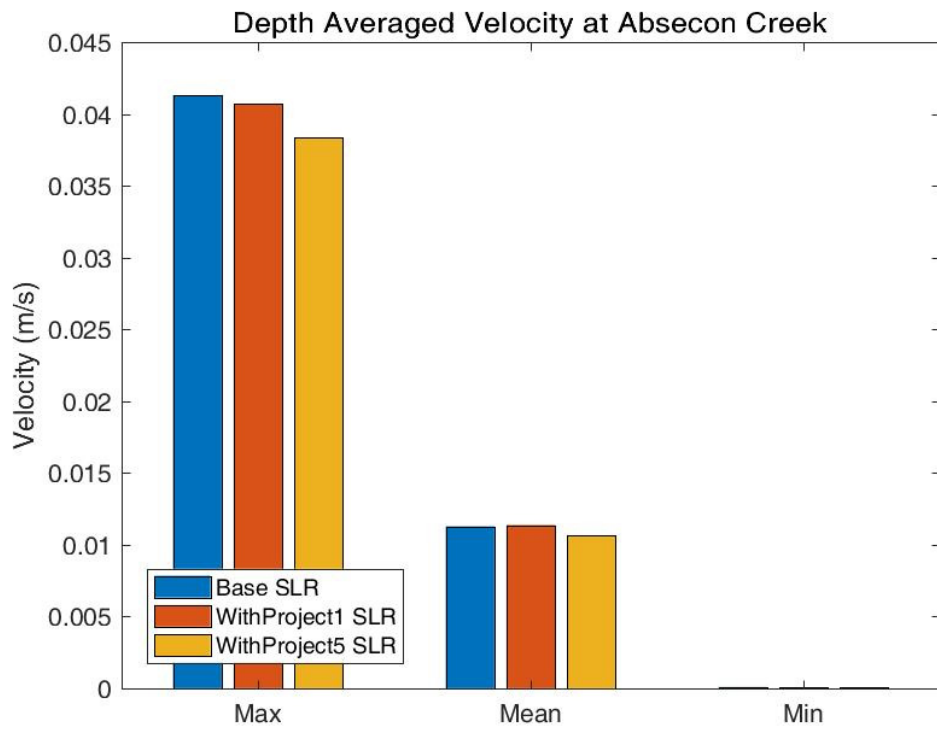


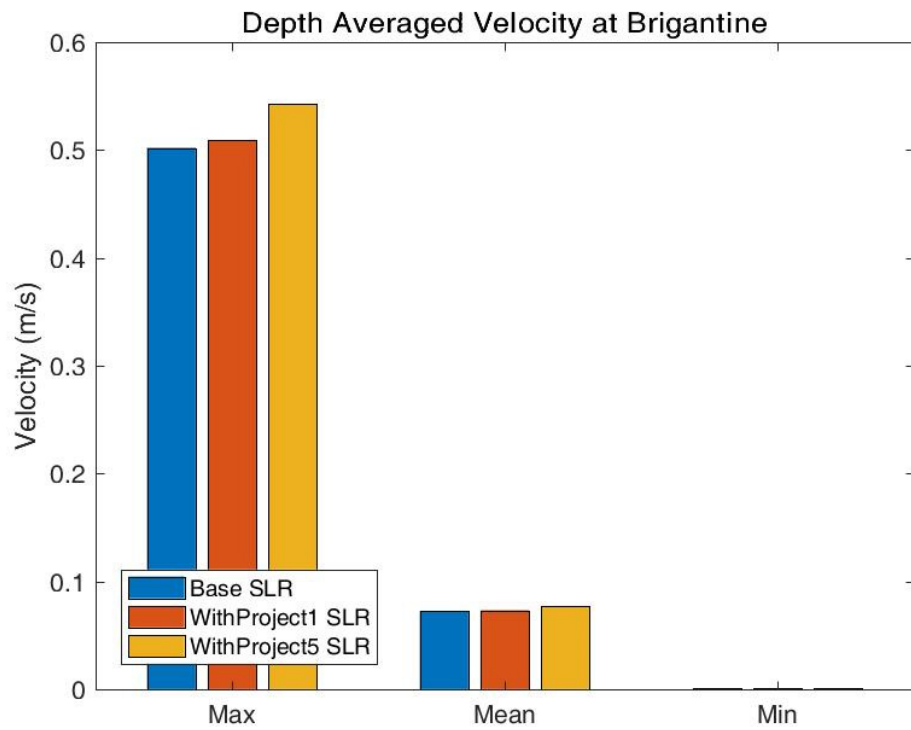
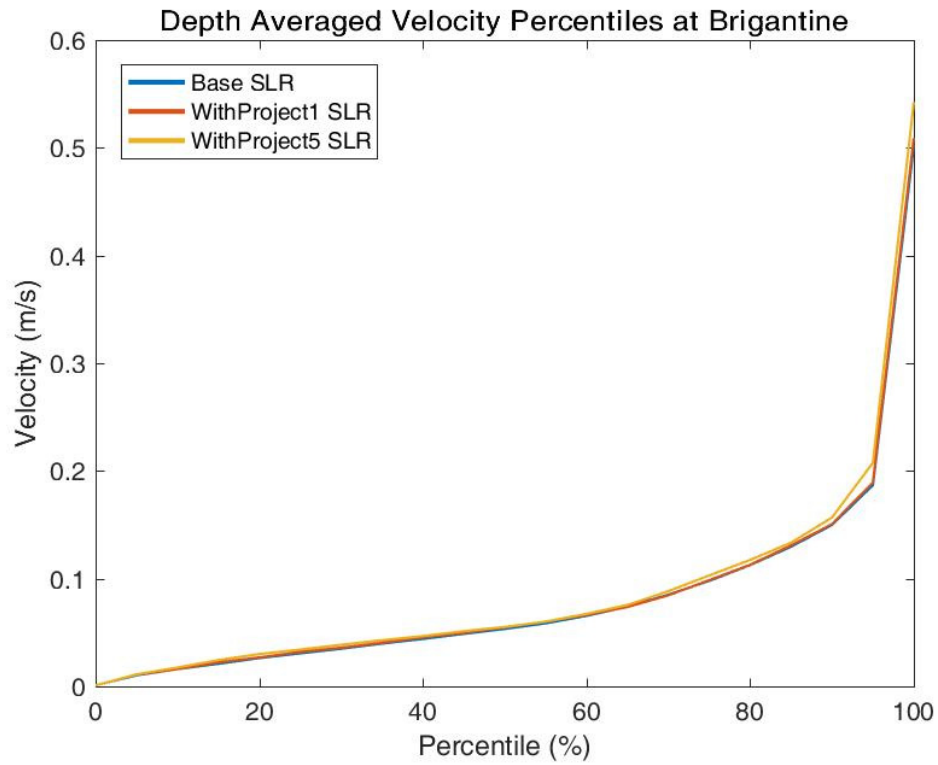


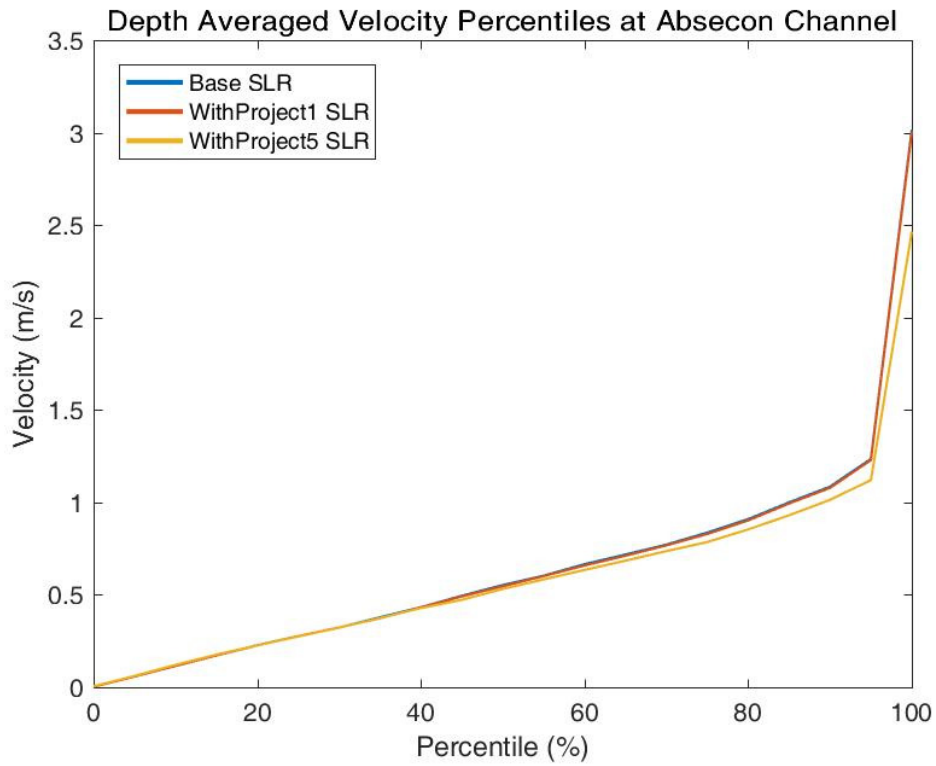
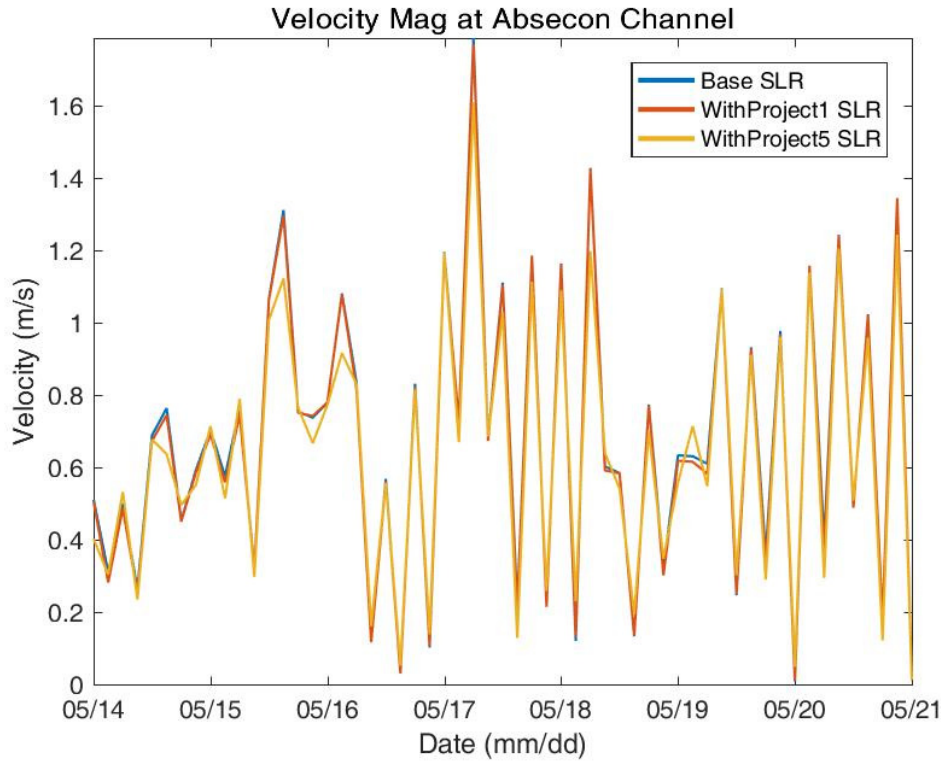


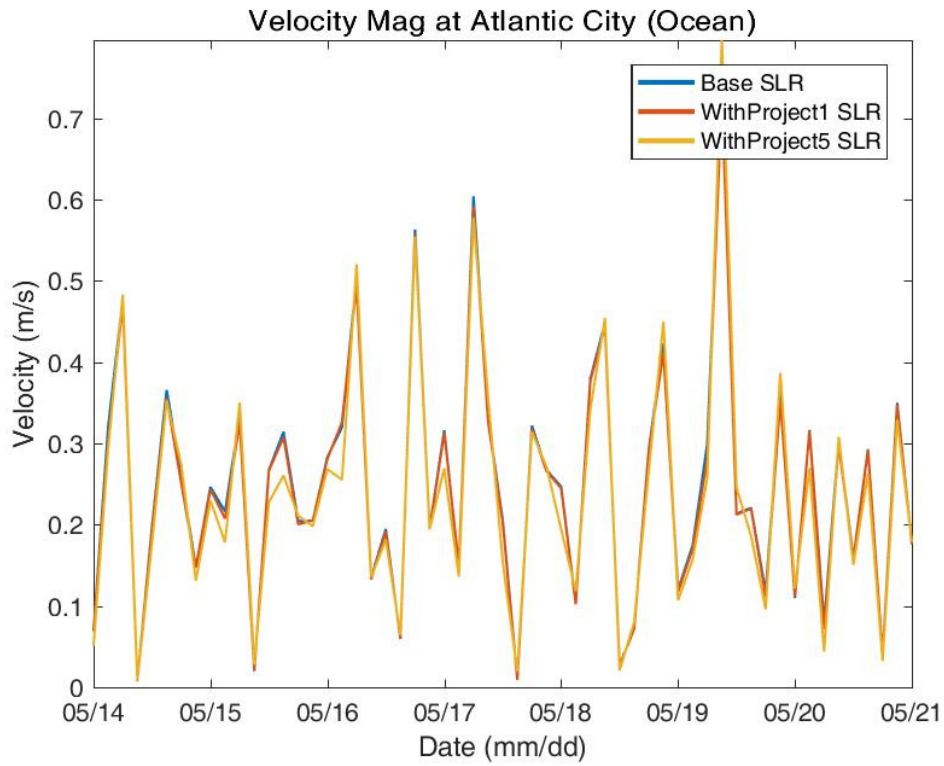
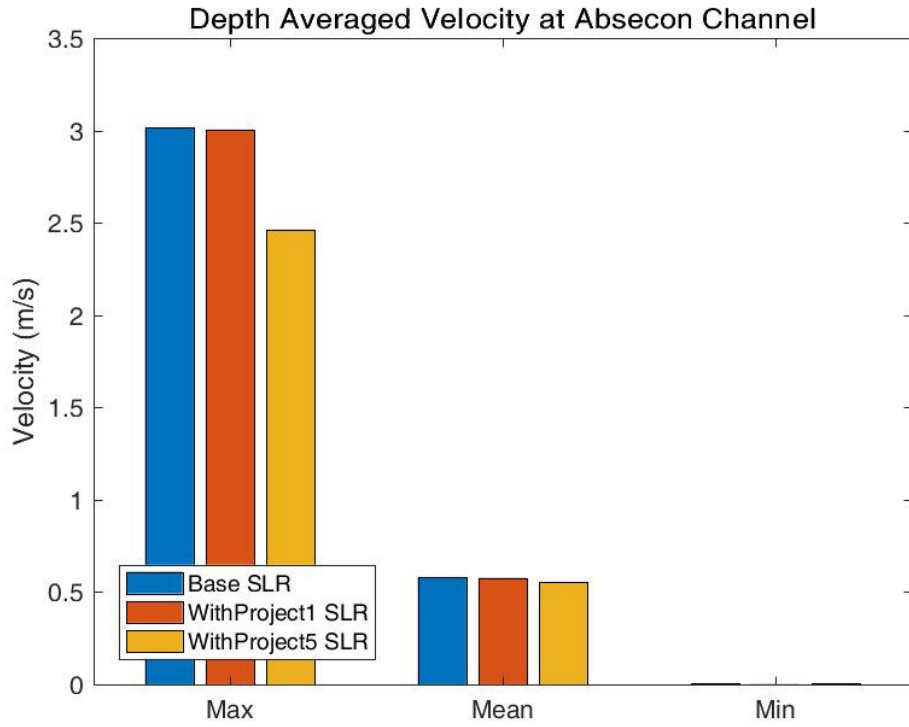


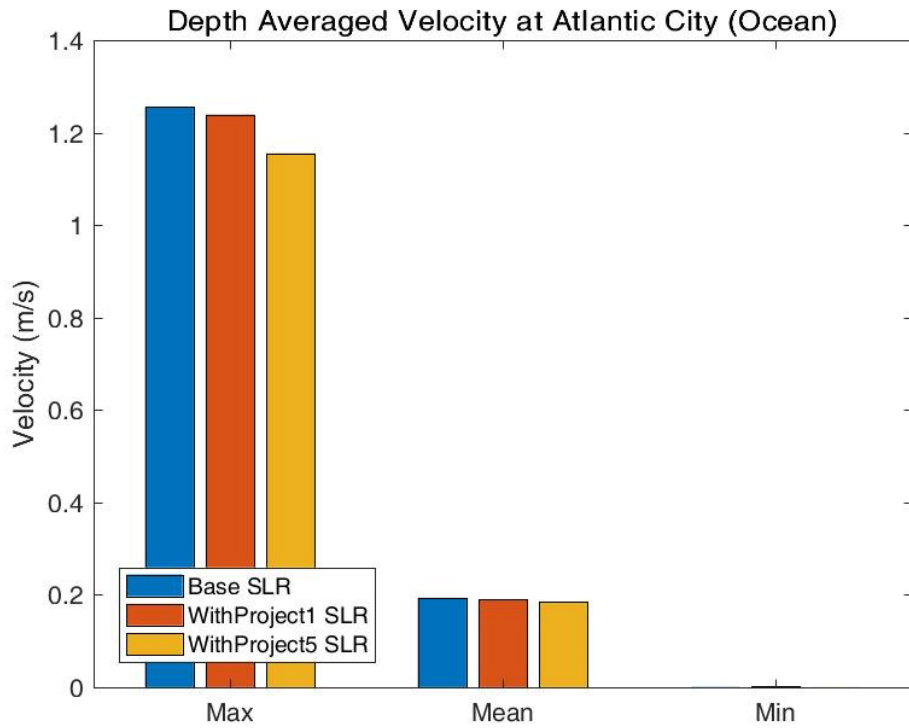
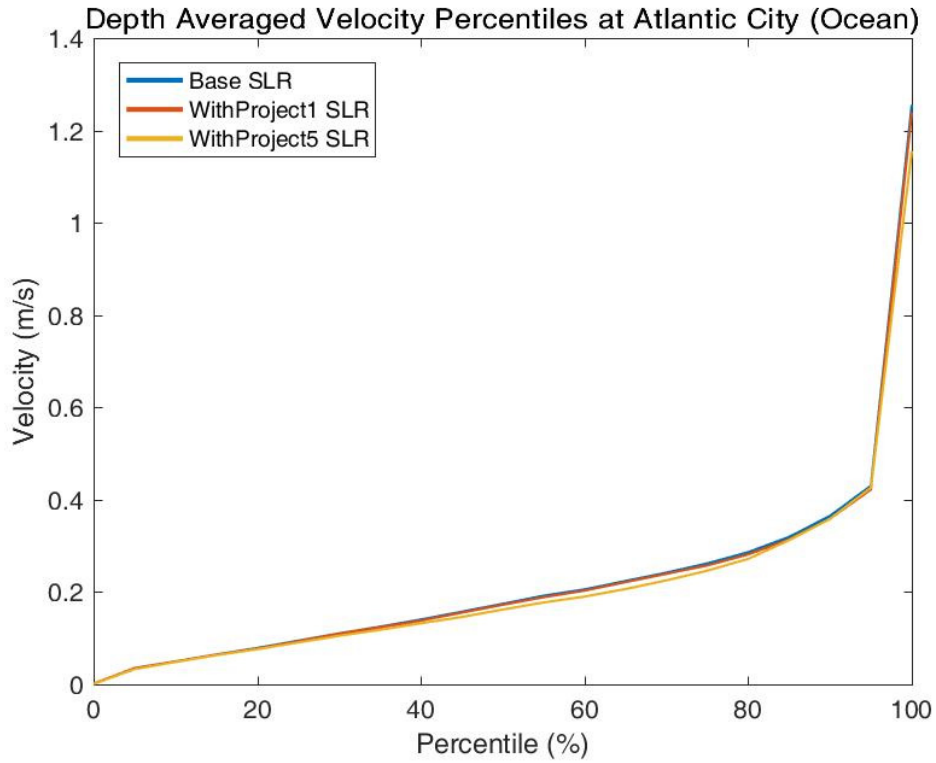


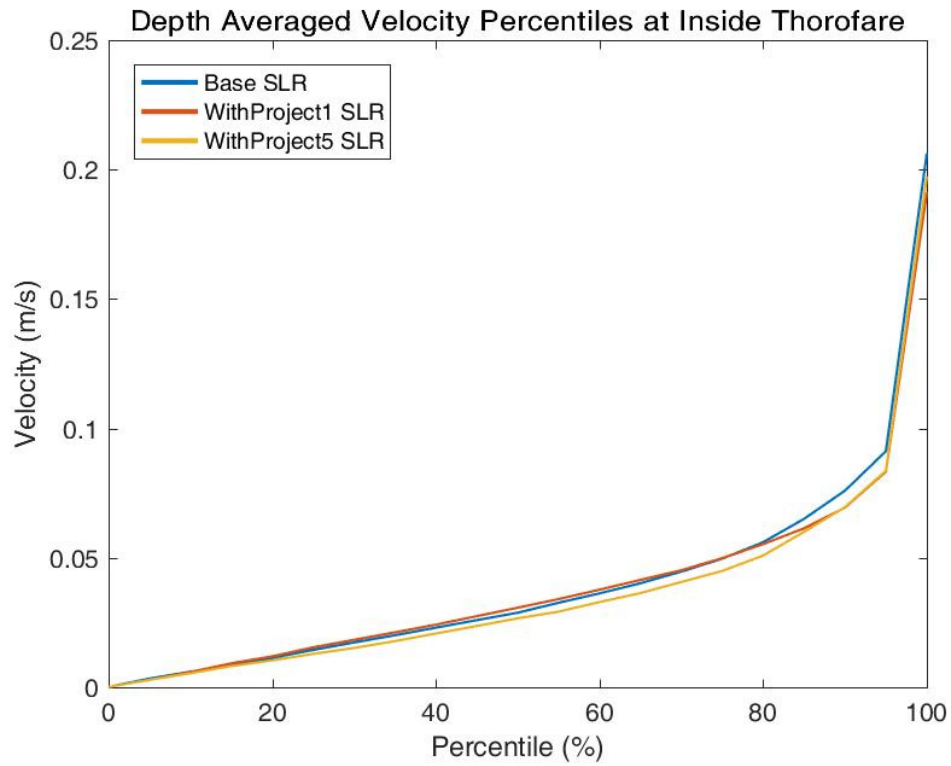
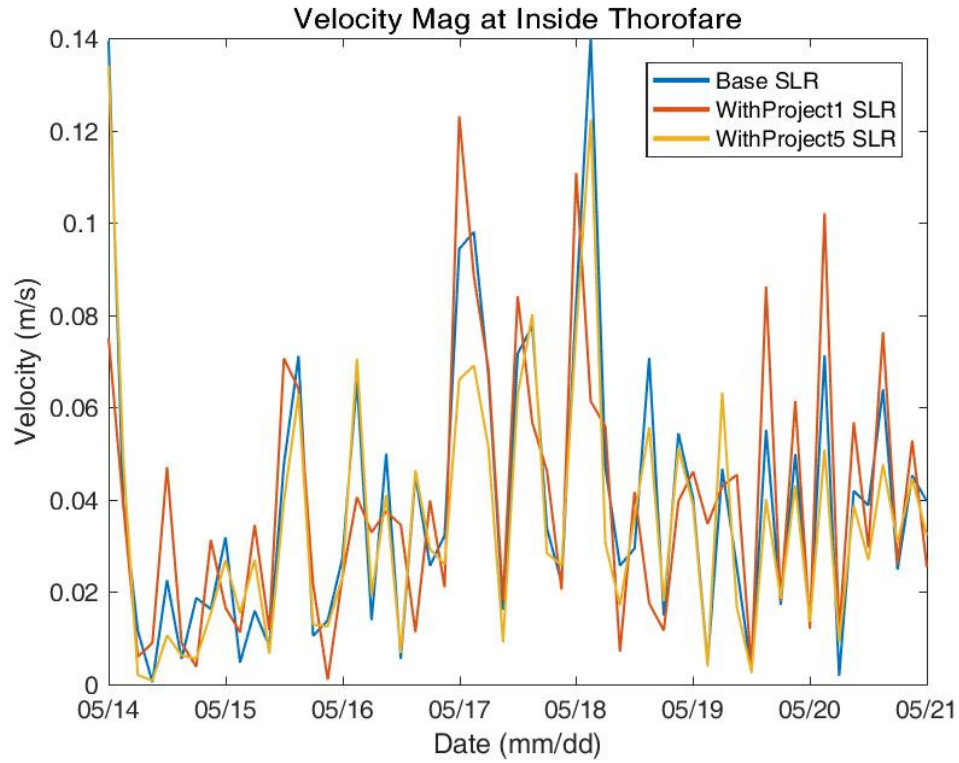


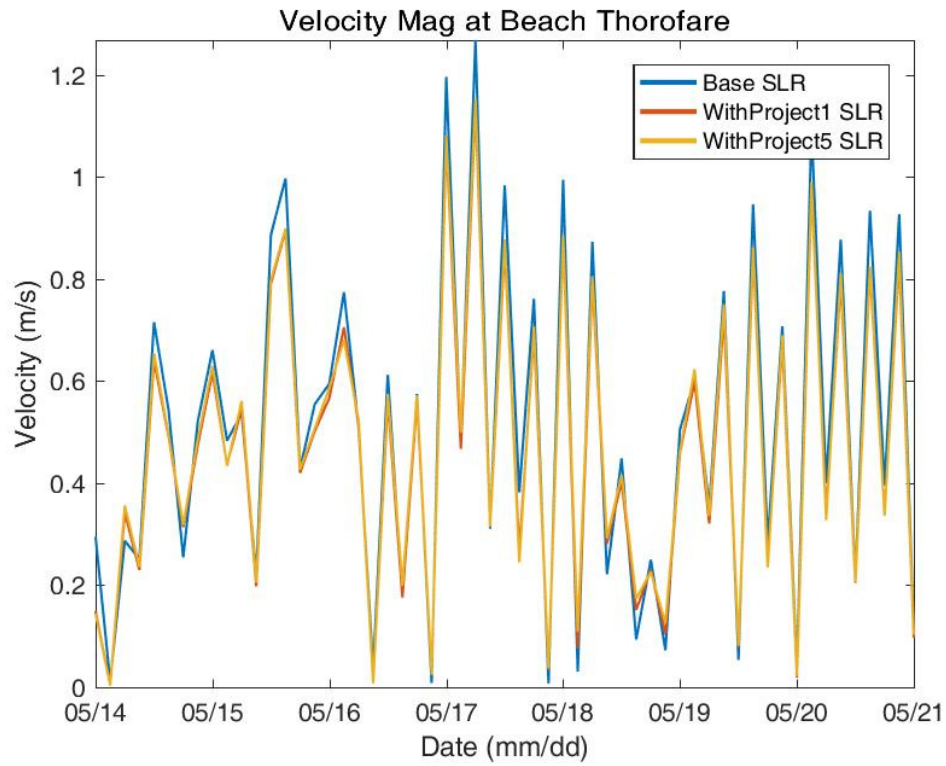
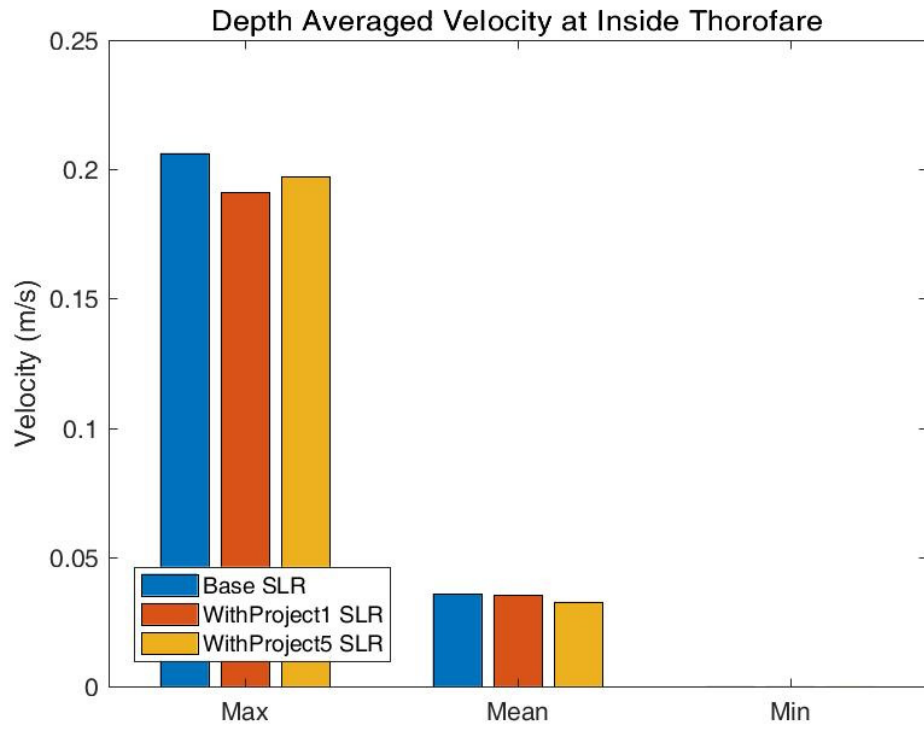


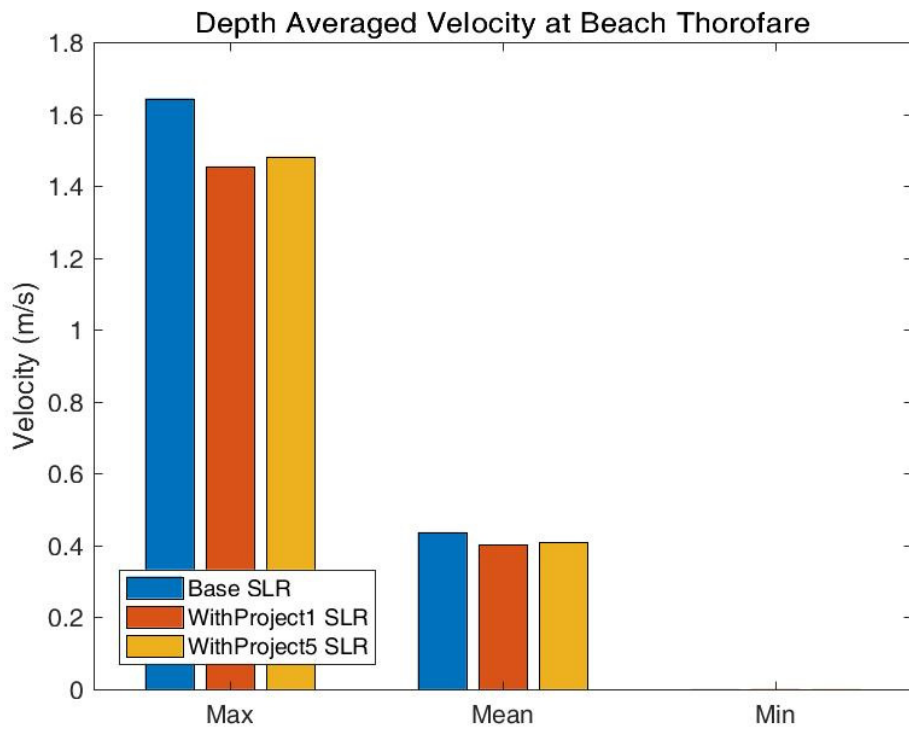
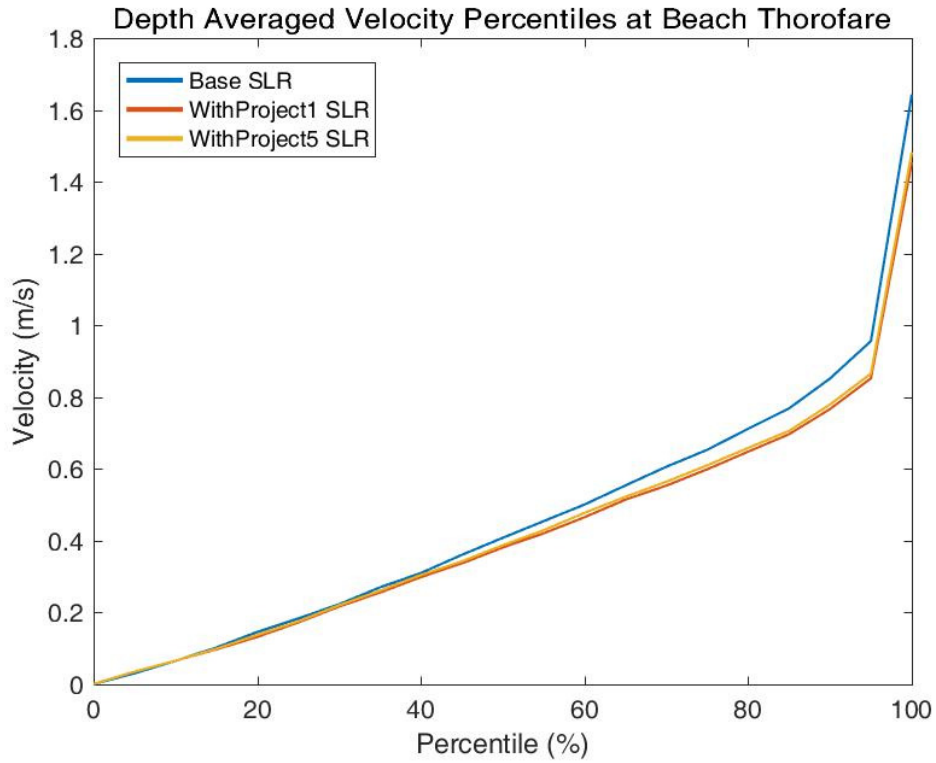


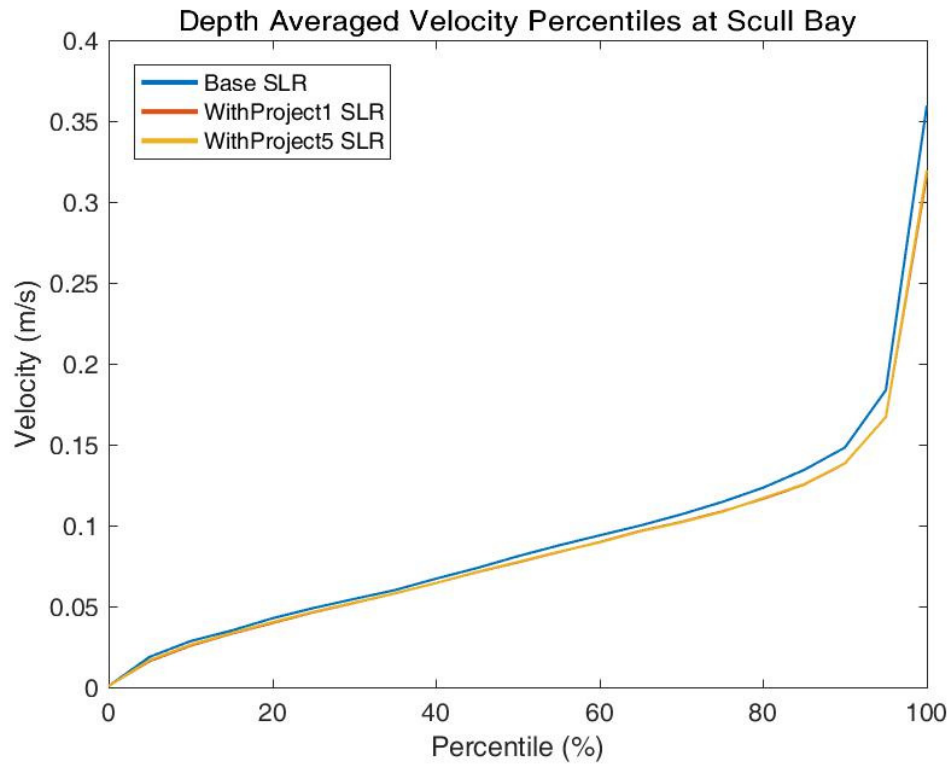
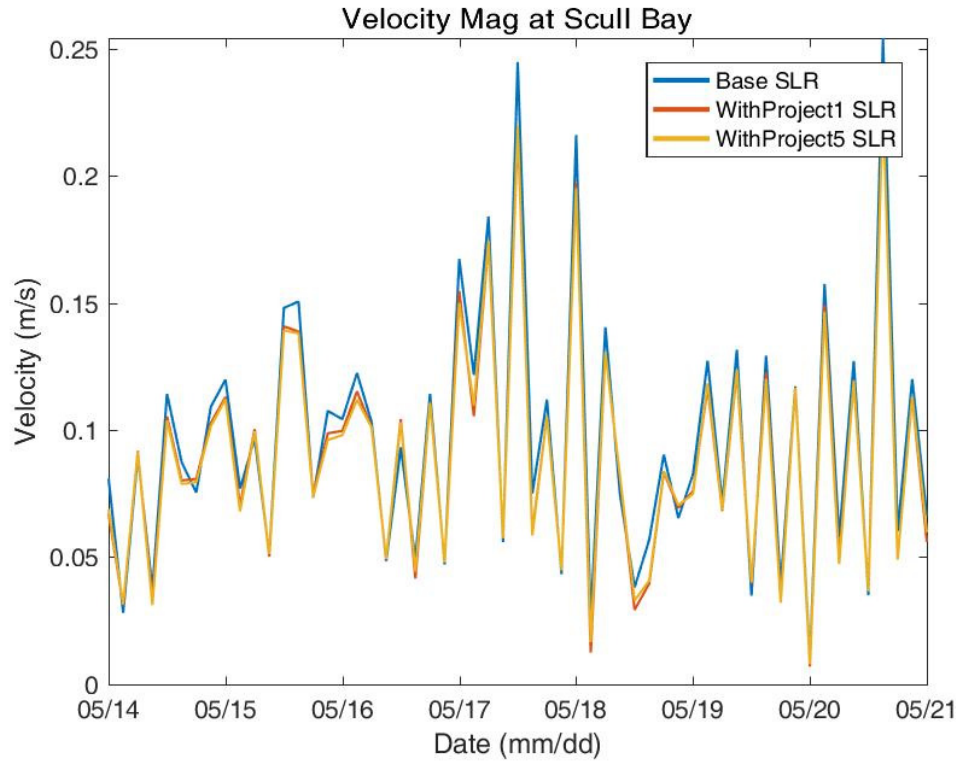


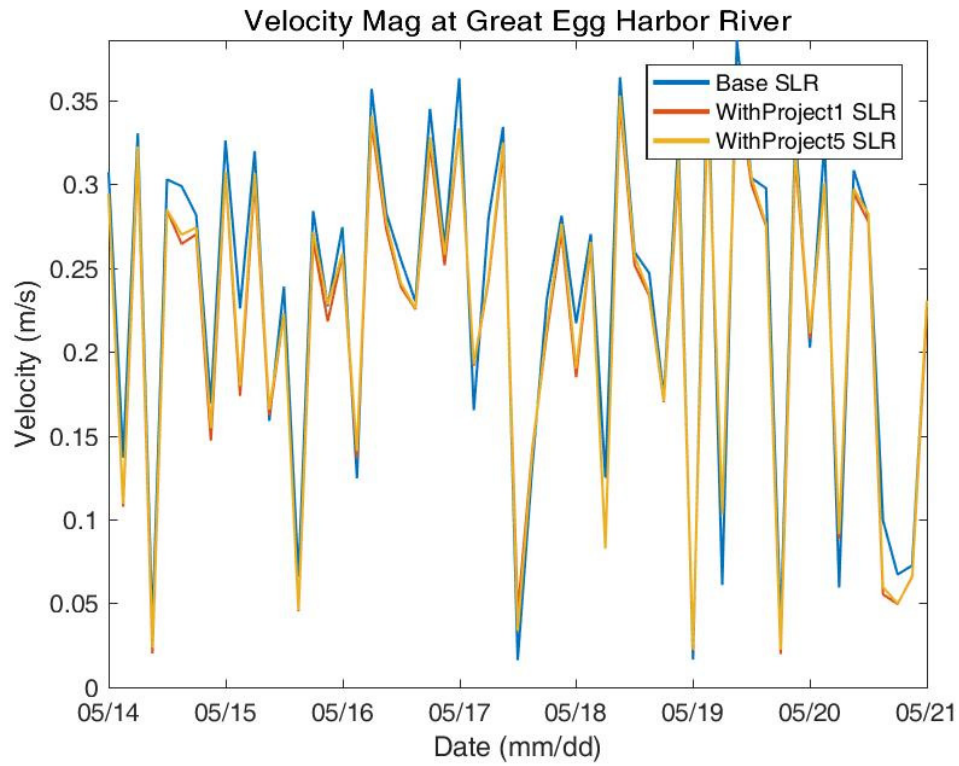
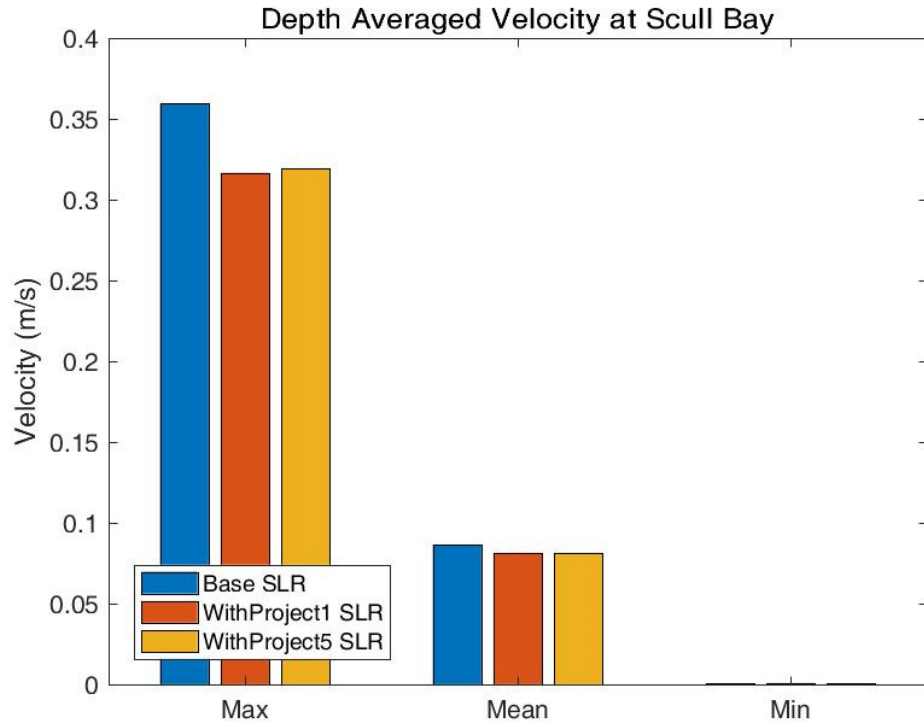


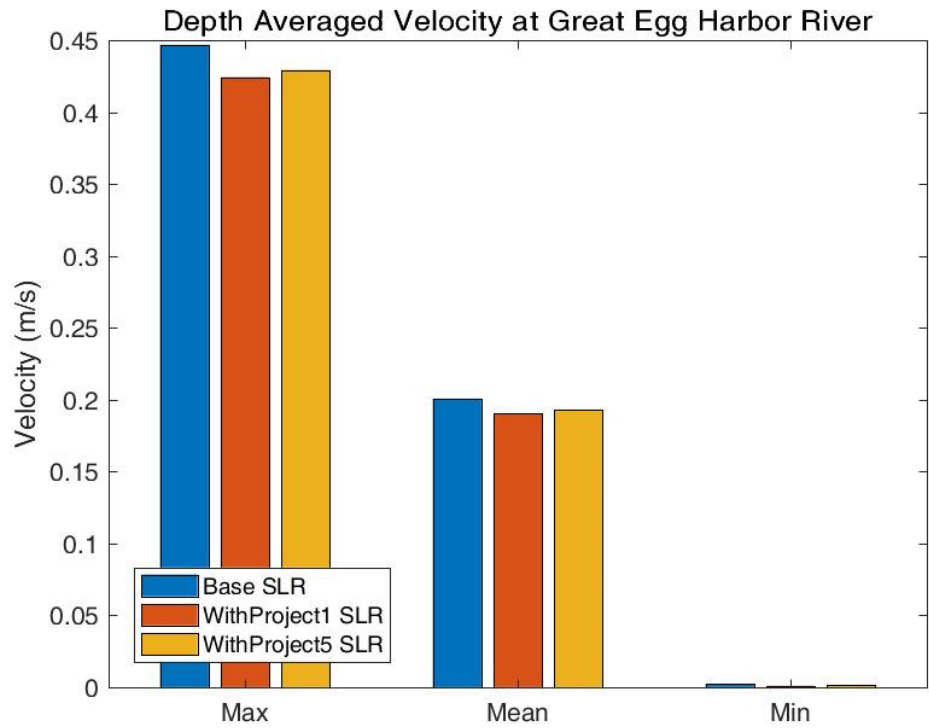
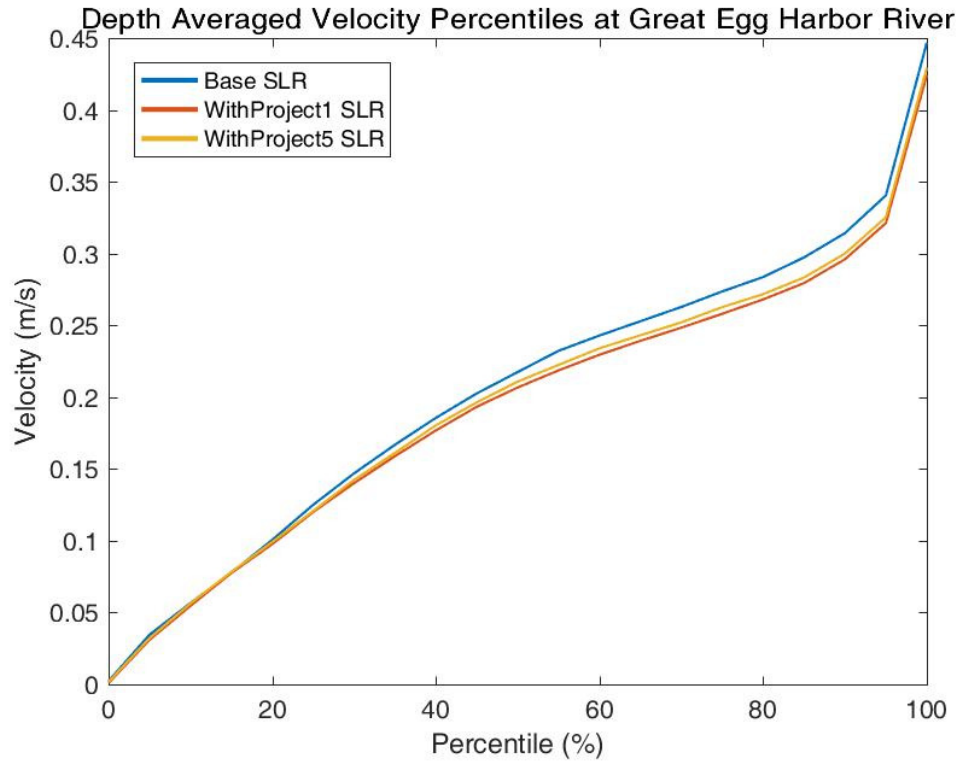


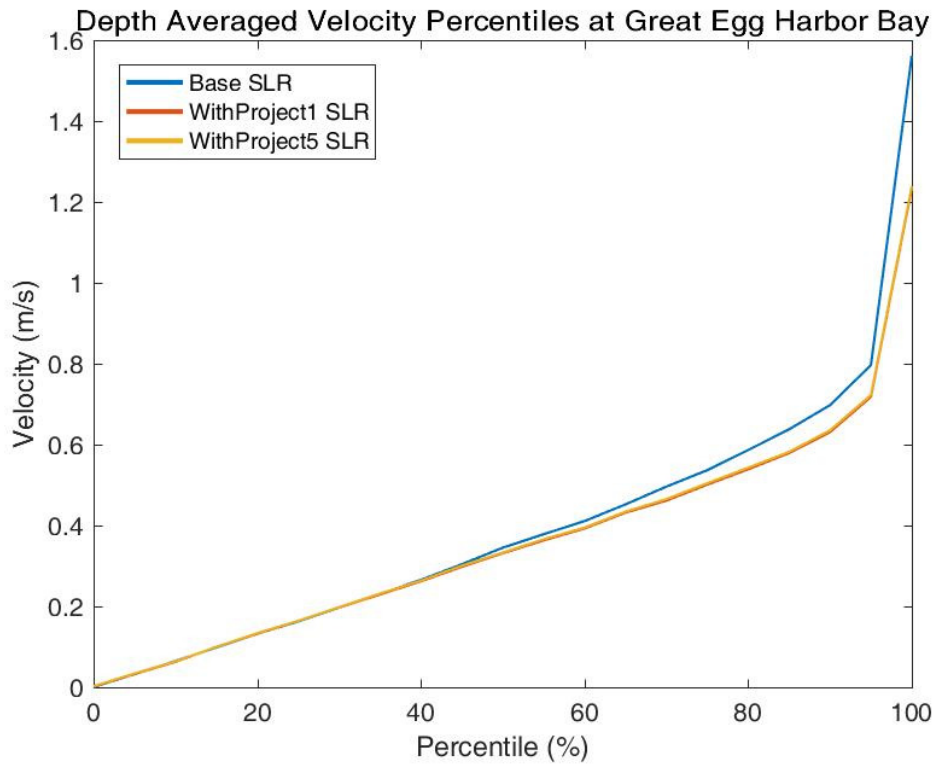
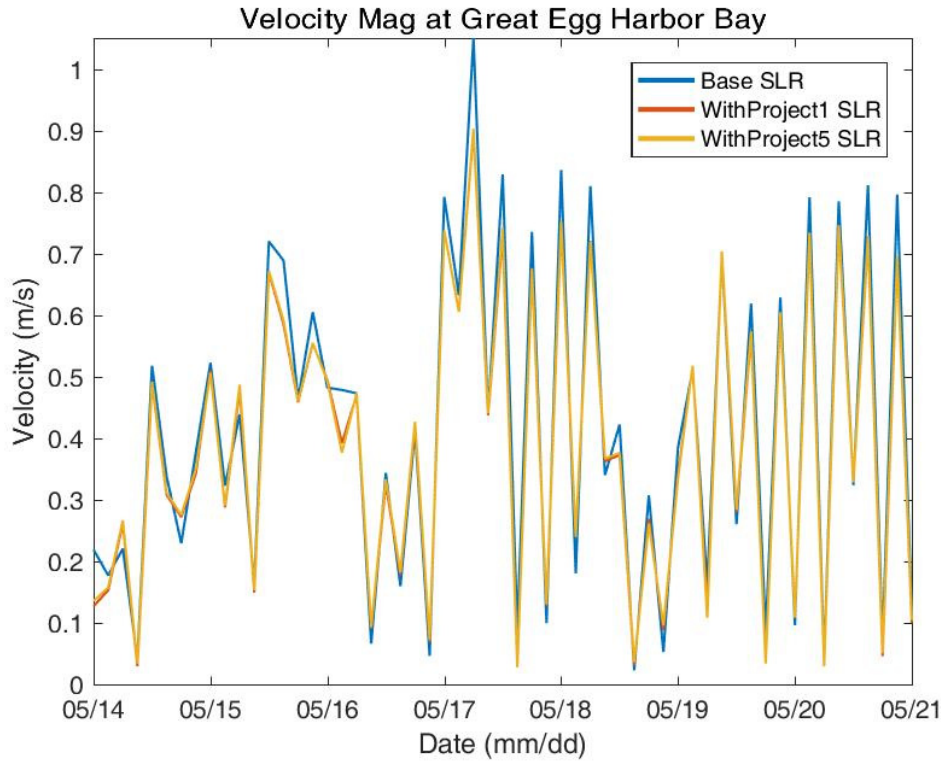


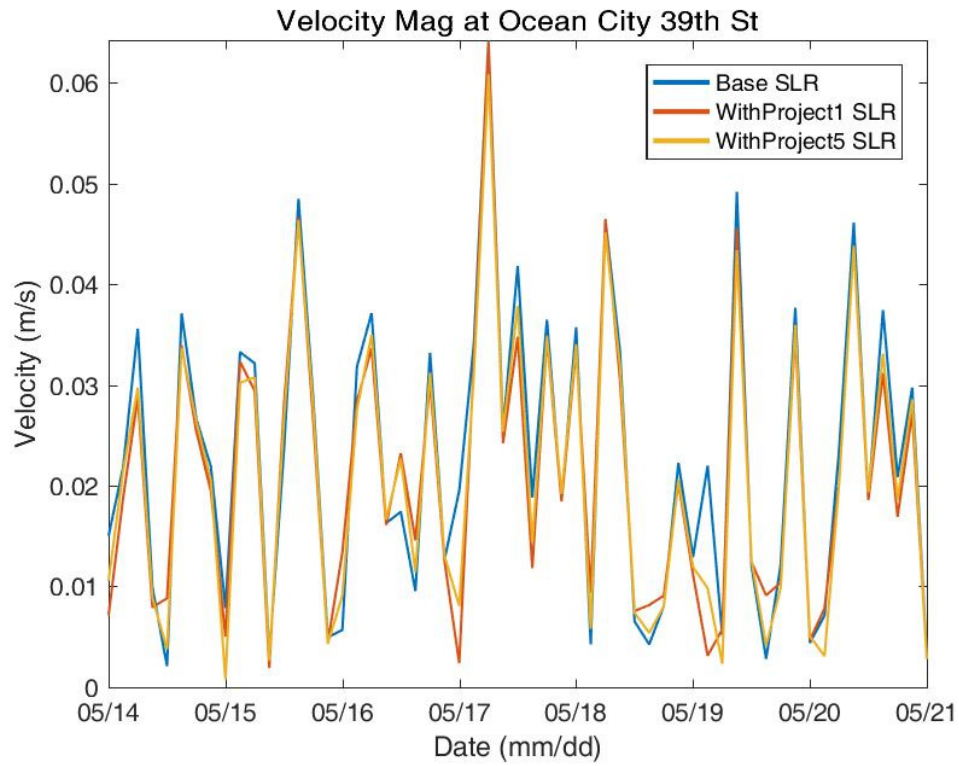
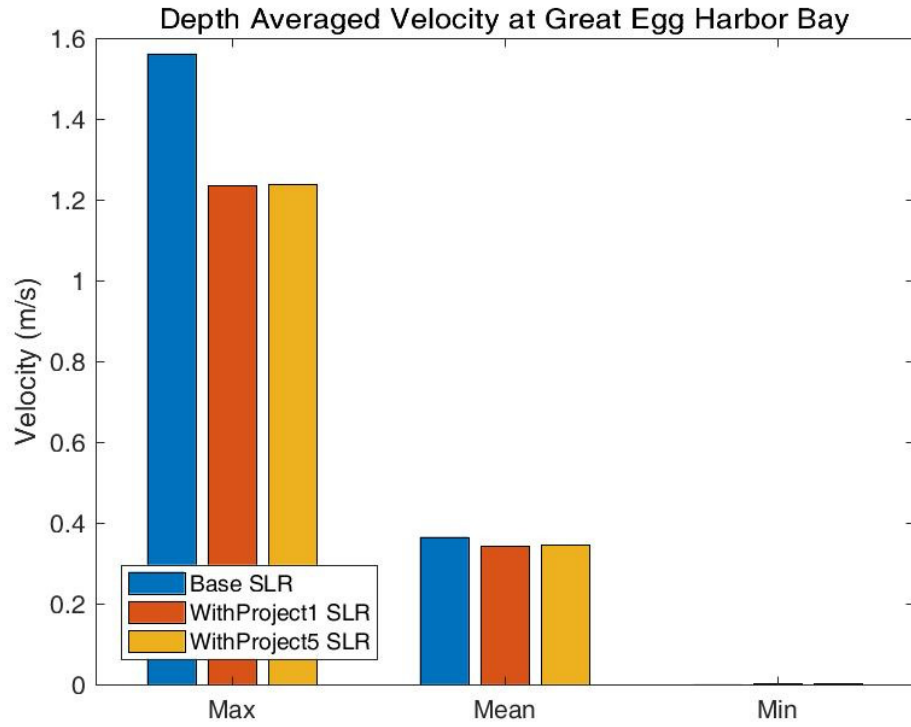


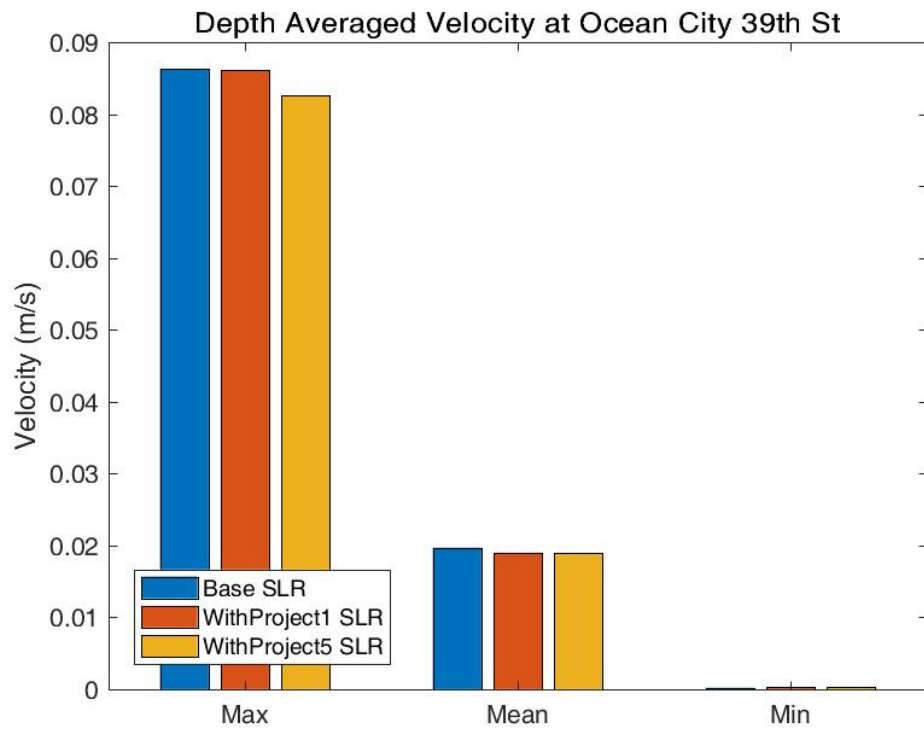
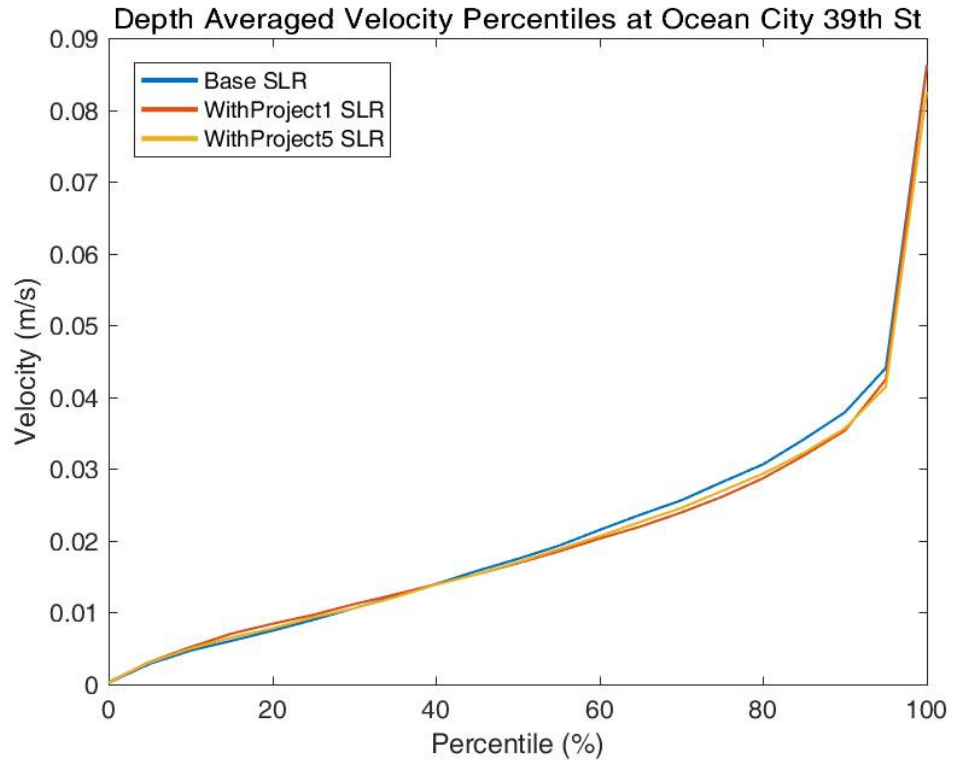


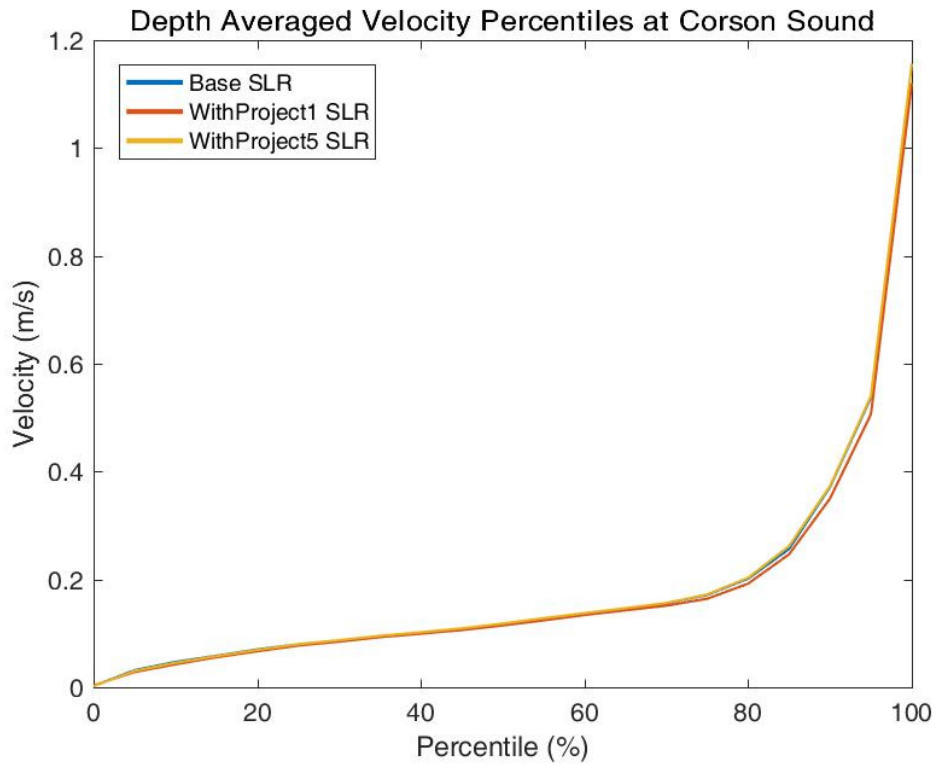
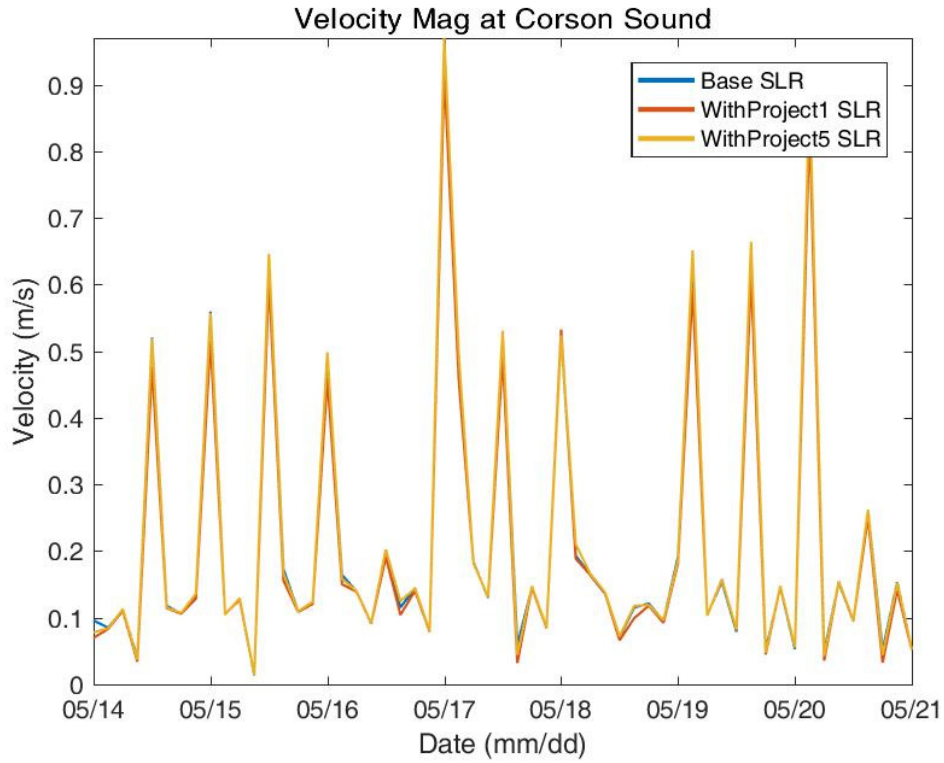


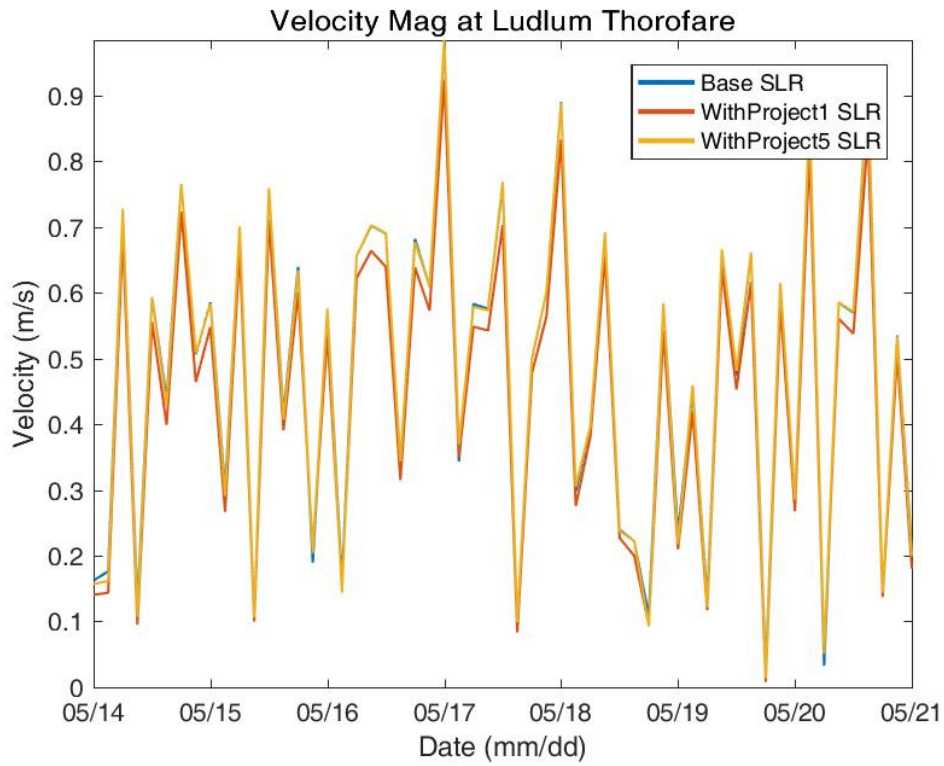
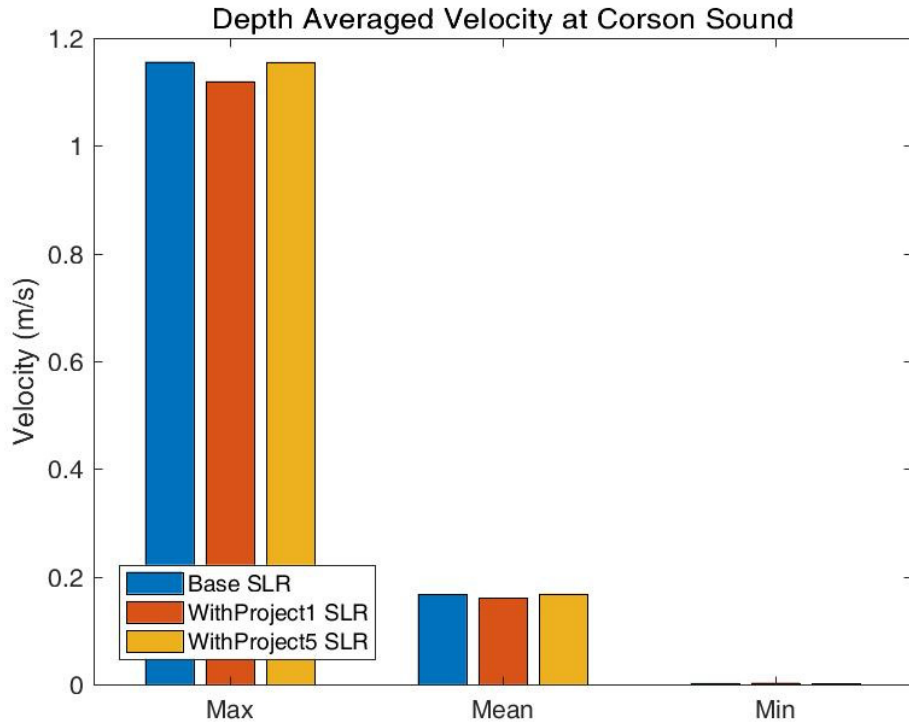


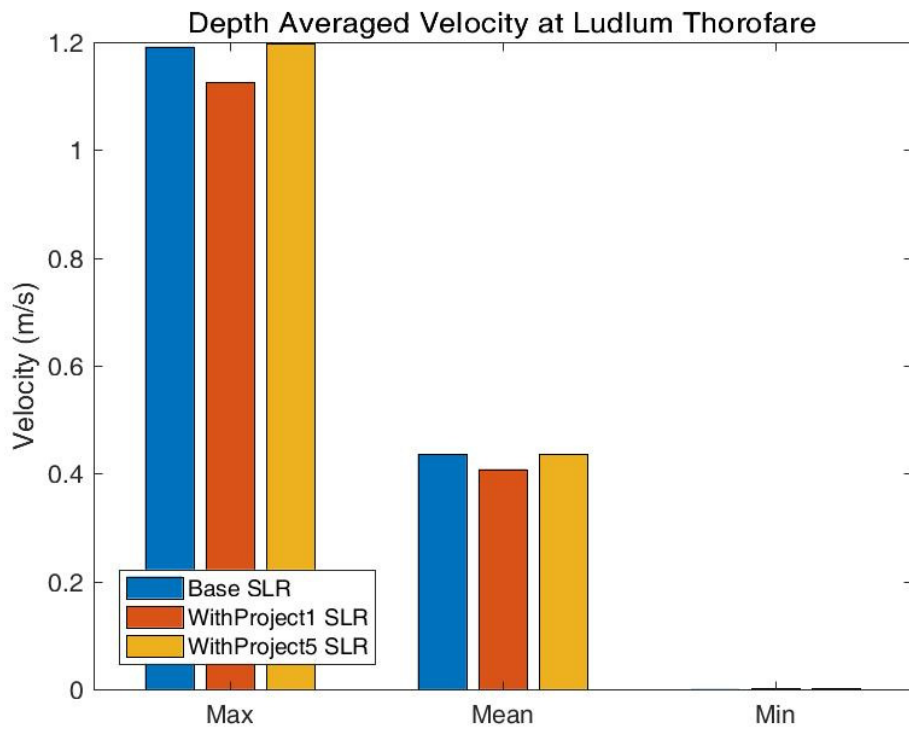
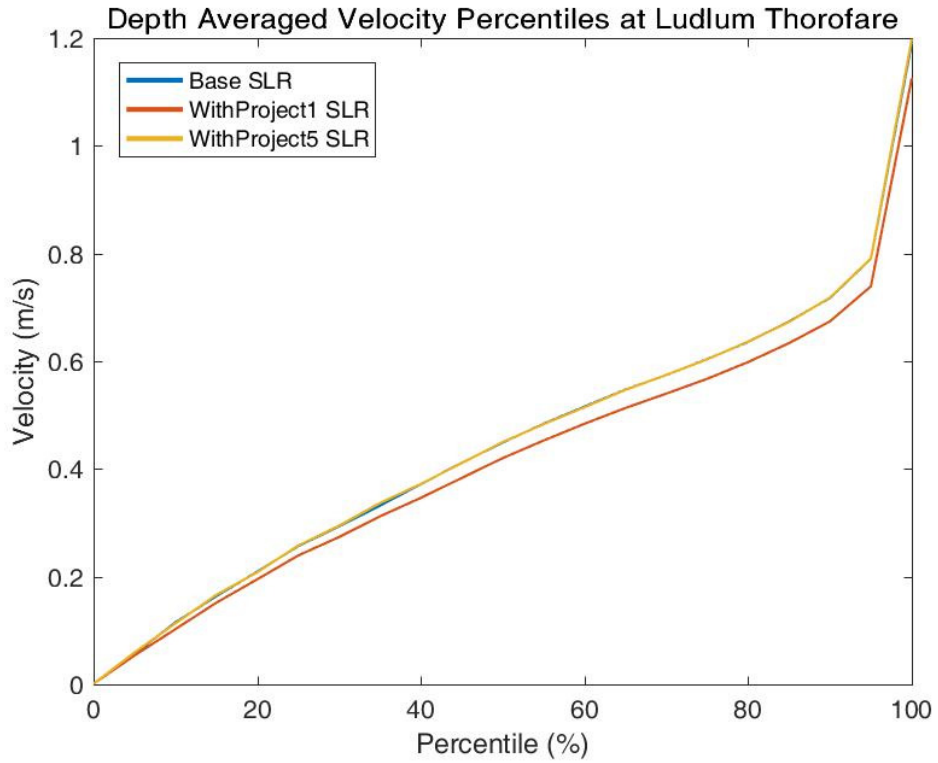


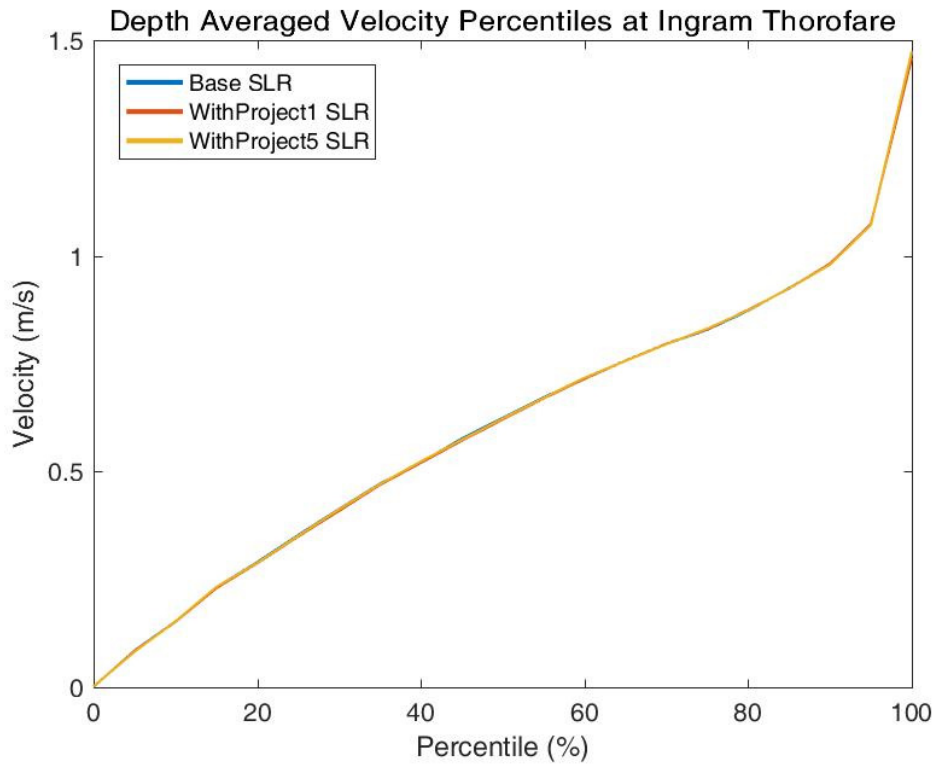
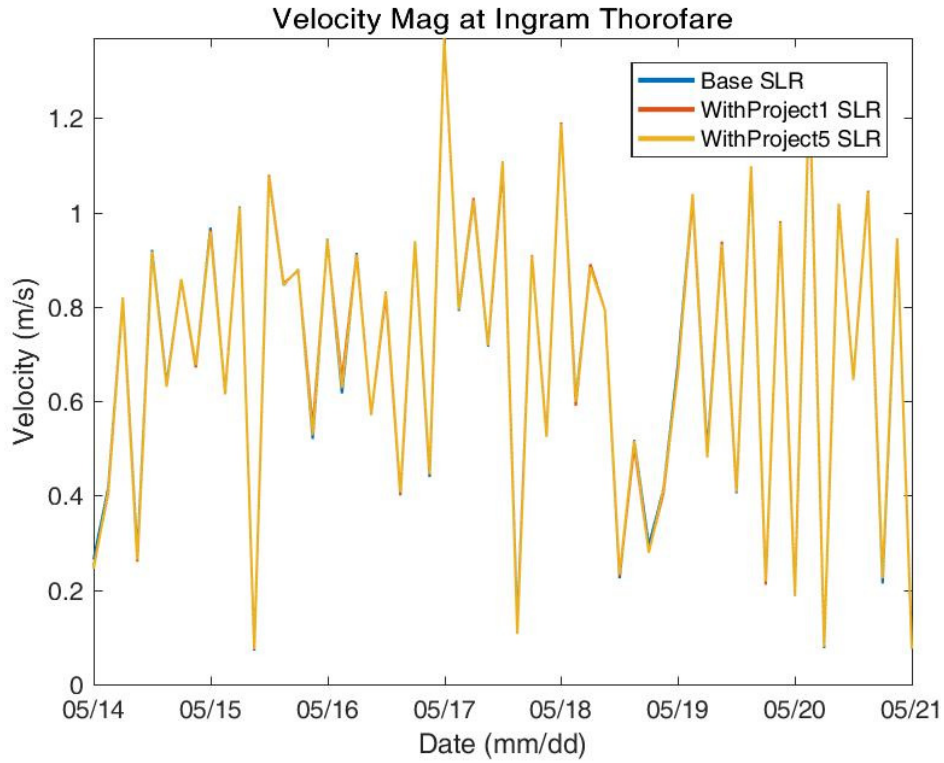


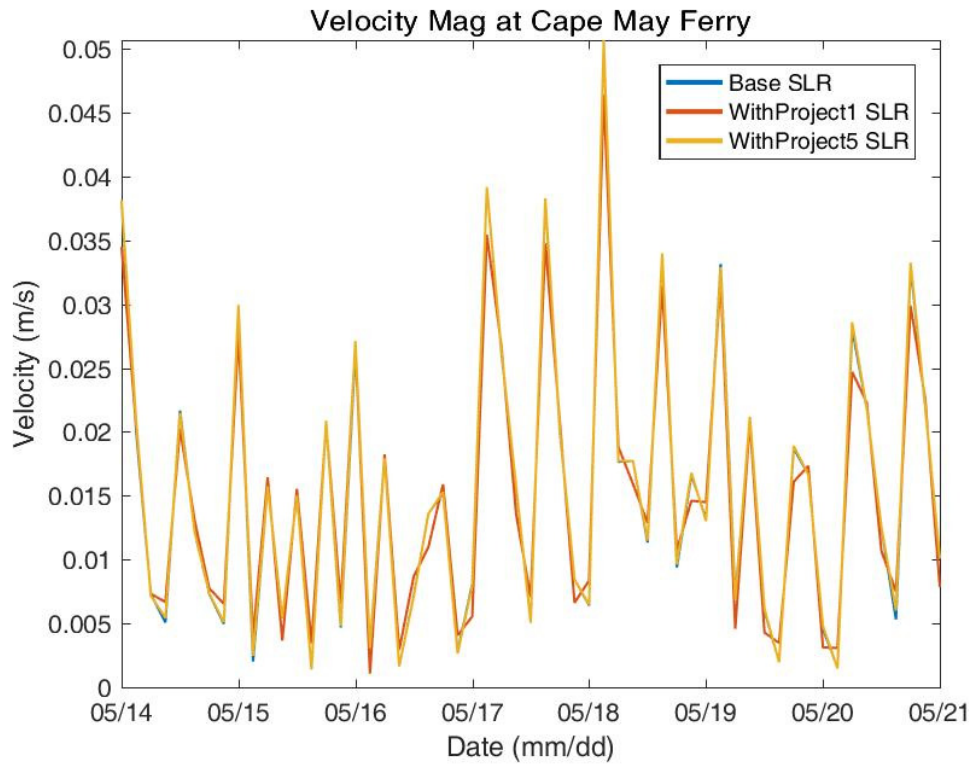
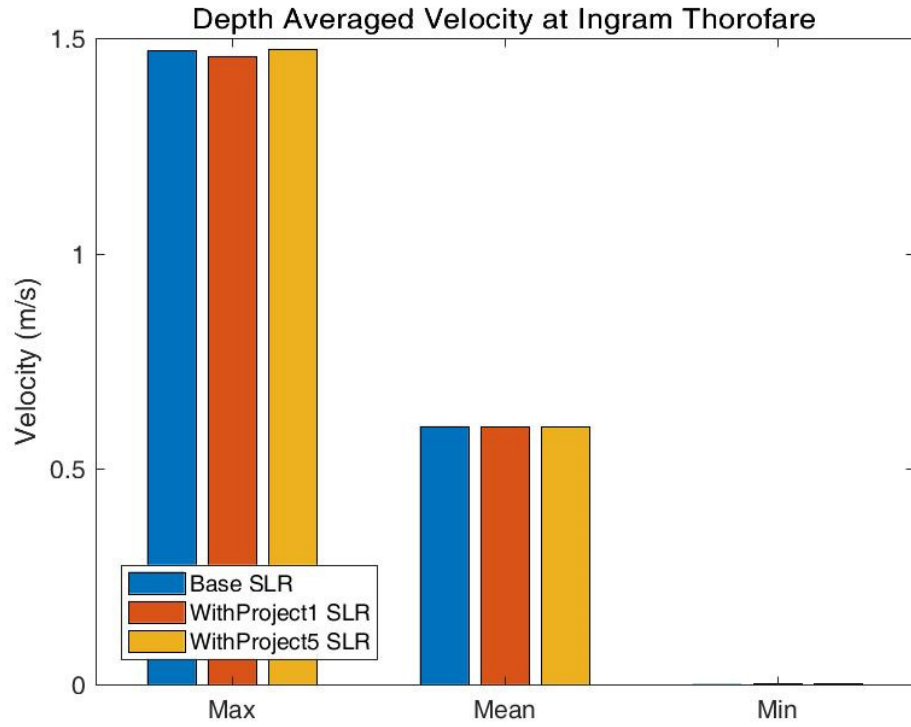


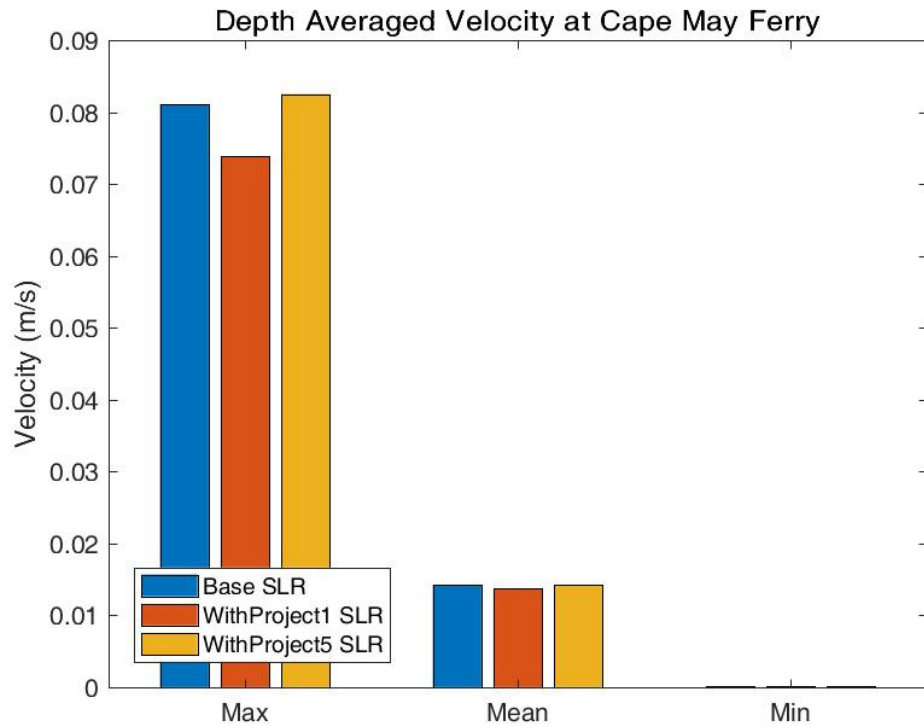
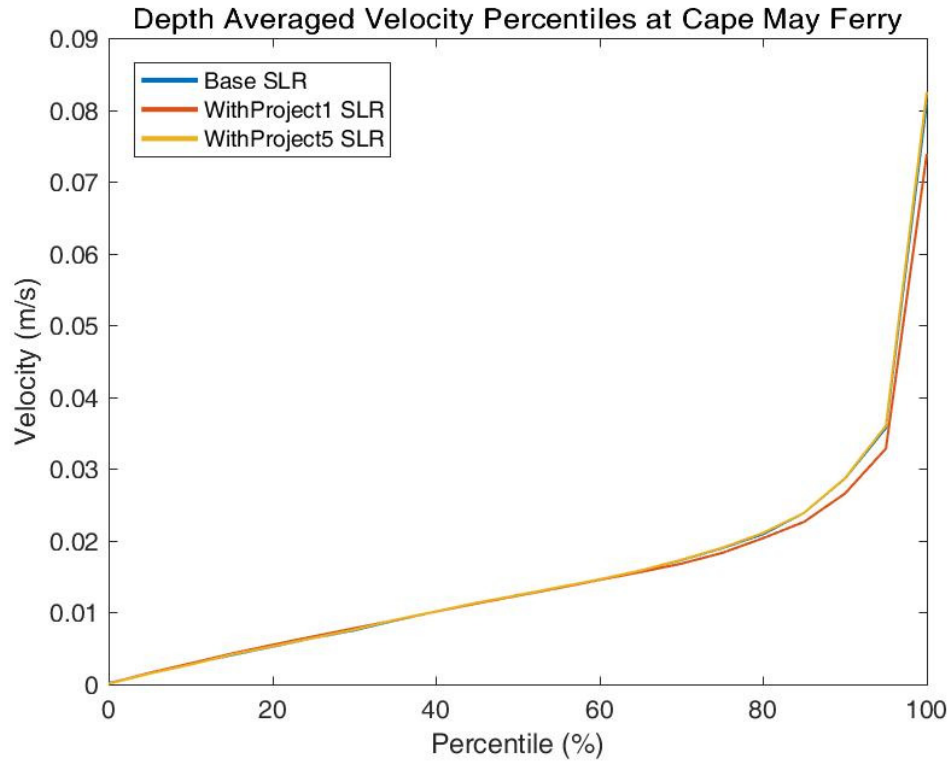


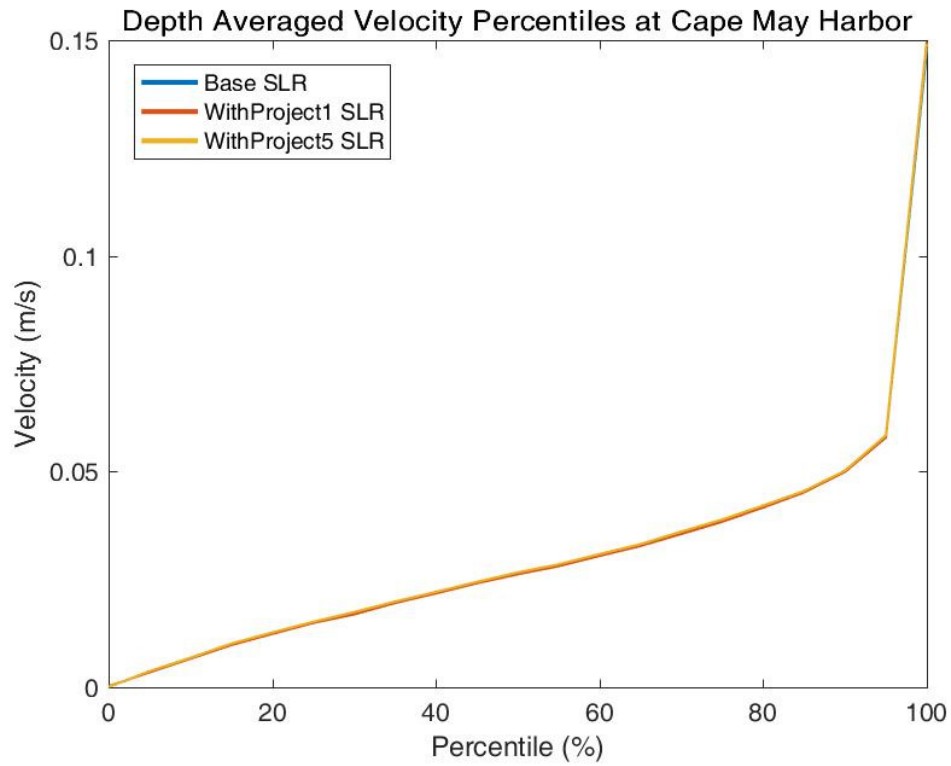
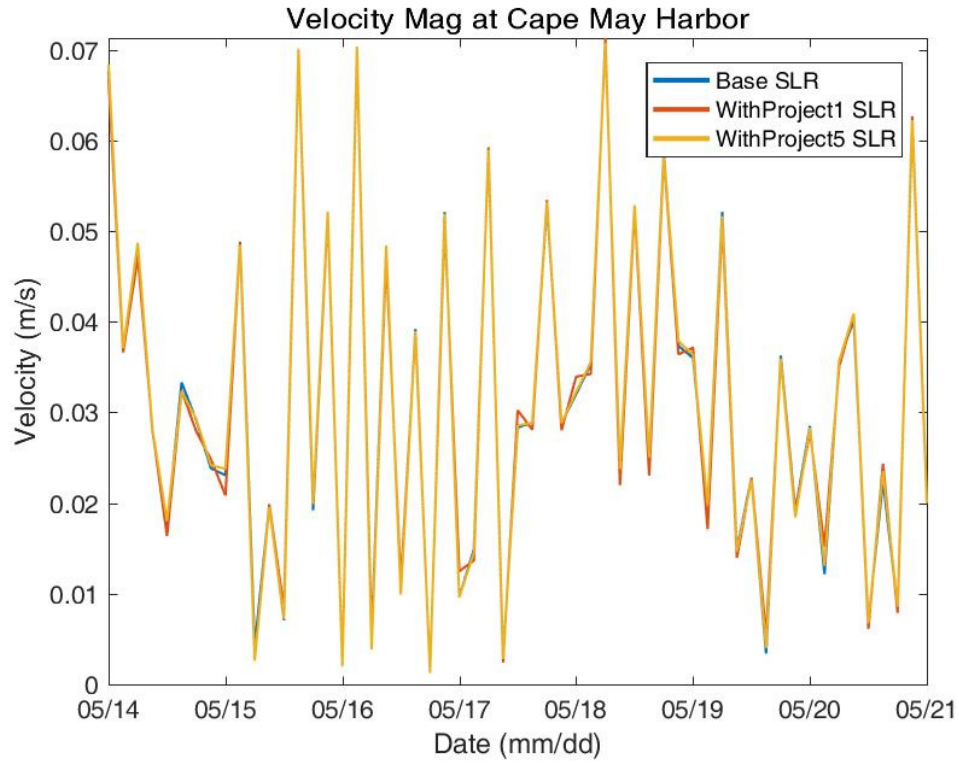


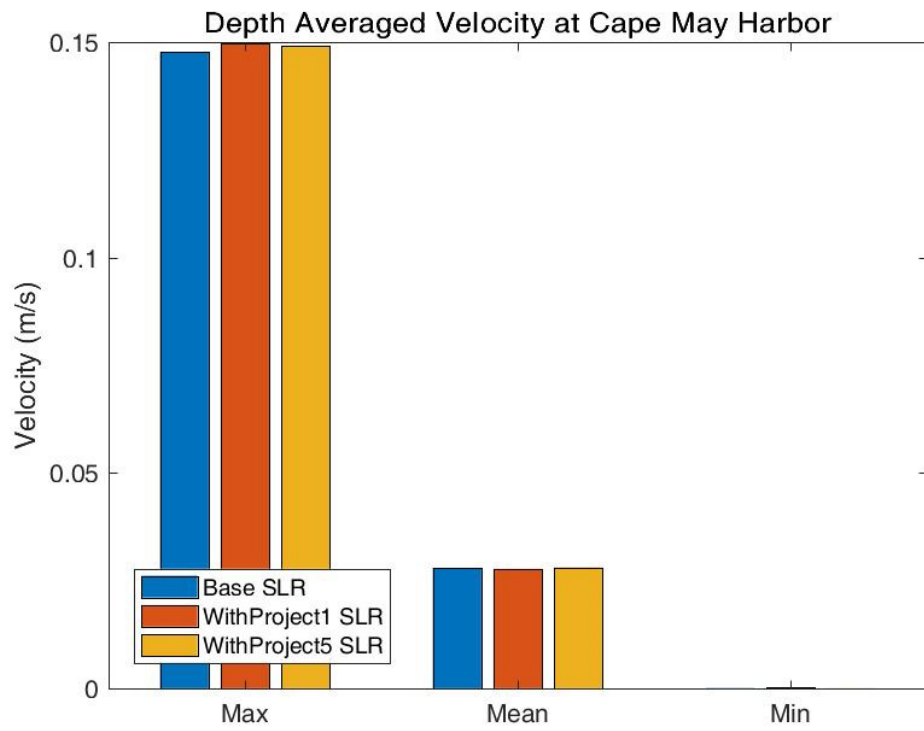






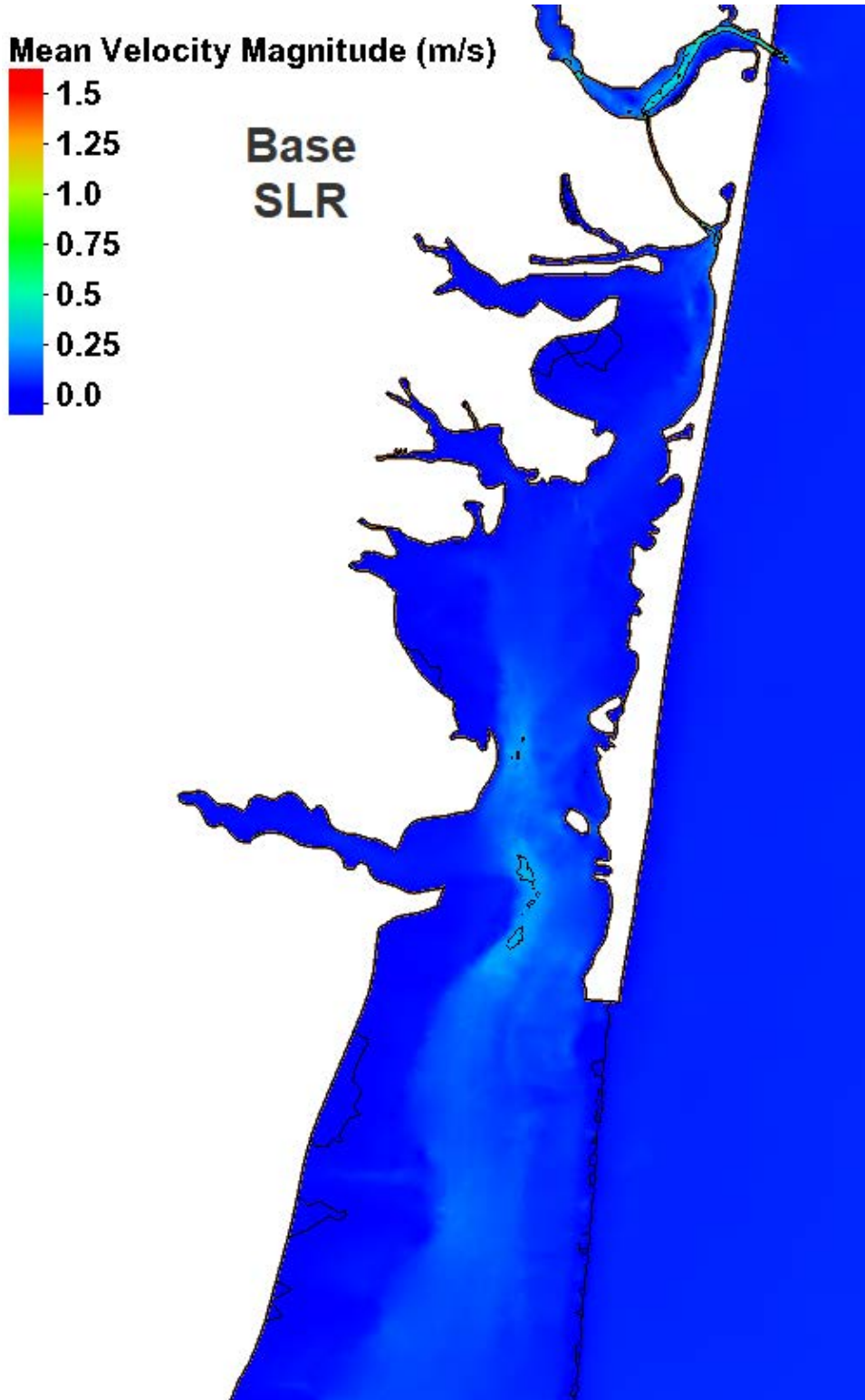


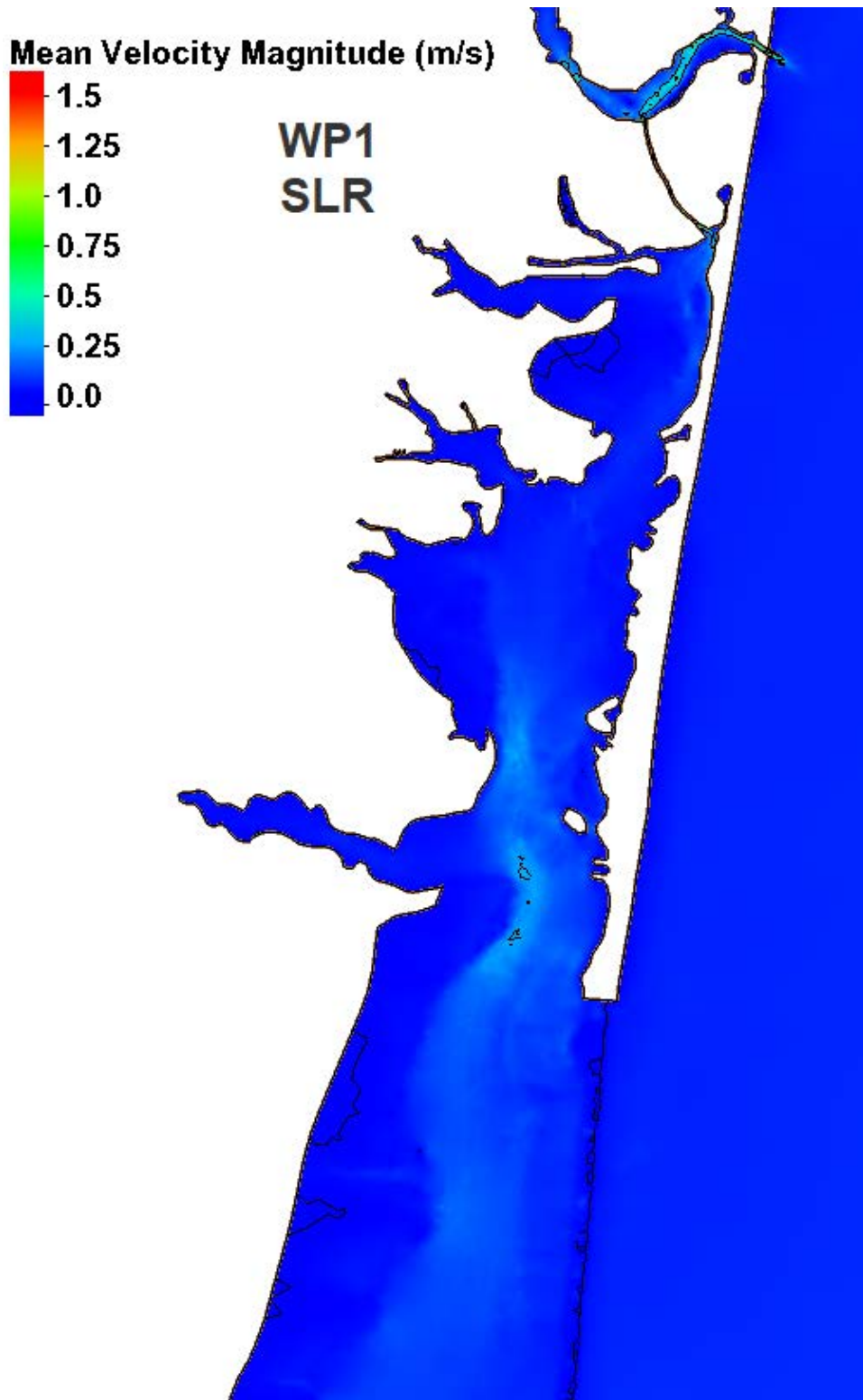


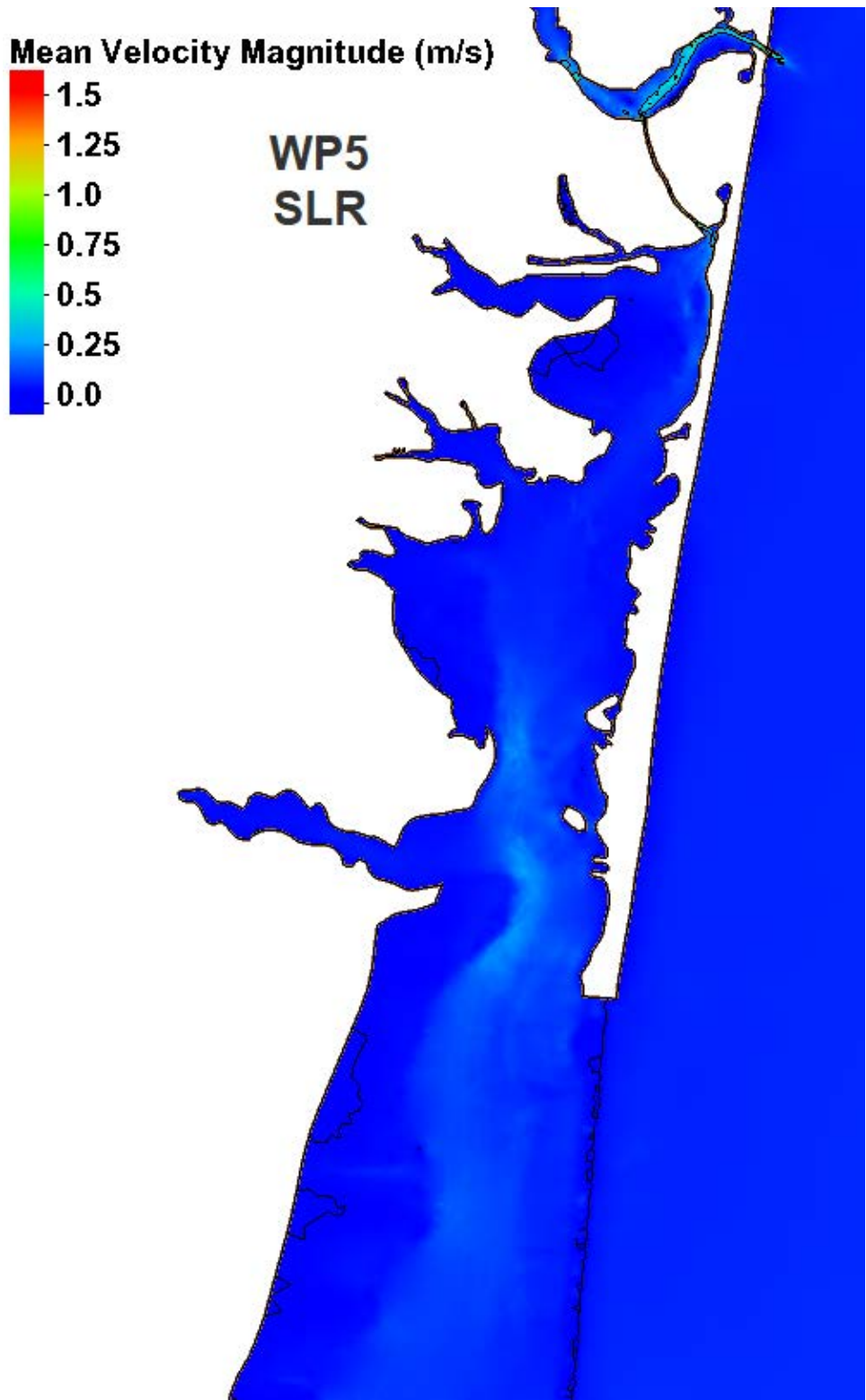


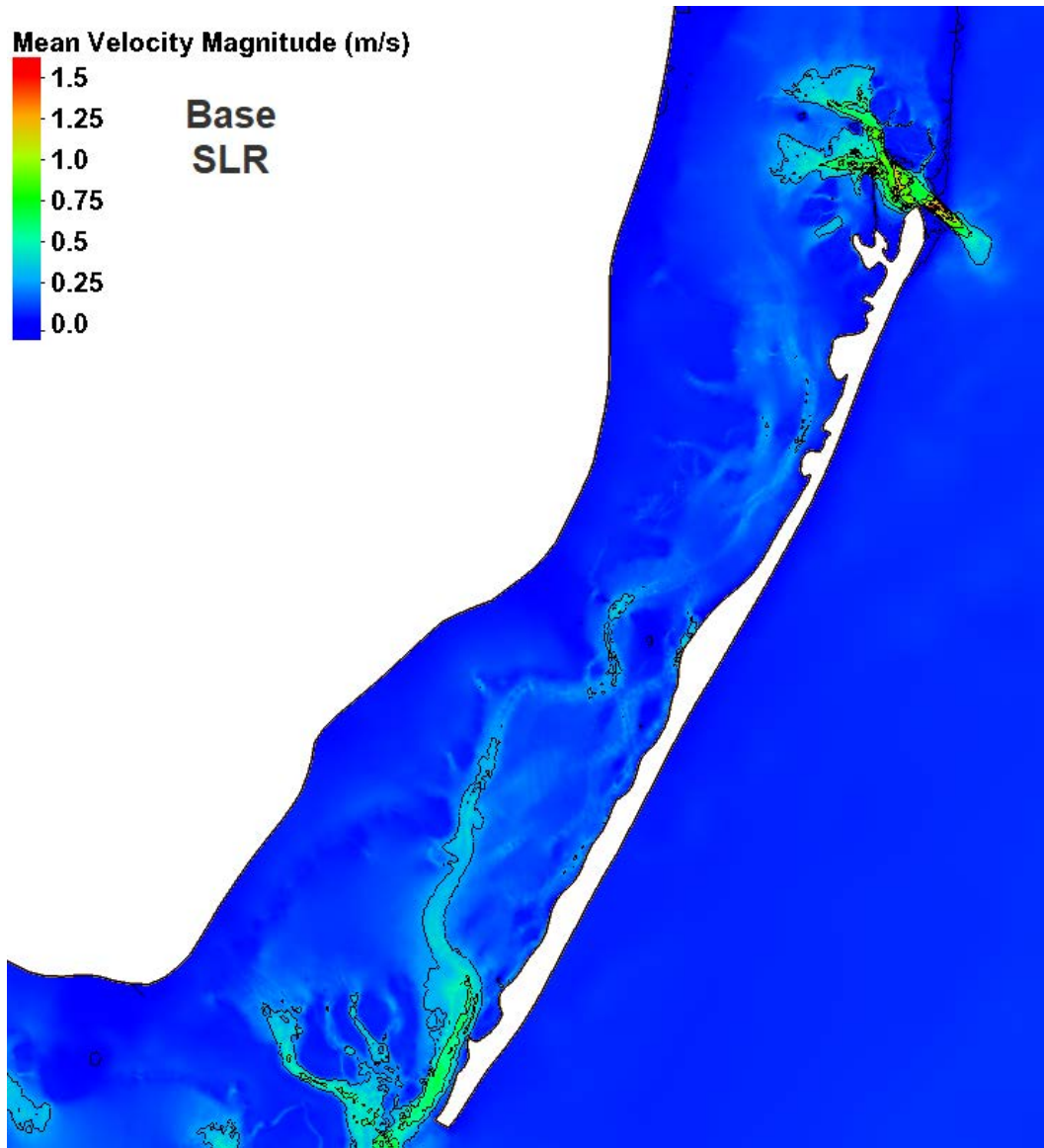
Regional Mean with Sea Level Rise

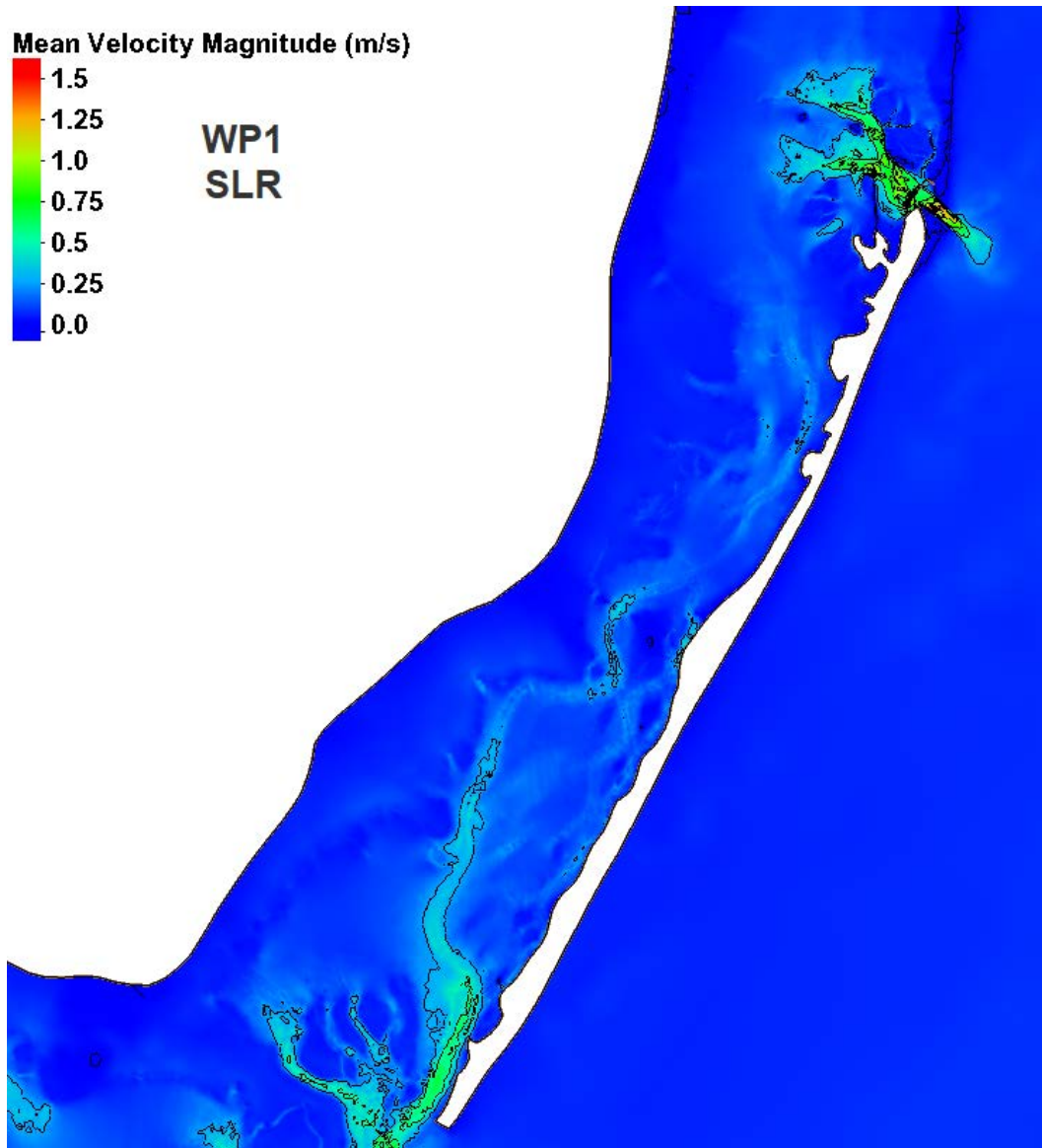
Northern Region (Manasquan and Barnegat)

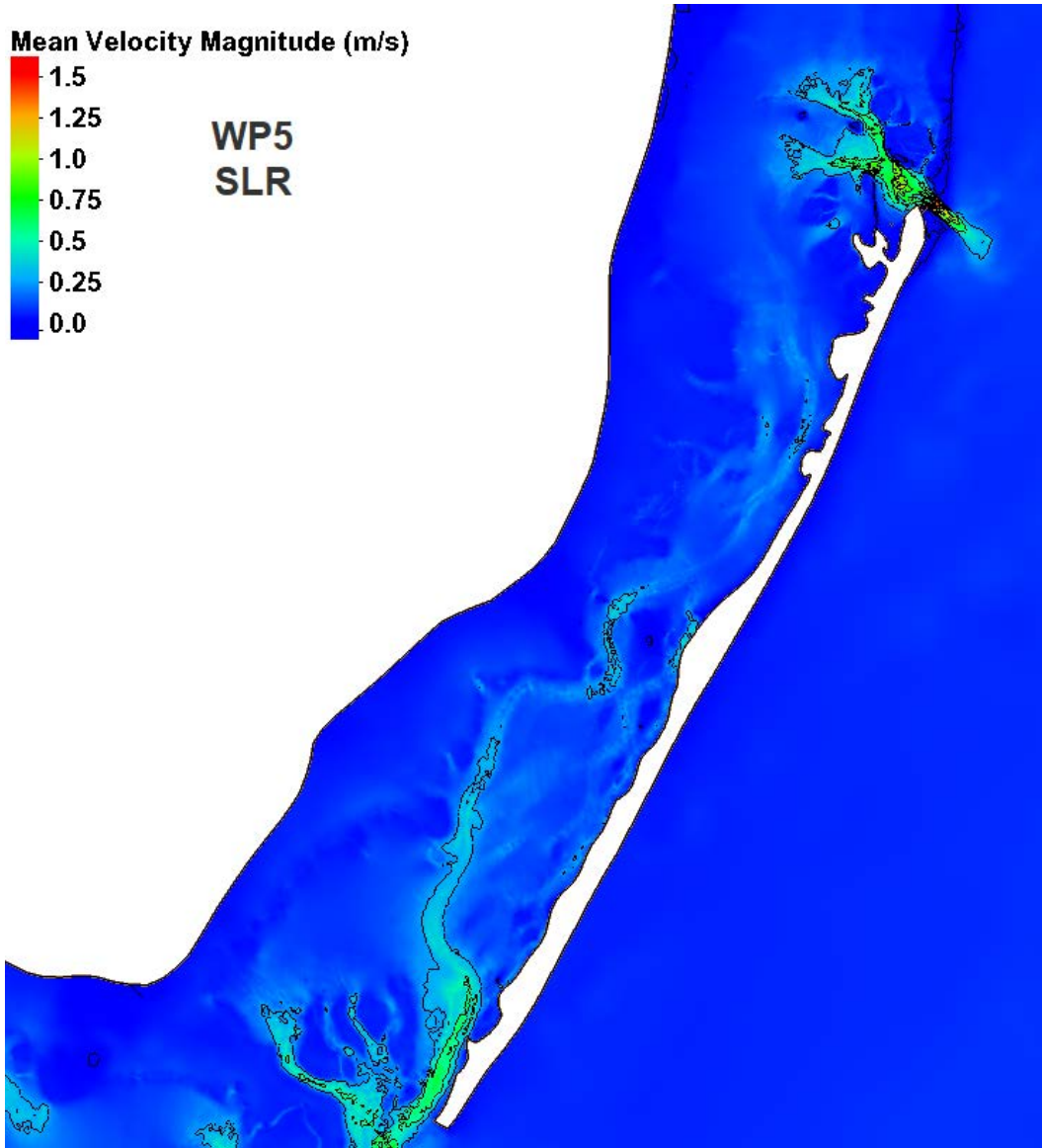




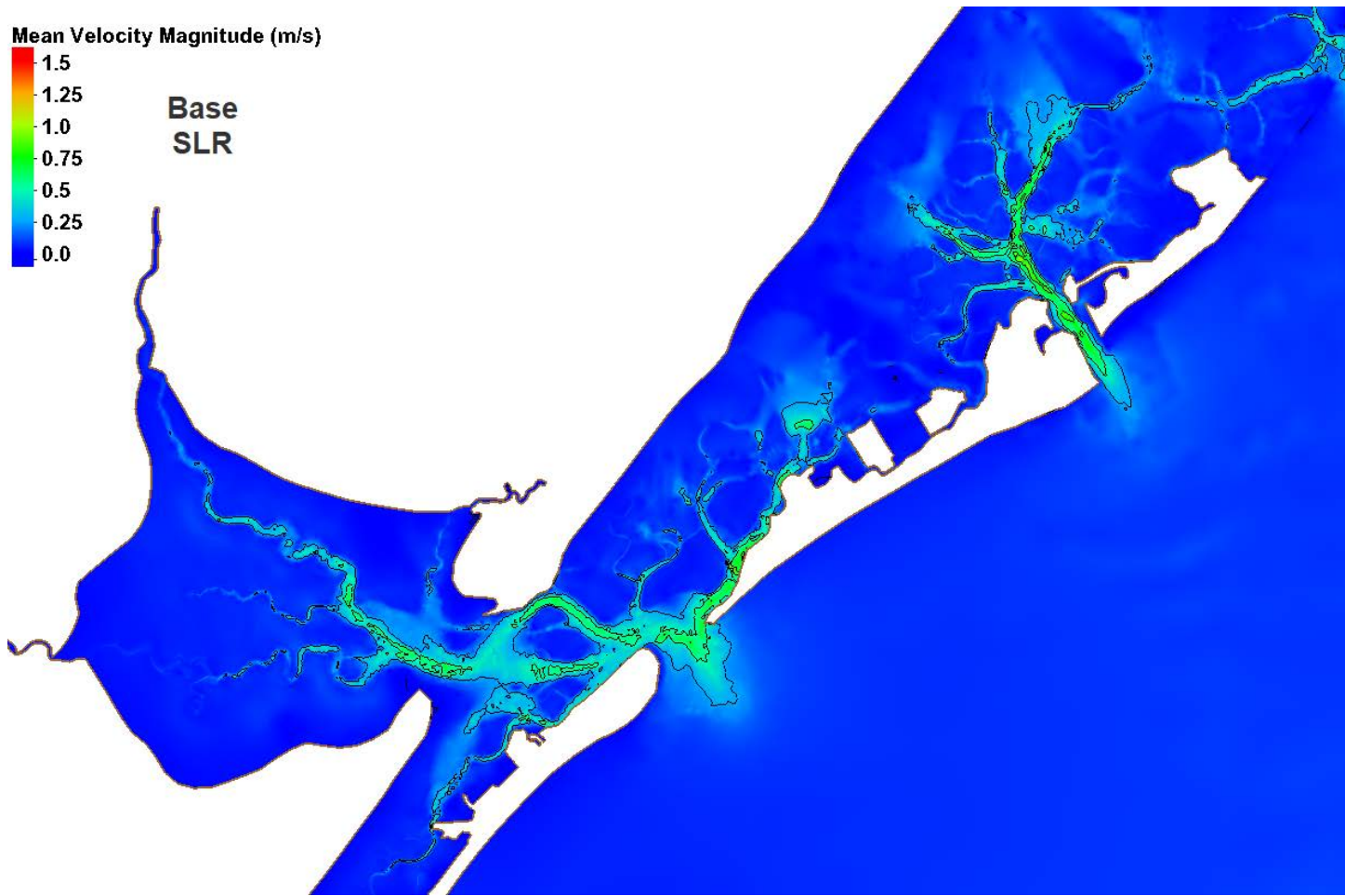


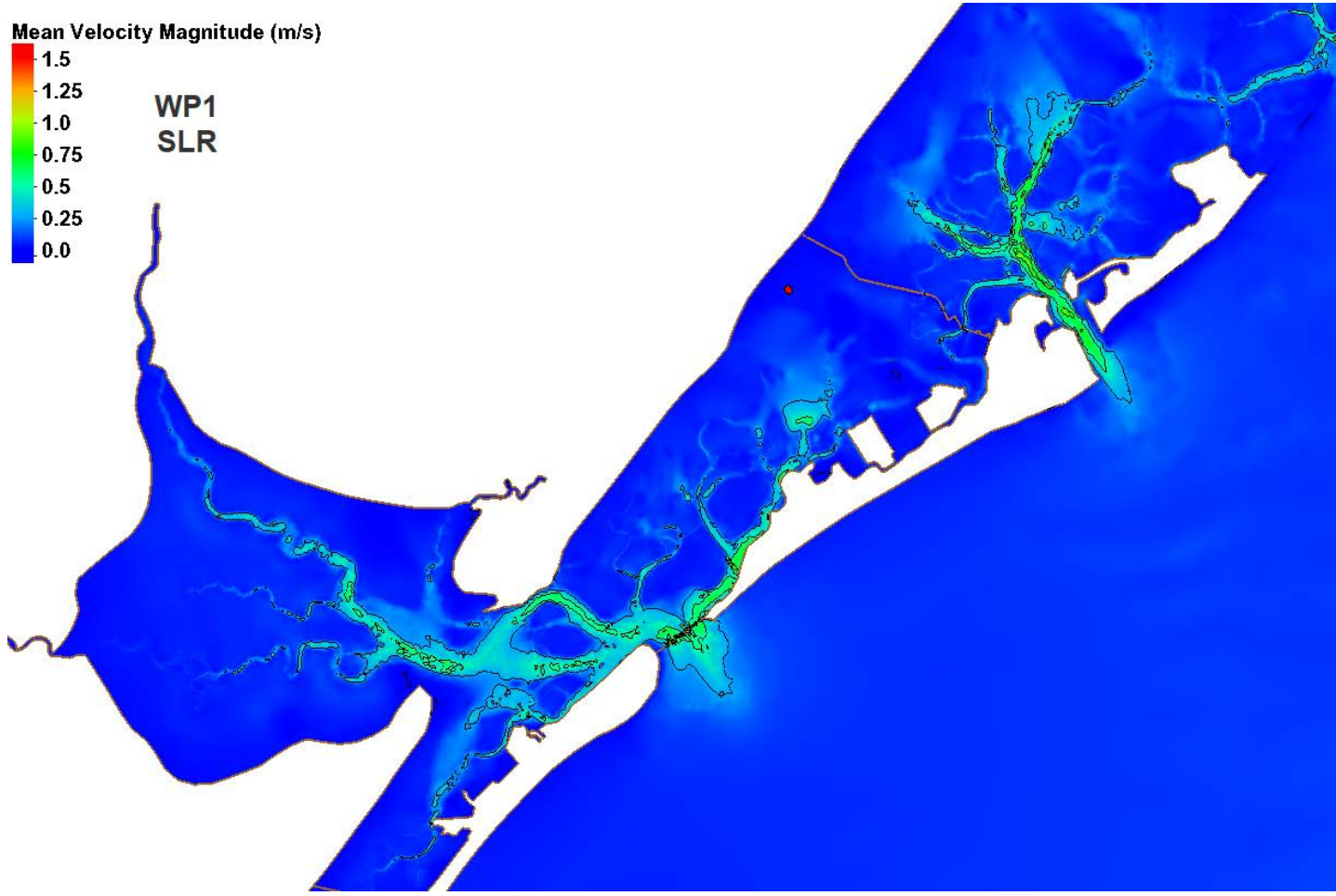


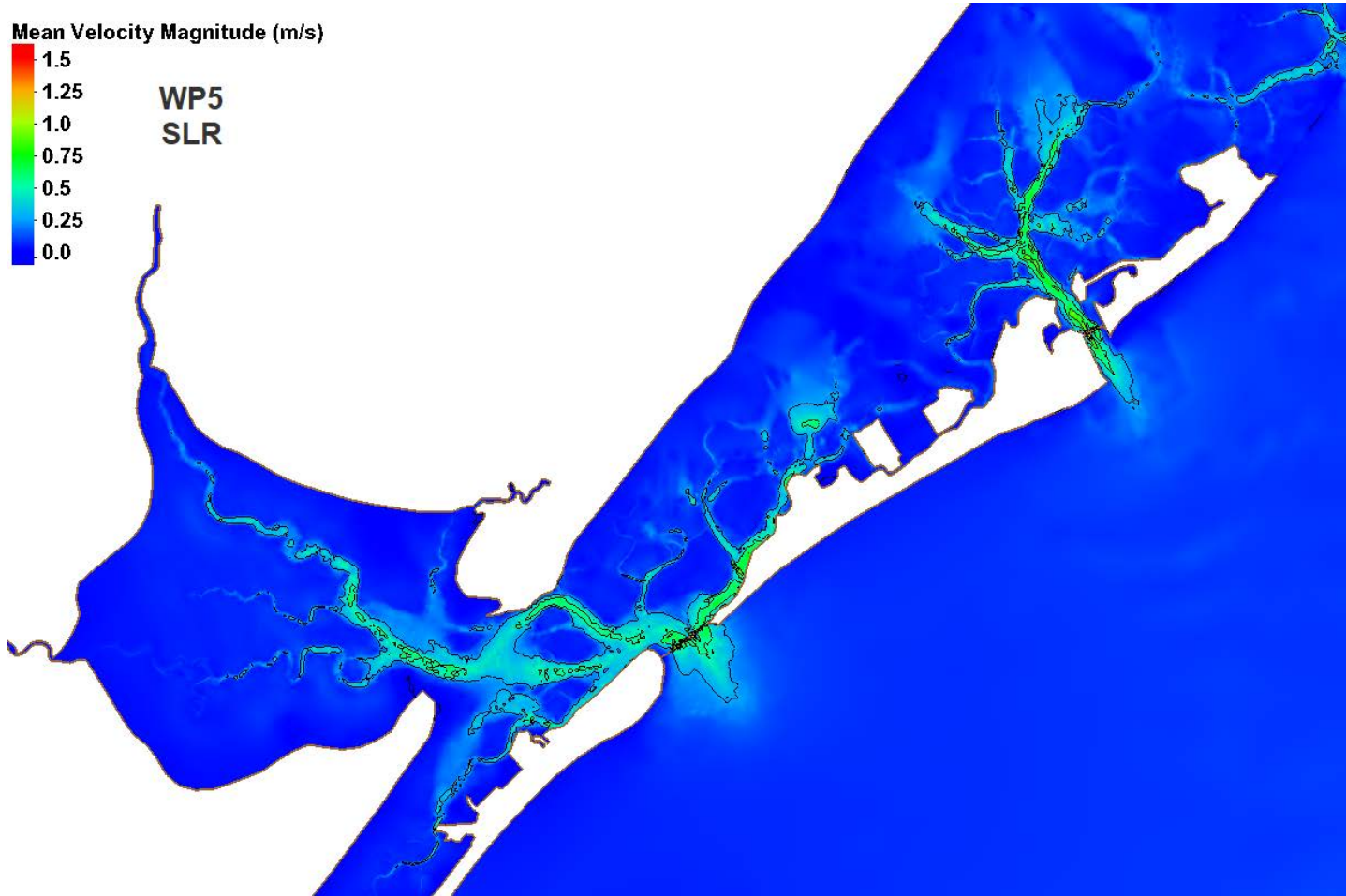




Central Region (Great Egg and Absecon)



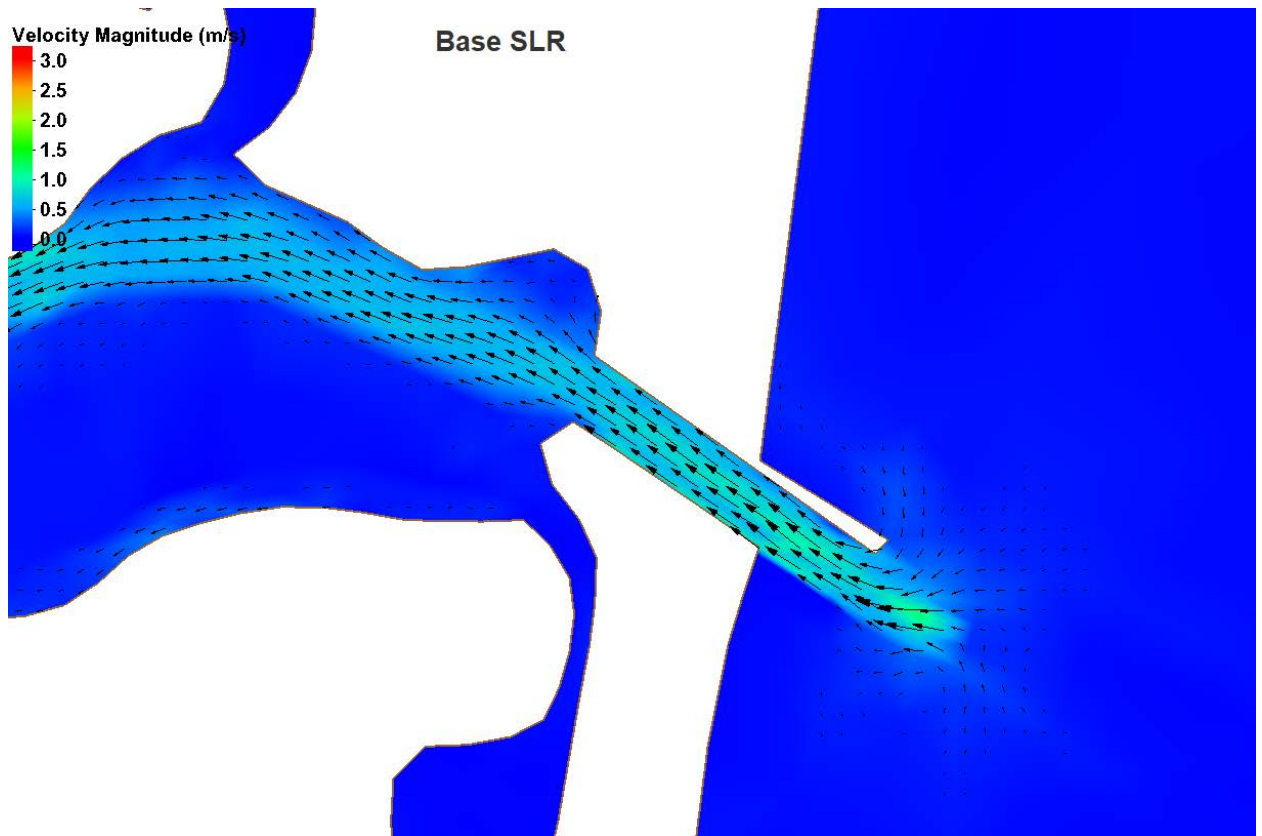


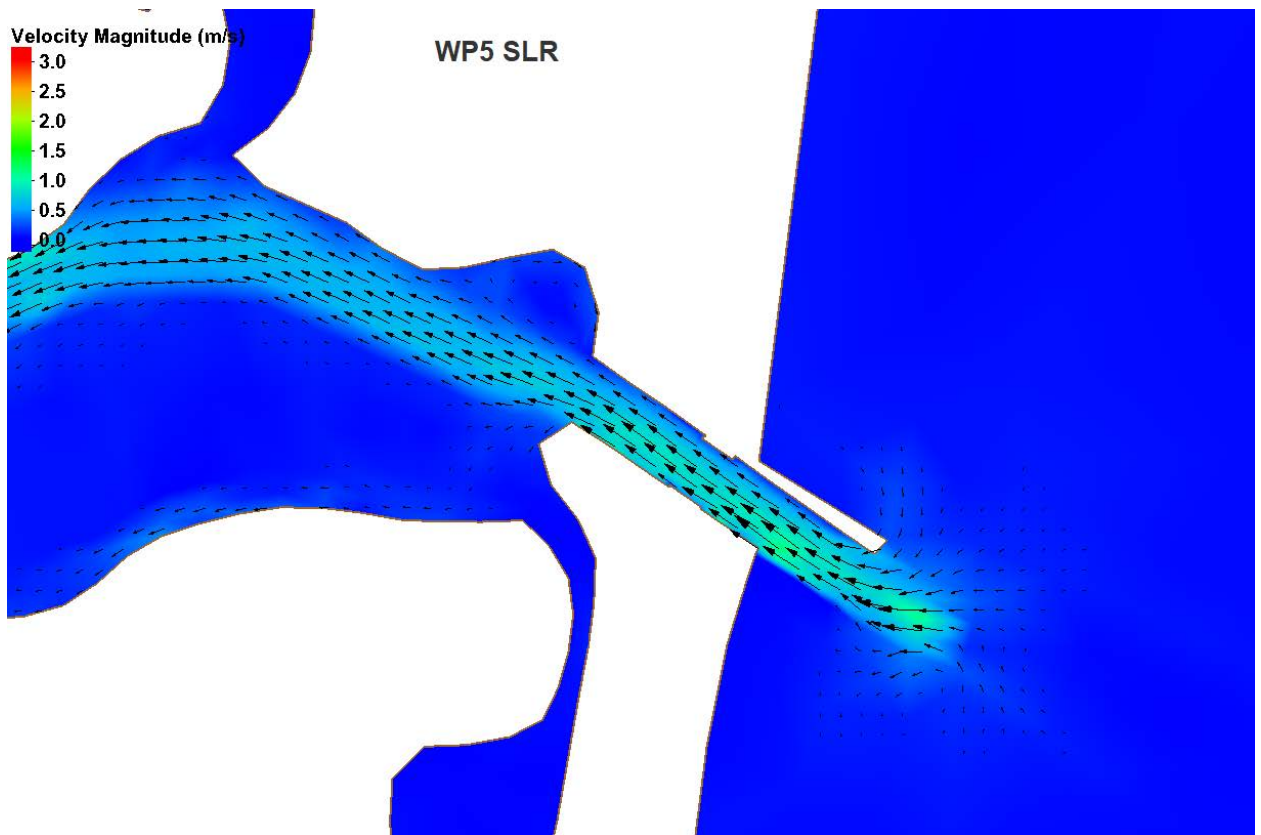
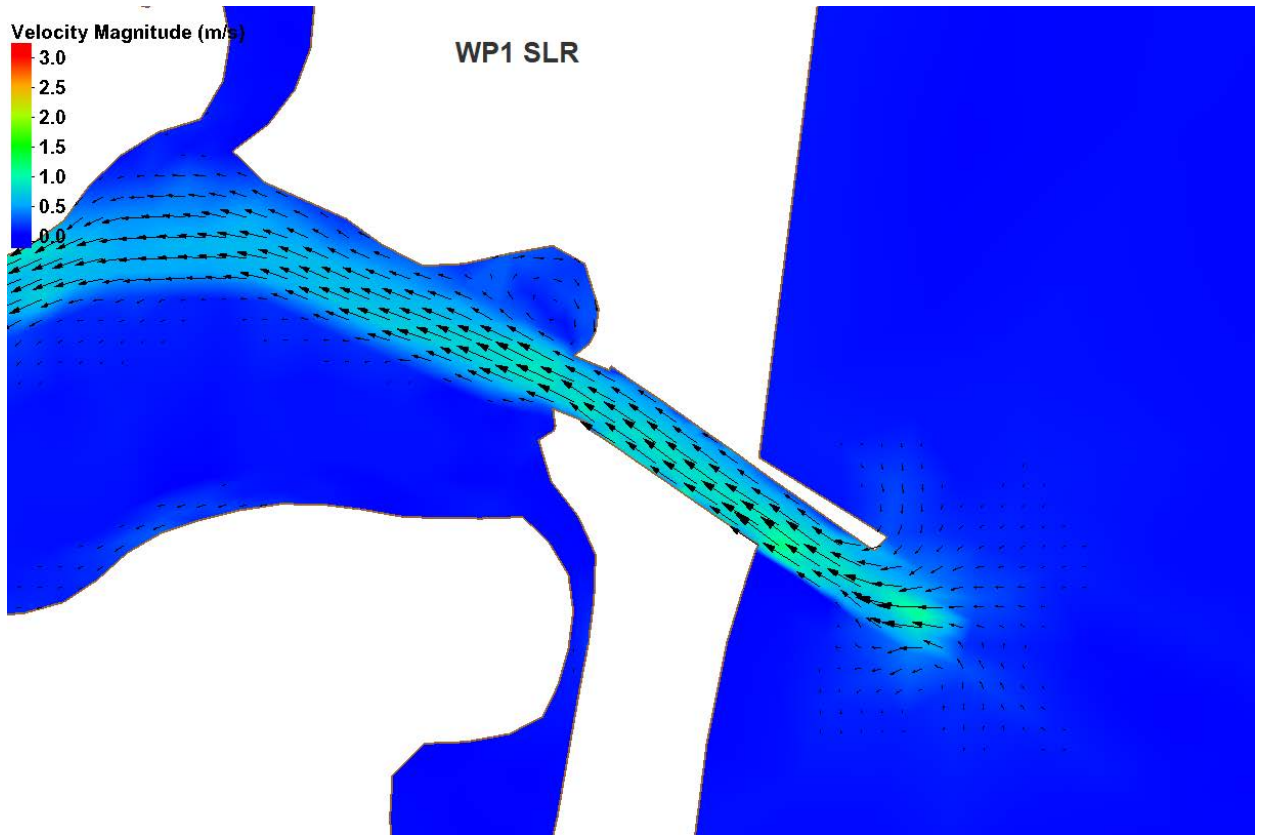


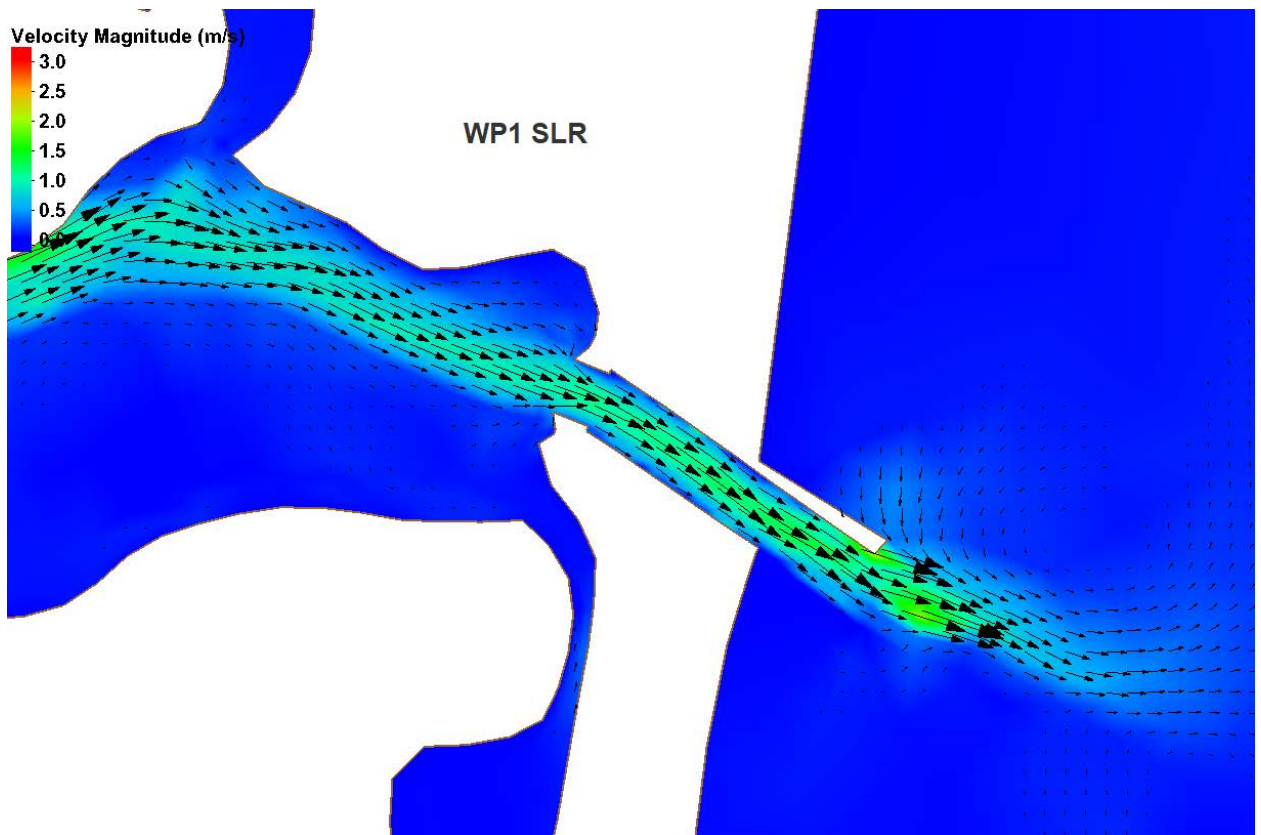
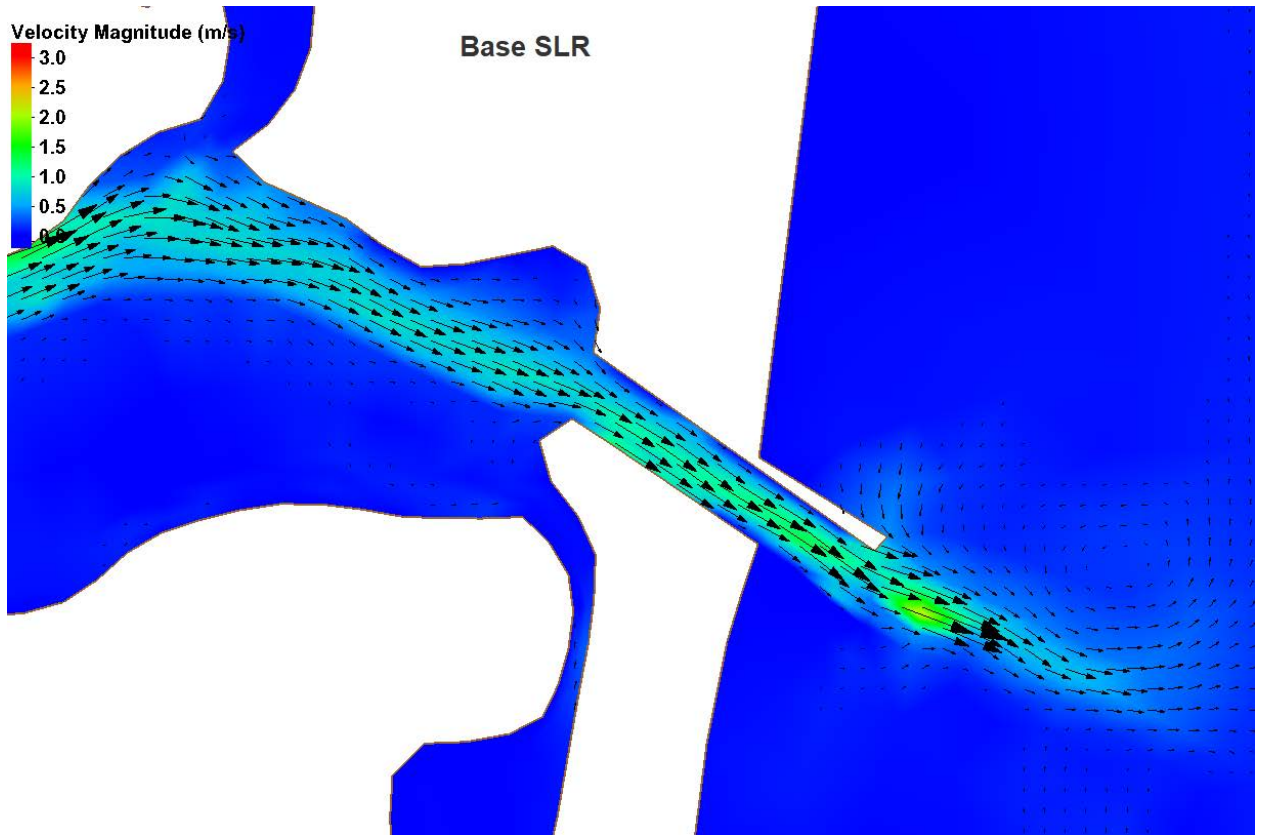
Flood/ebb Velocity Comparison at Structures with Sea Level Rise

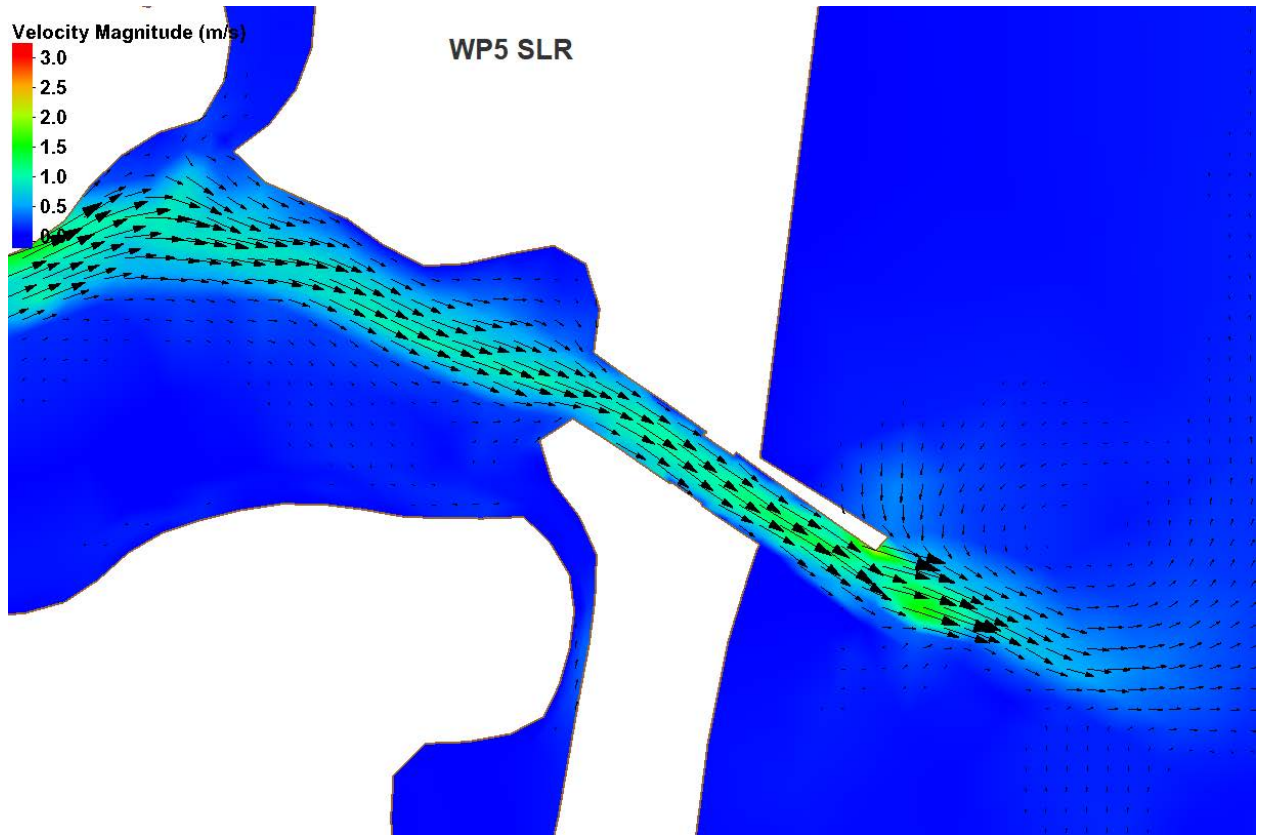
Flood directed flow is in toward the bays and ebb directed flow is out into the Atlantic Ocean. A representative maximum flood (16 April 12:00) and ebb time (16 April 18:00) is shown for all of the structure locations for velocity magnitude and direction comparison. These are contoured from 0 to 3 m/s with vectors scaled to the magnitude and shown on a grid.

Manasquan

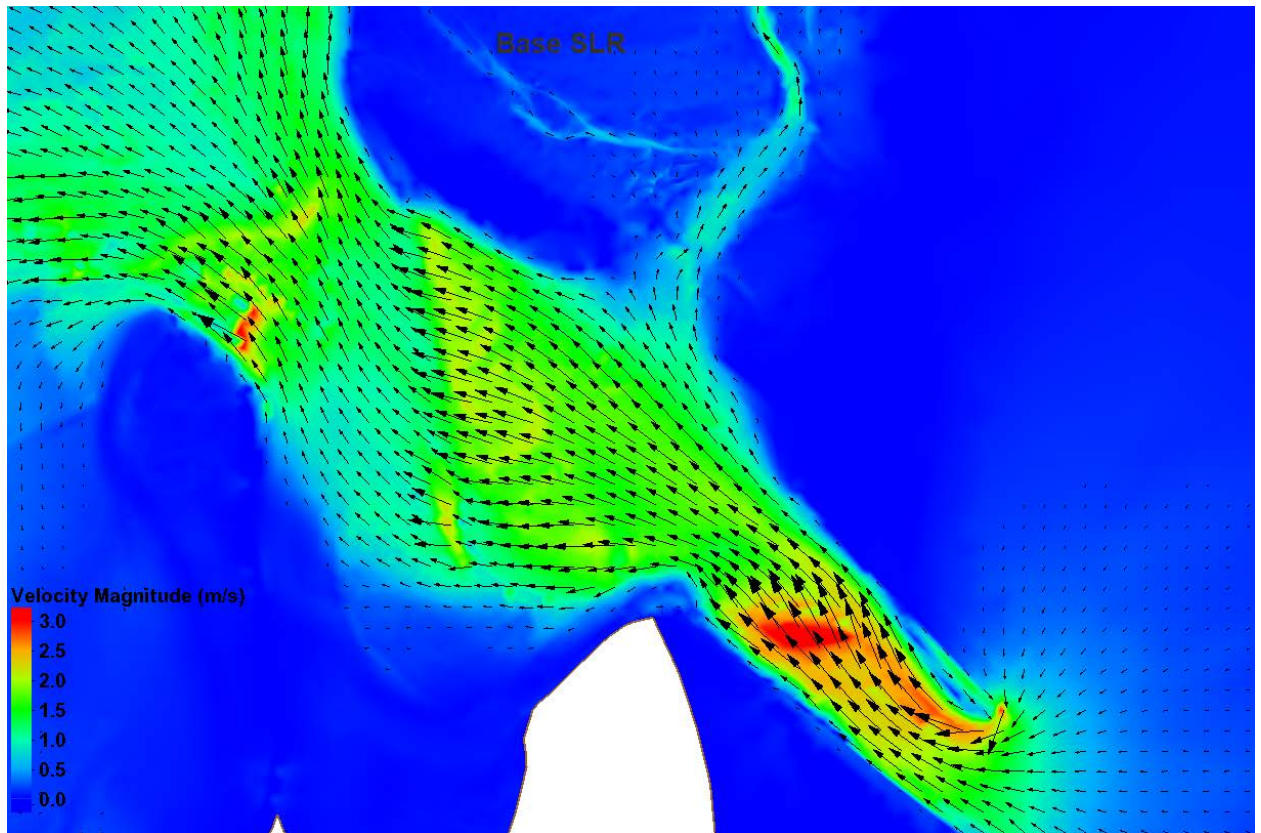


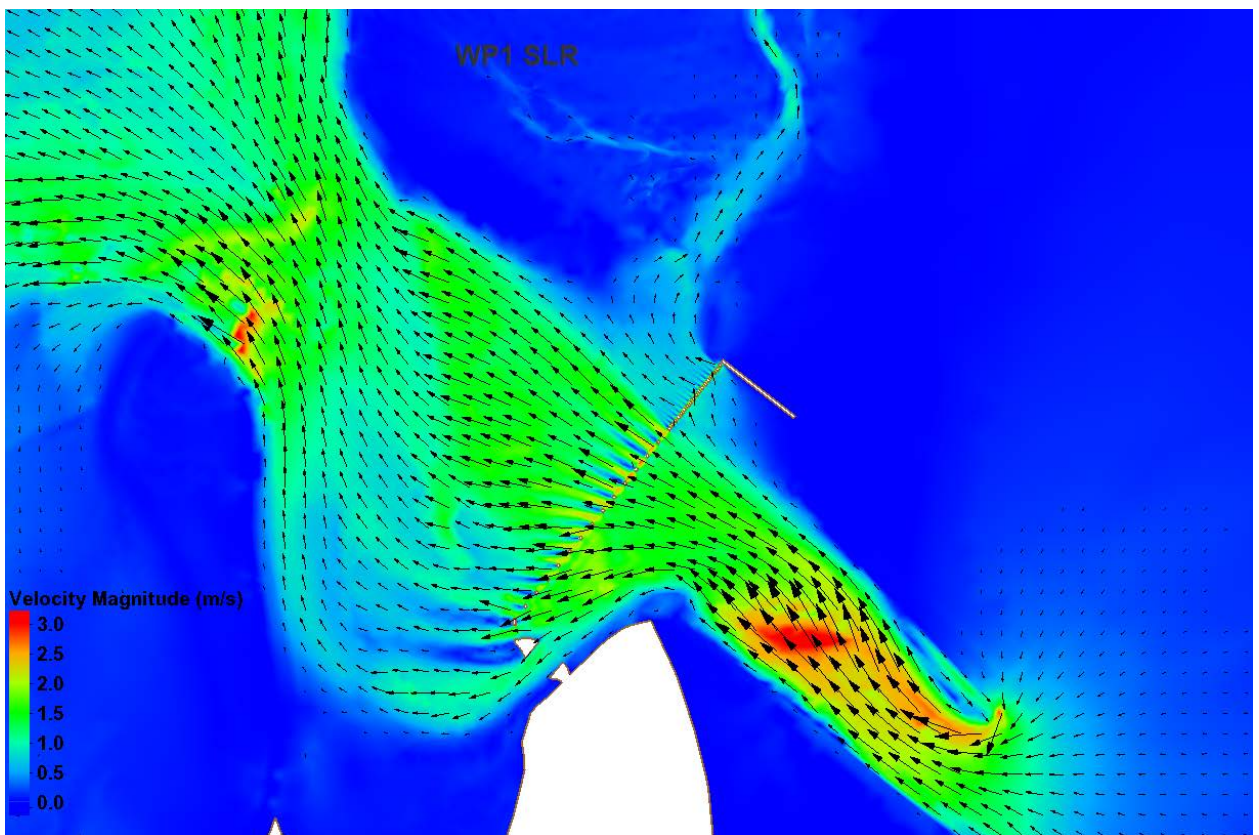
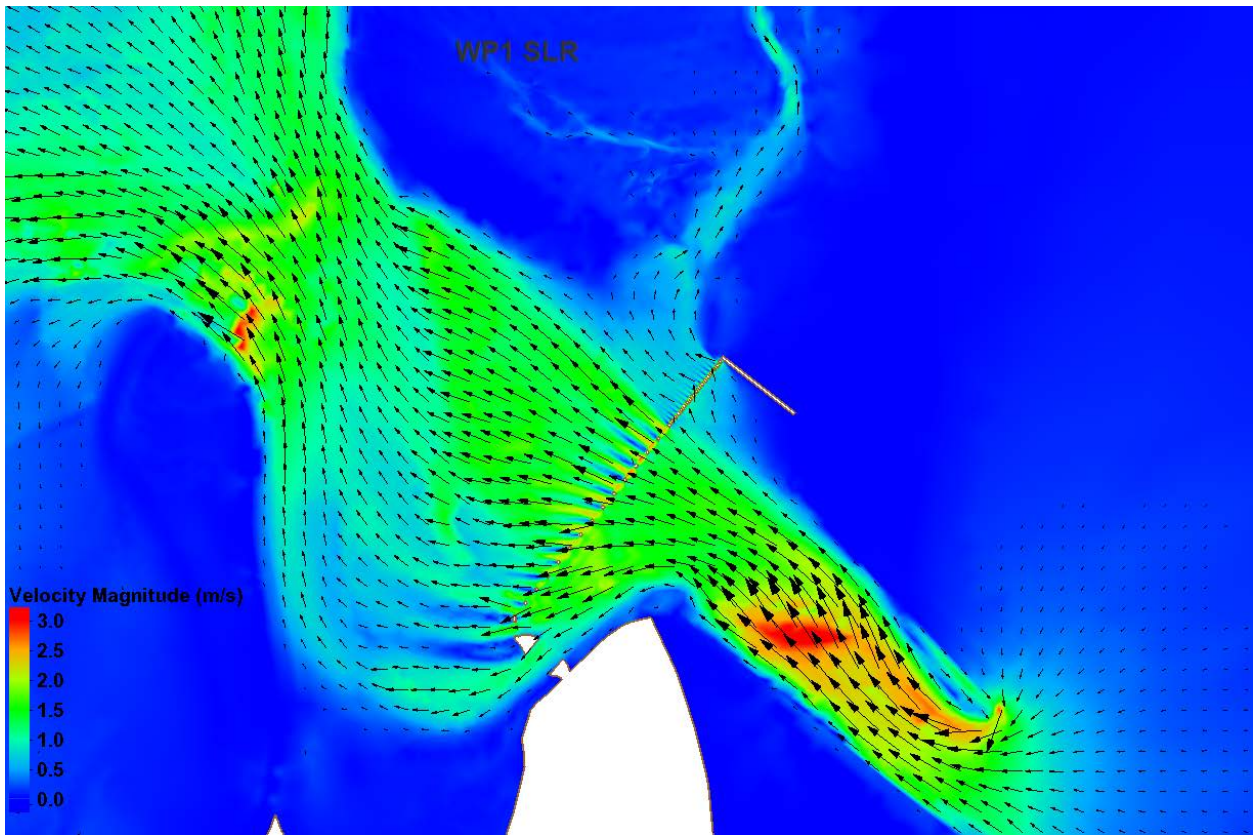


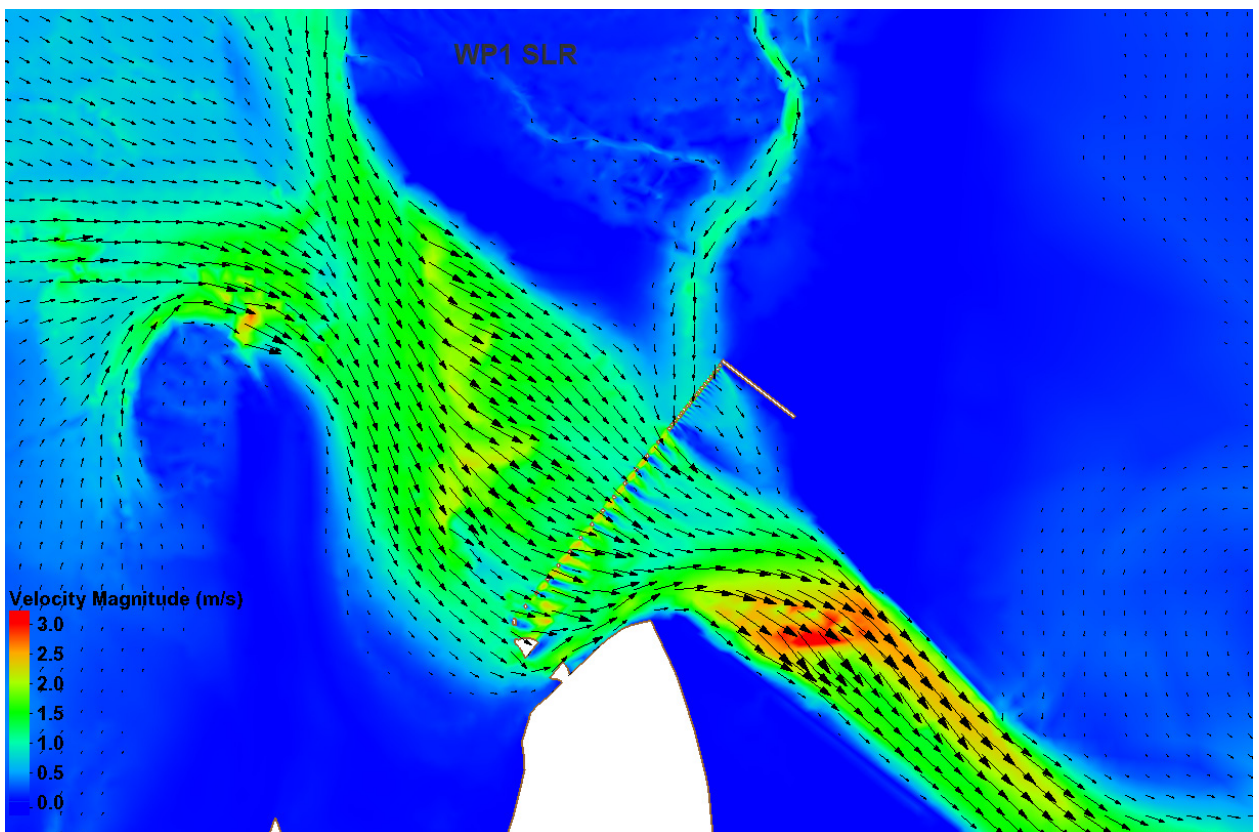
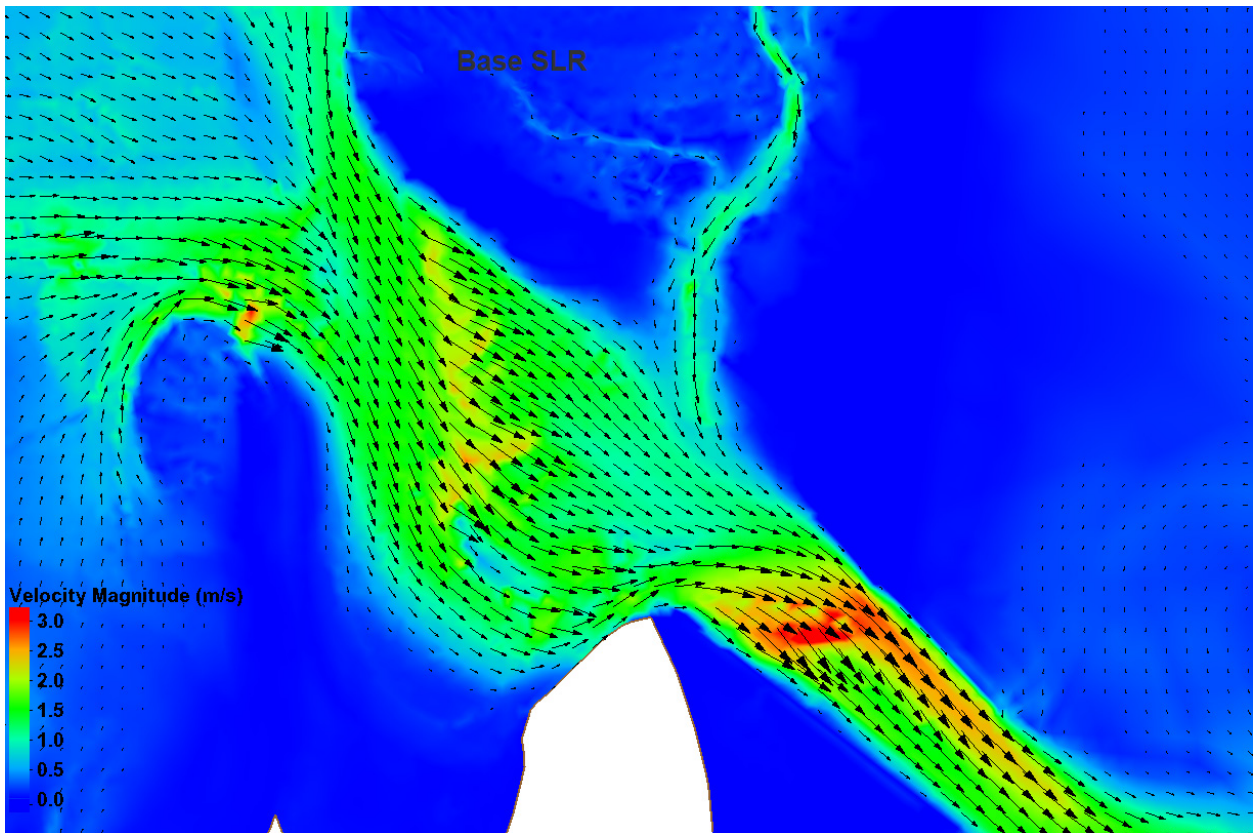


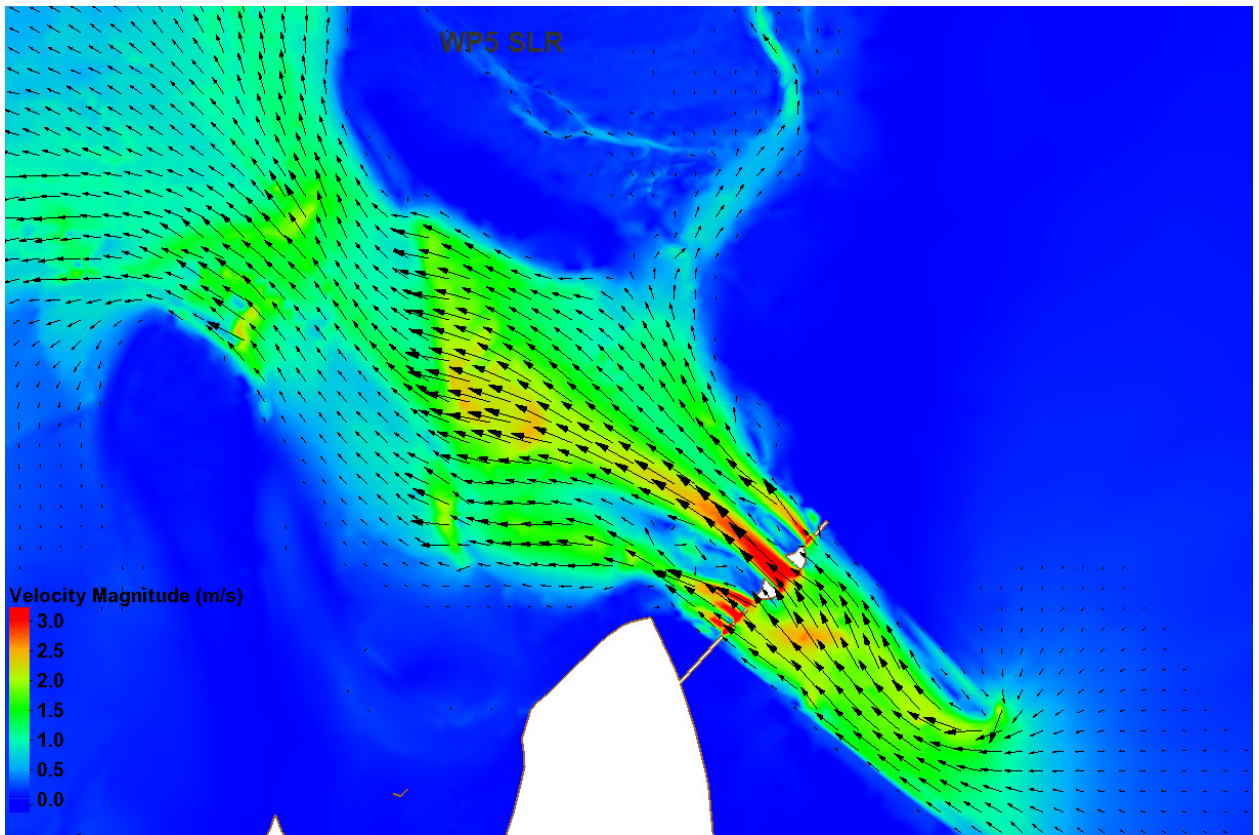


Barnegat

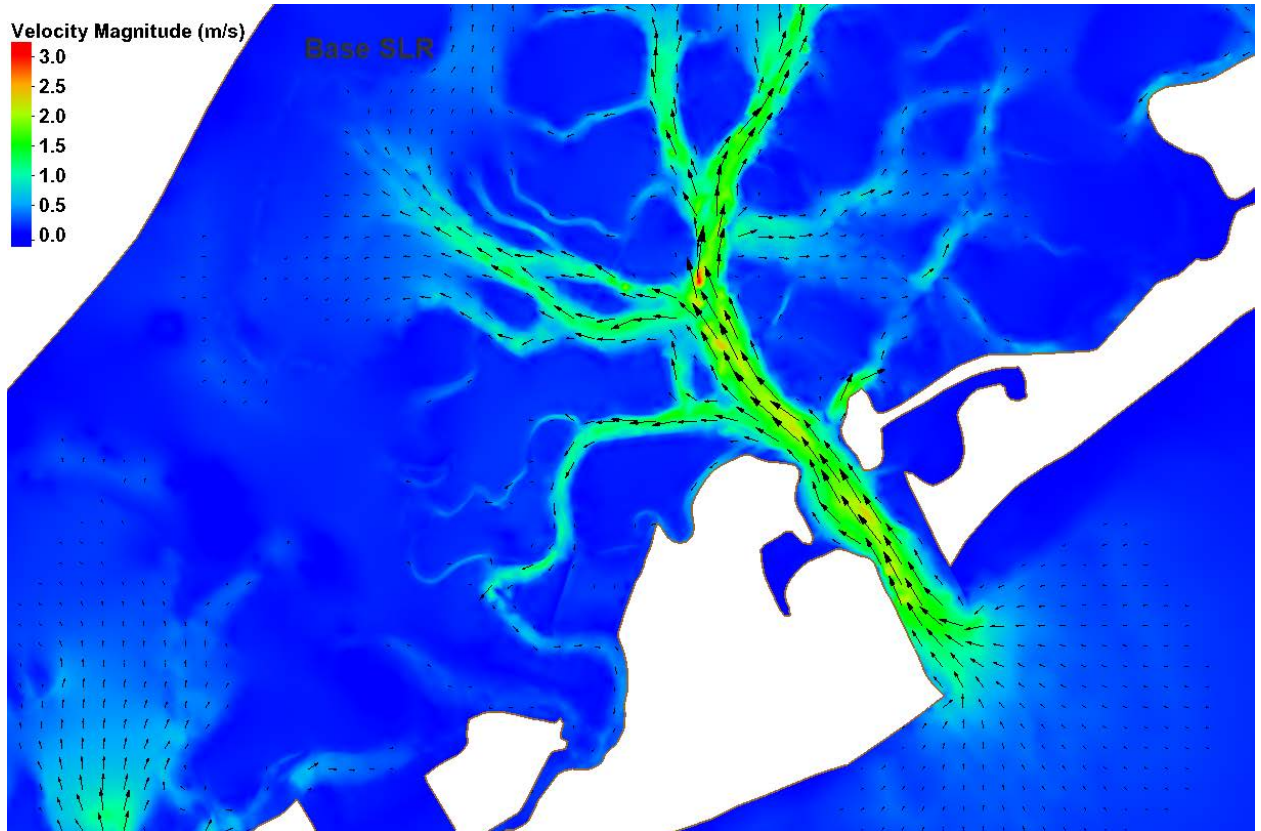


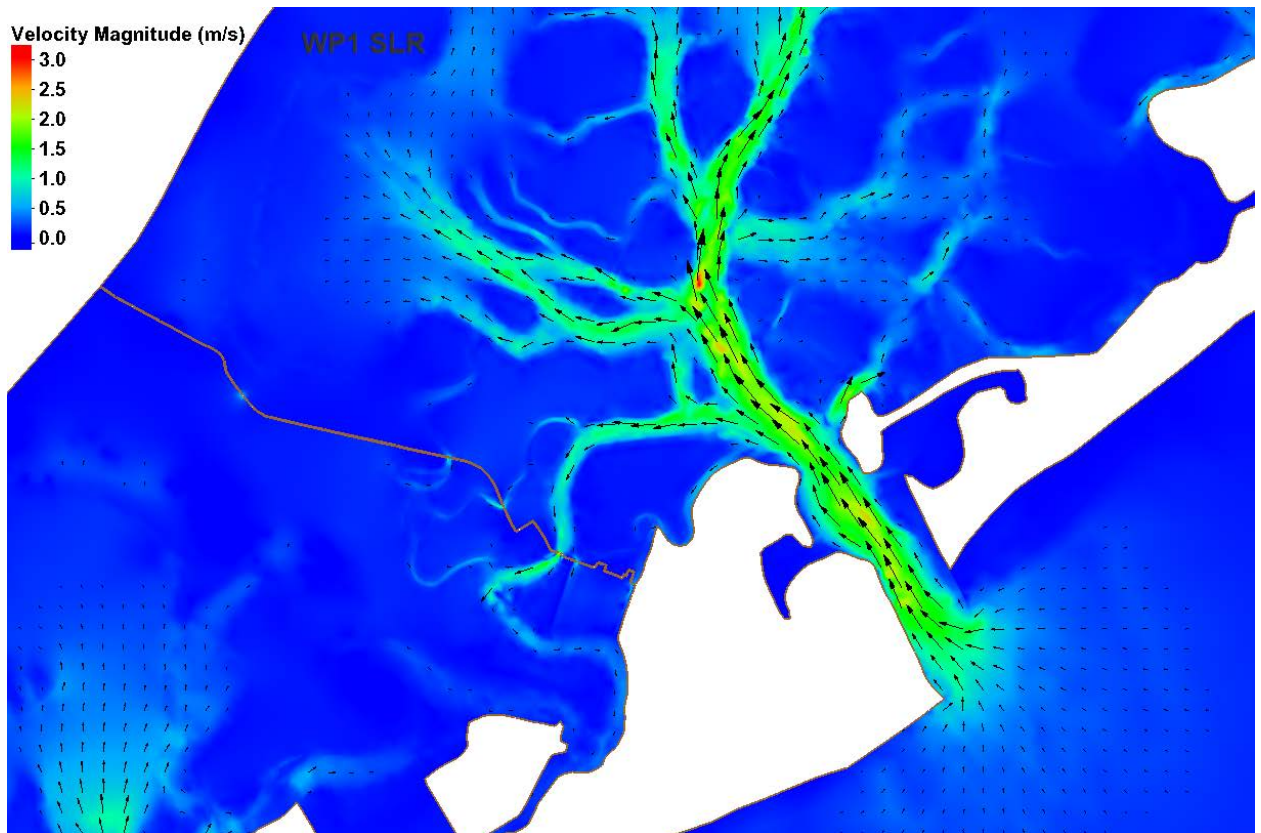
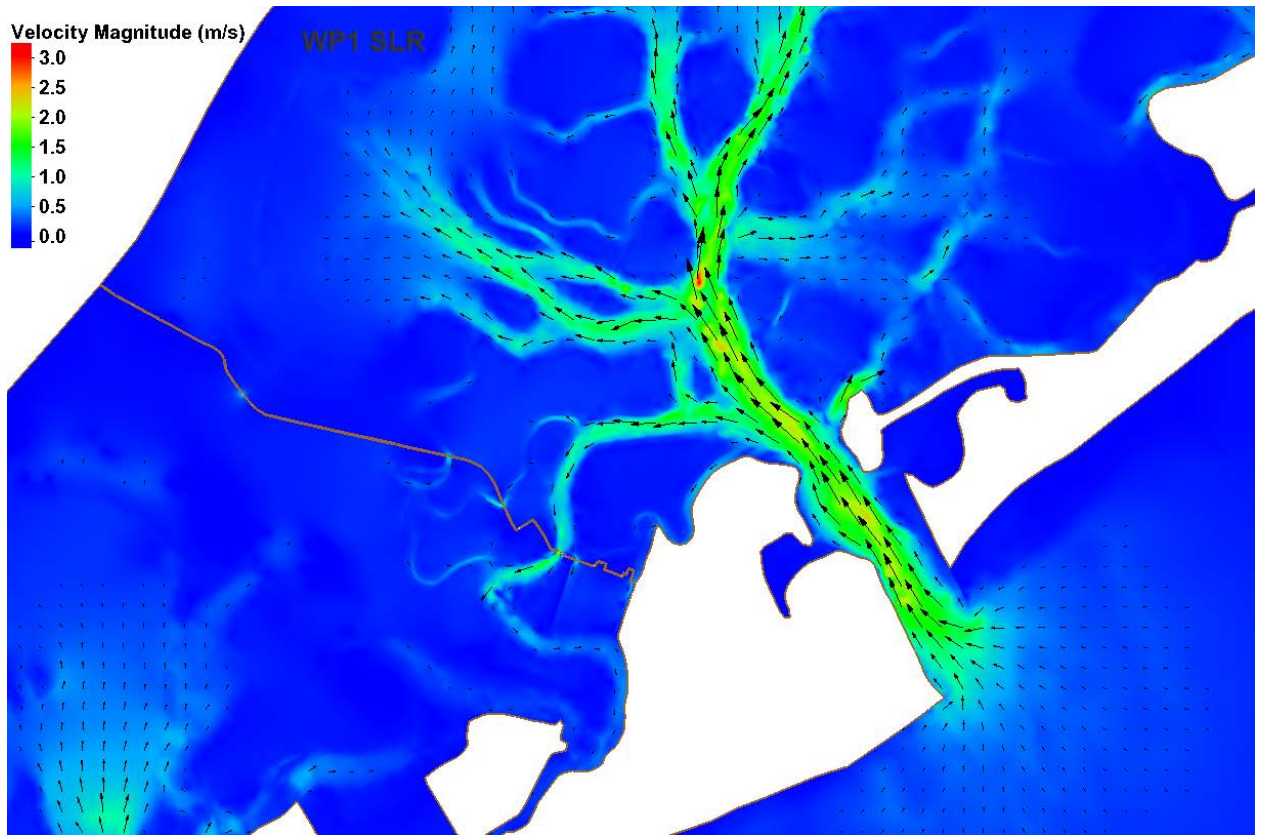


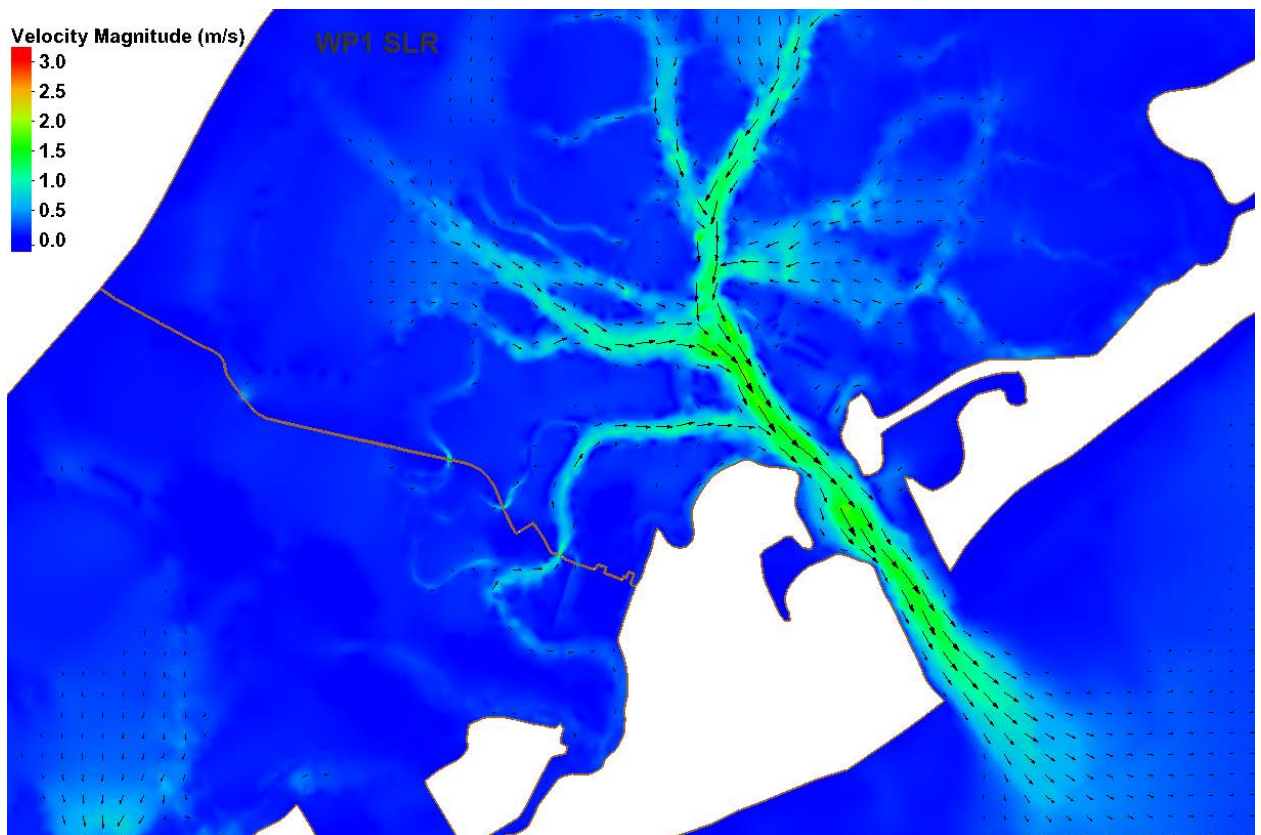
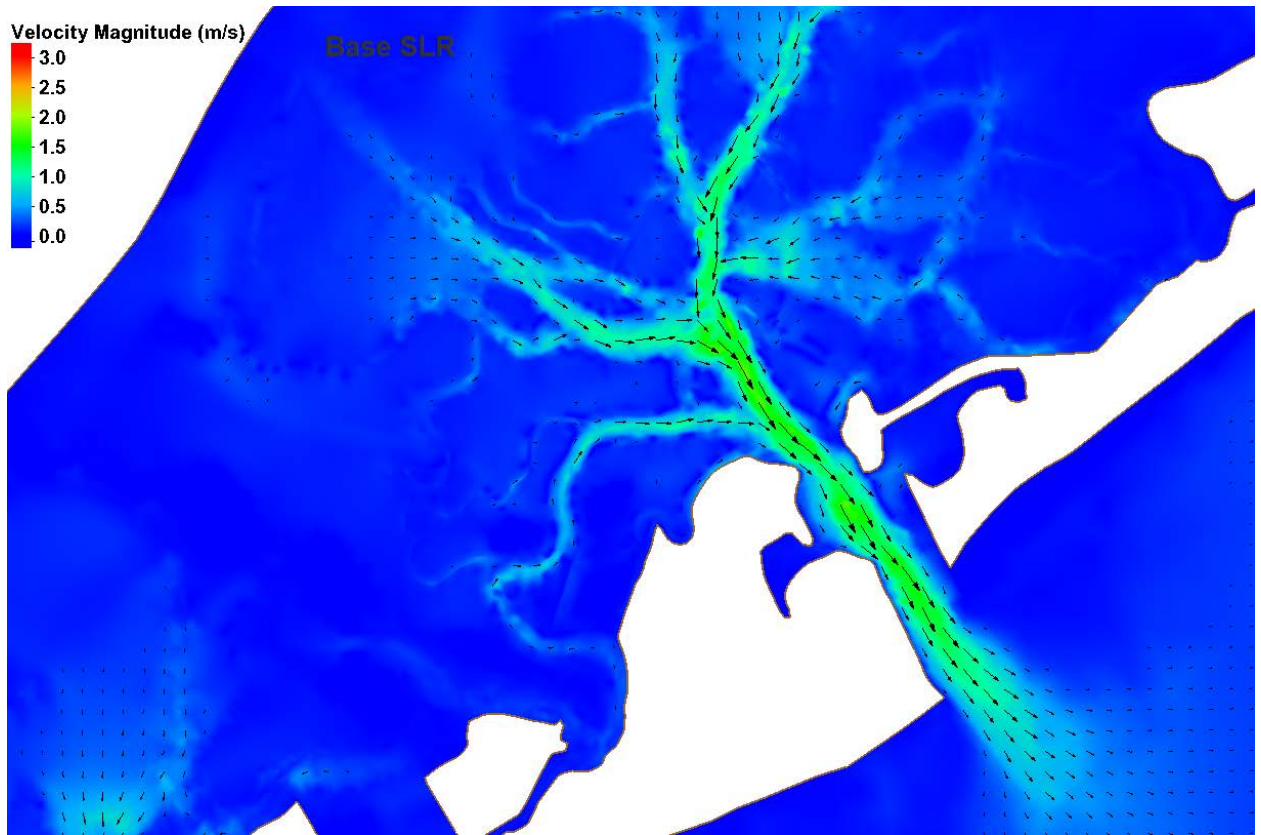


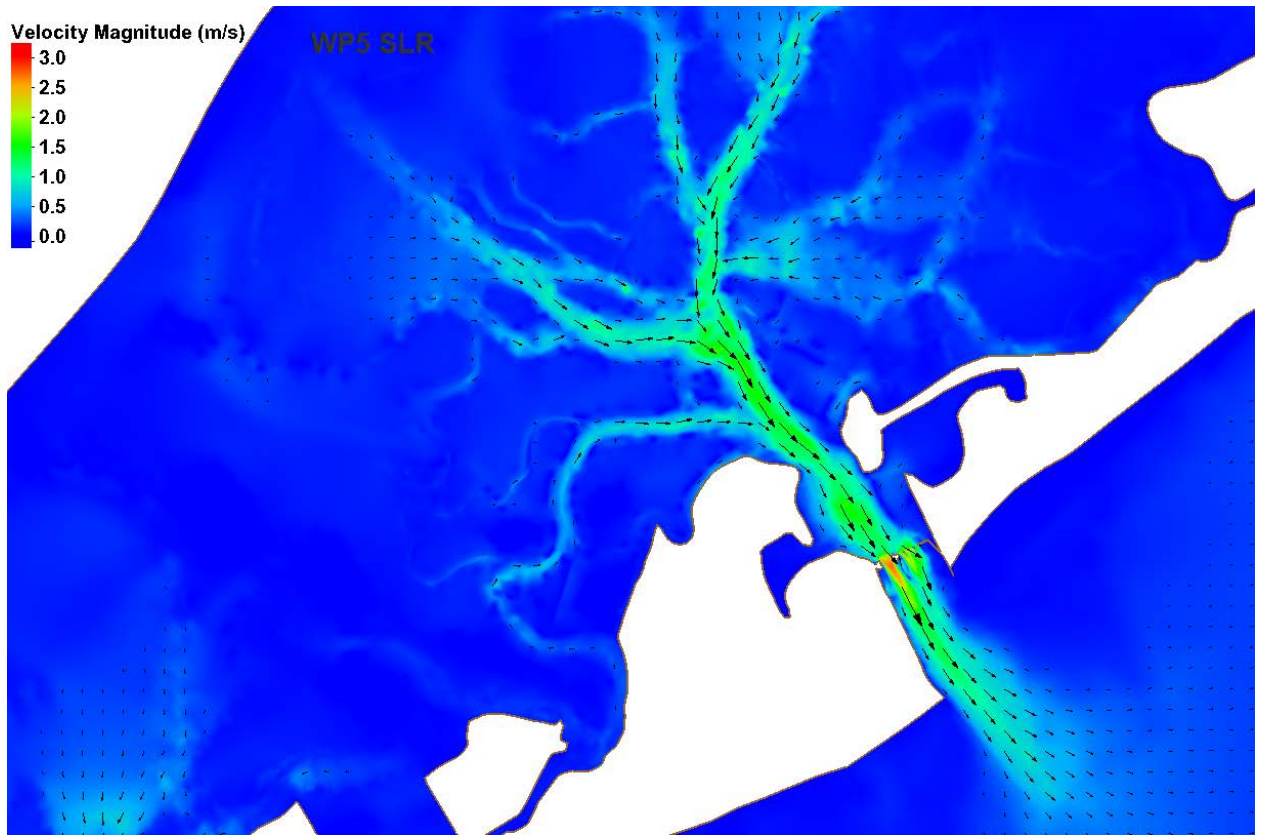


Absecon and Absecon Bay Blvd

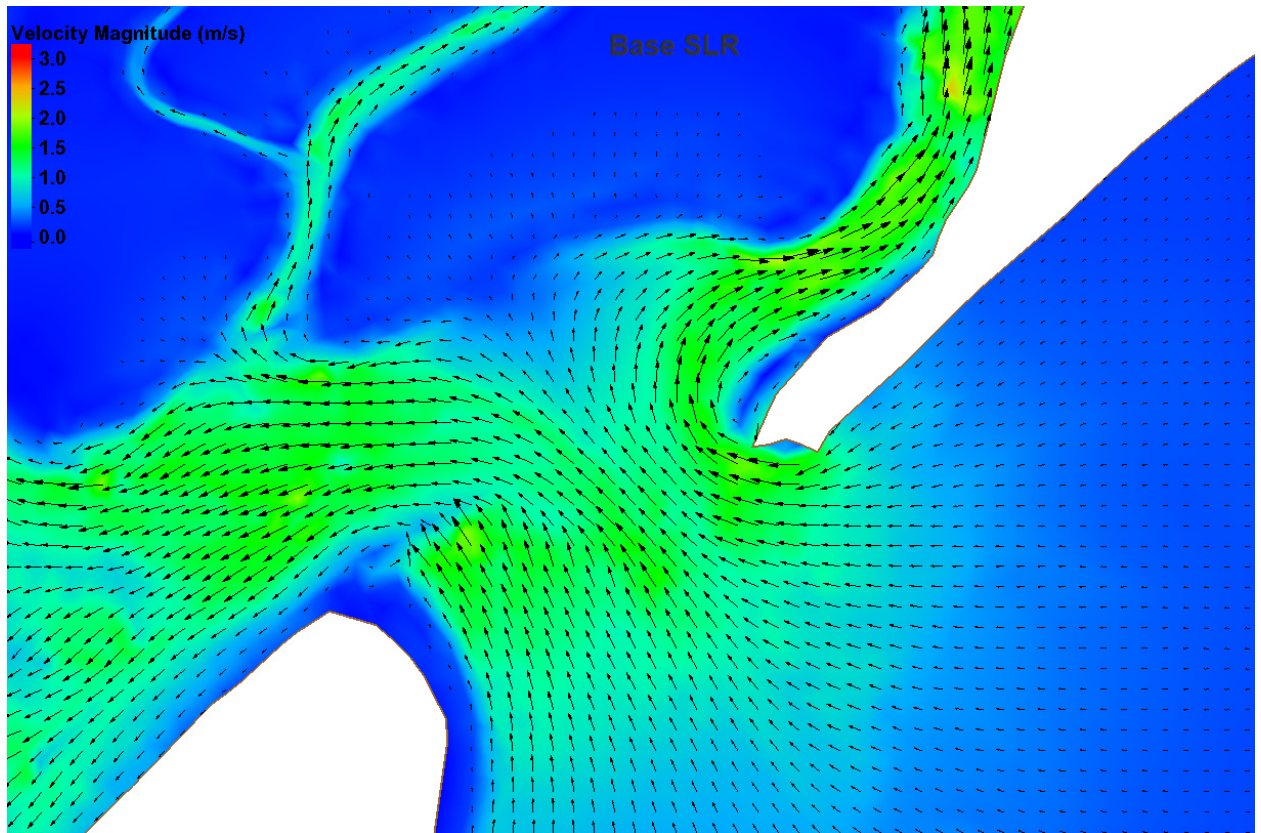


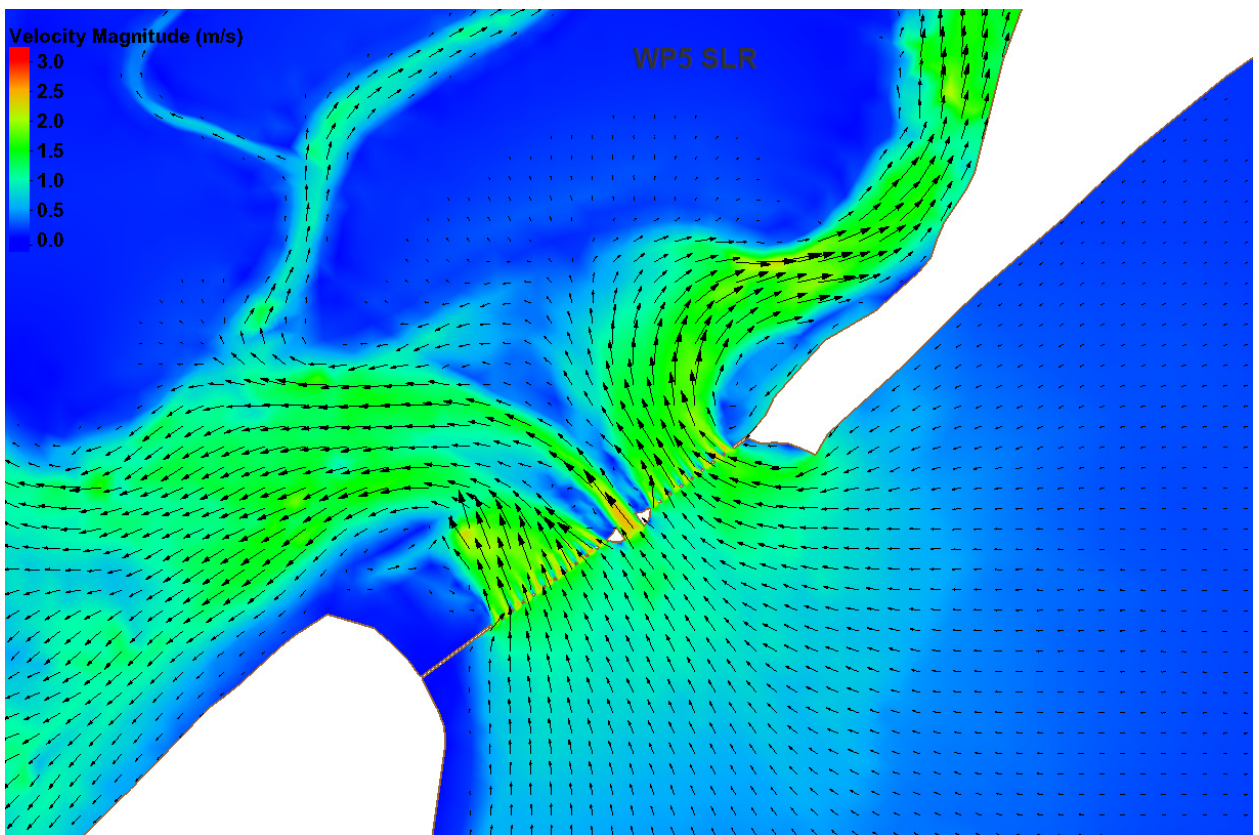
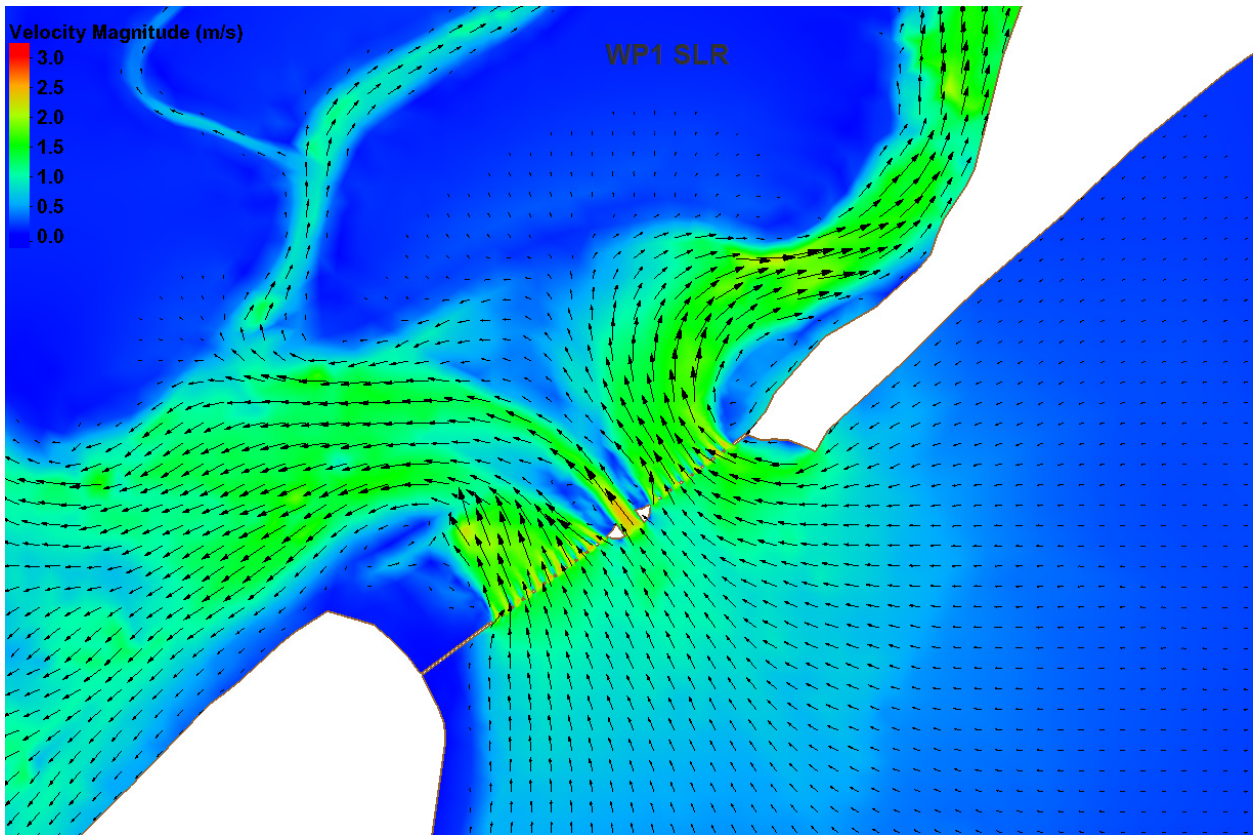


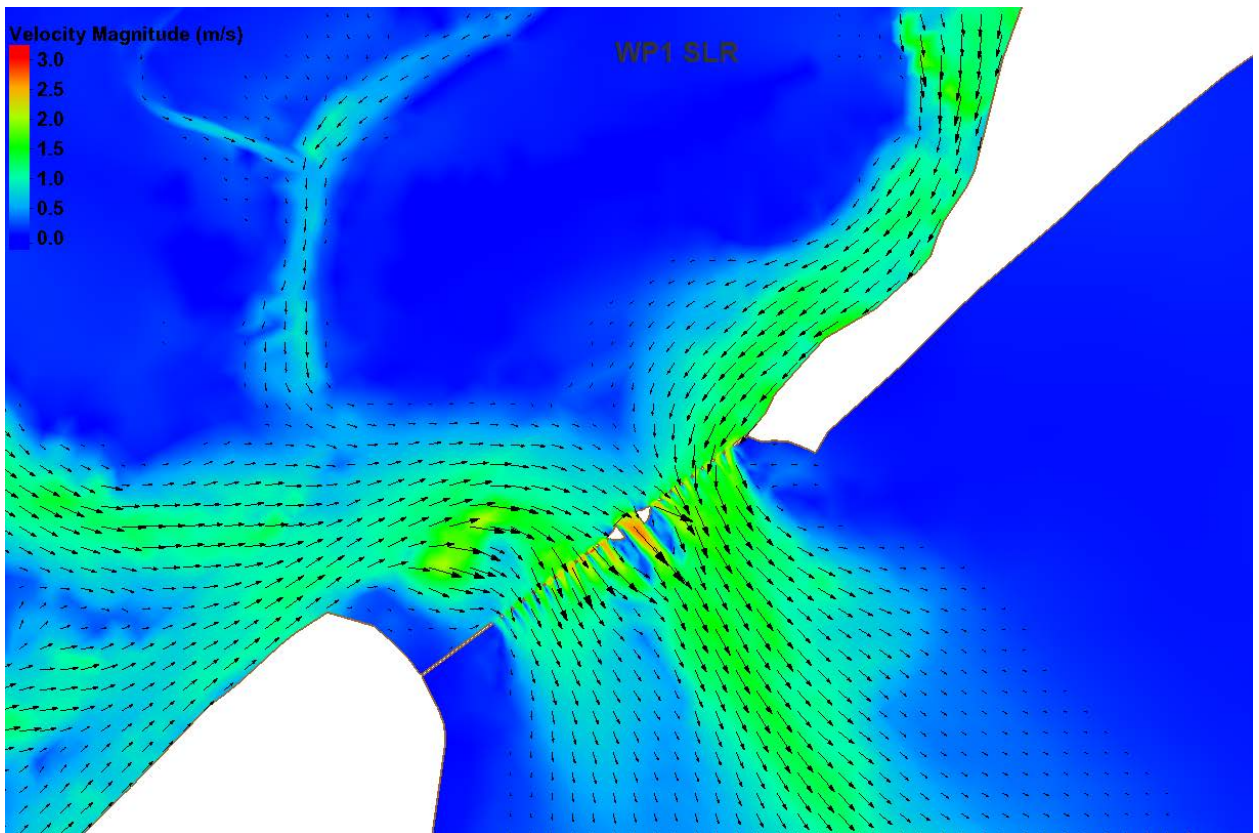
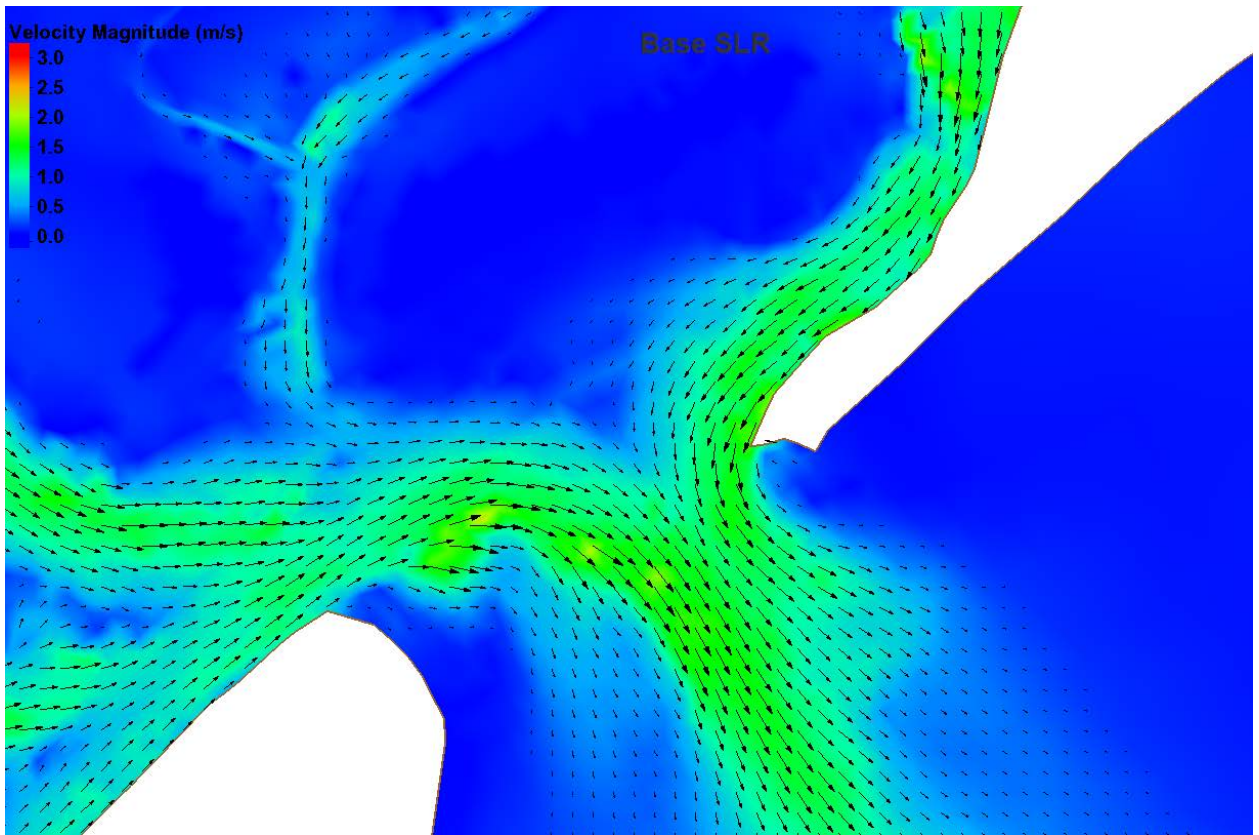


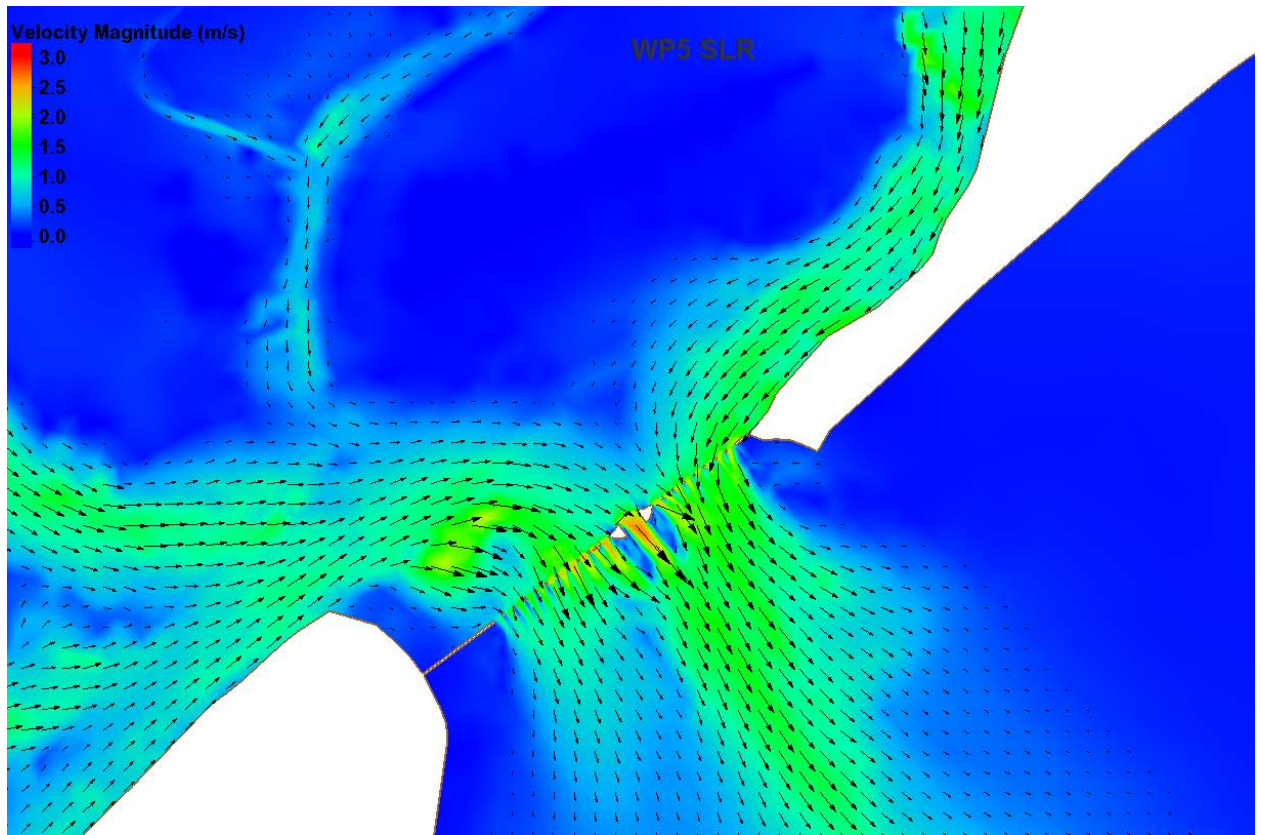


Great Egg

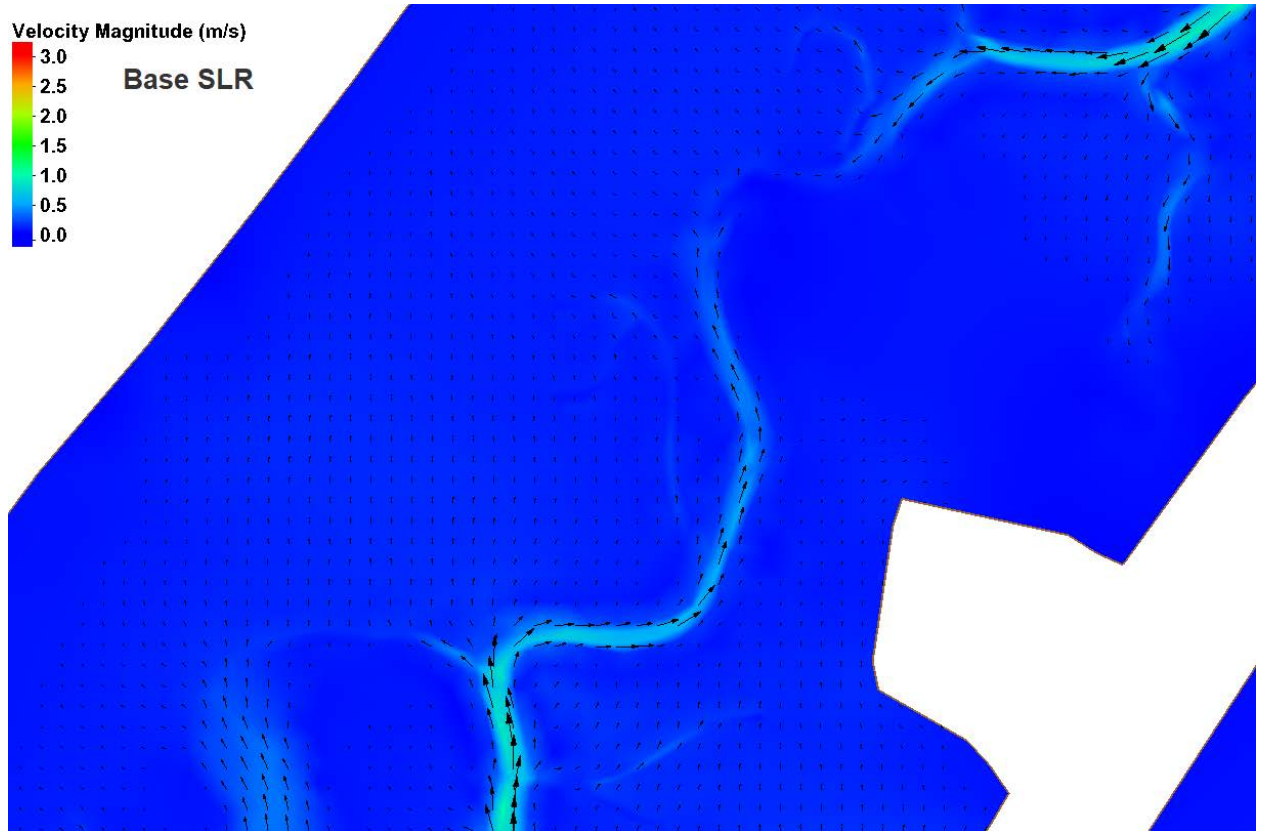


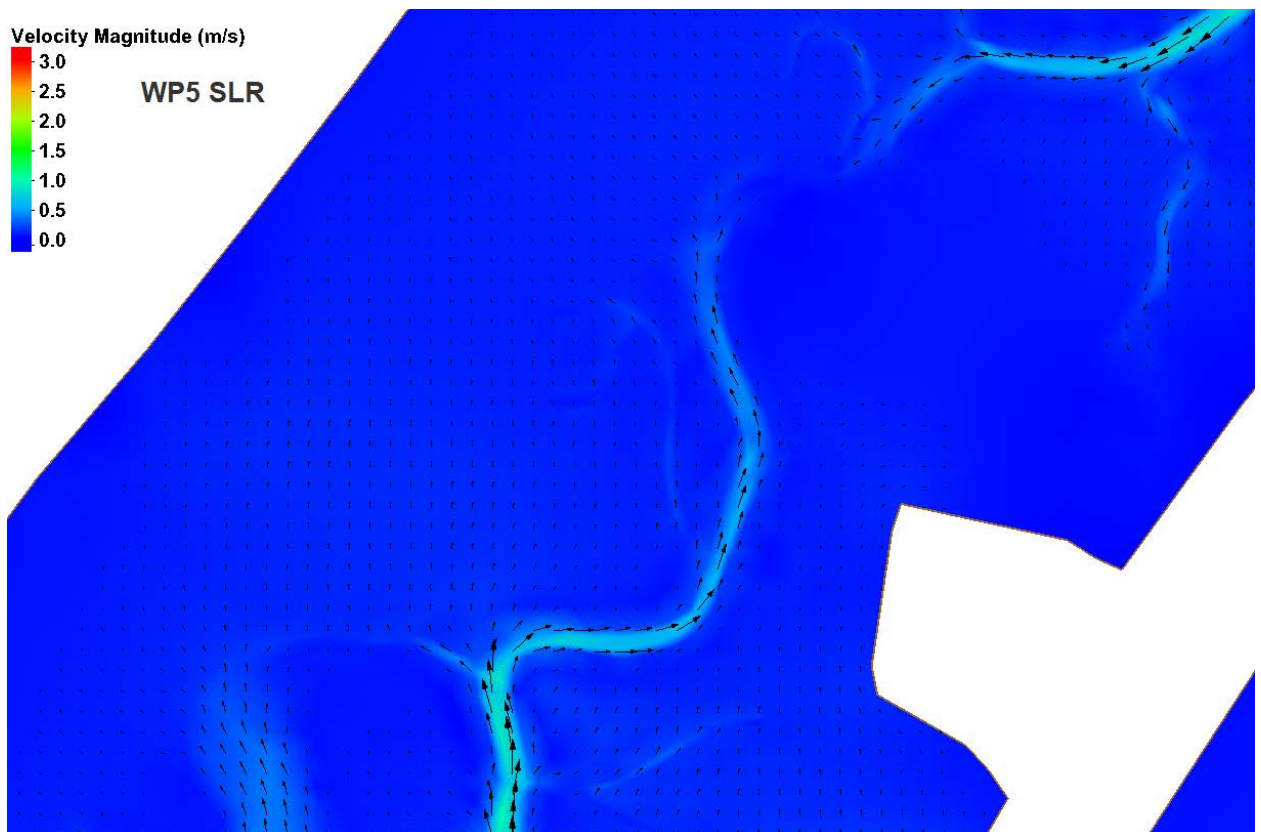
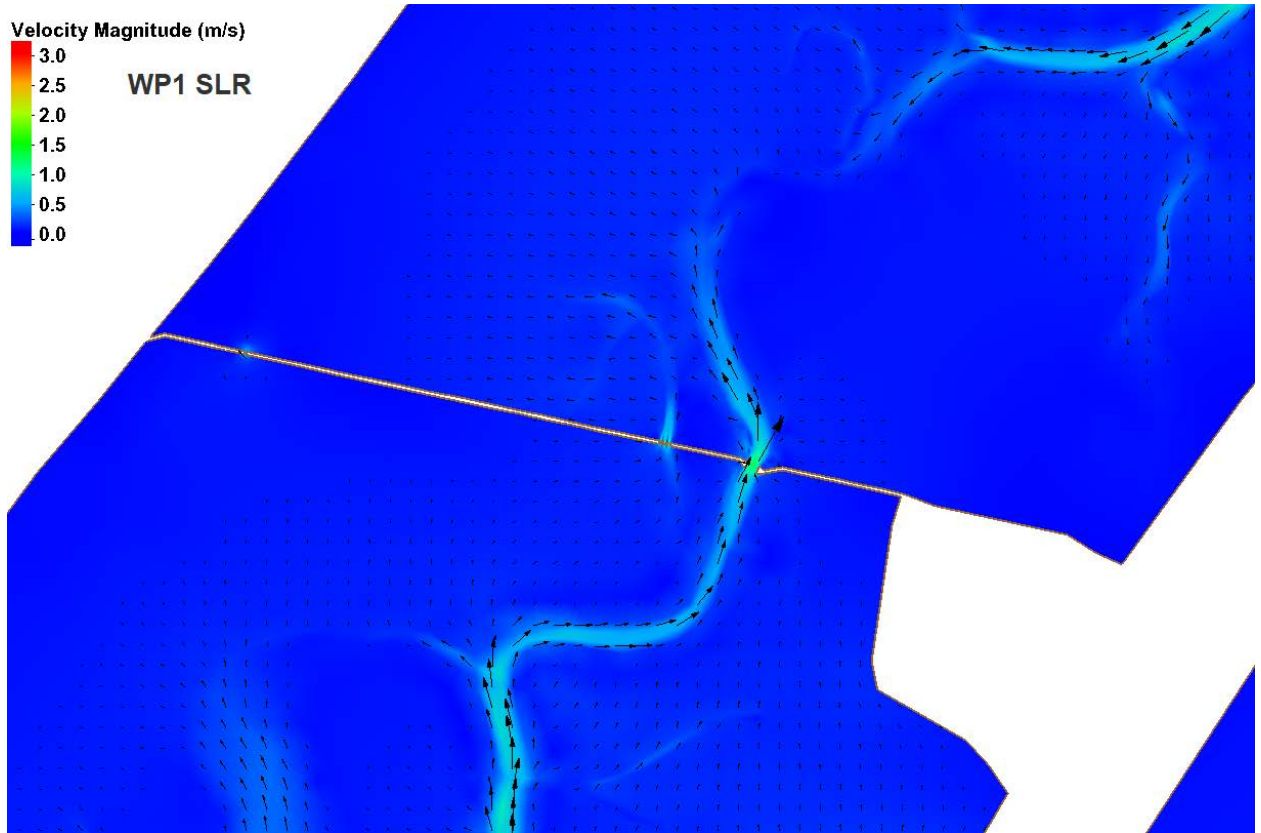


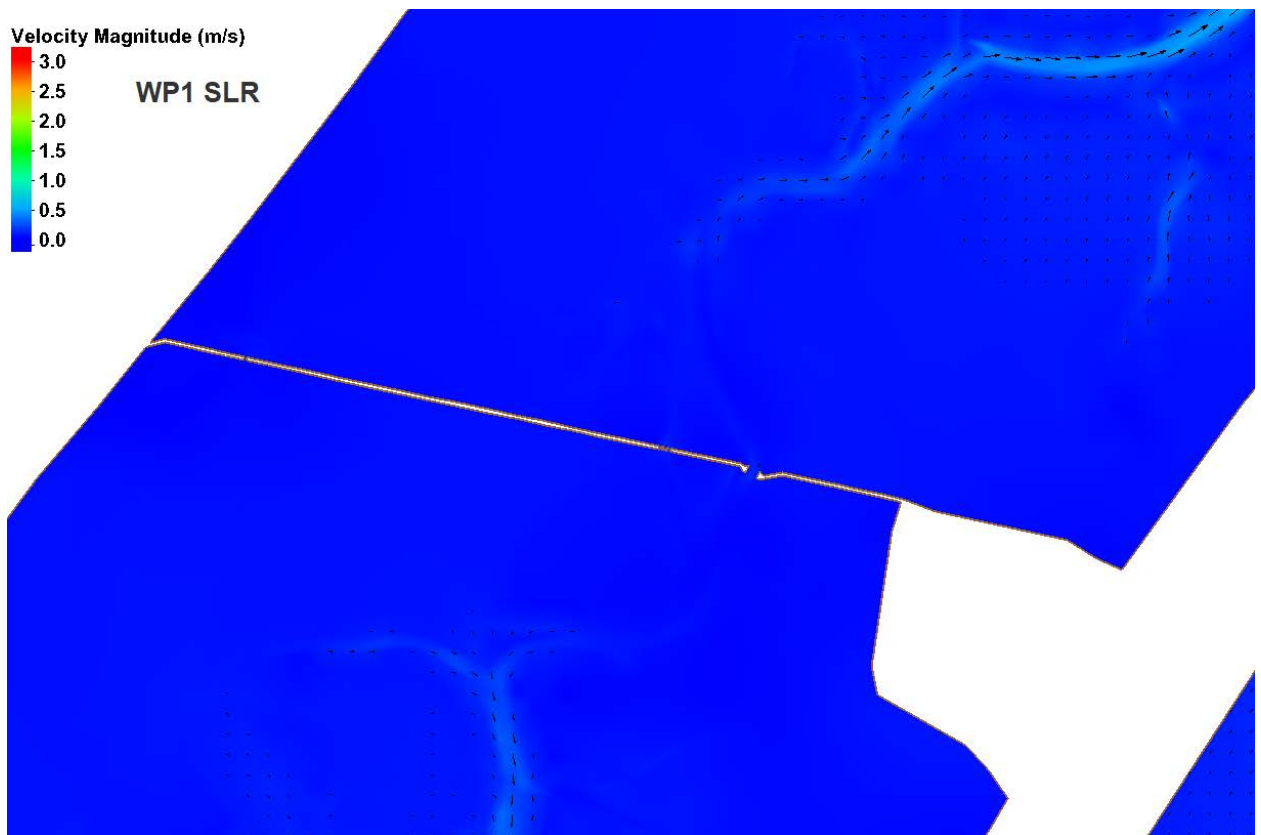
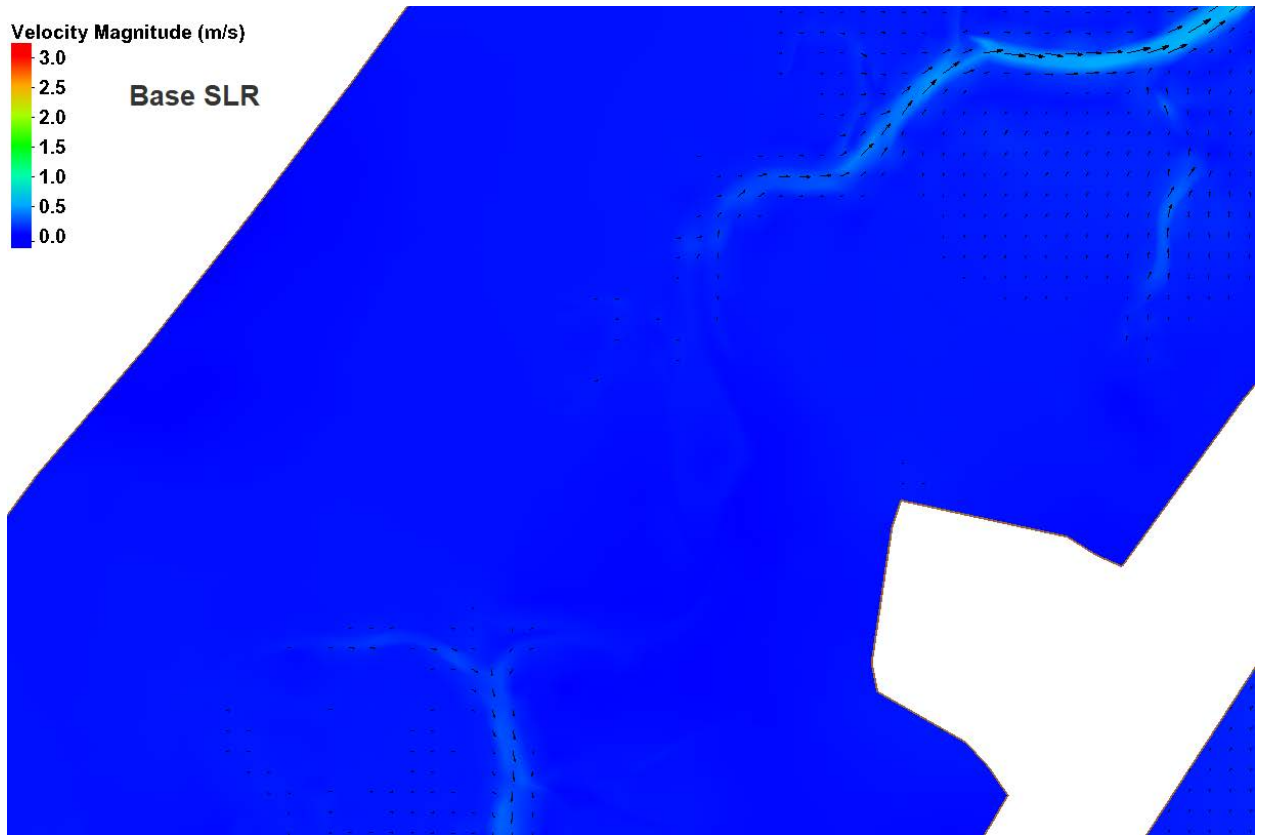


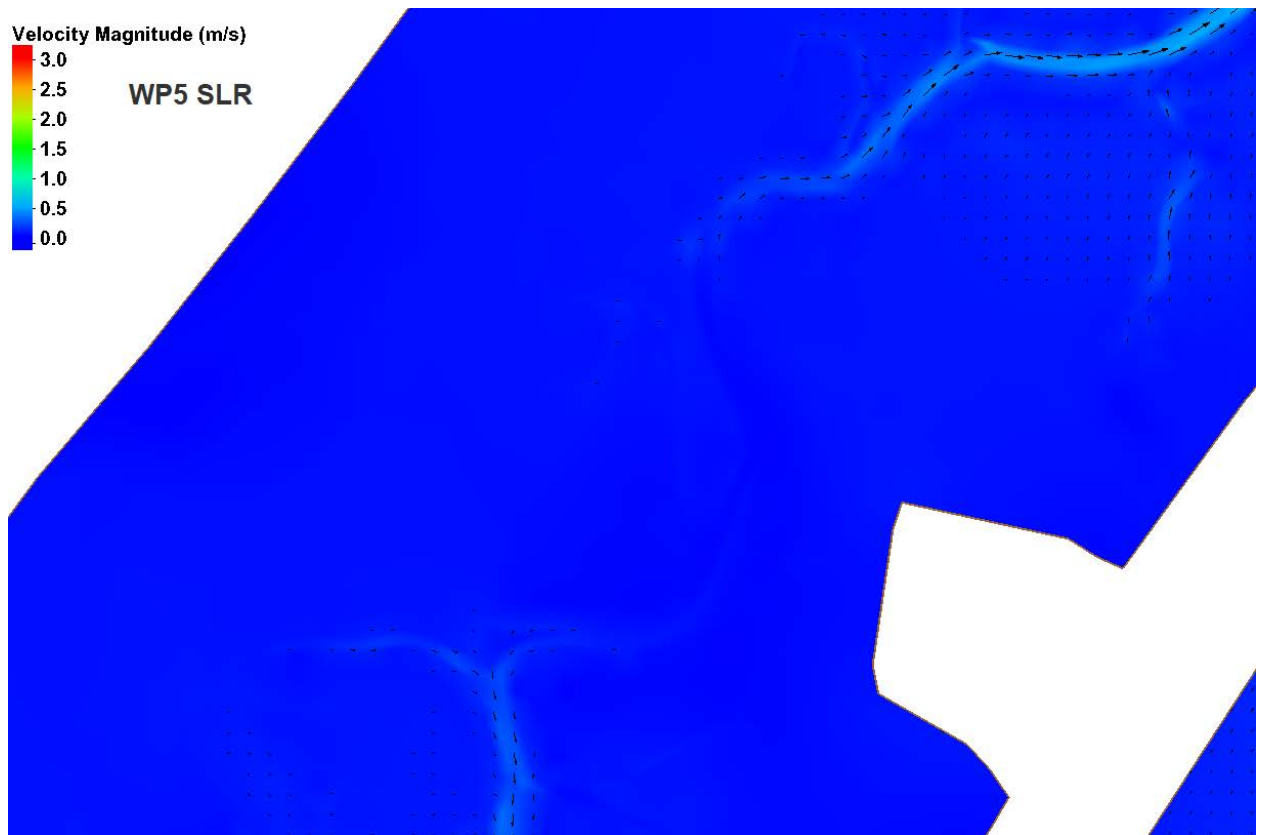


72nd Street









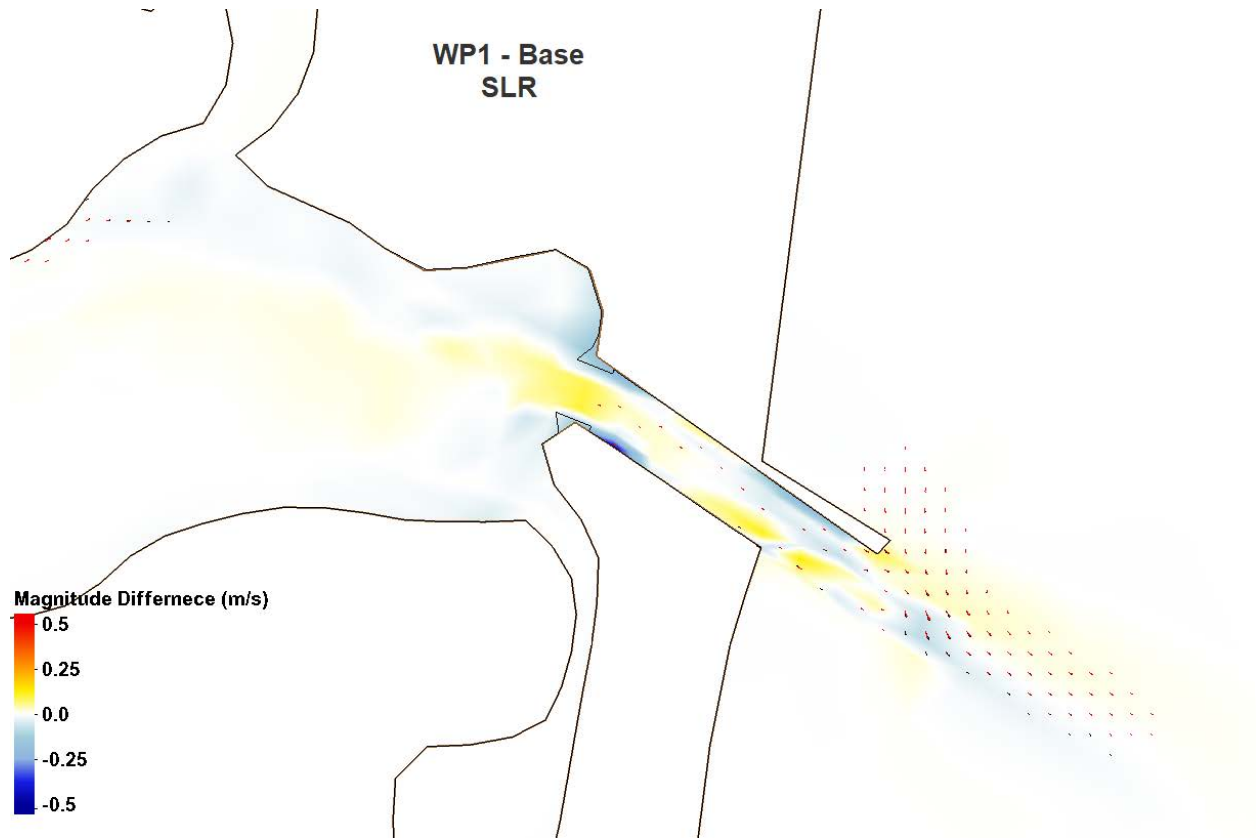
Residual Velocity at Structures with Sea Level Rise

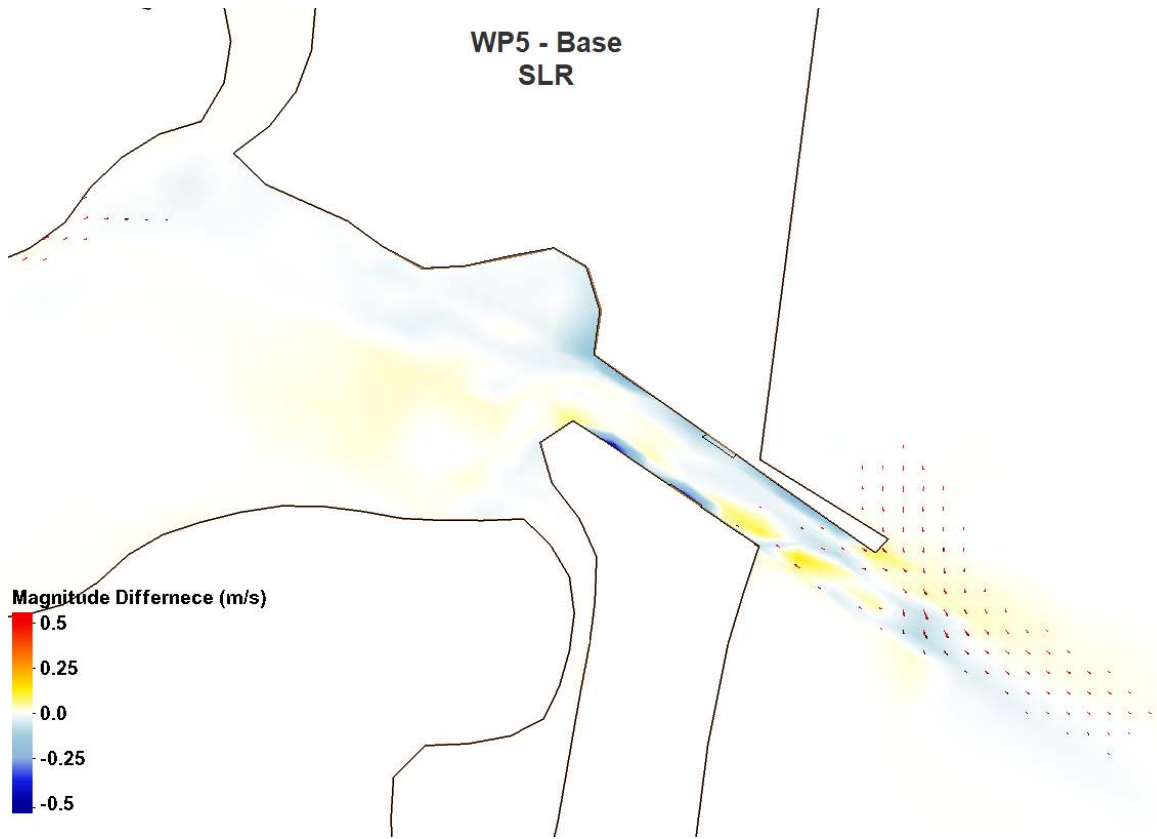
Residual velocity is the velocity that remains when the tidally varying velocity has been averaged out. This vector defines the predominant flow direction and speed of a particle of water. Although the tide will cause the particle to move back and forth, there is generally a flow direction that is a little stronger than the other, allowing for a particle to migrate along a certain path. The depth averaged velocity comparisons for Base and With Project alternatives are shown below. The red vectors indicate the direction of the alternative residual velocity and the black vectors, the Base. The contours represent the difference in the velocity magnitudes – alternative minus Base such that positive values (reds/yellows) indicate the alternative residual velocity magnitude is greater and negative values (blues) indicate that the Base residual velocity magnitude is greater.

Residual velocity comparisons for the structure locations – Manasquan, Barnegat, Absecon, Great Egg, Absecon Bay Boulevard, and 72nd Street –

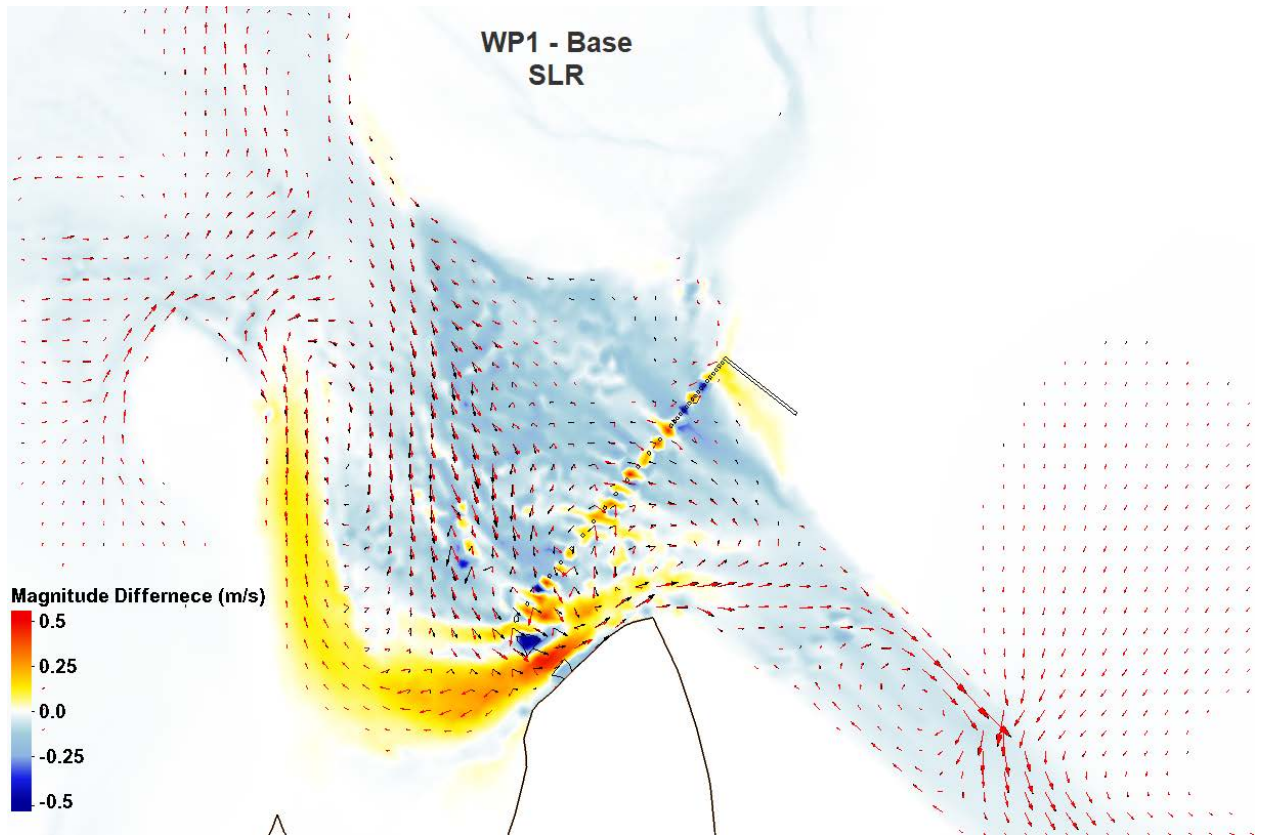
are shown for all alternatives. Velocity vectors are scaled to be comparable.

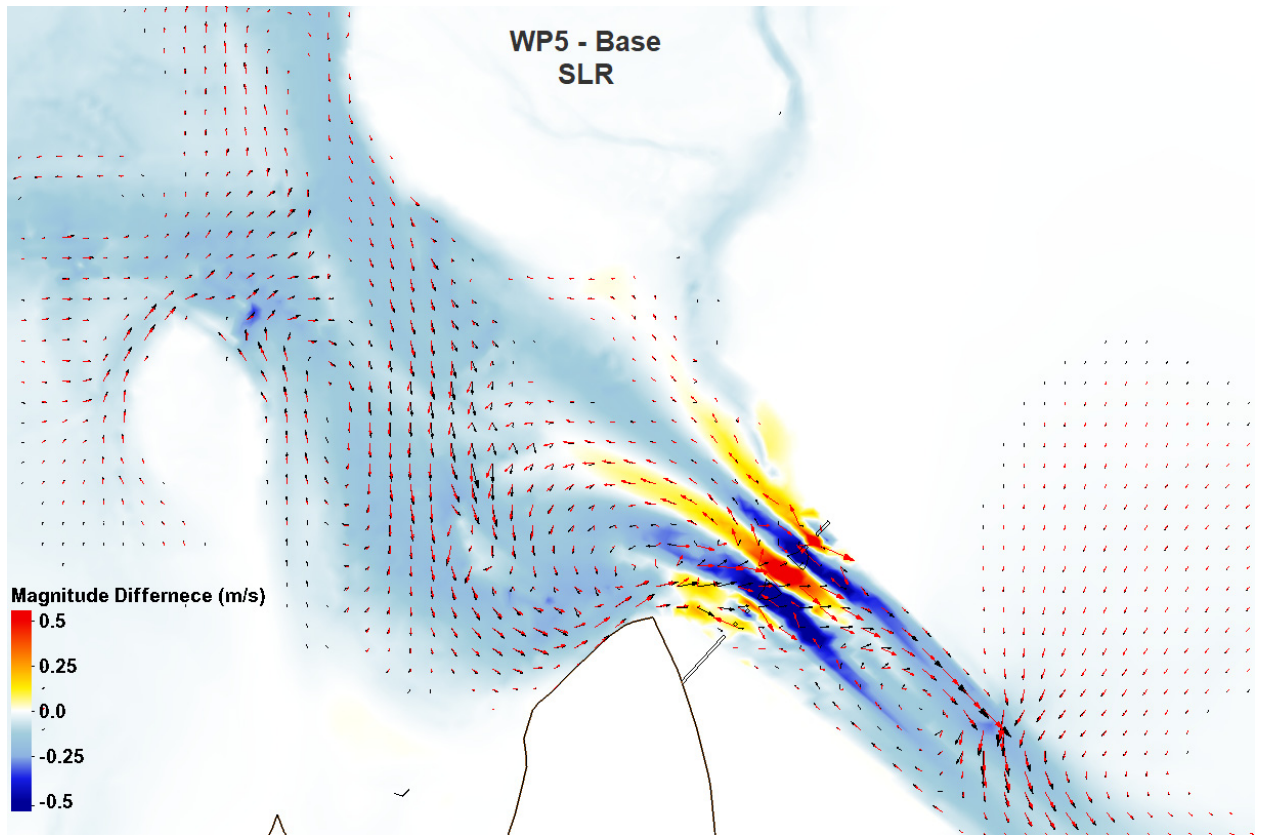
Manasquan



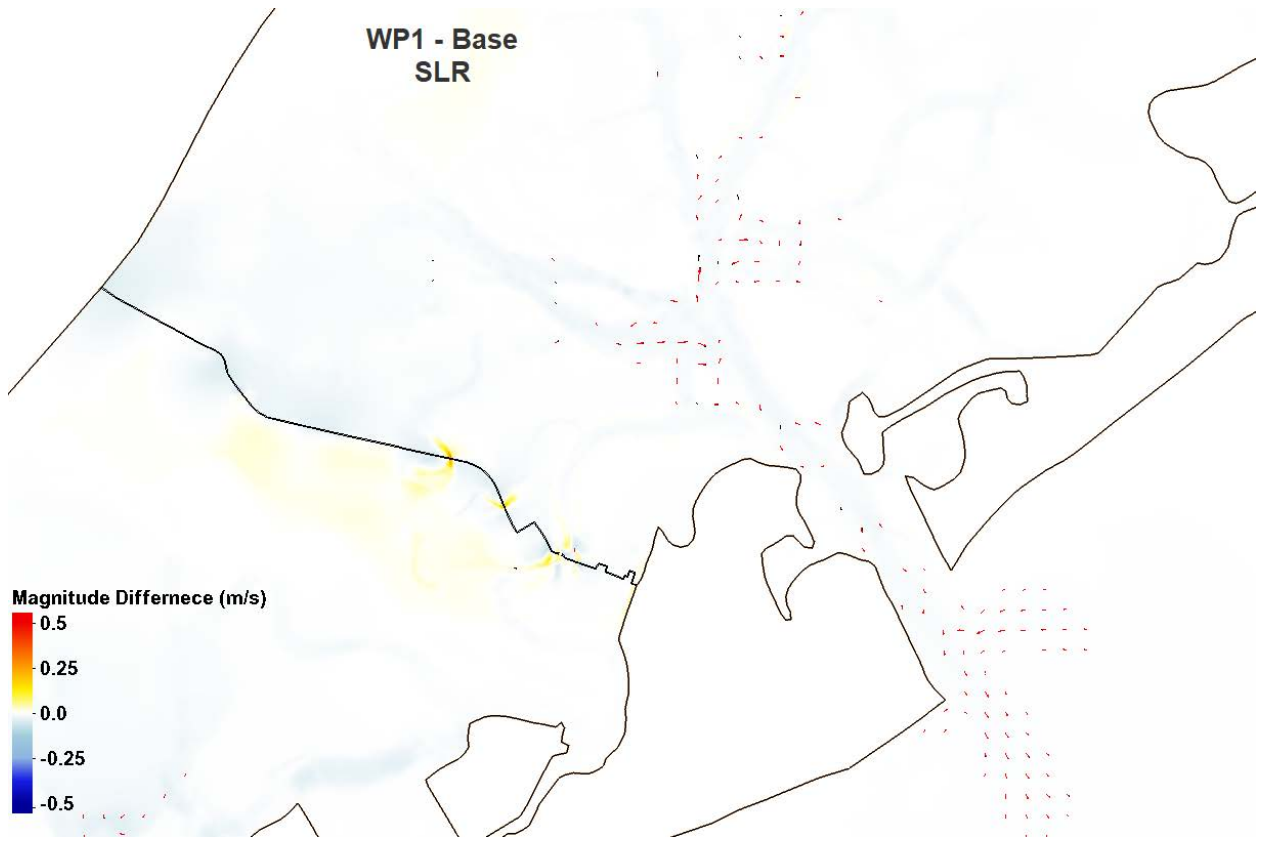


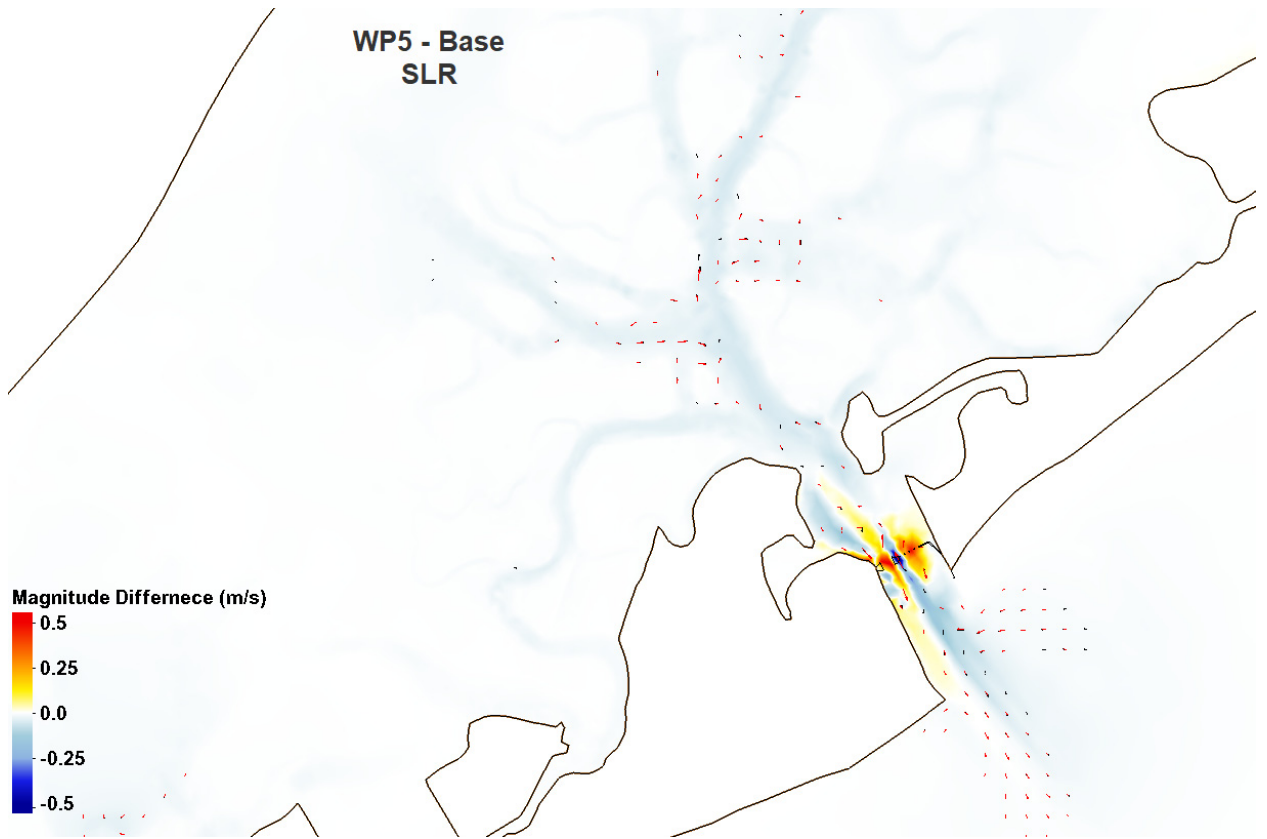
Barneгат



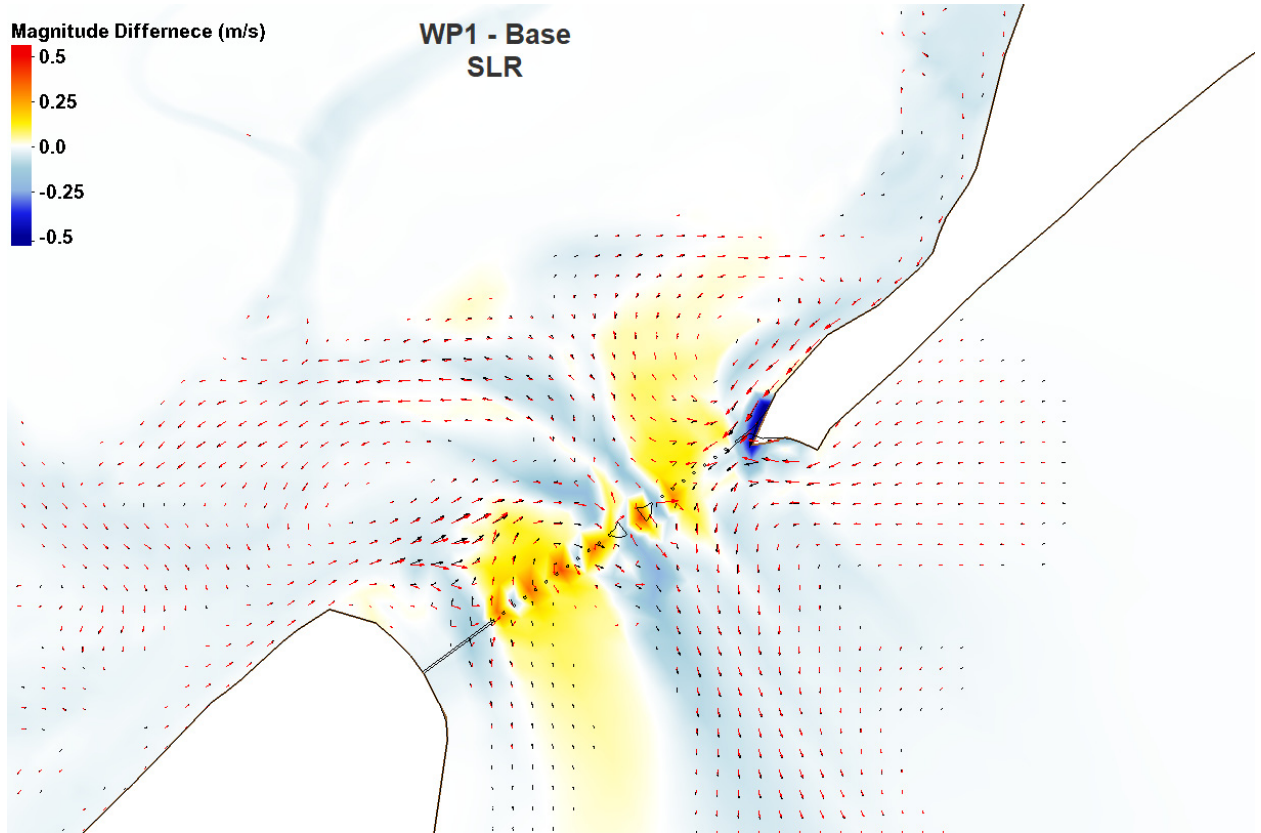


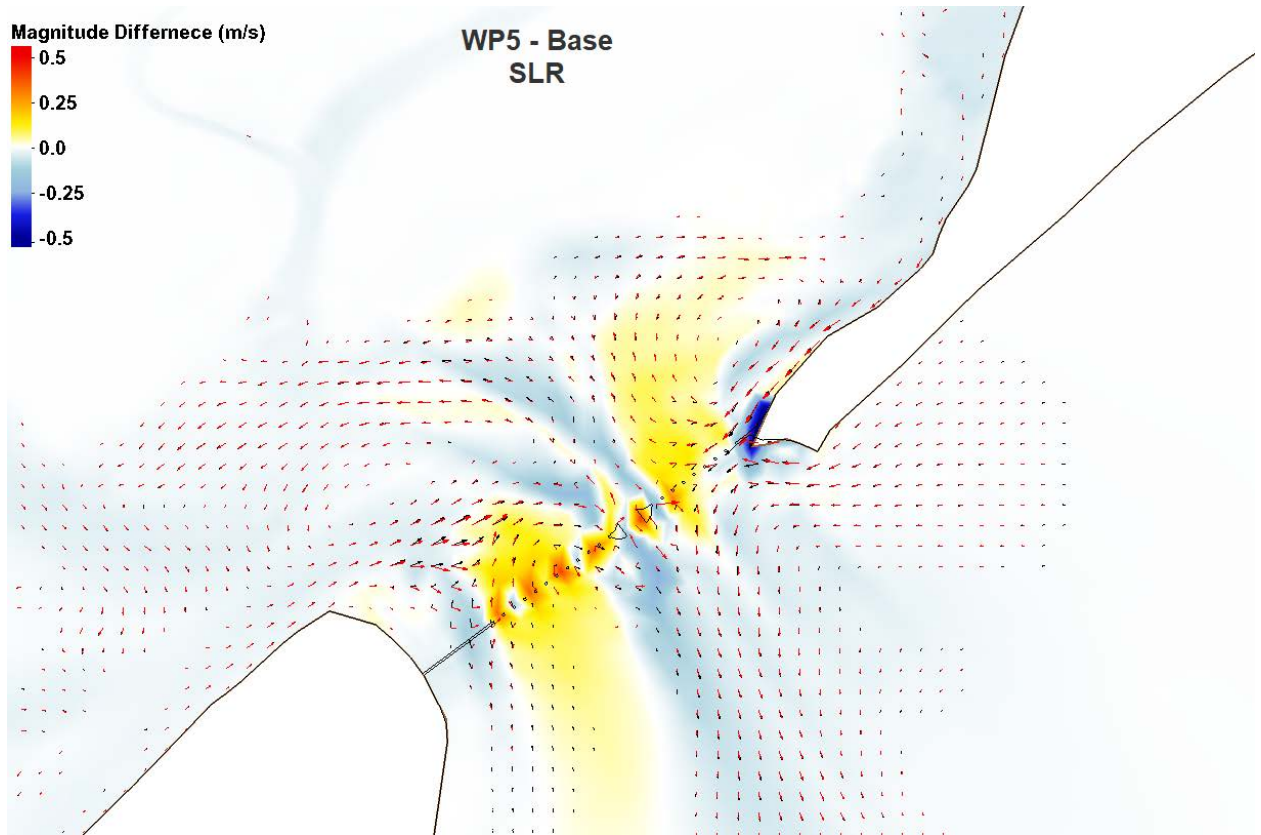
Absecon and Absecon Bay Blvd





Great Egg





72nd Street

WP1 - Base
SLR





Appendix G: Field Data Collection Report

FIELD REPORT ADCP DATA COLLECTION NEW JERSEY INLETS

Prepared by

Anthony M. Priestas

USACE Engineer Research and Development Center
Coastal and Hydraulics Laboratory
Field Data Collection and Analysis Branch

Introduction

This field report describes the operations, data collection, and data analysis efforts for surveys of flood and ebb velocities through three New Jersey back barrier inlets: Great Egg (GE), Little Egg (LE), and Barnegat Bay (BB). Velocity data were collected across specified transects at each of the three sites. Surveys were conducted continuously for 13 hours to capture flow directions and magnitudes across a full tidal cycle.

Summary of work

Three field teams, each consisting of a boat captain and ADCP operator, were deployed to collect the data. The personnel for each field team is provided in Table 1 and the schedule of work is provided in Table 2.

Table 15. Crew and vessels used in the field operation.

Location	Personnel	Role	Vessel
Barnegat Inlet	Chris Callegan	Boat Captain	R/V Curtis
	Kelsey Fall	ADCP Operator	
Little Egg Inlet	Charles Ellis	Boat Captain	R/V T. Waller
	Michael Ramirez	ADCP Operator	
Great Egg Harbor Inlet	Thomas Kirklin	Boat Captain	R/V Clara Jean
	Anthony Priestas	ADCP Operator	

The specific tasks of this work unit were:

- Completion of 13-hour ADCP surveys at specified transects
- Collection of Conductivity, Temperature, and Depth (CTD) profiles near the deepest location for each ADCP transect
- Data processing and visualization

Table 16. Schedule of work.

Sunday, February 17	Depart CHL
Tuesday, February 19	Arrive in New Jersey; launched vessels and performed instrument checks
Wednesday, February 20	Inclement weather day
Thursday, February 21	Survey
Friday, February 22	Depart New Jersey
Saturday, February 23	Arrive CHL
Monday, April 1	Completion of data processing and reporting

Site conditions

During the time of data collection, weather conditions ranged from cloudy to partly cloudy with no precipitation. Air temperatures ranged from 2.5-8° C, and the water temperature was approximately 4° C. Following the passage of a cold front and winter storm, winds (Figure 1) were mostly out of the west to west-northwest from 1.5 – 5 m/s (3-11 mph) as

measured at Cape May, NJ. Water elevations were slightly higher (mean of 0.19 m) than predicted. Strong winds produced moderate chop to choppy conditions within the bays; ocean waves entering Great Egg Inlet (T-3) were commonly 1.5 – 2 m based on visual observations. The rough sea conditions coupled with strong currents resulted in some missing ensembles, but not enough to significantly affect the average velocity and discharge results.

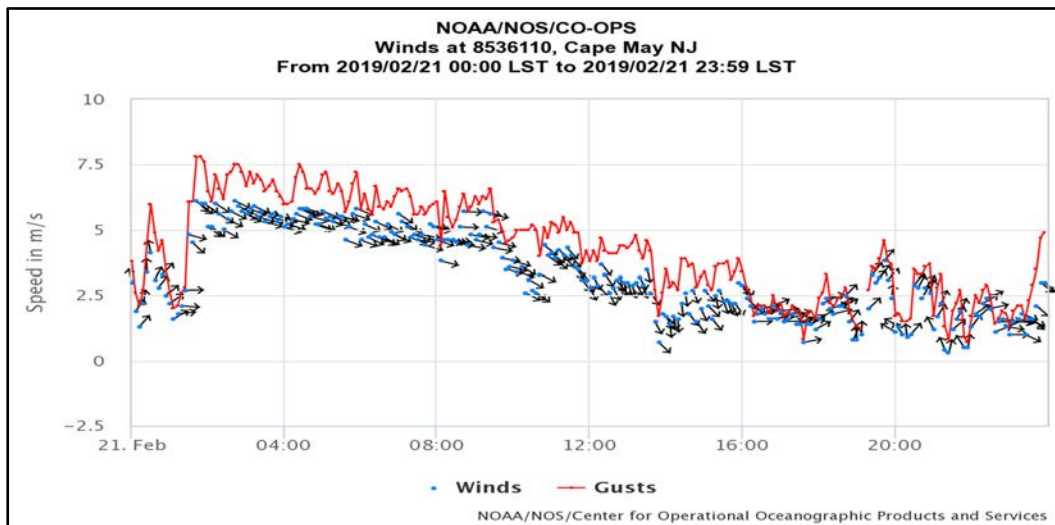


Figure 93. Wind speed vectors and gust magnitudes measured at Cape May, New Jersey, February 21, 2019.

General methods

Survey procedure

ADCP measurements were collected on February 21, 2019 across specified transects at each location. Data were collected across four transects each at Great Egg and Little Egg inlets, and one transect at Barnegat Inlet. Surveying began at approximately 1130 UTC (0630 EST) and ended near 2400 UTC (1900 EST). Survey directions are indicated by the arrows within the location maps. Velocity measurements were collected using a vessel-mounted, 1200 kHz Sentinel ADCP by Teledyne RD Instruments. The velocity measurement directions were co-registered with an external Trimble GPS system. The blanking distance was 0.25 m and the bin spacing was set to 0.25 m.

Salinity and temperature profiles were collected near the deepest part of each transect using a YSI Castaway CTD probe, which collects data at a frequency of 5 Hz. The CTD probe is designed to free fall at approximately 1 m/s.

Data processing

ADCP data were initially post-processed using Teledyne's WinRiver II software to evaluate data quality, ensure consistent velocity direction conventions, and to remove from further analysis transects that were aborted or erroneous. Depth-averaged velocities and .kmz files

for GIS visualizations were obtained using custom Matlab-based routines developed within the FDCAB of ERDC-CHL. Depth-averaged velocities were obtained by averaging the velocity bins within each ADCP ensemble; additional horizontal averaging was done by averaging every three ensembles.

CTD data were uploaded to the CastAway-CTD software and exported as .mat and .csv files as is; no further post-processing was conducted on the data as spikes and outliers are handled internally prior to data export. Temperature and salinity data are presented as depth profiles and as color maps as a function of depth and time. CTD data are not available for Little Egg Inlet due to instrument loss.

Data products

Multiple processed data products were generated for each inlet. They are as follows:

- Discharge summaries for each transect (.pdf)
- Depth averaged velocities for each ensemble (ASC.TXT)
- Depth averaged velocities, horizontally averaged by every three ensembles (ASC.TXT)
- CTD files and summaries for each transect (.CSV, .mat, .kml)

The values in the velocity files (ASC.TXT) correspond to the following headers and units listed in Table 1.

Table 17. Explanation of headers in velocity data files.

Date time							UTM [m]		Z [m]	Umag	Udir	u	x	z	Err	bckscttr
YY	MM	DD	hh	mm	ss	ms	X	Y	Z	cm/s	Deg	cm/s	cm/s	cm/s	cm/s	counts

Great Egg Inlet

Fifty-seven profiles were collected across four transects. Measurement cycles began at T-1 and continued counterclockwise, ending at T-2. Measurements began at approximately 1145 UTC (0645 EST) and ended near 2400 UTC (1900 EST). The start times of each measurement cycle at T-1 is mapped to the position of the tidal frame in Figure 3. Representative bottom profiles and examples of the flow structures and magnitudes near peak flood and ebb are provided in Figures 4-7.



Figure 94. Location map of Great Egg Inlet. All ADCP data were collected in the directions indicated by the arrow.

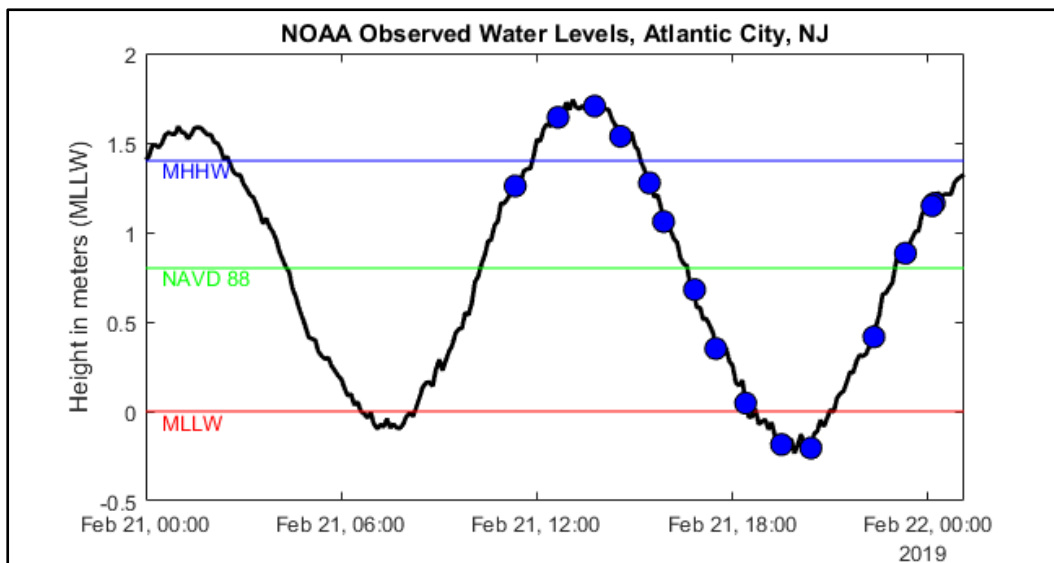


Figure 95. ADCP coverage of the tidal cycle at Great Egg Inlet. Start time of each ADCP measurement cycle (blue dot) is shown relative to the tidal frame. Times are in Universal Coordinated Time.

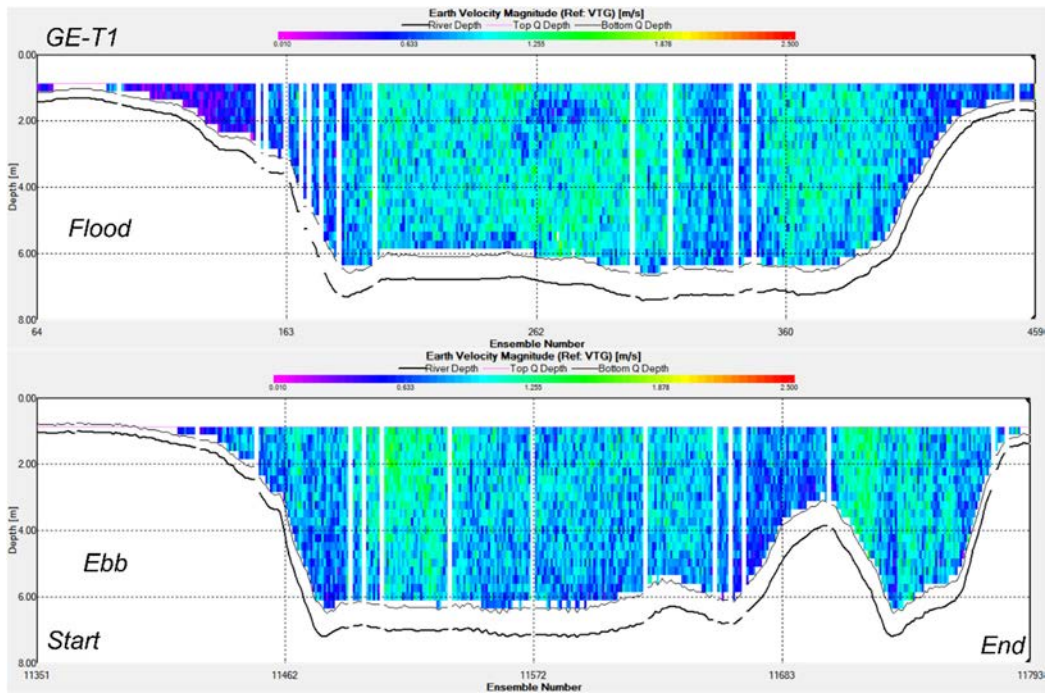


Figure 96. ADCP profiles of GE-T1 near peak flood (upper) and ebb (lower) tides, 12:53 and 15:55 UTC, respectively. Velocity scale 0.01 – 2.5 m/s. Note that variability in channel morphology was due to slight changes in start and end bank positions as dictated by water level and accessibility.

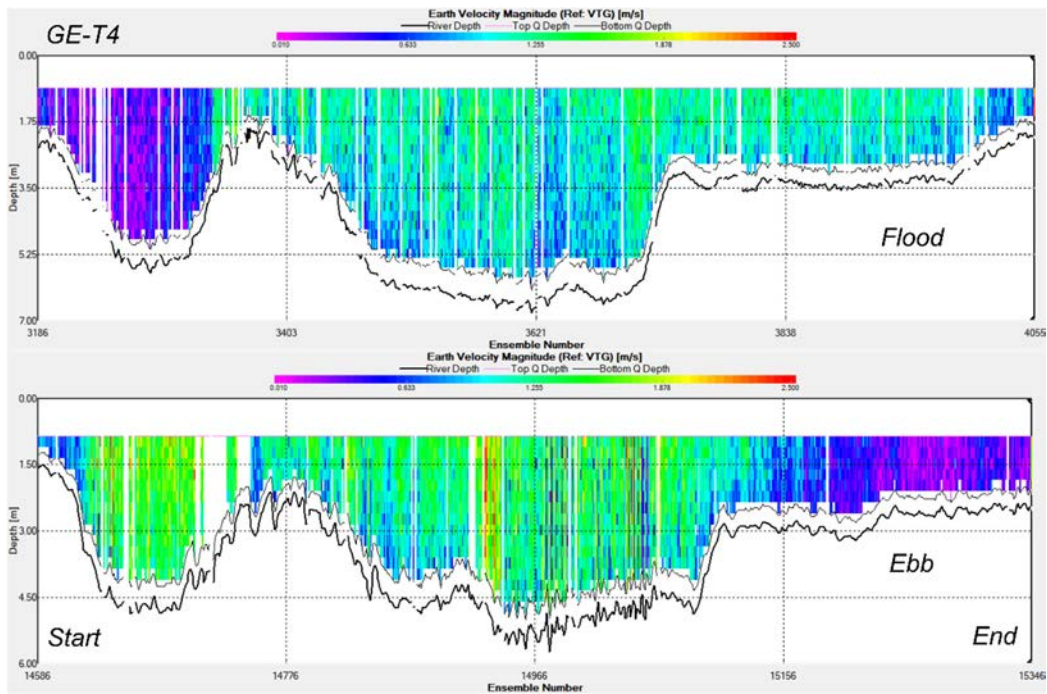


Figure 97. ADCP profiles of GE-T4 near peak flood (upper) and ebb (lower) tides, 11:56 and 18:49 UTC, respectively. Velocity scale 0.01 – 2.5 m/s.

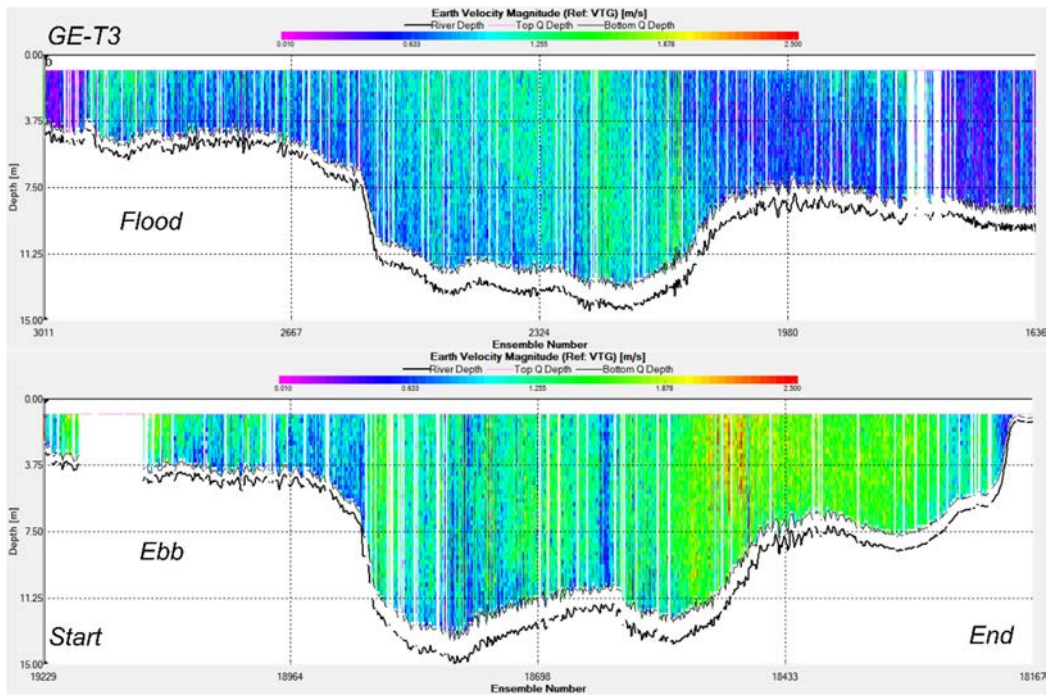


Figure 98. ADCP profiles of GE-T3 near peak flood (upper) and ebb (lower) tides, 12:13 and 17:08 UTC, respectively. Velocity scale 0.01 – 2.5 m/s.

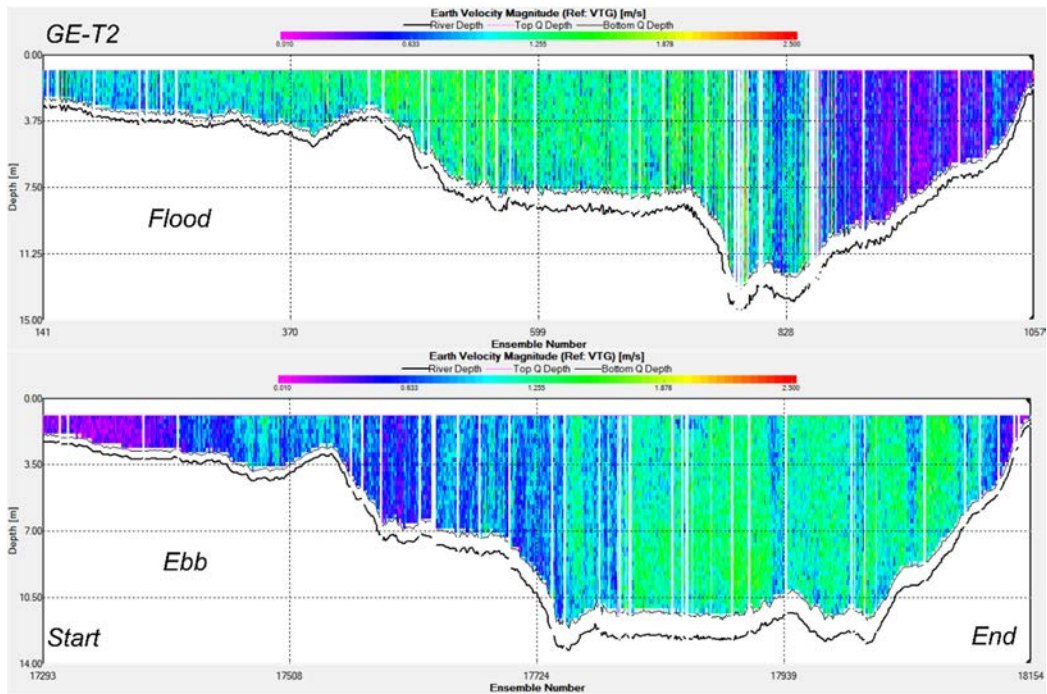


Figure 99. ADCP profiles of GE-T2 near peak flood (upper) and ebb (lower) tides, 12:30 and 16:30 UTC, respectively. Velocity scale 0.01 – 2.5 m/s.

Table 18. Generalized Summary of Velocity Data – GE Inlet

Transect No.	Width [m], mean (SD)	Area [m ²], mean (SD)	Peak Mean Flood Vel. [m/s]	Peak Mean Ebb Vel. [m/s]	Mean Flow Dir. (Flood/Ebb) [deg]		Peak Discharge (Flood/Ebb) [m ³ /s]	
1	166 (29)	544 (92)	-0.82	0.83	13	190	-509	473
4	771 (45)	2391 (483)	-0.72	0.93	62	228	-2123	2131
3	1541 (323)	11542 (2891)	-0.50	0.53	311	115	-6395	6572
2	907 (30)	5750 (556)	-0.79	0.80	228	62	-4870	4261

Table 19. Transect 1 - Generalized Summary of CTD Data – GE Inlet

Cast time (EST)	Start latitude	Start longitude	Mean Temp [C]	Depth [m]	Mean Salinity [PSU]
2/21/2019 18:22	39.31208	-74.5594	4.68	3.59	28.36
2/21/2019 17:31	39.31214	-74.5593	5.01	3.45	26.76
2/21/2019 16:40	39.31224	-74.5591	5.41	2.56	25.43
2/21/2019 15:45	39.31209	-74.5591	5.87	2.70	26.92
2/21/2019 15:45	39.31245	-74.5591	Invalid	Invalid	Invalid
2/21/2019 14:39	39.31209	-74.5593	5.77	3.00	27.35
2/21/2019 13:44	39.3123	-74.5592	5.54	2.70	27.27
2/21/2019 12:42	39.31216	-74.5593	5.21	3.30	27.31
2/21/2019 11:40	39.31228	-74.5593	4.78	3.44	27.90
2/21/2019 10:47	39.31217	-74.5593	4.45	3.59	28.91
2/21/2019 9:56	39.31218	-74.5593	4.17	3.89	29.85
2/21/2019 8:48	39.31181	-74.5592	4.06	3.44	29.99
2/21/2019 7:55	39.31202	-74.5594	3.99	3.88	30.04
2/21/2019 6:50	39.31203	-74.5595	3.93	3.74	29.92
2/21/2019 5:45	39.31208	-74.5593	3.74	3.59	29.48
2/21/2019 5:39	39.31198	-74.5586	Invalid	Invalid	Invalid

Table 20. Transect 2 - Generalized Summary of CTD Data – GE Inlet

Cast time (EST)	Start latitude	Start longitude	Mean Temp [C]	Depth [m]	Mean Salinity [PSU]
2/21/2019 18:54	39.30874	-74.5392	4.25	3.14	29.97
2/21/2019 18:00	39.30904	-74.5386	4.36	2.99	29.87
2/21/2019 17:08	39.30869	-74.5393	4.58	2.84	29.20
2/21/2019 16:14	39.30867	-74.5384	5.01	2.55	25.68
2/21/2019 15:16	39.30883	-74.5385	5.05	2.54	28.09
2/21/2019 14:20	39.30872	-74.5389	5.10	2.39	28.14
2/21/2019 13:25	39.30863	-74.5389	4.90	2.24	28.43
2/21/2019 13:23	39.3078	-74.5397	Invalid	Invalid	Invalid
2/21/2019 12:19	39.30875	-74.5387	4.74	2.40	28.99

2/21/2019 11:25	39.30867	-74.5388	4.47	2.54	29.12
2/21/2019 10:34	39.30863	-74.539	4.22	2.69	29.53
2/21/2019 9:22	39.30856	-74.5392	4.09	2.99	29.91
2/21/2019 8:30	39.30865	-74.5391	3.99	3.14	29.92
2/21/2019 7:40	39.30873	-74.539	3.94	3.43	29.94
2/21/2019 6:33	39.30882	-74.539	3.91	3.44	29.89

Table 21. Transect 3 - Generalized Summary of CTD Data – GE Inlet

Cast time (EST)	Start latitude	Start longitude	Mean Temp [C]	Depth [m]	Mean Salinity [PSU]
2/21/2019 18:45	39.30357	-74.5467	4.30	9.53	29.80
2/21/2019 17:50	39.30371	-74.5468	4.35	8.66	29.51
2/21/2019 16:59	39.30345	-74.5462	4.80	8.82	28.00
2/21/2019 16:05	39.30289	-74.5456	4.97	6.49	26.63
2/21/2019 15:07	39.30288	-74.5445	4.97	5.71	24.72
2/21/2019 14:07	39.3028	-74.5447	4.94	5.91	27.20
2/21/2019 13:06	39.30271	-74.5446	4.86	6.10	28.72
2/21/2019 12:08	39.30224	-74.5446	Invalid	Invalid	Invalid
2/21/2019 11:13	39.30265	-74.5457	4.40	10.87	29.55
2/21/2019 10:21	39.30244	-74.5454	4.25	9.94	29.98
2/21/2019 9:12	39.30147	-74.5437	4.02	10.26	29.94
2/21/2019 8:19	39.30261	-74.5461	4.00	8.60	30.09
2/21/2019 7:28	39.30267	-74.5463	3.93	11.87	30.14
2/21/2019 6:20	39.30284	-74.5467	3.93	10.58	30.11

Table 22. Transect 4 - Generalized Summary of CTD Data – GE Inlet

Cast time (EST)	Start latitude	Start longitude	Mean Temp [C]	Depth [m]	Mean Salinity [PSU]
2/21/2019 18:35	39.30055	-74.5553	4.50	5.38	29.47
2/21/2019 17:41	39.30032	-74.5559	4.62	3.89	28.91
2/21/2019 16:50	39.3008	-74.5557	4.87	5.24	28.07
2/21/2019 15:55	39.3006	-74.556	4.99	4.81	23.86
2/21/2019 14:55	39.3005	-74.5564	4.92	4.51	24.28
2/21/2019 13:57	39.30051	-74.5565	4.72	5.69	26.65
2/21/2019 12:55	39.30066	-74.5565	4.60	5.09	27.96
2/21/2019 11:57	39.30059	-74.5562	4.51	5.54	28.93
2/21/2019 11:04	39.30061	-74.5562	4.25	5.24	29.79
2/21/2019 10:09	39.30062	-74.5562	4.03	6.13	29.97
2/21/2019 9:00	39.30059	-74.5559	3.96	6.13	29.95
2/21/2019 8:09	39.30065	-74.5556	3.93	5.38	29.92
2/21/2019 7:20	39.30075	-74.5553	3.85	5.83	29.95
2/21/2019 6:09	39.30062	-74.5558	3.86	4.78	29.50

2/21/2019 6:01	39.302	-74.5562	3.85	4.03	29.67
----------------	--------	----------	------	------	-------

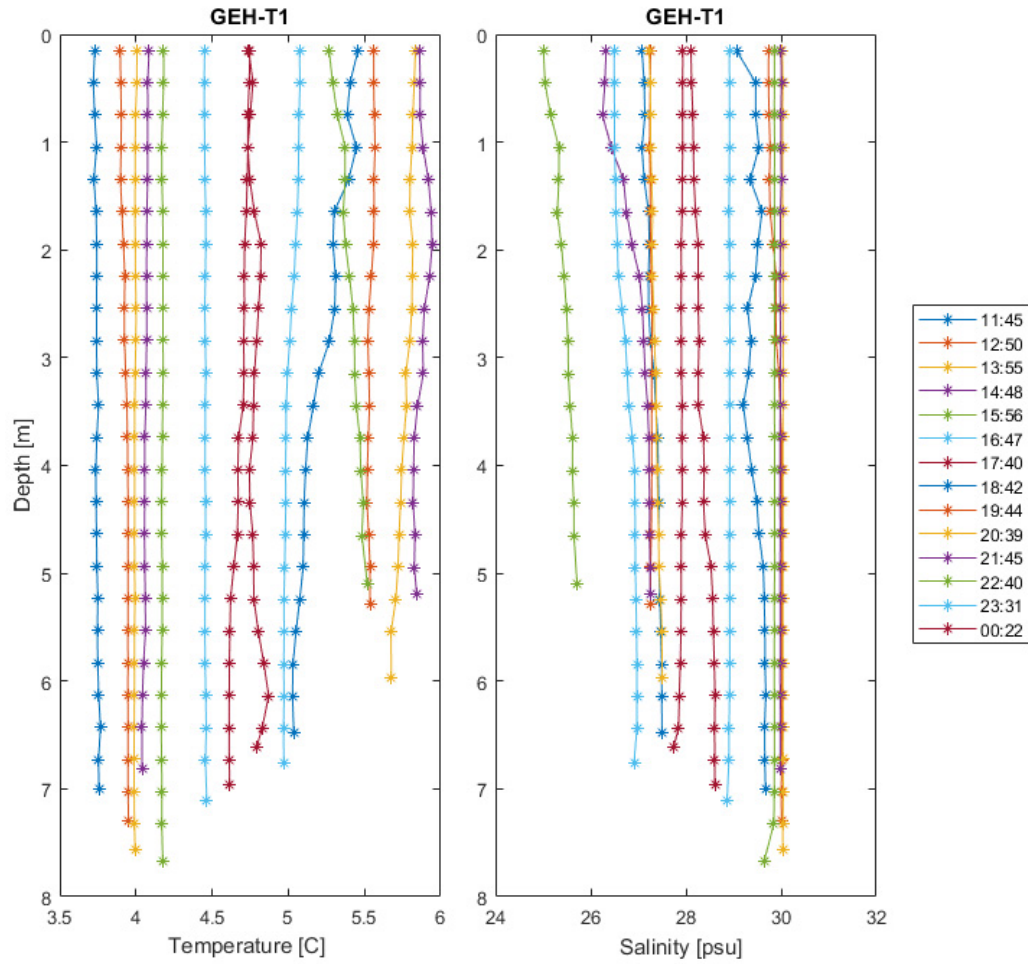


Figure 100. Salinity and temperature profiles at GEH Transect 1. Times refer to Local Standard Time.

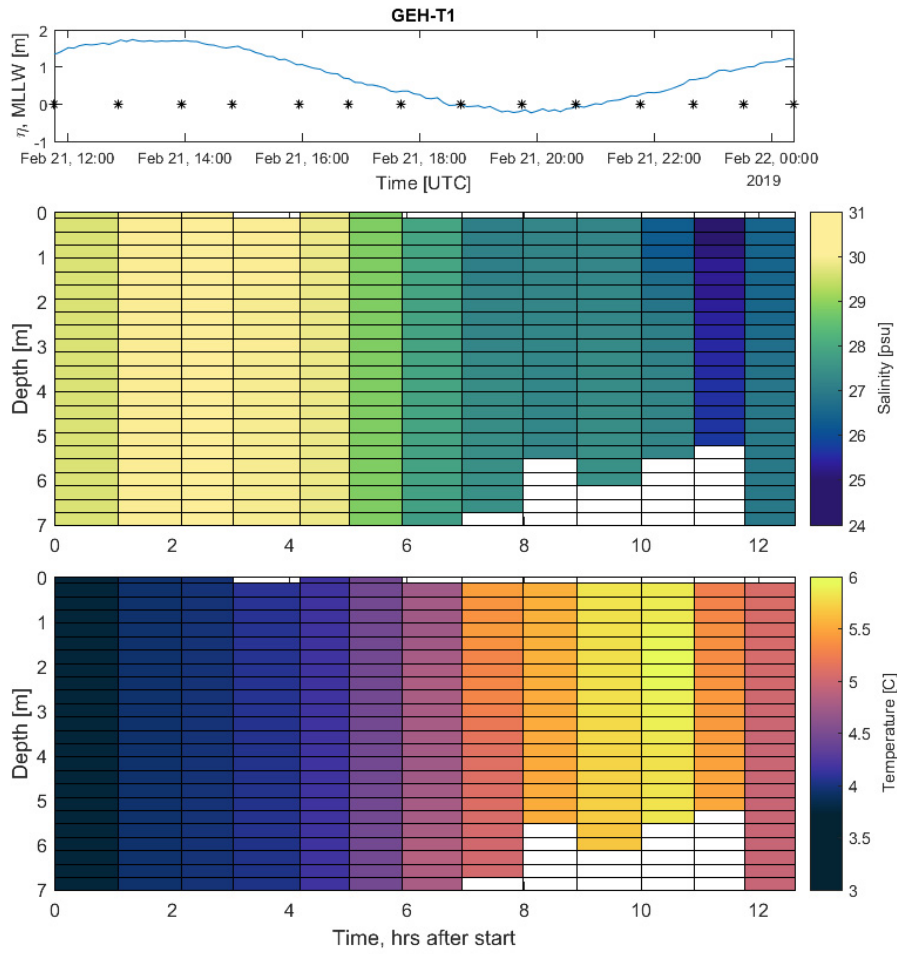


Figure 101. Salinity and temperature distributions as a function of depth and time at GEH Transect 1. Black dots on the upper panel indicates starting cast time.

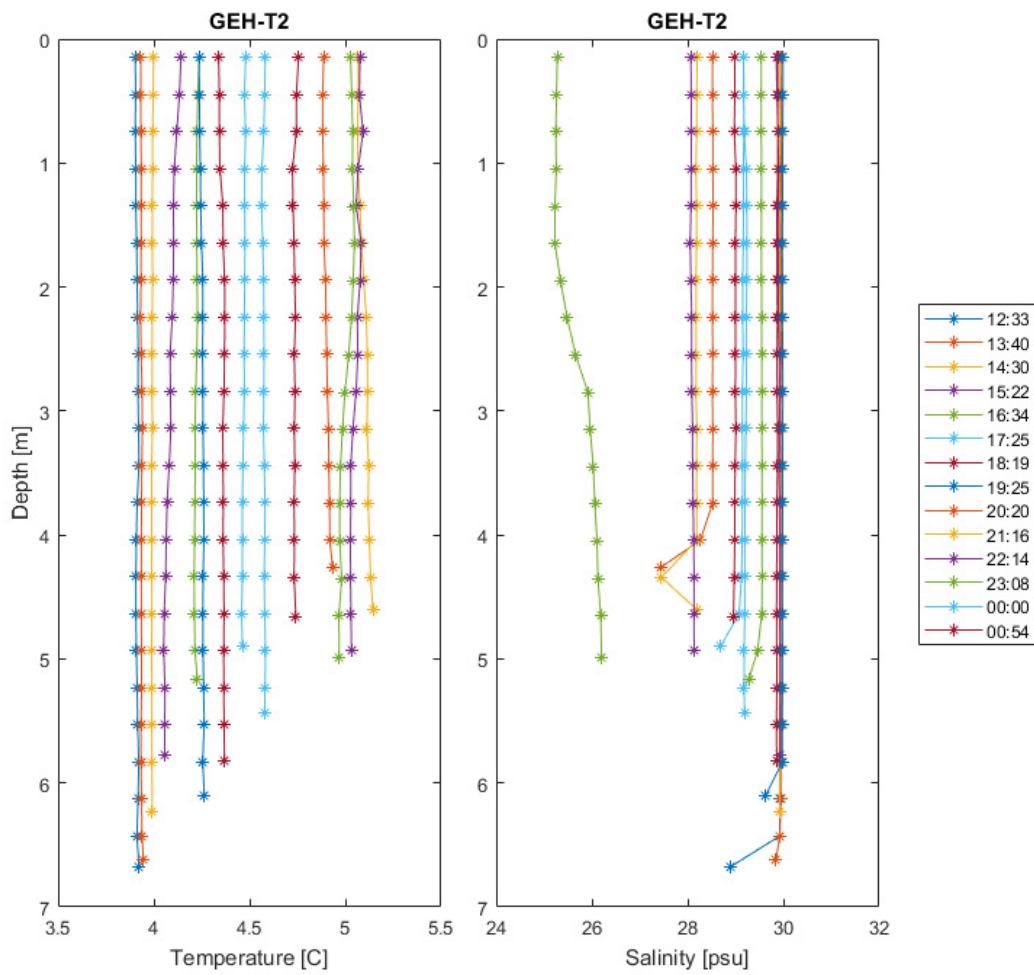


Figure 102. Salinity and temperature profiles at GEH Transect 2. Times refer to Local Standard Time.

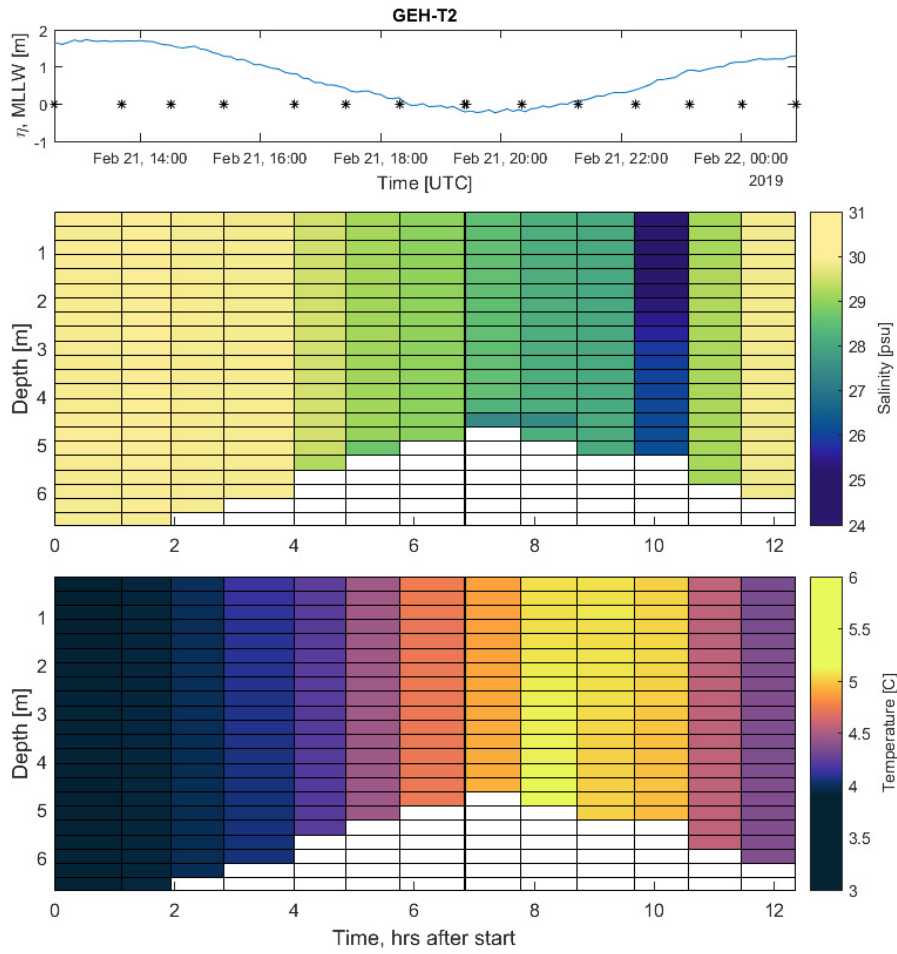


Figure 103. Salinity and temperature distributions as a function of depth and time at GEH Transect 2. Black dots on the upper panel indicates starting cast time.

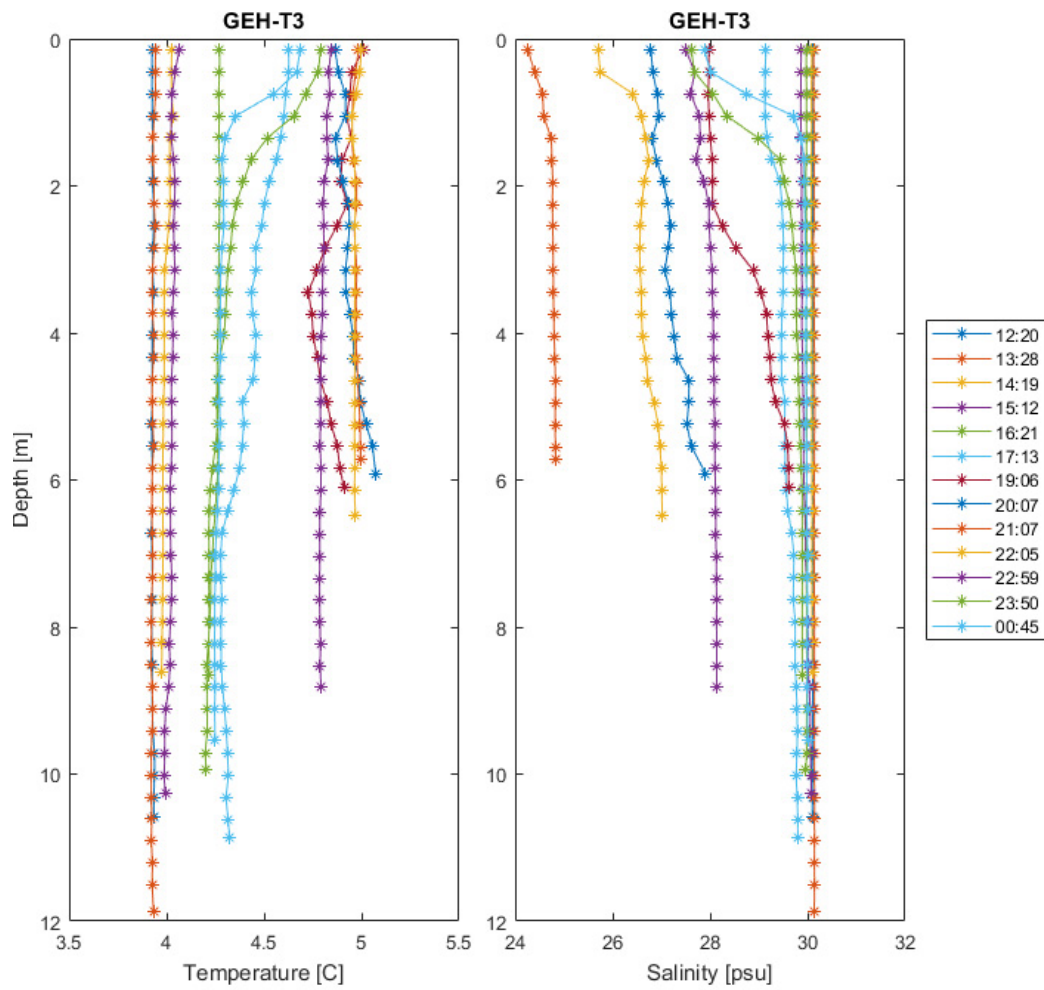


Figure 104. Salinity and temperature profiles at GEH Transect 3. Times refer to Local Standard Time.

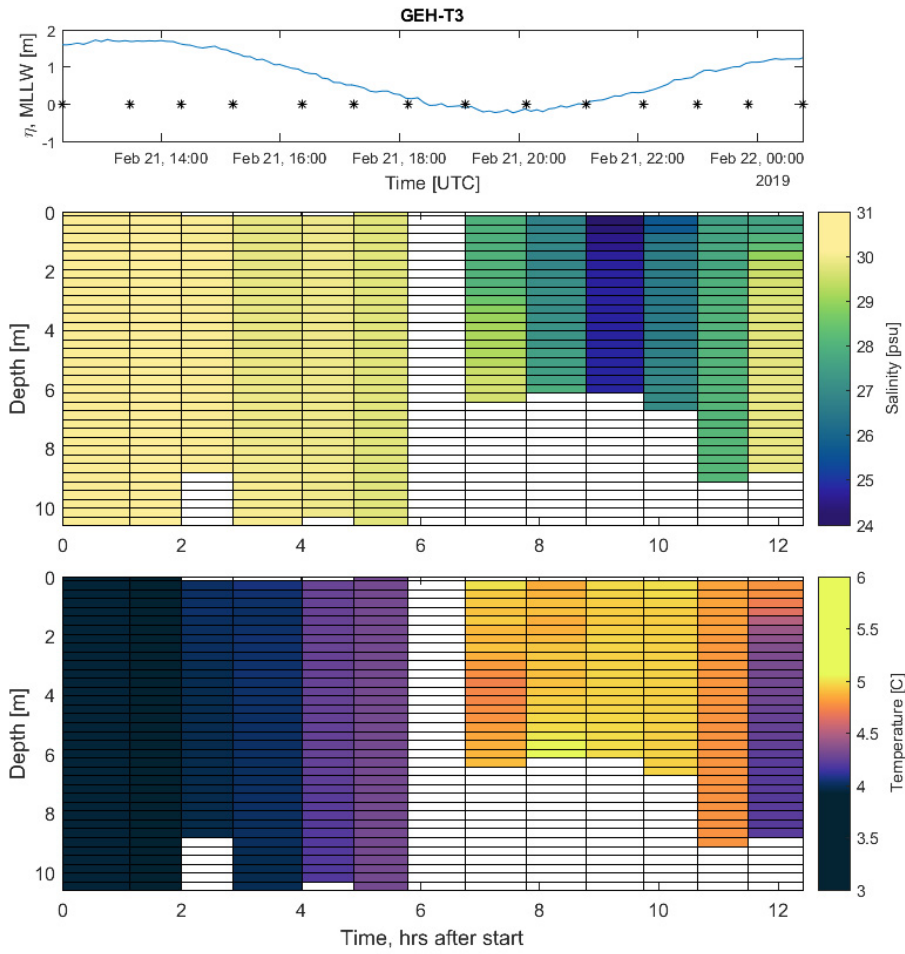


Figure 105. Salinity and temperature distributions as a function of depth and time at GEH Transect 3. Black dots on the upper panel indicates starting cast time.

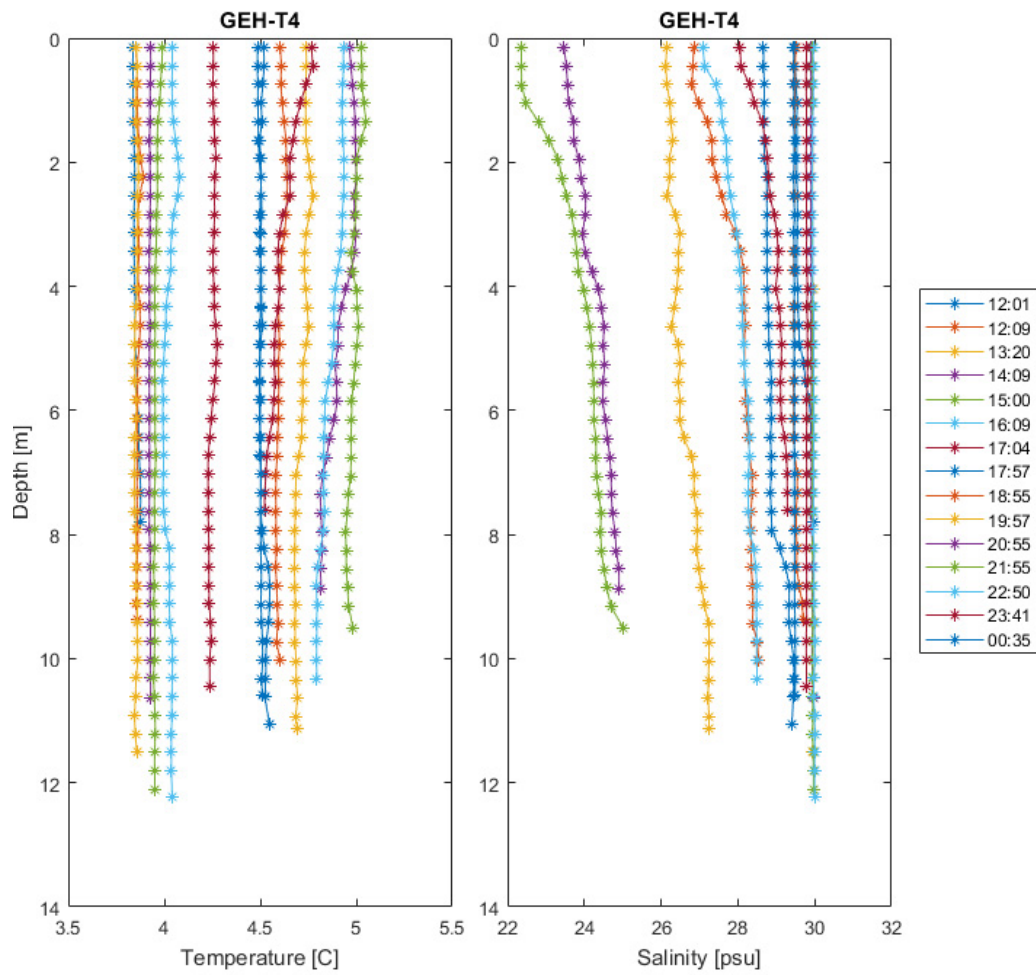


Figure 106. Salinity and temperature profiles at GEH Transect 4. Times refer to Local Standard Time.

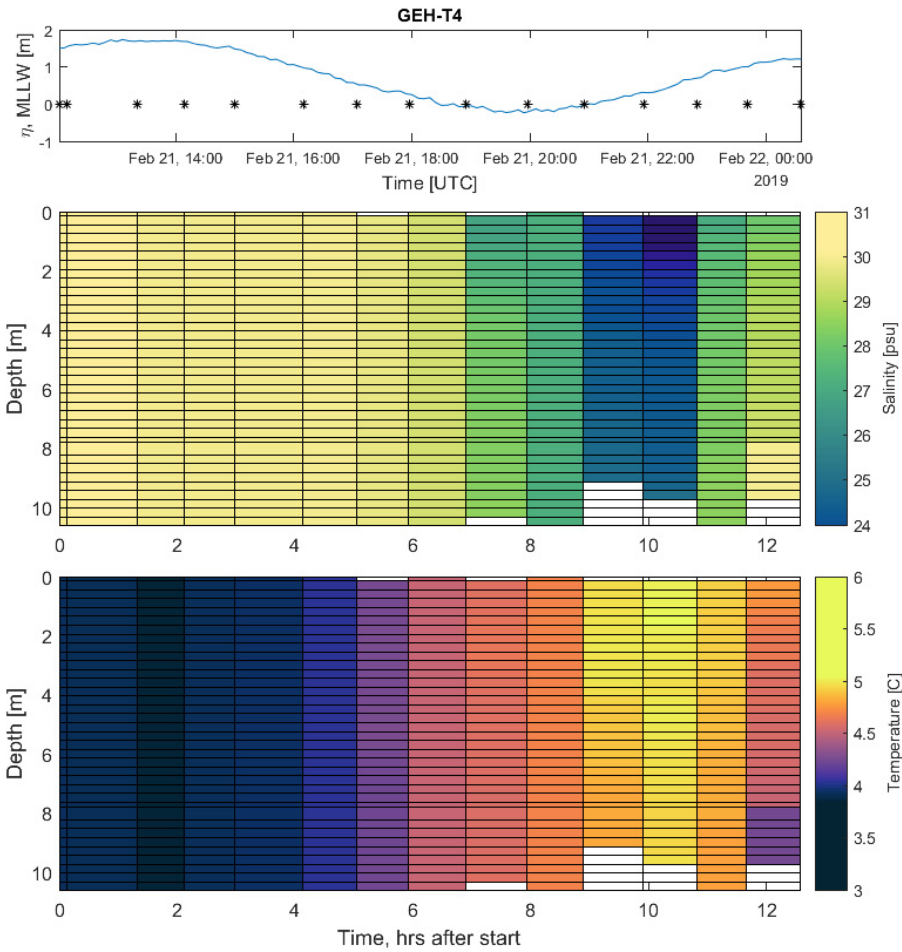


Figure 107. Salinity and temperature distributions as a function of depth and time at GEH Transect 4. Black dots on the upper panel indicates starting cast time.

Little Egg Inlet

Thirteen ADCP profiles were collected across each of four transects at Little Egg Inlet; measurement cycles began T-1 and continued clockwise as shown in Figure 16. Coverage of the tidal cycle is shown in Figure 17. No CTD data were collected as the instrument was lost during the first cast. Profiles of the velocity magnitudes near peak flood and ebb stages are shown in Figures 18-21. Summarized velocity and discharge data are shown in Table 9.

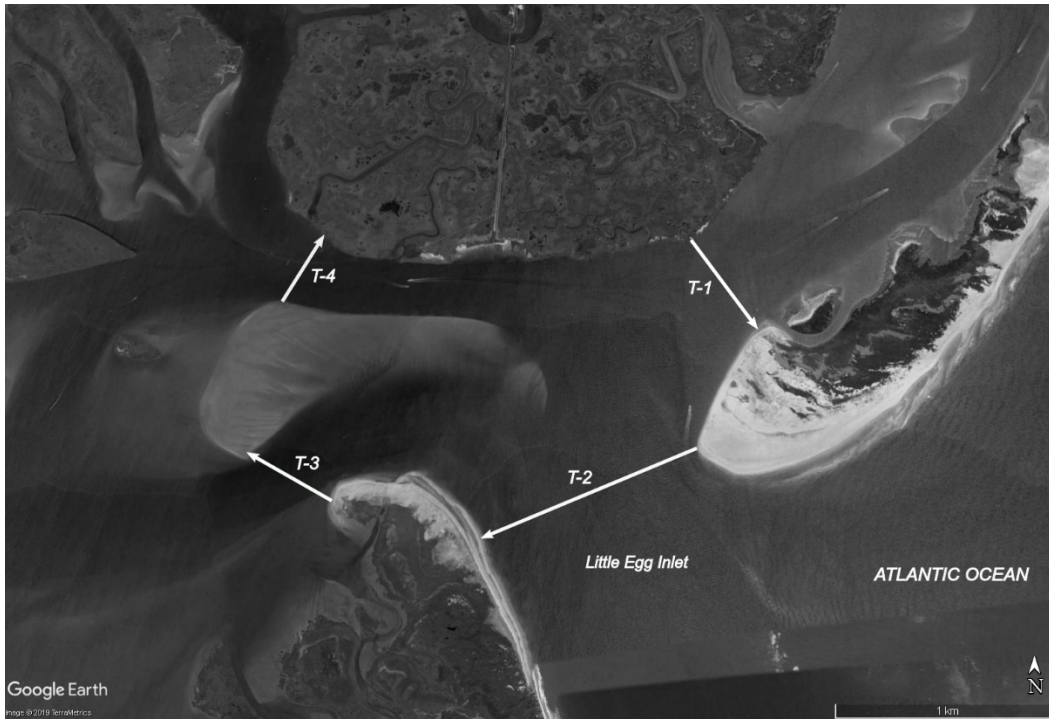


Figure 108. Location map of Little Egg Inlet. All ADCP data were collected in the directions indicated by the arrow.

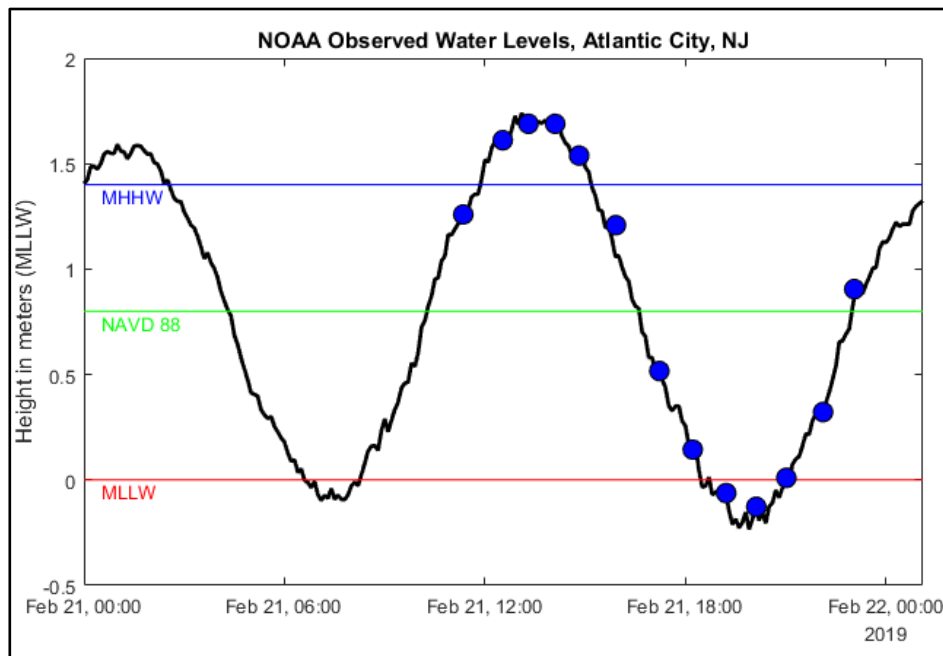


Figure 109. ADCP coverage of the tidal cycle at Little Egg Inlet. Start time of each ADCP measurement cycle (blue dot) is shown relative to the tidal frame. Times are in Universal Coordinated Time.

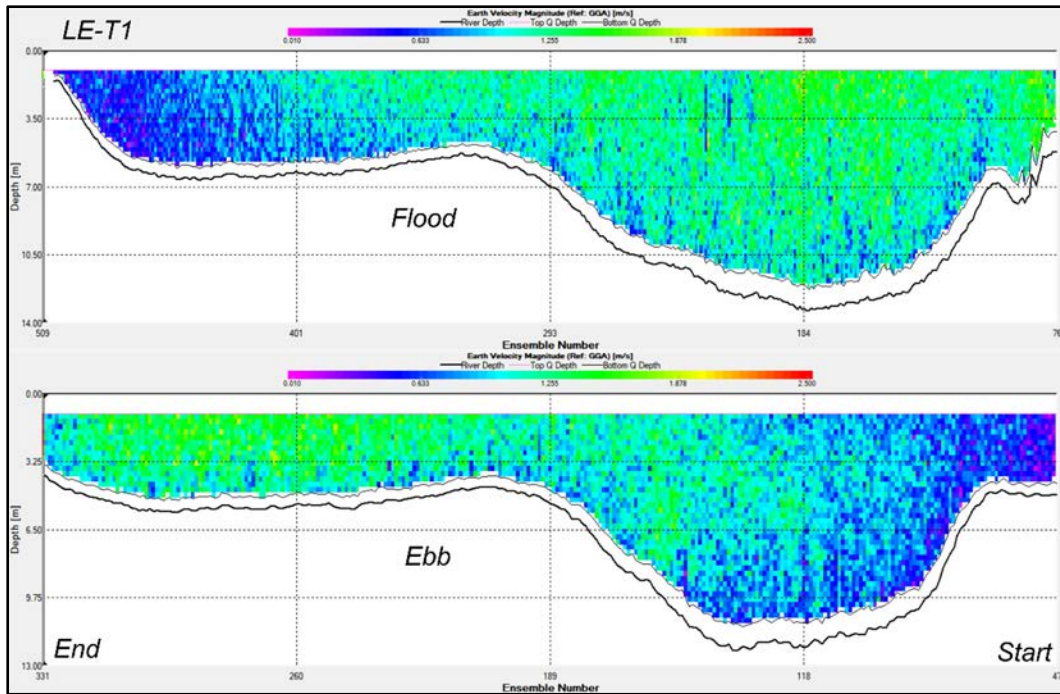


Figure 110. Profiles of LE-T1 near peak flood (upper) and ebb (lower) tides, 11:21 and 18:13 UTC, respectively. Velocity scale is 0.01 to 2.5 m/s.

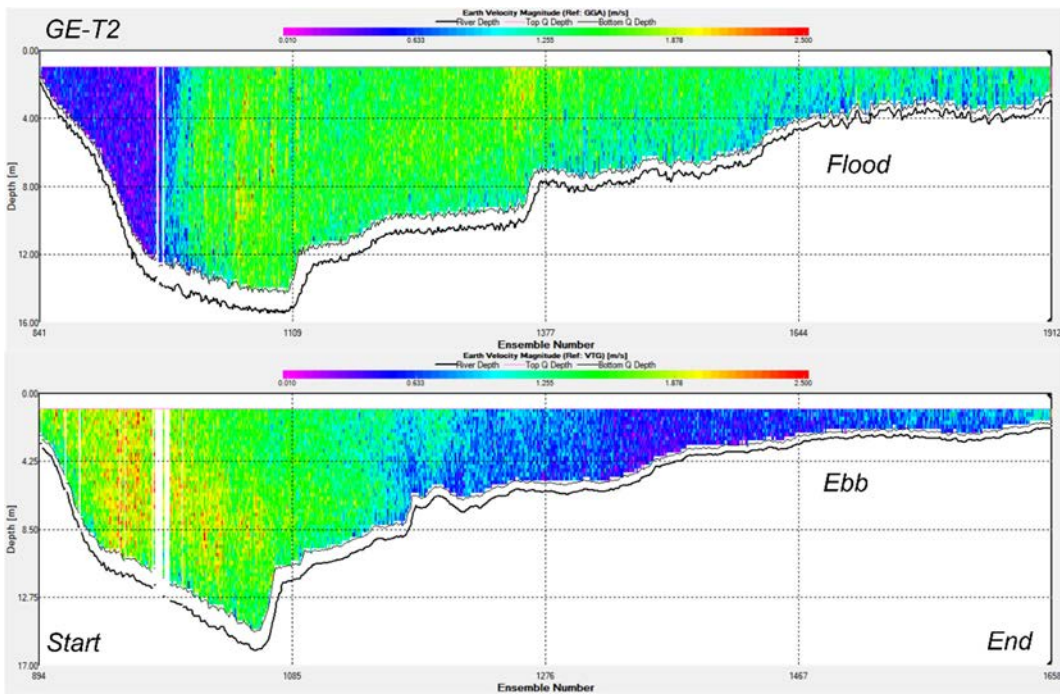


Figure 111. Profiles of LE-T2 near peak flood (upper) and ebb (lower) tides, 12:51 and 18:26 UTC, respectively. Velocity scale is 0.01 to 2.5 m/s.

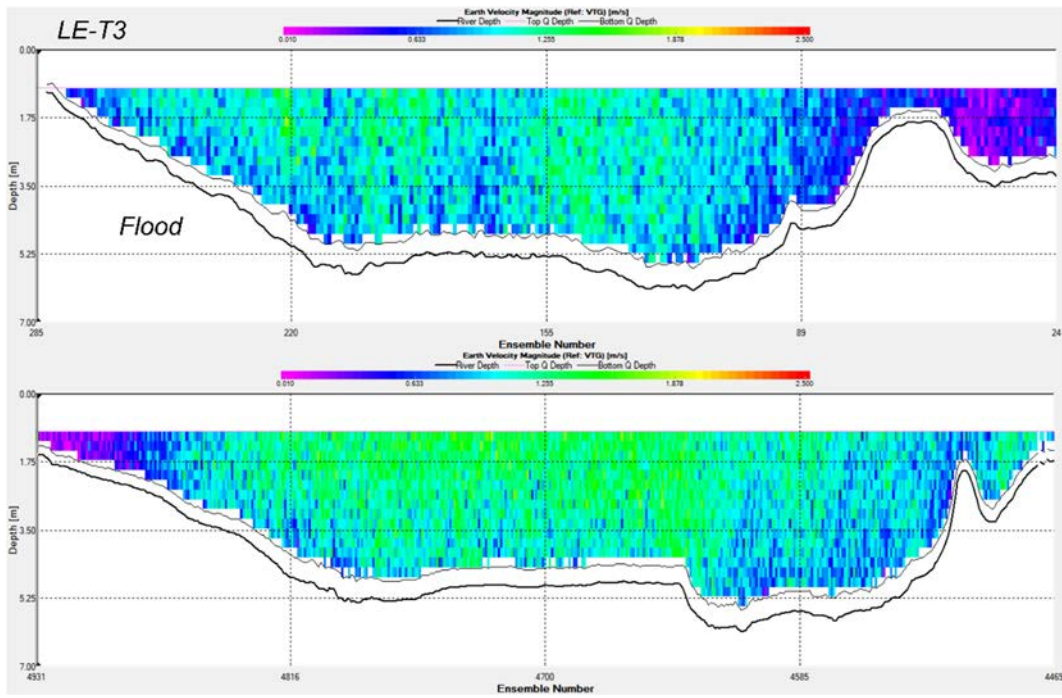


Figure 112. Profiles of LE-T3 near peak flood (upper) and ebb (lower) tides, 13:02 and 18:39 UTC, respectively. Velocity scale is 0.01 to 2.5 m/s.

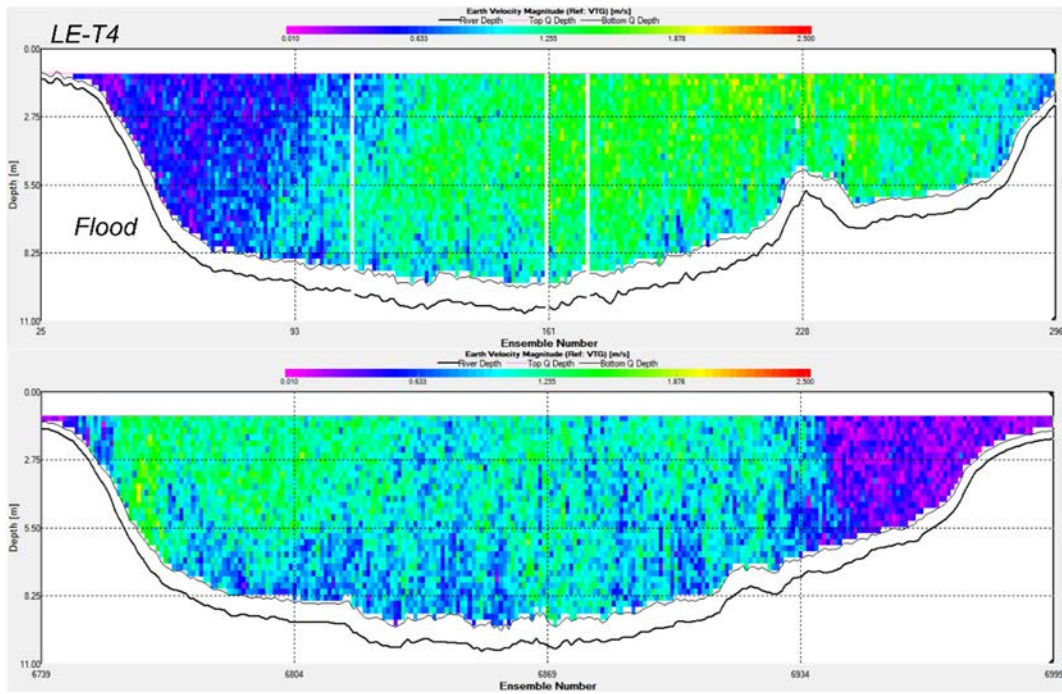


Figure 113. Profiles of LE-T4 near peak flood (upper) and ebb (lower) tides, 13:09 and 18:51 UTC, respectively. Velocity scale is 0.01 to 2.5 m/s.

Table 23. Summarized velocity and discharge data for Little Egg Inlet.

Transect No.	Width [m], mean (SD)	Area [m ²], mean (SD)	Peak Mean Flood Vel. [m/s]	Peak Mean Ebb Vel. [m/s]	Mean Flow Dir. (Flood/Ebb) [deg]		Peak Discharge (Flood/Ebb) [m ³ /s]	
1	536 (122)	4176 (943)	-1.02	0.89	48	213	-4817	3675
2	1134 (51)	7841 (692)	-1.07	1.10	345	174	-9028	8171
3	429 (21)	1864 (214)	-0.79	0.91	234	54	-1566	1556
4	399 (15)	3304 (151)	-1.00	0.84	293	103	-3388	2739

Barnegat Inlet

Fourteen ADCP profiles were completed at T-1. Measurement cycles began along the right descending bank and in the direction shown by the arrow (Figure 22). Tidal coverage is shown in Figure 23. Profiles of the velocity magnitudes near peak flood and ebb stages are shown in Figure 24. Summary velocity and discharge data are shown in Table 10.



Figure 114. Location map of Barnegat Inlet. All ADCP data were collected in the direction indicated by the arrow.

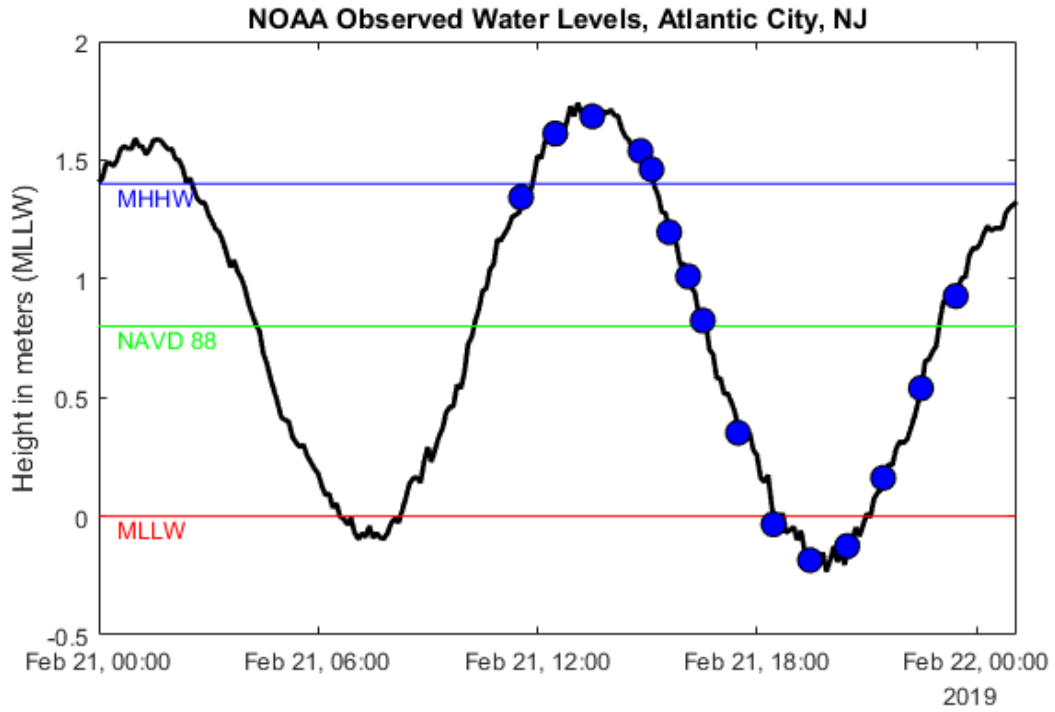


Figure 115. ADCP coverage of the tidal cycle at Barnegat Inlet. Start time of each ADCP measurement cycle (blue dot) is shown relative to the tidal frame. Times are in Universal Coordinated Time

Table 24. Summarized velocity and discharge data for Barnegat Inlet

Transect No.	Width [m], mean (SD)	Area [m ²], mean (SD)	Peak Mean Flood Vel. [m/s]	Peak Mean Ebb Vel. [m/s]	Mean Flow Dir. (Flood/Ebb) [deg]		Peak Discharge (Flood/Ebb) [m ³ /s]	
1	400 (14)	2755 (219)	-1.04	1.08	305	106	-3224	2747

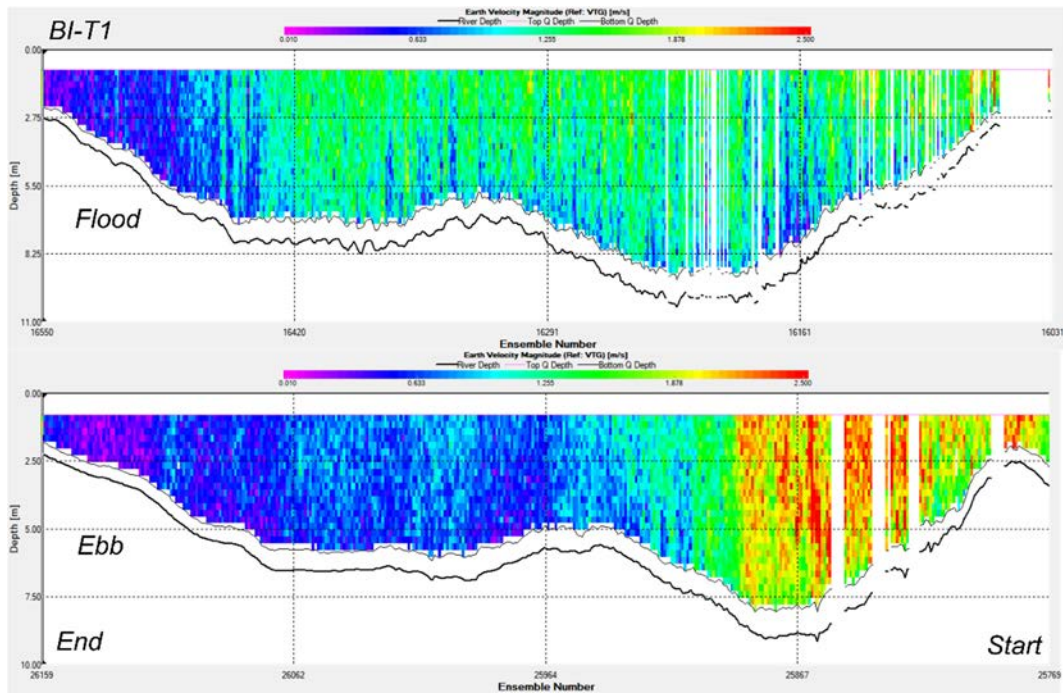


Figure 116. Profiles of BI-T1 near peak flood (upper) and ebb (lower) tides, 13:26 and 19:24 UTC, respectively. Velocity scale is 0.01 to 2.5 m/s.

Table 25. Transect 1 – Generalized Summary of CTD Data - Barnegat Inlet

Cast time (UTC)	Start latitude	Start longitude	Mean Temp [C]	Depth [m]	Mean Salinity [PSU]
2/21/2019 22:32	39.76566	-74.1021	5.0	6.48	25.83
2/21/2019 22:32	39.76564	-74.1022	5.0	6.45	25.81
2/21/2019 21:29	39.76582	-74.1024	5.1	6.98	26.06
2/21/2019 20:36	39.76571	-74.1012	5.1	5.08	27.01
2/21/2019 20:35	39.76576	-74.1023	5.2	6.01	26.82
2/21/2019 19:30	39.7658	-74.1023	5.2	8.09	28.96
2/21/2019 18:31	39.76588	-74.1018	4.8	6.23	29.75
2/21/2019 18:30	39.76595	-74.1025	4.8	5.44	29.78
2/21/2019 17:32	39.76588	-74.1026	4.5	5.59	29.72
2/21/2019 17:31	39.76599	-74.1031	4.5	5.23	29.76
2/21/2019 16:34	39.76566	-74.1024	4.3	6.06	29.82
2/21/2019 16:34	39.76581	-74.1025	4.3	5.29	29.82
2/21/2019 15:39	39.76597	-74.1028	4.3	6.13	29.73
2/21/2019 15:38	39.76572	-74.1025	4.2	5.26	29.72
2/21/2019 14:51	39.76589	-74.1031	4.2	5.96	29.65
2/21/2019 14:51	39.76558	-74.1025	4.2	5.67	29.62
2/21/2019 13:34	39.76576	-74.103	4.1	6.17	29.41
2/21/2019 13:33	39.76533	-74.1024	4.1	4.97	29.40
2/21/2019 12:34	39.76595	-74.1032	4.1	6.49	29.17

2/21/2019 12:33	39.76565	-74.1026	4.0	4.40	29.12
2/21/2019 12:31	39.76525	-74.1021	Invalid	Invalid	Invalid
2/21/2019 11:43	39.76587	-74.1028	4.0	6.76	29.29
2/21/2019 11:40	39.76584	-74.1027	4.1	5.51	29.30
2/21/2019 11:39	39.76566	-74.1025	4.0	2.36	29.18
2/21/2019 11:39	39.76571	-74.1025	Invalid	Invalid	Invalid

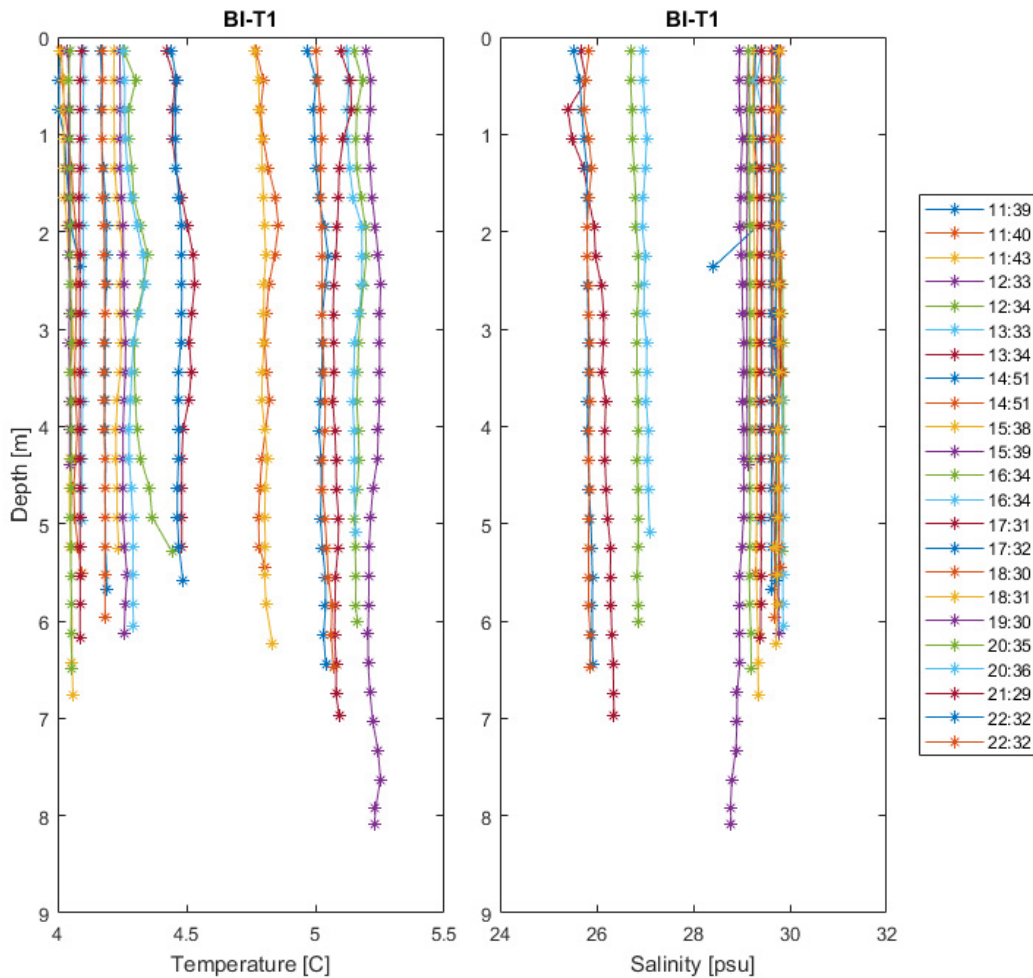


Figure 117. Salinity and temperature profiles at Barnegat Inlet. Times refer to UTC.

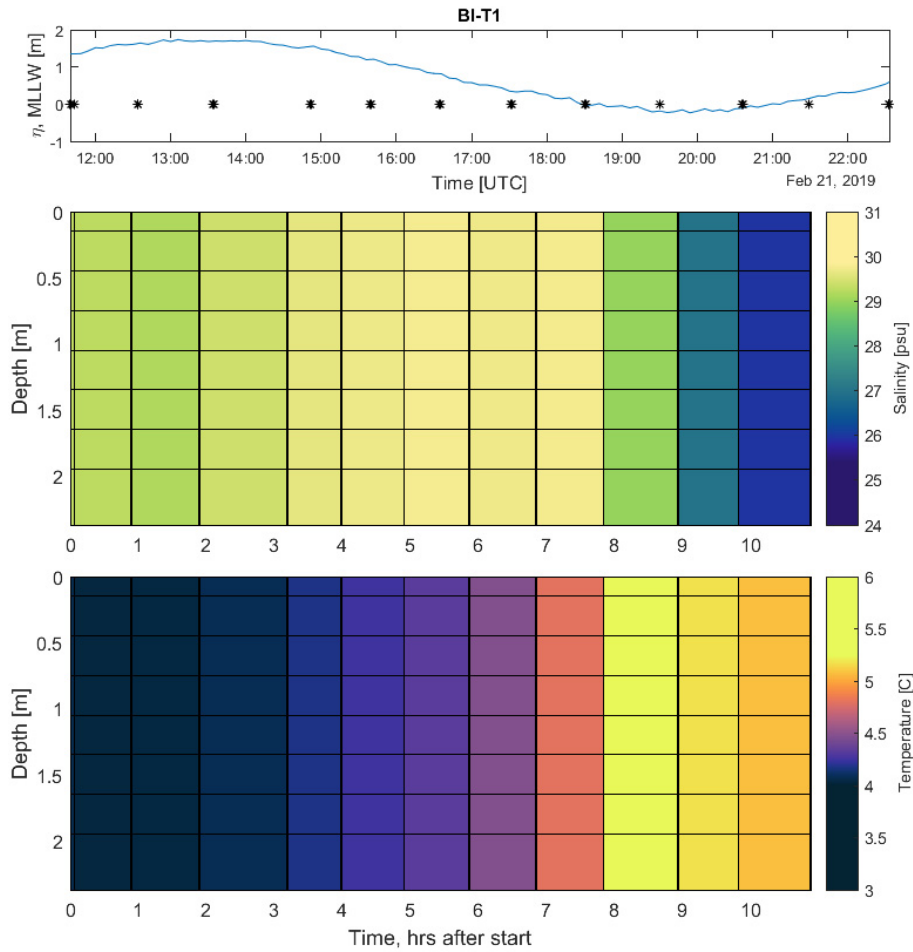


Figure 118. Salinity and temperature distributions as a function of depth and time at Barnegat Inlet. Black dots on the upper panel indicates starting cast time.

Point of Contact

Anthony M. Priestas
Research Physical Scientist
Field Data Collection and Analysis Branch
Anthony.M.Priestas@usace.army.mil
601-634-2978

REPORT DOCUMENTATION PAGE WILL BE INSERTED HERE.

H-2) NUMERICAL STORM SURGE MODELING AND
PROBABILISTIC ANALYSIS FOR EVALUATING PROPOSED
NEW JERSEY BACK BAYS INLET CLOSURES

ERDC/CHL TR-20-XX

1 Coastal and Hydraulics Laboratory



**US Army Corps
of Engineers®**
Engineer Research and
Development Center

Numerical Storm Surge Modeling and Probabilistic Analysis for Evaluating Proposed New Jersey Back Bays Inlet Closures

Gregory Slusarczyk, Mary A. Cialone, Norberto C. Nadal-Caraballo, and
Robert W. Hampson

January 2021

Numerical Storm Surge Modeling and Probabilistic Analysis for Evaluating Proposed New Jersey Back Bays Inlet Closures

Gregory Slusarczyk, Mary A. Cialone, Norberto C. Nadal-Caraballo, and Robert W. Hampson

*Coastal and Hydraulics Laboratory
U.S. Army Engineer Research and Development Center
3909 Halls Ferry Rd
Vicksburg, MS 39180-6199*

Final report

Approved for public release; distribution is unlimited.

Abstract:

The U.S. Army Corps of Engineers (USACE) Philadelphia District (NAP) and the New Jersey Department of Environmental Protection (NJDEP) are currently engaged in the New Jersey Back Bays (NJBB) Coastal Storm Risk Management CSRM (CSRM) Feasibility Study. The USACE Engineer Research and Development Center, Coastal and Hydraulics Lab (ERDC-CHL) conducted a numerical hydrodynamic modeling and probabilistic hazard analysis study to evaluate the effectiveness of storm surge barriers in reducing water levels in the NJBBs. The numerical modeling study included the simulation of water levels and a comparison of water surface elevations and corresponding annual exceedance frequency (AEF) between existing conditions and six final project alternatives. Results from the hydrodynamic simulations and probabilistic analysis are presented herein.

Table of Contents

Abstract:	iii
List of Figures and Tales	vi
Preface	xi
1.1- Introduction	1
1.2 – Project Objectives	3
2 – Storm Selections	5
2.1. Selection of Reduced Storm Set	5
2.2. Overview of Water Level Reconstruction and Development of Hazard Curves	7
2.3 – Reconstruction of Still Water Levels for Without-Project (Base) Condition	10
2.3.1 – Estimation of Wave Setup	11
2.3.2 – Tropical Cyclones	14
2.3.3 – Extratropical Cyclones	19
2.4 – Reconstruction of Water Levels for With-Project Alternatives	21
2.4.1 – Tropical Cyclones	22
2.4.2 – Extratropical Cyclones	27
3 – ADCIRC Grid Details and Model parameters	33
3.1 – Phase I - Iteration 1	39
3.1.1 – Configurations of proposed structures	41
3.1.2 – Grids	42
3.2 – Phase I - Iteration 2	43
3.2.1 – Configurations of proposed structures	44
3.2.2 – Grids	48
3.3 – Phase I - Iteration 3	48
3.3.1 – Configurations of proposed structures	49
3.3.2 – Grids	51
3.4 – Phase II	51
3.4.1 - Configurations of proposed structures	51
3.4.2 – Simulated Storms	53
3.4.3 – Grids	53

4.1 – Maximum Storm Surge Results – Iteration 1	56
4.2 – Maximum Storm Surge Results – Iteration 2	75
4.3 – Maximum Storm Surge Results – Iteration 3	90
4.4 – Maximum Storm Surge Results – Phase II	102
4.4.1 – SWL Hazard Curves	115
5 – Conclusions	119
6 – References	120
APPENDIX	122

List of Figures

Figure 1: NJBB Study Area.	3
Figure 2: Location of five select NJBB save points.	10
Figure 3: NACCS TC SWL with and without wave setup for NJBB SP 36 (base condition).	11
Figure 4: NACCS TC SWL with and without wave setup for NJBB SP 29 (base condition).	12
Figure 5: TC SWL wave setup correction for NJBB SP 36 (base condition).	13
Figure 6: TC SWL wave setup correction for NJBB SP 29 (base condition).	14
Figure 7: NJBB to NACCS TC SWL ratios for SP 36 (base condition).	15
Figure 8: NJBB to NACCS TC SWL ratios for SP 29 (base condition).	16
Figure 9: GPM input/output relationship.	17
Figure 10: Base condition GPM validation metrics for TC SWL at 180 NJBB save points.	18
Figure 11: NJBB vs. NACCS TC SWL for NJBB SP 36 (base condition).	19
Figure 12: NJBB vs. NACCS TC SWL for NJBB SP 29 (base condition).	20
Figure 13: Estimated XC SWL NJBB SP 36 (base condition).	21
Figure 14: Estimated XC SWL NJBB SP 29 (base condition).	21
Figure 15: NJBB All-Closed to base condition TC SWL ratios for SP 36.	23
Figure 16: NJBB All-Closed to base condition TC SWL ratios for SP 29.	23
Figure 17: NJBB All-Closed-Less-2 to base condition TC SWL ratios for SP 36.	24
Figure 18: NJBB All-Closed-Less-2 to base condition TC SWL ratios for SP 29.	24
Figure 19: All-Closed GPM validation metrics for TC SWL at 180 NJBB save points.	26
Figure 20: All-Closed-Less-2 GPM validation metrics for TC SWL at 180 NJBB save points.	27
Figure 21: NJBB All-Closed vs. base condition TC SWL for SP 36.	28
Figure 22: NJBB All-Closed vs. base condition TC SWL for SP 29.	28
Figure 23: NJBB All-Closed-Less-2 vs. base condition TC SWL for SP 36.	29
Figure 24: NJBB All-Closed-Less-2 vs. base condition TC SWL for SP 29.	29
Figure 25: Estimated NJBB XC SWL vs. NACCS XC SWL for SP 36 (All-Closed).	31
Figure 26: Estimated NJBB XC SWL vs. NACCS XC SWL for SP 29 (All-Closed).	31
Figure 27: Estimated NJBB XC SWL vs. NACCS XC SWL for SP 36 (All-Closes-Less-2).	32
Figure 28: Estimated NJBB XC SWL vs. NACCS XC SWL for SP 29 (All-Closed-Less-2). ..	32
Figure 29: Outline plot showing the boundary of the ADCIRC grid.	33
Figure 30: Boundary of ADCIRC grid showing New Jersey coast.	34
Figure 31: Chesapeake Bay before (left) and after (right) de-refining.	35
Figure 32: Long Island before (left) and after (right) de-refining.	35
Figure 33: NJBB save points (North).	36
Figure 34: NJBB save points (South).	36
Figure 35: The representative time series plot of water surface elevation (save point #31) for Hurricane Sandy (between October 25 and November 1, 2012): NACCS (red) vs NJBB-Base (blue) [m].	36

Figure 36: The time-series plot with the greatest difference in maximum water level (save point #56) for Hurricane Sandy (between October 25 and November 1, 2012): NACCS (red) vs NJBB-Base (blue) [m]	37
Figure 37: Schematic of NJBB Study Area	40
Figure 38: Schematic of All Closed Less 2.....	42
Figure 39: Base Grid before implementing Townsends Inlet closure. The red contour indicates the position of the future weir-pairs, the black line is the centerline of the structure.	43
Figure 40: The ADCIRC grid implementing Townsends Inlet closure. The green contour shows the weir-pairs, the black line is the centerline of the structure.....	43
Figure 41: Schematic of All Closed, All Closed Less 2, N3+S3, N4+S4, N5+S5, and N6+S6.	46
Figure 42: Schematic of N7+S7, S8, S9, S10, C3, and C4.	47
Figure 43: Schematic of C5, C6, and C7.	48
Figure 44: Schematic of All Closed, All Closed Less 2, N3+S3, N7+S4, C3, and C4.	50
Figure 45: Schematic of North, Central 1, and Central 2.	52
Figure 46: Bathymetry and topography in Barnegat Bay before the update.....	54
Figure 47: Bathymetry and topography in Barnegat Bay after the update.	54
Figure 48: Rte. 72 Causeway - design.....	55
Figure 49: Rte. 72 Causeway – ADCIRC implementation	55
Figure 50: NJBB Hydraulic Reaches (red dots indicate save points).	57
Figure 51: Maximum water elevation for Synthetic Storm 434: Base Grid (left), Barnegat Inlet Closed (center), and difference between Barnegat and Base (right)	59
Figure 52: Maximum water elevation for Synthetic Storm 636: Base Grid (left), Barnegat Inlet Closed (center), and difference between Barnegat and Base (right)	59
Figure 53: Dot plot: maximum water level for the Base condition vs maximum water level with Barnegat Inlet closed (the colors of the dots indicate different storms)	60
Figure 54: Selected save points in Barnegat Bay for time series plots.....	61
Figure 55: Storm 434: Time series plots for station (save point) 139.	62
Figure 56: Storm 434: Time series plots for station (save point) 68.	63
Figure 57: Storm 434: Time series plots for station (save point) 152.	63
Figure 58: Storm 434: Time series plots for station (save point) 156	64
Figure 59: Storm 636: Time series plots for station (save point) 139	65
Figure 60: Storm 636: Time series plots for station (save point) 68	66
Figure 61: Storm 636: Time series plots for station (save point) 152	66
Figure 62: Storm 636: Time series plots for station (save point) 156	67
Figure 63: Maximum water elevation for Synthetic Storm 99: Base Grid (left), Townsends Inlet Closed (center), and difference between Townsends and Base (right)	69
Figure 64: Maximum water elevation for Synthetic Storm 636: Base Grid (left), Townsends Inlet Closed (center), and difference between Townsends and Base (right)	69
Figure 65: Dot plot: maximum water level for the Base condition vs maximum water level with Townsends Inlet closed (the colors of the dots indicate different storms)..	70

Figure 66: locations of the save points used for evaluation of the Townsends closure with the time series plots	71
Figure 67: Storm 99: Time series plots for station (save point) 104	72
Figure 68: Storm 99: Time series plots for station (save point) 91	72
Figure 69: Storm 636: Time series plots for station (save point) 104	73
Figure 70: Storm 636: Time series plots for station (save point) 91	74
Figure 71: Maximum water elevation for Synthetic Storm 99: Base Grid (left), All Closed (center), and difference between All Closed and Base (right)	76
Figure 72: Maximum water elevation for Synthetic Storm 99: Base Grid (left), N3S3 (center), and difference between N3S3 and Base (right)	77
Figure 73: Maximum water elevation for Synthetic Storm 636: Base Grid (left), N3S3 (center), and difference between N3S3 and Base (right)	78
Figure 74: Maximum water elevation for Synthetic Storm 524: Base Grid (left), N3S3 (center), and difference between N3S3 and Base (right)	79
Figure 75: Maximum water elevation for Synthetic Storm 434: Base Grid (left), N4S4 (center), and difference between N4S4 and Base (right)	80
Figure 76: Maximum water elevation for Synthetic Storm 434: Base Grid (left), N5S5 (center), and difference between N5S5 and Base (right)	81
Figure 77: Maximum water elevation for Synthetic Storm 636: Base Grid (left), N5S5 (center), and difference between N5S5 and Base (right)	81
Figure 78: Maximum water elevation for Synthetic Storm 434: Base Grid (left), N6S6 (center), and difference between N6S6 and Base (right)	82
Figure 79: Maximum water elevation for Synthetic Storm 434: Base Grid (left), N7S7 (center), and difference between N7S7 and Base (right)	83
Figure 80: Maximum water elevation for Synthetic Storm 636: Base Grid (left), N7S7 (center), and difference between N7S7 and Base (right)	83
Figure 81: Maximum water elevation for Synthetic Storm 636: Base Grid (left), S8 (center), and difference between S8 and Base (right)	84
Figure 82: Maximum water elevation for Synthetic Storm 636: Base Grid (left), S9 (center), and difference between S9 and Base (right)	84
Figure 83: Maximum water elevation for Synthetic Storm 636: Base Grid (left), S10 (center), and difference between S10 and Base (right)	85
Figure 84: Maximum water elevation for Synthetic Storm 434: Base Grid (left), C3 (center), and difference between C3 and Base (right)	86
Figure 85: Maximum water elevation for Synthetic Storm 524: Base Grid (left), C3 (center), and difference between C3 and Base (right)	86
Figure 86: Maximum water elevation for Synthetic Storm 434: Base Grid (left), C4 (center), and difference between C4 and Base (right)	87
Figure 87: Maximum water elevation for Synthetic Storm 524: Base Grid (left), C4 (center), and difference between C4 and Base (right)	87
Figure 88: Maximum water elevation for Synthetic Storm 434: Base Grid (left), C5 (center), and difference between C5 and Base (right)	88
Figure 89: Maximum water elevation for Synthetic Storm 524: Base Grid (left), C5 (center), and difference between C5 and Base (right)	88

Figure 90: Maximum water elevation for Synthetic Storm 434: Base Grid (left), C6 (center), and difference between C6 and Base (right).....	89
Figure 91: Maximum water elevation for Synthetic Storm 434: Base Grid (left), C7 (center), and difference between C7 and Base (right).....	90
Figure 92: Phase I – Iteration 3: Shark River SWL Hazard Curves.....	91
Figure 93: North Region and Save Points	93
Figure 94: Phase I – Iteration 3: North Configurations SWL Hazard Curves.....	94
Figure 95: Central Region and Save Points.....	97
Figure 96: Phase I – Iteration 3: Central Configurations SWL Hazard Curves	97
Figure 97: South Region and Save Points	100
Figure 98: Phase I – Iteration 3: South Configurations SWL Hazard Curves.....	101
Figure 99: Typical change in maximum water level: North – Storm 349	102
Figure 100: Change in maximum water level: North – Storm 524 with water behind the surge barrier	103
Figure 101: Dot plot: maximum water level for the Base condition vs maximum water level with Barnegat and Manasquan Inlets closed (the colors of the dots indicate different storms)	104
Figure 102: Typical change in maximum water level: C1 – Storm 469.....	105
Figure 103: Change in maximum water level: C1 – Storm 99 with greater reduction in the rivers.....	107
Figure 104: Change in maximum water level: C1 – Storm 433 water level increase seaward of surge barriers.....	108
Figure 105: Change in maximum water level: C1 – Storm 636 with water behind the surge barrier	108
Figure 106: Dot plot: maximum water level for the Base condition vs maximum water level with Absecon and Great Egg Inlets closed (the colors of the dots indicate different storms)	109
Figure 107: Dot plot: maximum water level for the Base condition vs maximum water level with Absecon and Great Egg Inlets closed (the colors of the dots indicate different storms)	110
Figure 108: Typical change in maximum water level: C2 – Storm 434.....	111
Figure 109: Dot plot: maximum water level for the Base condition vs maximum water level with Absecon Blvd bay closure, 52nd Street bay closure, and Great Egg Inlet closed (the colors of the dots indicate different storms).....	112
Figure 110: Dot plot: maximum water level for the Base condition vs maximum water level with Absecon Blvd bay closure, 52nd Street bay closure, and Great Egg Inlet closed (the colors of the dots indicate different storms).....	113
Figure 111: Storm 433 maximum water level envelope for Configurations C1 (left) and C2 (right).....	114
Figure 112: Storm 433 difference in maximum water level compared to Base: C1 (left) and C2 (right).....	114
Figure 113: Storm 636 difference in maximum water level compared to Base: C1 (left) and C2 (right).....	115
Figure 114: Phase II North Region SWL Hazard Curves.....	117

Figure 115: Phase II Central Region SWL Hazard Curves..... 118

Preface

This report describes engineering studies that were conducted by the U.S. Army Engineer Research and Development Center, Coastal and Hydraulics Laboratory (ERDC/CHL), Vicksburg, MS, for the U.S. Army Engineer District, Philadelphia (NAP), and New Jersey Department of Environmental Protection (NJDEP). This study develops a numerical hydrodynamic modeling and probabilistic hazard analysis study to evaluate the effectiveness of storm surge barriers in reducing water levels in the NJBBs.

This report was prepared by Gregory Slusarczyk of the Coastal Processes Branch (CPB), Flood & Storm Protection Division (HF), Mary A. Cialone of the Technical Programs Office, Norberto C. Nadal-Caraballo of the Harbors, Entrances & Structures Branch (HESB), Navigation Division (HN), and Robert W. Hampson of NAP. During the study and publication of this report Ms. Ashley E. Frey and Dr. Cary A. Talbot were chiefs of the CPB and HF, respectively, and Mr. James Gutshall and Dr. Jackie Pettway were chiefs of the HESB and HN, respectively. Col. Jeffrey R. Eckstein was the Deputy Director and Dr. Ty V. Wamsley was the Director of CHL.

Yan Ding, Victor Gonzalez, and Ashley E. Frey reviewed this report.

Col. Ivan Beckman was ERDC Commander when this report was prepared. Col. Teresa A. Schlosser was ERDC Commander at time of publication. Dr. David W. Pittman was ERDC Director.

Unit Conversion Factors

1.1-- Introduction

The U.S. Army Corps of Engineers (USACE) Philadelphia District (NAP) and the non-federal sponsor, New Jersey Department of Environmental Protection (NJDEP), are currently engaged in the New Jersey Back Bays (NJBB) Coastal Storm Risk Management CSRM Feasibility Study. The NJBB study area is one of nine focus areas identified in the North Atlantic Coast Comprehensive Study (NACCS) (Cialone et al. 2015; Nadal-Caraballo et al. 2015) for additional analyses by USACE to address coastal flood risk.

The NACCS was authorized under the Disaster Relief Appropriations Act, PL 113-2, in response to Hurricane Sandy. The Act provided the USACE with up to \$20 Million to conduct a study with the goal to (1) reduce flood risk to vulnerable coastal populations, and (2) promote resilient coastal communities to ensure a sustainable and robust coastal landscape system, considering future sea level change and climate change scenarios.

As part of the NACCS, the US Army Engineer Research and Development Center, Coastal and Hydraulics Lab (ERDC-CHL) completed a coastal storm wave and water level modeling effort and quantification of coastal hazards for the U.S. North Atlantic Coast. That modeling study provided nearshore wind, wave, and water level estimates and the associated marginal and joint probabilities critical for effective coastal storm risk management. The modeling effort involved the application of a suite of high-fidelity numerical models within the Coastal Storm Modeling System (CSTORM-MS) to 1050 synthetic tropical storms and 100 historical extra-tropical storms. Documentation of the numerical modeling effort is provided in Cialone et al. (2015) and documentation of the probabilistic modeling and coastal hazards quantification is provided in Nadal Caraballo et al. (2015). Products of the study can be viewed or downloaded from the Coastal Hazards System (CHS) website: <https://chs.erdcdren.mil> (Nadal-Caraballo et al. 2020).

The NJBB study area, [Figure 1](#), extends along 177 km (110 miles) of the New Jersey coast and encompasses 2460 km² (950 square miles) of land, wetlands, open water, and coastal lakes across parts of five counties and 90 municipalities. There are approximately 235,000 structures and a

permanent population of about 700,000 within the study area. Twelve inlets provide hydraulic connections between the Atlantic Ocean and the back bays, making all of the back bays susceptible to flooding from the ocean. During coastal storms, elevated ocean water levels propagate through the inlets into the back bays, causing flood damage that is a function of the geographic extent, duration, and height of the ocean storm surge. Hurricane Sandy in 2012 demonstrated that in addition to the coastal flood risk posed to public and private infrastructure, there is a significant life-safety risk posed by coastal storms and the flooding that they cause.

The objective of the NJBB CSRM Study is to investigate CSRM problems and solutions to reduce damages from coastal flooding that affects population, critical infrastructure, critical facilities, property, and ecosystems. CSRM measures under consideration include Non Structural, Structural, and Natural and Nature Based Features (NNBFs). This report solely describes one of such structural measures that is inlet closure, constructed at one or more inlets in the study area. Due to the complex network of inlets and bays that control the flow of water between the ocean and back bays, NAP requested assistance from ERDC-CHL in evaluating the effectiveness of inlet closures in reducing water levels in the NJBB study area. More specifically, NAP wanted ERDC-CHL to quantify the potential reduction in back-bay flooding with the implementation of inlet closures during storm events, determine how effective inlet closures are at reducing water levels if other inlets are open, and determine if multiple inlet closures could be more effective at reducing water levels in the NJBB system. To answer these questions ERDC-CHL leveraged the existing NACCS CSTORM- MS and the CHS synthetic storm suite and probabilistic analysis tools as a starting point for this study. This report documents two consecutive stages, the Phase I and Phase II, of the NJBB study, focused on evaluation of the impact of Structural measures (individual and multiple inlet closures) on back bay water levels.



Figure 1: NJBB Study Area.

1.2 – Project Objectives

The objective of this numerical modeling study is to evaluate the effectiveness of inlet closures at reducing water levels in the NJBB study area. The numerical modeling and probabilistic analysis study was completed in two phases: Phase I between the Alternatives Milestones Meeting (AMM) and Tentatively Selected Plan-In Progress Review (TSP-IPR)

milestones, and Phase II between the TSP-IPR and TSP milestones. In Phase I, an iterative modeling approach was devised to allow a large number of inlet closures and potential inlet closure combinations to be evaluated before converging on a smaller final set of inlet closure alternatives.

The Phase I iterative modeling approach began with model simulations of individual inlet closures to improve understanding of the hydraulic influence of each inlet on back-bay water levels. The second iteration evaluated a large number of possible inlet closure combinations, before moving on to the 3rd iteration where a smaller final set of closure alternatives were evaluated with a larger suite of storms. Model simulations for the final set of alternatives was used to develop frequency distributions of peak water levels that may be applied in economic analyses of flood damages and benefits. In summary, the three iterations for Phase I were as follows:

- Iteration 1: Model the hydraulic influence of each barrier island inlet on back-bay water levels by modeling one inlet at a time.
- Iteration 2: Model the effectiveness of a large set of possible inlet closure combinations at reducing back-bay water levels.
- Iteration 3: Model the effectiveness of a final set of inlet closure alternatives with a larger storm suite and develop frequency distributions of peak water levels.

The iterative modeling approach is made feasible by utilizing a very small subset of 10 extreme cyclones for Iterations 1 and 2 to evaluate a large number of inlet closure configurations. The CHS Probabilistic Coastal Hazard Analysis (PCHA) tools that are further explained in Section 2 of this report were used to identify a more robust reduced storm set (RSS) consisting of 60 tropical cyclones for Iteration 3 in order to develop still water level hazard (SWL) curves. SWL is defined as the aggregation of the storm surge, including wave setup, and the astronomical tide water level components. Details on how the SWL components were determined in the present study are discussed in [2.2. Overview of Water Level Reconstruction and Development of Hazard Curves](#).

During Phase II, the model bathymetry was updated in Barnegat Bay and at several of the inlets with more recent survey data. After updating the model bathymetry, the same set of 60 tropical cyclones from Phase I –

Iteration 3 was simulated with CSTORM-MS and hazard curves generated for the baseline and the three primary storm surge barrier configurations in the Focused Array of Alternatives.

To achieve the project objectives, the NACCS CSTORM-MS was applied with modifications to the ADCIRC grid, ADCIRC bathymetry, and storm suite as presented herein. All CSTORM-MS applications in this study applied the ADCIRC-Only (no waves were included in the model) option to generate storm surge water levels. ADCIRC is a two-dimensional, depth-averaged ADvanced CIRCulation (ADCIRC) model (Luettich et al., 1991).

2 -- Storm Selections

The New Jersey Back Bays (NJBB) Coastal Storm Risk Management (CSRM) feasibility study sought the evaluation of various with-project alternatives that include individual and multiple inlet closures, as discussed in [3 -- ADCIRC Grid Details and Model parameters](#). The NJBB study made use of existing still water level (SWL) data, hydrodynamic modeling setup, and probabilistic analysis tools developed for the NACCS (Nadal-Caraballo et al. 2015; Cialone et al. 2015). Updating SWL hazard statistics for NJBB, both without- and with-project, the Coastal Hazards System (CHS) Probabilistic Coastal Hazard Analysis (PCHA) framework for the North Atlantic region requires the simulation of both Tropical Cyclone (TC) and eXtratropical Cyclone (XC) induced SWL. The NACCS Full Storm Suite (FSS) consists of 1,050 synthetic TCs and 100 historical XCs. SWL hazard curves are initially developed for TCs and XCs independently, and are subsequently integrated to compute Combined Cyclone (CC) SWL hazard curves. The next section discusses DoE approach employed in the selection of the RSS.

2.1. Selection of Reduced Storm Set

For the NJBB CSRM study, two separate RSS of 10 and 60 TCs were sought. The goal of storm selection, as implemented in this study, was to find the optimal combination of storms given a predetermined number of storms to be sampled (e.g., 60 TCs). In other words: out of a 1,050-TC FSS,

which storms should be sampled to constitute the 60-TC RSS? The number of storms sampled for each RSS was limited by budget and/or schedule constraints and informed by previous DoE studies. The storm selection process was performed using the DoE approach documented in Taflanidis et al. (2017), and Zhang et al. (2018). The DoE compares the RSS SWL hazard curves to benchmark hazards curves corresponding to the FSS at a given number of specific locations or save points. The difference between the RSS hazard curves and FSS benchmark curves is minimized by initially sampling a small subset of TCs (e.g., 10), and then iteratively adding additional TCs (e.g., 10 by 10, as needed) until the difference is significantly reduced or becomes negligible. The save points where the hazard curve optimization take place correspond to critical locations within the study area. The number of required save points typically ranges from 50 to 200.

Following are the general steps in the DoE approach used for the selection of the TC RSS:

1. Identify a set of save points within the study area where the DoE optimization is to be performed.
2. Develop or use existing TC SWL hazard curves for the FSS.
3. Determine the number of TCs to be sampled.
4. Develop new hazard curves for the RSS.
5. Select the annual exceedance frequency (AEF) range of at which the RSS and FSS hazard curves will be compared. Differences can be computed along the entire hazard curves, segment of the hazard curve, or at specific AEFs; e.g., 0.02 to 0.002 storms/year, equivalent to 50 to 500 years.
6. Calculate errors between RSS and FSS hazard curves at predetermined AEFs.
7. Conduct an iterative optimization analysis to evaluate the benefit of increased RSS size; e.g., 10 by 10, from 10 to 60 TCs.
8. Once the sought number of storms is reached (e.g. 60), in order to evaluate overall RSS performance, the RSS selected through optimization indicated in step 7 is compared to multiple RSS where TCs are sampled in a single batch.
9. Complete storms selection by choosing the optimal RSS from step 8.

10. The selected storms (60-TC RSS) are simulated in ADCIRC and the results used to reconstruct hazard curves for NJBB without- and with-project conditions.

The methodology for reconstruction of the NJBB SWL and the development of updated hazard curves is described in the next sections.

2.2. Overview of Water Level Reconstruction and Development of Hazard Curves

The process of reconstructing the SWL hazard curves for NJBB began with the selection of reduced storm sets (RSS) using design of experiments (DoE) approach. For the NJBB study, two RSS of 10 and 60 TCs, respectively, were identified. The 10-TC RSS was used as part of a sensitivity analysis for initial screening of with-project alternatives (Iteration 1 and 2). For Iteration 3, ADCIRC simulations of SWL without-waves were conducted for the 60-TC RSS in order to perform a comprehensive evaluation of select with-project alternatives. Relying only on RSS simulations would result in increased uncertainty relative to the FSS. Therefore, a key component of the methodology used in this study for the reconstruction of hazard curves is the application of surrogate modeling or metamodeling (e.g., Taflanidis et al. 2014; Kim et al. 2015) for the estimation of the FSS with-project SWL. More specifically, results from new NJBB hydrodynamic simulations corresponding to the 60-TC RSS were used to train and validate Gaussian Process Metamodel (GPM) (Jia et al. 2015) that is then used to estimate the SWL of the FSS. The GPM leverages the TC parametrization scheme that allows for tropical storms and hurricanes to be described in terms of climatological characteristics and atmospheric forcing including intensity, size, track path, and angle of approach. Following are the main steps in the reconstruction of NJBB TC SWL hazard curves at individual save points:

- 1.1 Conduct hydrodynamic surge-only simulations of the 60-TC RSS.
- 1.2 Since the NJBB simulations excluded waves, in order to estimate the contribution of wave setup, a regression model is fitted to previous NACCS SWL results with and without waves.

- 1.3 Add wave setup by correcting the NJBB SWL without-waves results through the application regression model established in the previous step.
- 1.4 NJBB simulations also excluded astronomical tide. Thus, NJBB simulation results were directly compared to NACCS results that also excluded tides, denoted here as WL (i.e., surge + wave). For base condition, compute the ratio ($K_{R,base}$) of NJBB WL to NACCS WL, where n is the RSS size:

$$K_{R,base} = \frac{1}{n} \sum_{i=1}^n \left(\frac{SWL_{RSS,NJBB,base}}{SWL_{RSS,NACCS,base}} \right)_i \quad \text{Eq. (1-a)}$$

For the assessment of with-project alternatives, $K_{R,alt}$ is computed as follows:

$$K_{R,alt} = \frac{1}{n} \sum_{i=1}^n \left(\frac{SWL_{RSS,NJBB,alt}}{SWL_{RSS,NJBB,base}} \right)_i \quad \text{Eq. (1-b)}$$

- 1.5 For base condition, compute the absolute difference ($K_{A,base}$) between NJBB SWL to NACCS SWL for the RSS:

$$K_{A,base} = \frac{1}{n} \sum_{i=1}^n (SWL_{RSS,NJBB,base} - SWL_{RSS,NACCS,base})_i$$

Eq. (2-a)

For the assessment of with-project alternatives, $K_{A,alt}$ is computed as follows:

$$K_{A,alt} = \frac{1}{n} \sum_{i=1}^n (SWL_{RSS,NJBB,alt} - SWL_{RSS,NJBB,base})_i$$

Eq. (2-b)

- 1.6 Train and validate GPM using the TC SWL ratios and absolute differences computed for the 60-TC RSS.
- 1.7 Use GPM results to estimate the TC SWL ratios and differences for the remaining of FSS (i.e., 1050 TCs – 60 TCs = 990 TCs).
- 1.8 The ratios and differences computed up to the previous step are used to estimate NJBB SWL (i.e., surge + waves + tide) by correcting existing NACCS SWL. Therefore, the reconstructed NJBB SWL and SWL hazard curves account for the astronomical tide component. For base condition, estimate the NJBB TC SWL for the FSS by correcting the NACCS SWL:

$$SWL_{FSS,NJBB,base} = \left[(SWL_{FSS,NACCS,base} \cdot K_{R,base}) + (SWL_{FSS,NACCS,base} + K_{A,base}) \right] / 2 \quad \text{Eq. (3-a)}$$

- 1.9 For with-project alternatives, estimate the NJBB TC SWL for the FSS by correcting the NACCS SWL:

$$SWL_{FSS,NJBB,alt} =$$

$$\left[(SWL_{FSS,NACC,base} \cdot K_{R,alt}) + (SWL_{FSS,NACCS,base} + K_{A,alt}) \right] / 2$$

Eq. (3-b)

- 1.10 Compute TC SWL hazard curves using joint probability analysis (e.g., PCHA).

The hydrodynamic simulations of SWL conducted for the NJBB did not include XCs. While it is possible to identify RSS of synthetic TC events to inform a joint probability model, given that XCs lack the well-defined vortex that characterizes TCs, the standard of practice for XCs is to sample historical events based on water level observations instead of relying on specific atmospheric forcing parameters. Following are the general steps for reconstructing NJBB XC SWL hazard curves on a per save point basis:

- 1.1 Using the new NJBB and previous NACCS hydrodynamic results, develop a regression model to establish the likely NJBB TC SWL attenuation or amplification (i.e., response variable) as a function of the NACCS TC SWL (i.e., predictor variable) at each evaluated save point.
- 1.2 Apply the regression model to estimate the NJBB XC SWL from the SWL results corresponding to the original 100 XCs simulated for NACCS.
- 1.3 Compute XC SWL hazard curves using extreme value analysis.

Finally, the combined cyclone (CC) SWL hazard curves are computed by integrating the individual TC and XC hazard curves at each save NJBB point. Examples of the SWL reconstruction are presented in the upcoming sections for five NJBB save points. The IDs and coordinates of these save points are given in [Table 1](#), while their locations are illustrated in [Figure 2](#).

Table 1: IDs and coordinates for select NJBB save points.

NJBB Save Point	NACCS Save Point	Lat (deg N)	Lon (deg W)	Depth (m, MSL)
36	11276	39.3698	74.4076	5.84
2	5380	39.3806	74.419	5.08
57	11360	39.3912	74.4302	4.98
50	11316	39.4103	74.4746	0.66
29	11249	39.4246	74.4857	-0.5



Figure 2: Location of five select NJBB save points.

2.3 -- Reconstruction of Still Water Levels for Without-Project (Base) Condition

The primary goal of the 60-TC RSS is to determine the change in storm surge and SWL hazards for the different NJBB alternatives based under consideration, leveraging from existing NACCS results for 1,050 TCs and 100 XCs. However, it is necessary to first reconstruct the base condition SWL to properly account for any changes arising from updated bathymetry and topography within the study area, and from modifications to the ADCIRC grid. Also, the new NJBB hydrodynamic simulations were conducted without the presence of waves. Therefore, NJBB SWL must be corrected for the lack of wave effects, such as wave setup. The processes of estimating wave setup and adding this component to the NJBB SWL simulations is presented in [2.3.1 – Estimation of Wave Setup](#). The reconstruction of TC and XC base condition SWL are discussed in [2.3.2 -- Tropical Cyclones](#) and [2.3.3 -- Extratropical Cyclones](#), respectively.

2.3.1 – Estimation of Wave Setup

Since the ADCIRC hydrodynamic simulations of the 60 TCs selected for NJBB were performed without waves, wave setup must be estimated and added to the TC SWL. The first step in the SWL reconstruction was to estimate the wave setup at each the 180 NJBB save points by first comparing NACCS TC SWL results with and without waves. The TC SWL with waves vs. TC SWL without waves relationships for NJBB save points 36 and 29 are shown in [Figure 3](#) and [Figure 4](#), respectively.

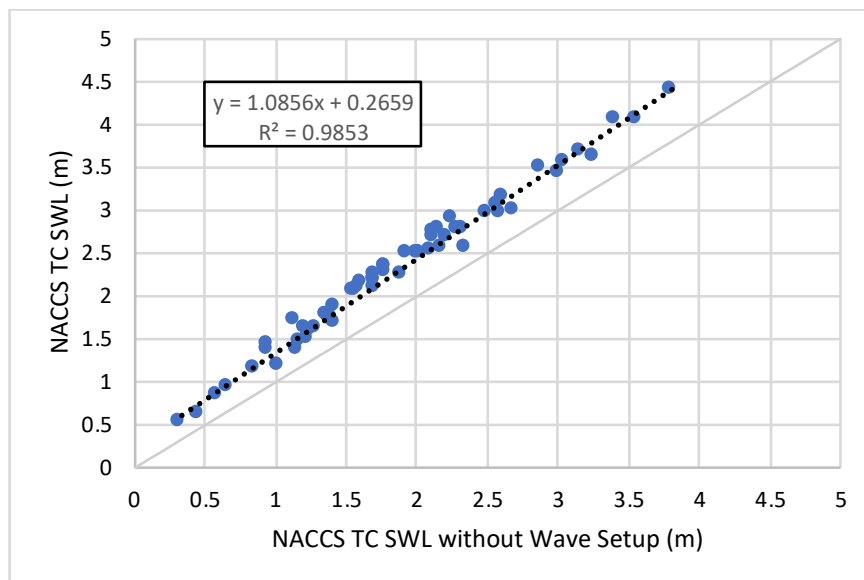


Figure 3: NACCS TC SWL with and without wave setup for NJBB SP 36 (base condition).

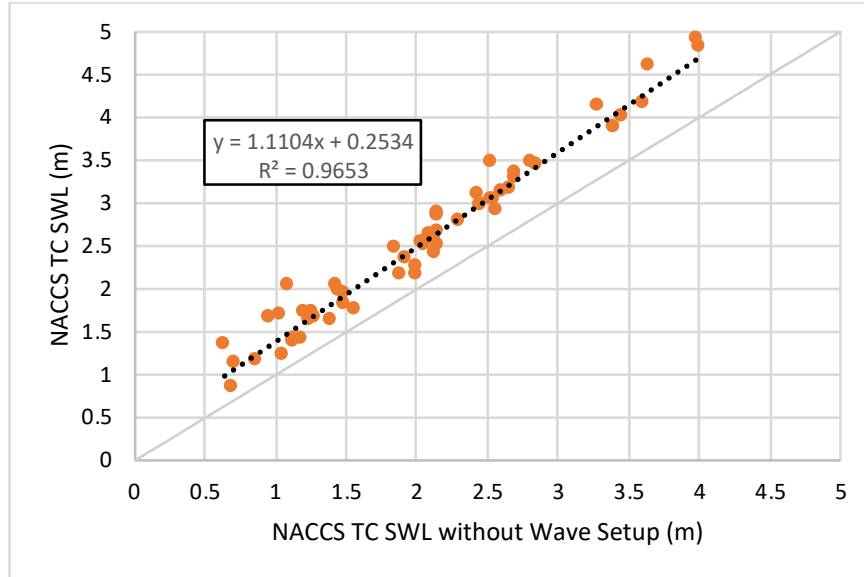


Figure 4: NACCS TC SWL with and without wave setup for NJBB SP 29 (base condition).

As seen in [Figure 3](#) and [Figure 4](#), the data plotted for both save points follow a linear trend with coefficients of determination (R^2) of 0.99 and 0.97, respectively. Therefore, wave setup was estimated by comparing NACCS TC SWL results with and without wave setup and developing a linear regression model for at each NJBB save point of the form:

$$Y = \beta_0 + \beta_1 X + \varepsilon$$

Eq. (4)

Where: Y = NACCS TC SWL with wave setup (i.e., response variable); X = NACCS TC SWL without wave setup (i.e., predictor variable); β_0 = intercept; β_1 = slope; and ε = aleatory error. The linear regression coefficients, β_0 and β_1 , and the coefficient of determination, R^2 , a goodness-of-fit metric, are presented in [Table 2](#).

Table 2: Linear regression coefficients and R^2 for TC SWL wave-setup correction (base condition).

NJBB Save Point	β_0 (m)	β_1	R^2
36	0.2659	1.0856	0.9853
2	0.1821	1.1644	0.9745

57	0.0957	1.2363	0.9725
50	0.2135	1.1511	0.9727
29	0.2534	1.1104	0.9653

The regressions models were then used to correct the NJBB simulations by adding wave setup to the TC SWL without-waves results. The aleatory error (ε) component in Eq. (4) was not accounted for in the wave-setup correction process. The NJBB TC SWL corrected for wave setup are presented in [Figure 5](#) and [Figure 6](#) for save points 36 and 29 as a function of the corresponding TC SWL without-waves values. At the save point locations evaluated in this study, the magnitude of the wave setup approximately ranged from 10% to 30% of the SWL.

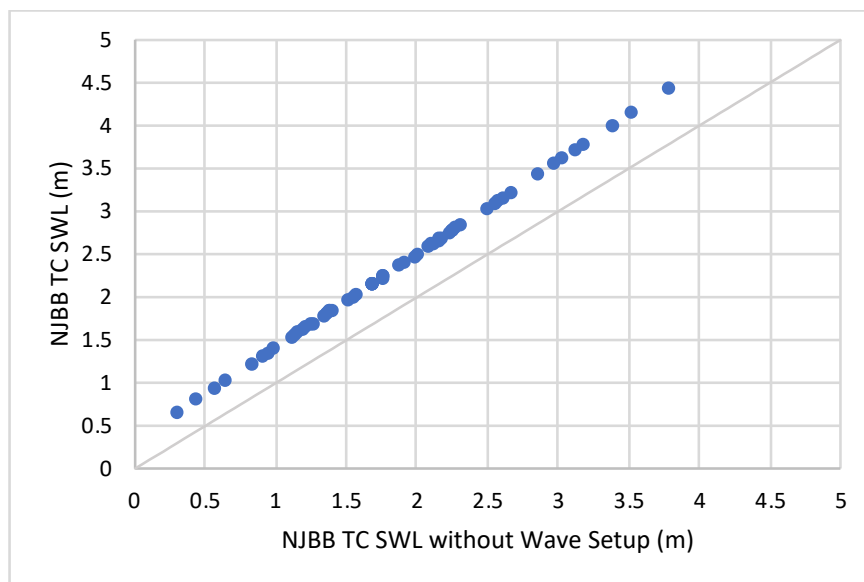


Figure 5: TC SWL wave setup correction for NJBB SP 36 (base condition).

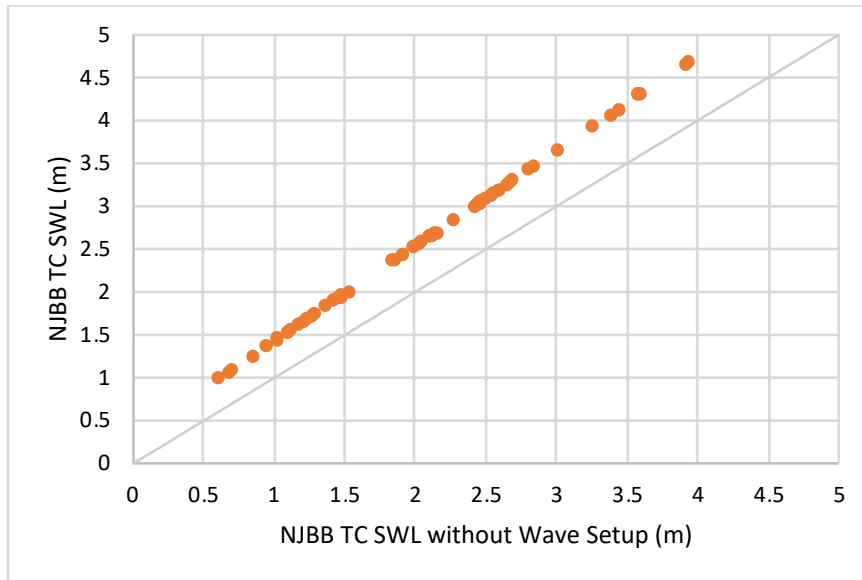


Figure 6: TC SWL wave setup correction for NJBB SP 29 (base condition).

2.3.2 -- Tropical Cyclones

After the NJBB simulations are corrected by adding wave setup, the next step in the SWL reconstruction process is the computation of NJBB TC SWL to NACCS TC SWL ratios ($K_{R,base}$) and absolute differences ($K_{A,base}$) for the different with-project alternatives. $K_{R,base}$ and $K_{A,base}$ are computed for the 60-TC RSS in order to estimate the SWL change (i.e., attenuation or amplification) resulting from these alternatives. The TC SWL ratios are plotted in Figure 7 and Figure 8 for save points 36 and 29, respectively. Note that both of these save points have a mean $K_{R,base}$ of 1.0, indicating net zero change in the NJBB TC SWL from relative to the NACCS TC SWL, as a result of modifications to the ADCIRC grid. Considering individual events within the 60-TC RSS, Figure 7 shows that most of the TC SWL ratios for save point 36, located at the entrance on the Absecon Inlet, lie within the 0.9 to 1.1 range, also demonstrating minimal change in SWL. Save point 29, located at the back end of Absecon Bay, shows a wider spread in the TC SWL ratios in Figure 8, with most SWL ratios ranging from 0.8 to 1.2, likely due to the modifications in the ADCIRC grid in conjunction to different combinations of TC atmospheric represented in the 60-TC RSS, but still presents a net SWL change of zero.

As observed in these figures, the relationship between the NJBB to NACCS TC SWL ratios (y-axis) and the NACCS TC SWL (x-axis) is not exclusively linear and the relationship can exhibit significant spread at some locations. Consequently, instead of relying on linear regression models, Gaussian Process Metamodels (GPMs) were trained for both $K_{R,base}$ and $K_{A,base}$, so SWL changes be estimated for the 1,050-TC FSS used in the development of updated SWL hazard curves for the NJBB study.

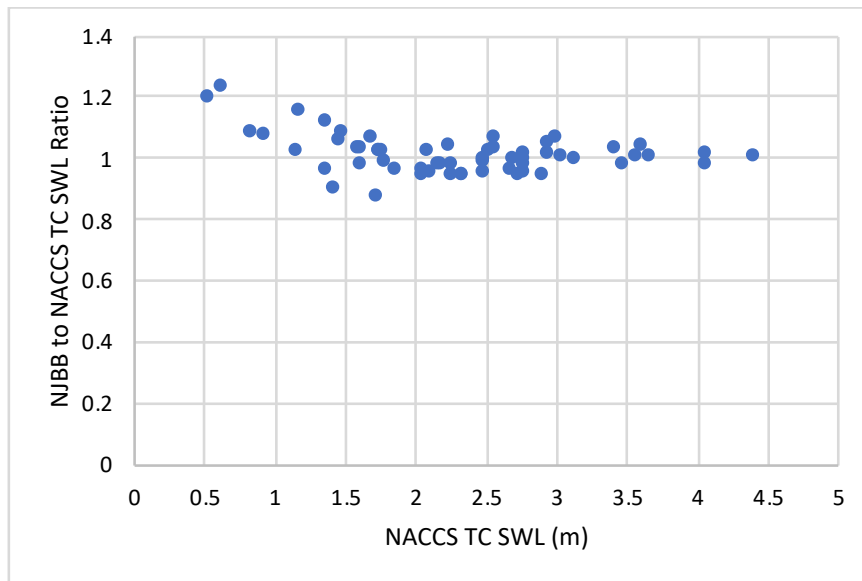


Figure 7: NJBB to NACCS TC SWL ratios for SP 36 (base condition).

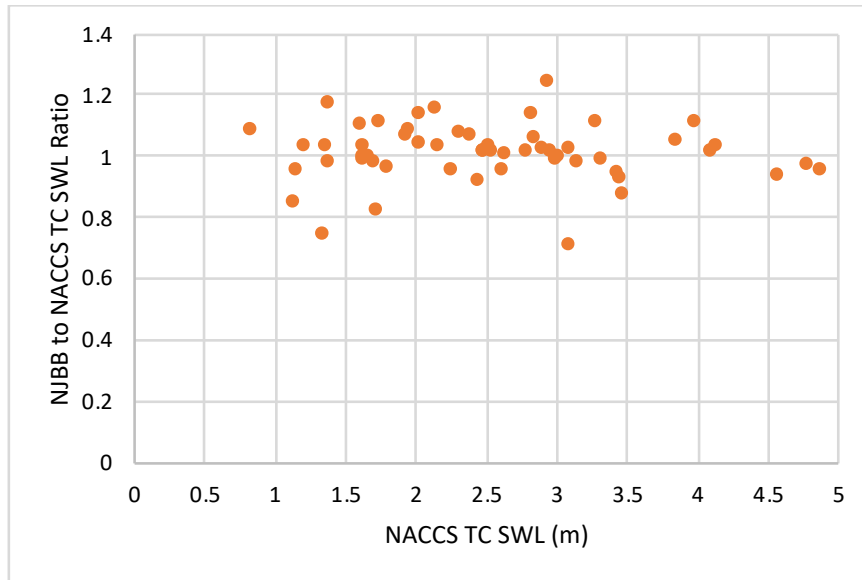


Figure 8: NJBB to NACCS TC SWL ratios for SP 29 (base condition).

GPM is a mathematical approximation for the input/output (x/z) relationship of a complex numerical model. It is formulated based on a database of simulations for complex process such as hurricane storm surge. This database is frequently referenced as experiments or support points, as shown in Figure 9. The basis for the GPM framework used in this study is the TC parametrization in the NACCS joint probability analysis (Nadal-Caraballo et al. 2015). The CHS synthetic TCs are the GPM input (x), while the output (z) are the CSTORM-MS water level simulation results. Each input/output pair constitutes a support point. Figure 9 shows a generalized input/output relationship, where support points are used to train a GPM and construct a 3-dimensional (3D) surface. Herein, the reconstruction of NJBB SWL is a 7-dimensional hyper-space, with six TC parameters as inputs and either $K_{R,base}$ or $K_{A,base}$ as a single output.

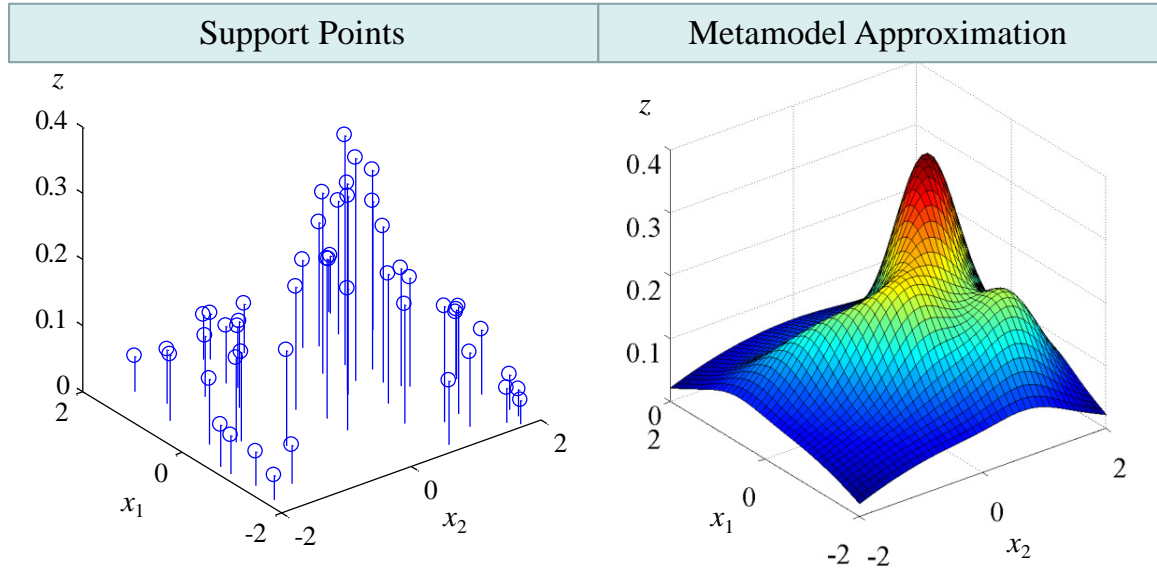


Figure 9: GPM input/output relationship.

As discussed in Nadal-Caraballo et al. 2015 and 2020, synthetic TCs are developed considering the historical climatology and characteristic storms of a specific region, and reflect likely combinations of storm intensity and size, track and landfalling location. The input vector (x) used in the training of GPM consists of the following TC parameters:

- Latitude of landfalling or bypassing reference location, x_{1at}
- Longitude of landfalling or bypassing reference location, x_{1on}
- Heading direction, θ
- Central pressure deficit, Δp
- Radius of maximum winds, R_{max}
- Translational speed, v_t

Training and validation of the GPM is discussed in details in Taflanidis et al. (2014); Jia et al. (2015); Taflanidis et al. (2017); and Zhang et al. (2018). The validation metrics for the GPM employed in this study were: coefficient of determination (R^2), mean absolute error (ME), and correlation coefficient (CC). Validation results for select NJBB save points and global validation values are given in Table 3. The GPM validation metrics for all 180 NJBB save points are plotted in Figure 10. Once trained, the GPM are used to estimate the water level response. SWL hazard curves for TCs were developed as described in Nadal-Caraballo et al. (2015).

Table 3: GPM validation for NJBB to NACCS TC SWL ratios (base condition).

NJBB Save Point	R ²	ME (m)	CC
36	0.8781	0.0172	0.9606
2	0.9179	0.0135	0.9695
57	0.8952	0.0167	0.964
50	0.8943	0.023	0.9634
29	0.6712	0.103	0.9427
All Save Points	0.8781	0.0172	0.9606

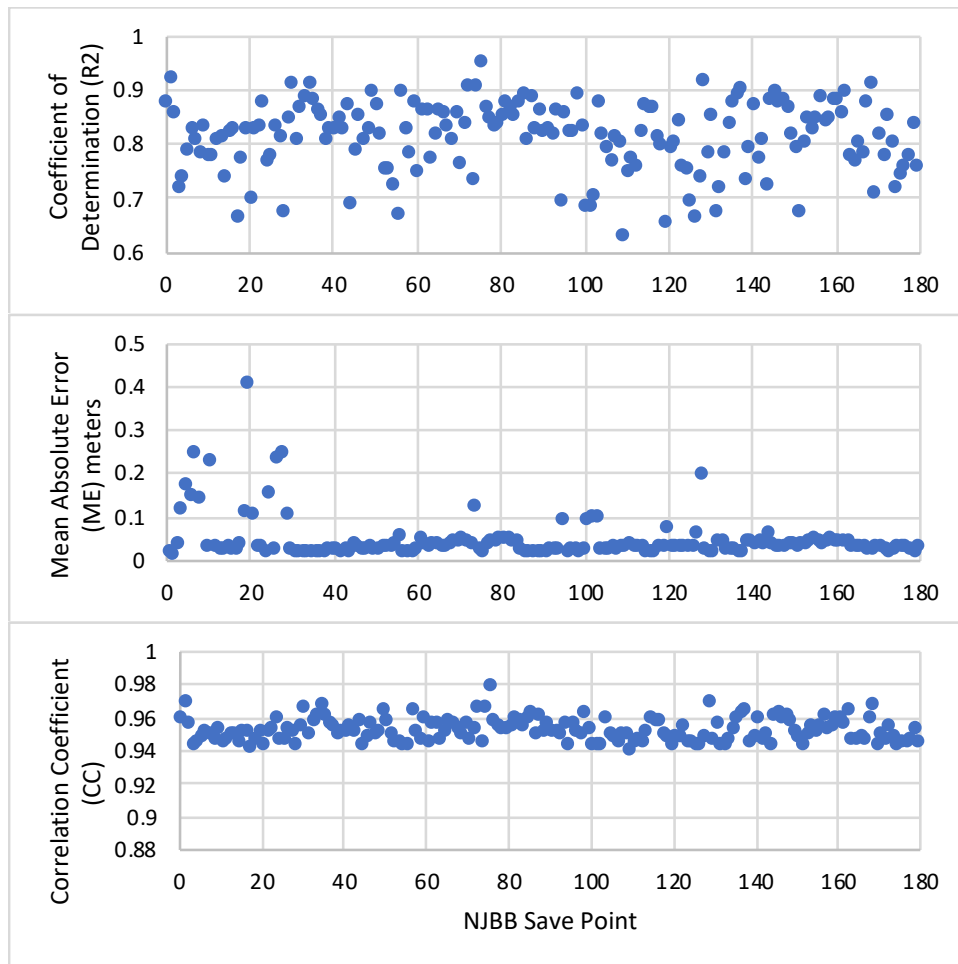


Figure 10: Base condition GPM validation metrics for TC SWL at 180 NJBB save points.

2.3.3 -- Extratropical Cyclones

The standard of practice for the assessment of XC storm surge and other coastal hazards does not require this storm population to be parametrized. Without a parametrization scheme, training of a GPM is unfeasible. Therefore, a regression model is used to estimate the general relationship between NJBB and NACCS SWL and, thus, the expected value of SWL attenuation or amplification, regardless of storm forcing. This allows the estimation of XC SWL for NJBB as a function of the previous NACCS results for 100 XCs. The NJBB TC SWL (corrected for wave setup) vs. NACCS TC SWL at save points 36 and 29 are shown in [Figure 11](#) and [Figure 12](#), respectively. The linear regression model coefficients, β_0 and β_1 , and the coefficient of determination, R^2 , are presented in [Table 4](#).

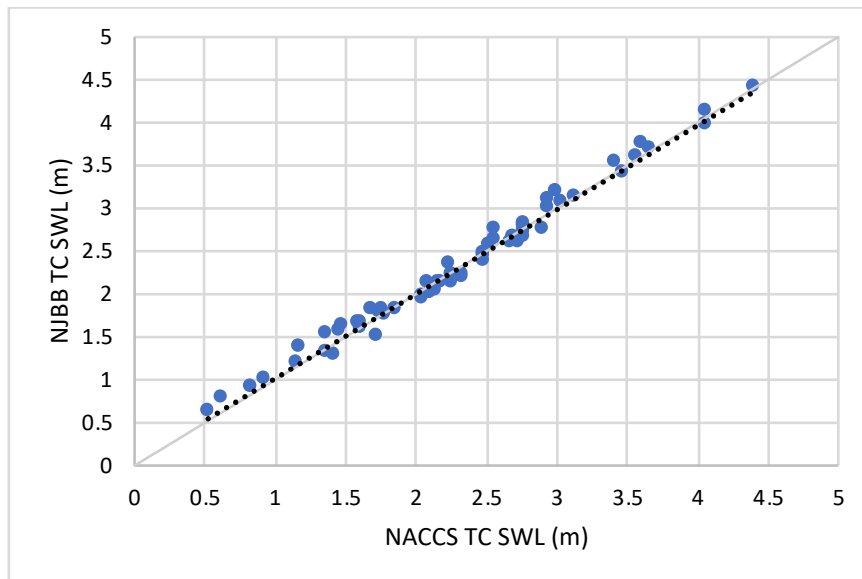


Figure 11: NJBB vs. NACCS TC SWL for NJBB SP 36 (base condition).

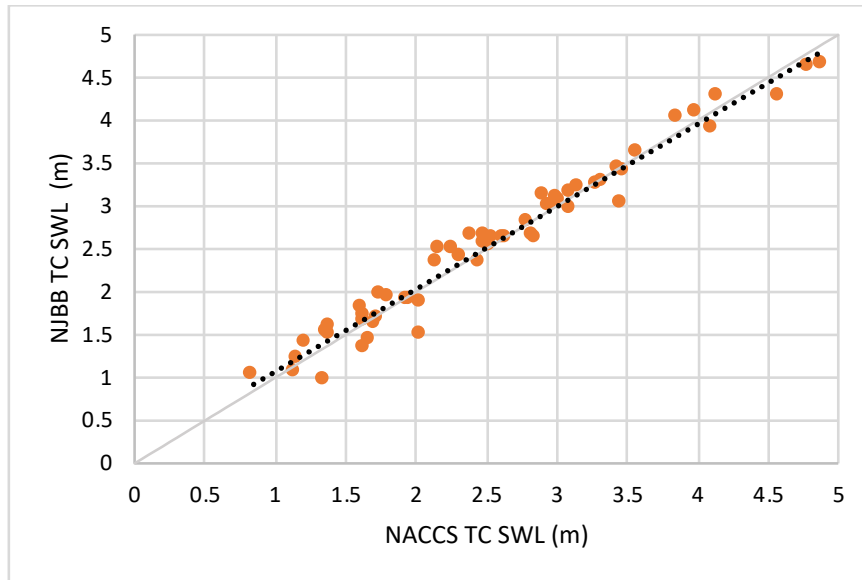


Figure 12: NJBB vs. NACCS TC SWL for NJBB SP 29 (base condition).

Table 4: Linear regression coefficients for estimation of NJBB XC SWL (base condition).

NJBB Save Point	β_0 (m)	β_1	R^2
36	0.0369	0.9828	0.9864
2	0.0987	0.9433	0.9782
57	0.0847	0.9555	0.9727
50	0.0815	0.9627	0.9705
29	0.1018	0.958	0.9647

The estimated NJBB XC SWL, as a function of NACCS XC SWL, are depicted in [Figure 13](#) and [Figure 14](#) for save points 36 and 29, respectively. SWL hazard curves for XCs and CC hazard curves were developed as described in Nadal-Caraballo et al. (2015).

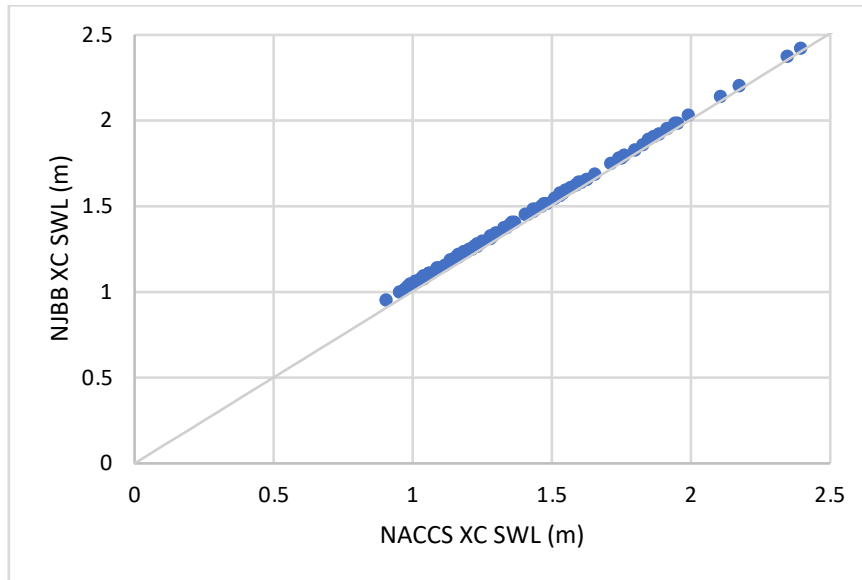


Figure 13: Estimated XC SWL NJBB SP 36 (base condition).

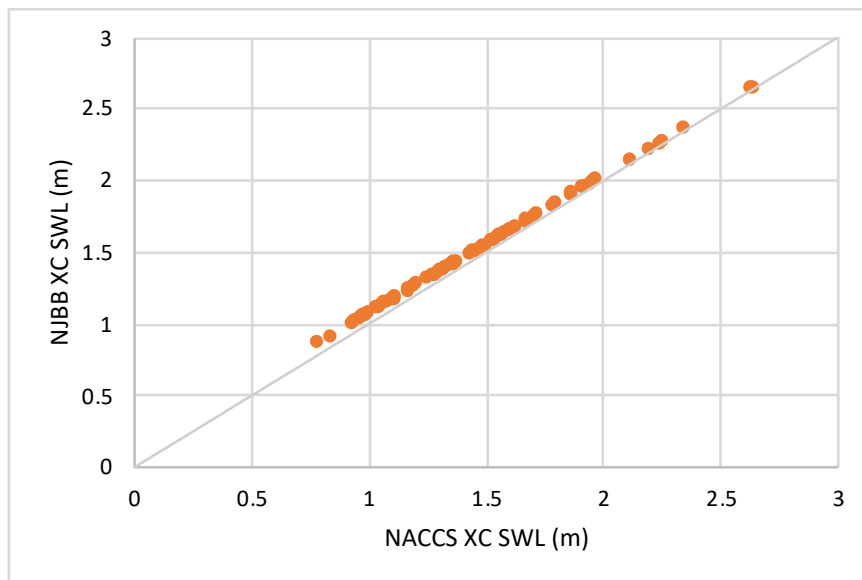


Figure 14: Estimated XC SWL NJBB SP 29 (base condition)

2.4 – Reconstruction of Water Levels for With-Project Alternatives

This section discusses the reconstruction of SWL for the different NJBB with-project alternatives. The processes of reconstructing TC and XC with-

project SWL are discussed in [2.4.1 -- Tropical Cyclones](#) and [2.4.2 -- Extratropical Cyclones](#), respectively. Results for the All-Closed (all inlets closed) and All-Closed-Less-2 (all inlets closed except Little Egg/Brigantine and Corson Inlet) alternatives are provided herein as examples of the application of this methodology.

2.4.1 – Tropical Cyclones

The methodology for training of GPM and reconstructing TC SWL for the with-project alternatives follows steps similar to the methodology previously discussed in [2.3.2 -- Tropical Cyclones](#) for reconstruction of the base condition TC SWL. However, wave setup estimation only needs to be done once for the base condition, as discussed in [2.3.1 – Estimation of Wave Setup](#), and the same per-save point regression models can be applied to correct the without-waves TC SWL values from the with-project alternatives. After the NJBB TC SWL is corrected for wave setup, the NJBB alternative to base TC SWL ratios ($K_{R,alt}$) and absolute differences ($K_{A,alt}$) for the 60-TC RSS are computed. Then, $K_{R,alt}$ and $K_{A,alt}$ are used as input in the training of the GPM for the different alternatives.

NJBB All-Closed alternative TC SWL to NJBB base condition TC SWL ratios are shown in [Figure 15](#) and [Figure 16](#) for save points 36 and 29, respectively. Save point 36 has a mean $K_{R,alt}$ of 1.05, resulting in a net SWL amplification of 5%. For save point 29, most of the resulting SWL ratios are in the 0.5 to 0.7 range with a mean $K_{R,alt}$ of 0.58, indicating that on average the All-Closed alternative reduced the SWL to 58% of the base condition SWL for this location. Likewise, the TC SWL ratios for the All-Closed-Less-2 alternative are illustrated in [Figure 17](#) and [Figure 18](#). For save point 36, the results at this location are virtually identical to the All-Closed alternative with a mean $K_{R,alt}$ of 1.05 and a net SWL amplification of 5%. Save point 29, however, shows most of the SWL ratios ranging from 0.7 to 1.1, with a mean $K_{R,alt}$ of 0.83, demonstrating that on average the All-Closed-Less-2 alternative resulted in the SWL being reduced to 83% of the base condition SWL at this location.

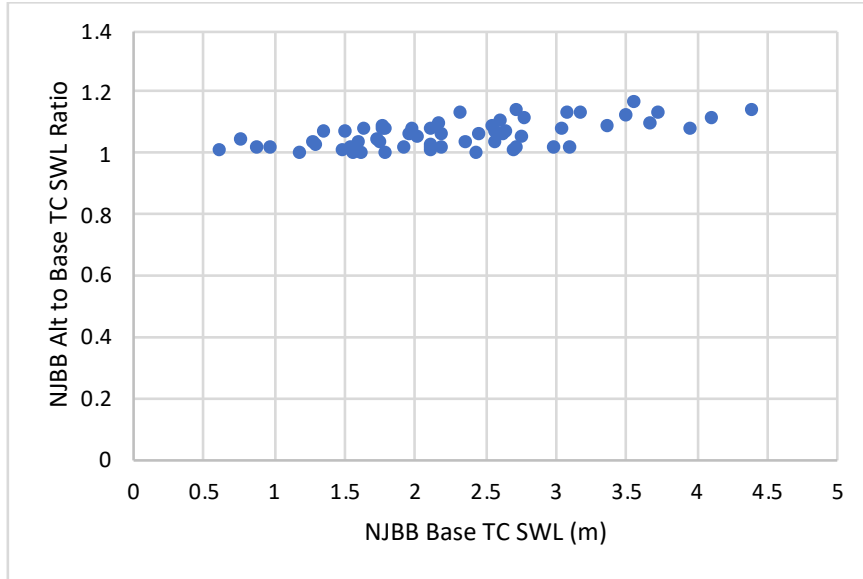


Figure 15: NJBB All-Closed to base condition TC SWL ratios for SP 36.

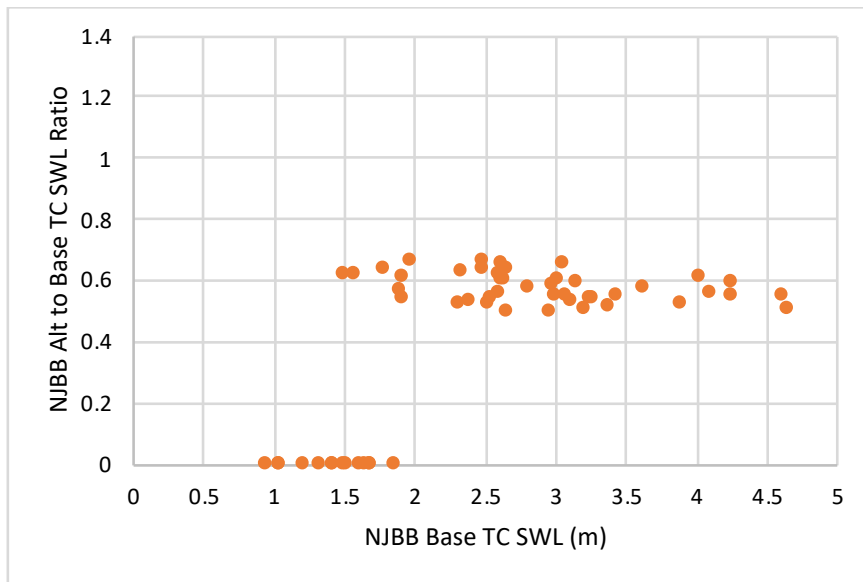


Figure 16: NJBB All-Closed to base condition TC SWL ratios for SP 29.

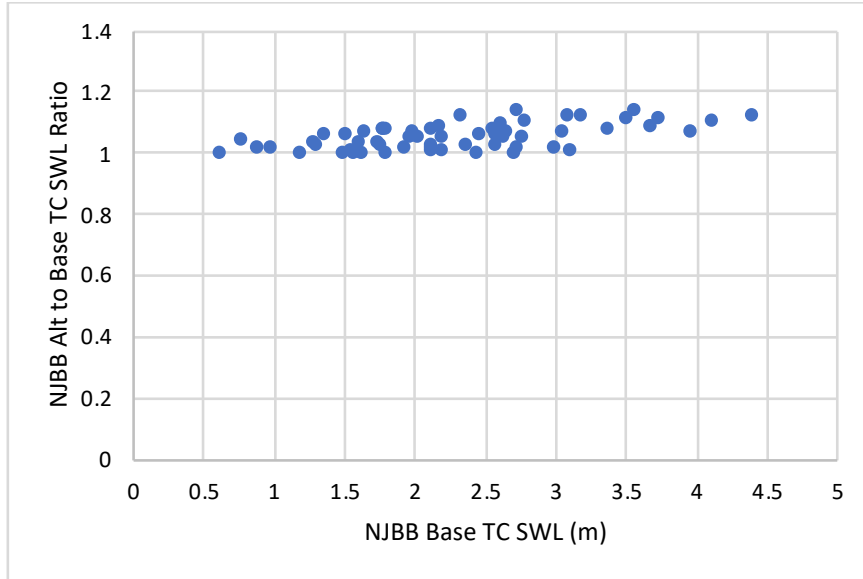


Figure 17: NJBB All-Closed-Less-2 to base condition TC SWL ratios for SP 36.

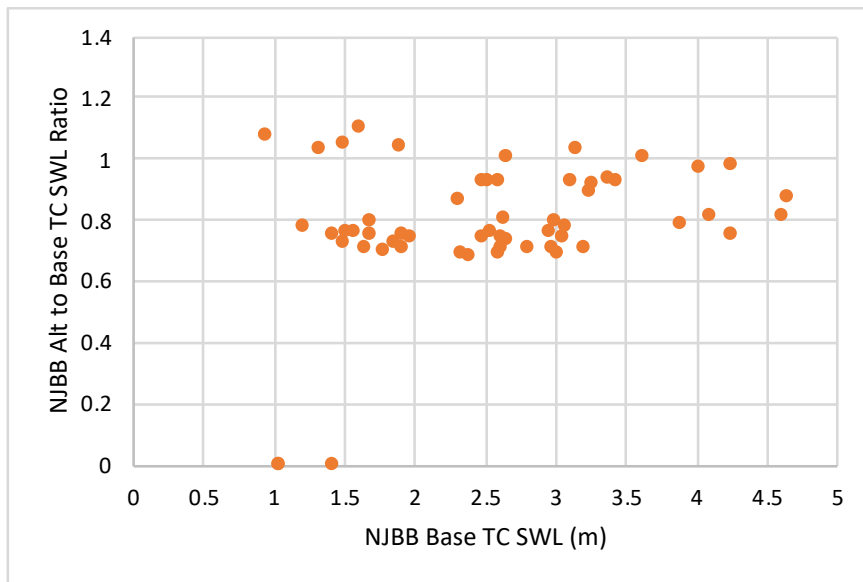


Figure 18: NJBB All-Closed-Less-2 to base condition TC SWL ratios for SP 29.

The validation metrics (R^2 , ME, and CC) for the GPM trained for the NJBB All-Closed with-project alternative are shown in [Table 5](#) for select NJBB save points, as well as global metrics accounting for all 180 save points. The validation metrics for the All-Closed-Less-2 alternative are given in [Table 6](#).

Table 5: GPM validation for All-Closed to base condition TC SWL ratios.

NJBB Save Point	R ²	ME (m)	CC
36	0.8859	0.0053	0.9615
2	0.9691	0.0649	0.9872
57	0.9599	0.079	0.984
50	0.924	0.0326	0.9758
29	0.776	0.2095	0.9377
All Save Points	0.8652	0.1354	0.9582

Table 6: GPM validation for All-Closed-Less-2 to base condition TC SWL ratios.

NJBB Save Point	R ²	ME (m)	CC
36	0.8816	0.0052	0.9605
2	0.9653	0.0516	0.9847
57	0.9708	0.0467	0.9869
50	0.9352	0.0393	0.9746
29	0.7461	0.1375	0.9456
All Save Points	0.8622	0.0956	0.9596

The NJBB All-Closed GPM validation metrics for all 180 NJBB save points are plotted in [Figure 19](#). The validation metrics for the All-Closed-Less-2 GPM are shown in [Figure 20](#). The TC with-project SWL hazard curves for were developed as described in Nadal-Caraballo et al. (2015).

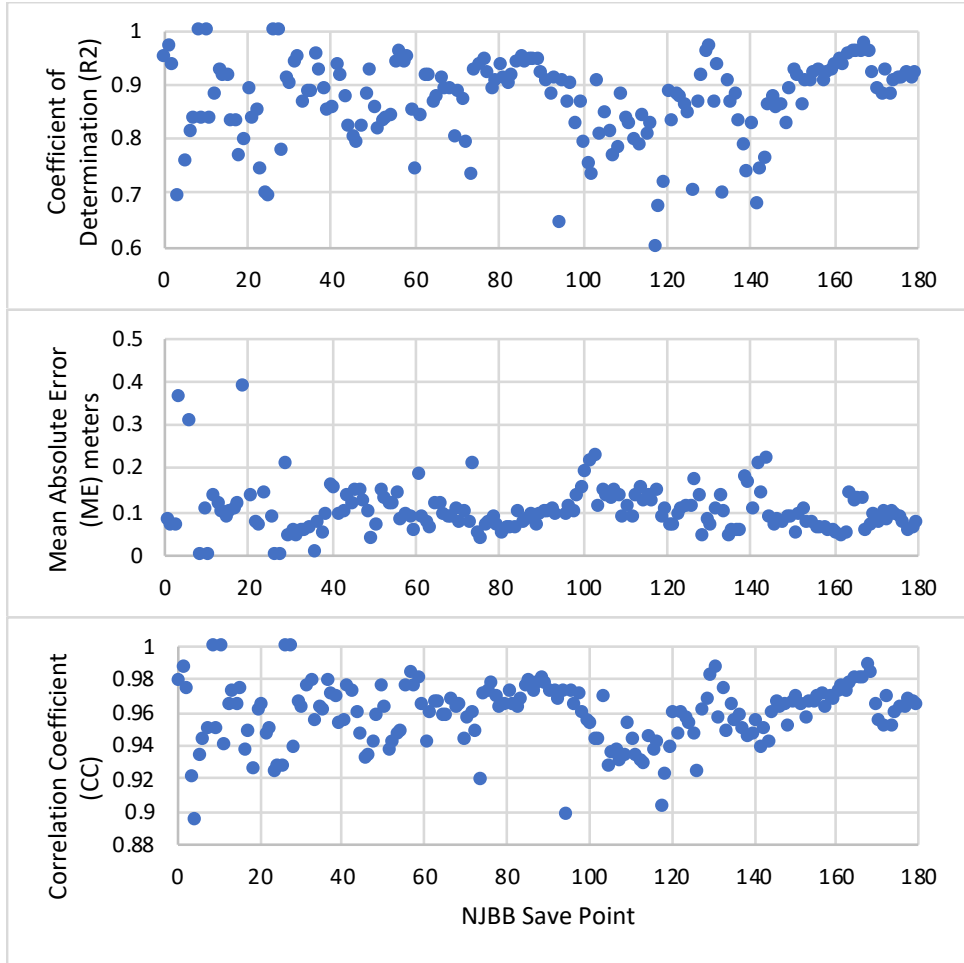


Figure 19: All-Closed GPM validation metrics for TC SWL at 180 NJBB save points.

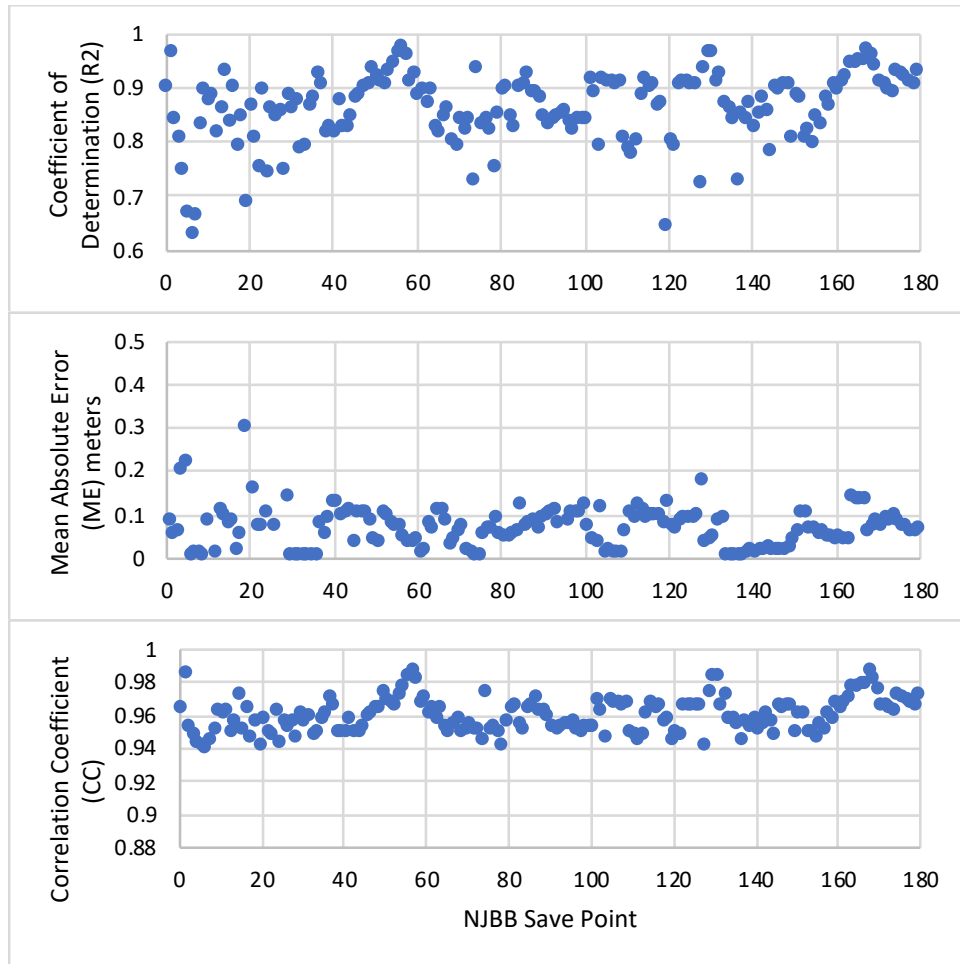


Figure 20: All-Closed-Less-2 GPM validation metrics for TC SWL at 180 NJBB save points.

2.4.2 -- Extratropical Cyclones

As discussed in [2.3.3 -- Extratropical Cyclones](#), XCs are not parameterized. Therefore, instead of employing GPM, which requires a set of input parameters to develop the input/output relationship, the reconstruction of XC SWL relies on regression models to: 1) add wave setup to the NJBB surge-only water levels for both base condition (as discussed in [2.3.3 -- Extratropical Cyclones](#)) and the different with-project alternatives; and 2) to establish the relationship between each NJBB with-project alternative TC SWL and the NJBB base condition TC SWL in order to estimate XC SWL. Considering the latter, the NJBB All-Closed TC SWL vs. base condition TC SWL are shown in [Figure 21](#) and [Figure 22](#) for save points 36 and 29, respectively. The NJBB All-Closed-Less-2 vs. base condition TC SWL for the same save points are shown in [Figure 23](#) and [Figure 24](#).

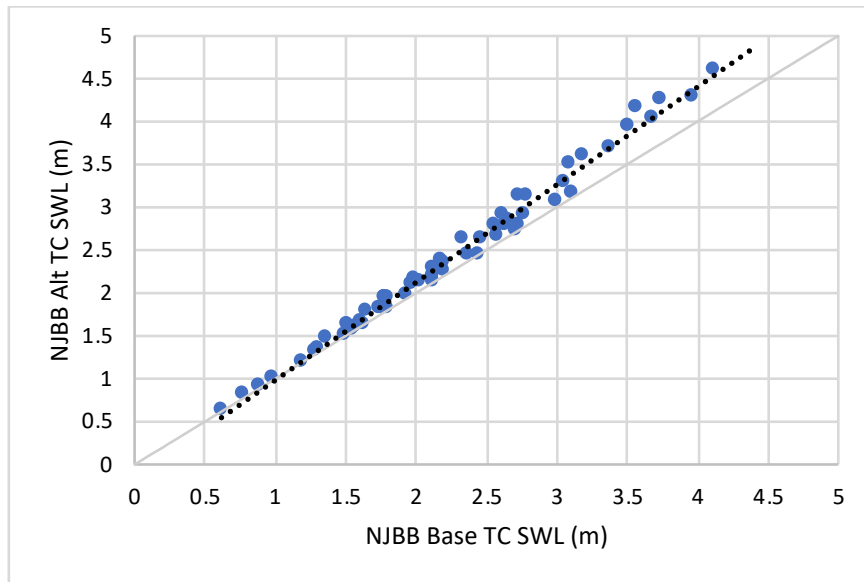


Figure 21: NJBB All-Closed vs. base condition TC SWL for SP 36.

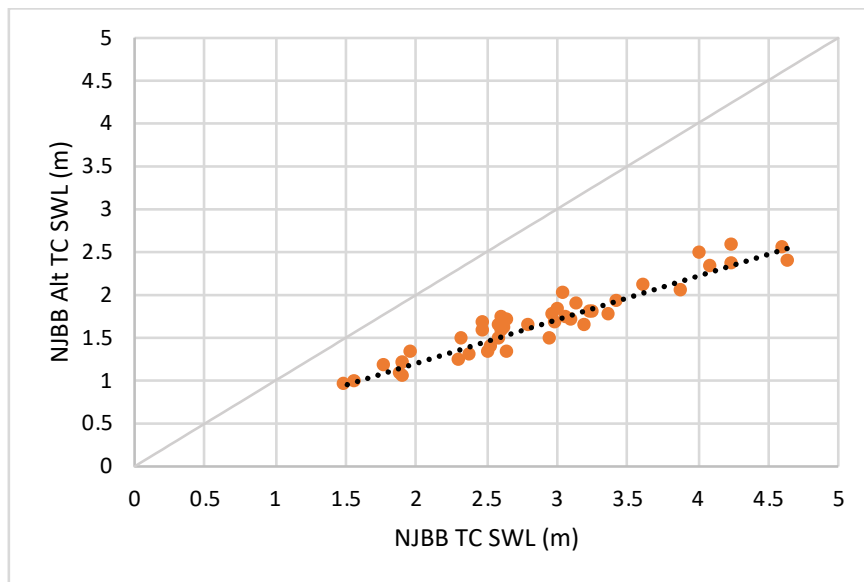


Figure 22: NJBB All-Closed vs. base condition TC SWL for SP 29.

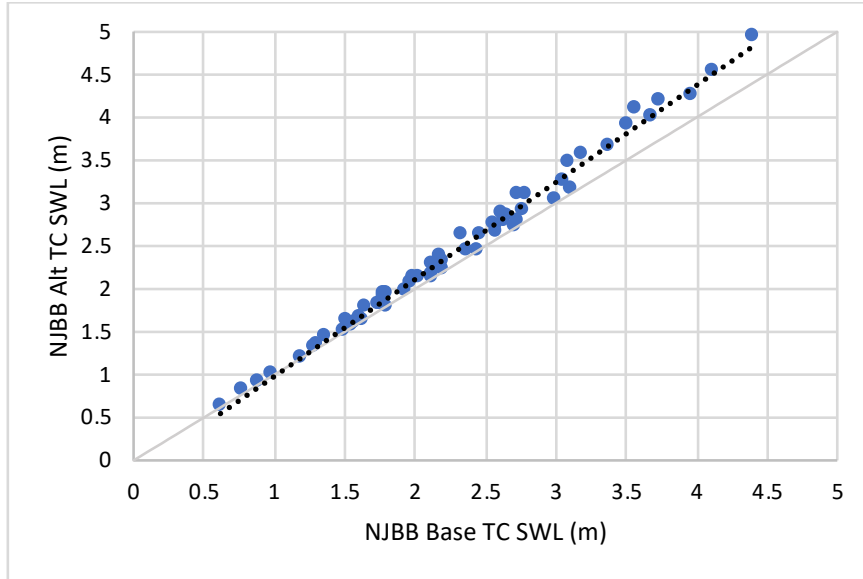


Figure 23: NJBB All-Closed-Less-2 vs. base condition TC SWL for SP 36.

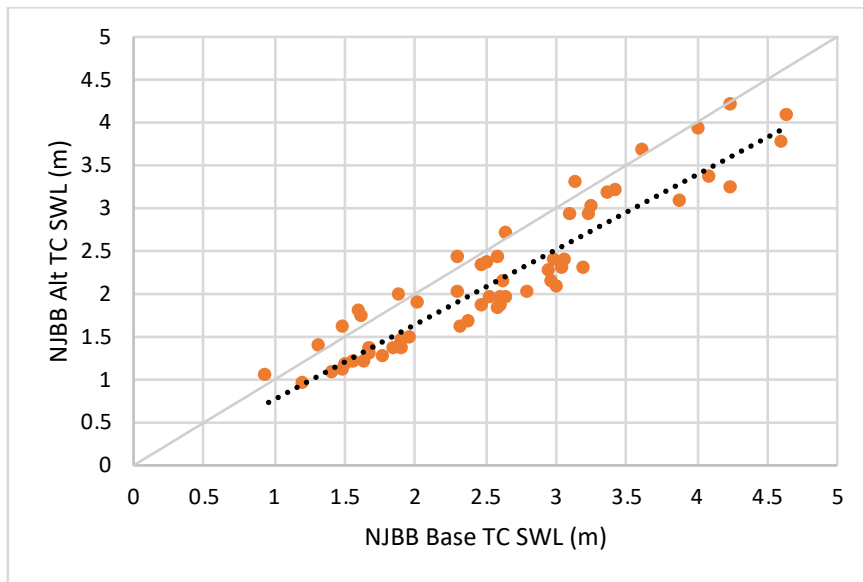


Figure 24: NJBB All-Closed-Less-2 vs. base condition TC SWL for SP 29.

The linear regression model coefficients, β_0 and β_1 , and the coefficient of determination, R^2 , for the NJBB All-Closed and All-Closed-Less-2 with-project alternatives are presented in Table 7 and Table 8, respectively. In the case of the All-Closed alternative, save point 29 remained dry until the

TC SWL reached an elevation of 1.42 m. This occurrence is shown in [Table 7](#) as elevation threshold. When estimating NJBB XC SWL for the All-Closed alternative, SWL less than this elevation are set to zero.

Table 7: Linear regression coefficients for estimation of NJBB XC SWL (All-Closed).

NJBB Save Point	β_0 (m)	β_1	R ²	Elevation Threshold (m)
36	-0.1825	1.1432	0.9898	–
2	0.4907	0.1299	0.0802	–
57	0.3535	0.1615	0.145	–
50	0.1298	0.4234	0.8713	–
29	0.1846	0.5069	0.908	1.42

Table 8: Linear regression coefficients for estimation of NJBB XC SWL (All-Closed-Less-2).

NJBB Save Point	β_0 (m)	β_1	R ²	Elevation Threshold (m)
36	-0.1593	1.1261	0.9911	–
2	0.1536	0.6603	0.3778	–
57	-0.144	0.808	0.5538	–
50	-0.1779	0.8664	0.8437	–
29	-0.1436	0.8831	0.8778	–

The estimated XC SWL for the NJBB All-Closed alternative as a function of NACCS XC SWL are shown in [Figure 25](#) and [Figure 26](#) for save points 36 and 29, respectively. The NJBB All-Closed-Less-2 XC SWL vs. NACCS XC SWL are shown in [Figure 27](#) and [Figure 28](#) for these two save points. The

with-project XC SWL hazard curves were developed as described in Nadal-Caraballo et al. (2015). The reconstructed CC SWL hazard curves for the with-project alternatives considered in NJBB Iteration 3 and the discussion of these results are presented in [4.3 -- Maximum Storm Surge Results – Iteration 3](#)

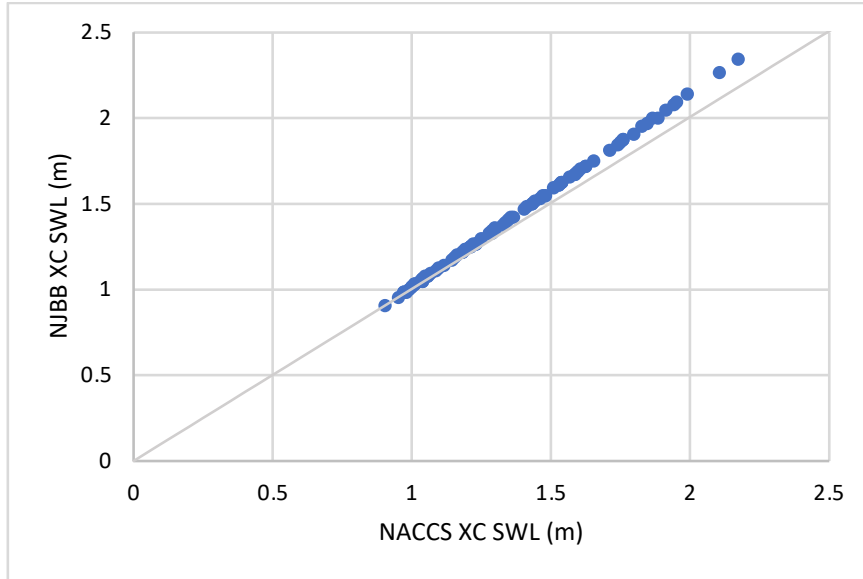


Figure 25: Estimated NJBB XC SWL vs. NACCS XC SWL for SP 36 (All-Closed).

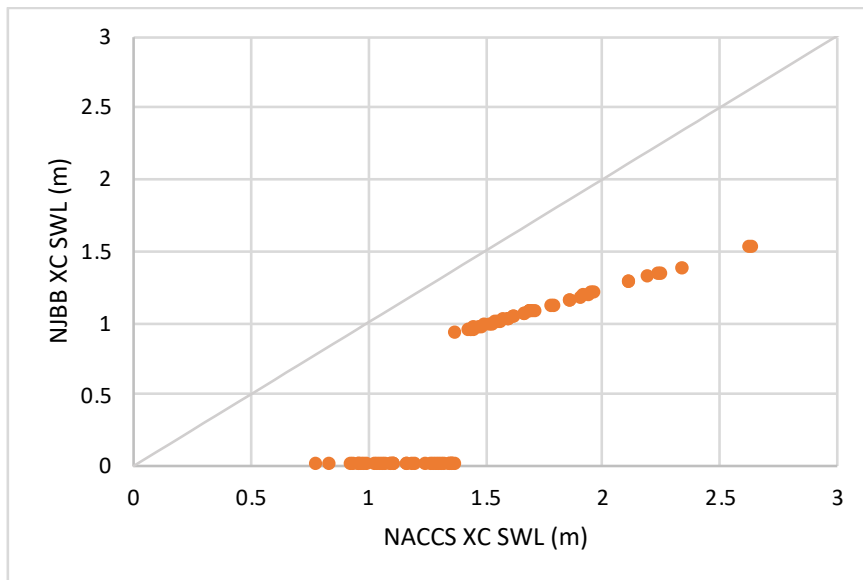


Figure 26: Estimated NJBB XC SWL vs. NACCS XC SWL for SP 29 (All-Closed).

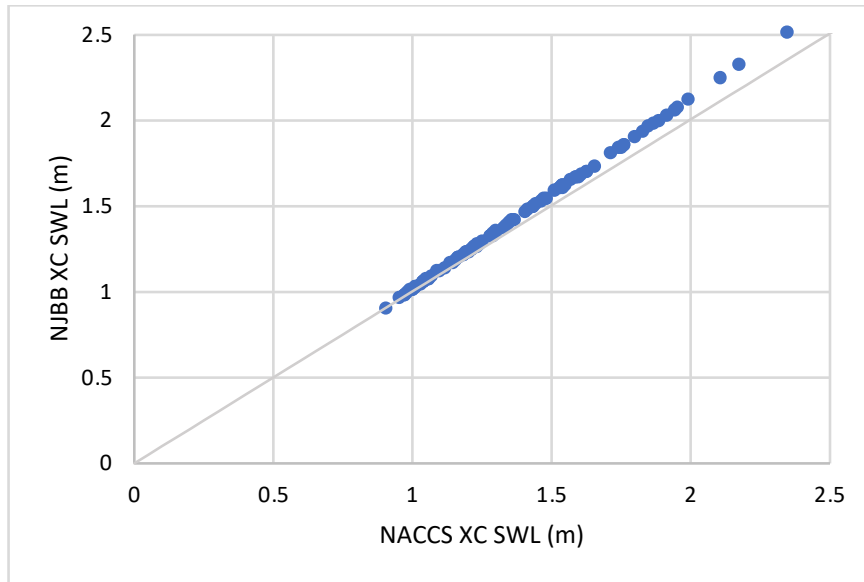


Figure 27: Estimated NJBB XC SWL vs. NACCS XC SWL for SP 36 (All-Closes-Less-2).

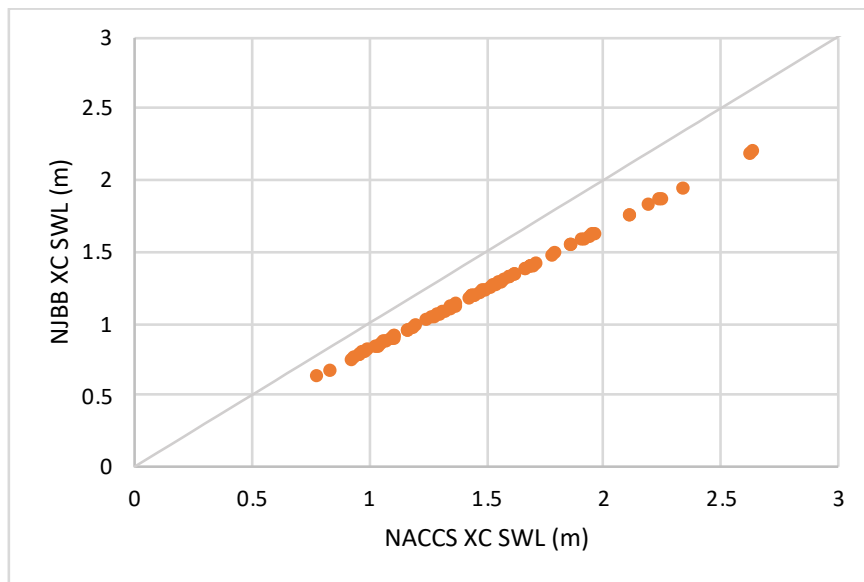


Figure 28: Estimated NJBB XC SWL vs. NACCS XC SWL for SP 29 (All-Closed-Less-2).

3 -- ADCIRC Grid Details and Model parameters

The computational domain for the NJBB study, shown in [Figure 29](#) was derived from the North Atlantic Coast Comprehensive Study (NACCS) ADCIRC grid and covers the North Atlantic Coast, Gulf of Mexico, and Caribbean Sea (Cialone et al. 2015). [Figure 30](#) shows the ADCIRC computational boundary in the New Jersey coastal area.



Figure 29: Outline plot showing the boundary of the ADCIRC grid.

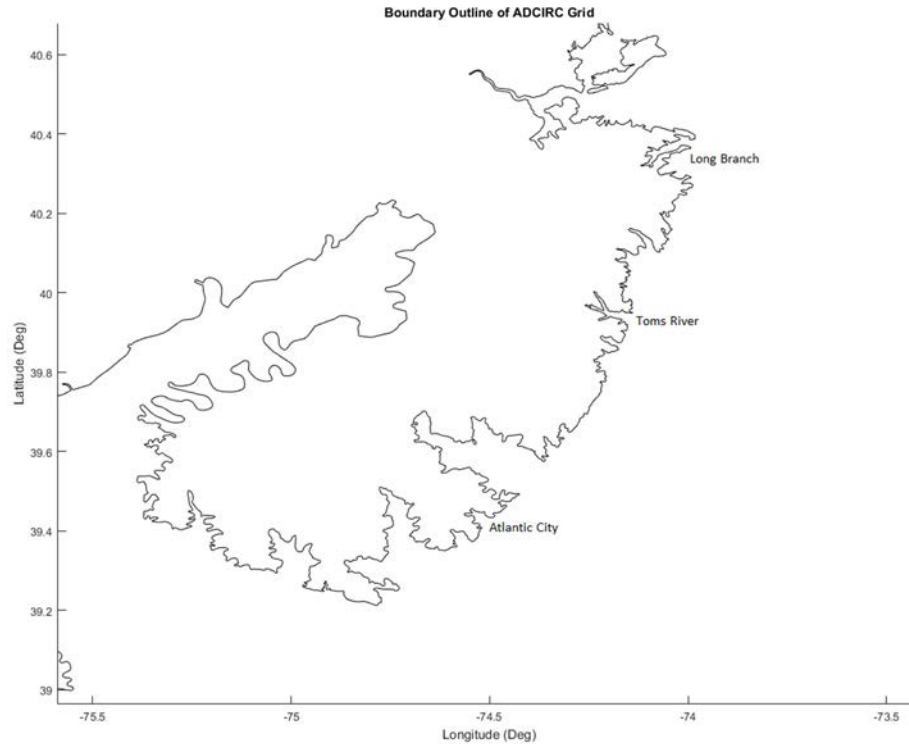


Figure 30: Boundary of ADCIRC grid showing New Jersey coast.

While the original NACCS grid boundary was maintained, Chesapeake Bay and coastal Long Island were subject to a “de-refining” procedure, which locally reduces grid resolution in areas that are distant from the area of interest. (Figure 31 and Figure 32 show grid resolution before and after de-refining in Chesapeake Bay and the coastal Long Island regions, respectively). The de-refining is performed in order to reduce model simulation times, while maintaining the flow volume exchange from the distant locations to and from the area of interest. The total number of 3.12 million nodes in the NACCS grid was reduced to 2.38 million (approximately a 24% reduction) in the NJBB grid due to the de-refining.

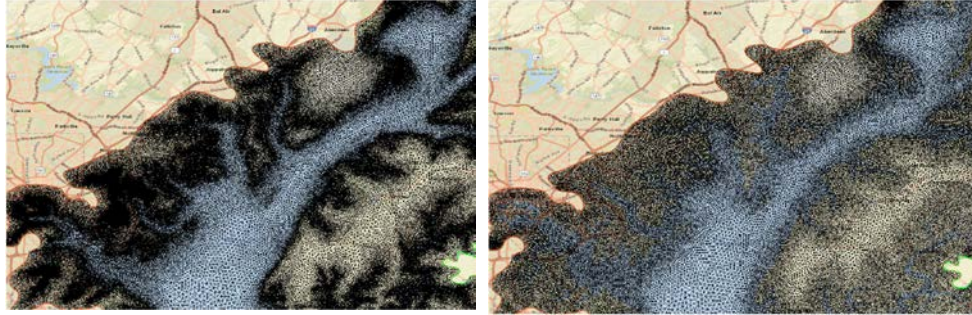


Figure 31: Chesapeake Bay before (left) and after (right) de-refining

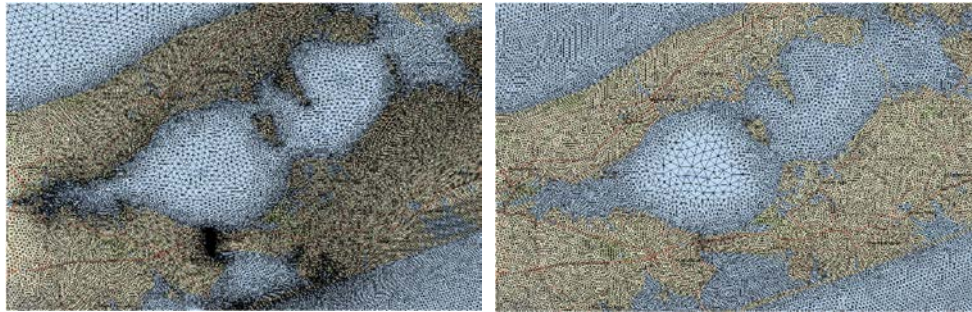


Figure 32: Long Island before (left) and after (right) de-refining

In order to show that the de-refining procedure did not significantly alter the model results in the region of interest, a comparison of “without-project condition” NJBB (further in this text referred to as the “Base Grid”) and NACCS water surface elevation time series was made for 59 save points (the locations of the save points are displayed in [Figure 33](#) and [Figure 34](#)) for a simulation of Hurricane Sandy. A representative plot comparing NJBB and NACCS water surface elevation time-series is shown in [Figure 35](#) for save point #31. A time-series plot for save point #56 shows the greatest difference in maximum water level ([Figure 36](#)). The absolute and relative differences of maximum water level between the NJBB Base and NACCS grids for the 59 save points are shown in [Table 9](#). The average absolute difference for maximum water level elevation was ~ 0.02 meters and the corresponding average relative difference was 1.02%. As mentioned above, the greatest difference in maximum water levels was observed at save point #56 (0.06 m, 3.64%).



Figure 33: NJBB save points (North)



Figure 34: NJBB save points (South)

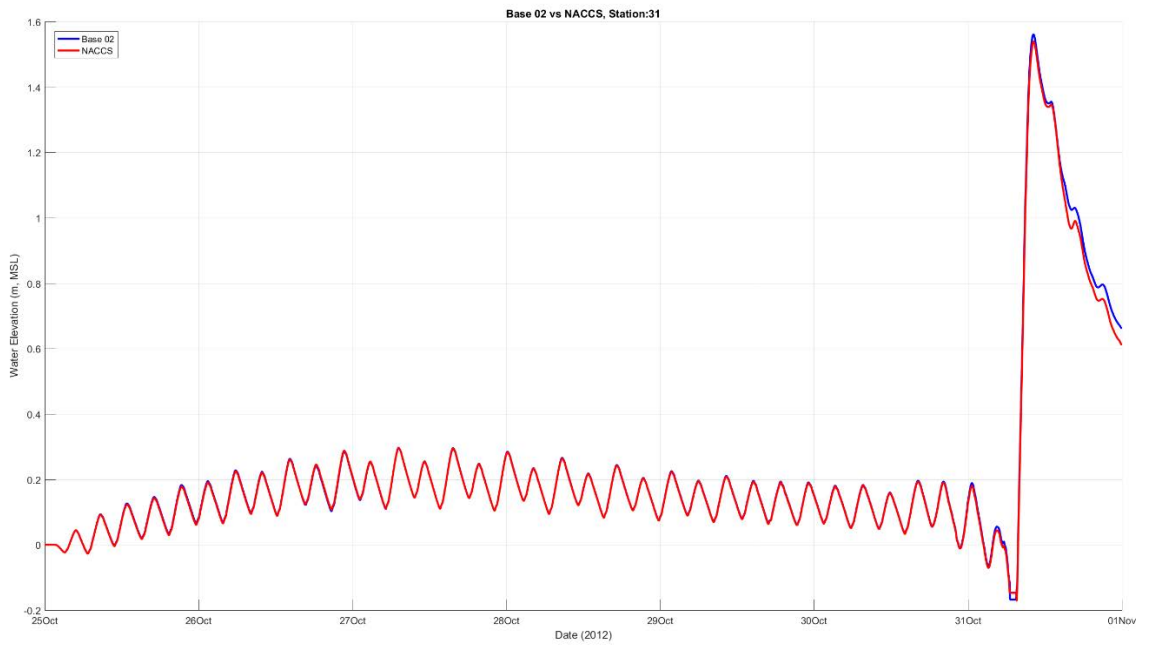


Figure 35: The representative time series plot of water surface elevation (save point #31) for Hurricane Sandy (between October 25 and November 1, 2012): NACCS (red) vs NJBB-Base (blue) [m]

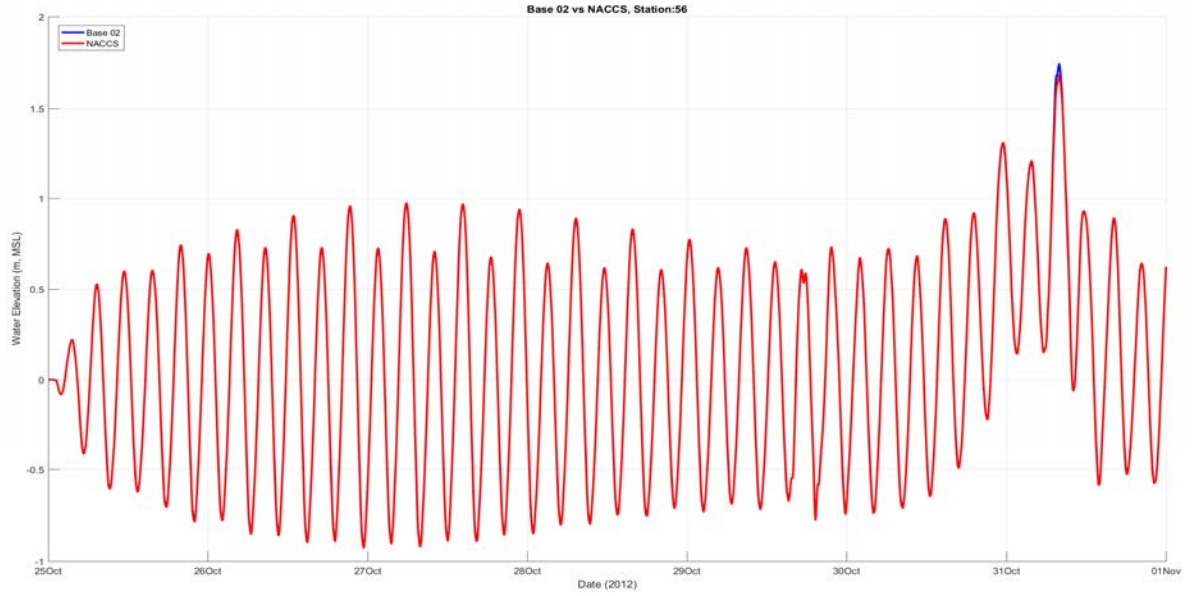


Figure 36: The time-series plot with the greatest difference in maximum water level (save point #56) for Hurricane Sandy (between October 25 and November 1, 2012): NACCS (red) vs NJBB-Base (blue) [m]

Table 9: Max difference for the peak surge in meters (col 2 & 4) and in percent (col 3 & 6) for the 59 save points.

Save point	Max diff for the peak surge [m]	Max diff for the peak surge [%]	Save point	Max diff for the peak surge [m]	Max diff for the peak surge [%]
1	0.0001	0.0057	31	0.0218	1.4149
2	0.0015	0.0641	32	0.0025	0.1281
3	0.0001	0.0056	33	0.0063	0.3089
4	0.0001	0.0047	34	0.0104	0.4976
5	0.0065	0.3046	35	0.0149	0.6872
6	0.0022	0.0891	36	0.0122	0.5639
7	0.0007	0.0290	37	0.0012	0.0550
8	0.0004	0.0148	38	0.0591	2.4807
9	0.0105	0.5733	39	0.0552	2.3636
10	0.0147	0.8114	40	0.0058	0.2558
11	0.0038	0.1826	41	0.0089	0.3470
12	0.0088	0.4643	42	0.0130	0.7530
13	0.0091	0.4186	43	0.0117	0.6502
14	0.0101	0.4159	44	0.0117	0.6018
15	0.0085	0.3359	45	0.0121	0.6631
16	0.0768	3.2408	46	0.0128	0.6898
17	0.0097	0.4189	47	0.0186	1.1292
18	0.0086	0.3661	48	0.0358	2.3804
19	0.0079	0.3189	49	0.0318	2.0249

20	0.0349	2.4429	50	0.0247	1.5213
21	0.0328	2.1922	51	0.0256	1.5390
22	0.0272	1.8349	52	0.0230	0.8527
23	0.0369	2.8029	53	0.0139	0.5206
24	0.0129	0.6702	54	0.0122	0.4576
25	0.0101	0.5200	55	0.0226	0.8173
26	0.0294	1.8812	56	0.0611	3.6394
27	0.0288	1.8832	57	0.0594	3.4429
28	0.0241	1.4965	58	0.0350	2.0400
29	0.0255	1.5253	59	0.0124	0.7130
30	0.0229	1.4401			

The final step in creating the Base Grid was to raise the barrier islands elevations from Manasquan to Lower Cape May Meadows to represent 2018 existing conditions with the recent construction of several USACE beach restoration projects (10-22 ft., NAVD88). [Table 10](#) gives a detailed description of the updated barrier islands elevations. All subsequent “surge barrier alternative” grids were constructed from the Base Grid. The NJBB Base Grid has a spatial resolution (element size) ranging from approximately 10 to 1000 m and MSL as a vertical datum. Finally, the dune heights ([Table 10](#)) were converted to meters and the vertical datum was adjusted to MSL by subtracting 0.12 m (based on NOAA Station 8534720 located in Atlantic City, NJ) before implementing the restored barrier islands into Base Grid.

Table 10: Elevation updates for New Jersey barrier island dunes to represent 2018 existing conditions.

Project	Location	Dune Height (ft, NAVD88)
Manasquan Inlet to Barnegat Inlet	Northern Point Pleasant Beach and Seaside Heights	18
Manasquan Inlet to Barnegat Inlet	Rest of Project Area	22
Barnegat Inlet to Little Egg Inlet	Long Beach Island	22
Brigantine Inlet to Great Egg Harbor Inlet	Brigantine Island	10
Brigantine Inlet to Great Egg Harbor Inlet	Atlantic City	14.75
Brigantine Inlet to Great Egg Harbor Inlet	Ventnor, Margate, Longport	12.75
Great Egg Harbor Inlet & Peck Beach	northern Ocean City	-
Great Egg Harbor Inlet to Townsends Inlet	southern Ocean City	12.8
Great Egg Harbor Inlet to Townsends Inlet	Strathmere and Sea Isle City	14.8
Townsends Inlet to Cape May Inlet	Avalon	14.75
Townsends Inlet to Cape May Inlet	Stone Harbor	14.75
Hereford Inlet to Cape May Inlet	Wildwood	16
Cape May to Lower Township	Cape May	-

Lower Cape May Meadows	Cape May Meadows	16.75
	Absecon Seawall	16
	Townsend's Seawall	11.7
	Hereford Seawall	11.7

The NACCS ADCIRC grid with the exception of the raised elevations of the barrier islands, mentioned in the preceding paragraph, was used as a topobathymetric data source. The source of the data used for modifying the barrier islands was the authorized dune and seawall heights for NAP projects.

3.1 – Phase I - Iteration 1

Iteration 1 began with model simulations of individual inlet closures to understand of the hydraulic influence of each inlet on surge propagation into the NJBB region and inform the development of multiple closure alternatives. One additional simulation that involved multiple inlet closures was included in Iteration 1, All Closed Less 2, at the request of NAP. This alternative gave insight into how openings at two of the most environmentally sensitive inlets, Little Egg/Brigantine and Corson, might limit the effectiveness of other inlet closures at reducing water levels in the study area. A schematic of the study areas tidal inlets and bay systems is shown in [Figure 37](#).



Figure 37: Schematic of NJBB Study Area

3.1.1 -- Configurations of proposed structures

Iteration 1 included the following closure configurations:

1. Base Conditions
2. Cape May Canal
3. Cape May Inlet
4. Hereford
5. Townsends
6. Corson
7. Great Egg
8. Absecon
9. Little Egg / Brigantine
10. Barnegat
11. Manasquan
12. Shark River
13. All Closed Less 2

A schematic of All Closed Less 2 is provided in [Figure 38](#), where the red lines representing closures.



Figure 38: Schematic of All Closed Less 2

3.1.2 -- Grids

A total of twelve proposed design structure layouts were modeled in addition to the existing condition (Base Condition) case for Iteration 1 as listed in the previous section. The grid modification process to implement a proposed closure was the same for all twelve structures, that is, the Base Grid was altered in the vicinity of the structure by adding “weir-pairs”, the ADCIRC subgrid feature that represents impermeable boundary type, to represent a storm surge barrier. This local modification of the Base Grid minimized the grid changes between the different alternatives. All weir-

pair structures were set to a +6.1 m (+20 ft) MSL elevation in Iteration 1. Implementing weir-pairs in ADCIRC maintains the stability of the model since the sub-grid scale formulation for weir-pairs prevents the model from transitioning from sub to supercritical flows during the course of the simulation in the event that the water elevation is high enough to overtop the structure. [Figure 39](#) and [Figure 40](#) show the same region of the ADCIRC grid before and after implementation of the weir-pairs, respectively. Simulations were initiated with the surge barriers in place and the surge barriers remained closed for the entire simulation. The simulation results are discussed in [4.1 -- Maximum Storm Surge Results – Iteration 1](#).

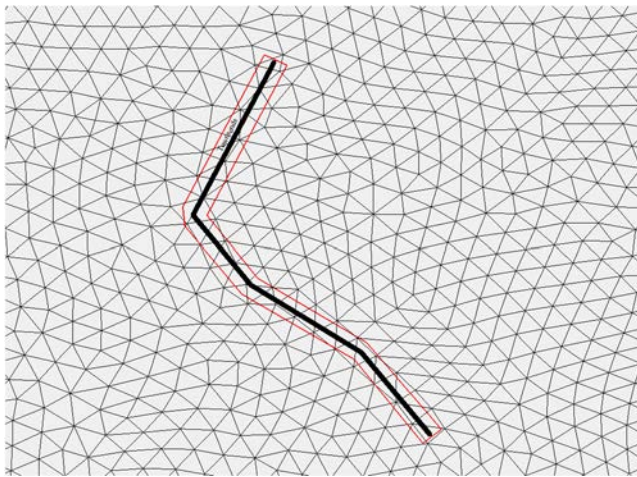


Figure 39: Base Grid before implementing Townsends Inlet closure. The red contour indicates the position of the future weir-pairs, the black line is the centerline of the structure.

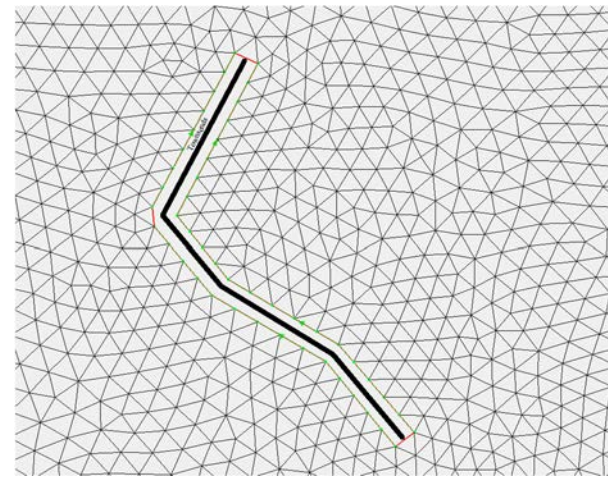


Figure 40: The ADCIRC grid implementing Townsends Inlet closure. The green contour shows the weir-pairs, the black line is the centerline of the structure

3.2 – Phase I - Iteration 2

A workshop with the CHL and the NJBB Project Delivery Team (PDT) was held on January 31, 2018 to review the model results from Iteration 1 and identify various closure configurations to be evaluated in Iteration 2. The PDT is an interdisciplinary group including project planners, biologists, hydraulic engineers, civil engineers, cost engineers, and project managers.

Many of the closure configurations for Iteration 2 were designed around leaving the most environmentally-sensitive inlets open: Little Egg/Brigantine, Corson, and Hereford. Closures across the interior bays, referred to as “bay closures”, were added to several configurations to reduce water levels for those configuration with the environmentally-

sensitive inlets remaining open. The study area was also divided into 3 regions (north (N), central (C), and south (S)) based on the relative hydraulic independence of the configurations identified for these regions. Since many of the configurations were designed around leaving Little Egg/Brigantine and Corson inlets open, these two inlets were natural boundaries for the three regions.

Model results from Iteration 1 indicated that the north and south configurations were independent of each other. Therefore, the north and south configurations could be combined into a single ADCIRC simulation without the results for the north or south configurations impacting the other region. Combining the north and south configurations reduced the total number of simulations required and High Performance Computer (HPC) demand.

A few of the closure configurations were intended as sensitivity simulations to help determine if certain closures may be omitted from configurations without significantly reducing the configurations effectiveness.

3.2.1 – Configurations of proposed structures

Iteration 2 included the following closure configurations:

1. All Closed ([Figure 41](#))
2. All Closed Less 2 - Simulated during Iteration 1 ([Figure 41](#))
3. N3 + S3 ([Figure 41](#))
4. N4 + S4 ([Figure 41](#))
5. N5 + S5 ([Figure 41](#))
6. N6 + S6 ([Figure 41](#))
7. N7 + S7 ([Figure 42](#))
8. S8 ([Figure 42](#))
9. S9 ([Figure 42](#))
10. S10 ([Figure 42](#))
11. C3 ([Figure 42](#))
12. C4 ([Figure 42](#))
13. C5 ([Figure 43](#))
14. C6 ([Figure 43](#))
15. C7 ([Figure 43](#))

A schematic of the Iteration 2 alternatives is provided in [Figure 41](#), [Figure 42](#), and [Figure 43](#) where the red lines represent closures.

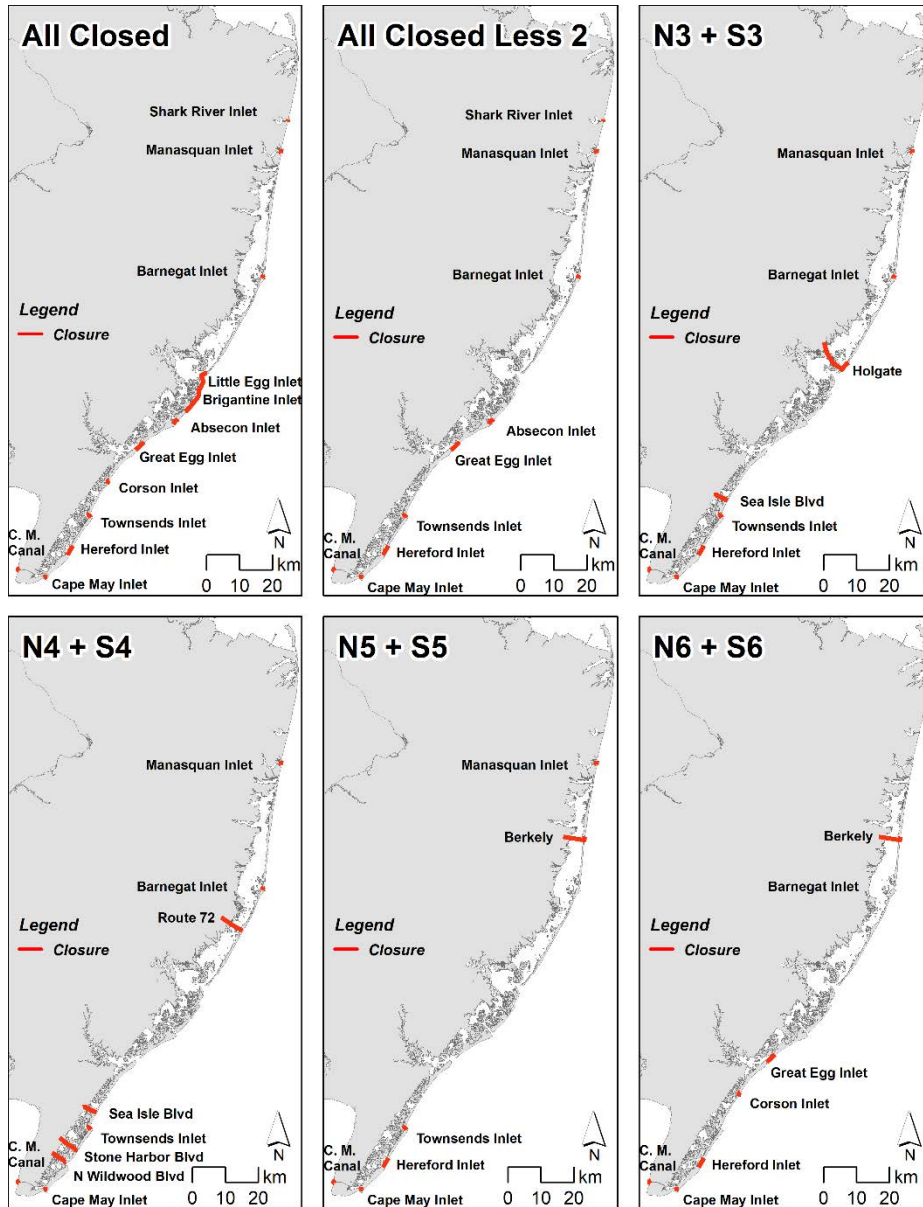


Figure 41: Schematic of All Closed, All Closed Less 2, N3+S3, N4+S4, N5+S5, and N6+S6.

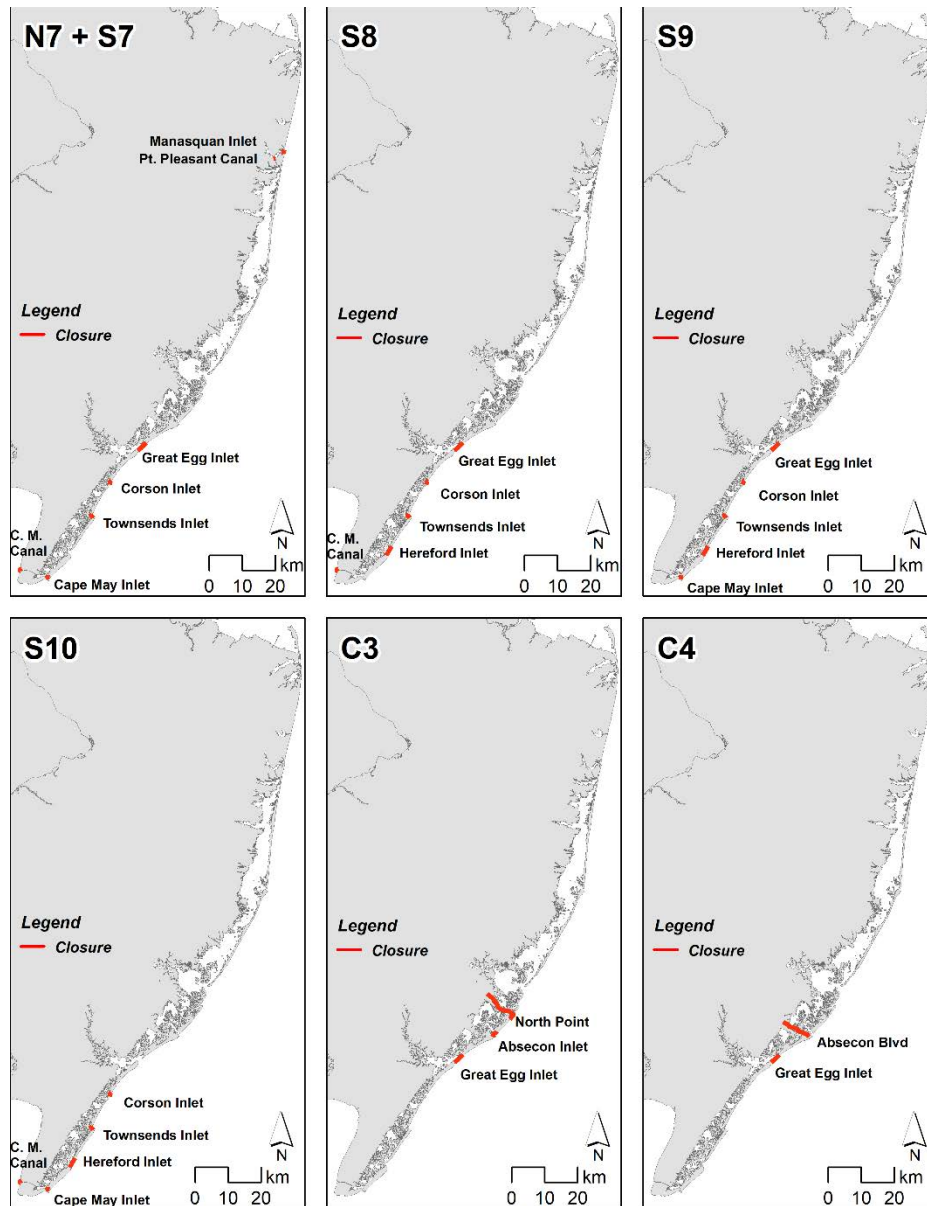


Figure 42: Schematic of N7+S7, S8, S9, S10, C3, and C4.

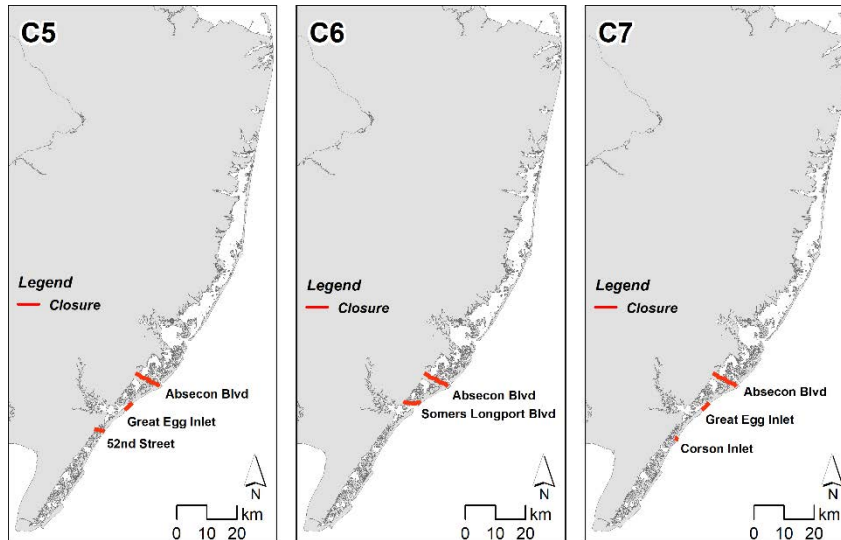


Figure 43: Schematic of C5, C6, and C7.

3.2.2 -- Grids

The grid development procedure for Iteration 2 closure configurations was the same as in [3.1.2 -- Grids](#), however, in this case multiple structures were implemented on a single grid. The simulation results are discussed in [4.2 -- Maximum Storm Surge Results – Iteration 2](#).

3.3 – Phase I - Iteration 3

A second workshop with the CHL, NJBB PDT, and non-Federal sponsor (NJDEP) was held on April 13, 2018 to review the model results from Iteration 2 and identify the final set of configurations for Iteration 3. The focus of this workshop was identifying the configurations that meet the NJBB study objectives and constraints, while also considering the environmentally-acceptable configurations likely to generate the greatest NED benefits (flood damages reduce minus project costs). Several configurations were still included in the Iteration 3 simulation suite, even though they are not likely to be environmentally acceptable (All Closed, N3, C3, and the majority of southern alternatives). This decision was made to ensure that configurations were not eliminated before a more thorough plan formulation approach is applied.

3.3.1 – Configurations of proposed structures

Iteration 3 included the following closure configurations:

1. All Closed ([Figure 44](#))
2. All Closed Less 2 ([Figure 44](#))
3. N3 + S3 ([Figure 44](#))
4. N7 + S4 ([Figure 44](#))
5. C3 ([Figure 44](#))
6. C4 ([Figure 44](#))

All of the Iteration 3 configurations were evaluated in Iteration 2, except N7S4, which is a combination of previously evaluated north and south configurations. A schematic of the Iteration 3 alternatives is provided in [Figure 44](#) where the red lines represent closures. These configurations were evaluated with the large (60) storm suite as described in [2 -- Storm Selections](#).

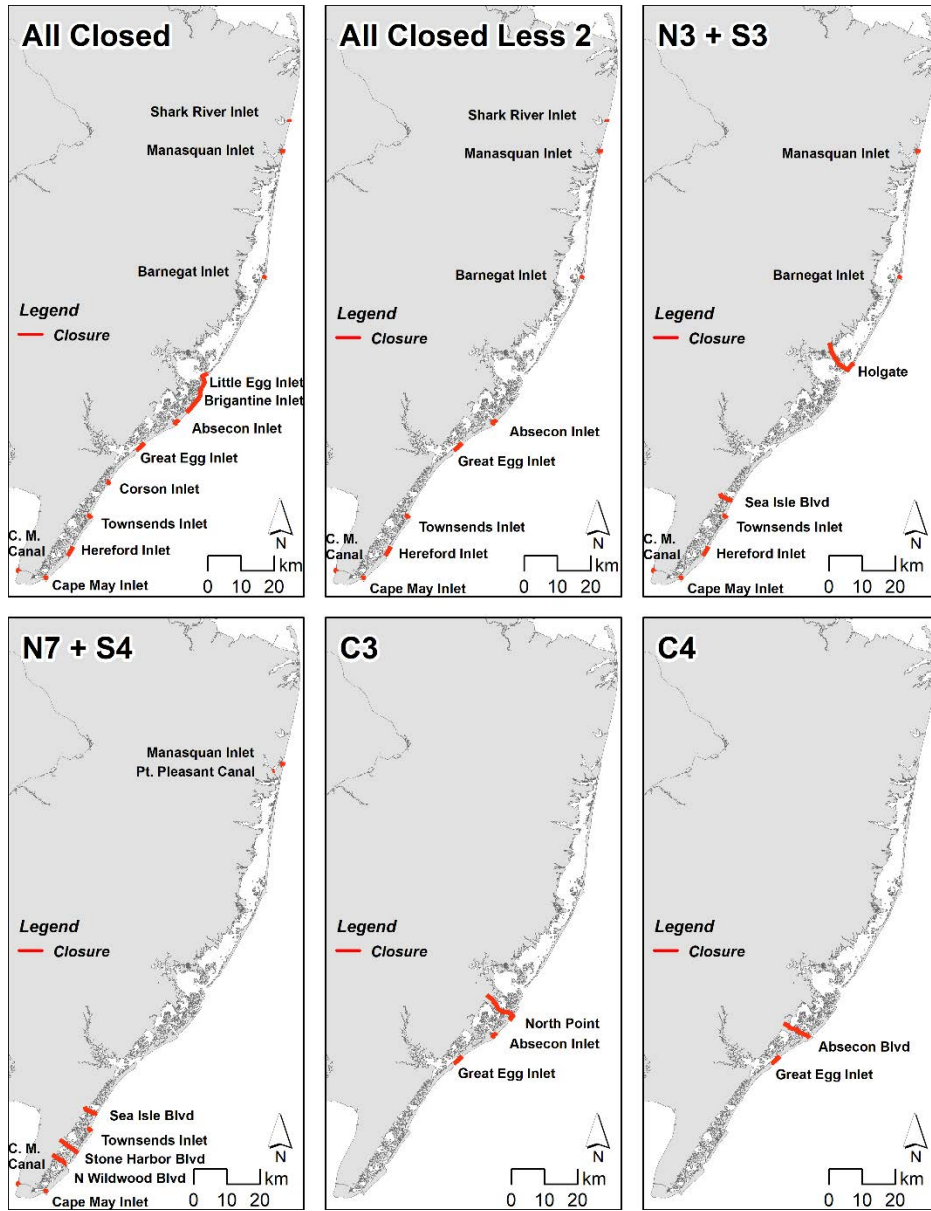


Figure 44: Schematic of All Closed, All Closed Less 2, N3+S3, N7+S4, C3, and C4.

3.3.2 -- Grids

The grid development procedure for Iteration 3 configurations was the same as in [3.1.2 -- Grids](#), however, this time multiple structures were implemented on a specific grid. The simulation results are discussed in [4.3 -- Maximum Storm Surge Results – Iteration 3](#).

3.4 – Phase II

The second phase of the New Jersey Back Bay (NJBB) numerical modeling effort was focused on updating the modeling results and hazard curves for the baseline conditions and remaining storm surge barrier alternatives in the Focused Array of Alternatives. During Phase II there was also an opportunity to update the model bathymetry in Barnegat Bay and at several of the inlets with more recent survey data. Initially, Phase II of the modeling study included tasks to evaluate NNBFs and the sensitivity of the modeling results to overwash and breaches at the barrier islands. However, the NNBF and overwash/breaching modeling efforts are not included in this technical report, but are documented in companion reports.

3.4.1 - Configurations of proposed structures

Phase II included the following four closure configurations:

1. Base. The NJBB Phase I Base Grid was modified in following ways 1) causeway barriers at Rte. 72, Absecon Blvd, Somers Longport Blvd, and 52nd St were implemented and 2) bathymetry was updated in the areas of Corson Inlet, Great Egg Inlet, Absecon Blvd, Brigantine, Little Egg Inlet, Lower Barnegat Bay, Barnegat Inlet, and Manasquan.
2. North (Figure 45). The North configuration included surge barriers at Manasquan Inlet and Barnegat Inlet in addition to the causeway at Rte. 72 to nearly enclose Barnegat Bay and Manahawkin Bay. The only openings to these bay areas are the 175-m, 750-m, and

- 220-m gap (listed from east to west) in the Rte. 72 causeway at the navigation channel location shown in [Figure 48](#) and [Figure 49](#).
3. Central 1 ([Figure 45](#)) supplemented the Base condition with surge barriers at Absecon Inlet and Great Egg Inlet, which nearly enclosed Lake Bay, Scull Bay, Great Egg Harbor Bay and Peck Bay. The only openings to these bay areas are 180-m and 200-m (east to west) gaps in the Absecon Blvd causeway, and a 900-m gap along Somers Longport Blvd causeway at the Beach Thorofare Channel location.
 4. Central 2 ([Figure 45](#)) supplemented the Base condition with only one surge barrier at Great Egg Inlet and converted the causeway closures to full bay closures at Absecon Blvd and 52nd St. This condition (Central 2) completely enclosed (“boxed off”) Lake Bay, Scull Bay, Great Egg Harbor Bay and Peck Bay.

A schematic of the closure alternatives are provided in [Figure 45](#), where the red lines represent closures. These configurations were evaluated with the large (60) storm suite as described in [2 -- Storm Selections](#).

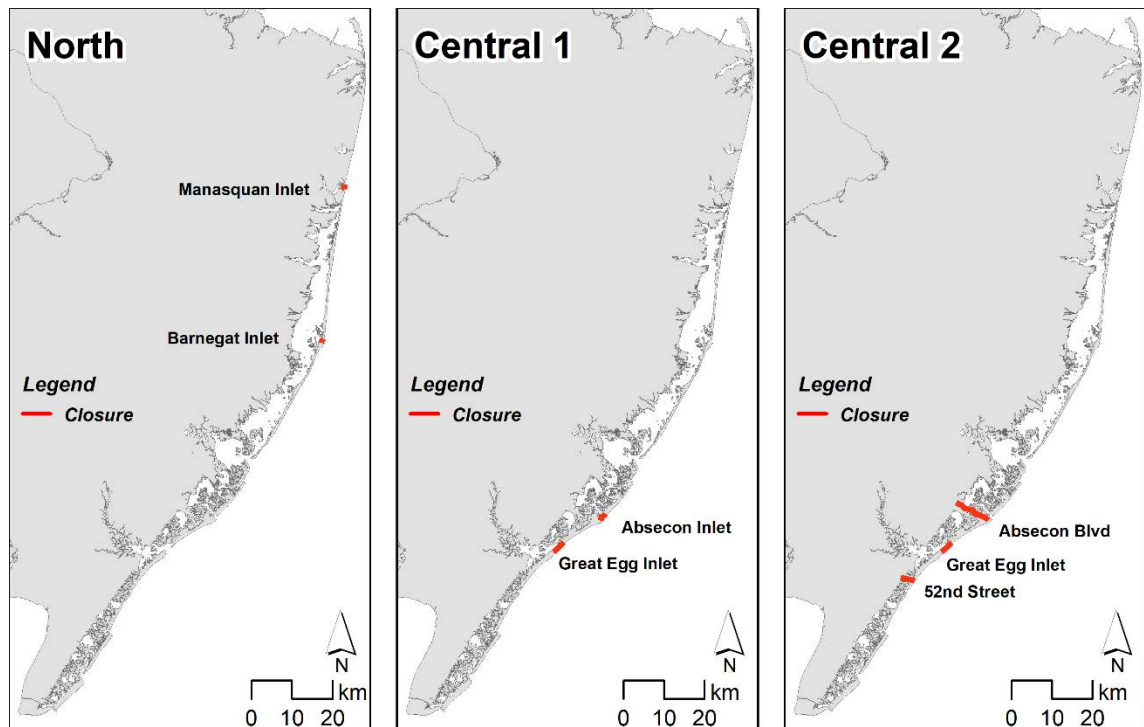


Figure 45: Schematic of North, Central 1, and Central 2.

3.4.2 – Simulated Storms

Synthetic Storms

The 60 storm suite that was determined in the NJBB Phase I ([2 -- Storm Selections](#)) numerical modeling by Design of Experiment methods was applied to the Base, Central 1, Central 2, and North grid configurations.

Historical Storms

Three historical storms were also selected for simulation to show water level response to actual events. The historical storm simulations included wind and tidal forcing. Hurricane Sandy and Extratropical (ET) NACCS Storms ET058 and ET060 (corresponding to October 1991 and December 1992), respectively were simulated for the Base, Central 1, Central 2, and North grid configurations.

3.4.3 – Grids

The grid development procedure for all four proposed design structure layouts was the same as in [3.1.2 -- Grids](#). However, the Base as well as the other three configurations also included bathymetry updates to the most recent NAP survey data for Corson Inlet, Great Egg Inlet, Absecon Blvd, Brigantine, Little Egg Inlet, Lower Barnegat Bay, Barnegat Inlet, and Manasquan. The causeway barriers at Rte. 72, Absecon Blvd, Somers Longport Blvd, and 52nd St were implemented as “weir-pairs”. [Figure 46](#) and [Figure 47](#) show the bathymetry and topography in Barnegat Bay before and after the bathymetric update, respectively, where blue indicates water depth and red indicates elevation. Note that the updated bathymetry and topography shows lower elevations of the marsh areas in this region (e.g., yellow colors change to green). [Figure 48](#) and [Figure 49](#) show the design and ADCIRC implementation of the Rte. 72 Causeway, respectively. The simulations results are discussed [4.4 -- Maximum Storm Surge Results – Phase II](#).

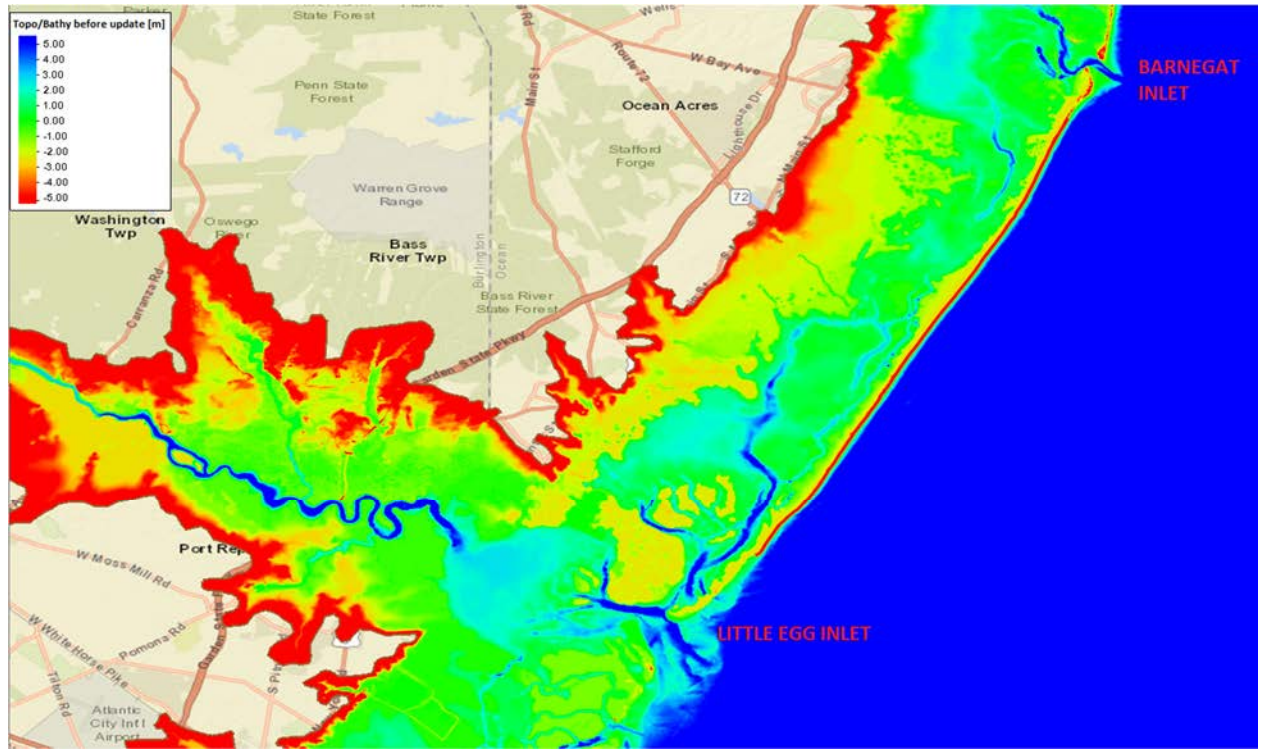


Figure 46: Bathymetry and topography in Barnegat Bay before the update.

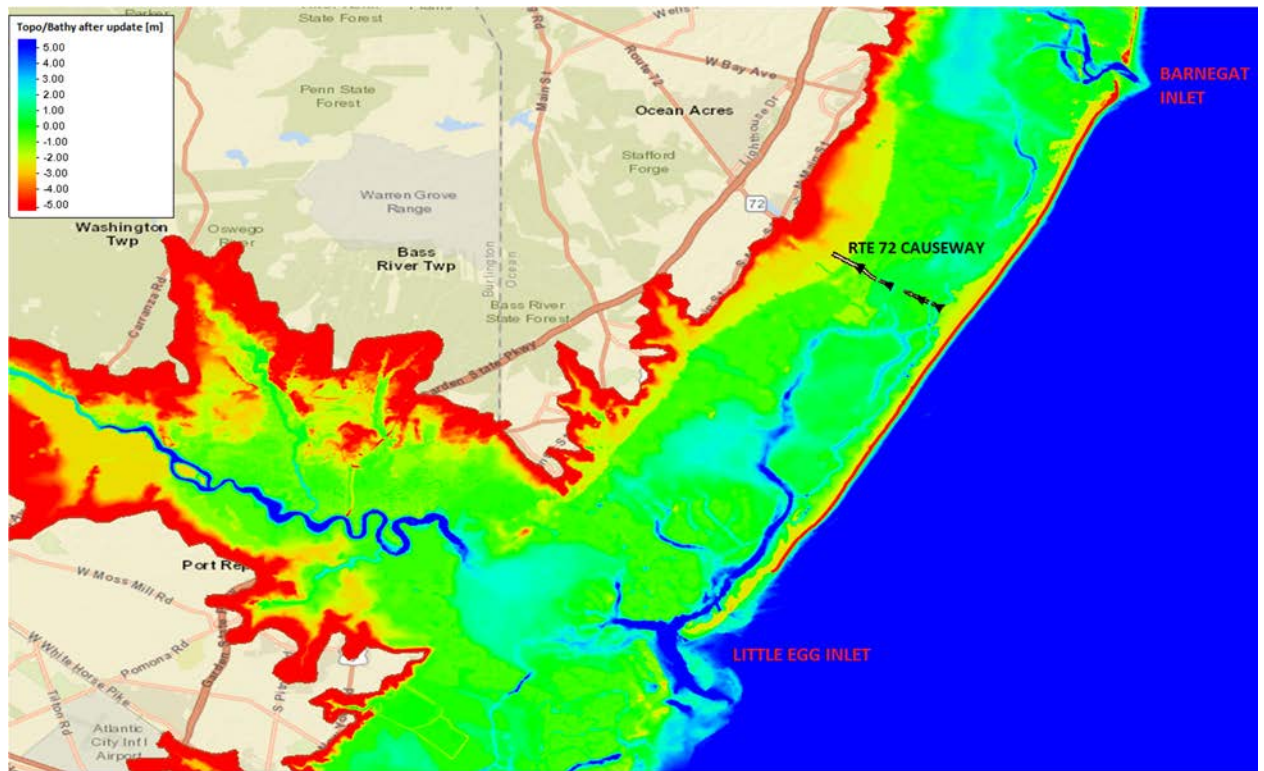


Figure 47: Bathymetry and topography in Barnegat Bay after the update.

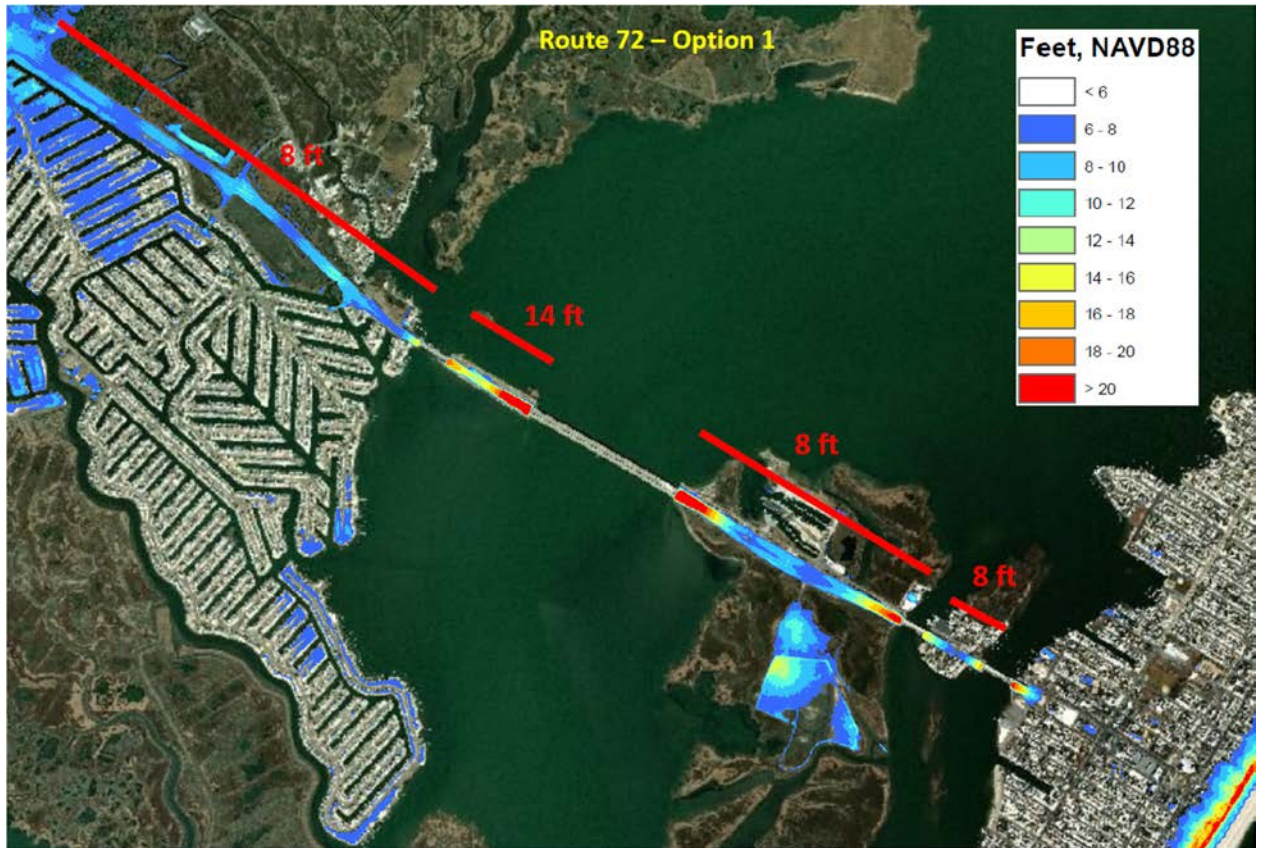


Figure 48: Rte. 72 Causeway - design



Figure 49: Rte. 72 Causeway - ADCIRC implementation

4.1 – Maximum Storm Surge Results – Iteration 1

The Iteration 1 numerical modeling task consisted in evaluating the impact on water levels in the NJBB of 1) individual inlet closures and; 2) closure of all inlets except LittleEgg/Brigantine and Corson Inlet using 10 storm events. The storm selection process was described in [2 -- Storm Selections](#) and the grid alternatives used in Iteration 1 were described in [3.1.1 -- Configurations of proposed structures](#). The following section describes the effect of closure configurations on maximum water level in the New Jersey back bays. The evaluation was made by analyzing the maximum water level in the overall project area as well as specific hydraulic reaches (shown outlined in black in [Figure 50](#)). The first stage of the analysis was based on comparing differences in the maximum water level for each closure condition relative to the base condition for the entire project area. Secondly, maximum water levels for the base condition at specific points in a hydraulic reach were compared to maximum water levels with a closure in place. These comparisons were referred to as “dot plots”, where each dot color represents one of the 10 storms and each individual dot represents a location in the hydraulic reach. Lastly, water level time series plots at specific points in the hydraulic reach were generated showing a comparison between the base condition and closure conditions. For the brevity of this document, only the Barnegat Inlet Closed and Townsend Inlet Closed configurations (Iteration 1) are provided and discussed with the above three types of plots. The complete set of maximum water level plots, difference plots, dot plots, and time series plots can be found in the Appendix.



Figure 50: NJBB Hydraulic Reaches (red dots indicate save points).

Shark River Inlet Closed versus Base Condition

Closure of Shark River Inlet individually had no impact on maximum water level for each of the 10 simulated storms beyond the immediate area behind (landward) of the closure location.

Manasquan Inlet Closed versus Base Condition

Closure of Manasquan Inlet individually had mixed results. For some storm events the closure was effective at reducing water levels. During other storm events that closure had little impact on maximum water levels and in a few instances resulted in higher water levels. The closure at Manasquan Inlet had no impact on Barnegat Bay. Results indicate that a standalone closure at Manasquan Inlet may not be effective.

Barnegat Inlet Closed versus Base Condition

Barnegat Inlet leads to the largest bay system in New Jersey which includes hydraulically connected Barnegat Bay, Manahawkin Bay, and Little Egg Harbor. Closing Barnegat Inlet provides the most significant maximum water level reduction in northern part of the bay system (0.32 to 0.67 m), moderate reduction observed in central section (Manahawkin Bay), and minimal reductions in Little Egg Harbor (0.07-0.26 m). This negligible reduction of maximum water level in the southernmost section of the bay system for most of the simulated storms is due to the surge entering through the open Little Egg/Brigantine Inlet. The only exception is Storm 636, that is, the maximum water elevation in Manahawkin Bay is substantially reduced due to strong north-to-south winds which pushes the water from the northern part of the bay system into Manahawkin Bay. For the Base configuration more water volume is directed southward since Barnegat Inlet is open and allows surge inflow. If, on the other hand, the inlet is closed (Barnegat Inlet configuration) less water can be transported southward to Manahawkin Bay which leads to the maximum water level reduction in that area.

[Figure 51](#) and [Figure 52](#) show maximum water elevation for the Base Grid (left), maximum water elevation with Barnegat Inlet closed (center), and the difference in maximum water elevations between Barnegat Inlet closed and the Base Grid (right) for tropical synthetic storms 434 and 636, respectively.

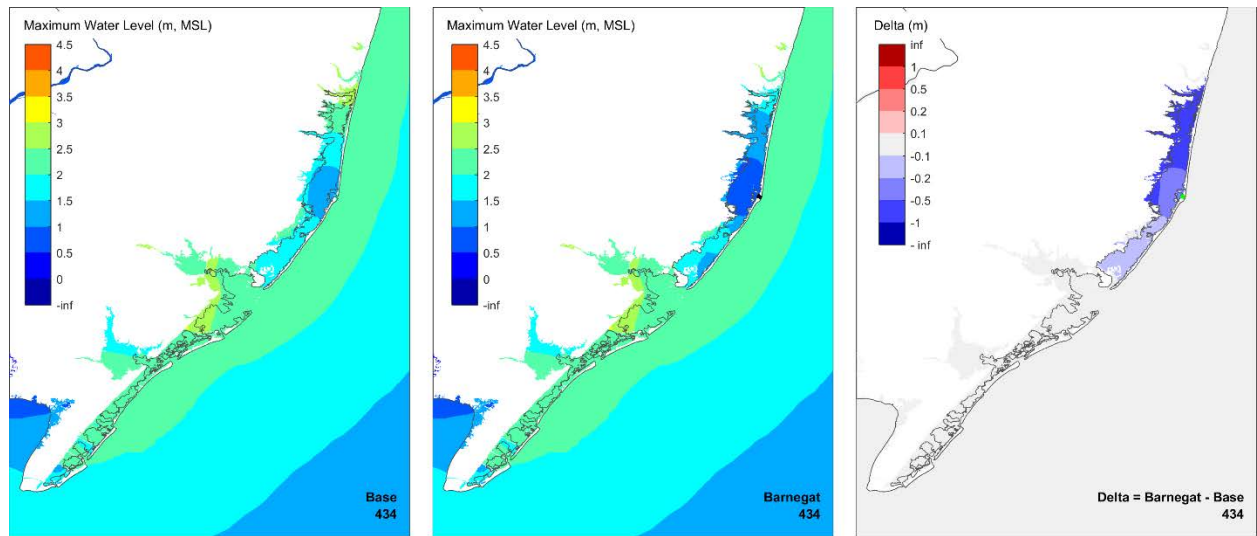


Figure 51: Maximum water elevation for Synthetic Storm 434: Base Grid (left), Barnegat Inlet Closed (center), and difference between Barnegat and Base (right)

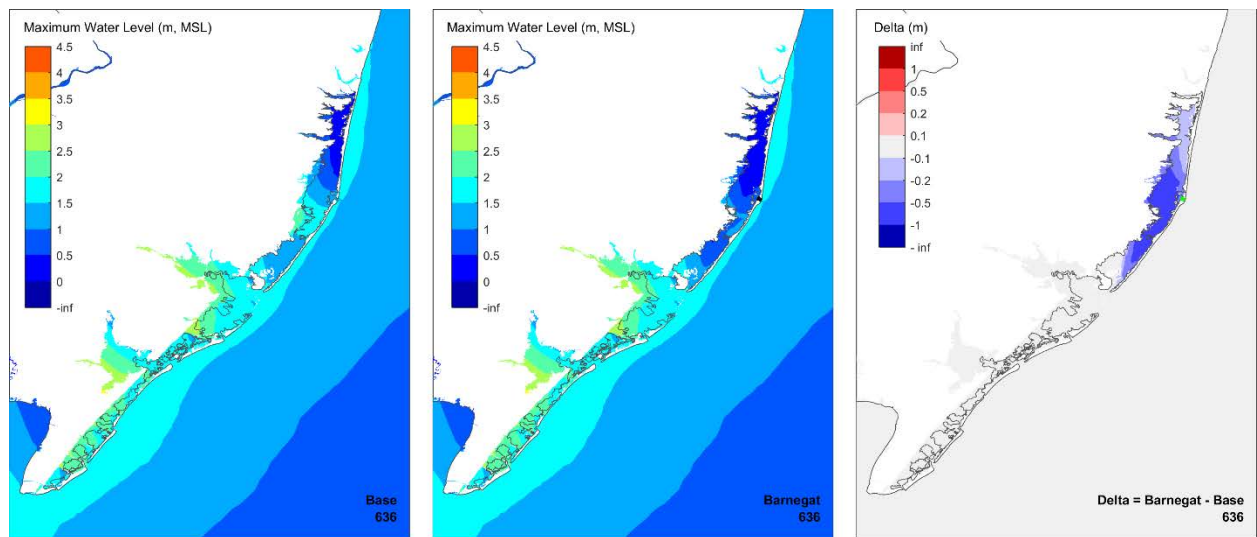


Figure 52: Maximum water elevation for Synthetic Storm 636: Base Grid (left), Barnegat Inlet Closed (center), and difference between Barnegat and Base (right)

Figure 53 shows maximum water levels at save point locations in the Barnegat hydraulic reach for the Base condition vs maximum water levels with Barnegat Inlet closed, referred to as a dot plot. Values below the 45 degree line indicate a reduction in maximum water level attributable to the closure. For this particular configuration the average reduction in maximum water level was 30% due to Barnegat Inlet being closed.

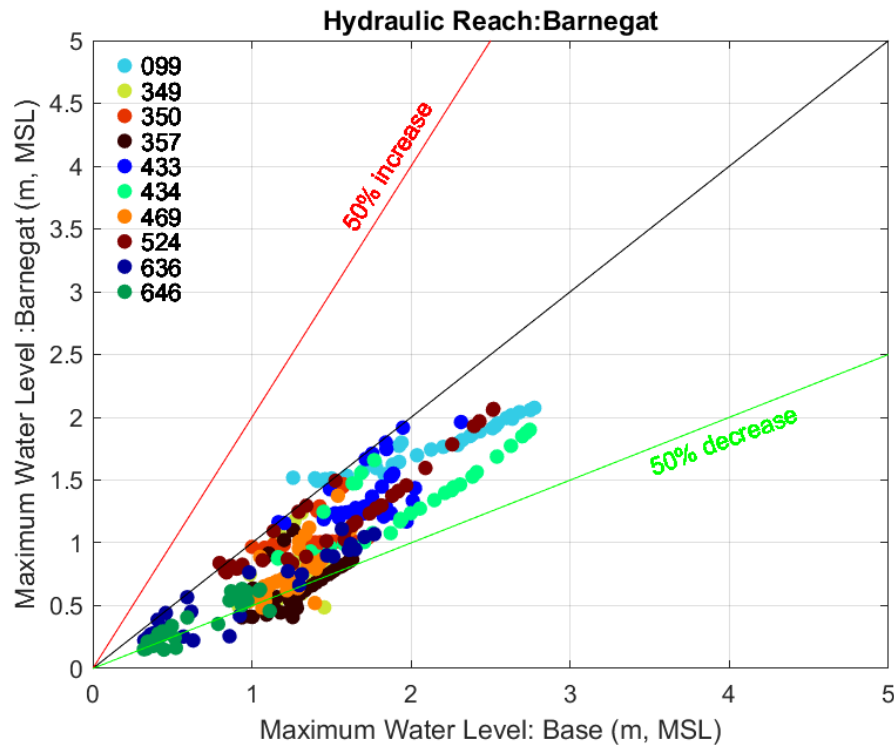


Figure 53: Dot plot: maximum water level for the Base condition vs maximum water level with Barnegat Inlet closed (the colors of the dots indicate different storms)

Figure 54 shows the locations of save points 139, 68, 152, and 156 in Barnegat Bay used for time series plots.

Figures Figure 55- Figure 58 show time series plots of water elevation at the selected stations (save points) for tropical synthetic storm 434. The red line indicates the Base Grid time series, the blue line shows the time series with Barnegat Inlet closed, the black line – the time series for All Closed Less 2, and the green line – the time series for All Closed.



Figure 54: Selected save points in Barnegat Bay for time series plots

Figure 55 depicts the time series at the southernmost save point (station 139), which indicates that this region only experiences a significant reduction in water level with all inlets closed. This region is greatly influenced by Little Egg/Brigantine Inlet. Moving northward, Figure 56 (station 68) indicates that this location is still influenced by Little Egg/Brigantine Inlet and only experiences significant reduction with all inlets closed (All Closed; Figure 44). There is a significant reduction in water surface elevation at station 152 (Figure 57) for all three closure configurations due to its proximity to the Barnegat Inlet closure. The initial

reduction in water level in the Base Grid at station 156 (Figure 58) is attributed to north-to-south winds transporting water southward away from this region. When the wind shifts, seiching occurs and water accumulates in this region with the most significant accumulation for the base condition.

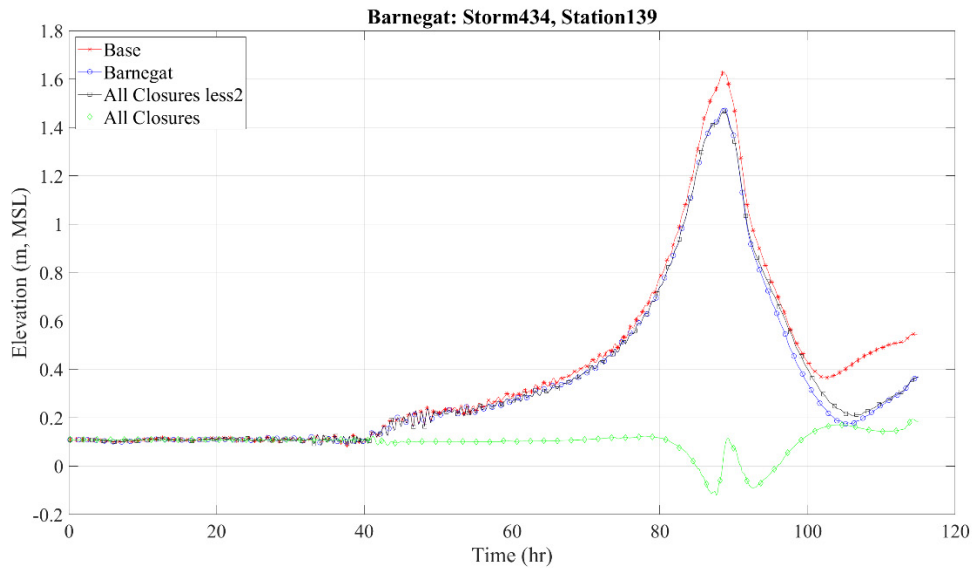


Figure 55: Storm 434: Time series plots for station (save point) 139.

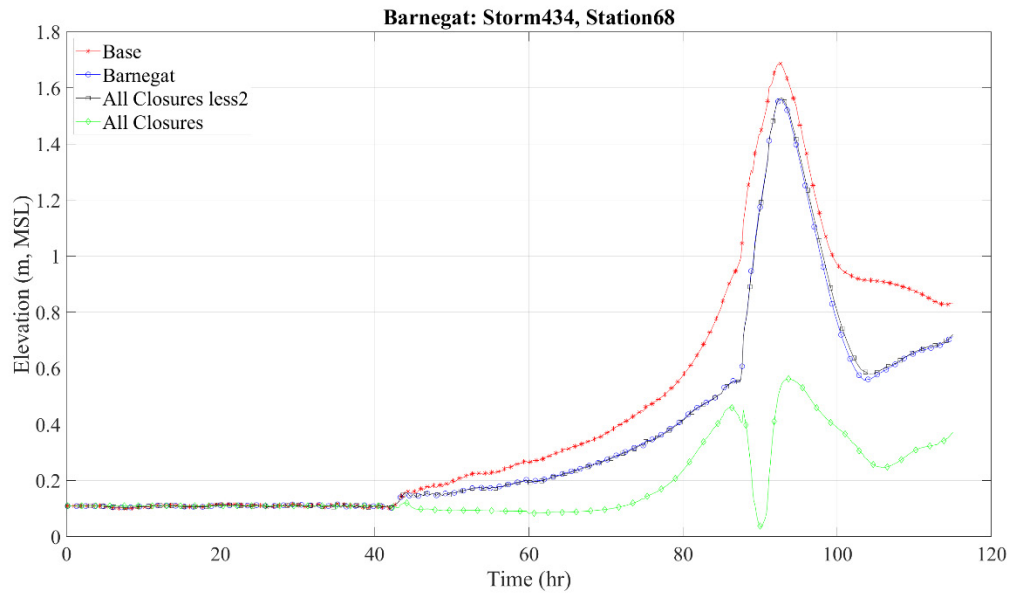


Figure 56: Storm 434: Time series plots for station (save point) 68.

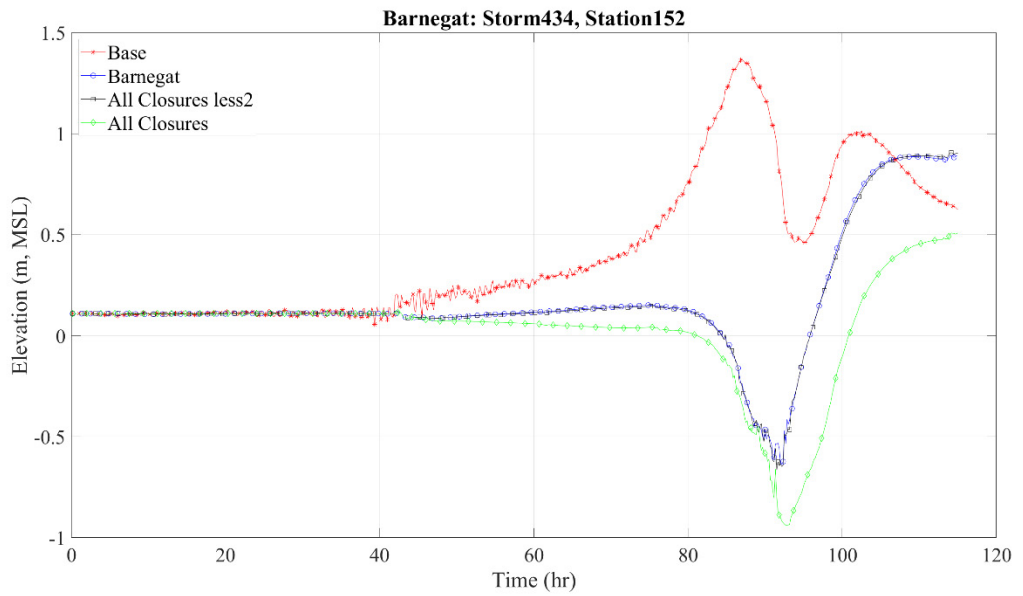


Figure 57: Storm 434: Time series plots for station (save point) 152.

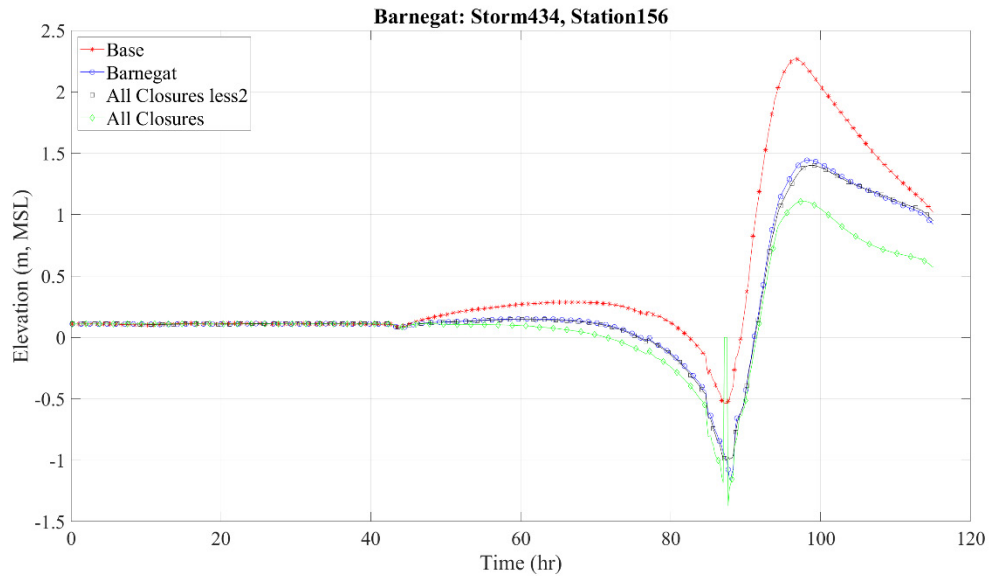


Figure 58: Storm 434: Time series plots for station (save point) 156

Figures [Figure 59](#)-[Figure 62](#) show the time series plots of water elevation for selected stations (save points) for tropical synthetic storm 636. The red line indicates the Base Grid time series, the blue line shows the time series with Barnegat Inlet closed, the black line – the time series of All Closed Less 2, and the green line – the time series of All Closed.

[Figure 59](#) depicts the time series at the southernmost save point (station 139), which indicates that this region experiences an initial reduction in water level with all inlets closed followed by an increase in water level due to seiching. However the maximum water level with all inlets closed is still lower compared to the water levels for the other closure configurations because of the smaller volume of water in the bay with all inlets closed. Moving northward, [Figure 80](#) (station 68) indicates that this location is still influenced by Little Egg/Brigantine Inlet as well as exposure to north-to-south winds. Therefore the water level response initially indicates convergence in the phasing of the peak response. After the peak, all configurations except All Closed allow water to escape through Little Egg/Brigantine Inlet. Conversely, the trapped water with All Closed elevates the water level 0.2 to 0.4 m above the base condition water level. At station 152 ([Figure 61](#)) the peak water level is less extreme due to its location in the bay and north-to-south winds.

The initial reduction in water level for all four configurations at station 156 (Figure 62) is attributed to strong north-to-south winds transporting water southward away from this region. When the wind shifts, water accumulates in this region with the most significant accumulation for the All Closed condition due to seiche of the trapped water. In actual inlet closure operations, the gates may be opened following the storm allowing the accumulated water to flow back into the ocean.

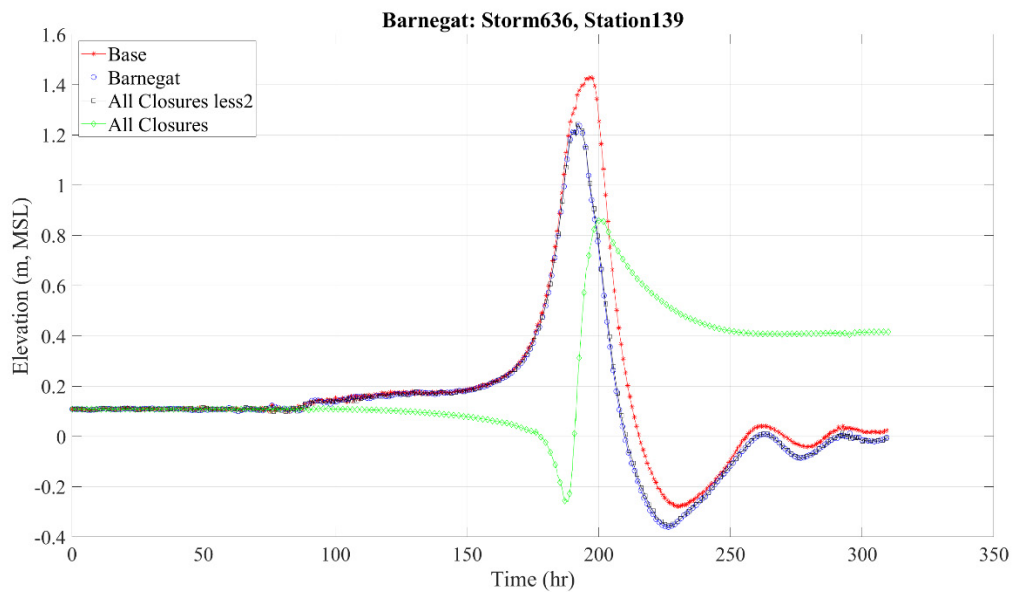


Figure 59: Storm 636: Time series plots for station (save point) 139

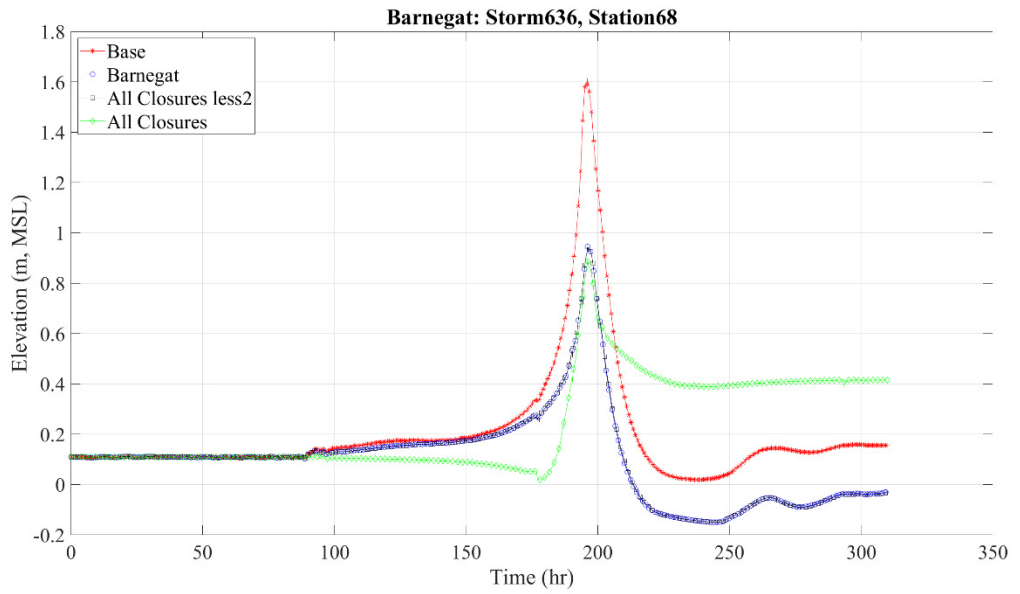


Figure 60: Storm 636: Time series plots for station (save point) 68

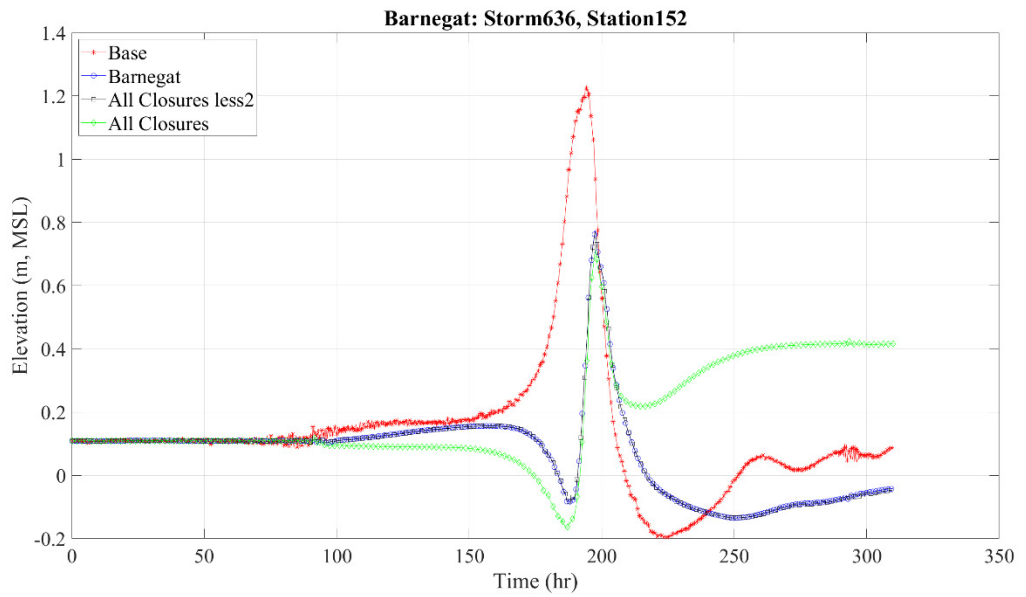


Figure 61: Storm 636: Time series plots for station (save point) 152

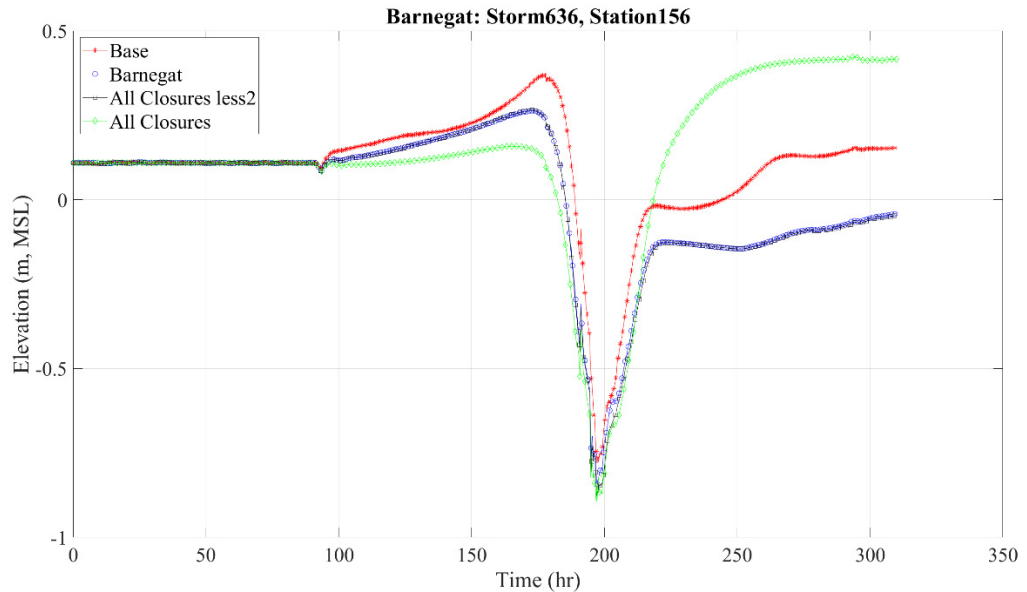


Figure 62: Storm 636: Time series plots for station (save point) 156

Little Egg/Brigantine Inlet

The implementation of a 15 km closure in the ADCIRC grid across Little Egg/Brigantine Inlet to inhibit surge propagation into the back bay areas was the most extensive closure evaluated in this study. The impact of the Little Egg/Brigantine closure on back-bay water levels was correspondingly extensive, with reductions in peak water level extending from the northernmost part of Barnegat Bay to Great Egg Inlet. The average reduction in Great Bay (bayward of the closure) was 1.3 m for all storms.

Absecon Inlet Closed versus Base Condition

Absecon Inlet is the first inlet south of the large opening at Little Egg/Brigantine, therefore the closure at Absecon Inlet can be influenced by flow through Little Egg/Brigantine. As such, closing Absecon Inlet can locally reduce water levels in Absecon Bay and vicinity, can be of no consequence to water levels, or can actually cause increased water levels, depending on the direction of storm winds. No change in water level with the closure in place is the result of water entering through Little Egg/Brigantine Inlet and propagating southward into Absecon Bay, thereby eliminating any positive impact of the closure. Increased water levels in

the bay with the inlet closures in place are caused by surge entering through Little Egg/Brigantine Inlet, propagating southward into Absecon Bay, then as the winds shift, surge cannot exit the bay due to the Absecon Inlet closure resulting in elevated water levels in the “protected” bay. This demonstrates the importance of considering multiple means of flow propagation into an embayment as well as the operation/timing of surge barrier closures.

Great Egg Harbor Inlet

Closing Great Egg Harbor Inlet can potentially have reductions in water level spanning northward to the bays near Atlantic City, southward to the bays near Sea Isle City, and eastward to the Great Egg Harbor River watershed, depending on the characteristics of the storm. The greatest reductions are in Great Egg Harbor, as expected.

Corson Inlet

Closing Corson Inlet can potentially have reductions in water level spanning northward to the bay near Ocean City/Great Egg Harbor Inlet and southward to the bay near Hereford Inlet. The greatest reductions are in Strathmere Bay near Corson Inlet, as expected

Townsend's Inlet

Closing Townsend's Inlet can potentially have reductions in water level spanning northward to Corson Inlet and southward to Cape May Harbor, depending on the storm characteristics (intensity, forward speed, direction, etc.). The greatest reductions are in Stites and Townsend's Sound which are closest to the closure at Townsend's Inlet, as expected.

[Figure 63](#) and [Figure 64](#) show maximum water elevation for the Base Grid (left), maximum water elevation for Townsend's Inlet closed (center), and the difference in maximum water elevations between Townsend's Inlet closed and the Base Grid (right) for tropical synthetic storms 99 and 636, respectively.

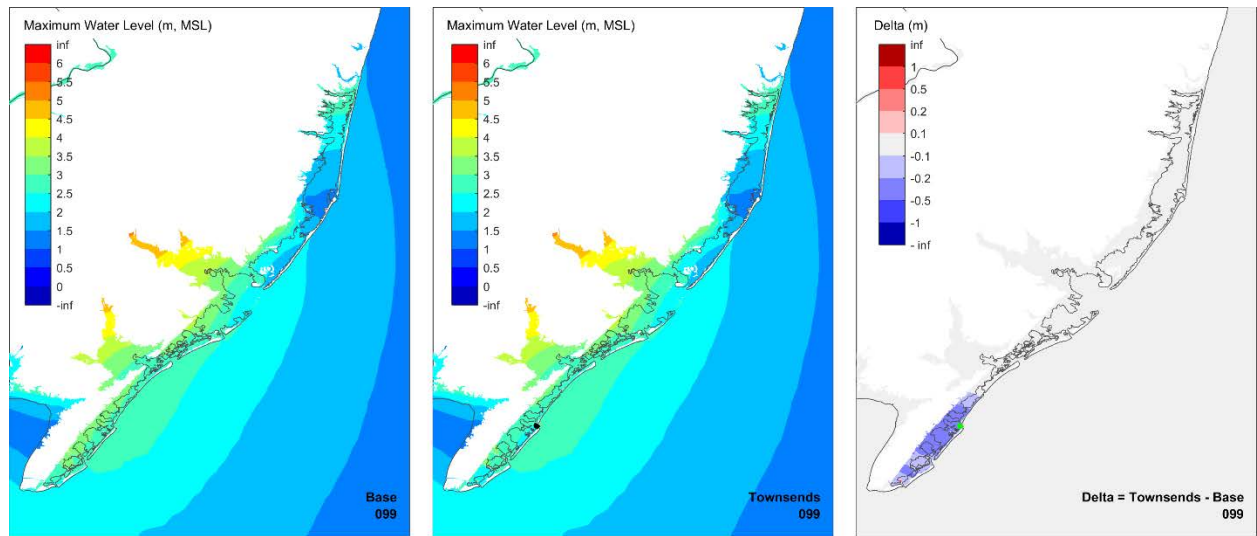


Figure 63: Maximum water elevation for Synthetic Storm 99: Base Grid (left), Townsend Inlet Closed (center), and difference between Townsend and Base (right)

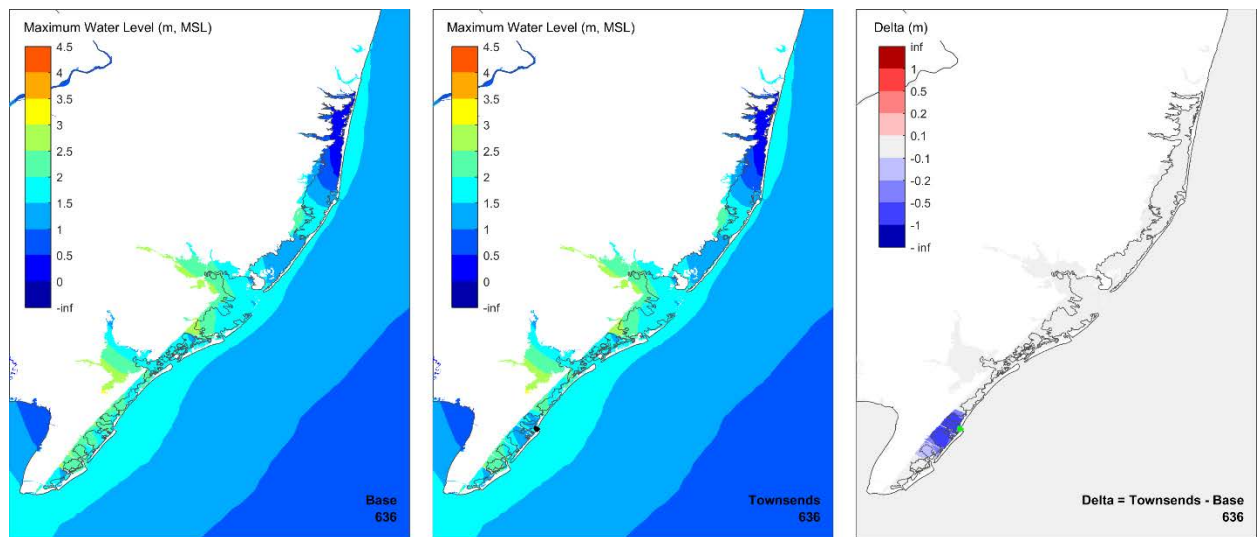


Figure 64: Maximum water elevation for Synthetic Storm 636: Base Grid (left), Townsend Inlet Closed (center), and difference between Townsend and Base (right)

Figure 65 shows maximum water levels at save point locations for the Base condition vs maximum water levels with Townsend Inlet closed, referred to as a dot plot. Values below the 45 degree line indicate a reduction in maximum water level attributable to the closure. For this particular configuration the average reduction in maximum water level was 26% due to Townsend Inlet being closed.

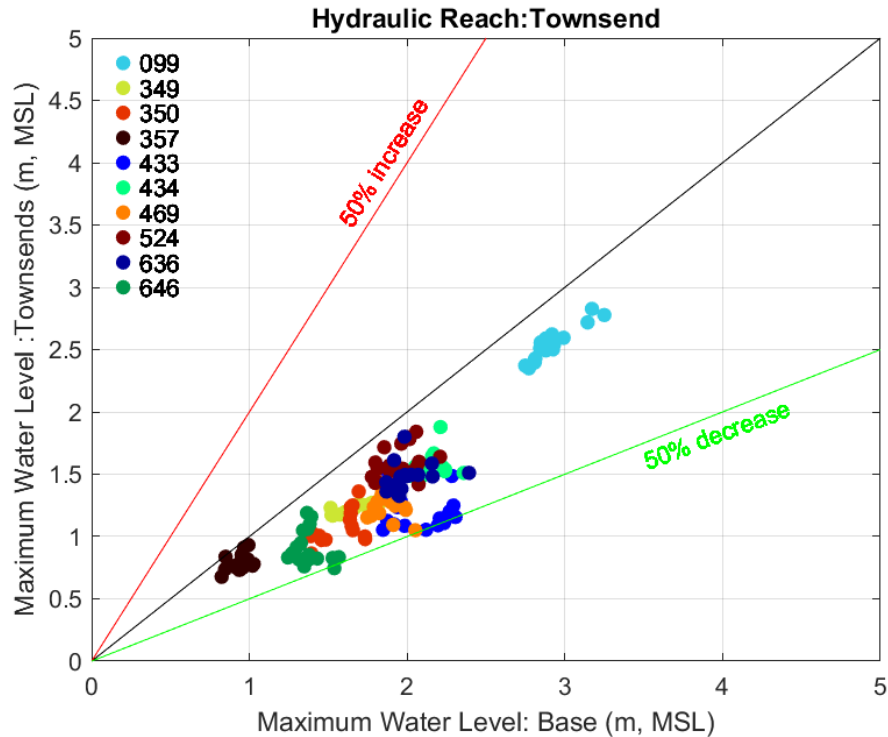


Figure 65: Dot plot: maximum water level for the Base condition vs maximum water level with Townsends Inlet closed (the colors of the dots indicate different storms)

Figure 66 shows the locations of the save points used to evaluate the Townsends closure with the time series plots.

Figure 67 and Figure 68 show time series plots of water elevation at selected stations (save points) for tropical synthetic storm 99. The red line indicates the Base Grid time series, the blue line shows the time series with Townsends Inlet closed, the black line – the time series for All Closed Less 2, and the green line – the time series for All Closed. The time-series plot for save point 104 clearly shows the effectiveness of the closures. First, the peak of water elevation for Base Grid (red) was reduced by 0.36 m (1.18 ft) (blue) due to implementation of the Townsend closure. Further reduction of an additional 0.47 m (1.54 ft) (black) was obtained by implementing All Closed Less 2 Grid. Finally, by closing all inlets (All Closed), the maximum water level was at 0.88 m (2.89 ft) (green) vs 2.91 m (9.55 ft) in Base Grid – with no closures implemented (red). Save point 91 displays similar behavior, however there is greater magnitude of the peak surge reduction

for All Closed Less 2 and All Closed comparing to the same scenarios for save point 104. This is due to the south-to-north direction of storm 99 winds. Therefore most of the water mass trapped in the bay system is shifted north toward save point 104 and away from save point 91.

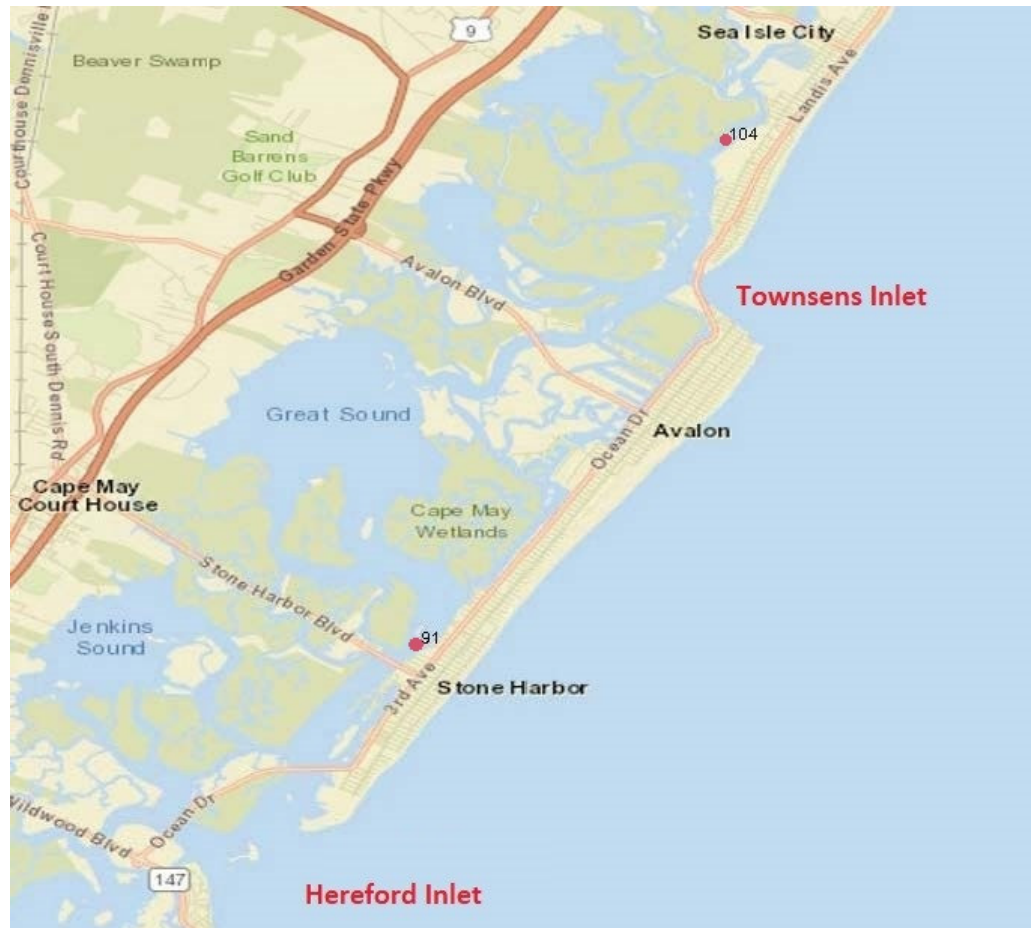


Figure 66: locations of the save points used for evaluation of the Townsends closure with the time series plots

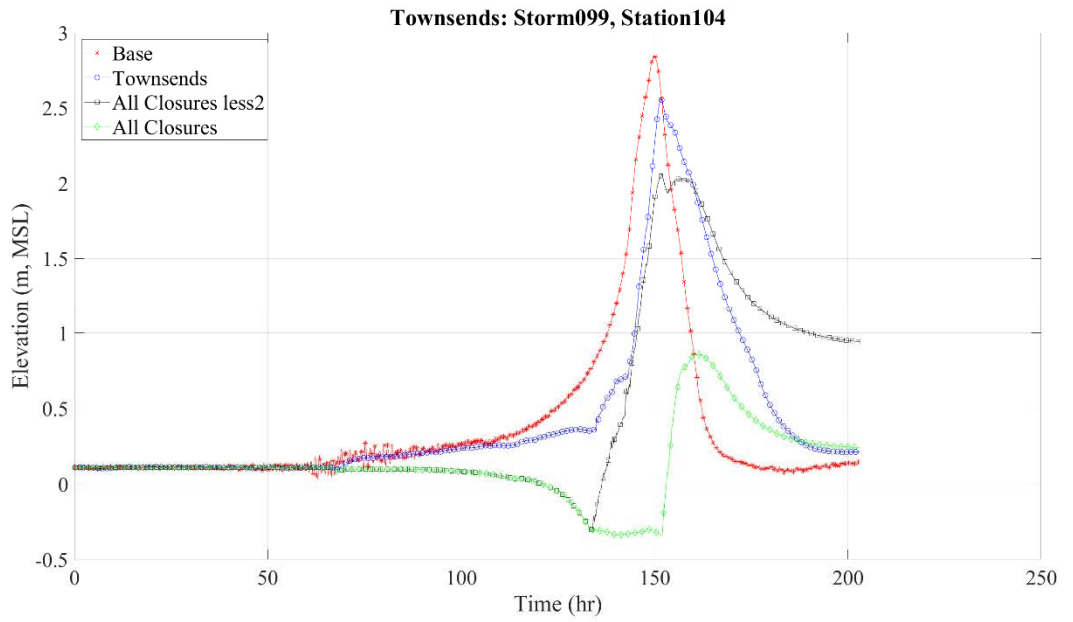


Figure 67: Storm 99: Time series plots for station (save point) 104

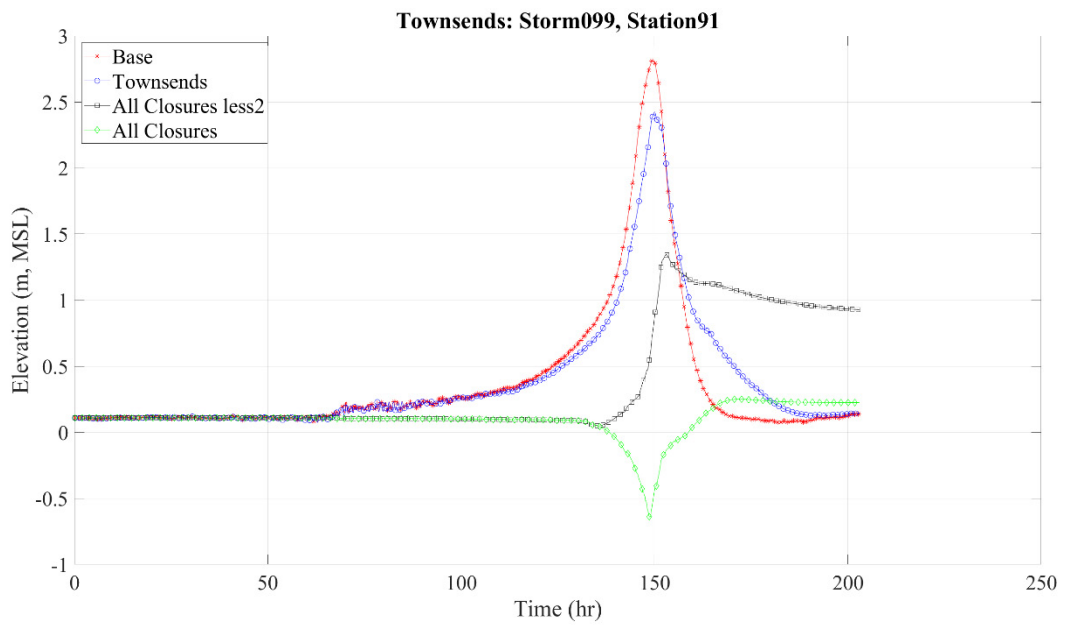


Figure 68: Storm 99: Time series plots for station (save point) 91

Figure 69 and Figure 70 show time series plots of water elevation at selected stations (save points) for tropical synthetic storm 636. The red line shows the Base Grid time series, the blue line shows the time series with Townsends Inlet closed, the black line – the time series for All Closed Less 2, and the green line – the time series for All Closed. The behavior shown on hydrographs in Figure 69 and Figure 70 is consistent with previous observations made for storm 99; the number of implemented storm surge barriers is positively correlated to the reduction in maximum water level. However, in this case the Base condition and Townsends Inlet closure conditions show very rapid flushing (very steep slope of red and blue lines after reaching the maximum water level) for both of the save points. This could be explained by the north-to-south wind direction and the geometry of Townsends and Hereford Inlets; the water being pushed southward by the wind can easily flow out through the much wider Hereford Inlet.

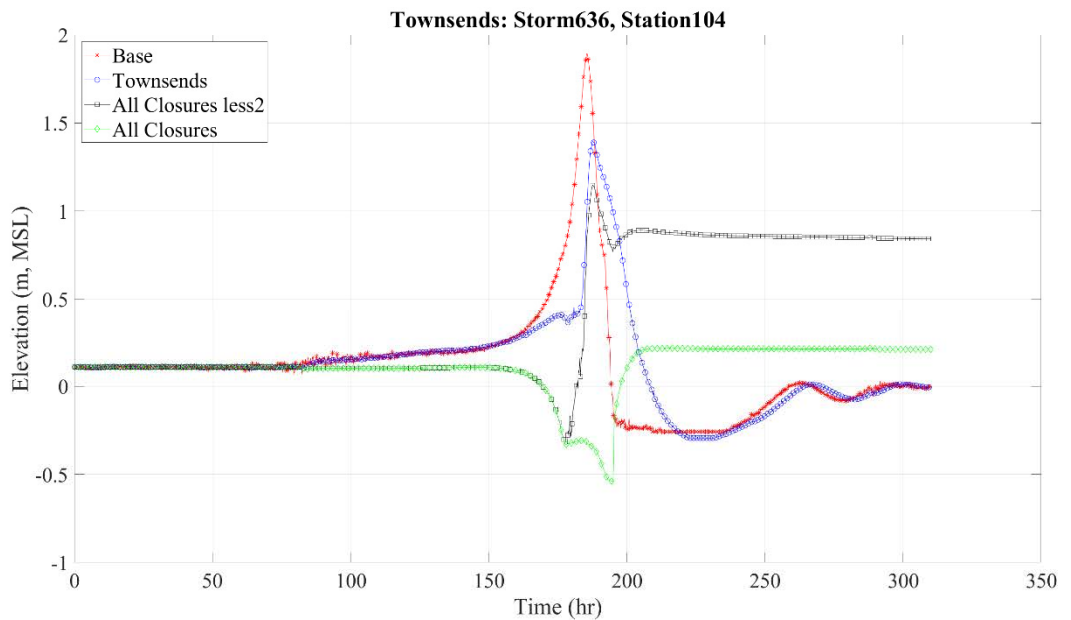


Figure 69: Storm 636: Time series plots for station (save point) 104

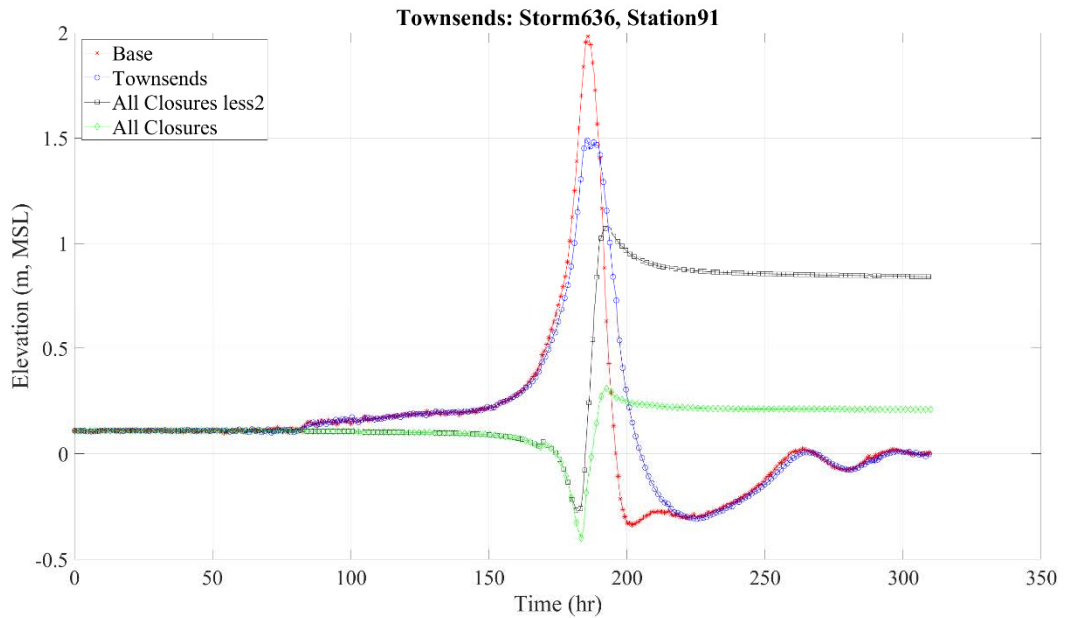


Figure 70: Storm 636: Time series plots for station (save point) 91

Hereford Inlet

Closing Hereford Inlet can potentially reduce water levels spanning northward to the bay near Corson Inlet and southward to the Cape May Harbor. The greatest reductions are in Jenkins Sound and Grassy Sound near Hereford Inlet, as expected.

Cape May Inlet

Similar to Absecon Inlet, closing Cape May Inlet can cause a reduction or an increase in maximum water levels, depending on the direction of storm winds and corresponding flows. Water entering Hereford Inlet or Cape May Canal could potentially be directed towards the Cape May Inlet closure and become trapped leading to elevated water levels. Other storms showed a reduction in water level in Cape May Harbor when flows entering nearby inlets were not directed to Cape May Harbor or were able to flow out through the Cape May Canal.

Cape May Canal

Closing Cape May Canal only had a null or detrimental effect on maximum water levels for the 10 storms simulated with this closure in place. Flow entering through Cape May Inlet and Hereford Inlet could potentially lose

the ability to flush through the canal, resulting in elevated water levels as was observed for Storm 99, 524, and 636.

All Closed Less 2 versus Base Condition

With all of the inlets closed except Corson Inlet and Little Egg/Brigantine Inlet, the reduction in maximum water level compared to the base condition with all the inlets open is significant in most of the New Jersey back bays, except in the vicinities of the open inlet areas. One notable exception is Storm 636 as was described in the evaluation of the Absecon Inlet closure. Surge entering Little Egg/Brigantine Inlet propagates southward into Absecon Bay, then becomes trapped from exiting Absecon Inlet due to the closure, again demonstrating the importance of closure operation/timing and taking into consideration multiple points of entry.

In summary, the analysis of Iteration 1 maximum surge envelopes, maximum values at save point locations, and water level time series focused on the evaluation of the ability of individual surge barriers to alter maximum water levels compared to a base condition with no closures in place. It was found that individual closures can reduce back bay flooding significantly, mainly in the bays closest to the closure location, but if other mechanisms allow flow into the bay then water level reductions can be less significant and closures can also trap water and prevent return flow out of the bays.

4.2 -- Maximum Storm Surge Results -- Iteration 2

The impact of combinations of inlet and bay closures on water levels in New Jersey back bays for 10 storm events was investigated in Iteration 2 (The storm selection process was described in [2 -- Storm Selections](#) and the grid alternatives used in Iteration 2 were described in [3.2.1 -- Configurations of proposed structures](#)) The following section describes the effect of the Iteration 2 closure combinations on maximum water level in the New Jersey back bays.

All Closed versus Base Condition

Closing all 11 inlets with surge barriers dramatically reduces maximum water levels in New Jersey Back Bays, most notably during Storm 99 (Figure 71), with an average reduction of 2.11 m (6.92 ft) over the entire NJBB system Inlet and an average reduction for all storms of 1.27 m (4.17 ft). Closing Little Egg/Brigantine Inlet dramatically reduced the potential for surge propagation into the Little Egg/Manahawkin/Barnegat Bay region. The overall average reduction for those regions doubled from 0.37 to 0.74 m (1.21 to 2.43 ft), with the greatest change (0.59 m ADDITIONAL average reduction) in Little Egg Harbor with all inlets closed. Maximum reductions are in the central portion of the study area (Great Bay) because of the extremely large Little Egg/Brigantine closure length. The average reduction in Great Bay for the 10 storms with all inlets closed was 1.31 m (4.3 ft).

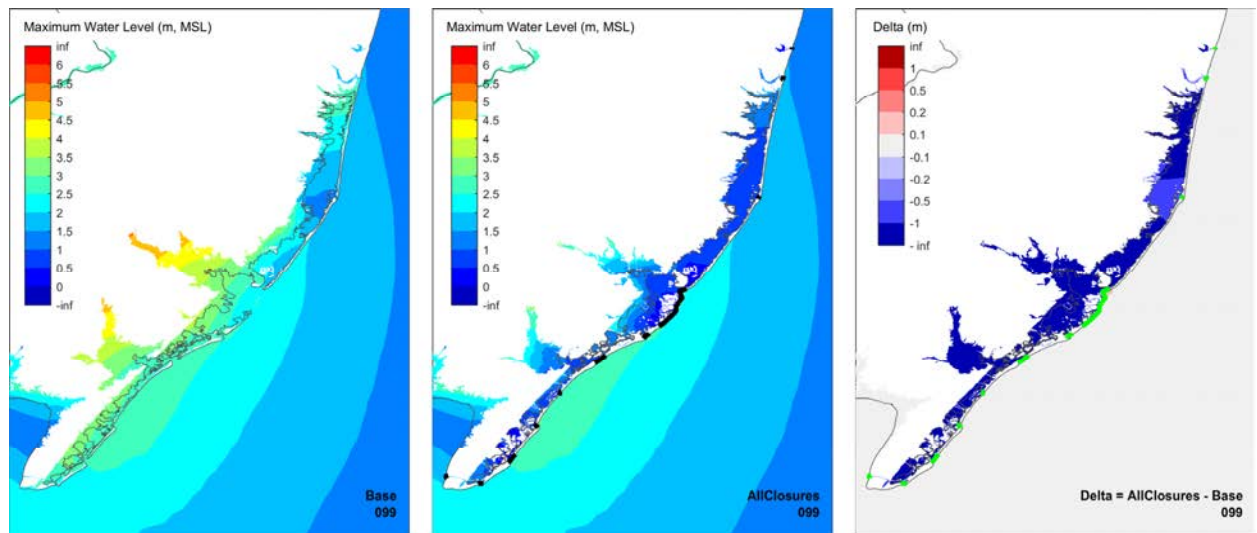


Figure 71: Maximum water elevation for Synthetic Storm 99: Base Grid (left), All Closed (center), and difference between All Closed and Base (right)

N3S3

The closures at Barnegat Inlet, Manasquan, and Holgate generally reduce water levels in Barnegat Bay for all 10 storms. The average reduction in maximum water level for this region is 0.67 m (2.2 ft). Some storms, such as 434 and 469 have a more uniform reduction in water level, whereas

other storms such as 99, 636, and 646 have a gradation in water level reduction due to a combination of wind direction over the bay, seiche, and barrier island overtopping.

For one of the storms (Storm 99, [Figure 72](#)), water level in the bay with the inlet closed is actually higher in the region of the bay immediately inside (bay side) of Barnegat Inlet. For this particular storm and closure configuration, overtopping of the barrier island near Barnegat Inlet elevates the maximum water level in the small region near the overtopping location.

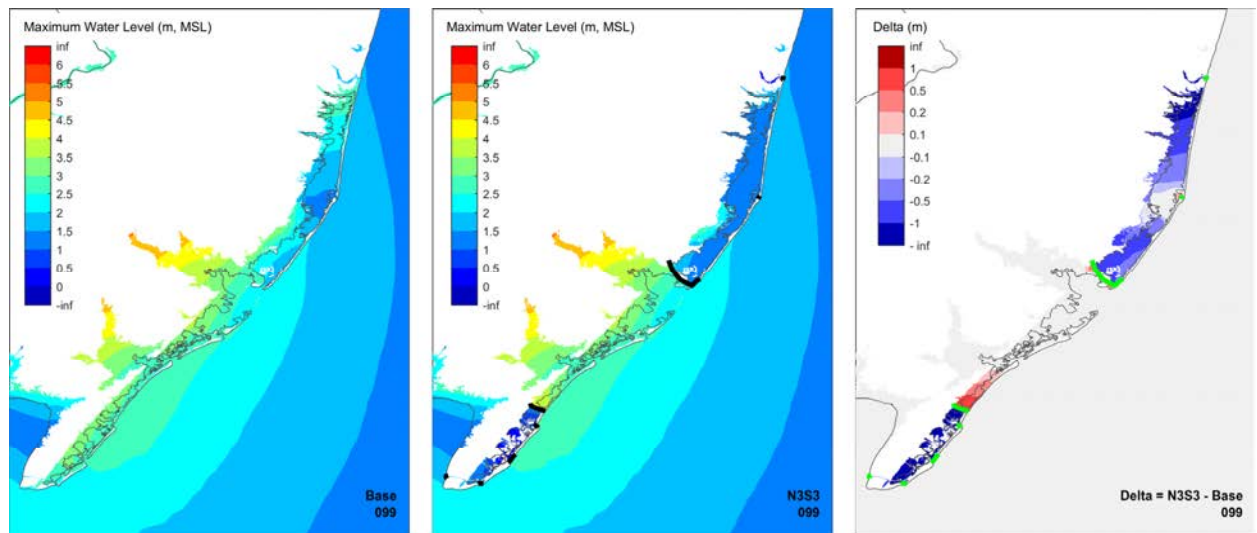


Figure 72: Maximum water elevation for Synthetic Storm 99: Base Grid (left), N3S3 (center), and difference between N3S3 and Base (right)

Storm 636 ([Figure 73](#)) shows little change in the north part of the bay from the base condition to the closure condition and the greatest reduction in Manahawkin Bay due to the north to south winds transporting flow into this region for the base condition and a smaller volume of water being transported into this region with the inlet closed. In addition, water levels are elevated inside the bay near the Holgate barrier due to the north to south winds and the Holgate barrier trapping water in the bay (behind the barrier).

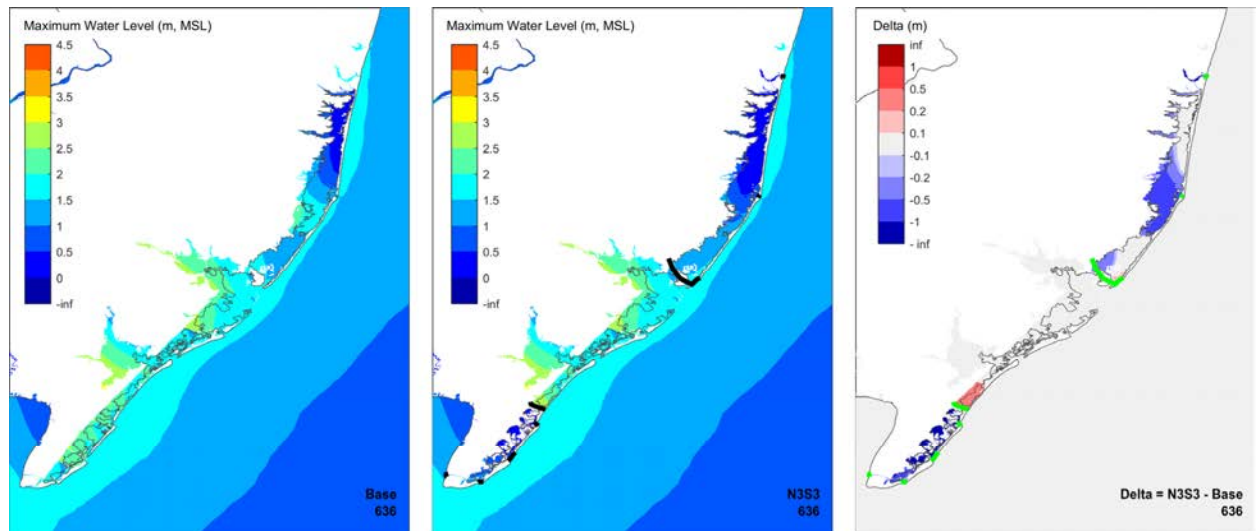


Figure 73: Maximum water elevation for Synthetic Storm 636: Base Grid (left), N3S3 (center), and difference between N3S3 and Base (right)

Even though the direction of Storm 646 is similar to Storm 636, it follows a path that is more seaward of Storm 636 and the resulting winds over Barnegat Bay are less intense. This results in more uniform water level reduction for the N3S3 configuration for this storm compared to the base condition as opposed to the large gradation in response for Storm 636.

In the south (S3) region, all inlets south of Sea Isle Blvd (Townsend, Hereford, Cape May, and Cape May Canal) are closed along with Sea Isle Blvd. Maximum water levels south of Sea Isle Blvd are greatly reduced (average reduction of 1.5 m), which is more uniform and more effective than the reduction in the northern region. The region north of Sea Isle Blvd experiences an increase in maximum water level due to storm winds directing flow towards this region, but the Sea Isle Blvd barrier blocks entry. However this surge buildup at Sea Isle Blvd is not present for Storms 433, 349, and 524 (Figure 74) due to several factors. The large translational speed of Storms 349 and 433 resulted in a short duration of strong winds over the bay and therefore insufficient wind forcing towards the Sea Isle Blvd closure. Though Storms 349 and 433 differed greatly in intensity, the short duration of winds over the bay for both storms led to similar impacts at the Sea Isle Blvd closure. For Storm 524, the storm track resulted in the major wind direction over the bay being from south to north, therefore water does not pile up on the Sea Isle Blvd closure as was observed for many of the other storms.

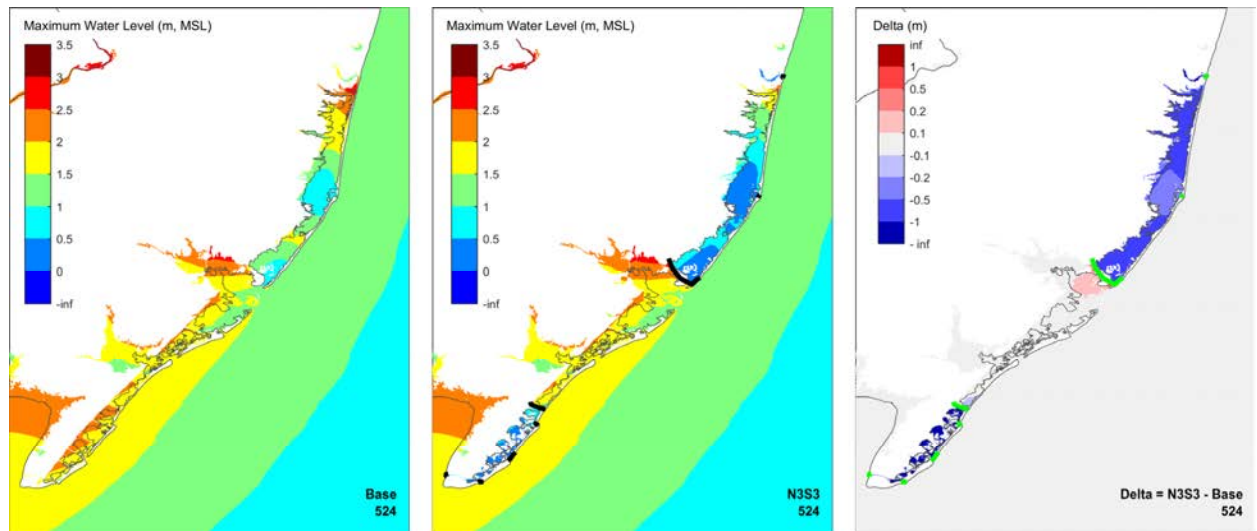


Figure 74: Maximum water elevation for Synthetic Storm 524: Base Grid (left), N3S3 (center), and difference between N3S3 and Base (right)

N4S4

For all storms in the northern portion of the area (N4), there is an increase in water level near the Rte. 72 closure. Due to the wind direction, Storms 99, 469, 434 (Figure 75), and 524 experience accumulation of water on the south side of the Rte. 72 closure, whereas Storms 636 and 646 experience accumulation inside the protected area (adjacent to the Rte. 72 closure on the north side). Other storms (357, 350, 433, and 349) experience accumulation on both sides of the Rte. 72 closure, due to seiche along the major North-South axis of Barnegat Bay. The Rte. 72 closure reduces the fetch length, thereby limiting the seiche amplitude compared to the base condition.

In the southern portion of the study area (S4), generally with the bay closures in place, there is a consistent decrease in maximum water level in all protected areas. In addition, the Sea Isle Blvd barrier prevents water from entering from the north, which leads to accumulation north of the Sea Isle Blvd barrier for most storms. As was previously described, Storms 349, 433, and 524 do not show accumulation at the Sea Isle Blvd barrier

mainly due to the forward speed of the storm and wind direction over the bay.

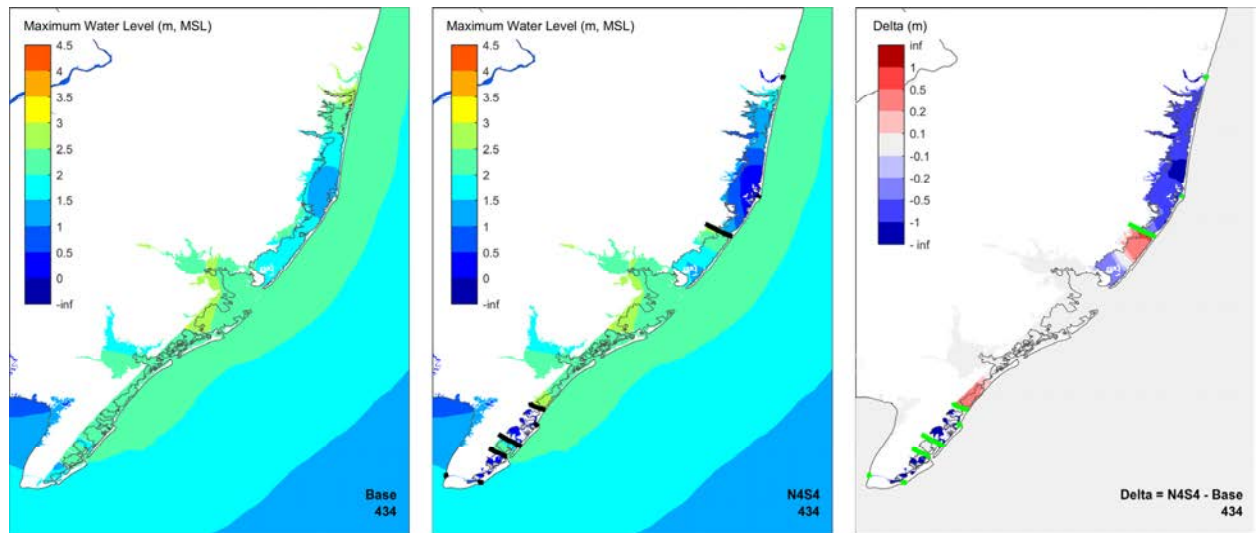


Figure 75: Maximum water elevation for Synthetic Storm 434: Base Grid (left), N4S4 (center), and difference between N4S4 and Base (right)

N5S5

Most storms show a decrease in water level north of the Berkeley barrier and an increase in water level south of the Berkeley barrier (the N5 closure; Figure 76). However, the response is reversed for Storm 636 (Figure 77) and 646 due to the wind direction from north to south over the bay for these two storms leading to increased water level north of the barrier and decreased water level south of the barrier. The S5 closure configuration is effective at reducing water level in the southern region. The average reduction in water level is 0.99 m (3.25 ft) in the southern region.

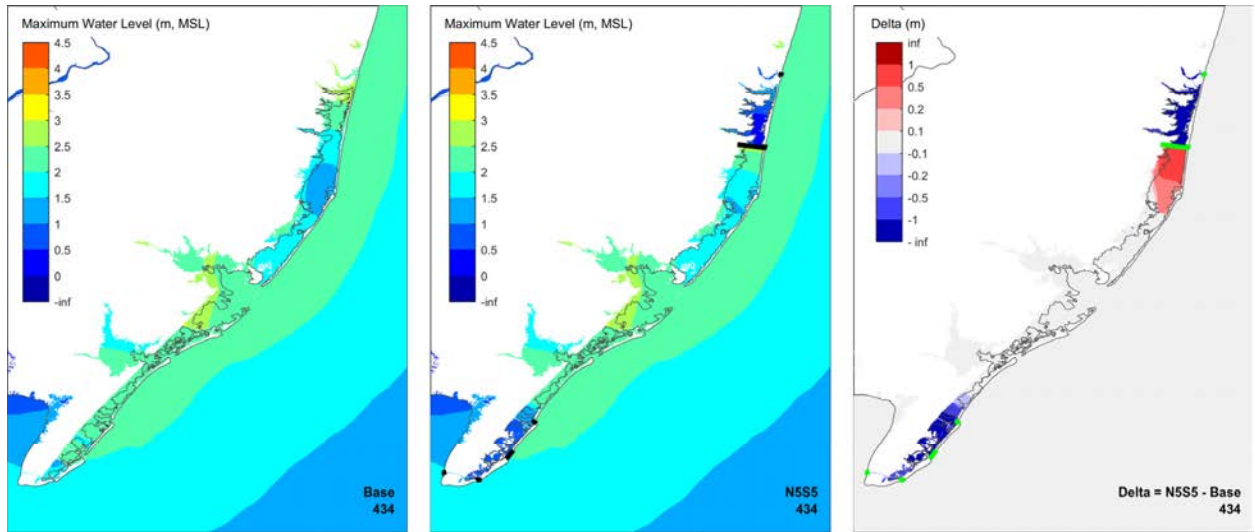


Figure 76: Maximum water elevation for Synthetic Storm 434: Base Grid (left), N5S5 (center), and difference between N5S5 and Base (right)

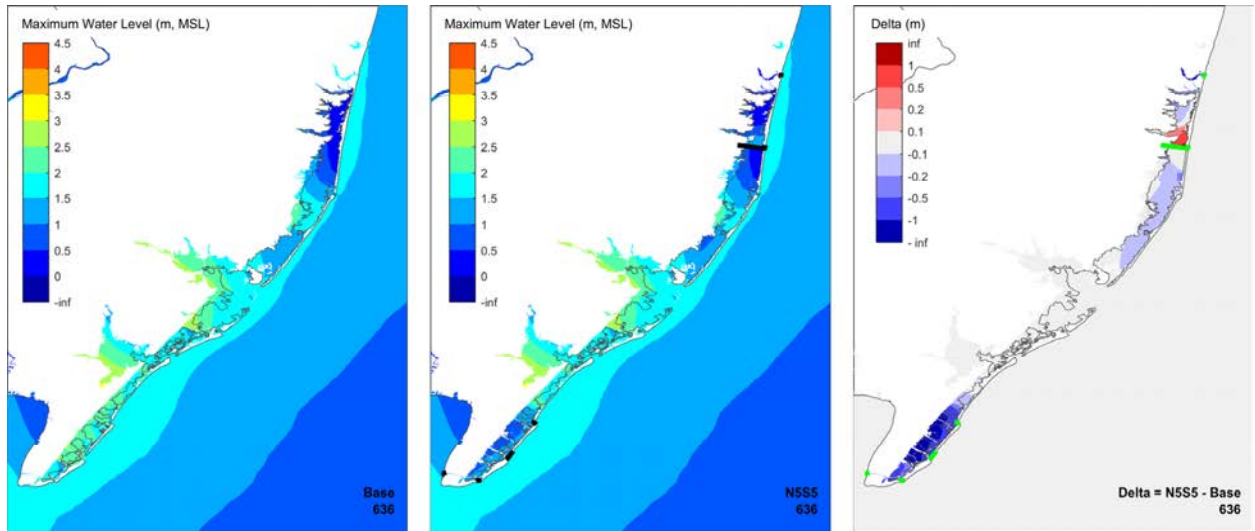


Figure 77: Maximum water elevation for Synthetic Storm 636: Base Grid (left), N5S5 (center), and difference between N5S5 and Base (right)

N6S6

The northern section of this closure configuration performs like the N5S5 configuration because of the presence of the Berkeley barrier in both cases. The primary difference is without a closure at Manasquan Inlet, storm surge in the Manasquan River is effectively the same as the base condition (Figure 78). The results of N6S6 also show that a closure at Manasquan Inlet has relatively little impact on storm surge in Barnegat Bay and is not essential to configurations with closures at Barnegat Inlet. For the southern section, there is a great reduction in water level in the bays

with the closures in place for most storms. One exception is Storm 357 which shows that the closures are less effective (not as necessary to be implemented) because this storm is distant from these closure locations and maximum surge levels were not significant even for the base condition with the inlets open.

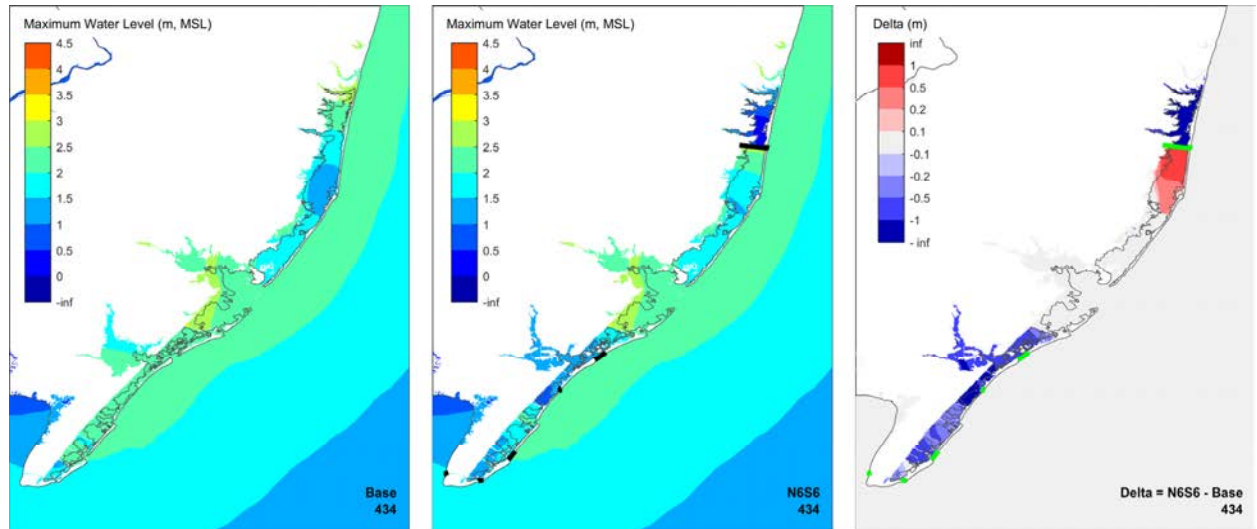


Figure 78: Maximum water elevation for Synthetic Storm 434: Base Grid (left), N6S6 (center), and difference between N6S6 and Base (right)

N7S7

Manasquan Inlet and Point Pleasant Canal closures only reduce water levels in a very limited region behind (bayward) of these closures (Figure 79). The southern region has two basic responses: 1) widespread reduction in peak water level due to the closures in place and 2) an increase in maximum water level in the Cape May area for a few storms (350 and 636, Figure 80) due to wind direction and slower storm speeds allowing flow

entering from the open area bayward of Hereford Inlet and transmitting that flow southward towards Cape May. With Cape May Inlet closed, the water is entrapped and maximum water levels increase in this region.

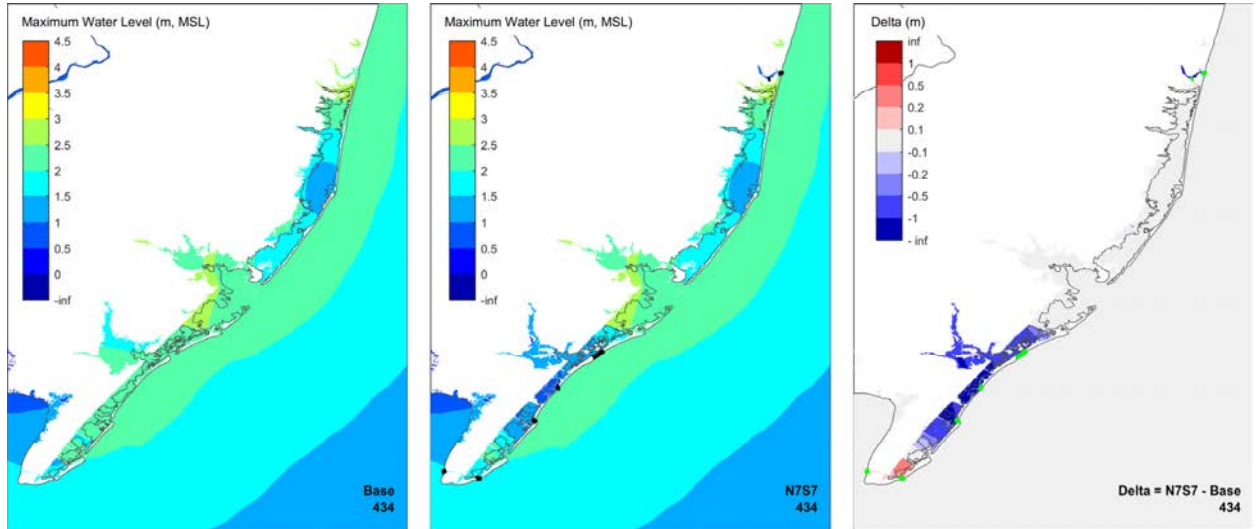


Figure 79: Maximum water elevation for Synthetic Storm 434: Base Grid (left), N7S7 (center), and difference between N7S7 and Base (right)

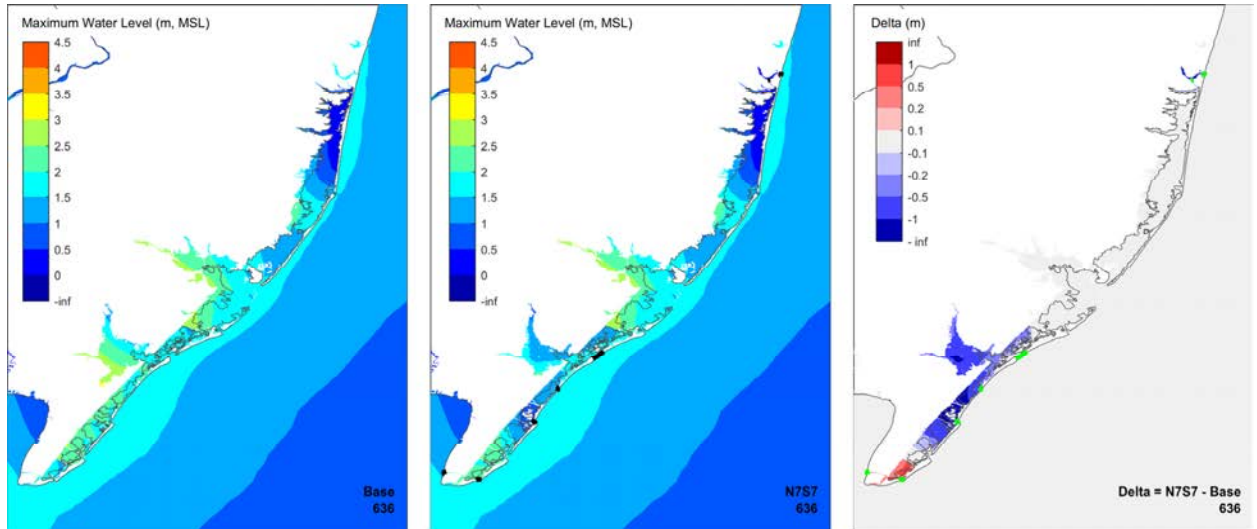


Figure 80: Maximum water elevation for Synthetic Storm 636: Base Grid (left), N7S7 (center), and difference between N7S7 and Base (right)

S8 and S9

These two configurations result in water level responses that are similar to N7S7 for all areas north of Hereford Inlet. There is significant reduction in water level in all south bay areas. It is interesting to note the difference in water level response for N7S7 versus S8 (Figure 81) and S9 (Figure 82) near Cape May for Storms 99, 350, 357, and 636 due to the opening at Hereford

for N7S7, Cape May Inlet for S8, and Cape May Canal for S9. For N7S7, the volume of water entering Hereford Inlet is pushed southward towards Cape May, where it is trapped by the Cape May Inlet and Cape May Canal closures. For S8 and S9, the supply of water from the Hereford Inlet region is eliminated by the Hereford Inlet closure, which reduces the volume of water that can be transported southward during these storms. In addition, the Cape May Inlet (S8) and Cape May Canal (S9) openings allow water to escape rather than build up as was observed for N7S7. For S8 and S9, water levels seaward of the closures increase by approximately 0.25 m (0.82 ft) for the most intense storm (Storm 433).

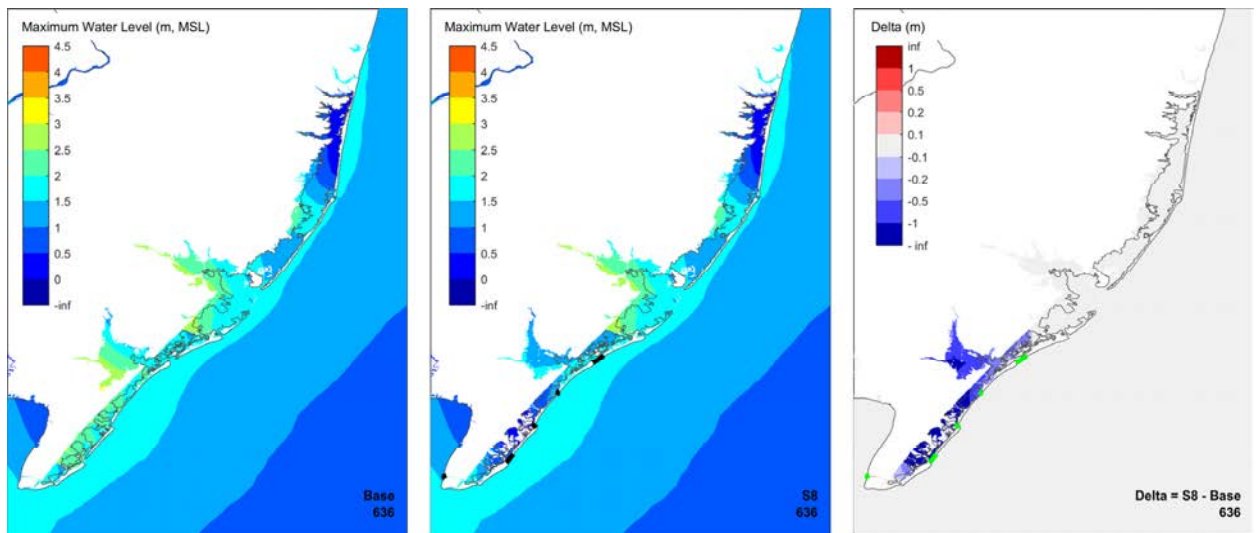


Figure 81: Maximum water elevation for Synthetic Storm 636: Base Grid (left), S8 (center), and difference between S8 and Base (right)

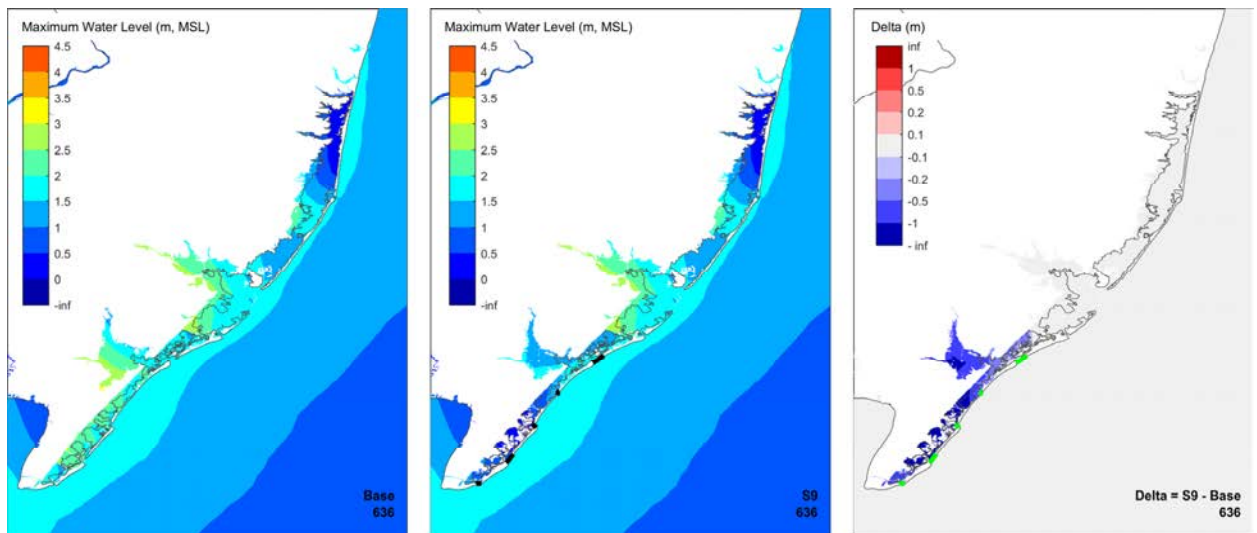


Figure 82: Maximum water elevation for Synthetic Storm 636: Base Grid (left), S9 (center), and difference between S9 and Base (right)

S10

For all storm events, there is significant reduction in peak water level for the protected areas (Figure 83). One interesting observation for this configuration is that leaving Great Egg Inlet open allows an escape route (flushing) of flow entering from other areas, rather than building up behind a closure. Also for Storm 433, allowing flow to enter the bays reduces the surge buildup on the barrier island side, seaward of the bays for this configuration.

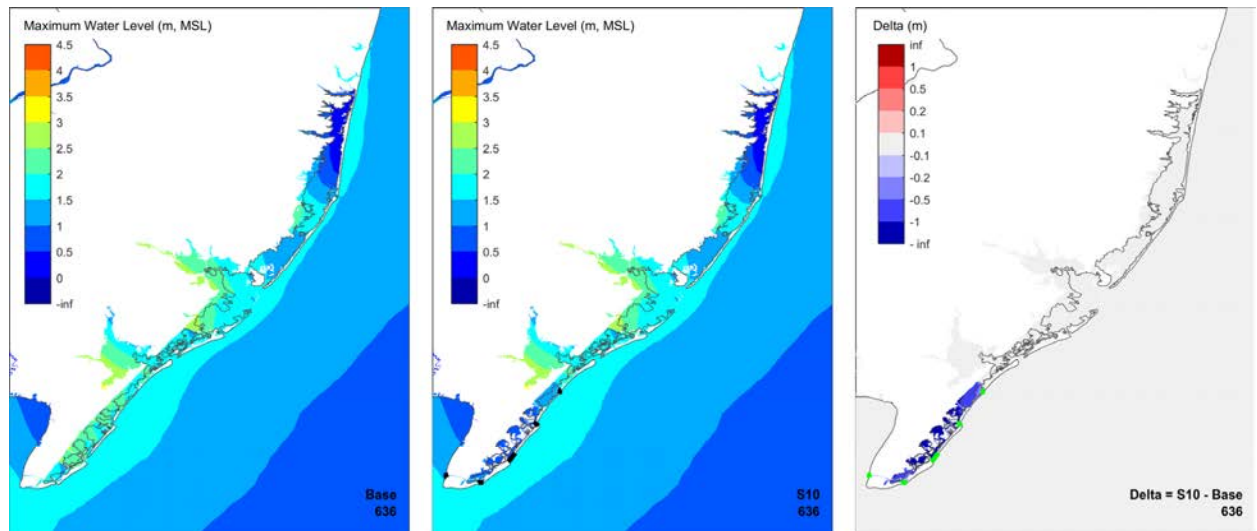


Figure 83: Maximum water elevation for Synthetic Storm 636: Base Grid (left), S10 (center), and difference between S10 and Base (right)

C3

This configuration generally led to a reduction in peak water level compared to the base condition for bay areas behind (bayward of) Absecon and Great Egg Inlets and an increase in peak water level north of North Point (Figure 84). One exception is Storm 524 (Figure 85) which did not show an increase in peak water level north of North Point due to wind direction. The greatest reduction in peak water level was observed for Storms 99, 350, 434, and 636 due to the slow forward speed of these events and Storm 433 due to its great intensity. All other storms showed a reduction in peak water level in the protected areas, however the reduction was less significant than the previously mentioned storms.

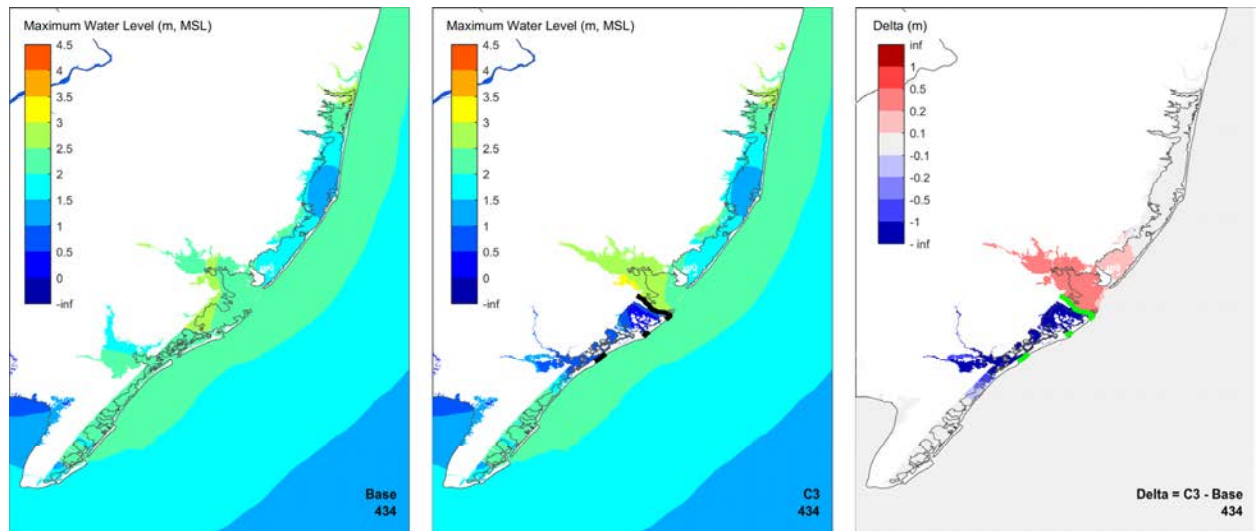


Figure 84: Maximum water elevation for Synthetic Storm 434: Base Grid (left), C3 (center), and difference between C3 and Base (right)

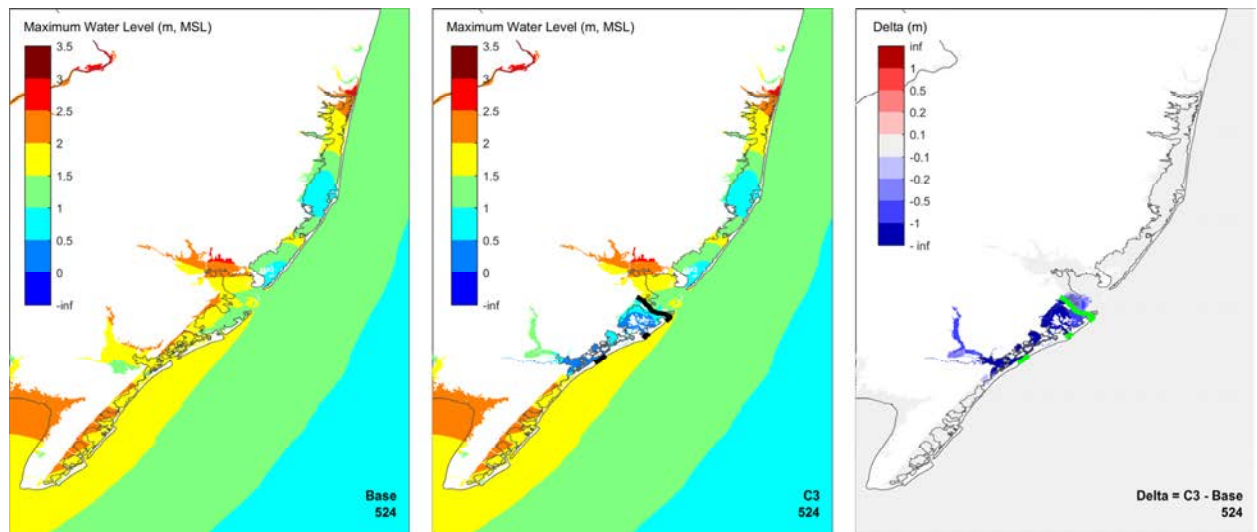


Figure 85: Maximum water elevation for Synthetic Storm 524: Base Grid (left), C3 (center), and difference between C3 and Base (right)

C4

This configuration responds similar to the C3 response. The primary difference is that an increase in peak water levels is observed in Absecon Bay with the bay closure moved south to Absecon Blvd (Figure 86 and Figure 87).

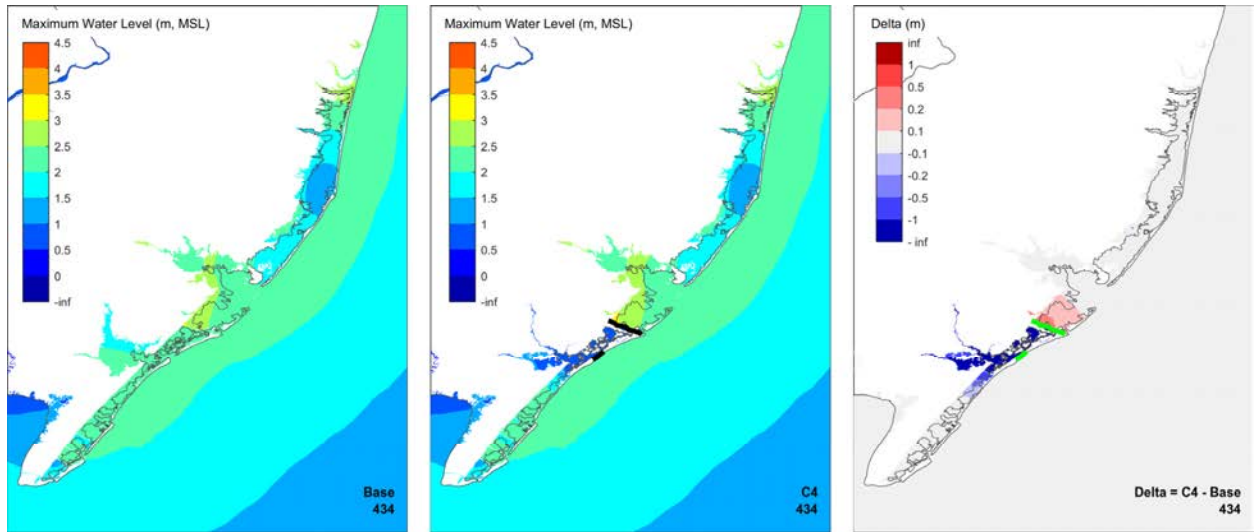


Figure 86: Maximum water elevation for Synthetic Storm 434: Base Grid (left), C4 (center), and difference between C4 and Base (right)

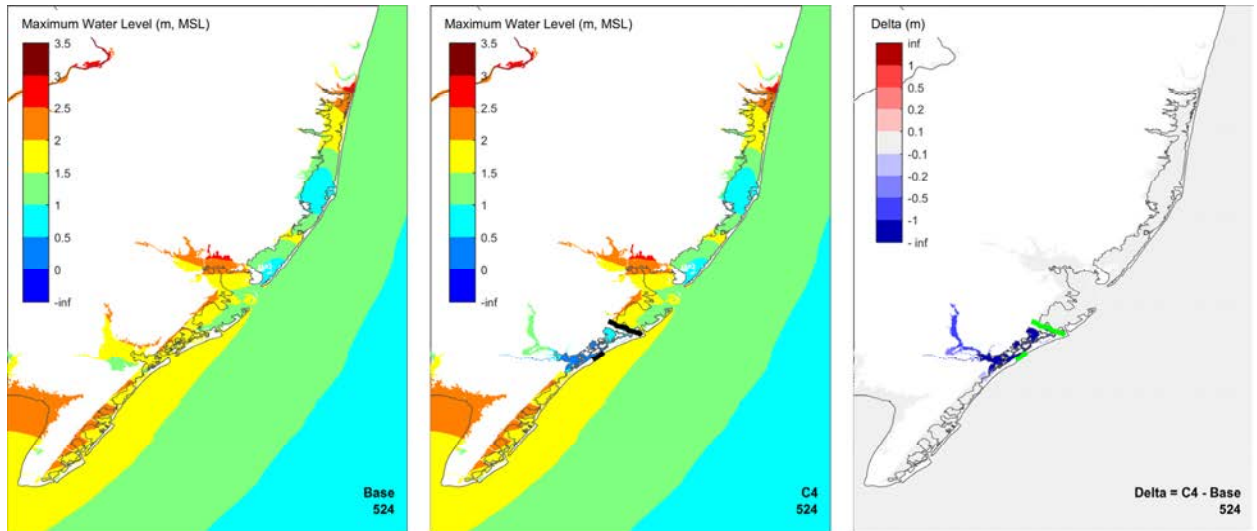


Figure 87: Maximum water elevation for Synthetic Storm 524: Base Grid (left), C4 (center), and difference between C4 and Base (right)

C5

In general, water levels are reduced within the bounds of the closures at Absecon Blvd, Great Egg, and 52nd St and water levels increase north of this region due to wind direction (Figure 88). Storm 433 results in increased

accumulation seaward of the closures for this high intensity storm. Storms 349 and 524 (Figure 89) show increased accumulation on the south side of the enclosed region due to the south to north wind direction over the bay for these storms. Storm 357 shows no closure-induced accumulation external to the closures because this storm made landfall distant from the C5 area.

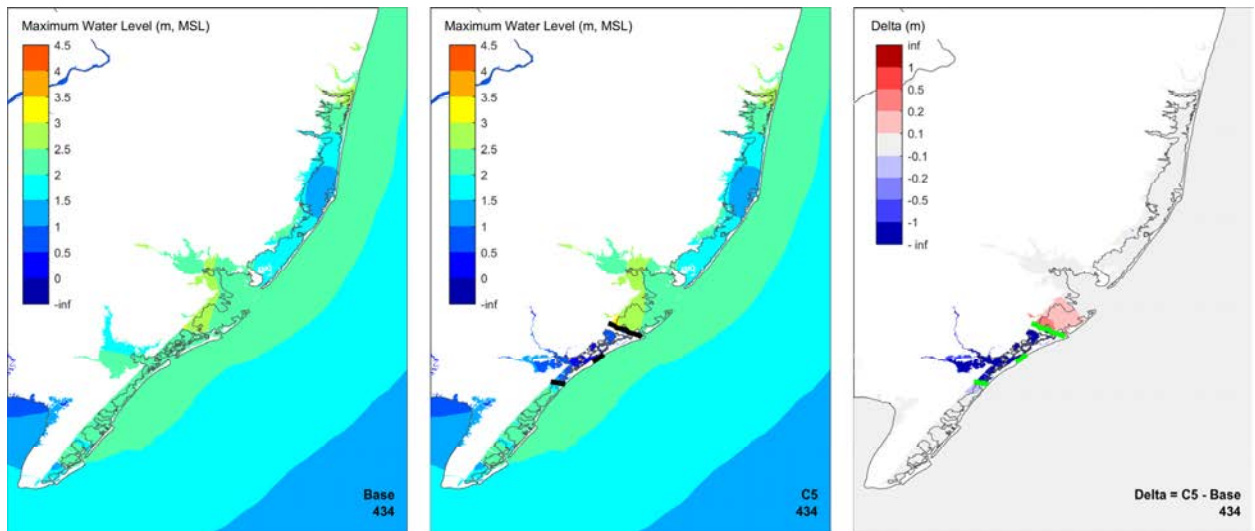


Figure 88: Maximum water elevation for Synthetic Storm 434: Base Grid (left), C5 (center), and difference between C5 and Base (right)

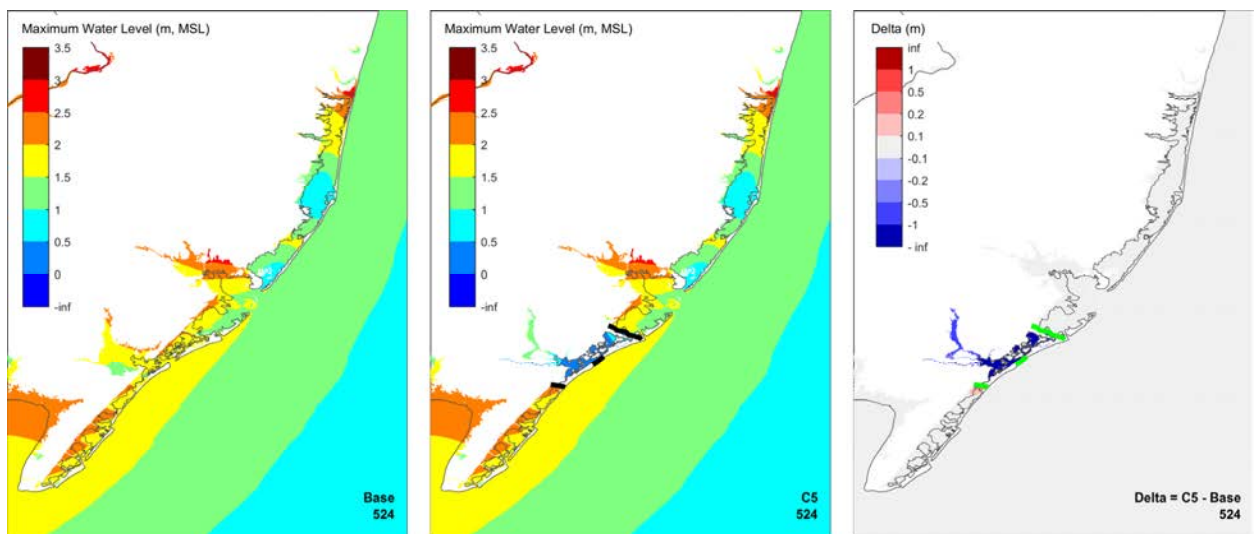


Figure 89: Maximum water elevation for Synthetic Storm 524: Base Grid (left), C5 (center), and difference between C5 and Base (right)

C6

In general, a very small section of the bay between Absecon Blvd and Somers Longport Blvd experiences a reduction in peak water level between

these closures and areas north of Absecon Blvd experience an increase in water level (Figure 90), except for Storm 349 which experiences an increase in water level on the south (Somers Longport Blvd) side of the closure due to wind direction. For Storm 433, there is an increase in water level external to the closures on both the north and south ends of the region due to the storms intensity. For Storm 99, there is an increase in maximum water level north of Absecon Blvd and reduction in water level south of Somers Longport Blvd. This is due to the wind direction. Normally water would pass north to south, however with the closures in place, the supply of water from the north is prevented from reaching the southern region, therefore resulting in a reduction in water level south of Somers Longport Blvd.

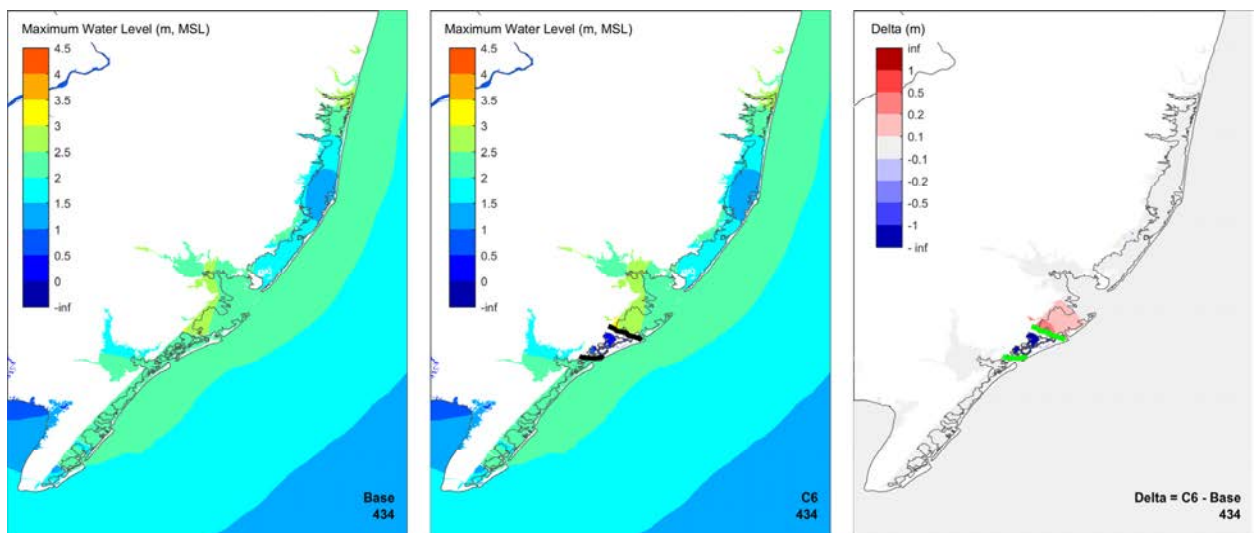


Figure 90: Maximum water elevation for Synthetic Storm 434: Base Grid (left), C6 (center), and difference between C6 and Base (right)

C7

This configuration responds similar to many of the other “C” configurations, with reduction in peak water level internal to the closures and an increase in peak water level external (north) of the Absecon Blvd closure, dependent on wind direction. The purpose of this configuration was to determine how a closure at Corson Inlet would impact peak water levels, north of the closure, at the southern end of Ocean City. A comparison of the results for C4 and C7 shows that the impact of closing Corson Inlet is limited to a relatively small area north of the inlet and does not significantly impact water levels in Great South Bay.

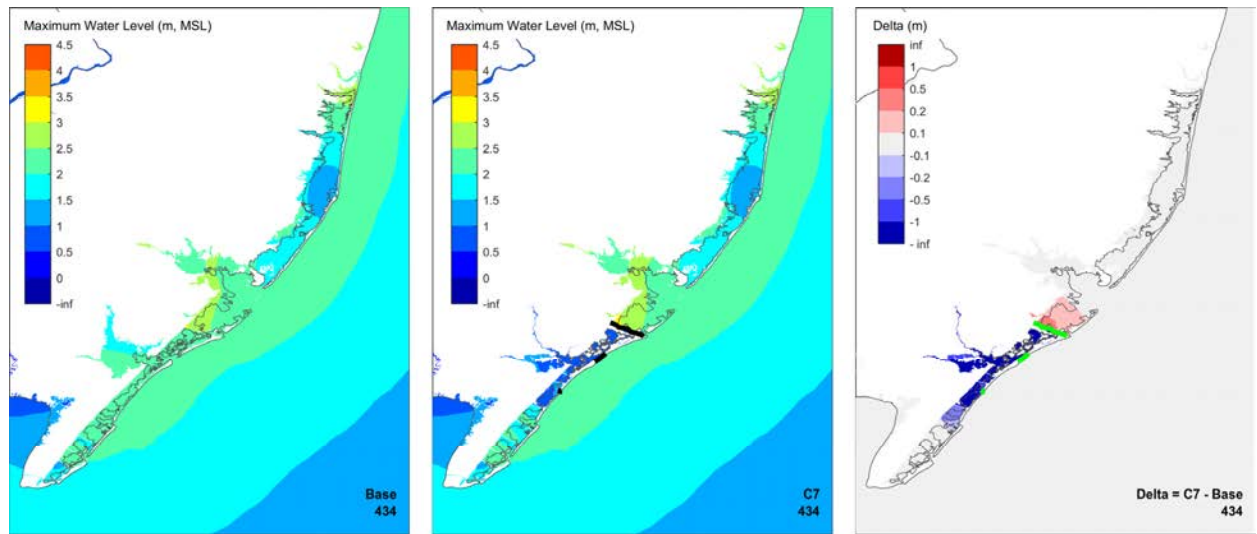


Figure 91: Maximum water elevation for Synthetic Storm 434: Base Grid (left), C7 (center), and difference between C7 and Base (right)

4.3 -- Maximum Storm Surge Results -- Iteration 3

The following section describes the effect of the Iteration 3 closure configurations on maximum water level in the New Jersey back bays. The storm selection process was described in [2 -- Storm Selections](#) and the grid alternatives used in Iteration 3 were described in [3.3.1 -- Configurations of proposed structures](#).

Shark River Region

The Iteration 3 model results for the All Closed Configuration confirmed earlier observations that a closure at Shark River is effective at reducing peak water levels inside the river entrance only. The still water level (SWL) hazard curve for both the baseline and All Closed configurations, [Figure 92](#), shows that a closure at Shark River effectively blocks storm surge from entering Shark River, with the 100-year SWL reduced from 3.2 m (MSL) in the base configuration to 1.0 m (MSL) in the All Closed configuration. Shark River Inlet is independent of all the other inlets so only one configuration, All Closed, was evaluated.

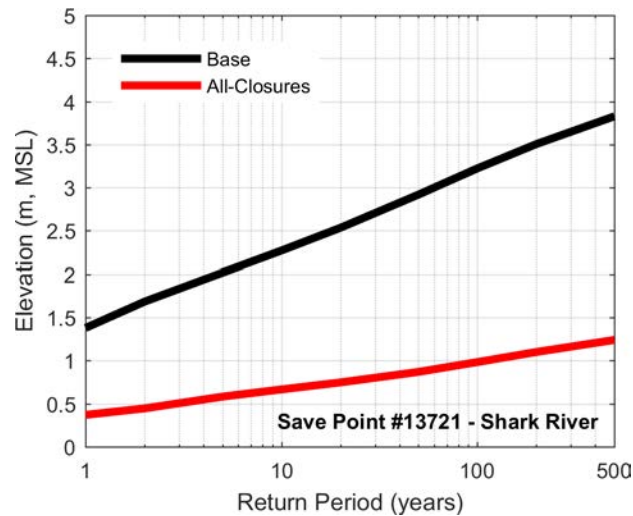


Figure 92: Phase I – Iteration 3: Shark River SWL Hazard Curves

North Region

Four north region configurations (All Closed, All Closed Less 2, N3S3, and N7S4) plus the base configuration were evaluated in Phase I - Iteration 3. The performance of the four configurations is characterized in this section by presenting the SWL hazard curves (Figure 94) at six locations throughout the North Region (Figure 93).

All Closed is generally the most effective configuration with significant reductions in SWL across the region. The hazard curves for the Base and All Closed configurations generally bracket the performance of all other configurations. Configurations that most resemble the All Closure configuration are more effective at reducing peak SWLs, thus their hazard curves are closest to the All Closure configuration. As noted during Iteration 2, even with all inlets closed, the potential for elevated SWL is not eliminated since overwash may occur at a few locations along Long Beach Island and winds are capable of generating seiches in the bay.

All Closed Less 2, closures at Manasquan Inlet and Barnegat Inlet, is nearly as effective as All Closed from Barnegat Light to Manasquan with significant reductions in SWL. However, peak SWLs from Surf City to Mystic Island are closer to the baseline condition, confirming an earlier observation that peak SWLs in lower Barnegat Bay are dominated by flow from Little Egg/Brigantine Inlet.

N3, closures at Manasquan Inlet, Barnegat Inlet, and a bay closure at Holgate, is similar in performance to All Closed and All Closed Less 2 from

Barnegat Light to Manasquan, with significant reductions in peak SWLs. The bay closure at Holgate significantly reduces peak SWLs along Long Beach Island, as observed in the Beach Haven and Surf City hazard curves. However, the potential for seiching and winds elevating water levels near the bay closure limits the effectiveness of the bay closure at the southern end of Long Beach Island (Beach Haven).

N7, closures at Manasquan Inlet and a bay closure at Point Pleasant Canal, is effective at reducing peak SWLs in Manasquan, with little or no effect on water levels in Barnegat Bay. It is noted that Point Pleasant canal, opening between Manasquan Inlet and Barnegat Bay, is still vulnerable to flooding from elevated water levels in Barnegat Bay.

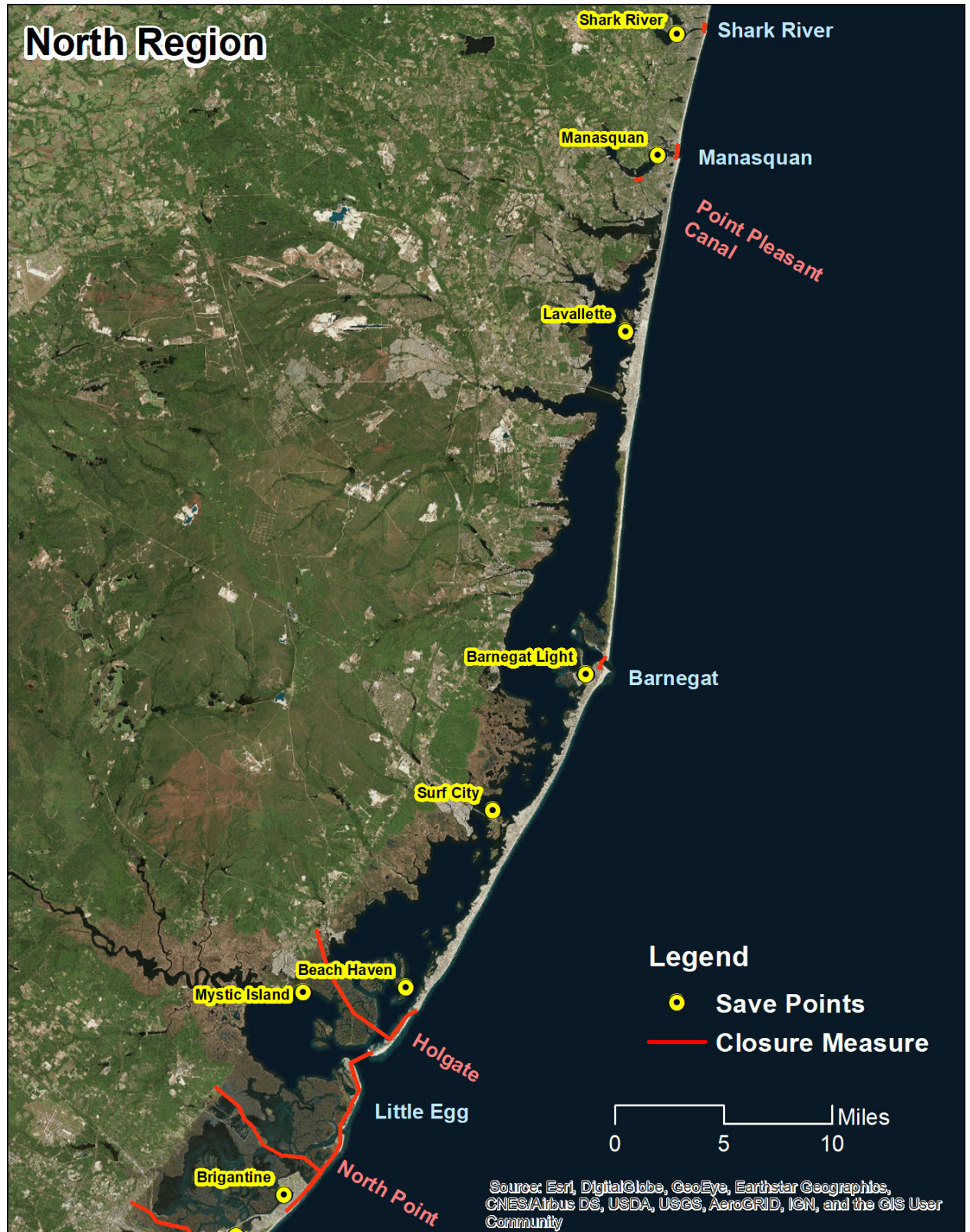


Figure 93: North Region and Save Points

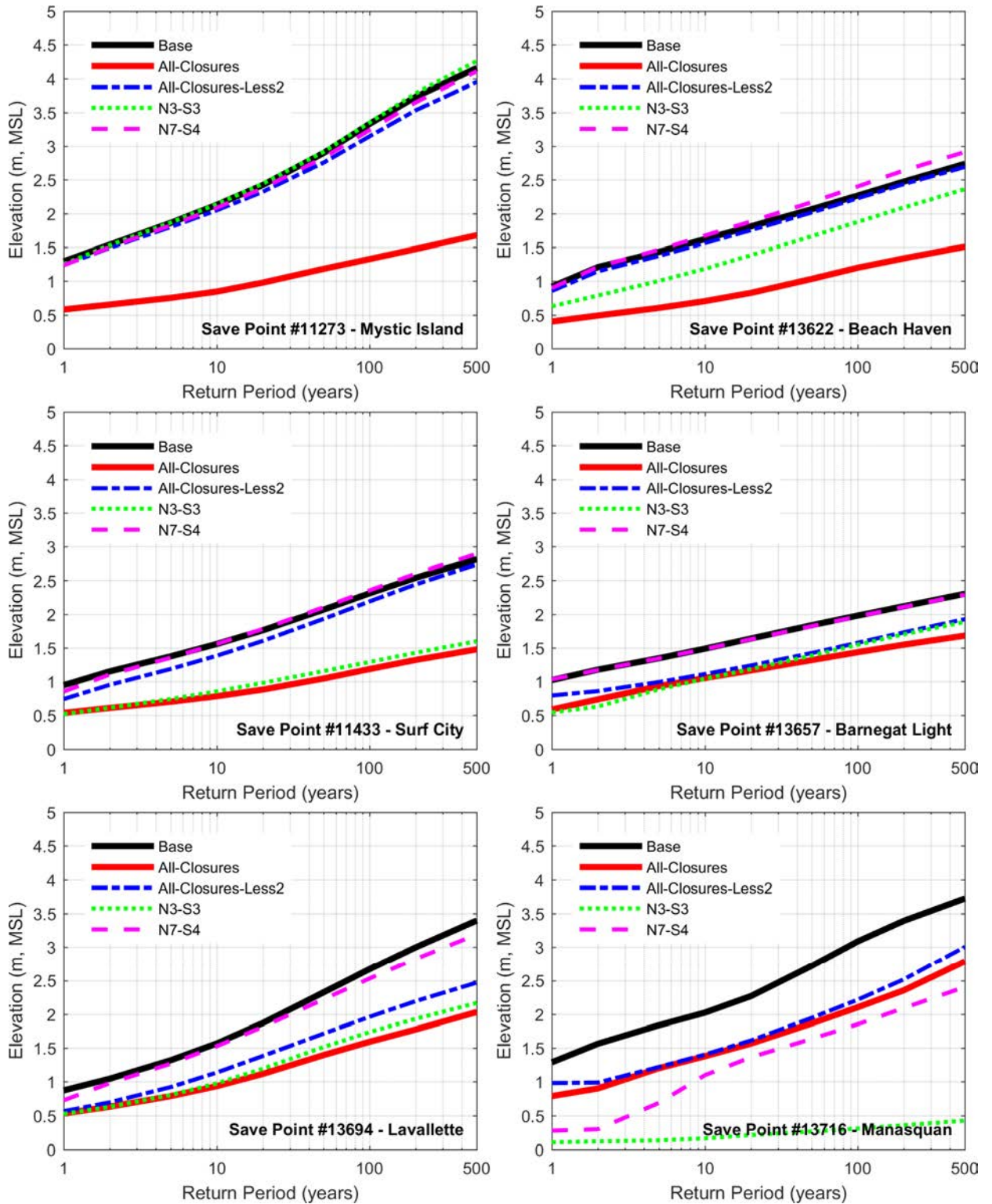


Figure 94: Phase I – Iteration 3: North Configurations SWL Hazard Curves

Central Region

Four Central Region configurations (All Closed, All Closed Less 2, C3, and C4) plus the base configuration were evaluated in Phase I - Iteration 3. The performance of the four configurations is characterized in this section by presenting the SWL hazard curves at six locations ([Figure 96](#)) throughout the Central Region ([Figure 95](#))

All Closed is generally the most effective configuration with significant reductions in SWL across the region. The hazard curves for the Base and All Closed configurations generally bracket the performance of all other configurations. Configurations with closures most similar to All Closed are more effective at reducing peak SWLs. As noted during Iteration 2, even when all the inlets are closed, the potential for elevated SWL is not eliminated since winds are capable of generating setup and seiches in the bay.

All Closed Less 2, with closures at Absecon Inlet and Great Egg Inlet, has peak SWLs that fall between the Base and All Closed peak SWLs. All Closed Less 2 is most effective in the immediate vicinity of Great Egg Inlet (Ocean City 4th St.) and less effective near Corson Inlet (Ocean City 43rd Street) and Little Egg Inlet (Brigantine) where peak SWLs are affected by flow through the open inlets.

C3, with closures at Absecon Inlet, Great Egg Inlet, and a bay closure at North Point, is more effective than All Closed at Brigantine and Absecon Inlet since the bay closure at North Point blocks the flow of storm surge from Little Egg/Brigantine Inlet. The North Point bay closure also reduces the potential for wind setup and large seiches (reduced fetch length) in Barnegat Bay. Peak SWLs at Atlantic City and Ocean City 4th St. are also lower than All Closed Less 2, and nearly equal to All Closed. Further south at Ocean City 43rd St, the peak SWLs are nearly the same as All Closed Less 2 with storm surge from Corson Inlet reducing the effectiveness of C3.

C4, with closures at Great Egg Inlet and a bay closure at Absecon Blvd, does not improve peak SWLs at Mystic Island, Brigantine, or Absecon Inlet, and has the potential to increase peak SWLs at these locations. South of Absecon Blvd, at Atlantic City and Ocean City and inside Great

Egg Harbor, C4 is effective at reducing peak SWLs with hazard curves that closely match C3.

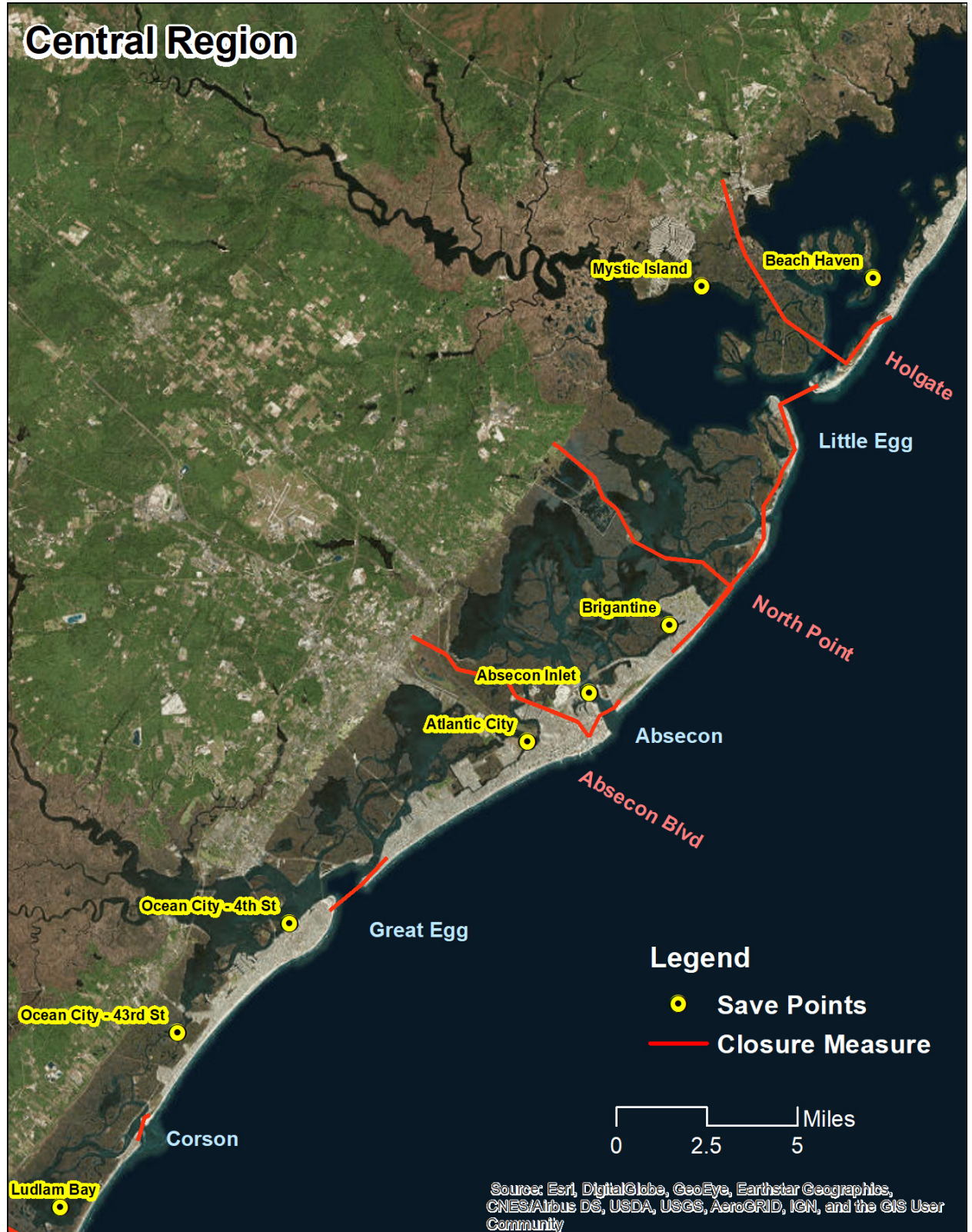


Figure 95: Central Region and Save Points

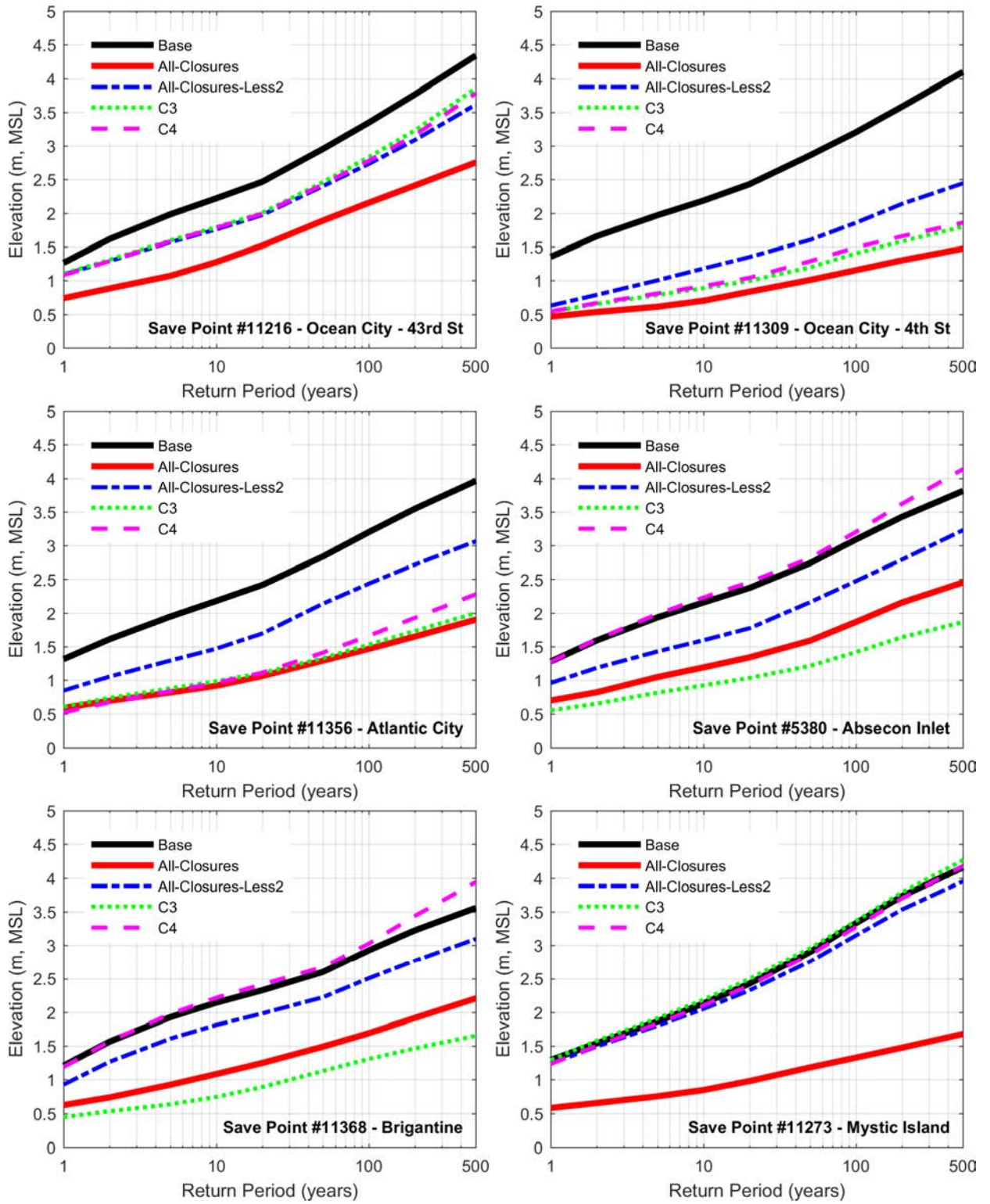


Figure 96: Phase I – Iteration 3: Central Configurations SWL Hazard Curves

South Region

Four configurations (All Closed, All Closed Less 2, S3, and S4) plus the base configuration are evaluated in Phase I - Iteration 3. The performance of the four configurations is characterized in this section by presenting the SWL hazard curves (Figure 98) at six locations throughout the South Region (Figure 97).

All Closed is generally the most effective configuration with significant reductions in SWL across the region. The hazard curves for the Base and All Closed configuration generally bracket the performance of all other configurations. Configurations with closures most similar to All Closed are more effective at reducing peak SWLs. As noted during Iteration 2, even though all the inlets are closed, the potential for elevated SWL is not eliminated since winds are capable of generating setup and seiches in the bay.

All Closed Less 2, with closures at Townsends Inlet, Hereford Inlet, Cape May Inlet, and Cape May Canal, are effective at reducing peak SWLs for the majority of the South Region. Elevated peak SWLs are observed at Ludlam Bay due to its proximity to Corsons Inlet (open) as well as at Cape May, where wind setup and seiching limit the effectiveness of even the All Closed configuration. Peak SWLs at Wildwood are reduced from approximately 3.3 m (MSL) to 1.3 m (MSL) at the 100-year return period. Similar reductions are observed at Stone Harbor, Mayville, and Sea Isle City.

S3, with closures at Townsends Inlet, Hereford Inlet, Cape May Inlet, Cape May Canal, and a bay closure at Sea Isle Blvd, is similar in performance to All Closed Less 2 except with a notable improvement at Sea Isle City. The bay closure at Sea Isle Blvd reduces peak SWLs south of the closure (Sea Isle City), but has the potential to increase peak SWLs in Ludlam Bay.

S4, with closures at Townsends Inlet, Cape May Inlet, Cape May Canal, and three bay closures at Sea Isle Blvd, Stone Harbor Blvd. and N. Wildwood Blvd, is designed to reduce peak SWLs in the South Region without a closure at Hereford Inlet which may be environmentally untenable. The three bay closures allow Hereford Inlet and Corson Inlet to remain open and block storm surge from propagating into the majority

of the bays in the South Region. S4 is the most effective configuration at Cape May, with peak SWLs below the All Closed configuration. At other locations, Wildwood, Stone Harbor, Sea Isle City, have peak SWLs that are similar to All Closed. The bay closures have the potential to increase peak SWLs on the exterior side of the closures, as observed at Mayville and Ludlam Bay.



Figure 97: South Region and Save Points

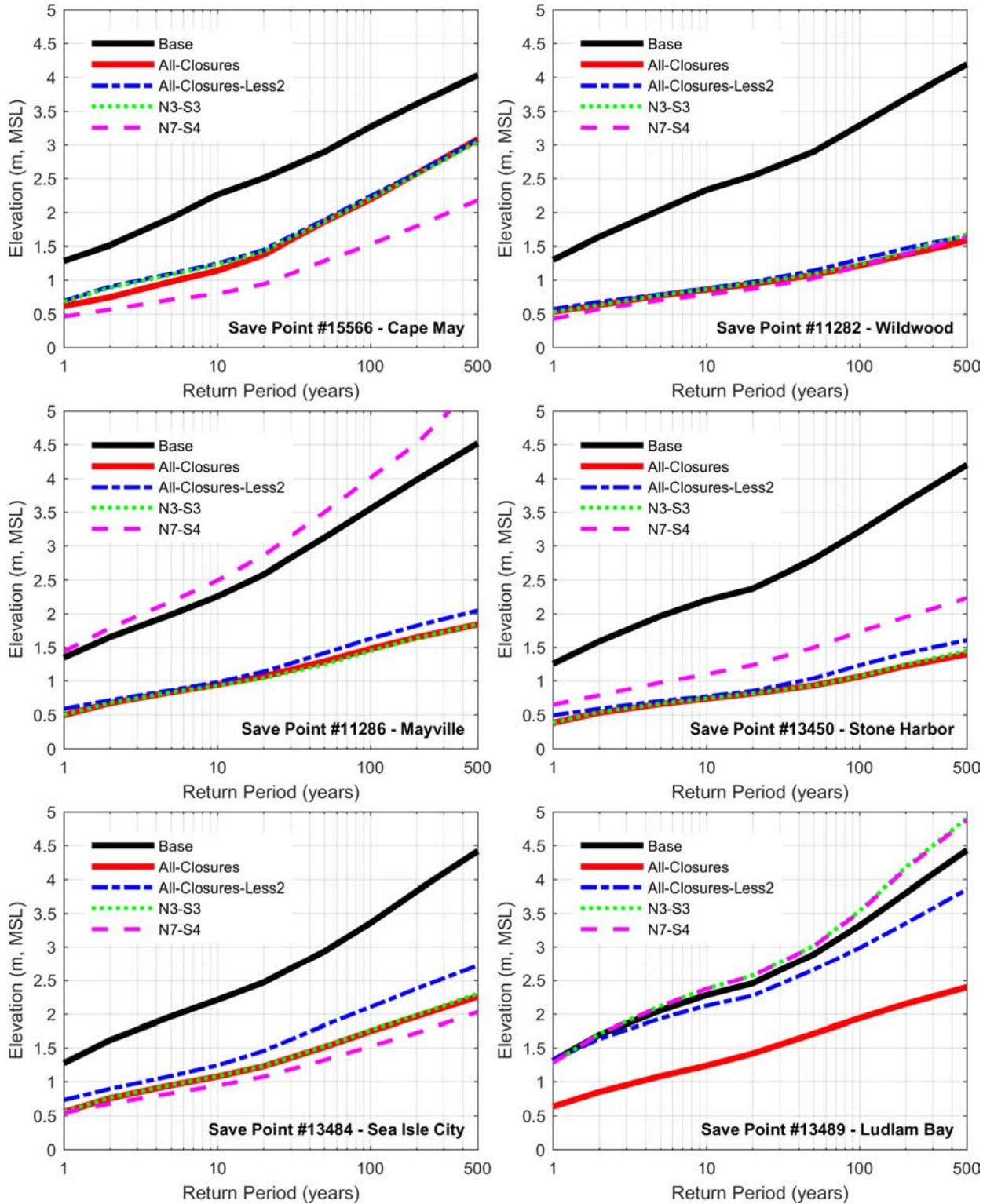


Figure 98: Phase I – Iteration 3: South Configurations SWL Hazard Curves

4.4 -- Maximum Storm Surge Results -- Phase II

The maximum water level response in the NJBB region for each alternative (Central 1, Central 2, and North described in [3.4.1 - Configurations of proposed structures](#)) was compared to the base condition for the suite of 60 storms described in [2 -- Storm Selections](#).

North:

Typical response:

The North Configuration enclosed Barnegat Bay and Manahawkin Bay with surge barriers at Barnegat Inlet and Manasquan Inlet and a causeway at Rte. 72, while leaving the navigation channel open at Rte. 72. This configuration provides for navigation, while limiting storm surge access to the bays and thus reduced maximum water level in the bays. The typical response to the simulated storms shows the average reduction in maximum water level in this 2-bay system is 0.49 m (1.61 ft) ([Figure 99](#)). For this particular storm (349) like many of the storms simulated, the reduction was greatest at the north end of Barnegat Bay.

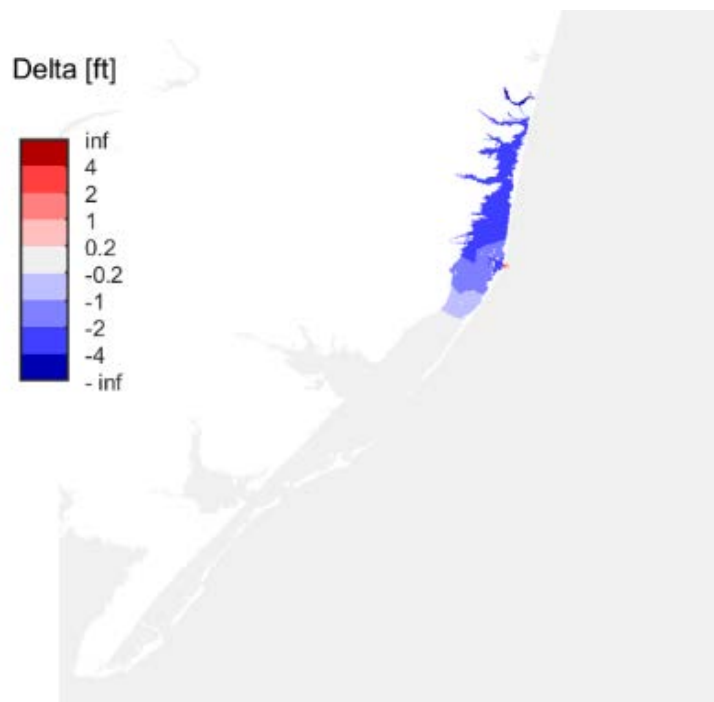


Figure 99: Typical change in maximum water level: North – Storm 349

Special Cases:

Some of the storms simulated with the North Configuration in place had greater reductions in the central or southern portion of the 2-bay system, depending on the predominant wind direction for the storm event. A few storms also showed trapping of surge behind the closed barrier at Barnegat Inlet, again, emphasizing the importance of the timing of opening and closing surge barriers before, during, and after an event (Figure 100)

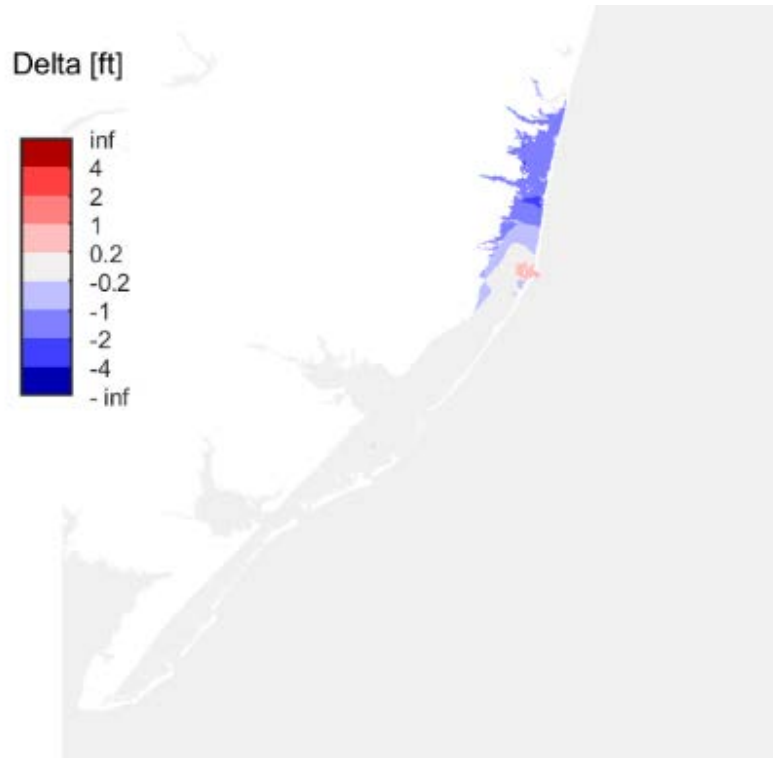


Figure 100: Change in maximum water level: North – Storm 524 with water behind the surge barrier

Figure 101 shows maximum water levels at save points for the Base condition vs maximum water levels with Barnegat and Manasquan Inlets closed, referred to as a dot plot. Values below the 45 degree line indicate a reduction in maximum water level attributable to the closure. For this particular configuration the average reduction in maximum water level in the Barnegat hydraulic reach was 35% due to Barnegat and Manasquan Inlets being closed.

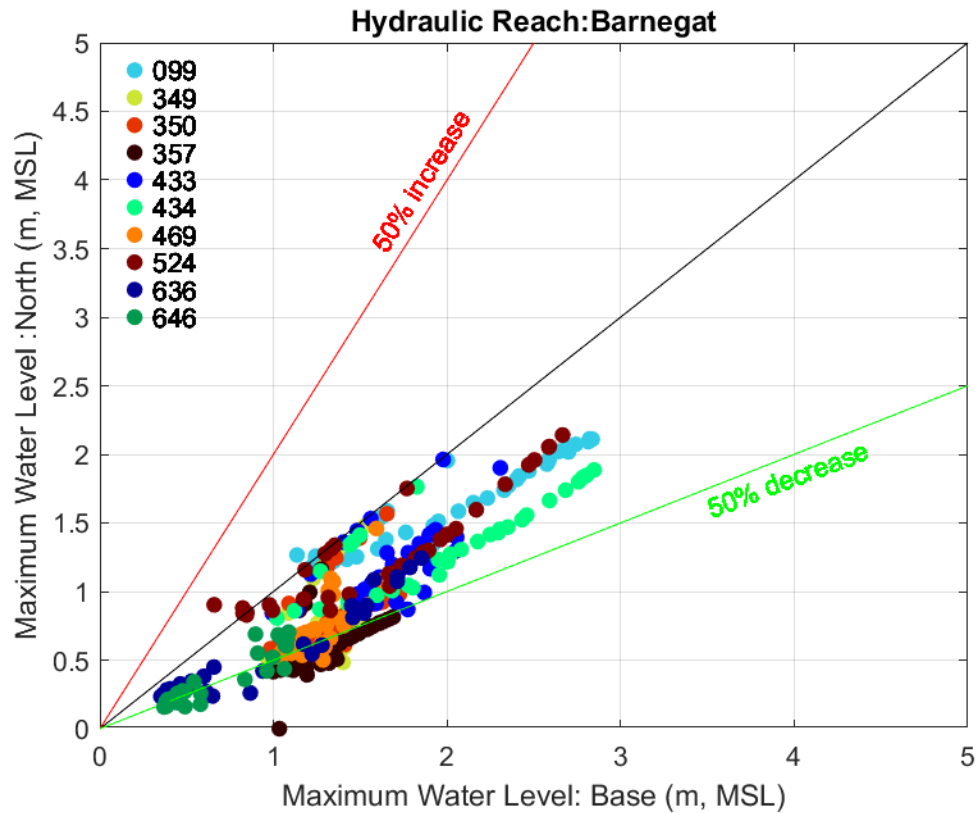


Figure 101: Dot plot: maximum water level for the Base condition vs maximum water level with Barnegat and Manasquan Inlets closed (the colors of the dots indicate different storms)

Central 1 (C1):

Typical response:

C1 nearly enclosed Lake Bay, Scull Bay, Great Egg Harbor Bay and Peck Bay with surge barriers and causeways, while leaving the navigation channels open. This condition provided a means for navigation while preventing or limiting access to the bays from storm surge and thus reduced maximum water level in the bays. The typical response to the simulated storms shows that the average reduction in maximum water level in Lake Bay, Scull Bay, Great Egg Harbor Bay and Peck Bay is 1.06 m (3.48 ft) (Figure 102; Storm 469). In addition, reductions in maximum water level were predicted to occur to a lesser degree in Absecon Bay and Reed Bay, transitioning from an average reduction “outside” of the Absecon Blvd causeway of 0.56 to 0.45 m (1.84 to 1.48 ft) in Reed Bay and negligible change in Great Bay. The 4-bay compartment area that is most protected also experienced reduced

average maximum water levels in the Mullica River and Wading River of 0.62 to 0.83 m (2.03 to 2.72 ft), respectively. Though flow could potentially enter through the navigation channel at the Absecon Blvd causeway and the 52nd St causeway, it could also exit through these openings; thus limiting the prevention of return flow or trapping surge in the bays.

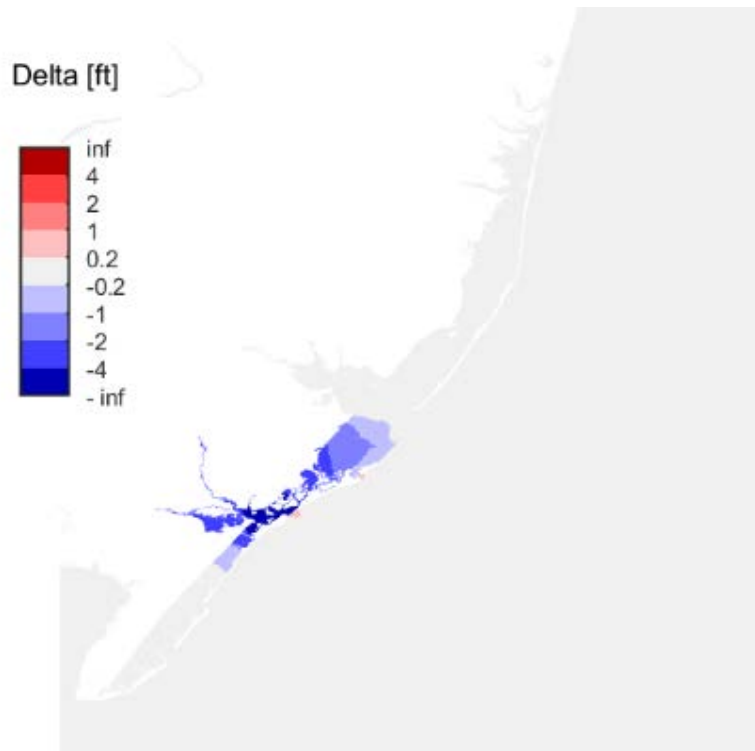


Figure 102: Typical change in maximum water level: C1 – Storm 469

Special cases:

Storm 99 is a slow-moving storm that tracked directly into Delaware Bay with a large central pressure deficit. These storm characteristics (path, forward speed, and central pressure deficit) resulted in strong, prolonged onshore winds for a large stretch of the New Jersey coastline located on the (right) side of the storm. The base condition simulation of this event showed extreme flooding in the 4-bay and 2-river system. The reduction in water level for this storm with Configuration C1 in place shows a greater extent of area with reduced water level in the 4-bay system than any of the other storms simulated, particularly in the Mullica and Wading Rivers (Figure 103). The typical water level reduction in the rivers was 0.62 to 0.83 m (2.03 to 2.72 ft), but the reduction for this storm was 1.02

to 1.27 m (3.35 to 4.17 ft) and extended into the overbank areas near the two rivers. The large reduction/protection from bay and river flooding for this event was due to the large extent of base condition flooding that was then prevented with the surge barriers in place. Other storms caused less base flooding, therefore the reductions were not as significant or extreme as this event.

For Configuration C1, Storm 433 responded typically within the 4-bay compartment, but showed an increase in water level seaward of the Absecon Inlet surge barrier of 0.46 m (1.51 ft), whereas the average increase in maximum water level seaward of the surge barrier for all 60 storms was only 0.12 m (0.39 ft) (Figure 104). This storm caused particularly large surge levels in the central New Jersey region, therefore the surge barriers served the purpose of preventing that volume of water from entering the bays. Thus, the water that was prevented from entering, exhibited the greatest levels seaward of the surge barrier and was also dispersed over a greater area in the Atlantic Ocean.

Storm 636 exhibited high maximum water levels with Configuration C1 in place in Reed Bay, Absecon Bay, Lake Bay, and Scully Bay (Figure 105). The wind direction for this particular storm allowed water to enter through Little Egg/Brigantine Inlet, winds then shifted north-to-south forcing flow into Reed and Absecon Bay, then winds shifted easterly trapping water behind the Absecon surge barrier. The storm characteristics and surge barrier configuration demonstrate the importance of understanding an approaching storm, knowing when to operate a surge barrier, and when to re-open a surge barrier.

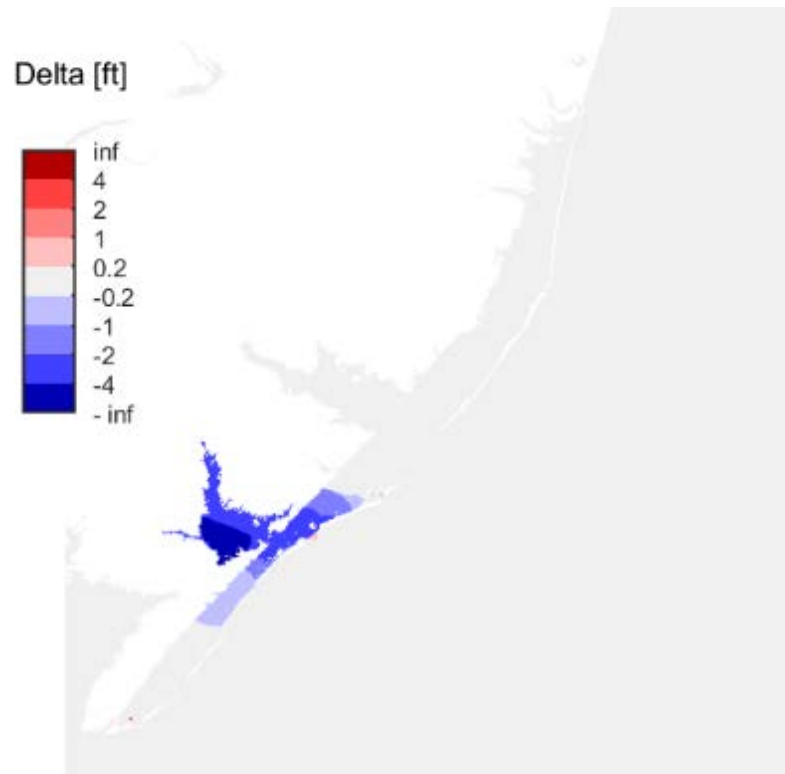


Figure 103: Change in maximum water level: C1 – Storm 99 with greater reduction in the rivers

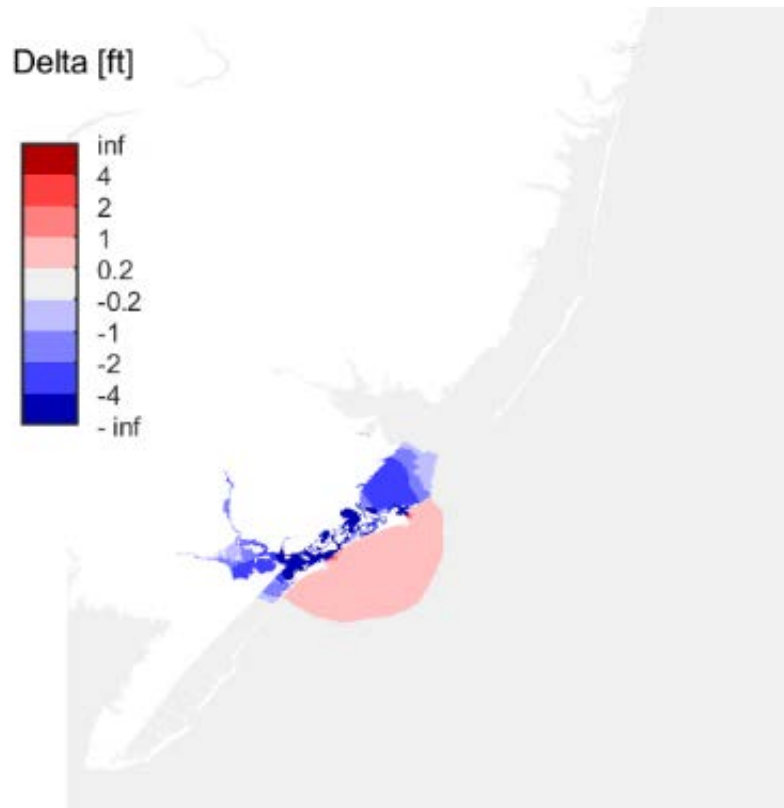


Figure 104: Change in maximum water level: C1 – Storm 433 water level increase seaward of surge barriers

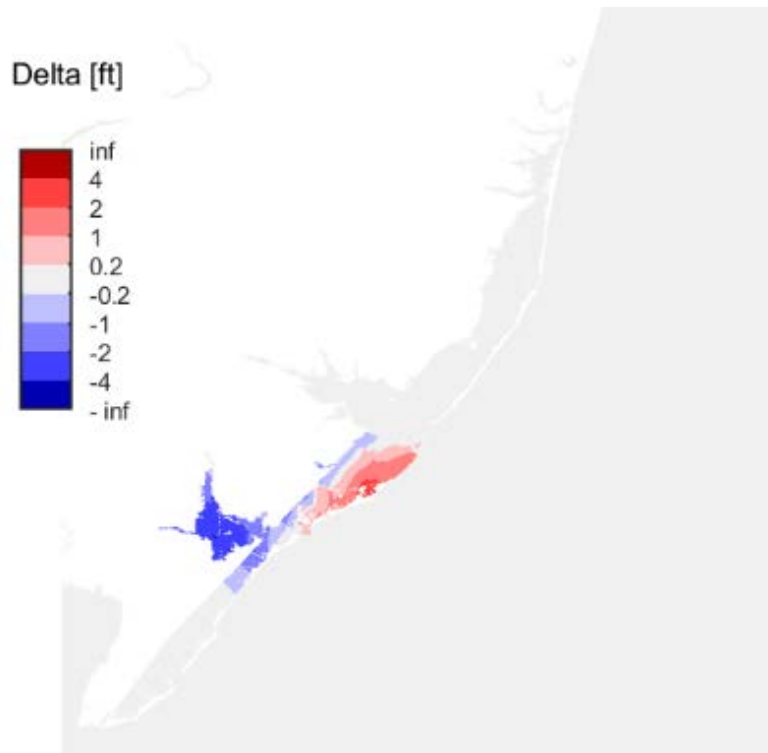


Figure 105: Change in maximum water level: C1 – Storm 636 with water behind the surge barrier

Figure 106 and Figure 107 show dot plots with Absecon and Great Egg Inlets being closed for Absecon and Great Egg hydraulic reaches, respectively. Values below the 45 degree line indicate a reduction in maximum water level attributable to the closures. For this particular configuration the average reduction in maximum water level in the Great Egg hydraulic reach was 51% and 16% in the Absecon hydraulic reach due to the inlet closures.

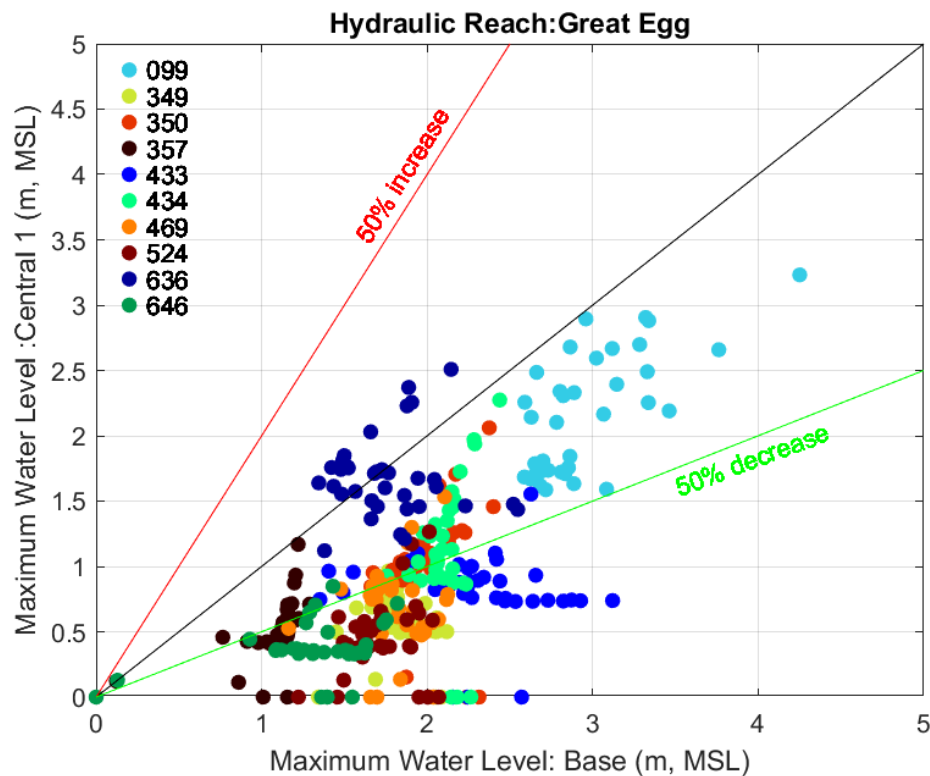


Figure 106: Dot plot: maximum water level for the Base condition vs maximum water level with Absecon and Great Egg Inlets closed (the colors of the dots indicate different storms)

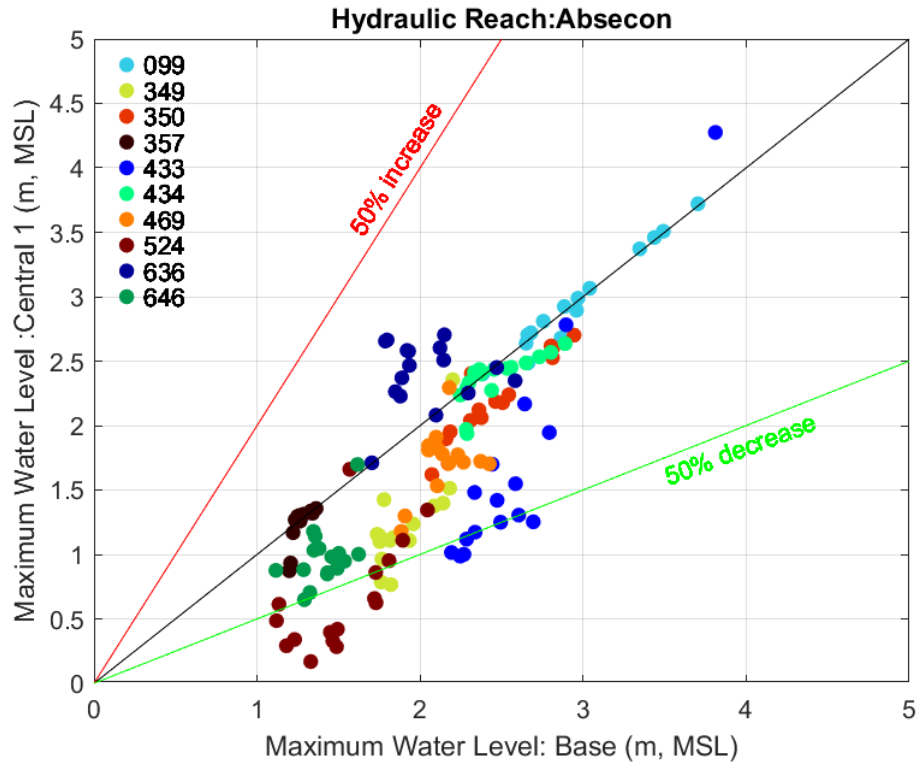


Figure 107: Dot plot: maximum water level for the Base condition vs maximum water level with Absecon and Great Egg Inlets closed (the colors of the dots indicate different storms)

Central 2 (C2):

Typical response:

Configuration Central 2 completely enclosed Lake Bay, Scull Bay, Great Egg Harbor Bay and Peck Bay with surge barriers and causeway closures. The typical maximum water levels relative to the base maximum water levels for C2 (Figure 108) are very similar to C1, with very slightly lower water levels where closed causeways prevent inflow and slightly higher water levels where closed causeways prevent outflow. The average reduction in water level over the 4-bay system is identical to the C1 value of 1.06 m (3.48 ft).

Though Absecon Bay and Reed Bay were protected with a surge barrier at Absecon Inlet for Configuration C1, this region is not protected from surge for Configuration C2 and average maximum water levels increase slightly from the Base condition in this area. The average water level reductions of 0.45 to 0.56 m (1.48 to 1.84 ft) observed for C1 are instead

replaced by modest increases of 0.03 to 0.06 m (0.1 to 0.2 ft) with Configuration C2 in place.

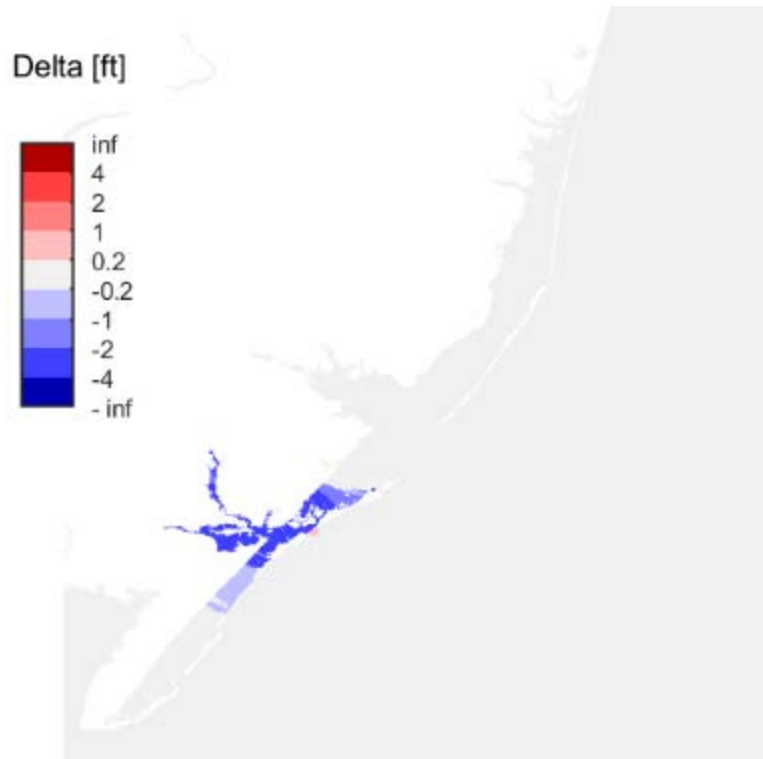


Figure 108: Typical change in maximum water level: C2 – Storm 434

Figure 109 and Figure 110 show dot plots with the 52nd Street bay closure, Absecon Blvd bay closure, and Great Egg Inlet being closed for the Absecon and Great Egg hydraulic reaches, respectively. Values below the 45 degree line indicate a reduction in maximum water level attributable to the closures. For this particular configuration the average reduction in maximum water level in the Great Egg hydraulic reach was 52% and 4% in the Absecon hydraulic reach due to the inlet closures.

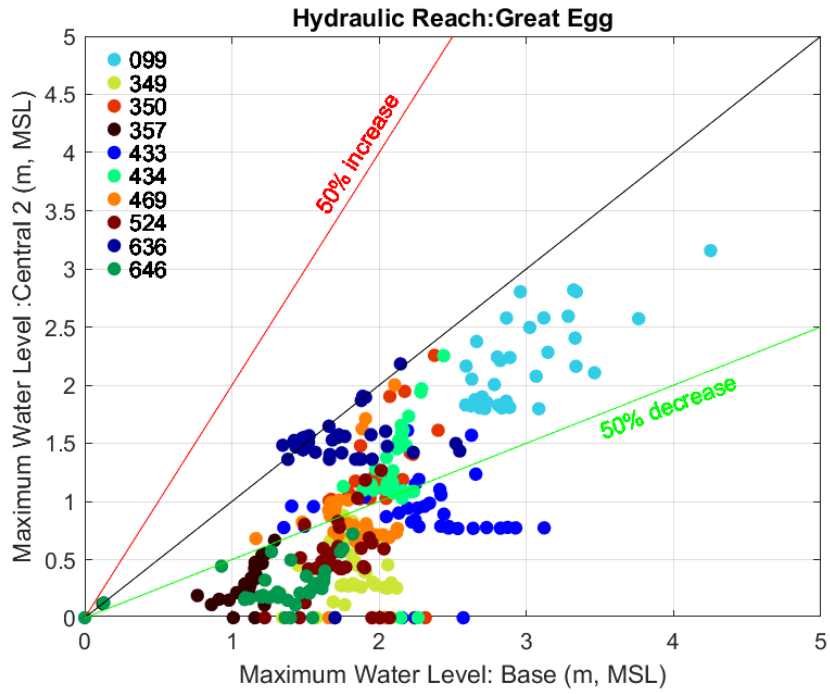


Figure 109: Dot plot: maximum water level for the Base condition vs maximum water level with Absecon Blvd bay closure, 52nd Street bay closure, and Great Egg Inlet closed (the colors of the dots indicate different storms)

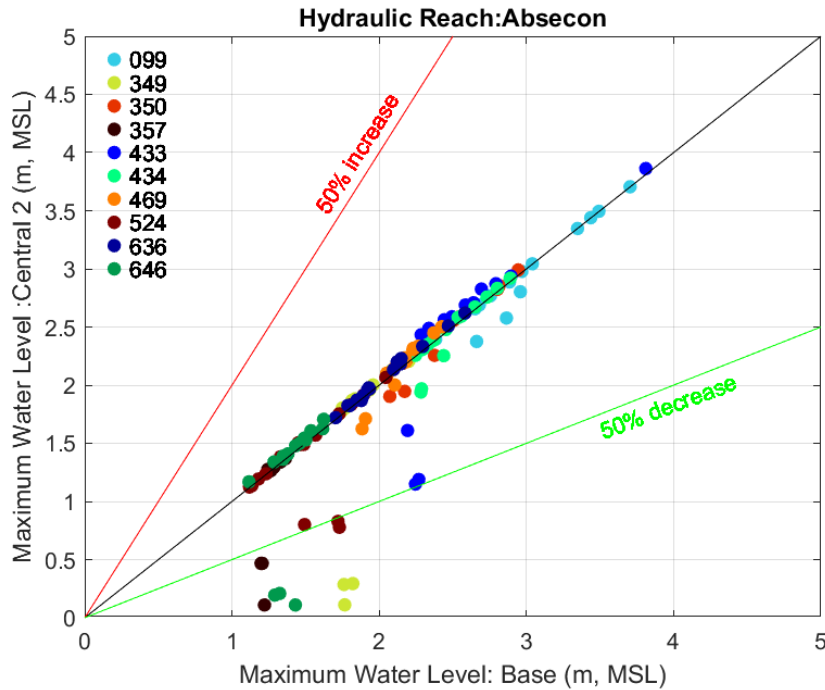


Figure 110: Dot plot: maximum water level for the Base condition vs maximum water level with Absecon Blvd bay closure, 52nd Street bay closure, and Great Egg Inlet closed (the colors of the dots indicate different storms)

Special Cases:

If we look beyond average results to a few specific storms, one can weigh the benefits of each configuration to specific approaching storms. Some Storms, such as Storm 433, illustrate the protection and vulnerability of Absecon and Reed Bay during a specific event (Figure 111). The average maximum water level in the bay for the Base condition during this event is approximately 2.57 m. With Absecon Inlet closed for case C1, the average maximum water level in the bay decreases to 1.67 m (0.9 m reduction), whereas for Configuration C2, the average maximum water levels actually increase to 2.75 m (0.09 increase). The increase is mainly caused by leaving the Absecon Inlet open for the C2 configuration and partially by converting the Absecon Blvd causeway into a full bay closure. The open inlet allows an additional volume of water to enter the bay and the bay closure prevents water distribution southward into Lake Bay.

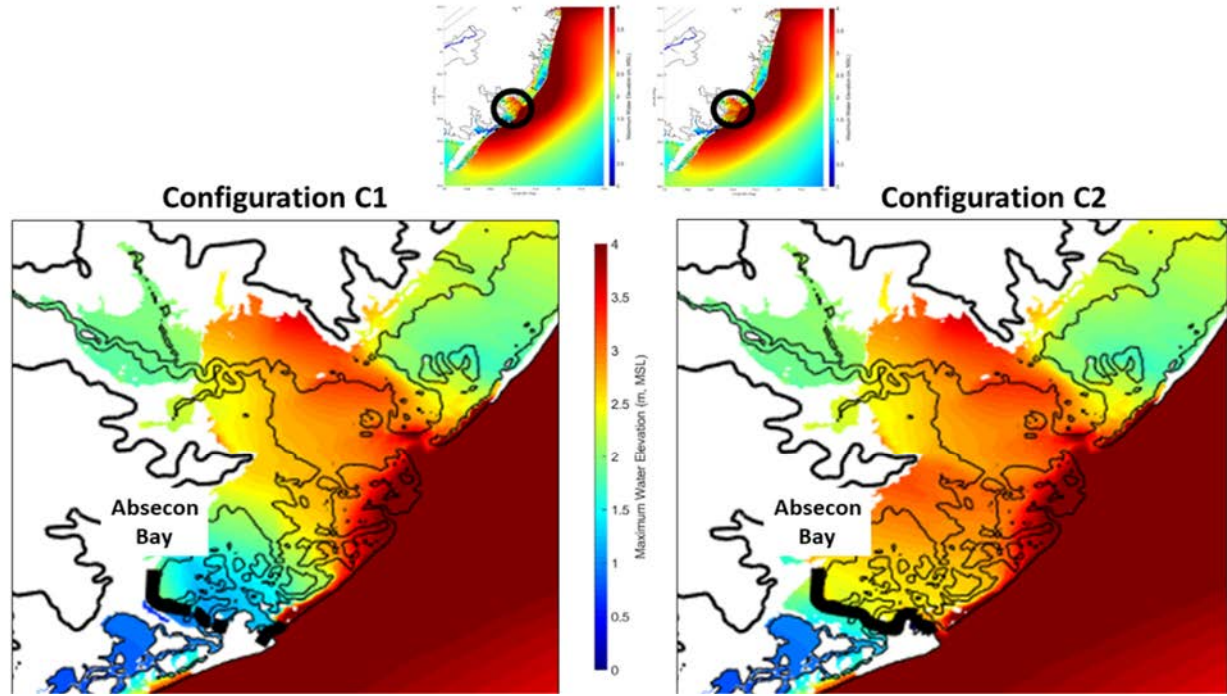


Figure 111: Storm 433 maximum water level envelope for Configurations C1 (left) and C2 (right)

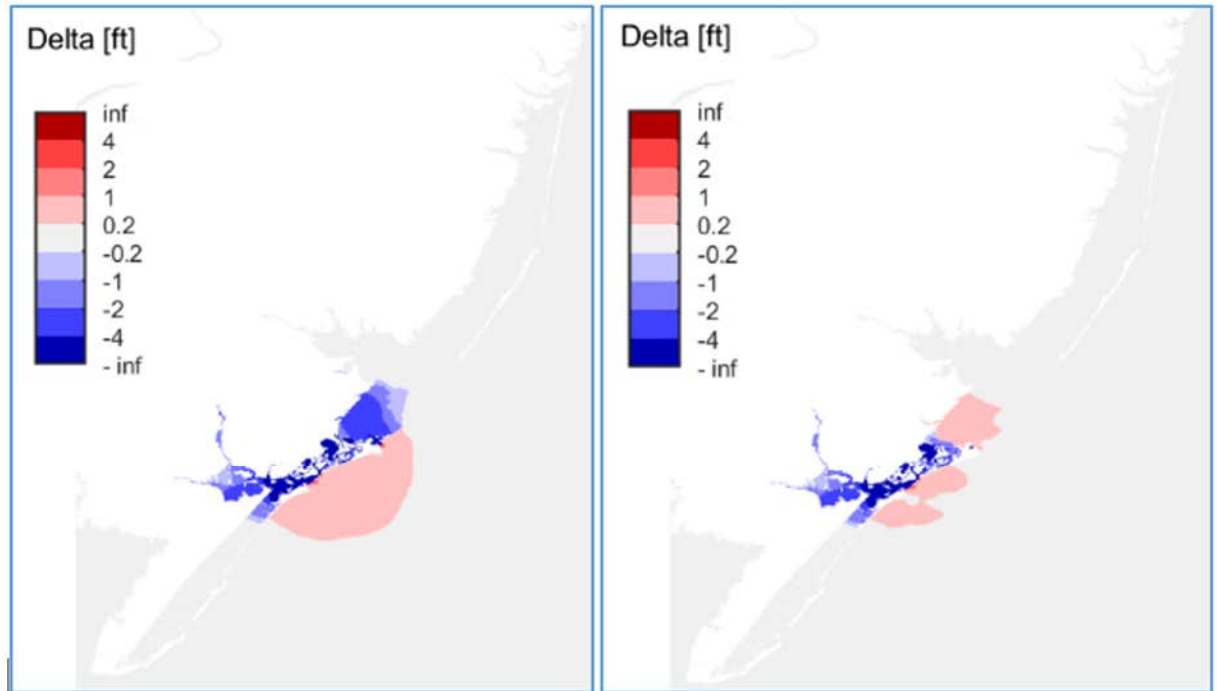


Figure 112: Storm 433 difference in maximum water level compared to Base: C1 (left) and C2 (right)

Other storm conditions, such as Storm 636, show more protection in Absecon Bay and Reed Bay for Configuration C2 compared to the protection from Configuration C1 (Figure 113). For this storm, flow through Little Egg/Brigantine Inlet is directed southward as the winds shift and then becomes trapped behind the surge barrier for Configuration C1 and flows outward for Configuration C2.

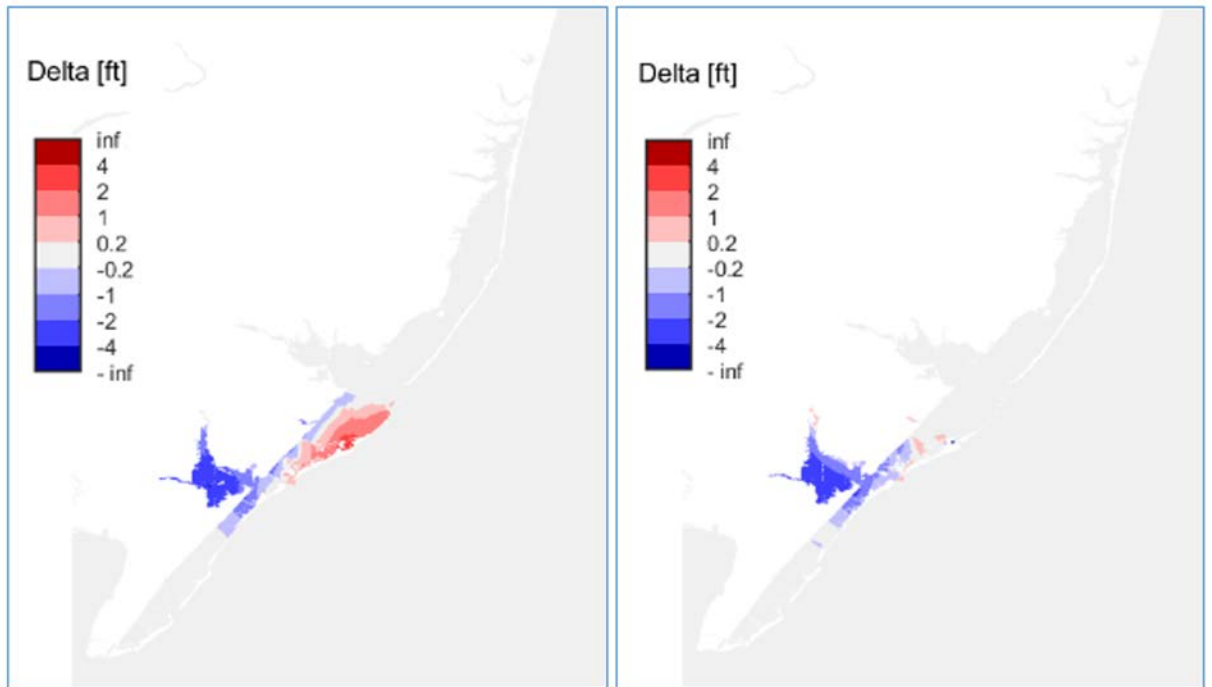


Figure 113: Storm 636 difference in maximum water level compared to Base: C1 (left) and C2 (right)

In summary, the overall benefit is the same for Configuration C1 and C2 internal to the 4-bay system and there is typically additional protection in Absecon Bay and Reed Bay with Configuration C1, except when north-to-south winds trap surge behind the Absecon Inlet surge barrier.

4.4.1 – SWL Hazard Curves

North Region

One closure configuration (North) plus the Base configuration were evaluated in Phase II. The performance of the North configuration is characterized in this section by presenting the SWL hazard curves (Figure

114)) at six locations throughout the North Region (Figure 93) for the North and base configurations.

The North configuration, with closures at Manasquan Inlet and Barnegat Inlet, produces similar results to All Closed Less 2 in the North Region. Peak SWLs in upper Barnegat Bay and Manasquan River are 0.5 to 1 m lower than the base conditions at the 100-year return period. The Peak SWLs in lower Barnegat Bay are only 0 to 0.25 m lower than the base conditions at the 100-year return period confirming earlier observations the peak SWLs in lower Barnegat Bay are dominated by flow through Little Egg/Brigantine Inlet.

Central Region

Two configurations (Central 1 and Central 2) plus the base configuration were evaluated in Phase II. The performance of each configuration is characterized in this section by presenting the SWL hazard curves (Figure 115)) at six locations throughout the Central Region compared to the Base (Figure 95).

The Central 1 configuration, with closures at Absecon Inlet and Great Egg Inlet, produces similar results to All Closed Less 2 in the Central Region. Peak SWLs in the area hydraulically controlled by Great Egg Inlet (most of Ocean City and Atlantic City) are 1 to 1.5 m lower than the base conditions at the 100-year return period. Peak SWLs in the vicinity of Absecon Inlet are approximately 0.5 m lower than the base conditions at the 100-year return period.

The Central 2 configuration, with closures at Great Egg Inlet and bay closures at Absecon Blvd and Southern Ocean City, produces similar results to Central 1 in the area hydraulically controlled by Great Egg Inlet (most of Ocean City and Atlantic City) indicating that the benefits of the bay closures are more localized. Peak SWLs in the vicinity of Absecon Inlet are nearly the same as the base conditions.

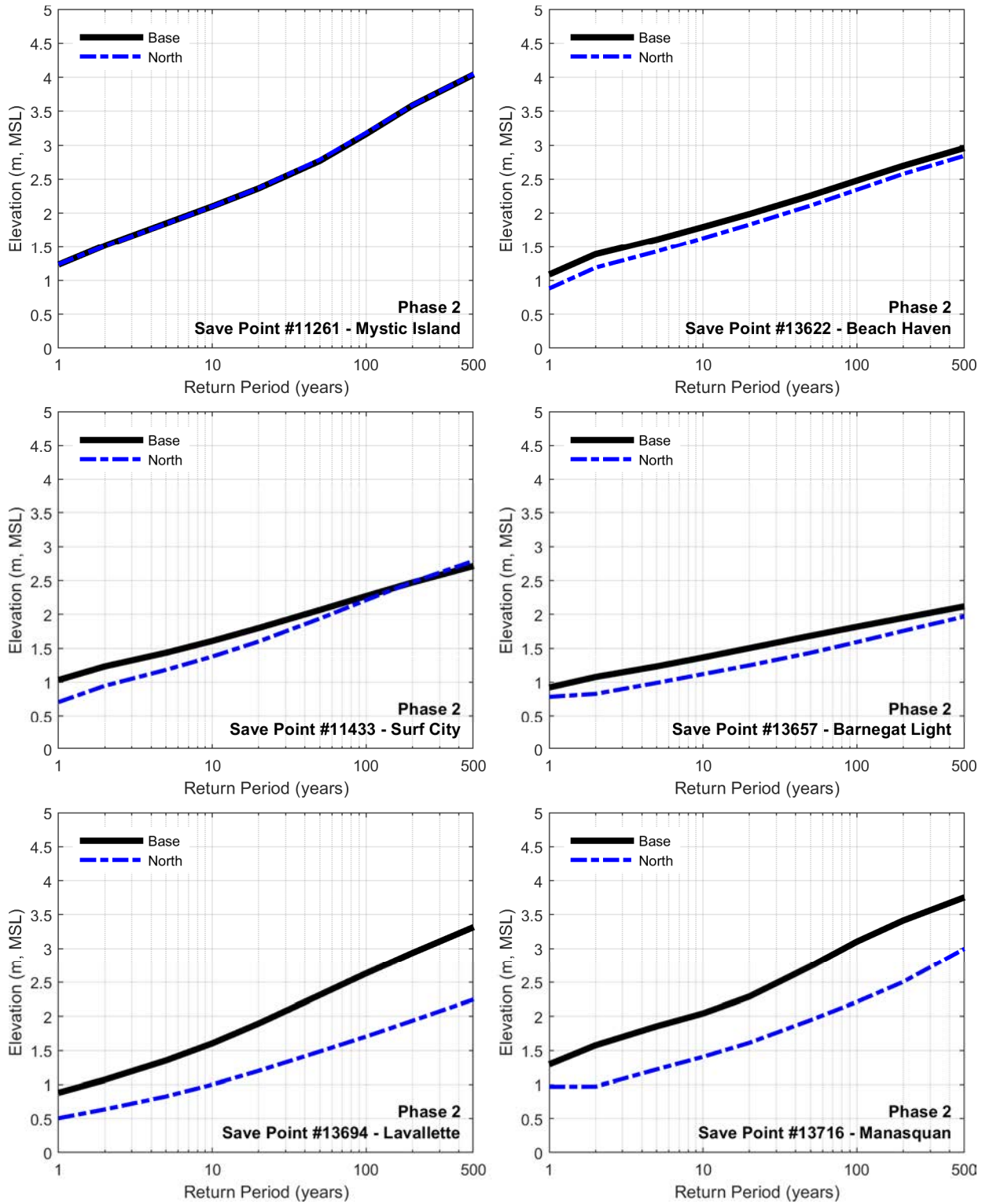


Figure 114: Phase II North Region SWL Hazard Curves

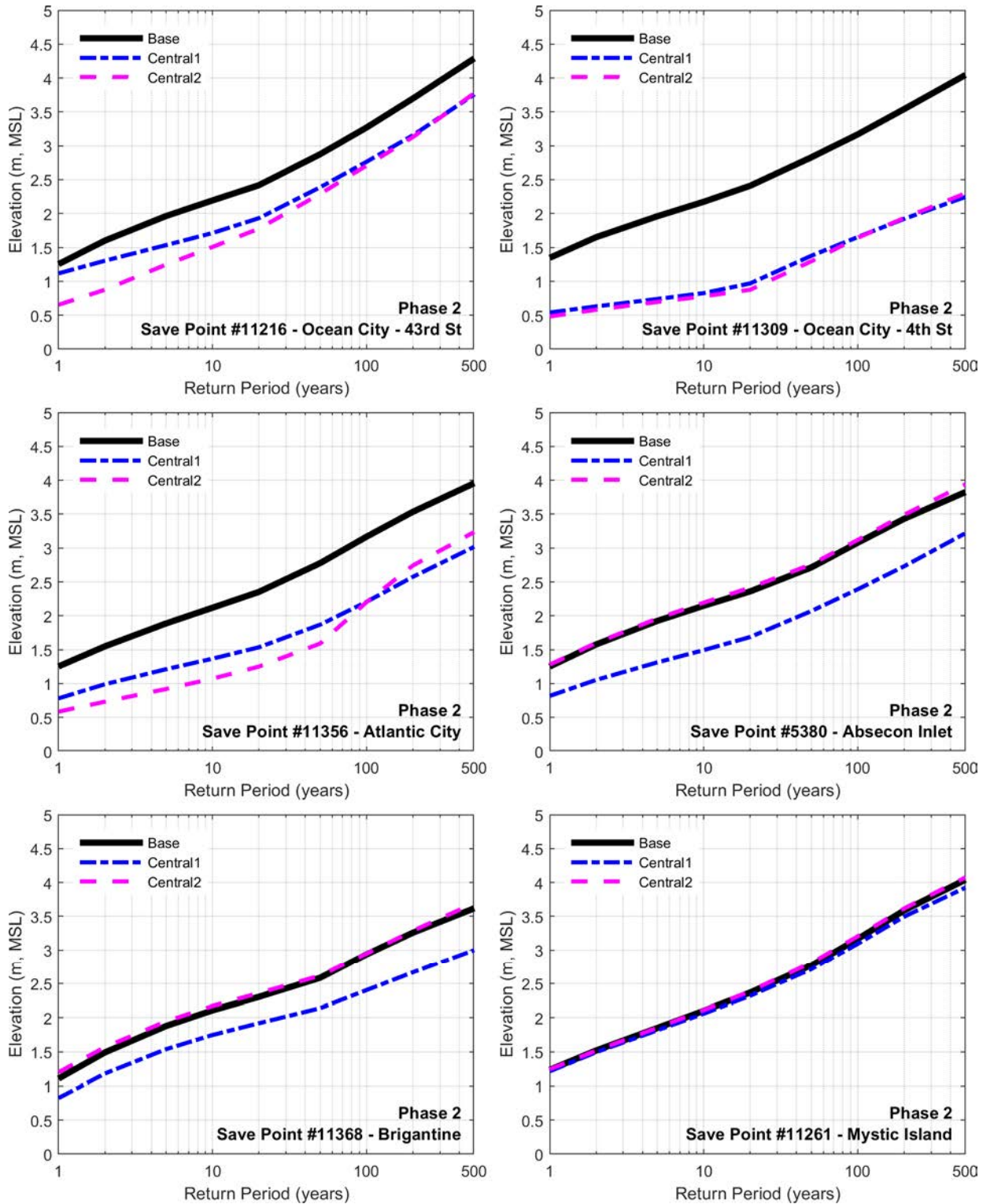


Figure 115: Phase II Central Region SWL Hazard Curves

5 -- Conclusions

The USACE Engineer Research and Development Center, Coastal and Hydraulics Lab (ERDC-CHL) conducted a numerical modeling study to evaluate the effectiveness of storm surge barriers in reducing water levels in the study area. ERDC-CHL leveraged the existing NACCS CSTORM-MS and the Coastal Hazards System (CHS) Probabilistic Coastal Hazard Analysis (PCHA) framework to complete the NJBB numerical hydrodynamic modeling and probabilistic analysis study. As part of this numerical modeling study the existing (base) condition water levels in the study area were updated (regenerated) from NACCS to ensure that the existing (base) and with-project water levels were consistent and derived from a common model, set of storms, and statistical evaluation.

The numerical modeling was completed in two phases: Phase I between the AMM and TSP-IPR milestones, and Phase II between the TSP-IPR and TSP milestones. In Phase I, an iterative modeling approach was devised that allowed a large number of inlet closures and potential inlet closure combinations to be considered before converging on a smaller final set of inlet closure alternatives.

Phase I, Iteration 1 focused on the ability of individual closures to alter maximum water levels compared to a base condition with no closures in place. It was found that individual closures can reduce back bay flooding, mainly in the bays closest to the closure location, but adjacent inlets may allow flow into the bay resulting in less significant water level reductions. Individual closures at Great Egg Inlet, Barnegat Inlet, and Shark River Inlet were most effective at reducing water levels in the back bays. Individual closures from Cape May to Corson Inlet were not as effective and may perform better as part of a system of closures. A closure at Manasquan Inlet was effective for storms where the predominant wind direction is from the north, however, storms with winds from the south could push storm surge up into northern Barnegat Bay, through the Point Pleasant Canal, and into the Manasquan River, limiting the closure's effectiveness.

Phase I, Iteration 2 focused on evaluating systems (multiple) of closures including cross-bay closures ("bay closures"). Many of the configurations were designed around leaving the most environmentally-sensitive inlets open: Little Egg/Brigantine, Corson, and Hereford. The numerical modeling results show that many of the Iteration 2 configurations are

effective at reducing back bay water levels. However, some of the configurations such as All Closed Less 2 showed considerable sensitivity to the storm and wind directions and it was unclear what the impact would be on the hazard curves. Iteration 2 also showed that many of the bay closures have the potential to increase surge on the unprotected side of the closure as surge piles up against the closure.

Phase I, Iteration 3 focused on the 6 configurations selected based on their ability to generate the greatest NED benefits (flood damages reduced minus project costs) and be environmentally acceptable. Using Gaussian process metamodeling (GPM) and a design of experiments (DoE) approach, CHL completed the frequency distributions of response for both the base and alternative configurations. An evaluation of the Iteration 3 hazards curves indicates that several of the configurations are effective at reducing peak still water levels and have the potential to generate significant economic benefits.

Phase II focused on the three primary storm surge barrier configurations in the NJBB Focused Array of Alternatives as well as refinements to the model bathymetry in Barnegat Bay and at several of the inlets with more recent survey data. An evaluation of Phase II CSTORM-MS simulations and water level frequency distributions confirm earlier observations that the configurations are effective at reducing peak still water levels and have the potential to generate significant economic benefits. However, the results for individual storm events vary and there is considerable sensitivity to the storm characteristics, particularly the wind direction. Future work is warranted to investigate the role storm surge barrier operations (timing, duration) have on water levels and the importance of understanding an approaching storm, knowing when to operate a surge barrier, and when to re-open a surge barrier.

6 -- References

Cialone, Mary A., Massey, T. Chris , Anderson, Mary E. , Grzegorzewski, Alison S. , Jensen, Robert E. , Cialone, Alan , Mark, David J. , Pevey, Kimberly C. , Gunkel, Brittany L. , McAlpin, Tate O. , Nadal-Caraballo, Norberto , Melby, Jeffrey A. , and Ratcliff, Jay J. (2015) "North Atlantic Coast Comprehensive Study (NACCS) coastal storm model simulations: Waves and water levels". U.S. Army Engineer Research and Development Center, ERDC/CHL TR-15-14.

- Jia, G., and Taflanidis, A.A. (2013) "Kriging metamodeling for approximation of high-dimensional wave and surge responses in real-time storm/hurricane risk assessment". *Computer Methods in Applied Mechanics and Engineering*, vol. 261-262, pp. 24-38.
- Jia, G., Taflanidis, A.A., Nadal-Caraballo, N.C., Melby, J.A., Kennedy, A.B., and Smith, J.M. (2015) "Surrogate modeling for peak or time-dependent storm surge prediction over an extended coastal region using existing database of synthetic storms". *Natural Hazards*, 81(2): 909-938.
- Kim, S.W., Melby, J.A., Nadal-Caraballo, N.C., and Ratcliff, J. (2015) "A time-dependent surrogate model for storm surge prediction based on an artificial neural network using high-fidelity synthetic hurricane modeling". *Natural Hazards*, 76(1): 565-585.
- Luettich, R.A., Birkhahn, R.H., and Westerink, J.J., 1991. Application of ADCIRC-2DDI to Masonboro Inlet, North Carolina: A brief numerical modeling study. Contractors Report to the US Army Engineer Waterways Experiment Station.
- Nadal-Caraballo, N.C.; Gonzalez, V.; Campbell, M.O.; Torres, M.J.; Melby, J.A., and Taflanidis, A.A., 2020. Coastal Hazards System: A Probabilistic Coastal Hazard Analysis Framework. *In: Malvárez, G. and Navas, F. (eds.), Global Coastal Issues of 2020. Journal of Coastal Research, Special Issue No. 95*, pp. XX-XX. Coconut Creek (Florida), ISSN 0749-0208.
- Nadal-Caraballo, N.C., Melby, J.A., Gonzalez, V.M., and Cox, A.T. (2015) "North Atlantic Coast Comprehensive Study – Coastal Storm Hazards from Virginia to Maine". Vicksburg, MS: U.S. Army Engineer Research and Development Center, ERDC/CHL TR-15-5.
- Taflanidis A.A., Jia, G., Nadal-Caraballo, N., Kennedy, A., Melby J., and Smith, J. (2014) "Development of Real-Time Tools for Hurricane Risk Assessment". *In Vulnerability, Uncertainty, and Risk*. M. Beer, S.K. Au, and J.W. Hall, ed. (Liverpool, UK, ASCE) 1341-1350.
- Taflanidis, A.A., Zhang, J., Nadal-Caraballo, N.C., and Melby, J.A. (2017) "Advances in surrogate modeling for hurricane risk assessment: storm selection and climate

change impact”. In proceedings of 12th International Conference on Structural Safety & Reliability, August 6-10, Vienna, Austria.

Zhang, J., Taflanidis, A.A., Nadal-Caraballo, N.C., Melby, J.A., Diop, F. (2018) “Advances in surrogate modeling for storm surge prediction: storm selection and addressing characteristics related to climate change”. *Natural Hazards*, 94(3): 1225-1253.

APPENDIX

H-3) RESIDENCE TIME ANALYSIS TO PREDICT IMPACT OF PROPOSED STORM PROTECTION STRUCTURES IN NEW JERSEY BACK BAYS (NJBB)



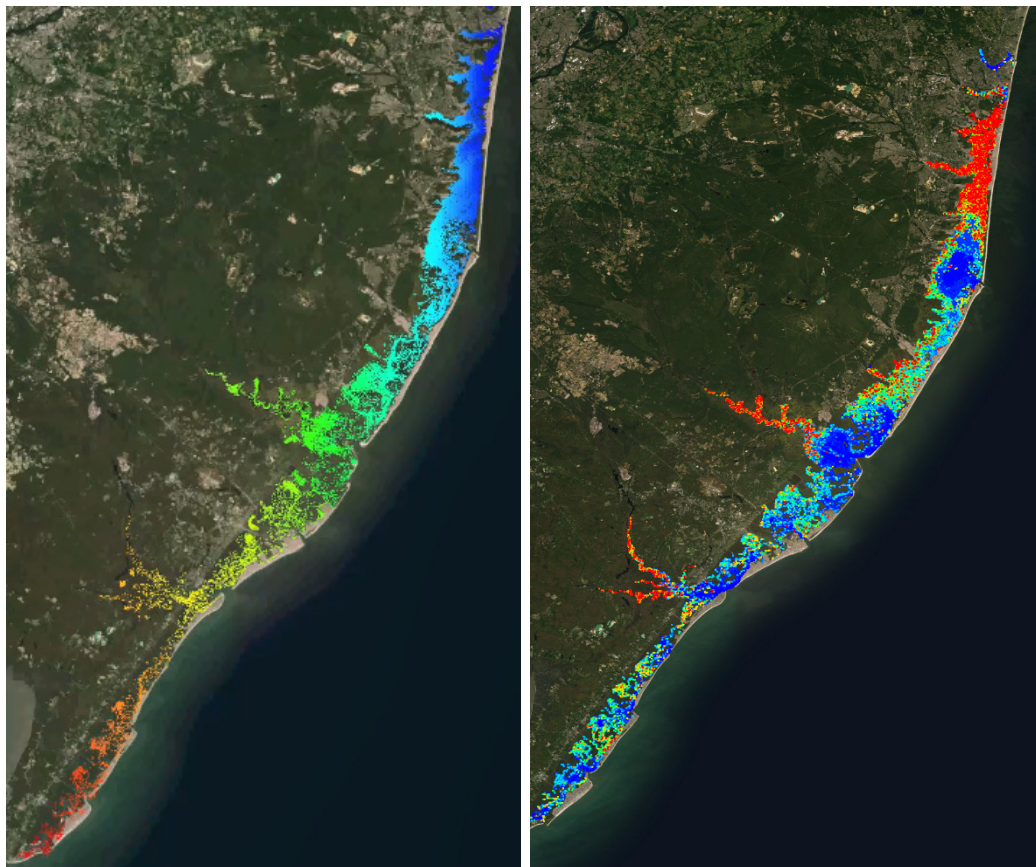
**US Army Corps
of Engineers®**
Engineer Research and
Development Center



DRAFT: Residence Time Analysis to Predict Impact of Proposed Storm Protection Structures in New Jersey Back Bays (NJBB)

Tahirih Lackey, Nathan Mays, Jennifer McAlpin, and Sung-
Chan Kim

February 2020



The U.S. Army Engineer Research and Development Center (ERDC) solves the nation's toughest engineering and environmental challenges. ERDC develops innovative solutions in civil and military engineering, geospatial sciences, water resources, and environmental sciences for the Army, the Department of Defense, civilian agencies, and our nation's public good. Find out more at www.erdclibrary.usace.army.mil.

To search for other technical reports published by ERDC, visit the ERDC online library at <http://acwc.sdp.sirsi.net/client/default>.

DRAFT: Residence Time Analysis to Predict Impact of Proposed Storm Protection Structures in New Jersey Back Bays (NJBB)

Tahirih Lackey, Nathan Mays, Jennifer McAlpin, and Sung-Chan Kim

*Coastal and Hydraulics Laboratory
U.S. Army Engineer Research and Development Center
3909 Halls Ferry Road
Vicksburg, MS 39180-6199*

Final report

Approved for public release; distribution is unlimited.

Prepared for U.S. Army Corps of Engineers, Philadelphia District
Under Work Unit

Abstract

The U.S. Army Engineer District, Philadelphia, requested the U.S. Army Engineer Research and Development Center, Coastal and Hydraulics Laboratory to analyze the impacts of proposed storm barriers in the New Jersey Back Bays (NJBB) on residence time of water particles within the system. The purpose of the residence time analysis would be to determine if proposed structures would increase areas of stagnation within NJBB, which might negatively affect the wetland habitat. The Particle Tracking Model (PTM), a Lagrangian particle tracker, is utilized to simulate transport of water particles out of the NJBB. Residence time analysis results show small difference between current conditions and with project conditions. An investigation of sea level rise (SLR), shows that flushing increases with SLR for all structural configurations.

DISCLAIMER: The contents of this report are not to be used for advertising, publication, or promotional purposes. Citation of trade names does not constitute an official endorsement or approval of the use of such commercial products. All product names and trademarks cited are the property of their respective owners. The findings of this report are not to be construed as an official Department of the Army position unless so designated by other authorized documents.

DESTROY THIS REPORT WHEN NO LONGER NEEDED. DO NOT RETURN IT TO THE ORIGINATOR.

Contents

Abstract	2
Figures and Tables	4
Preface	5
1 Introduction	7
Background	7
Objective	7
Approach.....	7
2 Methodology	9
Lagrangian Particle Tracking (PTM).....	9
<i>Simulation Details</i>	9
<i>ADH Hydrodynamic and Bathymetry</i>	10
<i>Particle Initial location</i>	12
<i>PTM Residence Time Traps</i>	14
Residence Time Calculations	16
<i>Residence Time Map</i>	16
<i>Average Residence Time Calculations</i>	19
Limitation of Modeling and Analysis Methods.....	20
3 Results	22
Particle Position Maps	22
Residence Time Contour Maps	24
Average Residence Time Analysis	28
Sea Level Rise Analysis.....	31
4 Summary and Conclusions	35
References	36
Appendix A: Plan Alternative Descriptions (Excerpt from McAlpin and Ross 2020)	37

Figures and Tables

Figures

Figure 1-1 Site Map of New Jersey Back Bay (NJBB)	8
Figure 2-1 ADH Mesh	11
Figure 2-2 ADH Bathymetry	12
Figure 2-3 (a) Initial Particle Locations, (b) Initial Particle locations Reduced to Back Bays and Channels, (c) Zoom in of Partiles in Back Bays and Channels.....	14
Figure 2-4 Residence Time Traps at each Inlets.....	16
Figure 2-5 Process of converting scatter point data to interpolated contoured mesh data	18
Figure 2-6 Average residence time polygons and initial particle locations	19
Figure 2-7 (a) Zoom in of Initial Particles, (b) Zoom in of adjusted particles that reach traps during the simulation.....	21
Figure 3-1 Particle position output (color coded based on initial location) at a) start time and then after b) 2 weeks c) 2 months, and d) 4 months.....	23
Figure 3-2 Base Case Particle Residence Time contour. Little Egg – Manasquan Inlet (Left) and Cape May Inlet – Absecon Inlet (Right).....	25
Figure 3-3 Particle Residence Time Contour Plots (Base – WP5). Little Egg – Manasquan Inlet.....	26
Figure 3-4 Particle Residence Time Contour Plots (Base – WP6). Cape May Inlet – Absecon Inlet.	27
Figure 3-5 Residence time contour maps of Base condition and Base SLR condition	32
Figure 3-6 Residence time contour map of Base SLR, WP1 SLR, WP4 SLR conditions	33

Tables

Table 2-1 Alternatives' Structures for NJBB regions.....	10
Table 2-2 Polygon ID and names.....	20
Table 3-1 Particle Residence Time (Days) - Base.....	29
Table 3-2 Alternatives' Average Residence Time (Days).....	30
Table 3-3 Alternatives' Difference (WP-Base) Residence Time (Days).....	31
Table 3-4 Alternatives' Average Particle Residence (Days)- SLR	34

Preface

The model investigation presented in this report was authorized and funded by the U.S. Army Corps of Engineers, Philadelphia District.

The work was performed at the U.S. Army Engineer Research and Development Center, Coastal and Hydraulics Laboratory (ERDC-CHL), Vicksburg, MS. At the time of publication of this report, Dr. Ty V. Wamsley was Director, and Mr. Jeffrey R. Eckstein was Deputy Director, ERDC-CHL. Direct supervision was provided by Dr. Cary Talbot, Chief, Flood and Storm Protection Division, and Ms. Ashley Frey, Chief, Coastal Processes Branch.

COL Teresa Schlosser was Commander of ERDC, and Dr. David W. Pittman was Director.

1 Introduction

Background

The U.S. Army Corps of Engineer Philadelphia District, (NAP) has a need to analyze possible hydrodynamic and water quality impacts of proposed storm barriers in the New Jersey Back Bays (NJBB) (Figure 1-1). Due to hurricane Sandy, there has been a push for more robust coastal protection along the Atlantic coastline. The North Atlantic Coast Comprehensive Study (NACCS) included a large scale storm surge modeling effort to analyze potential flooding due to various storm conditions (Cialone et al. 2017). The NACCS risk study identified several areas of further detailed evaluation. NJBB is one of the areas identified by NACCS. This area extends from Brick, NJ, to the southern tip of the state at Delaware Bay. The area of interest includes the inlets where the Atlantic Ocean joins the back bays as well as the area between the barrier islands and the mainland where large areas of wetland habitat reside.

An in-depth hydrodynamic study was performed to investigate velocity, water surface elevation, and salinity due to the proposed structures (McAlpin and Ross 2020). However, it was determined that a key component to understanding ecological impacts to NBJJ would be to perform a residence time analysis.

Objective

In 2018, NAP requested the ERDC-CHL perform numerical analysis to investigate changes in residence time and flushing within NJBB due to proposed storm surge protection measures. The purpose of the residence time analysis would be to determine if proposed structures would increase areas of stagnation within NJBB, which might negatively affect the wetland habitat. The goal of this effort is therefore, to investigate residence time for the current conditions and compare results with a series of project conditions that differ due to various potential structures (gates, barriers, etc) under consideration by NAP.

Approach

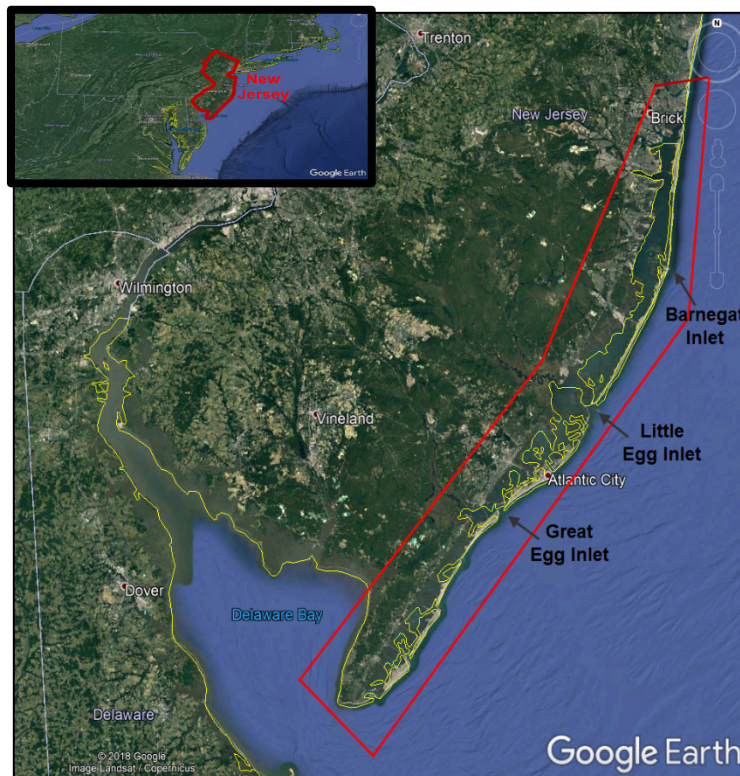
Residence time is determined utilizing a Lagrangian transport modeling approach. The Particle Tracking Model (PTM) (McDonald et al 2006, Gailani et al 2016, Lackey et al 2008), a Lagrangian particle tracker

developed by ERDC-CHL is utilized to simulate transport of water particles within the NJBB out into the ocean. Previous residence time analysis has been performed for a subsection of the upper NJBB (Defne and Ganju 2015). This work looks at the entire NJBB system.

Residence time calculations are performed utilizing PTM transport output from a four month simulation. A two-dimensional (2D) Adaptive Hydraulics (AdH) model provided hydrodynamic forcing for particle transport (McAlpin and Ross 2020). Sensitivity analysis to model parameters were performed and documented.

Chapter 2 describes Lagrangian transport modeling as well as analysis methods and techniques. Chapter 3 documents results in terms of residence time maps and average residence time tables. Comparison of current conditions, project conditions, and sea level rise conditions are presented. Chapter 4 provides a summary and conclusion of this effort.

Figure 1-1 Site Map of New Jersey Back Bay (NJBB)



2 Methodology

This chapter provides a description of the methods, techniques, and technologies used to perform the residence time calculation for the NJBB area. To determine the residence time in the different regions within the NJBB area, the transport calculations were performed using the Particle Tracking Model (PTM). PTM transport output was post processed and subsequently analyzed to determine residence time.

Lagrangian Particle Tracking (PTM)

PTM is a Lagrangian particle tracker designed to allow the user to simulate particle transport processes in coastal, estuarine, and riverine environments. PTM has been developed for applications which focus on both neutrally buoyant constituents and particles with mass such as sediment. The model contains algorithms that appropriately represent transport, settling, deposition, mixing, and resuspension processes in nearshore wave/current conditions.

Within this work particles are transported as passive (neutrally buoyant) which means they are only impacted by the velocities provided as model input and do not settle in the water column. Required model inputs for PTM to determine residence time are bathymetry, hydrodynamics, initial location of particles, and residence time traps.

Simulation Details

Four month simulations (July 1- October 31, 2019) were performed for this work. Each simulation utilized hydrodynamics developed for one of ten conditions:

1. Base (current) condition (1 simulation)
2. With Project 1-6 conditions (6 simulations)
3. Sea level Rise conditions for base and With Project 1 and 5. (3 simulations)

Each alternative describes a specific set of structures placed within the system (Table 2-1). The details of these structures are presented as an excerpt from (ADH reference) in Appendix A.

Table 2-1 Alternatives' Structures for NJBB Regions

Closure Location	Model Configuration Number					
	WP1	WP2	WP3	WP4	WP5	WP6
Manasquan Inlet	A1	A1	A1	A1	B1	A1
Barnegat Inlet	A1	A2	A3	A4	B1	C1
Absecon Inlet					A1	A2
Great Egg Inlet	A1	A2	A3	B1	A1	A1
Absecon Bay Blvd	A1	A1	A1	A1		
72 nd Street	A1	A1	A1	A1		

After extensive sensitivity analysis, the model was run with a timestep of 15 seconds and approximately 76,000 particles.

ADH Hydrodynamic and Bathymetry

The ADaptive Hydraulics model was used to determine water surface elevation and velocities needed for PTM input. The bathymetry for NJBB is represented in an ADH Mesh (Figure 2-1). An extensive report has been developed which described ADH modeling effort including model validation, calibration, boundary conditions (reference ADH draft report). One year of ADH hydrodynamic results were provided for PTM input to determine transport for the base condition and each of the alternatives.

Figure 2-1 ADH Mesh

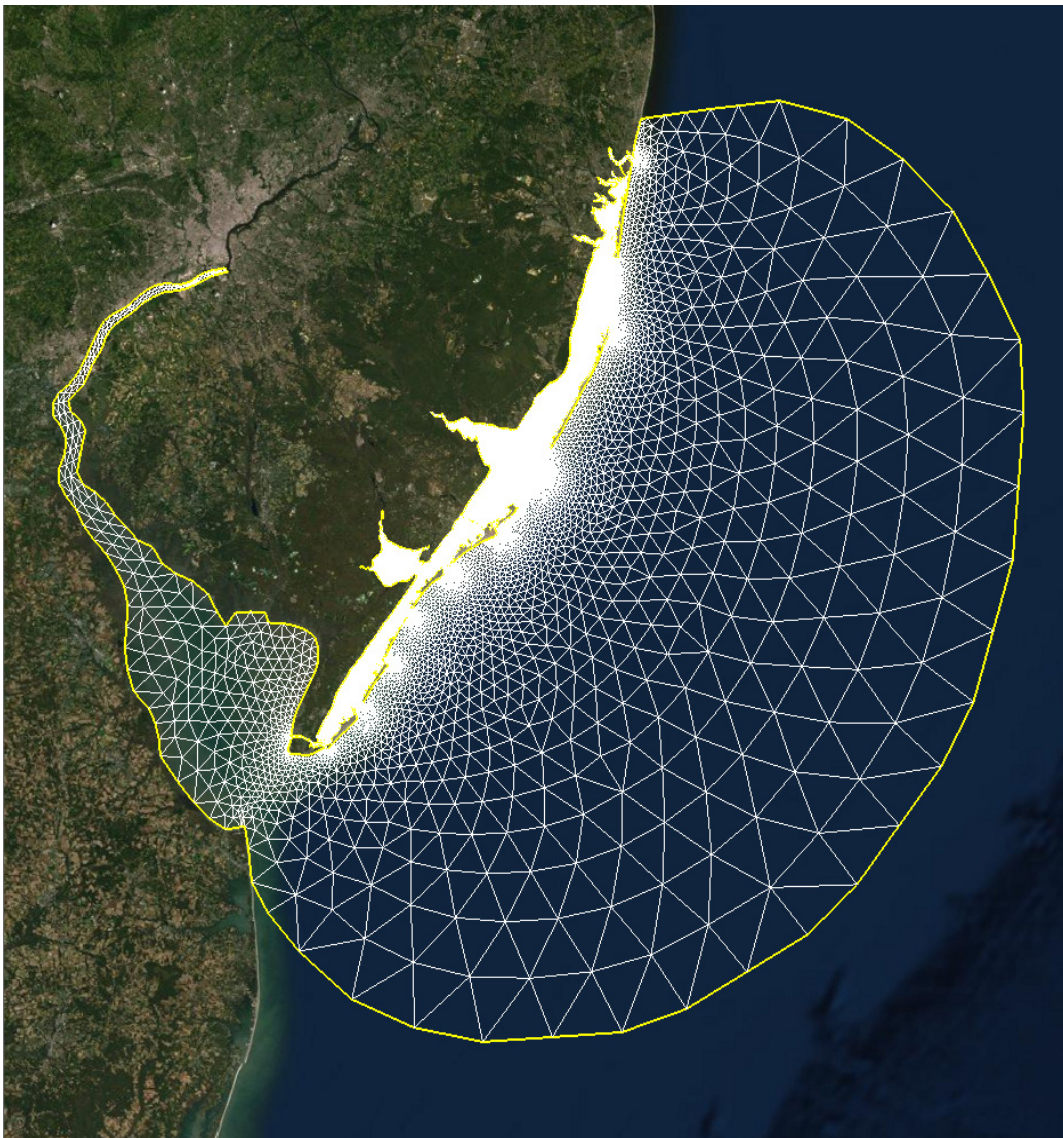
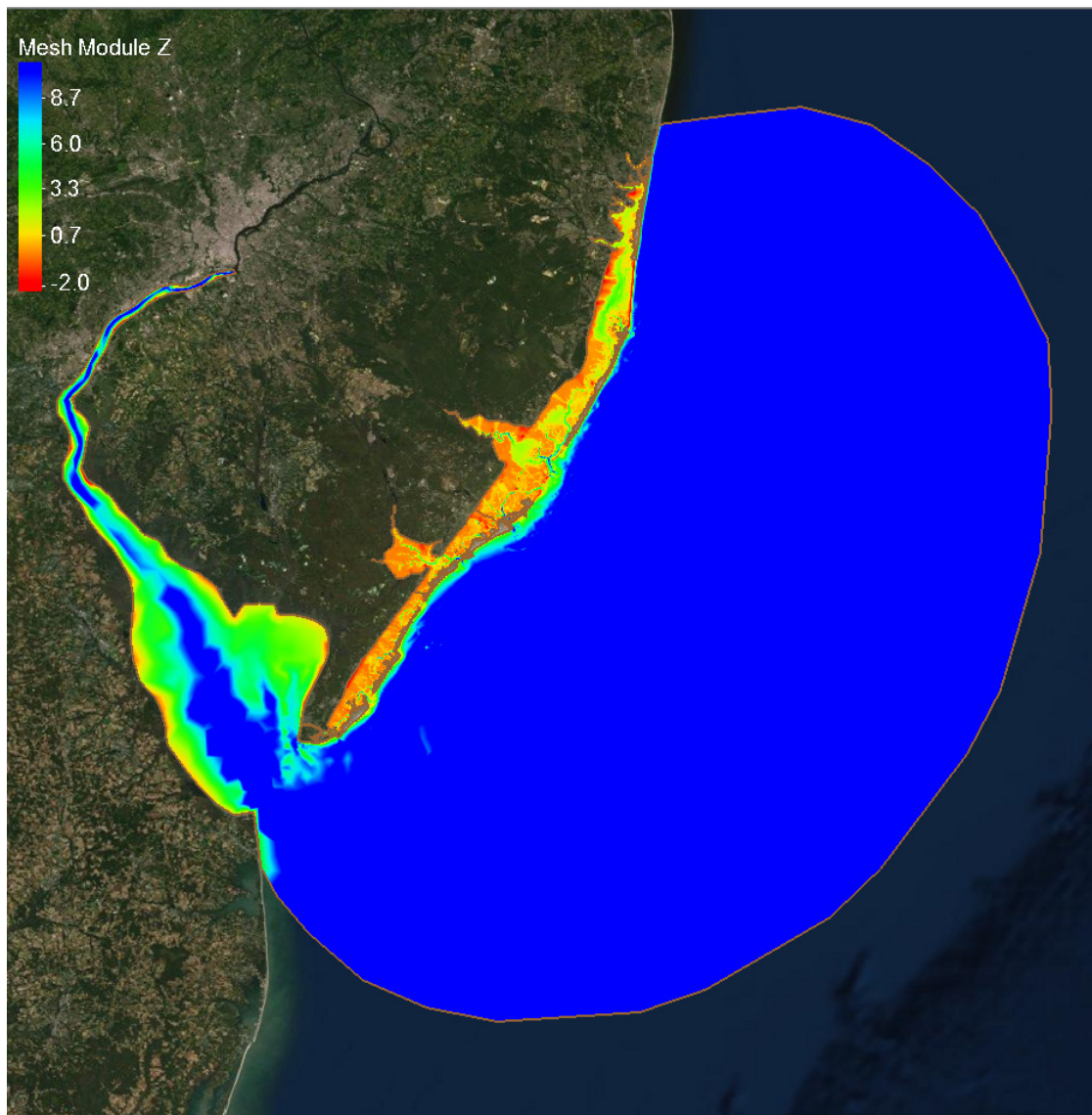


Figure 2-2 shows the ADH hydrodynamic modeling domain with contoured bathymetry. Areas in blue designate the ocean boundary to the NJBB and some deeper areas in the river. Areas in green show the backbays and channels. Areas in yellow and red designate the wetland regions.

Figure 2-2 ADH Bathymetry

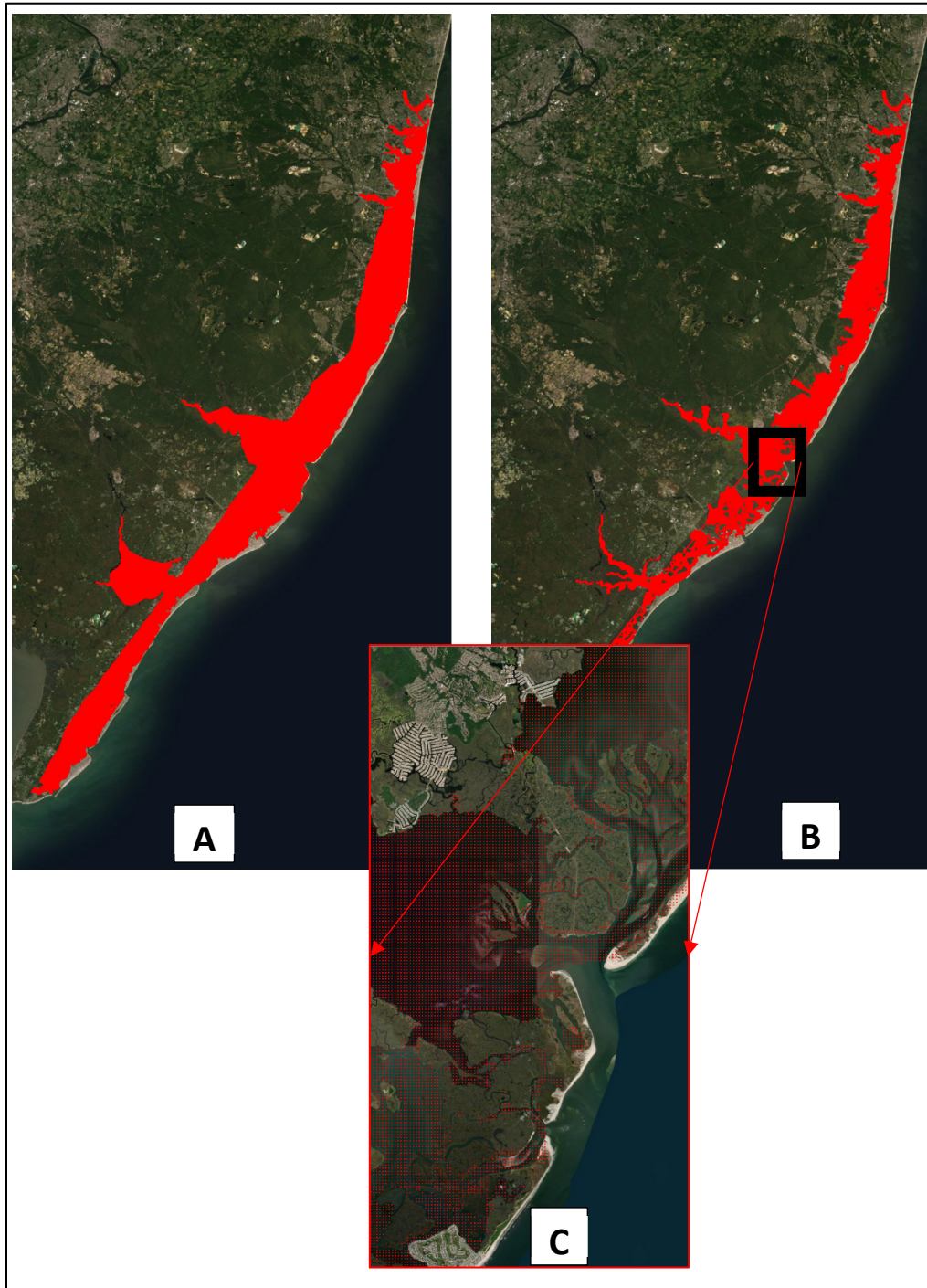


Particle Initial location

PTM takes initial particle location for this work as a series of x, y, z coordinates based on user input. The particles positions originally considered for this project are seen in Figure 2-3a (Particle locations are shown in red). These particles incorporate the entire NJBB area shown within the bathymetry and hydrodynamic section. However, the initial particle locations were reduced to particles introduced in areas which have been defined as back bays and channels in the ADH hydrodynamic section (shown in yellow and green in figure 2-2). The particles from this reduced

set have a greater chance of being transported by the velocities because they are predominately “wet”. Figure 2-3 c shows a zoomed in area of the initial particle locations. Particles are spaced 100 meters apart in both x and y-directions. Particles are introduced at the top of the water column. All particles are introduced at the same time at the beginning of the simulation (time T_0).

Figure 2-3 (a) Initial Particle Locations, (b) Initial Particle locations Reduced to Back Bays and Channels, (c) Zoom in of Partiles in Back Bays and Channels



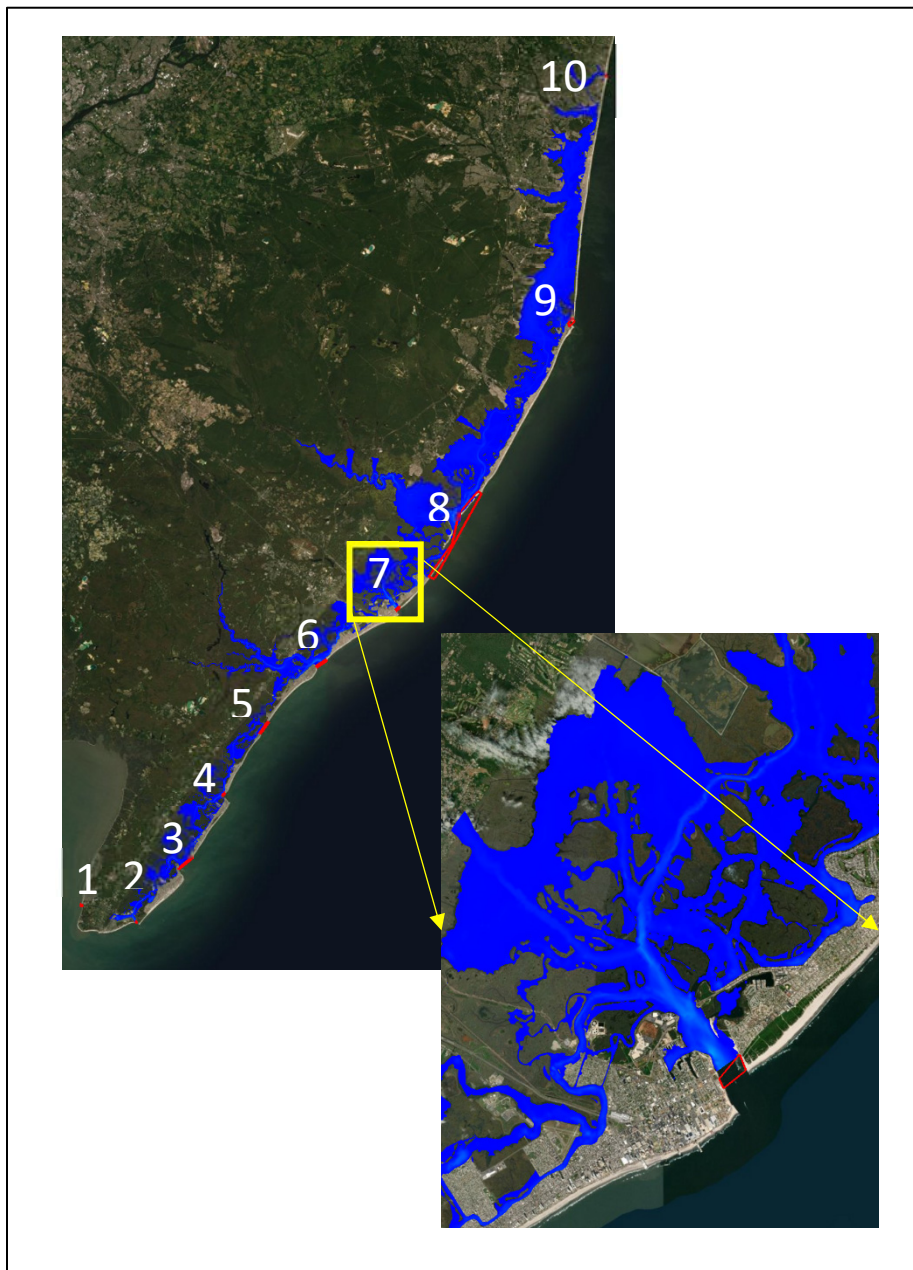
PTM Residence Time Traps

Residence time traps were placed at each inlet or area where particles might exit the NJBB. PTM uses “traps” to determine when particles pass

through specified areas of the domain. When particles pass through the traps, the model flags the particle ID, trap location, and date/time. This date/time is the residence time for the particles T_r .

Ten residence time traps were developed for this project (Figure 2-4). The traps are placed at the inlets of the NJBB and described for the model as polygons (shown in red). As particles enter the polygon they are considered recruited and are no longer a part of the simulation for efficiency. That is, particles are not modeled after they move through the traps into the ocean. Figure 2-4 shows a zoomed in view of the trap designated as trap 7.

Figure 2-4 Residence Time Traps at each Inlets



Residence Time Calculations

Residence Time Map

Residence time contour maps were created to visually differentiate the varying residence time of areas with the NJBB and then to compare and contrast the base conditions with the alternatives. As described in the

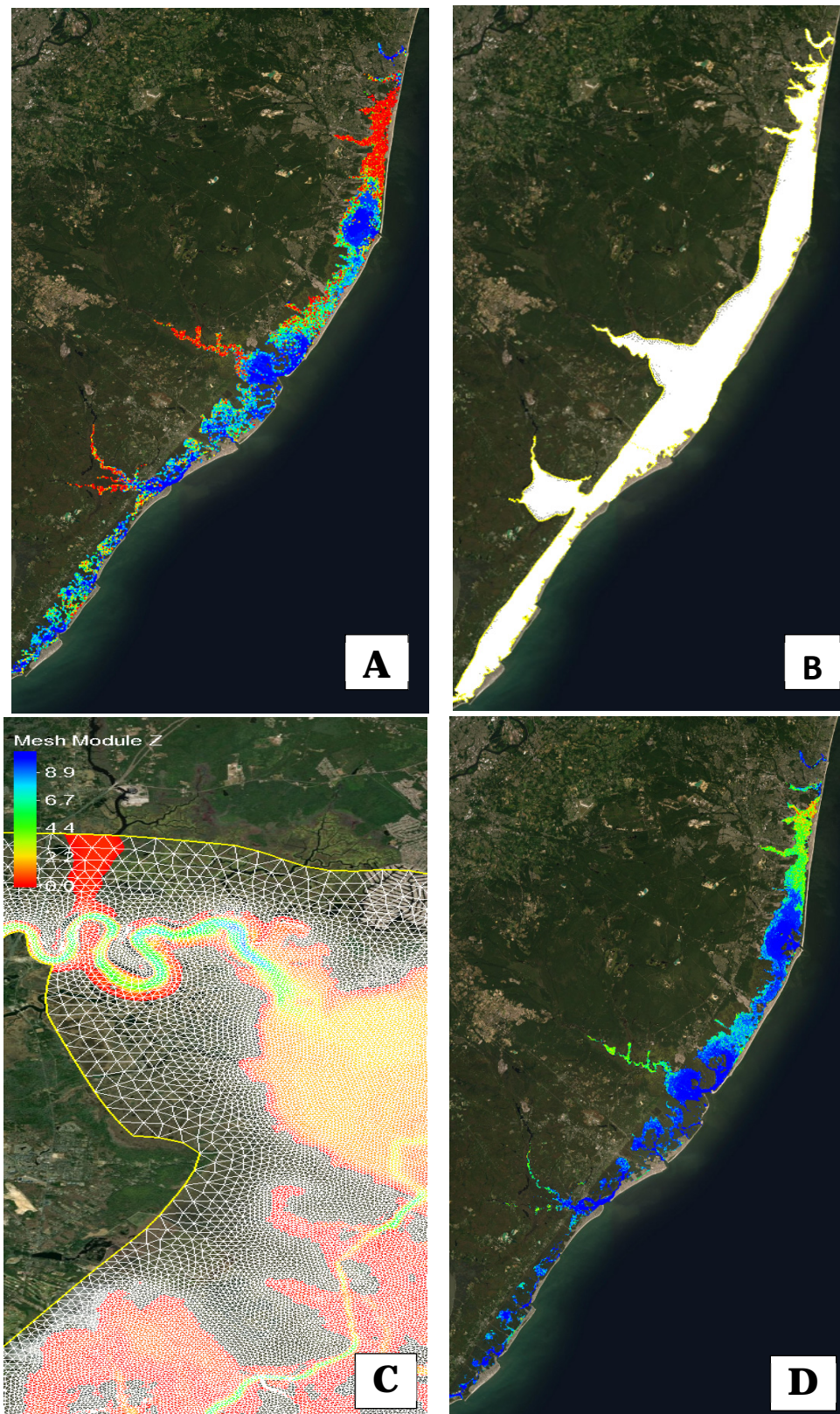
previous section, the PTM model identifies the time and location that each particle initiated within the system, exits the system. The initial time that particles were introduced T_0 into the system was subtracted from the time of the particle exiting the system T_r to determine the residence time of the particle RT_i .

$$RT_i = T_r - T_0 \quad (1)$$

That information was post processed (using a MatLab script) and the residence time was mapped back to the initial particle location (Figure 2-5 a). The resulting scatter set was then interpolated onto the ADH mesh (Figure 2-5b). For efficiency, this larger grid was reduced to only the NJBB area. In addition, only cells that were previously designated back bays and channels were for mapping. Figure 2-5 c shows a zoomed in area of the NJBB. The interpolation mesh is layered on top of contours designating the Back Bay and channel region. Only the colored areas were mapped for the residence time analysis. The results of the scatter set interpolation onto the mesh is shown in Figure 2-5 d.

Several interpolation techniques were investigated (linear, weighted). It was ultimately determined that the nearest neighbor technique introduced the least amount of error. With this technique the residence time associated with a mesh cell is based on the residence time of the closest initial particle location. It should be noted that within our area of interest the mesh cell size ranged from approximately 25m to 125m across. In most of the Back Bay area there was at least one particle in each cell. In areas where there are multiple particles within a grid cell, the residence time is averaged. In some instances the closest particle may be in a neighboring cell.

Figure 2-5 Process of converting scatter point data to interpolated contoured mesh data



Average Residence Time Calculations

Quantitative results were determined using average residence time calculations. Average residence time was calculated within a series of polygons (defined by NAP) (Figure 2-6a). Each polygon is populated with initial particle locations (Figure 2-6b). The residence times assigned to those particles were averaged based on the particles contained within the polygon. The average residence time of each polygon is denoted ART_p .

$$ART_p = \frac{\sum_{i=1}^{N_p} RT_i}{N_p} \quad (2)$$

Here N_p is the number of particles initially located in a polygon that also reached a trap. RT_i is the residence time of particle “ i ” located within that polygon at the beginning of the simulation.

Figure 2-6 Average residence time polygons and initial particle locations

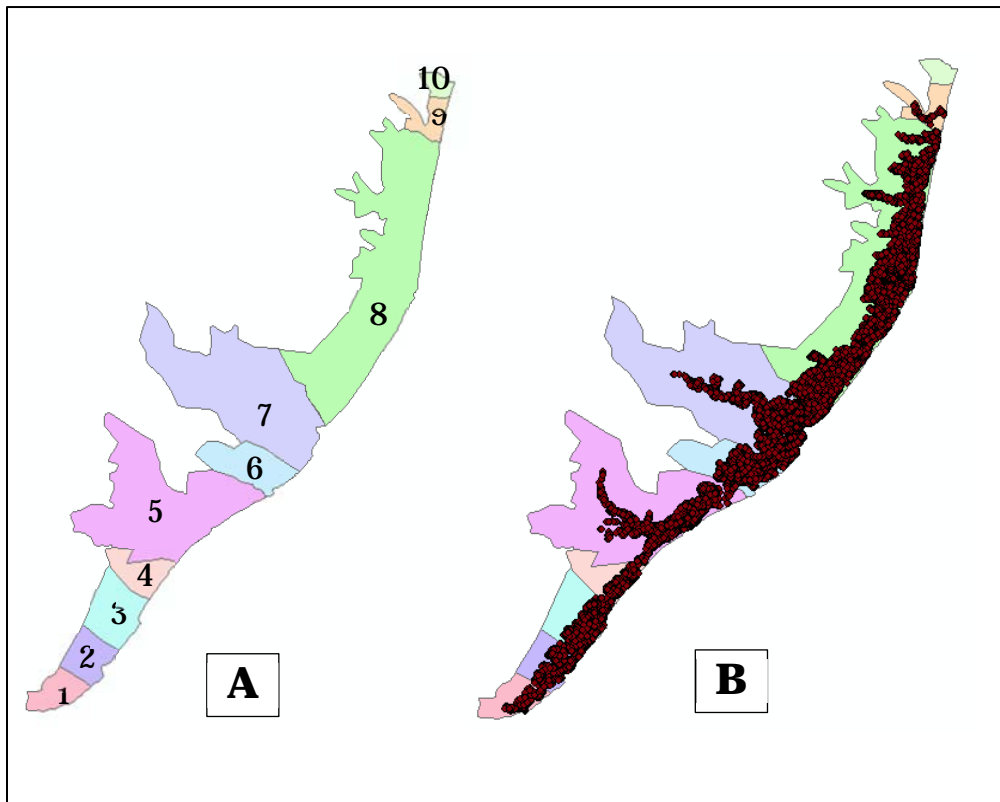


Table 2-2 Polygon ID and names

Polygon ID	Polygon Location
1	Cape May
2	Hereford
3	Townsend
4	Corson
5	Great Egg Harbor Bay
6	Absecon Bay
7	Great Bay
8	Barnegat Bay
9	Manasquan River
10	Shark

Limitation of Modeling and Analysis Methods

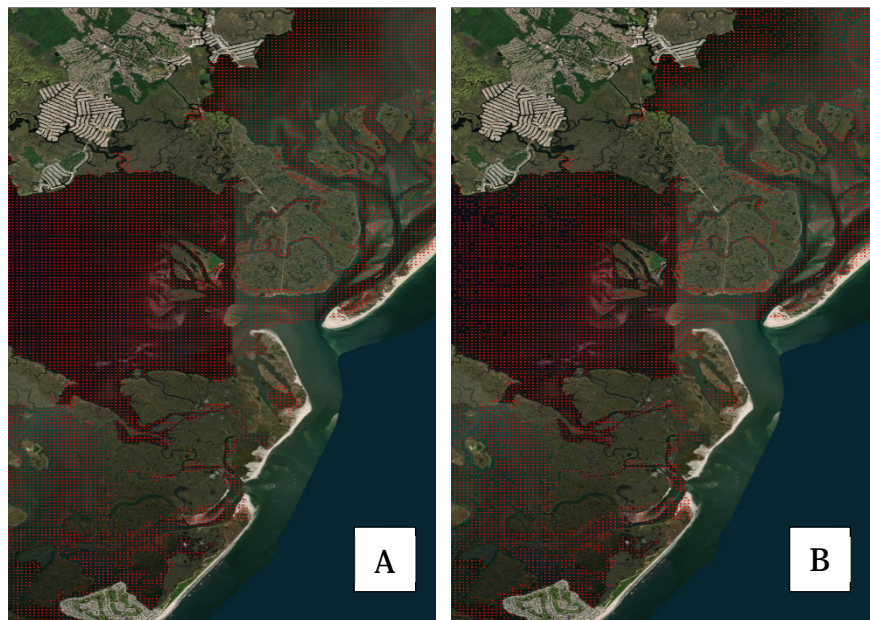
Although the previously described method is a reasonable technique utilized to obtain residence time information, there are several limitations that should be discussed.

Lagrangian particle transport for passive particles is entirely dependent on hydrodynamics. Hydrodynamic calculations within the Back Bay area are complex. The method used for the AdH calculations to predict this complicated flow is consistent with generally accepted hydrodynamic modeling techniques. However, when dealing with this type of system (which includes marsh and wetlands) this method is primarily used for determining water surface elevation and velocities near the inlets where validation data is most likely available. Unfortunately, field data measurements for bathymetry and velocity are often sparse (or non-existent) within the marsh area in Back Bays. In addition, to correctly calculate velocities in marsh regions for transport, the roughness values representing the marsh may need to be adjusted at each mesh cell. Without this level of detailed information, it is recognized that the accuracy of velocities are limited.

In addition, the PTM model has limited capacity to accurately transport particles in areas that are wet and dry. During the simulation, particles may potentially be transported into a cell that dries. The particle will attempt to resuspend, if it subsequently fills with water. However, depending on the velocity and the water surface elevation, the particle may be “stuck” for the remainder of the simulation or take longer to exit the system. In addition, some particle may have issues when interacting with mesh boundaries or become isolated in areas of recirculation for long time periods.

Analysis methods were adjusted to account for these particles. If a particle did not reach a trap during the simulation, it was no longer utilized in contour mapping or average residence time calculations. Figure 2-7a shows a zoomed in area of the initial particle locations. Figure 2-7b shows the adjusted initial locations accounting for particles that did not make it to traps during the simulation. Several areas of blank spots are visible.

Figure 2-7 (a) Zoom in of Initial Particles, (b) Zoom in of adjusted particles that reach traps during the simulation



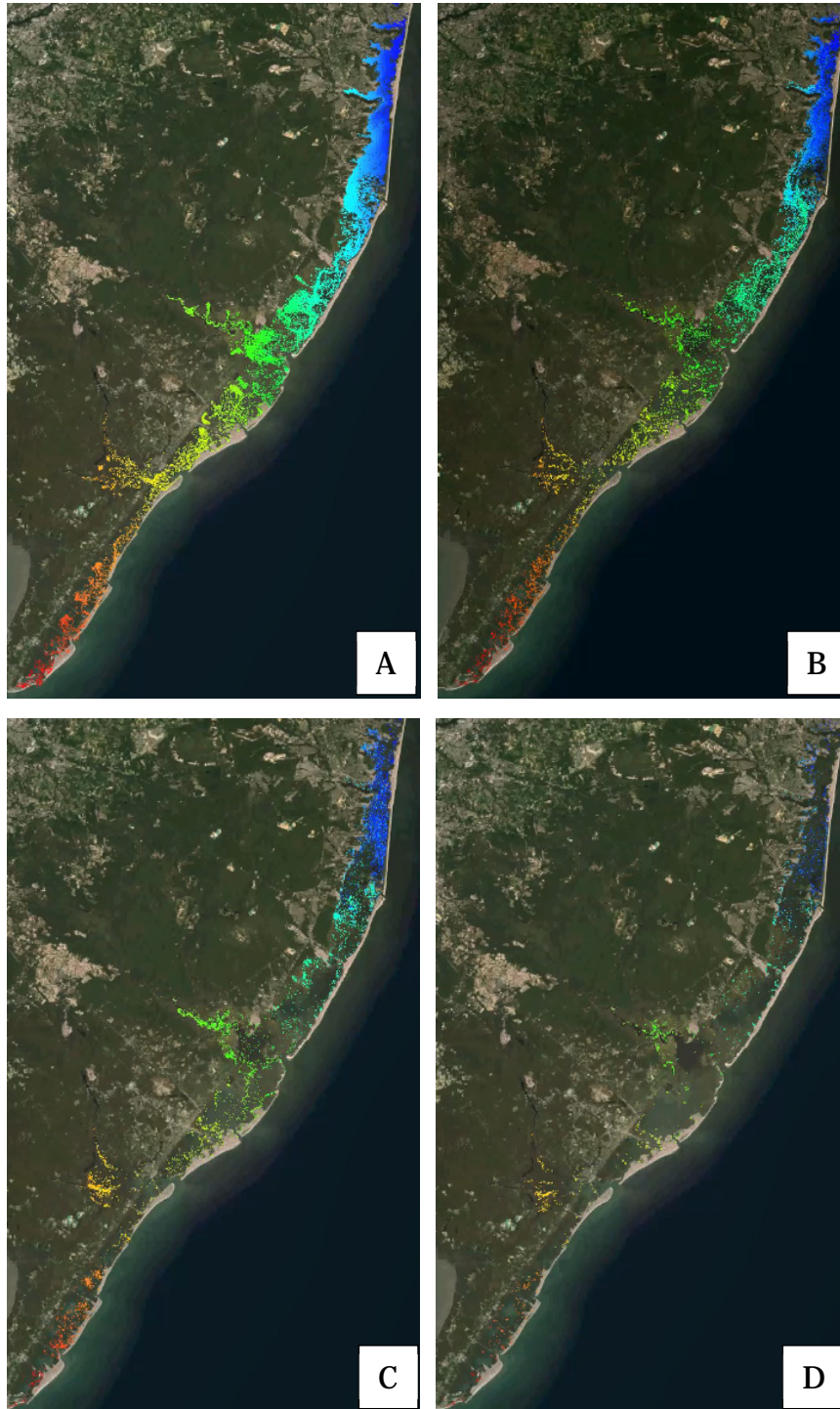
3 Results

Model results are shown as particle position maps, maps of residence time, and average residence time tables. For the residence time analysis, the results from the base case are described first and then compared to the alternative structure conditions. Finally the sea level rise results are presented.

Particle Position Maps

PTM particle position output is shown in figure 3-1. Particles are color coded based on particle initial location. Figure 3-1 shows the particles at the beginning of the simulation. As expected the particles cover the entire area “wet” area. Within two weeks, particles (primarily) within the lower region have begun to exit the system via the inlets. After two months, a good percentage of particles in the lower region have exited the system except for some particles (red and orange) which are slower to move out of the system. In the upper region many of the blue particles still remain in the system. After 4 months, most of the particles have exited the system. There are some particles still visible in the system which most likely represent particles which are “stuck” in marsh areas due to wetting and drying, or due to interactions with the mesh boundaries.

Figure 3-1 Particle position output (color coded based on initial location) at a) start time and then after b) 2 weeks c) 2 months, and d) 4 months



Residence Time Contour Maps

Base case residence time is shown in Figure 3-2. Contour levels range from minimum of 0 days to 80 days. Areas with a residence time of greater than 80s were incorporated within that maximum bin. Because the region is large, the maps were separated into two main areas. The upper region encompasses Little Egg to Manasquan Inlet and the lower regions contains Cape May Inlet to Absecon Inlet. The particles that are at near the opening of the inlet, exit out the system within 0 – 9 days. Particles that are initiated in-between inlets take longer to exit the system. The particles in the upper region near Barnegat Inlet seem to have the longest residence time. There are also some red areas designating longer residence near Townsend Inlet. Particles that are farther into the back channels inland from Little Egg Inlet also appear red. However reasonably due to distance into the marsh areas and the limitations of the model to predict transport for such a distance, the exact residence time would be too difficult to accurately determine. It is reasonable to assume that the residence time is longer than the residence time of areas further downstream towards the inlet. Therefore the overall trends seem realistic.

The contour plots for the Base case compared to WP1-6 upper region (Little Egg – Manasquan Inlet) and lower region (Cape May Inlet – Absecon Inlet) are shown in Figures 3-3 and 3-4. Visually there appears to be very little difference between the conditions. This suggest that overall the trends for particles exiting the system don't change much. Particles near the inlets exit first within 10 days and particles that are further away from the inlet take longer to exit the system. To gain further quantitative results, average residence time analysis was performed.

Figure 3-2 Base Case Particle Residence Time contour. Little Egg – Manasquan Inlet (Left) and Cape May Inlet – Absecon Inlet (Right)

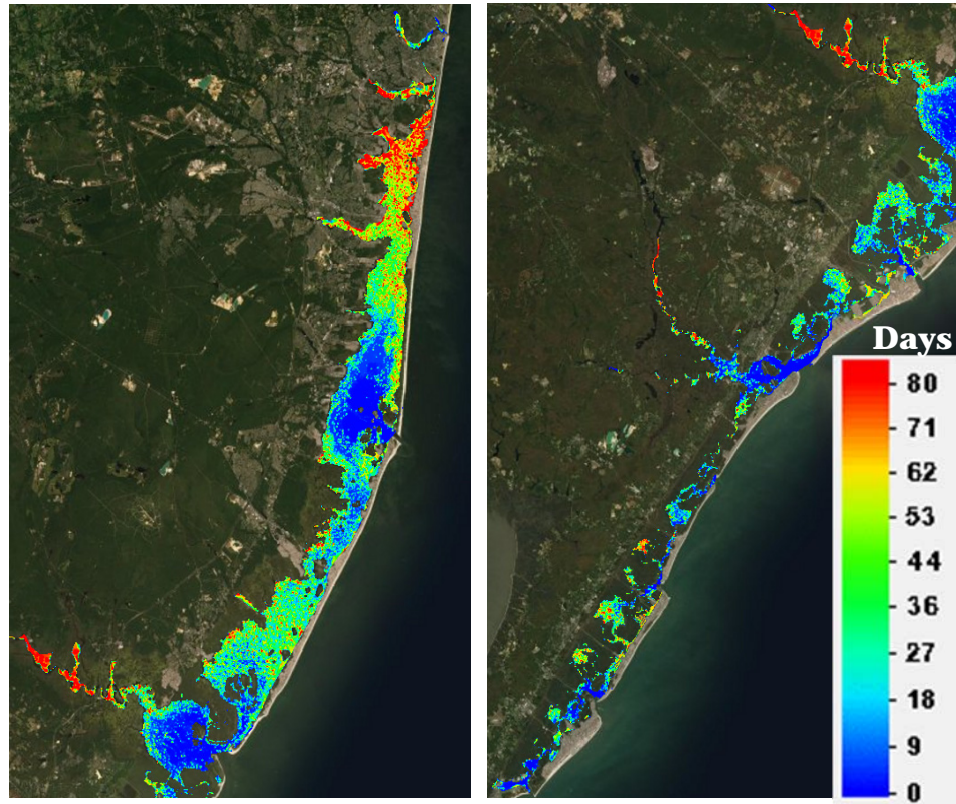


Figure 3-3 Particle Residence Time Contour Plots (Base - WP5). Little Egg - Manasquan Inlet

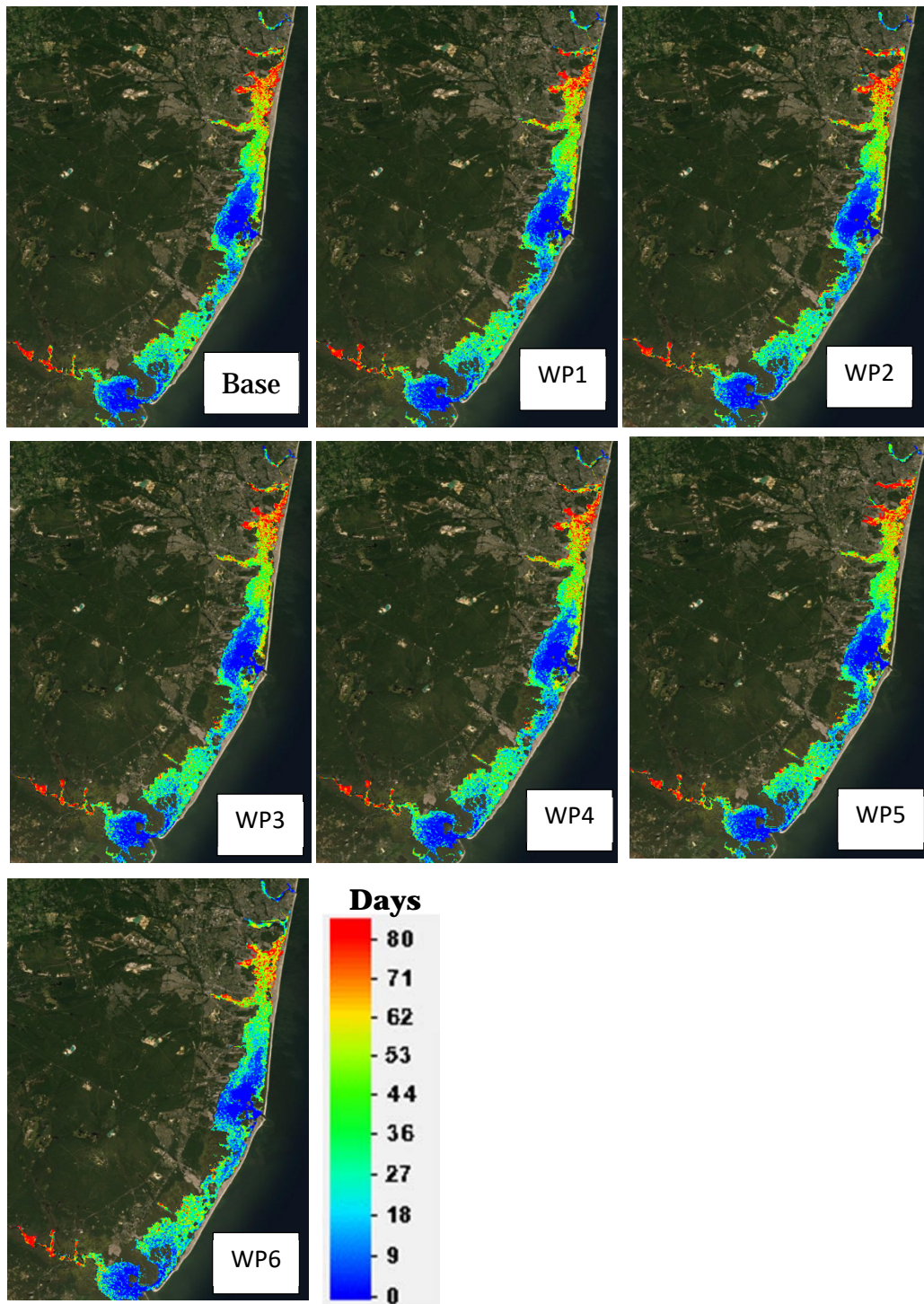
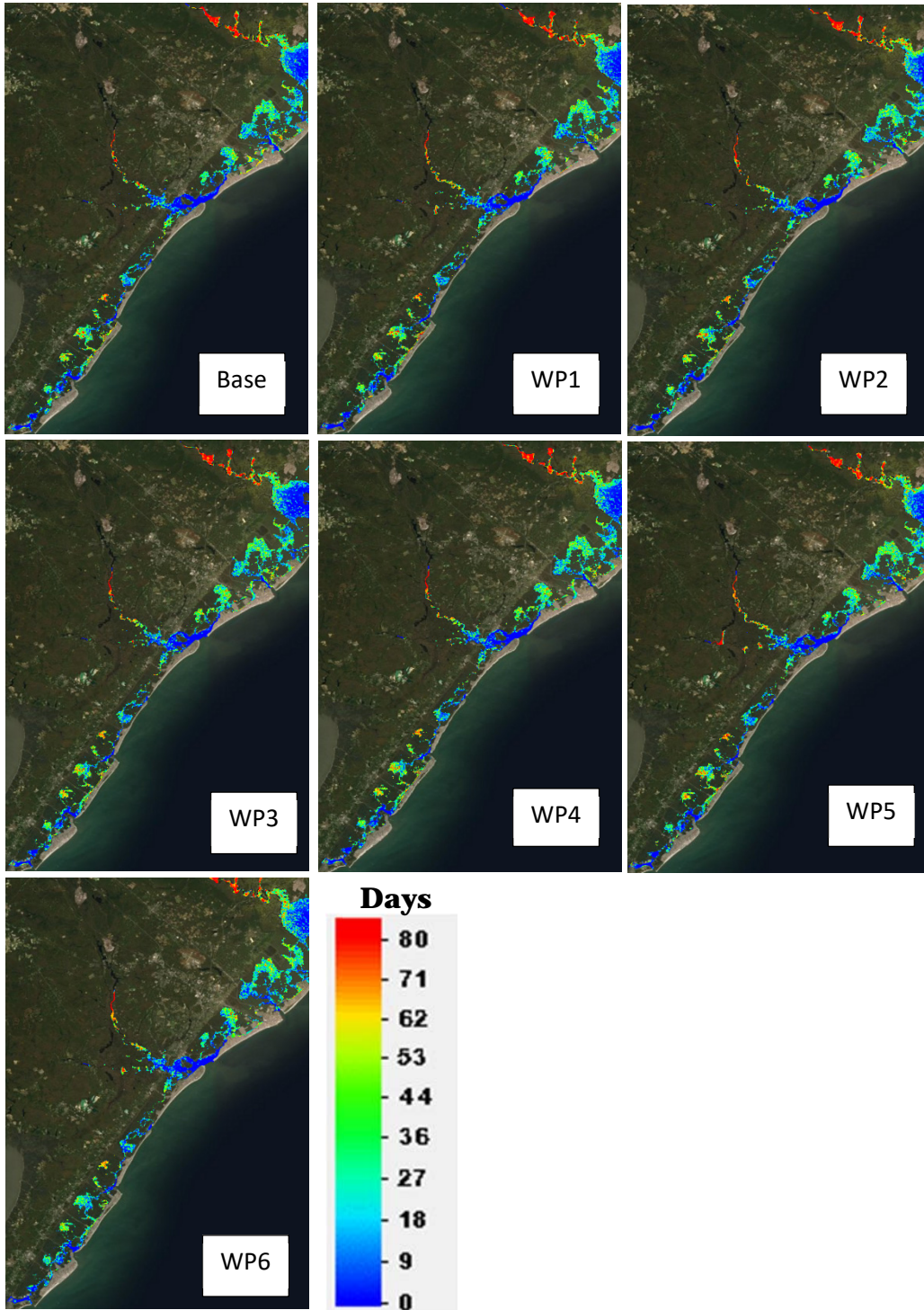


Figure 3-4 Particle Residence Time Contour Plots (Base - WP6). Cape May Inlet - Absecon Inlet.



Average Residence Time Analysis

The average residence time (ART) results for each of the polygons depicted in Figure 2-6a is shown for the Base case in Table 3-1. This table includes sensitivity statistics. The simulation for the base case was run five times and a sensitivity analysis was performed to determine the model sensitivity based on innate randomness. Model randomness results from several sources such as the random walk diffusion algorithms contained in PTM. If particles are transported into areas that wet and dry, then may deposit. Because of the wet/dry transport limitations, the particle may stay in the marsh areas for different lengths of time.

The first column of Table 3-1 is the location/name given for each polygon. Column two is the mean of the ART. The subsequent columns are for the minimum, maximum, range, and standard deviation respectively.

Results show that the highest average residence time is Townsend (approximately 36 days) and the lowest residence time is calculated at Cape May (approximately 11 days). It should be noted that these polygons are not the same size. More particles are in larger polygons than in smaller polygons. The Cape May polygon represents a small overall area where all of the particles were reasonably close to the inlet. A relatively small residence time is a logical result. The area of the Townsend polygon is also relatively small. However, Figure 3-2 shows that there are some areas of long residence time within that polygon. Because of the small overall area of the polygon, particles with long residence time may have a larger impact to the overall residence time calculation. The sensitivity analysis shows that this area also has a range of 4.39 days, which is relatively large compared to other areas such as Barnegat and Great Egg. Another relatively small region that has a large range (6.75 days) of residence time, is the Manasquan River polygon. Particles exiting from this area showed a tendency to interact with the mesh boundaries. Confidence in accurate residence time within the area is therefore low.

Table 3-1 Particle Residence Time (Days) - Base

Particle Residence Time (Days) - Base					
Location	Mean	MIN	Max	RANGE	SD
Cape May	10.88	10.05	11.83	1.78	0.97
Hereford	24.96	23.73	26.71	2.98	1.25
Townsend	35.97	34.82	39.21	4.39	2.16
Corson	19.14	17.77	21.46	3.69	1.60
Great Egg Harbor Bay	19.59	19.26	19.94	0.68	0.38
Absecon Bay	26.20	25.52	27.96	2.44	1.18
Great Bay	20.03	19.13	20.57	1.44	0.62
Barnegat Bay	30.48	30.31	30.70	0.39	0.16
Manasquan River	29.66	26.24	32.99	6.75	3.84

Comparison of average residence time is presented in Tables 3-2 and 3-3. Table 3-2 shows the Base case calculated residence time for each area as well as the results from the alternative configuration. For the sake of discussion purposes each configuration described in Table 2-1 will be denoted as With Project 1-6 or simply WP1-6. Results show that the WP 1-6 conditions follow similar trends to the Base condition. The Cape May polygon has the shortest residence time and the Townsends polygon has the largest residence time. However, because of low confidence in the Townsends area and Manasquan River area, these results will not be the focus on much discussion.

Table 3-2 Alternatives' Average Residence Time (Days)

Alternatives' Average Residence Time (Days)							
Location	Base	Wp1	Wp2	Wp3	Wp4	Wp5	Wp6
Cape May	10.88	9.85	9.57	11.66	11.66	10.96	12.68
Hereford	24.96	26.95	26.22	28.63	28.63	26.81	25.7
Townsend	35.97	39.89	38.85	39.34	39.34	40.04	25.17
Corson	19.14	23.95	24.24	21.98	21.98	22.58	17.93
Great Egg Harbor Bay	19.59	22.09	22	23.03	23.03	22.18	22.89
Absecon Bay	26.2	27.92	25.55	29.13	29.13	29.32	25.54
Great Bay	20.03	19.09	19.4	19.18	19.18	19.86	23.24
Barnegat Bay	30.48	29.55	28.97	29.62	29.62	29.85	24.76
Manasquan River	29.66	27.37	17.05	28.2	28.2	27.94	21.28

Table 3-3 presents a more accessible comparison of Base case and alternatives condition residence. Each column shows the difference (Difference = Project Value – Base Case ART) in residence time. The second column shows the range (in days) of residence time from the sensitivity analysis to give perspective to each of the results. For example, although the Cape May WP1 results differ from the Base case by -1.03. The sensitivity analysis shows that these two values can be described as similar. For most of the conditions, the results for the ART appear to be similar to the base case results. One potential difference might be shown at Great Egg Harbor Bay. Residence time seems to have increased between 2.5-3.5 days despite relatively low sensitivity in the base condition. One reason for this might be that the Great Egg inlet discharge values are larger for the Base case than for the WP conditions (McAlpin and Ross 2020).

Table 3-3 Alternatives' Difference (WP-Base) Residence Time (Days)

Alternatives' Difference (WP-Base) Residence Time (Days)							
Location	Base Sensitivity (Range)	Wp1	Wp2	Wp3	Wp4	Wp5	Wp6
Cape May	1.78	-1.03	-1.31	0.78	0.78	0.08	-1.8
Hereford	2.98	1.99	1.26	3.67	3.67	1.85	-0.74
Townsend's	4.39	3.92	2.88	3.37	3.37	4.07	10.8
Corson	3.69	4.81	5.1	2.84	2.84	3.44	1.21
Great Egg Harbor Bay	0.68	2.5	2.41	3.44	3.44	2.59	-3.3
Absecon Bay	2.44	1.72	-0.65	2.93	2.93	3.12	0.66
Great Bay	1.44	-0.94	-0.63	-0.85	-0.85	-0.17	-3.21
Barnegat Bay	0.39	-0.93	-1.51	-0.86	-0.86	-0.63	5.72
Manasquan River	6.75	-2.29	-12.61	-1.46	-1.46	-1.72	8.38

Sea Level Rise Analysis

The impact of Sea Level Rise (SLR) was investigated to determine the ultimate impact of structures on residence time. Figure 3-5 shows a comparison between the base condition and the base condition with SLR taken into consideration. The comparison shows that there is a decrease in overall residence time (more blue regions) for SLR conditions. Potentially this may be because there is less wetting and drying and more flow through the wetland areas due to the predicted conditions. This is supported by the results from the average residence time calculations (Table 3-4). The average residence time for the Base case for all areas ranges from 5 to 20 days for the SLR conditions. For the current Base case conditions the results range from 10 to 36 days.

Comparison of SLR base condition to the SLR WP1 and SLR WP5 alternatives (Figure 3-6 and Table 3-4) shows great similarities. The average residence time shows difference between the SLR base condition and the SLR WP1 and SLR WP5 conditions that range from 0.3 to 2 days. There is one outlier at Manasquan River. However, it has already been acknowledged the model performed poorly in this area. The overall

residence time values remain much lower than their previously described counter parts (WP1 and WP5).

Figure 3-5 Residence time contour maps of Base condition and Base SLR condition

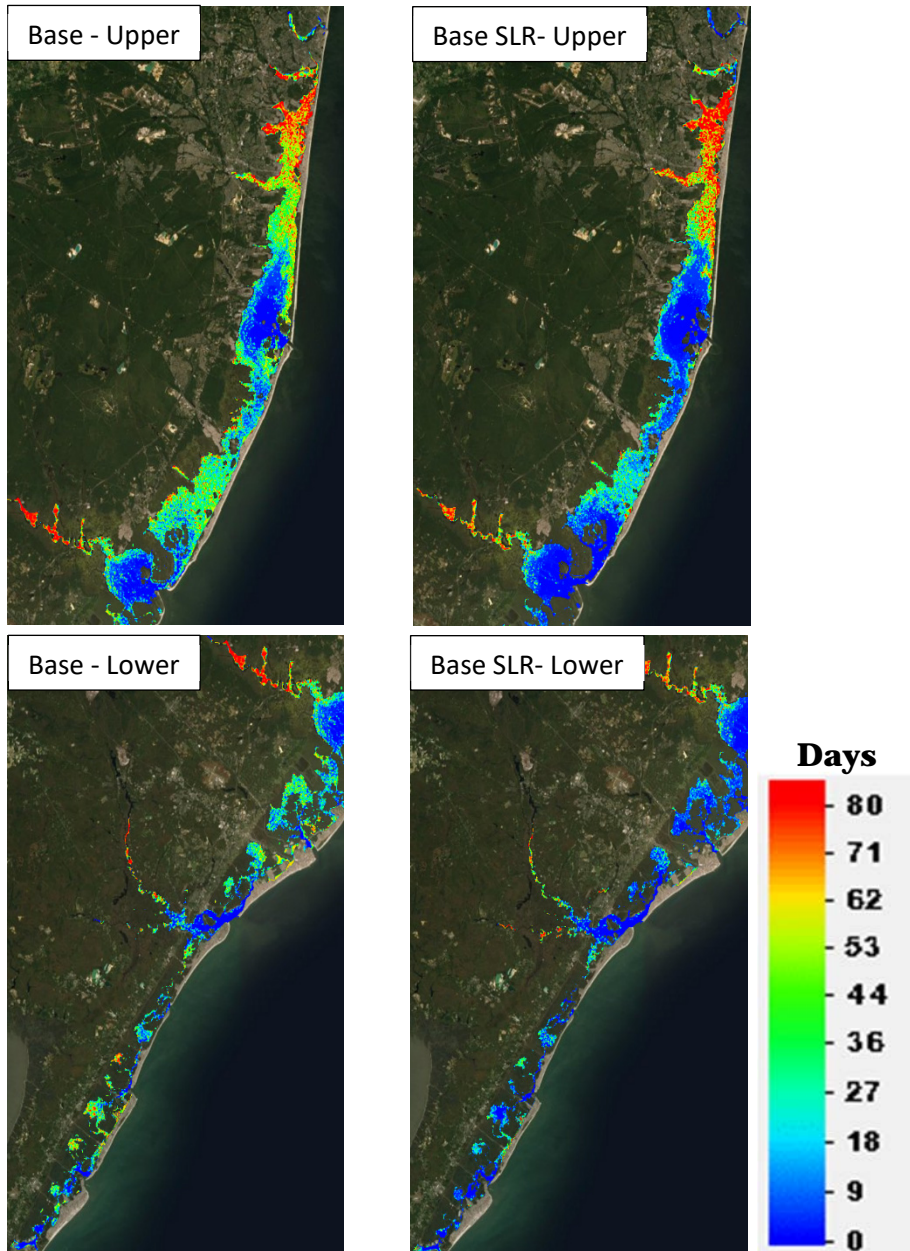


Figure 3-6 Residence time contour map of Base SLR, WP1 SLR, WP4 SLR conditions

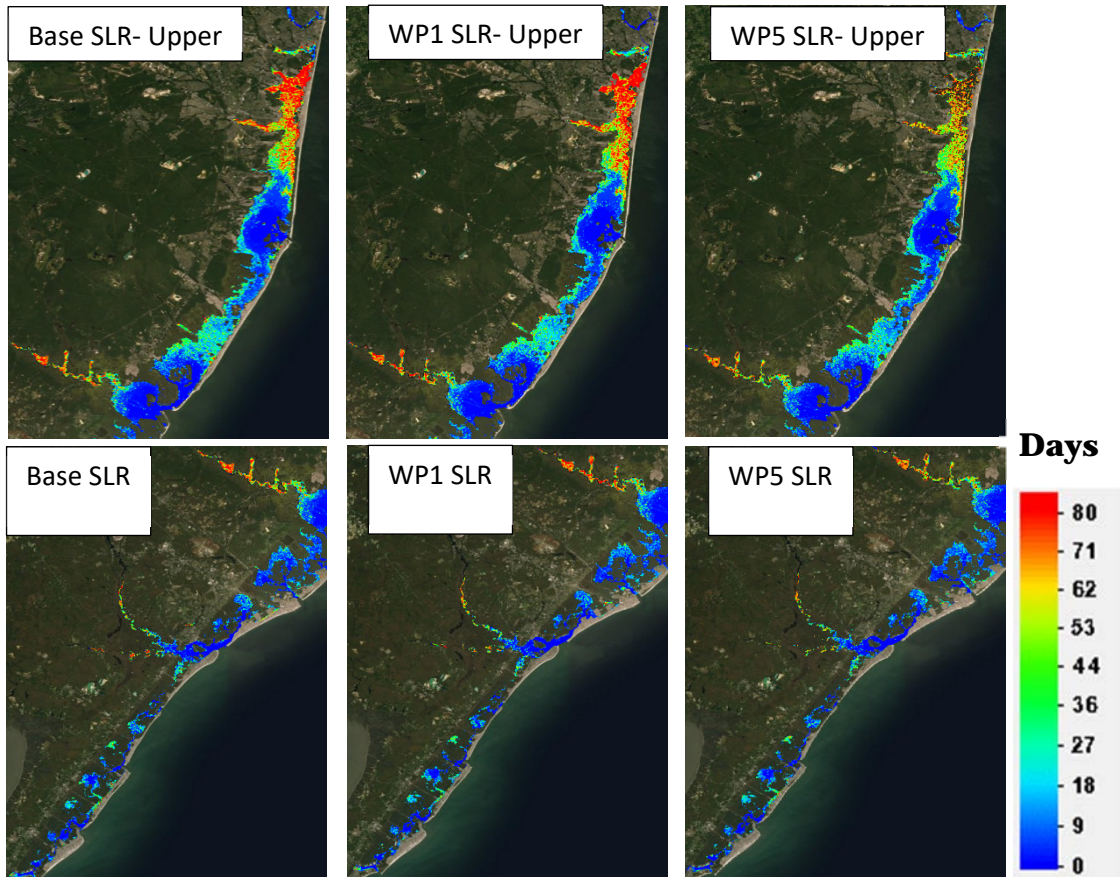


Table 3-4 Alternatives' Average Particle Residence (Days)- SLR

Alternatives' Average Particle Residence (Days)- SLR				
Location	Base	Base SLR	Wp1 SLR	Wp5 SLR
Cape May	10.88	7.09	6.40	6.61
Hereford	24.96	7.73	7.19	8.10
Townsend	35.97	13.57	12.48	13.26
Corson	19.14	10.16	8.05	8.58
Great Egg Harbor Bay	19.59	14.14	13.36	14.63
Absecon Bay	26.20	8.06	6.78	8.29
Great Bay	20.03	9.84	11.00	10.32
Barnegat Bay	30.48	20.53	20.16	21.60
Manasquan River	29.66	5.57	1.41	4.74

4 Summary and Conclusions

The U.S. Army Engineer Research and Development Center, Coastal and Hydraulics Laboratory performed residence time analysis to better understand the impacts of proposed storm barriers in the New Jersey Back Bays (NJBB) on wetland habitat within the system. The purpose of the residence time analysis would be to determine if proposed structures would increase areas of stagnation within NJBB, which might negatively affect the wetland habitat.

Residence time results for current (base) conditions were compared with a series of project conditions that differ due to various potential structures (gates, barriers, etc) under consideration by NAP. Residence time calculations were performed utilizing the Particle Tracking Model (PTM) transport output from a four month simulation. PTM, a Lagrangian particle tracker developed by ERDC-CHL, simulated transport of water particles within the NJBB out into the ocean. Residence time contour maps and average residence time within specified polygons were developed to compare and contrast the different conditions.

Sensitivity analysis was performed to better understand model precision for the base condition. This analysis showed that for average residence time calculations within developed polygons, model results could differ between 0.4-3.7 days (outliers were removed). Lack of validation for the hydrodynamic forcing within NJBB and the inability of the model to realistically simulate transport in areas which experience wetting and drying were two factors that impacted sensitivity. Residence time results showed little different within the determined sensitivity. Residence time for base (current) conditions were similar to with project conditions. There were some outliers. However those differences could be explained due to model limitations. The investigation of sea level rise (SLR), showed that residence time decreases significantly with SLR for all structural configurations.

References

- Cialone, Mary A., Alison S. Grzegorzewski, David J. Mark, Mary A. Bryant, and Thomas C. Massey. 2017. Coastal-Storm Model Development and Water-Level Validation for the North Atlantic Coast Comprehensive Study. *Journal of Waterway, Port, Coastal, and Ocean Engineering*, Volume 143 Issue 5. September 2017.
- Defne, Zafer and Ganju, Neil K. (2014) Quantifying the residence time and flushing characteristics of a shallow, back-barrier estuary: Application of hydrodynamic and particle tracking models. *Estuaries and Coasts*. Volume 38, Issue 5. Pages 1719-1734.
- Gailani, J.Z., T.C. Lackey, D.B. King, D. Bryant, S.-C. Kim, and D.J. Shaf-er. (2016) Predicting Dredging Effects to Coral Reefs in Apra Harbor, Guam: Sediment Exposure Modeling. *Journal of Environmental Management*. Volume 168, 1 March 2016, Pages 16-26
- Lackey, T. C. and Smith, S. J (2008) "Application of the Particle Tracking Model to Predict the Fate of Dredged Suspended Sediment at the Willamette River" Proceedings Western Dredging Association Twenty-Eighth Annual Technical Conference, St. Louis, MO, USA.
- McAlpin, Jennifer and Ross, C. (2020) Analysis of Proposed Storm Protection Structures on the Hydrodynamics and Salinity in New Jersey Back Bays (NJBB). Technical Report TR-20-xx. U.S. Army Engineer Research and Development Center, Vicksburg, MS. *Draft*
- MacDonald, N.J., Davies, M.H., Zundel, A.K., Howlett, J.C., Demirbilek, Z., Gailani, J.Z., Lackey, T.C., Smith, J., 2006. PTM: Particle Tracking Model: Model theory, implementation, and example applications. In: Technical Report TR-06-20. U.S. Army Engineer Research and Development Center, Vicksburg, MS.
- Savant, G., R. C. Berger, T. O. McAlpin, and C. J. Trahan. 2014. Three-Dimensional Shallow Water Adaptive Hydraulics (AdH-SW3): Hydrodynamic Verification and Validation. ERDC/CHL TR-14-7. Vicksburg, MS: U.S. Army Engineer Research and Development Center.

Appendix A: Plan Alternative Descriptions (Excerpt from McAlpin and Ross 2020)